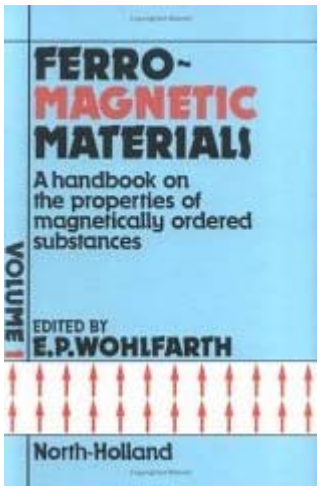

Handbook of Magnetic Materials, Volume1

North-Holland Publishing Company, 1980

Edited by: E.P Wohlfarth
ISBN: 978-0-444-85311-0

PREFACE

This Handbook on the Properties of Magnetically Ordered Substances, *Ferromagnetic Materials*, is intended as a comprehensive work of reference and textbook at the same time. As such it aims to encompass the achievements both of earlier compilations of tables and of earlier monographs. In fact, one aim of those who have helped to prepare this work has been to produce a worthy successor to Bozorth's classical and monomental book on Ferromagnetism, published some 30 years ago. This older book contained a mass of information, some of which is still valuable and which has been used very widely as a work of reference. It also contained in its text a remarkably broad converage of the scientific and technological background.

One man can no longer prepare a work of this nature and the only possibility was to produce several edited volumes containing review articles. The authors of these articles were intended to be those who are still active in research and development and sufficiently devoted to their calling and to their fellow scientists and technologists to be prepared to engage in the heavy tasks facing them. The reader and user of the Handbook will have to judge as to the success of the choice made.

One drawback of producing edited volumes is clearly the impossibility of having all the articles ready within a time span sufficiently short for the whole work, once ready, to be up-to-date. This is an effect occurring every time an editor of such a work engages in his task and has been found to be particularly marked in the present case, as might have been expected. Hence a decision was made to edit the first two volumes of the projected four volume work on the basis of the articles available about the end of 1978. Again, the reader must judge whether on balance the lack of a complete logical order of the articles in these two volumes is outweighed by their immediacy and topicality. The future of the work is in the hands of the remaining authors. The projected remaining two volumes will complete a broad and comprehensive coverage of the whole field.

Each author had before him the task of producing a description of material properties in graphical and tabular form in a broad background of discussion of

the physics, chemistry, metallurgy, structure and, to a lesser extent, engineering aspects of these properties. In this way, it was hoped to produce the required combined comprehensive work of reference and textbook. The success of the work will be judged perhaps more on the former than on the latter aspect. Ferromagnetic materials are used in remarkably many technological fields, but those engaged on research and development in this fascinating subject often feel themselves as if in a strife for superiority against an opposition based on other physical phenomena such as semiconductivity. Let the present Handbook be a suitable and effective weapon in this strife!

I have to thank many people and it gives me great pleasure to do so. I have had nothing but kindness and cooperation from the North-Holland Publishing Company, and in referring only to P.S.H. Bolman by name I do not wish to detract from the other members of this institution who have also helped. In the same way, I am deeply grateful to many people at the Philips Research Laboratory, Eindhoven, who gave me such useful advice in the early stages. Again, I wish to mention in particular H.P.J. Wijn and A.R. Miedema, without prejudice. Finally, I would like to thank all the authors of this Handbook, particularly those who submitted their articles on time!

E.P. Wohlfarth
Imperial College.

TABLE OF CONTENTS

chapter 1

IRON, COBALT AND NICKEL

E.P. WOHLFARTH
Department of Mathematics
Imperial College of Science and Technology
London SW7
UK

Ferromagnetic Materials, Vol. 1
Edited by E.P. Wohlfarth

CONTENTS

1. Summary of theoretical background

1.1. Introduction

The magnetism of the three ferromagnetic transition metals iron, cobalt and nickel is archetypal to the whole subject of metallic magnetism. It would seem necessary, if not sufficient, to understand the properties of these pure metals before attempting to understand those of the ferromagnetic transition metal alloys. As a result of this evident expectation great controversy has surrounded the three metals for many decades. The question used to be whether the magnetic carriers were localized or itinerant. Each of these views had its eminent proponent, such as Van Vleck on the one hand and Slater on the other. These heated arguments have died down since the 1950's, but even now it is by no means the case that iron, cobalt and nickel are fully understood. In fact, the magnetic properties of a considerable number of alloys are, surprisingly, more readily amenable to a reasonably simple interpretation than those of the pure metals. The reasons for this situation include the following:

(1) The three metals are either strong (nickel, cobalt), or almost strong (iron) itinerant electron ferromagnets. Hence the exchange splitting between the + and − spins is relatively large (see section 1.3). The application of one-electron, or Stoner theory is thus less certain than for the more weakly itinerant alloys and is even then algebraically and computationally less clear since no Landau expansion of the free energy is possible. (2) The influence on the magnetic properties of collective and many body effects, such as spin waves and spin fluctuations, is not only likely to be more important than for the weakly itinerant alloys but also to be itself less amenable to theoretical treatment. (3) The challenge of iron, cobalt and nickel is so clear that more attention has been paid to these materials than to others, so more experimental facts have to be explained.

Nevertheless, the controversy is now less heated and is more concerned with the relative importance of itinerancy and localization and of single particle and many body effects below the Curie temperature and with the apparent degree of order present above. Slater's emphatic belief that the Curie temperature itself is unrelated to the exchange splitting, although slowly being accepted as being true by some, continues to arouse some opposition from others. For all these reasons the ferromagnetism of iron, cobalt and nickel continues to provide the major

challenge in the field of metallic magnetism, in the same sense as before that any advance in understanding this difficult subject of the pure metals will surely help in understanding the more weakly itinerant alloys.

In this summary of the theoretical background a brief discussion of the calculation of energy bands and the Fermi surface is followed by the basics of one-electron or Stoner theory. The central parameter in this theory is the Stoner–Hubbard parameter I and a brief account is given of factors contributing to this energy (exchange and correlation), which in turn determines the exchange splitting between + and − spins. Theoretical values of these parameters for iron, cobalt and nickel are listed here while a summary of the experimental values obtained by the various possible measurements is given in later parts of this article. Since Stoner theory is too simple in some respects a brief discussion is given of results beyond this model, particularly those concerning spin waves and spin fluctuations. The theory of spin waves in metals is briefly outlined and calculated values of the spin wave stiffness D are tabulated. Experimental values are given later in section 2.7. This summary is kept deliberately brief in view of the nature of this Handbook which militates against an extensive theoretical treatment in favour of a more descriptive discussion of the physics of magnetic materials which serves as a background to the tabulation and graphical representation of their actual properties.

1.2. Calculation of energy bands and Fermi surface

There have been very many energy band calculations for iron and nickel, but fewer for cobalt. References to some of these are given by Callaway and Wang (1977a) for the former, including those carried out by themselves using the local exchange model of itinerant electron magnetism. Two approximations to the exchange potential were used, namely the so-called Kohn–Sham–Gaspar (KSG) potential which is basically derived from Slater exchange (Xα) here with α close to $\frac{2}{3}$, and the so-called von Barth–Hedin (vBH) potential which includes correlation. These methods are regarded at the time of writing as the most reliable for these metals. Table 1 summarizes the results for nickel. Detailed comparison with experiment is possible by reference to the later discussions. It suffices to note that (i) the magnetic moment as calculated by either method is reasonable,

TABLE 1
Band calculations for Ni (Callaway and Wang 1977a)

Potential	Moment (μ_B)	ΔE	$N(E_F)$	H_i
KSG($\alpha = \frac{2}{3}$)	0.65	0.88	22.9	−69.7
vBH	0.58	0.63	25.4	−57.4

ΔE, exchange splitting at top of band (eV).
$N(E_F)$, density of states at Fermi energy (states/atom/Ry).
H_i, difference in + and − spin densities at the nucleus, expressed as an effective hyperfine field (kG).

although better for vBH. (ii) The exchange splitting ΔE is sensitive to the potential and may be considerably larger than some but not all experimental values, discussed later; the explicit questions regarding the magnitude of ΔE remain central to the theory of the properties of the ferromagnetic transition metals. (iii) The density of states $N(E_F)$ lies below that obtained from the specific heat (see below) by a factor corresponding to an electron–phonon enhancement factor $\lambda \simeq 0.60$, which is very reasonable. (iv) The effective hyperfine field H_i is also reasonable when compared to experiment (see §2.2).

Wang and Callaway (1977) calculated the density of states curve for nickel on the basis of these two potentials, and the result for the vBH potential is shown in fig. 1 where the curve applies to both spin directions. Figure 2 shows cross-sections of the Fermi surface of nickel in a (100) plane. The agreement with experiment is generally good, although the d↓ heavy hole pocket shown by contour b has not been observed and may be an artifice of the potentials which are suggested to be insufficiently anisotropic.

Another band calculation on Ni has been reported by Marshall and Bross (1978), using an interpolation scheme and the Hubbard (1963) Hamiltonian for the ferromagnetic metal. The results agree better with experiment than those of Wang and Callaway (1977), e.g. the absence of the heavy hole pocket. The gap Δ, defined by eq. (9), comes out smaller at 175 meV, though still twice as large as given by the spin polarized photoemission data discussed in section 4.1. and the neutron data, section 2.7. The authors feel they can account for this remaining difference.

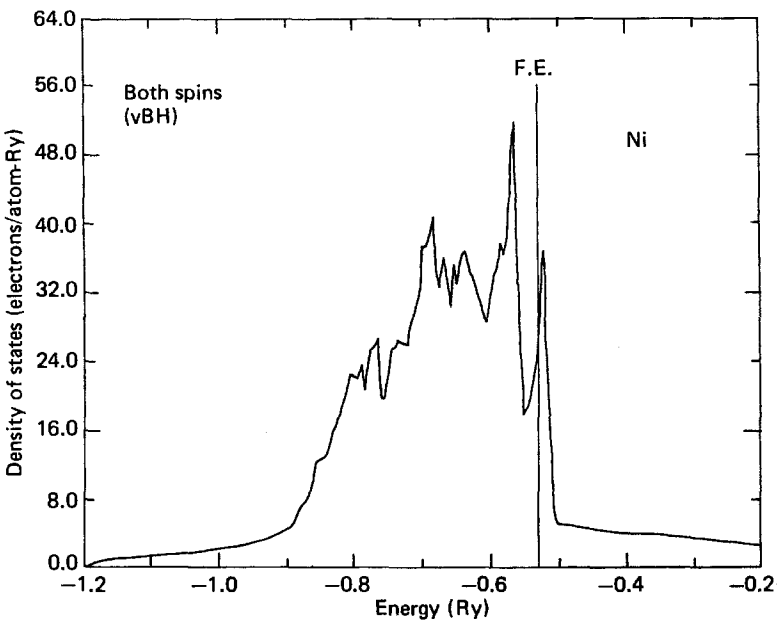

Fig. 1. Density of states curve for both spin directions of nickel using vBH potential (Wang and Callaway 1977).

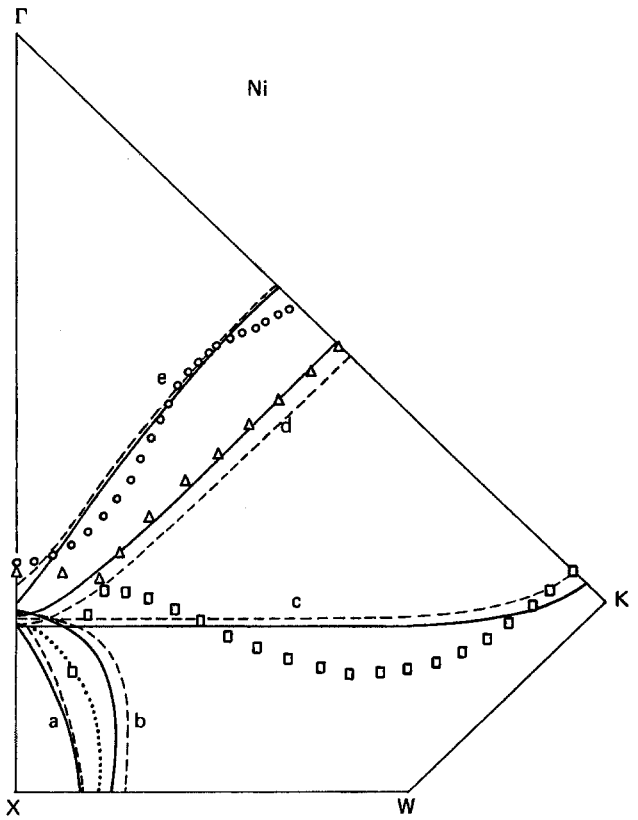

Fig. 2. Cross-sections of the Fermi surface of nickel in the (100) plane (Wang and Callaway 1977). Dashed lines KSG potential, solid lines vBH potential. Triangles, squares, dotted line, experimental data of Stark (see Gold 1974) and Tsui (1967). (a) $X_{5\downarrow}$ hole pocket; (b) $X_{2\downarrow}$ hole pocket; (c) major d ↓ hole surface; (d) sp ↑ surface; (e) sp ↓ surface.

For iron similar results are shown in table 2. Comparison with experiment, where possible, is given later. The question of the exchange splitting ΔE is even more critical for iron than for nickel; as before the calculated values are sensitive to the potential and tend to be somewhat above those given, without too much confidence, by the various possible observations described below. The electron–phonon enhancement factor λ is about 0.70.

TABLE 2
Band calculations for bcc Fe (Callaway and Wang 1977a,b)

Potential	Moment (μ_B)	ΔE	$N(E_F)$	H_i
KSG($\alpha = \frac{2}{3}$)	2.30	2.68	15.4	−343
vBH	2.25	2.21	16.0	−237

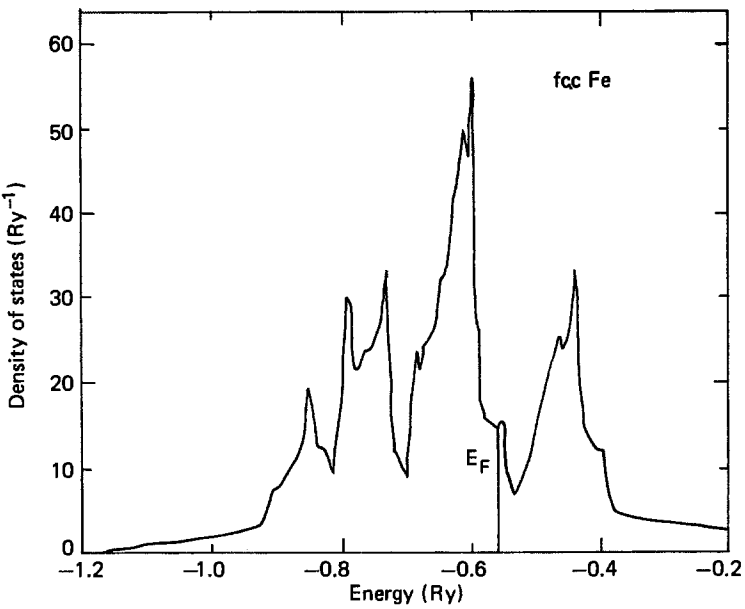

Fig. 3. Density of states curve for both spin directions of bcc iron using vBH potential (Callaway and Wang 1977a,b).

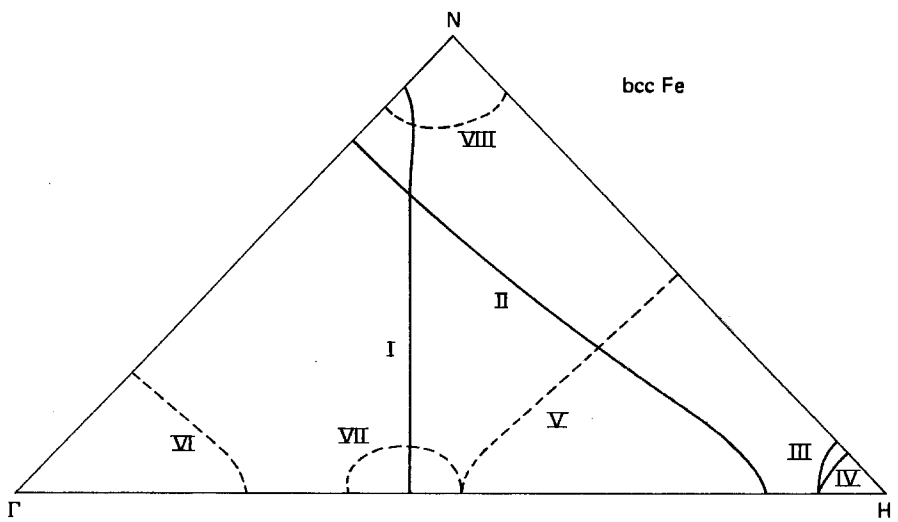

Fig. 4. Cross-section of the Fermi surface of bcc iron in the (100) plane (Callaway and Wang 1977a,b), using vBH potential. Solid lines, majority spin; dashed lines, minority spin. See original papers for notation. See also fig. 23.

Figure 3 shows the density of states curve for iron and fig. 4 a cross-section of the Fermi surface in the (100) plane. Comparison with experiment is given in the original publications (Callaway and Wang 1977a,b).

Brief reference only need be made here to energy band calculations for fcc

iron (Dalton 1970, Madsen et al. 1975) and to those for hcp iron, a phase which is produced at high pressures of the order of 100 kbar (Madsen et al. 1975, Fletcher and Addis 1974). Although the calculations for the latter do not contain the exchange and correlation potentials as in the Callaway calculations the location of the Fermi energy at a very pronounced dip in the density of states curve leaves little doubt that this high pressure phase of iron has no spin ordering at all, in agreement with observation (Williamson et al. 1972).

There is no comparably accurate band calculation for hcp cobalt. Two calculations (Wong et al. 1969, Wakoh and Yamashita 1970) based on different philosophies which both use the KKR method, were compared and contrasted by Wohlfarth (1970). Due to differences in the potential the values of the exchange splitting come out as 1.35 eV and 1.71 eV for the two respective calculations. Reference to the 1970 paper shows why both these values should be regarded as too large; a "best" estimate of 1.05 eV was thus proposed. Later Ishida (1972) reported a band calculation for hcp cobalt using again a KKR based method. The result of a *rigid* splitting of the paramagnetic energy bands, which is surely too simple, leads nevertheless to an exchange splitting of 1.13 eV, in excellent agreement with this best value. Figure 5 shows the *paramagnetic* density of states curve of hcp cobalt (full curve). Due to the fact that both crystal structures are close packed the density of states curves are very similar. The hcp curve is in good agreement with that of the earlier calculations. The electron–phonon enhancement factor λ comes out anomalously low at 0.14 in both calculations. Figure 6 shows the calculated Fermi surface of the majority spin band of hcp cobalt.

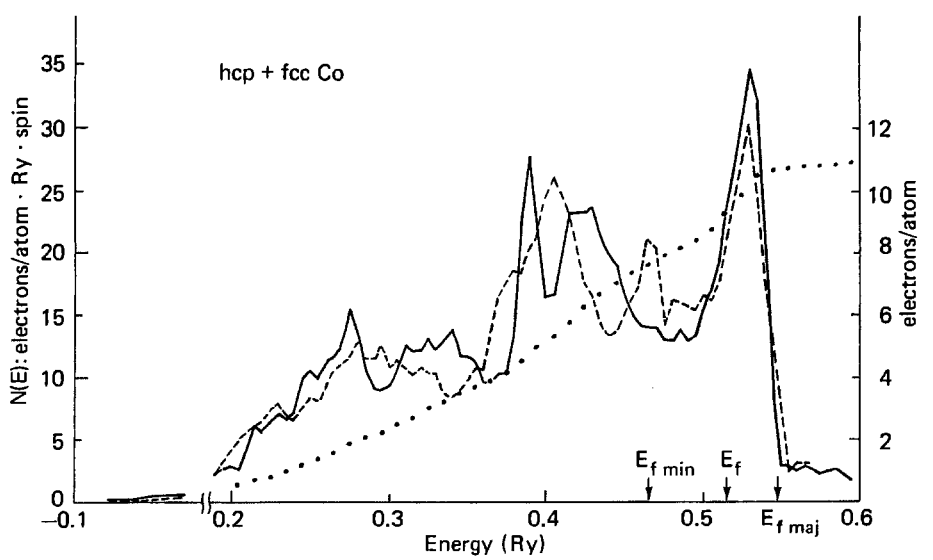

Fig. 5. Density of states curve of paramagnetic hcp cobalt (Ishida 1972), full curve; the density of states curve of paramagnetic fcc cobalt is shown by the dashed curve.

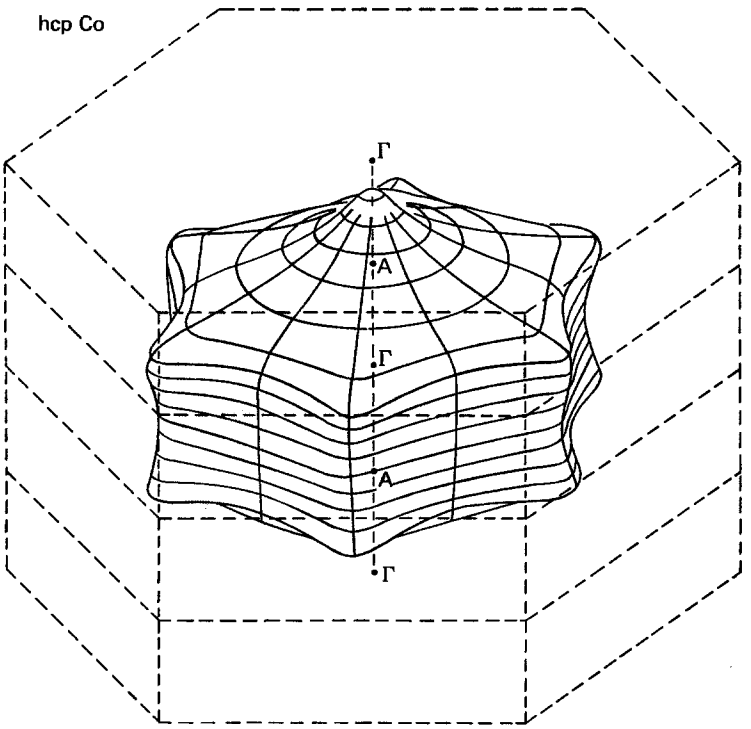

Fig. 6. Fermi surface of the majority spin band of hcp cobalt (Ishida 1972).

Table 3 collects the values of ΔE regarded as most reasonable on the basis of these band calculations for iron, cobalt and nickel. It also gives the resulting values of the Stoner–Hubbard parameter $I = \Delta E/\mu_S$, where μ_S is the saturation magnetization in μ_B. Even considering that the values of ΔE and I for iron and nickel are probably too high when considering the later experimentally derived values, it seems clear that I varies relatively little for these three metals. The origins of I are briefly discussed in the next section.

TABLE 3
Values of ΔE and I derived from band calculations[d)]

Metal	Fe	Co	Ni
ΔE (eV)	2.2[a)]	1.1[b)]	0.6[c)]
I (eV)	1.0	0.65	1.0

[a)]Taken from table 2, vBH potential.
[b)]Taken from Wohlfarth (1970) and Ishida (1972).
[c)]Taken from table 1, vBH potential.
[d)]An alternative compilation is due to Eastman (1979).

1.3. The Stoner model, origin of splitting energy

The Stoner model as applied to ferromagnetic metals and alloys is the basis of a simple scheme for correlating their magnetic properties. Section 1.4 describes briefly some approximations going beyond the Stoner model and 1.5 concentrates specifically on spin waves which were not a part of the original philosophy. The model is based on the following assumptions:

(1) The itinerant electrons are distributed among the energy levels described by density of states curves which are given by the band calculations of the type given in section 1.2. The carriers of magnetism in iron, cobalt and nickel are the holes in these 3d bands.

(2) The interactions between the itinerant electrons may be described by a molecular field approximation, with a molecular field H_m proportional to the magnetization. Specifically

$$H_m = \tfrac{1}{2} n I \zeta / \mu_B \tag{1}$$

with an associated molecular field energy per atom

$$E_m = -\tfrac{1}{4} n^2 I \zeta^2. \tag{2}$$

Here n is the number of holes per atom, ζ is the relative magnetization and I is the Stoner–Hubbard parameter whose origins are to be discussed below.

(3) At finite temperatures the distribution of particles among the energy levels is given by Fermi–Dirac statistics.

On this basis a number of physically significant results is derived by very elementary means and the most basic of these will now be summarized. Other consequences of the model will be discussed in later sections.

(1) The saturation magnetization at 0 K is given by

$$\mu_S = n \zeta_0 \tag{3}$$

expressed in Bohr magnetons per atom. Here ζ_0 is the relative magnetization at 0 K which equals 1 for a strong itinerant ferromagnet (Ni, Co) and is less than one for a weak itinerant ferromagnet (Fe).

(2) The spontaneous magnetization below the Curie temperature T_c depends on the temperature T through the Stoner equations

$$\tfrac{1}{2} n (1 \pm \zeta) = \int_0^\infty N(E)\, dE [\exp\{(E - \mu \mp \tfrac{1}{2} n I \zeta)/kT\} + 1]^{-1} \tag{4}$$

where $N(E)$ is the density of states and μ the chemical potential. Equations (4) can be solved numerically or analytically for the quantity $\zeta(T)$ after μ is eliminated. Solutions of (4) for differing $N(E)$ curves have been obtained by Stoner (1938), Wohlfarth (1951) and by Shimizu et al. (1965). It is found that curves of $\zeta(T)$ are rather insensitive to $N(E)$ and have a close resemblance to the observed curves of the ferromagnetic transition metals. However, there are significant and serious differences in detail (see sections 2.1 and 2.2) and it is

proposed to summarize here possible reasons for these differences. For a more detailed discussion see Shimizu (1977): (i) The molecular field energy E_m is a more complicated function of the magnetization ζ than given by (1); specifically

$$E_m = -\tfrac{1}{4}n^2 I\zeta^2(1 + \tfrac{1}{2}A\zeta^2 + \tfrac{1}{4}B\zeta^4 + \cdots). \tag{5}$$

The coefficient A was first introduced by Hunt (1953) to the same end and was later estimated theoretically by Wohlfarth (1953) and Bradbury and Edwards (1969) for nickel where its value is of the order 0.1. Unfortunately, Shimizu (1977) requires values of B which are inordinately large to bring about agreement for the observed $\zeta(T)$ curve of iron and cobalt. His discussion of this anomaly is still open to argument. (ii) The Stoner model as used here does not contain the effect of spin wave excitations although these are a natural consequence of the itinerant electron model as such (see section 1.5). These excitations contribute to the magnetization reduction at finite temperatures although, as discussed in sections 2.1 and 2.2, the relative importance of spin wave and Stoner excitation in iron, nickel and cobalt is at present impossible to assess.

(3) The Curie temperature T_c is given by

$$I\int_0^\infty N(E)\left|\frac{\partial f(T_c)}{\partial E}\right| dE = 1 \tag{6}$$

where f is the Fermi function given in (4) but with $\zeta = 0$. The validity of this formula in giving the Curie temperature for iron, cobalt and nickel is discussed below (see table 4). Although there is by no means any certainty it seems that T_c may be given more in terms of spin wave excitations than by this relationship in the case of the ferromagnetic transition metals; in contrast the Curie temperature of weak itinerant ferromagnets was suggested (Wohlfarth 1977a) to be more closely represented by (6) in its low temperature form.

(4) The paramagnetic susceptibility χ at $T > T_c$ is given by

$$\chi^{-1} = \left[2\mu_B^2\int_0^\infty N(E)\left|\frac{\partial f}{\partial E}\right| dE\right]^{-1} - \frac{I}{2\mu_B^2}. \tag{7}$$

Although it has just been surmised that T_c (corresponding to $\chi^{-1} = 0$) is not apparently given by this formalism the calculations of χ reported by Shimizu (1977) are impressive. Figures 7a,b shows the calculated χ^{-1}, T curves for Ni, fcc Fe, bcc Fe and fcc Co based on reasonable $N(E)$ curves, on values of I determined by T_c through (6) and on constant additional susceptibilities (of orbital and other origins) also introduced to fit T_c. The measured points are taken from reliable measurements. Shimizu makes the valid point that the observed χ^{-1}, T curves for these metals by no means obey a Curie–Weiss law by showing that $d\chi^{-1}/dT$, T curves show a very pronounced temperature dependence.

The origin of the electron interaction I is of course central to the whole discussion of the ferromagnetism of the transition metals. As such it has been

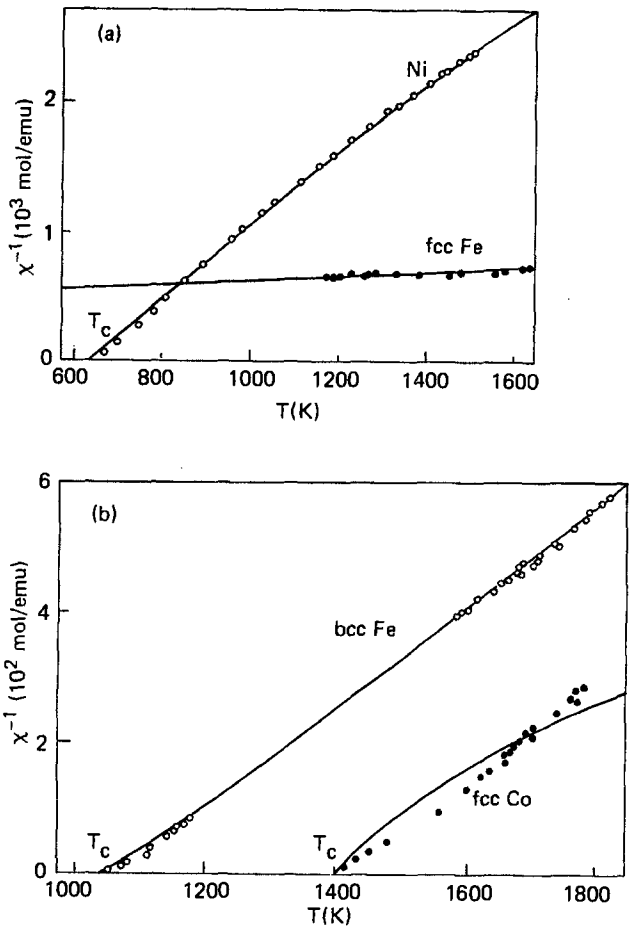

Fig. 7. Paramagnetic susceptibility for (a) Ni and fcc Fe, (b) bcc Fe and fcc Co (Shimizu 1977). Measured data are indicated and are discussed further in section 2.4.

the subject of intense study for several decades. Only a brief account can be given here which summarizes the theoretical background and the resulting numerical values of I and the exchange splitting ΔE. Experimental values will be given where appropriate in later sections.

There is agreement that I is determined by exchange and correlation arising from many body interaction effects; what remains an issue is how best to approximate these effects so as to make them amenable to actual calculation. Reviews of the origins of I are given by Wohlfarth (1953), Herring (1966) and Edwards (1977). For a simple discussion the tight binding approximation is felt to be appropriate for metals such as nickel with nearly filled 3d bands. For these the most important interaction is the intra-atomic Coulomb interaction I_{mm} for two localized wave functions ϕ_m. Other contributions regarded as important are intra-atomic exchange interactions (Hund's rule) I_{mn} and interatomic nearest

neighbour Coulomb interactions. In order of increasing importance Herring's rough estimate of this last contribution (about 1 eV) is surely much too large since the influence of conduction electron screening would act so as to reduce it drastically. This effect has not been fully investigated. The Hund's rule term is particularly important in iron and cobalt where the large number of holes per atom allows this interaction to take place freely. The intra-atomic Coulomb term, estimated at about 20 eV, is also severely reduced by two effects, namely again the effect of conduction electron screening and, secondly, the effect of correlation which is not included in this (Hartree–Fock) estimate of I_{mm}. A very rough estimate for the screening effect by Edwards (1977) leads to a modified intra-atomic Coulomb interaction of, say, 5 eV. The correlation problem is one of great theoretical difficulty especially since the interaction is of the order of the width of the 3d band (see figs. 1, 3 and 5). Kanamori (1963) (see also Hubbard 1963) showed that for the low density limit the ground state properties of the itinerant electron ferromagnet may be treated in the Hartree–Fock approximation if the bare interaction I_b is replaced by an effective interaction I_{eff} given by

$$I_{eff} = I_b/(1 + GI_b) \qquad \text{where} \qquad G \simeq \tfrac{1}{2} \int_{E_F} \frac{N(E)}{E} \, dE \tag{8}$$

and where $N(E)$ is the density of states for the holes in the 3d band. In the limit $I_b \to \infty$, this formula shows that the effective interaction is determined only by G^{-1}, i.e. by the band structure. If $I_b = 5$ eV, $G = 0.5$ eV^{-1} then $I_{eff} = 1.4$ eV. For nickel where the low density limit is reasonable there are three energy bands containing about 0.2 holes/atom each so that an average value of I for use in the Stoner model would be about 0.5 eV. This agrees well with some estimates based on experiment and on band calculations as shown in table 3. The step-by-step reduction of the intra-atomic Coulomb interaction from 20 eV to 0.5 eV is reasonable though very rough at all steps. For nickel the Hund's rule (intra-atomic exchange) contribution to the molecular field is small due to the small number of holes. For cobalt and iron this semiquantitative discussion is not justified since the Kanamori formalism only applied at low densities and since the Hund's rule contribution will be relatively large. Hence no estimates of I have been made along these lines.

For all three ferromagnetic metals the local spin density functional formalism underlying the band calculations of Callaway (1977) has been used explicitly to estimate the Stoner–Hubbard parameter I.

Gunnarson (1976, 1977) applied this formalism to the ferromagnetic transition metals using various reliable band calculations. He finds that the exchange splittings ΔE and the corresponding parameter I are only weakly dependent on the wave vector thus giving a justification for the Stoner model in which, in its original form, this dependence was absent; as discussed by Wohlfarth (1953) the parameter A in (5) also represents a weak wave vector dependence. Table 4 gives the values of I and $IN(E_F)$ for the local spin density functional formalism

TABLE 4
Values of I derived from the local spin density functional formalism (Gunnarson 1976, 1977)

Metal	Fe	Co	Ni	Pd
I (eV)	0.92	0.99	1.01	0.70
$IN(E_F)$	1.5–1.7	1.6–1.8	2.1	0.8
T_c K (calc.)	4400–6200	3300–4800	2900	–
Note that similar calculations by Andersen et al. (1977) give the following values of I				
I (eV)	0.91	–	0.99	0.72

for Fe, Co, Ni and also Pd. From (7) the Stoner criterion for ferromagnetism

$$IN(E_F) \geq 1 \qquad (7)^*$$

involves the density of states at the Fermi energy E_F. In agreement with this criterion the table makes the first three metals ferromagnetic and Pd paramagnetic. By contrast, Gunnarson's calculation of this product using the $X\alpha$ method makes Pd ferromagnetic (!) and gives much larger values of I for all four metals, since this method does not contain the correlation effects which militate against ferromagnetism. The values of I agree well with those of table 3 for Fe and Ni but not so well for Co, presumably since this was obtained in table 3 by rather less reliable and less consequent methods. However, it is still possible that all 3 values of I given in tables 3 and 4, especially that for nickel, may still be too large when it comes to explaining some properties of these metals. This uncertainty may be particularly relevant when considering the Curie temperature on the basis of these calculations and relation (6). The calculated values are also given in table 4 and those observed in table 5; the difference is dramatically obvious. If I is really too large its reduction would then reduce T_c, actually more rapidly than linearly as shown by relation (6). On the other hand, if I is indeed as large as given in table 4 then T_c would clearly have to be determined by causes other than those underlying the Stoner model which involves single particle excitations; this problem is discussed below.

Some indication of the correctness of estimates of the exchange splitting ΔE is given as follows. The value of ΔE determines that of the energy gap Δ of strong itinerant ferromagnets, given by

$$\Delta = \Delta E - E_F^+ \qquad (9)$$

where E_F^+ is the Fermi energy for the + spins. Using the band calculations of Callaway and Wang (1977a) for nickel table 1 gives $\Delta E = 0.63$ eV from the vBH potential and this calculation also gives $\Delta \sim 300$ meV. The spin polarized photoemission data and the neutron data, respectively, discussed in sections 4.1 and 2.7, demand, however, that $\Delta \leq 100$ meV as was pointed out by Wohlfarth (1971,

1977b), so that a distinct problem exists. Either all band calculations discussed are thus wrong to this order or they demand for some physical problems the influence of the many body effects discussed in this connection by Edwards (1978) and summarized below. This discussion (see section 1.5) stresses that the calculation of the spin wave stiffness D for nickel and its alloys demand the *large* values of I and ΔE obtained from band calculations and given in tables 1, 3 and 4 rather than a *smaller* value $\Delta E \sim 0.63 - (0.3 - 0.1) \sim 0.4$ eV which would be crudely demanded by the photoemission and neutron measurements. This is, in fact, an estimate of ΔE for nickel which had been suggested in an earlier analysis (Wohlfarth 1965) and which leads to a better value of T_c than is given in table 4. For nickel, therefore, the problem is this: Is $\Delta E \sim 0.6$ eV or ~ 0.4 eV?

If T_c is not given by the Stoner model it would have to be that temperature where the other principle elementary excitation of the system of itinerant electrons, the spin waves or magnons, go soft. However, the neutron measurements which are discussed in section 2.7 seem to show that spin waves exist a long way above T_c in nickel and iron. It is therefore difficult to understand T_c itself in terms of spin wave softening. Edwards (1976b) proposed that the elementary excitations which soften at T_c are not the usual spin waves but rather other more low lying modes. In this model the band structure enters explicitly; 3 two-dimensional ferromagnetic sub-bands are regarded as coupled by an effective intraatomic Hund's rule exchange interaction to give long range magnetic order. This coupling breaks down at T_c and long wavelength two-dimensional spin waves are then thermally excited within sub-bands. The model was applied specifically to fcc nickel where the Hund's rule term is small. Further developments would be concerned with the possibility of applying this model to bcc iron where ordinary spin waves also exist above T_c and where Hund's rule effects are, as discussed in section 1.4, much larger due to the larger number of holes.

In this section the Stoner model has been discussed, and the various methods of estimating the parameter I which occur were described, together with numerical estimates of this central quantity of the model. It was shown that these estimates are still rather uncertain. The model itself was used to obtain the temperature dependence of the magnetization and of the susceptibility from 0 K to temperatures above T_c, these being the basic observables. Further discussion of these quantities follows below with reference to the actual experimental observations. However, such observations are available together with similarly based theoretical discussions, for many other fundamental properties of the ferromagnetic transition metals. These will again be discussed in the appropriate sections with reference to the experimental values.

1.4. Results beyond the Stoner model, many body effects

Among several attempts to go beyond the Stoner model for the ferromagnetism of the transition metals the following three will be mentioned here: (i) The direct influence of the Hund's rule interaction, (ii) spin fluctuation effects, (iii)

electron–magnon interactions. In section 1.5 spin waves themselves will be discussed.

The direct influence of Hund's rule exchange interaction, called J, has been discussed by Edwards (1970) who recalls that Hubbard (1963, 1964a,b) had proposed a strong interaction model for d bands of width W if $I/W \geqslant 1$. For an atomic d^{10-r} configuration the band is split into two, the lower and upper bands containing $10-r$ and r states per atom, respectively. A metal with $10-r-n$ electrons per atom ($n < 1$) may be described as having n itinerant holes in the lower band and r holes on each atom in the upper band, these having localized spins coupled by Hund's rule. For cobalt and iron, $r = 1$ and 2, respectively; for nickel this mechanism does not occur. The effective exchange integral giving the energy of interaction between the localized spins and the itinerant holes is $J_{\text{eff}} = J - \frac{1}{10}W$. The itinerant electrons themselves interact via the mechanisms discussed in section 1.3, involving I. The problem of the magnetism of this system of localized and itinerant electrons is the same as that of giant moment systems like Fe in Pd (Doniach and Wohlfarth 1967) and using this formalism the following parameters for cobalt are needed for interpreting the properties of this metal: $I_{\text{eff}} \sim 0.6$ eV, $J_{\text{eff}} \sim 0.2$ eV, $\Delta E \sim 0.6$ eV. The value of J_{eff} is close to that for Fe in Pd; an estimate of this integral for iron is roughly 50 meV.

A description of iron and cobalt involving respectively 2 and 1 localized spins is clearly beyond Stoner. The validity of this description would require further consideration of the properties of alloys of these metals. Sakoh and Edwards (1975) applied it to a calculation of the magnetization and susceptibility of iron and cobalt; here the direct superexchange between the localized spins is also included although it has a value of only about 10 meV.

Another theoretical description of the ferromagnetism of itinerant electrons involves the effect of spin fluctuations. This model was discussed in detail by Moriya and Kawabata (1973a,b,c) and reviewed by Moriya (1977a,b). Application is made both to weak and strong itinerant ferromagnets. The spin fluctuations considered have the same character as paramagnons in strongly enhanced paramagnetic metals (Doniach and Engelsberg 1966) and spin waves in ferromagnetic metals, see section 1.5. Although the theory is developed generally, explicit calculations for quasi-free electrons are necessary for obtaining numerical results. In applying this theory to nickel as an example of a strong itinerant ferromagnet it is found that the spin fluctuations here behave like a set of localized moments. The presence of these fluctuations clearly acts so as to make it easier for the magnetization to vanish when the temperature is raised in comparison with the situation where these fluctuations are absent as in the Stoner model. Hence the Curie temperature is lower than is given by relation (6). The fact that such a decrease is demanded by the facts of table 4 may or may not be explicable in this way. The same goes for the result of the theory that the susceptibility above T_c approximately follows a Curie–Weiss law and that it predicts the observed persistence of spin wave like modes above T_c. Application of this theory to weak itinerant ferromagnets was also made by these authors (see also Ramakrishnan 1974, Yamada 1974, Gumbs and Griffin 1976, Dzy-

aloshinsky and Kondratenko 1976) but is outside the present scope. For nickel the suspicion remains that the complicated band structure, for example its quasi-two-dimensional character (see section 1.3), is not sufficiently a part of the analysis. As for paramagnons (de Chatel and Wohlfarth 1973) the band structure may well act so as to attenuate the fluctuation effects in the strong itinerant ferromagnets, at least.

The third discussion beyond Stoner concerns electron–magnon interactions. This many body problem was discussed with reference to nickel by Edwards and Hertz (1973), and the results have been summarized by Edwards (1978) in referring to the apparently small energy gap Δ demanded by the spin polarized photoemission data discussed in section 4.1 and the neutron date of section 2.7. As was mentioned in section 1.3 the band calculations imply much larger values of Δ for nickel and this difference may arise from a many body effect of this sort which the band calculations referred to do not encompass. Edwards and Hertz consider a hole in the − spin band making a virtual transition to the + spin Fermi level during which process a magnon is emitted. The energy of the scattering states is the Fermi energy plus the magnon energy, and a bound state splits off below the scattering states. The energy of the magnons involved may be estimated as (Edwards 1977) about 90 meV so that $\Delta \lesssim 90$ meV, whatever the band calculation may give. This estimate agrees excellently with the estimates based on the above two sets of measurements (Wohlfarth 1971, 1977b). In addition, the frequency dependence of the − spin hole self energy increases its effective mass compared to its band structure value so that there is some reason for having the normalized density of states at the band edge rising more sharply than is given in the absence of this many body effect. This sharper rise also seems to be demanded by the photoemission data. This sophisticated many body effect (see also Celasco and Corrias 1976) is thus apparently relevant in discussing the actual physical properties of nickel. Much further theoretical and experimental work, also for cobalt, is needed to be sure.

1.5. Spin waves

Spin waves, or magnons, are the elementary excitations of ferromagnetic metals which arise in addition to the single particle excitations of the Stoner model. The excitations are of bound electron–hole pairs and are characterized by the dispersion relation giving the energy $\hbar\omega(q)$ as a function of the wave vector q. For small values of q, i.e. long wavelength magnons, the dispersion relation for ferromagnets is

$$\hbar\omega(q) = Dq^2 \tag{10}$$

where D is the spin wave stiffness. This characteristic quantity is as fundamental in specifying the magnetism of the transition metals as is the saturation magnetization and the Curie temperature.

Spin waves enter the physics of the ferromagnetic transition metals in the

following ways:

(1) The magnetization decreases as a function of the temperature according to the famous law

$$\zeta(T) = \zeta(0)\{1 - \alpha T^{3/2} - O(T^{5/2})\} \tag{11}$$

where $\alpha \sim D^{-3/2}$. Experimental results are given in section 2.1. This decrease adds, linearly to lowest order, to that given by the Stoner equations. As was discussed in section 1.3, the Curie temperature may be determined, at least in part, by spin wave excitations.

(2) The specific heat, again additive to that from the itinerant electrons, also goes as $T^{3/2}$. Experimental results are given in section 3.5.

(3) Spin waves can scatter neutrons and are thus best observable by neutron techniques; these enable the spin wave stiffness D to be measured most accurately (see section 2.7).

(4) Proper high frequency excitation of metallic films produces spin wave resonance effects (see the chapter by Hoffmann, volume 3/4).

(5) Spin wave scattering of electrons also enters the electrical resistance (see section 3.6).

Theoretical calculations of the spin wave dispersion relation and of the stiffness are much more difficult than for the Heisenberg model where only a direct exchange integral enters to determine the energy scale. For metals the band structure gives rise to severe complications. In addition, the exact nature of the electron interactions is not established, as was discussed in sections 1.3 and 1.4. The resulting approximations are reflected in the theoretical expressions for spin wave energies.

Most generally the spin wave energy $\hbar\omega$ is given by the pole of the dynamic susceptibility, i.e. by

$$\chi^{-1}(q, \omega) = 0. \tag{12}$$

This function will be discussed in section 2.7 with reference to theoretical calculations and to the neutron measurements on nickel and iron. The dispersion curve, rising initially parabolically as given by relation (10), has been found theoretically and experimentally to deviate from this initial variation at shorter wavelengths. Eventually it will meet the downward going single particle excitations and this occurs at a characteristic wave vector q_{max}. For shorter wavelengths the electron–hole pairs dissociate into independent particles on entering the continuum of single particle excitations. The wave vector q_{max} is also observable by neutron scattering, see section 2.7.

Calculations of D have been made on several levels of sophistication. For a strong itinerant ferromagnet (Ni, Co) but with a single band and cubic crystal symmetry Edwards (1967) found that

$$D = \frac{1}{3n}\left\{\frac{1}{2}\sum_k \nabla^2\epsilon_k - \sum_k \frac{|\nabla\epsilon_k|^2}{\Sigma_-(k, \omega)} - \text{cross terms}\right\}. \tag{13}$$

Here n is the number of electrons, ϵ_k the band structure, Σ_- a self energy for the

– spins taken at energies $\hbar\omega$ depending on the approximation, and the summation is over occupied + spin states. In the random phase approximation and still for a single band strong itinerant ferromagnet Σ is replaced by the exchange splitting ΔE. For the more reasonable multiband case and for weak itinerant ferromagnets the problem becomes considerably more difficult and reference may be made to the following publications: Wakoh (1971), iron, cobalt and nickel. For nickel, agreement with experiment is within a factor about 2 using an exchange splitting of about 0.5 eV, i.e. lower than the value of table 3. For iron and cobalt the calculated values of D are much lower than those measured. The random phase approximation was used for a multiband model. Thompson and Mook (1970), George and Thompson (1970) and Thompson and Myers (1967) also reported RPA multiband calculations for iron, cobalt and nickel, respectively. Agreement of D with experiment was only attained by including interatomic exchange integrals (of the order of 16 meV for iron and cobalt). Their inclusion would also improve agreement in the calculations of Wakoh just referred to since this interaction is clearly one which acts towards stable ferromagnetism and thus increases D. On the other hand, use of another parameter is clearly not too satisfactory especially since the RPA itself may be at fault in causing the differences between theory and experiment. For nickel more sophisticated calculations of D have been reported by Wang and Callaway (1976) which are based on the local density functional formalism referred to in section 1.2. The calculated value of D is within a few percent of that observed, but with an exchange splitting ΔE about 0.8–0.9 eV, as given as the larger value in table 1. Since Riedinger and Nauciel-Bloch (1975) also require a large ΔE value of this order to obtain the experimental value of D for nickel, Edwards (1978) expresses the belief that different values of ΔE should in fact be sensibly used for a quasi-static quantity like spin wave stiffness and for such dynamic effects as photoemission where, as already pointed out in section 1.3, smaller values of ΔE are required. The arguments are based on the use of different expressions for ω in relation (13). Again, therefore, the exchange splitting is the key quantity in describing spin wave dispersion in the ferromagnetic metals.

Further discussions of spin waves are given in the appropriate sections below.

This very brief summary of the theoretical background should suffice to indicate the grave complications which arise in trying to establish a fully meaningful description of the experimental and empirical facts which will be the subject of the rest of this chapter. Where necessary, further aspects of the theory will be discussed by reference to specific results.

2. Fundamental properties

2.1. Magnetization at 0 K *and at finite temperatures*

For iron and nickel, measurements of the saturation magnetization at 0 K with the greatest claim to accuracy were summarized by Danan et al. (1968) whose

best values, with methods of measurement and analysis, are given in emu/g and in μ_B as in table 5. No such detailed analysis is available for hcp cobalt and the data in table 5 are based on the results of Myers and Sucksmith (1951). Although fcc cobalt is not stable at 0 K a rough estimate of its saturation magnetization at that temperature may be made by a linear extrapolation of the data for the fcc Ni–Co alloys (Wohlfarth 1949), giving about $1.80\mu_B$, an increase of about 5%.

These values of the saturation magnetization at 0 K are determined by the number of holes in the d-band, i.e. by the band structure and the exchange splitting, and by the g-factor. The latter is discussed in section 3.1. The change of the magnetization of cobalt resulting from the crystal structure transformation between the two close packed phases must follow similar principles.

The temperature dependence of the magnetization $M(T)$ of iron was measured by Aldred and Froehle (1972) up to room temperature and in fields up to 14 kOe. The data were best fitted as follows

$$M(H, T) - M(0, 0) = -\frac{g\mu_B}{\rho}\left[\frac{kT}{4\pi D(T)}\right]^{3/2} F\left(\frac{3}{2}, \frac{kT}{g\mu_B H}\right). \tag{14}$$

Here ρ is the density, $F(n, t)$ is given by

$$F(n, t) = \sum_{m=1}^{\infty} m^{-n}\, e^{-m/t} \tag{15}$$

and $D(T)$, the temperature dependent spin wave stiffness, is given by

$$D(T) = D(0) - D_1 T^2. \tag{16}$$

The values of $D(0)$, 311 ± 10 meV Å^2, and of $D_1 = (6.1 \pm 0.8) \times 10^{-4}$ meV Å^2 K^{-2}, are in good agreement with those obtained by Stringfellow (1968) from neutron measurements (see also section 2.7). The basis of this analysis is that the low temperature magnetization of iron is determined by spin wave excitations with a temperature dependent spin wave stiffness $D(T)$ determined by the itinerant model. The Stoner excitations contribute a term to $M(H, T)$ going as T^2 but this is apparently too small to be observed; see also Edwards (1974) and the

TABLE 5
Fundamental magnetic properties of iron, cobalt and nickel

	Fe	Co	Ni
Saturation magnetization emu/g	221.71 ± 0.08	162.55	58.57 ± 0.03
Saturation magnetization $\mu_B(q_s)$	2.216	1.715	0.616
Curie temperature T_c K	1044 ± 2	1388 ± 2	627.4 ± 0.3
kT_c meV	90.0	119.6	54.1
Number of magnetic carriers from Curie–Weiss law, q_c	2.29	2.29	0.90
q_c/q_s	1.03	1.34	1.46
Value of q_c for liquids	3.42	2.11	1.72
Spin wave stiffness D meV Å^2 (at room temperature)	280	510	455

discussion of de Haas–Van Alphen measurements in section 4.2. A discussion of these two contributions to $M(H, T)$ was given by Thompson et al. (1964) and by Mathon and Wohlfarth (1968).

Aldred and Froehle (1972) also fitted their data for iron on the basis of spin wave theory but with (i) D independent of T and (ii) a term in $T^{5/2}$ in addition to that, going as $T^{3/2}$, in (14). The coefficient of $T^{5/2}$ is related to the coefficient of q^4 in the spin wave dispersion relation. Although a fit of the magnetization data is again possible, the value of D and of the coefficients of $T^{5/2}$ and thus of q^4 disagree with those measured by neutrons (Stringfellow 1968, Shirane et al. 1968, Collins et al. 1969). Hence this analysis is less satisfactory.

For nickel similar measurements were carried out by Aldred (1975). The results differ from those for iron since the change of the magnetization with temperature appears not to be given only by spin wave excitations with a stiffness determined from neutron scattering. Using these measurements (Minkiewicz et al. 1969, Mook et al. 1973) and the resulting values of $D(0)$ and D_1 in relation (16), 555 meV Å^2 and 11.5×10^{-4} meV Å^2 K^{-2}, respectively, the change of magnetization $M(0, T) - M(0, 0)$ coming from spin waves is only about half that observed when $T = 300$ K. Aldred (1975) thus analyzed his data in terms of additional Stoner excitations. The change of $M(T)$ of a strong ferromagnet such as nickel varies as $e^{-\Delta/kT}$ (Thompson et al. 1964), where Δ is the energy gap discussed in section 1. A value of $\Delta = 14$ meV is required to give some agreement with the neutron data, although a more detailed discussion reveals this analysis to be unsatisfactory. In any case, larger values of Δ are suggested

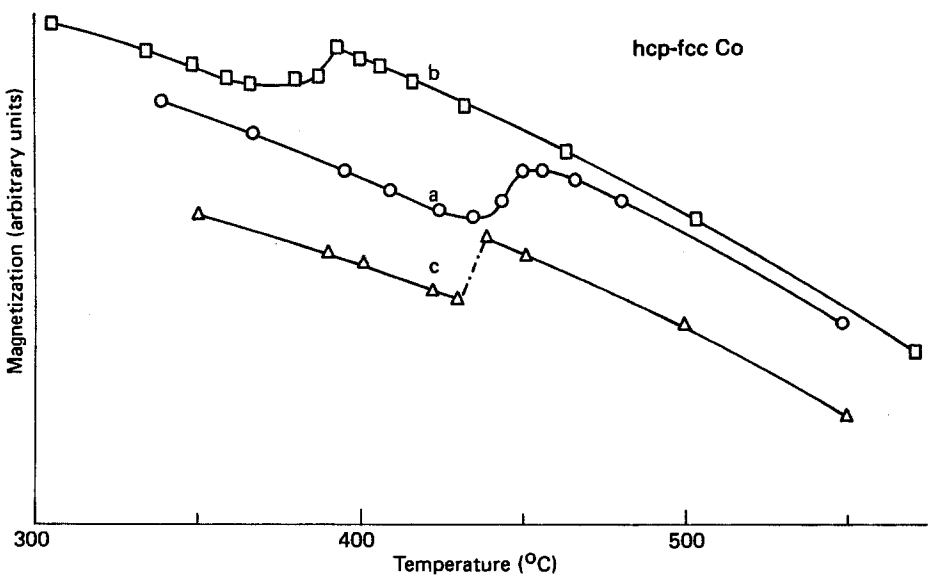

Fig. 8. Magnetization, temperature curve of cobalt on passing through the hcp–fcc phase transition (Myers and Sucksmith 1951). (a) Heating, (b) cooling, (c) heating of a single crystal specimen.

by all the other measurements. A somewhat better agreement is obtained if the contribution to $M(T)$ from the Stoner excitations goes as T^2 which, however, implies that nickel is a weak itinerant ferromagnet (Thompson et al. 1964) and this seems unlikely. Hence the problem of the temperature dependence of the magnetization of nickel remains unsolved. Further results based on NMR measurements are discussed in section 2.2.

For cobalt there exists no such detailed analysis and this would clearly be welcome.

The measurements of $M(T)$ just discussed refer to low temperatures. Between this range of temperatures and the Curie point the $M(T)$ curves for iron and nickel vary without special features. This variation can clearly not be interpreted satisfactorily before the low temperature variation is fully understood. Even then it would not be clear how the relative weights of spin wave excitations and of Stoner excitations, where these arise to any extent, vary with T. For cobalt special features of $M(T)$ do arise and these are related to the crystal structure change from hcp to fcc, as shown in fig. 8 (Myers and Sucksmith 1951); this clearly shows secondary effects having their own intrinsic interest.

The final disappearance of $M(T)$ occurs at the Curie temperature which will be discussed in section 2.3.

2.2. Hyperfine fields

Hyperfine fields of the ferromagnetic transition metals may be measured using nuclear magnetic resonance and Mössbauer techniques. The values of these fields at a given temperature and their temperature variation are both of interest.

A review (one of many!) of the measurements and their interpretation was given by Feldmann et al. (1971). Typical values of the hyperfine fields of the three metals are given in table 6, expressed as a resonance frequency ν_T, where T is the temperature; later measurements by Riedi (1973, 1977) are also included. The review gives a useful summary of the various contributions to the hyperfine field and this is reproduced in table 6. The existence of so many contributions clearly makes it difficult to estimate the hyperfine fields accurately; nevertheless, as shown in tables 1 and 2, such calculations have been performed.

The temperature dependence of the hyperfine fields is usually expressed in terms of that of the magnetization $M(T)$, since roughly the two quantities should vary similarly

$$\frac{\nu_T}{\nu_0} = A_T \frac{M(T)}{M(0)} \tag{17}$$

where A_T is called the hyperfine coupling constant. If A_T were really a constant, NMR techniques would provide a much more accurate way of measuring the temperature dependence of the magnetization than static measurements of $M(T)$. For iron Riedi (1973) showed that below 32 K ν_T follows a $T^{3/2}$ law with a coefficient in good agreement with that from static and spin wave measurements;

TABLE 6
Hyperfine fields of the ferromagnetic transition metals (taken from Feldmann et al. 1971, Riedi 1973, 1977)

	ν_T (frequency MHz)	T K
Fe (Feldmann et al.)	45.6	300
(Riedi 1973)	45.468	297.6
Co hcp (Feldmann et al.)	210–215	298–398
fcc (Feldmann et al.)	217–223	298–398
Ni (Feldmann et al.)	26.096	300
(Riedi 1977)	26.216	292.4

Summary of contributions to the hyperfine field (Feldmann et al.):
(*i*) *Local field* (a) external, (b) demagnetizing, (c) Lorentz.
(*ii*) *Conduction electrons* (a) Contact interaction due to polarization by 3d electrons via RKKY, (b) dipole interaction with orbital momentum of non-s electrons.
(*iii*) *Electrons in unfilled shells* (a) Electronic spin-dipole contribution from surrounding ions, (b) intrinsic electronic spin-dipole contribution, (c) dipole interaction with the orbital momentum, (d) contact interaction of s-electrons hybridized with the d-band.
(*iv*) *Closed inner shells* Contact interaction with polarized s-electrons.

thus $D(0)$ equals 316 ± 5 meV Å^2 on this basis, compared to the value 311 ± 10 reported in section 2.1. Hence in this temperature range $A_T = 1$ to within the experimental accuracy. Between 32 and 400 K, however, A_T varies with temperature according to the relation

$$A_T = 1 - (6.58 \times 10^{-9}\, T^{5/2}) + O(T^{7/2}). \tag{18}$$

The form of this relationship was given by Edwards (1976a) as arising from spin wave excitations and the action of the important contributions to the hyperfine field given in table 6.

For nickel Riedi (1977) showed that $A_T = 1$ to within the experimental error up to 300 K ($\sim \frac{1}{2}T_c$). The discrepancy between the neutron and static measurements of the magnetization discussed in section 2.1 was confirmed by the hyperfine field measurements, i.e. these continue to point to important single particle excitations in nickel, still without being able to describe these satisfactorily. A further difficulty in all cases is that measurements of the hyperfine field have to be corrected for constant volume/constant pressure effects at higher temperatures, necessitating accurate high pressure NMR measurements.

For cobalt there are no recent measurements of the temperature dependence but earlier ones (Feldmann et al. 1971) point to a constant A_T up to 400 K.

2.3. Curie temperature

The Curie temperature T_c of the ferromagnetic transition metals has often been measured and table 5 shows one reliable measurement in each case, namely iron

(Arajs and Colvin 1964), fcc cobalt (Colvin and Arajs 1965) and nickel (Kouvel and Comly 1968). There is no reliable estimation of T_c for hcp Co which is normally unstable there.

The values of kT_c also shown in table 5 demonstrate clearly the difficulty of interpreting the origin of this critical temperature, namely its small value compared to other key energies such as the exchange splitting or the interaction energy I or the band width. For example, the significant ratio $\Delta E/2kT_c$ is about 12 for iron and about 5 for cobalt and nickel. Although this ratio can easily be well above 1 in the itinerant electron model, and clearly is so for weak itinerant ferromagnets, such large values are not so easy to understand in the present cases in particular for iron. Alternatively, the Gunnarson (1976, 1977) estimates of T_c given in table 4 are clearly much larger than those observed. Hence, although an interpretation of T_c in terms of single particle excitations is not impossible, the alternative interpretation of T_c in terms of spin wave softening may appear to be more likely. Indeed, there is a qualitative correlation between T_c and the spin wave stiffness D in iron *alloys* (Wohlfarth 1966) which may also point in this direction. Maybe the absence of this correlation for nickel alloys is significant in pointing to a single particle origin of T_c in nickel after all. For nickel, indeed, $\Delta E/2kT_c$ is less than for iron and the high field data discussed in section 2.5 may also be relevant. Nevertheless, it seems clear that there is little certainty in any attempt to estimate the Curie temperatures for these three metals on any reliable theoretical basis. Attempts to do so (for example, by Capellmann 1979) continue, however, to be made.

2.4. *Susceptibility at $T > T_c$; Curie–Weiss constant*

The paramagnetic susceptibilities of fcc and bcc Fe, fcc Co and Ni are given in fig. 7 (Shimizu 1977, taken from Arajs and Colvin 1963 and Nakagawa 1956). The point is made by Shimizu that these curves do not obey the Curie–Weiss law (see his fig. 3) but that the observed curves may be explained on the basis of the itinerant model plus an additional constant susceptibility, perhaps of orbital origins. The whole question of the status of the Curie–Weiss law in the framework of this model was also discussed by Wohlfarth (1974). It was argued, in some agreement with Simizu, that the law, observed over limited or extended temperature ranges, is not incompatible with this model. Nevertheless, the controversy continues to bedevil the theory of the magnetic properties of the transition metals; see, for example, Moriya (1977a,b). If the law is observed even if only over limited temperature ranges, as is the case for the curves shown in fig. 7, it is convenient to characterize these curves by a Curie–Weiss constant, a resulting effective moment p_{eff} and a resulting number of magnetic carriers q_c, given by

$$p_{\mathrm{eff}}^2 = q_c(q_c + 2). \tag{19}$$

On the basis of comparisons of this number of carriers with that obtained from the saturation magnetization at low temperatures, q_s (see table 5), Rhodes and

Wohlfarth (1963) (see also Wohlfarth 1978a), were able to give a systematic discussion of the magnetic properties of ferromagnetic metals and alloys. The values of q_c, q_s and q_c/q_s are given in table 5 from which it appears, as is of course well known, that this ratio is greater than 1 but not as excessively so as for the weak itinerant ferromagnets discussed in the above papers. On the basis of this systematic discussion it was concluded that if q_c/q_s is as close to 1 as is the case here, and if the Curie temperature T_c is above about 500 K the whole scheme can not be used to distinguish between itinerancy or localization of the magnetic carriers. Hence the Curie–Weiss constant and thus q_c can only be regarded as formally convenient parameters for these metals. The discussion is only meaningful on a much more fundamental basis.

Apart from these data it is of interest to discuss briefly the susceptibility behaviour of iron, cobalt and nickel on passing through the melting point. Measurements are available by Nakagawa (1956), Briane (1973) and Müller (1978). For iron the susceptibility increases by 5% compared to the value for the γ-phase extrapolated to the melting point and decreases by 31% compared to the δ-phase which is stable just below the melting point. For cobalt the decrease of the susceptibility at the melting point is 6% and for nickel there is an increase of 2%, as shown in fig. 9. The changes of the susceptibilities on melting are thus small compared to those of solids with the same structure (γFe, Co, Ni) and the

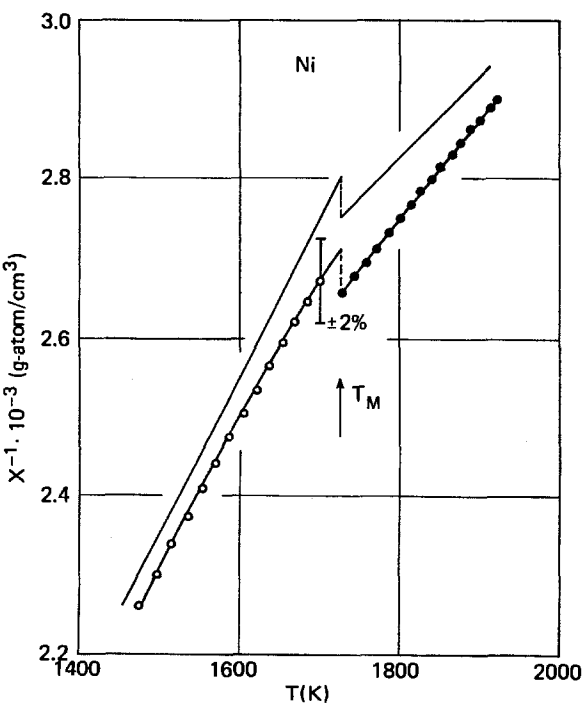

Fig. 9. Inverse susceptibility, temperature curve of nickel above and below the melting point (Müller 1978, Briane 1973).

sign of the changes is not systematic. The inverse susceptibility, temperature curves of the liquid ferromagnets obey the Curie–Weiss law and the corresponding values of q_c are shown in table 5. The differences from the q_c values of the solid metals are large for iron and nickel; a similar situation also occurs for palladium (Müller 1978). There is no deep going theory of these two effects (small change of absolute value and larger change of temperature derivative). Briane (1973) appeals to a very simple model calculation of Adachi and Aisaka (1973) which involves a smoothing out of the fine structure of the density of states curve on melting. This approach, which has also been suggested for amorphous ferromagnets (Wohlfarth 1978b), seems very reasonable and Briane showed that it can explain quantitatively his measurements on Fe–Ni alloys.

2.5. High magnetic field effects; high field susceptibility

At high magnetic fields H the magnetization of the itinerant ferromagnets iron, cobalt and nickel continues to increase with H, a phenomenon known as the paraprocess (this term is particularly popular in Germany and Russia but not in the Anglo-Saxon countries!). The following contributions to the resulting high field susceptibility χ_{hf} have been considered:

Pauli spin paramagnetism of d-electrons, χ_P ($\equiv\chi_0$ at 0 K)
Van Vleck orbital paramagnetism χ_{VV}
Pauli spin paramagnetism of s-electrons
Diamagnetism, of several origins
Susceptibility due to spin–orbit coupling
Susceptibility due to spin wave excitations.

At low temperatures only the first two contributions are significant in practice. Rebouillat (1972) has given an extensive account of his own, and others' measurements and also of the results of various theoretical estimates. A later analysis for cobalt was given by Fekete et al. (1976) on the basis of Knight shift measurements. Table 7 gives a summary of these results. The contribution χ_0 arises from the itinerancy of the d-electrons and is given as a generalization of the usual exchange enhanced paramagnetic susceptibility (7) by the relation (Wohlfarth 1962, Gersdorf 1962)

$$\chi_0^{-1} = (4\mu_B^2)^{-1}\{N(E^+)^{-1} + N(E^-)^{-1}\} - I/2\mu_B^2. \tag{20}$$

For strong ferromagnets $N(E^+) \simeq 0$ (only a small contribution from the s-electrons remains) and χ_0 will be small. For weak ferromagnets larger values of χ_0 are expected, as is clear on physical grounds. The temperature dependence of the high field susceptibility was discussed by Shimizu (1977) but the effects are complicated partly due to the growing importance of spin wave excitations. The Van Vleck orbital susceptibility has been discussed by Place and Rhodes (1971) and by Mori (1971) as well as by Rebouillat (1972) and Fekete et al. (1976). This susceptibility is largest for metals such as chromium and vanadium near the

TABLE 7
High field susceptibility of iron, cobalt and nickel (Rebouillat 1972, Fekete et al. 1976)

	Fe	Co	Ni
χ_0	69	0	0
	93	23	55
	98	30–40	76–114
	86	114	
		65	
χ_{vv}	84	240	80
	133	240	82
	110	240	48–45
	131	129	
	159	202	
$\chi_0 + \chi_{vv}$	–	240	80
	202	263	137
	203	270–280	124–159
	229	243	
	245	267	
χ_{hf}(obs.)	266	265	116
	231		129
	305		110

All susceptibilities are in units emu/mol $\times 10^6$. The data are taken from the two references given which tabulate estimated and observed values from several sources, fully quoted. The precise methods of estimation are too complicated to be given here.

centre of the periodic table but is certainly also important, as shown in table 7, for iron, cobalt and nickel.

The experimental and theoretical results are rather complicated since the measurements are not easy and since the theoretical estimations rely on many other factors (densities of states, exchange splittings, etc.). Hence it is not easy to discern clear trends. On the whole χ_0 tends to be larger for Fe than for Co and Ni since the latter are, from other evidence, strong itinerant ferromagnets. However, as Fekete et al. (1976) point out for cobalt (where they have $\chi_0 = 65$, $\chi_{vv} = 202$ as shown in table 7), this metal seems from their evidence to be a weak itinerant ferromagnet, so that the several complications do not allow a clear decision to be reached on this point. Again, χ_{vv} seems to be larger for cobalt than for nickel and iron. Nevertheless, the observed values agree surprisingly well with those estimated as the sum of $\chi_0 + \chi_{vv}$ at 0 K so that this seems to be well established as a reasonable explanation of the observations.

High field magnetization measurements for nickel near the Curie point have been reported by Ponomarev and Thyssen (1977) and for iron and nickel by Hatta and Chikazumi (1976, 1977). The former report measurements in fields up to 320 kOe and find that between 550 and 700 K the magnetization M as a

function of H and T follows the Landau theory of phase transitions previously applied by Edwards and Wohlfarth (1968) to weak itinerant ferromagnets, a reasonable result since M is also small near the Curie point of nickel. The Landau coefficients were found to vary systematically with temperature, going as T^2 in a temperature interval both above and below T_c which would imply important and significant effects due to single particle excitations. From an analysis of the data the exchange splitting came out as 0.33 eV and the high field susceptibility as 570×10^{-6} emu/mol. This last value is about 5 times the experimental values given in table 7 since it refers to a fictitious paramagnetic nickel. Hatta and Chikazumi (1976, 1977) also fit their high field data (up to 180 kOe) with a Landau theory and discuss these data on the basis of a localized model of ferromagnetism. The critical exponents (see section 2.6) deduced from these data for both iron and nickel were found to be close to the classical values. This is in contrast to other measurements in lower fields and is ascribed to the influence of the high fields in removing the effects of short range order near T_c.

2.6. Critical exponents near the Curie point

Near the Curie point the magnetic properties are characterized by a set of critical exponents, some of which will now be defined and tabulated; for further details see, for example, Stanley's book (1971).

Susceptibility χ at $T > T_c \sim (T - T_c)^{-\gamma}$
Magnetization M at $T < T_c \sim (T_c - T)^{\beta}$
$M(H)$ at $T = T_c \sim H^{1/\delta}$
Specific heat C_H at $T \gtrless T_c \sim |T - T_c|^{-\alpha}$
Correlation length ξ at $T \gtrless T_c \sim |T - T_c|^{-\nu}$
Pair correlation function at $T = T_c \sim r^{-(d-2+\eta)}$ (r = distance, d = dimensionality)
Spin wave stiffness D at $T < T_c \sim (T_c - T)^{x}$.

Values of γ, β, ν, η and x have been given for all three metals by Glinka et al. (1977) on the basis of their own and others' measurements. The value of δ is given by the scaling law

$$\delta = 1 + \gamma/\beta. \tag{21}$$

The values of α have been tabulated by Barmatz et al. (1975) and Ahlers and Kornblit (1975). All these values are given here in table 8. Note that this discussion is not fully rigorous (there are strictly two γ values, two η values and two α values for $T \gtrless T_c$ and (21) is debatable) but it suffices for the present context. The values are mean values weighed subjectively and no errors are given. Glinka et al. (1977) give a very useful review of the data tabulated here and conclude that although some features are reasonable from the point of view of scaling (e.g. β, γ and ν are well related by a scaling law) several features of these data are still not clear. Thus it does not seem clear why the value of γ for (cubic!) cobalt is close to that, 1.24, for the three-dimensional Ising model while

TABLE 8
Critical exponents (Glinka et al. 1977, Barmatz et al. 1975, Ahlers and Kornblit 1975)

Exponent	Fe	Co	Ni
γ	1.33	1.21	1.32
β	0.38	0.42	0.38
δ*	4.50	3.88	4.47
α	−0.12	−0.07**	−0.094
ν	0.70	0.65	–
η	0.07	0.10	–
x	0.37	0.39	0.39

*Values of δ from eq. (21).
**See section 3.5; the Rushbrooke inequality is used as an equality (Rocker and Schöpgens 1969).

the values for iron and nickel are closer to that, 1.38, for the isotropic Heisenberg model. Although there is no absolute theoretical certainty, the temperature dependence of the spin wave stiffness constant D, characterized by x, seems exceedingly close to that of M, characterized by β, so as to lead one to succumb to the temptation to postulate

$$D(T) \sim M(T) \qquad (T \sim T_c). \tag{22}$$

This result follows immediately from random phase approximations used in discussing spin wave energies.

2.7. Dynamic susceptibility; spin wave dispersion and stiffness

The use of neutron scattering techniques allows the elementary excitations of the ferromagnetic metals (single particle, spin wave) to be investigated and the dynamic susceptibility $\chi(\boldsymbol{q}, \omega)$ to be measured. An excellent summary of the present situation has been given by Windsor (1977) who summarizes the techniques of neutron scattering and what measurements are possible by each of these. Of immediate interest is the spin wave stiffness D defined by (10); calculations of D were described in section 1.5.

Spin wave stiffnesses may also be measured by the spin wave resonance measurements on thin films described more fully in the chapter by Hoffmann (volume 3/4). All the evidence points to the fact that these values are less reliable than those obtained by neutron measurements which will now be further discussed.

For iron triple axis measurements of D have been given by Collins et al. (1969) and by Mook and Nicklow (1973). The 1969 room temperature data are given in table 5 and agree excellently with those of 1973; in the earlier measurements the coefficient of the next term in the expansion of $\hbar\omega_q$, going as q^4, was also given but Windsor (1977) cautions against the use of such an expansion. The

measurements of Mook and Nicklow were taken to higher wave vectors corresponding to spin wave energies about 110 meV. The spin wave intensity was found to fall off slowly with increasing energy until about 80 meV where the intensity decreased rapidly by about an order of magnitude. It was proposed that this sudden decrease is caused by the entry of the spin wave mode into the continuum of single particle excitations, as discussed in section 1.5, where the entry was said to occur at a spin wave energy $\hbar\omega_{q\,\max}$. A band theoretical estimate of this energy was reported by Thompson and Mook (1970) and others (cf. below). Lynn (1975) reported similar measurements for an Fe(12% Si) crystal and less detailed for pure Fe as a function of temperature. Outside the long wavelength, low q range, where $D(T)$ varies as $|T - T_c|^x$ with x given in table 8, (i) the spin wave dispersion does not fit a quadratic + quartic dependence on q very well, (ii) spin waves exist as excitations up to and above the Curie temperature T_c, with no further renormalization with $T > T_c$. The measurements to show this result were obtained at $1.4T_c$. It was also found that the spin wave intensity dropped off sharply at an energy about 100 meV (for Fe–Si, cf. about 110 meV for Fe), but that this critical energy $\hbar\omega_{q\,\max}$ hardly changed at all on increasing the temperature from 295 K to 1240 K = $1.28T_c$. These data, shown in fig. 10, are extremely surprising since on a simple basis no excitations should persist so far above T_c.

For hcp cobalt there are several reported values of D and a value obtained by

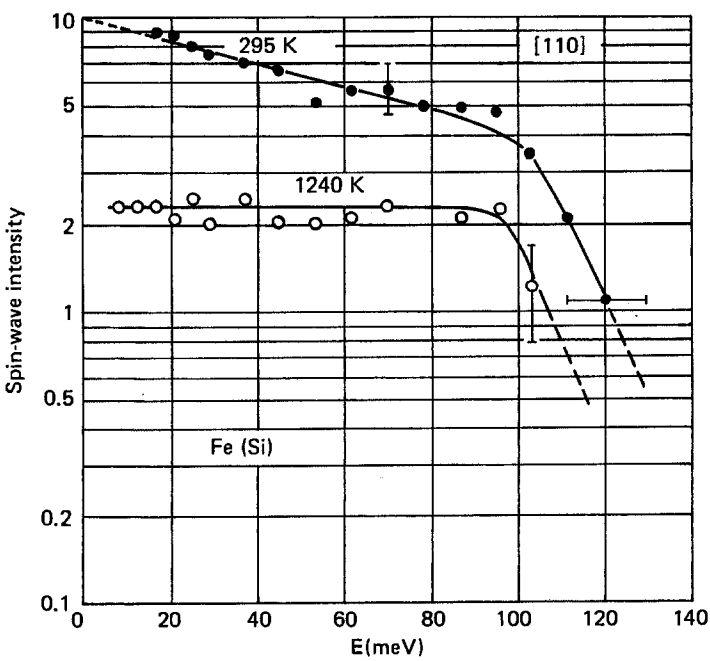

Fig. 10. Spin wave intensity against energy at 295 K and 1240 K = $1.28T_c$ for Fe (Si) (Lynn 1975).

triple axis measurements is given in table 5 (Shirane et al. 1968). In spite of Windsor's caution it may be mentioned that the coefficient of q^4 is considerably larger than is implied by a localized model of ferromagnetism (this point was still worth making in 1968!). There is also a report of D for fcc Co(+8% Fe), namely 371 meV Å^2 using the triple axis spectrometer.

For nickel there are several and differing values of D which have been analyzed carefully by Aldred (1975) who gives the room temperature value deduced from the triple axis data of Minkiewicz et al. (1969) and Mook et al. (1973) and shown in table 5 as the most reliable. Mook et al. also measured the temperature dependence of the spin wave dispersion through the Curie temperature. As for iron (Lynn 1975) there are two interesting results. The spin wave intensity at room temperature drops very rapidly at an energy about 80 meV, which is explained as the entry of the spin wave mode into the continuum of single particle excitations. This energy is significant as being roughly a measure of the energy gap Δ discussed in sections 1.3, 3.7 and 4.1 where it is shown to be in good agreement with some other estimations. However, as shown in fig. 11, it was also found that this energy did not decrease as the temperature was raised to over 700 K (Mook (1978) reports that spin wave modes persist up to $2T_c$ in Ni which are broadened and somewhat lower in energy than for the modes below T_c).

There are several possible interpretations of the surprising persistence of spin waves above T_c occurring in iron and nickel. One of these is the model of Edwards (1976b) discussed in section 1.3, another the spin fluctuation model of Moriya and Kawabata (Moriya 1977a,b) discussed in section 1.4 and a third is a theory of Korenman et al. (1977). In the last there is short range magnetic order above T_c on a scale characterized by an inverse length about 0.25 Å^{-1} so that a

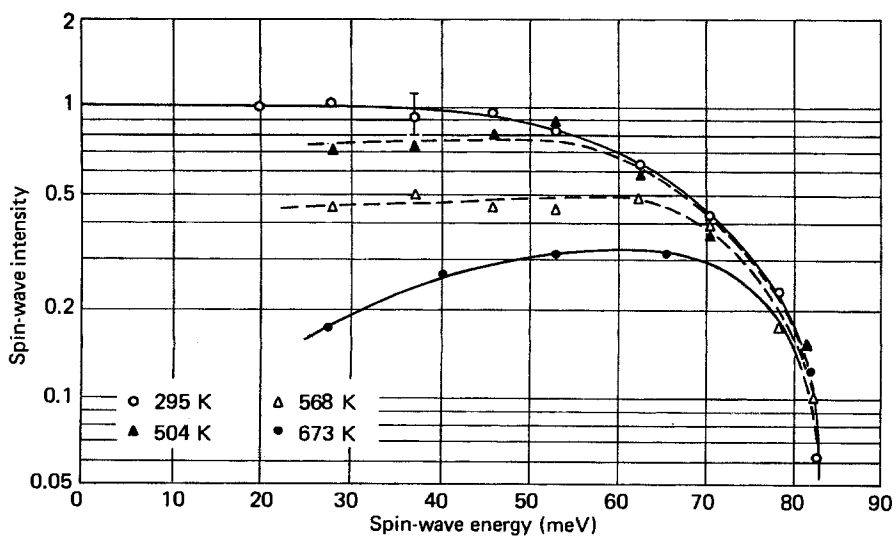

Fig. 11. Spin wave intensity against energy at various temperatures for Ni (Mook et al. 1973).

typical wavelength of the fluctuation is as much as 25 Å. It seems hard to believe in such large regions of coherence at $2T_c$. However, Capellmann (1979) has claimed to have calculated T_c for Fe and Ni on the basis of a similar model, in good agreement with experiment.

As mentioned in section 2.5 there is evidence from high field measurements that the magnetization of Ni near T_c follows closely a temperature and field dependence given by single particle excitations. It remains to correlate these two sets of data but it should be noted that the spin wave excitations would in any case be removed in these high fields.

The more general way of systematically regarding spin wave excitations is via the dynamic susceptibility $\chi(q, \omega)$ since its pole leads to the energy of spin waves as already pointed out in section 1.5. For iron calculations of this function have been given by Cooke et al. (1975). The calculation was based on a Slater–Koster interpolation scheme for the paramagnetic metal and a *rigid* splitting of 1.94 eV for the d-states resulting from screened wave vector dependent Coulomb interactions which differ for states of different symmetry (cf. ΔE for iron in table 2); the splitting of states other than d-states are themselves wave vector dependent. The calculations of $\chi(q, \omega)$ were carried out using standard numerical procedures and the results were used to calculate the neutron cross-section and spin wave energies. These were in good agreement with observation (Mook and Nicklow 1973) including a drop of intensity at about 120 meV. Hence Cooke et al. deduce that the itinerant model gives a good account of spin wave excitations in iron well below T_c. This conclusion is surprising in view of the suspicion that Hund's rule terms are highly important for Fe, as discussed in §1.4.

For nickel the dynamic susceptibility was discussed by Lowde and Windsor (1970) and Cooke and Davis (1973). The former reported a rather monumental research programme where the dynamic susceptibility of nickel was investigated by the neutron time-of-flight technique and by a band calculation based on a tight binding interpolation method and the random phase approximation. In the calculation the effective intra-atomic Coulomb interaction was taken to be slightly wave vector dependent. Figure 12 shows contours for the calculated and measured spin correlation function given by the imaginary part of the dynamic susceptibility, above and below T_c. Lowde and Windsor show how for any region in the space away from the origin the passage of the Curie temperature is much less catastrophic than for the static limit. Although the calculation and the measurements were carried out several years ago they represent the only such analysis ever reported for an itinerant ferromagnet. The agreement with experiment is quantitatively not perfect. Nevertheless, an RPA calculation was able to describe the broad features of the neutron data including the Curie point passage. Perhaps the later neutron data focussing attention on the persistence of spin waves above T_c should be reconsidered on this earlier basis.

Cooke and Davis (1973) (see also Cooke 1973) reported similar calculations for nickel using better band calculations, again a wave vector dependent effective interaction but covering only low temperatures. The agreement with the neutron data is again good.

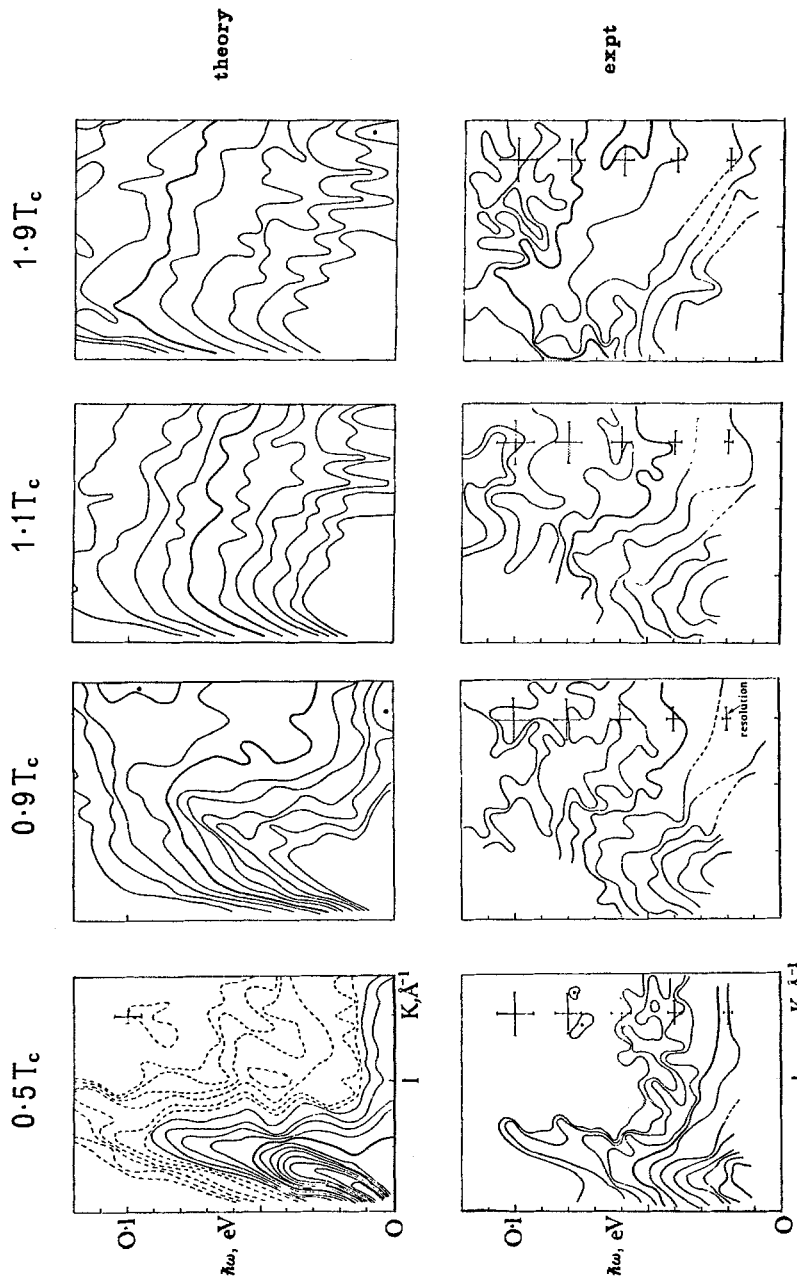

Fig. 12. Theoretical and experimental spin correlation functions for nickel, above and below the Curie point (Lowde and Windsor 1970).

TABLE 9
Magnetic moments of iron, cobalt and nickel from neutron measurements of spin densities (Shull and Yamada 1962, Moon 1964, Mook 1966)

	Fe	Co	Ni
Moment of 3d electrons (μ_B)	2.39	1.99	0.620
Moment of 4s electrons (μ_B)	−0.21	−0.28	−0.105

Note: The total moments differ somewhat from those in table 5 but the difference is within the experimental error.

2.8. Spin densities from neutron measurements

Spin densities of iron, cobalt and nickel have been measured using polarized neutron diffraction, (Shull and Yamada 1962, Moon 1964, Mook 1966). The resulting form factors were found to agree with calculated free atom form factors provided the magnetic moments are distributed among the 3d and 4s electrons as shown in table 9. The negative 4s magnetizations are relatively large. This last result is rather unexpected and has been found difficult to interpret theoretically. Thus Wakoh and Yamashita (1966) obtained a negative value of $-0.073\mu_B$ for iron but Duff and Das (1971) obtained a positive value for the same metal.

This review of the fundamental properties of iron, cobalt and nickel reveals a wealth of experimental information and a limited success in understanding these observations. The future will undoubtedly add new results in both directions.

3. Secondary magnetic properties

It is impossible to give here a complete treatment of the very many secondary magnetic properties of iron, cobalt and nickel nor to give complete tabulations of the relevant numerical values. Instead a fairly subjective approach is taken in tabulating and discussing selected quantities regarded as relevant and as reasonably reliable, both from the experimental and theoretical point of view. More detailed discussions of some data are given in Landolt-Börnstein (1962) and in the excellent article of Carr (1966).

3.1. g and g′ factors

The gyromagnetic ratio g' is measured by direct magnetomechanical experiments (Einstein–de Haas) and g by ferromagnetic resonance. They are related by the Kittel–Van Vleck formula

$$1/g' + 1/g = 1. \tag{23}$$

Scott (1962, 1966), Scott and Sturner (1969), Reck and Fry (1969) and related papers summarize measurements of g' for the metals and their alloys and those for the metals are given in table 10. This also contains average values of g given by the above authors and by Meyer and Asch (1961) and the corresponding values of $g/(g-1)$ which must be compared with g' according to (23). The table also contains Reck and Fry's estimates of the orbital magnetizations. It is seen that (23) holds excellently and that the orbital magnetizations are relatively large.

Values of g and g' have been calculated several times on the basis of the itinerant electron model including spin–orbit coupling effects. For iron and nickel Singh et al. (1976) obtained for g' and g the values 1.95 and 2.06 and for nickel 1.86 and 2.16; the agreement for nickel is better than for iron, as seen from table 10. For cobalt Ishida (1972) estimates g to be 2.11.

Using magnetic resonance studies on a nickel crystal it has been reported by Rodbell (1965) that g is independent of temperature and frequency, although this constant value is equal to 2.22 ± 0.03, compared to the best estimate of table 10.

3.2. *Linear magnetostriction*

For cubic crystals the linear strain introduced by the appearance of magnetization is written in a standard notation as follows (Becker and Döring 1939) in terms of the direction cosines α_i of the magnetization and β_i of the strain

$$\begin{aligned}\Delta l/l = {} & h_0 + h_1(\alpha_1^2\beta_1^2 + \quad + \quad - \tfrac{1}{3}) + 2h_2(\alpha_1\alpha_2\beta_1\beta_2 + \quad +) \\ & + h_3(\alpha_1^2\alpha_2^2 + \quad + \quad - \tfrac{1}{3}) \qquad \text{for nickel} \\ & + h_3(\alpha_1^2\alpha_2^2 + \quad +) \qquad \text{for iron} \\ & + h_4(\alpha_1^4\beta_1^2 + \quad + \quad + \tfrac{2}{3}(\alpha_1^2\alpha_2^2 + \quad +) - \tfrac{1}{3}) \\ & + 2h_5(\alpha_1\alpha_2\alpha_3^2\beta_1\beta_2 + \quad +). \end{aligned} \tag{24}$$

If, as is usual, only h_1 and h_2 are significant, then the usual magnetostriction coefficients λ_{100} and λ_{111} are given in terms of these coefficients by

$$\lambda_{100} = \tfrac{2}{3}h_1 \quad , \quad \lambda_{111} = \tfrac{2}{3}h_2.$$

TABLE 10

Values of g', g, $g/(g-1)$ and orbital magnetizations, according to the papers of Scott (1962, 1966), Scott and Sturner (1969), Reck and Fry (1969), and Meyer and Asch (1961)

	g'	g	$g/(g-1)$	$\mu_{orb}(\mu_B)$
Fe	1.919	2.091	1.916	0.0918
Co	1.838	2.187	1.842	0.1472
Ni	1.835	2.183	1.845	0.0507

Alternative representations of this expression have been given by Gersdorf (1961) and by du Trémolet de Lacheisserie (1970).

Values of h_1 to h_5 have frequently been obtained for iron and nickel. For iron two sets of measurements using strain gauges are considered here. Figure 13 gives results of measurements by Williams and Pavlovic (1968) over a wide temperature range (note the slightly different notations $A_1 = h_1$, $A_2 = 2h_2$, $A_3 = h_3$, $A_4 = h_4$, $A_5 = h_5$). Table 11 gives values of h_1, h_2 and h_3 at room temperature, these being due to Gersdorf (1961) who did not obtain values of h_4 and h_5 although these were small ($\sim 1 \times 10^{-6}$) for dilute iron alloys. The various data for iron were compared and contrasted by du Plessis et al. (1971) who concentrated on the high temperature peak in $A_1 = h_1$ shown in fig. 13. A theoretical interpretation of this peak in a general framework of localized electrons, due to Callen and Callen (1963), could not be tested using the available experimental data.

For nickel there are again several measurements and those of Lee and Asgar (1971) and Bower (1971) (see also Franse and Stop 1970) can be quoted here with confidence. The room temperature values are given in table 11 and the temperature variation of all five coefficients in fig. 14. The agreement between the data of table 11 is within the experimental uncertainty. Both Lee and Asgar and Bower state categorically that the temperature dependence of the h_i coefficients can not be explained on the basis of Callen and Callen's localized model.

For cobalt several notations for the magnetostriction coefficients exist (du Trémolet de Lacheisserie 1970) and one proposed by Bozorth (1954) is used here since the measurements of Hubert et al. (1969) are given in terms of this

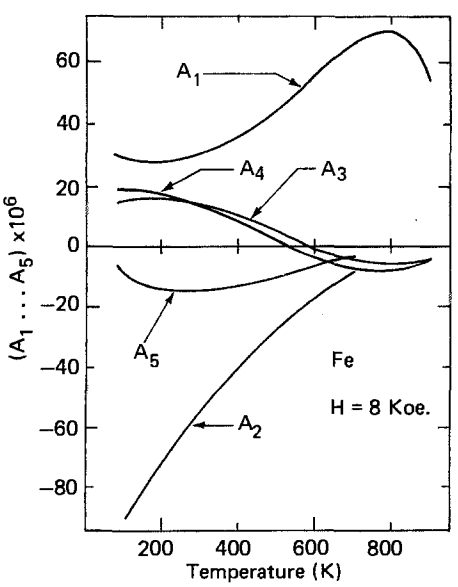

Fig. 13. Magnetostriction coefficients $A_1 \ldots A_5$ for iron (Williams and Pavlovic 1968). Note $A_1 = h_1$, $A_2 = 2h_2$, $A_3 = h_3$, $A_4 = h_4$, $A_5 = h_5$.

TABLE 11
Magnetostriction coefficients for Fe and Ni at room temperature

$10^6 \times$	h_1	h_2	h_3	h_4	h_5
Fe (Gersdorf 1961)	36.2	−34.0	2	–	–
Ni 1 (Lee and Asgar 1971)	−94.3	−42.5	−0.7	+0.2	+1.5
Ni 2 (Lee and Asgar 1971)	−93.9	−43.7	−0.3	−1.4	+1.2
Ni (Bower 1971)	−98.5	−43.1	+0.1	+3.4	+0.2

Magnetostriction coefficients for Co at room temperature (Hubert et al. 1969)

$10^6 \times$	λ_A	λ_B	λ_C	λ_D
	−50	−107	+126	−105

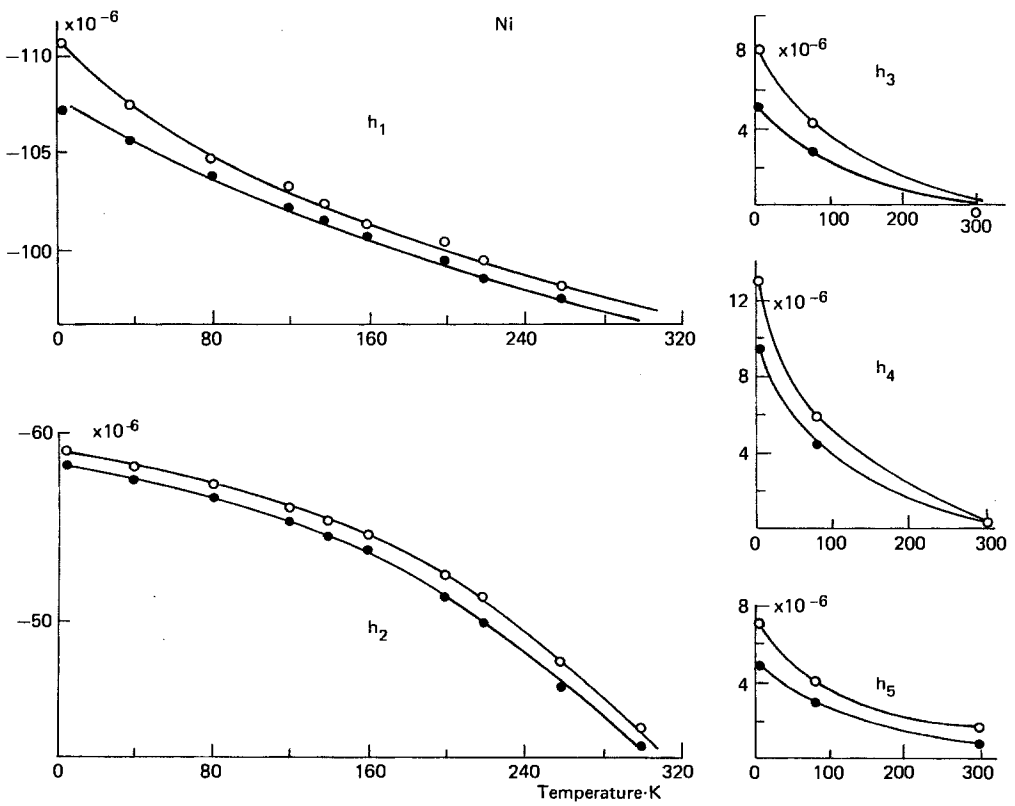

Fig. 14. Magnetostriction coefficients $h_1 \ldots h_5$ for nickel (Lee and Asgar 1971).

notation. This is

$$\begin{aligned}\Delta l/l = {} & \lambda_A[(\alpha_1\beta_1 + \alpha_2\beta_2)^2 - (\alpha_1\beta_1 + \alpha_2\beta_2)\alpha_3\beta_3] \\ & + \lambda_B[(1-\alpha_3^2)(1-\beta_3^2) - (\alpha_1\beta_1 + \alpha_2\beta_2)^2] \\ & + \lambda_C[(1-\alpha_3^2)\beta_3^2 - (\alpha_1\beta_1 + \alpha_2\beta_2)\alpha_3\beta_3] \\ & + 4\lambda_D[(\alpha_1\beta_1 + \alpha_2\beta_2)\alpha_3\beta_3] \end{aligned} \tag{25}$$

where the z or 3 axis is the hexagonal c-axis, the x or 1 axis the a-axis and y or 2 is perpendicular to x and z. Values of $\lambda_A \ldots \lambda_D$ at room temperature are given in table 11. The temperature dependence of these four coefficients is given by Hubert et al. (1969) and is again shown not to follow that predicted by Callen and Callen.

This inability of a localized model of ferromagnetism to explain the temperature dependence of these magnetostriction coefficients is natural. However, there exist as yet no band theoretical calculations of this dependence and, indeed, there is no very reliable calculation at 0 K. Fletcher (1955) (see also Gersdorf 1961) reported a calculation of h_1 and h_2 for nickel and, after a correction (Fletcher 1961), obtained the following values

$$h_1 = -70.0 \times 10^{-6} \qquad h_2 = -16.6 \times 10^{-6}$$

which agree as well as could be expected with the values of table 11. The calculation was based on that of a band structure of nickel with spin–orbit interactions treated by second order perturbation. The high values of h_1 and h_2 for nickel have led to the use of this metal in several applications, in particular in the construction of transducers for the conversion of electrical to mechanical energy at ultrasonic frequencies. Probably the largest single application is that of echo-sounding and underwater detection (Anon. 1961).

3.3. Magnetocrystalline anisotropy

Magnetocrystalline anisotropy may be measured by several different techniques, such as torque curves, magnetization curves and ferromagnetic resonance. In view of the importance of this property of ferromagnetic materials there are many measurements for the three metals Fe, Co and Ni, especially the last.

In a standard way, for the cubic metals the anisotropy energy may be written

$$E_a = K_1 s + K_2 p + K_3 s^2 + K_4 sp + K_5 s^3 + K_6 p^2 + \cdots \tag{26}$$

where $\quad s = \alpha_1^2\alpha_2^2 + \quad + \quad , p = \alpha_1^2\alpha_2^2\alpha_3^2$

with α_1, α_2, α_3 the direction cosines of the magnetization with respect to the crystal axes. Usually at most K_1, K_2 and K_3 are considered, but Franse and de Vries (1968) and Franse (1969) considered the influence of higher order terms for nickel, for which they are vitally important at low temperatures ($\lesssim$100 K). Aubert et al. (1976) and Gersdorf and Aubert (1978) very carefully produced a series of coefficients to describe the anisotropy at 4 K. The data in table 12 refer to room temperature where the usual representation continues to apply.

For iron, the older literature is given by Bozorth (1951) and in Landolt-Börnstein (1962), covering, in particular, measurements above room temperature. More recent measurements seem to have concentrated more on room temperature and below. It is impossible to assess accuracy and table 12 gives the values of K_1, K_2 and K_3 of Escudier (1973) at room temperature. The value of K_1 agrees excellently with an earlier one by Graham (1958) who also gives $K_2 = (0 \pm 50) \times 10^3$. Measurements by Sato and Chandrasekhar (1957), however, give $K_2 = 71 \times 10^3$ at room temperature, showing, in agreement with the earlier literature, that K_2 is virtually undetermined for iron. Escudier (1973) concludes that K_2 and K_3 are very small compared to K_1 and that a single anisotropy constant suffices to describe the anisotropy energy between 4 K and room temperature with good accuracy.

The temperature dependence of K_1 due to Escudier (1973) over the range 4 to 300 K agrees very well with that given in Bozorth (1951) over the wider range 0 to 800 K and Escudier's data are given in fig. 15. These two sets of data lead to the well-known result that $K_1(T)$ varies much more rapidly than $M(T)$ and a brief discussion of this result is given below.

For nickel there are considerably more measurements and Escudier's and Franse and de Vries' (1968) room temperature data are given in table 12. The agreement between these two sets of data is excellent.

The temperature dependence of K_1 for nickel given by Escudier from 4 to 300 K is shown in fig. 16. The value of K_1 at 4 K is here -1.26×10^6 erg/cm^3 whereas Franse and de Vries (1968) give -1.22×10^6 at the same temperature. Thus $K_1(T)$ is well established (ferromagnetic resonance measurements of K_1 for nickel by Rodbell (1965) are in good agreement with these static measurements) and, again, the variation is very rapid compared to that of $M(T)$. In both papers the influence of higher order terms is carefully analyzed.

Low temperature values of $K_3(T)$ are given by Amighian and Corner (1976) and Birss et al. (1977), and of $K_2(T)$ and $K_3(T)$ by Escudier (1973).

TABLE 12
Anisotropy constants at room temperature in erg/cm^3

	K_1	K_2	K_3	Author
Iron	4.81×10^5	1.2×10^3	-1.2×10^3	Escudier (1973)
Nickel	-5.48×10^4	-2.47×10^4	-0.3×10^3	Escudier (1973)
Nickel	-5.7×10^4	-2.3×10^4 / -2.6×10^4	0	Franse and de Vries (1968)
Cobalt	4.12×10^6	1.43×10^6	(K_3') 0.31×10^6	Sievert and Zehler (1970)
	M_1 emu/cm^3	$(M_{111} - M_{100})/M_0$		
Iron	0.781	−0.015%		
Nickel	0.246	0.017%		

Room temperature values due to Escudier (1973).

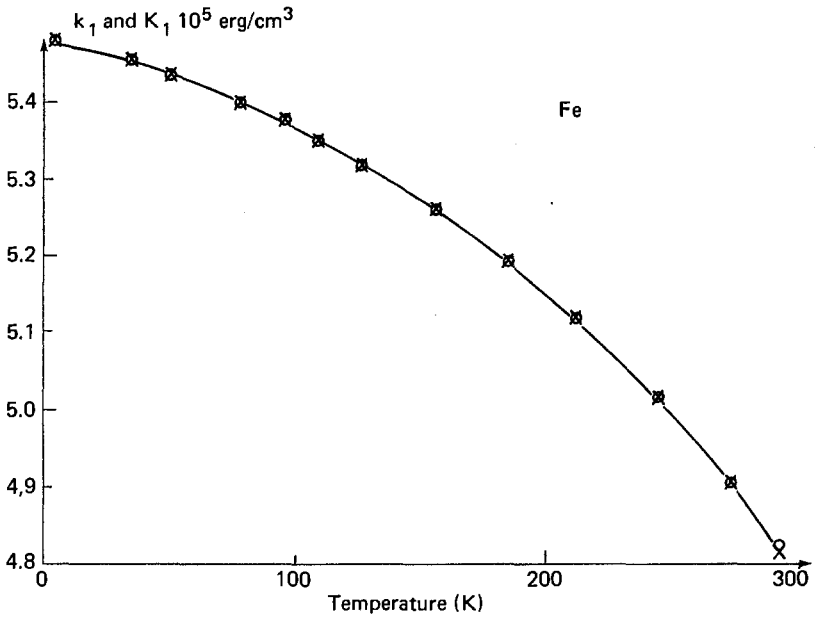

Fig. 15. Temperature dependence of K_1 for iron (Escudier 1973).

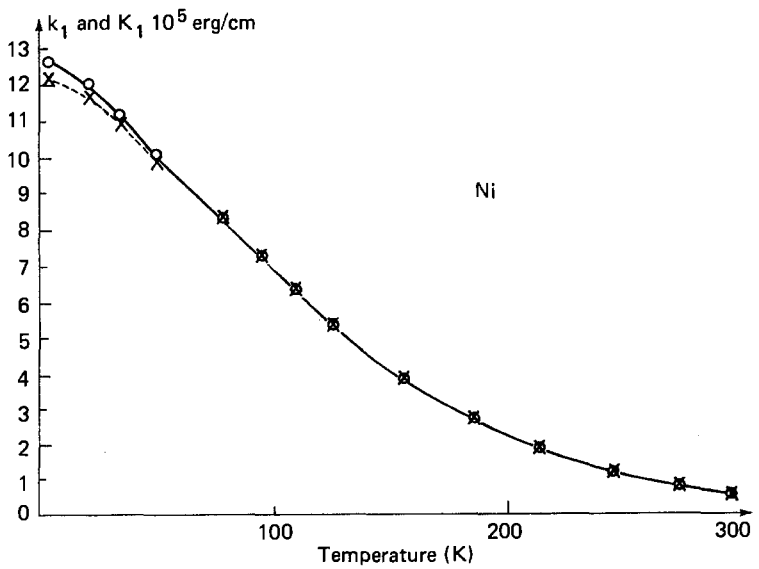

Fig. 16. Temperature dependence of K_1 for nickel (Escudier 1973).

For hcp cobalt the anisotropy energy is written as

$$E_a = K_1 \sin^2\theta + K_2 \sin^4\theta + K_3' \sin^6\theta + K_3 \sin^6\theta \cos 6\phi + \cdots \quad (27)$$

(Smit 1959) where θ and ϕ are polar angles with respect to the c and a axes. There are several measurements of K_1 and K_2 and table 12 gives the room temperature values of K_1, K_2 and K_3' due to Sievert and Zehler (1970). These values agree reasonably well with those of Honda and Masumoto (1931) reanalyzed by Sucksmith and Thompson (1954) and those of Barnier et al. (1961a). The temperature dependence of K_1 and K_2 due to Barnier et al. is shown in fig. 17. It is seen that $K_1(T)$ vanishes at 516 K, above which temperature the c-axis ceases to be easy. As shown by Barnier et al. (1961b), between 518 K and 598 K the easy axis lies along the generator of a cone of semivertical angle $\sin^{-1}(-K_1/2K_2)^{1/2}$ (Smit 1959) and this interesting behaviour is fully analyzed. At

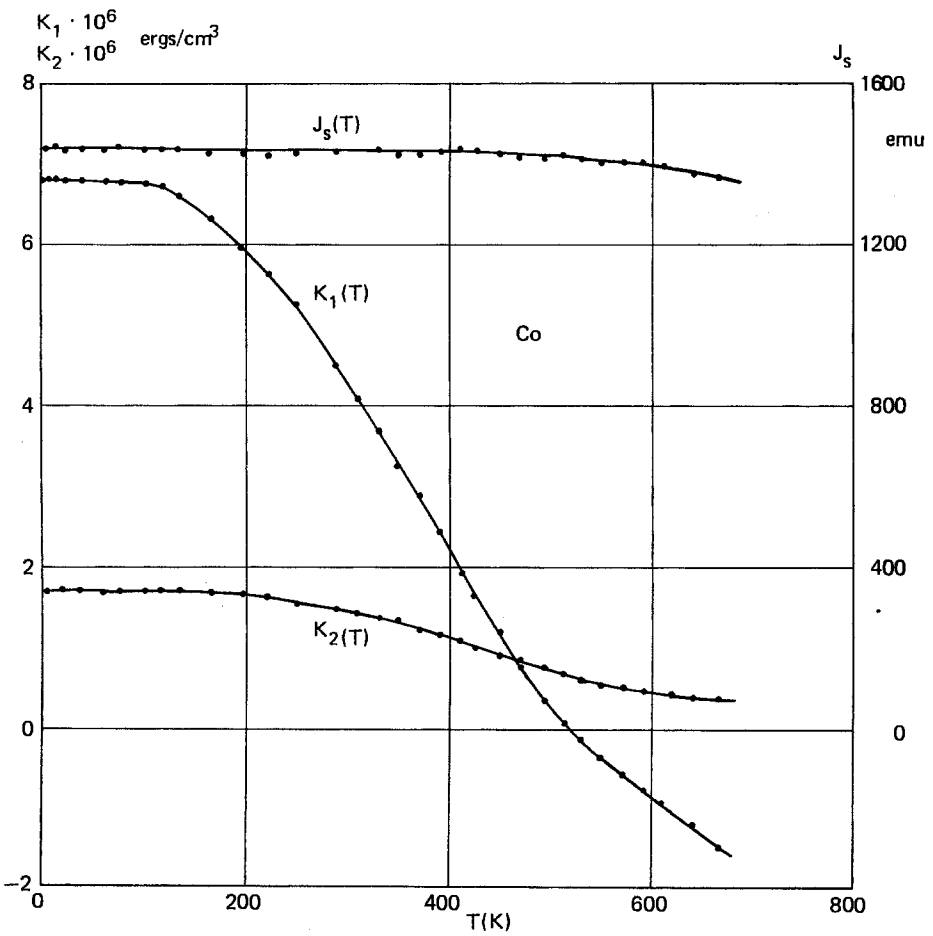

Fig. 17. Temperature dependence of K_1 and K_2 for hcp cobalt (Barnier et al. 1961a).

even higher temperatures cobalt becomes fcc (see fig. 8) and values of K_1 and K_2 between about 750 K and 1200 K have been given by Sucksmith and Thompson (1954). Both K_1 and K_2 are negative over this temperature range as is the case for fcc Ni (table 12) (see the relevant graphs in Landolt-Börnstein 1962; also see Carr 1966).

Aubert (1968) has discovered an anisotropy in the magnetization of nickel crystals and Escudier (1973) continued this work for nickel and iron. He represented the anisotropic part of the magnetization as

$$\Delta M = M_1 s + M_2 p + M_3 s^2 + \cdots \tag{28}$$

analogous to (26), and obtained the temperature dependence of M_1 for these two metals. The room temperature values are given in table 12 which also contains the corresponding values of the ratio of the change of the magnetization between the two crystal directions noted to the magnetization itself. The effect is seen to be small.

The theory of the anisotropy and its temperature variation has been given in terms of localized models (Carr 1966) which relate the K_1 coefficients directly to the magnetization $M(T)$. The agreement with experiment of the several formula given was analyzed for iron by du Plessis (1971) who plotted the exponent $n(T)$ to which the reduced magnetization $M(T)/M(0)$ has to be raised to yield $K_1(T)/K_1(0)$ (this tortuous procedure is historically based). The agreement is poor with all the versions of a localized model but also with one band model calculation (Mori 1969) which, however, Mori et al. (1974a,b) have since extended. For cobalt Barnier et al. (1961a,b) found none of the several localized models representative of the experimental data of fig. 17. In view of the strong itinerancy of the d-electrons in these metals this result is not surprising. However, it cannot be claimed that this very complicated problem has yet been fully solved using the itinerant model. Here calculations of the anisotropy coefficients have frequently been carried out (for a review for nickel, see Kondorsky 1974). The calculations include the following representative ones: Fletcher (1954, 1961), Slonczewski (1962), Furey (1967), Mori et al. (1974a,b), Kondorsky and Straube (1973), Gersdorf (1978) and others; the work of Furey is particularly remarkable but has never been published! The calculations are based on the following concepts:

Magnetic anisotropy is a result of spin–orbit coupling as is the case for the g-shift and linear magnetostriction. For cubic crystals calculations of K_1 require 4th order perturbation by the spin–orbit coupling of the unperturbed energy bands. As was first pointed out qualitatively by Fletcher (1954) and Fletcher and Wohlfarth (1962) large contributions to $K_1, \ldots$ are expected where there is a band degeneracy and these would be rapidly reduced by raising the temperature. This prediction was later verified by the several calculations quoted above. The temperature dependence is thus clearly not immediately related to a power of the magnetization and needs to be computed by direct methods of perturbation theory with temperature included by Fermi statistics. (The later trend "beyond Stoner" has clearly not yet reached this difficult problem.) Another way to smear

out the Fermi distribution is by alloying, which introduces mean free path effects. Hausmann and Wolf (1971) thus proposed a relationship between K_1 and residual resistivity and they, as well as Franse et al. (1974), found this verified by experiment. The perturbation calculations at 0 K and at finite temperatures require an independent knowledge of the spin–orbit coupling parameter, the energy band structure and the temperature dependent exchange splitting. The agreement of these calculations with experiment is good on the whole, as shown by reference to the calculations quoted.

Finally reference only is made to energy band calculations of the surface anisotropy of nickel by Bennett and Cooper (1971) and Takayama et al. (1976). This topic is discussed further by Hoffmann (volume 3/4).

3.4. Magnetoelastic effects

There is a variety of elastic properties of the ferromagnetic transition metals which are influenced by their magnetism. The effects are in general small compared to the observations on Invar alloys (Nakamura, volume 3/4). Nevertheless the results are significant and will now be briefly discussed.

3.4.1. Pressure dependence of fundamental properties

The Curie temperature of the three metals under pressure has been measured several times and reference is made to the results of Leger et al. (1972). For iron and cobalt it was found that dT_c/dP is essentially zero (Leger et al. quote 0 ± 0.03 K/kbar for Fe at 0 kbar and 0 ± 0.05 for Co at 0 and 60 kbar). For nickel at 0 kbar dT_c/dP is quoted as 0.36 ± 0.02 K/kbar at zero pressure and 0.17 ± 0.02 at 80 kbar. The increase of T_c of nickel at this high pressure is 25 K compared to the value at zero pressure, i.e. $T_c = 652$ K. The only simple theoretical formula for these three metals which is based on the itinerant model is that of Lang and Ehrenreich (1968) which is easily obtained by relating T_c to the energy band structure under pressure. It reads

$$dT_c/dP = \tfrac{5}{3} K T_c \tag{29}$$

where K is the compressibility. For nickel the calculated value is thus 0.60 K/kbar which agrees as well as can be expected with the above observations at zero pressure. For iron and cobalt the calculated values, 0.96 and 1.2 K/kbar, respectively, disagree with the observed null results, and there is at present no theoretical interpretation of the null data for these two metals.

The pressure dependence of the saturation magnetization is important in its own right and also by reference to the volume magnetostriction, since

$$\left(\frac{\partial M}{\partial P}\right)_H = -\left(\frac{\partial \omega}{\partial H}\right)_P \tag{30}$$

where ω is the volume strain. Direct measurements of $\partial M/\partial P$ have frequently been carried out and reference is made here to the measurements on nickel and iron by Tatsumoto et al. (1962). They obtained for the room temperature values

of the logarithmic derivative $\partial \ln M/\partial P - 2.4 \times 10^{-4}\,\mathrm{kbar}^{-1}$ for nickel and -3.0 in the same units for iron. The agreement with other measurements is only fair. The value of $\partial \ln T_c/\partial P$ for nickel is 5.7×10^{-4} in the same units, there being no clear reason for these two quantities being of the same order and sign for a strong itinerant ferromagnet. The temperature dependence of this logarithmic derivative was measured for nickel and iron by Tatsumoto et al. (1963) and found to be weak but smooth between 200 and 370 K.

Values of the pressure derivative of the saturation magnetization for cobalt were obtained by Kouvel and Hartelius (1960). Saturation for a polycrystalline specimen was achieved in 13 kOe and for a single crystal already in 3 kOe, yielding $\partial \ln M/\partial P = -2.2 \times 10^{-4}\,\mathrm{kbar}^{-1}$. Hence the values of this quantity for the three ferromagnetic metals are remarkably constant.

The pressure dependence of some other properties of iron, cobalt and nickel has also been measured and reference may be made to the crystalline anisotropy and linear magnetostriction. There are some differences in the results of different authors due to the obvious experimental difficulties. For Ni and Fe Franse and Buis (1970) (see also Kawai and Sawaoka 1968) give $\partial \ln K_1/\partial P$ at room temperature as -0.75 and $-0.50 \times 10^{-2}\,\mathrm{kbar}^{-1}$, respectively while for Co Sawaoka (1970) gives -0.60×10^{-2}; see also Kadomatsu et al. (1971). Such variations may follow from the strong influence of degeneracies on K discussed in section 3.3. Franse and Buis also give values of $\partial h_1/\partial P$ for Ni and Fe, where h_1 is defined by (24). Anderson (1966) gives values of the hyperfine field of Fe, Ni and Co under pressure.

3.4.2. Volume magnetostriction

The volume magnetostriction $\partial\omega/\partial H$ has been measured for binary alloys between Fe, Co and Ni by Stoelinga (1967) (see also Stoelinga et al. 1965) and by Fawcett and White (1968) for iron, cobalt and nickel at 4.2 K. In all cases high fields have had to be applied to reach saturation where $\omega \sim H$; this is the region of the paraprocess (see section 2.5). For polycrystalline specimens $\partial\omega/\partial H = 3h_0' +$ anisotropic terms, where h_0 is the magnetostriction coefficient defined in (24) (Stoelinga 1967) and the prime denotes a derivative with respect to H. The question of isotropy etc., is discussed in the above publications and by Hölscher and Franse (1979), giving the following values of $\partial\omega/\partial H$ at 4 K for Fe, Co and Ni, respectively: 4.5, 7.2 and $1.2 \times 10^{-10}\,\mathrm{Oe}^{-1}$. The value for cobalt leads to $\partial \ln M/\partial P = -3.4 \times 10^{-4}\,\mathrm{kbar}^{-1}$, compared to the directly observed value -2.2 quoted above. The temperature dependence of $\partial\omega/\partial H$ has been studied particularly for nickel (Stoelinga 1967, Tange and Tokunaga 1969). This quantity decreases from the above positive value, changes sign at about 440 K to reach very large negative values as the Curie point is approached.

The value of $\partial\omega/\partial H$ at low temperatures was proposed by Gersdorf (1961) to follow from the Landau theory of phase transitions which gives (Wohlfarth 1968) (see also Shimizu 1978)

$$\partial\omega/\partial H = 2KCM_T\chi_T. \tag{31}$$

Here K is the compressibility, M_T the saturation magnetization and χ_T the high field susceptibility both at temperature T, and C the magnetoelastic coupling constant defined by these authors. Although this Gersdorf formula correctly relates the volume magnetostriction to the paraprocess via the high field susceptibility it is not obviously justified to use the Landau theory for the ferromagnetic metals at low temperatures. It is, however, in order to apply this theory to materials with low values of the magnetization like Invar (see Nakamura, volume 3/4). However, near the Curie temperature the Landau theory is expected to apply (outside critical regions!) and Shimizu (1978) gives a detailed analysis. Mathon (1972) analyzed the data of Tange and Tokunaga (1969) by considering two processes under pressure, namely an s–d transfer and a change of the width of the d-band which influences the electron interactions. For the latter, Mathon (1972), Shimizu (1978) and others used the Kanamori theory of correlation effects (Kanamori 1963) and a dependence of the band width on volume characterized by an effective Grüneisen constant $\sim\frac{5}{3}$ (Heine 1967); this also occurs in relation (29). The correlation effects treated by the methods of the spin density functional formalism referred to in sections 1.2 and 1.3 lead to an effective interaction between the itinerant electrons which is only weakly dependent on volume. These methods have been used by Janak and Williams (1976) and Andersen et al. (1977) to estimate bulk moduli, volume magnetostrictions, etc., for magnetic materials, including iron, cobalt and nickel. Janak and Williams's so-called giant internal magnetic pressure is, apart from the compressibility, nothing more than the magnetostrictive volume strain. It is defined by them, as by Gersdorf (1961), Wohlfarth (1968), Shimizu (1978) and others in terms of the Landau theory. The values of this calculated pressure are 212, 182 and 10 kbar for Fe, Co and Ni, respectively. Shimizu (1978) claims, however, that these values are too large, due to the volume independence of the correlation effect which was assumed. This problem was also discussed by Friedel and Sayers (1978) and is fundamentally important.

3.4.3. Thermal expansion

The three problems partially relevant to magnetism are the low temperature values, the variation over a wide temperature range and the critical behaviour near T_c. At low temperatures the following values of the electronic Grüneisen parameter γ_e are relevant and are taken from the review of Collins and White (1964): 2.1, 1.9 and 2.0 for Fe, Co and Ni, respectively. These values were proposed by Shimizu (1974) to be close to the ubiquitous $\frac{5}{3}$ discussed in sections 3.4.1,2. Shimizu (1978) also discussed the temperature variation of the magnetic contribution to the thermal expansion of the three metals, comparison being made with the observed data of Kohlhaas et al. (1967). These measurements show very pronounced anomalies of the thermal expansion coefficient near the Curie point. This anomaly has been studied very carefully for nickel by Kollie (1977) from the point of view of critical phenomena. Critical indices α and α' were defined in the usual way (Stanley 1971) and were both found to be equal to

-0.093 ± 0.010, in excellent agreement with the specific heat based values given in table 8.

3.4.4. Elastic constants

The relevant magnetic problems concerning the elastic constants of the three ferromagnetic transition metals are essentially the changes introduced by the onset of magnetic order at the Curie temperature. For Young's modulus this is the well known ΔE effect. Measurements of single crystal elastic constants C_{11}, C_{12} and C_{44}, of relevant combinations and/or of elastic moduli have frequently been carried out and a good review of the older literature is given by Kneller (1962). For iron there are later measurements by Dever (1972), and fig. 18 shows the results for $C' = \frac{1}{2}(C_{11} - C_{12})$ and C_{44}. It is seen that C_{44} changes very little at T_c while C' has a positive anomaly of about 12% (measured as usual by extrapolating the data above T_c to very low temperatures and comparing with

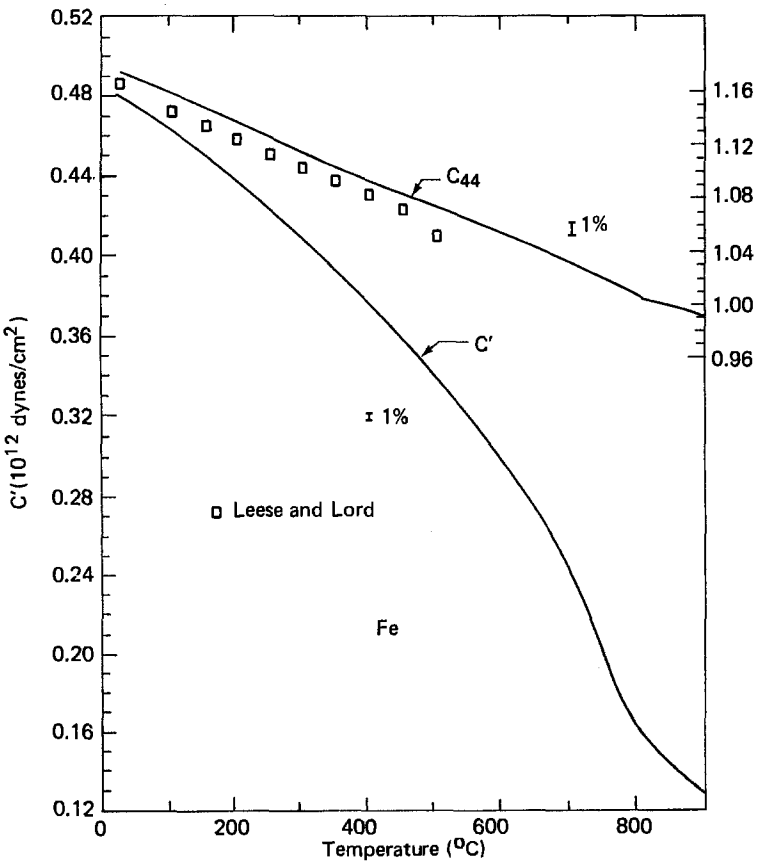

Fig. 18. Temperature dependence of $C' = \frac{1}{2}(C_{11} - C_{12})$ and C_{44} for iron (Dever 1972). The squares are data of Leese and Lord (1968).

the actual values at this temperature). For nickel the data of Alers et al. (1960) give again only a very small (positive) anomaly for C_{44} and a rather larger one, about +5%, for C'. Yamamoto and Taniguchi (1955) measured Young's modulus for Ni–Co alloys and observed a relatively large value of about +10% for nickel but a very small value (<1%) for hcp cobalt ($\Delta E/E$ decreases dramatically during the fcc/hcp phase transition). Hence the three metals display positive elastic coefficient anomalies at the Curie point which are frequently very small but may reach values $\sim +10\%$. This is in complete contrast with Invar (see Nakamura, volume 3/4) for which negative anomalies which may be very large are commonly observed.

The theoretical interpretation of the data is extremely difficult since the elastic constant anomalies have a number of contributing terms. The classical ΔE effect arises from domain processes ruled by the linear magnetostriction (Kneller 1962). This effect is generally assessed and removed by carrying out measurements in saturating magnetic fields (see for example Alers et al. 1960). The remaining anomaly is related to the volume magnetostriction in several complicated ways (Wohlfarth 1976, Hausch 1977) but a theory based on the itinerant model is being developed (Pettifor and Roy 1978). This relates the magnitude and sign of the anomaly to the structure and filling of the density of states curve but treats exchange and correlation by the spin density functional method. Using this same method Janak and Williams (1976) obtained the giant pressures (i.e. volume magnetostriction) referred to in section 3.4.2 and Shimizu (1978) claims that the resulting bulk modulus anomaly ΔB which is closely related to this pressure disagrees with experiment whereas his own thermodynamic analysis (similar to that of Hausch and Wohlfarth) is claimed to be more consistent. As already stated Friedel and Sayers (1978) ascribe the differences to the different volume dependences of exchange and correlation inherent in different models (Kanamori, spin density functionals, . . .).

Further experimental work on magnetoelasticity in iron due to de Vallera (1978) Gale et al. (1978), is concerned with the neutron observed changes of the phonon spectrum on passing through the Curie point.

3.5. Thermal properties

3.5.1. Specific heat

The low temperature specific heat of iron, cobalt and nickel was measured by Dixon et al. (1965) and the results are reproduced in table 13. Here the specific heat is expressed as

$$C = \gamma T + \beta T^3 + \alpha T^{3/2} + \kappa T^{-2} \tag{32}$$

where the γ term is electronic, the β term phonon (leading to the Debye temperature θ_D), the α term spin wave, and the κ term hyperfine (leading to an effective field H_{eff}). The accuracy of the values tabulated is fully discussed by Dixon et al. No comparison has since been made with later measurements and with other ways of estimating α (related to the spin wave stiffness D) and with κ

TABLE 13
Low temperature specific heat data (Dixon et al. 1965)

	Fe	Co	Ni
γ(mJ deg^{-2} mol^{-1})	4.741	4.38	7.028
θ_D K	472.7*	460.3	477.4*
α(mJ deg$^{-5/2}$ mol^{-1})	0.021*	–	0.011*
H_{eff} (kOe)	–	223.2	–

*Specimen *I*, use of eq. (32) by least squares.

(measurable by NMR and Mössbauer spectroscopy). The Debye temperature θ_D was carefully estimated from elastic constants by Konti and Varshni (1969) and Wanner (1970). Values of γ were discussed in some of the band calculations referred to in section 1.2 (see also below). These values of γ refer, of course, to the ferromagnetic state of the metals and thus contain a magnetic contribution given in terms of density of states by (Stoner 1939, Shimizu 1977)

$$\gamma_m = \gamma_{ferro} - \gamma_{para}$$

where
$$\gamma_{ferro} = \tfrac{1}{3}\pi^2 k^2 [N(E^+) + N(E^-)] \qquad (33)$$
$$\gamma_{para} = \tfrac{2}{3}\pi^2 k^2 N(E_F)$$

where E_F is the paramagnetic and $E^{\pm}$ the ferromagnetic Fermi energies. The ratio $\gamma_{para}/\gamma_{ferro}$ for a strong itinerant ferromagnet like nickel is expected to be $\sim$2; a realistic estimate for nickel was given by Jacobs and Zaman (1976) as 2.3. The calculated value of γ_{ferro} can not be immediately compared with experiment due to the electron–phonon enhancement effect (Grimvall 1976) which is uncertain for these three metals but for which estimates were given in section 1.2.

Nevertheless, the magnetic contribution to the low temperature γ value given by (33) is simple compared to the value of this contribution over the whole range of temperatures up to and above T_c (Stoner 1939, Shimizu 1977) although Shimizu gave calculated curves for iron and nickel. Measurements of the *total* specific heat over this broad temperature range have often been reported and fig. 19 shows the data of Braun and Kohlhaas (1965) (see also Braun 1964, and Braun et al. 1968). The Curie temperatures (and other phase transitions) are visible; the critical behaviour near T_c is discussed below. Great difficulties arise in analyzing such curves into constituent contributions analogous to the low temperature analysis given by (32). This unfortunate situation arises due to the complicated temperature dependences involved, the large number of possible contributions and the possibility of short range ordering effects above the Curie temperature. Analyses have, however, been bravely attempted by Stoner (1936), Braun and Kohlhaas (1965), Shimizu (1977) and others. Two other attempts concerning nickel and iron, respectively, are due to Jones et al. (1974) and Grimvall (1975, 1976). Jones et al. analyzed the specific heat data of several authors over the range 0 to 1200 K and deduced a paramagnetic γ versus T curve by having the

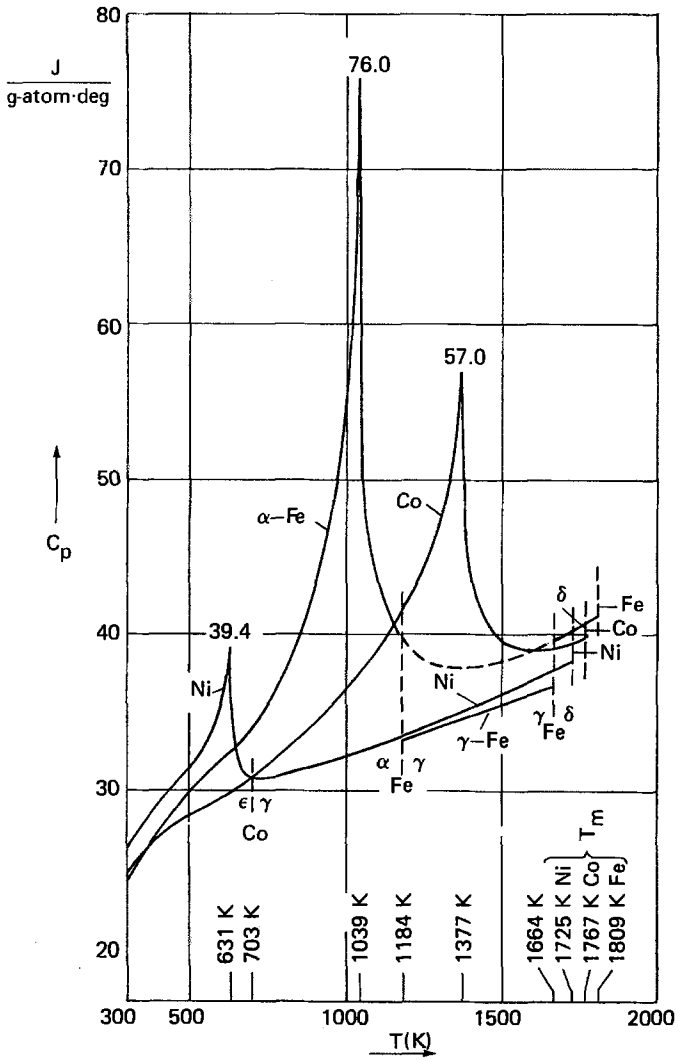

Fig. 19. Specific heat of iron, cobalt and nickel (Braun et al. 1968).

high temperature harmonic phonon contribution given by the Debye theory and estimating the anharmonic phonon contribution from thermal expansion data. The $\gamma(T)$ curve peaks at T_c and runs into a calculated curve (from the band calculations of Zornberg (1970)) at higher temperatures, being in excellent agreement with this at 1200 K, about $2T_c$. The calculated entropy of this temperature is 9.6 J/mol K, in excellent agreement with that obtained from the experimental data, namely 9.9 in these units. Since this calculated entropy is based on a single particle itinerant model Jones et al. (1974) conclude that this is a good model at these high temperatures. This is in contrast to the discussions of

Korenman et al. (1977) and the motivation for this work, namely the observation of spin waves above T_c discussed in section 2.7, but it agrees with the magnetic measurements of Ponomarev and Thyssen (1977) discussed in section 2.5.

For iron Grimvall (1975, 1976), however, concludes that the thermodynamic data require persistent disordered localized magnetic moments in the paramagnetic phases. This conclusion in turn was criticized by Sakoh and Shimizu (1977) who concluded that there was no need to invoke entropy contributions from localized moments in the high temperature regimes; Grimvall's conclusion was claimed to arise due to insufficient account having been taken of the peaks in the density of states curve for this metal (see fig. 3). The experimental data for the three ferromagnetic metals above the Curie points have even been taken into the liquid state by Vollmer et al. (1966) and the measured heat of melting should also be considered in future analyses of the vexed problem: can thermodynamic data give reliable information on the degree of localization of magnetic moments above the Curie point?

Near T_c the most important question is the magnitude of the critical exponents α and α' (Stanley 1971) and values of α (taken to equal α') for iron and nickel are given in table 8; both are seen to be rather small and negative. Measurements of these exponents have frequently been carried out and those of Shacklette (1974) (Fe) and Connelly et al. (1971) (Ni) are to be regarded as reliable as they agree with this compilation which covers a wider range of observations. For cobalt the situation is slightly less satisfactory. Kraftmakher and Romashina (1966) obtained a logarithmic dependence of the specific heat near T_c, i.e. $\alpha = \alpha' = 0$, while Rocker and Schöpgens (1969) obtained $\alpha = -0.1$ from the measurement of Braun (1964). The exponent may also be estimated using "the Rushbrooke inequality as an equality" (Stanley 1971, Rocker and Schöpgens 1969)

$$\alpha = \alpha' = 2 - 2\beta - \gamma. \tag{34}$$

This relation gives values for iron and nickel in quite reasonable agreement with those tabulated in table 8. Taking account of the residual differences, (34) and table 8 give for cobalt $\alpha = \alpha' = -0.07 \pm 0.02$ which is close to that of Rocker and Schöpgens (1969).

A further critical exponent, ζ, not listed in table 8, relates the change of the specific heat at field H compared to that in zero field,

$$C_H - C_0 \sim H^{-\zeta}. \tag{35}$$

Mathon and Wohlfarth (1969) (see also Ho 1971) considered earlier measurements on nickel of Korn and Kohlhaas (1969) and, although qualitative agreement with their critical exponent analysis was established the data were insufficient to establish the value of ζ which had to be obtained from the formula (Stanley 1971)

$$\zeta = \frac{2 - 2\beta - \gamma}{\beta + \gamma} = \frac{\alpha}{\beta + \gamma} \tag{36}$$

giving $\zeta = -0.06$, i.e. extremely small. For cobalt also Rocker and Schöpgens (1969) were unable to deduce values of ζ from the measurements of Braun (1964) and used (36) to obtain $\zeta = -0.05$. The measurements of Korn and Kohlhaas (1969) on iron in a magnetic field have not been analyzed in this way but relation (36) gives (using table 8) $\zeta = -0.07$; within the accuracy of measurement the value of ζ is thus the same for all the ferromagnetic transition metals.

3.5.2. Magnetocaloric effect

Mathon and Wohlfarth (1969) analyzed the magnetocaloric effect of nickel on the basis of the Kouvel–Comly (1968) equation of state which includes the critical exponents discussed and tabulated in section 2.6. A general relation for the resulting temperature change ΔT is given in terms of the magnetization M_H and the results are compared with the classical data of Weiss and Forrer (1926) which had earlier been expressed in terms of the classical formula

$$\Delta T \sim M_H^2 - M_0^2. \tag{37}$$

The agreement had long been known to be rather unsatisfactory, and the use of the non-classical critical exponents of Kouvel and Comly led to considerable improvement, including curvature effects at low fields H. When

$$T = T_c \qquad M_0 = 0 \qquad \Delta T \sim M^{\pi} \tag{38}$$

where $\pi = 2 + (\gamma - 1)/\beta$.

Using Kouvel and Comly's critical exponents, $\pi = 2.90$, compared to the observed value (Weiss and Forrer 1926) $\pi = 2.75$ and the classical value $\pi = 2$. Noakes and Arrott (1973) remeasured the magnetocaloric effect for nickel near T_c and found $\pi = 2.78$. Rocker et al. (1971) reanalyzed all the measurements of the magnetocaloric effect from the Kohlhaas school in terms of critical exponents and obtained the following values for π: 2.32, 2.58 and 2.82 for Fe, Co and Ni, respectively. The range of values of π using (38) and their own experimental values of β and γ is rather wide but includes these direct values for which a fundamental determination on the basis of renormalization group methods is awaited.

3.6. Transport properties

3.6.1. Electrical resistance

The article by Campbell and Fert (volume 3/4) includes an authoritative account of the microscopic mechanisms through which magnetism influences transport properties. In addition, this work summarizes the experimental data in concentrated transition metal alloys of iron, cobalt and nickel. It suffices, therefore, to include here only a representative set of typical data for the pure metals and to summarize the relevant theoretical ideas. The subject of the electrical properties of ferromagnetic metals is in principle very difficult since the scattering proces-

ses involved add their own inherent difficulties to those involved in the magnetism itself.

The electrical resistivity ρ of the three metals has frequently been measured and fig. 20 gives the data of Kierspe et al. (1967). All three curves show an anomalous drop of ρ below the Curie point. For cobalt the crystal structure change is clearly seen. These data have been excellently verified in independent measurements by Schröder and Giannuzzi (1969). The crystal structure change $(\alpha - \gamma)$ in iron was shown up in resistivity data of Arajs and Colvin (1964a). Very remarkable measurements of ρ in the solid and liquid phases and going up to the boiling point (!) were reported by Seydel and Fucke (1977).

Kierspe et al. (1967) and others have derived curves giving $d\rho/dT$ over a wide range of temperatures, and found a fairly complicated behaviour. For all three metals $d\rho/dT \sim T$ (i.e. $\rho \sim T^2$) at temperatures well below T_c. For iron and nickel a sharp maximum in $d\rho/dT$ occurs somewhat below T_c. For cobalt no such sharp maximum in the temperature derivative was observed; in fact, the derivative curve became horizontal and finally decreased right through the T_c region. Kierspe et al. draw an analogy with some rare earth metals (see chapter 3 by Legvold). The Curie temperature region itself was investigated for iron by Shacklette (1977) from the point of view of the Fisher–Langer (1968) prediction that $d\rho/dT$ varies near T_c in the same way as the specific heat, i.e. specified by the critical index α, and found this prediction to be verified with α as in table 8. For nickel, as Shaklette states, the situation is less clear: Thus Zumsteg and

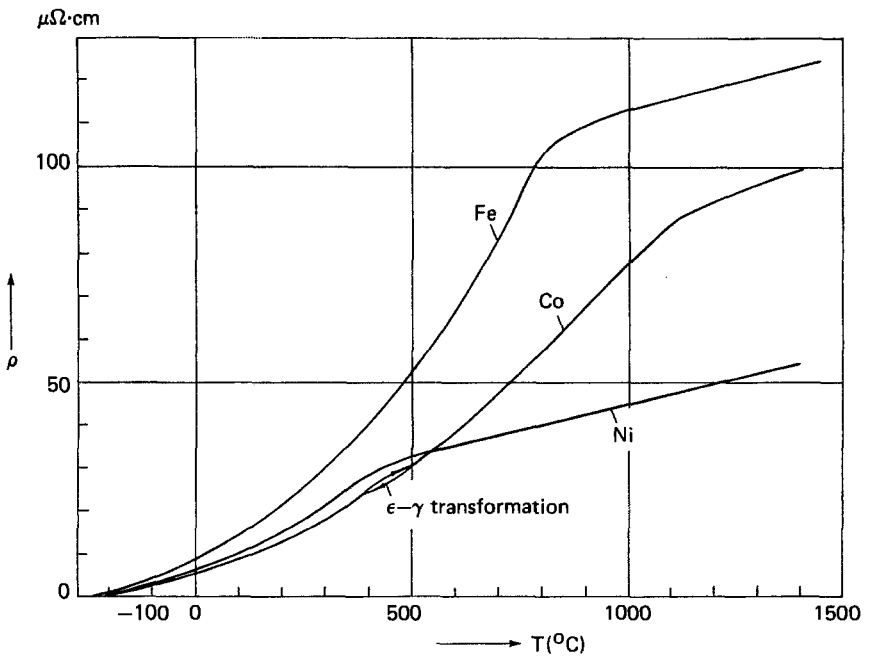

Fig. 20. Electrical resistivity of iron, cobalt and nickel (Kierspe et al. 1967).

Parks (1970) also claim to have verified this prediction but the α (and α') values derived from $d\rho/dT$ are not those regarded as reliable in table 8.

The T^2 dependence of the resistivity at low temperatures appears clear from the data of Kierspe et al. (1967). Measurements specifically directed towards this end have also been obtained. Thus Radakrishna and Nielsen (1965) measured the electrical resistivity of cobalt up to 6 K and found an important T^2 contribution. This verifies earlier data of White and Woods (1959) who had evidence from this term also for iron and nickel.

As more fully discussed by Campbell and Fert (volume 3/4) the special features of the electrical resistivity of ferromagnetic metallic materials may be understood on the following basis:

(1) The current is carried in the main by the s-electrons due to their lower effective mass (by ~ 10) compared to that of the d-electrons.

(2) These conduction electrons are scattered by the itinerant d-electrons.

(3) Below T_c the scattering d-electrons act in two groups with + and − spin thus leading to the observed dependence of the resistivity on magnetization (spin disorder scattering effect).

(4) The T^2 dependence of the resistivity arises from the scattering in a very general way. The same dependence also arises from a scattering process involving spin waves. Hence the scattering processes can not be distinguished in this way.

For the last point Radakrishna and Nielsen (1965) estimated the contribution to the T^2 term coming from magnon scattering to be about 15% of the total in the case of cobalt. Up-to-date estimations of this effect for all three metals would be desirable using reliable evidence on the spin wave spectrum. On the other hand, estimations of the T^2 term coming from scattering by d-electrons, due to Hasegawa et al. (1965) also deserves updating having regard to later information about the band structure, exchange splitting and the phonon spectrum.

3.6.2. Hall effect

Hall effect measurements on the three ferromagnetic metals have been summarized by Hurd (1972); see also Hurd (1974) and Cohen et al. (1973). Table 14 is extracted from Hurd's massive tabulation, the selection being made so as to fit

TABLE 14
Room temperature Hall effect coefficients (Hurd 1972)

	R_0*	R_1*	Authors
Fe	+0.23	+7.22	Volkenstein and Fedorov (1960)
Fe	+0.18	+4.35	Dheer (1967)
Co	−0.84	+0.24	Volkenstein and Fedorov (1960)
Ni	−0.5	−6.05	Volkenstein and Fedorov (1960)
Ni	−0.56	−5.0	Huguenin and Rivier (1965)

*In units $10^{-12}\ \Omega$ cm/G.

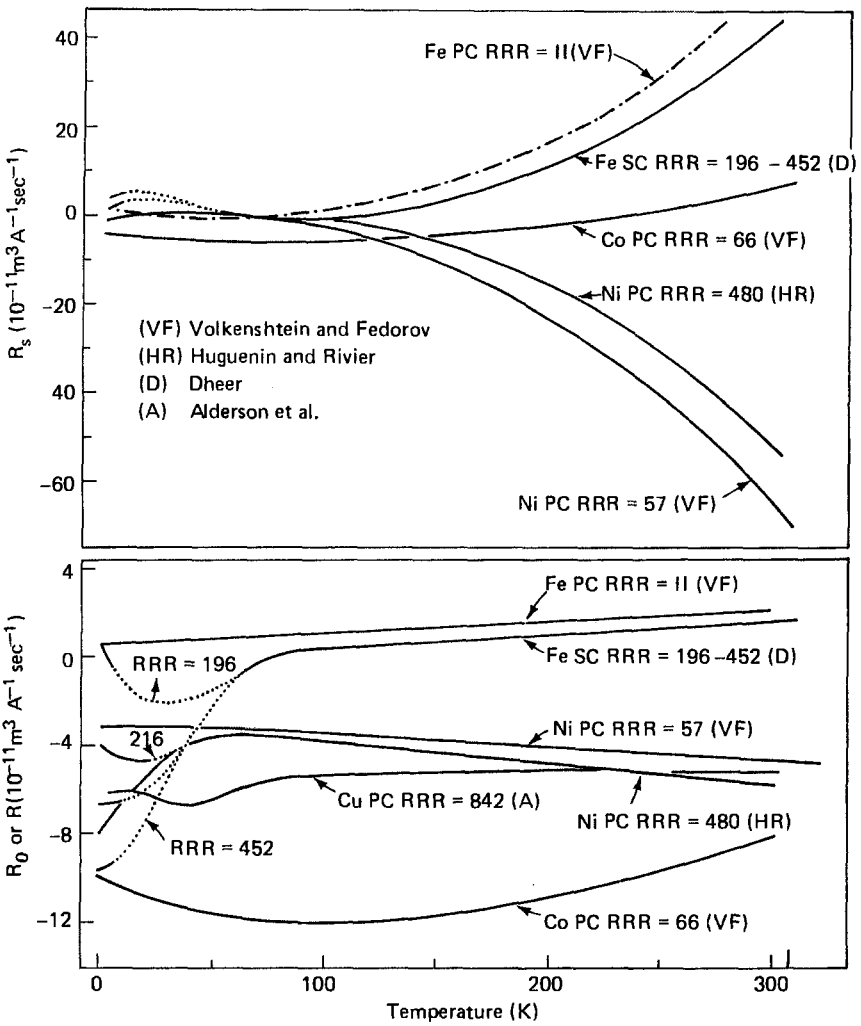

Fig. 21. Hall effect coefficients R_0 and R_1 of iron, cobalt and nickel (Hurd 1972).

with the temperature dependence of the tabulated quantities shown in fig. 21, also taken from Hurd (1972).

What is tabulated are the two coefficients R_0 and R_1 defined as ordinary and extraordinary coefficients of the Hall resistivity ρ_H in the form

$$\rho_H = R_0 H + R_1 M \tag{39}$$

where H is the (internal) field and M the magnetization; sometimes ρ_H is written as

$$\rho_H = R_0 B + 4\pi R_S M \tag{39}^*$$

where B is the applied B-field, and R_S is the spontaneous Hall coefficient. The

coefficient R_0 is thus the one occurring in ordinary metals while R_S is characteristic of magnetism.

The theory of these effects is very difficult and has long been the subject of controversy. A review is given by Hurd (1972) and by Campbell and Fert, (volume 3/4). To summarize the discussion of Hurd, the interpretation of the observations involves a scattering mechanism for the itinerant charge carriers together with an appropriate spin–orbit interaction to produce the required asymmetry leading to a transverse electric field which has the macroscopic properties of the effect in ferromagnetic metals. Theories of the anomalous effect have been given along these lines by Karplus and Luttinger (1954), Smit (1955) and Kondorsky (1969). A general result is that the coefficient R_S in (39*) is proportional to the square of the resistivity which for iron holds approximately above about 50 K (Volkenstein and Fedorov 1960, Dheer 1967) but not at lower temperatures. Theoretical papers referring in particular to both R_0 and R_1 of this metal are those of Irkhin et al. (1967), Fivaz (1968) and Cottam and Stinchcombe (1968); they are too complicated to summarize here but the summary by Hurd may be referred to. For nickel the Hall effect has helped in establishing the Fermi surface (see section 4.7); thin film effects related to the Hall effect are discussed by Hoffman (volume 3/4).

3.6.3. Other effects

As in the article of Campbell and Fert (volume 3/4) reference will be made to measurements of the thermoelectric power and the thermal conductivity, magnetoresistance in thin films being discussed by Hoffmann (volume 3/4). Schröder and Giannuzzi (1969) reported measurements of the Seebeck coefficient of iron, cobalt and nickel over a broad temperature range near the Curie temperature and observed, in agreement with other data, that this coefficient has a pronounced maximum close to T_c. The thermoelectric power of iron was analyzed by MacInnes and Huguenin (1973) in terms of the treatment of Fisher and Langer (1968) of the scattering of electrons from spin fluctuations which arise near the Curie point and which lead to the observed maximum in this case. Low temperature values of the thermoelectric power of cobalt by Radakrishna and Nielsen (1965) showed that no contributions due to magnon drag (Roesler 1964) arise in this case. The thermal conductivity of all three metals was measured by White and Woods (1959) and found to increase anomalously with temperatures in ranges $\geqslant \frac{1}{2}\theta_D$ where that of nonferromagnetic metals approximately reaches an asymptotic value. Richter and Kohlhaas (1964) found that near the Curie point the thermal conductivity and the resulting Lorentz number show a very marked anomalous peak extending over only 10 degrees. For nickel Papp et al. (1977) derived the thermal conductivity from measurements of the heat diffusivity and found that near T_c the temperature dependence differed markedly from that derived from the Wiedemann–Franz law. Low temperature data for nickel were also reported by Radakrishna and Nielsen (1965) and here the thermal conductivity followed closely a linear law $\kappa = 0.30T$ W/cm K. The Lorentz number was close to the "theoretical" value.

Due to the great difficulties involved in interpreting these data it seems best to leave them to speak for themselves. It is indeed unfortunate that no conclusions can be drawn regarding such theoretical problems as the relative importance of single particle and spin wave excitations below T_c and of spin wave phenomena above.

3.7. Optical properties

Magneto-optic effects and the magneto-optical conductivity are important for thin magnetic films and are discussed by Hoffmann (volume 3/4). The discussion is here limited to a few measurements on one of the ferromagnetic metals which have a bearing on the theoretical problems referred to in the earlier parts of this article, namely band structures, exchange splittings, and their temperature dependence. This section is thus in a way to be regarded as part of section 4, related to relevant electronic properties. Since the subject matter is only peripheral to magnetism, only nickel will be briefly discussed. For this metal Wang and Callaway (1974) calculated the diagonal and the off-diagonal elements of the optical conductivity tensor, including in their band calculation spin–orbit coupling effects (these also arise, of course, in other branches of magnetism as discussed earlier). The calculations give a pronounced peak in the real part of the xx component of the conductivity tensor at 0.8 eV, being a direct measure of the exchange splitting. No such peak was observed but an incipient manifestation of it was claimed to have been seen in the data of Lynch et al. (1971) which led to an exchange splitting of about 0.5 eV (see table 3). The evidence for this is not too firm and the wide scatter of the many experimental curves reproduced by Wang and Callaway (1974) shows that optical measurements do not provide a wholly reliable guide to the magnetism of nickel. The same caution may also have to be exercised regarding the following relevant papers. Shiga and Pells (1969) interpreted the temperature dependence of their measured optical absorption spectrum of nickel (specifically the width of a pronounced peak at 5 eV) by a temperature dependent exchange splitting which vanished at the Curie temperature. The low temperature value of this ΔE was 0.46 eV, whose closeness to the above value may be a coincidence. These data, showing a marked change in the optical absorption with temperature, were discussed in relation to other data by Fadley and Wohlfarth (1972) in a concise review of changes at T_c which will be referred to below.

The final example of optical data which have relevance to magnetism is the work of Stoll (1972) who aimed at obtaining the value of the energy gap Δ referred to in sections 1.3, 1.4 and 1.5. The analysis of his optical spectrum to answer the question: "Where to where is Δ?" is clearly in part debatable but a minimum value of 50 meV and an average value of 80 meV are claimed, and these are in excellent agreement with the *lower* values obtained from photoemission (see section 4.1) and neutron (section 2.7) data but much less than that from the band calculations of Callaway and Wang (1977a) discussed in sections 1.2 and 1.3, i.e. 300 meV. It remains to unravel this situation in the future.

Optical data of this type are thus not wholly conclusive but have led to a number of estimates of the exchange splitting which may be significant. The difficulties in this field are related to specimen purity and the analysis of the observed data which are often complicated.

4. Relevant electronic properties

This article will now be completed by a necessarily brief account of some relevant electronic properties of iron, cobalt and nickel. The aim of this extensive work, often based on very sophisticated experimental techniques, is to try to obtain information on the following matters:

(1) Energy band structure and band width
(2) Exchange splitting, and its temperature dependence
(3) Spin polarization of the electrons
(4) Fermi surface
(5) Wave functions and momentum distribution.

4.1. Solid state spectroscopy

4.1.1. Ultraviolet photoemission spectroscopy

This technique which when using angle resolution is popularly known as ARPSUPS, has been used to investigate points (1) and (2) above.

The bandwidth of nickel was measured using this advanced technique by Smith et al. (1977). The value obtained by a reasonable assignment of the observed peaks of the photoemission spectrum was 4.3 eV which is in good agreement with the calculated values of the band width (see fig. 1). It is considerably larger than the earlier UPS value of Eastman (1972), 3.3 eV, and values obtained by other techniques (see for example Fadley and Shirley 1971). The good agreement of Smith's value, if substantiated, will obviate the need for invoking many body effects! These measurements differ from the earlier ones in revealing a new peak at low energies which is claimed to be significant. Future work will be directed towards the direct measurement not just of the bandwidth but also of the actual structure, i.e. an attempt at details of density of states curves. Some results along these lines are already available, for example in the measurements of iron by Kevan et al. (1978) and on nickel by Williams et al. (1978). Even the former, who compare their data with a band calculation on iron (see fig. 3), admit that some features are missing while others are present which can not be explicitly accounted for. For a review, see Eastman (1979).

Explicit searches for the (low temperature) exchange splitting have been carried out for all three metals. For nickel Heimann and Neddermeyer (1976) gave arguments for assigning an exchange splitting of 0.3 eV to their observed spectra, this being on the low side of the arguments of section 1.3 and certainly less than the value 0.6 eV of table 3. An independent measurement of ΔE was

reported by Dietz et al. (1978), using two different photon energies 10.2 and 16.8 eV. Unfortunately, the exchange splitting (at the top of the d-band) depends on this energy, having values 0.35 and 0.49 eV, respectively. The higher value is claimed to be more reliable and both are significantly less than the value of table 3. Himpsel et al. (1979) and Eastman et al. (1978) (see also Eastman 1979) have reported what are probably at the time of writing the most accurate UPS data for Ni. They find ΔE at low temperatures to have a value of 0.31 eV and the gap Δ, defined by (9), to be close to that suggested by Wohlfarth (1977b) to bring about agreement with the spin polarized photoemission and neutron data discussed in sections 4.1 and 2.7, respectively. However, ΔE decreases to about half its low temperature value above T_c; see below.

For iron, the measurements of Kevan et al. (1978) have already been referred to. The exchange splitting was not explicitly deduced. This was done, however, in the measurements of Pessa et al. (1976) when combined with other data. The analysis is complicated due to this combination of techniques and the value $\leqslant 1.9$ eV has a debatable significance; it agrees well, however, with table 3. In a later paper Heimann and Neddermeyer (1978) return to the statement that an estimation of exchange splitting is not possible on the basis of UPS data alone, although here single crystal faces of iron were investigated.

For cobalt Heimann et al. (1977) obtained photoemission spectra which had again to be combined with other data, in the following way: A very well defined peak at -0.3 eV (relative to the Fermi energy) obtained in the measurements was identified with the sharp peak in the density of states curve of the majority spin band (see fig. 5 for the paramagnetic density of states curve). X-ray data of Turtle and Liefeld (1973) were felt to give the same peak for the minority spin band, occurring at $+0.7$ eV and thus giving $\Delta E = 1.0$ eV, in good agreement with table 3.

All these values are thus claimed to give evidence for exchange split bands but the actual values of the corresponding energy are not yet sufficiently reliable to feel fully confident about their significance.

Apart from the low temperature value of ΔE its variation through the Curie point has been vigorously studied since on the basis of Stoner theory ΔE should vanish at T_c. Measurements on nickel are available from Pierce and Spicer (1970, 1972) and Rowe and Tracy (1971), and for both nickel and iron by Petersson et al. (1976) and Petersson and Erlandsson (1978), and are fully reported by Petersson (1977).

Pierce and Spicer measured the position of the leading peak of the photoelectron energy distribution curve below and above T_c and observe no change within the experimental uncertainty; a theoretical curve was shown to give a shift of about 0.2 eV over the same temperature range which is much greater than this uncertainty. Petersson et al. studied in a similar way both iron and nickel using higher photon energies and again found no shifts of the order expected from an exchange splitting which varies as the (single particle) magnetization. Thus fig. 22 shows their data for the (100) face of Ni above and below T_c. Rowe and Tracy used photon energies close to those where Shiga and Pells (1969) observed

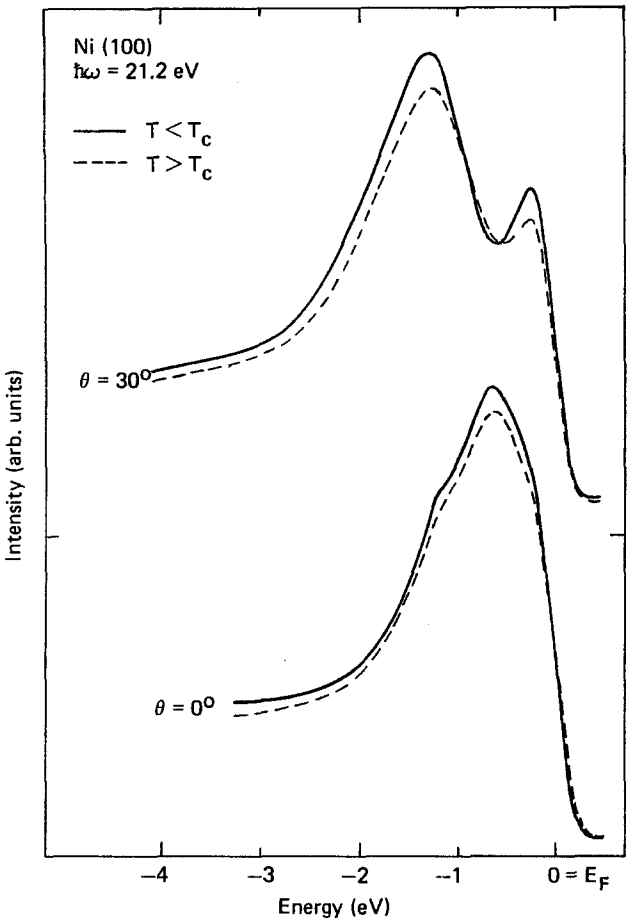

Fig. 22. Angular resolved electron distribution curves of nickel (Petersson 1977).

optical absorption anomalies (see section 3.7), i.e. 4–5 eV. They observed very marked (essentially "critical") changes of the d-band peak and width exactly at T_c, there being no such effect at this temperature for palladium used as a control. This observation has not yet been explained and it is not clear how it bears on the problem of the exchange splitting and its temperature variation.

As a result of these observations Fadley and Wohlfarth (1972) were motivated to ask the question: What changes in the ferromagnetic transition metals at the Curie point? They discuss a wide range of experimental observations for which such changes do, or do not, occur. Where they do not it was suggested that during the process the following may happen to cause the anomaly:

(1) Final state effects related to localized holes in the valence bands or core states.

(2) Life time effects, in that the solid state spectroscopy measurements have a time scale of the order 10^{-14}–10^{-16} s, whereas for the more static measurements

(e.g. of hyperfine fields or of the static magnetization) showing changes at T_c the time scales are much longer.

Clearly, a further possibility of interpreting these data is related to the persistence of magnetism above the Curie temperature which is evidenced by the neutron data discussed in section 2.7. A more satisfactory analysis of these solid state spectroscopy data will require consideration of the whole range of measurements discussed for the three ferromagnetic transition metals in this article. This would lead to an updating of the review of Fadley and Wohlfarth (1972); see Eastman (1979).

4.1.2. X-ray photoemission spectroscopy

The XPS method has been used in particular by Fadley and Shirley (1968, 1970) to give information on the structure of d-bands of transition metals. Despite the improved XPS resolution using the angular resolved technique (Fadley et al. 1976) the UPS data discussed in section 4.1.1 seem, in view of the higher resolution and the higher state of development, to be more relevant when discussing the influence of the Curie point.

4.1.3. Soft X-ray studies

The SXS method is, of course, most widely used to determine band structure. For iron, cobalt and nickel such measurements were reported by Cuthill et al. (1967) and McAlister et al. (1975). There was evidence for considerable structure, some of which could be identified with band calculations. In McAlister et al.'s paper measured and calculated d-band widths were compared. There was good overall agreement for iron and cobalt, but for nickel the lower band width of 3.3 eV reported in section 4.1.1 as coming from the earlier UPS measurements was also seen by SXS. The latter UPS data of Smith et al. (1977) gave a width of 4.3 eV as already reported, and this is in good agreement with the calculated values plotted by McAlister et al. Clearly, SXS should be repeated for nickel.

Measurements of the spectra of Fe on crossing the Curie point have been reported by McAlister et al. (1972) and by Kaihola and Pessa (1978). Unfortunately, these give opposing results in that the Americans find a shift of the bands which can be identified with a temperature dependent exchange splitting while the Finns find that characteristic features of the $M_{2,3}$ and L_3 emission spectra remain unchanged. The latter results would tend to agree with the UPS data reported in section 4.1.1.

4.1.4. Spin polarization of photoelectrons

This technique was pioneered by a Swiss group at ETH Zürich and nothing can detract from their achievement of constructing the sophisticated apparatus to this end. The earlier measurements (Alder et al. 1973, Siegmann 1975) had the polarization of the photoemitted electrons positive and decreasing with increasing energy. This result was in contrast to the prediction of Wohlfarth (1971), later also made by Smith and Traum (1971), that for nickel (and cobalt) the polarization should be negative for energies close to the Fermi energy (where the

majority spin band is full) and should change sign to become positive at an energy about 2Δ above the Fermi energy. Later measurements from the (100) face of a single crystal of nickel (Eib and Alvarado 1976) show precisely this behaviour thus showing that the earlier results arose from the inadequacy of the polycrystalline specimens. Wohlfarth (1977b) (see also Moore and Pendry 1978) deduced from these data a value of $\Delta = 75$ meV, in good agreement with the neutron and optical data discussed in sections 2.7 and 3.7, respectively. As discussed in section 1.4 the fact that this value is much less than that given by the band structure calculations of Callaway and Wang (1977a,b) (about 300 meV for Ni) may or may not be due to the many body effect of electron–magnon interactions. If not, the band calculations themselves may be at fault. Alternatively, Dempsey and Kleinmann (1977) ascribe the single crystal nickel data to the emission of the photoelectrons almost exclusively from the surface layer. This proposal in turn was severely criticized by Edwards (1978), and the problem remains at the centre of interest at the time of writing.

Eib and Reihl (1978) measured the spin polarization of photoelectrons from the (111) face of an iron single crystal, obtaining +60% at threshold. The authors regard this as proof of the applicability of the itinerant model to iron; in fact, it also implies that iron is a weak itinerant ferromagnet, with $\Delta = 0$ (Wohlfarth 1971).

4.1.5. Other related techniques

Two other techniques have been applied to the problem of the emission of electrons from ferromagnets and the relationship of the results to the theory of their magnetism. These are field emission and tunnelling through superconducting layers. Neither of these methods is as useful as the photoemission technique described in section 4.1.4. It was first clearly pointed out by Politzer and Cutler (1970, 1972) (and also stressed by Wohlfarth (1971, 1977b)) that "field emission from... nickel is largely due to the free-electron-like s–p band", and "the free electron (field) transmission coefficient is roughly 1 or 2 orders of magnitude greater than the 3d transmission coefficient". Hence neither of these techniques bears directly on the problems related to the d-band and its exchange splitting, except through the effect of hybridization between these two groups of electrons (Hertz and Aoi 1973). Oddly, there has been no attempt to relate these measurements of the properties of the s–p electrons with the neutron-observed moments given in table 9.

In view of this inadequacy of these two techniques it suffices merely to refer to some papers and point out one unusually interesting outcome of the tunnelling measurements:

Field emission: Gleich et al. (1971), Chobrok et al. (1977), Campagna et al. (1976), Landolt and Campagna (1977), Politzer and Cutler (1970, 1972), and Chazalviel and Yafet (1977).

Tunnelling: Tedrow and Meservey (1973), Paraskevopoulos et al. (1977), and Hertz and Aoi (1973).

The measurements using the tunnelling technique on pure iron, cobalt and nickel (Tedrow et al.) shows a phenomenological correlation between the

observed polarization and the magnetization. Extension to nickel alloys by Paraskevopoulos et al. showed this correlation to be remarkably well preserved. There is at present no theoretical interpretation of this clear-cut result. Perhaps the tunnelled electrons feel a strong field outside the ferromagnet which is proportional to its bulk magnetization.

A final technique was used to measure the electron spin polarization from nickel surfaces by using electron capture by scattered deuterons (Eichner et al. 1978). The observed polarization was found to be experiment and sample dependent and also varied drastically with the crystal face, having a maximum value of +96% from the (110) plane. The authors interpreted these early results on the basis of one-dimensional densities of states, but the technique is only in its infancy.

4.2. The Fermi surface, especially de Haas–Van Alphen technique

The Fermi surface studies on iron, cobalt and nickel have been reviewed by Gold (1974) and Young (1977). The two most widely used techniques are magnetoresistance and de Haas–Van Alphen effect. As far as the present article is concerned, the matters of greatest interest are the exchange splitting and its temperature dependence. Some of the calculated Fermi surfaces of iron, cobalt and nickel are given in figs. 3, 6 and 1, respectively and these are discussed in section 1.2.

For iron Gold et al. (1971) reported extensive de Haas–Van Alphen studies which they were able to analyze satisfactorily using an older band calculation (Wood 1962) rigidly exchange split by 2.0 eV; this value is in reasonable agreement with the entry in table 3. The corresponding Fermi surfaces for the majority and minority spin bands are shown in fig. 23. The minority spin band contains about 3 electrons per atom and its Fermi surface is surprisingly similar

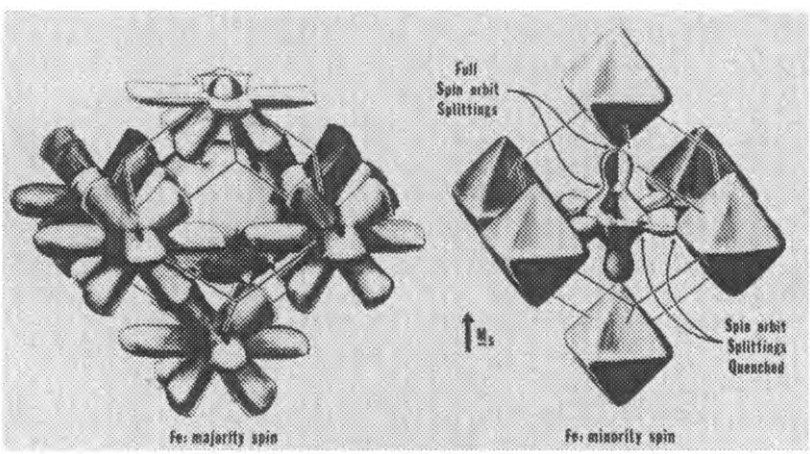

Fig. 23. Fermi surfaces of iron used to interpret de Haas–Van Alphen data (Gold 1974). See also fig. 4.

to that of molybdenum and tungsten containing the same number, implying that rigid splitting is a good approximation. Other de Haas–Van Alphen measurements for iron by Baraff (1973) and magnetoresistance measurements by Coleman et al. (1973) are also discussed in the above reviews where the discussion is too technical to reproduce here. The low temperature dependence of ΔE is discussed below.

For cobalt the Fermi surface was measured and the results analyzed by a band structure calculation of Batallan et al. (1975) who claimed that it gives a better account of their observations than those described in section 1.2. The calculation led to a rigid exchange splitting 1.39 eV, only slightly above the value of table 3; it also gives, incidentally, an energy gap value for this strong itinerant ferromagnet of 14 meV, a value which should be confirmed by independent measurements. The calculated minority spin Fermi surface resembles that of hcp rhenium. The calculated structures give a reasonable account of the de Haas–Van Alphen frequencies, particularly for the neck at the point Γ in the majority spin Fermi surface. Spin–orbit interactions were also taken into account in the calculations and in analyzing the measurements to explain the electron orbits around L in the minority spin band. Other de Haas–Van Alphen measurements on cobalt were reported by Anderson et al. (1973) who found that Ishida's band calculation (1972), described in section 1.2, was unable to account for the observations.

For nickel de Haas–Van Alphen and other measurements have frequently been reported. Tsui (1967) was able to make observations on the copper-like necks of the majority spin band, and Fawcett and Reed (1962) obtained evidence on these necks from magnetoresistance measurements. A minority spin hole pocket associated with the level X_5 was investigated by Tsui (1967) and Hodges et al. (1967). The discussion involves consideration of spin–orbit coupling effect as is the case for the other two metals (see fig. 23). This problem was considered by Zornberg (1970) and Ruvalds and Falicov (1968). Stark (see Gold 1974, Wang and Callaway 1974) observed de Haas–Van Alphen oscillations arising from large central orbits of the majority and minority bands which led him to postulate a rigid exchange splitting of the d-bands. The band calculation of Zornberg (1970) also gave good agreement with many observations of the Fermi surface of nickel, the rigid exchange splitting being here 0.4–0.6 eV. These values are less than or equal to that given in table 3. Other Fermi surface studies and the relationship to band calculations are discussed for iron and nickel by Callaway and Wang (1977a). Cyclotron resonance experiments by Goy and Grimes (1973) were discussed by Wang and Callaway (1974).

The temperature dependence of the exchange splitting of iron was measured in a remarkable study by Lonzarich and Gold (1974) over the temperature range 1–4.2 K. Specifically, the minority spin lens sheets of the Fermi surface (see fig. 23) were investigated, and the variation of the de Haas–Van Alphen frequency over this temperature range was found to be less than the resolution of the experiment, one part in 10^5. If the exchange splitting was proportional to the *total* magnetization then a change of one part in 10^4 would be expected.

Edwards (1974) showed that, while the change of the total magnetization δM is given by

$$\delta M = \delta M_{SP} + \delta M_{SW} \tag{40}$$

coming from single particle and spin wave excitations, the change of the exchange splitting ΔE is given by

$$\frac{\delta(\Delta E)}{\Delta E} = \frac{1}{M_0}\left[\alpha \delta M_{SP} + \beta \frac{kT}{\Delta E} \delta M_{SW}\right] \tag{41}$$

where α and β are ~ 1. Hence at low temperatures the exchange splitting depends almost entirely on the change of the single particle magnetization which was discussed in section 2.1 and which may well be small enough to agree with the observations.

4.3. Miscellaneous techniques

4.3.1. Plasma losses, work function

The review of Fadley and Wohlfarth (1972) was concerned with a number of physical properties of the ferromagnetic transition metals which do, or do not vary, at the Curie temperature. Among these the characteristic plasma losses are relevant and Heimann and Hölzl (1971) have claimed that for the (111) face of nickel the volume loss energy shows an anomalous change at T_c of the order of ΔE. On the other hand, the temperature dependence of the work function of this metal (Christmann et al. 1974) shows no anomaly at all at the Curie point. These and other related findings discussed earlier by Fadley and Wohlfarth (1972) can not yet be regarded as having been explained satisfactorily; they should continue to be regarded as having a close relationship to the results of solid state spectroscopy discussed in section 4.1.

4.3.2. Compton profile

Measurements of the Compton profile of transition metals give information on the momentum distribution and the wave functions. They are thus a valuable supplement to theoretical and experimental band structure determinations. Such measurements for iron were reported by Phillips and Weiss (1972) and for nickel by Eisenberger and Reed (1974). The results were analyzed in relation to band calculations by Rath et al. (1973) and Wang and Callaway (1975). Sakai and Ono (1977) were able to measure the momentum distribution of the magnetic electrons in iron and observed a negative conduction electron polarization as also given by the neutron scattering experiments summarized in table 9.

4.3.3. Positron annihilation

This technique enables Fermi surfaces and momentum distributions to be measured and is thus complementary to the studies of sections 4.2 and 4.3.2. For iron Mijnarends (1973) obtained detailed information on both properties. His data were in good agreement with calculations based on the band structure of

Wood (1962). He also claims that there is no need to invoke a negative polarization of the conduction electrons, contrary to the data of Sakai and Ono (1977) and those given in table 9.

Spin distribution studies in ferromagnetic metals by polarized positron annihilation experiments were also reported by Berko and Mills (1971). For cobalt Szuszkiewicz et al. (1976) have obtained only preliminary data which they are unable to relate to a Fermi surface. For nickel Kontrym-Sznajd et al. (1975) again report only preliminary data. One striking result is the claim that in the 5th zone an electron regrouping is visible at the Curie point. This finding would be sensational if confirmed.

Acknowledgements

I am grateful to D.M. Edwards and D.M. Newns for their valuable advice.

References

Adachi, K. and T. Aisaka, 1973, Proc. Conf. Liquid Metals, Tokyo, p. 313.

Ahlers, G. and A. Kornblit, 1975, Phys. Rev. **B12**, 1938.

Alder, H., M. Campagna and H.C. Siegmann, 1973, Phys. Rev. **B8**, 2075.

Aldred, A.T., 1975, Phys. Rev. **B11**, 2597.

Aldred, A.T. and P.H. Froehle, 1972, Intern. J. Mag. **2**, 195.

Alers, G.A., J.R. Neighbours and H. Sato, 1960, J. Phys. Chem. Solids, **13**, 40.

Amighian, J. and W.D. Corner, 1976, J. Phys. **F6**, L309.

Andersen, O.K., J. Madsen, U.K. Poulsen, O. Jepsen and J. Kollar, 1977, Physica **B86–88**, 249.

Anderson, D.H., 1966, Solid State Comm. **4**, 189.

Anderson, J.R., J.J. Hudak and D.R. Stone, 1973, A.I.P. Conf. Procs. **10**, 46.

Anon., 1961, Nickel-containing magnetic materials, International Nickel Publ. no. 2144.

Arajs, S. and R.V. Colvin, 1963, J. Phys. Chem. Solids **24**, 1233.

Arajs, S. and R.V. Colvin, 1964a, J. Appl. Phys. **35**, 2424.

Arajs, S. and R.V. Colvin, 1964b, Phys. Stat. Sol. **6**, 797.

Aubert, G., 1968, J. Appl. Phys. **39**, 504.

Aubert, G., et al., 1976, Phys. Rev. **B14**, 5314.

Barmatz, M., P.C. Hohenberg and A. Kornblit, 1975, Phys. Rev. **B12**, 1947.

Barnier, Y., R. Pauthenet and G. Rimet, 1961a, C. R. Acad. Sci., Paris, **252**, 2839.

Barnier, Y., R. Pauthenet and G. Rimet, 1961b, C. R. Acad. Sci., Paris, **253**, 400.

Barraff, D.R., 1973, Phys. Rev. **B8**, 3439.

Batallan, F., I. Rosenman and C.B. Sommers, 1975, Phys. Rev. **B11**, 545.

Becker, R. and W. Döring, 1939, Ferromagnetismus (Springer, Berlin).

Bennett, A.J. and B.R. Cooper, 1971, Phys. Rev. **B3**, 1642.

Berko, S. and A.P. Mills, 1971, J. de Phys. **32-C1**, 287.

Birss, R.R., G.J. Keeler and C.H. Sheppard, 1977, Physica **B86–88**, 257.

Bower, D.I., 1971, Proc. Roy. Soc. **A326**, 87.

Bozorth, R.M., 1951, Ferromagnetism (Van Nostrand, Princeton).

Bozorth, R.M., 1954, Phys. Rev. **96**, 311.

Bradbury, D.A.J. and D.M. Edwards, 1969, Phys. Lett. **30A**, 301.

Braun, M., 1964, Thesis, Cologne.

Braun, M. and R. Kohlhaas, 1965, Phys. Stat. Sol. **12**, 429.

Braun, M., R. Kohlhaas and O. Vollmer, 1968, Z. Angew. Phys. **25**, 365.

Briane, M., 1973, C. R. Acad. Sci. Paris **276**, 139; **277**, 695.

Callaway, J. and C.S. Wang, 1977a, Physica **B91**, 337.
Callaway, J. and C.S. Wang, 1977b, Phys. Rev. **B16**, 2095.
Callen, H.B. and E.R. Callen, 1963, Phys. Rev. **129**, 578; **132**, 991.
Campagna, M., T. Utsumi and D.N.E. Buchanan, 1976, J. Vac. Sci. Technol. **13**, 193.
Capellmann, H., 1979, Z. Phys. **34**, 29.
Carr, W.J., 1966, Handbuch der Physik **18/2**, 274.
Celasco, M. and M. Corrias, 1976, Nuovo Cimento **33B**, 807.
Chazalviel, J.N. and Y. Yafet, 1977, Phys. Rev. **B15**, 1062.
Chobrok, G., M. Hoffmann, G. Regenfus and R. Sizmann, 1977, Phys. Rev. **B15**, 429.
Christmann, K., G. Ertl and O. Schober, 1974, Z. Naturforsch, **29a**, 1516.
Cohen, G., B. Giovannini and D. Sorg, 1973, L'effet Hall extraordinaire (Univ. Geneva).
Coleman, R.V., R.C. Morris and D.J. Sellmyer, 1973, Phys. Rev. **B8**, 317.
Collins, J.G. and G.K. White, 1964, Progr. Low Temp. Phys. **4**, 450.
Collins, M.F., V.J. Minkiewicz, R. Nathans, L. Passell and G. Shirane, 1969, Phys. Rev. **179**, 417.
Colvin, R.V. and S. Arajs, 1965, J. Phys. Chem. Solids, **26**, 435.
Connelly, D.L., J.S. Loomis and D.E. Mapother, 1971, Phys. Rev. **B3**, 924.
Cooke, J.F., 1973, Phys. Rev. **B7**, 1108.
Cooke, J.F. and H.L. Davies, 1973, A.I.P. Conf. Procs. **10**, 1218.
Cooke, J.F., J.W. Lynn and H.L. Davies, 1975, A.I.P. Conf. Procs. **24**, 329.
Cottam, M.G. and R.B. Stinchcombe, 1968, J. Phys. **C1**, 1052.
Cuthill, J.R., A.J. McAlister, M.L. Williams and R.E. Watson, 1967, Phys. Rev. **164**, 1006.
Dalton, N.W., 1970, J. Phys. **C3**, 1912.
Danan, H., A. Herr and A.J.P. Meyer, 1968, J. Appl. Phys. **39**, 669.
de Chatel, P.F. and E.P. Wohlfarth, 1973, Comments Sol. State Phys. **5**, 133.
Dempsey, D.G. and L. Kleinmann, 1977, Phys. Rev. Lett. **39**, 1297.
de Vallera, A.M.B.G., 1978, Thesis, Cambridge.
Dever, D.J., 1972, J. Appl. Phys. **43**, 3293.
Dheer, P.N., 1967, Phys. Rev. **156**, 637.
Dietz, E., U. Gerhardt and C.J. Maetz, 1978, Phys. Rev. Lett. **40**, 892.
Dixon, M., F.E. Hoare, T.M. Holden and D.E. Moody, 1965, Proc. Roy. Soc. **A285**, 561.
Doniach, S. and S. Engelsberg, 1966, Phys. Rev. Lett. **17**, 750.
Doniach, S. and E.P. Wohlfarth, 1967, Proc. Roy. Soc. **A296**, 442.
Duff, K.J. and T.P. Das, 1971, Phys. Rev. **B3**, 2294.
du Plessis, P. de V., 1971, J. Phys. Chem. Solids **32**, 1691.
du Plessis, P. de V., P.E. Viljoen and L. Alberts, 1971, J. Phys. **F1**, 328.
du Trémolet de Lacheisserie, E., 1970, Ann. Phys. Paris **5**, 267.
Dzyaloshinsky, I.E. and P.S. Kondratenko, 1976, J.E.T.P. **70**, 1987.
Eastman, D.E., 1972, Electron spectroscopy (North-Holland, Amsterdam) p. 487.
Eastman, D.E., 1979, Proc. ICM Munich, J. Mag. Mag. Mat., to be published.
Eastman, D.E., F.J. Himpsel and J.A. Knapp, 1978, Phys. Rev. Lett. **40**, 1514.
Edwards, D.M., 1967, Proc. Roy. Soc. **A300**, 373.
Edwards, D.M., 1970, Phys. Lett. **33A**, 183.
Edwards, D.M., 1974, Can. J. Phys. **52**, 704.
Edwards, D.M., 1976a, J. Phys. **F6**, L185.
Edwards, D.M., 1976b, J. Phys. **F6**, L289.
Edwards, D.M., 1977, Physica **B91**, 3.
Edwards, D.M., 1978, Proc. Toronto Conf., Inst. P. Conf. Procs. **39**.
Edwards, D.M. and J.A. Hertz, 1973, J. Phys. **F3**, 2191.
Edwards, D.M. and E.P. Wohlfarth, 1968, Proc. Roy. Soc. **A303**, 127.
Eib, W. and S.F. Alvarado, 1976, Phys. Rev. Lett. **37**, 444.
Eib, W. and B. Reihl, 1978, Phys. Rev. Lett. **40**, 1674.
Eichner, S., C. Rau and R. Sizmann, 1978, Proc. Toronto Conf., Inst. P. conf. Procs. **39**.
Eisenberger, P. and W.A. Reed, 1974, Phys. Rev. **B9**, 3237.
Escudier, P., 1973, Thesis, Grenoble.
Fadley, C.S. and D.A. Shirley, 1968, Phys. Rev. Lett. **21**, 980.
Fadley, C.S. and D.A. Shirley, 1970, Phys. Rev. **A2**, 1109.
Fadley, C.S. and D.A. Shirley, 1971, Electronic

density of states, N.B.S. Special Publ. **323**, 163.
Fadley, C.S. and E.P. Wohlfarth, 1972, Comments Sol. State Phys. **4**, 48.
Fadley, C.S., R.J. Baird, L.F. Wagner and Z. Hussain, 1976, Proc. Noordwijk Photoemission Symp. p. 201.
Fawcett, E. and W.A. Reed, 1962, Phys. Rev. Lett. **9**, 336.
Fawcett, E. and G.K. White, 1968, Solid State Comm. **6**, 509.
Fekete, D., A. Grayovsky, D. Shaltiel, U. Goebel, E. Dormann and N. Kaplan, 1976, Phys. Rev. Lett. **36**, 1566.
Feldmann, D., H.R. Kirchmayr, A. Schmolz and M. Velicescu, 1971, I.E.E.E. Trans. Magnetics **7**, 61.
Fisher, M.E. and J.S. Langer, 1968, Phys. Rev. Lett. **20**, 665.
Fivaz, R.C., 1968, J. Appl. Phys. **39**, 1278.
Fletcher, G.C., 1954, Proc. Phys. Soc. **67**, 505.
Fletcher, G.C., 1955, Proc. Phys. Soc. **68**, 1066.
Fletcher, G.C., 1961, Proc. Phys. Soc. **78**, 145.
Fletcher, G.C. and R.P. Addis, 1974, J. Phys. **F4**, 1951.
Fletcher, G.C. and E.P. Wohlfarth, 1962, J. Phys. Soc. Japan **17**, B-1, 36.
Franse, J.J.M., 1969, Thesis, Amsterdam.
Franse, J.J.M. and N. Buis, 1970, Colloq. Int. C.N.R.S. **188**, 371.
Franse, J.J.M. and G. de Vries, 1968, Physica, **39**, 477.
Franse, J.J.M. and M. Stolp, 1970, Phys. Lett. **32A**, 316.
Franse, J.J.M., G. de Vries and T.F.M. Kortekaas, 1974, Proc. I.C.M. Moscow **3**, 84.
Friedel, J. and C.M. Sayers, 1978, J. Physique **39**, L-59.
Furey, W.N., 1967, Thesis, Harvard.
Gale, S.J. et al., 1978, Proc. Toronto Conf. Inst. P. Conf. Procs. **39**.
George, P.K. and E.D. Thompson, 1970, Intern. J. Mag. **1**, 35.
Gersdorf, R., 1961, Thesis, Amsterdam.
Gersdorf, R., 1962, J. Phys. Radium **23**, 726.
Gersdorf, R., 1978, Phys. Rev. Lett. **40**, 344.
Gersdorf, R. and G. Aubert, 1978, Physica **95B**, 135.
Gleich, W., G. Regenfus and R. Sizmann, 1971, Phys. Rev. Lett. **27**, 1066.
Glinka, C.J., V.J. Minkiewicz and L. Passell, 1977, Phys. Rev. **B16**, 4084.
Gold, A.V., 1974, J. Low Temp. Phys. **16**, 3.
Gold, A.V., L. Hodges, P.T. Panousis and D.R. Stone, 1971, Int. J. Mag. **2**, 357.
Goy, P. and C.C. Grimes, 1973, Phys. Rev. **B7**, 299.
Graham, C.D., 1958, Phys. Rev. **112**, 1117.
Grimvall, G., 1975, Physica Scripta, **12**, 173.
Grimvall, G., 1976, Physica Scripta **14**, 63; **13**, 59.
Gumbs, C. and A. Griffin, 1976, Phys. Rev. **B13**, 5054.
Gunnarson, O., 1976, J. Phys. **F6**, 587.
Gunnarson, O., 1977, Physica **B91**, 329.
Hasegawa, A., S. Wakoh and J. Yamashita, 1965, J. Phys. Soc. Japan **20**, 1865.
Hatta, S. and S. Chikazumi, 1976, J. Phys. Soc. Japan **40**, 52.
Hatta, S. and S. Chikazumi, 1977, J. Phys. Soc. Japan, **43**, 822.
Hausch, G., 1977, J. Phys. **F7**, L127.
Hausmann, K., 1970, Phys. Stat. Sol. **38**, 809.
Hausmann, K. and M. Wolf, 1971, J. Physique **32**, C-1, 539.
Heimann, B. and J. Hölzl, 1971, Phys. Rev. Lett. **26**, 1573.
Heimann, P. and H. Neddermeyer, 1976, J. Phys. **F6**, L257.
Heimann, P. and H. Neddermeyer, 1978, Phys. Rev. **B18**, 3537.
Heimann, P., E. Marschall, H. Neddermeyer, M. Pessa and H.F. Roloff, 1977, Phys. Rev. **B16**, 2575.
Heine, V., 1967, Phys. Rev. **153**, 673.
Herring, C., 1966, Magnetism 4 (G.T. Rado and H. Suhl, eds.) (Academic Press, New York).
Hertz, J.A. and K. Aoi, 1973, Phys. Rev. **B8**, 3252.
Himpsel, F.J., J.A. Knaap and D.E. Eastman, 1979, Phys. Rev. **B19**, 2919.
Ho, J.T., 1971, Phys. Rev. Lett. **26**, 1485.
Hodges, L., D.R. Stone and A.V. Gold, 1967, Phys. Rev. Lett. **19**, 655.
Hölscher, H. and J.J.M. Franse, 1979, J. Phys. F., to be published.
Honda, K. and H. Masumoto, 1931, Sci. Rep. Tohoku Univ. **20**, 322.
Hubbard, J., 1963, Proc. Roy. Soc. **A276**, 238.
Hubbard, J., 1964a, Proc. Phys. Soc. **84**, 455.
Hubbard, J., 1964b, Proc. Roy. Soc. **A277**, 237.
Hubert, A., W. Unger and J. Kranz, 1969, Z. Phys. **224**, 148.
Huguenin, R. and D. Rivier, 1965, Helv. Phys. Acta **38**, 900.
Hunt, K.L., 1953, Proc. Roy. Soc. **A216**, 103.

Hurd, C.M., 1972, The Hall effect in metals and alloys (Plenum, New York).
Hurd, C.M., 1974, Adv. Phys. **23**, 315.
Irkhin, Y.P., A.N. Voloshinsky and S.S. Abelsky, 1967, Phys. Stat. Sol. **22**, 309.
Ishida, S., 1972, J. Phys. Soc. Japan **33**, 369.
Jacobs, R.L. and N. Zaman, 1976, private communication.
Janak, J.F. and A.R. Williams, 1976, Phys. Rev. **B14**, 4199.
Jones, R.W., G.S. Knapp and R. Maglic, 1974, Int. J. Magnetism, **6**, 63.
Kadomatsu, H., E. Tatsumoto, H. Fujii and T. Okamoto, 1971, J. Phys. Soc. Japan **31**, 1403.
Kaihola, L. and M. Pessa, 1978, unpublished.
Kanamori, J., 1963, Progr. Theor. Phys. **30**, 275.
Karplus, J. and J.M. Luttinger, 1954, Phys. Rev. **95**, 1154.
Kawai, N. and A. Sawaoka, 1968, J. Phys. Chem. Solids **29**, 575.
Kevan, S.D., P.S. Wehner, and D.A. Shirley, 1978, Solid State Comm. **28**, 517.
Kierspe, W., R. Kohlhaas and H. Gonska, 1967, Z. Angew. Phys. **24**, 28.
Kneller, E., 1962, Ferromagnetismus (Springer, Berlin).
Kohlhaas, R., P. Dünner and N. Schmitz-Pranghe, 1967, Z. Angew. Phys. **23**, 245.
Kollie, T.G., 1977, Phys. Rev. **B16**, 4872.
Kondorsky, E.I., 1969, Soviet Physics J.E.T.P. **28**, 291.
Kondorsky, E.I., 1974, I.E.E.E. Trans. Magnetics **10**, 132.
Kondorsky, E.I. and E. Straube, 1973, Soviet Physics J.E.T.P. **36**, 188.
Konti, A. and Y.P. Varshni, 1969, Can. J. Phys. **47**, 2022.
Kontrym-Sznajd, G., H. Stachowiak, W. Wierzchowski, K. Petersson, N. Thrane and G. Trumpy, 1975, Appl. Phys. **8**, 151.
Korenman, V., J.L. Murray and R.E. Prange, 1977, Phys. Rev. **B16**, 4048.
Korn, J. and R. Kohlhaas, 1969, Z. Angew. Phys. **26**, 119.
Kouvel, J.S. and J.B. Comly, 1968, Phys. Rev. Lett. **20**, 1237.
Kouvel, J.S. and C.C. Hartelius, 1960, J. Appl. Phys. **35**, 940.
Kraftmakher, Y.A. and T.Y. Romashina, 1966, Soviet Phys. Sol. State **8**, 1562.
Landolt-Börnstein, 1962, **2**, 9/1.
Landolt, M. and M. Campagna, 1977, Phys. Rev. Lett. **38**, 663.
Landolt, M., Y. Yafet, B. Wilkens and M. Campagna, 1978, Sol. State Comm. **25**, 1141.
Lang, N.D. and H. Ehrenreich, 1968, Phys. Rev. **168**, 605.
Lee, E.W. and M.A. Asgar, 1971, Proc. Roy. Soc. **A326**, 73.
Leese, J. and A.E. Lord, 1968, J. Appl. Phys. **39**, 3986.
Leger, J.M., C. Loriers-Susse and B. Vodar, 1972, Phys. Rev. **B6**, 4250.
Lonzarich, G. and A.V. Gold, 1974, Can. J. Phys. **52**, 694.
Lowde, R.D. and C.G. Windsor, 1970, Adv. Phys. **19**, 813.
Lynch, D.W., R. Rosei and J.H. Weaver, 1971, Solid State Comm. **9**, 2195.
Lynn, J.W., 1975, Phys. Rev. **B11**, 2624.
McAlister, A.J., J.R. Cuthill, R.C. Dobbyn, M.L. Williams and R.E. Watson, 1972, Phys. Rev. Lett. **29**, 179.
McAlister, A.J., J.R. Cuthill, R.C. Dobbyn, M.L. Williams and R.E. Watson, 1975, Phys. Rev. **B12**, 2973.
MacInnes, W.M. and R. Huguenin, 1973, Phys. Lett. **44A**, 51.
Madsen, J., O.K. Andersen, U.K. Poulsen and O. Jepsen, 1975, A.I.P. Conf. Procs. **29**, 327.
Marschall, E. and H. Bross, 1978, Physica Stat. Sol. b, **90**, 241.
Mathon, J., 1972, J. Phys. **F2**, 159.
Mathon, J. and E.P. Wohlfarth, 1968, Proc. Roy. Soc. **A302**, 409.
Mathon, J. and E.P. Wohlfarth, 1969, J. Phys. **C2**, 1647.
Meyer, A.J.P. and G. Asch, 1961, J. Appl. Phys. **32**, 330S.
Mijnarends, P.E., 1973, Physica **63**, 235.
Minkiewicz, V.J., M.F. Collins, R. Nathans and G. Shirane, 1969, Phys. Rev. **182**, 624.
Mook, H.A., 1966, Phys. Rev. **148**, 495.
Mook, H.A., 1978, Proc. Toronto Conf. Inst. P. Conf. Procs. **39**.
Mook, H.A. and R.M. Nicklow, 1973, Phys. Rev. **B7**, 336.
Mook, H.A., J.W. Lynn and R.M. Nicklow, 1973, Phys. Rev. Lett, **30**, 556.
Moon, R.M., 1964, Phys. Rev. **136**, A195.
Moore, I.D. and J.B. Pendry, 1978, J. Phys. **C11**, 4615.
Mori, N., 1969, J. Phys. Soc. Japan, **27**, 307.
Mori, N., 1971, J. Phys. Soc. Japan **31**, 359.
Mori, N., Y. Fukuda and T. Ukai, 1974a, J. Phys. Soc. Japan **37**, 1263.

Mori, N., T. Ukai and H. Yoshida, 1974b, J. Phys. Soc. Japan **37**, 1272.
Moriya, T., 1977a, Physica **B86–88**, 356.
Moriya, T., 1977b, Physica **B91**, 235.
Moriya, T. and A. Kawabata, 1973a, J. Phys. Soc. Japan **34**, 639.
Moriya, T. and A. Kawabata, 1973b, J. Phys. Soc. Japan **35**, 669.
Moriya, T. and A. Kawabata, 1973c, Proc. I.C.M. Moscow **4**, 5.
Müller, M., 1978, Thesis, Basel.
Myers, H.P. and W. Sucksmith, 1951, Proc. Roy. Soc. **A207**, 427.
Nakagawa, Y., 1956, J. Phys. Soc. Japan **11**, 855.
Noakes, J.E. and A. Arrott, 1973, A.I.P. Conf. Procs. **10**, 899.
Papp, E., G. Szabó and G. Tichy, 1977, Solid State Comm. **21**, 487.
Paraskevapoulos, D., R. Meservey and P.M. Tedrow, 1977, Phys. Rev. **B16**, 4907.
Pessa, M., P. Heimann and H. Neddermeyer, 1976, Phys. Rev. **B14**, 3488.
Petersson, L.G., 1977, Thesis, Linköping.
Petersson, L.G. and R. Erlandsson, 1978, Phys. Rev. **B17**, 3006.
Petersson, L.G., R. Melander, D.P. Spears and S.B.M. Hagström, 1976, Phys. Rev. **B14**, 4177.
Pettifor, D.G. and D.M. Roy, 1978, Solid State Comm. **27**, 677.
Phillips, W.C. and R.J. Weiss, 1972, Phys. Rev. **B6**, 4213.
Pierce, D.T. and W.E. Spicer, 1970, Phys. Rev. Lett. **25**, 581.
Pierce, D.T. and W.E. Spicer, 1972, Phys. Rev. **B6**, 1787.
Place, C.M. and P. Rhodes, 1971, Phys. Stat. Sol. (b) **47**, 475.
Politzer, B.A. and P.H. Cutler, 1970, Surface Sci. **22**, 277.
Politzer, B.A. and P.H. Cutler, 1972, Phys. Rev. Lett. **28**, 1330.
Ponomarev, B.K. and V.G. Thyssen, 1977, Soviet Phys. J.E.T.P. **46**, 173.
Radakrishna, P. and M. Nielsen, 1965, Phys. Stat. Sol. **11**, 111.
Ramakrishnan, T.V., 1974, Phys. Rev. **B10**, 4014.
Rath, J., C.S. Wang, R.A. Tawil and J. Callaway, 1973, Phys. Rev. **B8**, 5139.
Rebouillat, J.P., 1972, Thesis, Grenoble.
Reck, R.A. and D.L. Fry, 1969, Phys. Rev. **184**, 492.
Rhodes, P. and E.P. Wohlfarth, 1963, Proc. Roy. Soc. **A273**, 247.
Richter, F. and R. Kohlhaas, 1964, Z. Naturforsch. **19a**, 1632.
Riedi, P.C., 1973, Phys. Rev. **B8**, 5243.
Riedi, P.C., 1977, Phys. Rev. **B15**, 5197.
Riedinger, R. and M. Nauciel-Bloch, 1975, J. Phys. **F5**, 732.
Rocker, W. and H.W. Schöpgens, 1969, Z. Angew. Phys. **28**, 1.
Rocker, W., R. Kohlhaas and H.W. Schöpgens, 1971, J. Physique **32**, C1, 652; Z. Angew. Phys. **32**, 164.
Rodbell, D.S., 1965, Physica **1**, 279.
Roesler, M., 1964, Phys. Stat. Sol. **7**, K75.
Rowe J.E. and J.C. Tracy, 1971, Phys. Rev. Lett. **27**, 799.
Ruvalds, J. and L.M. Falicov, 1968, Phys. Rev. **172**, 508.
Sakai, N. and K. Ono, 1977, J. Phys. Chem. Solids **42**, 770.
Sakoh, M. and D.M. Edwards, 1975, Phys. Stat. Sol. (b) **70**, 611.
Sakoh, M. and M. Shimizu, 1977, Phys. Stat. Sol. (a) **44**, 511.
Sato, H. and B.S. Chandrasekhar, 1957, J. Phys. Chem. Solids **1**, 228.
Sawaoka, A., 1970, Colloq. Int. C.N.R.S. **188**, 379.
Schröder, K. and A. Giannuzzi, 1969, Phys. Stat. Sol. **34**, K133.
Scott, G.G., 1962, Rev. Mod. Phys. **34**, 102.
Scott, G.G., 1966, Phys. Rev. **148**, 525.
Scott, G.G. and H.W. Sturner, 1969, Phys. Rev. **184**, 490.
Seydel, U. and W. Fucke, 1977, Z. Naturforsch. **32a**, 994.
Shacklette, L.W., 1974, Phys. Rev. **B9**, 3789.
Shacklette, L.W., 1977, unpublished.
Shiga, M. and G.P. Pells, 1969, J. Phys. **C2**, 1847.
Shimizu, M., 1974, Phys. Lett. **50A**, 93.
Shimizu, M., 1977, Physica **B91**, 14.
Shimizu, M., 1978, J. Phys. Soc. Japan **45**, 1520.
Shimizu, M., A. Katsuki and H. Yamada, 1965, J. Phys. Soc. Japan **20**, 396.
Shirane, G., V.J. Minkiewicz, R. Nathans, 1968, J. Appl. Phys. **39**, 383.
Shull, C.G. and Y. Yamada, 1962, J. Phys. Soc. Japan, **17**, B-III 1.
Siegmann, H.C., 1975, Phys. Rep. **17C**, 37.
Sievert, J.D. and V. Zehler, 1970, Z. Angew. Phys. **30**, 251.

Singh, M., J. Callaway and C.S. Wang, 1976, Phys. Rev. **B14**, 1214.
Slonczewski, J.C., 1962, J. Phys. Soc. Japan **17**, B-I, 34.
Smit, J., 1955, Physica **21**, 877.
Smit, J., 1959, J. Phys. Radium **20**, 362.
Smith, N.V. and M.M. Traum, 1971, Phys. Rev. Lett. **27**, 1388.
Smith, R.J., J. Anderson, J. Hermanson and G.J. Lepeyre, 1977, Solid State Comm. **21**, 459.
Stanley, H.E., 1971, Phase transitions and critical phenomena (Oxford University Press, Oxford).
Stoelinga, J.H.M., 1967, Thesis, Amsterdam.
Stoelinga, J.H.M., R. Gersdorf and G. de Vries, 1965, Physica **31**, 349.
Stoll, M.P., 1972, Phys. Lett. **38A**, 260.
Stoner, E.C., 1936, Phil. Trans. Roy. Soc. **A235**, 165.
Stoner, E.C., 1938, Proc. Roy. Soc. **A165**, 372.
Stoner, E.C., 1939, Proc. Roy. Soc. **A169**, 339.
Stringfellow, M.W., 1968, J. Phys. **C1**, 950.
Sucksmith, W. and J.E. Thompson, 1954, Proc. Roy. Soc. **A225**, 362.
Szuszkiewicz, S., B. Rosenfeld and G. Kontrym-Sznajd, 1976, Acta. Phys. Polon. **A50**, 719.
Takayama, H., K. Bohnen and P. Fulde, 1976, Phys. Rev. **B14**, 2287.
Tange, H. and T. Tokunaga, 1969, J. Phys. Soc. Japan, **27**, 554.
Tatsumoto, E., H. Fujiwara, H. Tange and T. Hirooka, 1963, J. Phys. Soc. Japan **18**, 1348.
Tatsumoto, E., H. Fujiwara, H. Tange and Y. Kato, 1962, Phys. Rev. **128**, 2179.
Tedrow, P.M. and R. Meservey, 1973, Phys. Rev. **B7**, 318.
Thompson, E.D. and H.A. Mook, 1970, J. Appl. Phys. **41**, 1227.
Thompson, E.D. and J.J. Myers, 1967, Phys. Rev. **153**, 574.
Thompson, E.D., E.P. Wohlfarth and A.C. Bryan, 1964, Proc. Phys. Soc. **83**, 59.
Tsui, D.C., 1967, Phys. Rev. **164**, 669.
Turtle, R.R. and R.J. Liefeld, 1973, Phys. Rev. **B7**, 3411.
Volkenstein, N.V. and G.V. Fedorov, 1960, Soviet Phys. J.E.T.P. **11**, 48.
Vollmer, O., R. Kohlhaas and M. Braun, 1966, Z. Naturforsch. **21a**, 181.
Wakoh, S., 1971, J. Phys. Soc. Japan, **30**, 1968.
Wakoh, S. and J. Yamashita, 1966, J. Phys. Soc. Japan **21**, 1712.
Wakoh, S. and J. Yamashita, 1970, J. Phys. Soc. Japan **28**, 115.
Wang, C.S. and J. Callaway, 1974, Phys. Rev. **B9**, 4897.
Wang, C.S. and J. Callaway, 1975, Phys. Rev. **B11**, 2417.
Wang, C.S. and J. Callaway, 1976, Solid State Comm. **20**, 255.
Wang, C.S. and J. Callaway, 1977, Phys. Rev. **B15**, 298.
Wanner, R., 1970, Can. J. Phys. **48**, 1270.
Weiss, P. and R. Forrer, 1926, Ann. Phys. Paris **5**, 153.
White, G.K. and S.B. Woods, 1959, Phil. Trans. Roy. Soc. **A251**, 273.
Williams, G.M. and A.S. Pavlovic, 1968, J. Appl. Phys. **39**, 571.
Williams, P.M., P. Butcher, J. Wood and K. Jacobi, 1978, unpublished.
Williamson, D.L., S. Buckshpan and R. Ingalls, 1972, Phys. Rev. **B6**, 4194.
Windsor, C.G., 1977, Physica **B91**, 119.
Wohlfarth, E.P., 1949, Phil. Mag. **40**, 1095.
Wohlfarth, E.P., 1951, Phil. Mag. **42**, 374.
Wohlfarth, E.P., 1953, Rev. Mod. Phys. **25**, 211.
Wohlfarth, E.P., 1962, Phys. Lett. **3**, 17.
Wohlfarth, E.P., 1965, Proc. I.C.M. Nottingham 51.
Wohlfarth, E.P., 1966, Quantum theory of atoms, molecules and the solid state (Academic Press, New York) p. 485.
Wohlfarth, E.P., 1968, J. Phys. **C2**, 68.
Wohlfarth, E.P., 1970, J. Appl. Phys. **41**, 1205.
Wohlfarth, E.P., 1971, Phys. Lett. **36A**, 131.
Wohlfarth, E.P., 1974, Comments on Solid State Phys. **6**, 123.
Wohlfarth, E.P., 1976, J. Phys. **F6**, L59.
Wohlfarth, E.P., 1977a, Physica **B91**, 305.
Wohlfarth, E.P., 1977b, Phys. Rev. Lett. **38**, 524.
Wohlfarth, E.P., 1978a, J. Mag. Mag. Mats. **7**, 113.
Wohlfarth, E.P., 1978b, I.E.E.E. Trans. Magnetics **14**, 933.
Wong, K.C., E.P. Wohlfarth and D.M. Hum, 1969, Phys. Lett. **29A**, 452.
Wood, J.H., 1962, Phys. Rev. **126**, 517.
Yamada, H., 1974, J. Phys. **F4**, 1819.
Yamamoto, M. and S. Taniguchi, 1955, Sci. Rep. Tohoku Univ. **7**, 35.
Young, R.C., 1977, Rep. Prog. Phys. **40**, 1123.
Zornberg, E.I., 1970, Phys. Rev. **B1**, 244.
Zumsteg, F.C. and R.D. Parks, 1970, Phys. Rev. Lett. **24**, 520.

chapter 2

DILUTE TRANSITION METAL ALLOYS; SPIN GLASSES*

J.A. MYDOSH AND G.J. NIEUWENHUYS

Kamerlingh Onnes Laboratorium
Rijksuniversiteit Leiden
Netherlands

*This work was supported in part by the Nederlandse Stichting voor Fundamenteel Onderzoek der Materie (FOM-TNO).

Ferromagnetic Materials, Vol. 1
Edited by E.P. Wohlfarth

CONTENTS

1. Introduction and description of terms

The subject of dilute transition metal alloys may be divided into two classes of interest. Firstly, non-interacting or very dilute 3d-magnetic impurities dissolved in a non-magnetic host can be classified under the general heading of the *Kondo effect* – a localized antiferromagnetic interaction of the isolated impurity spins with the surrounding conduction electrons. Secondly and of prime importance in this article, we consider the impurity spin–spin interactions which lead to *giant moment* ferromagnetism and *spin glass* "freezing". These latter two cases represent different examples of magnetic ordering – the first a long range, but non-uniform, ferromagnetic alignment; the second a random arrangement of frozen spin-orientations. Both of these effects depend strongly on the conduction electrons to propagate the magnetic interactions over large distances. The boundary between these two dissimilar states of magnetism is controlled by the magnetic behaviour of these itinerant electrons. If this behaviour is such that the indirect interaction is ferromagnetic over long distances, the long range, albeit non-uniform, ferromagnetic ordering may be expected at rather low concentrations. However, for smaller concentrations (i.e. longer distances between impurities), the interaction has an oscillatory nature and spin glass ordering will prevail. Therefore, for each system a *percolation limit* can be defined (a critical concentration above which long range order occurs, but for smaller concentrations the spin glass state is found) which will strongly depend upon the properties of the host material. For some alloys (the giant moment systems), this limit will be very low; yet, for other alloys this limit can be as large as the nearest neighbour percolation concentration, since only the direct interactions can support a long range ferro- or antiferromagnetic order. As the percolation limit is approached from below, large magnetic clusters are formed and randomly freeze out at low temperatures. Here the nomenclature *mictomagnetism* or *cluster glass* is used. Thus, the magnetic properties of the host material and the concentration of the magnetic component decisively determine the type of magnetism which may exist in the alloy.

1.1. Kondo effect and weak moments

For very dilute concentrations of 3d-impurities in a non-magnetic matrix, the

magnetic spins may be treated as isolated from each other. This leaves only an interaction with the itinerant conduction electrons which may be described by an s–d exchange Hamiltonian, $\mathcal{H} = -JS \cdot s$. Here $J(<0)$ is an antiferromagnetic exchange coupling, and S and s represent the 3d local moment spin and the conduction electron spin, respectively. At high temperatures the impurities behave like free (paramagnetic) moments. However, below a characteristic temperature, specific for each alloy system, the impurity becomes non-magnetic due to its interaction with the conduction electrons. This temperature is known as the Kondo temperature T_K and it signifies the breakdown of higher order perturbation theory which is used to calculate the physical properties from the s–d Hamiltonian. In the calculations, $T_K = (D/k_B)\exp(-1/N(0)|J|)$ where D is the band width ($\simeq$ the Fermi energy, E_F, or temperature T_F), and $N(0)$ is the conduction electron density of states at the Fermi surface. For $T < T_K$ the appearance of logarithmic divergences in the calculations denotes a broad temperature transition to a quasi-bound state which is unable to strongly respond to external magnetic fields (non-magnetic) and possesses an enhanced electron scattering cross-section (resistivity minimum at low temperatures).

An alternative approach to the interaction between a local moment and the conduction electrons is the localized spin fluctuation model. Here the local spin fluctuates in amplitude at a rate τ_{sf}^{-1} where τ_{sf} is the spin fluctuation lifetime. When this rate is greater than the orientation changes produced by thermal fluctuations $k_B T$, the impurity spin appears non-magnetic and there is additional conduction electron scattering. As before a broad temperature interval separates the magnetic from the non-magnetic regime, and an analogous temperature may be defined as $T_{sf} = h/(k_B \tau_{sf})$.

These two models give quite similar experimental predictions, and for the present article we can assume the two characteristic temperatures to be equal. Thus, for $T \gg T_K$, good magnetic moments exist, i.e. $\mu = g\mu_B\sqrt{S(S+1)}$, while for $T \ll T_K$, the moments becomes "weak" and lose their magnetic character.

The occurrence of the Kondo effect is thereby a hindrance to spin–spin interactions and magnetic ordering. In table 1 a collection of Kondo temperatures is given for many of the alloy systems which exhibit interaction and ordering effects at sufficiently high concentration. Below this temperature the moments are "weak" and cannot simply interact with each other. Of course, we can greatly eliminate the role of the Kondo effect and weak moments by increasing the concentration and creating good moments via a strongly magnetic local environment: for, T_K (single impurity) $\gg T_K$ (pair) $\gg T_K$ (triple), etc.

The enormous amount of literature on the Kondo effect has been summarized in several review articles beginning with Van den Berg (1964) and later Daybell and Steyert (1968), Heeger (1969), Kondo (1969), Van Dam and Van den Berg (1970), and Fischer (1970, 1971). More recent reviews include the collection of papers in Magnetism V (Rado and Suhl, editors, 1973), Rizzuto (1974), Grüner (1974) and Grüner and Zawadowski (1974).

TABLE 1
Isolated impurity Kondo (spin fluctuation) temperatures for important dilute alloy systems

Host	Impurity:	V	Cr	Mn	Fe	Co	Ni	
		Noble metal–transition metal						
Cu		1000 K	2 K	10 mK	30 K	500 K	>1000 K	
Ag		—	10 mK	$<10^{-6}$ K	5 K	—	—	
Au		300 K	1 mK	$<10^{-6}$ K	0.2 K	500 K	>1000 K	
		Transition metal–transition metal						
Mo			—	10 K	1 K	25 K		simple
Rh			—	10 K	50 K	1000 K		simple
Pd			100 K	10 mK	20 mK	0.1 K		exchange enhanced
Pt			200 K	0.1 K	0.3 K	1 K		exchange enhanced

1.2. Giant moments

The term giant moment describes the unique behaviour of dissolving a single, localized, magnetic moment in a non-magnetic host and thereby producing a net moment much greater than that due to the bare magnetic impurity alone. This overall moment is the sum of the localized moment plus an induced moment in the surrounding host metal. For the description of a large number of experimental properties, these magnetic entities (impurity moment plus polarization cloud) can be considered as one magnetic moment which is then called "giant". A typical example of such a system is PdFe in which the Fe moment is approximately $4\mu_B$; yet experiments on PdFe reveal moments $\simeq 12\mu_B$. Thus, via a strong, parallel, itinerant electron polarization extending for about 10 Å, the Fe moment induces a small ($\simeq 0.05\mu_B$) moment on the 200 or so surrounding Pd atoms. Figure 1 sketches a static giant moment. Since this interaction is ferromagnetic the Kondo effect is unimportant, and ferromagnetism occurs at very low (0.1 at.% Fe) concentration due to the long range, indirect, ferromagnetic interactions. This behaviour represents the simplest type of ferromagnetic ordering to appear in a dilute, random alloy.

Sometimes the term giant moment is also used for the large magnetic entities which are caused by chemical clustering of magnetic atoms or groups of nearest neighbours needed to produce a moment (local environment). In this article we will use "giant moment" only for those moments associated with one "good moment" impurity.

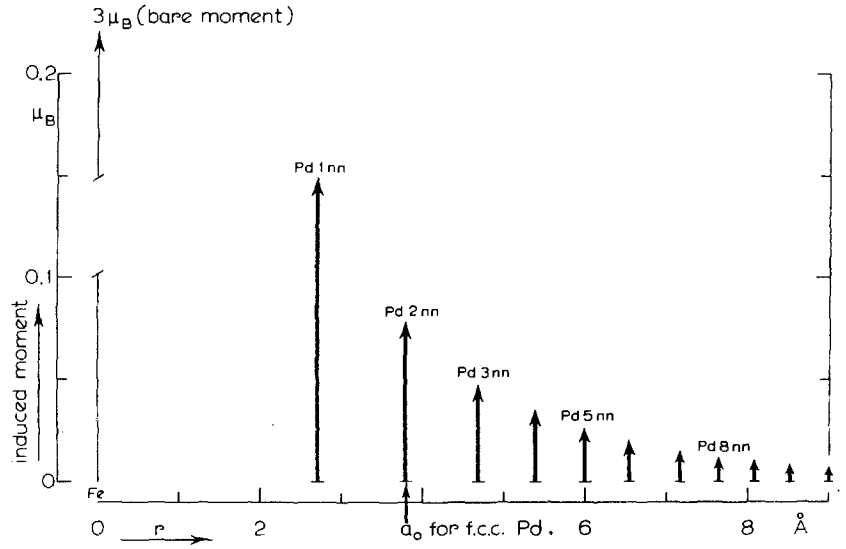

Fig. 1. Giant moment polarization cloud (schematic).

1.3. Spin glasses

Due to the newness of the concept spin glass*, there is less agreement on its exact meaning. For the purposes of this article, we offer the following working definition: a spin glass is a random, metallic, magnetic system characterized by a random freezing of the moments without long range order at a rather well-defined freezing temperature T_f. Mathematically, the above may be expressed (Sherrington 1976) as $\overline{|\langle S_i \rangle|} \neq 0$ for $T < T_f$, and $\overline{\langle S_i \rangle \langle S_j \rangle} \to 0$ as $|\boldsymbol{R}_i - \boldsymbol{R}_j| \to \infty$, where $\langle\ \rangle$ refers to a thermodynamic average, $|\ |$ is the amplitude modulus and $\overline{}$ a configuration average over all sites. The first equation demonstrates the random, but static, freezing of the spins, $\boldsymbol{S}_i$, below T_f, while the second shows that, although short range magnetic order may be present, there is no long range order, and the macroscopic moment for a spin glass in zero external field is always zero. Here we shall only treat metallic systems which are composed of at least one transition metal component. A schematic representation of a spin glass alloy is shown in fig. 2. The spin glass state is a new phase which is not possible in a translationally invariant system. Much of the experimental behaviour is probably related to the existence of a large number of low-lying energy states which are metastable for the reorientation of small groups of spins. The analogy, apparent from the word "glass", is with similar low lying metastable states believed to be important in the low temperature properties of "real" glasses (Anderson et al. 1972).

*This term was first suggested by B.R. Coles to be applied to the strange magnetic behaviour of the weak moment AuCo system (Bancroft 1970). Simultaneously, this expression appeared, again at Coles' instigation, in a paper from Anderson (1970) linking localization in disordered systems with the magnetic alloy problem.

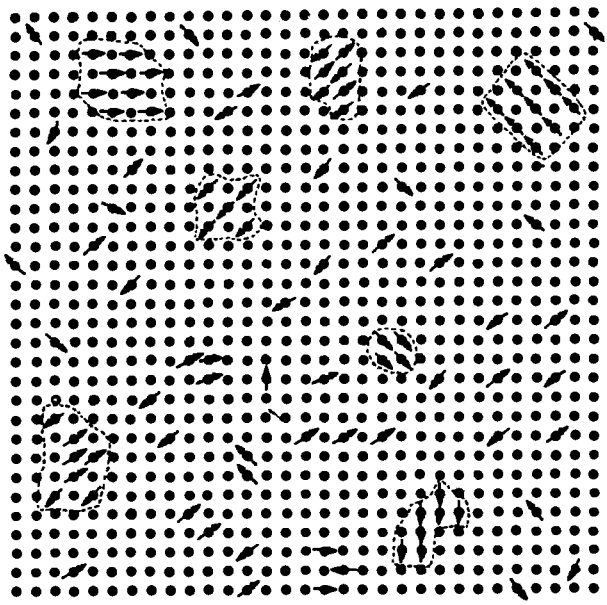

Fig. 2. Spin glass with mictomagnetic clusters (2-dimensional square lattice).

A more specific description of a canonical or archetypal spin glass has been suggested by Rivier (1974). Consider a moderately concentrated magnetic alloy, e.g. Cu or Au with about 0.1 to 10 at.% Mn or Fe. The magnetic impurities are interacting with each other by polarizing the conduction electrons – the RKKY (Ruderman and Kittel 1954, Kasuya 1956, Yosida 1957) interaction, which has the form

$$\mathfrak{J}(r) = 6\pi Z J^2 N(0)\left[\frac{\sin(2k_F r)}{(2k_F r)^4} - \frac{\cos(2k_F r)}{(2k_F r)^3}\right].$$

Here Z is the number of conduction electrons per atom, J is the s–d exchange, $N(0)$ the density of states per atom per spin of the host metal, k_F the Fermi momentum and r the distance away from an impurity. $\mathfrak{J}(r)$ is oscillatory and of infinite range (neglecting mean free path effects). The RKKY interaction between two impurities is shown in fig. 3. Note that the alignment may be parallel or antiparallel depending upon the separation between the impurities. Since the magnetic impurities have random positions in the lattice at low concentrations, the effective molecular field, $\boldsymbol{H}$, is a superposition of contributions from all the impurities in the alloy, due to the infinite range interaction. Furthermore, $\boldsymbol{H}$ has a distribution of magnitudes, $P(H)$, and a random distribution of directions because of the oscillatory nature of the RKKY. The range of the magnetic order corresponds to the size of a wave packet built from superposing all the RKKY contributions with random phase. Such a wave packet has a local character, thus, the system has at most short range, but no long range, order. This gives the random freezing or orientations of the spin glass moments. The freezing tem-

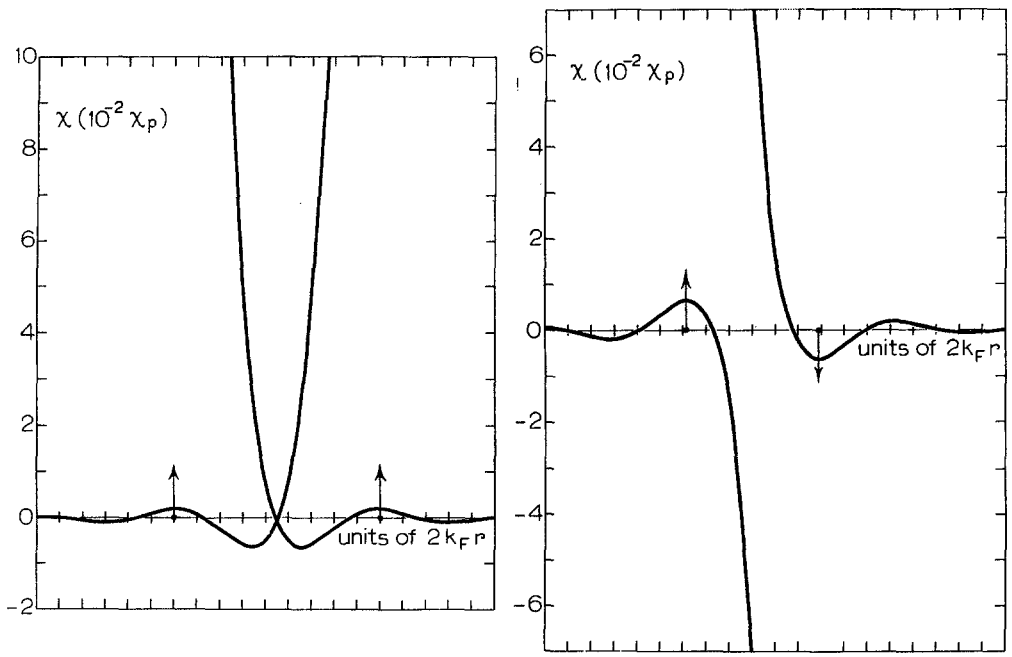

Fig. 3. Ruderman–Kittel–Kasuya–Yosida (RKKY) interaction between two impurities in terms of the Pauli susceptibility χ_P.

perature arises from a very simple model of D.A. Smith (1974, 1975). By considering only the amplitude of the RKKY, $\mathfrak{J}'(r) = A/r^3$, we have the strength of the interaction as a function of distance. For a low concentration alloy the average distance of impurity separation is $\bar{r} \propto (1/c)^{1/3}$. Again we use the thermal disorder energy, $k_B T$, which now destroys the correlations between the spins, on average, $\bar{r}$ apart. In other words, the molecular field from a spin S acting at a distance $\bar{r}$ on another spin S must be greater than thermal values for freezing to occur. At the freezing temperature, $\mathfrak{J}'(\bar{r}) = k_B T_f$ or $T_f = c(A/k_B)$. This means that no matter what the concentration is there will always exist a temperature for which the RKKY interaction will be dominant and cause this random freezing. Here only good moments are assumed, i.e. $T_K = 0$.

The same type of primitive reasoning may be applied to the giant moment alloys. Except at very large distance (very small concentrations), the conduction electron polarization is always positive (see fig. 1). So there can only exist a ferromagnetic order when these all-parallel polarization clouds contain more than one impurity. However, the functional form of $\mathfrak{J}(r)$ for a giant moment is more complicated (see section 4). Nevertheless, the same procedure of setting $k_B T_c = \mathfrak{J}(\bar{r})$ (where T_c is the Curie temperature) may be used to calculate $T_c(c)$ (Nieuwenhuys 1975).

An important difference between the giant moments and spin glasses becomes clear by examining the itinerant electron polarizations sketched in figs. 1 and 3.

For any arbitrary distance (except again the very largest), the conduction electrons surrounding a giant moment are always positively polarized, and a long range, ferromagnetic order will result. In the spin glass case with its RKKY polarization (fig. 3) the oscillations introduce an element of "conflict", also called "frustration" (Toulouse 1977), among the randomly positioned impurities. This encounter of competing positive and negative alignments is essential to the formation of the spin glass state. We need not solely restrict ourselves to the RKKY interaction for any mixture of opposite interactions when combined with the spatial randomness can produce the conflict leading to the spin glass phase.

1.4. Mictomagnets and cluster glasses

As the concentration of magnetic impurity is increased, there is a greater statistical chance of the impurity being first or second nearest neighbour to another impurity. Since the wave functions for the 3d electrons have a finite extent, i.e., not fully localized as for example with 4f electrons, there is an interatomic overlap and a direct magnetic exchange results. This adds a short range interaction which can couple neighbouring impurities ferro- or antiferromagnetically, depending upon the particular 3d element (and the neighbour position). Thus, magnetic clusters can form as a result of concentration fluctuations in a random alloy. In addition, at these larger concentrations short range chemical or atomic order and even chemical clustering (non-solubility of the alloy) may occur. Such deviations from randomness can greatly influence the local magnetism.

It has been experimentally found for a number of typical spin glass alloys that both of the above mechanisms produce a predominance of the ferromagnetic coupling and very large effective moments $\simeq$20–20,000μ_B form. When the magnetic behaviour is dominated by the presence of such large magnetic clusters, the terms mictomagnet or cluster glass have been used in the literature. Figure 2 shows some of these clusters within the dotted lines embedded in the spin glass matrix. At sufficiently low temperature, these clusters will freeze with random orientations in a manner analogous to the spin glass freezing. However, the mictomagnetic phase is especially sensitive to its metallurgical state. Heat treatments, with various times, temperatures and cooling rates, along with plastic deformation can greatly affect the cluster formation and magnetic behaviour. Of special interest here are the hard magnetic properties such as the peculiar displaced hysteresis loops and the remanence and irreversibilities in the magnetization.

The origin of mictomagnetism goes back to a series of early investigations by Kouvel (1963) and his "ensemble of domains" model. More recently, Beck (1971, 1972a,b, Tustison 1976, Tustison and Beck 1976, 1977) who coined the word "mictomagnetism", has extended the experiments with careful consideration of the metallurgical state and invoked the concept of a random freezing. Coles and co-workers (Murani et al. 1976a) use the name "cluster glass" to describe similar very large moment effects in more concentrated alloys. Sometimes in the

literature the term giant moment is applied to these mictomagnetic clusters. We in this article reserve giant moment solely for *induced* moment systems, introduced in section 1.2. Since mictomagnetism and cluster glass refer to alloys of higher concentration, this concept will not receive great attention in the following sections. For, as our title states, we limit ourselves to dilute alloys, that is, concentrations less than 10 at.% magnetic component.

1.5. Percolation and long range magnetic order

For the sake of completeness, let us proceed and further increase the number of magnetic atoms. At some given concentration for the particular crystal structure, each magnetic site will have at least one magnetic nearest neighbour. When such a macroscopic connection or uninterrupted chain extends from one end of the crystal to the other, the percolation limit (that concentration for which there is a non-zero probability that a given occupied site belongs to an unbounded cluster) has been reached. The schematic lattice in fig. 2 is far below the site percolation concentration which, for a square lattice, requires 58% of the total sites to be occupied (Essam 1972). Another type of percolation in bond percolation where an interaction or bond which couples two particular sites is present or absent. Then the closed bonds must continue in a macroscopic path through the crystal. Bond percolation is useful in describing the conductivity process (metal–insulator transition in disordered systems).

The magnetic consequences of percolation are that a long range but highly inhomogeneous magnetic order occurs. Thus, there can be no spin glass or mictomagnetic state above the percolation limit. However, loose magnetic clusters and weakly coupled "spines" to the central chain are present which can behave in a mictomagnetic way and perturb the long range properties. For a simple nearest neighbour ferromagnetic interaction in a face centered cubic lattice. e.g. AuFe, the percolation concentration is between 16 and 19 at.% (Essam 1972, Duff and Cannella 1973a,b, Sato and Kikuchi 1974), above which we have a ferromagnet. With antiferromagnetic bonding (fcc crystal), e.g. CuMn, a much larger concentration is necessary. For, the fcc (triangular) symmetry is unfavourable for antiferromagnetic order and many spins are needed to build this, coherent, long range, two sub-lattice structure in fcc space. Here the percolation limit is $\simeq$45 at.% (Sato and Kikuchi 1974), above which we have an antiferromagnet.

As mentioned before a modified concept of percolation is sometimes applied to the giant moment alloys. Now, the extent of the giant moment polarization will represent the magnetic entity. When the concentration of magnetic impurities is such that the clouds of one impurity include other impurities and a ferromagnetic path reaches from one end of the sample to the other, percolation is obtained. Here, of course, the critical concentration will be very small due to the large size (many lattice sites) of the induced polarization, see fig. 1.

Percolation theory has been reviewed by Essam (1972) and Kirkpatrick (1973). Present interest concerns the behaviour of the loose spins and the "spines", and

their effect on the overall properties of the system. Since percolation and the resulting long range order require a non-dilute concentration, $c > 10$ at.%, we shall not discuss these concepts in any detail.

2. Listing of alloy systems

2.1. Noble metals with transition metal impurities

We begin with the well-studied noble metal–3d transition metal alloys, and invoke two criteria to find the simplest spin glass behaviour*: (a) "good moment" systems, i.e. the Kondo temperature should be less than $\simeq 1$ K, so that no complications are encountered with the weakening of the local moments at low temperatures, and (b) a favourable solubility such that at least 10 at.% of the 3d metal may be dissolved in the noble metal host. This latter criterion, in conjunction with a proper homogenization process, provides for a random distribution of impurities and eliminates difficulties with chemical clustering. In table 2 the various combinations of noble metal solvent–3d solute are given. Besides the archetypal examples of CuMn and AuFe, there are only three other uncomplicated spin glass systems, shown by a "good" in table 2: AuCr, AuMn and AgMn. The experimental properties, e.g. low field susceptibility (Cannella and Mydosh 1974a,b) and the electrical resistivity (Ford and Mydosh, 1974a,b, 1976a, Mydosh et al. 1974) are very similar for these five alloy systems. By referring to table 2, problems are encountered for many of the other combinations, with either the Kondo temperature (see table 1) or especially the solubility limit, represented by XT and XS, respectively.

However, a number of special cases exist, as for example with CuFe which possesses a rather poor solubility and a $T_K \simeq 30$ K, but nonetheless shows the

TABLE 2
Spin glass combinations

	Noble metal–transition metal					
Host \ Impurity:	V	Cr	Mn	Fe	Co	Ni
Cu	XS	XS	GOOD	XS+T	XS	XT
Ag	XS	XS	GOOD	XS	XS	XS
Au	XT	GOOD	GOOD	GOOD	XS+T	XT

"GOOD" represents the most favourable combinations, XS or XT means that the spin glass behaviour is limited by lack of solubility or too high a Kondo (fluctuation) temperature, respectively.

*Since the noble metals are all diamagnetic, there is little tendency here to induce magnetic polarization on the host sites. Thus, giant moment behaviour will not occur.

magnetization characteristics of a mictomagnet (Mishra and Beck 1973). The high T_K means that isolated or single Fe atoms cannot participate in the magnetic interactions, yet Fe pairs or triplets may (Tournier 1974). Such interaction effects are very difficult to observe due to the small probability of finding "pairs" at low concentration and the utmost in experimental sensitivity (SQUID devices) and ultra low temperatures ($\simeq$10 mK) are required (Hirschkoff et al. 1971a,b, Frossati et al. 1975, 1976, Tholence and Tournier 1976). The deviations from randomness (precipitation of Fe for $c \geq 1$ at.%) are reflected in the low field susceptibility by the sharp peaks at the freezing temperature, T_f, changing into broad maxima (Cannella and Mydosh 1974a). Also, in this more complete category, we would include AuCo for which the Co solubility is poor, but not as bad as CuFe. The difficulty here is with the very large – few hundred Kelvin – Kondo (or spin fluctuation) temperature. As before T_K is strongly dependent upon the local environment, i.e. the number of Co nearest neighbours. In order to reduce $T_K \leq 1$ K for AuCo (Tournier 1974), a triplet is required; then, modified spin glass behaviour is observed (Cannella and Mydosh 1974a, Boucai et al. 1971). For this system an effective magnetic concentration of Co triplets should be used instead of the actual one.

A non-noble metal system which may be grouped with the above collection is ZnMn. Specific heat (du Chatenier 1964, F.W. Smith 1973, 1974a) and magnetic susceptibility (F.W. Smith 1974b) show all the characteristics of a spin glass. Although the solubility of Mn in Zn is rather limited (in the thousand ppm region), the hexagonal crystal structure is important to elucidate the anisotropy mechanisms present. Another special system ZrMn which has recently been investigated via magnetization and magnetoresistance also exhibits many spin glass properties (Jones et al. 1977).

2.2. Transition metal–transition metal combinations

By using the previous criteria of good moments and high solubility, binary combinations of transition metals may be examined for favourable examples of spin glass and giant moment systems. Table 3 gives a collection of the various possibilities. Beginning with the giant moment alloys, a further requirement is an exchange enhanced host. That is, at first, a large density of itinerant d-states should be near the Fermi energy, $N(0)$, such that there is a large Pauli paramagnetic susceptibility $\chi_P = 2\mu_B^2 N(0)$. Secondly, an intra-atomic exchange, $\bar{I}$, should be present on the host sites. This results in an exchange enhanced susceptibility $\chi = \chi_P \{1 - \bar{I}N(0)\}^{-1}$, where the factor $\{1 - \bar{I}N(0)\}^{-1} \equiv \Xi$ is the Stoner enhancement factor. For Pd, $\Xi = 10$, while for Pt, $\Xi = 3$. This means that only Pd or Pt hosts will produce the giant moment polarization. The simplest giant moment systems are PdFe($\mu_{eff} \simeq 12\mu_B$), PdCo($\mu_{eff} \simeq 10\mu_B$) (Nieuwenhuys 1975) and PtFe($\mu_{eff} \simeq 6\mu_B$) (Crangle and Scott 1965).

An especially interesting situation is with PdMn where for $c < 3$ at.% Mn the giant moment ($\mu_{eff} \simeq 7.8\mu_B$) ferromagnetism prevails (Nieuwenhuys 1975, Star et al. 1975). However, upon further increasing the Mn concentration ($c > 4$ at.%),

TABLE 3
Transition metal–transition metal spin glass/giant moment combinations

Host \ Impurity	Cr	Mn	Fe	Co	
Mo	XT	SG	SG	XS+T	simple
Rh	XT	SG	XT	XT	simple
Pd	XT	GM+SG	GM	GM	exchange enhanced
Pt	XT	SG	GM	SG	exchange enhanced

SG and GM represent favourable combinations for spin glass or giant moment behaviour. Note the strong, mixed behaviour of PdMn. XS or XT means solubility or too high a Kondo (fluctuation) temperature limits the appearance of both the spin glass or giant moment states.

the probability of having two Mn atoms at first or second (or even third) nearest neighbours increases. This then supplies the essential element of "conflict" or "frustration" for the appearance of the spin glass phase. For, Mn nearest neighbours couple antiparallel and thereby produce the competing Mn–Mn antiferromagnetic exchange to the longer ranged ferromagnetic giant moment polarization (Coles et al. 1975, Zweers and van den Berg 1975, Zweers et al. 1977). Hence, PdMn may be regarded as an example of a non-RKKY spin glass with two completely different exchange mechanisms (Nieuwenhuys and Verbeek 1977). An anomalous mixed phase with peculiar experimental properties occurs between 3 and 4 at.% (Guy and Howard 1977, Nieuwenhuys et al. 1979).

The platinum host alloys and their smaller exchange enhancements tend more readily towards spin glass and weak moment behaviour. For example, PtMn has a good moment and conflicting exchanges, and thus shows typical spin glass effects (Wassermann and Tholence 1976, Tholence and Wassermann 1977). On the contrary, PtCo is a weaker moment system which, when stabilized by increasing the Co-concentration, becomes a (semi) giant moment ferromagnet ($\mu_{\text{eff}} \simeq 4\mu_B$) (Crangle and Scott 1965, Swallow et al. 1975, Williams et al. 1975a,b). Here there is some recent evidence that a spin glass state may exist between the weak and giant moment phases (Rao et al. 1976).

A similar pair of systems are PdCr and PtCr; both have very weak moments in the dilute limit: $T_K(\text{PdCr}) \approx 200$ K and $T_K(\text{PtCr}) \approx 400$ K (Star 1971). Moreover, as the Cr concentration is increased, the total room temperature susceptibility at first decreases, and then, with sufficient Cr present, increases (Hagasawa 1970, Van Dam 1973). A simple interpretation can be made in terms of the following model (Mydosh 1976). Cr impurities, when introduced into the Pd or Pt host, locally "blot out" the uniform exchange enhancement, but in this process the Cr loses its magnetic moment (weak moment with a high T_K). Only when the Cr concentration is large enough to provide a suitable Cr local environment does a stable or good Cr moment appear, now however, in a non-enhanced Pd or Pt

matrix, and thus, the RKKY oscillating interaction can occur leading to a spin glass state at low temperature. Here there is no giant moment phase, if anything, the word "dwarf" or "destroyed" moment is more applicable. The Cr concentration necessary to produce the spin glass type of order is at least 7 at.% Cr in Pd (Roshko and Williams 1975), and $\simeq$17 at.% Cr in Pt (Roshko and Williams 1977).

At this point we should also mention the weak, but nonetheless giant moment PdNi alloys. For $c < 2$ at.% Ni there is no local moment associated with the Ni, and such alloys represent a canonical example of a localized spin fluctuation system (Lederer and Mills 1968). Above 2.2 at.% Ni, giant moment ferromagnetism ($\mu_{\text{eff}} \simeq 2.5\mu_B$) appears with a rapidly increasing Curie temperature $T_C(c)$ (Crangle and Scott 1965). The model used here is that the Ni atoms belonging to nearest neighbour groups of three or more are magnetic and produce, by polarization effects, giant moments (Chouteau 1976).

The word *weak* as used in this article refers to the "environment" model stipulation that a particular number of Ni, Co, Fe, Mn or Cr nearest neighbours are present to produce the local magnetic moment which is per se a magnetic cluster. This descriptive model may further be applied to the higher concentration alloys such as CuNi, RhNi, VFe and VMn. For the majority of systems there is a general concentration dependence from non-magnetic, weak moments, to an intervening spin glass or mictomagnetic regime, to finally, a long range ferromagnetic (Ni, Co, Fe) or antiferromagnetic (Mn, Cr) order.

Returning to the dilute alloys and considering the simple hosts Mo and Rh, table 3 lists three favourable candidates for spin glass behaviour: MoMn, RhMn and MoFe. The latter system has already been found to exhibit typical spin glass properties (Amamou et al. 1976, Ford and Schilling 1976, Caudron et al. 1977). Since the host metals are not exchange enhanced, a giant moment regime is not possible here. The special cases of RhFe (Murani et al. 1970, Rusby 1974) and RhCo (Coles et al. 1974) are weak moments and require a sufficiently large concentration of magnetic impurity ($\simeq$1 at.% Fe and 20 at.% Co) before spin glass behaviour manifests itself. Little is known about Cr in Mo or Rh and we would speculate that they fit into the general scheme of weak moments (Coles et al. 1971) which become spin glasses above a definite concentration.

2.3. Ternary and special transition metal alloys

A few additional systems should be briefly cited to complete this survey of giant moments and spin glass alloys. By utilizing certain binary combinations for the host, the exchange enhancement can be greatly increased. For example, $Ni_3Ga(\Xi = 35)$ and $Ni_{74}Al_{26}(\Xi = 25)$ (the stoichiometric compound is an itinerant ferromagnet), when diluted with Fe impurities all yield super-giant moments. Neutron and Mössbauer measurements give values of μ_{eff} up to $80\mu_B$ (Cable and Child 1973, Ling and Hicks 1973, Liddell and Street 1973).

The same procedure may be employed to generate really giant moments by doping Fe into CuNi, RhNi or PdNi hosts where the Ni concentration is kept

below that for ferromagnetism. There is yet another method to increase the exchange enhancement of Pd and that is alloying with a few percent Rh ($\Xi = 12$ for $Pd_{95}Rh_5$). However, the extra electron scattering caused by the Rh prevents any significant increase in the μ_{eff} produced with the inclusion of Fe. Conversely, the exchange enhancement of Pd or Pt may be reduced and even totally destroyed (diamagnetic susceptibility) by alloying with silver or charging with hydrogen. Thus, for 60 at.% Ag substitutional in Pd (Hoare et al. 1953, Mehlmann et al. 1973) and an interstitial H/Pd ratio of 0.65 (Jamieson and Manchester 1972), the host is diamagnetic (pseudo-noble metal-like), and the further addition of 3d-impurities, Co, Fe, Mn or Cr, leads to the formation of the spin glass state (Budnick et al. 1974, Levy and Rayne 1975, Mydosh 1974, 1976, Burger et al. 1975, 1976). Thus, the strong, positive polarization of the giant moment system (fig. 1) is altered into the weaker oscillations of the RKKY interaction (fig. 3). This leads us to the general conclusion that the spin glass phase is the most common in random dilute alloys. However, with the selection of a particular host, and there are very few of these available, a large exchange enhancement may be attained, which makes the creation of the giant moment and the resulting ferromagnetism possible. Nevertheless even for the simple PdFe system, at very dilute Fe concentrations, the large distance, rather small negative conduction electron polarization (Moriya, 1965b, Kim and Schwartz 1968) can lead to a conflicting interaction and the spin glass state. A recent investigation of the high (0.28 at.% Fe) giant moment and the low (0.015 at.% Fe) spin glass concentration differences has been carried out via positive muon depolarization experiments (Nagamine et al. 1977a,b,c).

Up until now we have considered crystalline (even single crystal) metallic systems with a random distribution of 3d-impurities. By relaxing the condition of lattice order, the problem of amorphous magnetism presents itself. A large assortment of disordered alloys may be fabricated in thin film form by quench-condensation or sputtering, and in bulk form by splat cooling. There exists adequate experimental evidence that a simple spin glass state does occur (Mydosh 1978). So far, however, amorphous systems with a large exchange enhancement have not been produced, thus preventing the study of giant moments in an amorphous host. We might expect here certain difficulties especially regarding the reduced mean free path and its effect on the conduction electron polarization.

2.4. Concentration regimes

It has become clear from the preceding sections that the concentration is most important in determining the magnetic state of the alloy. Consider now a concentration regime division for a conducting non-enhanced, magnetic alloy. Figure 4 gives such a schematic representation. At the very dilute magnetic concentrations (ppm) there are the isolated impurity-conduction electron couplings, which result in the Kondo effect. This localized interaction causes a weakening or fluctuation of the d-electron spin, and below the Kondo tem-

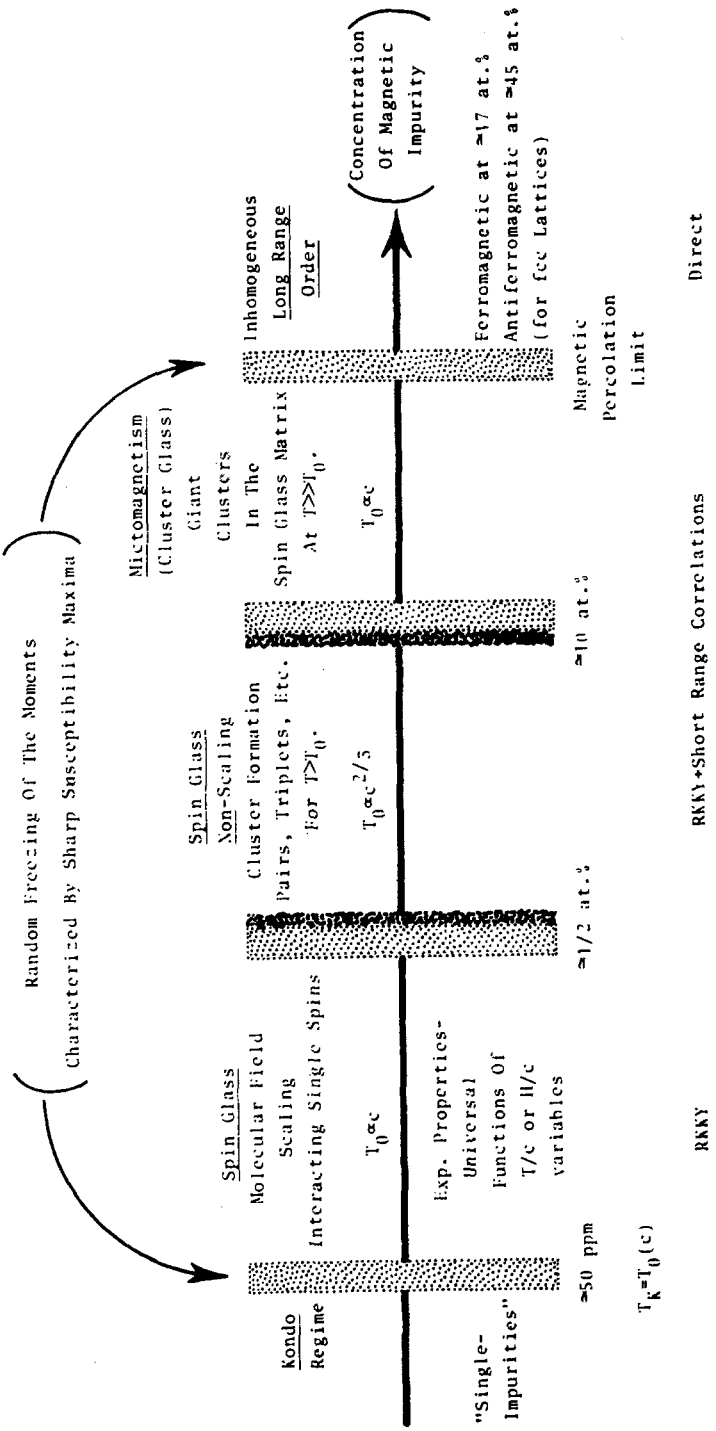

Fig. 4. Various concentration regimes for a non-exchange enhanced magnetic alloy illustrating the different types of magnetic behaviour which occur.

perature the impurity appears non-magnetic. Thus, the Kondo effect prevents strong impurity interactions which are the basic ingredients of the spin glass problem. Nevertheless, the local environment model tells us that there will be "pairs" (or "triplets") which possess a much lower T_K than the singles. These good moment pairs may then interact with other pairs and give rise to spin glass behaviour. Therefore, in principle, there is no lower concentration limit to spin glass consequences, until we run out of measurement response or temperature. Usually, however, we take $T_K \simeq T_f(c_0)$ as the concentration, c_0, below which the Kondo effect plays a large role in modifying the spin glass behaviour (Larsen et al. 1977).

Up to a concentration of a few thousand ppm ($\simeq 0.5$ at.%); a "scaling" approach (Souletie and Tournier 1969), based upon the RKKY exchange is particularly appropriate to the problem of interacting impurities. This means that the measurable properties (magnetization, specific heat, remanence, etc.) are universal functions of the concentration scaled parameters T/c and H_{ext}/c; in addition $T_f \propto c$. At low temperature $T \ll T_f$ and with the incorporation of dipolar interactions ($\propto 1/r^3$), which also scale with c, the magnetic behaviour may be nicely described within the model of Néel super-paramagnetism (Tholence and Tournier 1974, 1977). Yet, a more general class of behaviour is present to much higher concentrations, namely the freezing process at T_f. Although the scaling regime and its associated model represent an adequate first order approximation at low c, it is the random freezing, persisting over an extended concentration range, which exhibits the most dramatic experimental effects (see section 3.2).

Figure 4 indicates these various concentrations for a typical noble metal–3d alloy. Here, we would employ the term spin glass almost up until the percolation limit above which a long range, but inhomogeneous ferro- or antiferromagnetic order occurs. The qualifying "almost" has to do with the existence of magnetic clusters 20–20,000μ_B just below the percolation concentration. When the magnetic behaviour is dominated by such clusters, the nomenclature mictomagnet or cluster glass is used to emphasize the anomalies generated by these very large magnetic clusters.

A temperature dimension should be added to fig. 4 in order to give it the character of a T–c phase diagram. In fig. 5 such a general scheme is shown. T_K represents an average Kondo temperature which decreases as a function of the concentration. For $T_K > T_f$, we have the weak moment concentration regime. Then as the local environment builds good moments ($c > c_0$), the spin glass regime appears; and finally above the percolation limit c_p, long range magnetic order is present. The giant moment alloys may also be included in this scheme with c_0 and c_p much less than in the previous example. In addition, the spin glass regime for a giant moment ferromagnet may compose only a very narrow concentration region. So by properly adjusting the values of c_0 and c_p, and scaling the three temperatures of interest T_K, T_f and T_c, any of the previously mentioned alloy systems may be described within the very general phase diagram depicted in fig. 5.

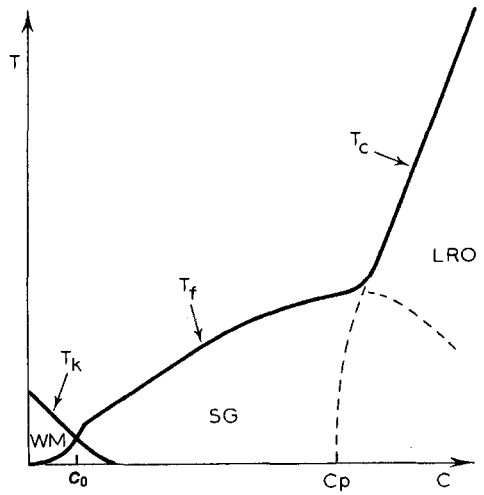

Fig. 5. General (schematic) $T-c$ phase diagram for a dilute magnetic alloy.

3. Experimental properties

3.1. Giant moment ferromagnetism

The giant moments associated with the 3d-transition metal atoms are directly related to the large magnetic susceptibility of the host metals in which they are dissolved. Therefore, in order to understand the magnetic properties of alloys exhibiting the giant moment phenomena, one should first understand the origin of these moments by treating the atomic physics of the 3d-atoms in a surrounding of highly polarizable, itinerant, host-electrons. This problem has been discussed for Co, Fe and Mn impurities in Pd and Pt by Moriya (1965b) and by Campbell (1968), while Kim (1970) attacked the many impurity problem, with special attention to PdNi. For the purpose of this introduction we adopt a description of the giant moment based mainly upon the linear response approximation. The occurrence of the giant moment is then depicted by assuming that the bare magnetic moment of the dissolved 3d-atom polarizes its surroundings, and the polarization, as a function of distance, is governed by the generalized magnetic susceptibility of the host material. If the host material were a normal metal in which the conduction electrons can be treated as free electrons, this susceptibility $\chi(r)$ is given by the RKKY formula (see section 1.3). In this case no significant polarization would be present, since the spatial integral over the susceptibility would approximate zero (neglecting the non-physical small distance divergence). However, if the intra-atomic exchange interactions between the band electrons are important, the generalized susceptibility will alter from the RKKY form to roughly (within the random phase approximation)

$$\chi(q, \omega = 0) = \frac{\chi_{\mathrm{RKKY}}(q)}{1 - \bar{I}\chi_{\mathrm{RKKY}}(q)} \tag{3.1}$$

where $\{1 - \bar{I}\chi_{\mathrm{RKKY}}(0)\}^{-1}$ defines the Stoner enhancement factor Ξ, and $\bar{I}$ is a measure for the strength of the intra-atomic exchange interaction (see Kittel 1968, Schrieffer 1968). The generalized susceptibility of the RKKY form is proportional to χ_{P} (the Pauli susceptibility) times the Lindhard function (Lindhard 1954), which for small values of q can be approximated by

$$u(q, 0) = \frac{1}{1 + \frac{1}{3}(q/2k_{\mathrm{F}})^2} \tag{3.2}$$

where k_{F} is the Fermi wave vector. Substituting eq. (3.2) into eq. (3.1), the exchange enhanced generalized susceptibility becomes

$$\chi(q, 0) = \frac{\chi_{\mathrm{P}}}{1 - \bar{I}\chi_{\mathrm{P}} + \frac{1}{3}(q/2k_{\mathrm{F}})^2}. \tag{3.3}$$

$\chi(r)$ may be calculated by taking the Fourier transform of eq. (3.3), the result being

$$\chi(r) = \chi_{\mathrm{P}} \frac{3k_{\mathrm{F}}^2}{\pi r} \exp(-r/\sigma) \tag{3.4}$$

where σ equals $(\frac{1}{3}\Xi)^{1/2}/2k_{\mathrm{F}}$.

Thus, in the case of an enhanced magnetic susceptibility of the host metal, the spatial integral of $\chi = \chi(q = 0)$ may considerably differ from zero, and lead to an extra net polarization in the host metal, and thus, to a giant moment. The magnitude μ_{eff} of the giant moment is given by (Takahashi and Shimizu 1965, Doniach and Wohlfarth 1967)

$$\mu_{\mathrm{eff}} = \mu_{\mathrm{bare}}(1 + \alpha\chi(q = 0)) \tag{3.5}$$

where μ_{bare} is the bare moment (as measured on an isolated atom in vacuum) of the dissolved magnetic atom and α is a coupling constant. Whether this giant moment will be sensed in an experiment as a magnetic unity, will be a point of future discussion. The simple relation given by eq. (3.5) breaks down when the itinerant electrons are very strongly polarized. Kim and Schwartz (1968) examined the spin polarization around a localized moment in a magnetized band. They concluded that the polarizability decreases with increasing polarization. This effect has experimentally been observed in Pd and Pt based alloys by a decrease of the total magnetic moment per impurity at increasing concentrations (see fig. 6). The ferromagnetic ordering occuring in alloys which exhibit the giant moment phenomena might now be explained by a model similar to that used to explain the spin freezing in the spin glasses (see section 1.3). On the other hand, Kim (1966) argues that the presence of the magnetic moments implies an extra exchange interaction between the band electrons and thus drives the alloy to itinerant ferromagnetism. In this formalism the extra exchange enhancement is obtained by eliminating the local moment-itinerant electron interaction via a

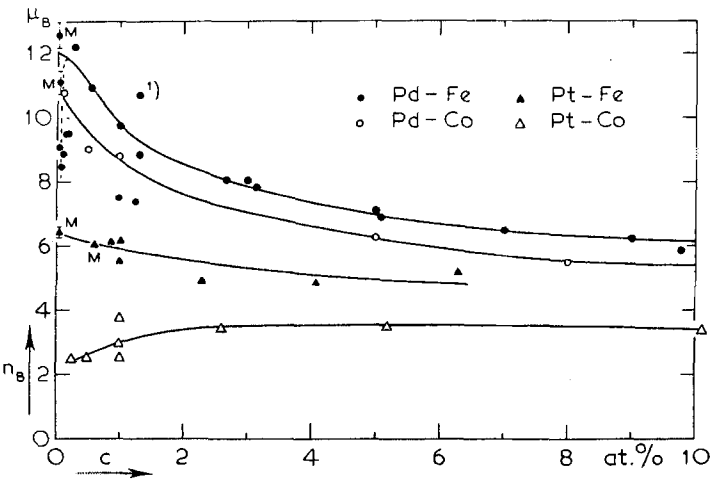

Fig. 6. Moment per solute atom n_B, expressed in Bohr magnetons, versus concentration. All data have been obtained from magnetization and susceptibility measurements, except those indicated by *M*, which have been deduced from Mössbauer experiments. Data sources: Crangle (1960), Crangle and Scott (1965), Bozorth et al. (1962), Clogston et al. (1962), Burger (1964), Craig et al. (1965b), Phillips (1965), McDougald and Manuel (1970), Craig et al. (1962), Maley et al. (1967), Kitchens et al. (1965), Foner et al. (1970). This figure has been taken from Boerstoel (1970).

canonical transformation. According to this point of view, PdFe dilute alloys would be an itinerant ferromagnet even if the Fe localized moments were in the paramagnetic state. A similar conclusion had already been reached by Rhodes and Wohlfarth (1963), by analysing experimental results on the basis of their intermediate model. Unfortunately, these authors used the high temperature susceptibility results, which later measurements showed to be inapplicable to deduce the magnetic moment (Nieuwenhuys et al. 1978). We will come back to this point in section 4.2.1.

No matter which of the models is adopted to explain the ferromagnetism, it is clear that the exchange enhancement of the host will create, at fairly small concentrations of magnetic atoms, a ferromagnetic order of the giant moments. Either the indirect interaction will be of long range and positive, or approached from another point of view, the host will be near the Stoner criterion for itinerant ferromagnetism. Takahashi and Shimizu (1965) developed a transparent molecular field model, which treats the giant moment problem in a simple way. They assumed the properties of the host to be independent of the magnetic concentration and the polarization to be uniform (no distance dependence). Denoting the interaction between the itinerant electrons by $\bar{I}$ and the interaction between the itinerant electrons and the localized impurities by α, they reach the following conclusions. Without magnetic ions, the susceptibility is given by $\chi_0 = \chi_P/(1 - \bar{I}\chi_P)$, and with magnetic impurities, the ferromagnetic phase transition taken place at $T_c = cg^2S(S+1)\mu_B^2\alpha^2\chi_0/3k_B$, where S is the magnetic quantum number and c the concentration of magnetic atoms. From a comparison with the experimental results these authors deduced that S should have

a small value (between 1–2) for Fe and Co dissolved in Pd. In the following sections the experimental results will be discussed within the framework sketched above. In section 4.2 we shall return to the theory.

3.1.1. Macroscopic properties

Experimental evidence for the existence of giant moments associated with 3d-impurities dissolved in exchange enhanced host materials can be obtained from magnetization and susceptibility, specific heat and transport measurements. The strength of the magnetic interaction in the alloy, causing ferromagnetism, is characterized by the value of the transition temperature, T_c. These T_c-values as a function of the concentration also contain information about the strength of the interaction as a function of the distance between impurities. The question whether the giant moment can be considered as a (dynamical) magnetic unit, might be answered by the value of the magnetic quantum numbers and the effective g-value, as will be discussed later on. Due to the large amount of previously reported experimental results (over 300), it is obviously impossible to discuss them all. Therefore, the main results of the experiments are tabulated in table A.1 in the appendix. In the following paragraphs we will restrict ourselves to the general features exhibited by the various properties, by taking examples from the Pd-based alloys. Then a general discussion of the other alloy systems will follow.

Magnetization and susceptibility

Let us focus attention on the simplest alloys: PdCo, PdFe and PdMn. The electronic structure of the Pd-atom consists of the krypton inert gas core surrounded by 10 (full shell) of 4d-electrons, however, the energy of the $(4d)^9(5s)^1$ configuration is only 1.3×10^{-19} J (1.3×10^{-12} erg) (or 0.8 eV) higher (McLennan and Grayson-Smith 1926). In metallic Pd the 5s and 5p states are lowered in energy due to the changed boundary conditions (Hodges et al. 1972), consequently the 5s and the 5p states will be filled up to the Fermi energy, causing the 4d-band to contain only 9.64 electrons per atom instead of 10. Therefore, the Fermi level will lie near the upper boundary of the narrow d-band, giving rise to a large density of states at the Fermi energy, and thus to a larger Pauli susceptibility than expected for normal metals. Due to the fact that the main part of the itinerant electrons at the Fermi level are strongly interacting 4d-electrons, the magnetic susceptibility is further increased by a factor of about ten, the so-called Stoner enhancement, $\mathcal{Z}$. This means that the intra-atomic interactions are only 10% too small to drive Pd into an itinerant ferromagnet. Therefore, Pd as host material is one of the best with which form giant moments alloys. Regarding Co, Fe and Mn on Pd there are two striking features in the experimental data from the magnetization measurements. The giant moment is fairly large (10–12μ_B per Co or Fe, and 7.8μ_B per Mn atom (Bozorth et al. 1961, McDougald and Manuel 1968, 1970, Star et al. 1975), and ferromagnetism persists down to fairly low concentrations ($\approx$0.1 at.%) (same references). The

critical concentration for ferromagnetism is thus very low compared to other alloys (AuFe). The magnetic susceptibility follows a modified Curie–Weiss law when allowance is made for the temperature dependence of the host susceptibility (Van Dam 1973). The incorporation of this temperature dependence can be done in two ways: either by assuming the Curie-effective moment, p_{eff}, to be simply proportional to the host susceptibility (Clogston et al. 1962), or by assuming p_{eff} to be equal to $p_{\text{eff}}^{(0)}(1+\alpha\chi_0)$ (Shaltiel et al. 1964). Thus, the excess susceptibility due to the magnetic impurities is represented by

$$\chi - \chi_{\text{Pd}}(T) = \frac{c p_{\text{eff}}^{0\,2}\alpha^2\chi_{\text{Pd}}^2(T)}{3k_{\text{B}}(T-\theta)} \quad \text{or} \quad \chi - \chi_{\text{Pd}} = \frac{c p_{\text{eff}}^{0\,2}(1+\alpha\chi_{\text{Pd}}(T))^2}{3k_{\text{B}}(T-\theta)}. \qquad (3.6,7)$$

In fig. 7 we reproduce the susceptibility of 1 at.% Co dissolved in Pd. The effective moment deduced in this manner from the Curie constant is in fair agreement with the value obtained from the saturation of the magnetization (see table A.1 in the appendix). However, there exists a large discrepancy between the paramagnetic Curie temperature, obtained from plots of χ^{-1} versus T and the ferromagnetic transition temperature deduced from Arrott plots (Arrott 1957). Also, the Arrott plots are not always the desired straight lines. These non-linear deviations become relatively larger as the concentration of magnetic atoms is reduced. This "difficulty" in determining T_c is presumably caused by the *width* of the transition to the ferromagnetic state, i.e. the transition from the paramagnetic state to the ferromagnetic one occurs gradually at lower concentrations, as is further revealed by other experiments. The *gradual* transition obviously finds its origin in the statistical concentration variations present in the alloy (which are relatively larger at lower concentrations) combined with the strong distance dependence of the magnetic interaction (being $r^{-1}\exp(-r/\sigma)$). Another remarkable aspect of the behaviour of the magnetization is its difficulty in achieving saturation at the higher concentrations. As an example we show (fig. 8) the magnetization as a function of temperature at different external magnetic

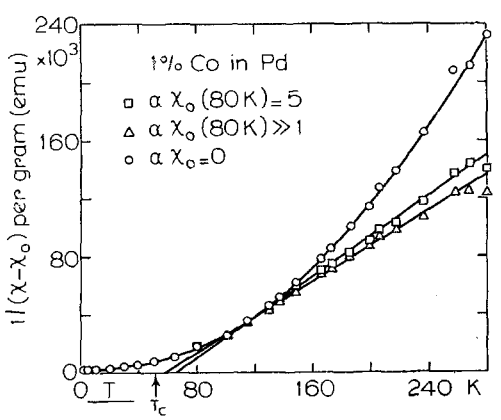

Fig. 7. $1/(\chi-\chi_0)$ curves for 1 at.% Co in Pd for different enhancement factors; the number of Bohr magnetons for $\alpha\chi_0(80\text{ K})=5$ and $\alpha\chi_0(80\text{ K})$ is 9.85 and 10.5, respectively; T_c was obtained from an Arrott plot of H/σ versus σ^2 (after Shaltiel et al. 1964).

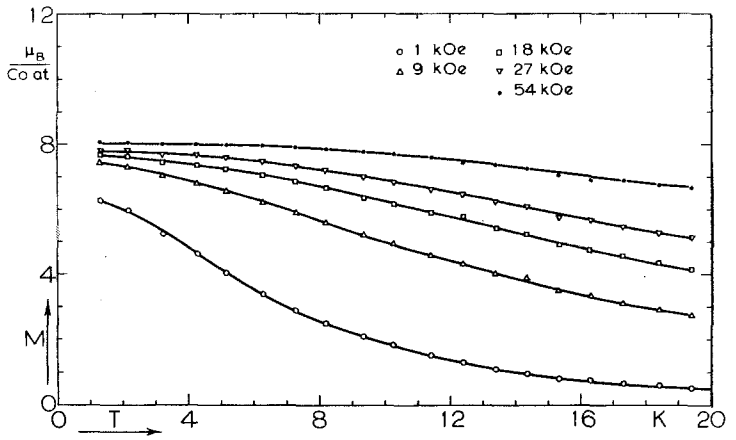

Fig. 8. Magnetization of PdCo 0.24 at.% as a function of temperature. (1 kOe = 0.1 T).

fields of PdCo 0.24 at.% as measured by Star (see Nieuwenhuys 1975). Even at 5.4 T (54 kOe) and $T = 1.5$ K the measured magnetization per Co atom is only $8\mu_B$, while the saturation magnetization per Co impurity (measured in alloys with lower concentration) is much higher, as can be seen from fig. 9 (also measured by Star, see Nieuwenhuys 1975). An explanation for this effect cannot be given straightforwardly without knowledge of the band structure of the alloy.

Apart from using the Curie–Weiss fit to determine the Curie temperature from the susceptibility, one can also use results for the susceptibility obtained at temperatures in the *vicinity* of T_c in very *small* external magnetic field ($B <$ 0.001 T [$B < 10$ G]) in most cases via the a.c. induction method (see e.g. Wiebes et al. 1964, or Maxwell 1965). The transition temperature is then found from the knee in the χ versus T curve in the case of a ferromagnet. This type of

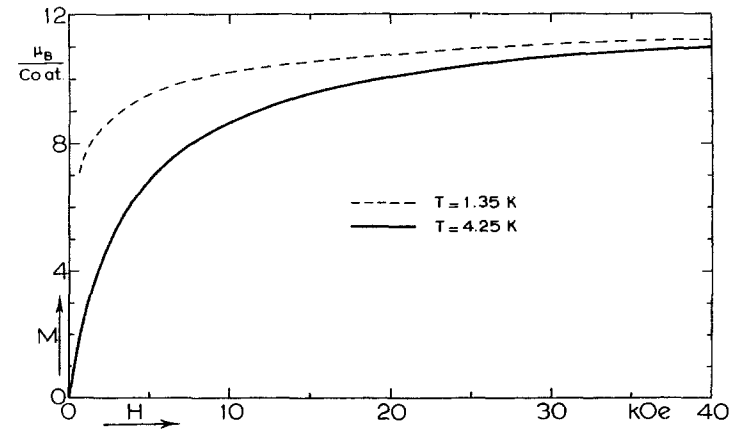

Fig. 9. Excess magnetization of PdCo 0.1 at.% at $T = 1.35$ K and $T = 4.25$ K as a function of temperature. The susceptibility of Pd has been assumed to be 7.42×10^{-4} emu/mol. No saturation of M_{imp} has been achieved, since dM_{tot}/dH_{ex} is 8.2×10^{-4} emu/mol at 50 kOe and 1.35 K.

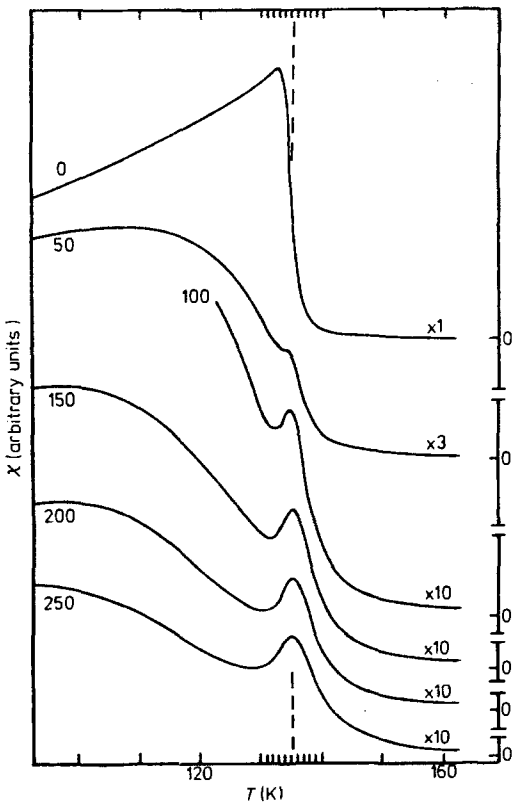

Fig. 10. $\chi(T)$ of PdCo 3 at.% for parallel fields up to 250 Oe, all taken during warming. The vertical scale has been multiplied by factors shown on the curves (1 Oe = 10^{-4} Tesla) (after Maartense and Williams 1976).

measurement has been applied to PdMn, PdCo and PdFe alloys by Burger and McLachlan (1973), to PdMn alloys by Nieuwenhuys (1975) and by Zweers et al. (1977), to PdAgFe alloys by Budnick et al. (1974), and to PdGd alloys by Cannella et al. (1975). Maartense and Williams (1976) used this susceptibility method for PdCo alloys in a somewhat different way. Their χ versus T curves did not show a knee sharp enough for an accurate determination of T_c. However, after applying a small dc magnetic field (up to 0.025 T [250 G]) the main χ versus T curve became rounded and an additional sharp peak appeared at a temperature which was then identified as T_c. The results found in this way are marked by an * in table A.1 in the appendix. In fig. 10 we reproduce the results obtained by Maartense and Williams (1976) on PdCo 3 at.% as an example of this low field methods.

Specific heat

Investigations of the specific heat of Pd-based giant moment alloys have been

carried out by Veal and Rayne (1964), Coles et al. (1965), Wheeler (1969), Boerstoel (1970), Chouteau et al. (1970), Boerstoel et al. (1972), Nieuwenhuys et al. (1972) and Nieuwenhuys (1975). Experiments on the specific heat of dilute alloys cannot be performed over a wide concentration range, since in order to deduce the extra specific heat due to the magnetic atoms, the specific heat of the host materials has to be subtracted. This latter contribution increases roughly proportional to T^3, so that in practical cases accurate specific

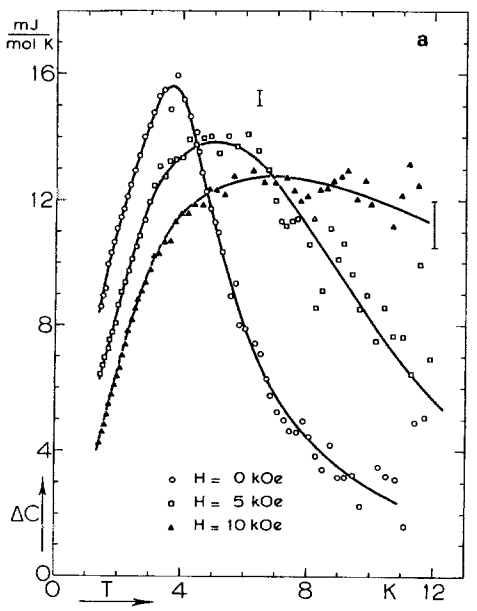

Fig. 11a. ΔC versus T for PdFe 0.23 at.% (1 kOe = 0.1 T).

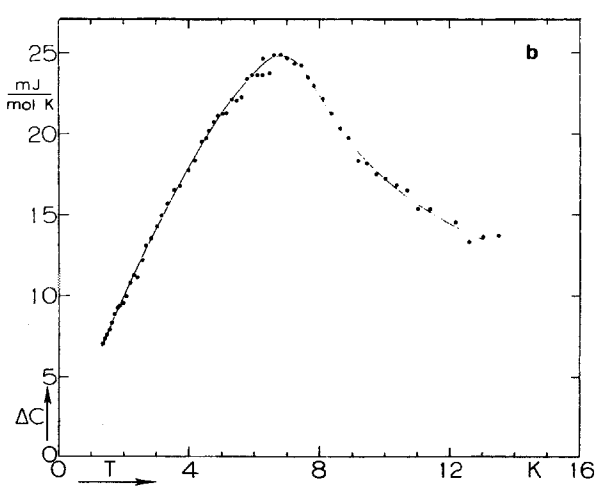

Fig. 11b. ΔC versus T for PdFe 0.35 at.% at zero external field.

measurements are limited to $T < 30$ K. This limitation implies that the measurements on Co and Fe which span T_c must be carried out for $c <$ 0.35 at.%, and for Mn up to 9 at.%. Typical curves for the specific heat of PdFe are shown in fig. 11, and for PdMn in fig. 12. As can be seen from the figs. 11a, b, the magnetic ordering in these dilute alloys gives rise to a wedge shaped maximum in the magnetic contribution to the specific heat. In the case of Mn the curves have much sharper "bending" as a function of temperature, but it should be noticed that the concentration of Mn is much higher than that of Fe. The broad maximum (in contrast to the λ-shaped peaks found in the pure ferromagnetic metal and many insulators with a translational invariant magnetic lattice) is obviously due to the gradual character of the magnetic transition in these random systems. The large magnitude of the magnetic moment of Fe is revealed by the relatively large field dependence of the specific heat. The magnetic entropy, $S_m = cR \ln(2S+1) = \int (C_m/T)\,dT$, deduced from the specific heat results agrees with a small value of the magnetic quantum number of the giant moment ($\frac{3}{2}$ for Co, 2 for Fe and $\frac{5}{2}$ for Mn). These small values for the entropy have been found by extrapolating the magnetic specific heat to higher temperatures as T^{-2}. Therefore, the conclusion must be drawn that the dynamics (e.g. the multiplicity) of the giant moments are mainly governed by the dynamics of the bare magnetic moment of the impurity. However, quantum numbers obtained from magnetization experiments by fitting the experimental data to a Brillouin function (incorporating an appropriate molecular field) are generally much higher (of order of 6) for Co and Fe in Pd. Remarkably, this contradiction does not exist in the case of Mn; an analysis of the specific heat (Boerstoel et al. 1972) as well as of the magnetization (Star et al. 1975) gives the same small quantum number ($\frac{5}{2}$).

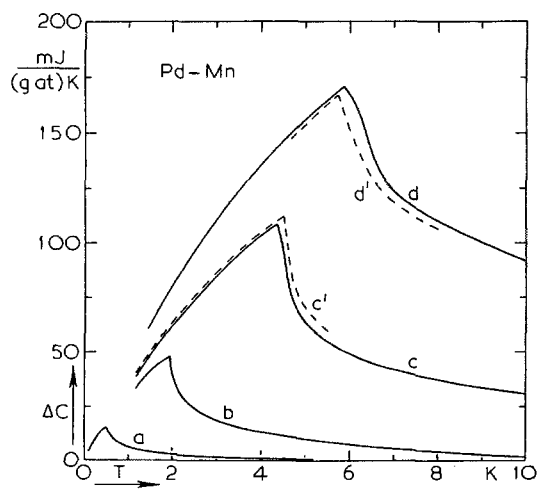

Fig. 12. ΔC versus T of PdMn alloys containing (a) 0.19 at.%, (b) 0.54 at.%, (c) 1.35 at.% and (d) 2.45 at.% at $H_{ex} = 0$. Curves c' and d' represent measurements after 220 hours homogenization at 1000°C subsequent to the usual homogenization (24 hours at 950°C) (after Boerstoel et al. 1972).

There have been several attempts to solve the observed discrepancy between the results for the magnetic quantum number as obtained from the specific heat and those from the magnetic measurements. Chouteau et al. (1970) have pointed out that the high temperature extrapolation as aT^{-2} is not correct for random alloys. These authors used an extrapolation according to $aT^{-2}+bT^{-1}$ to analyse their results on PdFe, and they obtained quantum numbers of order $\frac{7}{2}$, which is still much smaller than those obtained from magnetic measurements. In the case of zero-field measurements the extrapolation as used by Chouteau et al. (1970) is correct, however, for measurements in large external fields (Boerstoel 1970); the coefficient b appeared to be much smaller than a. Koon (1974) has called attention to the point that due the randomness of the alloy, there are a number of magnetic moments still coupled at temperatures far above T_c. Therefore, the specific heat will only contain part of the total entropy and this results in too small a magnetic quantum number. Koon's argument is certainly correct for measurements not extending to about 10 times T_c. However, if the measurements are extended up to 30 times T_c (as was done by Boerstoel (1970) in the case of PdCo 0.075 at.%) we estimate the error in the entropy obtained to be 4%, resulting in an error in the magnetic quantum number of only 15%.

Specific heat experiments on dilute alloys in large external magnetic fields may reveal an answer to this discrepancy. From the results of these experiments the magnetic quantum number can be calculated via the entropy content, and since the specific heat should (apart from details) behave like $B_{ex}(dM/dT)$, a Brillouin function fit as used in the analysis of the magnetic measurements can be made. Such experiments have been carried out by Boerstoel et al. (1972), Nieuwenhuys et al. (1973) and Nieuwenhuys (1975) on PdMn, PtCo, PtFe and PdCo very dilute alloys. In fig. 13 the results are shown of an experiment on PdMn 0.19 at.%, and in fig. 14 on PdCo 0.075 at.%. The dashed line in both figures

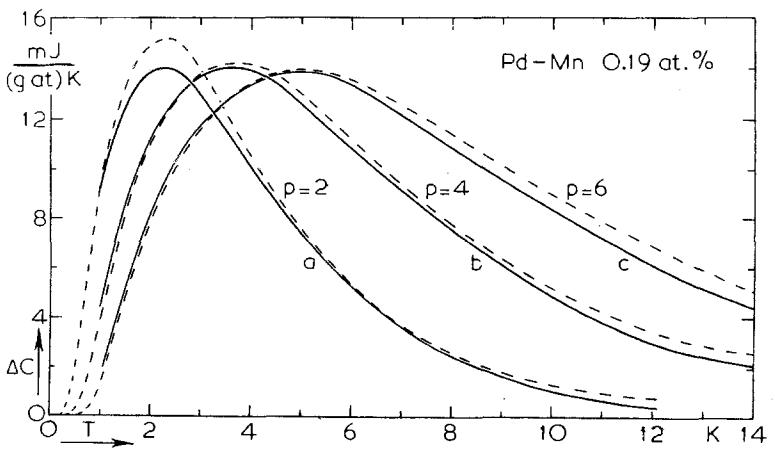

Fig. 13. ΔC versus T of PdMn 0.19 at.% at (a) $B = 0.9$ T [9 kOe], (b) $P \simeq 1.8$ T [18 kOe] and (c) B = 2.7 T[27 kOe]. Full curves: experiment, dashed curves: Schottky specific heat (after Boerstoel 1970).

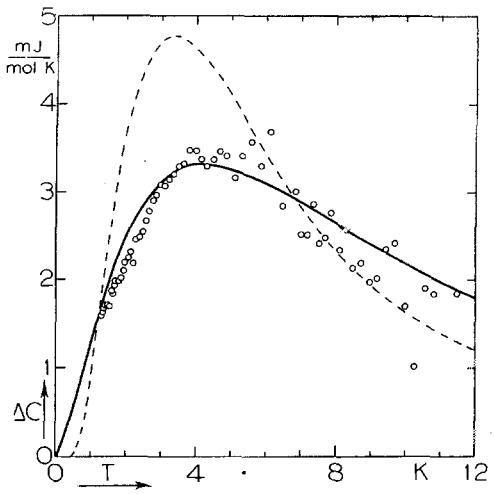

Fig. 14. ΔC versus T of PdCo 0.075 at.% at $B = 1.8$ T [18 kOe]. Circles: experimental results obtained by Boerstoel (1970), dashed curve: Schottky specific heat, full curve: results of a model calculation (Nieuwenhuys 1975).

represents the calculated Schottky specific heat (after correction for internal fields). From this work it is clear that in the case of PdMn the results based on the specific heat are in complete agreement with the Brillouin function based on the magnetic quantum number deduced from the entropy (Boerstoel et al. 1972). As mentioned earlier, there is no discrepancy present between the magnetization analysis and the entropy analysis for PdMn (Star et al. 1975). However, the other alloys investigated (PdFe, PdCo, PtMn and PtCo) did *not* behave according to Brillouin functions with S obtained from the entropy, and *also not* when a larger S (as obtained from magnetization) was used. From this investigation it has to be concluded that the magnetic entities associated with giant moments *do not* (generally) *behave in agreement with the appropriate Brillouin functions*, i.e. in agreement with statistical mechanics applied to *stable well-quantized* magnetic moments. In this respect the PdMn alloys are an exception. It then follows that the excellent fits of the magnetization (and the related splitting in the Mössbauer effect) to Brillouin functions with large values for the magnetic quantum number *are to be considered with great care.* An attempt to describe the behaviour of the single giant moments has been put forth by Nieuwenhuys (1975). In this approach the induced moment is assumed to be time dependent; a time dependence which may or may not be followed by the bare moment. Results of calculations based upon this model can explain the observed specific heat (see fig. 14) and the magnetic measurements. Unfortunately, no additional experimental nor theoretical support for this model has been provided up until now.

Electrical resistivity and thermopower

Measurements of the resistivity in the vicinity of the transition temperature on alloys of Pd with Co, Fe or Mn have been carried out by Sarachik and Shaltiel

(1967), Wilding (1967), Mydosh et al. (1968), Williams and Loram (1969a,b), Williams (1970), Kawatra and Budnick (1970), Grassie et al. (1971), Nieuwenhuys et al. (1972), Koon et al. (1972, 1973), Mydosh (1974), Coles et al. (1975) and Nieuwenhuys (1975). In general the scattering of conduction electrons by ordered magnetic impurities is smaller than in the non-ordered case. Therefore, a decrease in the electrical resistance is expected, and also observed, when the temperature is lowered below the ordering temperature. It should be noted that in the case of the giant moments alloys, the d-like itinerant electrons hardly contribute to the electrical conduction, because of their larger effective mass. Therefore, the whole giant moment acts as a scattering source for the conduction electrons (being s-like). In fig. 15 a typical curve for the resistance as a function of temperature for Pd-based alloys is shown. There are mainly two ways of deducing the transition temperature from the resistivity versus tem-

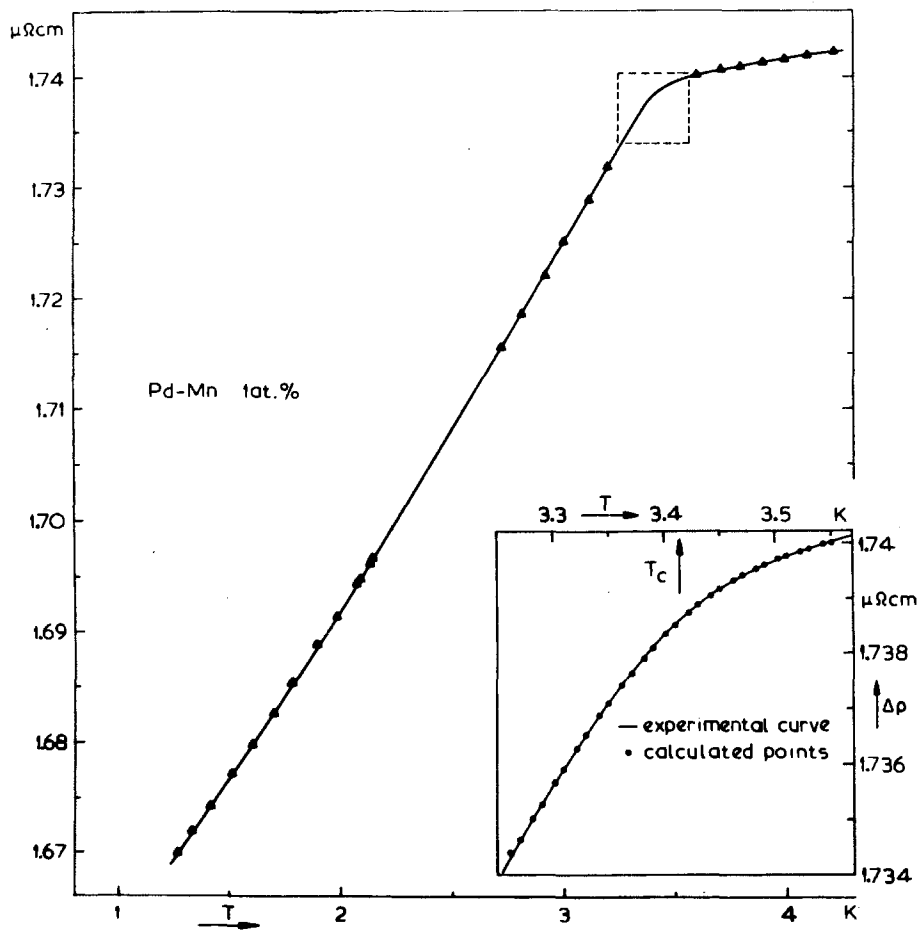

Fig. 15. The incremental resistivity $\Delta\rho$ of PdMn 1.0 at.% versus T (after Nieuwenhuys and Boerstoel 1970).

perature curve. One is identifying T_c with that temperature where the curve bends (in table A.1 denoted by "knee"), the other is defining the transition temperature as that temperature where the temperature derivative of the excess resistivity attains its maximum value (denoted by $d\Delta\rho/dT$). The first method originated from the molecular field theory (see e.g. Smart 1966) and the calculations by Yosida (1957a,b); the latter one from a theory by Fisher and Langer (1968), according to which the specific heat and $d\rho/dT$ should behave in the same way at temperatures in the vicinity of T_c. For sharp transitions the two methods will result in the same temperature; for broader transitions discrepancies will occur. In addition, the electrical resistivity gives a measure of the relative broadness of the transition. As mentioned earlier, this relative broadness is expected to be larger at lower concentrations.

Measurements on PdFe (Mydosh et al. 1968, Kawatra et al. 1968, 1970) and on PdMn (Nieuwenhuys 1975), shown in figs. 16a,b, confirm this picture. The resistivity can also be used to determine the type of magnetic ordering. The so-called resistivity step, $(\Delta\rho(T = T_c) - \Delta\rho(T = 0))$, depends on the character (ferromagnetic, antiferromagnetic or mixed) of the ordering. We will come back to this point.

Measurements of the thermopower, Q, of Pd-based alloys as a function of temperature have been performed by Gainon and Sierro (1970). These measurements do not add more new information about the magnetic ordering than electrical resistance does. There are indications that dQ/dT behaves similar to $d\rho/dT$ and gives significance to the speculation that a "divergence" in the temperature derivative of a particular transport property determined the critical temperature (Tang et al. 1971, Parks 1972).

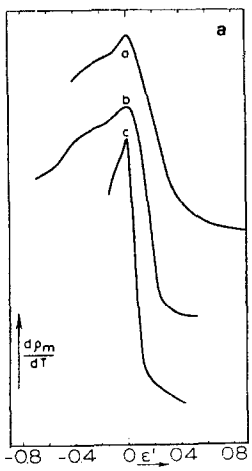

Fig. 16a. $d\Delta\rho/dT$ as a function of $\epsilon = (T - T_c)/T_c$. Curve (a) refers to PdFe 0.25 at.%, (b) to PdFe 0.5 at.% and (c) to PdFe 3 at.%. Data sources: Mydosh et al. (1968), Kawatra et al. (1969 and 1970).

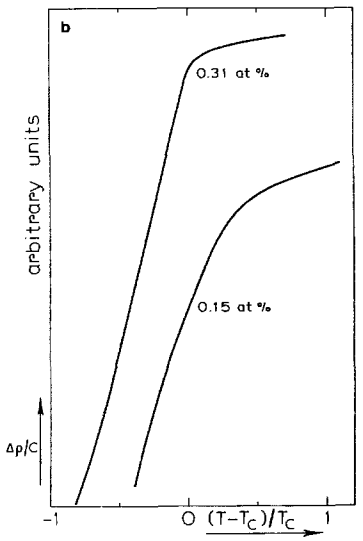

Fig. 16b. The incremental resistivity of PdMn 0.15 at.% and 0.31 at.% as functions of $\epsilon = (T - T_c)/T_c$.

3.1.2. Microscopic properties

Mössbauer effect (ME), nuclear orientation (NO) and NMR (on impurity atoms)

With both the Mössbauer effect and the nuclear orientation method it is possible to measure the effective magnetic field at the nucleus. Suitable Mössbauer nuclei are ^{57}Co, and ^{57}Fe. ^{54}Mn is useful for the nuclear orientation studies. Mössbauer effect studies of giant moment systems have been performed by: Nagle et al. (1962) on PdCo, Craig et al. (1962) on PdFe, Kitchens et al. (1965) on PtFe, Craig et al. (1965a) on PdFe, Craig et al. (1965b) on PdFe, Woodhams et al. (1966) on PdFe, Maley et al. (1967) on PdFe and PtFe, Dunlap and Dash (1967) on PdCo, Segnan (1967) on PtFe, Trousdale et al. (1967) on PdFe, Alekseevski et al. (1968) on PdSnCo (also NO), Reivari (1969) on PdCo, Carlow and Meads (1969) on PdFe, Clark and Meads (1970) on PdRhFe, Ericsson et al. (1970a) on PtFe, PtCo, PdCo and PdFe, Ericsson et al. (1970b) on PtCo and PtFe, Erich et al. (1970) on PdNi, Maletta (1972) on (Ni_3Ga)Fe, Tansil et al. (1972) on PdNi, Liddell and Street (1973) on (Ni_3Ga)Fe and (Ni_3Al)Fe, Levy et al. (1974) on PdAgFe, Scherg et al. (1974) on PtFe and by Gierisch et al. (1977) on PdFe.

Nuclear orientation studies have been carried out by: Cracknell et al. (1967) on PdCo, Gallop and Campbell (1968) on PtCo, Balabanov et al. (1969) on PdSnCo, Ali et al. (1974) on PtCo, Thomson and Thompson (1976, 1977) on PdMn and PdHMn, Flouquet et al. (1977, 1978) on PdCo and PdMn and by Benoit et al. (1977) on PdCo and PdMn. Finally nuclear magnetic resonance experiments on the nuclei at the impurity sites have been done by: Ehara (1964) on PdCo, Budnick et al. (1966) on PdFe, Skalski et al. (1968) on PdFe and Katayama et al. (1976) on PdNiCo.

It has been experimentally demonstrated that the observed splitting of the Mössbauer resonance is proportional to the macroscopic magnetization of the impurities. The great advantage of the Mössbauer effect over the macroscopic magnetization measurements is that it can be carried out on very dilute samples and if necessary in zero external field. Using the Mössbauer effect it could be proven that the giant moments also exist in the paramagnetic state (very dilute alloys), and a spontaneous magnetization occurs (in zero field) below the ferromagnetic transition temperature (e.g. PdCo, Dunlap and Dash (1967) and PdFe, Craig et al. (1965) and Trousdale et al. (1967)). It should be noted that the ratio between the effective magnetic field at the nucleus, $H_{\text{eff}}^{\text{sat}}$, and the magnetic moment, M_{sat}, is not known with great accuracy. Fits of the Mössbauer effect results to Brillouin functions therefore contain an extra parameter ($H_{\text{eff}}^{\text{sat}}/M_{\text{sat}}$). Bearing in mind the discussion about the difficulty to describe the magnetization of most of the giant moment alloys by a Brillouin function, the conclusions from fits of Mössbauer effect data to Brillouin functions should be considered with some care. Particularly, a wrong choice of the magnetic quantum number may greatly influence the results for the saturation moment (Nieuwenhuys 1975).

The Mössbauer effect and especially the nuclear orientation method enable (or sometimes force) the experimentalists to go to very low temperatures, where, if Kondo or spin fluctuation effects play a role, discrepancies from normal behaviour should be found (e.g. an unexpected decrease of the magnetic moment with decreasing temperature). Apart from the macroscopic behaviour the first indications for such anomalous behaviour have been found by Maley et al. (1967) in PtFe. Additional evidence has also been found by Gallop and Campbell (1968), Ali et al. (1974), Scherg et al. (1974), Flouquet et al. (1977a) for PdFe, PtCo and PdCo. Further, the measurements of the nuclear magnetic resonance of the host metal nuclei in PtCo by Graham and Schreiber (1966, 1968) did show a decreasing moment with decreasing temperature. On the other hand, nuclear orientation experiments by Benoit et al. (1977) and by Flouquet et al. (1977b) proved that PdMn behaves within the experimental error as it should according to a Brillouin function with $J = \frac{5}{2}$ and $g = 3$, thus in complete agreement with magnetization and specific heat observations. In the row of the 3d-metal giant moments Mn forms an exception, due to its normal behaviour.

As long as it was assumed that $|H_{\text{eff}}/H_{\text{eff}}^{\text{sat}}|$ is proportional to $|M/M_{\text{sat}}|$ interpretations of the results obtained from ME, NO or NMR measurements could be made fairly easily in terms of the magnetization, provided appropriate allowance was made for relaxation effects compared to the time window of the experiment. Difficulties in the interpretation arise when the magnitude and the sign of the effective field at the nuclei of the impurities are considered. We reproduce here table 4, published by Katayama et al. (1976), of the experimental hyperfine fields. According to these authors the positive sign of the hyperfine fields on Co and Ni in Pd is a puzzle. The rules, which these systems are expected to follow, are well established from measurements on a large number of ferromagnetic alloys (Kobayashi et al. 1966). Also the other systems mentioned in the table do follow these rules. Two possible origins for the positive contribution to the hyperfine

TABLE 4
Experimental values of the hyperfine fields (1 kOe = 0.1 T)

System	Experimental H_{eff} (kOe)
PdMn	−360*
PdFe	−304
PdCo	+230
PdNi	+190
PtMn	−375*
PtFe	−316
PtCo	−180

*Gallop (1969).

field can be suggested. One cause may be a strong s–d interaction, so that via this interaction the 4s-electrons give rise to a positive polarization. It is, however, unreasonable to assume such an interaction to be present in PdNi and PdCo and not in e.g. PdFe or PdMn. Another possible explanation may be an orbital momentum at the impurity site. Such orbital moments would be associated with the quadrupole effect due to the non-spherical distribution of electrons at the magnetic site. Indications for quadrupole effects have been found in the Mössbauer effect on PdNi (Tansil et al. 1972) and in the NMR investigations on PdCo by Katayama et al. (1976). Also the observed magnetocrystalline anisotropy, observed in the ferromagnetic resonance (Baggauley and Robertson 1974) and in the electrical resistivity (Senoussi et al. 1977) point towards orbital moments for PdCo and PdNi. Why PdCo and PtCo behave differently in this respect is still a puzzling question.

Electron paramagnetic resonance (EPR)

For the giant moment alloy systems, only the electron paramagnetic resonance of Mn in Pd has been intensively investigated, and one observation on PdFe has been reported. (The intensive EPR investigation on Pd-rare earth systems, reported in the literature (see Taylor 1975) falls beyond the scope of this chapter.)

The interpretation of the electron paramagnetic resonance in dilute magnetic alloys may be hindered by the so-called "bottleneck effect" (Hasegawa 1959). This effect is caused by the different strengths of the coupling of the conduction electrons to the impurity and the coupling of the conduction electrons to the lattice, which joins the resonances of the impurity and conduction electrons and leaves them disconnected from the lattice. However, Coles et al. (1975) concluded from their experiments that PdMn is not bottlenecked. The first detailed investigation of the EPR in PdMn has been carried out by Shaltiel and Wernick (1964), later such investigations were extended by Cottet (1971). Large positive g-shifts have been found by these authors and also more recently by Alquie et al. (1974) (see table 5). The influence of the magnetic ordering on the EPR

TABLE 5
Summary of EPR data for Mn in Pd

Reference	Conc. (at.%)	Frequency GHz	g-value	$\frac{d\Delta H}{dT}$ (GK^{-1})
Shaltiel et al. (1964)	2	9	2.08	—
Cottet (1971)	0.23	35	2.18	—
	0.5		2.15	95
	1.0		2.12	80
	1.5		2.12	80
	2.0		2.12	70
Shaltiel, Wernick (1964)	2	50	2.105	—
Alquié et al. (1974)	0.1	10.9	2.12	55
	1		2.12	—
	2		2.12	40
Coles et al. (1975)	0.6	9	2.15 ± 0.02	50
	0.9		2.14 ± 0.01	62
	2.3		2.13 ± 0.01	55
	2.5		2.15 ± 0.01	57
	3.75		2.14 ± 0.02	40
	4.6		2.16 ± 0.02	47
	5.5		2.16 ± 0.02	58
	6.0		2.16 ± 0.02	52
	7.0		2.17 ± 0.03	—

($1\ GK^{-1} = 10^{-4}\ T\ K^{-1}$).

properties of PdMn has been studied in detail by Coles et al. (1975). The rather peculiar magnetic ordering as a function of concentration is clearly revealed by the EPR results. Taylor (1975) has reviewed the area of EPR on magnetic ions in metals and in particular the PdMn system. The collection of these various data are given in table 5 which is taken from the review of Taylor (1975).

The origin of the large positive g-shifts might be the same as that of the giant moment itself. However, assuming no bottleneck effect, the g-values in EPR are still smaller than those deduced from the specific heat (Nieuwenhuys 1975) and magnetization (Star et al. 1975), using $g_{\text{eff}} = g(1 + \alpha\chi_{\text{Pd}})$. Very recently this discrepancy has been eliminated by the experiments of Alquie et al. (1978). They observed EPR in very dilute PdMn alloys and from their results it can be concluded that PdMn is at least partly bottlenecked, since (i) the observed field for resonance is temperature dependent, (ii) the variation of the linewidth with T is non-linear, and (iii) the coupling to the lattice can be increased by cold working or addition of Pb. From the analysis of these results, the authors find that the g-value of bare Mn is 2.1 and that of the Pd d-band electrons is 2.25, which implies that the true (unbottlenecked) Korringa g-value and linewidth slope for Mn in Pd are $g_K = 3.1$ and $d\Delta H/dT = 0.3\ T/K$ [= 300 Gauss/K]. Note that this g_K is in excellent agreement with the effective g-values obtained from magnetization and specific heat.

An observation of the electron paramagnetic resonance of Fe in Pd has been

reported by Devine (1976, 1977), who obtained from his experiments a g-value of 2.15 and a slope of the linewidth, $d\Delta H/dT$, of 0.0031 T/K [31 G/K] when extrapolated to zero concentration. From these values he calculated an exchange parameter, which is in agreement with that obtained from resistivity measurements. Note also that the g-value observed in EPR is much smaller than the value needed to describe the giant moments. Although we assume on the basis of other experimental results that the observation of EPR in PdFe might be possible, there is some doubt about Devine's result, since the temperature at which his observations were possible did not exceed 5 times T_c. At these temperatures small ferromagnetic clusters (due to short range order) have been observed in PdFe (Malozemoff and Jamet 1977, Nieuwenhuys 1975). In spite of many efforts, the paramagnetic resonance of none of the other giant moment systems has yet been observed.

Nuclear magnetic resonance (host metal nuclei)

Investigations of the nuclear magnetic resonance of the host metal nuclei have been carried out by Itoh and Kobayashi (1966) on PtFe, PtCo, PdFe and PdCo, by Graham and Schreiber (1966, 1968) on PtCo and by Sablik et al. (1973) on PdFe. Two kinds of information may be extracted from these investigations. The resonance frequency contains information about the effective magnetic field at the host nuclei (thus at some distance from the magnetic atoms) and from the relaxation rate, information about the influence of the impurity atoms on the electron–nuclei interaction can be deduced.

Itoh and Kabayashi (1966) found a broad resonance spectra for PtFe 1 at.% in the ferromagnetic phase, in which several maxima could be observed. By assuming these maxima to be due to the different neighbours shells (the maximum at the highest frequency due to the first nearest neighbour Pt with respect to Fe, etc.), a plot of the relative polarization at the Pt atoms as a function of the distance from a Fe atom can be made. We have reproduced this plot in fig. 17. This graph confirms the generally accepted picture of giant

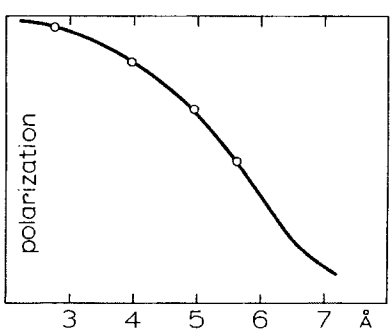

Fig. 17. Relative polarization of Pt atoms as a function of the distance from the Fe impurity (after Itoh and Kobayashi 1966).

moments. According to Itoh and Kabayashi (1966) similar results have been obtained for PtCo, PdFe and for PdCo. They observed a relaxation rate, T_1T, of 0.13 s K in PdFe which is slightly larger than that of pure Pd(0.11 s K, Narath et al. 1966). They did not investigate the concentration dependence of the relaxation rate in PdFe, contrary to Sablik et al. (1973) who found large concentration dependencies of the relaxation rate, resulting in a sharp maximum at 0.5 at.%. These latter authors ascribe this maximum in T_1T to a concentration dependent intra-atomic Coulomb interaction in PdFe. The Fe atoms are supposed to increase this interaction at the lowest concentration, whereas at higher concentrations the saturation of the polarization of the Pd atoms plays a role. The combination of the two effects causes the maximum in T_1T.

Positive muon spin rotation (μ^+SR)

One of the most recent techniques to investigate internal magnetic fields in magnetic substances is the μ^+SR. This method consists of implanting a beam of μ^+ into the alloy and then measuring the Larmor precession frequency (proportional to the magnetic field at the μ^+ site) by observing oscillations in the emitted positron intensity ($\mu^+ \rightarrow e^+ + \tilde{\nu} + \nu$ in 2.2 μs) at some fixed angle. For an extended description of this technique the reader is referred to Kossler (1975) and Yamazaki (1977). For the purpose of this chapter it is important to note that this new technique enables the experimentalists to measure the (mean) magnitude and the width of the distribution of internal fields, almost without disturbing the magnetic system.

Two PdFe samples (0.015 at.% and 0.28 at.%) have been investigated by Nagamine et al. (1977a,b,c). They find that the relative widths of the internal field distribution are 18.5 and 3 for 0.015 and 0.28 at.% sample, respectively. The authors consider this result as an evidence for the spin glass ordering in the more dilute sample. (Theoretically, spin glass-like ordering is expected at the lowest concentration (Nieuwenhuys 1978).) However, it should be noted, as mentioned earlier in this chapter, that the distribution of internal fields becomes much broader with decreasing concentration, albeit the interaction may remain ferromagnetic for the main part. In section 4.1 this distribution has been calculated.

Diffuse magnetic neutron scattering

In this article we have been attempting to describe the phenomena observed in giant moment systems by assuming these giant moments to consist of a bare magnetic moment due to the solvent atom itself surrounded by a cloud of partly polarized host material atoms. Evidence for the existence of such magnetic entities may be obtained from diffuse neutron scattering measurements. An extensive description of this and other neutron scattering techniques can be found in Marshall and Lovesey's book (1971). Diffuse neutron scattering experiments have been performed by Cable et al. (1965) and by Phillips (1965) on PdFe alloys, by Low (1965, 1969), Low and Holden (1966) and Hicks et al. (1968) on PdFe and PdCo alloys, by Aldred et al. (1970) on PdNi alloys, by Cable and Child (1972) on (Ni_3Ga)Fe, by Ling and Hicks (1973) on (Ni_3Al)Fe compounds,

by Dorofeyev et al. (1976) on PdFe alloys, by de Pater et al. (1975) and by Cable and David (1977) on PdMn alloys.

From these measurements it became clear that the bare moment of Fe and Co is of order of $3\mu_B$. According to de Pater et al. (1975) the bare moment of Mn in Pd is about $5\mu_B$, in agreement with specific heat and with EPR investigations. Cable and David (1977) performed scattering experiments with polarized neutrons, thereby avoiding possible errors due to critical scattering. They conclude a bare moment of $4\mu_B$ for Mn in Pd, however, they did assume a rather small number of antiferromagnetically coupled Mn atoms (in view of the magnetization results of Star et al. (1975)), which may have caused an underestimate of the bare moment. The rest of the giant moment is spatially distributed over the matrix. A plot of this spatial distribution for PdFe and PdCo as obtained by Low and Holden (1966) is reproduced in fig. 18. In view of this plot it seems evident that our picture of the giant moments is basically correct as confirmed by neutron scattering data. Similar results have been obtained for Fe in Ni_3Ga by Cable and Child (1972), who also reported a large critical scattering amplitude at temperatures in the vicinity of T_c.

Although no adequate theory for the critical scattering phenomena exists (certainly not for critical scattering in random dilute alloys) this scattering is obviously related due to the divergence of the magnetic susceptibility at T_c (and the large increase in the fluctuations and correlations of the magnetization). The dependence of the critical scattering amplitude on the scattering vector, q, contains information on the correlation length of the magnetic ions. In very recent experiments Verbeek et al. (1978b) and Verbeek (1979) investigated the critical scattering in PdMn and in PdFe. Their preliminary conclusions are that the scattering amplitude is sharply peaked as a function of temperature, and that the correlation lengths for these random ferromagnetic alloys are extremely large (more than 20 Å). Remarkably, the critical magnetic neutron scattering is

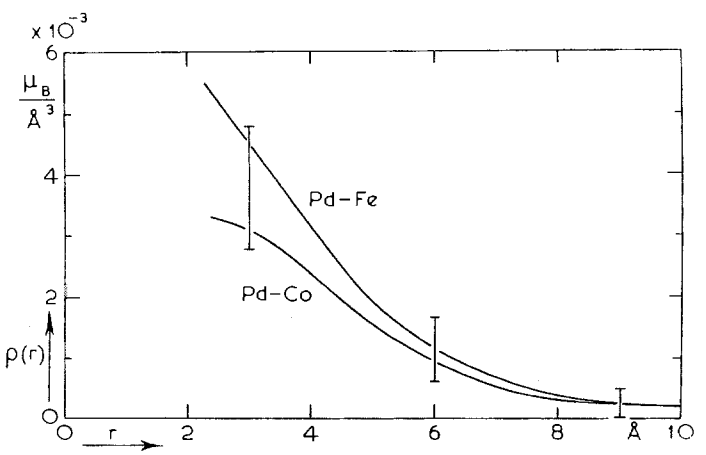

Fig. 18. Magnetic moment density as a function of the distance from the solute site in dilute PdFe and PdCo alloys (after Low and Holden 1966)

the only sharply peaked property of dilute PdFe alloys observed up to now. These experiments also showed that critical scattering effects should be taken into account when analyzing small angle scattering on "single" moments, such as those performed by Low and Holden (1966). Nevertheless, the general picture of the giant moment is not destroyed by these latest experiments [see Verbeek (1979)].

3.1.3. Curie temperature determination and properties of other giant moment systems

As previously mentioned, the determination of T_c of dilute Pd-based alloys with Co, Fe and Mn (and also of the other dilute giant moment alloys) is not always straightforward. The broadness of the transitions to ferromagnetism makes it possible to obtain different results from different experiments. Nevertheless, the concentration dependence of T_c can be explained rather well in the case of Pd-based alloys. As discussed in section 3.1, the interaction strength as a function of distance is given by $r^{-1}\exp(-r/\sigma)$. From microscopic experiments (see section 3.1.2) σ is known to be of order of 3 Å for Pd. Assuming $J(r_0)$ to be proportional to $r_0^{-1}\exp(-r_0/\sigma)$, where r_0 is the mean distance between the magnetic impurities, a comparison with the experimental values can be made (Nieuwenhuys 1975) and this is shown in fig. 19. It should be noted that at still larger concentrations T_c will increase less rapidly than proportional to c since then the d-band becomes magnetically saturated and the magnitude of the moment per atom decreases.

So far the discussion has been mainly restricted to Pd-based alloys with Fe,

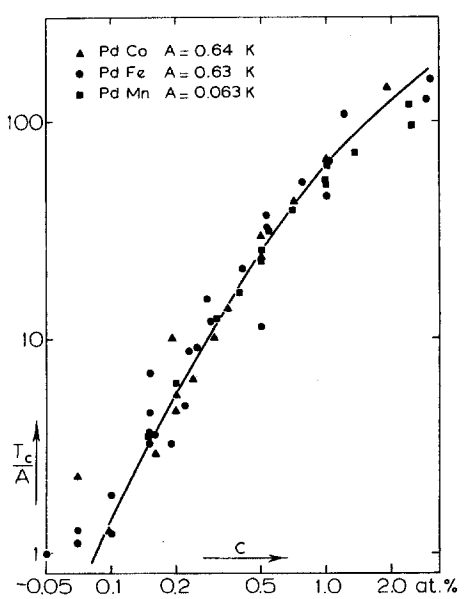

Fig. 19. The ferromagnetic transition temperature of PdCo (▲), of PdFe (●) and of PdMn (■) as a function of the concentration. The solid line results from a calculation by Nieuwenhuys (1975).

Co or Mn, we now briefly consider the properties of the other giant moment systems. The related alloy PdNi has special features. This system is characterized by a critical concentration for the occurrence of magnetic moments, which might be explained by a high spin fluctuation temperature. Detailed descriptions of the work on PdNi alloys may be found in papers by Chouteau et al. (1968a,b), Schindler and Mackliet (1968), Aldred et al. (1970), Van Dam (1973), Chouteau et al. (1974), Beille and Chouteau (1975), Murani et al. (1974) and Chouteau (1976). The general view of this system is a model in which single Ni atoms and pairs are not magnetic, but groups of three or more neighbouring atoms are magnetic (due to the stabilization of the fluctuations by a more magnetic local environment (Chouteau, 1976)). This means that the transition non-magnetic⇄magnetic occurs gradually, the largest change as a function of concentration is found at 2.3 at.% Ni (Murani et al. 1974). On the other hand, Ododo (1978) used the Landau expansion of the Gibbs free energy to analyze the experimental data on PdNi. He concludes a critical concentration of 2.8 at.% Ni, which coincides with the maximum in the linear term of the specific heat as a function of concentration (Van Dam 1973).

Theoretical calculations on the PdNi system considering a possible critical concentration have been carried out by Harris and Zuckermann (1972), Kato and Shimizu (1972), Levin et al. (1972), Edwards et al. (1973), and Kato and Mathon (1976). In the first three papers the zero-temperature susceptibility has been calculated within the CPA approximation. Kato and Shimizu used a numerical procedure to include a more realistic generalized susceptibility for Pd, while the others used an approximation for $\chi(q)$. All these three works find or assume a critical concentration for PdNi of about 2.3 at.%. Edwards et al. (1973) used the Landau expansion for the free energy to calculate the susceptibility of PdNi. Their results indicate a critical concentration of 1.8 at.%. Finally, Kato and Mathon (1976) have argued that no critical concentration is present in PdNi alloys, since the results obtained thus far are due to spurious solutions of the Landau equations. This then brings us back to the gradual change in the magnetic properties of PdNi mentioned above. These results on PdNi force us to consider the stability of the magnetic moments as a function of concentration. The instability (or non-existence) of magnetism, i.e. weak moments, is generally characterized by a spin fluctuation temperature, T_{sf} which is concentration dependent, (see section 1.1).

In the electrical resistivity terms proportional to $\log(T/T_{sf})$ (Kondo or spin fluctuation type) and in the magnetization (and Mössbauer effect) temperature dependent magnetic moments have been found. In most cases a decrease of the magnetic moments has been observed below T_{sf}. Investigations of this effect on a variety of Pd and Pt based alloys have been performed by Gallop and Campbell (1968); (PtCo); Shen et al. (1969) (PtCo); Loram et al. (1971) (PdCo); Loram et al. (1972) (PtFe); Tissier and Tournier (1972) (PtCo); Costa-Ribiero et al. (1974) (PtCo); Scherg et al. (1974) (PtFe); Ali et al. (1974) (PtCo); Swallow et al. (1975) (PtCo), and Williams et al. (1975a,b) (PtCo). Williams (1976) has proposed an explanation for this non-stable behaviour based on the configura-

tion-fluctuation approach (Hirst 1970, 1971). According to Williams the spin fluctuations/Kondo behaviour of the giant moments might be caused by configuration fluctuations of the bare moments. In fig. 20 we reproduce his graph of the characteristic temperature versus alloy composition. We also ascribe the peculiar paramagnetic behaviour of PdCo, PtCo, PdFe and PtMn alloys to such weak moment effect. It can be seen that PdMn has the lowest characteristic temperature, which would agree with the experimental results of a stable moment.

Since the magnitude of the giant moment is given by $\mu = \mu_{bare}(1 + \alpha\chi_0)$ it is very interesting to compare the results obtained on Pd-based alloys to results on alloys with host materials of which the exchange enhancement, Ξ, can be varied. Base materials with the highest exchange enhancement factors (of order of 35) are Ni_3Al and Ni_3Ga (de Boer et al. 1967, 1969, de Chatel and de Boer 1970). The magnetic moment per dissolved Fe atom in these base materials is expected to be very large, as has also been found from magnetization measurements (Schinkel et al. 1968, Maletta and Mössbauer 1970, Schalkwijk et al. 1971, Maletta 1972, Cable and Child 1972, Liddell and Street 1973, Ling and Hicks 1973). In table 6 we collect the results as obtained by several authors.

It is of course important to determine whether the assumption of μ being proportional to $(1 + \alpha\chi_0)$ holds for these giant moment systems. Since Ni_3Ga compounds can be made with slightly different compositions, thereby changing χ_0 over a wide range, this assumption can be tested on $(Ni_3Ga)Fe$ and other similar alloys, as has been carried out by Schalkwijk et al. (1971). In fig. 21 their plot of μ versus χ_0 is reproduced, from which it is clear that the linear response picture of the giant moment holds fairly well. On the basis of this experimental result one would expect similar behaviour for Pd-type alloys.

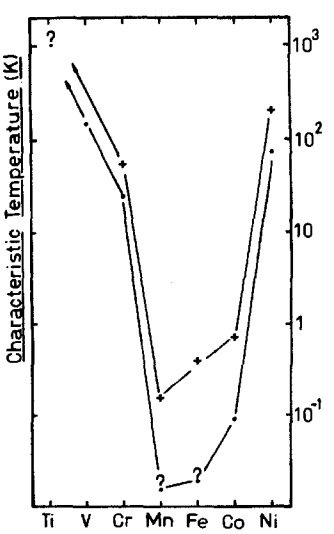

Fig. 20. The estimated characteristic temperature (in K) for various 1st transition series impurities in Pd (·) and Pt (+) (after Williams 1976).

TABLE 6
Magnetic moments per dissolved Fe atom in Ni_3Al and Ni_3Ga base materials

Alloy		Method	Reference	T_c [K]	μ [μ_B]
$(Ni_{74.0}Ga_{26.0})Fe$	10 ppm	Mössb.	Liddell and Street (1973)		21
$(Ni_{74.5}Ga_{25.5})Fe$	10 ppm	Mössb.	Liddell and Street (1973)		69
$(Ni_{75.1}Ga_{24.9})Fe$	10 ppm	Mössb.	Liddell and Street (1973)		84
$(Ni_{75}Ga_{25})Fe$	20 ppm	Mössb.	Maletta (1972)		58
$(Ni_{75}Ga_{25})Fe$	250 ppm	Mössb.	Maletta (1972)	11	40
$(Ni_{75}Ga_{25})Fe$	0.05 at.%	Magn.	Schinkel et al. (1968)	13.4	36
$(Ni_{75}Ga_{25})Fe$	0.1 at.%	Magn.	Schinkel et al. (1968)	27	29
$(Ni_{75}Ga_{25})Fe$	0.1 at.%	NS	Cable and Child (1972)	28	33
$(Ni_{75}Ga_{25})Fe$	0.2 at.%	Magn.	Schinkel et al. (1968)	41	24
$(Ni_{75}Ga_{25})Fe$	0.9 at.%	NS	Cable and Child (1972)	80	9.5
$(Ni_{75}Ga_{25})Fe$	1 at.%	Magn.	Schinkel et al. (1968)	85	12
$(Ni_{73.5}Al_{26.5})Fe$	10 ppm	Mössb.	Liddell and Street (1973)		25
$(Ni_{74}Al_{26})Fe$	10 ppm	Mössb.	Liddell and Street (1973)		32
$(Ni_{74.5}Al_{25.5})Fe$	10 ppm	Mössb.	Liddell and Street (1973)		34
$(Ni_{74.5}Al_{25.5})$		Magn.	Ling and Hicks (1973)	16	
$(Ni_{74.5}Al_{25.5})Fe$	0.2	Magn.	Ling and Hicks (1973)	46	18
$(Ni_{74.5}Al_{25.5})Fe$	0.5	Magn.	Ling and Hicks (1973)	70	14
$(Ni_{74.5}Al_{25.5})Fe$	1	Magn.	Ling and Hicks (1973)	79	8

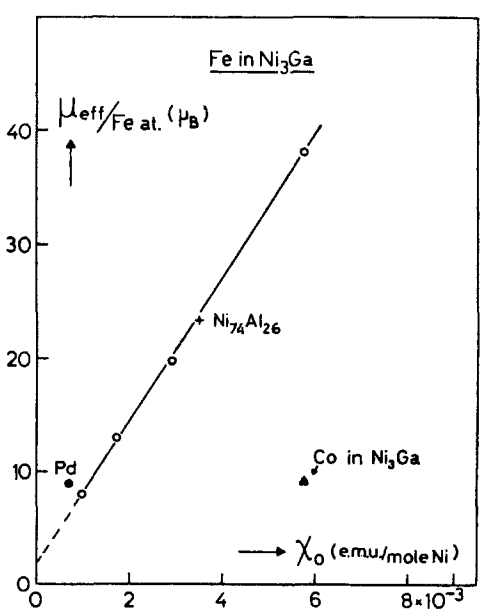

Fig. 21. Effective moments per iron atom as a function of the host matrix susceptibility per mol nickel. Values for iron in palladium and in $Ni_{74}Al_{26}$ and for Co in $Ni_{75}Ga_{25}$ are included for comparison (after Schalkwijk et al. 1971).

Susceptibility measurements on PdAg and on PdRh alloys (Budworth et al. 1960, Doclo et al. 1969) have shown an increase in the susceptibility compared to that of pure Pd upon alloying with Rh ($c < 5$ at.%) and a decrease upon alloying with Ag. Specific heat investigations (Hoare and Yates 1957, Budworth et al. 1960, Huq and Moody 1977, Verbeek private communication) do show qualitatively the same behaviour for the contribution of the $\gamma \propto N(0)$-term. Since the transition temperature is proportional to the magnitude of the susceptibility, similar influences on T_c are to be expected upon alloying with Ag or Rh. Other metals, like Cu, Sn and Pt act in the same way as Ag. Therefore, a number of studies have focussed on these alloys, (see table A.1 in the appendix, "other alloys"). The main features of these investigations are:

(i) The magnitude of the giant moment is not proportional to the matrix susceptibility (Guertin and Foner 1970).

(ii) The transition temperatures are not proportional to the matrix susceptibility (Nieuwenhuys 1975).

(iii) At higher Ag concentrations, PdAgFe alloys become a spin glass (Budnick et al. 1975).

The first two results can be explained by the fact that one does not only change the matrix susceptibility upon alloying, but also introduces extra scattering centres in the alloy, so that a direct comparison to pure Pd becomes impossible.

As mentioned in section 1.3 the oscillatory character of the interaction (RKKY) may become important in giant moment alloys at the lowest concentration (large distance between magnetic moments, see also section 4.2. For PdFe this concentration may be 0.05 at.% or smaller (Chouteau et al. 1971, Nieuwenhuys 1978). For Pt-based alloys, this concentration is much larger because of the smaller exchange enhancement. A great number of the Pt-based alloys mentioned in table A.1 order like spin glasses. For Co and Fe in Pt the boundary may be 0.5–1 at.%. The PtMn system forms an exception again since at small concentration this is a spin glass because of the RKKY oscillations and at larger concentrations it is a spin glass due to direct antiferromagnetic interactions (to be discussed below). Spin glass behaviour is therefore found over the whole concentration range (Sarkissian and Taylor 1974, Tholence and Wassermann 1977).

Indirect (RKKY type) interactions are not the only possible antiferromagnetic interaction. Direct (nearest neighbour) interaction between Mn-ions are also antiferromagnetic. This fact leads to a peculiar type of spin glass in PdMn at higher concentrations (also in PtMn). It was already known from magnetization measurements by Rault and Burger (1969) that PdMn alloys with concentrations larger than 8 at.% did order antiferromagnetically. This could be interpreted by assuming that the direct Mn–Mn coupling (being of great importance at these concentrations) is antiferromagnetic, in contrast to the ferromagnetic indirect interactions, which prevail at larger distances between the magnetic ions. The resistivity measurements by Williams and Loram (1969a,b) made clear that also at smaller concentrations a partly antiferromagnetic ordering was present. This was deduced from the fact that the resistivity step $[\Delta\rho(T = T_c) - \Delta\rho(T = 0)]$ was

smaller than expected on the basis of measurements in strong external fields. Later on the work of Coles et al. (1975), of Zweers and Van den Berg (1975) and of Star et al. (1975) showed that antiferromagnetic interactions are important in PdMn alloys as soon as the concentration is larger than 0.5 at.%. Star et al. (1975) and Nieuwenhuys and Verbeek (1977) concluded from various experimental results that up to the third nearest neighbour distances the interaction between Mn atoms is dominated by the direct antiferromagnetic interaction. This causes PdMn alloys in the concentration range from 3 to 10 at.% to be peculiar alloys in which the direct antiferromagnetic and the indirect ferromagnetic interactions are of comparable importance. Therefore, in this concentration range, PdMn may be called a spin glass, for a discussion of which one is referred to section 3.2.

3.2. Spin glass freezing

Although interacting dilute alloys have been investigated over many years, it was only recently that sharp effects were found at well-defined temperatures. In order to explain an additional (linear at low temperatures) contribution to the specific heat of AgMn (de Nobel and du Chatenier 1959) and CuMn (Zimmermann and Hoare 1960), Marshall (1960), and Klein and Brout (1963) developed molecular field theories for these systems using a probability distribution $P(H)$ of internal fields. Study of the susceptibility in fields around 0.1 T [1000 G] revealed a broad maximum at a temperature where the magnetic remanence disappeared (Lutes and Schmit 1964). These results were interpreted within the random molecular field model (Klein 1964, 1968, 1969 and Klein and Shen 1972). Further experiments of Kouvel (1960, 1961) on magnetization, remanence, resistivity and field cooling showed peculiar properties, as for example, a displaced hysteresis loop. This led Kouvel (1963) to suggest a model which describes the magnetic properties in terms of mutually interacting ferromagnetic and antiferromagnetic domains. In this model the susceptibility maximum corresponds to the disappearance of a strong magnetic anisotropy.

By employing a very low field (≈ 0.5 mT[$\approx$ 5G]) ac susceptibility technique, Cannella et al. (1971) discovered sharp peaks in the temperature dependence of the susceptibility. A sensitive external magnetic field dependence of χ was also observed in the T-region of the peak (Cannella and Mydosh 1972). Even for applied fields as small as 0.01 T [100 G], a noticeable smearing of the χ-peak occurred, and the susceptibility behaviour approached that of the previous measurements by Lutes and Schmit (1964). These results were then correlated with a series of earlier Mössbauer investigations (Borg et al. 1963, Craig and Steyert 1964, Gonser et al. 1965, Violet and Borg 1966, Window 1969, 1970, Window et al. 1970) which also found magnetic transitions characterized by the sudden onset of hyperfine splitting at well-defined temperatures. The susceptibility peak temperature agreed well with the Mössbauer splitting temperature (Borg and Kitchens 1973). Initially, there was certain confusion as to the nature of the magnetic ordering. The sharpness of the experimental effects indicated a

long range antiferromagnetic order, and the connotation antiferromagnetism was often applied. However, Arrott (1965, 1966) by analyzing his neutron scattering data had already pointed out the absence of long range magnetic order in these types of alloys. Random alignments of frozen spins were extracted from the analysis of the Mössbauer lines and their intensity ratios (Borg 1970). Thus, the ideas of randomness, disorder and amorphism became articulated in the concept "spin glass", and a most intriguing question presented itself: order out of randomness?

We now proceed to discuss the various experiments performed on spin glass systems. A division is made here between the macroscopic and microscopic properties. In addition, three regions of temperature are noted: above, below and at the freezing temperature. Finally a simple phenomenological model is used to describe the freezing process and a collection of freezing temperatures for some characteristic alloys is given.

3.2.1. Macroscopic properties

Susceptibility

We limit ourselves to the low field (<0.01 T[100 G]) susceptibility χ and include the Faraday and other high field methods in the section on magnetization. The first measurements in small fields were carried out by Cannella et al. (1971, 1972) using a very sensitive, low audio frequency, mutual inductance bridge which required a driving field of ≈ 0.5 mT [5 G]. The temperature dependences for a series of AuFe alloys are shown in fig. 22. This figure further represents the typical behaviour for all the spin glass alloys (Cannella and Mydosh 1973,

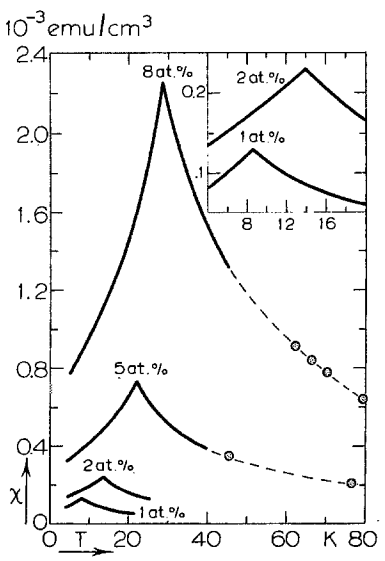

Fig. 22. Low field susceptibility $\chi(T)$ for four AuFe alloys. After Cannella and Mydosh (1972).

1974a,b). The remarkable feature of these measurements is the sharp, cusp-like peak which occurs. Such distinct temperature effects were totally unexpected on the basis of the random molecular field model and the previous high field Faraday susceptibility. The magnitude of the peak is rather small. Above the peak temperature which we denote as the freezing temperature T_f, a modified Curie–Weiss form, $\chi = ng^2\mu_B^2 S(S+1)/3k_B(T-\theta)$, may be obtained with both S and θ functions of the concentration. n is the density of magnetic atoms, S their spin angular momentum (for simplicity we neglect possible orbital contributions), and θ the paramagnetic Curie temperature.

At low temperatures, $\chi(T) = \chi(0) + bT^n$ with $n \approx 2$. Thus χ extrapolates to a finite value for $T \to 0$ and a ratio $\chi(0)/\chi(T_f) \approx 0.6$ is obtained for magnetic concentrations between ≈ 0.1 and a few atomic percent. These measurements have been extended to a variety of spin glass alloys which show the same general characteristics, and a collection of the important parameters are listed in table 7. The disadvantage of the mutual induction method is that for $T \gg T_f$ its accuracy is severely limited, and we are unable to follow the high temperature

TABLE 7
Salient parameters obtained from low field susceptibility measurements on noble metal-based spin glasses

	c[at.%]	T_f[K]	$P_{eff} = g\mu_B\sqrt{S(S+1)}$	$\chi(0)/\chi(T_f)$	θ[K]
AgMn	0.25	—	4.5 ± 0.5	—	~0
	0.5	2.7	4.2 ± 0.5	—	~1
	1.0	5.1	5.5 ± 0.5	0.58	~0
	2.0	9.0	6.5 ± 0.5	0.57	~2
	5.0	17.6	6.8 ± 0.5	0.48	~2
	10.0	30.8	7.4 ± 0.5	0.42	~6
CuMn	0.1	1.8	5.5 ± 0.5	0.58	~−2
	0.2	3.0	—	0.58	—
	0.5	6.4	5.4 ± 0.5	~0.5	~0
	1.3	12.3	6.0 ± 0.5	0.53	~0
	5.2	27.8	8.0 ± 1.0	0.50	~2
	8.8	42.5	10.0 ± 1.0	0.29	~9
	10.3	45.0	11.0 ± 1.0	0.28	~6
AuMn	0.2	1.6	—	—	—
	0.5	3.5	7.0 ± 1.0	0.60	~0
	1.1	5.7	7.3 ± 0.5	~0.65	~1
	2.0	8.3	10.6 ± 1.0	0.60	~−1
	5.7	17.5	11.5 ± 1.0	0.25	~7
	10.3	29.3	>20	0.12	—
AuFe	0.1	2.1	~3.3	0.60	~0
	0.2	3.0	~3.3	0.60	~0
	0.5	5.4	~3.3	0.60	~0

TABLE 7 (*contd.*)

	c [at. %]	T_f[K]	$P_{eff} = g\mu_B\sqrt{S(S+1)}$	$\chi(0)/\chi(T_f)$	θ[K]
AuFe	0.9	8.5	3.4	0.50	~ -2
	1.0	9.0	—	—	—
	2.0	13.9	3.6	0.50	~ -1
	5.0	22.2	4.9	0.39	~ 1.5
	7.6	27.9	7.1	0.27	~ 4
	12.0	36.0	11.4	0.11	~ 12
	13.0	38.0	15.5	0.11	~ 17
AuCr	0.2	4.1	4.0 ± 0.5	0.67	~ 0
	0.6	11.3	3.5 ± 0.5	0.68	~ 0
	0.9	14.3	4.4 ± 0.5	0.68	~ -5
	1.8	25.0	4.1 ± 0.5	0.69	~ -11
	3.5	40.0	—	—	—
	3.7	41.5	—	0.75	—
	6.1	60.0	—	~ 0.75	—
	10.8	92.0	—	—	—
AuCo	2.0	—	1.3 ± 0.2	—	—
	3.0	1.7	—	—	—
	4.0	3.2	—	—	—
	5.0	4.1	3.0 ± 0.5	0.28	~ -1
	7.0	6.7	4.5 ± 0.5	0.34	~ 2
CuFe	0.3	2.3	—	0.58	—
	0.7	5.0	6.0 ± 0.5	0.50	~ -2
	0.8	5.2	7.5 ± 1.0	—	~ -1
	1.0	6.0	7.5 ± 0.5	0.30	~ 0

Curie–Weiss tail. Furthermore, at very low concentrations ($\lesssim 0.1$ at.%), this method does not possess sufficient sensitivity, so superconducting quantum interferometry devices (SQUID) must be used. A series of such experiments have been able to follow the freezing temperature down to 10 mK with reduced concentrations $\gtrsim 10$ ppm (Hirschkoff et al. 1971a, b, c, Doran and Symko 1974a, b, Frossati et al. 1976). The SQUID technique (working sensitivity 10^{-6} emu/g) is in fact a magnetometer which requires an external field bias 1.0–10 mT [10–100 G]. So, at these very low T and c, a step, rather than a cusp, appears in the $M(T)/H$ dependence. This signifies a complete smearing of the freezing process with external field. At frequencies up to a few thousand Hz there was no apparent frequency dependence in χ (Cannella and Mydosh 1974a,b).

Another approach to the low field susceptibility has been to refine the Faraday method whereby fields of only ≈ 2.0 mT [20 G] are needed to perform measurements sensitive enough to detect the spin glass freezing. Using this static procedure, Guy (1975, 1977a,b, 1978) has observed a sharp peak in $\chi(T)$, confirming the a.c. method, under short time conditions. Nevertheless, when the

magnetization $M(H)$ is allowed to come into long time (a few hours) equilibrium at each temperature, a quite different behaviour of $\chi(T)$ is found for $T < T_f$. These experiments demonstrate that the true equilibrium ground state of a spin glass is obtainable only in zero field $\chi(T) = \lim_{H\to 0}[M(T)/H]$. For, the application of a very small static fields perturbs this state, and over a long time scale the spin glass slowly relaxes into a new metastable state. This occurs for $T \leq T_f$ and marks the onset of remanence, irreversibilities and thermomagnetic history.

Magnetization

There exists a large number of magnetization experiments which have been carried out long before the term spin glass came into use. A sampling of the general behaviour is given below. At high temperatures, M is initially linear in H and bends off at large fields. A simple Brillouin function does not easily fit the data. Instead a modified form was proposed by Beck (1972a,b), Mukhopadhyay et al. (1975) and Mukhopadhyay and Beck (1975)

$$M(H, T) = \chi_0 H + \bar{\mu} c' B\left[\bar{\mu}, \frac{H + \lambda(M - \chi H)}{T}\right]$$

(the parameters in this equation are χ_0 a field independent susceptibility, $\bar{\mu}$ the average moment with a concentration c' and λ a molecular field constant). Despite the four adjustable parameters, it is very difficult to obtain good agreement with the experimental data over a significant temperature interval. This prompted Beck to treat the magnetization in terms of dynamical clusters which begin forming at very high temperatures due to local correlations between the spins. By tabulating $\bar{\mu}$ and c' as the temperature is reduced, one obtains a growth of the average moments and a decrease in their concentration (Mukhopadhyay et al. 1975). The cluster formation ($\bar{\mu}$ and c' values) is strongly dependent upon the heat treatment used, and only for $T \gg T_f$ is the free ion paramagnetic moment found.

The M–H curves show the usual curvature as the temperature is reduced (Careaga et al. 1966, Borg and Kitchens 1973, Franz and Sellmyer 1973, de Mayo 1974). However, it is extremely difficult to saturate the magnetization even at very low temperatures and fields above 10 T [100 kG]. Here dM/dH remains finite. These magnetization studies yield no dramatic changes as the temperature is lowered through T_f, provided the measurements are begun in zero external field. Once field cooling and field cycling methods are used remanence, irreversibilities and relaxation appear at $T \leq T_f$. This marks a distinct contrast to the high temperature ($T > T_f$) behaviour where none of these effects occur.

Another way of handling the high field, high temperature magnetization is via the virial expansion theory of Larkin et al. (1970, 1971). They developed the free energy in a power series of the concentration in order to investigate the RKKY interaction on the thermodynamic functions of a dilute magnetic alloy. For $g\mu_B H \gg k_B T \gg cJ'$, the approach to saturation of the magnetization is predicted to be $M = g\mu_B Sc\{1 - [2(2S + 1)cJ'/g\mu_B H]\}$. F.W. Smith (1974a,b,c, 1976) has

carried out magnetization and susceptibility ($\chi = ng^2\mu_B^2 S(S+1)/3(k_B T + cJ')$ from the Larkin et al. theory) measurements on a variety of alloys systems where the above (weak interaction) limits are valid. From this analysis the scaling behaviour is verified and the magnitude of the RKKY exchange J' can be determined for each system.

Remanence and irreversibilities

Below the freezing temperature for a spin glass, a remanent magnetization and an irreversible susceptibility are found (Tholence and Tournier 1974, Guy 1977b). The isothermal remanent magnetization (IRM) is obtained by cycling an external field $0 \rightarrow H \rightarrow 0$, and then measuring the magnetization. A saturation in the IRM is observed for sufficient large H which depends upon the alloy concentration. The thermoremanent magnetization (TRM) is a field cooling effect for which the sample temperature is reduced from $T > T_f$ to $T < T_f$ in field H. At this lower temperature H is set equal to zero and the magnetization measured. Here saturation is reached in a lower external field. Figure 23 illustrates this behaviour for a typical spin glass. From the TRM, an irreversible susceptibility may be defined as $\chi_{ir} = \mathrm{TRM}(H)/H$. By adding χ_{ir} to $\chi = \lim_{H \to 0}(M/H)$ (called the reversible susceptibility), the total susceptibility, χ_{tot}, may be indirectly obtained. χ_{tot} is simply constant for $T < T_f$ and thus the characteristic step or "kink" appears in $\chi_{tot}(T)$ at T_f.

The hysteresis loops in fig. 24 further show these remanences and irreversibilities. Part (a) is the zero field cooled M–H character; the inner portion being reversible up until a certain threshold value of the external field is exceeded, then a small hysteresis and IRM develops (outer loop of part (a)). Part (b) represents a field cooled spin glass with a displaced hysteresis loop. The positive M value for $H = 0$ is the TRM, and there is a rather sharp switching to negative M values for a relatively small (much less than the field cooling field) oppositely applied field. This displacement is a dramatic illustration of the unidirectional

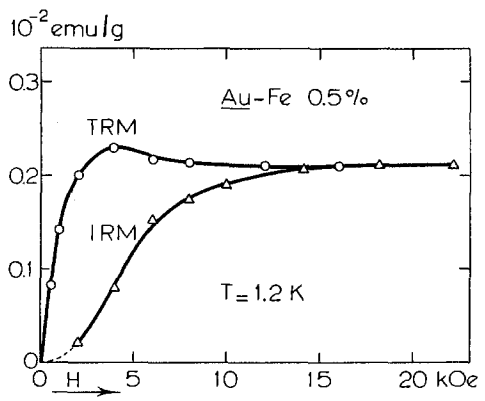

Fig. 23. Field dependences of the thermoremanent magnetization (TRM) (field cooling) and isothermal remanent magnetization (IRM) (field cycling) for AuFe at $T \ll T_f$. After Tholence and Tournier (1974).

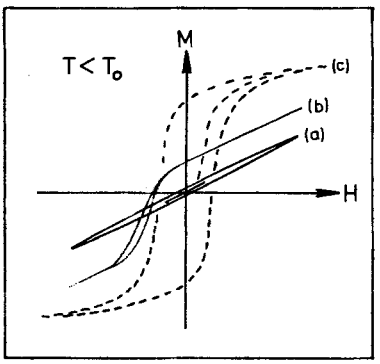

Fig. 24. Schematic hysteresis loops for (a) zero-field cooled spin glass, (b) field cooled spin glass, and (c) a ferromagnet. After Mydosh (1975).

exchange anisotropy caused by the field cooling and freezing process. For comparison, a typical ferromagnetic loop with its virgin curve is given in part (c). It should be noted that all of the above properties are functions both of the temperature and the concentration.

A time dependence of the magnetization, and of both the IRM and TRM, is observed which varies in a manner which differs from the usual, simple, exponential form (Borg and Kitchens 1973). A better fit (Guy 1977a) to the low field decay data is $M(T, t) = M_0(T) - \sigma(T) \log t$. This means that a spin glass has a long-time relaxation into its new equilibrium state when perturbed with an external field. Guy (1978) has further studied the behaviour of $\sigma(T)$ and found a maximum in this decay coefficient at $0.6T_f$ for both the IRM and TRM. Plots of σ/M_0 versus T suggest the existence of two temperature regimes above and below $0.8T_f$. The magnetic measurements in the low temperature region may be qualitatively described using an activation model with a distribution of energy barriers for non-interacting particle moments (Street and Woolley 1949). The implications from Guy's experiments are that the spin glass behaviour far below T_f is quite similar to a blocked super-paramagnet and that the relaxation effects are intrinsic to the nature of the frozen state. Thus, any first principles theory full treating the spin glass alloys must not only consider the freezing behaviour at T_f, but also these magnetic viscosity effects occurring at low temperatures.

Specific heat

Early measurements (de Nobel and du Chatenier 1959, Zimmermann and Hoare 1960) of the magnetic contribution to the specific heat, C_m, showed a linear low temperature dependence which was approximately independent of the concentration. A broad maximum in C_m developed at higher temperatures and the very high temperature fall off was proportional to $1/T$ (F.W. Smith 1974a). It was initially thought that the maximum in C_m indicated the freezing temperature T_f. However, the recent measurements of C_m and χ on the same samples showed that the maximum appeared at a temperature significantly larger than T_f. The most sensitive present day experiments disclose that nothing happens at T_f.

Figure 25 illustrates this point along with the overall C_m behaviour. At best, a good correlation could be obtained for one system PdMn (Zweers et al. 1977) where a maximum in C_m/T ($= dS_m/dT$, S_m is the magnetic entropy) occurred at the freezing temperature. This correlation was less apparent for the other spin glass systems with a knee developing at $\approx T_f$. The experiments of Wenger and Keesom (1975, 1976) further revealed a significant magnetic specific heat contribution well above T_f. When converted into entropy change, $S_{max} = cR \ln(2S+1)$, a large percentage ($\approx$70%) of S_{max} was already developed above T_f. This indicates the presence of short range magnetic order or correlations for $T \gg T_f$ which take away some degrees of spin freedom giving S_{max}. These specific heat results create a special challenge for both experimentalists and theorists. For even the revised cluster or fluctuation theories show a small effect in C_m at T_f which would require a unique measurement sensitivity. The application of an external magnetic field shifts the maximum in C_m to higher temperatures and slightly smears the general shape (Trainor and McCollum 1975).

At very low temperatures ($T \lesssim 1$ K), there is evidence of deviations from the strict linear temperature dependence, e.g. in certain cases C_m extrapolates to negative values as $T \to 0$ (Wenger and Keesom 1976). Furthermore, in the amorphous $GdAl_2$ spin glass a clear $T^{3/2}$ term has been seen (Coey et al. 1977). Thus, the limiting temperature variation would be $C_m \propto T^n$ with $n > 1$. Measurements in the opposite temperature extreme $T \gg T_f$ show a $1/T$ dependence which is slower than the $1/T^2$ Schottky tail. For low enough concen-

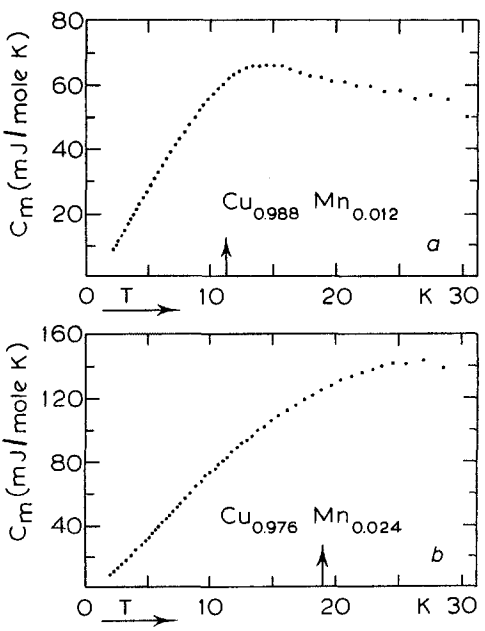

Fig. 25. Magnetic specific heat for two CuMn spin glass alloys. The arrows represent the freezing temperature as obtained from the susceptibility peak. After Wenger and Keesom (1976).

trations, the specific heat scales as $C_m/c = f(T/c, H/c)$ over the entire temperature range. This scaling behaviour was predicted by Souletie and Tournier (1969) and Larkin and Khmel'nitskii (1970, 1971). Finally, relaxation effects have also been observed in the specific heat and heat flux (Nieuwenhuys and Mydosh 1977). A sudden ΔH will result in long time scale ($\propto \log t$) relaxation to a new metastable state as with the magnetization.

Resistivity

The electrical resistivity of a dilute transition metal alloy is an easily measurable, yet difficult to interpret, quantity. First of all an estimate must be made of the non-magnetic contributions to the alloy's resistivity, i.e. residual, phonons and deviations from Matthiessen's rule. Then an important component of the magnetic resistivity $\Delta\rho$ due to the Kondo effect $\Delta\rho_K \propto -\ln T/T_K$ must be considered. This results in a negative temperature coefficient of the resistivity, $d(\Delta\rho_K)/dT < 0$. For the spin glass alloys, the interaction between the spins gradually breaks up the resonant, single impurity, Kondo scattering and at a certain temperature T_m, a maximum develops in $\Delta\rho$. This signifies the dominance of the spin disorder scattering freezing-out over the Kondo effect.

The interplay in the resistivity between the Kondo effect and the spin glass interactions has been investigated via the application of high pressures (Schilling et al. 1976, 1977, Larsen 1976, Larsen et al. 1977). Pressure always causes an increase in T_K while leaving the impurity–impurity interactions relatively unchanged. A theory due to Larsen (1976) relates T_m to the average RKKY interaction energy, $\Delta_c \propto f(c)J^2/D$, via T_K. Thus, $T_m \approx \Delta_c \ln(\Delta_c/T_K) \gg T_f$.

Figure 26 illustrates the overall behaviour of the approximate magnetic resistivity $\Delta\rho(T)$ for a series of CuMn alloys. Such general temperature and concentration dependences are typical for all the 3d spin glass systems (Mydosh et al. 1974, Ford and Mydosh 1976, Laborde 1977). By starting from the limit $T \to 0$, there is a substantial residual resistivity $\Delta\rho_0$ per at.% of magnetic impurity. A magnetic (spin-split) virtual bound state of the 3d impurities along with disorder scattering from the randomly frozen spins gives this large, magnetic, residual component. As the temperature is increased, $\Delta\rho(T, c) = c\Delta\rho_0 + A(c)T^{3/2}$ where $A(c)$ decreases very slowly with increasing concentration. Some evidence has been offered for the appearance of a limiting T^2 dependence at the lowest temperatures $\lesssim 0.3$ K (Laborde and Radhakrishna 1973, 1974). A theory of Rivier and Adkins (1975) has ascribed the low temperature $\Delta\rho$ behaviour to long wavelength elementary excitations which are diffusive in character. These excitations are highly damped, non-coherent (independent) localized spin fluctuations which scatter the conduction electrons. For the temperature region about T_f, a strong rapidly rising $\Delta\rho$ roughly proportional to T is found. There exists no definite indication for $\Delta\rho$ or $d(\Delta\rho)/dT$ of the spin glass freezing temperature. In general, the maximum value of $d(\Delta\rho)/dT$, which characterizes the Curie or Néel temperatures of long range ordered substances, lies at a temperature considerably below the freezing temperature (see fig. 26). For yet higher temperatures, a much slower $\Delta\rho(T)$ variation gradually leads to

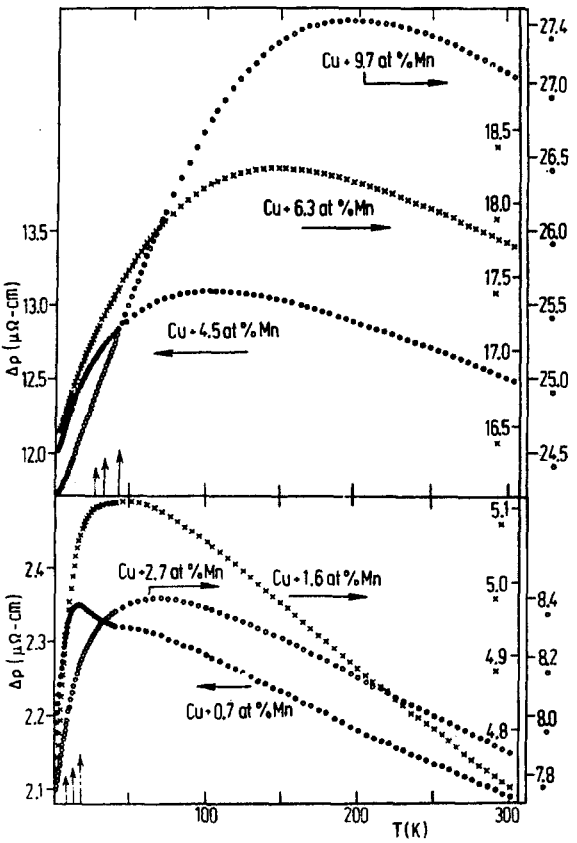

Fig. 26. Overall temperature variation of the magnetic resistivity, $\Delta\rho$, for six CuMn alloys. The arrows represent the freezing temperatures as determined by the susceptibility peak. After Ford and Mydosh (1976).

the maximum in $\Delta\rho$ at T_m, followed by a continuous fall-off as room temperature is reached. Because of the logarithmic nature of the Kondo effect, this negative slope tail in $\Delta\rho$ can extend over a wide temperature range especially for these larger concentrations. Here the strong thermal disorder, $k_B T$, breaks many of the impurity–impurity interactions. The large changes in $\Delta\rho$ for $T \gg T_f$ means the average magnetic scattering is constantly varying. Once again, consistent with the specific heat we have experimental evidence that correlations and magnetic clusters are progressively destroying the Kondo scattering and reducing the paramagnetic spin disorder scattering. In other words, there is a growth of magnetic short range order as T_f is approached from above.

Hall effect (magnetoresistance)

The anomalous part of the Hall effect due to the spin–orbit coupling between the conduction electron and the localized moments may be used to study spin glass alloys. This coupling results in an asymmetric or skew scattering for those

moments aligned with a magnetic field perpendicular to the current flow. Thus, a transverse voltage is developed which reflects the degree of alignment in the magnetic field (Fert and Friederiech 1976). For a random arrangement of moments there is no average skew component. A series of such experiments on a variety of noble metal alloys has been carried out by McAlister and Hurd (1976a,b), Hurd and McAlister (1977) and McAlister (1978). They measured the temperature dependence of the Hall effect in different external fields. Since the normal Hall coefficient (the linear Lorentz contribution) is at least 10 times less than the anomalous part, the skew scattering effects may be followed down to low temperatures and fields. The low magnetic fields are necessary to avoid smearing the spin glass freezing. In fig. 27 some of these measurements are shown. At high temperatures, the thermal disorder randomizes the local moments and the skew scattering is small. At T_f, there is a clear drop in the skew scattering due to the random freezing of the moments. Here the applied field is not strong enough to produce significant deviations from the random freezing directions. Note, however, the substantial broadening effects as the external field is increased to 0.1 T [1000 G]. A definite similarity appears between the anomalous Hall resistivity and the susceptibility $\chi(H)$. Good and consistent agreement of the freezing temperature obtained from Hall measurements exists with the other methods of extracting T_f. The sensitivity of this transport

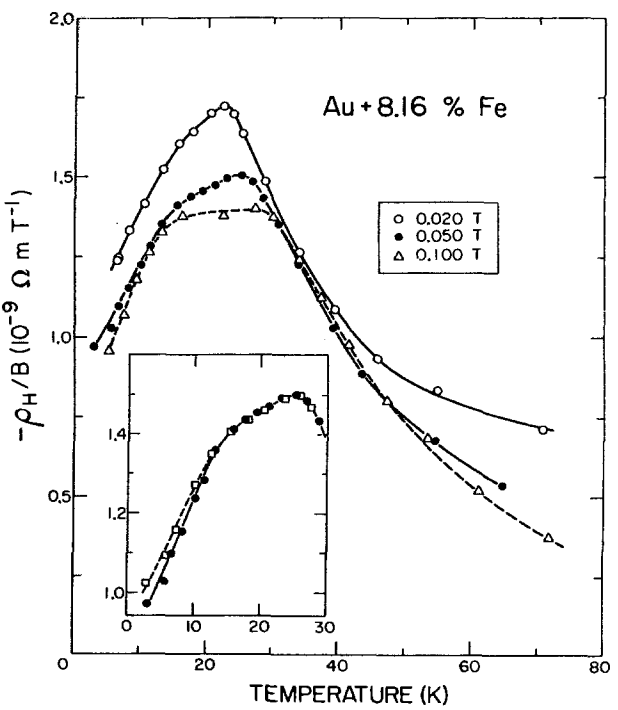

Fig. 27. Temperature dependence of the total Hall resistivity divided by the applied field strength for Au + 8 at.% Fe. After McAlister and Hurd (1976).

property, when compared to the others, e.g. resistivity and thermopower, in indicating the freezing process is due to the smallness of the non-magnetic contribution. For the Hall effect the normal component is negligible, and phonon or electron diffusion (which greatly dominate the total resistivity and thermopower) do not play a role.

Little recent experimental effort has been devoted to magnetoresistance measurements in the spin glass alloys. The magnetoresistance is an important property in the Kondo effect where an external field destroys the Kondo state. Thus a strong negative magnetoresistive effect is observed which demonstrates the alignment of the local moments in an external field and a reduction of the fluctuations and spin disorder scattering (Daybell 1973). Similar behaviour is observed for the higher concentration spin glass alloys where the very large external fields (8–13 T [80–130 kG]) distort the random orientations and give gradually varying temperature and field dependences (Welter and Johnen 1975, Li and Paton 1976). Thus, the overall magnetoresistance character may be related to the magnetization $M(\mu H/k(T+\theta))$. A similar comparison was performed for ZrMn by Jones et al. (1977).

Thermoelectric power

The most sensitive of the transport properties is the thermoelectric power, Q. Dilute Kondo alloys exhibit strong anomalies with a large, roughly concentration independent, peak in $|Q|$ near T_K (Daybell 1973). The sign of Q due to the magnetic scattering, is opposite that from ordinary potential scattering. When these effects are combined with the electron diffusion and phonon drag contributions, Q becomes a rather complicated quantity. Fortunately, the magnetic component usually dominates the others making a qualitative analysis possible.

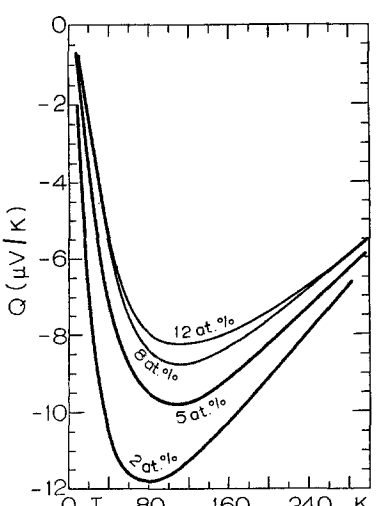

Fig. 28. Thermoelectric power dependence on the temperature for four AuFe alloys. After Cannella and Mydosh (1972).

Using AuFe as a prototype spin glass, we can discuss the general thermopower behaviour. Figure 28 illustrates the temperature dependence of Q for four concentrations of AuFe (Cannella et al. 1970, Cannella and Mydosh 1972). As the concentration is increased and spin glass effects appear, this maximum in $|Q|$ is at first slowly shifted to higher temperatures. Above ≈ 0.2 at.% there is a rapid increase, with $T_{|Q|max}$ around 100 K. $T_{|Q|max}$ is always much greater than T_f. The magnitude of Q at $T_{|Q|max}$ remains relatively constant until about 1 at.%, above which it decreases (see fig. 28).

Other spin glass alloys which have been studied, AuMn (MacDonald et al. 1962) and CuMn (Kjekshus and Pearson 1962), show similar behaviour allowing for certain changes in the overall sign of the various contributions to Q. An example of these general trends is the AuCr system (Ford et al. 1973), where the maximum in $|Q|$ is distorted into an obvious change of slope at $T \gg T_f$, due to the presence of additional scattering mechanisms. Extended and systematic investigations of the many different spin glass systems is presently lacking Nevertheless with the now available data, we may draw the following conclusions:

(a) There is no indication of the freezing process from the thermopower*, and

(b) The high temperature peaks in $|Q|$ suggest the presence of correlations and interactions among the spins well above T_f. Both of these statements are fully consistent with the interpretation and results of the resistivity measurements. An interacting pair description of the thermopower has been given by Matho and Béal-Monod (1974). This theory treats the sign changes and maxima in Q and derives a scaling in c/T for Q when interaction effects are present.

Ultrasonic experiments

Ultrasonic measurements are very sensitive to magnetic phase transitions and have provided much useful information regarding the critical behaviour. There exist thermodynamic relations which relate the temperature dependence of the sound propagation to the specific heat. For typical magnetic ordering (long range), a sharp maximum in the ultrasonic attenuation and a clear minimum in the ultrasonic velocity have been observed at T_c or T_N. By employing the high resolution (1 part in 10^7) of this technique, the spin glass freezing for different systems has been studied by Thomas et al. (Moran and Thomas 1973, Hawkins et al. 1976, 1977, Hawkins and Thomas 1978). For AuFe, CuMn and AuMn, a noticeable change of velocity occurred for an external field variation $0 \rightarrow 0.6$ T [6 kG], but only for temperatures below T_f. There was no sign of anomalous behaviour in the longitudinal wave sound velocity at 30 MHz as the temperature was varied through T_f in zero external field. However, for AuCr ($c = 4.6$ and 11 at.% Cr), small deviations from background did occur at T_f. These minima required the utmost in sensitivity to detect, still they permitted a consistent (with other measurements) determination of the freezing temperature.

*Very recently Foiles (1978) has proposed the temperature at which the thermoelectric power reverses sign to indicate the freezing temperature.

The general shape of the minima was similar, yet quite rounded, to those observed for long range ferro- or antiferromagnetic phase transitions. Two conclusions are indicated from these experimental results. Firstly, there are certain field dependent excitations which exist for $T < T_f$ and they clearly affect the magnetoelastic coupling down to the lowest temperatures, 4 K. Secondly, for a particular alloy – AuCr $c \geq 4$ at.% – the freezing process is plainly evident from the ultrasonic velocity. This would further suggest a corresponding maximum in the specific heat at T_f. Additional measurements are needed to better resolve the ultrasonic–spin glass situation.

3.2.2. Microscopic properties

Mössbauer effect

The Mössbauer technique measurements were the first to indicate the existence of "magnetic transitions" in AuFe and CuFe alloys (Borg et al. 1963, Gonser et al. 1965). While the early macroscopic methods all exhibited certain anomalies in the low temperature properties, none were at that time able to resolve the question of a magnetic transition. However, the Mössbauer studies showed that a clear hyperfine field splitting occurred at a distinct temperature. This hyperfine field can be related to the local spontaneous magnetization, and an $M(T)$ functional fit was obtained which did not differ much from that of pure ferromagnetic iron – see fig. 29. Nevertheless, the spin alignment (ferro- or antiferromagnetic) can not be distinguished in a Mössbauer measurement without using an external magnetic field. Such a study by Craig and Steyert (1964) showed a peculiar type of antiferromagnetic (weak, canted) ordering to occur. A number of other Mössbauer investigations (Violet and Borg 1966, 1967, Ridout 1969, Borg 1970, Window 1972) focused upon the nature of the magnetic ordering. At low temperatures a random distribution of magnetic moments was determined on the basis of the intensity ratios of the Mössbauer hyperfine spectrum. Significant departures from randomness were observed due to the application of an external magnetic field (Borg 1970). An unique freezing temperature was found which coincided with the T_f extracted from the low field susceptibility (Borg and Kitchens 1973, Window 1975).

Additional systems were investigated with a variety of Mössbauer isotopes ^{197}Au and ^{119}Sn in order to further probe the magnetic ordering (Borg and Pipkorn 1969, Window 1969, 1970, Window et al. 1970). The one feature common to all these measurements is a sharp transition temperature (Window 1975).

The low temperature ($T \ll T_f$) Mössbauer studies have also given information regarding the local spin arrangements within the ground state. Here the important result is that for AuFe, the anisotropic part of the exchange interaction between nearest neighbour Fe atoms determines the direction of the magnetization of these Fe moments. A comparison with computer simulation signified this anisotropy to be of dipolar-like form (Window 1972, 1973).

The main thrust of the present day Mössbauer work is towards exotic

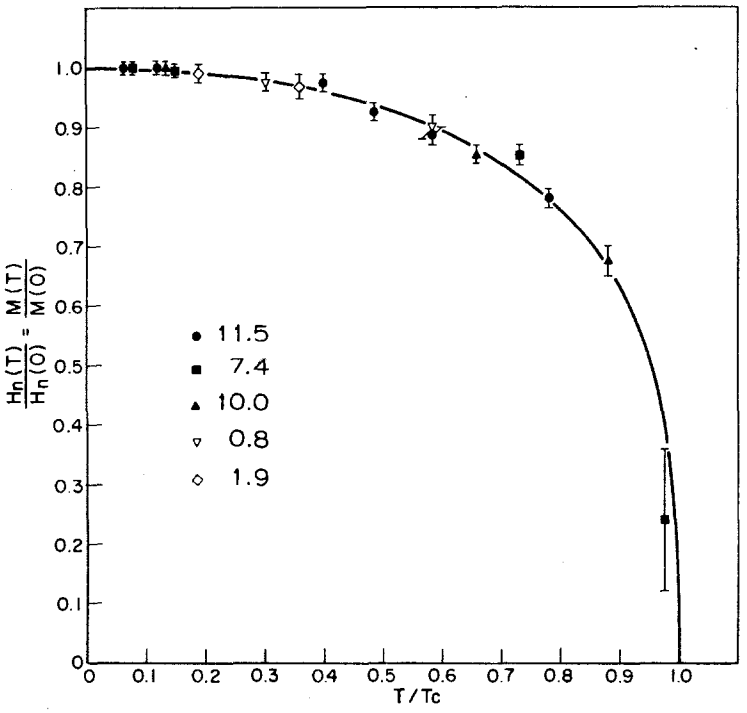

Fig. 29. Normalized temperature dependence ($T_c = T_f$) of the hyperfine splitting (proportional to the magnetization) determined from the Mossbauer effect for five Fe concentrations in Au. After Borg et al. (1963).

systems, especially the rare earth Mössbauer elements. It would be worthwhile to perform one last very sensitive measurement through the freezing transition to test the sharpness and consistency of T_f.

Nuclear magnetic resonance

Up until recently it has not been possible to follow the temperature dependence of an NMR signal for a typical spin glass alloy. In the past few years the host NMR technique has made available linewidths and relaxation of ^{63}Cu in dilute CuMn (0.1 to 1 at.% Mn) over a wide temperature range. The first of these investigations by MacLaughlin and Alloul (1976) at the lower end of this concentration decade reported no abrupt increase in linewidth below T_f. There were, however, decreases in the longitudinal and transverse NMR relaxation times and a gradual variation of the resonance intensity through T_f. The former linewidth result was interpreted as being in disagreement with the notion of a cooperative freezing at T_f of spin orientations, while the latter results indicated important modifications of the impurity spin dynamics for $T > T_f$. A difficulty with these experiments was the necessity of performing the resonance in

external fields* larger than 0.18 T [1.8 kG] which will greatly smear out the freezing process. In addition, certain nuclei were lost from the observed resonance, and this presented a further problem with the data analysis.

More recent measurements of the inhomogeneous broadening of the Cu NMR linewidth were carried out by Levitt and Walstedt (1977) on a higher concentration ≈ 1 at.% CuMn alloy. Here definite evidence was found for a low temperature frozen configuration of Mn spin, i.e. distribution of hyperfine fields which are static on a time scale of 10^{-4} s. Also a dramatic decrease of the spin echo transverse decay time constant, T_2, was observed at T_f, along with indications of short range order and fluctuation slowing down in the region around T_f. MacLaughlin and Alloul (1977a,b) extended their experiments to include these higher concentration alloys, and good agreement was obtained with Levitt and Walstedt. This then leaves open the question as to why such a drastic change in the NMR behaviour occurs between concentrations of 0.2 and 0.6 at.% Mn in Cu, particularly when the macroscopic measurements χ, ρ, C_m show nothing unusual in this concentration regime. Very recently Bloyet et al. (1978) have reported NMR results which indicate a well-defined T_f below which all impurities interact and behave collectively.

Positive muon spin rotation (μ^+SR)

The precession of polarized muons can be used to determine the distribution of local fields within a spin glass alloy. This new and highly sensitive technique gives a measure of the direct magnetic dipolar fields and the contact field from the RKKY polarized conduction electrons.

A series of AuFe and CuMn alloys have been studied in this manner by Fiory and co-workers (Murnick et al. 1976, Fiory 1976). In fig. 30 μ^+ depolarization rate and Δ data for AuFe are shown as a function of temperature. $\Delta = (\gamma_\mu T_2^*)^{-1}$, where γ_μ is the muon's gyromagnetic ratio and T_2^* is the μ^+ depolarization time. The appearance of local fields causes Δ to increase via additional depolarization. Note the abrupt change in Δ near T_f as determined from the low field susceptibility. Furthermore the temperature width of the transition increases with applied magnetic field. There are also field cooling effects giving a large constant depolarization rate below T_f. At the lowest temperatures the extrapolated limits of Δ are consistent with random, static spin configurations over the characteristic time of measurement, here ≈ 0.1 μs.

Nagamine et al. (1977a,b,c) have further used the μ^+SR technique to probe the conduction electron polarization in PdFe. The temperature dependence of the local fields showed a significant difference between a 0.28 at.% Fe and a 0.015 at.% Fe sample. The reason for this change in behaviour was attributed to conduction electron spin oscillations of the RKKY in the lower concentration alloy. Thus, here a spin glass state is indicated at very low temperatures, in contrast to the giant moment ferromagnetism (no negative oscillations in the

*New measurements by Alloul (1979) have studied the formation of the spin glass state in CuMn by field cooling the sample and then performing NMR with the field set to zero.

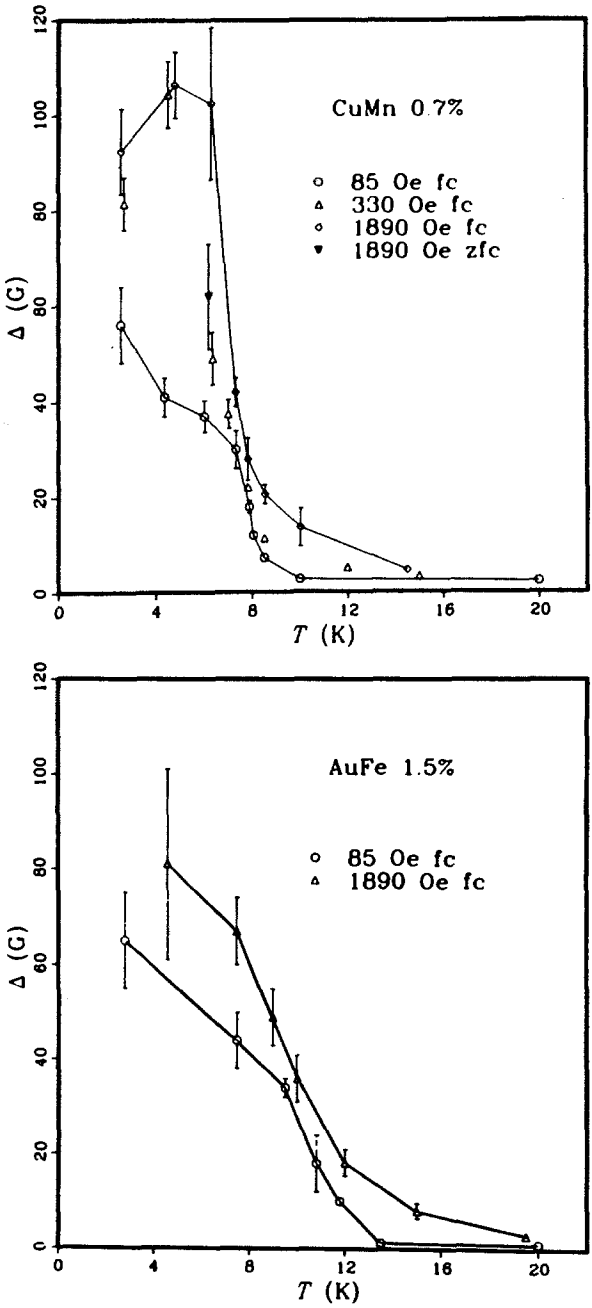

Fig. 30. μ^+ depolarization rate, expressed as a line-width in Gauss, plotted against sample temperature for several values of applied magnetic field. T_f is 7.7 K for CuMn and 11.6 K for AuFe. fc and zfc mean field cooling and zero field cooling, respectively. After Murnick et al. (1976).

conduction electron polarization) of the 0.28 at.% Fe in Pd sample. See section 3.1.2.

Neutron scattering

With the availability of very high flux reactors, the problem of neutron absorption in the noble metals has been alleviated and neutron studies on the most typical AuFe and CuMn spin glasses are now on hand. We begin first with the high temperature ($T \gg T_f$) measurements. By using diffuse scattering of unpolarized neutrons in AuFe with zero external field, two quasi-elastic lines were found with different linewidths (Scheuer et al. 1977a,b). The broad line was interpreted as due to the fast relaxation process of single spins, while the narrow (or slower) one represents the effect of spin clusters (pairs, triplets, etc., averaged collectively). Both linewidths have a Korringa-like linear T-dependence (with different slopes), but as the temperature is lowered towards T_f the intensity of the slower (cluster) linewidth grows at the expense of the faster one.

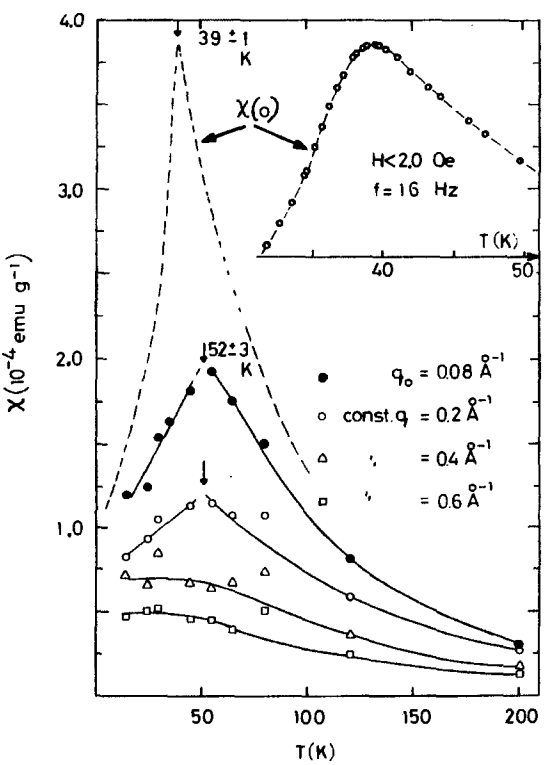

Fig. 31. Wave vector dependent susceptibility $\chi(q)$ as a function of temperature for a Cu + 8 at.% Mn alloy. Also included is the low field ac susceptibility $\chi(0)$. After Murani and Tholence (1977).

A series of neutron scattering experiments by Murani and co-workers (Murani and Thoulence 1977, Murani 1976, Murani et al. 1976b) have focused directly on the temperature region near T_f. By employing time-of-flight spectrometry and a separation analysis, the integrated quasi-elastic, elastic and total cross-sections have been determined at various temperatures for a Cu + 8 at. % Mn spin glass. The results show a smoothly decreasing quasi-elastic component as the temperature is reduced under about 80 K, while the elastic cross-section begins to increase below this temperature. Since $T_f \approx 40$ K, this behaviour indicates a diminution of the fast relaxing spin component, i.e. paramagnetic spins, at $T \approx 2T_f$. Again such behaviour is fully consistent with the other high temperature measurements in suggesting local correlations and the building of magnetic clusters. By properly calibrating the scattering cross-section, the static wave vector dependent susceptibility $\chi(q)$ may be obtained as a function of temperature. Figure 31 illustrates this $\chi(q, T)$ dependence. Also included in fig. 31 is the static $q = 0$, low field and frequency (ac) susceptibility. Of importance here is the strong q dependence of χ. At large q-values (very small regions of real space), there is no indication of the freezing process. However as q is reduced, a maximum starts to appear in χ. The best neutron determination for the temperature of the maximum is 50 K with q as small as possible. Yet the $q = 0$ susceptibility gives a $T_f = 40$ K. The reason for this temperature difference is intimated by the various times of the two measurements; the ac $\chi(q = 0)$ using audio frequencies, has a typical time constant of 10^{-2} s, while for the neutron scattering the instrumental energy resolution sets the time constant scale at about 10^{-11} s. Thus, the very fast neutron scattering will see the fastest or non-interacting spins. Once these become correlated (dynamic-correlation times greater than 10^{-11} s) with sizes greater than 1/0.08 Å, the scattering cross-section and $\chi(q)$ are insensitive to these magnetic entities and will drop. On the other hand, the static susceptibility has its very long measurement time and is particularly responsive to the largest of the magnetic clusters. Therefore, $\chi(0)$ detects the freezing of the largest clusters at T_f, afterwards it falls off with further reduction of the temperature. So it would seem that the freezing process represents the cooperative "locking-in" and growth stoppage for these largest clusters, while the neutrons are mainly responding to the smallest and fastest of the spins. At $T \to T_f$, these latter spins are too small in number to adequately contribute to $\chi(q)$. Here the cluster growth rate and relaxation time play an important role, and the 10 K difference between the two types of measurements may be considered as a wide temperature range slowing down. This results in a rather smeared "critical phenomenon" with a much larger $\epsilon = (T - T_c)/T_c$ region that is normally found.

Another neutron scattering investigation (Murani 1976) has been the small angle measurements on Au + 10 and 13 at. % Fe. Here the temperature variation of the small angle scattering intensity is determined for various values of q. By assuming the observed scattering to be mainly quasi-elastic, the intensity is then proportional to $\chi(q)T$ with a fairly long measurement time constant $\sim 10^{-3}$ s. The results show a maximum in $\chi(q)$ which is especially clear for the lowest

q-values. By estimating a characteristic temperature from the $\chi(T)$ maximum, the smallest q-values give the largest T_{max}. This range of temperatures indicates that the largest clusters freeze out first, while there are small entities (single spins or localized excitations) which can contribute to $\chi(q)$ at a lower temperature. There is fair agreement between the values of the freezing temperature for the $\chi(q \to 0)$ maximum and the low field a.c. susceptibility (see Soukoulis et al. 1978), but for these rather high Fe concentrations (beginning of the mictomagnetic regime), it is most difficult to carry out an exact comparison of the various samples and measurements. A wider series of neutron studies on lower concentrated alloys would be most useful.

Finally, some very recent diffuse inelastic neutron (time of flight) measurements, have been begun at the lowest temperatures (Scheuer et al. 1977c). The first results indicate the presence of magnetic excitations in a spin glass for $T \ll T_f$. A well-defined excitation peak was found in a Cu + 5 at. % Mn sample at a rather large energy $\hbar\omega = 4.2\,\text{meV} = 49\,\text{K} > T_f = 27\,\text{K}$. The preliminary analysis shows little dispersion with ω being constant for three different q-values. This suggests non-propagating ($d\omega/dq = 0$) localized modes. For an alternative description see Verbeek et al. (1978c).

Electron spin resonance

ESR measurements on the magnetic ions in CuMn, AgMn, AuMn, etc., offer another method with which to study the spin dynamics of a spin glass. Although there are certain difficulties with the "bottleneck" effect, once this is broken, a direct study of the interacting magnetic impurities becomes possible. The early work of Owen et al. (1957) already contained many indications of spin glass behaviour, e.g. a shifting of the ESR line to lower fields below the "ordering" temperature along with hysteresis and field cooling affecting the ESR results. A continuously variable temperature spectrometer was used by Griffiths (1967) to obtain the complete temperature dependences for CuMn. He found a well-defined maximum in the signal amplitude at a temperature where the ESR-linewidth, ΔH, showed a weak minimum and a line shift became apparent. This "characteristic" temperature is well above the freezing temperature determined from other measurements. It would seem that the temperature and concentration variation of ΔH exhibits the same general form for many spin glasses. At high temperature, there is the usual Korringa thermal broadening $\Delta H \propto T$. However, as the temperature is reduced, deviations from linearity appear and result in a low T concentration dependent minimum with ΔH still increasing at the lowest temperatures (≈ 1 K). Such behaviour, often referred to in the literature as "ordering effects", indicates a change in the spin relaxation rate to larger values due to spin–spin interactions as $T \to T_f$ from above. In a complete experimental review, Taylor (1975) has discussed the general area of ESR for magnetic ions in metals. Nevertheless a systematic investigation and connection with theory of ESR effects in simple spin glasses is presently lacking. Much more work has been carried out on the rare earth ions.

A final point regarding microwave frequencies has to do with the frequency

dependence of the low field susceptibility $\chi(\omega)$. At present there has been no $\chi(\omega)$ experiments from the audio frequency range $\approx 10^2$ Hz through the radio bands up to the microwave frequencies 10^{10} Hz. Such a study would be most useful in determining the spin dynamics and relaxation of a spin glass near T_f^*.

Nuclear orientation

At very low temperatures (mK), the nuclear sub-states are unequally populated. Upon the radioactive decay of certain elements, e.g. ^{54}Mn and ^{60}Co, this unequal population produces an anisotropy in the γ-ray radiation pattern. This distribution of radiation is proportional to the local magnetic hyperfine field which orients the nuclei; and thereby probes the field seen by the atom or ion. The method of nuclear orientation (NO) may be directly used in very dilute Mn spin glass alloys or it may be employed as a hyperfine field probe of other interacting impurities.

In a series of nuclear orientation experiments using ^{54}Mn in Pd and Au, and ^{60}Co in Pd, Flouquet et al. (1977, 1978) have measured the temperature dependence ($\approx$3–25 mK) of the effective field $H_{\text{eff}} = H_{\text{hf}} + H_{\text{ext}}$ from the γ- anisotropy. A strong decrease in H_{eff}, due to local misalignments of the hyperfine field axes, occurred at low temperature. This indicated the presence of the random spin glass freezing which prevents a full alignment of H_{hf}. Such spin glass effects were clearly seen below 10 mK for as little as 10 ppm Mn and as little as 3 ppm Fe parasitic impurity.

Further NO investigations by Thompson et al. (1976, 1978) and Thomson et al. (1976) were carried out on PdHMn and PtMn. Mn in the former system was much more difficult to orient (a greater misalignment) with an external field at low temperatures than unhydrogenated PdMn. The authors found it necessary to assume a distribution, random in direction and Gaussian in magnitude for the local field on the Mn ions, i.e. $H_{\text{eff}} = H_{\text{ext}} + H_{\text{random}}$. The distribution half-width was four times larger with hydrogen charging than without. Thus, the NO studies showed that although both PdHMn and PdMn are spin glasses at sufficiently low T and c, the hydrogenation greatly increases the strength of the random freezing. From macroscopic measurements (Mydosh 1974) we know the same to be true for PdHFe and PdFe. For PtMn, a good spin glass, a preferential nuclear spin ordering axis was found in the absence of an external field. This suggests that, on a microscopic level, the spins do not freeze into a fully random array, but that a local anisotropy exists and gives the spins a preferred direction. Certainly, additional work is necessary to pinpoint the mechanism for this frequently occurring and often postulated anisotropy.

3.2.3. The freezing process

Before proceeding with the theory of random alloys, we can collect the previous survey of experimental results into a phenomenological description of the

*Currently, the frequency dependence of the low field susceptibility is the subject of intense interest (see Dahlberg et al. 1979).

freezing process. First, as the temperature is lowered from $T \gg T_f$, many of these randomly positioned and freely rotating spins build themselves into locally correlated clusters or domains which can then rotate as a whole. The remaining loose spins serve to transmit the long range interactions between the clusters. We note that this cluster growth process is strongly dependent upon the alloy randomness and the temperature, and does not represent the well-defined "chemical particles" of Néel super-paramagnetism, although this model might easily be adopted to the dynamical cluster case. As $T \to T_f$, the various spin components begin to interact with each other over a longer range and the system seeks its ground state configuration for the particular distribution of spins. This means a favourable set of random alignment axes into which the spins or clusters can lock. The freezing takes place in both the spatial and time dimensions with the largest and slowest of these dynamically growing clusters responsible for the sharp effects at T_f. Experimental techniques which are not sensitive to these clusters, such as the specific heat and the resistivity, will give no clear indication of the freezing process. The neutron scattering measurements, which essentially determine $\chi(q, \omega)$ and thus the response as a function of r and t, show a wide range of behaviour depending upon the particular space or time region. A unique feature of the spin glasses seems to be the wide temperature and concentration regimes within which the spatial and temporal correlations are varying.

The exact nature of the freezing process is presently unresolved, and there are three main schools of thought which focus on this problem. The first model (Tholence and Tournier 1974, 1977) extends the Néel description of super-paramagnetism to the random metallic systems. Domains are formed and the freezing is a result of a distribution of blocking temperatures, T_B, at which these domains cannot overcome an energy barrier, E_B, governed by the anisotropy energy and the interaction with the external field. The anisotropy is basically provided by the dipolar coupling, although cluster shape anisotropy could also play a role. Transitions over the barrier require thermal activation. If the domain is blocked for a time greater than a typical measurement time, τ_m, it is frozen, $E_B(T_B) = k_B T_B \ln(\text{const.}\ \tau_m)$. For a distribution of E_B's or T_B's, as is required for the spin glass case, the maximum T_B determines T_f. The application of the Néel theory to spin glasses and a review of its fundamental concepts has been recently discussed by Guy (1977a, 1978).

The second approach (Edwards and Anderson 1975) replaces the randomly situated moments and the oscillatory RKKY interaction with a regular lattice of spins which have a Gaussian probability of exchange interaction strengths $P(J)$. Here the statistical mechanics of phase transitions may be invoked, and various critical phenomena and exponents for the thermodynamic quantities can be calculated near T_f. More exact and sophisticated treatments based upon this starting point have been recently obtained (Sherrington and Kirkpatrick 1975, Harris et al. 1976, Luttinger 1976, Thouless et al. 1977). A final model which we propose here for the spin glass freezing would draw heavily upon comparison with the solidification process of real glasses, e.g. a "window glass". Now there

is no distinct phase transition, but a gradual change in the behaviour of the viscosity, density, volume, etc., as the molten liquid is cooled into an amorphous solid. Most important in this model are the irreversibilities and the dependences of the experimental properties upon rates and directions of the temperature variation. At present there are no direct references or detailed comparisons on the possible similarities of these two "glass" systems. A first test of such behaviour would be to measure the low field spin glass susceptibility near T_f as a function of various cooling and heating rates, dT/dt, beginning both above and below T_f.

At the lowest temperatures $T \ll T_f$, most measurements exhibit irreversibilities and relaxation time effects. Since the process of cluster growth has now stopped,

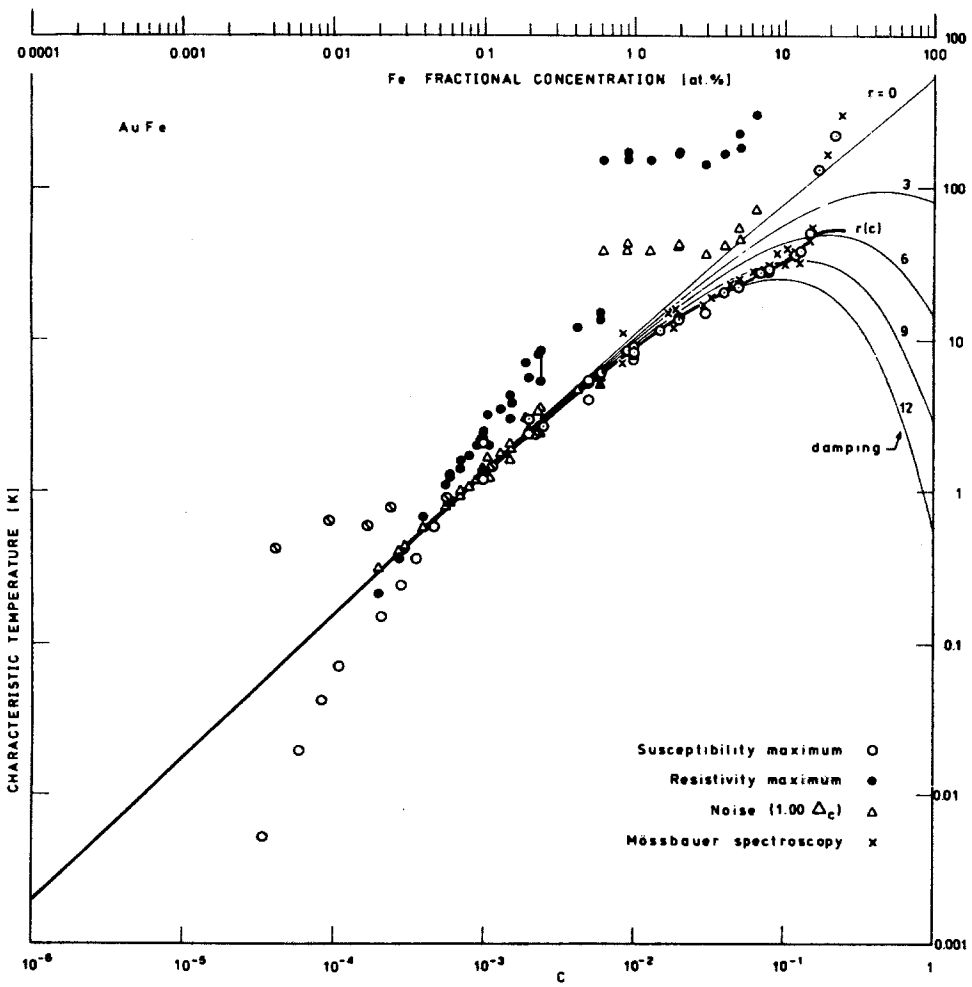

Fig. 32. Collection of characteristic temperatures for AuFe alloys over the complete concentration range. After Larsen (1978a).

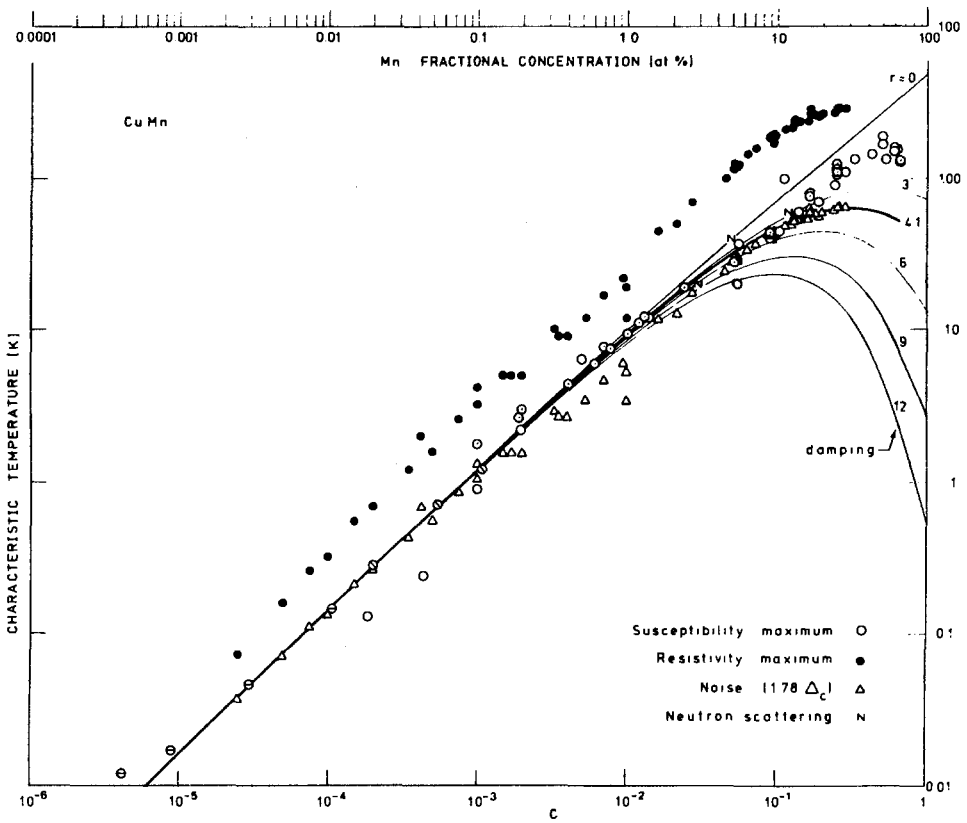

Fig. 33. Collection of characteristic temperatures for CuMn alloys over the complete concentration range. After Larsen (1978b).

the model of Néel super-paramagnetism can be used to describe many of the frozen spin glass properties. In addition to this classical energy barrier process, magnetic excitations involving diffusive, highly damped spin fluctuations are also present. These localized modes are probably related to quantum mechanical tunnelling through the energy barrier.

A collection of freezing temperatures for the two most-studied spin glasses, AuFe and CuMn, and a theoretical model to calculate the concentration dependence of T_f have been given by Larsen (1977, 1978a,b). This calculation begins by relating $k_B T_f$ to the RKKY interaction envelope $\Delta(r) \propto 1/r^3$ which is consistent with the Edwards and Anderson expression for the freezing temperature $k_B T_f = \frac{1}{12}\{(2S+1)^4 - 1\}^{1/2}\{\Sigma_j \Delta_{ij}^2\}^{1/2}$. By considering the mean free path, λ, (self) damping $e^{-r/\lambda}$ of the RKKY interaction, and the effect of fluctuations in the nearest neighbour distances, $T_f(c)$ can be evaluated for the entire concentration range. Figures 32 and 33 illustrate the results of Larsen. The solid lines represent

the theory with a scaling parameter $r(c)$ which may be obtained from the experimental residual resistivity. The measured T_f-points are determined from the susceptibility maximum, the Mössbauer effect and neutron scattering. Another theory of Larsen (1976, Larsen et al. 1977) connects the temperature of the resisistivity maximum with the freezing temperature. The results of this "noise" theory give an additional set of data points for T_f in figs. 32 and 33. As can be seen by comparing these two figures CuMn is a well-behaved spin glass over the full 5 orders of magnitude of concentration. For CuMn, the Kondo temperature is very low ($\approx 10^{-2}$ K), so that there is little competition between Kondo and spin glass effects down to the lowest concentration. Since the long range magnetic order in CuMn is of the antiferromagnetic type, its "percolation limit" is $\approx$45 at. % (see section 1.5), and there are no deviations at the high concentration limit. The opposite is true for AuFe which has $T_K = 0.2$ K and thus shows a significant depression of T_f below this T_K. Furthermore, due to 17 at.% percolation for ferromagnetism, an upward departure from the theoretical line results at the high concentration limit in AuFe.

4. Theory of random alloys

A complete survey of the theory of dilute giant moment systems and spin glasses should contain a description of the existence of the magnetic moments in metals (i.e. deal with the atomic physics in a metallic environment), their interactions with the itinerant electrons, their direct and indirect interactions among themselves, and, finally, the ordering phenomena due to these interactions. It is obvious that such a thorough treatment is beyond the scope of the present article. Even if the interaction between "good" magnetic moments is known, the theoretical description of the ordering phenomena is fairly complicated due to random positions of the magnetic atoms in the host matrix.

In order to make this theoretical section consistent with the lines used in the experimental sections, we shall divide this section into two parts. In the first we will describe a random molecular field theory which gives the magnetic phase diagrams of ferromagnetic/spin glass alloys, and which roughly describes the experimental phenomena. In the second part we will give a limited review of the important literature on the theory of these alloys.

4.1. Random molecular field model

In this model it is assumed that the bare magnetic moments exist and are stable. Due to direct and/or indirect correlations there is an interaction between each pair of magnetic moments i and j, denoted by J_{ij}. This J_{ij} is assumed to depend only on the distance between the magnetic moments, $J_{ij} = J(r_{ij})$. If the spin operator of the magnetic moment i is denoted by $\hat{S}_i$ (S instead of the total angular momentum for simplicity; we do not in principle exclude orbital momenta), then the Hamiltonian (without external magnetic field) can be written

as

$$\mathcal{H} = -\sum_{i>j} 2J(r_{ij})\hat{S}_i \cdot \hat{S}_j. \tag{4.1}$$

The zeroth order approximation to the solution of this Hamiltonian is the molecular field approximation. Then, the Hamiltonian is written as

$$\mathcal{H} = -\sum_i \bar{H}\hat{S}_i$$

$$\text{where } \bar{H} = \sum_{j\neq i} J(r_{ij})\langle S_j\rangle.$$

This approximation may give a solution for ferromagnetic ordering with $J(r_{ij}) > 0$, but it will lead to wrong results in the case of a spin glass because of the oscillatory character of $J(r_{ij})$. To obtain results from this Hamiltonian one should go to better approximations.

Two important approaches have been suggested in recent years. One is due to Edwards and Anderson (1975) in which they treated the Hamiltonian assuming a Gaussian distribution of J_{ij}, according to $P(J_{ij}) \propto \exp(-J_{ij}^2/2J^2)$. On the basis of this distribution of J_{ij} they could (via a replica technique and applying the $n \to 0$ trick) derive an expression for the free energy and found that a phase transition occurred at $T = J/k_B$. Many theoretical papers, investigating the so-called Edwards and Anderson model, have appeared since then, including a quantum mechanical version and computer simulations (see next section). Sherrington and Southern (1975) and Sherrington and Kirkpatrick (1975) investigated a mixed ferromagnet/spin glass system by using a slightly different distribution function

$$P(J_{ij}) = \frac{1}{J(2\pi)^{1/2}} \exp\left\{-\frac{(J_{ij} - J_0)^2}{2J^2}\right\} \tag{4.2}$$

and these authors derived a phase diagram, according to which the alloy may become a spin glass or a ferromagnet depending on the ratio between $\tilde{J}_0$ and $\tilde{J}$, where $\tilde{J}_0$ equals zJ_0 and $\tilde{J} = J\sqrt{z}$, and z is the effective number of neighbours. We reproduce this phase diagram in fig. 34.

Another approach to the spin glass problem (called at that time the dilute alloy problem) has been made by Klein (1968), based on the Random Molecular Field Approximation (RMFA) introducted by Marshall (1960). In this approximation the probability is calculated that a magnetic moment (taken to be at the origin) senses a molecular field between H and $H + dH$. This probability is then given by $P(H)\,dH$. It should be noted that $P(H)$ is temperature dependent, since it depends upon the direction of the magnetic moments, which must be calculated via the $P(H)$, leading to coupled integral equations for $P(H)$ and the magnetization. This technique (Marshall 1960, Klein and Brout 1963) has been more recently applied to giant moment alloys by Korenblitz and Shender (1972) and by Nieuwenhuys (1975).

In order to characterize magnetic alloys it would be sufficient to calculate the

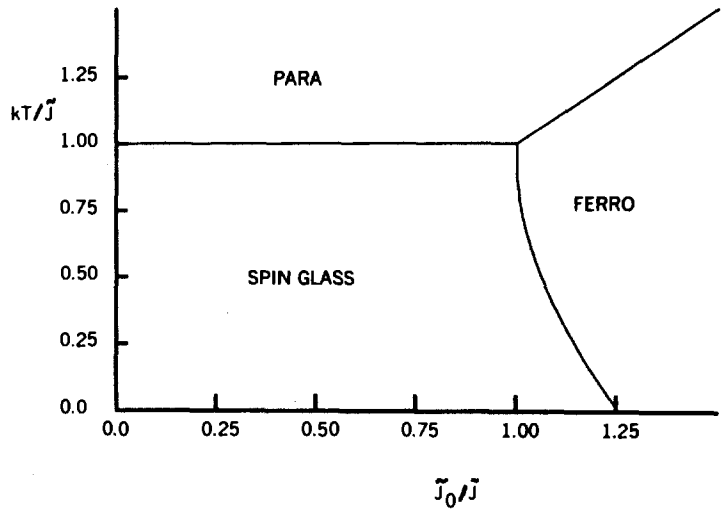

Fig. 34. Phase diagram of spin glass/ferromagnet. After Sherrington and Kirkpatrick (1975).

$P(J_{ij})$ curve, deduce the mean value and the width, multiply these by z and $\sqrt{z}$ respectively to obtain $\tilde{J}_0$ and $\tilde{J}$and compare these values with the phase diagram given by Sherrington and Kirkpatrick (1975). Unfortunately, it is rather difficult to calculate $P(J_{ij})$ even if the distance dependence of the interaction is known. Obviously, the distribution will be sharply peaked at $J_{ij} = 0$, since the major part of the mutual distances is relatively large. Therefore, an effective interaction range has to be defined, and the resulting $P(J_{ij})$ will depend on the choice of this interaction range. Recently, however, Klein (1976) showed that if one calculates the $P(H)$ on the basis of the distribution $P(J_{ij})$ as used by Sherrington and Kirkpatrick (1975) and then calculates the properties of the system by the RMFA, the results are identical to those obtained by Sherrington and Kirkpatrick (1975) using the $n \to 0$ expansion. If ferromagnetic ordering prevails the molecular field distribution at $T = 0$ as found by Klein (1976) is given by

$$P(H) = \frac{1}{(2\pi z)^{1/2}} \exp\left\{-\frac{(H - zJ_0)^2}{2zJ^2}\right\}. \tag{4.3}$$

Bearing in mind that the parameters entering the phase diagram are given by zJ_0 and $J\sqrt{z}$, it might be sufficient to calculate $P(H)$ at $T = 0$ for any given alloy, and then to use the mean and the width to deduce its location in the phase diagram.

The interaction as a function of the distance can be calculated assuming that the indirect interaction is governed by the generalized susceptibility of the itinerant electrons. Afterwards the total interaction can be formed by incorporating the direct short range interactions. The generalised susceptibility of itinerant electrons, which may be considered as a free electron gas is given by the RKKY formula (see section 1.3). For the itinerant electrons with intra-atomic exchange enhancement the susceptibility can be calculated according to

Schrieffer (1968) via the random phase approximation (see section 3.1). Since we are now interested in giant moment alloys as well as in spin glasses, we cannot use (as in section 3.1) the approximation of the Lindhard function for small q, but we have to include its complete form

$$F(q) = \frac{1}{2} + \frac{k_F}{2q}\left(1 - \frac{q^2}{4k_F^2}\right) \ln\left|\frac{2k_F + q}{2k_F - q}\right|. \tag{4.4}$$

Once the distance dependence of the interaction is known (after inclusion of the direct interaction) the $P(H)$ at $T = 0$ may be calculated according to Klein (1968) applying a method developed by Margenau (1935). We shall follow Margenau's paper. The molecular field acting on a magnetic moment in the origin is given by

$$\sum_j J_{ij}|\mu_j| = \sum_j J(r_{ij})|\mu|. \tag{4.5}$$

Assuming a homogeneous distribution of n magnetic moments in a volume V, the probability can be written as

$$P(H)\,\mathrm{d}H = (4\pi/V)^n \int \cdots \int r_1^2 \ldots r_n^2 \,\mathrm{d}r_1 \ldots \mathrm{d}r_n. \tag{4.6}$$

The integration extends over the range of r values such that

$$H - \tfrac{1}{2}\,\mathrm{d}H < \sum_j J(r_{ij})|\mu| < H + \tfrac{1}{2}\,\mathrm{d}H.$$

By using the Dirichlet representation of the δ-function, the integration can be extended over the whole volume

$$P(H)\,\mathrm{d}H = \frac{1}{\pi}\left(\frac{4\pi}{V}\right)^n \int \cdots \int r_1^2 \ldots r_n^2 \,\mathrm{d}r_1 \ldots \mathrm{d}r_n \times \int_{-\infty}^{+\infty} \mathrm{d}\rho \frac{\sin(\frac{1}{2}\rho\,\mathrm{d}H)}{\rho} \exp\left[-\mathrm{i}H\rho + \mathrm{i}\rho|\mu| \sum_j J(r_{ij})\right]. \tag{4.7}$$

Taking the limit for $\mathrm{d}H \to 0$ and writing $\mathrm{e}^{\mathrm{i}\rho|\mu|J(r)}$ as $[1 - (1 - \mathrm{e}^{\mathrm{i}\rho|\mu|J(r)})]$ this becomes

$$P(H) = \frac{1}{2\pi}\left(\frac{4\pi}{V}\right)^n \int_{-\infty}^{+\infty} \mathrm{d}\rho\, \mathrm{e}^{-\mathrm{i}H\rho}\left\{\int [1 - (1 - \mathrm{e}^{\mathrm{i}\rho|\mu|J(r)})] r^2\,\mathrm{d}r\right\}^n. \tag{4.8}$$

The term in the brackets may be written as

$$\int [1 - (1 - \mathrm{e}^{\mathrm{i}\rho|\mu|J(r)})] r^2\,\mathrm{d}r = \frac{V}{4\pi}\left(1 - \frac{D}{V}\right) \tag{4.9}$$

where $$D = 4\pi \int_0^\infty (1 - \mathrm{e}^{\mathrm{i}\rho|\mu|J(r)}) r^2\,\mathrm{d}r.$$

If we let the volume of the system go to infinity, while maintaining the density

$n_1 = n/V$ constant, we reach

$$\lim_{n\to\infty}\left(1-\frac{n_1 D}{n}\right)^n = e^{-n_1 D}$$

thus $$P(H) = \frac{1}{2\pi}\int_{-\infty}^{+\infty} d\rho\, e^{-iH\rho - n_1 D}. \tag{4.10}$$

From this distribution function the parameters for the phase diagram can be calculated straightforwardly.

We have calculated the generalized susceptibility within the random phase approximation (see section 3.1) as a function of $2k_F r$, on the basis of eq. (4.4). In fig. 35 this suceptibility, multiplied by $(2k_F r)^3$ for clarity of the graph, is shown for several values of the Stoner enhancement factor, Ξ. Then, by assuming $J(r)$ to be proportional to this susceptibility, the $P(H)$ curves have been computed, using eq. (4.9) and (4.10), for several values of the concentration (or density n_1). The calculated mean value ($\int HP(H)\,dH$) and width ($\{\int H^2 P(H)\,dH - \overline{H}^2\}^{1/2}$), then determine the position of the alloy in the phase diagram. Note that no adjustable parameters have been used in this model. The results are shown in fig. 36 for $\Xi = 1$ and $\Xi = 10$, respectively. In fig. 36a we have used the lattice spacing and Fermi wave vector for AuFe. As can be seen from the graph the freezing

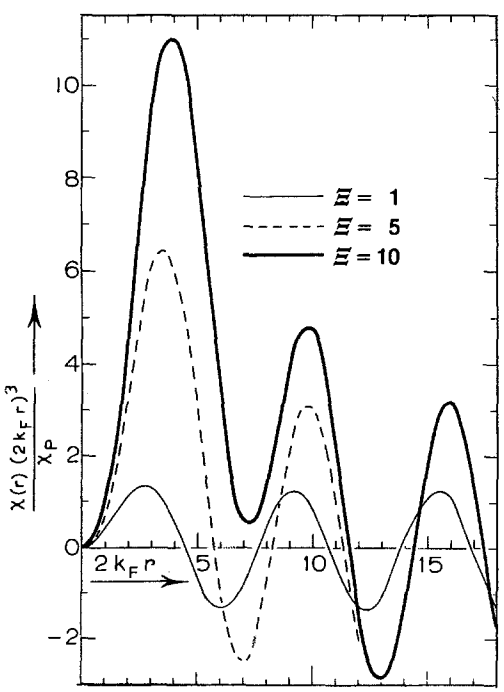

Fig. 35. The generalized susceptibility multiplied by $(2k_F r)^3$ as a function of $2k_F r$ for three values of the Stoner enhancement factor, Ξ.

temperature is proportional to $c^{0.52}$, for this limited concentration region, which is in fair agreement with the results from experiments, see section 3.2.3. In fig. 36b the parameters have been chosen, corresponding to the properties of Pd-based alloys. Clearly, the spin glass phase exists up to rather high concentrations of impurities, in contrast to the experimental observation. Investigating the possible causes of this disagreement, it can be noted that:
(i) The calculated ratio of the width of the $P(H)$ and its mean value is in fair agreement with the results obtained with the help of μ^+-depolarization by Nagamine et al. (1977a,b) on PdFe 0.015 and 0.25 at.%.
(ii) The form of the $P(H)$ obtained for the Pd-based alloys differs considerably from that used by Sherrington and Kirkpatrick (1975), in that it is not at all symmetric about the mean value of H.
The first fact gives us some confidence in the calculation of $P(H)$, so that combined with the second one, we conclude that the Sherrington–Kirkpatric phase diagram cannot be used with extensive parameters in the case of a "non-symmetric" $P(H)$.

In order to improve the calculated phase diagram we have to go one step backwards. Let the mean absolute value of the local magnetization be denoted m ($m = |\langle\mu\rangle|$) and the mean value of the bulk magnetization by M. Then the equations for m and M read (Klein 1976)

$$m = \int_{-\infty}^{+\infty} P(H)\left|B_S\left(\frac{\mu H}{k_B T}\right)\right| \mathrm{d}H \tag{4.11}$$

$$M = \int_{-\infty}^{+\infty} P(H) B_S\left(\frac{\mu H}{k_B T}\right) \mathrm{d}H \tag{4.12}$$

where $B_S(x)$ is the appropriate Brillouin function. The calculation of $P(H)$ may then be based on the following approximation. If n is the total number of magnetic moments then on the average there will be $n_\uparrow = \frac{1}{2}n[1 + (M/m)]$

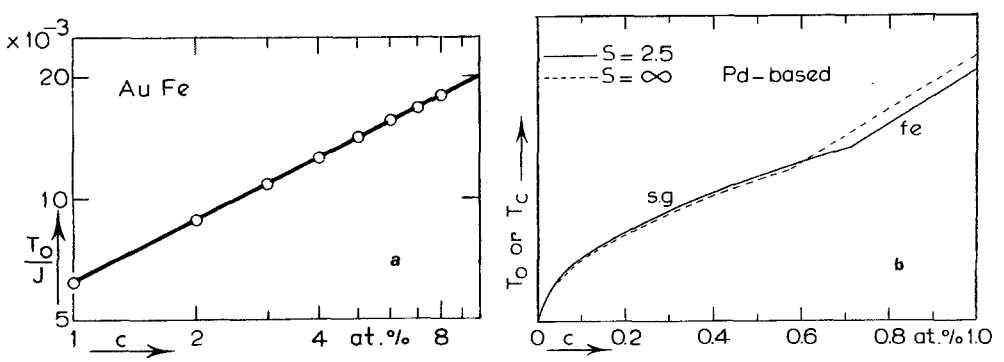

Fig. 36. The *calculated* phase diagram for (a) an alloy (AuFe) with $\Xi = 1$ and (b) for an alloy (PdMn) with $\Xi = 10$. For $\Xi = 1$ the ordered phase is the spin glass one; for $\Xi = 10$ the spin glass exists up to about 0.6 at.% (depending on the magnetic quantum number).

moments pointing in the upward direction and $n_\downarrow = \frac{1}{2}n[1-(M/m)]$ in the downward direction. Noting that $D(\rho)$ changes into $D(-\rho)$, if the sign of the interaction changes, $P(H)$ will be given by

$$P(H) = \frac{1}{2\pi}\int_{-\infty}^{+\infty} d\rho \exp\{-iH\rho - n_\uparrow D(\rho) - n_\downarrow D(-\rho)\} \tag{4.13}$$

where $$D(\rho) = 4\pi \int_0^\infty (1 - e^{i\rho m J(r)}) r^2 \, dr. \tag{4.14}$$

Equations (4.11)–(4.14) can be solved numerically to obtain an improved phase diagram (Nieuwenhuys 1978). In conclusion, the random molecular field model is potentially able to predict a wide range of properties of alloys from spin glasses to giant moment ferromagnets.

4.2. Survey of additional theories

4.2.1. Giant moments

The magnetic phenomena in giant moment alloys have several aspects: the ferromagnetism at low concentrations (far below the nearest neighbour percolation limit), the influence of direct interactions, spin waves, and the occurrence of the giant moment itself. This section has therefore been divided in the following parts: (a) ferromagnetism and spin waves, (b) the giant moment, and (c) short range interactions.

(*a*) *Ferromagnetism and spin waves*

As explained in section 3.1 the ferromagnetism in giant moment alloys is obviously correlated to the large susceptibility of the host materials. A transparent and mathematically simple model has been developed by Takahashi and Shimizu (1965). These authors began with the following approximations:
(i) The rigid band model can describe the 4d band.
(ii) Direct interactions between the dissolved magnetic atoms can be neglected.
(iii) The interaction among 4d electrons and between the 4d electrons and the magnetic atoms is independent of the composition of the alloy.
(iv) The bare moment is localized on the dissolved atoms and the induced polarization is uniform over the alloy.
The interaction among the 4d electrons is denoted by I; that between 4d electrons and the localized moments by α. Then the energy of the 4d electrons is given by

$$E = \mu_B(\alpha M_i + I M_d + B_{ex})$$

where M_i and M_d are the magnetization of the localized magnetic moments and of the 4d electrons, respectively, and B_{ex} is an external magnetic field.

Restricting ourselves to low temperatures, small concentrations and weak

external magnetic field, we may write

$$M_i = N_i g \mu_B S B_S[g\mu_B S(\alpha M_d + B_{ex})/k_B T] \tag{4.15}$$

$$M_d = \chi_P(IM_d + \alpha M_i + B_{ex}) \tag{4.16}$$

where χ_P is the Pauli susceptibility, and N_i the number of magnetic ions. From the last equation it can easily be seen that for zero N_i (no impurities) the susceptibility will become

$$\chi_0 = \chi_P/(1 - I\chi_P). \tag{4.17}$$

For small arguments of the Brillouin function we may write for M_i

$$M_i = C(\alpha M_d + B_{ex})/T \tag{4.18}$$

where $C = N_i g^2 \mu_B^2 S(S+1)/3k_B$.

Combining eqs. (4.16) and (4.18) the total susceptibility, $\lim(M_d + M_i)/B_{ex}$, as $B_{ex} \to 0$, is found to be

$$\chi = \chi_0 + \frac{C(1+\alpha\chi_0)^2}{(T - \alpha^2 C\chi_0)}. \tag{4.19}$$

When the denominator of this expression vanishes, the total susceptibility diverges, indicating a transition to ferromagnetism. The transition temperature is then given by

$$T_c = N_i g^2 \mu_B^2 S(S+1)\alpha^2\chi_0/3k_B. \tag{4.20}$$

The numerator of the second term of eq. (4.19) can be written as $N_i p_{eff}^2$, where

$$p_{eff} = g\mu_B\{S(S+1)\}^{1/2}(1 + \alpha\chi_0) \tag{4.21}$$

which is the expression for the giant moment used throughout this present paper.

This model put forth by Takahashi and Shimizu (1965) contains the main features of the static properties of giant moment alloys. It also withstands remarkably well a comparison with experimental results; except that the absolute value of the transition temperature appears to be too high. This is obviously due to the assumed uniformity of the polarization. If instead of χ_0 a function $\chi(r)$ is used, where r is some mean value of the distance between the magnetic impurities, the agreement is much improved, as shown in fig. 19.

The model of Takahashi and Shimizu does not solve the itinerant/localized duality of the magnetic ordering phenomena. The same duality is found in the description of pure ferromagnetic metals (see e.g. Herring 1966).

It is interesting to note that from eqs. (4.16) and (4.18) one may derive

$$M_i = C\{B_{ex}(\alpha\chi_0 + 1) + \alpha^2\chi_0 M_i\}/T \tag{4.22}$$

showing that $\alpha^2\chi_0$ may be regarded as an effective molecular field coefficient in a localized picture, leading to an expression for T_c identical to eq. (4.20). On the other hand, we may write

$$M_d = \frac{\chi_P}{1 - \{I + C\alpha^2/T\}\chi_P}\left\{\frac{C\alpha}{T} + 1\right\} B_{ex}. \tag{4.23}$$

Defining $\{I + C\alpha^2/T\}$ as an effective d–d interaction, the itinerant criterion for ferromagnetism will be given by

$$\chi_P\{I + C\alpha^2/T\} = 1 \tag{4.24}$$

which again results in the identical expression for T_c.

Kim (1966) has calculated the properties of the ferromagnetic alloys based on the interaction Hamiltonian: $\mathcal{H}_{int} = J \Sigma \sigma(\chi_j) S_j$ (σ is the spin density operator and J is a parameter measuring the interaction between the d-electrons of the local moment and the itinerant electrons). He then uses a canonical transformation to eliminate $\mathcal{H}_{int}$, leading to an effective interaction among the d-electrons of the host plus the RKKY interaction. From here he calculates the susceptibility of the band, which diverges at a temperature T_c again given by eq. (4.20) (using $\alpha = 2J/N_d g^2 \mu_B^2$).

Later, Long and Turner (1970) have pointed out that in calculating the effective molecular field acting on the ith magnetic moment, one should be careful to exclude the field due to the polarization induced by the ith moment itself. Therefore, the susceptibility to be incorporated in eq. (4.20) should be

$$\chi(q = 0) - \chi(r = 0) \tag{4.25}$$

or more exactly

$$\sum_q \sum_{j \neq i}^{N_i} \chi(q) \exp\{iq(r_i - r_j)\}.$$

These authors obtain smaller values for the transition temperature via a procedure similar to the one used by us to calculate fig. 19 and the one used in section 4.1.

The localized/itinerant duality has been the subject of a paper by Rhodes and Wohlfarth (1965). As a criterion for itinerancy of the magnetism they used the ratio of the magnetic moment deduced from the measured Curie-constant and that obtained from saturation experiments. For localized magnetism this ratio is of order 1. For itinerant (intermediate) magnetism it is larger than 1. Their conclusion is that PdFe and PdCo should be treated as itinerant (intermediate) magnets. However, if we apply the same criterion to the experimental results obtained by Chouteau et al. (1974) and by Star et al. (1975), we have to conclude that low concentrated PdFe, PdCo and PdMn alloys should be treated as localized magnets (Nieuwenhuys et al. 1978).

So far the occurrence of a lower critical concentration for magnetic order has not been mentioned. Experiments on PdNi alloys (see section 3.1) have made clear that such a critical concentration exists (here 2.3 at.% Ni). This problem has been treated theoretically by Kim (1970). He extended the Anderson model (Anderson 1961) to the many-impurity case, including also d–d intra-atomic interactions. His conclusion is that as soon as the alloy obeys the Anderson–Wolff–Clogston criterion for the occurrence of localized moments it will also

order magnetically. So there is no lower critical concentration for magnetic ordering, but rather one for the appearance of localized magnetic moments (see also Chouteau 1976).

The dynamic properties of giant moment ferromagnetism have been treated by Doniach and Wohlfarth (1967), Cole and Turner (1969), and Long and Turner (1970). Their starting point is again the Hamiltonian $\mathcal{H} = J \Sigma_j \sigma(\chi_j) S_j$. According to Stringfellow (1968), J is approximately 2.4×10^{-20} J [$= 2.4 \times 10^{-13}$ ergs = 0.15 eV] in the case of PdFe. Note that the model of Doniach and Wohlfarth does not possess the restrictions necessary for the Takahashi and Shimizu approximation. After solving this Hamiltonian and including the d–d intra-atomic interaction

$$\chi(q, \omega) = \frac{1}{N_d} \sum_k \frac{f_{k,\uparrow} - f_{k+q,\downarrow}}{\omega - (E_k - E_{k+q})} \tag{4.26}$$

(leading to the Lindhard function for a parabolic band) χ becomes (ignoring exchange-enhancement for the moment)

$$\chi(q, \omega) = \frac{1}{N_d} \sum_k \frac{f_{k,\uparrow} - f_{k+q,\downarrow}}{\omega - (E_k - E_{k+q}) - IM'_d - 2JM'_i} \tag{4.27}$$

where M'_d and M'_i are the reduced magnetizations of the d-electrons and of the localized impurities, respectively. To obtain the enhanced susceptibility, the usual random phase approximation has to be applied. It should be noted that for $\omega \to 0$ eq. (4.27) is similar to the one used by Kim (1966).

From the calculation of the susceptibility, Doniach and Wohlfarth (1967) conclude two spin wave modes, a low frequency acoustical one and a high frequency optical one. Cole and Turner (1969) have pointed out that the results of Doniach and Wohlfarth (1967) for the acoustic mode are only valid for $q \ll q_{min}$, since a distinction has to be made between the ranges of q-values because of the polarization of the Fermi sea. The borderline q_{min} is given by $q_{min} = M_d / 2E_F N_d$. For the appropriate ranges the spin wave spectrum is characterized by $\omega_{ac} = Dcq^2$, where D is the spin wave stiffness constant, and by $\omega_{opt} = \omega^0_{opt} - D_{opt} q^2$, where $\omega_{opt} = JM'_d + 2JM'_i$.

Long and Turner (1970) have calculated the electrical resistivity due to spin waves, and obtained results proportional to $T^{3/2}$. On the basis of a molecular field approximation the resistivity is found to be proportional to T at temperatures just below T_c. Recently, Korenblitz and Shender (1976) have obtained an expression for D based on a model with essential ingredients: the random position of the magnetic moments, and an exchange interaction between these moments falling off exponentially with distance. Using percolation theory ideas, they arrive at the conclusion that for very low concentrations D should vary exponentially with c, while for the higher concentrations a linear dependence on c should be found. This latter conclusion is in agreement with those of the other calculations mentioned above.

Considering the experimental values of D, rather different results have been deduced from the various measured properties, e.g. for 1 at.% PdFe values

between 2×10^{-42} J m^2 [$= 2 \times 10^{-31}$ erg cm$^2 = 15$ K Å^2] and 10^{-40} J m^2 [$= 10^{-29}$ erg cm$^2 = 700$ K Å^2] have been reported (see Stringfellow 1968, Long and Turner 1970, T.F. Smith et al. 1970, Skalski et al. 1970, Williams and Loram 1971, Williams et al. 1971, 1973, Colp and Williams 1972, Williams 1972, Star et al. 1975). Nevertheless, considering the concentration dependence obtained by the different workers, a reasonable agreement with the predicted results is obtained.

(*b*) *The giant moment*

Throughout this article it has been assumed that the giant moment could be described as a localized bare moment due to the magnetic impurity which polarizes the surrounding host. In the case of large host susceptibility this polarization can be much larger than the bare moment itself. A theoretical basis for this picture emerges by treating the localized magnetic moment and its interaction with the surroundings. The Virtual Bound State (VBS) model (Mott 1949, Friedel 1958) has provided a sound framework for the understanding of the existence of localized moments. This VBS picture has been translated into mathematical models by Anderson (1961), Wolff (1961) and by Clogston et al. (1962). Later Hirst (1970, 1971) suggested that these calculations might overemphasize the itinerant character of the localized moments. Reviews on this subject may be found in the fifth volume of Magnetism (Wohlleben and Coles 1973, Blandin 1973).

With the existence of the localized moment established, the interaction with the host metal may be denoted as (following Doniach and Wohlfarth 1967)

$$\mathcal{H}_{\text{int}} = J \sum_i \sigma(r_i^{\text{Fe}}) S_i \tag{4.28}$$

where r_i^{Fe} is the lattice site of S_i and σ is the spin density operator. From this Hamiltonian, Doniach and Wohlfarth (1967) derive, within the linear response approximation

$$\mu = g\mu_B S(1 + \alpha\chi_{\text{Pd}}) \tag{4.29}$$

where $\alpha = 2J/Ng^2\mu_B^2$. Note that χ_{Pd} also governs the spatial extension of the moment. Similar results have been obtained by Giovannini et al. (1964), Takahashi and Shimizu (1965) (see section 4.2.1 (a) and Clogston et al. 1962). Zuckermann (1971) has added an extra term $\beta\chi_{\text{loc}}$ to $1 + \alpha\chi_{\text{Pd}}$, representing a local extra enhancement of the host susceptibility due to the presence of the magnetic atom. Kim and Schwartz (1968) have gone beyond the linear response approximation by considering the susceptibilities of the spin-up and spin-down electrons separately within the random phase approximation. They showed that the magnitude as well as the range of the induced polarization decreased with increasing total magnetization of the itinerant electrons. This result explains the decreasing moment per dissolved Fe-atom with increasing concentration in PdFe.

Suhl (1975) interprets the occurrence of giant moments within the Landau–

Ginsburg theory of second order phase transitions, as thermodynamic fluctuations. The starting point is also the Hamiltonian given in eq. (4.28). From this calculation he obtains results similar to those of Kim and Schwartz (1968).

The origin of the effective exchange interaction J has been discussed by Moriya (1965b) and later by Campbell (1968). Clogston et al. (1962) have ascribed this interaction entirely to exchange effects, implying J to be positive. This completely neglects possible negative values of J (e.g. Kondo effect). Moriya (1965b) has further treated the induced moment problem by incorporating into the Anderson model (Anderson 1961) or into the Wolff model (Wolff 1961) a five-fold degeneracy of the impurity level and the intra-atomic exchange interaction of the host metal. Based on the investigation of the "two localized moment" problem by Alexander and Anderson (1964) and by Moriya (1965a), he treats the interaction between the host and the magnetic atom as due to covalent admixture. In addition there is of course the usual exchange interaction (always positive), but this is expected to be a minor contribution to the total interaction. Moriya reaches the conclusion that the induced moment equals a constant δM times the generalized susceptibility. The constant δM is determined by two major terms: one due to the energy shift of the impurity levels, giving an antiparallel polarization, and the other due to the admixture between the band and the impurity levels, giving a positive polarization. The results for δM appear to be essentially independent of the choice of the starting model (Anderson or Wolff) and of the shape of the density of states. The number of d-electrons in the host metal and impurity atom determine for the major part the sign and magnitude of δM. From his calculations Moriya (1965b) was able to explain the giant moment of Fe and Co in Pd and the negative polarization in PdCr, and to predict a smaller but positive polarization of Mn in Pd, the latter being confirmed by experiments (Star et al. 1975). Thus, the calculations by Moriya provide a basis for the "giant moment" phenomenon and its spatial extension.

(c) *Short range or direct interactions*

In the foregoing paragraphs it has been accepted that the indirect RKKY-type interactions are the main cause of the magnetic ordering in dilute alloys. However, experiments on, e.g., PdMn have shown that direct interactions can play a role at concentrations larger than 1 at.%. As mentioned above, Alexander and Anderson (1964) and Moriya (1965a) have treated the problem of two neighbouring localized magnetic moments. Moriya generalized the Anderson model for the case of a five-fold degenerate d-orbitals. The effective exchange can then be calculated as due to d–d covalent admixture. The conclusions are that atoms with nearly half-filled d-shells couple antiferromagnetically for any value of the magnetic moment; the heavier atoms (with nearly filled d-shells) couple ferromagnetically. This is in agreement with the antiferromagnetism of Cr and Mn and the ferromagnetism of Co, Fe and Ni.

For alloys in general, it again appears that the chance of ferromagnetic coupling increases with increasing number of d-electrons. From this calculation, the antiferromagnetic coupling between Mn-pairs dissolved in Pd or Pt is

explained. As mentioned in section 3.1 this coupling is responsible for the spin glass behaviour at higher concentrations. Remarkably, going one step further, it appears that the coupling between Fe, Co or Mn and the Pd-*atoms* is ferromagnetic and that between Cr and Pd-*atoms* is antiferromagnetic. So even this completely localized picture accounts for the observed giant moments, which emphasizes the insensitivity of the sign of the induced polarization to the band structure.

4.2.2. Spin glass alloys

The stimulation of an intense theoretical interest in the spin glass problem began with the Edwards–Anderson (EA) (1975) model. These authors replaced the random occupancy of lattice sites coupled via the oscillating RKKY interaction by a model of a regular lattice with random bonds or interaction strengths. Thus, a simple Hamiltonian results: $\mathcal{H} = -\Sigma_{i,j} J_{ij} \boldsymbol{S}_i \cdot \boldsymbol{S}_j - g\mu_B H \Sigma_i S_i^z$ where the distribution of the J_{ij} is random, i.e. $P(J_{ij})$ is a Gaussian. The solution for the free energy

$$F = \overline{F\{J_{ij}\}} = \int P(J)F(J)\,\mathrm{d}J = \int P(J)\{-k_B T \ln[\mathrm{Tr}\exp(-\mathcal{H}/k_B T)]\}\,\mathrm{d}J$$

is rather difficult and has been the subject of various methods of calculation. These involve such techniques as the replica trick, mean field and renormalization group treatments, and exactly soluble spherical and ring diagram models. A number of review papers have appeared which elaborate the mathematics and methods of the EA model (Sherrington 1976, Fischer 1977, Binder 1977a, Anderson 1977, Aharony 1978). In these treatments the order parameter which appears at the freezing temperature, T_f, is defined as $q = \overline{\langle S_i \rangle^2}$ where $\langle\ \ \rangle$ and $\overline{}$ represent a thermal and a configurational average, respectively (see section 1.3). This order parameter is different from the usual phase transition order parameter, $\langle S_i \rangle$, and thereby causes non-ordinary critical phenomena and exponents.

The mean random field (MRF) (probability distribution model, see section 4.1) approximation has recently been extended within the framework of the EA model (Klein 1976). The magnetic properties which are easily obtained from the MRF approach are similar to those derived from the EA free energy solutions. When a cut-off of a nearest neighbor distance for the closest approach between two impurities is invoked, a finite freezing temperature is found instead of $T_f = \infty$ as with earlier MRF calculations (Riess and Klein 1977).

A second theoretical model is based upon a random site representation for which J_{ij} depends upon the atoms at the end of the bonds (Mattis 1976, Luttinger 1976, Aharony and Imry 1976). Writing J_{ij} as $J\epsilon_i\epsilon_j$ where $\epsilon_i = 1$ for an A-atom and $\epsilon_i = -1$ for a B-atom, we have the Hamiltonian

$$\mathcal{H} = -\sum_{i,j} J\epsilon_i\epsilon_j \boldsymbol{S}_i \cdot \boldsymbol{S}_j - g\mu_B H \sum_i S_i^z.$$

By transforming to a new spin and field variable $\tau_{i,j} \equiv \epsilon_{i,j} \boldsymbol{S}_{i,j}$ and $H_i \equiv H\epsilon_i$, the

Hamiltonian becomes an ordinary Heissenberg Hamiltonian in a random (up–down) field

$$\mathcal{H} = -J \sum_{i,j} \tau_i \cdot \tau_j - g\mu_B \sum_i H_i \tau_i^z.$$

For unequal concentrations of A or B atoms ($\bar{\epsilon}_i \neq 0$), a ferromagnetic phase will appear. However, with equal concentration $\bar{\epsilon}_i = 0$, but $\overline{|\epsilon_i|} = 1$, and the spin glass phase is possible. Here the order parameter is the ordinary one $\langle \tau_i \rangle \equiv \overline{|\langle S_i \rangle|}$. Furthermore, exact solutions of the above Hamiltonian are accessible to give the full thermodynamic behaviour.

A final technique, which is especially suitable to the "randomness" of the spin glasses, is that of Monte Carlo computer simulation. Basically the Monte Carlo method amounts to a numerical determination of the thermal average of a given physical quantity. Here the usual integrals are replaced by a finite sum over an "importance" sampling of points in phase space. This specific sampling is chosen with a probability $\exp(-U/k_B T)$ (where U is the interaction potential). Then for a sufficiently large number of these points, a good approximation can be obtained for the thermal average. The choice of these "importance" points according to the above probability is made from a Markov process in which a chain of points is constructed using a transition probability W consistent with the detailed balance condition. The problem is now to choose an appropriate W for the given physical situation. In addition, in order to better determine the accuracy and degree of convergence, a time is associated with the steps in the Markov chain. This leads to a master-equation-governed probability that the system is in a particular state at a particular time. Thus, the dynamics of the physical quantity into equilibrium may be followed via the Monte Carlo steps (Binder 1974). Using the EA Gaussian $P(J)$, many of the spin glass properties have been calculated by Binder and co-workers (Binder and Stauffer 1976, Binder and Schroder 1976a,b, Binder 1977a,b). The computer simulations which are primarily based upon the EA model give a better agreement with the experimental results than the analytic calculations of the same properties. Yet there is still much to be accomplished before a complete theoretical description of the spin glass phenomenon is attained.

4.3. Conclusions and future directions

In the preceeding sections we have introduced the important concepts and physical models used to describe the two different ways in which magnetic ordering can occur in dilute transiton metal alloys. Then a survey was presented of the various systems in which such ordering appears. This was followed by a review of the salient experimental features which manifest themselves and which lend support to our picture of giant moment ferromagnetism and spin glass freezing. Finally an introduction was given to the random molecular field model – a very useful theoretical method to calculate the general properties of

random magnetic alloys. Within the framework of this model and by using realistic, distant-dependent exchange interactions $J(r)$ much of the experimental behaviour may be simply obtained. In addition, a summary of other theoretical approaches and some of the modern techniques were briefly described. The Appendix with table A.1 gives a complete listing of measurements performed on giant moment alloys and their most characteristic parameters.

While there exists a number of older theories describing the giant moment formation and the low temperature behaviour, the magnetic ordering phenomenon can be nicely discussed within a percolation representation which is very similar to certain spin glass models. The main difference is that for the giant moment case $J(r)$ strongly favours parallel orientations, so a ferromagnetic, infinite cluster or chain is formed. The spin glass freezing required random orientations within the infinite cluster. Here additional work is needed and hopefully a synthesis of these two magnetic states will be attained via percolation theory. Presently the spin glass problem is receiving enormous attention especially from the theoretical side and it is impossible to mention in this article all the recent calculations and methods. There is further a great deal of controversy concerning which of two general approaches is most suitable for the spin glass behaviour. Although the phenomenological super-paramagnetic model gives a good description of the low temperature spin glass behaviour, it fails to meet the requirements of a sharp freezing and dynamical cluster growth above the freezing temperature. On the other hand, the extension of the critical phenomenon or phase transition theories while focusing upon the freezing behavior has only begun to include the very low or very high temperature regimes. It must then be left to future investigations to resolve these spin glass disputes.

The experimental situation is moving into a second generation of highly sophisticated and accurate measurements. Present attention is centering on dynamical and time dependent effects employing the most modern of techniques, e.g. neutron scattering, μ^+SR etc. The results of these studies will certainly stimulate the theoretical progress and offer ways of distinguishing between the various models and calculations. A very recent experimental discovery has been the transition of giant moment ferromagnetism into a spin glass state by reducing the temperature in an alloy of constant concentration (Verbeek et al. 1978a). This effect seems to be a general property of magnetic alloys, where at a certain concentration there will be paramagnetism $\rightarrow T_c \rightarrow$ ferromagnetism $\rightarrow T_f \rightarrow$ spin glass transitions, see fig. 5.

In brief both the giant moment and spin glass problems remain a topical area of magnetism and a better understanding will continue to develop in the coming years. The convergence in the description of these two types of magnetism is now underway and we might shortly expect a consistent and complete picture of the dilute magnetic component alloy, which also contains the rare earths as solute.

Appendix A: table A.1 on the main properties of "giant moment" alloys

In table A.1 data on the transition temperature, the saturation moment per dissolved magnetic atom, the magnetic quantum number and the effective g-value are collected. As in most cases with dilute alloy systems, the borderline between giant moment alloys and other alloys (e.g. spin glasses) is not sharp. Some alloys, which exhibit the phenomena of a giant moment do not order ferromagnetically at any of the concentrations under consideration. In spite of this difficulty we have included these alloys in the table for completeness. Therefore, in a number of cases T_c should be read as T_f, the spin glass freezing temperature. The first column gives the concentration of the magnetic atoms in at.% (or in parts per million if indicated), and the second column, an abbreviation of the experimental method. The meaning of the abbreviations are: Mössb.: Mössbauer effect; s.h.: specific heat; res.: electrical resistivity; d $\Delta\rho/\mathrm{d}T$: temperature derivative of the electrical resistivity; magn.: magnetization measurements; sucs.: susceptibility measurement; F.M.R.: ferromagnetic resonance; Arrott: T_c determined by means of an Arrott plot; W.F.: T_c determined applying the Weiss–Forrer method; model: T_c determined using model calculations; infl.: T_c determined as that temperature at which $\Delta\rho$ starts to deviate from a straight line as a function of T with increasing temperature; max.: T_c defined as that temperature at which ΔC or d $\Delta\rho/\mathrm{d}T$ attains its maximum value; knee: T_c defined as that temperature where a knee can be found in the resistivity versus temperature curve; W.M.F.: T_c determined from Weiss Molecular Field model calculations; N.O. means nuclear orientation experiments.

In the third column the reference is given. The fourth, fifth, sixth and seventh columns contain the values reported for the transition temperature in K, for the saturation moment μ in μ_B, for the total magnetic quantum number J and for the effective g-value g_{eff}, respectively. In the last part of table A.1 ("other alloys") the alloy composition is given in first column, and the fourth and fifth columns list the transition temperature and the magnetic moment, respectively. The magnetic quantum number and the effective g-value have been omitted here. We have used the "unit" μ_B for the magnetic moment per dissolved atom, instead of S.I. units, in order to facilitate comparison between the alloys. If one wishes to calculate the magnetic moment per unit of volume, one should remember that this is given by $\mu\mu_B N\rho c/(100\,M)$, where $\mu_B = 9.274096 \times 10^{-24}\,\mathrm{JT}^{-1}$ [$9.274096 \times 10^{-21}\,\mathrm{erg\,G}^{-1}$], N is Avogadro's number $= 6.022169 \times 10^{26}\,\mathrm{kmole}^{-1}$ [$6.022169 \times 10^{23}\,\mathrm{mole}^{-1}$], μ is the number of Bohr magnetons per dissolved atom, c the concentration in at.%, ρ the density of the alloy and M the molar mass of the alloy. The magnetic quantum number J is obtained from specific heat experiments by evaluating the magnetic entropy and assuming it equal to $cR\ln(2J+1)$. From magnetic measurements this quantity is obtained by fitting the experimental data to a Brillouin function. A table of the saturation moment and transition temperature of Fe dissolved in "Ni_3Al" and in "Ni_3Ga" can be found in section 3.1.3 (table 6).

TABLE A.1: Main properties of "giant moment" alloys
Main properties of Pd–Co alloys

Conc. (at. %)	Exp. method	Reference	Transition temperature (K)	Saturation moment (μ_B)	Magn. quantum number.	Eff. g-value
0.07	Mössb.	Dunlap and Dash (1967)	1.55			
0.075	s.h.	Nieuwenhuys et al. (1972)			1.2	
0.098	res.(infl.)	Williams and Loram (1969a,b)	0.8			
0.1	magn. (Arrott)	Bozorth et al.(1961)	7	10.8		
0.16	s.h. (model)	Nieuwenhuys et al. (1972)	1.84		1.35	5.3
0.19	Mössb.	Dunlap and Dash (1967)	6.5			
0.2	$d\Delta\rho/dT$ (model)	Nieuwenhuys et al. (1972)	3.5			
0.2	res. (infl.)	Williams and Loram (1969a,b)	2.95			
0.24	s.h. (model)	Nieuwenhuys et al. (1972)	4.16		1.44	6.7
0.3	magn.	Bozorth et al. (1962)	22			
0.3	res. (infl.)	Williams and Loram (1969a,b)	6.45			
0.35	s.h. (max.)	Nieuwenhuys et al. (1972)	8.8		1.35	
0.4	susc. (θ)	Alekseevski et al. (1968)	10			
0.49	Mössb.	Dunlap and Dash (1967)	18.8			
0.5	magn. (Arrott)	Bozorth et al. (1961)	25	9		
0.5	res. (infl.)	Williams and Loram (1969a,b)	16.2			
0.7	res. (infl.)	Williams and Loram (1969a,b)	27.5			
1	susc.	Gerstenberg (1958)	253	3.3		

Main properties of Pd–Co alloys (contd.)

Conc. (at. %)	Exp. method	Reference	Transition temperature (K)	Saturation moment (μ_B)	Magn. quantum number.	Eff. g-value
1	magn. (Arrott)	Bozorth et al. (1961)	90	8.9		
1	magn. (Arrott)	Shaltiel et al. (1964)	52	10		
1.0	res. (infl.)	Williams and Loram (1969a,b)	44.0			
1	F.M.R.	Bagguley and Robertson (1974)	70			
1.5	susc (θ)	Alekseevski et al. (1968)	60			
1.5	F.M.R.	Bagguley and Robertson (1974)	85			
1.91	Mössb.	Dunlap and Dash (1967)	90			
2	susc. (θ)	Alekseevski et al. (1968)	95			
3	susc.	Gerstenberg (1958)	305	3.5		
3	Mössb.	Nagle et al. (1962)	130			
3	susc*	Maartense and Williams (1976)	135.1			
3.5	susc (θ)	Alekseevski et al. (1968)	150			
4	susc*	Maartense and Williams (1976)	169.5			
4.5	Mössb.	Dunlap and Dash (1967)	186			
5	susc.	Gerstenberg (1958)	323	3.5		
5	magn.	Bozorth et al. (1961)		6.2		
5	susc (θ)	Alekseevski et al. (1968)	180			
5	susc*	Maartense and Williams (1976)	188.6			

Main properties of Pd–Co alloys (contd.)

Conc. (at. %)	Exp. method	Reference	Transition temperature (K)	Saturation moment (μ_B)	Magn. quantum number.	Eff. g-value
7	susc.	Gerstenberg (1958)	353	3.4		
7	susc (θ)	Alekseevski et al. (1968)	220			
7.5	susc*	Maartense and Williams (1976)	252.2			
8	magn.	Bozorth et al. (1961)		5.3		
8	Mössb.	Nagle et al. (1962)	275			
8.3	susc (θ)	Alekseevski et al. (1968)	250			
8.6	susc (θ)	Alekseevski et al.(1968)	260			
10	magn. (W.F.)	Grube and Winckler (1935)	300			
10.4	susc (θ)	Alekseevski et al. (1968)	285			
13	magn.	Bozorth et al. (1961)		4.7		
15	Mössb.	Nagle et al. (1962)	423			

Main properties of Pd–Fe alloys

0.6 ppm	Mössb.	Gierisch et al. (1977)		12.9	6	
7 ppm	Mössb.	Gierisch et al. (1977)		12.9	6	
7.6 ppm	N.O.	Flouquet et al. (1977)			5	2
0.005	susc.	Chouteau and Tournier (1971)	0.016			

Main properties of Pd–Fe alloys (contd.)

Conc. (at. %)	Exp. method	Reference	Transition temperature (K)	Saturation moment (μ_B)	Magn. quantum number.	Eff. g-value
0.007	susc.	Chouteau and Tournier (1971)	0.036			
0.009	susc.	Chouteau and Tournier (1971)	0.054			
0.01	Mössb.	Craig et al. (1962)		12.6	6.5	2.4
0.01	magn. (Arrott)	McDougald and Manuel (1968)	0.44	4.5	16	2
0.01	magn. (W.M.F.)	McDougald and Manual (1970)	0.22			
0.01	susc.	Chouteau and Tournier (1971)	0.059			
0.013	susc.	Chouteau and Tournier (1971)	0.097			
0.018	susc.	Chouteau and Tournier (1971)	0.16			
0.02	susc.	Chouteau and Tournier (1971)	0.2			
0.02	magn. (Arrott)	Chouteau and Tournier (1971)	0.055			
0.03	susc.	Chouteau and Tournier (1971)	0.39			
0.03	magn. (Arrott)	Chouteau and Tournier (1971)	0.115			
0.035	magn. (Arrott)	Chouteau and Tournier (1971)	0.13			
0.043	magn. (Arrott)	Chouteau and Tournier (1971)	0.2			
0.05	magn. (Arrott)	McDougald and Manuel (1968)	0.6	6	8.5	2
0.05	magn. (W.M.F.)	McDougald and Manuel (1970)	0.55			
0.06	s.h.	Chouteau et al. (1970)			3.5	
0.06	magn. (Arrott)	Chouteau and Tournier (1971)	0.41			

Main properties of Pd–Fe alloys (contd.)

Conc. (at. %)	Exp. method	Reference	Transition temperature (K)	Saturation moment (μ_B)	Magn. quantum number.	Eff. g-value
0.068	magn. (Arrott)	Chouteau and Tournier (1971)	0.47			
0.07	magn. (Arrott)	McDougald and Manuel (1968)	0.78	7	8.5	2
0.07	magn. (W.M.F.)	McDougald and Manuel (1970)	0.67			
0.1	Mössb.	Maley et al. (1967)		11.1	3.76	2.95
0.1	magn. (Arrott)	McDougald and Manuel (1968)	1.08	8.5	8.5	2
0.1	magn. (W.M.F.)	McDougald and Manuel (1970)	1.1			
0.1	$d\Delta\rho/dT$ (max.)	Kawatra and Budnick (1970)	0.7			
0.15	magn. (Arrott)	Crangle and Scott (1965)	4.3			
0.15	$d\Delta\rho/dT$ (max.)	Wilding (1967)	2			
0.15	magn. (Arrott)	McDougald and Manuel (1968)	2.12	10	8.5	2
0.15	magn. (W.M.F.)	McDougald and Manuel (1970)	2.2			
0.16	res. (knee)	Williams and Loram (1969a,b)	2.8			
0.16	s.h. (model)	Nieuwenhuys et al. (1972)	2.2		1.6	6.3
0.19	s.h. (max.)	Coles et al. (1965)	2			
0.2	res. (knee)	Mydosh (1974)	2.5			
0.22	Mössb.	Trousdale et al. (1967)	3.5			
0.22	$d\Delta\rho/dT$ (model)	Nieuwenhuys et al. (1972)	3			
0.23	res. (knee)	Williams and Loram (1969a,b)	5.4			

Main properties of Pd–Fe alloys (contd.)

Conc. (at. %)	Exp. method	Reference	Transition temperature (K)	Saturation moment (μ_B)	Magn. quantum number.	Eff. g-value
0.23	s.h. (max.)	Nieuwenhuys (1975)	3.7		2	
0.25	$d\Delta\rho/dT$ (max.)	Kawatra and Budnick (1970)	4.2			
0.25	F.M.R.	Bagguley and Robertson (1974)	20			
0.28	magn. (Arrott)	Crangle and Scott (1965)	9.5			
0.29	$d\Delta\rho/dT$ (max.)	Wilding (1967)	7.5			
0.35	s.h. (max.)	Nieuwenhuys (1975)	6.7		2.1	
0.4	Mössb.	Trousdale et al. (1967)	17			
0.41	res. (knee)	Williams and Loram (1969a,b)	13.0			
0.5	F.M.R. (W.F.)	Bagguley and Robertson (1968)	29			
0.5	$d\Delta\rho/dT$ (max.)	Mydosh et al. (1968)	7			
0.53	Magn. (Arrott)	Crangle and Scott (1965)	23			
0.53	$d\Delta\rho/dT$ (max.)	Wilding (1967)	20			
0.54	res. (knee)	Williams and Loram (1969a,b)	20.1			
0.78	res. (knee)	Williams and Loram (1969a,b)	32.6			
1	susc.	Gerstenberg (1958)	238	4.1		
1	magn. (Arrott)	Clogston et al. (1962)	39	9.7		
1	susc.	Clogston et al. (1962)	55	11.3		
1	magn. (Arrott)	Shaltiel et al. (1964)	56	11.5		

Main properties of Pd–Fe alloys (contd.)

Conc. (at. %)	Exp. method	Reference	Transition temperature (K)	Saturation moment (μ_B)	Magn. quantum number.	Eff. g-value
1	F.M.R. (W.F.)	Bagguley and Robertson (1968)	60			
1	$d\Delta\rho/dT$ (max)	Mydosh et al. (1968)	28			
1	Mössb.	Clark and Meads (1970)	33.3		5	
1	Mössb.	Levy et al. (1974)	37.3	8.1		
1	res (knee)	Mydosh (1974)	30			
1.03	$d\Delta\rho/dT$ (max)	Wilding (1967)	40			
1.25	magn. (W.F.)	Crangle (1960)	66			
1.25	magn.	Bozorth et al. (1962)	65			
1.26	Mössb.	Craig et al. (1965)	90			
1.5	F.M.R.(W.F.)	Bagguley and Robertson (1968)	69			
1.7	F.M.R.(W.F.)	Bagguley and Robertson (1968)	112			
1.7	F.M.R.	Bagguley and Robertson (1974)	89			
2	magn	Bozorth et al. (1962)	90			
2	Mössb	Clark and Meads (1970)	64.5			
2.8	Mössb.	Carlow and Meads (1969)	95			
2.65	Mössb.	Craig et al. (1965)	90		1	
3	susc.	Gerstenberg (1958)	253	4.4		
3	$d\Delta\rho/dT$ (max.)	Kawatra et al. (1969)	97			

Main properties of Pd–Fe alloys (contd.)

Conc. (at. %)	Exp. method	Reference	Transition temperature (K)	Saturation moment (μ_B).	Magn. quantum number.	Eff. g-value
3.16	magn. (W.F.)	Crangle (1960)	122			
3.25	magn.	Bozorth et al. (1962)	125			
4	Mössb.	Trousdale et al. (1967)	85			
4	F.M.R.(W.F.)	Bagguley and Robertson (1968)	140			
4.0	Mössb.	Carlow and Meads (1969)	106			
5	susc.	Gerstenberg (1958)	273	4.4		
5.11	magn. (W.F.)	Crangle (1960)	162			
5.8	Mössb.	Carlow and Meads (1969)	146			
6	$d\Delta\rho/dT$ (max.)	Kawatra et al. (1969)	162			
6.4	Mössb.	Carlow and Meads (1969)	147			
7	susc.	Gerstenberg (1958)	288	4.3		
7.2	Mössb.	Carlow and Meads (1969)	168			
7.5	Mössb.	Trousdale et al. (1967)	170			
9.78	magn. (W.F.)	Crangle (1960)	236			
9	$d\Delta\rho/dT$ (max.)	Kawatra et al. (1969)	212			
9.5	Mössb.	Carlow and Meads (1969)	220			
10.3	Mössb.	Carlow and Meads (1969)	246			
12.3	Mössb.	Carlow and Meads (1969)	282			

Main properties of Pd–Fe alloys (contd.)

Conc. (at. %)	Exp. method	Reference	Transition temperature (K)	Saturation moment (μ_B)	Magn. quantum number.	Eff. g-value
13	Mössb.	Trousdale et al. (1967)	300			
15.75	magn. (W.F.)	Crangle (1960)	377			

Main properties of Pd-Mn alloys

Conc. (At. %)	Exp. method	Reference	Transition temperature (K)	Saturation moment (μ_B)	Magn. quantum number.	Eff. g-value
1 ppm	N.O.	Benoit et al. (1977)			2.5	3
0.05	magn.susc.	Star et al. (1975)	0.18	7.4	1.5	3.15
0.054	magn.susc.	Star et al. (1975)	0.24	7.3	2.4	3.18
0.08	s.h. (W.M.F.)	Boerstoel et al. (1972)			2.2	2.6
0.08	magn.susc.	Star et al. (1975)	0.39	7.8	2.4	3.18
0.15	res. (knee)	Nieuwenhuys (1975)	0.22			
0.19	s.h. (W.M.F.)	Boerstoel et al. (1972)			2.9	2.8
0.2	res. (knee)	Nieuwenhuys (1975)	0.39			
0.23	magn.susc.	Star et al. (1975)	1.33	8.0	2.5	2.97
0.31	res. (knee)	Nieuwenhuys (1975)	0.76			
0.4	res. (knee)	Nieuwenhuys (1975)	1.03			

Main properties of Pd–Mn alloys (contd.)

Conc. (at. %)	Exp. method	Reference	Transition temperature (K)	Saturation moment (μ_B)	Magn. quantum number.	Eff. g-value
0.45	magn.	Rault and Burger (1969)	1.41			
0.49	magn.susc.	Star et al. (1975)	2.66	6.6	1.9	2.91
0.49	magn. (Arrott)	Star et al. (1975)	1.55			
0.5	res. (knee)	Sarachik and Shaltiel (1967)	1.6			
0.5	res. (knee)	Nieuwenhuys (1975)	1.44			
0.54	s.h.	Boerstoel et al. (1972)	1.98		2.31	3.0
0.65	res. (knee)	Nieuwenhuys (1975)	2.05			
0.7	res. (knee)	Nieuwenhuys (1975)	2.48			
0.96	magn.susc.	Star et al. (1975)	4.56	6.9	3.4	2.84
0.96	magn. (Arrott)	Star et al. (1975)	3.45			
1	res. (knee)	Sarachik and Shaltiel (1967)	3.6			
1	res. (knee)	Nieuwenhuys and Boerstoel (1970)	3.41			
1.05	res. (knee)	Williams and Loram (1969 a,b)	3.9			
1.2	magn.	Rault and Burger (1969)	4.95			
1.33	magn. susc.	Star et al. (1975)	7.48	6.8	2.1	2.86
1.33	magn. (Arrott)	Star et al. (1975)	4.54			
1.35	s.h.	Boerstoel et al. (1972)	4.48		2.37	3.2
1.8	magn.	Rault and Burger (1969)	7.5			

Main properties of Pd–Mn alloys (contd.)

Conc. (at. %)	Exp. method	Reference	Transition temperature (K)	Saturation moment (μ_B)	Magn. quantum number.	Eff. g-value
2.4	res. (knee)	Williams and Loram (1969 a,b)	7.35			
2.45	s.h.	Boerstoel et al. (1972)	5.78		2.33	
2.45	magn. susc.	Star et al. (1975)	7.12	5.7	2.2	2.65
2.45	magn. (Arrott)	Star et al. (1975)	6.14			
2.7	s.h. (max.)	Zweers and Van den Berg (1975)	4.75			
2.91	res. (knee)	Williams and Loram (1969 a,b)	7.71			
3	susc.	Gerstenberg (1958)	60	4.6		
3	Magn. (Arrott)	Shaltiel et al. (1964)	8	6.3		
3	susc.	Burger and McLachlan (1973)	7.3			
3.0	s.h. (max.)	Zweers and Van den Berg (1975)	4.5			
3.3	s.h. (max.)	Zweers and Van den Berg (1975)	4.8			
3.75	res. (knee)	Coles et al. (1975)	6.3			
3.78	magn.	Rault and Burger (1969)	6			
4.0	s.h. (max)	Zweers and Van den Berg (1975)	7.5			
4	susc.	Zweers et al. (1977)	2.2			
4.1	res. (knee)	Coles et al. (1975)	4.5			
4.6	magn.(Arrott)	Coles et al. (1975)	1.2			
4.95	magn. (θ)	Rault and Burger (1969)	3.9			

Main properties of Pd-Mn alloys (contd.)

Conc. (at. %)	Exp. method	Reference	Transition temperature (K)	Saturation moment (μ_B)	Magn. quantum number.	Eff. g-value
5	susc.	Gerstenberg (1958)	63	2.1		
5.5	s.h. (max.)	Zweers and Van den Berg (1975)	10.4			
6	susc.	Zweers et al. (1977)	3.9			
6.5	susc. (max.)	Coles et al. (1975)	2.6			
6.75	magn. (θ)	Rault and Burger (1969)	1.17			
8	susc.	Zweers et al. (1977)	5.7			
8.5	susc. (max.)	Coles et al. (1975)	5.2			
9.5	s.h. (max.)	Zweers and Van den Berg (1975)	16.2			
10	magn.	Rault and Burger (1969)	4			
10	susc.	Zweers et al. (1977)	8.8			
10.5	susc. (max.)	Coles et al. (1975)	8.7			
11	susc.	Burger and McLachlan (1973)	9.7			
15	magn.	Rault and Burger (1969)	13			
25	magn.	Rault and Burger (1969)	25			

Main properties of Pd–Ni alloys

Conc. (at. %)	Exp. method	Reference	Transition temperature (K)	Saturation moment (μ_B)	Magn. quantum number.	Eff. g-value
2.25	magn.	Murani et al. (1975)	0 ± 0.1			
2.35	magn.	Murani et al. (1975)	0.3			
2.42	magn.	Murani et al. (1975)	0.85			
2.5	magn.	Crangle and Scott (1965)	12			
3	magn.	Bozorth et al. (1962)	32			
3	magn.	Murani et al. (1975)	12.5			
3.33	magn.	Crangle and Scott (1965)	27	1.6		
3.5	magn.	Murani et al. (1975)	22			
4.29	magn.	Crangle and Scott (1965)	59	2.4		
5	magn.	Bozorth et al. (1962)	75			
5	F.M.R.	Bagguley and Robertson (1974)	160			
5.55	magn.	Crangle and Scott (1965)	88	2.5		
11.78	magn.	Crangle and Scott (1965)	177	2.2		

Main properties of Pt–Co alloys

Conc. (at. %)	Exp. method	Reference	Transition temperature (K)	Saturation moment (μ_B)	Magn. quantum number.	Eff. g-value
0.0414	susc. (θ)	Tissier and Tournier (1972)	-1.6	$5.11_{(p_{eff})}$		
0.061	susc.	Swallow et al. (1975)		5.1-6.3		
0.067	s.h.	Nieuwenhuys et al. (1973)			0.98	
0.0807	susc. (θ)	Tissier and Tournier (1972)	-1.45	$5.14_{(p_{eff})}$		
0.163	susc. (θ)	Tissier and Tournier (1972)	-1	$5.3_{(p_{eff})}$		
0.271	susc. (θ)	Tissier and Tournier (1972)	0	$5.38_{(p_{eff})}$		
0.312	susc. (θ)	Tissier and Tournier (1972)	0.6	$5.56_{(p_{eff})}$		
0.5	magn.	Bozorth et al. (1962)	4			
0.5	susc.	Tsiovkin and Volkenshteyn (1965)		5.8		
0.5	s.h.	Nieuwenhuys et al. (1973)			1.05	
0.51	magn.	Crangle and Scott (1965)	2.7	2.5		
0.662	susc. (θ)	Tissier and Tournier (1972)	5.15	$5.68_{(p_{eff})}$		
0.7	magn.	Bozorth et al. (1962)	6			
0.8	s.h. (max.)	Nieuwenhuys et al. (1973)	3		0.92	
0.8	susc.	Rao et al. (1976)	2.75			
0.878	susc. (θ)	Tissier and Tournier (1972)	10.2	$5.78_{(p_{eff})}$		
0.88	s.h.	Wheeler (1969)	3.2		0.8	
0.99	magn.	Crangle and Scott (1965)	6.8	2.9		

Main properties of Pt–Co alloys (contd.)

Conc. (at. %)	Exp. method	Reference	Transition temperature (K)	Saturation moment (μ_B)	Magn. quantum number.	Eff. g-value
1	magn.	Bozorth et al. (1962)	12			
1.2	susc.	Rao et al. (1976)	8.4			
2	susc.	Rao et al. (1976)	22.8			
2.60	magn.	Crangle and Scott (1965)	39	3.4		
3.9	F.M.R.	Bagguley and Robertson (1974)	67			
5	magn.	Bozorth et al. (1962)	135			
5	susc.	Rao et al. (1976)	96			
5.17	magn.	Crangle and Scott (1965)	104	3.5		
10.2	magn.	Crangle and Scott (1965)	218	3.4		
15.2	magn.	Crangle and Scott (1965)	315	3.2		
20.1	magn.	Crangle and Scott (1965)		3.0		

Main properties of Pt–Fe alloys

Conc. (at. %)	Exp. method	Reference	Transition temperature (K)	Saturation moment (μ_B)	Magn. quantum number.	Eff. g-value
0.01	Mössb.	Scherg et al. (1974)		6.31	2.34	
0.05	res.	Swallow et al. (1971)			2.3	3.1

Main properties of Pt–Fe alloys (contd.)

Conc. (at. %)	Exp. method	Reference	Transition temperature (K)	Saturation moment (μ_B)	Magn. quantum number.	Eff. g-value
0.1	Mössb.	Maley et al. (1967)		6.46	3	2.17
0.45	magn.	Crangle and Scott (1965)	3.3			
0.5	magn.	Bozorth et al. (1962)	10			
0.5	susc.	Tsiovkin and Volkenshteyn (1965)		5.8		
0.87	magn.	Crangle and Scott (1965)	5.4	6.2		
1	magn.	Bozorth et al. (1962)	18			
1	Mössb.	Segnan (1967)	7			
1	res.(dρ/dT)	Kawatra et al. (1970)	5			
1	magn.	Koon and Gubser (1975)	4			
1.8	res.(dρ/dT)	Kawatra et al. (1970)	10			
2.3	magn.	Crangle and Scott (1965)	21.5	4.9		
3	magn.	Bozorth et al. (1962)	47			
3	Mössb.	Segnan (1967)	32			
3	res.(dρ/dT)	Kawatra et al. (1970)	25			
4.07	magn.	Crangle and Scott (1965)	59	4.9		
4.5	F.M.R.	Bagguley and Robertson (1974)	85			
4.8	Mössb.	Segnan (1967)	75			
5	res.(dρ/dT)	Kawatra et al. (1970)	65			

Main properties of Pt–Fe alloys (contd.)

Conc. (at. %)	Exp. Method	Reference	Transition temperature (K)	Saturation moment (μ_B)	Magn. quantum number.	Eff. g-value
6.3	magn.	Crangle and Scott (1965)	104	5.2		
6.8	Mössb.	Segnan (1967)	120			
7	res.(dρ/dT)	Kawatra et al. (1970)	107			
10	Mössb.	Segnan (1967)	170			
10	res.(dρ/dT)	Kawatra et al. (1970)	165			
12	Mössb.	Segnan (1967)	190			
12	res.(dρ/dT)	Kawatra et al. (1970)	200			
13	Mössb.	Segnan (1967)	200			
15	Mössb.	Segnan (1967)	200			
15	res.(dρ/dT)	Kawatra et al. (1970)	220			

Main properties of Pt–Mn alloys

Conc. (At. %)	Exp. method	Reference	Transition temperature (K)	Saturation moment (μ_B)	Magn. quantum number.	Eff. g-value
0.26	s.h. (max.)	Sacli et al. (1974)	0.39		3	
0.36	s.h.	Nieuwenhuys et al. (1973)			2.4	
0.47	s.h. (max,)	Sacli et al. (1974)	0.63		2.4	

Main properties of Pt–Mn alloys (contd.)

Conc. (at. %)	Exp. method	Reference	Transition temperature (K)	Saturation moment (μ_B)	Magn. quantum number.	Eff. g-value
0.5	susc.	Tsiovkin and Volkenshteyn (1965)		5.7		
0.5	susc.	Wassermann and Tholence (1977)	0.4	6		2.5
0.67	s.h. (max.)	Sacli et al. (1974)	0.87		2.4	
0.8	susc.	Wassermann and Tholence (1977)	0.8			
0.88	s.h. (max.)	Nieuwenhuys et al. (1973)	2		2.4	
0.97	s.h. (max.)	Sacli et al.(1974)	1.97		2.2	
1.35	s.h. (max.)	Sacli et al. (1974)	2.76		2.2	
1.64	s.h. (max.)	Nieuwenhuys et al. (1973)	4			
2.5	susc.	Wassermann and Tholence (1977)	2.5			

Other alloys

Alloy	Exp. method	Reference	T_c (K)	μ (μ_B)
$Mo_{0.99}Fe_{0.01}$	susc.	Clogston et al. (1962)	-4	2.1
$(Mo_{0.9}Pd_{0.1})Fe_{0.01}$	susc.	Clogston et al. (1962)	-33	11.2
$(Mo_{0.8}Pd_{0.2})Fe_{0.01}$	susc.	Clogston et al. (1962)	-10	6

Other alloys (contd.)

Alloy	Exp. method	Reference	T_c (K)	μ (μ_B)
$(Mo_{0.6}Pd_{0.4})Fe_{0.01}$	susc.	Clogston et al. (1962)	-5	2.6
$(Pd_{0.995}Ag_{0.005})Fe_{0.01}$	Mössb.	Levy et al. (1974)	34.6	7.8
$(Pd_{0.9975}Ag_{0.0025})Mn_{0.01}$	res. (knee)	Nieuwenhuys (1975)	3.3	
$(Pd_{0.995}Ag_{0.005})Mn_{0.01}$	res. (knee)	Nieuwenhuys (1975)	3.1	
$(Pd_{0.99}Ag_{0.01})Mn_{0.01}$	res. (knee)	Nieuwenhuys (1975)	2.8	
$(Pd_{0.98}Ag_{0.002})Fe_{0.0012}$	magn.	Guertin and Foner (1970)		7.2
$(Pd_{0.975}Ag_{0.025})Fe_{0.01}$	Mössb.	Levy et al. (1974)	29.9	7.1
$(Pd_{0.975}Ag_{0.025})Fe_{0.01}$	susc.	Budnick et al. (1974)	25.3	$12(p_{eff})$
$(Pd_{0.96}Ag_{0.04})Fe_{0.001}$	magn.	Guertin and Foner (1970)		7.4
$(Pd_{0.9}Ag_{0.1})Co_{0.01}$	magn.	Bozorth et al. (1962)	57	2.5
$(Pd_{0.9}Ag_{0.1})Fe_{0.0014}$	magn.	Guertin and Foner (1970)		4.7
$(Pd_{0.9}Ag_{0.1})Fe_{0.01}$	Mössb.	Levy et al (1974)	20.1	6.1
$(Pd_{0.9}Ag_{0.1})Fe_{0.01}$	susc.	Budnick et al. (1974)	17.6	$13(p_{eff})$
$(Pd_{0.75}Ag_{0.25})Fe_{0.01}$	susc.	Clogston et al. (1962)	12	8.3
$(Pd_{0.75}Ag_{0.25})Fe_{0.01}$	Mössb.	Levy et al. (1974)	7.5	4.9
$(Pd_{0.75}Ag_{0.25})Fe_{0.01}$	susc.	Budnick et al. (1974)	6.5	$16(p_{eff})$
$(Pd_{0.67}Ag_{0.33})Fe_{0.01}$	susc.	Budnick et al. (1974)	4	$17(p_{eff})$
$(Pd_{0.5}Ag_{0.5})Fe_{0.01}$	susc.	Budnick et al. (1974)	3.3	$15(p_{eff})$

Other alloys (contd.)

Alloy	Exp. method	Reference	T_c (K)	μ (μ_B)
$(Pd_{0.98}Ag_{0.01}Rh_{0.01})Fe_{0.001}$	magn.	Guertin and Foner (1970)		9.5
$(Pd_{0.94}Ag_{0.03}Rh_{0.03})Fe_{0.001}$	magn.	Guertin and Foner (1970)		7.4
$(Pd_{0.8}Ag_{0.1}Rh_{0.1})Co_{0.01}$	magn.	Bozorth et al. (1962)	18	5.5
$(Pd_{0.95}Cu_{0.05})Co_{0.01}$	magn.	Bozorth et al. (1962)	32	6.1
$(Pd_{0.9}Cu_{0.1})Co_{0.01}$	magn.	Bozorth et al. (1962)	23	5
$(Pd_{0.8}Cu_{0.2})Co_{0.01}$	magn.	Bozorth et al. (1962)	5	3.3
$(Pd_{0.7}Cu_{0.3})Co_{0.01}$	magn.	Bozorth et al. (1962)	3	2.3
$Pd_{0.99}(Co_{0.5}Fe_{0.5})_{0.01}$	magn.	Bozorth et al. (1962)	67	8.8
$Pd_{0.99}(Co_{0.5}Ni_{0.5})_{0.01}$	magn.	Bozorth et al. (1962)	32	5
$Pd_{0.9955}Fe_{0.0035}Mn_{0.001}$	s.h. (max)	Verbeek (1978)	7	
$Pd_{0.994}Fe_{0.0035}Mn_{0.0025}$	s.h. (max)	Verbeek (1978)	8.3	
$Pd_{0.9915}Fe_{0.0035}Mn_{0.005}$	s.h. (max)	Verbeek (1978)	8.6	
$Pd_{0.99}(Mn_{0.5}Fe_{0.5})_{0.01}$	magn.	Bozorth et al. (1962)	22	8
$Pd_{0.99}(Mn_{0.67}Fe_{0.33})_{0.01}$	magn.	Bozorth et al. (1962)	15	7
$(Pd_{0.8}Mo_{0.2})Fe_{0.01}$	susc.	Clogston et al. (1962)	0	6.1
$(Pd_{0.6}Mo_{0.4})Fe_{0.01}$	susc.	Clogston et al. (1962)	-9	4.1
$(Pd_{0.55}Mo_{0.45})Fe_{0.01}$	susc.	Clogston et al. (1962)	-15	3
$(Pd_{0.95}Pt_{0.05})Fe_{0.001}$	magn.	Guertin and Foner (1970)		9.5

Other alloys (contd.)

Alloy	Exp. method	Reference	T_c (K)	μ (μ_B)
$(Pd_{0.925}Pt_{0.075})Fe_{0.0008}$	magn.	Guertin and Foner (1970)		9.7
$(Pd_{0.9}Pt_{0.1})Fe_{0.0013}$	magn.	Guertin and Foner (1970)		5.7
$(Pd_{0.8}Pt_{0.2})Fe_{0.001}$	magn.	Guertin and Foner (1970)		4.4
$(Pd_{0.8}Rh_{0.2})Co_{0.01}$	magn.	Bozorth et al. (1962)	17	6
$(Pd_{0.6}Rh_{0.4})Co_{0.01}$	magn.	Bozorth et al. (1962)	6	3
$(Pd_{0.99}Rh_{0.01})Mn_{0.0065}$	res. (knee)	Nieuwenhuys (1975)	2.15	
$(Pd_{0.98}Rh_{0.02})Mn_{0.0065}$	res. (knee)	Nieuwenhuys (1975)	1.8	
$(Pd_{0.97}Rh_{0.03})Mn_{0.015}$	res. (knee)	Nieuwenhuys (1975)	3.7	
$(Pd_{0.96}Rh_{0.04})Mn_{0.0065}$	res. (knee)	Nieuwenhuys (1975)	1.4	
$(Pd_{0.96}Rh_{0.04})Mn_{0.015}$	res. (knee)	Nieuwenhuys (1975)	3	
$(Pd_{0.95}Rh_{0.05})Mn_{0.015}$	res. (knee)	Nieuwenhuys (1975)	2.5	
$(Pd_{0.94}Rh_{0.06})Mn_{0.015}$	res. (knee)	Nieuwenhuys (1975)	1.4	
$(Pd_{0.98}Rh_{0.02})Fe_{0.001}$	magn.	Guertin and Foner (1970)		11.9
$(Pd_{0.95}Rh_{0.05})Fe_{0.0005}$	magn.	Guertin and Foner (1970)		11.4
$(Pd_{0.95}Rh_{0.05})Fe_{0.0009}$	magn.	Guertin and Foner (1970)		10
$(Pd_{0.95}Rh_{0.05})Fe_{0.01}$	susc.	Clogston et al. (1962)	49	12.7
$(Pd_{0.9}Rh_{0.1})Fe_{0.01}$	susc.	Clogston et al. (1962)	33	11.4
$(Pd_{0.8}Rh_{0.2})Fe_{0.01}$	susc.	Clogston et al. (1962)	14	9.6

Other alloys (contd.)

Alloy	Exp. method	Reference	T_c (K)	μ (μ_B)
$(Pd_{0.6}Rh_{0.4})Fe_{0.01}$	susc.	Clogston et al. (1962)	1	7.1
$Pt_{0.99}(Co_{0.75}Fe_{0.25})_{0.01}$	magn.	Bozorth et al. (1962)	12	5.6
$Pt_{0.99}(Fe_{0.5}Co_{0.5})_{0.01}$	magn.	Bozorth et al. (1962)	12	4.8
$Pt_{0.99}(Fe_{0.75}Mn_{0.25})_{0.01}$	magn.	Bozorth et al. (1962)	8	5.5
$Rh_{0.99}Fe_{0.01}$	susc.	Clogston et al. (1962)	-14	2.2
$(Rh_{0.7}Pd_{0.3})Fe_{0.01}$	susc.	Clogston et al. (1962)	-2	4.5
$(Rh_{0.55}Pd_{0.45})Fe_{0.01}$	susc.	Clogston et al. (1962)	-2	5.9

References

Aharony, A., 1978, J. Mag. and Mag. Mat. **7**, 198.

Aharony, A. and Y. Imry, 1976, Solid State Commun. **20**, 899.

Aldred, A.T., B.D. Rainford and M.W. Stringfellow, 1970, Phys. Rev. Lett. **16**, 897.

Alekseevskii, N.E., Yu.A. Samerskii, A.P. Kir'yanov and V.I. Tsebro, 1968, JETP Letters **8**, 403.

Alexander, S. and P.W. Anderson, 1964, Phys. Rev. **133**, A1594.

Ali, M., W.D. Bremer, E. Klein, A. Benoit, J. Flouquet, O. Taurian and J.C. Gallop, 1974, Phys. Rev. **B10**, 4659.

Alloul, H., 1979, Phys. Rev. **42**, 603.

Alquié, G., A. Kreisler, G. Sadoc and J.P. Burger, 1974, J. Physique Lett. **35**, L69.

Alquié, G., A. Kreisler and J.P. Burger, 1978, Solid State Commun. **26**, 265.

Amamou, A., R. Caudron, P. Costa, J.M. Friedt, F. Gautier and B. Loegel, 1976, J. Phys. F **6**, 2371.

Anderson, P.W., 1961, Phys. Rev. **124**, 41.

Anderson, P.W., 1970, Mat. Res. Bull. **5**, 549.

Anderson, P.W., 1977, *Amorphous magnetism II* (R.A. Levy and R. Hasegawa, eds.) (Plenum Press, New York) p. 1.

Anderson, P.W., B.I. Halperin and C.M. Varma, 1972, Phil. Mag. **25**, 1.

Arrott, A., 1957, Phys. Rev. **108**, 1394.

Arrott, A., 1965, J. Appl. Phys. **36**, 1093.

Arrott, A., 1966, *Magnetism IIB*, (G.T. Rado and H. Suhl, eds.) (Academic Press, New York) p. 295.

Bagguley, D.M.S. and J.A. Robertson, 1968, Phys. Lett. **27A**, 516.

Bagguley, D.M.S. and J.A. Robertson, 1974, J. Phys. **F4**, 2282.

Balbanov, A.E., N.N. Delyagin, A.L. Yerzinkyan, V.P. Perfenova and V.S. Shpinel, 1969, Sov. Phys. JETP **28**, 1131.

Bancroft, M.H., 1970, Phys. Rev. **B2**, 2597.

Beck, P.A., 1971, Met. Trans. **2**, 2015;

Beck, P.A., 1972a, J. Less-common Met. **28**, 193.

Beck, P.A., 1972b, Magnetism in alloys (P.A. Beck and J.T. Weber, eds.) (TSM-AIME, New York) p. 211.

Beille, J. and G. Chouteau, 1975, J. Phys. F **5**, 721.

Benoit, A., M. Chapellier, J. Flouquet, M. Ribault, O. Taurian, J. Sanchez and J.L. Tholence, 1977, Physica **86–88B**, 487.

Binder, K., 1974, Adv. Phys. **23**, 917.

Binder, K., 1977a, Festkörperprobleme, Advances in solid state physics, vol. XVII (J. Treusch, ed.) (Vieweg, Braunschweig) p. 55.

Binder, K., 1977b, Z. Physik B **26**, 339.

Binder, K. and K. Schröder, 1976a, Solid State Commun. **18**, 1361.

Binder, K. and K. Schröder, 1976b, Phys. Rev. B **14**, 2142.

Binder, K. and D. Stauffer, 1976, Phys. Lett. **57A**, 177.

Blandin, A., 1973, Magnetism V (H. Suhl, ed.) (Academic Press, New York) ch. II.

Bloyet, D., E. Varoquaux, C. Vibet, O. Avenel and M.P. Berglund, 1978, Phys. Rev. Lett. **40**, 250.

Boerstoel, B.M., 1970, Thesis, University of Leiden, unpublished.

Boerstoel, B.M., J.J. Zwart, and J. Hansen, 1972, Physica **57**, 397.

Borg, R.J., 1970, Phys. Rev. **B1**, 349.

Borg, R.J. and T.A. Kitchens, 1973, J. Phys. Chem. Solids **34**, 1323.

Borg, R.J. and D.N. Pipkorn, 1969, J. Appl. Phys. **40**, 1483.

Borg, R.J., R. Booth and C.E. Violet, 1963, Phys. Rev. Lett. **11**, 464.

Boucai, E., B. Lecoanet, J. Pilon, J.L. Tholence and R. Tournier, 1971, Phys. Rev. **B3**, 3834.

Bozorth, R.M., P.A. Wolff, D.D. Davis, V.B. Compton and J.H. Wernick, 1961, Phys. Rev. **122**, 1157.

Bozorth, R.M., D.D. Davis and J.H. Wernick, 1962, J. Phys. Soc. Japan, **17**, Suppl. B-I, 112.

Budnick, J.I., J. Lechaton and S. Skalski, 1966, Phys. Lett. **22**, 405.

Budnick, J.I., V. Cannella and T.J. Burch, 1974, AIP Conf. Proc. **18**, 307.

Budworth, D.W., F.E. Hoare, and J. Preston, 1960, Proc. Roy. Soc. A **257**, 250.

Burger, J.P., 1964, Ann. Physique **9**, 345.

Burger, J.P. and D.S. McLachlan, 1973, Solid State Commun. **13**, 1563.

Burger, J.P., D.S. McLachlan, R. Mailfert and B. Souffaché, 1975, in Low temperature physics LT-14, vol. 3 (M. Krusins and M. Vuorio, eds.) (North-Holland, Amsterdam) p. 278.

Burger, J.P., S. Senoussi and B. Souffaché, 1976, J. Less-common Met. **49**, 213.

Cable, J.W. and H.R. Child, 1973, AIP Conf. Proc. **10**, 1623.
Cable, J.W. and L. David, 1977, Phys. Rev. **B16**, 297.
Cable, J.W., E.O. Wollan and W.C. Koehler, 1965, Phys. Rev. **138**, A755.
Campbell, I.A., 1968, J. Phys. C **1**, 687.
Cannella, V. and J.A. Mydosh, 1972, Phys. Rev. **B6**, 4220.
Cannella, V. and J.A. Mydosh, 1973, AIP Conf. Proc. **10**, 785.
Cannella, V. and J.A. Mydosh, 1974a, AIP Conf. Proc. **18**, 651.
Cannella, V. and J.A. Mydosh, 1974b, Proc. Int. Conf. Mag. vol. 2, (Publ. House Nauka, Moscow) p. 74.
Cannella, V., J.A. Mydosh and M.P. Kawatra, 1970, J. Appl. Phys. **41**, 1421.
Cannella, V., J.A. Mydosh and J.I. Budnick, 1971, J. Appl. Phys. **42**, 1689.
Cannella, V., T.J. Burch and J.I. Budnick, 1975, AIP Conf. Proc. **24**, 464.
Careage, J.A., B. Dreyfus, R. Tournier and L. Weil, 1966, in Low temperature physics LT-10, vol. IV (M.P. Malkov, ed.) (Moscow) p. 284.
Carlow, J.S. and R.E. Meads, 1969, J. Phys. C **2**, 2120.
Caudron, R., P. Costa, B. Loegel, J.L. Tholence and R. Tournier, 1977, Physica **86–88B**, 833.
Chouteau, G., 1976, Physica **84B**, 25.
Chouteau, G. and R. Tournier, 1971, J. Physique, C **32**, 1002.
Chouteau, G., R. Fourneaux, K. Gobrecht and R. Tournier, 1968a, Phys. Rev. Lett. **20**, 193.
Chouteau, G., R. Fourneaux, R. Tournier and P. Lederer, 1968b, Phys. Rev. Lett. **21**, 1082.
Chouteau, G., R. Fourneaux and R. Tournier, 1971, in Low temperature physics LT-12 (E. Kandra, ed.) (Academic Press of Japan) p. 769.
Chouteau, G., R. Tournier and P. Mollard, 1974, J. Physique, **C4–35**, 185.
Clark, P.E. and R.E. Meads, 1970, J. Phys. **C 3**, S308.
Clogston, A.M., B.T. Matthias, M. Peter, H.J. Williams, E. Corenzwit and R.C. Sherwood, 1962, Phys. Rev. **125**, 541.
Coey, J.M.D., S. von Molnar and R.J. Gambino, 1977, Solid State Commun. **24**, 167.
Cole, H.S.D. and R.E. Turner, 1969, J. Phys. C **2**, 124.
Coles, B.R., J.H. Waszink and J.W. Loram, 1965, Proc. Int. Conf. Mag. 1964 (IPPS, London) p. 165.
Coles, B.R., S. Mozumder and R.L. Rusby, 1971, in Low temperature physics LT-12 (E. Kandra, ed.) (Academic Press of Japan) p. 737.
Coles, B.R., A. Tari and H.C. Jamieson, 1974, in Low temperature physics LT-13, vol. 2 (K.D. Timmerhaus, W.J. O'Sullivan and E.F. Hammel, eds.) (Plenum, New York) p. 414.
Coles, B.R., H. Jamieson, R.H. Taylor and A. Tari, 1975, J. Phys. **F 5**, 565.
Colp, M.E. and G. Williams, 1972, Phys. Rev. **B5**, 2599.
Costa-Ribeiro, P., M. Saint-Paul, D. Thoulouse and R. Tournier, 1974, in Low temperature physics LT-13, vol. 2 (K.B. Timmerhaus, W.J. O'Sullivan and E.F. Hammel, eds.) (Plenum, New York) p. 521.
Cottet, H., 1971, Thesis, University of Geneva, unpublished.
Cracknell, M.F., J.C. Gallop and G.V.H. Wilson, 1967, Phys. Lett. **24A**, 719.
Craig, P.P. and W.A. Steyert, 1964, Phys. Rev. Lett. **13**, 802.
Craig, P.P., D.E. Nagle, W.A. Steyert and R.D. Taylor, 1962, Phys. Rev. Lett. **9**, 12.
Craig, P.P., B. Mozer and R. Segnan, 1965a, Phys. Rev. Lett. **14**, 895.
Craig, P.P., R.C. Perisho, R. Segnan and W.A. Steyert, 1965b, Phys. Rev. **138**, A1460.
Crangle, J., 1960, Phil. Mag. **5**, 335.
Crangle, J. and W.R. Scott, 1965, J. Appl. Phys. **38**, 921.
Dahlberg, E.D., M. Hardiman, R. Orbach and J. Souletie, 1979, Phys. Rev. Lett. **42**, 401.
Daybell, M.D. and W.A. Steyert, 1968, Rev. Mod. Phys. **40**, 380.
Daybell, M.D., 1973, in Magnetism V (G.T. Rado and H. Suhl eds.) (Academic Press, New York) p. 136.
De Boer, F.R., C.J. Schinkel and J. Biesterbos, 1967, Phys. Lett. **25A**, 606.
De Boer, F.R., C.J. Schinkel and J. Biesterbos, 1969, J. Appl. Phys. **40**, 1049.
De Chatel, P.F. and F.R. de Boer, 1970, Physica **48**, 331.
De Mayo, B., 1974, J. Phys. Chem. Solids **35**, 1525.
De Noble, J. and F.J. du Chatenier, 1959, Physica **25**, 969.
De Pater, C.J., C. Van Dijk and G.J. Nieuwenhuys, 1975, J. Phys. **F 5**, L58.

Devine, R.A.B., 1976, Solid State Commun. **19**, 351.
Devine, R.A.B., 1977, J. Phys. F **7**, 461.
Doclo, R., S. Foner and A. Narath, 1969, J. Appl. Phys. **40**, 1206.
Doniach, S., and E.P. Wohlfarth, 1967, Proc. Roy. Soc. A **296**, 442.
Doran, J.C. and O.G. Symko, 1974a, AIP Conf. Proc. **18**, 980.
Doran, J.C. and O.G. Symko, 1974b, Solid State Commun. **14**, 719.
Dorofeev Yu, A., A.Z. Men'shikov and S.K. Sidorov, 1976, Fiz. Metal Metalloved **40**, 978.
Du Chatenier, F.J., 1964, Thesis, University of Leiden, unpublished.
Duff, K.J. and V. Cannella, 1973a, in Amorphous Magnetism (H.O. Hooper and A.M. de Graaff, eds.) (Plenum, New York) p. 207.
Duff, K.J. and V. Cannella, 1973b, AIP Conf. Proc. **10**, 541.
Dunlap, B.D. and J.G. Dash, 1967, Phys. Rev. **155**, A460.
Edwards, D.M., J. Mathon and E.P. Wohlfarth, 1973, J. Phys. F **3**, 161.
Edwards, S.F. and P.W. Anderson, 1975, J. Phys. F. **5**, 965.
Ehara, S., 1964, J. Phys. Soc. Japan **19**, 1313.
Erich, U., J. Göring, S. Hüfner and E. Kankeleit, 1970, Phys. Lett. **31A**, 492.
Ericsson, T., M.T. Hirvoren, T.E. Katila and P. Reivari, 1970a, in Low temperature physics LT-12 (E. Kandra, ed.) (Academic Press of Japan) p. 765.
Ericsson, T., M.T. Hirvonen, T.E. Katila and V.K. Typpi, 1970b, Solid State Commun. **8**, 765.
Essam, J.W., 1972, in Phase transitions and critical phenomena, vol. 2 (C. Domb and M.S. Green eds.) (Academic Press, New York) p. 197.
Fert, A. and A. Friederich, 1976, Phys. Rev. **B13**, 397.
Fiory, A.T., 1976, AIP Conf. Proc. **29**, 229.
Fischer, K., 1970, in Springer tracks in modern physics, vol. 54, (G. Höhler, ed.) (Springer, Berlin) p. 1.
Fischer, K., 1971, Phys. Stat. Sol. B, **46**, 11.
Fischer, K., 1977, Physica **86–88B**, 813.
Fisher, M.E., and J.S. Langer, 1968, Phys. Rev. Lett. **20**, 665.
Flouquet, J., O. Taurian, J. Sanchez, M. Chapellier and J.L. Tholence, 1977, Phys. Rev. Lett. **38**, 81.
Flouquet, J., M. Ribault, O. Taurian, J. Sanchez and J.L. Tholence, 1978, Phys. Rev. **B18**, 54.
Foiles, C.L., 1978, Phys. Lett. **67A**, 214.
Foner, S., E.J. McNiff, Hr. and R.P. Guertin, 1970, Phys. Lett. **31A**, 466.
Ford, P.J. and J.A. Mydosh, 1974a, J. Physique **35**, C4, 241.
Ford, P.J. and J.A. Mydosh, 1974b, Proc. Int. Conf. Mag. vol. 2, (Publ. House Nauka, Moscow) p. 79.
Ford, P.J. and J.A. Mydosh, 1976, Phys. Rev. **B14**, 2057.
Ford, P.J. and J.S. Schilling, 1976, J. Phys. F **6**, L 285.
Ford, P.J., J.R. Cooper, N. Jungfleish and J.A. Mydosh, 1973, Solid State Commun. **13**, 857.
Franz, J.M. and D.J. Sellmeyer, 1973, Phys. Rev. **B8**, 2083.
Friedel, J., 1958, Nuovo Cimento **7**, 287.
Frossati, G., J.L. Tholence, D. Thoulouse and R. Tournier, 1975, in Low temperature physics LT-14, vol. 3 (M. Krusins and M. Vuorio, eds.) (North-Holland, Amsterdam) p. 370.
Frossati, G., J.L. Tholence, D. Thoulouse and R. Tournier, 1976, Physica **84B**, 33.
Gainon, D. and J. Sierro, 1970, Helv. Phys. Acta **43**, 541.
Gallop, J.C., 1969, Thesis, University of Oxford, unpublished.
Gallop, J.C. and I.A. Campbell, 1968, Solid State Commun. **6**, 831.
Gerstenberg, D., 1958, Ann. Phys. **2**, 236.
Gierisch, W., W. Koch, F.J. Litterst, G.M. Kalvius and P. Steiner, 1977, J. Mag. and Mag. Mat. **5**, 129.
Giovannini, B., M. Peter and J.M. Schrieffer, 1964, Phys. Rev. Lett. **12**, 736.
Gonser, V., R.W. Grant, C.J. Meecham, A.M. Muir and H. Wiedersich, 1965, J. Appl. Phys. **36**, 2124.
Graham, L.D. and D.S. Schreiber, 1966, Phys. Rev. Lett. **17**, 650.
Graham, L.D. and D.S. Schreiber, 1968, J. Appl. Phys. **39**, 963.
Grassie, A.D.C., G.A. Swallow, G. Williams and J.W. Loram, 1971, Phys. Rev. **B3**, 4154.
Griffiths, D., 1967, Proc. Phys. Soc. **90**, 707.
Grube, G., and D. Winckler, 1935, Z. Electrochem. **41**, 52.
Grüner, G., 1974, Adv. Phys. **23**, 941.
Grüner, G. and A. Zawadowski, 1974, Rep. Prog. Phys. **37**, 1497.

Guertin, R.P. and S. Foner, 1970, J. Appl. Phys., **41**, 917.
Guy, C.N., 1975, J. Phys. **F 5**, L242.
Guy, C.N., 1977a, Physica, **86–88B**, 877.
Guy, C.N., 1977b, J. Phys. **F 7**, 1505.
Guy, C.N., 1978, J. Phys. **F 8**.
Guy, C.N. and W. Howard, 1977, in Amorphous magnetism II (R.A. Levy and R. Hasegawa, eds.) (Plenum, New York) p. 169.
Harris, R. and Zuckerman, 1972, Phys. Rev. **B5**, 101.
Harris, A.B., T.C. Lubensky and J.-H. Chen, 1976, Phys. Rev. Lett. **36**, 415.
Hasagawa, H., 1959, Prog. Theor. Phys. **27**, 483.
Hawkins, G.F. and R.L. Thomas, 1978, J. Appl. Phys. **49**, 1627.
Hawkins, G.F., T.J. Morgan and R.L. Thomas, 1976, AIP Conf. Proc. **29**, 235.
Hawkins, G.F., T.J. Morgan and R.L. Thomas, 1977, in Amorphous magnetism II (R.A. Levy and R. Hasegawa, eds.) (Plenum, New York) p. 117.
Heeger, A.J., 1969, in Solid state physics, vol. 23 (F. Seitz, D. Turnbull and H. Ehrenreich, eds.) (Academic Press, New York) p. 283.
Herring, C., 1966, Magnetism IV (G.T. Rado and H. Suhl, eds.) (Academic Press, New York) Ch. VI.
Hicks, T.J., T.M. Holden and G.G. Low, 1968, J. Phys. C **1**, 528.
Hirschkoff, E.C., O.G. Symko and J.C. Wheatley, 1971a, J. Low Temp. Phys. **5**, 155.
Hirschkoff, E.C., M.R. Shanaberger, O.G. Symko and J.C. Wheatley, 1971b, Phys. Lett. **34A**, 397.
Hirschkoff, E.C., M.R. Shanaberger, O.G. Symko and J.C. Wheatley, 1971c, J. Low Temp. Phys. **5**, 545.
Hirst, L.L., 1970, Phys. Kondens. Materie **11**, 255.
Hirst, L.L., 1971, Z. Phys. **241**, 9.
Hoare, F.E. and B. Yates, 1957, Proc. Roy. Soc. **A 240**, 42.
Hoare, F.E., J.C. Matthews and J.C. Walling, 1953, Proc. Roy. Soc. **216**, 502.
Hodges, L., R.E. Watson and H. Ehrenreich, 1972, Phys. Rev. B **5**, 3953.
Huq, M. and D.E. Moody, 1977, Physica **86–88B**, 485.
Hurd, C.M. and S.P. McAlister, 1977, in Amorphous magnetism II (R.A. Levy and R. Hasegawa, eds.) (Plenum, New York) p. 47.
Itoh, J. and S. Kobayashi, 1966, in Low temperature physics LT-10 (M.P. Malkov, ed.) (Moscow) p. 186.
Jamieson, H.C. and F.D. Manchester, 1972, J. Phys. **F 2**, 323.
Jones, H.C., A.G. Montgomery, I.B. Lin, J.W. Loe, H. Nadler and R.R. Hake, 1977, Phys. Rev. **B16**, 1177.
Kasuya, T., 1956, Prog. Theor. Phys. **16**, 45.
Katayama, M., K. Kumagai, T. Kohara, K. Asayama, I.A. Campbell, N. Sano, S. Kobayashi and J. Itoh, 1976, J. Phys. Soc. Japan **40**, 429.
Kato, T. and J. Mathon, 1976, J. Phys. **F 6**, 221.
Kato, T. and M. Shimizu, 1972, J. Phys. Soc. Japan, **33**, 363
Kawatra, M.P. and J.I. Budnick, 1970, Int. J. Mag. **1**, 61.
Kawatra, M.P., J.I. Budnick and J.A. Mydosh, 1968, Phys. Rev. **B2**, 1587.
Kawatra, M.P., S. Skalski, J.A. Mydosh and J.I. Budnick, 1969, J. Appl. Phys. **40**, 1202.
Kawatra, M.P., J.A. Mydosh, J.I. Budnick and B. Madden, 1970, in Low temperature physics LT-12 (E. Kandra, ed.) (Academic Press of Japan) p. 773.
Kim, D.J., 1966, Phys. Rev. **149**, 434.
Kim, D.J., 1970, Phys. Rev. **B1**, 3725.
Kim, D.J. and B. Schwartz, 1968, Phys. Rev. Lett. **20**, 201.
Kirkpatrick, S., 1973, Rev. Mod. Phys. **45**, 574.
Kitchens, T.A. W.A. Steyert and R.D. Taylor, 1965, Phys. Rev. **138**, A 167.
Kittel, C., 1968, in Solid state physics, vol. 22 (F. Seitz, D. Turnbull and H. Ehrenreich, eds.) (Academic Press, New York) p. 1.
Kjekshus, A. and W.B. Pearson, 1962, Can. J. Phys. **44**, 2293.
Klein, M.W., 1964, Phys. Rev. **136**, A 1156.
Klein, M.W., 1968, Phys. Rev. **173**, A 552.
Klein, M.W., 1969, Phys. Rev. **188**, A 933.
Klein, M.W., 1976, Phys. Rev. **B14**, 5008.
Klein, M.W. and R. Brout, 1963, Phys. Rev. **132**, 2412.
Klein, M.W. and L. Shen, 1972, Phys. Rev. **B5**, 1174.
Kobayashi, S., K. Asayama and J. Itoh, 1966, J. Phys. Soc. Japan **21**, 65.
Kondo, J., 1969, in Solid state physics, vol. 23, (F. Seitz, D. Turnbull and H. Ehrenreich, eds.) (Academic Press, New York) p. 183.
Koon, N.C., 1974, AIP Conf. Proc. **18**, 302.
Koon, N.C. and D.U. Gubser, 1975, AIP Conf. Proc. **24**, 94.

Koon, N.C. and A.I. Schindler, 1973, Phys. Rev. **B8**, 5257.
Koon, N.C., A.I. Schindler and D.L. Mills, 1972, Phys. Rev. **B6**, 4241.
Korenblitz, I.Ya., and E.F. Shender, 1972, Sov. Phys. JETP **35**, 1017.
Korenblitz, I.Ya. and E.F. Shender, 1976, Sov. Phys. JETP **44**, 819.
Kossler, W.J., 1975, AIP Conf. Proc. **24**, 788.
Kouvel, J.S., 1960, J. Appl. Phys. **31**, 1425.
Kouvel, J.S., 1961, J. Phys. Chem. Solids **21**, 57.
Kouvel, J.S., 1963, J. Phys. Chem. Solids **24**, 795, and experimental references therein.
Laborde, O., 1977, Thesis, University of Grenoble, unpublished.
Laborde, O. and P. Radhakrishna, 1973, J. Phys. F **3**, 1731.
Laborde, O. and P. Radhakrishna, 1974, Proc. Int. Conf. Mag. vol. 4, (Publ. House Nauka, Moscow) p. 82.
Larkin, A.I. and D.E. Khmel'nitskii, 1970, Zh. Eksp. Teor. Fiz. **58**, 1789 (Sov. Phys. JETP **31**, 958).
Larkin, A.I. and D.E. Khmel'nitskii, 1971, Zh. Eksp. Teor. Fiz, **60**, 846 (Sov. Phys. JETP **33**, 458).
Larsen, U., 1976, Phys. Rev. **B14**, 4356.
Larsen, U., 1977, Solid State Commun. **22**, 311.
Larsen, U., 1978a, Phys. Rev. **B18**, 5014.
Larsen, U., 1978b, to be published.
Larsen, U., P.J. Ford, J.S. Schilling and J.A. Mydosh, 1977, in Amorphous magnetism II (R.A. Levy and R. Hasegawa eds.) (Plenum, New York) p. 85.
Lederer, P. and D.L. Mills, 1968, Phys. Rev. **165**, 837.
Levin, K., R. Bass and K.H. Bennemann, 1972, Phys. Rev. **B6**, 1865.
Levitt, D.A. and R.E. Walstedt, 1977, Phys. Rev. Lett. **38**, 178.
Levy, R.A. and J.A. Rayne, 1975, Phys. Lett. **53A**, 329.
Levy, R.A., J.J. Burton, D.I. Paul and J.I. Budnick, 1974, Phys. Rev. **B9**, 1085.
Li, P.L. and B.E. Paton, 1976, Phys. Lett. **56A**, 225.
Liddell, P.R. and R. Street, 1973, J. Phys. F **3**, 1648.
Lindhard, J., 1954, Kgl. Danske Videnskab. Selskab. Mat.-fyss. Medd. **28**, 8.
Ling, P.C. and T.J. Hicks, 1973, J. Phys. F **3**, 697.
Long, P.D. and R.E. Turner, 1970, J. Phys. C **3**, S 127.
Loram, J.W., G. Williams and G.A. Swallow, 1971, Phys. Rev. **B3**, 3060.
Loram, J.W., R.J. White and A.D.C. Grassie, 1972, Phys. Rev. **B5**, 3659.
Low, G.G., 1965, Proc. Int. Conf. Mag. (IPPS London) p. 133.
Low, G.G., 1969, Adv. Phys. **18**, 371.
Low, G.G. and T.M. Holden, 1966, Proc. Phys. Soc. **89**, 119.
Lutes, O.S. and J.S. Schmit, 1964, Phys. Rev. **134**, A 676.
Luttinger, J.M., 1976, Phys. Rev. Lett. **37**, 778.
Maartense, I. and G. Williams, 1976, J. Phys. F **6**, L121.
MacDonald, D.K.C., W.B. Pearson and I.M. Templeton, 1962, Proc. Roy. Soc. A **266**, 161.
MacLaughlin, D.E. and H. Alloul, 1976, Phys. Rev. Lett. **36**, 1158.
MacLaughlin, D.E. and H. Alloul, 1977a, Physica **86–88B**, 839.
MacLaughlin, D.E. and H. Alloul, 1977b, Phys. Rev. Lett. **38**, 181.
McAlister, S.P., 1978, J. Appl. Phys. **49**, 1616.
McAlister, S.P. and C.M. Hurd, 1976a, Solid State Commun. **19**, 881.
McAlister, S.P. and C.M. Hurd, 1976b, Phys. Rev. Lett. **37**, 1017.
McDougal, M. and A.J. Manuel, 1968, J. Appl. Phys. **39**, 961.
McDougal, M. and A.J. Manuel, 1970, J. Phys. C **3**, 147.
McLennan, J.C. and H. Grayson-Smith, 1926, Proc. Roy. Soc. A **112**, 110.
Maletta, H., 1972, Z. Physik **250**, 68.
Maletta, H. and R.L. Mössbauer, 1970, Solid State Commun. **8**, 143.
Maley, M.P., R.D. Taylor and J.L. Thompson, 1967, J. Appl. Phys. **38**, 1249.
Malozemoff, A.P. and J.P. Jamet, 1977, Phys. Rev. Lett. **39**, 1297.
Margenau, H., 1935, Phys. Rev. **48**, 755.
Marshall, W., 1960, Phys. Rev. **118**, 1519.
Marshall, W. and S.W. Lovesey, 1971, The theory of thermal neutron scattering (Clarendon Press, Oxford).
Matho, K. and M.T. Beal Monod, 1974, in Low temperature physics LT-13, vol. 2 (K.D. Timmerhaus, W.J. O'Sullivan and E.F. Hammel eds.) (Plenum, New York) p. 475.
Mattis, D.C., 1976, Phys. Lett. **56A**, 421.
Maxwell, E., 1965, Rev. Sci. Instr. **36**, 553.
Mehlmann, R., H. Husemann and H. Brodowsky, 1973, Ber. Bunsenges. Phys. Chem. **77**, 36.

Mishra, S. and P.A. Beck, 1973, Phys. Stat. Sol. A **19**, 267.
Moran, T.J. and R.L. Thomas, 1973, Phys. Lett. **45A**, 413.
Moriya, T., 1965a, Prog. Theor. Phys. **33**, 157.
Moriya, T., 1965b, Prog. Theor. Phys. **34**, 329.
Mott, N.F., 1949, Proc. Roy. Soc. A **62**, 416.
Mukhopadhyay, A.K. and P.A. Beck, 1975, Solid State Commun. **16**, 1067.
Mukhopadhyay, A.K., R.D. Shull and P.A. Beck, 1975, J. Less-common Met. **43**, 69.
Murani, A.P., 1976, Phys. Rev. Lett. **37**, 450.
Murani, A.P., 1977a, J. Mag. and Mag. Mat. **5**, 95.
Murani, A.P., 1978a, to be published.
Murani, A.P., 1978b, J. Appl. Phys. **49**, 1604.
Murani, A.P. and J.L. Tholence, 1977, Solid State Commun. **22**, 25.
Murani, A.P., A. Tari and B.R. Coles, 1970, J. Phys. C **2**, S159.
Murani, A.P., A. Tari and B.R. Coles, 1974, J. Phys. F **4**, 1769.
Murani, A.P., S. Roth, P. Radhakrishna, B.D. Rainford, B.R. Coles, K. Ibel, G. Goeltz and F. Mezei, 1976a, J. Phys. F **6**, 425.
Murani, A.P., G. Goelt and K. Ibel, 1976b, Solid State Commun. **19**, 733.
Murnick, D.E., A.T. Fiory, W.J. Kossler, 1976, Phys. Rev. Lett. **36**, 100.
Mydosh, J.A., 1974, Phys. Rev. Lett. **33**, 1562.
Mydosh, J.A., 1976, AIP Conf. Proc. **29**, 239.
Mydosh, J.A., 1978, J. Mag. and Mag. Mat. **7**, 237.
Mydosh, J.A., J.I. Budnick, M.P. Kawatra and S. Skalski, 1968, Phys. Rev. Lett. **21**, 1346.
Mydosh, J.A., P.J. Ford, M.P. Kawatra and T.E. Whall, 1974, Phys. Rev. B **10**, 2845.
Nagamine, K., N. Nishida, S. Nagamiya, O. Hashimoto and T. Yamazaki, 1977a, Phys. Rev. Lett. **38**, 99.
Nagamine, K., N. Nishida, R.S. Hayano and T. Yamazaki, 1977b, Physica **86–88B**, 489.
Nagamine, K., N. Nishida and T. Yamazaki, 1977c, in Amorphous magnetism II (R.A. Levy and R. Hasegawa, eds.) (Plenum, New York) p. 29.
Nagasawa, H., 1970, J. Phys. Japan **28**, 1171.
Nagle, D.E., P.P. Craig, P. Barrett, D.F.R. Cochran, C.E. Olsen and R.D. Taylor, 1962, Phys. Rev. **125**, 490.
Narath, A., A.T. Fromhold, Jr. and E.D. Jones, 1966, Phys. Rev. **144**, 428.
Nieuwenhuys, G.J., 1975, Adv. Phys. **24**, 515.
Nieuwenhuys, G.J., 1978, Phys. Lett. **67A**, 237.
Nieuwenhuys, G.J. and B.M. Boerstoel, 1970, Phys. Lett. **33A**, 147.
Nieuwenhuys, G.J. and J.A. Mydosh, 1977, Physica, **86–88B**, 880.
Nieuwenhuys, G.J. and B.H. Verbeek, 1977, J. Phys. F **7**, 1497.
Nieuwenhuys, G.J., B.M. Boerstoel, J.J. Zwart, H.D. Dokter and G.J. van den Berg, 1972, Physica **62**, 278.
Nieuwenhuys, G.J., M.F. Pikart, J.J. Zwart, B.M. Boerstoel and G.J. van den Berg, 1973, Physica **69**, 119.
Nieuwenhuys, G.J., J.A. Mydosh and E.P. Wohlfarth, 1978, Phys. Lett. **66A**, 221.
Nieuwenhuys, G.J., B.H. Verbeek and J.A. Mydosh, 1979, J. Appl. Phys. **50**, 1685.
Ododo, J.C., 1978, Solid State Commun. **25**, 25.
Owen, J., M.E. Brown, V. Arp and A.F. Kip, 1957, J. Phys. Chem. Solids **2**, 85.
Parks, R.D., 1972, AIP Conf. Proc. **5**, 630.
Phillips, W.C., 1965, Phys. Rev. **138**, A1649.
Rado, G.T. and H. Suhl, eds., 1973, Magnetism V (Academic Press, New York).
Rao, K.V., O. Rapp, Ch. Johannesson, J.I. Budnick, T.J. Burch and V. Cannella, 1976, AIP Conf. Proc. **29**, 346.
Rault, J. and J.P. Burger, 1969, C.r. hebd. Séanc Acad. Sci, Paris **269**, series B, 1085.
Reivari, P., 1969, Phys. Rev. Lett. **22**, 167.
Rhodes, P. and E.P. Wohlfarth, 1963, Proc. Roy. Soc. **A273**, 247.
Ridout, M.S., 1969, J. Phys. C **2**, 1258.
Riess, I. and M.W. Klein, 1977, Phys. Rev. **B15**, 6001.
Rivier, N., 1974, Wiss Z. Tech. Univ. Dresden **23**, 1000.
Rivier, N. and K. Adkins, 1975, J. Phys. F **5**, 1745.
Rizzuto, C., 1974, Rep. Prog. Phys. **37**, 147.
Roshko, R.M. and G. Williams, 1975, in Low temperature physics LT-14, vol. 3, (M. Krusius and M. Vuorio, eds.) (North Holland, Amsterdam) p. 274.
Roshko, R.M. and G. Williams, 1977, Physica **86–88B**, 829.
Ruderman, M.A. and C. Kittel, 1954, Phys. Rev. **96**, 99.
Rusby, R.L., 1974, J. Phys. F **4**, 1265.
Sablik, M., S. Skalski and J.I. Budnick, 1973, Phys. Rev. **B8**, 2222.
Sacli, O.A., D.J. Emerson and D.F. Brewer, 1974, J. Low. Temp. Phys. **17**, 425.

Sarachik, M.P. and D. Shaltiel, 1967, J. Appl. Phys. **38**, 1155.
Sarkissian, B.V.B. and R.H. Taylor, 1974, J. Phys. **F 4**, L243.
Sato, H. and R. Kikuchi, 1974, AIP Conf. Proc. **18**, 605.
Schalkwijk,M.S., P.E. Brommer, G.J. Cock and C.J. Schinkel, 1971, J. Physique **32**, C1, 997.
Scherg, M., E.R. Seidel, F.J. Litterst, W. Gierisch and G.M. Kalvius, 1974, J. Physique **35**, C6, 527.
Scheuer, H., M. Loewenhaupt and W. Schmatz, 1977a, Physica **86–88B**, 842.
Scheuer, H., M. Loewenhaupt and W. Just, 1977b, J. Mag. and Mag. Mat. **4**, 77.
Scheuer, H., M. Loewenhaupt and J.B. Suck, 1977c, J. Mag. and Mag. Mat. **6**, 100.
Schilling, J.S., P.J. Ford, U. Larsen and J.A. Mydosh, 1976, Phys. Rev. **B14**, 4368.
Schilling, J.S., P.J. Ford, U. Larsen and J.A. Mydosh, 1977, in Amorphous magnetism II (R.A. Levy and R. Hasegawa, eds.) (Plenum, New York) p. 95.
Schindler, A.I. and C.A. Mackliet, 1968, Phys. Rev. Lett. **20**, 15.
Schinkel, C.J., F.R. de Boer and J. Biesterbos, 1968, Phys. Lett. **26A**, 501.
Schrieffer, J.R., 1968, J. Appl. Phys. **39**, 642.
Segnan, R., 1967, Phys. Rev. **160**, A404.
Senoussi, S., I.A. Campbell and A. Fert, 1977, Solid State Commun. **21**, 269.
Shaltiel, D. and J.H. Wernick, 1964, Phys. Rev. **136**, A245.
Shaltiel, D., J.H. Wernick, H.J. Williams and M. Peter, 1964, Phys. Rev. **135**, A1346.
Shen, L., D.S. Schreiber and A.J. Arko, 1969, Phys. Rev. **179**, 512.
Sherrington, D., 1976, AIP Conf. Proc. **29**, 224.
Sherrington, D. and S. Kirkpatrick, 1975, Phys. Rev. Lett. **35**, 1792.
Sherrington, D. and B.W. Southern, 1975, J. Phys. **F 5**, L49.
Skalski, S., J.I. Budnick and J. Lechaton, 1968, J. Appl. Phys. **39**, 965.
Skalski, S., M.P. Kawatra, J.A. Mydosh and J.I. Budnick, 1970, Phys. Rev. **B2**, 3613.
Smart, J.S., 1966, Effective field theories of magnetism, (W.B. Saunders, London).
Smith, D.A., 1974, J. Phys. **F 4**, L266.
Smith, D.A., 1975, J. Phys. **F 5**, 2148.
Smith, F.W., 1973, Solid State Commun. **13**, 1267.
Smith, F.W., 1974a, Phys. Rev. **B9**, 942.
Smith, F.W., 1974b, Phys. Rev. **B10**, 2034.
Smith, F.W., 1974c, Phys. Rev. **B10**, 2980.
Smith, F.W., 1976, Phys. Rev. **B13**, 2976.
Smith, T.F., W.E. Gardner and H. Montgomery, 1970, J. Phys. **C**, Suppl., **3**, S 370.
Soukoulis, C.M., G.S. Grest, and K. Levin, 1978, Phys. Rev. Lett. **41**, 568.
Souletie, J. and R. Tournier, 1969, J. Low Temp. Phys. **1**, 95.
Star, W.M., 1971, Thesis, University of Leiden, unpublished.
Star, W.M., S. Foner and E.J. McNiff, Jr., 1975, Phys. Rev. **B12**, 2690.
Street, R. and J.C. Woolley, 1949, Proc. Phys. Soc. **A62**, 562.
Stringfellow, M.W., 1968, J. Phys. **C 1**, 1699.
Suhl, H., 1975, Appl. Phys. **8**, 217.
Swallow, G.A., G. Williams, A.D.C. Grassie and J.W. Loram, 1971, J. Phys. **F 1**, 511.
Swallow, G.A., G. Williams, A.D.C. Grassie and J.W. Loram, 1975, Phys. Rev. **B11**, 337.
Takahashi, T. and M. Shimizu, 1965, J. Phys. Soc. Japan, **20**, 26.
Tang, S.H., P.P. Craig and T.A. Kitchens, 1971, Phys. Rev. Lett. **28**, 593.
Tansil, J.E., F.E. Obenshain and G. Czjzek, 1972, Phys. Rev. **B6**, 2796.
Taylor, R.H., 1975, Adv. Phys. **24**, 681.
Tholence, J.L. and R. Tournier, 1974, J. Physique **35**, C4, 229.
Tholence, J.L. and R. Tournier, 1976, Physica, **84B**, 3.
Tholence, J.L. and R. Tournier, 1977, Physica **86–88B**, 873.
Tholence, J.L. and E.F. Wassermann, 1977, Physica **86–88B**, 875.
Thomson, J.O. and J.R. Thompson, 1976, AIP Conf. Proc. **29**, 342.
Thompson, J.R. and J.O. Thomson, 1977, AIP Conf. Proc. **34**, 20.
Thomson, J.R., J.O. Thomson and P.G. Huray, S. Nave and T.L. Nichols, 1978, J. Phys. **F8**. 169.
Thouless, D.J., P.W. Anderson and R.G. Palmer, 1977, Phil. Mag. **35**, 593.
Tissier, B. and R. Tournier, 1972, Solid State Commun. **11**, 895.
Toulouse, G., 1977, Comm. on Phys. **2**, 115.
Tournier, R., 1974, in Low temperature physics LT-13, vol. 2 (K.D. Timmerhaus, W.J. O'Sullivan and E.F. Hammel, eds.) (Plenum, New York) p. 257.
Trainor, R.J. and D.C. McCollum, 1975, Phys. Rev. **B11**, 3581.

Trousdale, W.L., T.A. Kitchens and G. Longworth, 1967, J. Appl. Phys. **38**, 922.
Tsiovkin, Yu.N. and N.V. Volkenshteyn, 1965, Phys. Metals Metallog. (USSR) (English translation) **19**, 45.
Tustison, R.W., 1976, Solid State Commun. **19**, 1075.
Tustison, R.W. and P.A. Beck, 1976, Solid State Commun. **20**, 841.
Tustison, R.W. and P.A. Beck, 1977, Solid State Commun. **21**, 517.
Van Dam, J.E., 1973, Thesis, University of Leiden, unpublished.
Van Dam, J.E. and G.J. van den Berg, 1970, Phys. Stat. Sol. A3, 11.
Van den Berg, G.J., 1964, in Progress in low temperature physics, vol. 4 (C.J. Gorter, ed.) (North-Holland, Amsterdam) p. 194.
Veal, B.W. and J.A. Rayne, 1964, Phys. Rev. **135**, A442.
Verbeek, B.H., 1978, Private communication.
Verbeek, B.H., 1979, Thesis, University of Leiden, unpublished.
Verbeek, B.H., G.J. Nieuwenhuys, H. Stocker and J.A. Mydosh, 1978a, Phys. Rev. Lett. **40**, 587.
Verbeek, B.H., C. van Dijk, B. Rainford and A.P. Murani, 1978b, J. Appl. Crystall. **11**, 637.
Verbeek, B.H., C. van Dijk, G.J. Nieuwenhuys and J.A. Mydosh, 1978c, J. Physique **39**, C6 918.
Violet, C.E. and R.J. Borg, 1966, Phys. Rev. **149**, 540.
Violet, C.E. and R.J. Borg, 1967, Phys. Rev. **162**, 608.
Wassermann, E.F. and J.L. Tholence, 1976, AIP Conf. Proc. **29**, 237.
Weiss, P. and M. Forrer, 1926, Ann. de Physique **5**, 153.
Welter, J.M. and F.J. Johnen, 1975, Cryogenics **15**, 28.
Wenger, L.E. and P.H. Keesom, 1975, Phys. Rev. **B11**, 3497.
Wenger, L.E. and P.H. Keesom, 1976, Phys. Rev. **B13**, 4053.
Wheeler, J.C.G., 1969, J. Phys. **C2**, 135.
Wiebes, J., W.S. Hulscher and H.A. Kramers, 1964, Appl. Sci. Res. **11**, 213.
Wilding, M.D., 1967, Proc. Phys. Soc. **90**, 801.
Williams, G., 1970, J. Phys. Chem. Solids **31**, 529.
Williams, G., 1972, Phys. Rev. **B5**, 236.
Williams, G., 1976, Solid State Commun. **19**, 821.
Williams, G. and J.W. Loram, 1969a, Solid State Commun. **7**, 1261.
Williams, G. and J.W. Loram, 1969b, J. Phys. Chem. Solids **30**, 1827.
Williams, G. and J.W. Loram, 1971, J. Phys. **F 1**, 434.
Williams, G., G.A. Swallow and J.W. Loram, 1971, Phys. Rev. **B3**, 3863.
Williams, G., G.A. Swallow and J.W. Loram, 1973, Phys. Rev. **B7**, 257.
Williams, G., G.A. Swallow and J.W. Loram, 1975a, Phys. Rev. **B11**, 344.
Williams, G., G.A. Swallow, A.D.C. Grassie and J.W. Loram, 1975b, AIP Conf. Proc. **24**, 447.
Window, B., 1969, J. Phys. **C 2**, 2380.
Window, B., 1970, J. Phys. **C 3**, 922.
Window, B., 1973, in Amorphous magnetism (H.O. Hooper and A.M. de Graaf, eds.) (Plenum, New York), p. 229.
Window, B., 1975, J. Mag. and Mag. Mat. **1**, 167.
Window, B., G. Longworth and C.E. Johnson, 1970, J. Phys. **C 3**, 2156.
Wohlleben, D.K. and B.R. Coles, 1973, in Magnetism V (G.T. Rado and H. Suhl, eds.) (Academic Press, New York) Ch. 1.
Wolff, P.A., 1961, Phys. Rev., **124**, 1030.
Woodhams, F.W.P., R.E. Meads and J.S. Carlow, 1966, Phys. Lett. **23A**, 419.
Yamazaki, T., 1977, Physica **86–88B**, 1053.
Yosida, K., 1957a, Phys. Rev. **106**, 893.
Yosida, K., 1957b, Phys. Rev. **107**, 396.
Zimmermann, J.E. and F.E. Hoare, 1960, J. Phys. Chem. Solids **17**, 52.
Zuckermann, M.E., 1971, Solid State Commun. **9**, 1861.
Zweers, H.A. and G.J. van den Berg, 1975, J. Phys. **F 5**, 555.
Zweers, H.A., W. Pelt, G.J. Nieuwenhuys and J.A. Mydosh, 1977, Physica **86–88B**, 837.

chapter 3

RARE EARTH METALS AND ALLOYS

S. LEGVOLD

Ames Laboratory-DOE
Department of Physics
Iowa State University
Ames, IA 50011
USA

Ferromagnetic Materials, Vol. 1
Edited by E.P. Wohlfarth

CONTENTS

1. Introduction

1.1. Epitome and tables

The rare earths, or lanthanides, are the trivalent 4f shell transition metals. Their magnetic properties stem from unpaired electrons in the 4f shell. The latter are relatively closely bound to the nucleus and so are shielded by the eight $5s^2$–$5p^6$ electrons and, to some extent, by the three 5d–6s valence electrons. In more picturesque language Nobel Laureate Van Vleck (1932) wrote that 4f electrons are "deeply sequestered" in the atom. This means that 4f electron wave functions are confined close to the nucleus and that wave function overlap with neighboring atoms in a lattice is vanishingly small. Therefore direct Heisenberg exchange does not occur. To account for the observed magnetic order in the rare earths, an indirect exchange mechanism via three 5d–6s conduction electrons is invoked. Strong evidence to support this view comes from the observed spin polarization of the conduction electrons. The elements which exhibit ferromagnetism are Gd, Tb, Dy, Ho, Er, fcc Pr and fcc Nd; of these rare earths, Dy and Ho have the highest magnetic moment per unit volume for all the elements; the magnitude of their magnetic moments is over fifty percent larger than that of iron. Unfortunately this high moment is attainable only at low temperatures and along the easy magnetic direction in single crystals.

Strong spin orbit coupling for the 4f electrons leads to low magnetic moments for the early (or light) members of the transition group; for these elements the total angular momentum quantum number is $J = L - S$ where the spin quantum number $S = \Sigma_i s_i$, the orbital quantum number $L = \Sigma_l m_l$ and the sums over the 4f electrons are made in accordance with Hund's rules*. Similarly, high magnetic moments are associated with the heavy rare earths for which $J = L + S$. La, which is the forerunner to the rare earths and which has an empty 4f shell and Lu, which has a full 4f shell, exhibit only typical conduction electron Pauli paramagnetism. Also included in the discussion are the closely related trivalent

*When electrons are in an incomplete shell and so have the same n, l quantum numbers then the "lowest lying" electronic state has (i) the maximum multiplicity, $2S + 1$, allowed consistent with the Pauli exclusion principle and (ii) the maximum L consistent with this multiplicity. (iii) For less than half filled shells $J = L - S$, otherwise $J = L + S$.

elements Sc and Y.

A wide variety of magnetic structures are displayed by the rare earth metals and their alloys. These range from simple ferromagnetism to complex sinusoidal and/or helical ordering; the magnetic structure sometimes involves sublattices. In many instances the magnetic ordering is incommensurate with the atomic ordering and this leads to sizeable physical property perturbations.

Because of the low magnetic moments of the light rare earths it is possible for electric crystal field effects to dominate the magnetic exchange interaction. This leads to a number of interesting observations, the most outstanding of which is the singlet ground state configuration found in pure samples of Pr.

In the following pages the intention is to give a reasonable accounting of the magnetic and transport properties of rare earth metals and their alloys. For more details on the theory and the experimental data, it may be necessary to consult the references. Several reviews have been published; there is the volume "Magnetic properties of the rare earth metals" edited by Elliott (1972). More recently, in chapter 3 of Gschneidner and Eyring (1978), Liu has reviewed lanthanide electronic structures while McEwen (chapter 6) has treated the

TABLE 1

Room temperature physical properties of the rare earth metals and their melting and boiling points*; dhcp = double-hexagonal close-packed, fcc = face-centered cubic, bcc = body-centered cubic, hcp = hexagonal close-packed

Rare earth metal	Z	Crystal structure	Lattice constants (Å) a_0	c_0	Metallic radius (Å)	Atomic volume** (cm^3/mol)	Density (g/cm^3)	Melting point (°C)	Boiling point (°C)
La	57	dhcp	3.7740	12.171	1.8791	22.603	6.145	918	3464
Ce	58	fcc	5.1610	—	1.8247	20.698	6.770	798	3433
Pr	59	dhcp	3.6721	11.8326	1.8279	20.804	6.773	931	3520
Nd	60	dhcp	3.6582	11.7966	1.8214	20.584	7.007	1021	3074
Pm	61	dhcp	3.65	11.65	1.811	20.248	7.260	1042	~3000
Sm	62	rhomb†	3.6290	26.207	1.8041	20.001	7.520	1074	1794
Eu	63	bcc	4.5827	—	2.0418	28.981	5.243	822	1529
Gd	64	hcp	3.6336	5.7810	1.8013	19.904	7.900	1313	3273
Tb	65	hcp	3.6055	5.6966	1.7833	19.312	8.229	1356	3230
Dy	66	hcp	3.5915	5.6501	1.7740	19.006	8.550	1412	2567
Ho	67	hcp	3.5778	5.6178	1.7661	18.753	8.795	1474	2700
Er	68	hcp	3.5592	5.5850	1.7566	18.450	9.066	1529	2868
Tm	69	hcp	3.5375	5.5540	1.7462	18.124	9.321	1545	1950
Yb	70	fcc††	5.4848	—	1.9392	24.843	6.965	819	1196
Lu	71	hcp	3.5052	5.5494	1.7349	17.781	9.840	1663	3402
Sc	21	hcp	3.3088	5.2680	1.6406	15.041	2.989	1541	2836
Y	39	hcp	3.6482	5.7318	1.8012	19.894	4.469	1522	3338

* After Beaudry and Gschneidner (1978).

** Data for coordination number 12.

† Rhombohedral is the primitive cell. The close-packed layer stacking is ABABCBCAC with symmetries chhchhchh in nine layers.

†† Low temperature form is hcp.

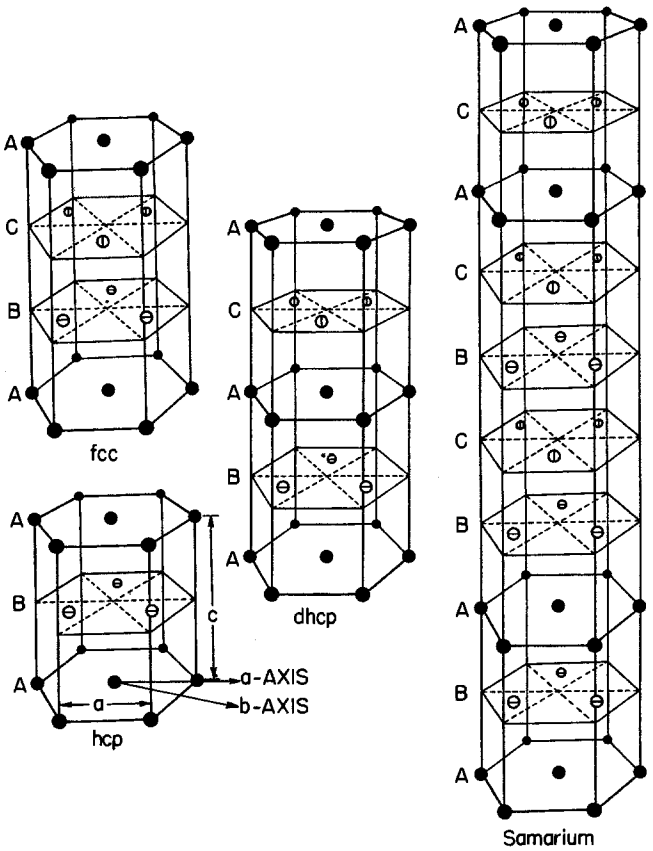

Fig. 1. Close packed crystal structures found in rare earth metals.

magnetic and magnetoelastic properties of the metals. Rhyne and McGuire (1972) have reviewed the magnetic properties as have Taylor and Darby (1972). A popular review has been prepared by Mackintosh (1977). The theory for the electronic properties has been reviewed by Dimmock (1971). In his book on soft magnetic materials Chen (1977) devotes a section to rare earth magnetism.

In many instances it is of importance to know the physical properties of the elements under discussion. These are shown in table 1 from chapter 2 of Gschneidner and Eyring (1978). The rare earths exhibit several close packed atom stacking arrangements. These are shown in fig. 1. The heavy elements are hcp at room temperature while the light elements prefer the dhcp (double hexagonal close packed) crystal structure. The room temperature crystal structures, lattice parameters, metallic radii, atomic volumes, densities, melting points, and boiling points are shown in the table. Reasonably smooth changes in the properties occur with increasing atomic number for the rare earths and the decreasing lattice parameters for the heavies heralds the "lanthanide contraction". Some irregular features can, however, be seen at once. Eu and Yb have

low melting points and this is related to the divalency of the metals wherein one of the conduction electrons migrates to the 4f shell to half fill the shell for Eu and to completely fill the shell for Yb. The crystal structure of Sm is an unusual nine layered affair with close packed layers ABABCBCAC giving atomic nearest neighbor symmetries chhchhchh on the respective planes. This is now called the samarium structure. Pm is radioactive and the boiling point given is an estimate.

In table 2 we give an extensive listing of the magnetic and related properties of the rare earth metals. It is convenient to use cgs units and to give the magnetic moments of the rare earths in Bohr magnetons; where $\mu_B = 9.27409 \times 10^{-21}$ erg/Oe $= 9.27409 \times 10^{-24}$ Joule per Tesla. Saturation magnetic moments per gram at absolute zero, $\sigma_{\infty,0}$, may be converted to the number of Bohr magnetons per atom N_{eff}, by use of $N_{eff} = A\sigma_{\infty,0}/5585$ where A is the atomic weight of the element. The table displays the total spin, S, of the 4f electrons, their total orbital angular momentum, L, their appropriately determined total angular momentum, J, the spectroscopic state designation, the Landé g value*, and the theoretical paramagnetic moment $g\sqrt{J(J+1)}$ along side the latest observed value. The table also shows the theoretical saturation magnetic moments which are given by gJ; these are shown in graphical form in fig. 2. The theoretical gJ values in the table differ from the observed values for the heavy elements because gJ does not include the conduction electron contribution mentioned earlier. Also shown are the values of $S(S+1)$ and $(g-1)^2J(J+1)$ (the de Gennes factor) for a comparison with the ordering temperatures T_N and T_c in the next columns. Since J is a good quantum number for localized magnetic moments, de Gennes (1966) proposed that the spin projection onto J should govern the magnetic interaction; this leads to the replacement of S with $(g-1)J$ in the theory of the rare earths.

The saturation magnetic moment for light rare earths is hard to obtain because

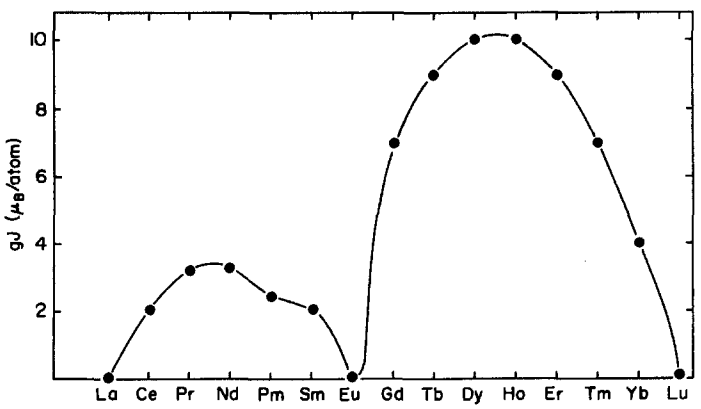

Fig. 2. Plot of the theoretical gJ saturation magnetic moments for tripositive rare earth ions in Bohr magnetons, μ_B, per atom.

* $g = 1 + \dfrac{[J(J+1)+S(S+1)-L(L+1)]}{2J(J+1)}$

TABLE 2
Magnetic properties of rare earth metals

Rare earth metal	Z	S	L	$J = L \pm S$	Spect.* state	Magnetic moment in Bohr magnetons/atom g	$g\sqrt{J(J+1)}$ obs.	gJ	obs.**	$S(S+1)$	† $(g-1)^2 \times J(J+1)$	Easy axis at 0 K	Hex. sites	T_N (K)	Cubic sites	T_c (K)	θ_P (K)		
La	57	0	0	0	$^1S_0$	–	0	–	0	–	0	0	–	–	*dhcp*	–	–			
Ce	58	$\frac{1}{2}$	3	$\frac{5}{2}$	$^2F_{5/2}$	$\frac{6}{7}$	2.54	2.51	2.14	–	0.75	0.18	–	13.7	††	12.5	–			
Pr	59	1	5	4	$^3H_4$	$\frac{4}{5}$	3.58	2.56	3.20	–	–	0.80	*a*	–		–	–			
Nd	60	$\frac{3}{2}$	6	$\frac{9}{2}$	$^4I_{9/2}$	$\frac{8}{11}$	3.62	3.4	3.27	–	3.75	1.84	*b*	19.9		7.5	–			
Pm	61	2	6	4	$^5I_4$	$\frac{3}{5}$	2.68	–	2.40	–	6.0	3.20	–	–		–	–			
Sm	62	$\frac{5}{2}$	5	$\frac{5}{2}$	$^6H_{5/2}$	$\frac{2}{7}$	0.85	1.74	0.71	–	8.75	4.46	*a*	109		14.0	–			
Eu^{+3}	63	3	3	0	$^7F_0$	–	–	–	0	–	12.0	0	–	–		–	–			
Eu^{+2}	63	$\frac{7}{2}$	0	$\frac{7}{2}$	$^8S_{7/2}$	2	7.94	8.48	7.0	5.9	15.75	15.8	⟨110⟩	*bcc*	90.4	–	–	$\parallel c$	$\perp c$	ave.
Gd	64	$\frac{7}{2}$	0	$\frac{7}{2}$	$^8S_{7/2}$	2	7.94	7.98	7.0	7.63	15.75	15.8	–		*hcp*	–	293.4	317	317	317
Tb	65	3	3	6	$^7F_6$	$\frac{3}{2}$	9.72	9.77	9.0	9.34	12.0	10.5	*b*		230.0	–	219.5	195	239	224
Dy	66	$\frac{5}{2}$	5	$\frac{15}{2}$	$^6H_{15/2}$	$\frac{4}{3}$	10.64	10.83	10.0	10.33	8.75	7.1	*a*		179.0	–	89.0	121	169	153
Ho	67	2	6	8	$^5I_8$	$\frac{5}{4}$	10.60	11.2	10.0	10.34	6.0	4.5	*b*		132.0	–	20.0	73.0	88.0	83
Er	68	$\frac{3}{2}$	6	$\frac{15}{2}$	$^4I_{15/2}$	$\frac{6}{5}$	9.58	9.9	9.0	9.1	3.75	2.6	–		85.0	–	20.0	61.7	32.5	42
Tm	69	1	5	6	$^3H_6$	$\frac{7}{6}$	7.56	7.61	7.0	7.14	2.0	1.2	*c*		58.0	–	32.0	41.0	−17.0	2
Yb	70	$\frac{1}{2}$	3	$\frac{7}{2}$	$^2F_{7/2}$	$\frac{8}{7}$	4.53	–	4.0	–	0.75	0.32	–		–	–	–	–	–	

* Spectroscopic state = $^{2S+1}X_J$ with X = S, P, D, F, G, H, I as L = 0, 1, 2, 3, 4, 5, 6 respectively.

** Antiferromagnetic ordering in the light rare earths prevents the measurement of the saturation magnetic moment.

† See text.

†† T_N for fcc Ce is 16.8 K.

of antiferromagnetic ordering. Very rough values might be forthcoming from neutron diffraction measurements. Finally, the last columns provide the paramagnetic ordering temperatures in the easy and hard directions for the heavy rare earths. References for this table will be listed when the individual elements are discussed.

We note, in passing, the existence of two Néel points for some of the light rare earth metals. These correspond to the ordering of the moments on different sublattices of different symmetries for the dhcp allotrope. This is one of the many interesting and curious magnetic phenomena associated with rare earth metals.

1.2. The indirect interaction, generalized susceptibility, and spin waves

In this section the contribution of the magnetic moments to the energy and magnetic ordering of rare earth metals is considered. We begin with a total Hamiltonian

$$H_{\text{tot}} = H_{\text{coul}} + H_{\text{exch}} + H_{\text{cf}} + H_{\text{ms}} + H_{\text{z}} \tag{1}$$

where the Coulomb interactions of the conduction electrons appear in the first term as discussed in the band structure of the next section, H_{exch} is the indirect exchange or RKKY interaction of concern in this section, H_{cf} is the crystalline ionic lattice electric field energy of the 4f electrons, H_{ms} is the magnetostriction or magnetoelastic contribution to the energy of the metal and H_{z} is the Zeeman energy in an applied magnetic field. The terms are written in order of decreasing strength, although the relative importance of some terms varies because of the $J = L - S$ spin orbit coupling for the light rare earths. The leading term, H_{coul}, is spin independent and therefore is not important for this discussion. We neglect it now in a discussion of the second term which gives the 4f electron magnetic exchange energy. The other terms in the Hamiltonian will also be neglected here even though we are aware that the crystal field term might be larger than the 4f exchange term for the light rare earths.

In the indirect exchange model the 4f electron spin at $\boldsymbol{R}_i$ interacts locally with and polarizes the 5d–6s conduction electrons which then interact in turn with the 4f electron spin at $\boldsymbol{R}_j$. This approach is needed because the 4f wave functions have insufficient overlap to give direct Heisenberg exchange. This can be seen in fig. 3 which shows the radial distribution probability for the 4f, 5d and 6s electrons out to the Wigner–Seitz radius (3.8 atomic units or 1.9 Å). On the other hand, the 4f–5d overlap (cross-hatched area) is adequate to yield a strong direct exchange between the local moment and the conduction electrons which can polarize the conduction band giving rise to an excess saturation magnetic moment and which, happily, takes on the appearance of direct exchange between local moments.

Following Kasuya (1966) the interaction may be written in the form

$$H_{\text{exch}} = -\sum_{i \neq j} \mathcal{J}(\boldsymbol{R}_i - \boldsymbol{R}_j)\boldsymbol{S}_i \cdot \boldsymbol{S}_j \tag{2}$$

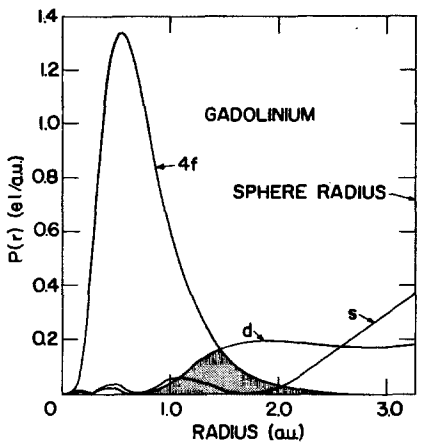

Fig. 3. Typical radial densities of S-like (Γ_1 state) and d-like wave functions; the shaded area shows the important d and f function overlap. After Harmon and Freeman (1974a).

where the 4f spin $\boldsymbol{S}_i$ is located at position $\boldsymbol{R}_i$ and the 4f spin $\boldsymbol{S}_j$ at $\boldsymbol{R}_j$ and $\mathcal{J}(\boldsymbol{R}_i - \boldsymbol{R}_j)$ is the exchange interaction function. At this point it may be recalled that the total angular momentum quantum number J is a good quantum number and proceed to use the projection of the spin on J as suggested by de Gennes (1966). To accomplish this we replace $\boldsymbol{S}_i$ by $(g-1)\boldsymbol{J}_i$ and work with the conventional form

$$H_{\text{exch}} = -\Sigma\, \mathcal{J}(\boldsymbol{R}_{ij})(g-1)^2 \boldsymbol{J}_i \cdot \boldsymbol{J}_j \tag{3}$$

with $\boldsymbol{R}_{ij} = \boldsymbol{R}_i - \boldsymbol{R}_j$. The procedure from here is to take the Fourier transform of the interaction function to get

$$\mathcal{J}(\boldsymbol{q}) = \sum_j \mathcal{J}(\boldsymbol{R}_{ij}) \exp\left[i\boldsymbol{q} \cdot \boldsymbol{R}_{ij}\right]. \tag{4}$$

This function can in principle be obtained directly from band structure calculations. However, the exchange matrix elements between states $\boldsymbol{k}$ and $\boldsymbol{k}'$ (such that $\boldsymbol{q} = \boldsymbol{k}' - \boldsymbol{k}$) are very difficult to work with and are frequently approximated as a constant or a simple function of $\boldsymbol{q}$. With this approximation one obtains for N atoms

$$\mathcal{J}(q) = (2/N)(g-1)^2 I_{\text{exch}}^2(q)\chi(q) \tag{5}$$

where I_{exch} is the approximate exchange matrix element for the interaction and where $\chi(q)$, the generalized susceptibility, has the form

$$\chi(q) = \frac{1}{N} \sum_k \frac{n_k - n_{k+q}}{E_k - E_{k+q}}. \tag{6}$$

In the latter we have taken $\boldsymbol{k}' - \boldsymbol{k} = \boldsymbol{q}$, n_k is the occupation number of electrons with momentum $\boldsymbol{k}$ and energy E_k in the conduction band. (If more than one band is involved, a band index with a sum on the index would be required.) Since the

matrix elements are not easily calculated, it is generally assumed that the matrix element I^2_{exch} does not vary, so that $\chi(q)$ plays the dominant role in determining magnetic ordering. It may be seen that those regions on the Fermi surface which make $\chi(q)$ large would likely come from flat parallel surfaces perpendicular to the c-axis (q is assumed along c here) so that many electrons could participate at a given q; such geometry is called "nesting". This is discussed in the next section which covers the bands and Fermi surfaces of the metals. For now we note the minimum in H_{exch} will occur for a maximum in $\chi(q)$, say at $q = Q$. When the maximum of $\chi(q)$ is at $q = Q = 0$ the ordering is ferromagnetic. If "nesting" occurs at $q = Q$, then $\chi(Q)$ will be a maximum and an antiferromagnetic (spiral or sinusoidal) type of ordering will give a minimum in energy.

Before proceeding to the consequences of the effects of $\chi(q)$ on magnetic ordering we examine the relationship between the exchange energy and the magnetic ordering temperature. This is obtained by equating H_{exch} from eq. (3) with the thermal energy. Hence

$$k_B T_0 = \tfrac{2}{3}\mathcal{J}(Q)(g-1)^2 J(J+1) \tag{7}$$

where k_B is Boltzmann's constant and T_0 is the magnetic ordering temperature. This suggests that the ordering temperatures should be proportional to the de Gennes factor $(g-1)^2 J(J+1)$. In fig. 4 the highest ordering temperatures for the heavy rare earths found in table 2 are plotted against the spin factors $S(S+1)$, solid circles, and $(g-1)^2 J(J+1)$, solid triangles. It is seen that the fit is better to

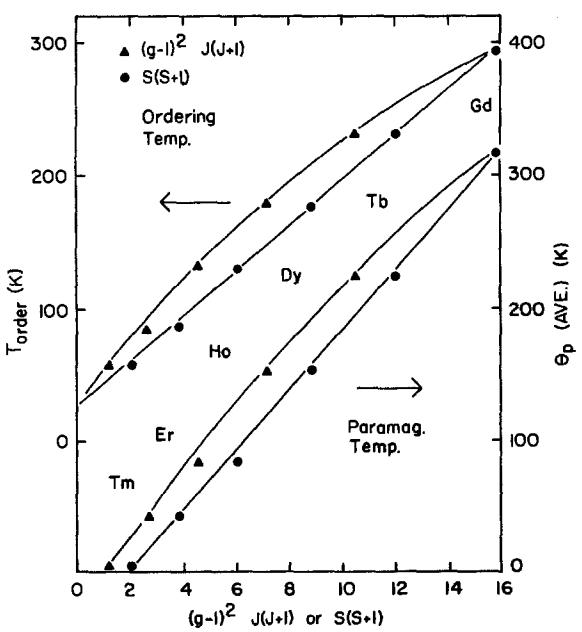

Fig. 4. Highest ordering temperatures and average paramagnetic Curie points of heavy rare earths versus de Gennes factor and versus $S(S+1)$. The fit to $S(S+1)$ appears to be superior.

the simple spin factor $S(S+1)$. This may be accidental because the possibility that $\mathcal{J}(Q)$ might be different for different elements has been neglected.

We can likewise examine the relationship between the average paramagnetic ordering temperatures from table 2 and the spin factors. We use $\theta_{p(ave.)} = \frac{1}{3}\theta_{p\parallel} + \frac{2}{3}\theta_{p\perp}$ and get the results shown in fig. 4. We see that in this case the fit to $S(S+1)$ is again superior. We explore this matter further in fig. 5 where we show the paramagnetic Curie points for H parallel to the c-axis and for H perpendicular to the c-axis for the heavy rare earths as a function of the de Gennes factor and of the simple spin factor. We see θ_p perpendicular to c is nearly linear in the plot against $S(S+1)$.

We examine next the form for $\mathcal{J}(R)$ when the assumption is made that the conduction electron band is free electron-like with $E(k) = \hbar^2k^2/2m$ (parabolic). We have in this simple case

$$\mathcal{J}(R) = (m|I|^2/4\pi^3R^4)[2k_FR\cos(2k_FR) - \sin(2k_FR)] \tag{8}$$

where k_F is the electron momentum at the Fermi level and m is the electron mass. This is the Rudermann–Kittel–Kasuya–Yosida (RKKY) form for the exchange interaction. It falls off as $1/R^3$ so has a somewhat limited range; for small k_FR, $\mathcal{J}(R)$ is proportional to $-1/k_FR$ so we get ferromagnetic ordering out to the first zero of the function in the bracket. We note also that the first term in the bracket is oscillatory with R so it can give anti- as well as ferromagnetic ordering.

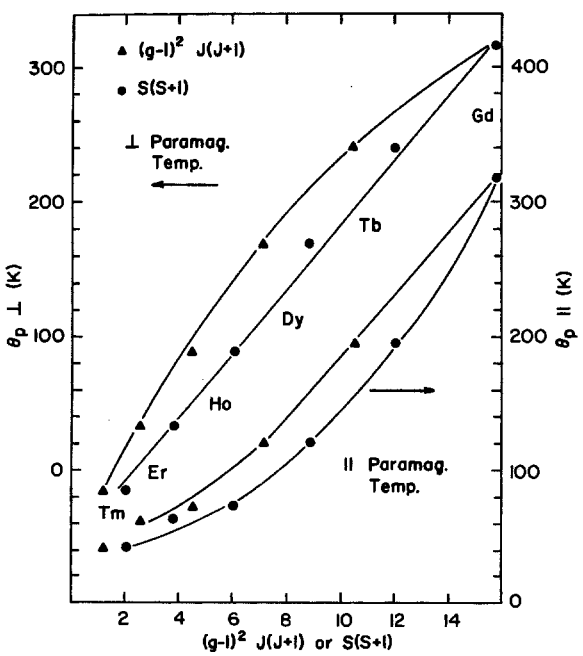

Fig. 5. Paramagnetic Curie points for H parallel to the c-axis and for H perpendicular to the c-axis for the heavy rare earths versus de Gennes factor and versus $S(S+1)$.

To examine magnetic order in greater detail we assume that the total angular momentum at site $\boldsymbol{R}_i$ is $\boldsymbol{J}$, that within the hexagonal layers we have aligned spin factors and that $\boldsymbol{J}$ makes angle θ with respect to $\boldsymbol{q}$ which is assumed along the c-axis of the hexagonal lattice. Let $\hat{z}$ be along the c-axis, $\hat{x}$ along a line of atoms or a-axis in the basal plane and $\hat{y}$ along the b-axis which is $\perp$ to the a-axis in the basal plane. The components of $\boldsymbol{J}$ at site $\boldsymbol{R}_i$ are

$$J_{iz} = J\cos\theta \tag{9}$$

$$J_{ix} = J\sin\theta\cos(\boldsymbol{q}\cdot\boldsymbol{R}_i + \varphi) \tag{10}$$

$$J_{iy} = J\sin\theta\sin(\boldsymbol{q}\cdot\boldsymbol{R}_i + \varphi) \tag{11}$$

with J the amplitude and φ an arbitrary phase angle at $\boldsymbol{R}_i = 0$. This describes a conical moment structure (Er or Ho at low temperature) with the turn angle related to $q = (2\pi/\lambda)\hat{q}$. For a planar spiral structure (Tb, Dy, Ho) $\theta = \frac{1}{2}\pi$ and $J_{iz} = 0$ with a turn angle again determined by q. For the ferromagnetic structure of Tb and Dy $\theta = \frac{1}{2}\pi$, and $q = 0$. It turns out that magnetic exchange alone cannot account for conical magnetic ordering. This can be seen by examining the exchange energy per atom

$$E_{\text{exch}} = -J^2[\mathcal{J}(q)\sin^2\theta + \mathcal{J}(0)\cos^2\theta]. \tag{12}$$

If $\mathcal{J}(q) > \mathcal{J}(0)$ then the exchange energy would be a minimum for $\theta = \frac{1}{2}\pi$, the planar spiral. On the other hand if $\mathcal{J}(0) > \mathcal{J}(q)$ the exchange is a minimum for $\theta = 0$, the ferromagnetic structure with the magnetic moment along the c-axis. Neither case gives a conical structure and so anisotropy energy and/or magnetoelastic energy is required to stabilize a conical structure.

The behavior of the moments when a magnetic field is applied to the planar spiral structure (Tb, Dy, Ho) is examined next. Large anisotropy confines the magnetic moment vectors to the basal plane, i.e., the c-axis is the very hard direction. Assume the magnetic field is applied along the b-axis in the basal plane. Progressive stages showing what happens to the spins of several layers of magnetic moments in the spiral phase of Ho are shown in a projection onto the basal plane in fig. 6. In part (a) of the figure the orientation of the moments for $H = 0$ are the solid vectors which tend to cluster around the easy b-axis directions and for a modest H are the dotted vectors. At higher fields there is an abrupt transition to the fan structure shown in fig. 6b. Then at even higher fields the pattern in (c) and (d) appears. The theory for this process is discussed by Cooper (1972). It is shown later how such fan structures affect the magnetization process in Ho.

In the cases of Tb, Dy, Ho and Er there is a transition from an antiferromagnetic phase to a ferromagnetic phase as the temperature is decreased. This comes about because of the difference in the temperature dependence of the exchange energy and of the magnetoelastic energies which both play a part in determining the magnetic ordering. The magnetoelastic energy favors ferromagnetism and is greater at low temperatures but falls off more rapidly as T

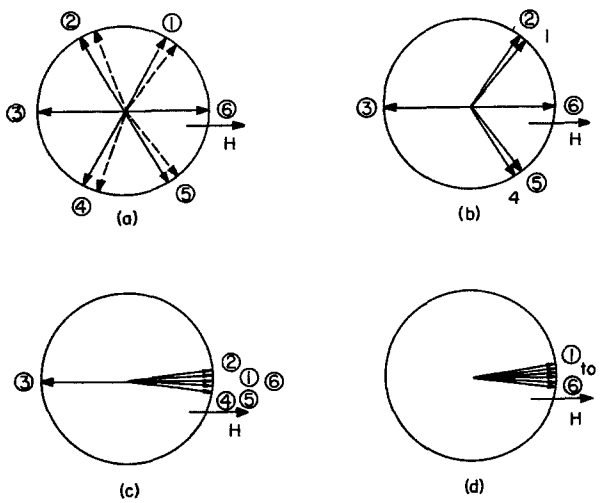

Fig. 6. Development of the fan structure for helically ordered magnetic moments. The diagram is appropriate for H along the b-axis of Ho at about 60 K. (a) The moments marked 2, 4, 5 bend toward the field in a weak field giving paramagnetic-like behavior. (b) When the field is higher the moments marked 2,4 jump to new positions creating a fan-like appearance. (c) Next the moments marked 1,2,4,5 become parallel to the field, (d) at high fields the antiparallel moments move to give total ferromagnetic alignment – an overall three step process.

increases than does the exchange energy which favors antiferromagnetic (spiral) ordering.

The planar spiral ordering in Tb exists over a temperature range of only 10 K and the spiral turn angle from layer to layer is small $\sim 18°$. The temperature range over which Dy and Ho are in the spiral phase is much greater. Cooper (1972) has discussed this phenomenon and has pointed out that the principal driving force for the helix to ferromagnetic transition in Dy and Tb comes from the cylindrical symmetry energy associated with the lowest order magnetostriction effect.

In fig. 7 polar graphs of 4f wave functions are shown. These explain the strong magnetic anisotropy associated with the rare earth metals other than Gd (which has a spherically symmetric half full 4f shell). The 4f electrons have three units of angular momentum and for partially full or partially empty shells give aspherical charge densities as can be seen in the figure. (In the absence of crystal fields we have rotational symmetry about the z-axis as indicated.) Indeed for one to three electrons in the shell the charge distribution is donut-like in shape. When we invoke near neighbor Coulomb repulsion between such aspherical charge distributions one sees at once a simple basis for understanding the strong magnetostriction, magnetoelastic and magnetic anisotropy effects which are observed.

We turn next to a brief discussion of spin wave physics. A detailed discussion

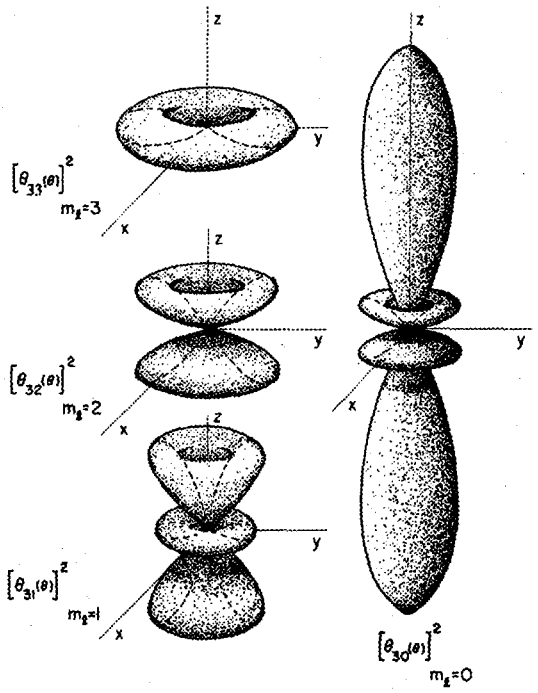

Fig. 7. The $[\Theta_{lm}(\theta)]^2$ probability orbitals for 4f electrons. For $m_l = 3$ the distribution is donut like. The $m_l = 0$ distribution is noticeably different from the others with high concentration along the z-axis. The θ dependence is uniform as sketched for zero crystal fields.

is given by Mackintosh and Møller in chapter 5 of the book edited by Elliott (1972). The manner in which spin waves, or magnons, arise is analogous to the manner in which phonons arise in the treatment of solids. In the latter case atoms are arranged in a lattice and interact via Coulomb forces making it possible for characteristic vibrations or standing waves to exist in the solid. The frequencies in a solid are of the order of 10^{12} Hz giving the disturbances a quantized energy $h\nu$ of about 4 mev. In the case of magnetic systems the magnetic moments on different lattice sites are coupled by way of the exchange interaction of eq. (2). This means that characteristic magnetic spin waves will be supported by a magnetic lattice. At absolute zero the magnetic moments are in their zero point energy state and we expect any disturbance of the ionic lattice to have a counterpart in the magnetic lattice. At low temperatures only long wavelength or low energy disturbances will be excited, i.e., the spins precess in a coupled manner and the spin wave propagates through the lattice. The name magnon is given to a quantized spin wave. It turns out that the energies of magnons are very much like those of phonons and the energy dependence on the q vector is also much like that of phonons so they have dispersion relationships, $E(q)$, which are reminiscent of phonon dispersion.

When the Hamiltonian of eq. (3) is second quantized and thermal disturbances are introduced in the case of a simple lattice, the energy takes on the form

$$H = -AJ^2\mathcal{J}(q=0) + J\sum_q [\mathcal{J}(q=0) - \mathcal{J}(q)]a_q^+ a_q \tag{13}$$

where a_q^+ is a creation operator for a spin wave of wave number q and a_q is the corresponding annihilation operator. The first term gives the ground state energy of the moments and the second gives the spin wave energy so the dispersion relationship is

$$E(q) = \hbar\omega(q) = J[\mathcal{J}(q=0) - \mathcal{J}(q)]. \tag{14}$$

The problem is more complicated in the case of the hcp lattice where there are two atoms per unit cell. In this case Mackintosh and Møller get dispersion relations which show two branches. The term acoustic is used to identify the lower branch for which the A and B lattice site moments are in phase, for small wavevectors, while the term optical is used to identify the upper branch for which the A and B site moments are 180° out of phase, for $q = 0$.

The dispersion relations depend on the type of ordering, so different curves for the ferromagnetic and helical phases encountered in the rare earths are expected.

A thermodynamic treatment of magnetic moments leads to a discussion of the entropy associated with the disorder generated by the spin waves. By the time the order disorder transformation (Curie point or Néel point) is reached, essentially all spin waves which can be supported are excited and the contribution of the spins to the entropy is nearly saturated. Short range order persists into the paramagnetic range so the specific heat levels off to the non-magnetic part (phonon and electronic) well above the ordering temperature. When the phonon and electronic parts of the specific heat for a magnetic material are subtracted from the total specific heat the magnetic portion is obtained. A step by step calculation of the energy added divided by the temperature gives the magnetic entropy. From statistical mechanics the total magnetic entropy S_{mag} comes out to be

$$S_{mag} = R\ln(2J+1) \tag{15}$$

where J is the total angular momentum quantum number and $2J+1$ is the spectroscopic multiplicity associated with the total angular momentum quantum number. We see from this that specific heat measurements are significant and useful in the study of magnetic systems.

1.3. Energy bands, Fermi surfaces and electrical resistivity

In the last section the exchange energy term in the Hamiltonian of eq. (1) was considered. This term was discussed first because of its importance in explaining many features of the magnetic ordering in rare earth metals. It turns out as suggested there that the Coulomb term in the Hamiltonian also plays a strong

and interesting part in the magnetic properties of the rare earth metals. One should certainly expect this because of the indirect exchange interaction wherein the 5d–6s conduction bands are intermediaries for coupling 4f moments to each other.

The most recent review of the band structure of the rare earths is given by Liu in chapter 3 of the book edited by Gschneidner and Eyring (1978). Earlier reviews have been given by Dimmock (1971) and by Freeman (1972). The bands of the related trivalent elements Sc and Y have been reviewed by Cracknell (1971).

Band calculations treat the conduction electron Coulomb term of the total Hamiltonian of eq. (1). We have

$$H_{\text{coul}} = \sum_i \frac{p_i^2}{2m} - \sum_i \sum_j \frac{Ze^2}{|\boldsymbol{R}_i - \boldsymbol{R}_j|} + \frac{1}{2} \sum_i \sum_{k \neq i} \frac{e^2}{|\boldsymbol{R}_i - \boldsymbol{R}_k|}. \tag{16}$$

Here m is the electron mass, p_i the electron momentum, $\boldsymbol{R}_i$ and $\boldsymbol{R}_k$ electron positions, $\boldsymbol{R}_j$ the position of the lattice nuclear (ionic) charge Z, and e the electronic charge. The first term is the electronic kinetic energy, the second term the Coulomb attraction energy and the last term the electronic Coulomb repulsion energy. For N atoms there are then ZN electrons all told.

Several approximations must be employed to make this many body system tractable. In the Born–Oppenheimer approximation the electron–phonon interaction is eliminated. The Hartree–Fock approximation using a Slater determinant wave function reduces the problem to an independent electron model which neglects electron–electron correlations of opposite spin electrons. An average single electron effective potential is required, i.e., the electron moves in an average but periodic potential due to the ions and to all the other electrons. The augmented plane wave method with a muffin tin potential as suggested by Slater (1937) has proved to be effective in the band calculations for the rare earths. This potential is spherically symmetric inside of non-overlapping muffin tin spheres around each ion and is constant outside the spheres.

Since the rare earths are beyond the middle of the periodic table they fall on the borderline for the appearance of relativistic effects. Some advantages accrue if a relativistic augmented plane wave method (RAPW) is employed to find the bands. This approach automatically includes spin orbit effects. APW and RAPW methods for calculating bands have been described by Mattheiss et al. (1968), Loucks (1967), Dimmock (1971) and by Callaway (1974).

When the APW method is employed the wave functions for the Schroedinger equation are spherical waves inside the muffin tin spheres and are plane Bloch type waves outside the spheres in the interstices. The two sets of wave functions are matched at the sphere surfaces and this leads to linear relations between the sets of coefficients. A variational treatment leads to homogeneous equations in the coefficients which must have a non-trivial solution. By fitting the solutions at wave vector points in the Brillouin zone a set of basis functions is found for the approximations. The points must be chosen judiciously to obtain accurate bands.

Historically, the bands for Gd were calculated first by Dimmock and Freeman

(1964). Gadolinium has the hcp structure as do Tb, Dy, Ho Er, Tm, and Lu. A simple diagram showing the relative energy levels and conduction band for Eu and Gd (Gd is typical of the heavy rare earths) is shown in fig. 8. We see that the 4f electrons exist in a very sharp band, which is essentially an atomic energy level, lying about 8 eV (electron volts) below the Fermi level in the 5d–6s conduction electron bands for Gd and about 2 eV below for Eu. The conduction electrons have some common qualitative features for all the heavy rare earths as well as for Sc and Y. There are, however, some very important small differences which have strong influences magnetically. These differences are related to the positions of some of the flat d-like bands relative to the Fermi energy. The Brillouin zone for the hcp lattice is also hcp for which the geometric symmetry points are shown in fig. 9.

Energy bands are dependent on $\boldsymbol{k}$ vectors; they are calculated along symmetry lines in the Brillouin zone and the energy bands are usually shown along these lines. The original Dimmock and Freeman (1964) paramagnetic (above $T_c = 293.4$ K) bands for Gd are shown in fig. 10. The general layout of the bands may be described as follows: Because the lowest energy band at Γ is broad in energy and rises in a fashion reminiscent of the parabolic band for nearly free electrons it is called an s-like band. The much flatter bands above this near E_F are d-like and these play a dominant role in the determination of the Fermi surface. Two bands intersect the Fermi level which is established when the three conduction electrons have been accommodated in the bands. It is seen that this occurs near T along Γ to K, near K and near Σ along M to Γ. By using a mesh of many points in the Brillouin zone the constant energy surface at E_F for such bands can be found. The Dimmock and Freeman (1964) Fermi surface for Gd in the extended

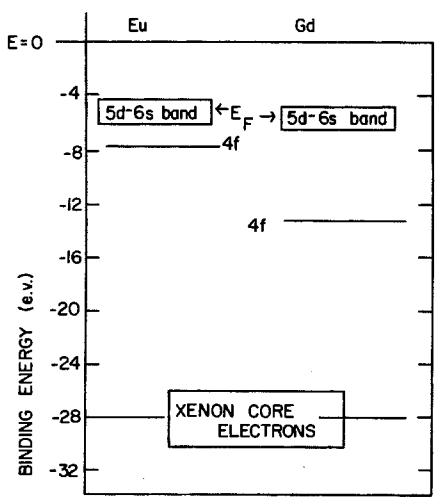

Fig. 8. Sketch of the pertinent energy levels for Eu and Gd. The positions of the 4f levels below E_F (the Fermi level) are based on XPS data of Héden et al. (1972) and of McFeely et al. (1973).

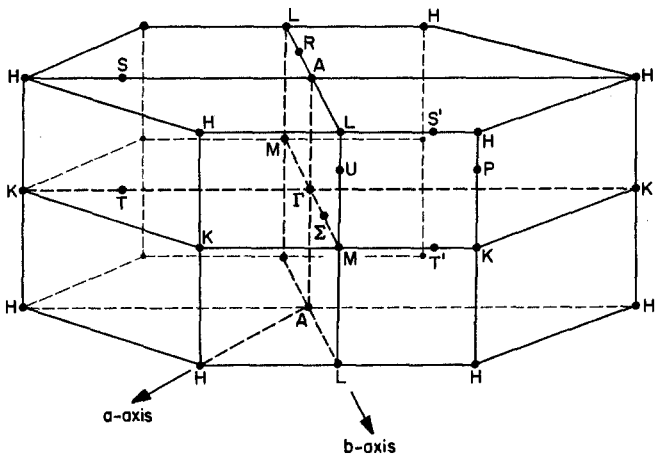

Fig. 9. Brillouin zone for the hexagonal close packed structure showing the standard symmetry points (an a-axis of the zone corresponds to a real lattice b-axis and a b-axis of the zone corresponds to a real lattice a-axis).

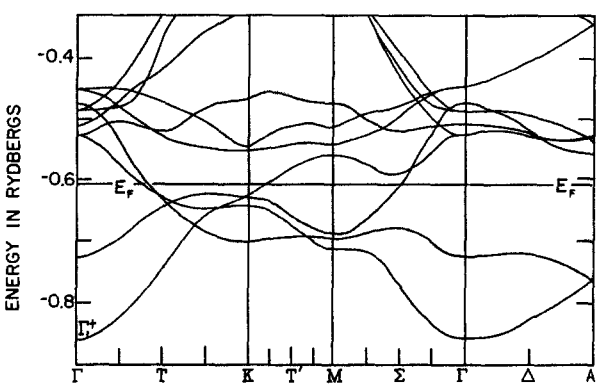

Fig. 10. The conduction electron energy bands for Gd calculated by Dimmock and Freeman (1964).

double zone scheme is shown in fig. 11. The surface is found by folding the bands between Γ and A into the extended zone ΓAΓ. It is an open hole surface and goes from one zone to the next with the states outside the surface occupied and the states inside empty. It is unusual that there are no other pieces or pockets of Fermi surface. The surface has a cylindrical tree trunk-like shape in the central ΓMK region which involves electrons in the steep bands of s–p character. Then going up or down along the c-axis, the trunk expands into arms or branches which extend out in the ALH planes and which exhibit a duck foot type of webbing between the arms near the trunk. Both the trunk and the webbing play important roles in the electrical conductivity, as might be expected since the conductivity comes from an integration of the electron Fermi velocity

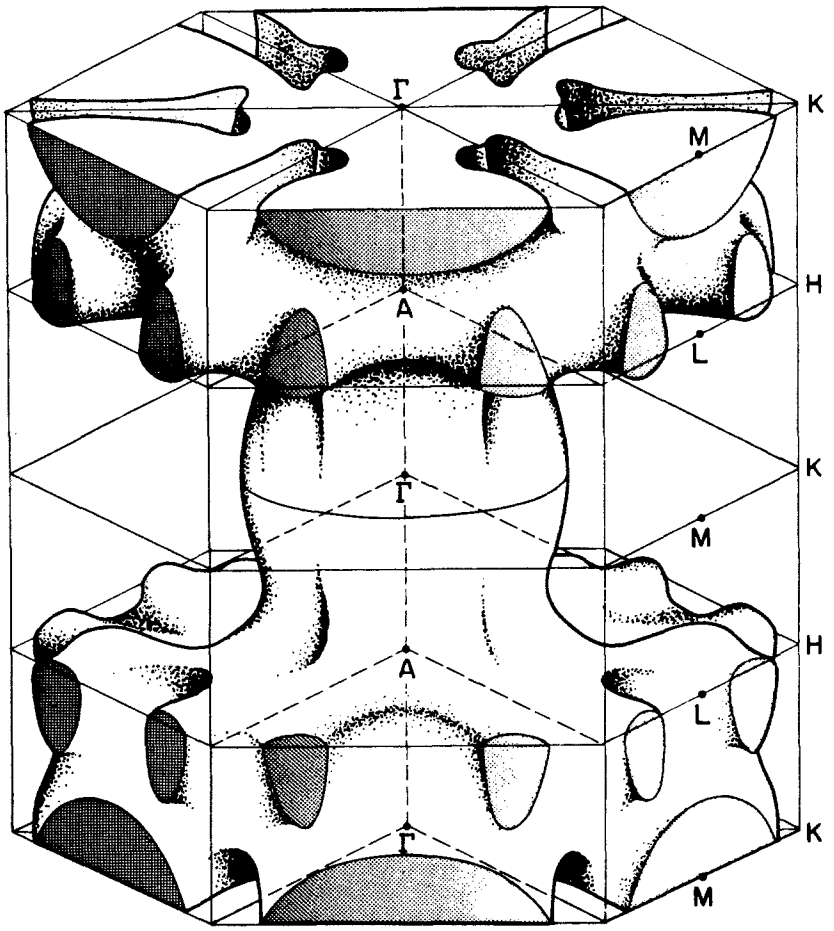

Fig. 11. Fermi surface of Gd as determined by Dimmock and Freeman (1964). This is a hole surface in the extended zone scheme with the states inside the surface empty and the states outside the surface occupied.

over the Fermi surface. Indeed the Fermi surface geometry explains the anisotropy found in the electrical resistivity, as seen later in this chapter. On the other hand it is principally the webbing feature which exhibits a strong interplay with magnetic ordering by way of the exchange energy term in the Hamiltonian and the effect this has on the periodic electron potential. More detailed discussions of these Fermi surface features for the hcp metals will be found later when the individual elements are treated.

The light rare earth metals, La, Ce, Pr and Nd, exhibit the crystal structure with ABAC stacking of hexagonal layers. The Brillouin zone is hexagonal and the symmetry points used are the same as those for hcp as shown in fig. 9. Since there are four atoms per unit cell in this situation there are four bands which

intersect the Fermi energy and thus contribute to the Fermi surface. The problem is formidable; even so the energy bands for La have been calculated by Fleming et al. (1968) using the RAPW method. The bands they found for La are shown in fig. 12. The bands near E_F are flat and so have d-like character and are reminiscent of the bands for Gd. Since the RAPW method was used it was not possible for them to fold the bands out into the extended zone as for Gd. The Fermi surface they found consisted of many pieces and pockets, so they chose to display only some cross sections of the surface in high symmetry planes. Their findings appear in fig. 13. They noted that the webbing feature associated

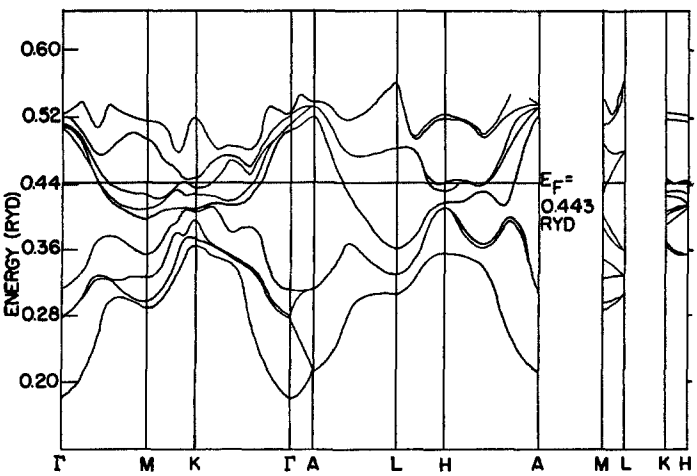

Fig. 12. Relativistic conduction electron energy bands for La calculated by Fleming et al. (1968).

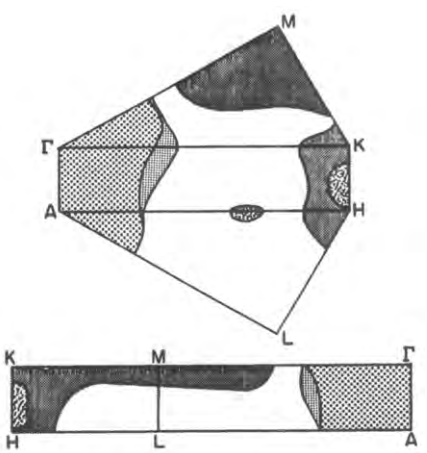

Fig. 13. Some cross sections of the Fermi surface of dhcp La with the high symmetry Brillouin zone planes as found by Fleming et al. (1968).

with the c-axis direction is missing and suggested this might be associated with the stabilizing of the dhcp structure. On the other hand, they noted that some of the surfaces depicted partially in fig. 13 could lead to a nesting in directions perpendicular to c which might account for some magnetic ordering observations for these metals.

Since the metal Eu is divalent and exhibits the bcc structure, it has been necessary to make a separate calculation for its bands. Freeman and Dimmock (1966) calculated bands for bcc Eu by the APW method and Andersen and Loucks (1968) used the RAPW method. The Brillouin zone for the bcc crystal is fcc and has the shape and point designation shown in fig. 14. The bands obtained by Andersen and Loucks are shown in fig. 15 and appear to be similar to the bands of the bcc transition metals. The Fermi surface they found is shown in fig. 16. There is a large electron surface centered around H which has the shape of a rounded cube and around P there is a similarly shaped hole surface with ellipsoids tetrahedrally attached on four of the corners. The flat pieces of the hole cube provides the nesting required to explain the observed magnetic structure of Eu. More recent Fermi surface calculations by Kobayasi et al. (1976) are in reasonable agreement with the earlier calculations above.

The element Yb is divalent in metallic form and has a full 4f shell so it is only weakly magnetic. It has been found by Bucher et al. (1970) and Kayser (1970) that the hcp structure is the stable form at very low temperatures. Jepsen and Andersen (1971) made a RAPW calculation for hcp Yb and found the bands shown in fig. 17. They also found that the Fermi surface consisted of a number

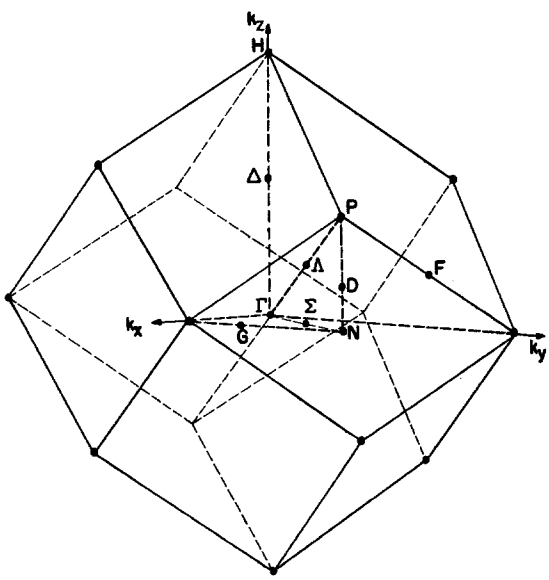

Fig. 14. Brillouin zone with symmetry points for the body centered cubic lattice. The point N is in the K_xK_y plane at the foot of the point P shown.

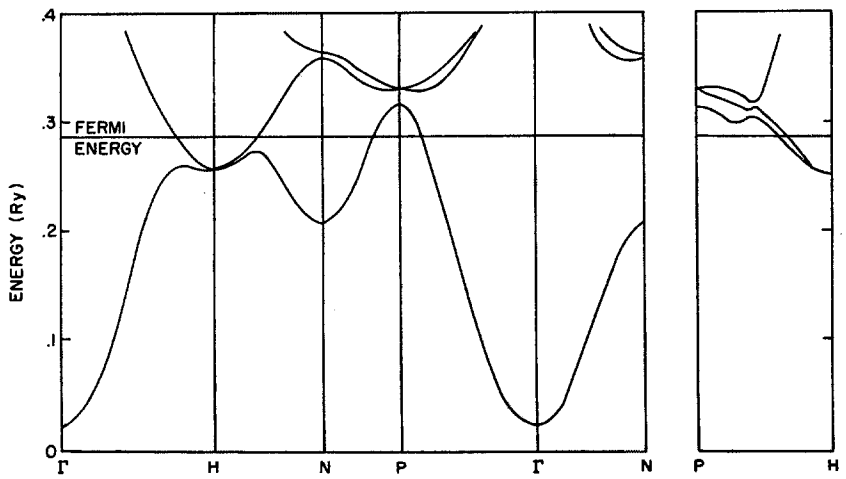

Fig. 15. Energy bands of Eu calculated by Andersen and Loucks (1968) using the relativistic augmented plane wave method.

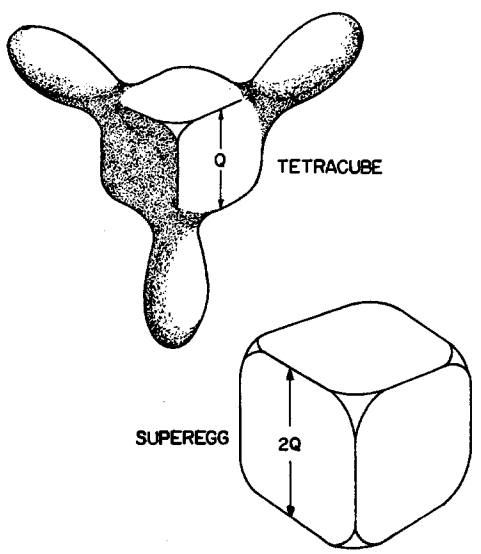

Fig. 16. Fermi surface for Eu determined by Andersen and Loucks (1968).

of pieces and pockets which were hard to picture. As might be inferred from the bands shown in the figure along Γ to K they calculated a high density of states at the Fermi level and they argue that this feature might account for the fcc to hcp transformation at low temperatures for Yb.

The element Ce is quite inscrutable from the band viewpoint. The element is fcc (γ-form) above 350 K, takes on the β form, which is dhcp, in the range

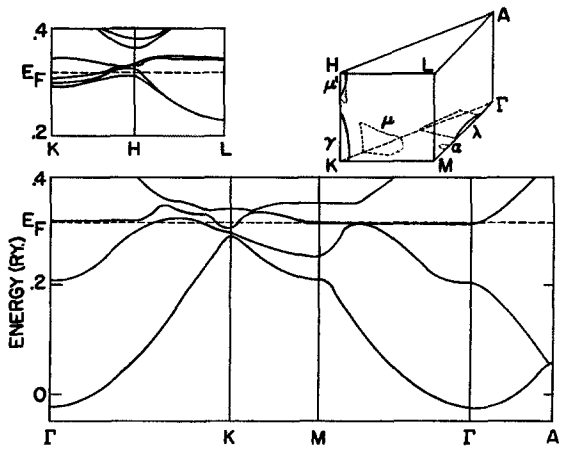

Fig. 17. Band structure, and (upper right) some features of the Fermi surface for hcp (low temperature phase) of Yb calculated relativistically by Jepsen and Andersen (1971).

50–350 K and collapses into a more dense fcc form (α) below 50 K. The f band falls close to the Fermi level and makes band calculations difficult.

Next a very brief outline of transport theory as related to the Fermi surfaces of rare earth metals is given. Reviews of the subject have been published by Meaden (1965, 1971). The indirect exchange mechanism leads naturally to a close correlation of conduction electron transport properties to the magnetic properties of the metals, i.e., the electrical resistivity exhibits anomalous behavior when changes in magnetic ordering occur. This makes it possible to determine magnetic ordering temperatures by way of electrical resistivity measurements. It should also be noted that at low temperatures the resistivity of magnetic metals should have a T^2 dependence according to Mannari (1959).

The usual Boltzmann equation treatment for determining electrical conductivity leads to

$$(\rho^{-1})_{ij} = \frac{e^2}{4\pi^3} \int_{E_F} \tau v_i \, \mathrm{d}S_j \tag{17}$$

where ρ is the resistivity tensor, e is the electronic charge, τ is the relaxation time of the conduction electrons, v_i is the component of the conduction electron velocity in the i direction at the Fermi surface and $\mathrm{d}S_j$ is the projection of the Fermi surface element in the j direction. As indicated above, the Fermi surfaces for the rare earths, particularly the hcp elements, are anisotropic and this leads to anisotropy in the electrical resistivity of the metals.

A wide variety of conduction electron scattering mechanisms influence the conductivity of the rare earths. The problem is usually treated by associating independent relaxation times with the different mechanisms so that the effective relaxation time for eq. (17) has the form

$$1/\tau = 1/\tau_0 + 1/\tau_p + 1/\tau_m. \tag{18}$$

Here τ_0 is due to impurity scattering and is related to the residual resistivity ρ_0, τ_p arises from phonon scattering and normally gives the low temperature resistivity dependence T^x, $x = 2$–5 along with linear temperature dependence at elevated temperatures and τ_m is related to magnon scattering. Magnons are quantized magnetic excitations (spin waves) so τ_m arises from magnetic spin disorder scattering. We assume an average conduction electron velocity, v_i, may be used. Then in the case of hexagonal crystal lattices the resistivity ρ_c along the c axis would have the form

$$\rho_c = A\left(1/\tau_0 \int_{E_F} dS_c + 1/\tau_p \int_{E_F} dS_c + 1/\tau_m \int_{E_F} dS_c\right) \tag{19}$$

where A is a constant. A similar expression gives ρ_b in the basal plane b direction. (The resistivity is found to be isotropic in the basal plane so $\rho_b = \rho_a$.) The ratio of the single crystal resistivities gives some information about Fermi surface geometry because

$$(\rho_b - \rho_{0b})/(\rho_c - \rho_{0c}) = \int_{E_F} dS_c \Big/ \int_{E_F} dS_b \tag{20}$$

with similar expressions for residual resistivities and for the high temperature slopes $d\rho/dT$ of ρ vs. T. For non-magnetic Y and Lu, Hall et al. (1959) found resistivity ratios ρ_a/ρ_c of 2 and 2.2 respectively from experiment. The shape of the Fermi surface of fig. 11 makes the numbers look reasonable.

As might be expected in the light of eqs. (17) and (19) and the fact that the rare earths are transition metals with relatively high density of states at E_F, these metals are poor conductors, particularly those which exhibit magnon scattering. The element Gd has a room temperature resistivity two orders of magnitude greater than Cu.

Of greatest significance for this chapter, however, is the effect of the exchange interaction and magnetic ordering on the Fermi surface. We recall that when the periodic lattice of ions (a Coulomb term) is introduced in free electron theory the wave functions take on the Bloch form and energy gaps appear at reciprocal lattice points, e.g., at $n\pi/a$ ($n = 1, 2, 3, \ldots$) in the one dimensional lattice whose atom spacing is a. It is therefore to be expected that the introduction of magnetic periodicity into the Hamiltonian by way of H_{exch} would lead to additional energy gaps at or near magnetic ordering temperatures. As suggested by Mackintosh (1963), Elliott and Wedgewood (1963), and Miwa (1963) such magnetically induced energy gaps lead to so called "superzones". Here one notes that the spins of a ferromagnetic material would have the same periodicity as the ionic lattice so dramatic superzone effects would be missing. However, if the magnetic lattice differs from the ionic lattice (as happens in most rare earths) pronounced effects on the conductivity are found. In the case of helical structures which

have q along the c-axis and which are incommensurate with the ionic lattice, the new magnetic energy gaps along the c-axis wipe out Fermi surface areas with c-axis projections and this strongly influences the resistivity in the c direction.

A striking illustration from work by Freeman et al. (1966) for hcp Tm is shown in fig. 18. The extra energy gaps wipe out a considerable amount of the Fermi surface projection in the c direction.

The manner in which the electrical resistivity is affected by this phenomenon has been treated by Elliott and Wedgewood (1963). They assumed a spheroidal Fermi surface and used first order perturbation theory along with eq. (3) plus eqs. (9), (10), (11) in the form

$$\langle J_j^x \rangle = M'J \cos(\boldsymbol{q} \cdot \boldsymbol{R}_j) \tag{21}$$

$$\langle J_j^y \rangle = M'J \sin(\boldsymbol{q} \cdot \boldsymbol{R}_j) \tag{22}$$

$$\langle J_j^z \rangle = MJ \cos(\boldsymbol{q} \cdot \boldsymbol{R}_j + \phi) \tag{23}$$

to get the position $\boldsymbol{d}$ of the magnetic superzone planes at

$$\boldsymbol{d} = \tfrac{1}{2}(\boldsymbol{\eta} \pm \boldsymbol{q}) \tag{24}$$

with $\boldsymbol{\eta}$ a reciprocal lattice vector. Here M' and M are temperature dependent moment amplitudes which may be found from neutron diffraction data and ϕ is a phase angle. They found the energy to be

$$2E(\boldsymbol{k}) = E(\boldsymbol{k}) + E(\boldsymbol{k} + 2\boldsymbol{\eta}) \pm \{[E(\boldsymbol{k}) - E(\boldsymbol{k} + 2\boldsymbol{\eta})]^2 + I_{\text{exch}}^2 J^2 M_{\pm}^2\}^{1/2} \tag{25}$$

where $E(k)$ is the unperturbed energy of an electron of wave vector $\boldsymbol{k}$, I_{exch} is the exchange matrix element of eq. (5) and where

$$M_{\pm}^2 = M^2 + 2M'^2 \pm 2M'(M^2 + M'^2)^{1/2}. \tag{26}$$

The energy gap from this is

$$\Delta = I_{\text{exch}} JM \pm . \tag{27}$$

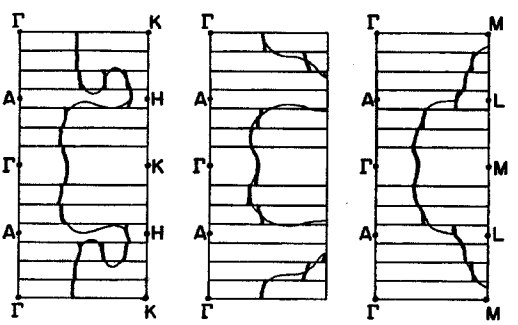

Fig. 18. Some of the vertical cross-sections of the Fermi surface for Tm. Light lines are for the original Fermi surface and the heavy lines are the result of magnetic superzone effects with the onset of antiferromagnetic ordering. After Freeman et al. (1966).

From eqs. (18), (19) and (24–27), the calculations for different crystallographic directions come out to be

$$\rho_b = \lambda_1 + \mu_1 T + U_1(1 - \tfrac{1}{2}M^2 - M'^2) \tag{28}$$

$$\rho_c = \frac{\lambda_2 + \mu_2 T + U_2(1 - \tfrac{1}{2}M^2 - M'^2)}{1 - \Gamma(M^2 + M'^2)^{1/2}} \tag{29}$$

$$\Gamma = (3\pi I_{\text{exch}} J/4E_F k_F) \sum_i |d_i|. \tag{30}$$

Here the sum is to be taken over all superzones which slice the Fermi surface, E_F is the Fermi energy, k_F is the electron wave vector evaluated at the Fermi surface and λ_1, μ_1, U_1, λ_2, μ_2, U_2 are adjustable parameters. The fits of the theory to the experiments are just fair and appear later with the discussion of the individual elements.

1.4. The crystal field

The first term in the Hamiltonian of eq. (1) provides for the Coulomb energy of the solid. Equation (16) treats the Coulomb energy of the three 5d–6s conduction electrons per atom in the ionic lattice. This does not include the Coulomb energy of the localized 4f electrons on a given atom due to the charges of all surrounding atoms in the lattice. Such a term, called the crystalline electric field term H_{cf}, must be added to make the picture more complete. (In a metal this term is small because the conduction electrons move so as to neutralize electric fields inside the metal. To find very large crystal field effects one turns to insulating or dielectric type compounds or matrices.) In the case of metals, we know that the symmetry of the lattice (hcp, dhcp, fcc) must be reflected in the description of the potential of the ionic lattice, and therefore also in the localized 4f electron wave functions. It is found that crystal fields have the effect of removing degeneracy and thereby diminishing (quenching) the orbital magnetic moment (recall that only $0.2\mu_B$ of $2.2\mu_B$ for iron comes from orbital moment). Strong LS coupling in the rare earths means that crystal fields may diminish both spin and orbital parts. The typical energy between the ground state and first excited crystal field state varies from 1 to 10 meV (10 K to 100 K) with the overall spread of all levels up to 20 meV. This should be compared to the exchange energy for Gd which is 25 meV.

It turns out that for the heavy rare earth elements from Eu to Tm, for which $J = L + S$, the exchange energy dominates the crystal field energy. The effect of crystal fields is most pronounced in the light rare earths for which $J = L - S$ and for which the exchange interaction is therefore small. Now J is a good quantum number and one looks to the crystal field to find the proper mixing of the $2J + 1$ degenerate m_J levels; or, to put it another way, the crystal field energy term is used to find the 4f wave function combination which will yield the appropriate energy levels. These then dictate the magnetic moment of the system.

The crystalline electric potential is of the Coulomb potential form. This is

expanded in tesseral harmonics which are directly related to spherical harmonics. Operator equivalents are used as suggested by Stevens (1952). Group theory arguments show that because of lattice symmetries most of the coefficients of these harmonics are zero. See, for example, Baker et al. (1958). For a hexagonal crystal only four terms remain, namely,

$$H_{cf} = B_2^0 O_2^0 + B_4^0 O_4^0 + B_6^0 O_6^0 + B_6^6 O_6^6 \tag{31a}$$

where the B's are parameters and the O's are operator equivalents, many of which have been tabulated by Hutchings (1964). When the c/a ratio is ideal and a point charge model for the ionic lattice is used this expression reduces to

$$H_{cf} = A_4^1 O_4^0 + A_6^1 [O_6^0 + \tfrac{77}{8} O_6^6] \tag{31b}$$

where the parameters A_4 and A_6 could, in principle, be calculated but are fitting parameters. For the hcp lattice and crystal field Hamiltonian of eq. (31b) Yosida (1964) gives a sample classical calculation where the operator equivalents are replaced by corresponding Legendre polynomials, $A_n^m P_{nm}$ and gets

$$H_{cf} = 2\alpha A_2^0 \langle r^2 \rangle J^2 P_2(\cos\theta) + 8\beta A_4^0 \langle r^4 \rangle J^4 P_4(\cos\theta) + 16\gamma A_6^0 \langle r^6 \rangle J^6 P_6(\cos\theta) + \gamma A_6^6 \langle r^6 \rangle J^6 \sin^6\theta \cos 6\phi. \tag{32}$$

Here θ is the polar angle from the c-axis and ϕ is the azimuthal angle from the a-axis, r is the radial distance, the brackets, $\langle\rangle$, designate the expectation value for 4f electrons, and α, β, γ are Stevens (1952) factors. The expression shows the anisotropy or angular dependence of the energy as it is related to the lattice geometry.

For a cubic lattice only two parameters, B_4 and B_6, are needed

$$H_{cf} = B_4(O_4^0 + 5O_4^4) + B_6(O_6^0 - 21O_6^4). \tag{33}$$

In such cases Lea et al. (1962) have suggested that convenient parameters are x, which gives the ratio of fourth to sixth order anisotropy, and W which gives the absolute scaling of the crystal field energy level scheme. They are given by

$$\frac{B_4}{B_6} = \left[\frac{x}{1-|x|}\right] \frac{F_6(J)}{F_4(J)} \qquad B_4 F_4(J) = xW \tag{34, 35}$$

where $F_4(J)$ and $F_6(J)$ are specified constants for a given J.

Most of the information about crystal field parameters for the heavy rare earths has come from studies of dilute alloys for which the exchange field is considerably weaker than the crystal field. Inelastic neutron scattering and magnetic susceptibility measurements have been used by Rathmann and Touborg (1977) and by Touborg (1977) for such studies. They got the hcp crystal field levels for 2at.% Er in a Sc host and in a Lu host. They found the admixture of m_J wave functions and the energy levels to be only slightly different in the two hosts, the main difference being in the height of the upper crystal field levels. As a typical case their results for Er in Sc are shown in fig. 19. Discussions of crystal field effects in the light rare earths appear in the sections describing the magnetic properties of these elements later in this chapter.

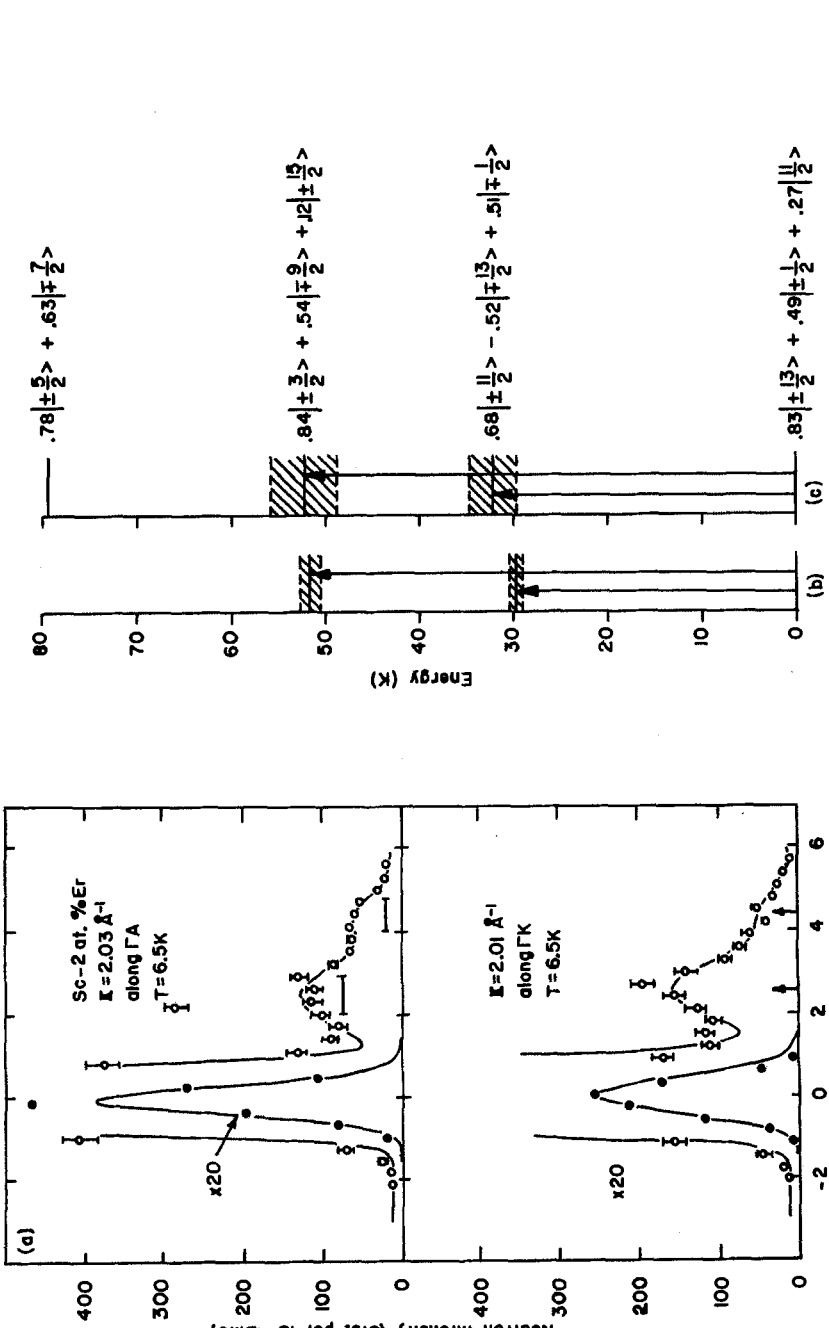

Fig. 19. (a) Inelastic neutron scattering spectra for Sc–2.0at.% Er. The experimental resolution and statistical uncertainties are indicated. The full lines are least-squares fits. (b) Transition energies with uncertainties obtained from the spectra in (a). (c) Crystal-field levels and wave functions calculated from the average crystal-field parameters in K for Sc host (table KK in Touborg 1977) $B_{20}/\alpha = -29.5 \pm 0.9$, $B_{40}/\beta = 9.9 \pm 1.9$, $B_{60}/\gamma = 19.8 \pm 1.5$, $B_{66} = \frac{77}{8} B_{60}$. The uncertainties in energy of the lowest levels and observable transitions at zero temperatures are indicated after Rathmann and Touborg (1977).

2. Magnetic properties of Eu, Gd, Tb, Dy, Ho, Er and Tm

This section begins with a brief description of the magnetic structures of the heavy rare earth metals as they have unfolded from neutron diffraction measurements. A review of this work has been prepared by Koehler (1972).

The seven 4f electrons of body centered cubic divalent Eu have parallel spins ($S = \frac{7}{2}$) which take on a helical configuration below the 90.4 K Néel temperature and the axis of the helix is along a ⟨100⟩ direction in the absence of an external field. This implies that the magnetic moments are in {100} planes. When a modest field is applied the axis of the helical spin structure takes the orientation of the field. A sketch of the magnetic structures of the heavy rare earths is given in fig. 20. The elements beyond Gd have strong magnetic anisotropy effects associated with the asymmetric charge distribution that goes with the 4f orbital electron wave functions which are donut-like for Tb and Dy and then become more complex for Ho, Er and Tm (see fig. 7).

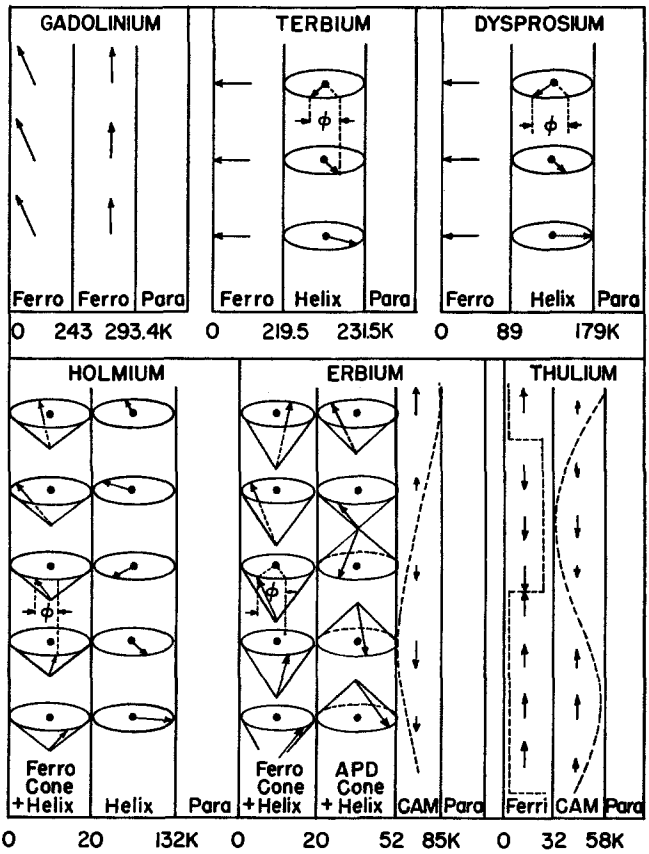

Fig. 20. Magnetic ordering in the heavy rare earths as found by neutron diffraction.

Gd is a simple ferromagnet. Like Eu it has the half filled 4f shell with seven parallel spins so $S = \frac{7}{2}$. The easy direction of magnetization lies along the c-axis of the hcp lattice just below the 293.4 K Curie temperature. The easy direction moves away from the c-axis for T below 240 K.

As shown in fig. 20 Tb is helical from 230 K to 219.5 K with the magnetic moments in the basal plane and the axis of the helix along the c-axis. Below 219.5 K the metal is ferromagnetic with the moments in the basal plane and with the easy direction along the b-axis. Dy has magnetic phases similar to those of Tb with the helical form extending from 179 K down to 89 K below which it is ferromagnetic with the moments in the basal plane and with the a-axis the direction of easy magnetization.

Starting with Ho a new magnetic phase develops. Just below the 132 K Néel point the helical structure of Tb is found; then at 20 K the moments take on a nearly conical ferromagnetic helical structure with a cone angle relative to the c-axis of 80°. Thus Ho has an antiferromagnetic moment component in the basal plane and a ferromagnetic component along the c-axis below 20 K.

As sketched in fig. 20 Er has an oscillatory (sinusoidal) c-axis component with an essentially random basal plane component below the 85 K Néel temperature and down to about 53 K where some squaring off of the wave sets in giving a quasi antiphase domain magnetic structure which extends down to about 20 K. Below this temperature a conical ferromagnetic structure is attained with the cone angle about 30° so that the c-axis moment comes out to be $7.6\mu_B$ or 0.84 times the full $9\mu_B$ expected.

In the case of Tm the moments have a sinusoidal modulation of the c-axis component just below the 58 K Néel point so it is much like Er. Then below 38 K the modulation of the c-axis component begins to square off and gradually takes on a strange ferrimagnetic like structure at 4.2 K wherein four moments up along c are followed by three moments down. This gives a net ferromagnetic component along c of one seventh the expected $7\mu_B$ or $1\mu_B$ at helium temperatures. This completes a brief survey of the heavy rare earths and we present next detailed information about the individual elements.

2.1. Europium

The rare earth Eu, atomic number 63, is a divalent metal and so has chemical properties like Ca. Hence, it is quite different from its neighboring elements among the lanthanides. The divalency stems from the migration of one of the 5d–6s conduction electrons to the 4f shell so as to half fill the shell because this configuration is highly stable and energetically favorable. One might then expect Eu to have magnetic properties akin to those of trivalent Gd which also has a half filled 4f shell and therefore has the same spectroscopic designation of $^8S_{7/2}$. Experimental measurements show otherwise. Why should this be so? The answer is found in differences (a) in crystal structure, (b) in atomic spacing and (c) in conduction electron d-bands. From table 1 it is seen that Eu is body centered cubic while Gd is hcp. The atomic spacing for Eu is 4.83 Å and that for

Gd is 3.63 Å which is important in determining the magnitude of the exchange energy as well as the sign of the spin coupling from the RKKY interaction of eq. (8). This helps to explain why Eu is found to be antiferromagnetic and Gd ferromagnetic. The divalent character of Eu as compared to the trivalent character of Gd means that fewer conduction electrons are available locally for the indirect exchange; in a study of Eu and Gd solutes in La, Legvold et al. (1977b) found this effect was large. A combination of the latter effect and the effect of atomic spacing explains the ratio of the Eu to Gd ordering temperatures which according to table 2 is 90.4 K to 292.3 K or about 1 to 3.

From X-ray photoemission spectroscopy (XPS) Héden et al. (1972) found the main 4f peak for Eu to be 2.1 eV below the Fermi level while McFeely et al. (1973) using (XPS) found the main peak for Gd at 7.7 eV below E_F. This shows the 4f electrons are much more tightly bound in Gd.

The magnetic moment of Eu in the form of small particles obtained by a filing technique was investigated by Nereson et al. (1964) using neutron diffraction methods. They found that the moments are ordered antiferromagnetically below 90.4 K, the Néel point. This transition is second order with a precipitous drop of the moment from 0.4 of the saturation value between 88 and 90.4 K. The moments are parallel to a cube face of the bcc lattice so that the axis of the helix (the screw axis) is perpendicular to the cube face and is therefore along a ⟨100⟩ direction. Just below T_N they found that the pitch of the helix (the q vector period) was $3.5a$, where a is the lattice parameter, and that the pitch gradually increased to $3.6a$ at 4.2 K corresponding to an interlayer turn angle of 50°. They found from their data that the magnetic moment per atom was only $5.9\mu_B$ which is well below the expected $7\mu_B$ for the $^8S_{7/2}$ ions. More recent neutron diffraction results on a Eu single crystal slab in an external magnetic field by Millhouse and McEwen (1973) corroborate the earlier findings and show that for fields H greater than 8 kOe the magnetic moments in domains move so as to be perpendicular to H; q for the helical moment arrangement is then parallel to H. At 4.2 K the q stays in this orientation when the magnetic field is turned off. The original helical arrangement returned when the sample temperature was elevated above 37 K.

From magnetic susceptibility measurements in the paramagnetic regime Johansson et al. (1971) found a moment of $8.48\mu_B$ which is higher than the $8.3\mu_B$ reported by Bozorth and Van Vleck (1960); both are high as compared to the expected $g\sqrt{S(S+1)}$ of $7.94\mu_B$ shown in table 2. This gives a surplus of $0.54\mu_B$ which is attributed to polarization of the 5d–6s conduction electrons. If conduction electron polarization is used to explain the low temperature moment of $5.9\mu_B$ as compared to the expected $7\mu_B$, an antiparallel localized 5d moment of $1.1\mu_B$ per atom is required. This is nearly twice the positive 5d band polarization found in ferromagnetic Gd at low temperatures. Such a large negative conduction electron polarization is difficult to understand and certainly calls for further investigation.

High field magnetization measurements by McEwen et al. (1973) on single crystal Eu at 4.2 K show the moment is linear with field from 2 to 20 T with the

moment then falling below linear behavior between 20 T and 35 T (350 kOe) where the moment reached was nearly $5\mu_B$ per atom. They expected the moment might saturate and reach the theoretical $7\mu_B$ at about 100 T (10^6 Oe).

Electrical resistivity data for Eu obtained by Curry et al. (1960) are shown in fig. 21. This is a nice example of the effect of spin wave scattering and of antiferromagnetism on the conductivity. The spin waves give rise to the rapid increase in the resistivity from 0 to 90.4 K, the Néel point, above which the spin disorder scattering saturates and approaches a constant. The slope of the resistivity curve at 300 K arises from phonon scattering alone. One may extrapolate this linear part back to the resistivity axis to obtain the total spin disorder scattering. Thus we have obtained a curve for the magnon resistivity alone for Eu by subtracting the nearly linear phonon resistivity. The result is the dashed curve of the figure which shows an interesting slow fall off to a constant value reflecting short range spin order-clustering or fluctuation effects up to 200 K. As a general rule it is expected that electrical resistivity versus temperature curves will always bend down toward the temperature axis when the temperature rises past an ordering temperature because of the spin disorder saturation effect. As suggested earlier this proves useful in exploring for ordering temperatures. The cusp in the resistivity curve near 90.4 K shows the effect of critical scattering and is also typical of antiferromagnetism where Fermi surface superzones play a role as described in the theory section earlier. Exactly how the Fermi surface pieces of fig. 6 are affected has not been determined. The Néel temperature of 90.4 K in table 2 is about the mean of the literature values.

The specific heat of Eu has been reported by Gerstein et al. (1967). Their results are shown in fig. 22 where we see a sharp peak at a temperature slightly below the 90.4 K Néel point with the curve tapering off gradually below the peak as the temperature is increased. If we estimate and subtract the phonon part

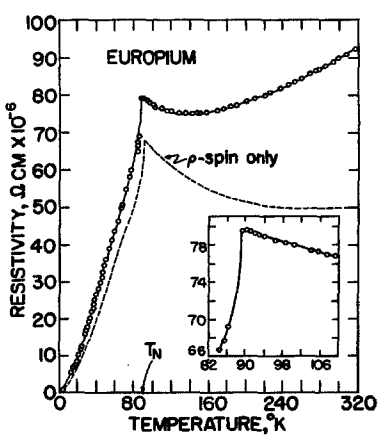

Fig. 21. Electrical resistivity of Eu as reported by Curry et al. (1960). The dashed curve is the spin only resistivity.

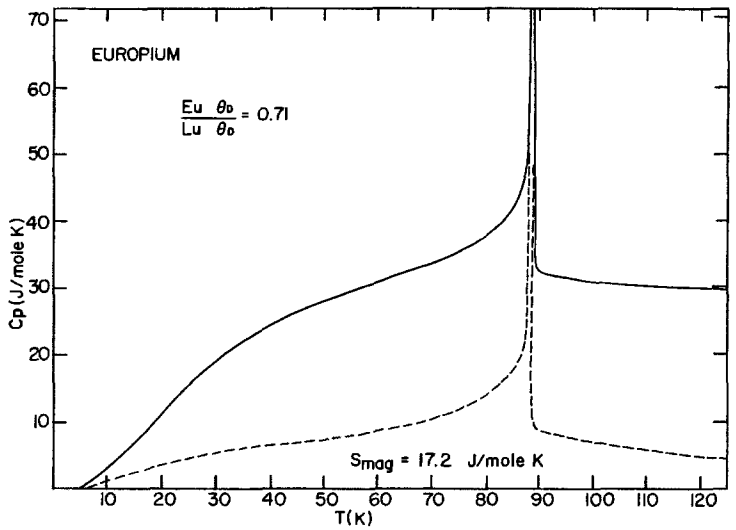

Fig. 22. The specific heat of Eu as determined by Gerstein et al. (1967). The dashed curve gives the spin only contribution.

using the ratio of 0.7 for the Debye temperature of Eu to that of Lu we get the magnetic heat capacity shown by the dashed curve. This choice of Debye temperature (116 K) was made so as to obtain a magnetic entropy S_{mag} for the dashed curve equal to the theoretical $S_{mag} = R \ln(2J + 1) = 17.2$ J/mole K. For Eu Rosen (1968) obtained a low temperature $\theta_D(0)$ of 177 K.

2.2. Gadolinium

The element Gd, atomic number 64, has a half filled 4f shell containing seven electrons and so has the spectroscopic designation $^8S_{7/2}$. It is the only rare earth which is a simple ferromagnet. It marks the start of the heavy rare earths which have the hcp crystal structure. The Curie temperature is 293.4 K (see table 2) and the direction of easy magnetization just below the Curie point is along the c-axis. Nigh et al. (1963) measured the temperature dependence of the magnetic moment of single crystals at several internal fields and obtained the results shown in fig. 23. As the temperature is lowered in an internal field of 100 Oe the observed magnetic moment rises sharply below the Curie point 293.4 K. Then as the easy direction moves away from the c-axis below 240 K the moment falls off to a minimum at 170 K and then rises at low temperatures. These results are in agreement with neutron diffraction observations made by Will et al. (1964) and by Cable and Wollan (1968) who found that Gd is indeed a simple ferromagnet and that the angle θ_c between the c-axis and the easy direction of magnetization changes with temperature. The data of the latter and the results of torque measurements on single crystals by Corner and Tanner (1976) are shown in the

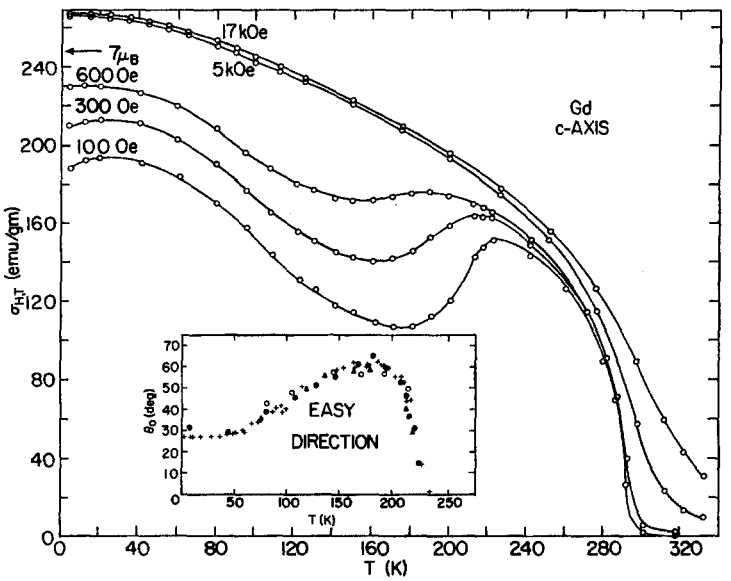

Fig. 23. Isofield magnetization data for Gd in the c-axis direction found by Nigh et al. (1963). The insert shows the temperature dependence of θ_c, the angle between the easy direction of magnetization and the crystal c-axis. The circles are from neutron diffraction measurements of Cable and Wollan (1968). The + and Δ symbols and the figure itself are from the work of Corner and Tanner (1976).

insert of fig. 23. Franse and Mihai (1977) found that the easy direction curve shifted downward when pressure was applied.

Nigh et al. (1963) found that the saturation magnetization followed the Bloch $T^{3/2}$ law from 50 K to 200 K and showed a $T^{2.2}$ fit in the temperature regime below 50 K. At 4.2 K they found a saturation moment of $7.55\mu_B$ which is to be compared with the expected gJ of $7\mu_B$. More recent measurements on electrotransported single crystals with very low oxygen content by Roeland et al. (1975a) and by White et al. (1975) give a saturation value of $7.63\mu_B$. The surplus moment of $0.63\mu_B$ is attributed to polarization of the 5d conduction electron bands. Fermi surface and band calculations by Harmon and Freeman (1974a, b) for ferromagnetic Gd have shown that the observed surplus moment is reasonable and explains the neutron diffraction form factor observations of Moon et al. (1972) on a single crystal of ^{160}Gd. (The separated isotope was used because the slow neutron capture cross section for natural Gd is 46 000 barns.)

De Haas–Van Alphen measurements which explored the Gd Fermi surface extremal orbits have been reported by Schirber et al. (1976, 1977), by Young et al. (1973), and by Mattocks and Young (1977). They were able to identify the orbits by fitting results to conduction electron spin up and spin down Fermi surfaces.

The paramagnetic moment found by Nigh et al. (1963) was $7.98\mu_B$, in close agreement with the $g\sqrt{S(S+1)}$ of $7.94\mu_B$. The paramagnetic Curie temperature

was 317 K for measurements both parallel to c and perpendicular to c, so paramagnetic Gd is isotropic as might be expected for the spherically symmetric 4f shell. The temperature dependence of the electrical resistivity they found is shown in fig. 24. Other measurements extending to 600 K by Maezawa et al. (1977) gave results much like those shown. Also the hump in the c-axis resistivity near T_c has been discussed by Zumsteg et al. (1970) as a lattice parameter effect. The dashed curve is the spin only resistivity obtained by the subtraction procedure described previously. The spin only resistivity in the c direction exhibits short range order fluctuation effects for some one hundred degrees K above the Curie point.

The separated isotope ^{160}Gd made it possible for Koehler et al. (1970) to ferret out the magnon dispersion curves for Gd. Their results at 78 K are shown in fig. 25 for different crystal directions and along the usual lines in the Brillouin zone. The lower curve from Γ to M is the "acoustic" branch and it shows no gap at Γ and is well behaved. The upper curve which has energy 14.6 meV at Γ is the so called optical branch. An ab initio calculation of the APW type has been made along ΓAΓ (c direction) by Lindgård et al. (1975) and their result (scaled to fit at A) is shown as the dashed curve of the figure.

There is a good correlation of the resistivity behavior of Gd with that of the specific heat as reported by Griffel et al. (1954) by Voronel et al. (1966) by Lewis (1970), by Simons and Salamon (1974) and by Wells et al. (1975). The Griffel et al. results are shown in fig. 26 where we display both the specific heat of Gd and the specific heat of Lu. The latter is from the work of Jennings et al. (1960) and is shown here so that the phonon plus conduction electron part only for Gd may

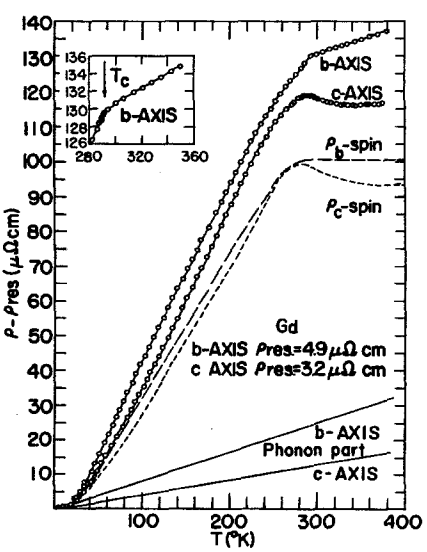

Fig. 24. Electrical resistivity of Gd single crystals as reported by Nigh et al. (1963). The dashed curves are the spin only resistivities.

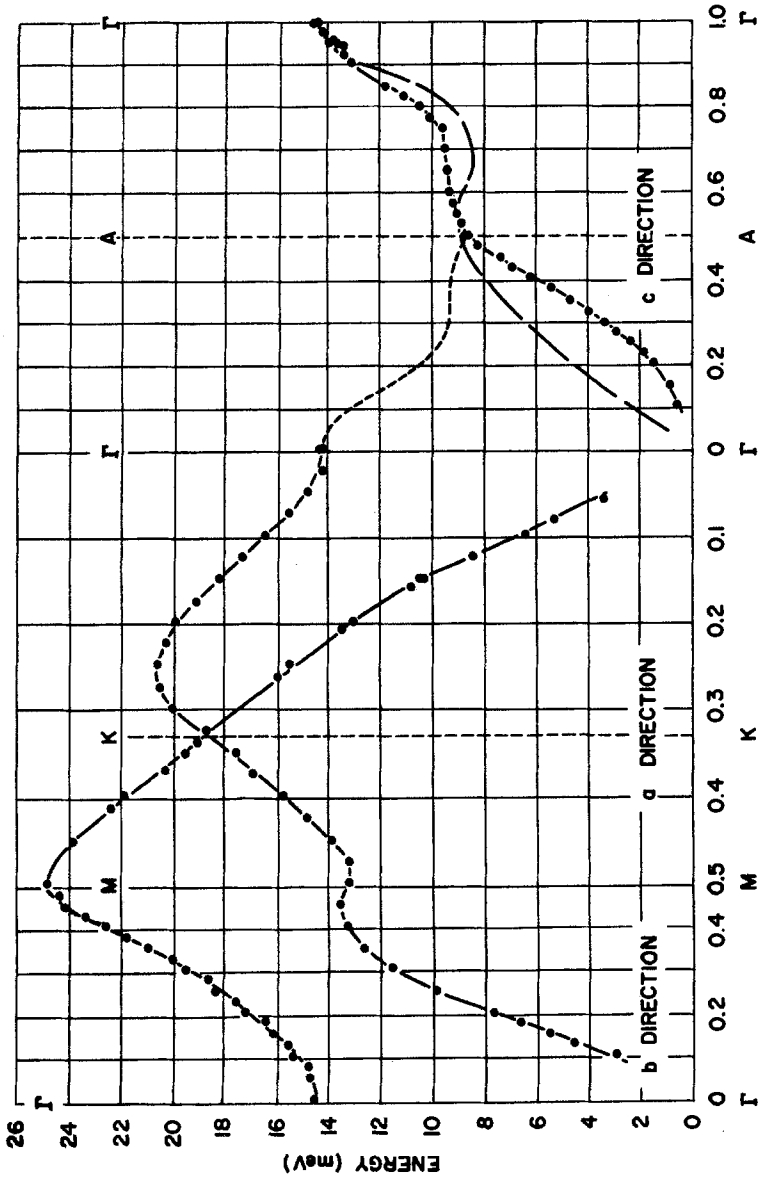

Fig. 25. The magnon dispersion curves for ^{160}Gd single crystals at 78 K as reported by Koehler et al. (1970).

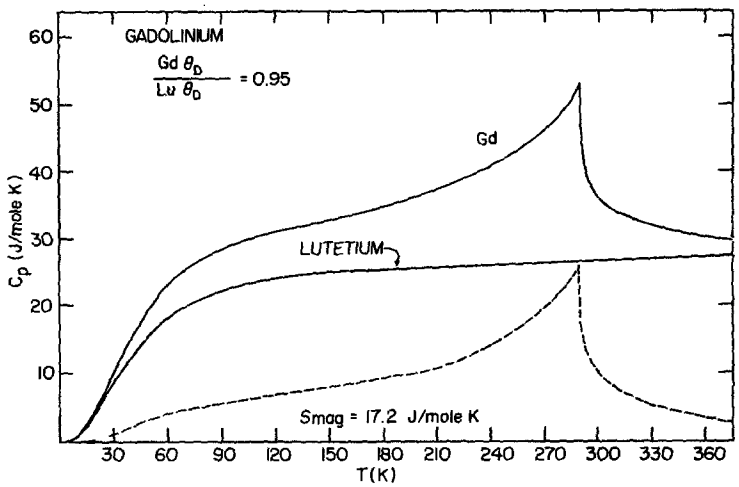

Fig. 26. Specific heat of Gd as reported by Griffel et al. (1954) and the specific heat of Lu for comparison. The latter is from the work of Jennings et al. (1960). The dashed curve is the magnetic contribution to the specific heat of Gd.

be subtracted out to give an estimate of the magnetic specific heat for Gd which is the dashed curve of the figure. The magnetic entropy computed from this curve turns out to be $S_{mag} = 17.2$ J/mole K which we obtained by using a ratio of Debye temperature of Gd to that for Lu of 0.95. The theoretical value $S_{mag} = R \ln(2S+1) = 17.3$ J/mole K for Gd. Debye temperatures for Lu have been reported by Lounasma (1964), and by Wells et al. (1976). It appears that at intermediate temperatures a Debye value of 166 K for Lu is appropriate.

2.3. Terbium

The element Tb has atomic number 65, crystallizes in the hcp structure and has eight electrons in the 4f shell, one beyond the half filled shell of Gd. The total orbital moment is therefore $L = 3$, the spin $S = 3$ and $J = L + S = 6$ making the spectroscopic designation $^7F_6$. Neutron diffraction measurements on Tb single crystals made by Koehler et al. (1963) showed that the magnetic moments formed a helical structure in the temperature interval from 219.5 K to 230 K, the Néel point. Below 219.5 K Tb is ferromagnetic with the moments in the basal plane. They found that the inter-layer turn angle in the helical phase is about 20° just below the Néel point and then decreases slightly with temperature to about 18° before rising again near the ferromagnetic transition at 219.5 K. This means that a q vector wave spans between 9 and 10 c-axis lattice parameters or about 20 layers. This orientation of the moments in Tb is not surprising in view of Coulomb repulsion associated with the toroid like charge distribution for the 4f electron of angular momentum $L = 3$. This single ion interaction leads to phenomenally high magnetic anisotropy and giant magnetostriction. The external

field required to magnetize Tb in the c direction is of the order of a million to ten million oersteds and one must not be surprised if single crystal samples leave their moorings or suddenly suffer recrystallization in the presence of strong fields along the c direction. This is also true for other heavy rare earth single crystals.

Isofield magnetization data obtained by Hegland et al. (1963) in the easy b-axis direction are shown in fig. 27. In an applied field of 50 Oe the magnetic moment versus temperature shows a sharp peak in the vicinity of 230 K which is typical of a Néel point marking the change from paramagnetism to antiferromagnetism. In this case it marks the onset of the helical magnetic structure as the temperature is lowered.

The critical external field required to suppress the helical phase in Tb is about 800 Oe. The isofield data at this field is shown in the insert of fig. 27 and is smooth while the one at 500 Oe shows a slight kink around the Néel point. The stability of the helical structure is tenuous on the basis of these and other observations including the very narrow temperature range over which the phase exists.

Below 219.5 K the isofield data show ferromagnetic behavior with the moment rising at low temperatures. The saturation magnetic moment found by the usual high field–low temperature extrapolation method $\sigma(H, T)$ versus $1/H$ with $1/H \to 0$ for several isotherms followed by $\sigma(\infty, T)$ versus T with $T \to 0$) comes out to be $9.34\mu_B$ compared with the expected gJ of $9.0\mu_B$ shown in table 2. The same surplus moment of $0.34\mu_B$, was found by Roeland et al. (1975a). The surplus is attributed to conduction band polarization and is down considerably from the $0.63\mu_B$ for Gd. One might expect at least $0.42\mu_B$ if the moment scaled according to the de Gennes factor or $0.48\mu_B$ if it followed the $S(S+1)$ factor. Since neither one seems to fit it must be assumed that the higher atomic number or the addition of 4f orbital moment causes a decrease in the local 5d conduction

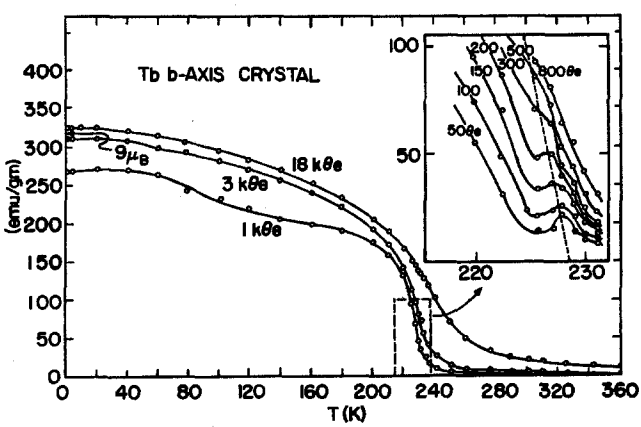

Fig. 27. Isofield magnetization data for the b-axis crystal of Tb as found by Hegland et al. (1963).

electron wave function overlap with the 4f wave functions. The importance of this overlap was seen in the suppression of superconductivity of La by Legvold et al. (1977b). The general decrease of the 5d band electron population across the rare earths has been described by Duthie and Pettifor (1977) and also by Lindgård (1977) who has pursued the theory of rare earth alloys. There is also the possibility that 4f orbital moment in Tb brings about a decrease in the 4f–5d interaction when compared with the spin only 4f band of Gd.

One of the outstanding differences between Tb and Gd is found in the anisotropy of the paramagnetic susceptibility. In the case of Tb the susceptibility in the basal plane is higher than that along the c-axis as can be seen in fig. 28 which shows the $1/\chi$ vs. T data of Hegland et al. (1963). This is contrasted with the isotropic character of the susceptibility of Gd single crystals above the Curie point. There are thus two paramagnetic Curie temperatures for Tb. Along the c-axis $\theta_p = 195$ K and in the basal plane the susceptibility is the same along the b-axis as along the a-axis and $\theta_p = 239$ K. The high temperature ($1/\chi$ vs. T) lines are parallel and the paramagnetic moment found is $9.77\mu_B$ which is slightly higher than the theoretical $9.70\mu_B$. The physical basis for two ordering temperatures has been discussed by Kasuya (1966) who proposed the crystal fields are responsible. Single ion anisotropy has been discussed by Rhyne (1972).

The electrical resistivities of single crystals of Tb have been reported by Hegland et al. (1963). Their results are shown in fig. 29. We have subtracted the phonon part to obtain the spin disorder resistivities which are shown as the dashed curves. In the insert the c-axis data near the Néel point are shown on an enlarged scale. The dramatic effect of an external magnetic field in the easy b-axis direction on the electrical resistivity along the c-axis is shown in the insert. The external field suppresses the helical phase and eliminates the superzone energy gaps near the Néel point. (The much higher field needed here to suppress the helical structure as compared to the 800 Oe field mentioned

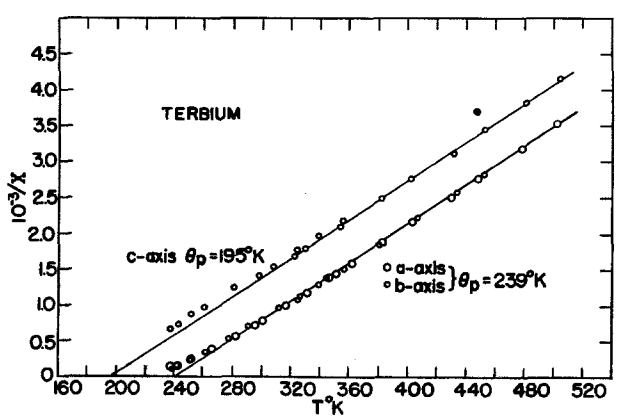

Fig. 28. The reciprocal of the paramagnetic susceptibility of a-, b-, and c-axis samples of Tb versus temperature as published by Hegland et al. (1963).

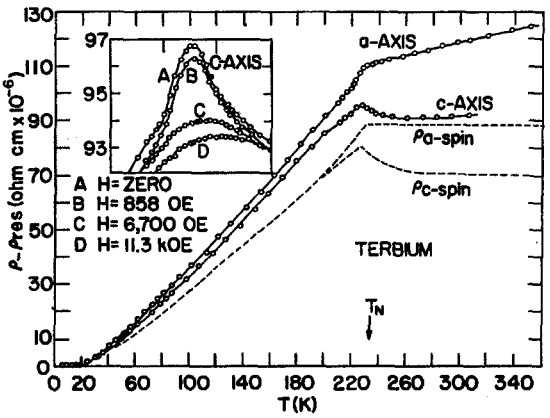

Fig. 29. The electrical resistivity of a- and c-axis crystals of Tb versus temperature as reported by Hegland et al. (1963). The dashed curves are the spin only resistivities.

earlier is the result of widely differing demagnetizing fields related to the different sample geometries.) The peak in the c-axis resistivity associated with the onset of magnetically induced energy gaps is very much like that in Eu near its Néel point. (The broad c-axis peak near T_c in Gd is generally attributed to short range order–disorder fluctuations; some of this is surely present above the Néel point in Tb also.)

The resistivity below 40 K displays some anomalies which have been discussed by Mackintosh (1963) who related this behavior to a spin wave energy gap in Tb. Magnetization calculations for Dy by Niira (1960) involved such an energy gap. More recent resistivity measurements on higher purity single crystals by Sze et al. (1969) and by Nellis and Legvold (1969) confirm the $q = 0$ spin wave energy gap and give a gap width of 1.9 meV. Inelastic neutron scattering data have been reviewed by Mackintosh and Møller (1972) and they show the magnon dispersion curves of fig. 30 for Tb. The energy gap of 2 meV is seen at 4.2 K in the lower branch for $q = 0$ at Γ, the center of the Brillouin zone.

The specific heat of Tb from 1.5 to 16 K has been reported by Wells et al. (1976). Jennings et al. (1957) made measurements over a wide temperature range and their data are shown in fig. 31. There appears to be a shoulder on the curve just above 219.5 K corresponding to θ_c and a characteristic sharp peak at 228 K corresponding to the Néel temperature. We have subtracted off the phonon and electron parts and show the magnetic part of the heat capacity as the dashed curve of the figure. The entropy computed from the dashed curve comes out to be 21.0 J/mole K; the theoretical $S = R \ln(2J + 1)$ is 21.3 J/mole K which does not include an allowance for conduction electron polarization. As shown in the figure the ratio of the Debye temperature for Tb to that of Lu used to obtain the good fit to theory was 0.93.

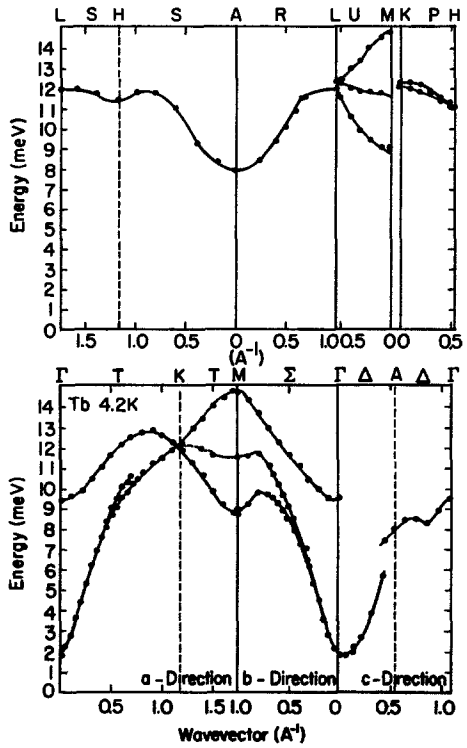

Fig. 30. Magnon dispersion curves for Tb along symmetry lines in the zone at 4.2 K (ferromagnetic phase). After Mackintosh and Møller (1972).

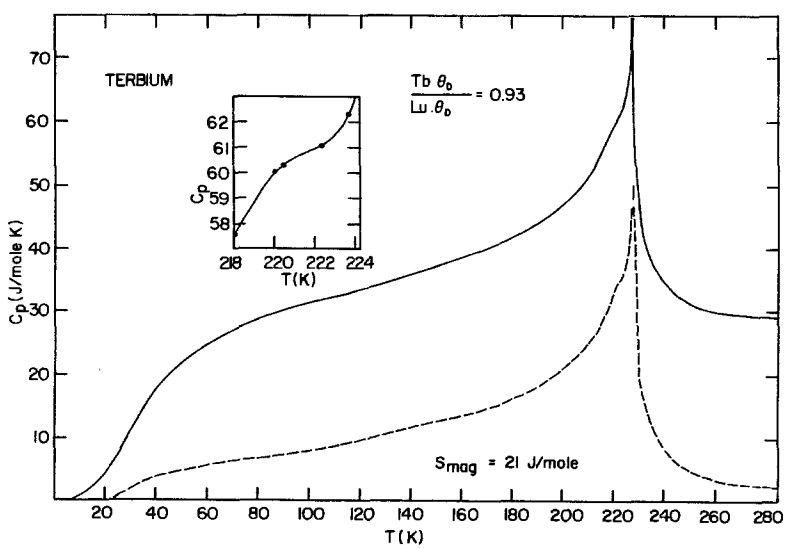

Fig. 30. Magnon dispersion curves for Rb along symmetry lines in the zone at 4.2 K (ferromagnetic curve gives the magnetic contribution.

2.4. *Dysprosium*

The 4f shell of the element Dy, atomic number 66, contains 9 electrons; there are 5 electrons with unpaired spins so $S = \frac{5}{2}$ and 2 electrons with z projection orbital angular momentum quantum numbers $m_l = 3$ and 2, respectively, making $L = 5$. This makes $J = L + S = \frac{15}{2}$ and the spectroscopic designation is $^6H_{15/2}$. The room temperature crystal structure is hcp, and at low temperatures in the ferromagnetic state there is a small departure from this to orthorhombic, as reported by Darnell (1963a, b).

Neutron diffraction results of Wilkinson et al. (1961) showed that the magnetic moments of Dy take on the helical structure below the 179 K Néel point as described previously in fig. 20. The helix axis is along c with the moments in the basal plane, and the interlayer turn angle just below the ordering temperature is 43.2°. The angle decreases with decreasing temperature down to 89 K at which it reaches 26.5°. Below 89 K Dy is ferromagnetic and the easy axis of magnetization is along an a-axis or $\langle 11\bar{2}0 \rangle$.

Magnetic measurements on single crystals of Dy have been made by Jew (1963). His a-axis isothermal magnetization data, taken in the temperature range where the helical structure is found, are displayed in fig. 32. As the applied field increases the moment rises linearly until a critical field for that temperature is reached, and then the moment rises sharply and ferromagnetic alignment is accomplished. Isofield data for the a-axis crystal from 90 K to 290 K are shown in fig. 33. In applied magnetic fields below 10 kOe the sharp peaks in the magnetic moment versus temperature curves shown in the insert of the figure fix the Néel point at 179 K. The rapid rise of the moment below 100 K in the 2 kOe field marks the transition from the helical phase to the ferromagnetic phase. An applied field greater than 12 kOe clearly suppresses the helical structure. We note the field required for this is considerably higher for Dy than for Tb where

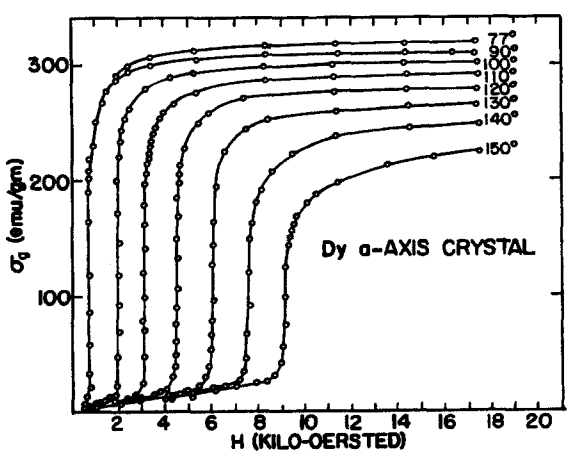

Fig. 32. Magnetization isotherms for the a-axis of Dy. After Jew (1963).

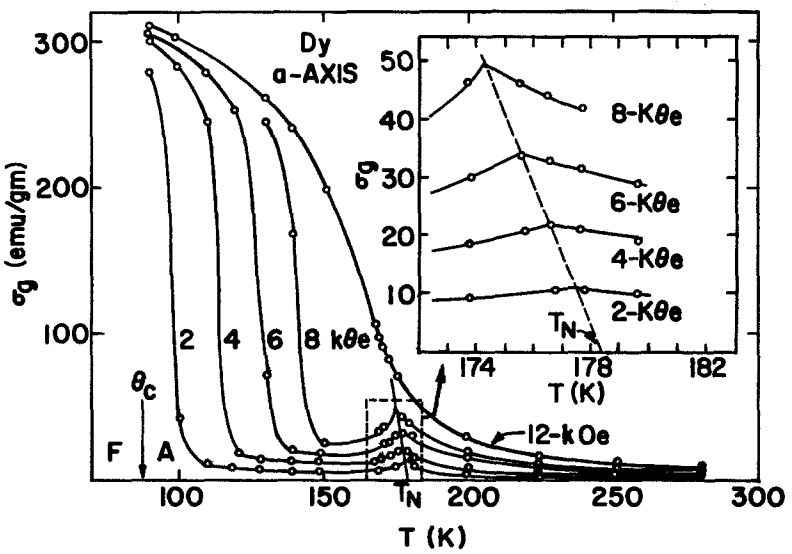

Fig. 33. Isofield magnetization data for the easy a-axis of Dy as reported by Jew (1963).

the critical field was less than 1 kOe; this result correlates well with the wider temperature span over which Dy has the helical structure as compared to the ten degree interval for Tb. In the insert of the figure the data near the Néel point are shown and the manner in which the cusp for different fields may be extrapolated to zero field to get the Néel point. Queen (1979) has used Dy of $R_{300}/R_{4.2}$ equal 80 to get the saturation magnetic moment of 358 emu per gram, the highest for any element and almost 1.6 times that for iron (which has about the same density); this moment corresponds to $10.4\mu_B$/atom which is $0.4\mu_B$/atom higher than the gJ value of $10\mu_B$. Again the $0.4\mu_B$ comes from 5d band polarization.

As in the case of Tb the susceptibility in the paramagnetic range along the b-axis was the same as that along the a-axis and the paramagnetic Curie temperature for both was 169 K. Along the c-axis the data gave a paramagnetic Curie temperature of 121 K thus demonstrating large anisotropy. The slopes of the Curie–Weiss lines gave a paramagnetic moment of $10.83\mu_B$ compared with the theoretical $10.64\mu_B$.

The electrical resistivity of Dy as determined by Boys and Legvold (1968) on single crystals with resistivity ratios 24 along the a-axis and 13 along the c-axis is shown in fig. 34. The data for the a-axis crystal are rather prosaic when compared with the c-axis data which demonstrate the dramatic superzone effects at the ferro to helical transition at 89 K as well as in the vicinity of the Néel point. The c-axis resistivity calculated by Elliott and Wedgwood (1963) in the manner described earlier is shown as the dot–dash curve; the general features are present but exaggerated in the theory. The spin disorder resistivity as found by subtracting the phonon resistivities appears in the figure as the

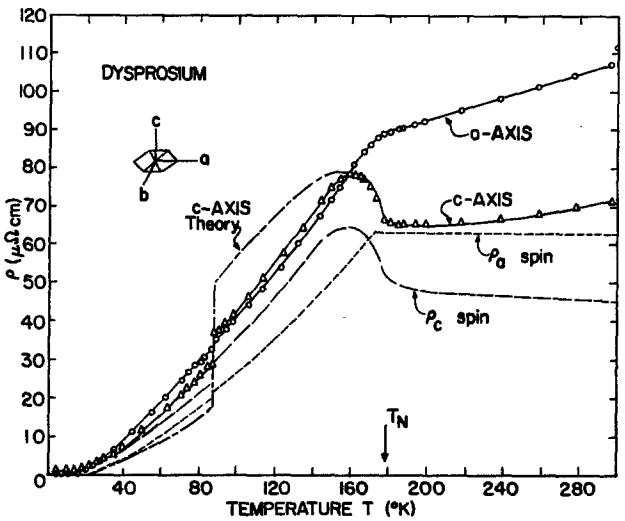

Fig. 34. Electrical resistivity versus temperature for single crystals of Dy as reported by Boys and Legvold (1968). The dashed curves are the spin only resistivity and the dot–dash curve is the Elliott and Wedgewood (1963) theoretical curve.

dashed curves. The sharp bend or knee in the *a*-axis resistivity marks the 179 K Néel point whereas there is only a barely detectable shift of the points at the 89 K ferromagnetic to antiferromagnetic transition. Hence, the Fermi surface area projections in the basal plane (*a* or *b*) directions are nearly unaffected by the onset of the superzones. Quite the opposite is apparent in the *c*-axis direction. By comparing the resistivity jump at 89 K to the total magnetic resistivity we estimate that nearly 30% of the Fermi surface projected in the *c* direction is wiped out by the helical structure, a remarkable effect.

Spin wave dispersion in Dy has been investigated by inelastic neutron diffraction by Nicklow et al. (1971a, b) and their results are shown in fig. 35. The data at 78 K in part (a) of the figure show an energy gap at $q = 0$ of 1.3 meV. The effect of this gap shows up in the electrical resistivity at low temperatures as in the case of Tb. In fig. 35b the Fourier transform of the exchange they obtained is shown; the curve at 98 K has a maximum at Q/q_{max} (see arrow) equal to about 0.17, which corresponds to a turn angle per layer in reasonably good agreement with the experimental finding. This demonstrates the significance of the generalized susceptibility $\chi(q)$ and its relationship to the magnetic structure as discussed in the theory section.

The specific heat of Dy was measured by Griffel et al. (1956) with results as shown in fig. 36. The spin only part in this case was obtained by assuming that Dy has the same Debye temperature as Lu; it is shown as the dashed curve. The large peak occurs at the 179 K Néel point with a smaller hump in evidence at the ferro-order to antiferro-order transition near 89 K. There is again a tail in the magnetic specific heat which extends above 179 K corresponding to short range ordering effects. The dashed curve yields a magnetic entropy of 22.6 J/mole K

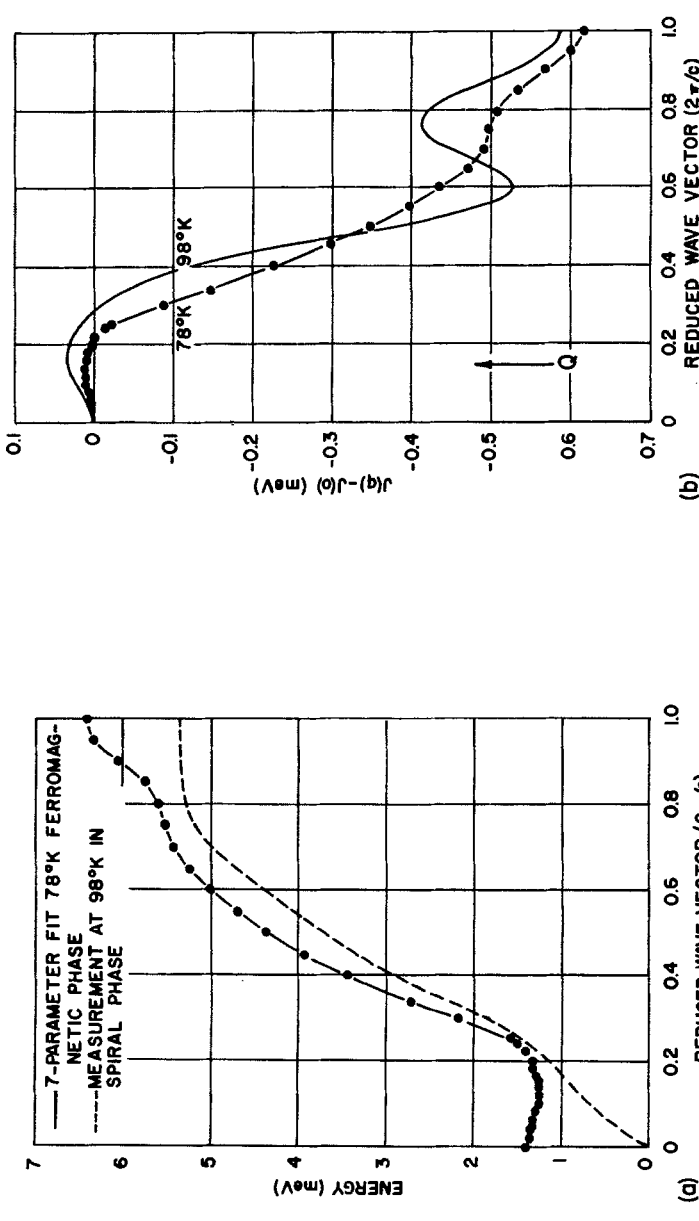

Fig. 35. Magnon curves in the *c* direction for ferromagnetic ^{163}Dy at 78 K and for helical ^{163}Dy at 98 K. The arrow denotes the helical wave vector *Q*. After Nicklow et al.

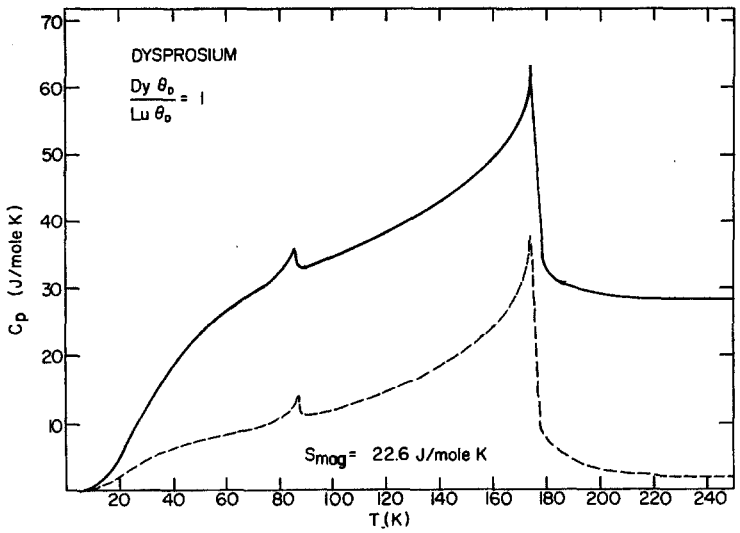

Fig. 36. Specific heat of Dy as published by Griffel et al. (1956). The dashed curve is the magnetic contribution.

which should be compared with the expected $S = R \ln(2J+1) = R \ln 16 = 23.0$ J/mole K.

2.5. Holmium

The element Ho has atomic number 67 and has 10 electrons in the 4f shell leading to $L = \Sigma m_l = 3+2+1 = 6$, $S = \frac{7}{2} - \frac{3}{2} = 2$, $J = L + S = 8$ and to the spectroscopic state $^5I_8$. The angular dependence of the 4f wave function of fig. 7 suggests that the three electrons beyond the half filled shell will begin to approach spherical symmetry and should show magnetic properties at least somewhat different from those of Dy and Tb. This turns out to be the case.

Neutron diffraction work by Koehler et al. (1966, 1967) showed that below the 132 K Néel point the magnetic moments lay in the basal plane and formed a spiral structure. Just below the Néel point the interlayer turn angle was 50°. As the temperature was lowered the turn angle decreased and at 20 K hit a low of 30°. Below 20 K the moments tilted out of the basal plane and formed a conical structure with a $1.7\mu_B$ ferromagnetic component along the c-axis and with a basal plane component of $9.5\mu_B$ in a distorted spiral so the half-cone angle was about 80°. The easy direction for Ho is along the b-axis and at 4.2 K an external field will induce the full expected $10\mu_B$ in this direction. In the presence of an external field the magnetic phase diagram of Ho is extremely complex, according to Koehler et al. (1967).

Results of isothermal magnetization measurements on a b-axis single crystal of Ho by Strandburg et al. (1962) are shown in fig. 37. Particularly interesting are the three bends or knees seen in the curves at 49.6 K and at 54.8 K. These come

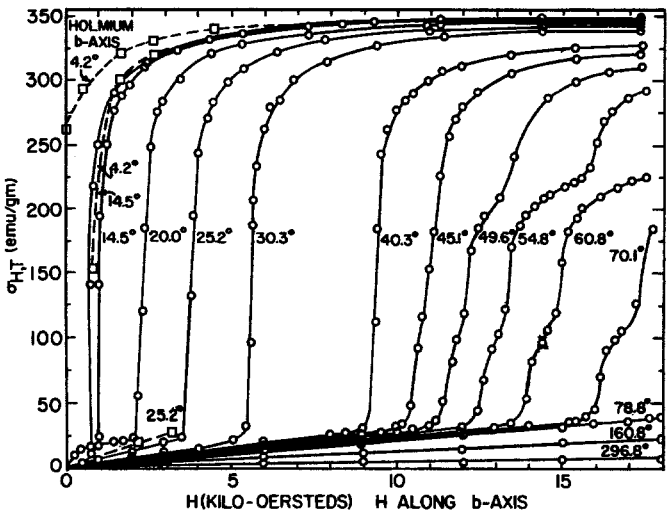

Fig. 37. Magnetization isotherms for single crystal Ho along the *b*-axis as published by Strandburg et al. (1962).

about because the magnetic moments jump from one set of easy *b*-axis directions or fan structure in the presence of the field to the next set of easy directions or fan structure closer to the field direction. (The fan structures involved are like those shown in fig. 6.) The dashed curve of fig. 37 at 4.2 K shows hysteresis and remanence when the field is decreased; i.e., the sample remains magnetized in the basal plane. Isofield data for *b*- and *c*-axis crystals are shown in fig. 38. The small cusps in the *b*-axis data near 132 K identify the Néel point. The fan structure effect is observable in this figure also, particularly for the 16 kOe *b*-axis data. The *c*-axis data in the insert show a relatively sharp rise in moment at the onset of the conical ferromagnetic phase which sets in at temperatures higher than 20 K when a field is applied along *c*.

The saturation magnetic moment at 4.2 K along the *a*-axis was $8.95\mu_B$, which is exactly cos 30° times the saturation moment of $10.34\mu_B$ found along the *b*-axis. This means that the moments stay along the *b*-axis even in the presence of a field along the *a*-axis and demonstrates anisotropy in the basal plane. In the case of Ho, then, we have a saturation moment $0.34\mu_B$ larger than the expected *gJ* of $10\mu_B$ and the surplus represents the polarization of the 5d conduction band electrons. For the *c*-axis the initial magnetization below 20 K was about $1.7\mu_B$ which is in good agreement with the neutron diffraction finding. In the paramagnetic range the $1/\chi$ versus T plots showed anisotropy with θ_p equal to 88 K for the *b*- and *a*-axis crystals and with θ_p equal to 73 K for the *c*-axis crystal. The paramagnetic moment was $11.2\mu_B$/atom for all three crystals. This is six percent higher than the theoretical $10.6\mu_B$ expected, indicating that some conduction electron polarization persists into the paramagnetic regime. Magnetic susceptibility measurements on Ho at high temperatures have been reported by St.

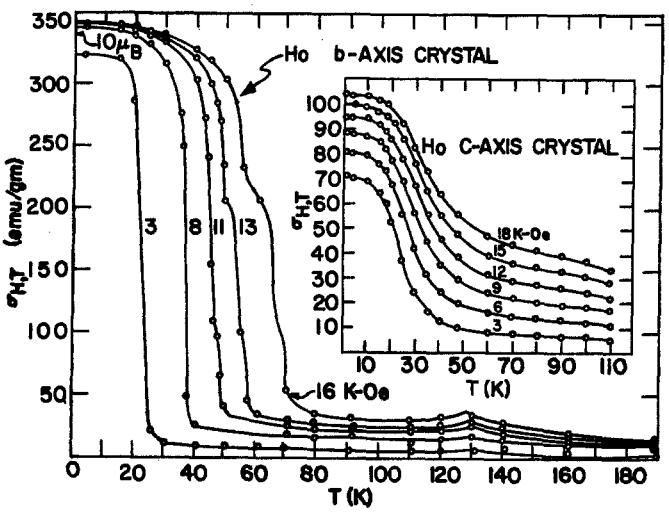

Fig. 38. Isofield data for single crystal Ho along *b*- and *c*-axis as reported by Strandburg et al. (1962).

Quinton (1973), by Kirchmayer and Schindl (1966), by Chechernikov (1962), and by Arajs and Miller (1960).

The electrical resistivity of Ho single crystals has been reported by Strandberg et al. (1962) and by Nellis and Legvold (1969). The results of the two sets of measurements are in substantial agreement. We show the results of the former in fig. 39; only a small disturbance was noticeable along the *c*-axis at 20 K where the conical phase forms. The *a*-axis resistivity typically changes slope at the Néel point and the *c*-axis resistivity has a broad hump below the Néel point, so the behavior is much like that for Dy. The dashed curves are the spin wave only resistivity curves and the dot–dash curve is the result of the Elliott and Wedgewood (1963) theory for the *c*-axis resistivity; in this case the fit is rather good. Of particular interest here is the substantial difference between the *a*-axis and *c*-axis spin wave only resistivity above 132 K. It is a manifestation of a sizeable change from Tb and Dy in the Fermi surface geometry; the trunk part, which gives the projection along an *a*-axis, has diminished in size and this decrease continues to be the case across the rest of the heavy rare earths.

Spin wave dispersion at 4.2 K for Ho with 10% Tb added to preserve the planar ferromagnetic structure has been reported by Mackintosh and Møller (1972), and their findings are shown in fig. 40. It is seen that at $q = 0$ there is a spin wave energy gap of the type found in Tb and Dy. Dispersion and $\mathcal{J}(q) - \mathcal{J}(0)$ curves for Ho in the helical phase are shown in fig. 41. We note there is no energy gap at $q = 0$ for the helical phase and there is a maximum in $\mathcal{J}(q) - \mathcal{J}(0)$ at q/q_{max} of about 0.22, confirming the helical ordering. Coupling of spin waves to giga-Hertz radiation has been studied by Akhavan and Blackstead (1976).

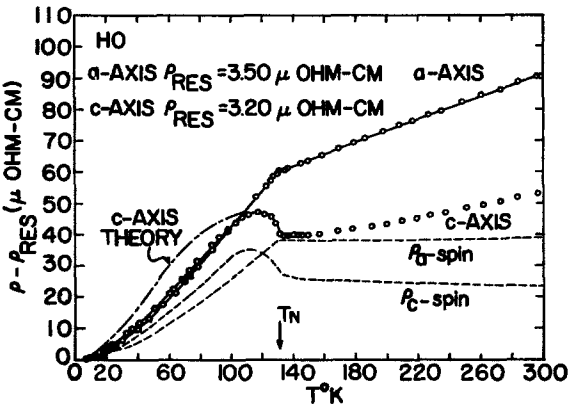

Fig. 39. Electrical resistivity, residual subtracted, versus temperature for Ho single crystals as measured by Strandburg et al. (1962). The dashed curves are the spin only contribution to the resistivity. The dot–dash curve is the resistivity calculated for the *c*-axis by Elliott and Wedgewood (1963).

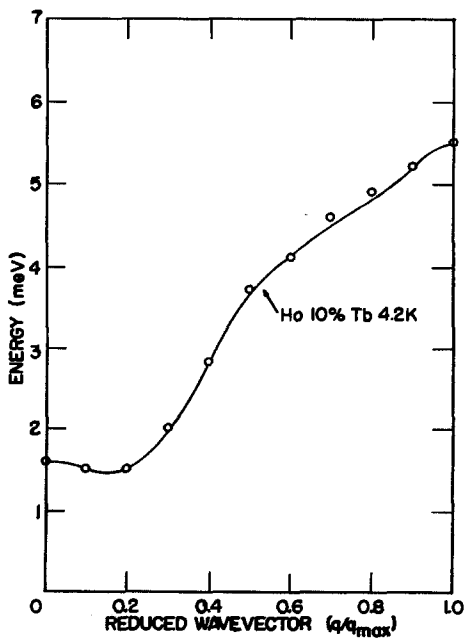

Fig. 40. Magnon dispersion curve at 4.2 K for Ho–10% Tb as reported by Mackintosh and Møller (1972).

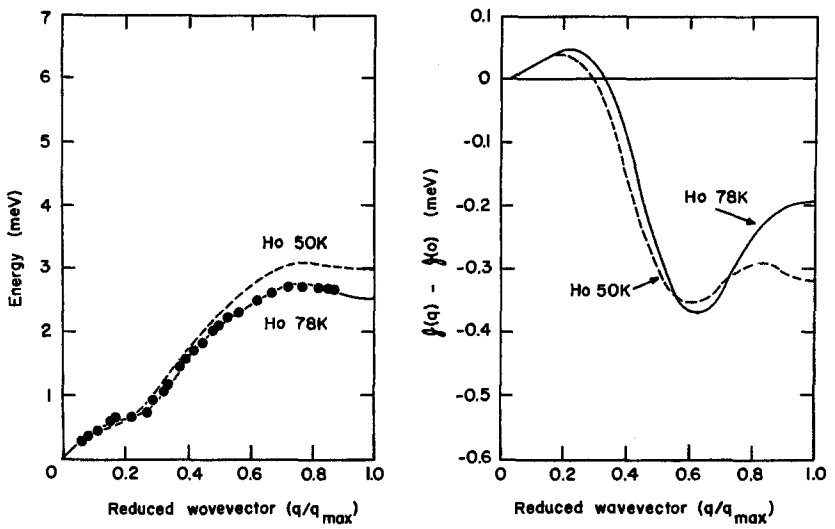

Fig. 41. Magnon dispersion curves and $\mathcal{J}(q) - \mathcal{J}(0)$ in the c direction for the helical phases of Ho as reported by Nicklow (1971) and by Nicklow et al. (1971a).

Gerstein et al. (1957) measured the heat capacity of Ho, with results as shown in fig. 42. The spin wave part is shown as the dashed curve of the figure. There is a very small peak at the 20 K conical ferro to helical transformation temperature and a very large peak at 130 K which is close to the Néel point. The entropy computed from the dashed curve gives a spin wave component of 23.8 J/mole K, and was obtained by use of a Debye temperature for Ho of 0.99 times that for Lu. The theoretical value of Ho is R ln 17 equal to 23.6 J/mole K.

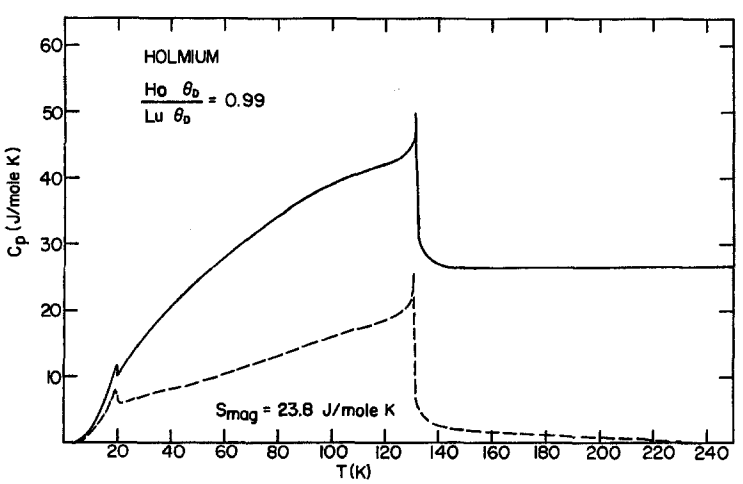

Fig. 42. Specific heat of Ho as measured by Gerstein et al. (1957). The dashed curve is the magnetic contribution to the specific heat.

2.6. Erbium

The spectroscopic designation for Er, atomic number 68, is $^4I_{15/2}$ since it has four 4f electrons beyond the half full shell of Gd. The quantum numbers are then $L = 6$, $S = \frac{3}{2}$ and $J = L + S = \frac{15}{2}$. The crystal structure is hcp. From neutron diffraction studies by Cable et al. (1965), by Habenschuss et al. (1974), and by Atoji (1974) it has been established that the magnetic structure of Er is quite complex. As the temperature of Er is lowered the component of the magnetic moment along the c-axis becomes ordered at 85 K in a sinusoidal manner with the q vector along the c-axis; this is called the c-axis modulated (CAM) structure. It is also found that the basal plane component remains random. At 53 K a squaring off of the c-axis component wave modulation takes place and the basal plane component is found to order helically as shown in fig. 20. This may be described as a quasi anti-phase domain structure. It is a peculiar structure for which several atomic layers having c components up (cones open upward) are followed by an equal number of atomic layers having c-axis components down (cones open downward). This structure changes from an incommensurate to commensurate form at 35 K and then transforms to conical ferromagnetism below 20 K. The c-axis component at 4.2 K is $7.6\mu_B$ and the basal plane component is $4.3\mu_B$, making the half cone angle about 30° and giving a total of $9.0\mu_B$, which is the expected full gJ value for Er.

Magnetic measurements on a c-axis single crystal of Er by Green et al. (1961) yielded isofield data as shown in fig. 43. The onset of antiferromagnetism is characterized by the usual cusp which is seen at 85 K in the low field curve. There is the usual shift of T_N to lower temperatures at the higher fields as well as a shift of the ferromagnetic state to higher temperatures in the applied field; an applied field favors the ferromagnetic state. A plot of the critical field required to

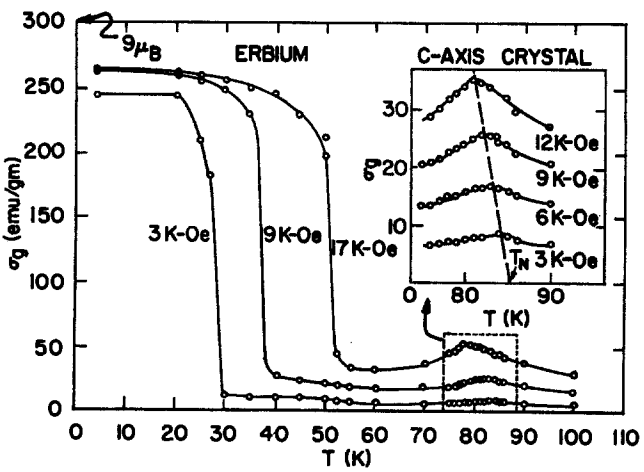

Fig. 43. Isofield magnetization data for a c-axis crystal of Er as reported by Green et al. (1961).

bring about ferromagnetic ordering at different temperatures is extrapolated to zero field to get about 19 K for the spontaneous ferromagnetic ordering temperature. In general there is some thermal hysteresis in this order–order transition so it is difficult to pinpoint the transition temperature. The magnetic moment of Er single crystals was measured by Rhyne et al. (1968) at 4.2 K in a field ranging up to 150 kOe. Their results showed that in the easy c-axis direction there was an initial sharp rise at low applied field up to $8\mu_B$ followed by a very gradual rise to almost $9\mu_B$ at an applied field of 130 kOe. In the hard basal plane direction there was one jump to a fan structure at about 17 kOe followed by a less rapid change in moment with field until about 120 kOe was reached when another relatively sharp rise took place but the applied field was not high enough for saturation to occur. These data demonstrate the strong anisotropy of Er which has foiled attempts to obtain the saturation moment. However, if the c-axis data of Rhyne et al. (1968) are extrapolated to $H = \infty$ $(1/H = 0)$ a saturation moment of $9.1\mu_B$ is found, and this is reasonable. The high temperature measurements of Green et al. (1961) also demonstrated anisotropy in the $1/\chi$ versus T plots which gave θ_p of 32.5 K along the a-axis and 61.7 K along the c-axis while the paramagnetic moment was the same for both crystals at $9.9\mu_B$, which is a little higher than the theoretical $9.6\mu_B$ for Er. It may be concluded that some conduction electron polarization is indeed manifested in Er just as in the other heavy rare earth metals. Jensen (1976) has made a five parameter molecular field calculation for Er to explain its magnetic behavior. Other such calculations have been made by Southern and Sherrington (1974).

Electrical resistivity results on single crystal Er by Boys and Legvold (1968) are shown in fig. 44. The c-axis data reflect the magnetic ordering phenomena beautifully. The onset of the modulated c-axis moment causes a sharp break in the curve at 85 K. Then as the temperature decreases a rapid rise in the resistivity continues down to 35 K, which marks the onset of the squared-up

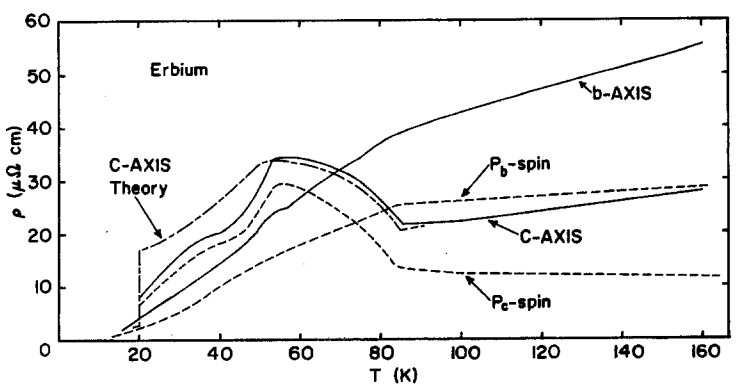

Fig. 44. Electrical resistivity of single crystal Er versus temperature as determined by Boys and Legvold (1968). The dashed curves are the spin only resistivity and the dot–dash curve is the c-axis resistivity calculated by Elliott and Wedgewood (1963).

c-axis magnetic moment modulation and the helical basal plane structure. The rapid drop in resistivity at 20 K marks the onset of ferromagnetism and the disappearance of superzone effects on the Fermi surface. The fit of Elliott and Wedgewood (1963) calculation for the c-axis is shown by the dot–dash curve; it again exaggerates the effect of the magnetic moment structure change at 20 K on the resistivity.

Spin wave dispersion in the c-axis direction for Er has been reported by Nicklow et al. (1971b). Their results for the conical phase are shown in fig. 45. There is no spin wave energy gap at $q = 0$ and there are two branches, one for $+q$ and one for $-q$. The data for the latter show a maximum in energy at a reduced wave vector q/q_{max} of 0.75.

The specific heat of Er according to work of Skochdopole et al. (1955) is found in fig. 46. There is a small peak at the 20 K order–order transition, a second small peak at 35 K where the moment squares up, another small peak at the 52 K helical ordering temperature and a large peak at the 86 K Néel point. The magnon specific heat is shown as the dashed curve and the entropy computed from the curve yields a magnetic portion of 22 J/mole K, which is smaller than the $R \ln(2J + 1)$ of 23.1 J/mole K, even though a Debye temperature for Er which

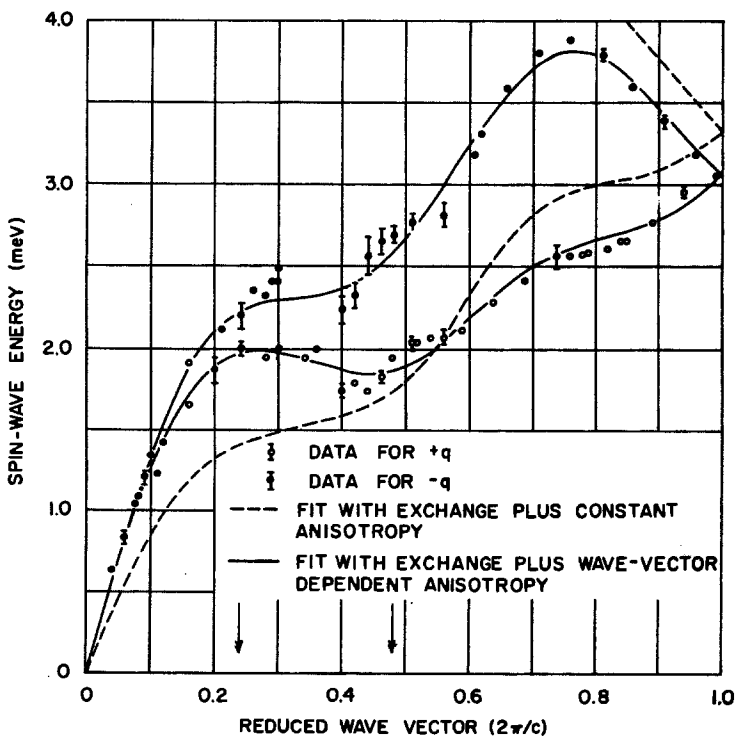

Fig. 45. Magnon dispersion curves in the c direction of the cone magnetic phase of Er reported by Nicklow et al. (1971b).

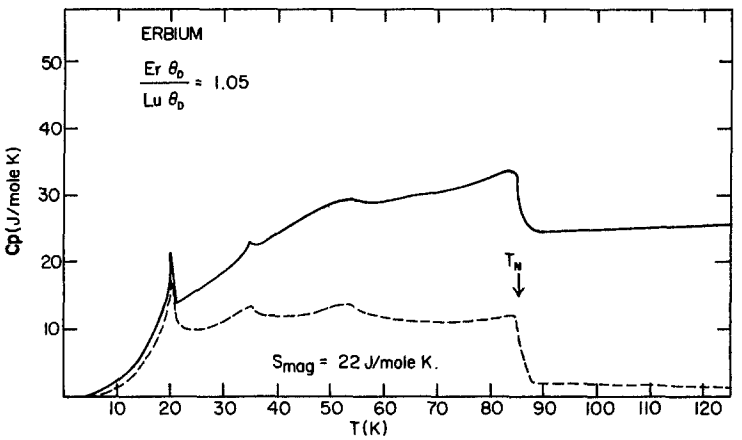

Fig. 46. Specific heat of Er as measured by Skochdopole et al. (1955). The dashed curve is the magnetic portion.

was 5 percent higher than that for Lu was used. It did not seem realistic to go to a higher Debye temperature to get a better fit.

2.7. Thulium

There are 12 electrons (two holes) in the 4f shell of Tm so there are two electrons with unpaired spin. The spectroscopic designation for the ion is $^3H_6$ since $L = 5$, $S = 1$ and $J = L + S = 6$.

Several neutron diffraction studies have been made on single crystals of Tm. Early work by Koehler et al. (1962) was followed by investigations on more pure samples by Brun and Lander (1969) and by Brun et al. (1970). The c-axis component of the magnetic moment becomes ordered below 58 K, the Néel point, with a sinusoidal variation of the magnitude just as in Er. The pattern is shown in fig. 20. The q vector just below 58 K is incommensurate with the ionic lattice but becomes commensurate with a seven layer-period below 32 K. There is also a squaring up of the sinusoidal structure between 40 K and 32 K before the seven layer pattern sets in. The odd feature for Tm is its combined antiphase domain-ferrimagnetic structure below 32 K which consists of four moments pointing up along c followed by three moments pointing down. Since the ionic moment is $7\mu_B$ this leaves a net of $1\mu_B$ in the c-axis direction for each seven layer period.

Magnetic moment measurements in fields up to 95 kOe on Tm single crystals have been reported by Richards and Legvold (1969). Their isofield data appear in fig. 47. The characteristic cusps in the low field data mark the Néel point at 58 K. In fields above 30 kOe the sinusoidal modulation of the moments disappears and a ferromagnetic ordering only takes place. In low applied fields along the easy c-axis direction there is a rise in the magnetic moment for T below 32 K marking the onset of the ferrimagnetic phase, and the magnetic moment at 4.2 K turns out

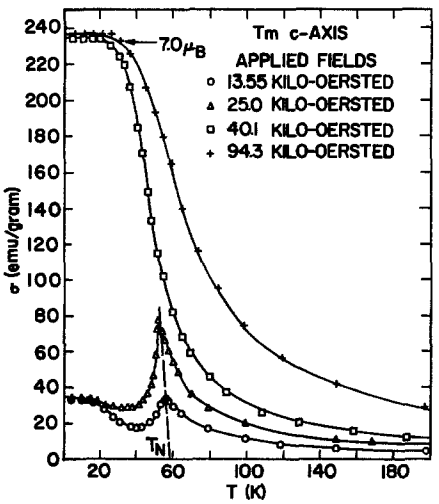

Fig. 47. Isofield magnetization data for a c-axis crystal of Tm as reported by Richards and Legvold (1969).

to be $1\mu_B$, in excellent agreement with the neutron diffraction result. In high fields at 4.2 K the saturation moment is $7.14\mu_B$, which is higher than the gJ value of $7\mu_B$ for Tm giving evidence again for conduction electron polarization. Their $1/\chi$ versus T plots as shown in fig. 48 gave a paramagnetic Curie point along the b-axis of -17 K and a paramagnetic Curie point along the c-axis of 41 K showing anisotropy which, like Er, is reversed from Tb, Dy, and Ho. The slopes were nearly identical and gave a paramagnetic moment of $7.6\mu_B$, to be compared with the $7.56\mu_B$ expected.

The electrical resistivities of Tm single crystals reported by Edwards and Legvold (1968) are shown in fig. 49. The usual knee in the basal plane resistivity, which proves to be about the most reliable method for finding the Néel point,

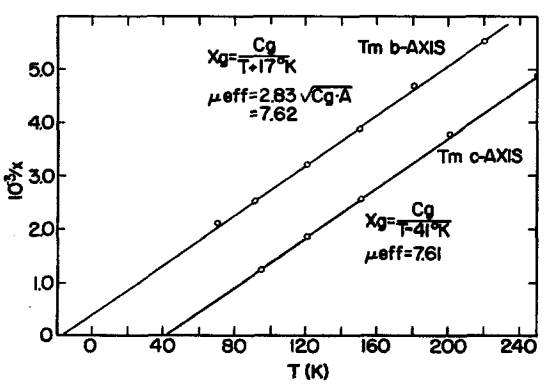

Fig. 48. The inverse susceptibility versus temperature in the paramagnetic range for Tm single crystals as given by Richards and Legvold (1969).

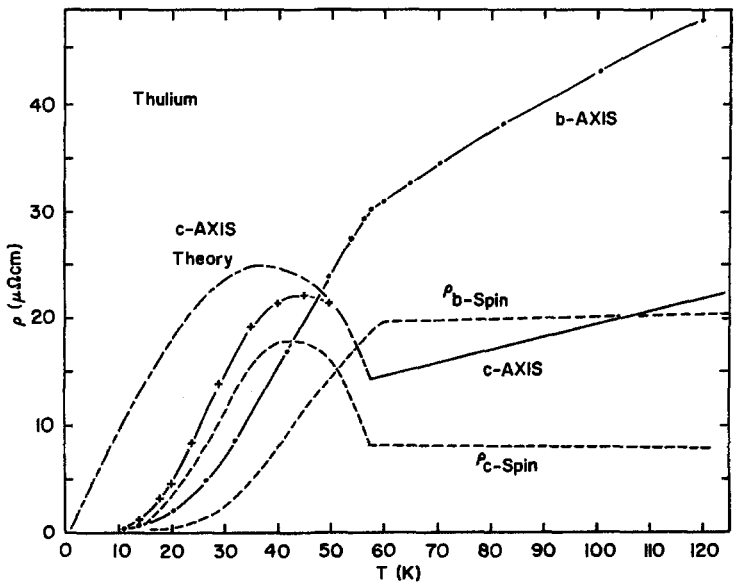

Fig. 49. Electrical resistivity versus temperature for single crystals of Tm as measured by Edwards and Legvold (1968).

occurs at 58 K. The *c*-axis resistivity reveals the very dramatic effect of the modulated magnetic moment along the *c*-axis. It shows up as a pronounced bump just below the Néel point. This is the superzone effect on the Fermi surface of Tm shown in fig. 18 and discussed in the theory section. The fit of the *c*-axis resistivity calculated from the theory of Elliott and Wedgewood (1963) is shown by the dot–dash curve of the figure. The shape is proper but the size is exaggerated. In neither resistivity curve is the 32 K onset of the ferrimagnetic commensurate *c*-axis modulation observable. However, there was a very noticeable spike at this temperature in Seebeck coefficient measurements of Edwards and Legvold (1968) on the *c*-axis sample. This was the first evidence for the 32 K commensurate to incommensurate transition in Tm and is a nice illustration of the high sensitivity of such measurements relative to magnetic and Fermi surface phenomena.

Spin dispersion data for Tm have not been obtained. The specific heat of the metal has been reported by Jennings et al. (1961). Their findings are shown in fig. 50. The magnetic part of the specific heat is shown as the dashed curve. It may be seen in the figure that any effect near 32 K is masked by the main magnetic specific heat peak near 58 K, the Néel point. The Debye temperature used to determine the magnetic specific heat was 0.985 times the Debye temperature of Lu. The dashed curve shows the result and gives an entropy of 21.4 J/mole K which comes close to the $R \ln(2J + 1)$ for Tm of 21.3 J/mole K.

This section on the high magnetic moment rare earths is concluded with a graph (fig. 51) showing the surplus magnetic moment plotted against $S(S + 1)$ and

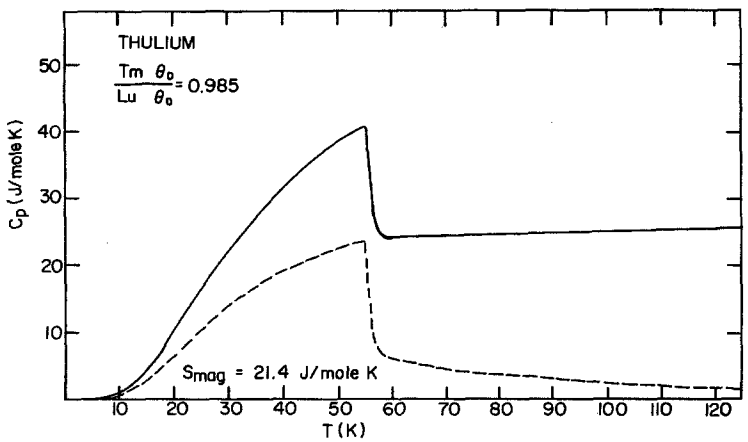

Fig. 50. Specific heat of Tm as measured by Jennings et al. (1961). The dashed curve is the magnetic part.

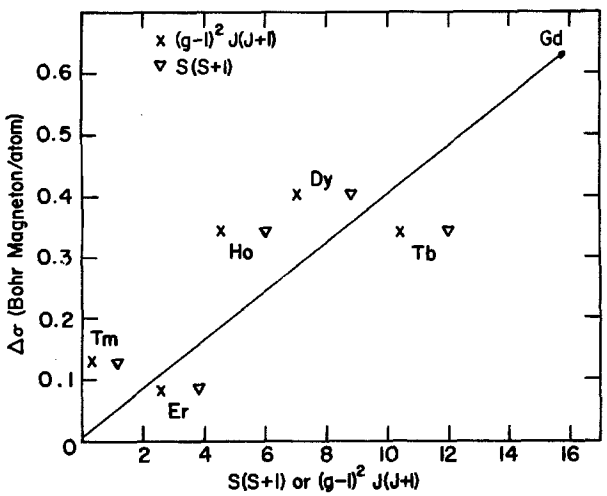

Fig. 51. Magnetic moment in excess of the theoretical gJ value vs the spin factors $(g-1)^2J(J+1)$ and $S(S+1)$.

against the de Gennes factor which one might expect the surplus moment as well as the highest magnetic ordering temperature to follow. We see that the value for Tb is much too low so some other factor plays a role in this matter.

3. Magnetic properties of Ce, Pr, Nd, Pm and Sm

Briefly, the magnetic properties of the light elements differ from the heavy elements in several ways. The crystal structures of the light elements favor the dhcp form with fcc appearing when samples are quenched from higher tem-

peratures. In the case of Sm there is the special nine layer structure which now bears the name of the element. From the magnetic viewpoint, another very significant difference is found in the total quantum number J which is given by $J = L - S$ for the light elements and this leads to very weak exchange interactions when compared with the heavies which have high moments and strong exchange effects. Finally, the relative strengths of the crystal fields to the exchange fields are much greater for the light elements because of the LS coupling they display. It is therefore anticipated that low ordering temperatures and very complex magnetic structures will occur because all of the effects just listed are intermixed. It is found, for example, that the presence of cubic sites and hexagonal sites in the dhcp and Sm structures can be quite significant in the magnetic ordering process. A very brief description of the individual elements follows:

The fcc (γ) form of Ce is paramagnetic down to a Néel point of 14.4 K; the dhcp (β) form is also paramagnetic but shows two ordering temperatures of 13.8 and 12.5 K. The condensed fcc (α) form shows a nearly constant paramagnetic susceptibility. In the case of Pr the fcc allotrope is ferromagnetic with a Curie point of 8.7 K while the stable dhcp form is the outstanding example of crystal field effects because it is now quite certain that pure samples of the metal take on the singlet configuration. In the latter case external fields can induce magnetic moments, and there is also a complication at very low temperatures because nuclear magnetic ordering occurs. Neutron diffraction measurements have shown that dhcp Nd has two antiferromagnetic ordering temperatures, one at 19.9 K and the other at 7.5 K, but specific heat measurements show that the complete story will likely be more complicated. The fcc allotrope of Nd is ferromagnetic with a T_c of 29 K. The element Pm, which is radioactive, has been found to have the dhcp crystal structure and there is a slight hint some type of magnetic ordering may take place around 90 K. In the case of Sm, which has the nine layer ABABCBCAC structure, there is evidence for a Néel point at 106 K with an additional transition of the Néel type at 14 K. As will be seen some features of the magnetic ordering in the light metals are just now emerging.

3.1. Cerium

In a word the element Ce is phenomenal – it exhibits at least five crystal structures, a valence variation from 4 down to 3, paramagnetism, antiferromagnetism, diamagnetism, and superconductivity. It is the only element which has both superconducting and magnetically ordered phases and the only solid known to have a critical point. It seems that one could spend a lifetime exploring cerium's ramifications. The physical properties of Ce have been reviewed by Gschneidner in the book edited by Parks (1977). The atomic number for Ce is 58 and the 4f level turns out to be very close to the Fermi level so that valence fluctuations can occur. It is normally expected that one electron will be in the 4f state for which the spectroscopic designation is $^2F_{5/2}$ with $L = 3$, $S = \frac{1}{2}$ and $J = L - S = \frac{5}{2}$. When the 4f electron migrates to the conduction band (it is

believed about 0.67 electron/atom actually moves) the element must be treated as a tetravalent metal – see the discussion of theory later on.

Any discussion of Ce must begin with the phase diagram shown in fig. 52. The most remarkable feature in the diagram is the appearance of a critical point at 20 atm and about 580 K; apparently no other solid has this feature. Next it is seen that at 1 atm pressure several crystal structures are encountered. At high temperatures the stable structure is bcc (δ from) with fcc (γ form) the stable allotrope from 1000 down to 350 K. The dhcp form is stable from 350 down to about 100 K. A very sluggish transformation to the dhcp (β form) is indicated by the dashed phase boundary lines. At low temperatures the collapsed fcc' (α form) is stable; the volume is about 12% smaller for this phase and the 4f level occupancy is about 0.4 electron/atom. At pressures beyond 50 kbar Ce takes on the α' phase and the 4f level occupancy is near zero; this phase is superconducting.

Returning to the behavior of Ce at 1 atm pressure it is found that for slowly decreasing temperatures, samples which are initially in the β form at room temperature collapse to the α form at about 50 K. Quickly cooled samples will remain dhcp at 4.2 K and upon slow warming will transform to α at about 18 K; hence to preserve the dhcp form the 15 to 60 K regime must be traversed rapidly. Indeed, use of rapid sample cooling to 4.2 K followed by rapid warming to room temperature and lengthy annealing at 350 K leads to the growing of the

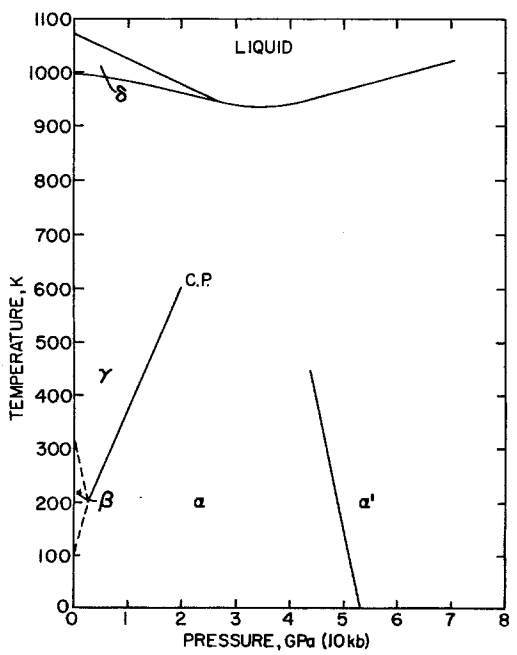

Fig. 52. Temperature–pressure phase diagram for Ce. For the phase transitions which are sluggish the dashed lines are the average of several observations. After Koskenmaki and Gschneidner (1978).

dhcp allotrope. The addition of 5at.% of La will preserve the dhcp allotrope once it has been formed. All of these observations are substantiated in figs. 53 and 54 which show resistivity observations reported by Burgardt et al. (1976). In fig. 53 the data for slow cool down and warm up show that γ has a lower resistivity at room temperature. If one starts at room temperature and follows the cool down–warm up cycle one sees the γ to α back to γ (plus a little β) transitions and the β to mixed β and α back to mixed β and γ (mostly β) at room temperature. In fig. 54 the data obtained with rapid cool down and warm up reveal the stability of the dhcp allotrope and the manner in which γ transforms upon cooling to α and then relaxes back to mixed β and γ upon warming up to room temperature. The remarkable resistivity of β Ce given in fig. 54 has been explained in terms of the Kondo effect by Liu et al. (1976).

After the procedures for preserving β Ce had been established Burgardt et al. (1976) were able to obtain magnetic susceptibility data for β Ce which is shown in fig. 55. The data in the insert show the onset of antiferromagnetic ordering at the 12.5 K Néel point. Specific heat measurements on β Ce by Tsang et al. (1976a, b) and extensive studies of Ce–La alloys by Petersen et al. (1978a) have shown that there is an additional ordering temperature at 13.7 K. The data of Petersen et al. (1978) are shown in fig. 56. At the higher La concentrations their samples contained some of the fcc phase which accounted for the third (upper) ordering temperature shown in the figure. The two ordering temperatures which appear at low La concentrations are associated with the dhcp form and are 12.5 and 13.7 K. They conjectured that the moments on the hexagonal sites became

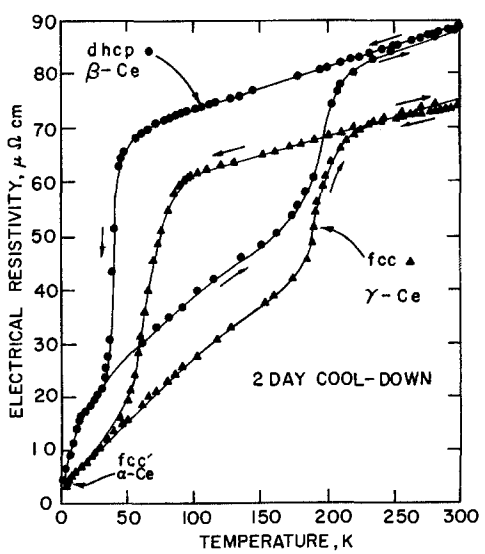

Fig. 53. Electrical resistivity versus temperature of β Ce and γ Ce for samples cooled down over a 2 day period and warmed up over 1.5 days. After Burgardt et al. (1976).

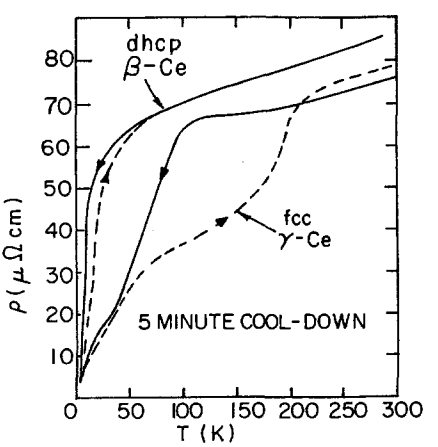

Fig. 54. Electrical resistivity versus temperature of β Ce and γ Ce for samples cooled from 298 to 4.2 K in five minutes. Warm up times were comparably short. After Burgardt et al. (1976).

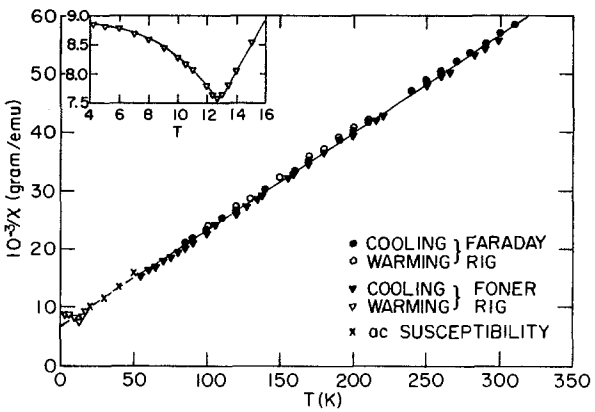

Fig. 55. The reciprocal of the magnetic susceptibility of β Ce versus temperature. The insert shows the details near the Néel temperature. After Burgardt et al. (1976).

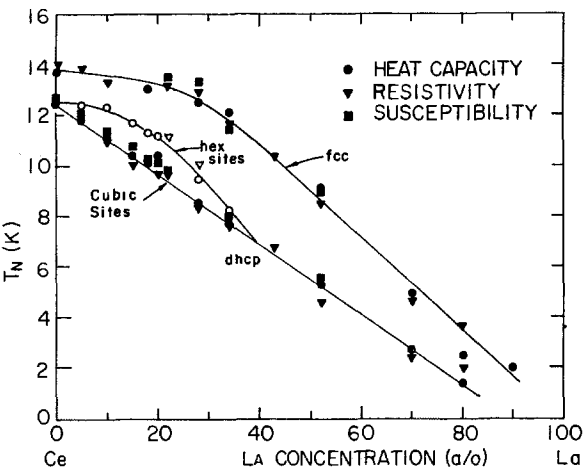

Fig. 56. Magnetic ordering temperatures of Ce–La alloys. After Petersen et al. (1978a, b).

ordered at 13.7 K and that the moments on the cubic sites became ordered at 12.5 K by analogy with the magnetic ordering first reported for Nd. This view is suspect because the most recent neutron diffraction findings on Nd by Bak and Lebech (1978) show small ordered moments appear on the cubic sites at the time that considerably larger moments become ordered on the hexagonal sites.

The high temperature slope of the $1/\chi$ versus T curve of fig. 55 yielded an effective Bohr magneton number μ_{eff} of $2.61\mu_B$ to be compared with the expected $2.54\mu_B$. If the linear portion of the $1/\chi$ versus T plot is extrapolated to the abscissa the paramagnetic Curie point found is -40 K.

The fcc (γ) phase of Ce has been investigated by Bates et al. (1955) and their

data for $1/\chi$ versus T are almost identical with the data for dhcp (β) Ce shown in fig. 55. They found $\theta_p = -42$ K and reported a $\mu_{eff} = 2.58\mu_B$ which are both very close to the values reported for β Ce. Direct measurements of the ordering temperature of cubic (γ) Ce have not been made. However, the upper ordering temperatures (marked fcc) of fig. 56 extrapolates to a Néel point of about 14.4 K at zero La concentration so this gives a good estimate of the behavior of pure γ Ce.

The α phase (collapsed fcc) of Ce is the low temperature–high pressure form. A 12% decrease in sample volume accompanies the γ Ce to α Ce transformation. As might be expected the collapsed cubic form is only weakly magnetic because the population of the 4f state is greatly diminished by the migration of electrons to the conduction band. The magnetic susceptibility of α Ce has been reported by Koskimaki and Gschneidner (1975) and their data are shown in fig. 57. There is no evidence of magnetic ordering in the temperature range covered. It was their appraisal that their sample was single phase α Ce and that the rather rapid rise in the susceptibility below 15 K was not attributable to magnetic impurities. They conjectured that this was a case of exchange enhanced susceptibility.

The heat capacity results of Tsang et al. (1976a, b) for β Ce, mentioned earlier, are shown in fig. 58. There is a sharp peak at the 12.5 K ordering temperature and a shoulder which comes from the ordering process at 13.7 K. In the case of γ Ce it would be difficult to obtain repeatable interpretable heat capacity data, but in the case of the collapsed cubic phase or (α Ce) the heat capacity has been measured by Koskimaki and Gschneidner (1975) with results which are shown by the lower curve in fig. 58 for the temperature range from 1.3–20 K. There is no evidence here, nor at higher temperatures, of any type of magnetic ordering, and the samples showed no evidence of β Ce contamination because the data show no anomaly at 12.5 K. From a C_P/T versus T^2 plot it was found that the electronic specific heat constant was 12.8 mJ/g atom K^2, one of the highest reported for a pure non-magnetic metal. This suggests a high density of states at

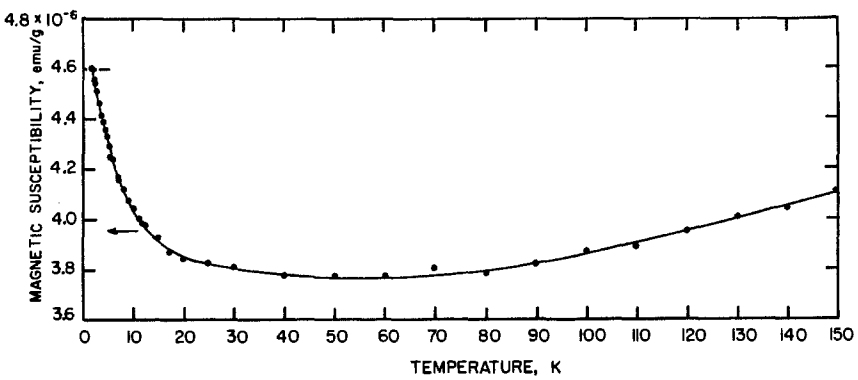

Fig. 57. Magnetic susceptibility of α Ce(fcc') versus temperature. After Koskimaki and Gschneidner (1975).

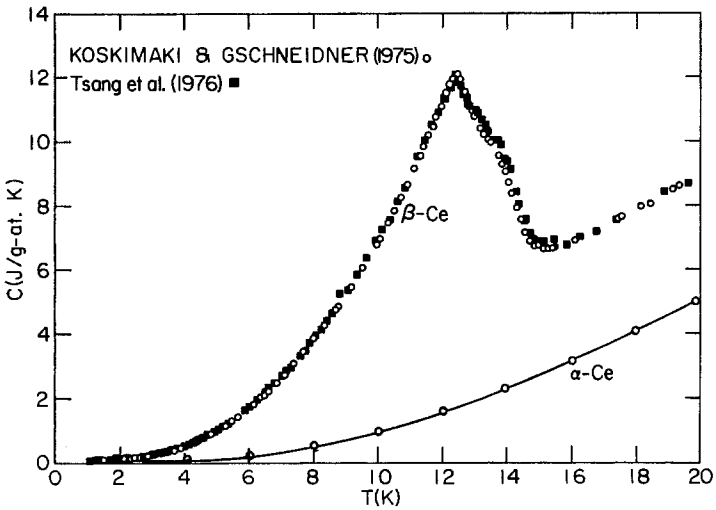

Fig. 58. Specific heat versus temperature for β Ce (dhcp) and for α Ce (fcc'). After Tsang et al. (1976a) for the β allotrope and after Koskimaki and Gschneidner (1975) for the α form.

the Fermi level leading one to believe a 4f band might be involved. The high pressure phase for Ce is denoted by α' and it is this phase which is believed to be truly tetravalent. This would be compatible with the observation of superconductivity in this allotrope by Wittig (1968) at a pressure of 50 kbar with T_c of 1.8 K.

Two different approaches to the formidable problem of generating a theory for the electronic properties of Ce have been made. The basic phenomenon which must be explained is the phase transition from the room temperature γ(fcc) phase to the collapsed α(fcc') phase with about 12% smaller volume.

Coqblin and Blandin (1968) used the Hartree–Fock approximation and Anderson's formalism for a treatment of virtual bound states (4f states). They discussed the γ to α phase transition in Ce in terms of electron promotion from a sharp 4f state to the conduction band.

Ramirez and Falicov (1971), Kiwi and Ramirez (1972) and Aliscio et al. (1973) also used the electron promotion approach. They assumed that atomic like 4f electrons were promoted to the conduction band when the solid went from γ to α, i.e., the atomic state changed from $4f^1\,(sd)^3$ for γ to $4f^n\,(sd)^{4-n}$ for α. They proposed that the change in occupation number n is caused by the short range part of the electron–electron interaction and assumed a linear relationship between n and the lattice constant. They used a free energy expression to calculate pressure and temperature effects and were able to get reasonable fits to experimental observations such as the critical temperature. They found the 4f electron populations of γ, α, and α' to be 0.98, 0.44, and 0.03 respectively. As mentioned earlier the generally accepted number for α Ce is 0.33.

Johansson (1974) proposed that the γ to α phase change is a Mott transition. He assumes that the 4f radial functions (see fig. 3) extend close to the cell

boundary for Ce and that thermal contraction and/or an applied pressure will cause neighboring 4f functions to overlap enough to give rise to a 4f band. He avers that the γ phase of Ce is on the high volume side of the Mott transition and that two conduction bands coexist in the condensed α phase. Johansson also says that the electron promotion model discussed above (i) does not provide the appropriate cohesive energy for Ce, (ii) assumes a 4f energy level close to E_F in conflict with the 1.8 eV found for this by Baer and Busch (1973), (iii) requires higher 5d–6s conduction electron numbers in the condensed α phase in conflict with positron annihilation data of Gustafson et al. (1969). It is noted that the 4f band model has been invoked to explain superconductivity in La and that for the parallel actinide elements a 5f band model has been proposed by Veal et al. (1973). Johansson suggested his model was compatible with the experimental results.

3.2. Praseodymium

The element Pr, atomic number 59, is the second in the series of rare earth elements and has two electrons in the 4f shell. The spin quantum number is $S = 1$ and $L = 3 + 2 = 5$, so $J = L - S = 5 - 1 = 4$ and the spectroscopic designation is $^3H_4$. The stable room temperature structure for Pr is dhcp. Nevertheless it was possible for Bucher et al. (1969) to obtain and retain the fcc allotrope by the rapid quenching process which arc melting over a cooled copper hearth provides. The normally expected high temperature phase (just below the melting point) is bcc just as is found for nearly all the rare earth metals.

The most remarkable feature of Pr is its singlet ground state in the dhcp allotrope. This state is characterized by the total quenching of magnetic moments by the crystal field effect. For this wave function configuration only induced paramagnetism occurs in modest applied fields. It turns out that the balance between the crystal field and magnetic exchange energies is so delicate that sample purity, both phase and chemical, is very critical and many measurements on impure samples have given misleading results. Indeed, McEwen (1978) induced a magnetic moment in Pr by straining a sample.

The singlet ground state was found for single crystal dhcp Pr by Johansson et al. (1970) using neutron diffraction. More recently, by way of magnetization measurements up to 8 T, Sakamoto et al. (1976) found the singlet state in a Pr sample cut from mother polycrystalline stock and in a single crystal grown from that stock. Very high field (33 T) magnetization measurements at 4.2 K on a dhcp single crystal of Pr have been reported by McEwen et al. (1973) who also observed the singlet state. Their results are shown in fig. 59 where it is seen that the a-axis is the easy direction and the c-axis is the hard direction of magnetization. The results of Sakamoto et al. are in good agreement with those shown in the figure. It should be noted that the magnetization curves emanate from the origin in a paramagnetic fashion. In the basal plane easy direction the magnetization appears to grow toward a saturation value of about $2.8\mu_B$ which is well below the theoretical $3.2\mu_B$ value. In the c-axis direction a sudden rise in

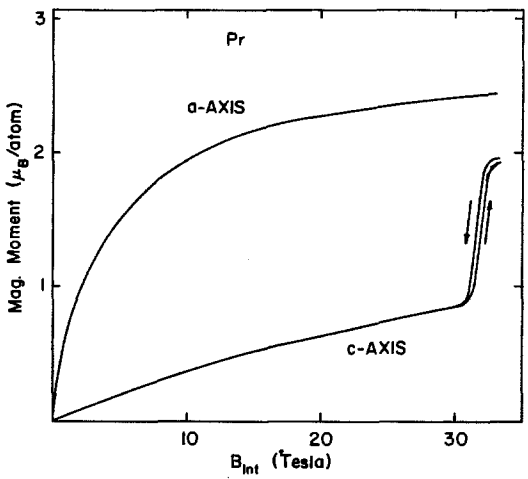

Fig. 59. High field magnetization data for single crystal Pr. After McEwen et al. (1973).

the moment at 31.5 T was found to have a hysteresis of 0.2 T at 4.2 K. The anomaly decreased with increasing temperature and vanished at 65 K. They attributed the magnetization jump to a first order transition on the hexagonal sites from a non-magnetic to a field induced magnetic phase (the term metamagnetic is now used to describe this type of magnetic material); they discussed some of the crystal field states which might be involved in the two phases.

Magnetization measurements on polycrystalline fcc and dhcp samples of Pr have been reported by Bucher et al. (1969). The normally expected form for pure Pr is the dhcp allotrope but by arc melting a sample of the metal over a cold Cu hearth Bucher et al. obtained a sample of the fcc allotrope. The results of their magnetic measurements are shown in fig. 60. The upper curve in the figure is for fcc Pr and shows the typical ferromagnetic jump to high magnetic moment in a weak field followed by the slow approach to saturation. The spontaneous moment they obtained was $0.76\mu_B$/atom which was about a fourth of the full value and was explained as a crystal field level effect. The lower curve of the

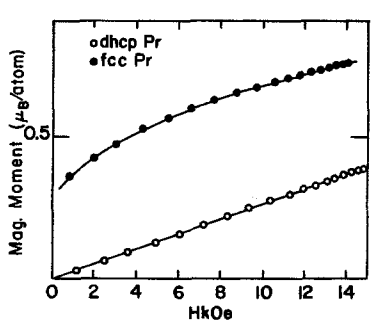

Fig. 60. Magnetic moment versus field at 1.43 K for dhcp and fcc Pr. After Bucher et al. (1969).

figure shows the nearly linear behavior with field of the polycrystalline Pr sample. The fields here are relatively weak which makes it difficult to make a quantitative comparison of these results with the very high field results on single crystals described above. Bucher et al. invoked crystal field properties to explain the absence of a specific heat anomaly for fcc Pr at the 8.7 K Curie point.

The temperature dependence of the initial magnetic susceptibilities found by Sakamoto et al. (1976) for single crystal dhcp Pr exhibited considerable anisotropy of the type found in the heavy rare earths. Their data along with results of previously reported investigations by Johansson et al. (1971) and by Andres et al. (1972) are shown in fig. 61. A very crude extrapolation to the abscissa of the nearly linear trend at 90 K yields paramagnetic ordering temperatures of about −20 K for the c-axis data and about 13 K for the a-axis data. These data do not extend high enough in temperature for a determination of the paramagnetic moment.

The reciprocal of the magnetic susceptibility of a sample of dhcp Pr as a function of temperature found by Bucher et al. (1969) in a field of 14.24 kOe is shown in the upper part of fig. 62. The slope of the linear part of the dhcp curve yields an effective moment of $3.65\mu_B$ which is very close to the theoretical $3.68\mu_B$ for Pr. There is a small difference in the slope of the high temperature linear part of the curve for the fcc allotrope which does not appear significant. In both phases it appears that the susceptibility is strongly affected by the crystal field levels of the 4f electrons and that all levels in both allotropes become occupied above about 100 K. The paramagnetic Curie point for dhcp Pr is about −10 K while that for fcc Pr is 8 K which is in good agreement with the observed 8.7 K Curie point.

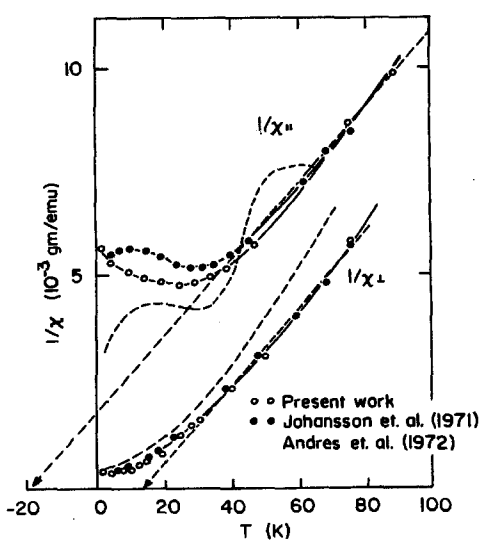

Fig. 61. Reciprocal of the magnetic susceptibility for a c-axis sample and for a basal plane sample of Pr. After Sakamoto et al. (1976).

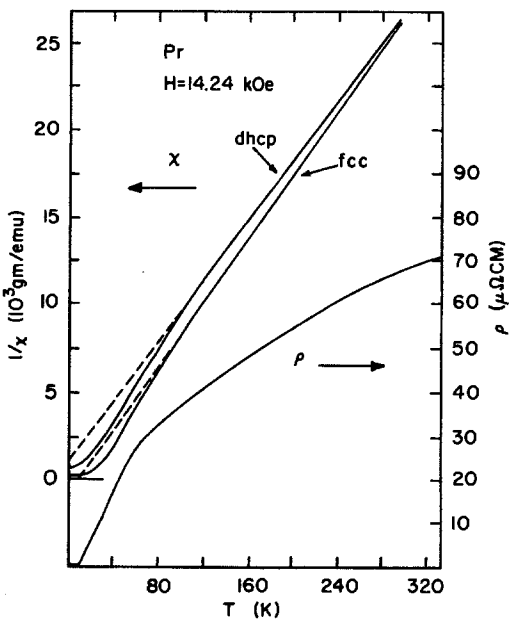

Fig. 62. At the top is the reciprocal of the magnetic susceptibility versus temperature for dhcp Pr and for fcc Pr. After Bucher et al. (1969). At the bottom is the electrical resistivity versus temperature of polycrystalline Pr. After Arajs and Dunmyre (1967).

The electrical resistivity of polycrystalline Pr has been reported by Arajs and Dunmyre (1967) and their results are shown in the bottom part of fig. 62. The curvature below 80 K is anomalous for a metal and is believed to represent the effect of the crystal field levels as they become occupied thermally. This interpretation goes hand in glove with the behavior of the susceptibilities in the upper part of the figure. One can conclude that the crystal field levels are within 100 K (about 8 meV) of the Fermi level in the metal.

Crystal field levels in a single crystal of Pr have been investigated by Rainford and Houman (1971) using inelastic neutron diffraction techniques along principal crystallographic directions. They found two types of dispersion curves and identified a single very flat curve at 8 meV with the cubic sites of the dhcp lattice and a more dispersive group of curves in the 1 to 4 meV range with the hexagonal sites. Houman et al. (1975b) have obtained additional, more detailed, results at 6.4 K on the dispersion relations for the hexagonal site magnetic excitons (these are the excitations of 4f electrons to higher energy crystal field states). Their results are shown in fig. 63. They identify the lower curve from Γ to M as being responsible for magnetic ordering when small amounts of Nd are added to Pr. These magnetic excitons play a strong role in the magnetic susceptibility and electrical resistivity results described previously.

Specific heat measurements on Pr have been reported by Parkinson et al. (1951). From their results Mackintosh (1971) has derived the magnetic part of the

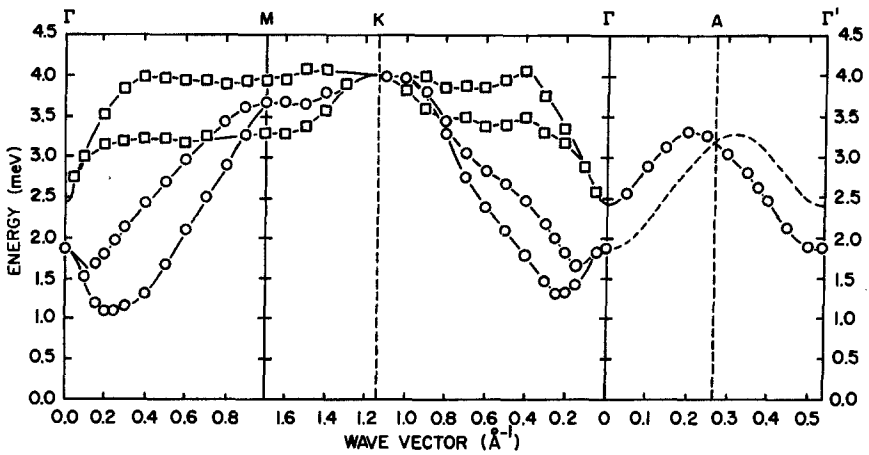

Fig. 63. Dispersion relations for the magnetic excitons propagating on the hexagonal sites in Pr at 6.4 K. The extended zone representation is used in the ΓA direction. After Houman et al. (1975b).

heat capacity as shown in fig. 64. Crystal field levels suggested to Mackintosh by B.D. Rainford for the different types of sites are also shown – both sites have singlet ground states as required in the absence of magnetic ordering in observations down to 1 K. Below this temperature nuclear magnetic ordering at the hexagonal sites in single crystal Pr has been reported by Lindelof et al. (1975) who found a λ type of anomaly in the heat capacity between 25 and 30 mK. They invoke a nucleus–ion–nucleus magnetic coupling which has been described by Murao (1972) and by Triplett and White (1973). Theory of the singlet ground state system has been treated by Cooper (1967), and by Bleaney (1963).

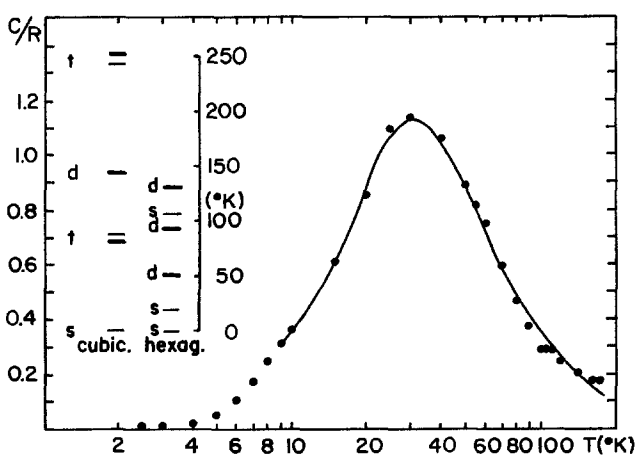

Fig. 64. Crystal field levels and magnetic heat capacity of Pr calculated by Rainford and Houman (1971) and shown by Mackintosh (1971). The s, d, t represent singlet, doublet, triplet states.

3.3. Neodymium

Since the element Nd, atomic number 60, has three electrons in the 4f shell it is a Kramers ion and cannot have the singlet ground state. The 4f electron quantum numbers are $L = 6$, $S = \frac{3}{2}$ and $J = L - S = \frac{9}{2}$ and the spectroscopic designation is $^4I_{9/2}$. The normal crystal structure for the pure metal is dhcp with ABAC stacking although Bucher et al. (1969) were able to obtain an fcc sample by the same arc melting process they used to obtain an fcc Pr sample as described in the previous section.

Just as in the case of Pr the crystal field interaction should be expected to influence and complicate the magnetic properties of Nd. The most recent neutron diffraction results of Bak and Lebech (1978) have confirmed earlier work of Moon et al. (1964) that antiferromagnetic ordering sets in at $T_N = 19.9$ K and have found (i) that the transition at T_N is second order, (ii) that moments on all sites are involved in the magnetic ordering with the size of the moments on the cubic (A) sites about 15% of the moments on the hexagonal (B, C) sites and with the c direction components on the cubic sites about this same order of magnitude, (iii) that there is a lattice distortion which accompanies the onset and growth in magnitude of the ordered magnetic moments, and (iv) that the metal has the "triple-q" magnetic structure. They found that the magnitude of the magnetic q vector varied from an incommensurate 0.144 at $T_N = 19.9$ K to an apparently commensurate 0.125 at 7.5 K which is the temperature at which Moon et al. had reported the onset of ordering on the cubic sites (they had interpreted their results at $T_N = 19.9$ K as the onset of ordering at the hexagonal sites). The beautiful magnetic moment pattern of the A layers and of the accompanying lattice distortion proposed by Bak and Lebech is shown in fig. 65, but this result has not been corroborated by other investigators. The in-plane magnetic moment components give the three leaf clover pattern in part (a) and the lattice distortion is the triangular pattern of part (b).

The behavior of the moments and lattice below 7.5 K was not explored. It is expected that other interesting effects will be seen on the basis of electrical resistivity and specific heat results described below.

Very high field magnetization data on single crystal Nd obtained at 4.2 K by McEwen et al. (1973) are shown in fig. 66. The easy direction of magnetization is along an a-axis. The insert in the figure shows the low field data at 4.2 K of Behrendt et al. (1957) on what is believed to be the first macroscopic rare earth single crystal grown. It is seen that the magnetization rises linearly with field at low field in line with antiferromagnetic requirements. There is a rapid rise in moment with field at about 10 kOe indicating that the external field has passed a critical level for some of the moments to jump into alignment with the field. In measurements up to 60 kOe at 4.2 K on single crystal Nd Johansson et al. (1970) obtained similar results and showed that along the a-axis two additional moment jumps occur, one at 20 kOe and the other at 30 kOe. This is reminiscent of the magnetization of Ho. The magnetic moment at 30 T along the easy axis is about

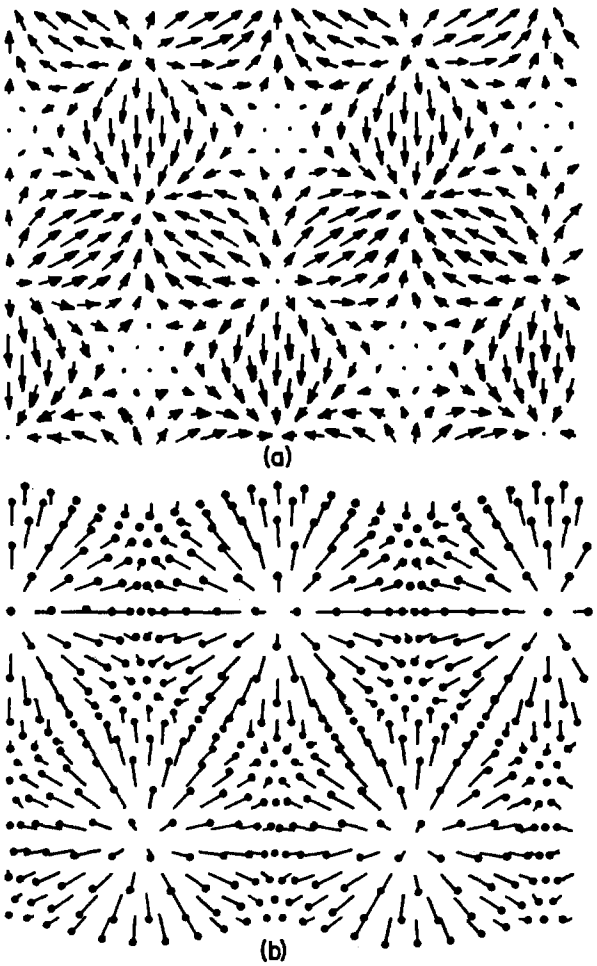

Fig. 65. (a) The magnetic structure of Nd below 19 K as proposed for the A sites of Nd by Bak and Lebech (1978). (b) The accompanying lattice distortion they proposed; the atoms are shifted to the dot end of the line.

$2.7\mu_B$ well below the theoretical saturation value of $3.27\mu_B$ which it appears to be approaching asymptotically.

In the paramagnetic range the reciprocal of the magnetic susceptibility found by Behrendt et al. (1957) was linear with temperature above 150 K with $\chi_\parallel = (1.19\times10^{-2})/(T+17)$ and $\chi_\perp = (1.20\times10^{-2})/(T+11)$ in cgs units. The paramagnetic moment yielded was $3.71\mu_B$ to be compared with the expected $3.62\mu_B$ from theory. Since the $1/\chi$ vs. T plots only settle down to linear form above 150 K one concludes that crystal field levels have an effect below this temperature. The two paramagnetic Curie points are $\theta_{p\parallel} = -17$ K and $\theta_{p\perp} = -11$ K so there is some two fold anisotropy in Nd. Above 20 K Behrendt et al. observed no basal plane anisotropy. Some basal plane anisotropy at 4.2 K may be seen in the low field

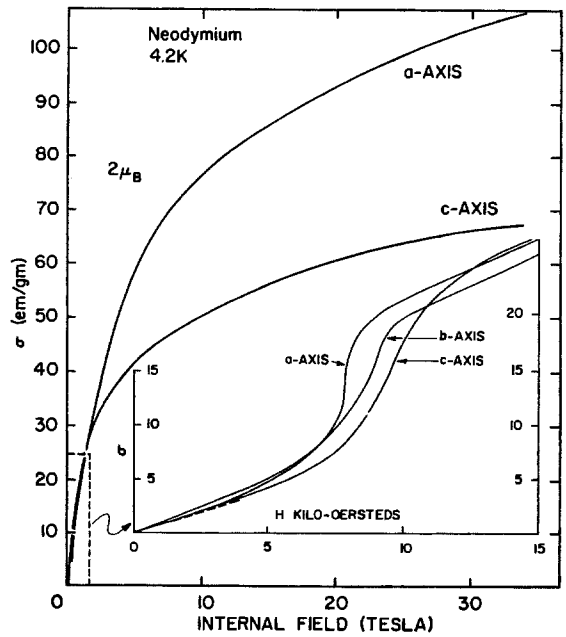

Fig. 66. High field magnetization data at 4.2 K for *a*-axis and *c*-axis crystals of Nd. After McEwen et al. (1973). In the insert the low field magnetization data at 4.2 K for *a*-axis, *b*-axis and *c*-axis crystals are shown. After Behrendt et al. (1957).

magnetization data in fig. 66 where the critical field for the magnetization jump at about 9 kOe is smaller along the *a*-axis than along the *b*-axis.

Results of specific heat measurements on electrotransport purified Nd by Forgan et al. (1979) are shown in fig. 67. There are five distinct specific heat anomalies or peaks in the 5 K to 8.5 K regime. The peaks are modified in the presence of an applied field of 2.8 kOe as shown in the lower part of the figure. Some of the peaks are more pronounced and the peak just below 8 K has apparently increased at the expense of the peak just above 8 K. The peak at 6.7 K seems to have shifted to a slightly lower temperature. Apparently low temperature data are dependent on thermal and magnetic history so the magnetic ordering is fraught with complexity and very precise neutron diffraction measurements will be needed if an understanding of the structures is to be found.

The electrical resistivity of Nd single crystals has been measured by Petersen et al. (1978) and their results are shown in fig. 68. The low temperature data shown in the insert shows sharp changes in slope at 6 K and 8 K which correspond to the two double specific heat anomalies. The individual specific heat peaks are too close for a resolution by resistivity methods. It thus appears that additional elastic, as well as inelastic, neutron diffraction and Seebeck coefficient measurements are essential if the low temperature magnetic properties of Nd are to be resolved.

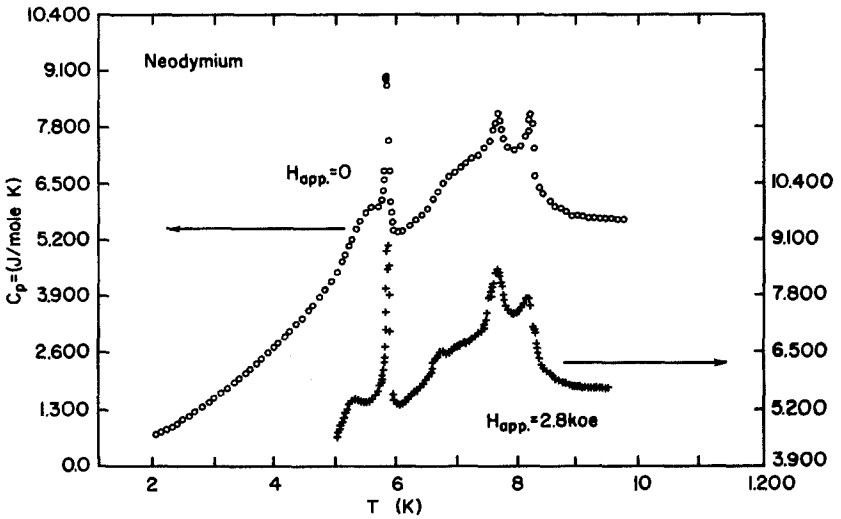

Fig. 67. Heat capacity of high purity Nd versus temperature. After Forgan et al. (1979).

3.4. Promethium

The information available on Pm is necessarily sparse because all known isotopes of the element are radioactive. The atomic number of Pm is 61 and it has four electrons in the 4f shell. The quantum numbers for this configuration are $L = 6$, $S = 2$ and $J = L - S = 4$ so the spectroscopic designation is $^5I_4$. It is known that the stable crystal structure is dhcp which is in keeping with the light rare earths. The expected saturation moment per atom, gJ, is $2.4\mu_B$.

Since Pm has an even number of 4f electrons it is not a Kramers ion and so might have magnetic properties like those of Pr. About the only information regarding the magnetic properties of Pm comes from a neutron diffraction study at Oak Ridge by Koehler et al. (1973). They carried out a variety of neutron diffraction experiments and established (i) that the crystal structure was dhcp, (ii) that any ordered moment in the temperature range 7.5 to 320 K had to be less than $0.4\mu_B$ and (iii) that a very small ferromagnetic moment might be present below an ordering temperature of 98 K. They noted that the latter would not be consistent with crystal field levels anticipated for the ground state of the metal.

3.5. Samarium

There are five electrons in the 4f shell of Sm so it has the spectroscopic designation $^6H_{5/2}$ with $S = \frac{5}{2}$, $L = 5$, and $J = L - S = \frac{5}{2}$. The crystal structure is rhombohedral but is generally treated as a nine layered hexagonal structure with stacking ABABCBCAC as shown on the right of fig. 1. This gives a succession of atomic site symmetries of chhchhchh, and this sequence plays a very strong role in the magnetic properties of the element.

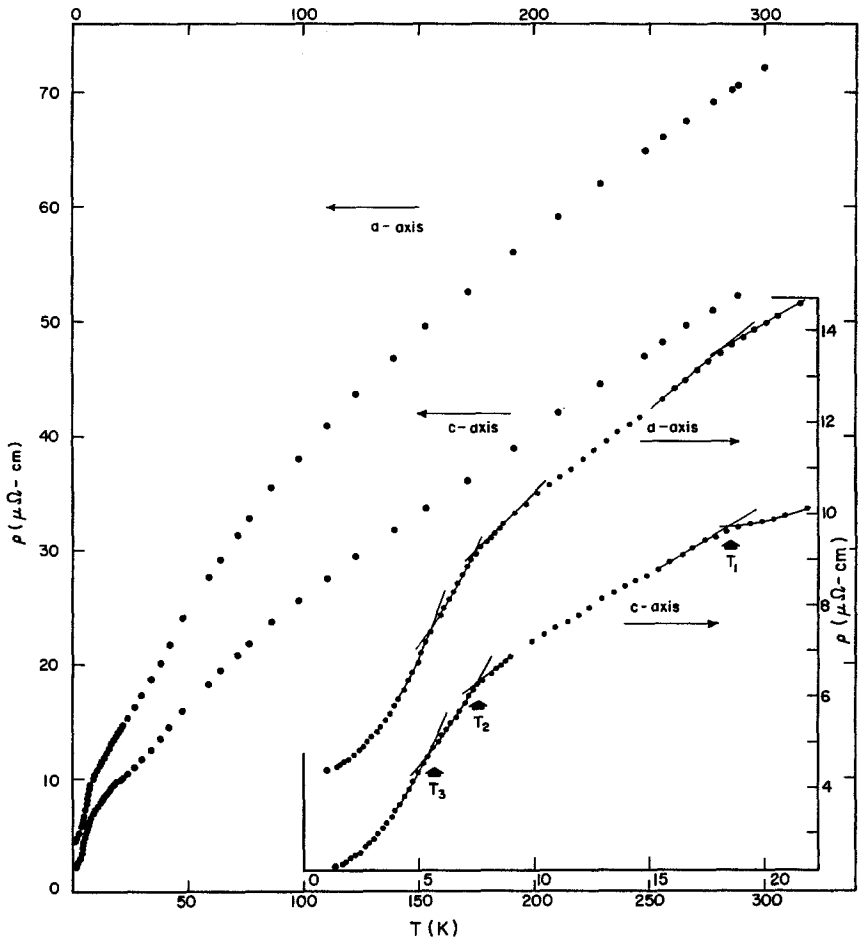

Fig. 68. Electrical resistivity of single crystal Nd versus temperature. After Petersen et al. (1978a, b).

Neutron diffraction measurements on a single crystal grown from metal enriched in ^{154}Sm have been made by Koehler and Moon (1972). The low magnetic moment of $gJ = \frac{5}{7}\mu_B$ per atom and the high neutron capture cross section of ordinary Sm prompted them to use a sample enriched in a low capture cross section isotope. They found that the moments on the hexagonal sites become ordered antiferromagnetically below a Néel point of 106 K. The moments pointed along the c-axis with two adjoining hexagonal site layers pointing in the plus c direction and then alternating to point along the minus c direction on the next pair of hexagonal layers and so on. This gives a magnetic moment sequence on the consecutive layers of $++0--0++\ldots$ where 0 means that no order moment exists on this cubic site layer and $-$ means the moment is pointed along the minus c-axis so it takes eighteen layers to make a magnetic cell. For this magnetic structure the exchange field is zero on the cubic

sites. It is not surprising then that the magnetic moments on the cubic sites do not become ordered until the temperature has been lowered to 13.8 K. The direction of the moments on these sites is also parallel to the c-axis; two rows of atoms perpendicular to the b-axis in a cubic site layer have plus c direction moments followed by two rows with minus c direction spins. This gives ferromagnetic layers in $(10\bar{1}1)$ planes (here the c-axis parameter spans 9 atom layers or three cubic site layers) with two adjacent planes having plus c direction moments followed by the next two adjacent planes with minus c direction moments and so on. The magnetic scattering amplitudes found yielded about $0.1\mu_B$ per atom as compared to the $0.71\mu_B$ expected. They propose that the spin part of the ionic moment plus the induced conduction electron spin polarization nearly cancels the orbital contribution to the total magnetic moment since here $J = L - S$.

The very low magnetic moment found by neutron diffraction is in good agreement with results of magnetization measurements on single crystal Sm reported by McEwen et al. (1973). Their work is shown in fig. 69. It is seen that Sm is extremely hard magnetically. In fields below 25 T (250 kOe) the moment rises nearly linearly with field and the a-axis is the easy direction of magnetization. However, with the applied field along the c-axis the magnetic moment makes a sizable jump near 30 T, indicating that the moments originally aligned opposed to the field have flipped and ferromagnetic alignment has been achieved. The moment at 32 T is about $0.12\mu_B$ per atim which is in good agreement with neutron scattering results as mentioned above. Magnetic susceptibility data along the c-axis of McEwen et al. (1974) show peaks at 14 and 109 K.

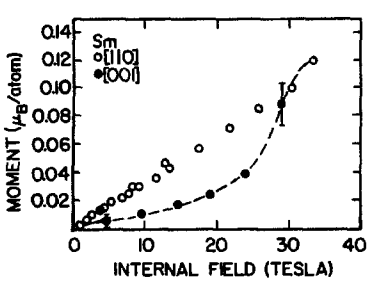

Fig. 69. High field magnetization data at 4.2 K for single crystal Sm. After McEwen et al. (1973).

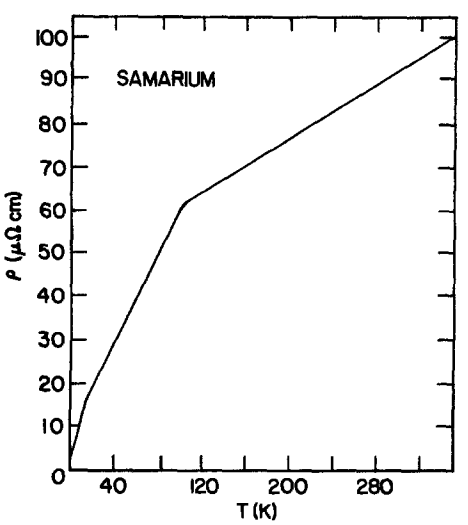

Fig. 70. Electrical resistivity versus temperature for polycrystalline Sm. After Arajs and Dunmyre (1966).

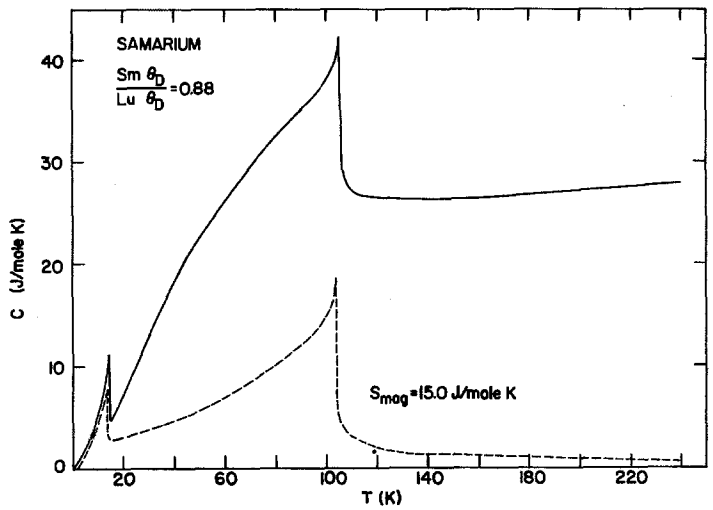

Fig. 71. Specific heat of Sm versus temperature. The dashed curve is the magnetic part of the specific heat obtained by the subtraction of the specific heat of Lu with a Debye temperature ratio θ_D for Sm to θ_D for Lu of 0.88. After Roberts (1957) and Jennings et al. (1959).

The electrical resistivity of polycrystalline Sm has been published by Arajs and Dunmyre (1966) and their results are shown in fig. 70. The knee at 14 K marks the low temperature ordering temperature associated with the cubic sites and the upper temperature knee at 106 K faithfully marks the hexagonal site ordering process. The high resistivity characteristic of the rare earths in general is also in evidence with the room temperature resistivity nearly 90μ ohm cm.

The specific heat of Sm has been measured by Roberts (1957) and by Jennings et al. (1959). The results shown in fig. 71 are a composite of both sets of data and show a small specific heat peak at 14 K with a much higher and broader peak at 106 K. This difference reflects the $\frac{1}{3}$ to $\frac{2}{3}$ ratio which would be expected because of the corresponding ratio of $\frac{1}{3}$ to $\frac{2}{3}$ cubic site to hexagonal site magnetic sublattice occupancy. The dashed curve at the bottom of the figure shows the magnetic part of the heat capacity found by subtracting the heat capacity of Lu adjusted by use of the ratio of θ_D for Sm to that for Lu of 0.88. This yielded the magnetic entropy of 15.0 J/mole K as compared with the $R \ln(2J + 1)$ value of 14.9 J/mole K.

This concludes the discussion of the elements which exhibit ionic magnetic moments. The weakly magnetic rare earth related elements are described next.

4. Magnetic properties of Sc, Y, Lu, La and Yb

The elements Sc, Y, and Lu are hcp trivalent metals and have a close relationship with the rare earth metals, particularly the heavy rare earths which have the same crystal structure. La is the trivalent forerunner of the rare earths while Yb

turns out to be divalent with a full 4f shell, and so departs from the main rare earths in its magnetic properties.

4.1. Scandium

The element Sc has atomic number 21; it is the third element of the fourth period in the periodic table and so has a valence of three. It is an early element in the 3d transition (iron) group of elements, has the hcp crystal structure and its three conduction electrons are found in 3d and 4s bands. These conduction electron bands are much like those of the hcp rare earths with which it generally will form solid solutions.

The early magnetic susceptibility measurements on Sc gave results which were very much sample dependent; in fact some of the samples even appeared to have a magnetically ordered phase. When purer samples became available the data were not quite as confusing. The results obtained by Spedding and Croat (1973) on single crystal Sc are shown at the top of the susceptibility versus temperature graph of fig. 72. It is seen that the a-axis has the higher susceptibility and so Sc is reminiscent of Tb, Dy, and Ho in this respect. The susceptibility increases almost linearly with decreasing temperature down to about 25 K, below which the behavior is more complex. This low temperature behavior is impurity sensitive and since the single crystals used contained 19 atomic ppm (parts per million) Fe and several atomic ppm magnetic rare earths it

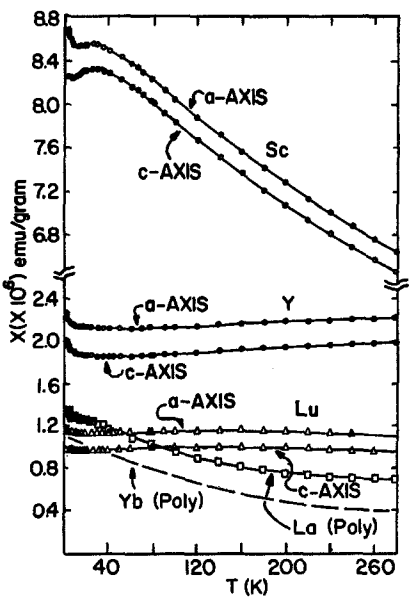

Fig. 72. Magnetic susceptibility versus temperature for Sc, Y, Lu, La, and Yb. After Spedding and Croat (1973) for Sc, Y, Lu, La; after Queen (1979) for Yb.

is very likely the low temperature anomaly will disappear in high purity electrotransported Sc. Indeed, heat capacity measurements of Tsang et al. (1976a, b) on electrotransported samples of Sc show no low temperature peak of the type which a sample containing 30 atomic ppm Fe exhibits. Thus one concludes that small quantities of magnetic impurities lead to sizable effects on the low temperature magnetic susceptibility of Sc, which appears to show enhancement at low temperatures much like Pd. One outcome of the susceptibility results for Sc has been a series of theoretical papers about the metal. Among these is a publication by Rath and Freeman (1975) who calculated the generalized susceptibility and the Fermi surface and one by Das (1976) who computed the magnetic susceptibility. These papers followed earlier calculations by Koelling et al. (1969) and Capellman (1970).

The electrical resistivity of electrotransported Sc single crystals has been determined by Queen (1979). The samples showed resistivity ratios $R_{300}/R_{4.3}$ of 270 for the c-axis sample, and 350 for the a-axis sample. His results are shown in fig. 73. The resistivity for the a-axis sample at room temperature is over twice as high as that for the c-axis sample reflecting the Fermi surface area effect. There is no evidence of any low temperature anomaly for either sample.

The well behaved heat capacity results found for Sc by Tsang et al. (1976a, b) may be compared to the heat capacities obtained by Jennings et al. (1960) for the related elements Lu, La, and Y if the data are adjusted according to Debye

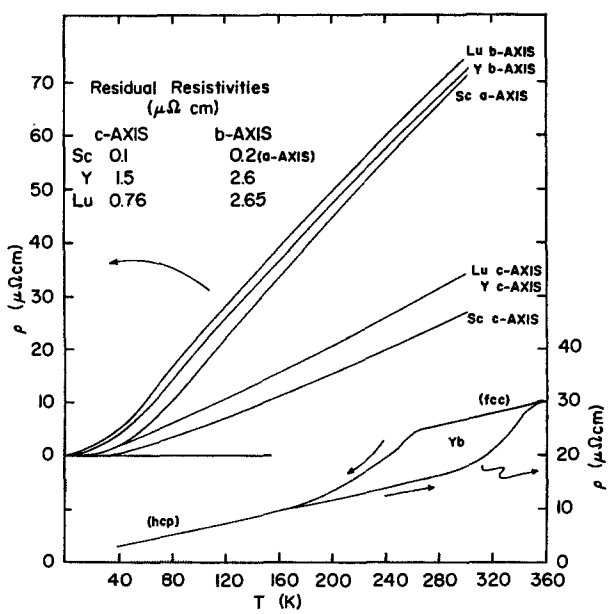

Fig. 73. Electrical resistivity versus temperature for polycrystalline Yb and for single crystals of Sc, Y, Lu. After Kayser (1970) for Yb; after Queen (1979) for Sc; after Hall et al. (1959) for Y; after Boys and Legvold (1968) for Lu.

temperatures (see fig. 26). It appears that Debye temperatures appropriate to specific heat data for Sc, Y, Lu, La and Yb are 347, 214, 166, 131, and 107 K, respectively.

4.2. Yttrium

The element Y has atomic number 39. It has the hcp crystal structure and is the trivalent element near the left end of the 4d electron transition elements of the fifth period of the periodic chart. The three conduction electrons of Y are in 5s and 4d bands and, as in the case of Sc, these bands are much like the 6s and 5d conduction electron bands of the heavy hcp rare earth metals. This close relationship makes solid solutions of Y with the rare earths possible. It also makes the purification problem difficult.

The magnetic susceptibility of single crystals of Y has been measured by Spedding and Croat (1973) with results as shown in the center section of fig. 72. The susceptibility drops only slightly with decreasing temperature in contrast with the behavior of Sc which is shown at the top of the figure and the magnitude is about a fourth of that for Sc. As in the case of Sc the a-axis susceptibility is higher than the c-axis susceptibility. The relatively sharp rise in the susceptibility below 15 K is very likely the effect of impurities in the samples. They reported 8 ppm Fe and about 10 ppm magnetic rare earth impurities. It appears that Pauli paramagnetism would account for the observed susceptibility of Y.

The electrical resistivity of single crystal Y has been reported by Hall et al. (1959). Their results are shown in fig. 73 where it may be seen that Y has higher resistivities than Sc although the anisotropy is about the same as that for Sc. The heat capacity of Y reported by Jennings et al. (1960) is essentially the same as that for Lu as shown in fig. 26 if it is scaled according to the Debye temperatures of 214 K for Y and 166 K for Lu.

4.3. Lutetium

The element Lu, atomic number 71, has the hcp structure and is the end point of the rare earth or lanthanide series. It has a full complement of 14 electrons in the 4f shell. Magnetic measurements on single crystals of Lu have been made by Spedding and Croat (1973). Their magnetic susceptibility results are shown towards the bottom of fig. 72. The data look very much like those for Y with almost no temperature dependence and with a magnitude almost exactly half that for Y for both the a-axis and c-axis results. In the case of Lu the three conduction electrons are in the characteristic rare earth 6s and 5d bands and Pauli paramagnetism of these conduction electrons accounts pretty much for the susceptibility. The difference in magnitude compared with Y is partially accounted for by the diamagnetism of the larger number of filled shells in Lu although a difference in the density of states at the Fermi level may also be a contributing factor. The slight upward turn of the susceptibility at very low

temperatures is again a likely consequence of the iron content of 17 ppm and the magnetic rare earth content of 5 ppm. Use of electrotransport methods to eliminate the Fe would be advantageous.

Results of electrical resistivity measurements on Lu single crystals as reported by Boys and Legvold (1968) are shown in fig. 73. The similarity of the Lu resistivities to those for Sc and Y is apparent in the figure and one may conclude that the Fermi surface projections must be nearly alike for all three elements. The heat capacity of Lu as found by Jennings et al. (1960) is shown in fig. 26.

4.4. Lanthanum

The forerunner to the rare earth elements is La, atomic number 57. It is normally considered to have an empty 4f shell, although some conjecture exists about the possibility of a 4f band just slightly above the Fermi level in the 6s and 5d conduction bands which are occupied by three conduction electrons. The most interesting property of La is its superconductivity with T_c of 6.17 K for the fcc form and 5.15 K for the dhcp form. The latter structure is the stable one at room temperature and is the form which is characteristic of the light rare earths. Considerable difficulty is encountered in the growing of La single crystals, and single crystal magnetic data have not been published. The results of magnetic susceptibility measurements on high quality polycrystalline La as published by Spedding and Croat (1973) are shown near the bottom in fig. 72. The susceptibility increases with decreasing temperature and crosses the curves for Lu at about 60 K. Again it is believed the rise in the susceptibility below 30 K is an impurity effect since the sample contained 6 ppm Fe and about 18 ppm magnetic rare earth elements. The electrical resistivity of polycrystalline La as reported by Legvold et al. (1977b) is shown in fig. 74. The resistivity of the dhcp allotrope is higher than that of the fcc form which contained 0.2at.% Gd to stabilize that

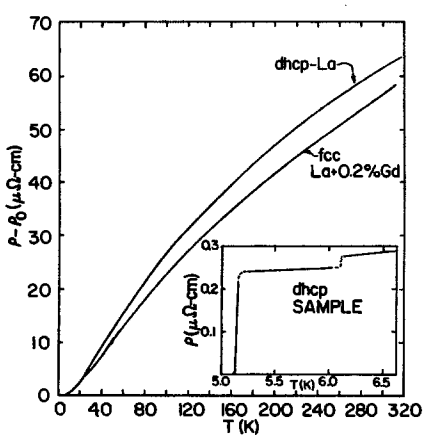

Fig. 74. Electrical resistivity versus temperature for dhcp La and fcc La alloyed with 0.2at.% Gd. After Legvold et al. (1977b).

allotrope. The insert of the figure shows the low temperature part of the dhcp sample resistivity. The small drop in resistivity at 6.17 K occurs at the superconducting transition of a small fraction of fcc crystallites in the sample while the large drop to zero at 5.15 K gives the superconducting transition temperature of the dhcp allotrope. The specific heat of La has been published by Parkinson et al. (1951) and discussed by Jennings et al. (1960). The latter found that the specific heat of La would scale to that of Lu if Debye temperatures of 131 K for La and 166 K for Lu were used.

4.5. Ytterbium

The rare earth element Yb has atomic number 70 and would normally have 13 electrons in the 4f shell. This configuration would yield $L = 3$, $S = \frac{1}{2}$ and $J = L + S = \frac{7}{2}$ for a spectroscopic designation of $^2F_{7/2}$. However, this trivalent configuration is not found in the metal because a lower energy configuration is accessible to the metal if one conduction (valence) electron migrates into the 4f shell to fill it. Hence Yb is a divalent metal with calcium-like properties. It is not highly magnetic and belongs in the class of Sc, Y, Lu, and La in this respect. The crystal structure of Yb below 270 K is hcp (α) while the fcc (β) form is stable between 300 and 1100 K. The low temperature (α) form was found and reported by Kayser (1970) and by Bucher et al. (1970). The resistivity results of Kayser are shown in fig. 73 where it is seen that considerable thermal hysteresis goes with the α–β–α transition.

Magnetic susceptibility measurements on a polycrystalline sample of Yb have been made by Queen (1979) and his results are shown as the dashed curve at the bottom of fig. 72. The problem of impurities was not serious even though analysis showed the sample contained about 30 ppm Fe and 15 ppm of magnetic rare earth impurities. No effect of a possible crystal structure change from fcc to hcp was seen. Heat capacity data for Yb have not been published.

This concludes the discussion of the magnetic properties of the pure rare earth and rare earth related elements.

5. Binary rare earth alloys

The fact that the trivalent rare earth metals (this excludes Eu and Yb) form solid solutions has made the study of a wide variety of rare earth alloys possible. The main difficulty encountered occurs when light elements which favor the dhcp crystal structure are alloyed with the heavy elements which favor the hcp structure. It is generally observed that for such mixtures of elements the samarium structure turns up in the middle concentration range.

The factors governing the ordering temperature of alloys must include electron mean free path effects according to the work of Legvold et al. (1977a). They found that (i) the saturation moments of Gd alloyed with Sc, Y, La, Lu, Mg, Yb, and Th correlated with the c/a ratio of the samples and (ii) that the ordering

temperatures did not correlate with c/a; rather, the drop in T_c (ΔT_c) was found to vary nearly linearly with sample residual resistivity. Their results are shown in fig. 75 for the excess saturation magnetic moment and in fig. 76 for the decrease in ordering temperature. Intra-heavy rare earth alloys should be relatively compatible and not suffer much from this phenomenon. A large number of such alloys has been investigated by Fujiwara et al. (1977). The ordering temperatures they obtained are shown in table 3. Their data and data of Koehler (1972) were used by Legvold (1978a) for fig. 77 which shows a plot of the ordering temperature (filled circles) *versus* average spin factor given by $C_1S_1(S_1+1)+C_2S_2(S_2+1)$. It is seen that the ordering temperatures of intra-heavy rare earths followed the straight line established by the pure elements as described earlier in fig. 4. Results on ordering temperatures for Gd–Y by Thoburn et al. (1958), for Tb, Dy, Ho, and Er–Y by Child et al. (1965), for Tb–Sc by Child and Koehler (1966), or Gd–Sc by Nigh et al. (1964) are also shown in the figure. The departure of the data for Gd–Sc, Tb–Sc, Gd–Y, and Tb–Y from the line for the elements was attributed to a combination of the two opposed effects discussed at the start of this section. One of the effects tended to raise the ordering temperature via enhanced 5d band polarization by Y, Lu, and to a smaller extent by Sc as attested by the increased surplus moment of fig. 75; the other effect, conduction electron scattering by solute atoms (see fig. 76), tended to lower the ordering temperature. The small atomic volume 15.03 cm^3/mole for Sc as compared to 19.88 for Gd, 19.86 for Y, or 17.8 for Lu makes it the most incompatible solute

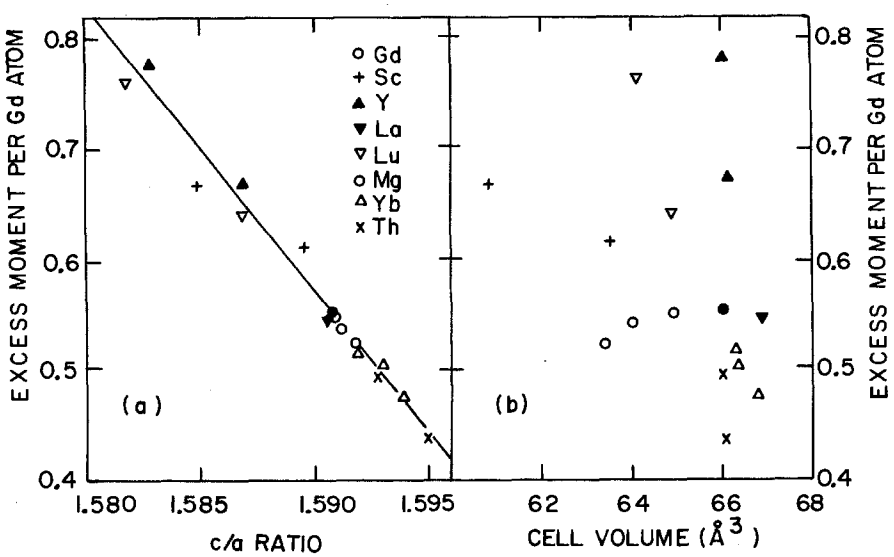

Fig. 75. (a) Excess magnetic moment per Gd atom in units of μ_B versus the unit-cell axis ratio c/a for Gd (polycrystal mother) and the Gd alloys. The symbols indicate the solute atom. (b) Excess magnetic moment per Gd atom in units of μ_B versus the unit-cell volume for Gd (polycrystal mother) and the Gd alloys. The symbols indicate the solute atom. After Legvold et al. (1977a).

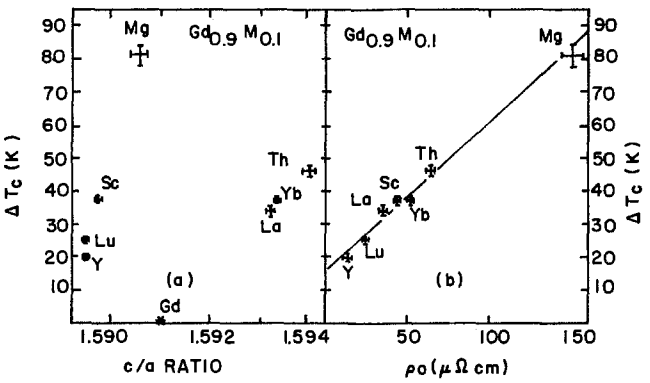

Fig. 76. (a) Depression of the Curie temperature ΔT_c of Gd alloys versus the hexagonal-lattice c/a ratio. The metal solute concentration is 0.1 for all samples as indicated by $M_{0.1}$. (b) Depression of the Curie temperature ΔT_c of Gd alloys vs. the residual resistivity. The equation for the straight line shown is $\Delta T_c = 15 + 0.46\rho_0$ in K, the dashed curve is from theory. After Legvold et al. (1977a).

and so it should lower the ordering temperature the most. In the insert of fig. 77 the residual resistivities of Gd and Tb alloyed with Y, Lu, and Sc give evidence for conduction electron scattering by these solute atoms.

The observation of Heisenberg exchange for heavy rare earth alloys prompted Legvold et al. (1979a) to reexamine the effect of spin disorder on the residual resistivity of dilute alloys. They measured the residual resistivity of one atomic percent of heavy rare earths in thorium. Results showed that the atomic volume difference between the host and the solute was a large contributor to the

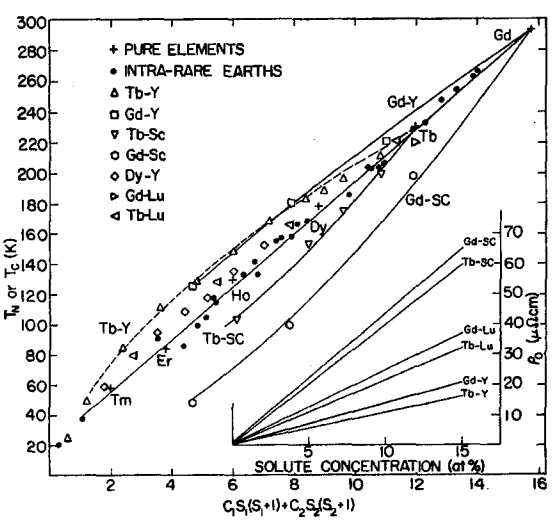

Fig. 77. Magnetic ordering temperatures for heavy rare earth alloys versus the spin factor $S(S+1)$. After Legvold (1979).

TABLE 3

Pressure effect on magnetism of heavy rare earth alloys. After Fujiwara et al. (1977)

	$\langle S(S+1)\rangle$	T_c	T_f	T_N	θ_p	$\frac{\Delta T_c}{\Delta P}$	$\frac{\Delta T_f}{\Delta P}$	$\frac{\Delta T_N}{\Delta P}$	$\frac{\Delta \theta_p}{\Delta P}$	n_{eff}	$\frac{1}{n_{eff}}\frac{\Delta n_{eff}}{\Delta P}$	Magnetic structure†
		(K)				(10^{-3} deg bar^{-1})					(10^{-6} bar^{-1})	
Gd	15.8	292.6			304	−1.56			−1.46	8.1		
Gd–50% Tb	13.9	262.4			270	−1.30				9.0		
Tb*	12			230.0	230			−0.86	−0.75	9.7	−0.96	HS
Gd–25% Dy	14	265.0			274	−1.10				8.8		
Gd–50% Dy	12.3	233.0			240	−1.00				9.5		
Gd–75% Dy	10.55		155.2	203.0	203		−1.06	−0.66	−0.51	10.2	−0.50	HS
Dy*	8.8		87.6	178.0	148		−1.28	−0.44	−0.17	10.7	−0.62	HS
Gd–25% Ho	13.35	253.8			265	−1.20				8.7		
Gd–25% Ho	10.9		172.0	206.7	213		−0.84	−0.76	−0.83	9.5	0.55	HS
Gd–75% Ho	8.95			168.6	158			−0.54	−0.40	10.1	−0.10	HS
Ho*	6.0			125.0	87			−0.40	−0.39	11.0	0.06	HS
Gd–25% Er	12.8	247.3			255	−1.05				8.4		
Gd–50% Er	9.8		171.0	184.8	200		−0.48	−0.66	−0.68	8.4	0.40	CAM
Gd–75% Er	6.8			131.8	111			−0.46	−0.72	9.4	0.60	CAM
Er*	3.8			82.0	39			−0.24	−0.53	10.2	0.34	CAM
Tb–50% Dy	10.4		150.8	204.4	201		−0.96	−0.61	−0.46	10.2	−0.80	HS
Dy–25% Ho	8.1			166.5	143			−0.42	−0.09	11.0	−0.50	HS
Dy–50% Ho	7.4			154.7	126			−0.40	−0.12	11.0	−0.30	HS
Dy–75% Ho	6.7			141.5	108			−0.40	−0.26	11.0	−0.05	HS
Dy–25% Er	7.55			156.5	126			−0.41	−0.20	10.8	−0.38	HS
Dy–50% Er	6.3			132.2	94			−0.38	−0.32	10.6	−0.05	HS
Dy–75% Er	5.05			103.4	63			−0.30	−0.48	10.4	0.15	HS
Ho–25% Er	5.45			113.5	73			−0.35	−0.46	10.9	0.15	HS
Ho–50% Er	4.9			98.6	54			−0.34	−0.56	10.7	0.28	HS
Ho–75% Er	4.35			84.6	42			−0.28	−0.55	10.4	0.30	HS
Tm	2.0			58	−17					9.9		CAM

† HS = Helical screw structure, CAM = c-axis modulated.

* H. Fuji, 1969, J. Sci. Hiroshima University, ser. A-II 33, 43.

observed residual resistivity. This led them to reexamine the data of Mackintosh and Smidt (1962) for heavy rare earths dissolved in Lu; when these results were adjusted for the volume effect the spin only residual resistivity was found to be proportional to $S(S+1)$. This outcome was explained classically by calculations which showed that the transit time of a conduction electron across a 4f function range (~ 1 Å) was $\sim 10^{-16}$ s, a value too short compared to the 10^{-14} s 4f spin precision time around J (the total 4f angular momentum) for the conduction electron to sample just the component of S along J, i.e., $(g-1)J$.

In an earlier study of a large number of hcp binary alloys Bozorth (1967) found that the magnetic ordering temperatures were proportional to the two-thirds power of the average de Gennes factor of the alloys. (He did not show a plot versus the average spin factor.) His results are shown in fig. 78 where it is seen again that the alloys of Gd with Sc and Tb with Sc depart from the universal $G^{2/3}$ factor dependence. The theoretical basis for the unexpected de Gennes factor dependence and the departure of the Sc alloys from the universal curve has been discussed by Lindgård (1977), who attributes the observed results to concentration dependent exchange interactions and to variations in the conduction electron density of states at the Fermi level as one goes across the series of elements. In table 4 the parameters found to be appropriate by

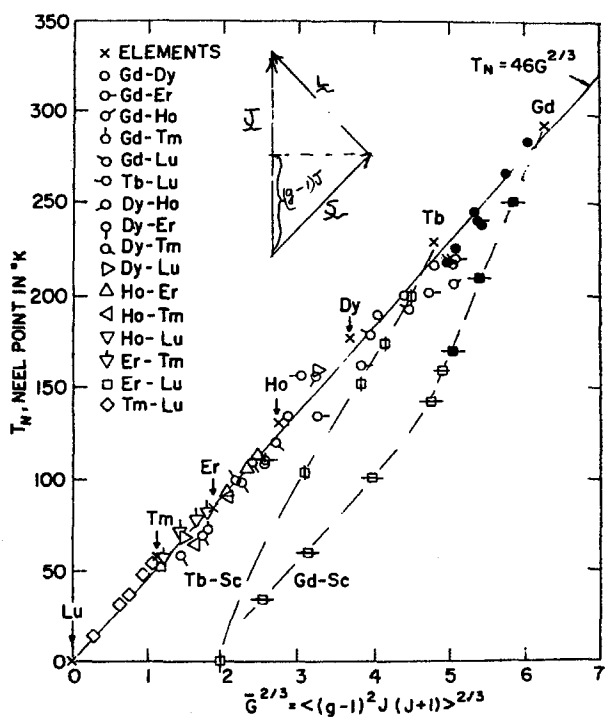

Fig. 78. Magnetic ordering temperature of intra-rare earth alloys versus the two thirds power of the average de Gennes factor. After Bozorth (1967).

TABLE 4

First the basic physical properties of the elements composing the various alloys are given. Next come the effective matrix elements j_{df} deduced in the present analysis and the corresponding averaged electrons generalized susceptibilities $\bar{\chi}_N(Q)$ and $\bar{\chi}_c(0)$. As described in the text the values are normalized with respect to the Gd values. The total density of states at the Fermi energy $\rho(\epsilon_F)$, calculated from the APW energy bands, is shown for comparison. A is a simple crystal-field correction. The crystal-field parameters B_1^0 are given below, in the complete crystal-field calculations the B_2^0 derived from $\Delta\theta$ for the pure elements have been used (after Lindgård 1977)

	Gd	Tb	Dy	Ho	Er	Tm	Lu	Y	Sc	Comments
4f electrons	7	8	9	10	11	12	14	0	0	
V (cm^3/mol)	19.91	19.30	19.03	18.78	18.49	18.14	17.79	19.95	15.04	See table 1
$r = c/a$	1.5910	1.5800	1.5732	1.5702	1.5692	1.5700	1.5832	1.5711	1.5921	See table 1
j_{df}(eV)	0.049	0.051	0.051	0.051	0.049	0.050	0	0	0	
$\bar{\chi}_c(Q)\left(\frac{\text{states}}{\text{eV}}\right)$	1.71	2.06	2.29	2.76	3.00	2.67	3.02	3.02	1.7	Lindgård (1977)
$\bar{\chi}_c(0)\left(\frac{\text{states}}{\text{eV}}\right)$	2.0	–	–	–	–	–	–	2.50	1.0	
$\rho(\epsilon_F)\left(\frac{\text{states}}{\text{eV}}\right)$	2.1	2.0	2.0	–	1.8	–	1.9	3.9	2.5	Band calculation Liu et al. (1971), Lindgård (1976) and Keeton and Loucks (1968)
$\rho_{exp}\left(\frac{\text{states}}{\text{eV}}\right)$	2.0	2.4	–	–	–	–	3.7	4.4	4.4	From C_v relative to Gd, Wells et al. (1975), (1976) and Gschneidner et al. (1978)
A (K)	0	15	16	5	13	45	–	–	–	
B_2^0(K)	0	0.90	0.63	0.17	−0.39	−1.40	–	–	–	From $\theta_{p\parallel} - \theta_{p\perp}$, Koehler (1972) p. 81; Tb, Ho by Hansen and Lebech (1976)
B_2^0(K)	0	1.04	0.65	0.23	−0.26	−1.04	–	–	–	Dilute Y alloys, Høg and Touborg (1974)
$B_4^0 \times 10^4$ (K)	0	8.61	−4.03	−2.26	3.02	11.1	–	–	–	–
$B_6^0 \times 10^5$ (K)	0	−1.52	1.04	−1.77	2.82	−7.62	–	–	–	–

Lindgård for the heavy rare earths are listed. The j_{df} of the table is the I_{exch} of eq. (5) and it is of high interest to note it is nearly constant across the series of hcp elements shown. There is a considerable spread in the calculated and experimental conduction electron density of states at the Fermi level for Lu, Y, and Sc. It should be noted that the ordering temperatures for the pure elements fall close to the universal curve in fig. 78.

A wide ranging series of alloys of La containing small concentrations of rare earths has been investigated in studies of their effect on the superconducting transition temperature of La. One study by Legvold et al. (1977b) showed that the interatomic electron 4f wave function overlap with the 5d wave functions would explain why one atomic percent trivalent Gd in La would depress T_c twice as much as an equal amount of divalent Eu even though both solutes had seven 4f electrons. In another study Legvold et al. (1978) found the dependence of the superconducting transition temperature of La was not a linear function of the de Gennes factor of the solute. Their double butterfly diagram of the superconducting transition temperature of fcc and dhcp La containing one atomic percent rare earth solutes is shown in fig. 79 and their plot of T_c versus the de Gennes factor and versus $S(S+1)$ is shown in fig. 80. Since the conduction band is essentially fixed here, the localized exchange interaction for each element will probably have to be calculated carefully to bring about agreement between experiment and theory.

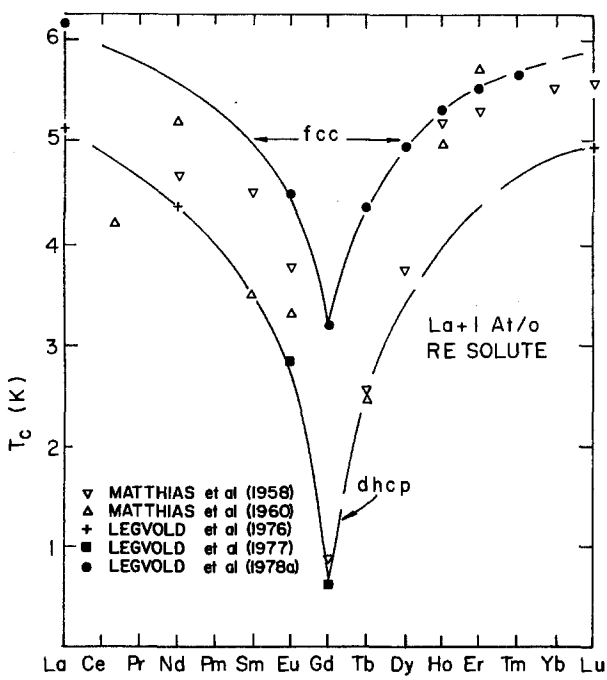

Fig. 79. Double butterfly plot of the superconducting transition temperature T_c versus rare earth element in the sequence of nominal number of 4f electrons. After Legvold et al. (1978).

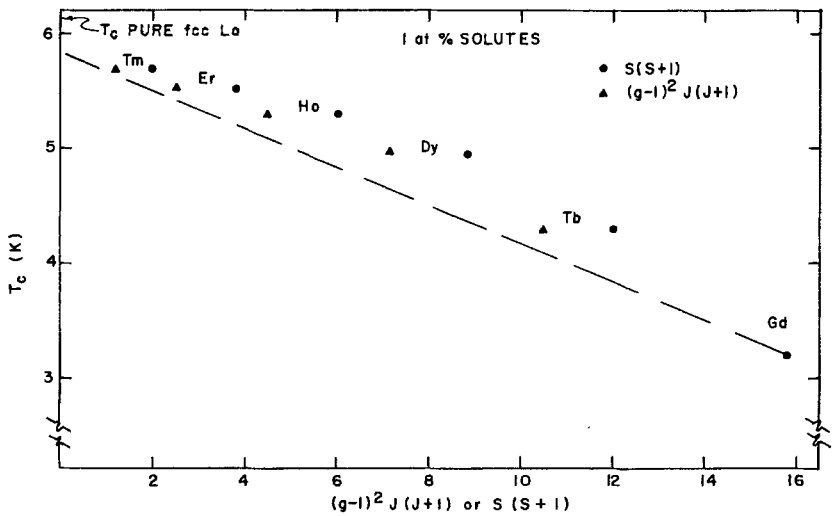

Fig. 80. Superconducting transition temperature versus the spin factors $S(S+1)$ and $(g-1)^2J(J+1)$ for 1at.% of heavy rare earth metals in fcc La. After Legvold et al. (1978).

A survey of much of the binary alloy work on the individual elements is given next.

5.1. Eu base alloys

Since Eu oxidizes rapidly it is not an easy element with which to work. Also it is divalent, belongs in the calcium family, and does not alloy readily with the other rare earths save for Yb which is also divalent.

The magnetic properties of Eu alloyed with Yb have been investigated by Legvold and Beaver (1979). The alloys contained 10 to 40at.% Eu and had the fcc form which is the room temperature form for Yb (Eu has the bcc structure). The isofield data they obtained for the 40 atomic percent Eu sample are shown in fig. 81. There is a peak in the magnetic moment which is interpreted as a Néel point marking the onset of a low temperature antiferromagnetic structure. The slope of the $1/\chi$ versus T plot shown gave a paramagnetic moment of $8.9\mu_B$ per Eu atom as compared to the expected $7.94\mu_B$ and the paramagnetic Curie temperature was 14 K. At lower Eu concentrations the magnetization curves gave indications of ferromagnetism in the samples in the low temperature regime. An example is shown in fig. 82 which shows the isothermal magnetization data for the $Eu_{0.2}Yb_{0.8}$ sample. From plots of σ^2 versus H/σ it was possible for them to obtain Curie temperatures for several of the samples. A plot of their Curie temperatures and Néel (isofield peak) temperatures is shown in fig. 83. A dashed curve is shown extending from the Néel points of the samples studied up to the Néel point of Eu. The dot–dash curve for θ_p extending out from 40% Eu is an estimate of the behavior leading down to the θ_p of -3.2 K

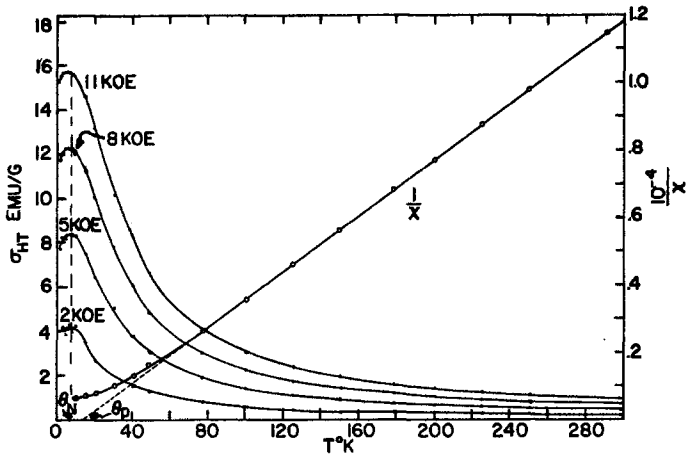

Fig. 81. Isofield magnetization data for 40at.% Eu in Yb. After Legvold and Beaver (1979).

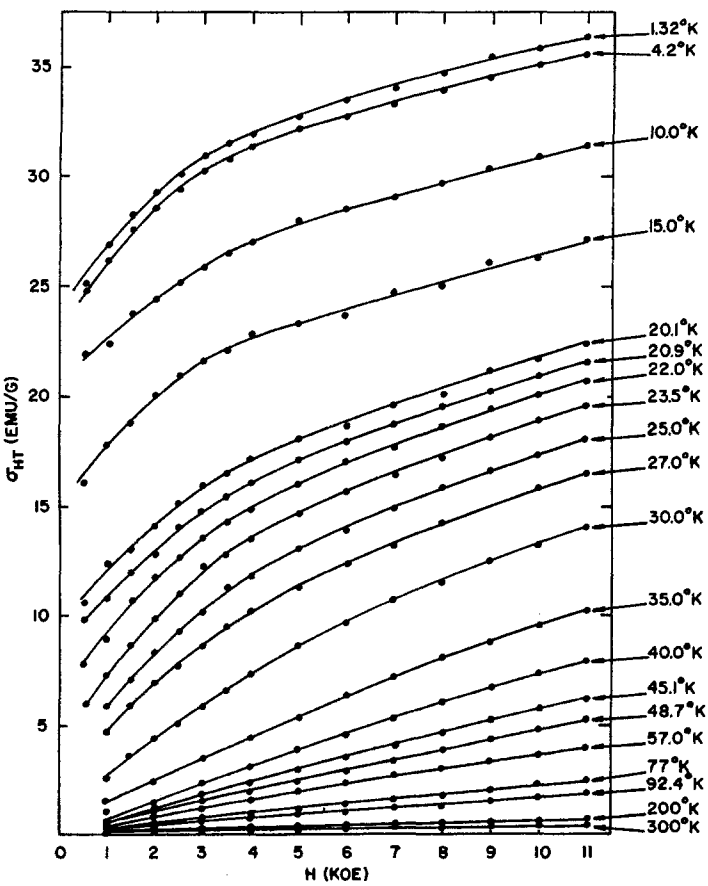

Fig. 82. Magnetization isotherms for 20at.% Eu in Yb. After Legvold and Beaver (1979).

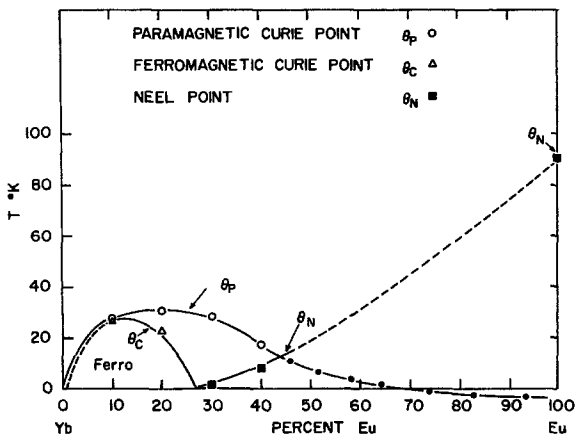

Fig. 83. Magnetic phase diagram for Yb–Eu alloys. After Legvold and Beaver (1979).

found for Eu from the susceptibility data between 300 and 400 K of Colvin et al. (1961).

5.2. Gd base alloys

A large number of binary alloy investigations involving Gd have been completed. The magnetic properties of Gd–Y and Gd–La alloys were reported by Thoburn et al. (1958). Data on Gd–Sc were reported by Nigh et al. (1964) and similar work on a few samples of Gd–Lu were employed in the study by Legvold et al. (1977a) described at the start of this alloys section. The results of these studies are shown in fig. 84. Alloys of Gd with Sc, Lu, and Y give ordering temperatures which are much alike. The data for La are quite different with a good part of the difference accounted for by the onset of the samarium crystal structure at a concentration of about 16at.% La. This difficulty holds for alloys of Gd with the light rare earths so these are not the simple solid solution type. The point of intersection of the curve for the ferromagnetic ordering temperature with the curve for the Néel points gives a potential Lifshitz point because the generalized susceptibility here has a true maximum at $Q = 0$ (ferromagnetism). The precipitous drop in the Curie temperature above the Lifshitz point concentration is a consequence of the generalized susceptibility dependence on the q vector. In the detailed magnetic phase diagrams a variety of critical points will be seen. Theoretical work on the magnetic properties expected for samples in the vicinity of such points has been reviewed by Hornreich (1979). There is some work reported by Mukamel and Krinsky (1976a, b), by Bak and Mukamel (1976), by Lindgård (1977) and by Redner and Stanley (1977). Figure 85 shows the results of a detailed study by Legvold et al. (1979b) of the Gd–Y system near 31 at.% Y. It is seen that the highest ordering temperature has a 5 K gap or drop at the changeover from ferromagnetic to helical ordering, apparently in this system the net magnetic interaction is ferromagnetic at high temperatures. Then, as the temperature is

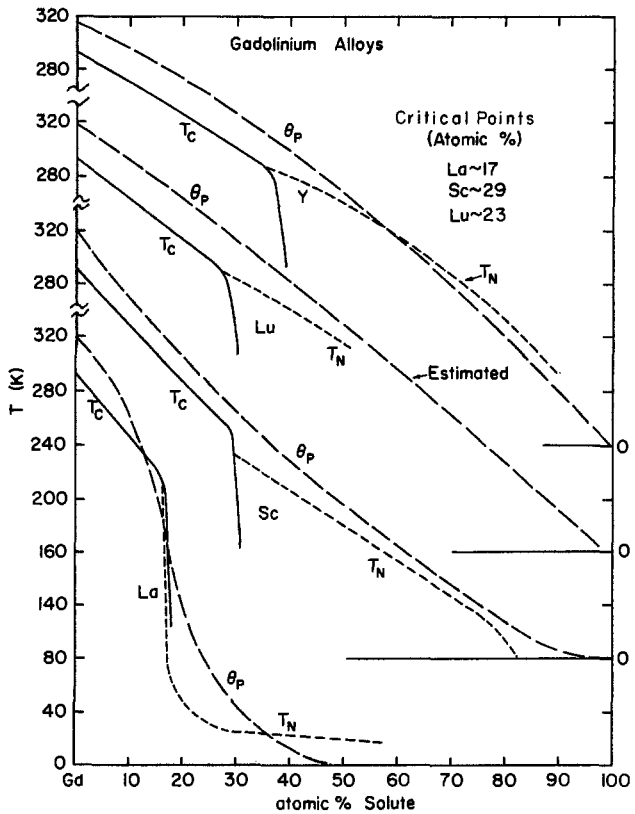

Fig. 84. Magnetic phase diagrams for Gd alloyed with Y, Lu, Sc, and La. After Thoburn et al. (1958) for Gd–Y and Gd–La; after Legvold et al. (1977a) for Gd–Lu; after Nigh et al. (1964) for Gd–Sc.

lowered the antiferromagnetic interaction (possibly the next nearest neighbor part) overtakes the ferromagnetic interaction (possibly the nearest neighbor part) and this automatically suppresses the highest ordering temperature. It appears that this alloy system shuns the Lifshitz requirements. This suggests that all systems should be explored near the critical concentration.

Magnetic data of Fujiwara et al. (1977) for Gd alloyed with Tb, Dy, Ho, and Er have been given in table 3, where the pressure dependence of the ordering temperatures as well as the ordering temperatures themselves are shown. The latter have been useful in the preparation of phase diagrams for heavy rare earth alloys of Gd as shown in fig. 86. The phase diagram for Gd alloyed with Tb is at the top of the figure. Data came from table 3 and from Burgardt and Legvold (1978). The diagram consists of the ferromagnetic phase below the T_c (Curie temperature) curve extending from 293.4 K for pure Gd across to 219.5 K for pure Tb. Paramagnetism exists above the T_c curve out to 94% Tb and 230 K, the Lifshitz point, and then above the dashed T_N curve which extends from this point to 23 K at 100% Tb. The dashed curve also marks the upper boundary of the triangular shaped helix structure region associated with pure Tb from 230 K

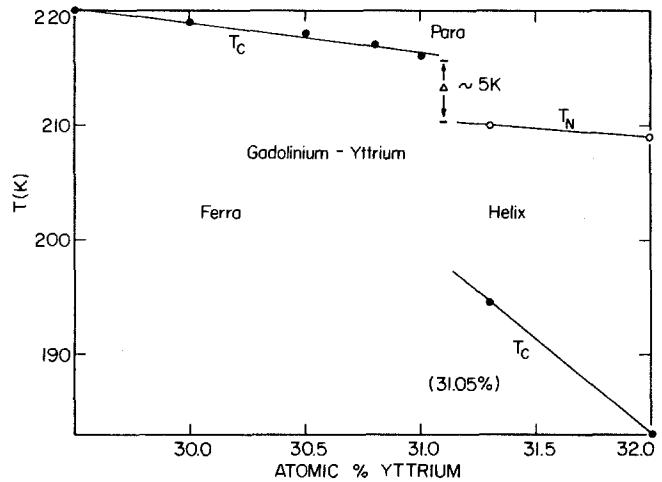

Fig. 85. Enlarged magnetic phase diagram for Gd alloyed with Y showing the temperature gap of 5 K near 31at.% Y. After Legvold et al. (1979b).

down to 219.5 K. Next from the top in fig. 86 is the Gd–Dy phase diagram which is just like that for Gd–Tb. The data of Fujiwara et al. (1977) given in table 3 were used in the drawing. The diagram shows ferromagnetism below the T_c curve which extends from 293.4 K for pure Gd across and down to 85 K for pure Dy. The T_N dashed line from the 225 K, 50% Lifshitz point to 179 K marks the upper boundary of the triangular helix region.

A displaced (downward) temperature scale has been used to avoid confusion for the other phase diagrams of fig. 86. For Gd–Ho the phase diagram is the third from the top in the figure and begins to show some complications at the Ho rich end. Data for the figure come from Fuji et al. (1976) as well as from Fujiwara et al. (1977) as shown in table 3. The T_c curve extends from the 293.4 K T_c point for pure Gd out to about 70% Ho where confusion sets in; Fuji et al. (1976) show the line extended along the dotted portion to the cone region but Fujiwara et al. show no T_c for 75% Ho. It must be concluded that samples show inhomogeneous magnetic behavior from 70% to 90% Ho. Even so, T_N is observable all the way from the 245 K, 25% Ho Lifshitz point out to the 132 K Néel point of pure Ho. Below the dashed T_N line the helix magnetic structure exists down to the questionable region below about 80 K. The ferromagnetic cone structure region extends from about 85% Ho up to pure Ho.

The phase diagram for Gd–Er as given by Fuji et al. (1976) shows much greater complexity to the right of the 36% Er, 206 K Lifshitz point. Apparently the single ion anisotropy of Er makes it magnetically incompatible with the elements Gd and Tb. It can be seen that the Lifshitz point marks the start of a region of unknown magnetic structure designated by the question mark. For Er concentrations from 60% to 100% a c-axis modulated (CAM) plus helix structure exists over a fairly large region and the CAM only phase of pure Er extends over a small triangular region back to 13% Gd (or 87% Er). Below 40 K a rather large

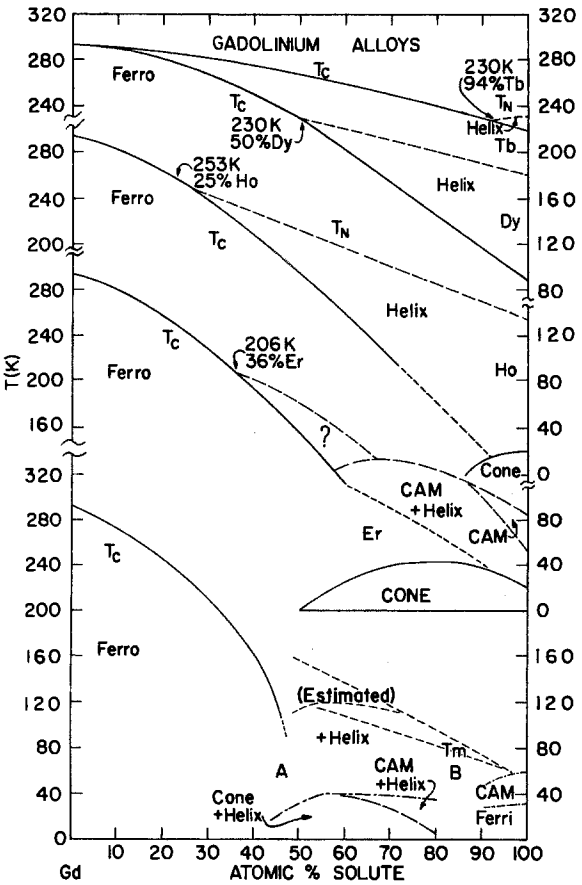

Fig. 86. Magnetic phase diagrams for Gd alloyed with Tb, Dy, Ho, Er and Tm. After Fujiwara et al. (1977) and Fuji et al. (1976) with some data for Gd–Tb after Burgardt and Legvold (1978).

region of conical ferromagnetism extends from 50% Er out to 100% Er. At 75% Er a region of inhomogeneous magnetic structure (apparently an unstructured system) extends from 40 K up to about 80 K. The structure there is not ferromagnetic because Fujiwara et al. (1977) did not report a T_c for the 75% Er sample.

The phase diagram for Gd–Tm at the bottom of fig. 86 is a tentative educated guess formulated in the absence of published data by extrapolation from the Gd–Er diagram and by incorporation of the changes suggested by the Tb–Er and Tb–Tm diagrams which have been published and which appear later here. The T_c curve extends out and downward from the T_c of 293.4 K for pure Gd and terminates near 45% Tm at the region (marked A) of inhomogeneous magnetic structure (perhaps amorphous like – or spin glass like) like that observed in Tb–Tm. There is likely a small cone plus helix region at low temperatures which extends from about 45% Tm out to 80% Tm where the magnetically inhomogeneous area B exists. A small CAM plus helix region is shown from 60 to

80% Tm. Also the CAM and ferrimagnetic phases of pure Tm must extend into the dilute Gd in Tm regime as shown.

Several papers on Gd alloyed with the light rare earth elements have appeared. In general the magnetic phase diagram for these alloys is like the diagram for Gd–La (fig. 84) with small changes in the concentration and temperature at the Lifshitz point. The concentration of solute at which the crystal structure changes from hcp to the Sm form also varies in about the same manner. Tissot and Blaise (1970) found that 7.3at.% of Pr in Gd had the hcp structure and was ferromagnetic with a Curie temperature of 254 K and that the Sm structure occurred for concentrations greater than 19.6at.% Pr. Magnetic measurements were not definitive at the higher concentration; for samples with more than 50at.% Pr there was no magnetic ordering down to 2 K. The magnetic moment of a hcp single crystal of 9at.% Pr alloyed with Gd was measured by Legvold et al. (1977c). They obtained a saturation moment of $6.63\mu_B$ at 4.2 K. This result compared favorably with the $6.60\mu_B$ obtained under the assumptions (i) that the saturation moment of the mother Gd stock was $7.55\mu_B$, (ii) that the magnetic moment of Pr has $3.2\mu_B$ per atom; and (iii) that the spins coupled parallel to each other so that the magnetic moments were opposed to each other. They observed further that at 4.2 K the easy direction of magnetization was along the *b*-axis and that there was a jump in the magnetization of the *c*-axis sample at an applied field value of 16 kOe which gave a measure of the anisotropy.

Magnetic measurements by Fujimori et al. (1974) on hcp Gd–Nd and Gd–Sm alloys showed that these alloys were very much alike and that the ferromagnetic Curie temperature dropped steadily from 293.4 K for pure Gd down to about 200 K at 25at.% Sm. Samples in the 30 to 50at.% solute range of Gd alloyed with La, Ce, Pr and Nd were rapidly quenched from the molten state by Speight (1970) who found they had the hcp structure with magnetic properties about like those one might extrapolate from the dilute hcp regions. His slowly cooled samples had the Sm structure and in an applied field of 8.4 kOe he found about 10 emu moment/gram for Gd with 30% Ce at 4.2 K, about half this for 35% Pr or 50% Nd. The latter two had broad peaks suggestive of Néel like behavior at about 12 K.

5.3. Tb base alloys

Since Tb has a Néel point at 230 K and then becomes ferromagnetic at 219.5 K the magnetic phase diagrams for Tb have a different appearance from those for Gd. At the top of fig. 87 the behavior of Tb alloyed with Pr, and La and with the tetravalent metal thorium is shown. The Nd and Pr alloy data were published by Curry and Taylor (1976). The La and Th data were obtained by Burgardt (1976). In all four cases the helical structure is eliminated when the concentration is high enough to reach the Lifshitz point. On the basis of susceptibility measurements of Speight (1970) on Tb–Pr and Tb–Ce alloys it is possible to conclude that the phase diagram for Tb–Ce would be like that for Tb–Pr in fig. 87. It is most interesting that such a small percent of Th should have such a strong effect. The

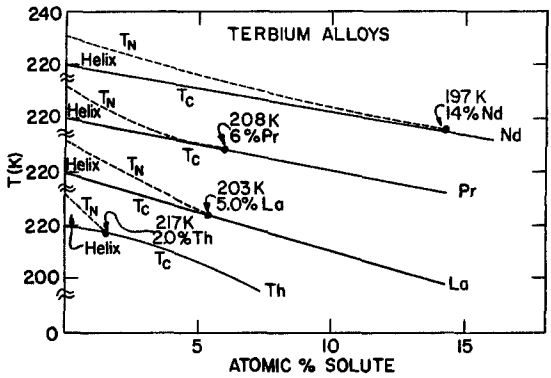

Fig. 87. Partial magnetic phase diagrams for Tb alloyed with Nd, Pr, La, and Th. After Curry and Taylor (1976) for Tb–Nd and Tb–Pr; after Burgardt (1976) for Tb–La; after Burgardt and Legvold (1975) for Tb–Th.

nesting feature of the Fermi surface for Tb is highly sensitive to an increased number of conduction electrons and explains this result. At higher concentrations of the light elements with Tb there is a change to the Sm type crystal structure which brings about large changes in the magnetic properties. In a neutron diffraction study at higher Pr concentration Curry et al. (1977) found that Tb_{55}–Pr_{45} had the Sm crystal structure, that the magnetic moment structure was helical at 4.2 K and that the turn angle was 60°. They also found that Dy and Ho alloyed with Pr and with Nd had zero magnetic moments on cubic site layers (recall the Sm magnetic structure) while moments on adjacent hexagonal site layers were parallel and in the basal plane; alternate pairs of hex site planes had antiparallel moments. They interpreted the latter results in terms of two contra-rotating helices with 60° turn angles on each helix.

In samples of 20% Pr in Tb and 25% Nd in Tb Achiwa and Kawano (1973) found that a martensitic transformation from the Sm structure to hcp took place at very low temperatures and that ordering was ferromagnetic in the hcp phase. Speight (1970) obtained hcp for such alloys by quenching from the molten state.

The magnetic ordering temperatures of Tb alloyed with the non-magnetic trivalent elements Y, Lu, and Sc are shown in fig. 88. For this figure most of the data were obtained through use of neutron diffraction by Child et al. (1965) for Y and Lu solutes and by Child and Koehler (1966) for Sc solutes; some low concentration solute data of Burgardt (1976) have also been used in the diagram. For all three solutes the helical structure is stabilized relative to the ferromagnetic structure. In fact some twenty to twenty five atomic percent of these solutes is sufficient to wipe out the ferromagnetic phase.

The magnetic phase diagrams for Tb alloyed with heavy rare earths are shown in fig. 89. As in the case of Gd the successive diagrams get more complicated. The data of Fujiwara et al. (1977) for Tb with 50% Dy established the plots of T_N and T_c for Tb–Dy which form a textbook example phase diagram with a linear change with alloying across the whole concentration range from one element to

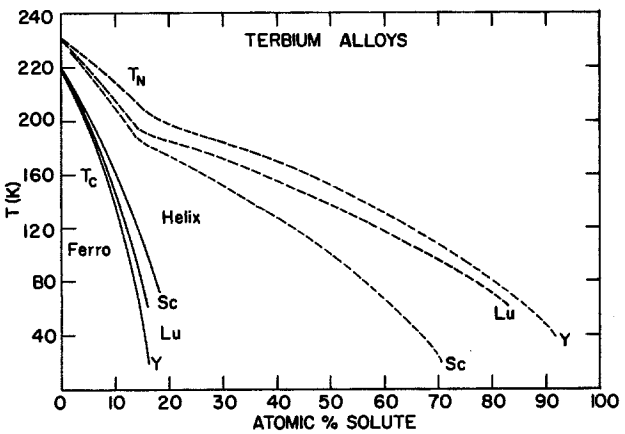

Fig. 88. Magnetic phase diagrams for Tb alloyed with Y, Lu, and Sc. After Child et al. (1965) and Child and Kœhler (1966).

the other. The data of Koehler (1972) for Tb–Ho and Tb–Er are shown in the middle of fig. 89. In the case of Tb–Ho the Néel points T_N go linearly from one element to the other but the curve for T_c has to reflect the fact that the planar ferromagnetic phase of Tb has to suffer a marked change to arrive at the low temperature conical ferromagnetic structure of Ho. The out of plane ferromagnetic phase observed at high Ho content at low temperatures seems to be in order. In a recent study of a Tb–50% Ho study Isci and Palmer (1977) found ordering temperatures in excellent agreement with those shown in the figure. The ordering temperatures found by Spedding et al. (1970) for several Tb–Ho samples are in good agreement with the results given here.

The magnetic phase diagram for Tb–Er is more complicated than that for Tb–Ho because of the difference in 4f charge densities and consequent single ion anisotropies of the constituent metals. The T_N data fall on a relatively smooth curve across the system out to about 90at.% Er where complications arise. The planar helix structure of Tb has to compete with the c-axis modulated (CAM) structure of Er. At low temperatures the conical structure shown for Er content above 50at.% involves Tb moments on a cone with an angle from the c-axis of the order of 80–85° and the Er moments on a cone with an angle from the c-axis of about 30°, according to an interpretation of NMR data of Sano et al. (1975). The diagram shows a CAM plus helix region between 80 and 100% Er and a small region where the Er CAM structure alone is found. Sherrington (1973) has suggested that the Er rich alloys may favor a tilted helix or tilted cone magnetic structure.

The magnetic phase diagram for Tb–Tm published by Hansen and Lebech (1976) is shown at the bottom of fig. 89. The T_N curve extends out to 75% Tm (to the vicinity of area marked B) where difficulties relating to finding magnetic order are encountered. In a similar fashion the curve for T_c extends rapidly downward from 219.5 K for pure Tb so that planar ferromagnetism disappears

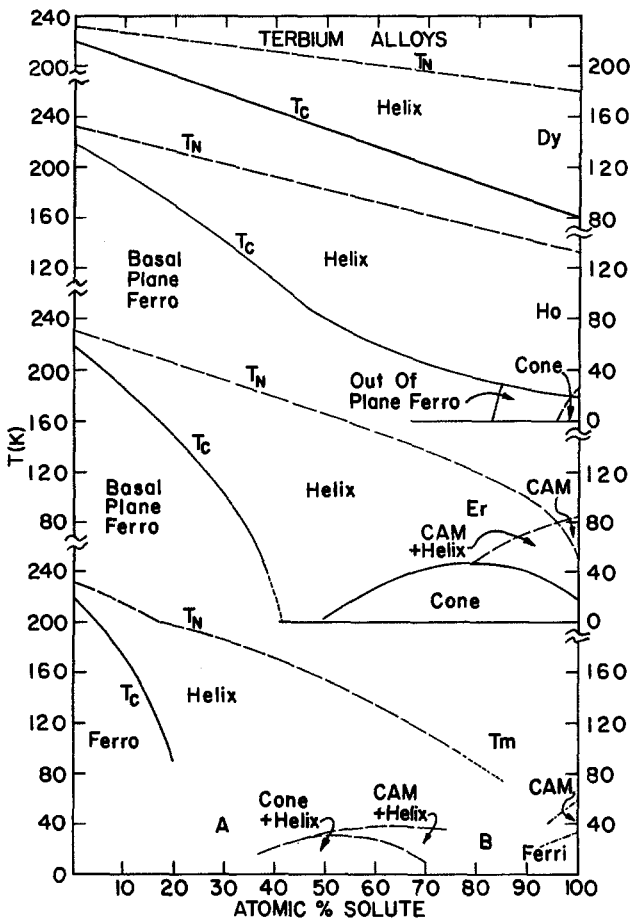

Fig. 89. Magnetic phase diagrams for Tb alloyed with Dy, Ho, Er and Tm. After Koehler (1972) for Tb alloyed with Dy, Ho, Er. After Hansen and Lebech (1976) for Tb–Tm alloys.

for concentrations of Tm higher than 20%, which is close to the magnetically inhomogeneous area marked A. At low temperatures a double cone plus helix phase (Tm varies from 9° to 13° from the c-axis and Tb varies from 86° and up) is found which extends from about 35 to 70at.% Tm with a very small adjacent area in which the CAM plus helix magnetic structure is found. There are also small regions at the Tm rich end in which the CAM and ferrimagnetic phases of Tm are found.

5.4. Dy base alloys

As in the case of Tb the element Dy has helical and planar ferromagnetic phases. However, the Néel point T_N and Curie temperature T_c are more widely separated and this affects the appearance of the magnetic phase diagrams in

which the helix is dominant. At the top of fig. 90 the magnetic phase diagram for Dy alloyed with Ho is shown as determined from the data of Fujiwara et al. (1977) and of Koehler (1972). The Néel point data fall on a line from 179 K for Dy down to the 132 K point for Ho. A small region on the lower left shows the planar ferromagnetic phase of Dy and a small area on the lower right shows the conical ferromagnetic phase of Ho which extends out to the left to about 10at.% Dy in Ho.

Next on the figure is the diagram for Dy alloyed with Er. The data are again from the work of Koehler (1972) modified to accommodate the results of Fujiwara et al. (1977). The T_N data fall on a line extending from 179 K for Dy toward the 85 K Néel point of Er with a departure from the line at 90at.% Er

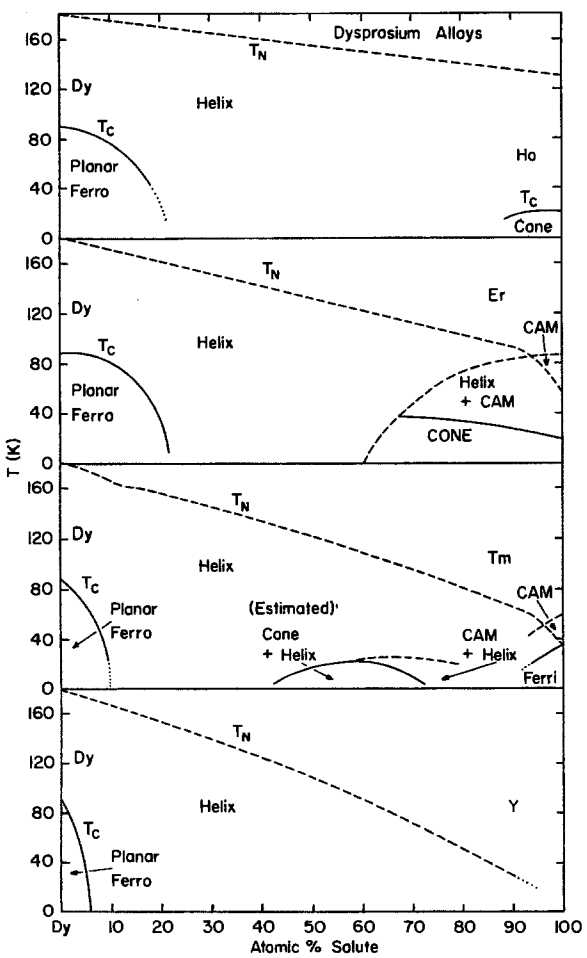

Fig. 90. Magnetic phase diagrams for Dy alloyed with Ho, Er, Tm, and Y. After Koehler (1972) and Fujiwara et al. (1977) for Dy alloyed with Ho, Er and after Child et al. (1965) for Dy–Y.

where the c-axis modulated moment phase of Er takes precedence over the helix favored by Dy. At the lower left of the diagram the planar ferromagnetic phase of Dy is again found. On the lower right of the diagram there is a region where the helix plus CAM coexist and a region at low temperatures where the stable magnetic structure is the conical ferromagnetic phase (a double cone phase with Er moments on one and Dy moments on the other).

Data on Dy–Tm alloys are unavailable so an attempt has been made to show what might be expected on the basis of the Tb–Tm phase diagram and the general patterns for these systems which seem to emerge. The estimated phase diagram shows T_N going nearly linearly from the Dy Néel point to the 58 K Néel point of Tm with a slight change at the Tm rich end where the CAM phase of Tm takes over. A smaller region of planar ferromagnetism at the lower left is compatible with the trend from Er to Tm to Y in the Tb phase diagrams. A small CAM plus helix region at low temperatures is postulated at the middle concentrations because this phase is found in the Tb–Tm diagram. Then on the lower right the CAM and ferri phases of pure Tm should be expected to carry over to about 10% of Dy in Tm.

At the bottom of fig. 90 is the Dy–Y magnetic phase diagram based on data of Child et al. (1965). The Néel point curve is slightly concave downward and heads toward zero for Y. The planar ferro region is estimated but is probably close; there was a sample at 5at.% Y in Dy for which the T_c point was not seen. This set the right hand limit for the planar ferro phase which certainly exists for small Y concentrations.

5.5. Ho base alloys

The phase diagram for Ho alloyed with Er, published by Koehler (1972), is shown at the top of fig. 91. The Néel point curve extends from 132 K for pure Ho and is slightly concave upward as it approaches the 85 K ordering temperature at the Er end of the diagram. The Er rich end at high temperatures has the c-axis modulated phase starting at about 80% Er. Then there is the mixed region of the helix plus the CAM form, and these have different ordering temperatures. Even so the helix form favored by Ho dominates the diagram. All across the bottom of the phase diagram it is seen that the cone structure exists. Since both Ho and Er have conical phases at low temperatures this feature was not unexpected. It is interesting that the T_c for the conical ferro phase reaches a value almost twice as high as for either one of the pure elements at the concentration midpoint.

Metallurgy difficulties with Tm leaves the Ho–Tm phase diagram to the best estimate approach which is found in the middle of fig. 91. There is little doubt about the position of the T_N line on the basis of the other diagrams but the cone and ferri phases at low temperature are probably in error. The compatibility of Ho and Er suggests that Ho and Tm might give the cone range shown. The CAM and CAM plus helix phases on the lower right of the diagram seem reasonable when Ho–Er and Ho–Tm are compared.

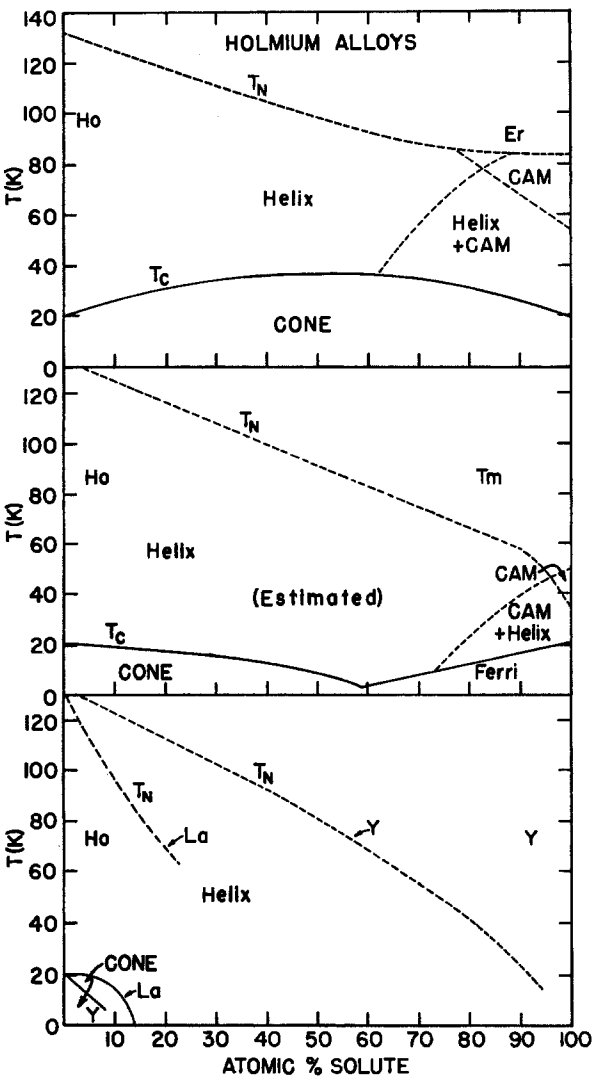

Fig. 91. Magnetic phase diagrams for Ho alloyed with Er, Tm and Y. After Koehler (1972) for Ho–Er, after Child et al. (1965) for Ho–Y, and after Kawano and Achiwa (1975) for Ho–La.

The Child et al. (1965) data for Ho–Y alloys are shown at the bottom of fig. 91. Outside the broad helix region only a small pocket of a conical ferromagnetic structure at the lower left of the diagram is proposed in the absence of data there. Also shown in the lower part of the figure are data of Kawano and Achiwa (1975) for Ho–La alloys. The curve for T_N drops more precipitously for the La alloys than for the Y alloys. The T_N and T_c points for Ho–Ce alloys are nearly coincident with those for Ho–La alloys up to 16at.% Ce, according to Kawano and Achiwa (1974).

5.6. Er base alloys

Since all of the earlier heavy elements have been discussed, only Er–Tm in that category remains. An estimate of the phase diagram for this system is shown at the top of fig. 92. The Néel temperature will most likely follow a nearly linear curve from the 85 K point of Er to the 58 K point of Tm as shown. A CAM plus helix region characteristic of Er at the lower left along with an extended cone region are conceivable. The conical phase has to merge with the ferrimagnetic phase characteristic of Tm at the Tm rich end.

At the bottom of fig. 92 the magnetic phase diagram for Er alloyed with Y is given as determined from the data of Child et al. (1965). The regular T_N curve which extends from the 85 K point for Er extends downward and heads toward zero for pure Y as should be expected. Just below T_N is the c-axis modulated phase of pure Er which borders the CAM plus helix of the basal plane components. A small cone phase characteristic of pure Er is shown at the lower left.

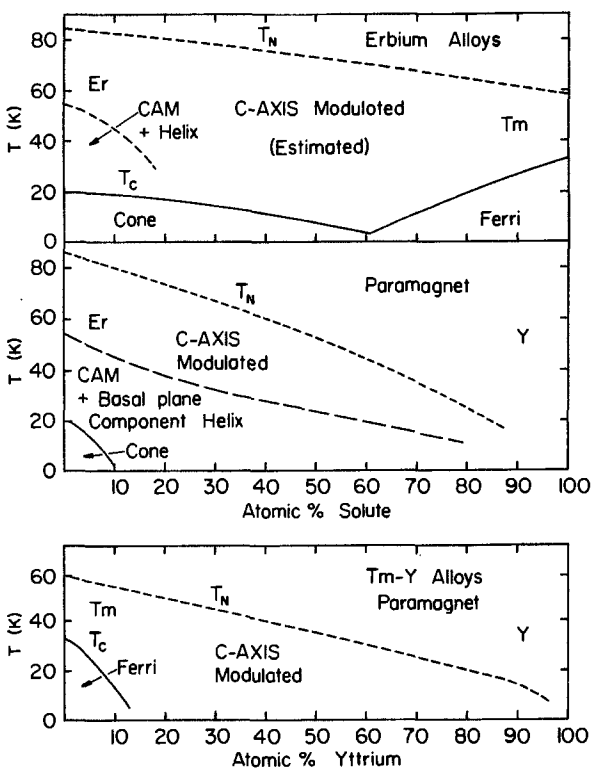

Fig. 92. Upper part: magnetic phase diagrams for Er alloyed with Tm and Y. After Child et al. (1965) for Er–Y. Lower part: magnetic phase diagrams for Tm alloyed with Y. After Child et al. (1965).

5.7. Tm base alloys

The only Tm base alloy left for display is the Tm–Y diagram shown at the bottom of fig. 92. It is based on data of Child et al. (1965) on 45% Y in Tm and 85% Y in Tm. The Néel points follow a linear pattern and tend toward zero for pure Y. Shown at the lower left is a smaller pocket of the ferrimagnetic phase of pure Tm which is expected to exist for Y concentrations up to about 10%.

All other Tm alloy information is covered in the preceding phase diagrams.

5.8. Light rare earth alloys

Some light–heavy rare earth alloy studies have been covered in the discussion of the heavy elements. Two intra-light rare earth investigations which have been reported give the ordering temperatures of Nd alloyed with Pr on the one hand and Nd alloyed with La on the other. Lebech et al. (1975) investigated several single crystals of Nd–Pr and found the results shown by the top curve of fig. 93. Starting at the 19.6 K ordering temperature for Nd the Néel temperature drops nearly linearly with Pr concentration as though Pr had a Néel point of 10 K. Then for Pr concentrations above 75at.% the Néel point drops precipitously toward the 0 K point actually found in pure unstrained Pr, as mentioned in the discussion of Pr earlier.

From magnetic and electrical resistivity measurements on several poly-

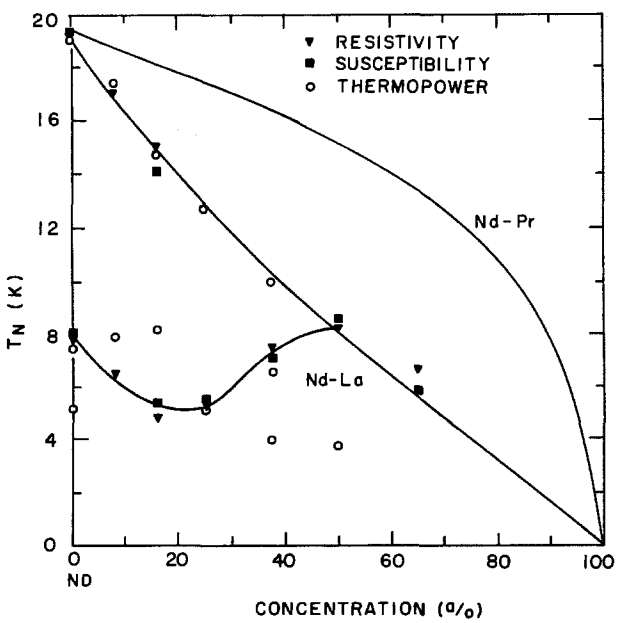

Fig. 93. Magnetic phase diagrams for Nd alloyed with La and with Pr. After Petersen et al. (1978a, b) for Nd–La and after Lebech et al. (1975) for Nd–Pr.

crystalline alloys of Nd with La, Petersen et al. (1977) found two ordering temperatures for La concentrations less than 50at.%. Their data are at the bottom of fig. 92 and show that above 50at.% La in Nd only one transition was observable. The system appeared to be inhomogeneous magnetically for La concentrations above 50at.%.

6. Magnetic anisotropy energy and magnetostriction

The large magnetic anisotropy of the hcp heavy rare earths has its origins in the asymmetrical charge distribution of the 4f electrons as shown in fig. 7. The magnetic anisotropy energy consists of the crystal field energy expressed in the appropriate macroscopic form; for hexagonal lattices the equation generally used is

$$H_{cf} = K_2^0 Y_2^0(\theta, \phi) + K_4^0 Y_4^0(\theta, \phi) + K_6^0 Y_6^0(\theta, \phi) + K_6^6[Y_6^6(\theta, \phi) + Y_6^{-6}(\theta, \phi)]. \tag{36}$$

Here the $Y_l^m(\theta, \phi)$ are normalized spherical harmonics and θ, ϕ are the polar coordinate angles of the magnetization relative to the c- and a-axes of the hexagonal lattice. The coefficients K_l^m have a complicated temperature dependence which has been described by Callen and Callen (1966). They give the expression

$$K_l^m(T) = K_l^m(0^\circ)\hat{I}_{l+1/2}[\mathscr{L}^{-1}(\sigma)] \tag{37}$$

where $\hat{I}_{l+1/2}$ is the reduced modified Bessel function of odd half integer order, $\mathscr{L}^{-1}(\sigma)$ is the inverse of the Langevin function and σ is the reduced magnetization $M(T)/M(0)$. At low temperatures the dependence on σ expected is $K_2^0(T) = K_2^0(0)\sigma^3$, $K_4^0(T) = K_4^0(0)\sigma^{10}$ and $K_6^0(T) = K_6^0(0)\sigma^{21}$ so the temperature dependence arises indirectly through the basic Brillouin function temperature variation of the reduced magnetization.

If the coefficients K_2^0 and K_4^0 are positive the magnetic moments lie in the basal plane as in the case of Tb and Dy. If these coefficients are negative (Er, Tm) the magnetic moments are aligned along or near the c-axis. If K_2^0 and K_4^0 are of opposite sign and about equal in magnitude the easy direction is on a cone around the c-axis. If there is a basal plane component of the magnetic moments then the sixth order terms determine the easy sixfold direction.

The experimental values of the anisotropy constants are shown in table 5. There is a considerable spread in some of the coefficients reported. As noted in the table the only data on Tm comes from dilute alloys and are likely lower than the Tm metal would show.

The temperature dependence of the magnetic anisotropy constants of Gd has been investigated by Mihai and Franse (1976). They used a torque method along with a magnetic anisotropy energy expression in the form

TABLE 5

The zero Kelvin magnetic anisotropy energy constants of eq. 33. All values are in units of 10^7 ergs/cm^3 (10^6 J/m^3). The temperature dependence via σ^n is also given where available

Element	K_2^0	σ^n	K_4^0	K_6^0	K_6^6	σ^n	Reference
Terbium	90	σ^4	5.4	–	0.19	–	Feron et al. (1970)
		–	–	–	0.23	σ^{15}	Houman et al. (1975)
	87	–	–	–	–	–	Rhyne and Clark (1967)
	76	–	−3.0	–	0.27	–	Roeland et al. (1975)
					0.30		Shepherd (1976)
Dysprosium	87	σ^3	6.4	–	−1.1	–	Feron et al. (1970)
	78	–	–	–	–	–	Rhyne et al. (1968)
	87	–	–	–	–	–	Rhyne et al. (1968)
					−1.4	σ^{26}	McEwen (1978)
Holmium	66	–	2.1	–	2.7	–	Feron et al. (1970)
	32	–	−1.7	−1.6	2.7	–	Rhyne et al. (1968)
					3.4	–	Cock (1976)
Erbium	−9.7	–	−4.1	5.1	−2.1	–	Jensen (1976)
Thulium	−30*	–	−3*	−6*	3.5*	–	Touborg and Høg (1974)
Gadolinium	−0.21	–	0.08	–	–	–	Feron et al. (1970)
	−0.14	–	0.07	−0.014	–	–	Mishima et al. (1975)
					0.0006	–	Graham (1967)

* The data for thulium are from dilute alloy measurements. In the cases of Tb and Dy the constants found this way were about one third the values found for the pure metals. The coefficients determined from paramagnetic susceptibility anisotropy data are also considerably lower than results of the more direct measurements.

$$E_A = K_0 + K_2 \sin^2\theta + K_4 \sin^4\theta + K_6 \sin^6\theta \cos 6\phi + \ldots \tag{38}$$

where θ and ϕ are the polar angles of the magnetization relative to the crystal c- and a-axes. For the torque data they found it convenient to use

$$L_A = C_1 \sin^2\theta + C_2 \sin^4\theta \tag{39}$$

where L_A is the torque and $C_1 = -(K_2 + K_4)$ and $2C_2 = K_4$. Their results for C_1 and C_2 are shown in fig. 94.

For a more detailed discussion of magnetic anisotropy energy see McEwen (1978).

The observation of giant magnetostriction in rare earths is directly related to their magnetic structure and the magnetic anisotropy energy. An analysis of single ion effects for hexagonal crystals has been made by Clark et al. (1963) and their expression in cartesian coordinates (x is along a, y along b, and z along c) for the magnetostriction correct to second order in the cosines α_i of the magnetization is

$$\begin{aligned} \Delta L/L = {} & [\lambda_1^{\alpha,0} + \lambda_1^{\alpha,2}(\alpha_z^2 - \tfrac{1}{3})](\beta_x^2 + \beta_y^2) + [\lambda_2^{\alpha,0} + \lambda_2^{\alpha,2}(\alpha_z^2 - \tfrac{1}{3})]\beta_z^2 \\ & + \tfrac{1}{2}\lambda^{\gamma,2}[(\alpha_x\beta_x + \alpha_y\beta_y)^2 - (\alpha_x\beta_y - \alpha_y\beta_x)^2] + 2\lambda^{\epsilon,2}(\alpha_x\beta_x + \alpha_y\beta_y)\alpha_z\beta_z. \end{aligned} \tag{40}$$

Here β_i are the direction cosines of the line of the strain measurement and the

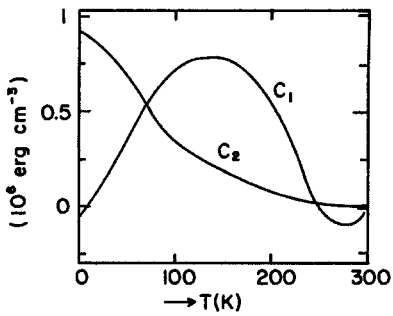

Fig. 94. Magnetic anisotropy energy constants C_1 and C_2 of eq. (39) for Gd versus temperature. After Mihai and Franse (1976).

coefficients $\lambda_i^{m,n}$ must be determined experimentally. The coefficient $\lambda_1^{\alpha,2}$ represents dilatations in the basal plane, $\lambda_2^{\alpha,2}$ represents dilatation along the c-axis, $\lambda^{\gamma 2}$ represents a distortion of the hexagonal symmetry into orthorhombic (circles go to ellipses), $\lambda^{\epsilon,2}$ represents shear in going along the c-axis, $\lambda_1^{\alpha,0}$ and $\lambda_2^{\alpha,0}$ are related to anomalous thermal expansion and exchange magnetostriction.

The temperature dependence of magnetostriction coefficients is like that for the magnetic anisotropy constants so has the form

$$\lambda(T) = \lambda(0)\bar{I}_{l+1/2}[\mathscr{L}^{-1}(\sigma)]. \tag{41}$$

Since the magnetic moments of Tb and Dy are essentially constrained to lie in the basal plane at low temperatures it has been necessary to go to higher order terms in $\Delta L/L$. For details see the chapter of the present volume on the magnetostrictive rare earth–Fe_2 compounds by A.E. Clark who gives the expression for $\Delta L/L$ out to sixth order in the direction cosines. It has also been necessary in these cases to use theoretical considerations to make extrapolations of paramagnetic data down to low temperatures to obtain some of the magnetostriction coefficients. It is noted that in some cases the coefficients can only be determined in combinations and are reported in this fashion. In table 6 the available magnetostriction coefficients are given.

TABLE 6
Magnetostriction coefficients at zero Kelvin in units of 10^{-3}

Element	$\lambda_1^{\alpha,2}$	$\lambda_2^{\alpha,2}$	$\lambda^{\gamma,2}$	$\lambda^{\epsilon,2}$	$\lambda_1^{\alpha,0}-\frac{1}{3}\lambda_1^{\alpha,2}$	$\lambda_2^{\alpha,0}-\frac{1}{3}\lambda_2^{\alpha,2}$	$\lambda^{\gamma,4}$
Gadolinium[a]	0.14	−0.13	0.11	0.02	–	–	–
Terbium[b]	−2.6[c]	9.0[c]	8.7	15.0[c]	−0.8	4.3	−2.1
Dysprosium[b]	–	–	9.4	5.5	−2.0	7.3	1.5
Holmium[b]	–	–	2.5[c]	–	−3.9	7.1	–
Erbium[b]	–	–	−5.1[c]	–	+0.3	6.2	–

[a] After Mishima et al. (1976).
[b] After Rhyne (1972).
[c] Extrapolated from paramagnetic range using single-ion theory.

In fig. 95a the temperature dependence of the coefficients for Gd found by Mishima et al. (1976) is shown. Here and in the table the magnitude of the coefficients is clearly an order of magnitude lower than for Tb or Dy. This is expected because Gd has the half full 4f shell and is spherically symmetric. The strain modes are shown in fig. 95b.

The data of Rhyne and Legvold (1965a) for Tb is displayed in fig. 96. The data for $\lambda^{\gamma,2}$ gave a good fit to $8.7\hat{I}_{5/2}[\mathscr{L}^{-1}(\sigma)]$ and those for $\lambda^{\gamma,4}$ to $-2.14\hat{I}_{9/2}[\mathscr{L}^{-1}(\sigma)]$.

In the case of Dy the results of Rhyne (1965) came out as shown in fig. 97. The data for $\lambda^{\gamma,2}$ gave a reasonably good fit to $9.4\hat{I}_{5/2}[\mathscr{L}^{-1}(\sigma)]$ and those for $\lambda^{\gamma,4}$ were close to $1.4\hat{I}_{13/2}[\mathscr{L}^{-1}(\sigma)]$.

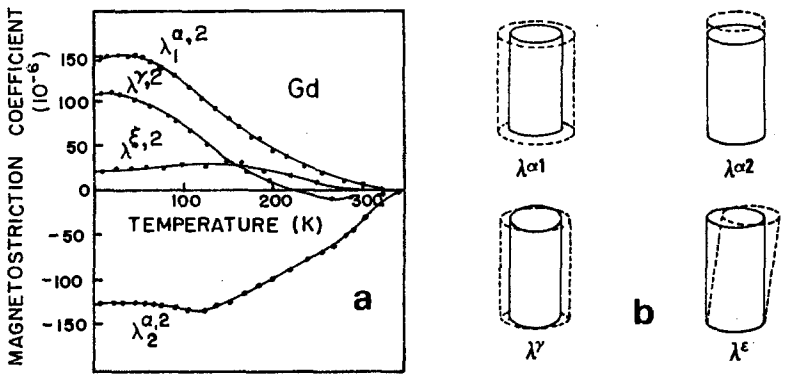

Fig. 95. (a) Magnetostriction coefficients for Gd versus temperature. After Mishima et al. (1976). (b) Strain modes associated with the hexagonal magnetostriction coefficients.

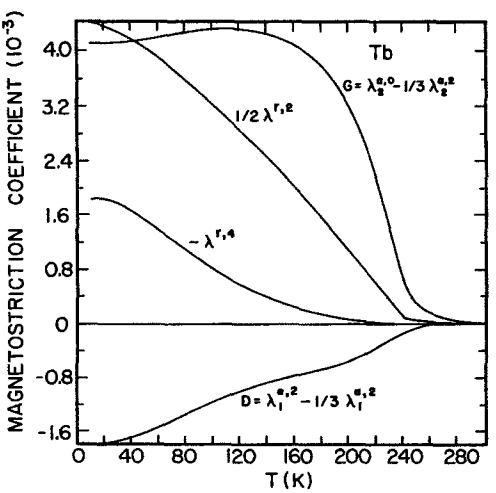

Fig. 96. Magnetostriction coefficients of Tb extrapolated to zero applied field versus temperature. After Rhyne and Legvold (1965a).

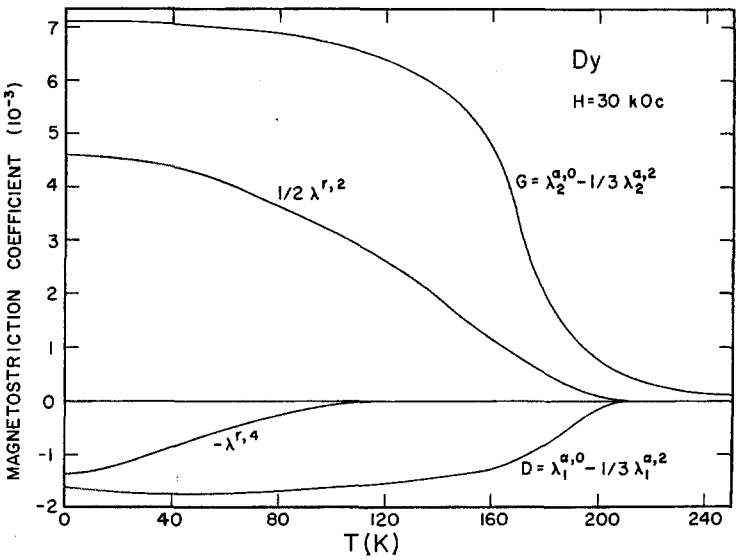

Fig. 97. Magnetostriction coefficients of Dy at 30 kOe versus temperature. After Rhyne (1965).

Magnetostriction data of Rhyne et al. (1967) for Ho are shown in fig. 98. Data for the strain gauge G along the a-axis are read on the right hand ordinate and data for G along the b- and c-axes are read on the left hand ordinate. Thermal contraction is indicated as T decreases from room temperature and then magnetically induced strains appear as T goes below the 132 K Néel point. For

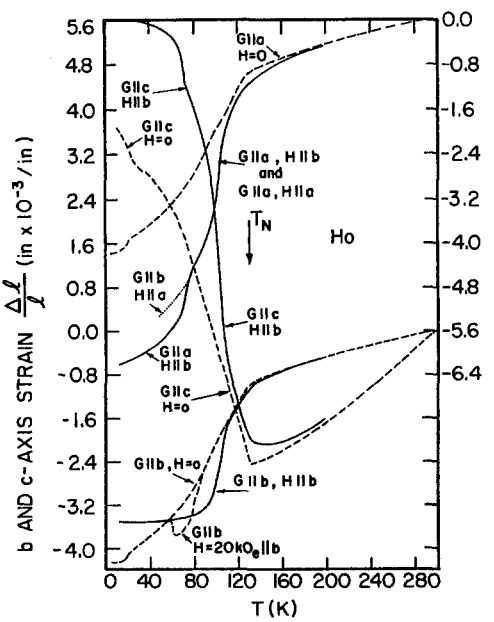

Fig. 98. Principal strains for Ho versus temperature. After Rhyne et al. (1967).

Er the magnetostriction data along *a*- and *c*-axes of Rhyne and Legvold (1965b) are shown in fig. 99. Their data with the strain gauge along the *b*-axis were like those along the *a*-axis. Again thermal contraction is indicated down to the 85 K Néel point.

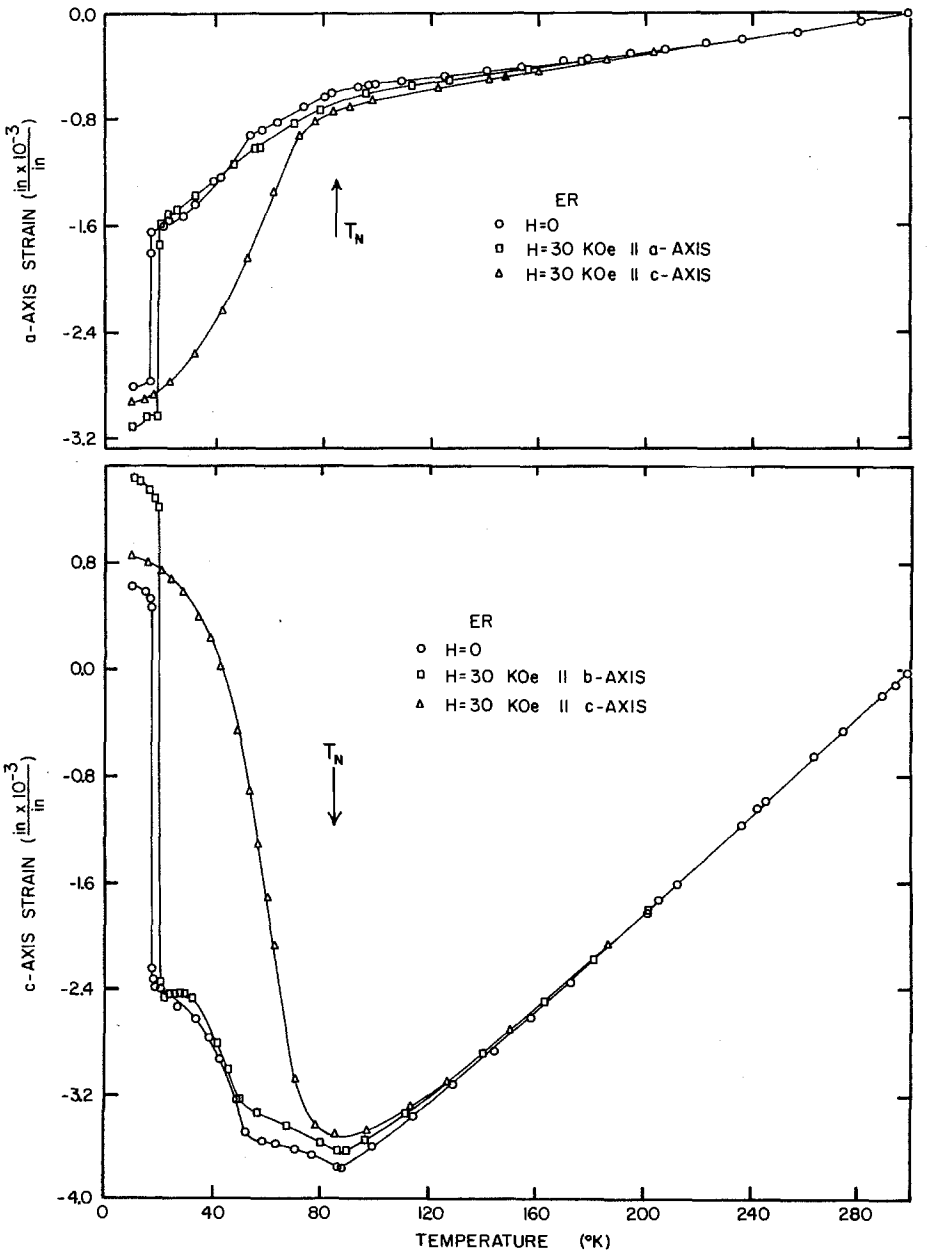

Fig. 99. The *c*- and *a*-axis strains of Er versus temperature. After Rhyne and Legvold (1965b).

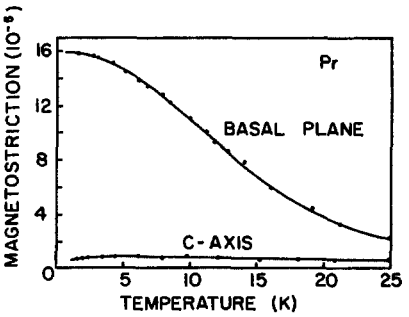

Fig. 100. Magnetostriction of Pr at 10 kOe (1 T) versus temperature. After Ott (1975).

In fig. 100 the magnetostriction data of Ott (1975) for Pr indicate that the 10 kOe (1 T) applied field induced a magnetic moment in this normally non-magnetic singlet state metal. The magnitude of the magnetostriction is seen to be about two orders of magnitude lower than for Tb. This concludes the discussion of magnetostriction.

Acknowledgements

The author is grateful to John Queen, Thomas Petersen, Paul Burgardt, and Prof. Burce Harmon of the Physics Department for help on the manuscript, to Karl Gschneidner, Jr., and Berni Evans of the Rare Earth Information Center for their help in the literature searches; to Roy L. Anderson, Kevin R. Shanks, and Dennis W. Sailsburgy for their help in the preparation of the figures; to Janet Hartman for typing the manuscript, and finally to his wife, Lavona, for her forebearance throughout the project. This work was supported by the U.S. Department of Energy, Office of Basic Energy Sciences, Materials Sciences Division.

References

Achiwa, N. and S. Kawano, 1973, J. Phys. Soc. Japan **35**, 303.

Akhavan, M. and H.A. Blackstead, 1976, Phys. Rev. B **13**, 1209.

Aliscio, B., A. Lopez and C.F.E. Ohmedo, 1973, J. Phys. F **3**, 1324.

Andersen, O.K. and T.L. Loucks, 1968, Phys. Rev. **167**, 551.

Andres, K., E. Bucher, J.P. Maita, L.D. Longinotti and R. Flukiger, 1972, Phys. Rev. B **6**, 313.

Arajs, S. and G.R. Dunmyre, 1966, Z. Naturforsch. **21**, 1856.

Arajs, S. and G.R. Dunmyre, 1967, J. Less Common Metals **12**, 162.

Arajs, S. and D.S. Miller, 1960, J. Appl. Phys. Suppl. **31**, 325S.

Atoji, M., 1974, Solid State Commun. **14**, 1047.

Baer, Y. and G. Busch, 1973, Phys. Rev. Lett. **31**, 35.

Bagguley, D.M.S. and P. Partington, 1975, J. Phys. F **5**, L39.

Bak, P. and B. Lebech, 1978, Phys. Rev. Lett. **40**, 800.

Bak, P. and D. Mukamel, 1976, Phys. Rev. B **13**, 5086.

Baker, J.M., B. Bleany and W. Hayes, 1958, Proc. Roy. Soc. (London) A **247**, 141.
Bates, L.F., S.J. Leach and R.G. Loasby, 1955, Proc. Phys. Soc. London B **68**, 859.
Behrendt, D.R., S. Legvold and F.H. Spedding, 1957, Phys. Rev. **106**, 723.
Beaudry and Gschneidner 1978
Bleaney, B., 1963, J. Appl. Phys. **34**, 1024.
Boys, D.W. and S. Legvold, 1968, Phys. Rev. **174**, 377.
Bozorth, R.M., 1967, J. Appl. Phys. **38**, 1366.
Bozorth, R.M. and J.C. Suits, 1964, J. Appl. Phys. **35**, 1039.
Bozorth, R.M. and J.H. Van Vleck, 1960, Phys. Rev. **118**, 1493.
Brun, T.O. and G.H. Lander, 1969, Phys. Rev. Lett. **23**, 1295.
Brun, T.O., S.K. Sinha, N. Wakabayashi, G.H. Lander, L.R. Edwards and F.H. Spedding, 1970, Phys. Rev. B **1**, 1251.
Bucher, E., C.W. Chu, J.P. Maita, K. Andres, A.S. Cooper, E. Buehler and K. Nassau, 1969, Phys. Rev. Lett. **22**, 1260.
Bucher, E., P.H. Schmidt, A. Jayaraman, K. Andres, J.P. Maita, K. Naseau and P.D. Dernier, 1970, Phys. Rev. B **2**, 3911.
Burgardt, P., 1976, unpublished Ph.D. thesis, Iowa State University, Ames, Iowa, 50011, USA.
Burgardt, P. and S. Legvold, 1975, AIP Conf. Proc. **24**, 418.
Burgardt, P. and S. Legvold, 1978
Burgardt, P., K.A. Gschneidner, Jr., D.C. Koskenmaki, D.L. Finnemore, J.O. Moorman, S. Legvold, C. Stassis and T.A. Vyrostek, 1976, Phys. Rev. B **14**, 2995.
Burgardt, P., S. Legvold, B.J. Beaudry and B.N. Harmon, 1979, Phys. Rev. B, to be published. (Lifshitz point of Gd Tb.)
Cable, J.W. and E.O. Wollan, 1968, Phys. Rev. **165**, 733.
Cable, J.W., E.O. Wollan, W.C. Koehler and M.K. Wilkinson, 1965, Phys. Rev. **140**, 1896.
Callaway, J., 1974, Quantum theory of the solid state, part A (Academic Press, New York) pp. 339–341.
Callen, H.B. and E.R. Callen, 1966, J. Phys. Chem. Solids **27**, 1271.
Capellman, H., 1970, J. Low Temp. Phys. **3**, 189.
Chechernikov, V.I., 1962, Fiz. Met. and Metallored **13**, 458. (Phys. Met. and Metallogr. **13**, 134.)
Chen, C.-W., 1977, Magnetism and metallurgy of soft magnetic materials (North-Holland, Amsterdam).
Child, H.R. and W.C. Koehler, 1966, J. Appl. Phys. **37**, 1353.
Child, H.R., W.C. Koehler, E.O. Wollan and J.W. Cable, 1965, Phys. Rev. **138**, A1655.
Clark, A.E., R. Bozorth and B. DeSavage, 1963, Phys. Lett. **5**, 100.
Cock, G.J., 1976, thesis, University of Amsterdam.
Colvin, R.V., S. Arajs and J.M. Peck, 1961, Phys. Rev. **122**, 14.
Cooper, B.R., 1967, Phys. Rev. **163**, 444.
Cooper, B.R., 1972, chapter 2 of Magnetic properties of rare earth metals (editor R.J. Elliott) (Plenum Press, New York and London).
Coqblin, B. and A. Blandin, 1968, Adv. Phys. **17**, 281.
Corner, W.D. and B.K. Tanner, 1976, J. Phys. C **9**, 627.
Cracknell, A.P., 1971, Adv. Phys. **20**, 1.
Culbert, H.V., 1967, Phys. Rev. **156**, 701.
Curry, R.G. and K.N.R. Taylor, 1976, Phys. Rev. B **14**, 4219.
Curry, M.A., S. Legvold and F.H. Spedding, 1960, Phys. Rev. **117**, 971.
Curry, R.G., M.W. Stringfellow and K.N.R. Taylor, 1977, Physica **86–88B**, 57.
Darnell, F.J., 1963a, Phys. Rev. **130**, 1825.
Darnell, F.J., 1963b, Phys. Rev. **132**, 1098.
Das, S.G., 1976, Phys. Rev. B **13**, 3978.
de Gennes, P.G., 1966, C. R. Acad. Sci. **247**, 1836.
Dimmock, J.O., 1971, in Solid state physics, (eds. H. Ehrenreich, F. Seitz and D. Turnbull) vol. **26**, 104.
Dimmock, J.O. and A.J. Freeman, 1964, Phys. Rev. Lett. **13**, 750.
Duthie, J.C. and D.G. Pettifor, 1977, Phys. Rev. Lett. **38**, 564.
Edwards, L.R. and S. Legvold, 1968, Phys. Rev. **176**, 753.
Elliott, R.J., ed., 1972, Magnetic properties of the rare earth metals (Plenum Press, New York, London).
Elliott, R.J. and F.A. Wedgewood, 1963, Proc. Phys. Soc. (London) **81**, 846.
Feron, J.L., G. Hug and R. Pauthenet, 1970, Z. Angew. Phys. **30**, 61.
Fleming, G.S., S.H. Liu and T.L. Loucks, 1968, Phys. Rev. Lett. **21**, 1524.
Forgan, E.M., C.M. Muirhead, D.W. Jones and K.A. Gschneidner, Jr., 1979, to be published.

Franse, J.J.M. and V. Mihai, 1977, Physica **86–88B**, 49.
Freeman, A.J., 1972, ch. 6 of Magnetic properties of rare earth metals (ed. R.J. Elliott) (Plenum Press, New York, London).
Freeman, A.J. and J.O. Dimmock, 1966, Bull. Am. Phys. Soc. **11**, 216.
Freeman, A.J., J.O. Dimmock and R.E. Watson, 1966, Phys. Rev. Lett. **16**, 94.
Fuji, H., Y. Hashimoto, A. Mishima, N. Shohata and T. Okamato, 1976, J. Phys. Soc. Japan **41**, 1179.
Fujimori, H., K. Goto and D.E.G. Williams, 1974, J. Phys. F **4**, 2152.
Fujiwara, H., H. Fujii, Y. Hidaka, T. Ito, Y. Hashimoto and T. Okamoto, 1977, J. Phys. Soc. Japan **42**, 1194.
Gerstein, B.C., M. Griffel, L.D. Jennings, R.E. Miller, R.E. Skochdopole and F.S. Spedding, 1957, J. Chem. Phys. **27**, 394.
Gerstein, B.C., F.J. Jelinek, J.R. Mullaly, W.D. Shickell and F.H. Spedding, 1967, J. Chem. Phys. **47**, 5194.
Graham, C.D., 1962, J. Phys. Soc. Japan **16**, 1310.
Graham, C.D., 1967, J. Appl. Phys. **38**, 1375.
Green, R.W., S. Legvold and F.H. Spedding, 1961, Phys. Rev. **122**, 827.
Griffel, M., R.E. Skochdopole and F.H. Spedding, 1954, Phys. Rev. **93**, 657.
Griffel, M., R.E. Skochdopole and F.H. Spedding, 1956, J. Chem. Phys. **25**, 75.
Gshneidner, Jr., K.A., and L. Eyring, eds., 1978, Handbook of the physics and chemistry of rare earths, (North-Holland, Amsterdam). See ch. 2, B.J. Beaudry and K.A. Gschneidner, Jr.; ch. 3, S.H. Liu; and ch. 6, K.A. McEwen.
Gschneidner, Jr., K.A., T.-W.E. Tsang, J.H. Queen, S. Legvold and F.A. Schmidt, 1978, Proc. Conf. on Rare Earths and Actinides, University of Durham (England) July 4–6, 1977.
Gustafson, D.R., J.D. McNutt and L.O. Roellig, 1969, Phys. Rev. **183**, 435.
Habenschuss, M., C. Stassis, S.K. Sinha, H.W. Deckman and F.H. Spedding, 1974, Phys. Rev. B **10**, 1020.
Hall, P.M., S. Legvold and F.H. Spedding, 1959, Phys. Rev. **116**, 1446.
Hansen, P. and B. Lebech, 1976, J. Phys. F **6**, 2179.
Harmon, B.N. and A.J. Freeman, 1974a, Phys. Rev. B **10**, 1979.
Harmon, B.N. and A.J. Freeman, 1974b, Phys. Rev. B **10**, 4849.
Hedén, P.O., H. Löfgren and S.B.M. Hagström, 1972, Phys. Stat. Sol. (b) **49**, 721.
Hegland, D.E., S. Legvold and F.H. Spedding, 1963, Phys. Rev. **131**, 158.
Høg, J. and P. Touborg, 1974, Phys. Rev. B **9**, 2952.
Hornreich, R.M., 1979, J. Magnetism and Magnetic Mat., Proc. of ICM 1979 (paper 7AII, to be published).
Houman, J.C.G. and R.M. Nicklow, 1970, Phys. Rev. B **1**, 3943.
Houman, J.G., J. Jensen and P. Touborg, 1975a, Phys. Rev. B **12**, 332.
Houman, J.G., M. Chapellier, A.R. Mackintosh, P. Bak, O.D. McMasters and K.A. Gschneidner, Jr., 1975b, Phys. Rev. Lett. **34**, 587.
Hsieh, Y.Y. and D.A. Pink, 1972, Solid State Commun. **11**, 783.
Hutchings, M.T., 1964, Solid State Physics **16**, 227.
Isci, C. and S.B. Palmer, 1977, J. Phys. Chem. Solids **38**, 1253.
Jennings, L.D., E.D. Hill and F.H. Spedding, 1959, J. Chem. Phys. **31**, 1240.
Jennings, L.D., E.D. Hill and F.H. Spedding, 1961, J. Chem. Phys. **34**, 2082.
Jennings, L.D., R.E. Miller and F.H. Spedding, 1960, J. Chem. Phys. **33**, 1849.
Jennings, L.D., R.M. Stanton and F.H. Spedding, 1957, J. Chem. Phys. **27**, 909.
Jensen, J., 1976, J. Phys. F **6**, 1145.
Jepsen, O. and O.K. Andersen, 1971, Solid State Commun. **7**, 731.
Jew, T.T., 1963, unpublished M.S. thesis, Iowa State University Library, Ames, Iowa, 50011, USA.
Johansson, B., 1974, Phil. Mag. **30**, 469.
Johansson, T., B. Lebech, M. Nielsen, H. Bjerrum Moller and A.R. Mackintosh, 1970, Phys. Rev. Lett. **25**, 524.
Johansson, T., K.A. McEwen and P. Touborg, 1971, J. de Phys. (Paris) Suppl. **32**, Cl-372-4, 372.
Kasuya, T., 1966, Magnetism, vol. IIB (eds. G.T. Rado and H. Suhl) (Academic Press, New York) p. 215.
Kawano, S. and N. Achiwa, 1974, J. Phys. Soc. Japan **37**, 569.
Kawano, S. and N. Achiwa, 1975, J. Phys. Soc. Japan **38**, 285.
Kayser, F.X., 1970, Phys. Rev. Lett. **25**, 662.

Keeton, S.C. and T.L. Loucks, 1968, Phys. Rev. **168**, 672.
Kirchmayr, H.R. and K.H. Schindl, 1966, Acta Phys. Austriaca **22**, 267.
Kiwi, M. and R. Ramirez, 1972, Phys. Rev. B **6**, 3700.
Kobayasi, S.-I., Fukuchi and S. Nagai, 1976, Solid State Commun. **20**, 589.
Koehler, W.C., 1972, ch. 3 of Magnetic properties of rare earth metals, (ed. R.J. Elliott) (Plenum Press, New York, London).
Koehler, W.C. and R.M. Moon, 1972, Phys. Rev. Lett. **29**, 1468.
Koehler, W.C., J.W. Cable, E.O. Wollan and M.K. Wilkinson, 1962, Phys. Rev. **126**, 162.
Koehler, W.C., H.R. Child, E.O. Wollan and J.W. Cable, 1963, J. Appl. Phys. **34**, 1335.
Koehler, W.C., J.W. Cable, M.K. Wilkinson and E.O. Wollan, 1966, Phys. Rev. **151**, 414.
Koehler, W.C., J.W. Cable, M.K. Wilkinson and E.O. Wollan, 1967, Phys. Rev. **158**, 450.
Koehler, W.C., R.M. Moon and H.R. Child, 1973, AIP Conf. Proc. **10**, 1319.
Koelling, D.D., A.J. Freeman and F.M. Mueller, 1969, Bull. Am. Phys. Soc. **14**, 360.
Koskimaki, D.C. and K.A. Gschneidner, Jr., 1975, Phys. Rev. B **11**, 4463.
Koskenmaki, D.C. and K.A. Gschneidner, Jr., 1978, ch. 4 of Handbook on the physics and chemistry of rare earths, vol. 1, (North-Holland, Amsterdam).
Lea, K.R., M.J.M. Leask and W.P. Wolf, 1962, J. Phys. Chem. Solids **23**, 1381.
Lebech, B., K.A. McEwen and P.-A. Lindgard, 1975, J. Phys. C **8**, 1684.
Legvold, S., 1979, Phys. Rev. B **19**, 446.
Legvold, S. and J.P. Beaver, 1979, Solid State Commun., to be published.
Legvold, S., B.N. Harmon, B.J. Beaudry, P. Burgardt, D.R. Younkin and H.W. White, 1977a, Phys. Rev. B **16**, 4986.
Legvold, S., B.J. Beaudry, J.E. Ostenson and B.N. Harmon, 1977b, Solid State Commun. **21**, 1061.
Legvold, S., P. Burgardt and B.J. Beaudry, 1977c, in Crystal field effects in metals and alloys (ed. A. Furrer) (Plenum, New York, London) p. 340.
Legvold, S., P. Burgardt, B.J. Beaudry and K.A. Gschneidner, Jr., 1977d, Phys. Rev. B **16**, 2479.
Legvold, S., R.W. Green, J.E. Ostenson and B.J. Beaudry, 1978, Phys. Rev. B **18**,
Legvold, S., J. Queen, B.J. Beaudry and B.N. Harmon, 1979a, J. Magn. Magnetic Mat., Proc. Int. Conf. on Magnetism (to be published).
Legvold, S., P. Burgardt and B.J. Beaudry, 1979b, J. Magn. Magnetic Mat., Proc. Int. Conf. on Magnetism (to be published).
Lewis, E.A.S., 1970, Phys. Rev. B **1**, 4368.
Lindelof, P.E., I.E. Miller and G.R. Pickett, 1975, Phys. Rev. Lett. **35**, 1297.
Lindgård, P.-A., 1976, in Magnetism in metals and metallic compounds (eds. J.T. Lopuszansky, A. Pekalski and J. Przystawa) (Plenum Press, New York) p. 203.
Lindgard, P.-A., 1977, Phys. Rev. B **16**, 2168.
Lindgård, P.-A., B.N. Harmon and A.J. Freeman, 1975, Phys. Rev. Lett. **35**, 383.
Liu, S.H., 1978, ch. 3 of Handbook of the physics and chemistry of rare earths (eds. K.A. Gschneidner and L. Eyring) (North-Holland, Amsterdam).
Liu, S.H., R.P. Gupta and S.K. Sinha, 1971, Phys. Rev. B **4**, 1100.
Liu, S.H., P. Burgardt, K.A. Gschneidner, Jr. and S. Legvold, 1976, J. Phys. F **6**, L55.
Loucks, T.L., 1967, Augmented plane wave method (Benjamin, New York).
Lounasma, O.V., 1964, Phys. Rev. **133**, A219.
Mackintosh, A.R., 1963, Phys. Lett. **4**, 140.
Mackintosh, A.R., 1971, J. de Phys. (Paris) Suppl. **32** C1, 482.
Mackintosh, A.R., 1977, Physics Today **30**, 23.
Mackintosh, A.R. and H. Bjerrum Møller, 1972, in ch. 5 of Magnetic properties of the rare earth metals (ed. R.J. Elliott) (Plenum Press, New York, London).
Mackintosh, A.R. and F.A. Smidt, 1962, Phys. Lett. **2**, 107.
Maezawa,K., K. Mori, K. Sato, Y. Saito and S. Wakabayashi, 1977, J. Phys. Soc. Japan (Letters) **43**, 1815.
Mannari, I., 1959, Prog. Theoret. Phys. (Kyoto) **22**, 335.
Mattheiss, L.F., J.H. Wood and A.C. Switendeck, 1968, Methods in Computation Physics **8**, 64.
Mattocks, P.G. and R.C. Young, 1977, J. Phys. F **7**, L19.
McEwen, K.A., 1978, ch. 6 or Handbook of the physics and chemistry of rare earths (eds. K.A. Gschneidner and L. Eyring) (North-Holland, Amsterdam).
McEwen, K.A., G.J. Cock, L.W. Roeland and A.R. Mackintosh, 1973, Phys. Rev. Lett. **30**, 287.

McEwen, K.A., P.F. Touborg, G.J. Cock and L.W. Roeland, 1974, J. Phys. F **4**, 2264.
McFeely, F.R., S.P. Kowalczyk, L. Ley and D.A. Shirley, 1973, Phys. Lett. **45A**, 227.
Meaden, G.T., 1965, Electrical resistance of metals (Plenum Press, New York).
Meaden, G.T., 1971, Contemp. Phys. **12**, 331.
Mihai, V. and J.J.M. Franse, 1976, Rev. Roum. Phys. **21**, 1041.
Millhouse, A.H. and K.A. McEwen, 1973, Solid State Comm. **13**, 339.
Milstein, F. and L.B. Robinson, 1967, Phys. Rev. **159**, 466.
Mishima, A., H. Fujii and T. Okamoto, 1975, J. Phys. Soc. Jap. **38**, 284; **39**, 873.
Mishima, A., H. Fujii and T. Okamoto, 1976, J. Phys. Soc. Jap. **40**, 962.
Miwa, H., 1963, Prog. Theoret. Phys. (Japan) **29**, 477.
Moon, R.M., J.W. Cable and W.C. Koehler, 1964, J. Appl. Phys. **35**, 1041.
Moon, R.M., W.C. Koehler, J.W. Cable and H.R. Child, 1972, Phys. Rev. B **5**, 997.
Mukamel, D. and S. Krinsky, 1976a, Phys. Rev. B **13**, 5065.
Mukamel, D. and S. Krinsky, 1976b, Phys. Rev. B **13**, 5078.
Murao, T., 1972, J. Phys. Soc. Japan **33**, 33.
Nellis, W.J. and S. Legvold, 1969, Phys. Rev. **180**, 581.
Nereson, N.G., C.E. Olsen and G.P. Arnold, 1964, Phys. Rev. **135**, A176.
Nicklow, R.M., 1971, J. Appl. Phys. **42**, 1672.
Nicklow, R.M., H.A. Mook, H.G. Smith, R.E. Reed and M.K. Wilkinson, 1969, J. Appl. Phys. **40**, 1452.
Nicklow, R.M., N. Wakabayashi, M.K. Wilkinson and R.E. Reed, 1971a, Phys. Rev. Lett. **26**, 140.
Nicklow, R.M., N. Wakabayashi, M.K. Wilkinson and R.E. Reed, 1971b, Phys. Rev. Lett. **27**, 334.
Nigh, H.E., S. Legvold and F.H. Spedding, 1963, Phys. Rev. **132**, 1092.
Nigh, H.E., S. Legvold, F.H. Spedding and B.J. Beaudry, 1964, J. Chem. Phys. **41**, 3799.
Niira, K., 1960, Phys. Rev. **117**, 129.
Ott, H.R., 1975, Solid State Commun. **16**, 1355.
Parkinson, D.A., F.E. Simon and F.H. Spedding, 1951, Proc. Roy. Soc. A207, 137.
Parks, R.D., 1977, ed., Valence instabilities and related narrow-band phenomena (Plenum, New York) p. 89.
Petersen, T.S., S. Legvold, K.A. Gschneidner, Jr., T.-W.E. Tsang and J.O. Moorman, 1978a, J. Appl. Phys. **49**, 2115.
Petersen, T.S., S. Legvold, K.A. Gschneidner, D.W. Jones, D. Fort and B.J. Beaudry, 1978b, to be published.
Queen, J.H., 1979, private communication.
Rainford, B.D. and J.G. Houman, 1971, Phys. Rev. Lett. **26**, 1254.
Ramirez, R. and L.M. Falicov, 1971, Phys. Rev. B **3**, 2425.
Rath, J. and A.J. Freeman, 1975, Phys. Rev. B **11**, 2109.
Rathmann, O. and P. Touborg, 1977, Phys. Rev. B **16**, 1212.
Redner, S. and H.E. Stanley, 1977, Phys. Rev. B **16**, 4901.
Rhyne, J.J., 1965, Ph.D thesis, Iowa State University Library, Ames, Iowa, 50011, USA.
Rhyne, J.J., 1972, ch. 4 of Magnetic properties of the rare earth metals (ed. R.J. Elliott) (Plenum Press, New York, London).
Rhyne, J.J. and A.E. Clark, 1967, J. Appl. Phys. **38**, 1379.
Rhyne, J.J. and S. Legvold, 1965a, Phys. Rev. **138**, A507.
Rhyne, J.J. and S. Legvold, 1965b, Phys. Rev. **140**, A2143.
Rhyne, J.J., S. Legvold and E.T. Rodine, 1967, Phys. Rev. **154**, 266.
Rhyne, J.J. and T.R. McGuire, 1972, IEEE Trans. Magnetics **8**, 105.
Rhyne, J.J., S. Foner, E.J. McNiff and R. Doclo, 1968, J. Appl. Phys. **39**, 892.
Richards, D.B. and S. Legvold, 1969, Phys. Rev. **186**, 508.
Roberts, L.M., 1957, J. Phys. B; Proc. Phys. Soc. London **70**, 343.
Roeland, L.W., G.J. Cock, F.A. Mueller, A.C. Moleman, K.A. McEwen, R.G. Jordon and D.W. Jones, 1975a, J. Phys. F **5**, L233.
Roeland, L.W., G.J. Cock and P.-A. Lindgard, 1975b, J. Phys. C **8**, 3427.
Rosen, M., 1968, Phys. Rev. **174**, 504.
Sakamoto, S., J. Nakai and Y. Nakagawa, 1976, J. Phys. Soc. Japan **40**, 686.
Sano, N., K. Shimizu, Y. Aoki and J. Itoh, 1975, J. Phys. Soc. Japan **39**, 93.
Schirber, J.E., F.A. Schmidt, B.N. Harmon and D.D. Koelling, 1976, Phys. Rev. Lett. **36**, 448.
Schirber, J.E., F.A. Schmidt, B.N. Harmon and D.D. Koelling, 1977, Phys. Rev. B **16**, 3230.

Shepherd, C.H., 1976, thesis, University of Salbord.
Sherrington, D., 1973, J. Phys. C **6**, 1037.
Simons, D.S. and M.B. Salamon, 1974, Phys. Rev. B **10**, 4680.
Skochdopole, R.E., M. Griffel and F.H. Spedding, 1955, J. Chem. Phys. **23**, 2258.
Slater, J.C., 1937, Phys. Rev. **51**, 846.
Southern, B.W. and D. Sherrington, 1974, J. Phys. F **4**, 1755.
Spedding, F.H. and J.J. Croat, 1973, J. Chem. Phys. **58**, 5514.
Spedding, F.H., Y. Ito and R.G. Jordan, 1970, J. Chem. Phys. **53**, 1455.
Speight, J.D., 1970, J. Less-Common Metals **20**, 251.
Stevens, K.W.H., 1952, Proc. Phys. Soc. (London) A **65**, 209.
St. Quinton, J.M.P., 1973, J. Phys. F **3**, 597.
Strandburg, D.L., S. Legvold and F.H. Spedding, 1962, Phys. Rev. **127**, 2046.
Sze, H.H., K.V. Rao and G.T. Meaden, 1969, J. Low Temp. Phys. **1**, 563.
Taylor, K.N.R. and M.I. Darby, 1972, Physics of rare earth solids (Chapman and Hall, London).
Thoburn, W.C., S. Legvold and F.H. Spedding, 1958, Phys. Rev. **110**, 1298.
Tissot, L. and A. Blaise, 1970, J. Appl. Phys. **41**, 1180.
Touborg, P., 1977, Phys. Rev. B **16**, 1201.
Touborg, P. and J. Høg, 1974, Phys. Rev. Lett. **33**, 775.
Triplett, B.B. and R.M. White, 1973, Phys. Rev. B **7**, 4938.
Tsang, T.-W.E., K.A. Gschneidner, Jr., D.C. Koskenmaki and J.O. Moorman, 1976a, Phys. Rev. B **14**, 4447.
Tsang, T.-W.E., K.A. Gschneidner, Jr. and F.A. Schmidt, 1976b, Solid State Comm. **20**, 737.
Van Vleck, J.H., 1932, Electric and magnetic susceptibilities (Oxford University Press, London).
Veal, B.W., D.D. Koelling and A.J. Freeman, 1973, Phys. Rev. Lett. **30**, 1961.
Voronel, A.V., S.R. Garber, A.P. Simkina and I.A. Charkina, 1966, translation Sov. Phys. JEPT **22**, 301.
Wells, P., P.C. Lanchester, D.W. Jones and R.G. Jordan, 1974, J. Phys. F **4**, 1729.
Wells, P., P.C. Lanchester, D.W. Jones and R.G. Jordan, 1976, J. Phys. F **6**, 11.
White, H.W., B.J. Beaudry, P. Burgardt, S. Legvold and B.N. Harmon, 1975, AIP Conf. Proc. **29**, 329.
Wilkinson, M.K., W.C. Koehler, E.O. Wollan and J.W. Cable, 1961, J. Appl. Phys. **32**, 48S.
Will, G., R. Nathans and H.A. Elperin, 1964, J. Appl. Phys. **35**, 1045.
Wittig, J., 1968, Phys. Rev. Lett. **21**, 1250.
Yang, T.-T and L.B. Robinson, 1969, Phys. Rev. **185**, 743.
Yosida, K., 1964, Progress in low temperature physics, vol. 4 (ed. C.J. Gorter) (North-Holland, Amsterdam) p. 265.
Young, R.C., R.G. Jordan and D.W. Jones, 1973, Phys. Rev. Lett. **31**, 1473.
Zumsteg, F.C., F.J. Cadieu, S. Marcelja and R.D. Parks, 1970, Phys. Rev. Lett. **25**, 1204.

chapter 4

RARE EARTH COMPOUNDS

K.H.J. BUSCHOW

Philips Research Laboratories
Eindhoven
Netherlands

Ferromagnetic Materials, Vol. 1
Edited by E.P. Wohlfarth

CONTENTS

1. Introduction

The number of stable binary intermetallic compounds in which one of the components is a rare earth element is of the order of a thousand. In the first place this large number is a result of the fact that the rare earths group comprises 15 elements, or even 16 if one includes the element yttrium. In the second place each of these 16 elements, when combined with a non-rare earth partner, can give rise to more than one compound, in general. Examples of binary systems are known which contain more than 10 different intermetallic compounds, each of these being characterized by a different composition and crystal structure. The reason for this is probably to be sought in the rather large metallic radii of the rare earths. Combination with elements of much smaller metallic radii then encompasses a much larger number of possible atomic arrangements of sufficiently high space filling than would be the case for two components of almost equal size. Furthermore, the stability of a given atomic arrangement will not be strongly influenced by symmetry requirements of the wavefunctions of the incomplete-shell electrons since the 4f electrons occur well to the interior of the rare earth atoms and their effect on the bonding can be taken as being relatively unimportant. Most important for the readiness with which the rare earths form compounds is the fact that their electronegativities (ϕ^*) are rather low compared with those of other metallic elements. Miedema et al. (1975, 1976, 1977) have proposed a simple model in which the heat of formation is given by

$$\Delta H = f(c)[-Pe(\Delta\phi^*)^2 + Q_0(\Delta n_{ws}^{1/3})^2 - R].$$

In this expression ϕ^* and $n_{ws}^{1/3}$ represent the electronegativity and the electron density parameter of the composing elements, respectively. The quantities P, Q_0 and R are approximate constants for large groups of alloy systems; e is the elementary charge. The function $f(c) = c(1-c)[1+\frac{1}{8}c^2(c-1)^2]$ is symmetric in the molar fraction c of the rare earth component. The large electronegativity difference between rare earth elements and other metals is the main reason why in most cases ΔH is negative, i.e. a compound is likely to exist. Values of ΔH calculated by Miedema et al. (1975, 1976, 1977) for various binary compounds are listed in table 1 (a slight adjustment has been made recently in the R values of the rare earth elements (Miedema et al. 1977)).

TABLE 1

Heat of formation of intermetallic compounds of Y (identical to Gd, calculated at three concentrations, 75at.% and 25at.% Y. In order to indicate the variation in ΔH for different (trivalent) rare earth metals, LaM and ScM have also been included. The heat of formation of other rare earths can be found by interpolation according to their molar volumes. ΔH is given in kcal/g-at. alloy. All data are from Miedema et al. (1977).

M = transition metal						M = non-transition metal					
M	Y_3M	LaM	YM	ScM	YM_3	M	Y_3M	LaM	YM	ScM	YM_3
Sc	+0	+3	+0	–	+0	Li	+1	+1	+3	+4	+2
Ti	+2	+9	+4	+2	+3	Na	+6	+5	+10	+12	+6
V	+3	+12	+6	+3	+5	Cu	−4	−7	−9	−10	−7
Cr	+2	−10	−4	−0	+3	Ag	−6	−10	−11	−12	−8
Mn	−0	+5	−0	−3	−0	Au	−13	−22	−26	−27	−16
Fe	−0	+7	−0	−4	−0						
Co	−4	−1	−7	−10	−6	Ca	+3	+0	+4	+6	+2
Ni	−5	−4	−10	−13	−9	Sr	+4	+2	+6	+8	+3
						Ba	+5	+2	+7	+9	+4
Y	–	+1	–	+0	–	Be	+0	+5	+1	−1	+1
Zr	+2	+7	+3	+1	+2	Mg	−2	−3	−3	−3	−2
Nb	+5	+17	+10	+6	+7	Zn	−7	−12	−13	−13	−10
Mo	+5	+17	+8	+4	+6	Cd	−9	−15	−15	−15	−10
Tc	−5	−2	−10	−14	−8	Hg	−11	−18	−18	−16	−12
Ru	−6	−3	−12	−15	−9						
Rh	−10	−12	−18	−21	−15	B	−8	−12	−15	−16	−15
Pd	−16	−23	−29	−30	−22	Al	−9	−14	−16	−16	−13
						Ga	−10	−16	−17	−16	−13
La	+1	–	+1	+3	+1	In	−10	−17	−16	−14	−10
Hf	+2	+9	+3	+1	+3	Tl	−10	−18	−16	−13	−10
Ta	+5	+17	+9	+6	+7						
W	+5	+17	+8	+3	+6	C	−6	−8	−12	−14	−11
Re	−5	+0	−8	−13	−6	Si	−10	−15	−18	−19	−12
Os	−5	−1	−9	−14	−7	Ge	−12	−20	−21	−20	−14
Ir	−10	−10	−18	−22	−14	Sn	−14	−22	−22	−20	−14
Pt	−16	−22	−29	−31	−21	Pb	−13	−23	−21	−18	−13
Th	+0	+3	+0	−0	+0	N	−21	−36	−39	−40	−27
U	+3	+11	+5	+2	+3	As	−19	−30	−32	−31	−23
Pu	+1	+6	+1	−0	+1	Sb	−18	−29	−28	−26	−18
						Bi	−16	−26	−24	−20	−15

The preparation of rare earth intermetallics is most conveniently performed by fusing the stoichiometric proportions of the composing metals in an arc furnace or in a levitation furnace. Combination of the metals by heating in a crucible (Al_2O_3, MgO or ThO_2) is less suitable owing to the rapid reaction of the rare earth component at elevated temperatures with the crucible material. In some cases one (or both) of the starting materials may possess a low heat of sublimation of evaporation (for example: Eu, Yb, Zn, Cd or Mg). Combination of the composing metals has then to be performed in a closed system consisting

of metals such as Ta or Mo. These latter two metals not only have a high melting point but in addition (as more or less follows from the large positive values of ΔH in table 1) do not react with the molten rare earth alloy.

A meaningful study of the physical properties of intermetallic compounds can only be made on single phase materials. Only a fraction of the compounds is in single phase condition after the melting together of the components. This is usually the case with congruently melting compounds such as for instance $LaAl_2$ in fig. 1. Incongruently melting compounds do not form directly from the melt. LaAl in fig. 1 is an example of such a compound. It is formed at 873°C by a so-called peritectic reaction between the primary $LaAl_2$ crystallites and a more La-rich liquid (44 at.% Al). Slow diffusion of the metal atoms at low temperatures prevents this peritectic reaction from reaching completeness during a normal cooling process. Single phase condition can be reached here by vacuum annealing at temperatures close to but below the peritectic reaction temperature (873°C in the case of LaAl). Sometimes the situation is more complicated. It is

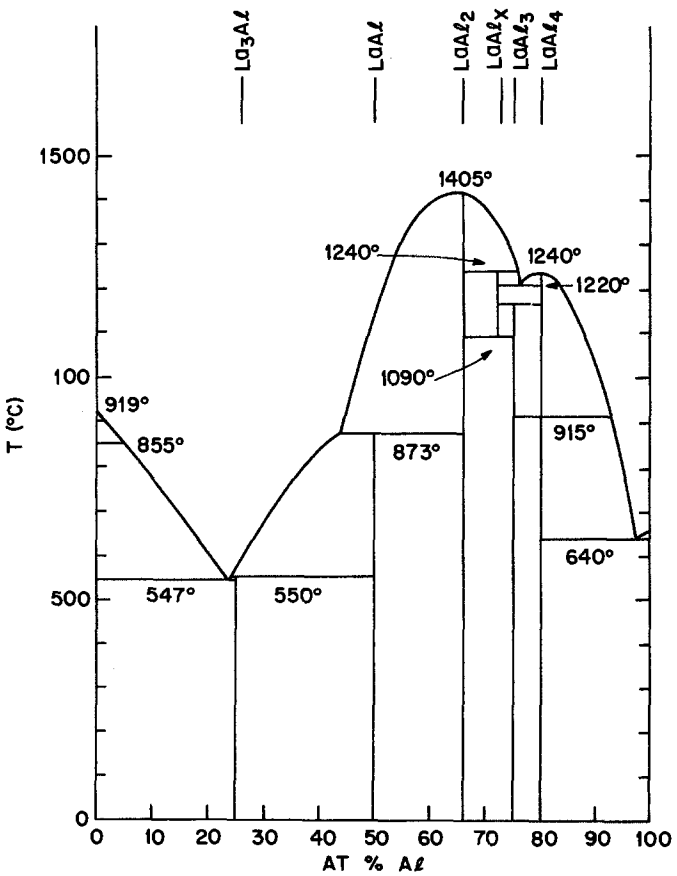

Fig. 1. Phase diagram of the La–Al system. The stoichiometric composition of $LaAl_x$ is approximately La_9Al_{11}. The compound $LaAl_4$ is slightly Al-deficient. Its actual stoichiometry corresponds to La_3Al_{11}.

seen in fig. 1 that La_9Al_{21} is also formed peritectically. In this case the vacuum annealing is strictly limited to the region between 1240° and 1090°C and subsequent quenching is required. The reason for this is the eutectoid decomposition of La_9Al_{21} into the adjacent phases $LaAl_2$ and $LaAl_3$ at 1090°C. The compound $LaAl_4$ is an example of a compound that needs heat treatment after melting, even though it melts congruently. At 915°C a structural phase transformation occurs. If the high temperature phase is desired, quenching from above this temperature is required. On the other hand, if one wishes to obtain the low temperature phase, one can remove residual amounts of the high temperature phase by annealing below the transformation temperature.

The examples given above may demonstrate that the availability of phase diagrams is often a great help in the preparation of single phase samples. Information on phase diagrams can be obtained from the books by Elliot (1965), Gschneidner (1961), Hansen (1958), Savitsky and Terekhova (1975), and Shunk (1969).

The most common crystal structures adopted by rare earth intermetallics have been collected together in table A.1 in the Appendix at the end of this review. The formulas of the compounds representing the structure type (column 1) have been written down in a manner that the sites of the first element correspond to the R sites in all cases. The last column of the table indicates with which non-rare earth component the rare earth partner can be combined in a particular structure type. For instance it can be derived from the table that RBe_{13}, RCo_{13} and RZn_{13} compounds exist, and that these have the cubic $NaZn_{13}$ structure with space group Fm3c. Very often the stability of a given crystal structure depends to a large extent on the relative size of the two components. In view of the lanthanide contraction of the rare earth it can happen that this particular structure does not persist through the whole lanthanide series. This is for instance the case with RCo_{13} which compound exists only for $R = La$. Alternatively one could say that, with the exception of $LaCo_{13}$, compounds of the type RCo_{13} are not stable with respect to R_2Co_{17} and elementary cobalt.

In the interpretation of magnetic data and, a fortiori, in the evaluation of hyperfine field data it is desirable to know the number of crystallographically non-equivalent R and M sites in a given compound. This can be derived from the data given in the fourth and fifth columns of table A.1. Again using the $NaZn_{13}$ structure type as an example, there is only a single rare earth site (a) but two different non-rare earth sites (b and i). The numbers in front of the parentheses indicate the occupation numbers. From these one can also find the number of formula units per unit cell. This is eight in the case of $NaZn_{13}$ and four in the case of Th_6Mn_{23}.

Some of the structure types listed are closely related. The crystal structures of Th_2Ni_{17}, Th_2Zn_{17}, Ce_2Ni_7, Gd_2Co_7, $CeNi_3$, $PuNi_3$ and $MgCu_2$ can be derived in a simple manner from the $CaCu_5$ type. For instance, the structure of Ce_2Ni_{17} (Th_2Ni_{17} type) is obtained from $CeNi_5$ ($CaCu_5$ type) by an ordered substitution of one third of the Ce sites by a pair of Ni atoms ($3\,CeNi_5 \rightarrow Ce_2Ni_2Ni_{15} = Ce_2Ni_{17}$). Another example is the CaB_6 type, which can be visualized as CsCl type with Ca

at the Cs sites and an octahedron of B atoms at the Cl sites. It falls outside the scope of this review to go into more detail regarding the various relationships of the structures given in table A.1. For this the reader is referred to excellent text books on this subject (Schubert 1964, Pearson 1958, 1972).

For the rare earth intermetallics the various representatives of the crystal structures of table A.1 are listed in tables A.2 and A.3 in the Appendix at the end of this review. The list is not complete in so far as it does not comprise those (few) groups of intermetallics for which no magnetic data are available in the literature.

In most of the compounds listed in tables A.2 or A.3 it is possible to replace the M component, or part of it, by a third component M' without changing the crystal structure. One speaks of pseudobinary compounds $R(M_{1-x}M'_x)_n$ if there exists a statistical distribution of M and M' atoms over the crystallographic site(s) available for the non-rare earth component. In some cases the substitution of M' atoms at M sites is not a random process but shows a preference for particular site(s) or for a particular coordination. If the preference is very pronounced these compounds can no longer be regarded as pseudobinaries but must be classified as ternary compounds. Apart from the ternary compounds that can be thought to arise from atomic ordering within pseudobinary compounds, compounds of a completely different composition and crystal structure exist which are in no way related to binary compounds.

No systematic studies have as yet been made of the magnetic properties of ternary compounds. The only exceptions are compounds of the type $RM_2M'_2$ and $RM_4M'_8$. The compounds $RM_2M'_2$ (M = Cr, Mn, Fe, Co, Ni, Cu, Ag and Au; M'_2 = Si, Ge) have the $ThCr_2Si_2$ structure derived from the $BaAl_4$ type (Rieger and Parthé 1969), in which the M atoms are restricted to the 4(d) sites and the M' atoms to the 4(e) sites (see table A.1). The compounds $RM_4M'_8$ have the $CeMn_4Al_8$ structure derived from the $ThMn_{12}$ type (Zarechnyuk and Krypiakevich, 1963). Here the M atoms (Cr, Mn, Fe and Cu) occupy the 8(f) sites while the M' atoms (Al) are accommodated at the 8(i) and 8(j) sites of the $ThMn_{12}$ structure (see table A.1, line 2). Representatives of both ternary series, together with a few other ternary compounds derived from the Fe_2P type (Dwight et al. 1968) are given in table A.4.

2. Compounds with non-magnetic elements

2.1. Interaction between the localized 4f moments

The spatial extent of the 4f electrons is very small in comparison to the interatomic spacings. There is no substantial overlap of the wave functions of 4f electrons centered on different atoms. This precludes a direct interaction between the localized moments. Two mechanisms have been proposed in which the 4f moment can interact in an indirect way. In the first of these, called the RKKY interaction, the magnetic coupling proceeds by means of spin polariza-

tion of the s-conduction electrons. In the second mechanism the spin polarization of the appreciably less localized rare earth 5d electrons plays an important role. These two mechanisms and their implications for the magnetic properties of the various intermetallic compounds, listed in tables A.2, A.3 and A.4 are briefly discussed below.

In its simplest form the RKKY theory was originally proposed by Ruderman and Kittel (1954) to describe the interaction between nuclear magnetic moments. Extensions to the model were made later on by Yosida (1957), Kasuya (1956) and DeGennes (1962a). In metal systems involving rare earth elements the localized rare earth spins S are engulfed by a sea of conduction electrons. These latter are spin polarized by the former through the exchange interaction

$$\mathcal{H} = -2J(q)s \cdot S \tag{1}$$

where s represents the spin of the Fermi surface conduction electrons and where the exchange integral $J(q) \equiv J(k' - k)$ depends on the wave vectors k and k' of the conduction electrons before and after scattering by the localized spin, respectively. This exchange interaction between localized spins and conduction electrons is treated as a perturbation on free conduction electron states. The conduction electron polarization is obtained by applying a first order perturbation to the free electron wave functions. The spatial spin up and spin down densities $|\psi^{\pm}(r)|^2$ of the conduction electrons are then given by

$$|\psi^{\pm}(r)|^2 = \tfrac{1}{2}N \pm (3n/16E_F) \sum_q J(q)f(q) \sum_i S_i(e^{iq\cdot(r-R_i)} + e^{-iq\cdot(r-R_i)}) \tag{2}$$

The sum over i counts the number of localized spins in the crystal. The other symbols in eq. (2) have the following meanings:

N: total number of conduction electrons present in a volume V,
n: average conduction electron to atom ratio,
E_F: Fermi level energy,
R_i: position vector of the i'th localized spin S_i.

The q'th Fourier component of the static free electron susceptibility $f(q)$ in this expression is given by

$$f(q) = 1 + \frac{4k_F^2 - q^2}{4k_F q} \ln \left| \frac{2k_F + q}{2k_F - q} \right| \tag{3}$$

k_F being the Fermi wave vector.

An analytical expression for the conduction electron spin polarization $P(r) \propto |\psi^{+}(r)|^2 - |\psi^{-}(r)|^2$ is obtained if $J(q)$ in eq. (2) is assumed to be a constant, $J(0)$

$$P(r) = -\frac{9n^2\pi J(0)}{2E_F} |\langle S_z \rangle| \sum_i F(2k_F \cdot |r - R_i|). \tag{4}$$

Due to the oscillating character of the function $F(x) = (x \cos x - \sin x)/x^4$ this spin polarization is spatially non-uniform. The spatial variation of $F(x)$ is shown graphically in fig. 2. In the bottom part of the figure the positions of several

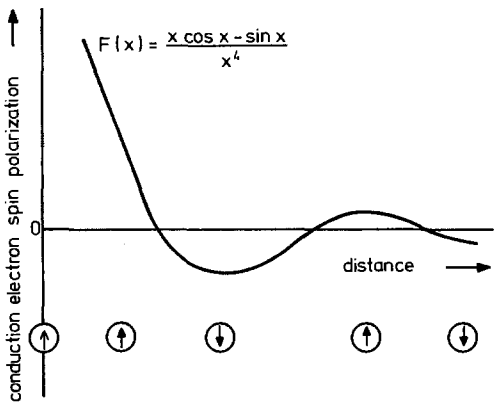

Fig. 2. Spatial variation of the RKKY function $F(x) = (x \cos x - \sin x)/x^4$. The position of several localized moments at a distance R_i from the central ion ($r = 0$) is indicated by arrows.

localized moments have been indicated. These may be visualized as representing 4f atoms residing in the first, second, third and fourth neighbour shells of the central 4f atom. If we consider, for instance, an interaction of the central 4f moment with only one of the neighbouring 4f moments, we see that this interaction will vary from one neighbour site to the other: the neighbour atom will orient its spin moment according to the local spin polarization, and the magnitude of the interaction is proportional to $P(r)$. For each localized moment, the total interaction with the other moments present in the crystal is obtained by summing the contributions originating from the conduction electron spin polarization produced by all the other moments at this particular site. The sign of this sum determines whether the 4f spin moments will ultimately order ferromagnetically or antiferromagnetically.

An expression for the paramagnetic Curie temperature θ_p can be obtained from a combination of the molecular field model (DeGennes 1962a, b) with the expression of the second order perturbed energy associated with the s–f exchange interaction (Yosida 1957)

$$\theta_p = -\frac{3\pi n^2 J(0)^2}{k_B E_F} S(S+1) \sum_i F(2k_F R_i). \tag{5}$$

If one includes in the total energy expression the hyperfine interaction between the s-conduction electrons and the nuclear magnetic moments (I), characterized by the Hamiltonian

$$\mathcal{H} = A(q)\boldsymbol{s} \cdot \boldsymbol{I} \tag{6}$$

one finds in a similar manner an expression for the hyperfine field H_N (Yosida 1957)

$$\boldsymbol{H}_N = -\frac{9\pi n^2 A J(0)}{2E_F g_n \mu_n} |\langle S_z \rangle| \sum_i F(2k_F R_i) \tag{7}$$

where the origin is chosen at the nuclear site that is considered, and where the summation runs over all the other lattice sites. A represents the effective hyperfine structure coupling constant, and g_n and μ_n are the nuclear g-value and the nuclear magneton, respectively.

In the magnetically non-ordered regime it is more appropriate to consider the Knight shift (K) rather than H_N. This quantity is given by (Jaccarino et al. 1960)

$$K = K_0[1 + J_{sf}(S \cdot J)\chi_f/2g_f\mu_B^2 J(J+1)] \tag{8}$$

where

$$J_{sf} = -12\pi n J(0) \sum_i F(2k_F R_i). \tag{9}$$

Here g_f is the rare earth ion Landé g-value, μ_B the Bohr magneton and K_0 the Knight shift due to Pauli paramagnetism only. The quantity χ_f is the 4f electron magnetic susceptibility.

The expression for the EPR g-shift due to the s–f interaction is given in the RKKY model by (Yosida 1957)

$$\Delta g = 3nJ(0)/2E_F. \tag{10}$$

The excess bulk magnetic moment due to the spin polarized conduction electrons can be expressed as (DeGennes 1962a)

$$\Delta M = 3nJ(0)(g_f - 1)J\mu_B/2E_F. \tag{11}$$

In the free electron model one has furthermore the following relation between k_F (or E_F) and n, N and V

$$k_F^3 = 3\pi^2 nN/V. \tag{12}$$

It follows from the above discussion that the RKKY model lends itself fairly well to a comparison with experimental data derived from magnetization measurements. In the first place it is to be noted that the paramagnetic Curie temperature, via the sum function $\Sigma_i F(2k_F R_i)$ in eq. (5), is structure dependent: It can be inferred from fig. 2 that the contributions due to the moments residing in the various neighbour shells largely cancel, but that this cancellation depends strongly on the radius of the neighbour atom shell and the number of 4f atoms present in it. The extent of this cancellation therefore differs from structure to structure and can lead to order of magnitude differences in the value for θ_p. In the second place it is seen that, through k_F appearing in eq. (5) the value of θ_p is also dependent on the number of conduction electrons, nN, present per unit cell volume V [see eq. (12)]. The effect of changes of k_F are most conveniently illustrated again by means of fig. 2. For larger or smaller k_F values, the distances, R, where the function $F(2k_F R)$ passes through zero, are reduced or increased, respectively. The oscillations are, as it were, compressed or expanded in the R direction. For a given structure, i.e. for fixed neighbour atom distances, this leads to an altered contribution for each of the neighbour shells, which can seriously affect the value of θ_p. The appearance of a wave number (k_F) rather

than just the number of conduction electrons is inherent in the long-range nature of the interaction expressed in eq. (5).

If a given intermetallic compound orders ferromagnetically at low temperatures one can compare the excess magnetization measured on top of the free ion value ($gJ\mu_B$) with the theoretical result given by eq. (11). Such a comparison is in general only restricted to ferromagnetic Gd compounds where moment reductions due to crystal field effects are absent.

It can furthermore be seen that via eqs. (7), (8) and (10) sufficient contact is also made with experimental results available from various resonance techniques such as NMR, the Mössbauer effect and EPR.

A different coupling scheme between the localized 4f moments was proposed by Campbell (1972). This scheme involves the 5d electrons of the rare earth elements. By means of ordinary f–d exchange the 4f moment induces a positive local d moment. The d electrons are by far less localized than the 4f electrons, and the mutual interaction between the d electrons (involving also d electrons on other rare earth sites) is in many respects similar to that encountered in normal d-transition metals. This implies that the 4f induced positive d electron polarization does not remain restricted to the particular atom in question but has a much larger spatial extent, at least if the rare earth concentration in the compound is sufficiently high to still guarantee overlap of the 5d electron wave functions. Campbell argues that since the d–d interaction is positive and since the f–d interaction occurs twice in the total coupling term between two R-moments, one ends up with a net positive indirect 4f–4f interaction. Apart from the fact that it predicts positive values of θ_p, this model in its present form is less well suited for comparison with the experimental data. The following requirements should be satisfied: If the above d–d coupling scheme is effective the 5d bands in the corresponding intermetallics should be partially filled. Part of the electrons at the Fermi level should exhibit therefore a pronounced d-character. Furthermore, partial filling of the narrow 5d bands implies a high density of states at the Fermi surface. It is sometimes possible to check the fulfillment of these two requirements by experiment. Although the contact of the d–d coupling scheme with the experimental situation is much more difficult to achieve than in the case of the RKKY scheme, it does not necessarily mean that the contributions of the former model to the 4f–4f coupling are less important compared to the latter. That the d electrons are indeed expected to play a significant role was for instance shown by band structure calculations performed on Gd by Harmon and Freeman (1974). According to these calculations all electron states on or very near the Fermi surface have 80–95% $l = 2$ character, implying a dominant role in the 4f moment coupling by the d-like electrons.

2.2. Crystal field effects

In an intermetallic compound the composing elements lose their valence electrons to the conduction band. In general one can speak therefore of a lattice of positive charges immersed in a sea of conduction electrons. The 4f electrons

residing on a given rare earth ion will experience the electric field produced by the screened charge of the surrounding ions. The effect of this electric field on the 4f wave functions leads in general to a complete or partial removal of the $(2J+1)$ fold degeneracy of the ground J multiplet level. Deviations from free ion behaviour can be expected therefore whenever the temperature decreases below a value smaller than the total splitting of the ground state after removal of the degeneracy mentioned. Since the spatial extent of the 4f wave functions is rather small, the crystal field splitting is small compared to the spin orbit interaction. The total angular momentum can therefore be taken as a good quantum number and the effect of the crystal field can be regarded as a small perturbation on the $(2J+1)$ fold degenerate wave functions $\langle J, J_z|$ of the ground multiplet.

The electrostatic potential $V_c(r)$ due to charges Z_j located at a distance R_j, for points close to the origin at the rare earth ion in question, can be given by

$$V(r) = \sum_j \frac{Z_j}{|R_j - r|}. \tag{13}$$

The perturbing crystal field Hamiltonian then is

$$\mathcal{H}_c = -e \sum_i V(r_i) \tag{14}$$

where the summation extends to all 4f electrons at r_i forming part of the rare earth ion considered.

This crystal field Hamiltonian is most conveniently represented by a series development in Tesseral harmonics f_{kq} through

$$\mathcal{H}_c = \sum_{k=0}^{\infty} \sum_{q=0}^{k} A_k^q \sum_i f_{kq}(r_i) \tag{15}$$

where the summation over i is to be performed again over all the 4f electrons. The unrenormalized f_{kq} are defined through

$$c_{k0} f_{k0}(r) = r^k Y_k^0(\theta, \phi) \tag{16a}$$

$$c_{kq} f_{kq}(r) = 2^{-1/2} r^k [Y_k^{-q}(\theta, \phi) + (-1)^q Y_k^q(\theta, \phi)] \tag{16b}$$

where $Y_k^q(\theta, \phi)$ are the standard normalized spherical harmonics. Most of the f_{kq} along with their normalization constants c_{kq} are given in the review by Hutchings (1964). For the rare earth elements the summation over k in eq. (15) may be restricted to $k \leqq 6$, since otherwise the matrix elements are zero, while the term with A_0^0 is irrelevant. In the more restricted point charge model the electric charges Z_j are identified with point charges located at the sites of the surrounding ions. The lattice coefficients A_k^q, following Stevens' (1953) conventions, are then given by

$$A_k^q = -e \frac{4\pi}{2k+1} c_{kq}^2 \sum_j Z_j \frac{f_{kq}(\boldsymbol{R}_j)}{R_j^{2k+1}}. \tag{17}$$

The point symmetry causes a number of A_k^q to vanish and requires, once the

quantization axis (z-axis) is chosen, the remaining A_k^q to differ by constant factors. For instance, for a cubic field with $z \parallel [001]$

$$\mathcal{H}_c = A_4^0[f_{40} + 5f_{44}] + A_6^0[f_{60} - 21f_{64}]. \tag{18}$$

In a hexagonal field the expressions are more complex in general. For instance, for rare earth ions residing at sites of point symmetry D_{6h} (such as in $CaCu_5$ type compounds) the Hamiltonian for $z \parallel [001]$ is

$$\mathcal{H}_c = A_2^0 f_{20} + A_4^0 f_{40} + A_6^0 f_{60} + A_6^6 f_{66}. \tag{19}$$

In these expressions f_{kq} is the shorthand notation for

$$\sum_i f_{kq}(r_i).$$

The calculation of the matrix elements of f_{kq} in the $\langle J, J_z|$ representation, for the general case that one wishes to include ground- as well as excited J-multiplet levels, has been reviewed by De Wijn et al. (1976a). Detailed information on such calculations can also be found in the book of Wybourne (1965).

In some cases it is sufficient to consider only the ground J-manifold of the 4f electrons. The matrix elements can then be derived by Stevens' (1953) method of operator equivalents via

$$\sum_i f_{kq}(r_i) = \theta_k \langle r^k \rangle O_k^q \tag{20}$$

where O_k^q are operators in terms of J_x, J_y and J_z. The quantities θ_k are multiplicative factors, characteristic of a given rare earth element. Values of θ_k are listed in the review by Hutchings (1964), while values of $\langle r^k \rangle$ have been calculated in the paper by Freeman and Watson (1962). An alternative notation for the Stevens multiplicative factors is $\theta_2 = \langle J \| \alpha \| J \rangle$, $\theta_4 = \langle J \| \beta \| J \rangle$ and $\theta_6 = \langle J \| \gamma \| J \rangle$; very often only the abbreviations α_j, β_j and γ_j are used. It has become common usage to represent the strength of the crystal fields by means of the coefficients $B_k = A_k \langle r^k \rangle$ so that eq. (15) now reads

$$\mathcal{H}_c = \sum_{k=0} \sum_{q=0} B_k^q O_k^q. \tag{21}$$

The coefficients B_k, through θ_k, still contain the specific properties of a given rare earth ion and hence are not constant in going through the rare earth series. Better quantities to specify the intensity of the crystal field in a given crystal structure are $A_4\langle r^4 \rangle$, $A_6\langle r^6 \rangle$ etc. In order to exclude also the variations of the quantities $\langle r^k \rangle$ from ion to ion one may use the reduced crystal field parameters $A_4 a^5$, $A_6 a^7$, etc., where a is the lattice constant (cubic compounds).

A somewhat different notation has been introduced by Lea et al. (1962). These authors considered crystal fields of cubic symmetry with $z \parallel [001]$ for which eq. (18) reduces to

$$\mathcal{H}_c = B_4(O_4^0 + 5O_4^4) + B_6(O_6^0 - 21O_6^4) \equiv B_4 O_4 + B_6 O_6. \tag{22}$$

This Hamiltonian was re-written by Lea et al. into the form

$$\mathcal{H}_c = W[xO_4/F_4 + (1-|x|)O_6/F_6] \tag{23}$$

where W is an energy scale factor and x represents the relative weight of the fourth- and sixth-order terms. The quantities F_4 and F_6 are numerical factors common to all matrix elements and values of these have been listed for all rare earths by Lea et al. (1962). The parameters W and x are related to the B_4 and B_6 coefficients by $Wx = B_4F_4$ and $W(1-|x|) = B_6F_6$; $0 < x < 1$.

The eigenfunctions and energies corresponding to the crystal field split states of the ground J-multiplet can be calculated by diagonalization of $\mathcal{H}_c$. Depending on whether one uses eq. (21) or eq. (23) the eigenfunctions and energies are obtained with $A_k\langle r^k\rangle$ or W and x as parameters, respectively. For the latter case the eigenfunctions have been listed for various x by Lea et al. These authors also give a schematic representation of the energy levels as a function of W and x.

At this point it is perhaps desirable to comment further on the fact that analyses of crystal field effects in terms of adjustable parameters, such as those mentioned above, are preferred to first principle calculations by means of point charges [eq. (17)]. In the first place it is rather difficult to predict the charge of a given element in a given compound on the grounds of its valency. Due to the differences in electronegativity of the composing elements, charge transfer takes place and the charge of a given ion is dependent for these reasons on the nature and the concentration of the partner element. Bucher and Maita (1973) showed that for simple ligand systems a correlation exists between the crystal field splitting associated with a given sign and magnitude of the ligand charges on the one hand and the electronegativities of the ligand elements on the other. Apart from this rather trivial difficulty, a rather fundamental problem regarding the applicability of eq. (17) is that in a metal the assumption of even screened point charges is highly unrealistic. For ligands containing d electrons in particular the charge distribution will not be the same in the various crystallographic directions, so that the strength of the actual crystal field may differ from that due to the point charges on the lattice sites. Extremely large deviations from the point charge model can be expected if there is a high density of 5d electrons at the rare earth site itself (Williams and Hirst 1969, Eagles 1975, Dixon 1973, Morin et al. 1974a, Devine 1974). Due to their large spatial extent, crystal field splitting of the 5d electron states will be much greater than that involving the 4f electrons. These 5d electrons will therefore occupy almost exclusively the symmetry state(s) having the lowest energy after the crystal field splitting (Williams and Hirst 1969). In view of the close proximity of the 5d electrons, symmetry and strength of the actual crystal field felt by the 4f electrons will in this case predominantly be determined by the charge distribution associated with the lowest crystal field state of the 5d electrons rather than by the ionic lattice.

In recent years it has become possible to obtain direct information on the level scheme of the crystal field split ground state by means of neutron scattering experiments. The $A_k\langle r^k\rangle$ parameters responsible for a given level scheme can

then be compared with point charge calculations. Very often it was found that the point charge model prediction is incorrect by more than an order of magnitude, or even by its sign (Morin et al. 1974a, Gross et al. 1977, Furrer 1975). For these reasons it has become no longer fashionable to analyse experimental data on crystal field effects by means of point charge considerations.

There are two main features that will make crystal field effects manifest in the experimental data. The first of these is a reduction of the rare earth's magnetic moment (in the sense of a definite decrease of the rare earth's moment length). The second feature is an often pronounced magnetocrystalline anisotropy. This, too, can give rise to a reduction of the bulk magnetic moment, even though the magnitude of the actual moment may be close to the free ion value. Direct information on the magnitude of the rare earth moment can be obtained from neutron diffraction experiments. In the tables it has been indicated on which compounds neutron diffraction data have been performed. In almost all cases the rare earth moment has been reported to be below the free ion value. A special case is formed by rare earth ions with an even number of electrons. Here the crystal field splitting can lead to a singlet ground state with zero magnetic moment. In the case of a non-negligible exchange interaction between the localized moments this can lead to interesting collective excitation behaviour (Wang and Cooper 1969, Buyers et al. 1975).

In order to describe the magnetocrystalline anisotropy in terms of crystal fields one has to take account of the fact that due to the presence of exchange interactions the Zeeman splitting and crystal field splitting may be of comparable magnitude. The exchange energy is determined by the Hamiltonian

$$\mathcal{H}_{ex} = 2\mu_B \boldsymbol{H}_{ex} \cdot \boldsymbol{S} \tag{24}$$

where H_{ex} represents the exchange field exerted on the R spin by the surrounding R- and M spins. It will therefore be necessary to include H_{ex} in the diagonalization procedure. The total perturbing Hamiltonian then becomes

$$\mathcal{H}_t = \mathcal{H}_c + \mathcal{H}_{ex}. \tag{25}$$

In routine computations the diagonalization is usually performed for many different directions $\boldsymbol{n}$ of $\boldsymbol{H}_{ex}$, keeping the quantities $A_k\langle r_k\rangle$ and H_{ex} as parameters. The resulting energy values E_i are subsequently used to calculate the partition function $Z(\boldsymbol{n}, T)$ and the Helmholtz free energy

$$F(\boldsymbol{n}, T) = -k_B T \ln Z(\boldsymbol{n}, T). \tag{26}$$

The direction of easy magnetization at a given temperature is the direction of $\boldsymbol{n}$ in which the free energy has its lowest value. Estimates of the magnitude of H_{ex} can often be obtained for the compound considered from magnetic data available for this or related compounds in literature. Limits for the parameters $A_k\langle r^k\rangle$ may be set by the requirement that, with a given set of $A_k\langle r^k\rangle$ values, a consistent description should be obtained for all the observed easy directions within a series of isostructural RM_n compounds.

Usually the bulk magnetocrystalline free energy $E(n, T)$ of a cubic system can be expanded into a power series of the direction consines α of the direction of magnetization n with respect to the cube edges

$$E(n, T) = K_0 + K_1(\alpha_1^2\alpha_2^2 + \alpha_2^2\alpha_3^2 + \alpha_1^2\alpha_3^2) + K_2\alpha_1^2\alpha_2^2\alpha_3^2 + K_3(\alpha_1^4\alpha_2^4 + \alpha_2^4\alpha_3^4 + \alpha_1^4\alpha_3^4) + \ldots \quad (27)$$

For a hexagonal system the free energy expression becomes

$$E(n, T) = K_0 + K_1 \sin^2\theta + K_2 \sin^4\theta + K_3 \sin^6\theta + K_4 \sin^6\theta \cos^6\phi \quad (28)$$

where θ and ϕ are the polar angles of n relative to the c-axis. The anisotropy constants K_i can be obtained by comparing $E(n, T)$ in these expressions with $F(n, T)$ of eq. (26) (Atzmony et al. 1973a). Both sides of eq. (28) are subsequently calculated for a number of different directions of n after which the quantities K_i can be derived by a fitting procedure. The temperature dependence of K_i can be obtained by repeating this treatment for different values of T. We note that temperature dependences of K_i of a more general character, such as considered for instance by Akulov (1936) and more recently by Callen and Callen (1971), are not included in the above treatment.

2.3. Magnetic properties

2.3.1. Compounds with group III elements

Magnetic investigations have been performed on rare earth boron compounds of the following compositions: RB_2, R_2B_5, RB_4, RB_6 *and* RB_{12}. The data available have been collected in table A.2a.

Compounds of the series RB_2 seem to be stable only in the case of rare earths with an atomic number smaller than that of Tb. Neutron diffraction performed on TbB_2 shows that this compound is a ferromagnet below $T_c = 151$ K with an easy direction of magnetization parallel to the c-axis of its hexagonal AlB_2 structure (Will 1977a). This suggests that the other RB_2 compounds of this series, in each of which a positive paramagnetic Curie temperature has been reported (Buschow 1977d), are also ferromagnets (see table A.2a). The results obtained on TbB_2 have furthermore shown that a considerable magnetic anisotropy can be present, giving rise to a large intrinsic coercive force.

Unlike the series RB_2 and R_2B_5 listed in table A.2a the series RB_4 is fairly complete. It is seen in the table that all magnetic rare earth elements give rise to antiferromagnetic ordering in RB_4. The only exception is PrB_4, which is ferromagnetic at low temperatures. The change in sign of the magnetic coupling within a series of rare earth compounds is highly uncommon and needs further comment. In the first place it seems less likely that the 5d electrons contribute significantly to the indirect coupling between the localized 4f moments in RB_4 since a large 5d electron density is improbable in view of the diamagnetic character of LaB_4 and LuB_4. The only alternative then left is a coupling via the RKKY mechanism (see section 2.1). It can be derived from eq. (5) that the sign of θ_p in the RKKY approach is determined by the lattice sum $\Sigma_i F(2k_F R_i)$. This

sum is subject to scarcely any changes if one proceeds through the whole series from LaB_4 to LuB_4 because k_F is proportional to a reciprocal lattice vector. The decrease of the lattice constants will therefore leave the products $k_F R_i$ more or less unchanged (this holds strictly in cubic structures and only approximately in structures of lower symmetry). The change in sign of θ_p within the RB_4 series seems therefore in conflict with the RKKY model.

Kaplan and Lyons (1963) have shown that the presence of an orbital momentum on the rare earth atoms can lead to a modified exchange interaction between the 4f moments. According to Levy (1969) this leads to an expression of the paramagnetic Curie temperature θ_p given by

$$\theta_p = (3k_B)^{-1} J(J+1)[(g-1)^2 Q_{0101} + (2-g)Q_{1010} + C_n^2 Q_{2121} + 2(g-1)(2-g)Q_{1001} + 2(g-1)C_n Q_{0121} + 2(2-g)C_n Q_{1021}]. \quad (29)$$

The quantities $Q_{p_1 k_1 p_2 k_2}$ are generalizations of the term $J(0)^2 \Sigma_i F(2k_F R_i)$ in eq. (5) and are defined in Levy (1969). They originate from pair interactions described by orbital and spin tensor operators of ranks p and k. Levy's extension of the RKKY approach has been used by Buschow and Creijghton (1972) to explain the sign reversal of θ_p in the RB_4 series. Confirmation of the applicability of an RKKY type exchange mechanism has also been derived from results of NMR (Creijghton et al. 1973) neutron diffraction (Schäfer et al. 1976a). In all these investigations the value of k_F was considered as a parameter since, in view of the presence of B–B bonds, no straightforward relation of k_F to the formal number of valence electrons [eq. (12)] can be expected.

The series RB_6 forms by far the most interesting series of the borides since it comprises compounds which are diamagnetic (R = La), antiferromagnetic (R = Ce, Pr, Nd, Gd, Tb, Dy and Ho) and ferromagnetic (R = Eu). The exceptional behaviour of EuB_6 is a result of the fact that this compound is a semiconductor (Matthias et al. 1968, Geballe et al. 1968). Instead of the normal RKKY mechanism responsible for the antiferromagnetic exchange in, for instance GdB_6, the Bloembergen–Rowland interaction (Bloembergen and Rowland 1955) seems more appropriate in the case of EuB_6 (Fisk 1971, Wood 1971). The relative importance of the two types of interactions was estimated by Glausinger (1975) on the basis of EPR in EuB_6. However, it appears that the contribution of the Bloembergen–Rowland type interaction is only moderate. The values observed for θ_p in RB_6, with R being trivalent, do not vary according to $S(S+1)$ or $(g-1)^2 J(J+1)$ as expected on the basis of eq. (5). This would suggest that an additional coupling mechanism involving the rare earth 5d electrons (see section 2.1) is present in these compounds. No evidence of any appreciable s–d exchange interaction was found, however, from EPR performed on $Gd_x La_{1-x} B_6$ (Sperlich et al. 1973).

Effects of short-range ordering in RB_6, derived from EPR and resistivity data (Fisk et al. 1971) are discussed by Taylor (1975) and Fisk et al. (1971). Finally we note that a rather complex situation is found in SmB_6, where Sm occurs in a so-called mixed valence state (Cohen et al. 1970, Chazalviel 1976). A more

detailed review of the magnetic properties of rare earth boron compounds, including the RB_{12} compounds, is given in Buschow (1977d).

The number of intermetallic compounds occurring in the various R–Al systems is considerable (Buschow and Van Vucht 1967). The magnetic properties of most of these compounds have been reported in the literature and the results are gathered in table A.2b. Rather high magnetic ordering temperatures are exhibited by the first members of the R_3Al_2 series. In Gd_3Al_2 the Curie temperature is even close to room temperature. Results of magnetic dilution studies performed with Gd_3Al_2 are discussed in terms of the RKKY approach in Buschow (1975a). Barbara et al. (1971a) showed that the high magnetocrystalline anisotropy in Tb_3Al_2, in conjunction with the comparatively low coupling strengths between the localized moments, can lead to a new type of magnetization process. It is well known that minimization of the magnetostatic energy requires that in zero applied field a ferromagnet decomposes into magnetic domains separated by walls whose thickness is determined by a compromise between the coupling energy and the anisotropy energy. In Tb_3Al_2 the domain walls are extremely thin and extend over a few interatomic distances only. There is a considerable difference in energy between positions in which the centre of the wall coincides with an atomic layer and positions in which the centre falls in between two atomic layers. Movement of the Bloch walls therefore involves the surmounting of an energy barrier. Consequently the magnetization process needs thermal activation. Macroscopically the existence of these narrow walls becomes manifest through the presence of large intrinsic coercive forces with a pronounced temperature dependence. This feature will be discussed in more detail in connection with TbGa below (see figs. 4 and 5).

It is apparent from the large number of references listed in table A.2b for RAl_2 that the compounds of this series have received considerable attention. In part this is due to the simple crystal structure of these compounds. It is also known that it is relatively easy to prepare RAl_2 samples in single phase condition.

Most of the results of magnetic investigations performed on these compounds could be explained by the presence of a ferromagnetic coupling between the 4f moments in conjunction with a crystal field splitting of about the same order of magnitude. For the characterization of the crystal fields in these compounds a reasonably consistent set of data is available, obtained by measurements of the specific heat (Hill and Machado da Silva 1969, Deenadas et al. 1971), the Al^{27} NMR (De Wijn et al. 1973, Kaplan et al. 1973), inelastic neutron scattering (Houmann et al. 1974) and by measurements of the magnetization in various directions on single crystals (Barbara et al. 1975a, b, 1977a, e, Cock et al. 1974). The level schemes shown in fig. 3 and the parameters listed in table 2 are based primarily on the single crystal data. (It was found that several of the RAl_2 compounds undergo a spontaneous cell distortion at low temperatures. This has been attributed to a minimization of the crystal field energy (Barbara et al. 1977c). With the exception of $CeAl_2$ the values of A_4a^5 and A_6a^7 listed in table 2 do not vary by more than a factor of about 2 from compound to compound. A relatively large error may be involved with the parameters of

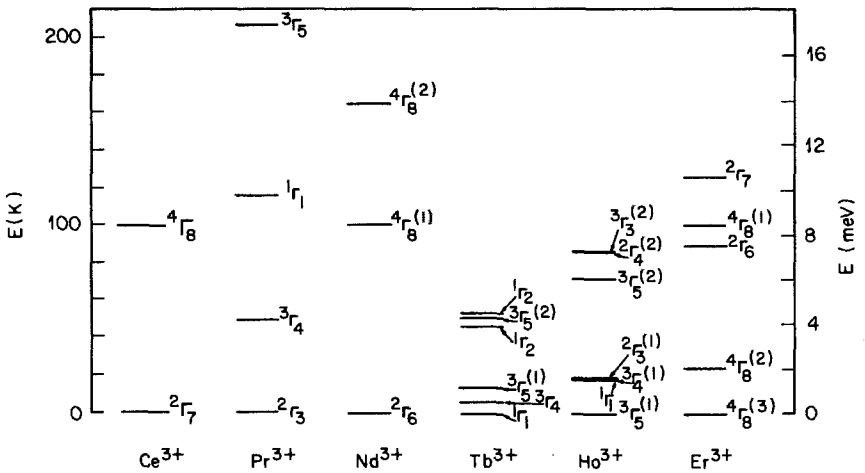

Fig. 3. Level scheme of the crystal field split ground J multiplet of several rare earth compounds of the type RAl_2. The degeneracy of the various levels is indicated by the left hand index of the level symbol. The level schemes correspond to the parameters given in table 2.

TABLE 2

Crystal field parameters of various cubic Laves phase compounds RAl_2. For a definition of the quantities listed see section 2.2.

Compound	Easy axis	B_4 (10^{-4} meV)	B_6 (10^{-4} meV)	x	W (meV)	A_4a^5 (10^6 meVÅ)	A_6a^7 (10^4 meVÅ)	References
$CeAl_2$	[111]	240	0	1	1.44	3.8	–	1,2,3
$PrAl_2$	[100]	−44	−88	0.70	−0.38	55	−4.3	4,5
$NdAl_2$	[100]	−10	40	−0.37	0.16	36	−3.8	6,4,7
$SmAl_2$	[111]	–	–	–	–	22	−2.0	8,4,9
$TbAl_2$	[111]	3.0	0.25	0.91	0.020	43	−1.6	4,5
$DyAl_2$	[100]	–	–	–	–	–	–	4,10
$HoAl_2$	[100]	−0.69	0.64	−0.32	0.013	42	−4.4	11,5
$ErAl_2$	[111]	1.10	−1.3	−0.26	−0.025	54	−6.3	4,5

1. Barbara et al. (1975a)
2. Hill and Machado da Silva (1969)
3. Deenadas et al. (1971)
4. Kaplan et al. (1973)
5. Purwins et al. (1976)
6. Cock et al. (1974)
7. Houmann et al. (1974)
8. De Wijn et al. (1973)
9. Buschow et al. (1973a)
10. Barbara et al. (1977d)
11. Barbara et al. (1976)

$SmAl_2$. For Sm^{3+} the separation between the multiplet J levels is rather close compared to the crystal field splitting. The crystal field analysis has therefore to be based on a mixing of excited J levels into the ground J multiplet due to the perturbing influence of crystal fields and exchange fields (De Wijn et al. 1976b, Malik et al. 1974) (see section 2.2). The data of $SmAl_2$ listed in the table are based on $A_4\langle r^4\rangle/k = 150$ K, $A_6\langle r^6\rangle/k = -150$ K derived from the combination of NMR data (De Wijn et al. 1973, Kaplan et al. 1973) and magnetic measurements (Buschow et al.

1973a). It is to be noted that the sixth order contribution is a consequence of the above-mentioned mixing and would otherwise be absent for $J = \frac{5}{2}$ ions. The parameter A_4a^5 of $CeAl_2$ does not fit in the series of values of the RAl_2 compounds. This deviation might be closely connected with the electronic structure of cerium in this compound. In general it can be said that most of the experimental data show cerium to be trivalent in $CeAl_2$. The fact that $CeAl_2$ is the only RAl_2 compound which orders antiferromagnetically (it has two phase transitions at 3.4 and 4.5 K (Walker et al. 1973, Barbara 1975a) and the fact that its electrical resistivity (van Daal and Buschow 1969, Maple 1969) has a remarkable temperature dependence suggests, however, that the interaction of the 4f and 5d(6s) electrons of Ce in $CeAl_2$ is nevertheless different from that in the other RAl_2 members.

Magnetic dilution experiments (Buschow et al. 1967, Maple 1969) and NMR data (Kaplan et al. 1973, Jaccarino et al. 1960, Dormann et al. 1973, McHenry et al. 1972) seem to favour an interpretation of the magnetic properties of RAl_2 in terms of the RKKY formalism. The s–f exchange integral [eqs. (5–10)] was found to vary slightly across the RAl_2 series. This was explained by Levy as being a result of orbital contributions to the s–f exchange and spin orbit coupling of the conduction electrons (Levy 1971). Kaplan et al. (1973) found evidence for the existence of about 10% anisitropy in the s–f exchange constant $J(0)$. This was correlated by these authors with the small helical antiferromagnetism superimposed on the ferromagnetic moment arrangement in $DyAl_2$ (Nereson et al. 1966). Evidence for the existence of a large anisotropic exchange contribution in $DyAl_2$ was also derived from single crystal data (Barbara et al. 1977b) and from EPR measurements on $Gd_{1-x}Dy_xAl_2$ (Nguyen et al. 1976). A further manifestation of higher order terms in the exchange Hamiltonian in RAl_2 compounds was found in $HoAl_2$ where, well below T_c, it leads to a change in easy direction (Barbara et al. 1975b, 1977b, Sankar et al. 1977).

Other experimental data support the notion that the magnetic interactions in the RAl_2 series are much more compounded than the simple RKKY approach outlined in section 2.1.1 would suggest: Magnon dispersion relations were studied by Bührer et al. (1973) on a single crystal of $TbAl_2$. An analysis of their data clearly shows a long-range oscillatory character of the exchange interaction but quantitative agreement with RKKY predictions is lacking. Dormann et al. (1973) also found that the conduction electron polarization around a 4f spin moment decreases less strongly with distance than expected on the grounds of the RKKY picture. Davidov et al. (1973a) were led to assume the presence of spin polarized d electrons residing in a narrow band in order to explain their EPR results on $Gd_{1-x}La_xAl_2$. A relatively large participation of d electrons to the exchange interaction finally follows from a comparison of the values of T_c and H_N (eqs. (5) and (7), respectively) in various rare earth compounds (Dormann et al. 1976). Some of the features sketched above were encountered in a variety of compounds other than RAl_2. For this reason we will postpone an evaluation of the validity of the RKKY approach in RAl_2 and give it together with an evaluation of the coupling mechanism in other compounds in section 2.3.5.

It can be seen from table A.2b that the ordering temperatures of the compounds RAl_3 and R_3Al_{11} are much lower than in RAl_2. The compounds $CeAl_3$ (Buschow et al. 1971a) and Ce_3Al_{11} (Van Daal and Buschow 1970c), like $CeAl_2$, show a rather anomalous temperature dependence of their resistivity. In $CeAl_3$ the resistivity increases with decreasing temperature and after reaching a maximum at about 35 K decreases steeply. Attempts have been made to explain this behaviour by means of the Kondo side band model, which describes Kondo exchange scattering of the conduction electrons in the presence of localized moments with a crystal field split ground state (Maranzana 1970). Alternative explanations are based on scattering on virtual bound 4f states of widths narrower than the crystal field splitting (Andres et al. 1975a). Evidence for the presence of crystal field splitting of the required magnitude (Maranzana 1970, Andres et al. 1975a) was obtained from inelastic neutron scattering experiments (Murani et al. 1977). It falls outside the scope of this book to review all the experimental and theoretical material accumulated on $CeAl_3$ and related compounds. The same holds with respect to the so-called mixed valence compounds $YbAl_3$ and $YbAl_2$ (Klaasse et al. 1976).

Inelastic neutron scattering experiments have been reported for $PrAl_3$ (Alekseev et al. 1976). The results disagree with the level scheme arrived at earlier by means of specific heat data (Mahoney et al. 1974).

The magnetic properties of rare earth gallium compounds are listed in table A.2c. The highest ordering temperatures are observed in RGa. Neutron diffraction performed on some of these compounds shows that at low temperatures the moment arrangement is not simply ferromagnetic (Barbara et al. 1971b). The magnetization processes are governed by the presence of narrow walls leading to a strongly temperature dependent intrinsic coercive force. A typical set of data (Barbara et al. 1971b) for a system containing narrow walls is shown in figs. 4

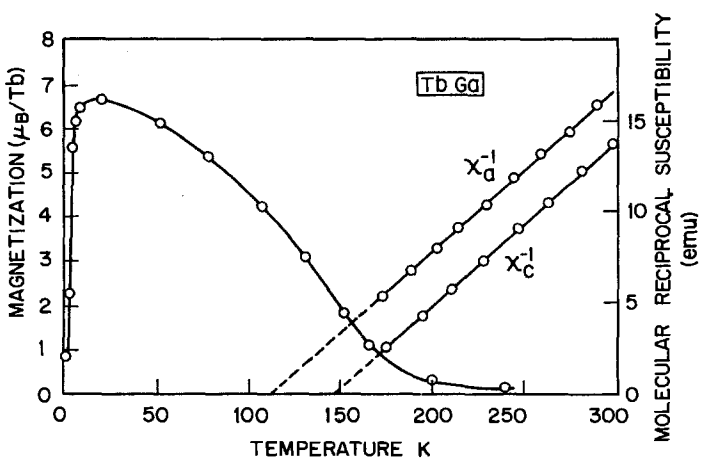

Fig. 4. Temperature dependence of the magnetization and the reciprocal susceptibility (measured in the a- and c-directions) of TbGa.

and 5. When the magnetization (σ) is measured with increasing temperature in an applied field smaller than the coercive field the σ versus T curves behave in a way similar to that shown in fig. 4. At the lowest temperature the thermal energy is not yet strong enough to surmount the energy barrier needed to move the narrow walls. This leads to the absence of an appreciable net magnetization in the low temperature region. The temperature at which σ rises strongly will be higher the lower the applied field. Furthermore, the typical initial rise in the σ versus T curves is generally absent if the sample is cooled in the presence of a magnetic field (Barbara et al. 1971a) prior to the measurements: At temperatures of sufficiently high thermal energy the field applied can remove all the walls from the sample so that the net magnetization is large. Upon subsequent cooling, wall movement will no longer be possible from a given temperature on, so that a situation with aligned moments, corresponding to a high net magnetization, is frozen-in. A further characteristic feature of a system composed of narrow walls is the rather field independent nature of the first part of the curve of initial magnetization at low temperatures (fig. 5). Increase of the net magnetization will only be possible by wall movement in directions corresponding to an increase in size of those domains for which the net magnetization is parallel to the applied field. Due to the presence of the energy barrier, wall propagation will become possible only above a critical field. This critical field is close to the coercive field and, in the same way as the latter, decreases strongly with temperature (see the inset of fig. 5). The origin of the presence of narrow walls is a high magneto-crystalline anisotropy energy, comparable in magnitude with the magnetic coup-

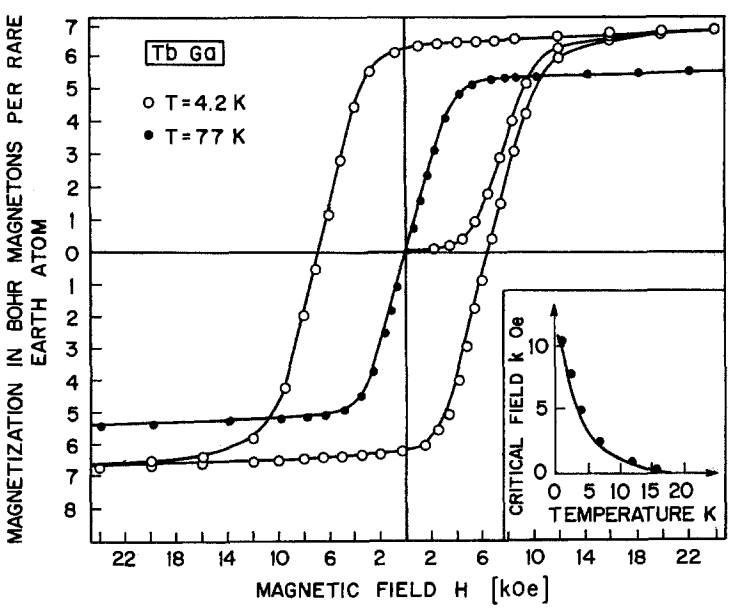

Fig. 5. Magnetic isotherms of TbGa at 4.2 K and 77 K. The inset shows the temperature dependence of the critical field, below which wall propagation is impeded. (Taken from Barbara et al. 1971b.)

ling energy (Barbara et al. 1971a). In rare earth intermetallics the former energy is the result of the crystal field interactions of moments containing an orbital contribution. No such effects are therefore expected in Gd compounds ($L = 0$ for Gd) and this is in keeping with experimental observations (Buschow and Van den Hoogenhof 1976, Barbara et al. 1972).

The compounds RGa_2 have extremely low magnetic ordering temperatures. It can be inferred from the data shown in table A.2c that the ordering is antiferromagnetic. Barbara et al. (1971c) report that $DyGa_2$ and $HoGa_2$ show metamagnetic behaviour below T_N. It has been found impossible to describe the magnetic properties of these compounds by means of the RKKY model (Buschow and Van den Hoogenhof 1976).

The rare earth rich R–In compounds order ferromagnetically at fairly high temperatures (table A.2d). In the equiatomic and indium rich R–In compounds magnetic ordering is antiferromagnetic. If one compares the θ_p values and the ordering temperatures T_N of the various RIn_3 compounds one finds that the values of $CeIn_3$ are greatly in excess of the expectations based on the DeGennes relation (Buschow et al. 1969a) (eq. (5) section 2.1). This suggests that the exchange interaction between the 4f electrons and the conduction electrons in $CeIn_3$ differs markedly from those in the remainder of compounds. An enhanced interaction of 4f and conduction electrons also becomes apparent from the Kondo-like resistivity anomaly reported for this compound (Van Daal and Buschow 1970). Crystal field splittings in $PrIn_3$ (Gross et al. 1977) and $NdIn_3$ (Lethuillier and Chaussy 1976a) were determined by inelastic neutron scattering and the results were compared with the crystal field data in other RX_3 (X = In, Tl, Pb, Sn). The overall splitting was found to decrease from In to Sn. Lethuillier and Chaussy (1976a) compared the crystal field data available for $CeIn_3$, $PrIn_3$ and $NdIn_3$ and ascribed the observed change in sign of the crystal field parameters $A_4\langle r^4\rangle$ and $A_6\langle r^6\rangle$ to an increasing energy difference between the 4f levels and the conduction band in this sense.

The rather few rare earth thallium compounds whose magnetic properties have been studied are listed in table A.2e. Inelastic neutron scattering performed on Pr_3Tl has shown that the lowest crystal field level is a (non-magnetic) singlet (Birgenau et al. 1972). The compound Pr_3Tl can be characterized as an induced moment ferromagnet (Andres et al. 1972) in which the singlet ground state is spontaneously polarized below about 11 K due to a slightly overcritical exchange interaction (Cooper 1972). In $PrTl_3$ (having the antistructure of Pr_3Tl) a singlet level is lowest (Gross et al. 1977) too, but the low exchange interaction between the Pr moments leads to Van Vleck paramagnetism only at low temperatures and magnetic ordering was found to be absent (Buschow, unpublished).

2.3.2. Compounds with group IV elements

Data of the magnetic and crystallographic properties of compounds between rare earths and Si or Ge are listed in tables A2.f and A2.g. The values of the effective moments (μ_{eff}) and the paramagnetic Curie temperature (θ_p) of Ce–Si and Ce–Ge compounds were derived by Ruggiero et al. (1964) from the thermal

variation of the reciprocal susceptibility in the temperature range 100–500 K. The reported μ_{eff} values are not far off from the free ion value of Ce^{3+} ($2.54\mu_B$), which indicates that Ce in this temperature range is primarily trivalent. It is remarkable, however, that the θ_p values are very often strongly negative, even though the θ_p values of the other (isostructural) rare earth compounds of the corresponding series have positive θ_p values. This may point to a coupling scheme which for the Ce^{3+} moments is different from that of the other R^{3+} moments in these compounds. Alternatively the deviating magnetic properties of the Ce compounds could be due to an intermediate valence state of the Ce ions, where an excited valence state with an effective moment μ_{eff} and degeneracy $2J+1$ is lying at an energy ΔE above the ground state, having an effective moment equal to zero and a degeneracy equal to 1. The susceptibility is then

$$\chi_{4f}(T) = N\mu_{eff}^2 c(T)/3k_B(T+\theta) \tag{30}$$

where

$$c(T) = (2J+1)\exp(-\Delta E/k_BT)/[1+(2J+1)\exp(-\Delta E/k_BT)]$$

and where N denotes the concentration of Ce atoms. According to this expression Curie–Weiss like behaviour should be observed at high temperatures with an effective moment close to the Ce^{3+} free ion value $\mu_{eff} = 2.54\mu_B$. In the model based on interconfigurational fluctuations (Hirst 1970) $c(T)$ is replaced by $c(T+\theta)$ and the positive quantity θ is a measure of the transition rate between the two valence states (Sales and Wohlleben 1975). It can account for the often large negative values of the Curie–Weiss intercepts observed for θ_p. A different interpretation of θ in eq. (30) is given in Havinga et al. (1973) and in Jefferson and Stevens (1976). Unfortunately the absence of low temperature susceptibility data (Ruggiero et al. 1964) precludes a further analysis of this interesting class of compounds.

Magnetic studies performed on compounds of the type R_5Si_3 and R_5Ge_3 other than $R = Ce$ show that these compounds do not order ferromagnetically at low temperatures, even though they have positive Curie–Weiss intercepts. Very often the temperature of the magnetization exhibits a cusp-like behaviour, indicative of antiferromagnetic ordering. Presumably the magnetic structure of these compounds is rather complex. The tendency of the magnetic isotherms at 4.2 K of Gd_5Si_3 and various R_5Ge_3 compounds to saturate in high field strengths (Ganapathy et al. 1976, Buschow and Fast 1967) shows that the antiferromagnetic interactions in these compounds are relatively weak. This agrees with the positive sign of the values of θ_p observed.

Rather high magnetic ordering temperatures are reached in R_5Si_4 (Holtzberg et al. 1967). The Curie temperature of Gd_5Si_4 is even above room temperature and exceeds that of Gd metal. In contrast, the R_5Ge_4 compounds have rather low ordering temperatures (Néel type). Again, the positive θ_p values show that the antiferromagnetic interaction may be rather weak.

Neutron diffraction performed on several equiatomic rare earth silicon compounds (Whung et al. 1970, 1971) has shown that these compounds order

antiferromagnetically. Antiferromagnetic order has also been reported (Buschow and Fast 1966) to occur in the compounds RGe with rare earth elements of an atomic number higher than that of Nd. The compounds PrGe and NdGe behave differently. In contrast to the compounds with a rare earth of a higher atomic number the paramagnetic Curie temperature of PrGe and NdGe are positive and the temperature dependence of the magnetization points to ferromagnetism. This sign reversal of θ_p within the RGe series shows that the magnetic interactions in RGe cannot be described by the simple RKKY approach (see eq. (5) in section 2.1 and the discussion given in section 2.3.1).

In the compounds RSi_2 and RGe_2 involving heavy rare earth elements, magnetic ordering seems to become antiferromagnetic (Yaguchi 1966, Sekizawa 1966, Sekizawa and Yasukochi 1966a). On the other hand, ferromagnetism has been reported in several members of the series RGe_2 when R is a light rare earth element (see table A.2g). The sign reversal of θ_p in the RGe_2 series is again indicative of a coupling scheme of the localized moments not describable in terms of the RKKY approach. The study of the magnetic properties of these compounds is considerably hampered, however, by the occurrence of at least four different structure types and in some cases by an off-stoichiometric composition of the compounds (Parthé 1967). It is interesting to note that the compounds $LaSi_2$, $LaGe_2$, YGe_2 and $ScGe_2$ have been reported to become superconducting at low temperatures (Matthias et al. 1958, Henry 1962).

Magnetic properties of rare earth compounds with tin and lead are listed in table A.2h. It can be seen from the table that the study of magnetic properties in R–Sn and R–Pb compounds has been focussed mainly on compounds of the relatively simple $AuCu_3$ structure. Magnetic ordering in these compounds occurs at rather low temperatures and is antiferromagnetic ($T_N < 25$ K). In $PrSn_3$, $NdSn_3$ and $NdPb_3$ the magnetic structure has been determined by neutron diffraction (Lethuillier 1974). Apart from $PrSn_3$ and $NdSn_3$ conclusions about the magnetic structure type could be derived by means of Sn Mössbauer spectroscopy in $SmSn_3$, $EuSn_3$ and $GdSn_3$ (Sanchez et al. 1976). In $SmSn_3$ the magnetic structure is antiferromagnetic of the first kind (like in $PrSn_3$ and $NdSn_3$) whereas it is more complicated in $EuSn_3$ (doubled unit cell) and in $GdSn_3$ (helical spin structure). In $CeSn_3$ no magnetic transition was found down to 1.6 K. The magnetic susceptibility of this compound exhibits a rather peculiar temperature dependence (Tsuchida and Wallace 1965, Borsa et al. 1967, Shenoy et al. 1970, Cooper et al. 1971). At about 135 K there is a broad maximum in the susceptibility followed by a rapid rise below about 30 K (see fig. 6). In the high temperature region ($T > 200$ K) Curie–Weiss behaviour is followed with $\mu_{eff} = 2.78\mu_B$/Ce and $\theta_p =$ 203 K (Ruggiero et al. 1964). The occurrence of the susceptibility maximum was first attributed to a $Ce^{3+} \rightarrow Ce^{4+}$ partial conversion associated with the thermal contraction of the lattice (Tsuchida and Wallace 1965). Recent high pressure susceptibility data show that the thermal expansion is not responsible for the magnetic–non-magnetic transition in $CeSn_3$ (Beille et al. 1977). The ^{119}Sn Mössbauer spectra obtained on this compound did not show significant changes of the isomer shift and the quadrupole interaction around 135 K (Shenoy et al. 1970).

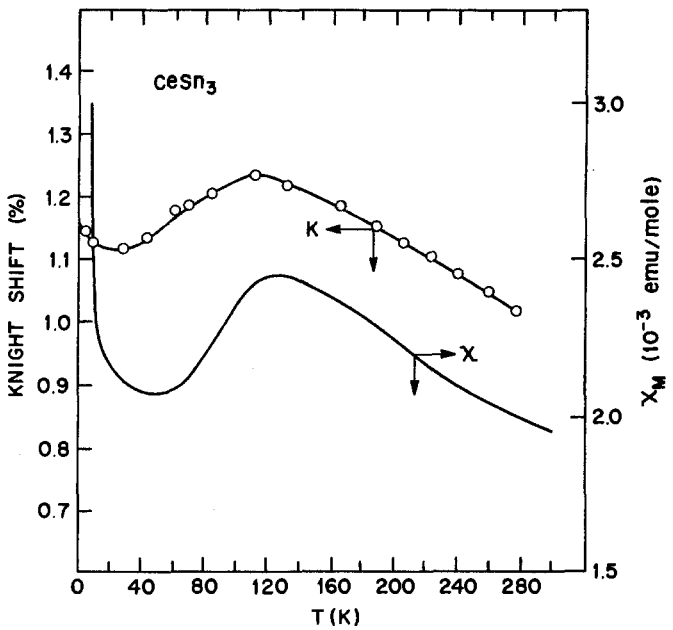

Fig. 6. The temperature dependence of the ^{119}Sn Knight shift and the magnetic susceptibility in $CeSn_3$ (taken from Malik et al. 1974).

This does not seem to preclude a temperature dependent valence state change in $CeSn_3$ since these two parameters appear to be hardly affected by the valence state of the R ions in RSn_3 (Sanchez et al. 1976). Most likely, therefore, is an explanation of the peculiar $\chi(T)$ behaviour in terms of an intermediate valence state. If the ground state corresponds to Ce^{4+} and the excited state to Ce^{3+} eq. (30) does indeed predict a maximum in $\chi(T)$ and furthermore can account for the large negative value of θ_p without involving magnetic ordering. It is to be noted that in this picture a maximum is also expected for the thermal average of the spin moment. This agrees with the temperature dependence of the Sn Knight shift observed in $CeSn_3$ (Malik et al. 1974). The close proximity of the 4f level to the Fermi level in $CeSn_3$ leads to interesting behaviour of the thermal variation of the electrical resistivity, thermoelectric power and the specific heat. These quantities have been reviewed recently by Malik et al. (1974).

Rather unusual magnetic behaviour is displayed by $SmSn_3$. The sign reversal of the Sn Knight shift, expected in compounds of Sm to occur close to 300 K, proved to be absent. This has been explained as being due to crystal field induced mixing of the $J = \frac{7}{2}$ multiplet into the $J = \frac{5}{2}$ ground state in the presence of exchange fields. For more details we refer to the reviews by Malik et al. (1974) and by De Wijn et al. (1976a).

2.3.3. Compounds with group Ia elements

It can be seen from table A.2i that the equiatomic rare earth copper compounds occur either in the cubic CsCl structure or in the orthorhombic FeB structure. Most of the compounds have negative Curie–Weiss intercepts, indicating antiferromagnetism at low temperatures, although a Néel type transition in the thermal variation of the magnetization has been discerned only in relatively few of these compounds (Walline and Wallace 1965, Chao et al. 1964, De Wijn et al. 1968, Pierre 1967, 1969, Burzo et al. 1972, Sekizawa and Yasukochi 1966b, Winterberger et al. 1971). Neutron diffraction performed on RCu with R = Tb, Dy, Ho and Er showed that in all cases the magnetic structure is antiferromagnetic, the magnetic propagation vector being $q = (\frac{1}{2}, \frac{1}{2}, 0)$ (Cable et al. 1964a, b, Winterberger et al. 1971, Yashiro et al. 1976, Pierre 1970). Attempts have been made to explain the magnetic properties of the CsCl type RCu compounds by means of the RKKY approach (De Wijn et al. 1968, Pierre 1969). This will be discussed in more detail in section 2.3.5, together with the results of band structure calculations (Belakhovsky et al. 1972).

The splitting of the crystal field levels in ErCu was studied by means of inelastic neutron scattering (Morin et al. 1974a). The results were compared with similar measurements made on the isostructural compounds ErAg and ErZn. In all three cases the parameters $A_4^0\langle r^4\rangle$ and $A_6^0\langle r^6\rangle$ were found to be negative (Γ_8 quartet level lowest). The sixth order term derived from these measurements exceeds the value obtained via point charge calculations by one order of magnitude (see also section 2.3.5).

With the exception of $LaCu_2$ all compounds RCu_2 have the orthorhombic $CeCu_2$ structure. Most of the compounds investigated show metamagnetic behaviour (Sherwood et al. 1964). The properties of $PrCu_2$ are unique in this series in that at low temperatures a cooperative Jahn–Teller effect occurs, driven by the strain coupling of the singlet crystal field states of the Pr^{3+} ion (Wun and Phillips 1974, Andres et al. 1976).

Attempts to explain the magnetic properties by means the RKKY model are based mainly on the results of a magnetic investigation of the series $Gd(Ni, Cu)_2$ (Poldy and Kirchmayr 1974). Although most of the changes in magnetic behaviour of this series can be explained satisfactorily, some difficulties are encountered when comparing the data of $GdCu_2$ ($\theta_p = 11$ K; $k_F = 1.39$ Å^{-1}) with those of $GdZn_2$ ($\theta_p = 68$; $k_F = 1.50$ Å^{-1}) since the picture proposed predicts a strong reduction of θ_p if the conduction electron concentration is increased in going from $GdCu_2$ to $GdZn_2$.

With the exception of $EuCu_5$ magnetic ordering in RCu_5 compounds occurs at rather low temperatures. An analysis of the magnetic properties in terms of the RKKY model (Van Steenwijk et al. 1977, Buschow et al. 1970) is hampered by the change in crystal structure from hexagonal to cubic between $EuCu_5$ and $GdCu_5$. The RKKY approach does not seem quite satisfactory for explaining all of the data (including hyperfine fields) in the case of the hexagonal compounds (Van Steenwijk et al. 1977).

Magnetic properties of R–Ag and R–Au compounds are listed in table A.2j.

Since the RAu and RAg compounds have similar electron concentration and crystal structure as the CsCl-type RCu compounds it is predicted by the RKKY model that the magnetic properties of RCu, RAg and RAu should be the same for a given R. Comparison of the corresponding Gd compounds in tables A.2i and A.2j shows indeed that the magnetic properties of GdCu and GdAg are not very different. In GdAu, however, the sign of θ_p is no longer negative, indicating that ferromagnetic interactions prevail in this compound. Furthermore, the lattice constant of GdAu is in between those of GdCu and GdAg. This seems to disagree with the view expressed by Sekizawa and Yasukochi (1966b), where θ_p is considered to be a slightly decreasing function when plotted versus increasing lattice constant in pseudobinary series based on these compounds. More recently it was found by means of Mössbauer effect spectroscopy that the CsCl structure in the RAu compounds is metastable and undergoes a low-temperature martensitic phase transformation to a close-packed FeB-like structure (Kimball et al. 1975). This difference in structure could partially account for the difference in magnetic properties between GdAu and GdAg or GdCu. On the other hand it cannot be excluded that the occurrence of a phase transformation upon cooling from room temperature to 4.2 K and vice versa, if extended over a relatively large temperature region, can lead to deviations from the true temperature dependence of the susceptibility associated with either one of the two phases. The same then holds with respect to the values of θ_p and μ_{eff} derived from such data.

Unlike the case with the RAu compounds, no martensitic type of structure transformation has been found in RAg compounds (Goebel et al. 1975, Ihrig and Methfessel 1976b). The first members of this series are nevertheless not far off structural instability. This follows from investigations on pseudobinary $R\mathrm{Ag}_{1-x}\mathrm{In}_x$ compounds (Ihrig and Methfessel 1976a, b, Ihrig et al. 1976b). Cubic to tetragonal transformations in these compounds are ascribed either to a band- or to a molecular Jahn–Teller effect associated with the e_g levels of the rare earth 5d electrons. It seems, however, that the situation can be even more complex in some cases, and that a distortive phase transition can also be driven by the 4f electrons in these compounds. Polarized neutron experiments on CeAg have shown that this compound undergoes a distortive cubic to tetragonal transition at 21 K, which is only slightly above the magnetic ordering temperature (Radhakrishna and Livet, unpublished). This transition has been ascribed to a cooperative Jahn–Teller effect involving the 4f electrons; together with the magnetic transition it has been described by means of a spin Hamiltonian involving dipolar as well as quadrupolar interactions (Ray and Silvadiere, 1976).

Extensive bulk magnetic and neutron diffraction measurements were made on PrAg by Brun et al. (1976). The compound PrAg is antiferromagnetic below about 11 K but undergoes a spin-flop transition in fields in excess of about 5 kOe (see fig. 7). A closer analysis of the data, using crystal field energy levels for Pr^{3+} derived from inelastic neutron scattering experiments (Brun et al. 1974b) revealed that the net exchange field on a Pr atom does not vary linearly with the magnetization M but also contains a substantial negative term in M^3. This was

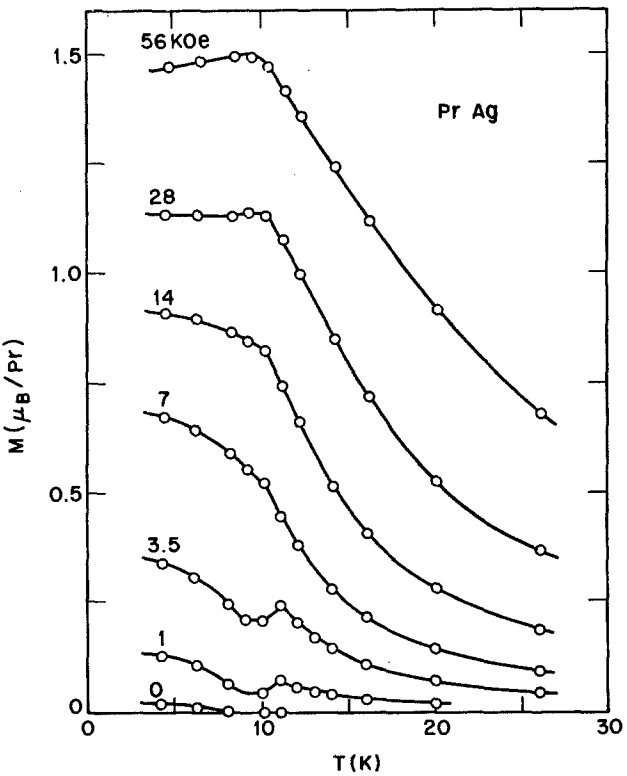

Fig. 7. Temperature dependence of the magnetic moment of PrAg in various field strengths (taken from Brun et al. 1974b).

taken as an indication that the spin Hamiltonian in the paramagnetic regime contains a positive biquadratic exchange term.

Further proof that the magnetism in the RAg compounds is not that simple comes from neutron diffraction studies performed by Nereson on HoAg and ErAg (Nereson 1963, 1973). There are two antiferromagnetic transitions at low temperature between which the magnetic ordering entails a sinusoidally modulated magnetization wave, propagating in the ⟨100⟩ direction. It is incommensurate with the chemical unit cell and is also temperature independent. A commensurate antiferromagnetic structure does exist, however, at temperatures below the lowest of the two transition points mentioned.

Information on the crystal field splitting and the exchange interaction in HoAg and ErAg has been obtained from inelastic neutron scattering experiments (Furrer 1975, Tellenbach et al. 1975). The analysis of the experimental data was based on a single-ion Hamiltonian similar to eqs. (22–25) in section 2.2 but where the term $\mathcal{H}_{ex}$ of eq. (25) was expressed as

$$\mathcal{H}_{ex} = -g_J \mu_B \boldsymbol{H}_m \boldsymbol{J}.$$

The molecular field H_m in this equation was approximated by $H_m = g_J \mu_B \lambda \langle J \rangle$,

where λ is the molecular field constant. Furthermore the crystal field Hamiltonian had to be expressed with respect to an axis other than a symmetry axis in cases where the magnetic moment was tilted away from the z-axis. The energy levels were calculated by diagonalizing $\mathcal{H} = \mathcal{H}_c + \mathcal{H}_{ex}$ and keeping H_m as a parameter. By means of fitting procedures, involving the experimental results obtained in the magnetically ordered and paramagnetic regime, the level schemes were obtained together with the corresponding molecular field parameters. In the case of ErAg Furrer has used the following expression: $H_m = 2(g_J\mu_B)^{-1}\Sigma_r n_r J_r \langle J \rangle$. Here n_r is the number of r'th nearest neighbours and J_r is the isotropic exchange constant with an ion of the r'th neighbour shell. By considering only neighbour interactions up to $r = 3$ and using the λ values corresponding to the paramagnetic, commensurate and incommensurate region, Furrer obtained the following results: $J_1 = -0.093$ meV, $J_2 = +0.049$ meV and $J_3 = -0.004$ meV. Qualitatively these parameters display the oscillatory behaviour expected on the basis of the RKKY formalism.

Antiferromagnetic ordering also exists in the compounds of the type RAg_2 and RAu_2 (see table A.2j). Numerous neutron diffraction studies performed on these materials by Atoji (1968a, b, 1969a, b, 1970, 1972a, b, c) have shown that the magnetic structures of these materials can be rather complex. Many of the compounds have more than one magnetic transition temperature and the magnetic structures are very often incommensurate with the crystallographic lattice.

No clear indication of the magnetic ordering type could be derived from magnetic measurements in RAu_3 and RAu_4 compounds (Sill and Prindeville 1975, Sill et al. 1971). The positive value of θ_p in the former and the peculiar magnetic isotherms found for some of the RAu_3 compounds suggest that the magnetic properties are again not free from complexity.

2.3.4. Compounds with Be, Mg and group IIa elements

A glance at the data in table 1 shows that the heat of formation of R–Be compounds derived from model calculations is close to zero. It is not surprising, therefore, that the number of existing rare earth beryllides is rather limited. The RBe_{13} compounds, whose magnetic properties are given in table A.2k are in fact the only stable rare earth beryllides known at present. Most of the data listed in table A.2k were obtained by Bucher et al. (1975). In low field strengths the magnetization of most of the compounds with heavy rare earth elements show a Néel type transition in their temperature dependence. The magnetic isotherms studied well below T_N are either concave upward or exhibit a step-like jump at some critical field strength. These features are reminiscent of spin flop transitions, leading eventually to a paramagnetic phase in high applied field strengths. Since the magnetocrystalline anisotropy energy can be regarded as appreciable compared with the exchange energy, the jump fields are proportional to the exchange: For RB_{13} with R = Tb, Dy, Ho the step-like jumps occur at about 8, 5 and 3 kOe, respectively. These values scale reasonably well with the corresponding T_N values. The occurrence of transitions from the antiferromagnetic via spin flop to the paramagnetic phase in relatively low magnetic fields is in keeping with the fact

that θ_p in the compounds considered takes positive rather than negative values and is furthermore close to the values of T_N. In the highest field strengths applied the magnetization corresponds to R moments smaller than the free ion values ($gJ\mu_B$). Presumably, saturation is not yet reached in the field-induced paramagnetic phase. This may be due to the presence of a large magnetocrystalline anisotropy and/or to a crystal field ground state with a moment smaller than $gJ\mu_B$. Bucher et al. (1975) ascribe the step-like jumps mainly to additional admixtures of excited crystal field states into the ground state or to Zeeman level crossing of adjacent crystal field levels as the field strength increases. The peculiar magnetic isotherm found for DyB_{13}, in particular, points strongly in this direction and makes it clear that a description of the magnetic properties in terms of spin flops is too crude a picture.

In their investigations of RBe_{13} compounds Borsa and Olcese (1973) reported the occurrence of ferromagnetism in $GdBe_{13}$. The discrepancy with the results of Bucher et al. is very likely due to the application of too high a field strength in the magnetization measurements, which could obscure the Néel type transition. Bucher as well as Borsa and Olcese found a rather peculiar temperature dependence of the susceptibility in $CeBe_{13}$ showing a maximum close to 140 K. In view of the anomalously low lattice constant (Bucher et al. 1975) and the temperature dependence of the ^9Be nuclear magnetic resonance and relaxation (Borsa and Olcese 1973) this $\chi(T)$ behaviour was ascribed to an intermediate valence state of the Ce ions, with a Ce^{3+}/Ce^{4+} ratio depending on the temperature. No further analysis of the $\chi(T)$ curve in $CeBe_{13}$ was given. Very probably the data can conveniently be explained under the assumption of two energy states, separated by ΔE, where the lower and higher states correspond to Ce^{4+} and Ce^{3+}, respectively. Straightforward application of eq. (30), then qualitatively leads to the required temperature behaviour of the susceptibility.

EPR investigations on rare earth beryllides have been reported by Bloch et al. (1976) and by Heinrich and Meyer (1977). The exchange constant $J(0)$ [see eq. (10)] was found to be positive in both investigations. Bloch et al. report in addition that this quantity varies significantly across the rare earth series.

Magnetic properties of rare earth magnesium compounds are displayed in table A.2ℓ. The magnetic properties of compounds of the type RMg have rather unusual features. In the first place there is a sign reversal of θ_p in going through the series (Buschow 1973b, Aleonard et al. 1976) which is difficult to understand in terms of the RKKY approach. Furthermore, none of the compounds with heavy rare earths can be regarded as truly ferromagnetic, although such behaviour is suggested by the observation of paramagnetic–ferromagnetic transition temperatures. Neutron diffraction measurements performed on several of these compounds show that TbMg is antiferromagnetic with a non-collinear spin arrangement (Aleonard et al. 1975, Schäfer et al. 1977) and DyMg antiferromagnetic with a collinear spin arrangement (Aleonard et al. 1976, Schäfer et al. 1976b). Magnetic ordering in HoMg also seems to be primarily ferromagnetic; a diffuse antiferromagnetic $(0, 0, \frac{1}{2})$ reflection indicates some tendency to antiferromagnetic short-range order (Aleonard et al. 1976). Schäfer et al. (1976b) report ErMg to be ferromagnetic at 4.2 K. Low-intensity antiferromagnetic reflection

lines, not commensurate with the lattice and increasing in intensity from 4.2 to 1.5 K, were observed by Aleonard et al. (1976). In several compounds, primarily in TbMg and DyMg, the magnetic isotherms at low temperatures indicate the presence of domain effects involving small domain walls such as described in the case of Tb_3Al_2 and TbGa in section 2.3.1. This severely hampers the interpretation of the neutron diffraction results.

A determination of the crystal field parameters in RMg was made by Aleonard et al. (1976) via magnetization anisotropy studies on single crystals. They found $A_4\langle r^4\rangle$ and $A_6\langle r^6\rangle$ to be negative and positive, respectively. Inelastic neutron scattering studies on ErMg led to the same result (Morin et al. 1976).

Complex magnetic behaviour has also been observed in GdMg, where crystal fields are absent (Aleonard et al. 1975, Buschow and Schinkel 1976, Buschow and Oppelt 1974, Morin et al. 1978, Pierre et al. 1979). High field magnetization measurements performed on $Gd_{1-x}La_xMg$ made it clear that the RKKY mechanism is not able to deal adequately with the magnetic properties of the RMg compounds (Buschow and Schinkel 1976).

Only some of the RMg_2 compounds are cubic (see table A.2ℓ). The ferromagnetic ordering temperatures are slightly lower than in the corresponding RMg compounds. $EuMg_2$ has a Néel type transition rather than a paramagnetic–ferromagnetic transition (Buschow et al. 1978). Since Eu in $EuMg_2$ is divalent, this possibly originates from a different conduction electron concentration. The too low saturation moments and the often peculiar temperature dependence of the magnetization below T_c indicate that the actual magnetic structure in RMg_2 may be more complicated than simply ferromagnetic. No neutron diffraction data have as yet been obtained on these compounds.

Magnetic ordering in RMg_3 compounds occurs at rather low temperatures and is antiferromagnetic. There is some doubt about the prevailing ferromagnetism reported in $GdMg_3$ and $TbMg_3$ (Buschow 1976), since this may be due to a contamination with the corresponding RMg_2 which can be suppressed by applying an excess of magnesium (Will et al. 1977b). Alternatively it is possible that magnetic ordering in RMg_3 depends strongly on deviations from the ideal site occupancy in the Fe_3Al structure type. More experiments are needed to clarify the situation.

The equiatomic rare earth zinc compounds have relatively high magnetic ordering temperatures, approaching room temperature in the case of GdZn (see table A.2m). Magnetic ordering is antiferromagnetic or ferromagnetic, depending on whether R in RZn belongs to the light or heavy rare earth elements, respectively. For the RZn compounds in which R = Ce, Pr or Nd the neutron patterns can be described by antiferronagnetic structures having a propagation vector (0, 0, $\frac{1}{2}$) (Buschow et al. 1975c, Morin et al., unpublished). As was discussed by Morin and de Combarieu (1975), this solution is not unique for a description of the neutron diffraction results in cubic materials. Doubling of the unit cell upon magnetic ordering can occur in more than one direction and lead to non-collinear spin structures. Crystal field effect considerations and results of

specific heat measurements reported by these authors favour a non-collinear antiferromagnetic structure with the moments along ⟨110⟩ at temperatures between T_N and 18 K. Below this temperature the moments in the non-collinear structure are assumed to point along ⟨111⟩. Magnetization measurements on single crystals and specific heat measurements have shown that in the ferromagnets TbZn and HoZn a similar rotation of the magnetic moment with temperature occurs at 65 K and 25 K, respectively (Morin and Pierre 1973, Morin et al. 1974b). An analysis of the experimental data was given in terms of a molecular field model including crystal field effects along lines analogous to those outlined at the end of section 2.2 [eqs. (22–26)]. The Hamiltonian $\mathcal{H}_{ex}$ of eq. (25) was put equal to $-g\mu_B H_{ex} J_z$, where $H_{ex} = ng\mu_B \langle J_z \rangle_T$. First an approximate value of H_{ex} was used in the diagonalization of eq. (25). From the level scheme a new value of the thermal average $\langle J_z \rangle_T$ was derived and used subsequently to solve the problem self-consistently in the various crystallographic directions. The crystal field parameters $A_4^0\langle r^4 \rangle$ and $A_6^0\langle r^6 \rangle$ derived from this analysis (Morin et al. 1974b) were found to be reasonably consistent with the crystal field parameters obtained by inelastic neutron scattering in ErZn (Morin et al. 1976).

Magnetic dilution studies have been reported of GdZn. The decrease of the magnetic ordering temperatures was found to proceed much faster with x in $Gd_{1-x}La_xZn$ than in $Gd_{1-x}Y_xZn$ (Eckrich et al. 1973, 1976). These results are in disagreement with a description of the magnetic properties of the RZn compounds by means of the RKKY formalism. This will be discussed in more detail in section 2.3.5, together with NMR data obtained on these materials (Eckrich et al. 1973, 1976).

The compounds RZn_2 crystallize in the orthorhombic $CeCu_2$ type of structure. Neutron diffraction performed on several of these compounds shows that the magnetic structure is in general rather complicated (Debray and Sougi 1972, 1973, Debray et al. 1970a, and unpublished) and entails incommensurate sinusoidal magnetic structures which in some cases give rise to a first order transition to a commensurate structure upon further cooling. Field induced metamagnetic transitions have been reported by Debray et al. (1975) to occur in $EuZn_2$, $DyZn_2$ and $TmZn_2$ (see fig. 8). It has been noted by Debray and Sakurai (1974) that the positive value of θ_p in RZn_2 is not expected on the basis of the RKKY approach if eq. (5) in section 2.2 is used in conjunction with eq. (12). Attempts have been made therefore to use an extended form of the RKKY theory which approximates the s–f exchange integral by the form factor of the local moment density and in addition considers a non-negligible interelectron interaction between the conduction electrons. The effect of this extension is to shift the node of the oscillating RKKY function in the k_F range appropriate to $GdZn_2$ towards slightly higher k_F values, thereby making θ_p positive at the free-electron value $k_F = 1.50$ Å^{-1} (see for instance fig. 1 in Debray and Sakurai 1974). It would be interesting to investigate how far this approach also leads to a consistent description for compounds of different conduction electron concen-

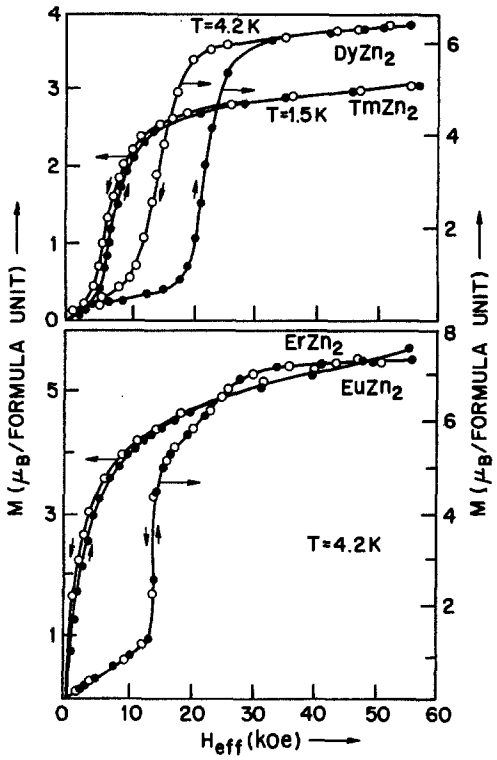

Fig. 8. Field dependence of the magnetic moment in $DyZn_2$, $TmZn_2$, $ErZn_2$ and $EuZn_2$. The data are taken from Debray et al. (1975).

tration such as $EuZn_2$ and $GdCu_2$. In these two compounds θ_p is still positive, even though the free electron k_F values are much lower than in $GdZn_2$ ($k_F = 1.38$ Å^{-1} and 1.40 Å^{-1} in $EuZn_2$ and $GdCu_2$, respectively).

Magnetization and electrical resistivity measurements performed by Stewart and Coles (1974) on the more dilute rare earth zinc compounds R_2Zn_{17} and RZn_{12} have shown that most of these compounds order antiferromagnetically at relatively low temperatures. In order to exclude effects of crystal fields, investigations into the presence of short-range order have been focussed mainly on the Gd compounds. Short-range order, also detected by ESR measurements (Taylor 1975, see also Fisk et al. 1971), was found to lead to deviations from normal Curie–Weiss behaviour at temperatures appreciably in excess of the Néel temperatures (Stewart and Coles 1974). Since $|\theta_p|$ in Gd_2Zn_{17} as well as in $GdZn_{12}$ is much larger than T_N, the presence of short-range order effects is not quite unexpected (Fisk et al. 1971).

Rare earth cadmium compounds of the composition RCd are similar in crystal structure and formal conduction electron concentration to the compounds RZn. It is not surprising therefore that the RCd compounds are also ferromagnetic (table A.2n) and that the ordering temperature of GdCd is almost the same as in

GdZn. Apart from those of GdCd, the magnetic properties of the other members of the RCd series appear to be more complex due to the presence of large crystal field induced magnetocrystalline anisotropies and incidentally also to transformations in their crystal structure. In almost all cases the temperature dependence of the magnetization below T_c was found to exhibit pecularities not expected for a normal ferromagnet (Buschow 1974, Alfieri et al. 1967). A cooperative Jahn–Teller effect from cubic to tetragonal symmetry has been reported by Lüthi et al. (1973). Unfortunately the unfavourable neutron cross-section of natural Cd seriously hampers magnetic structure determinations by means of neutron diffraction studies in all these materials.

Magnetic data pertaining to the members of other RCd series are still rather incomplete. The same holds for RHg compounds. The few examples available in the literature are listed in the second part of table A.2n.

2.3.5. Discussion

It is obvious from the results described in the preceding sections that the magnetic properties of the various rare earth intermetallics are governed mainly by two different entities: the crystal field splitting and the indirect exchange interaction between the localized moments. Rather compounded situations can be expected in cases where the crystal field splitting and the indirect exchange interaction are of the same order of magnitude. Unfortunately this applies to a rather large number of the compounds discussed above.

It is gratifying that in recent years single crystals of some of the compounds have become available by means of which reliable data regarding the crystal field splitting could be obtained via measurements of the magnetization anisotropy. Considerable progress in this field has also been made thanks to inelastic neutron scattering experiments. In some special cases such experiments have even led to useful results when performed in the magnetically ordered regime on compounds in which the exchange interaction between the localized moments, though smaller than the crystal field splitting, is rather large. In such cases information on the crystal field effects and the indirect exchange coupling could be extracted simultanously. It should be emphasized that the progress made with respect to crystal field effects is predominantly in the experimental field. Most of the new data have contributed considerably in showing that the point charge model is less well applicable to the present compounds. A unique model by means of which crystal field splittings can be predicted is still lacking. The difficulties one has to cope with in setting up such a model are demonstrated in comparative studies, such as for instance given in the paper by Morin et al. (1976): the fourth order potential term $A_4\langle r^4\rangle$ in various CsCl type ErX compounds (X = Rh, Pd, Ag, Cu, Zn, Mg) becomes less negative in the sequence Rh to Mg and changes its sign between Zn and Mg, whereas the $A_6\langle r^6\rangle$ term remains negative and of the same order of magnitude in all compounds. No such behaviour is expected if one takes into account merely the effective ligand charges, even if derived from APW calculations. Seemingly of more importance are the Coulombic terms arising from the anisotropic charge distribution of the conduction electrons. The in-

creasing localization of the 3d(4d) electrons due to the X component, as well as the progression in filling of the rare earth 5d band in the sequence Rh to Mg, lead at least to the correct trend in the $A_4\langle r^4\rangle$ values observed (Morin et al. 1976). The origin of the large $A_6\langle r^6\rangle$ is still obscure. Apart from the contributions mentioned above, proper cognizance should be taken of contributions due to the anisotropic exchange between the 4f electrons and the conduction band (Morin et al. 1976, Freeman 1972, Devine and Ray 1977).

Intuitively one would expect that the strong localization of the 4f electrons justifies a description of the coupling between 4f moments in terms of the RKKY model discussed in section 2.1. This model entails a non-uniform conduction electron spin polarization, leading to an oscillatory distance dependence of the exchange coupling between the localized moments. Qualitatively these features are in agreement with the observation of different Knight shifts in compounds of more than one crystallographically inequivalent site (Van Diepen et al. 1969) and with the oscillatory behaviour of the coupling constant between localized moments derived from neutron scattering experiments (Bührer et al. 1973, Furrer 1975). In the last decade numerous attempts have been made to understand the magnetic interactions in rare earth intermetallics in a more quantitative way by comparing the magnetic properties with results of NMR measurements and using eq. (5) in combination with either eq. (7) or eq. (8) and solving for $J(0)$ and k_F (see for instance De Wijn et al. 1968). Similar information regarding $|J(0)|$ and k_F has also been extracted from neutron diffraction studies by calculating the k_F dependence of the stability of various magnetic structures and comparing the results of these calculations with the trends observed experimentally (see for instance Pierre 1969). Results of such analyses were satisfactory in general but mostly resulted in values of the parameter k_F slightly different from those (k_F^0) derived by means of the free electron model [eq. (12)]. These discrepancies were ascribed to a non-spherical Fermi surface. In such cases it is more appropriate to sample $J(q)f(q)$ in eq. (2) over all the extremal surface calipers. Instead of a singularity at $q = 2k_F^0$, singularities will occur at values both smaller and larger than $2k_F^0$, so that $J(0)$ as well as k_F take the form of an average (see also Watson 1967). Recently numerous experimental data have been reported in the literature which are more seriously in conflict with the RKKY approach. Most of the reported discrepancies pertain to CsCl type compounds. Examples of experimental results on bulk material are: the sign reveral of θ_p in the series GdX with X = Cu, Ag or Au; the sign reversal in the series RMg and the strongly non-linear θ_p behaviour in magnetic dilution experiments on $Gd_{1-x}La_xMg$ (Buschow and Schinkel 1976), $Gd_{1-x}La_xZn$ and $Gd_{1-x}Y_xZn$ (Eckrich et al. 1973, 1976). Furthermore, a consistent description by means of the RKKY model of the θ_p sign reversal in series like $GdAg_{1-x}Zn_x$ or $GdCu_{1-x}Zn_x$ necessitates a similar change in sign of the hyperfine field at the non-magnetic site. This is not found experimentally (Oppelt et al. 1972). Experimental (Goebel et al. 1975, Dormann and Buschow 1976, Weimann et al. 1973, Davidov et al. 1970) as well as theoretical (Hasegawa and Kübler 1974, Tannous et al. 1976, Ray 1974) indications have been obtained that the dis-

crepancies with the RKKY formalism originate from a relatively large participation of the rare earth 5d electrons in the indirect exchange interaction. These results are interesting in so far as in these CsCl type compounds the crystal field splitting and the crystallographic structure transformations (Ihrig and Methfessel 1976a, b) seem largely to depend on the electronic properties of the 5d electrons, too. In order to check how far the 5d electrons participate in the indirect exchange interaction in other than CsCl type compounds, Dormann et al. (1977a) extended their NMR investigation to several ferromagnetic Gd compounds of the cubic $MgCu_2$ type. They found a strong correlation between the magnitude of θ_p and the sign of the transferred hyperfine field H_N at the Gd site (see fig. 9). This correlation is based on the fact that the hyperfine interaction constants of s and d electrons are positive and negative, respectively. The results of a further analysis of their data suggest that the RKKY interaction is much weaker than hitherto assumed and leads to magnetic ordering temperatures of only moderate strength. Reasonably large values are only obtained in the presence of a

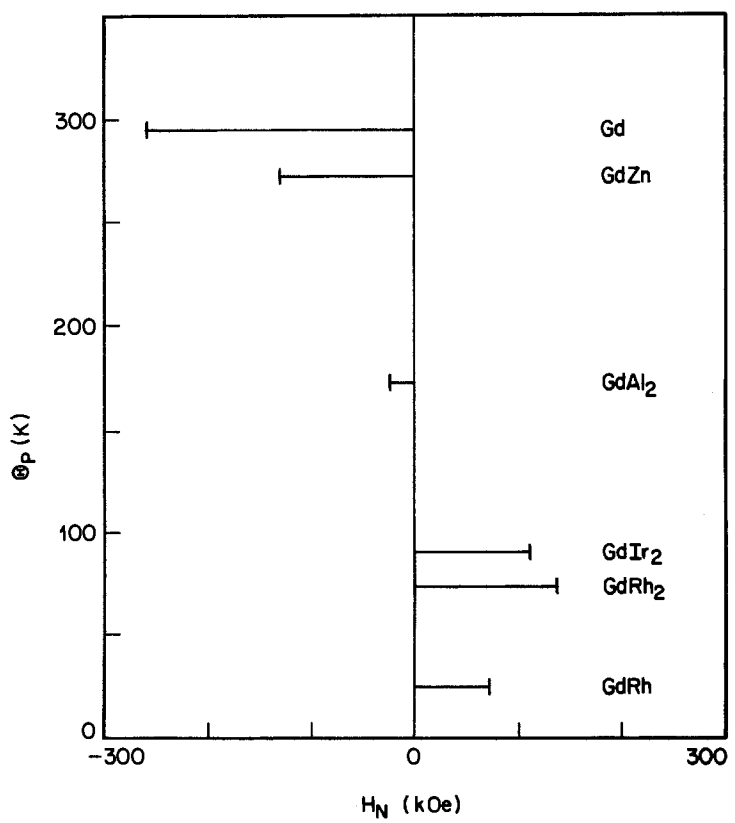

Fig. 9. Correlation between the paramagnetic Curie temperature (θ_p) and the transferred hyperfine field at the Gd site (H_N) in various Gd compounds.

participation of 5d electrons in the indirect coupling between the localized moments.

In a way all these results seem rather frustrating. Initially rare earth intermetallics and their magnetic properties were believed to represent standard examples of the RKKY coupling scheme. From the discussion given above it would appear that the predictive value of the RKKY coupling scheme is actually rather limited and that for an a priori description of the magnetic properties in the rare earth intermetallics a knowledge of details of their band structure would be required.

3. Compounds with d transition metals

3.1. Exchange interaction in metal systems containing d electrons

It may be inferred from the data listed in table 1 that the combining of rare earths and d transition metals leads to the formation of stable intermetallic compounds, provided the latter do not belong to the first few members of the transition metal series. In the case of transition metals of the 3d type stable R–M compounds have been observed only when M represents Mn, Fe, Co or Ni. The unpaired 3d electrons of the transition metal component give rise to a magnetic moment in most cases. The magnetic interactions in R–M compounds comprise therefore three different types: the R–R interaction, the R–M interaction and the M–M interaction.

The R–R interaction is the weakest of the three types mentioned. As a matter of fact it is similar to the indirect interaction between the localized 4f moments in compounds belonging to the group of intermetallics discussed in the preceding sections. In cases of a purely RKKY type exchange the R–R coupling will be weak but may reach somewhat higher values if the indirect exchange proceeds via the 5d electrons. An impression of the strength of the R–R coupling in R–M compounds is given by the ordering temperatures in compounds in which there is no moment on the M atoms. Such a situation is reached in several $R\mathrm{Ni}_n$ compounds ($n \leq 2$). These have ordering temperatures well below 100 K, in general.

Three different schemes have been proposed for the coupling between the R and M moments. In the first scheme (Buschow 1971b, Wallace 1968) the coupling is assumed to proceed via polarization of the s conduction electrons. The 4f–s interaction was taken to be of the spatial non-uniform RKKY type; the 3d–s interaction was assumed to be positive (Wallace 1968) or of the same type as the 4f–s interaction (Buschow 1971b). In the second scheme (Campbell 1972) the 5d electrons of the rare earth elements play an important role. Through ordinary 4f–5d exchange the localized 4f spins produce a positive local 5d spin polarization. The 4f–3d coupling then arises indirectly via the 3d–5d interaction. Campbell (1972) argues that with respect to the 5d electronic properties one can consider the rare earth elements as belonging to the first half of a d-transition

metal series. Since the elements M = Fe, Co or Ni belong to the second half of such a series, one expects a negative 5d–3d interaction, making the overall 3d–4f spin coupling antiferromagnetic. Possible exceptions to this rule may occur with Mn compounds since this element belongs to the first half of the 3d transition metal series. In general considerable electron transfer from the rare earths to Mn may take place in view of the large electronegativity difference between these elements (Miedema et al. 1977). It is reasonable to assume that this electron transfer would be accompanied by a more complete filling of the 3d electron states of the Mn atoms. In R–Mn compounds manganese might therefore behave as a 3d element belonging to the second half of the transition series, too, and like iron, cobalt and nickel give rise to an antiferromagnetic coupling between the R and M spin moments.

A third coupling scheme has been proposed by Szpunar and Kozarzewski (1977). In their model the localized rare earth spin interacts with d electrons that are accommodated in narrow bands formed essentially with the 5d and 3d states of the rare earth and transition element atoms, respectively. In order to be able to apply the coherent potential approximation it was furthermore assumed that the average magnetic moments of the transition metal atoms and rare earth atoms do not depend on the various types of sites in which these atoms can be accommodated in the crystal structure of the R–M compounds. The magnetic moments corresponding to the "alloys" were calculated within the molecular field and Hartree–Fock approximations. It was found that the model leads to an antiparallel coupling between the rare earth spin and the transition metal moment in rare earth compounds based on M = Ni, Co and Fe, independent of the R/M ratio. A model dealing with the temperature dependence of the magnetization of rare earth transition metal compounds has been given by Szpunar and Lindgard (1977).

In contrast to the second and third coupling schemes mentioned above no uniform behaviour regarding the sign of the coupling between the R and M moments emerges from the first scheme. The reason for this is that this scheme is based on analytical expressions of the RKKY type interaction like eq. (4) in section 2.1. The sign of the 4f induced s electron polarization at the transition metal site depends on the sign of $J(0)$ as well as on the sign of the lattice sum $\Sigma_i F(2k_F|r - R_i|)$ appearing in eq. (4) of section 2.1. It can be expected therefore that the R–M coupling is sensitive to changes in crystal structure and electron concentration. Guided by ^{27}Al Knight shift results on RAl_2 compounds reported by Jaccarino et al. (1960) [which have shown the rare earth induced s electron polarization to be negative at the Al sites], Wallace (1968) has proposed that a negative s electron polarization prevails also at the transition metal sites in R–M compounds. With a positive s–3d interaction the overall 4f–3d coupling would then be antiferromagnetic.

It is worth noting that also the model proposed by Szpunar and Lindgard bears some features of an RKKY type interaction. In this case, too, the exchange interaction has been taken to be independent of k and q ($J(q) = J(0)$, see section 2.1), but contrary to the first scheme no analytical expressions have been used in

which structural details are considered explicitly. As a matter of fact the effect of atomic ordering of the R and M atoms into well-defined crystal structures has been disregarded completely.

A critical assessment of the validity of the three proposed coupling schemes will be given at the end of section 3.

The M–M interaction is by far the strongest one in the R–M compounds. This is a direct consequence of the spatial extent of the 3d electron wave functions being considerably larger than the 4f electron wave functions. The 3d electron wave functions of neighbouring atoms show a strong overlap, which leads to 3d electron bands rather than to 3d levels. The relatively strong effective Coulomb repulsion between the 3d electrons in these bands can favour situations in which the number of spin up and spin down electrons is no longer equal and leads to the formation of a magnetic moment. Possible situations are schematically represented in fig. 10. For the sake of clarity, s electron bands, in which $N(E)$ is considerably lower, have been omitted in this figure. The relative filling of the bands is determined by the Fermi energy, indicated by horizontal bars. The magnitude of the magnetic moment (μ) is proportional to $\int_0^{E_F} [N(E)\uparrow - N(E)\downarrow] \, dE$, where the integration extends from the bottom of the 3d band up to the Fermi energy. In fig. 10a the Fermi energy is much higher than the top of the 3d band; both sub-bands are filled completely and $\mu = 0$. In case (b) the Fermi level is low enough to allow for a partial depletion of the 3d band. The effective Coulomb repulsion between the 3d electrons can be too weak, however, to give rise to band splitting. The result is no magnetic moment since the number of spin up and spin down electrons is equal. A comparison of the shaded areas corresponding to the number of spin up and spin down electrons in situations (c) and (d) shows that in these cases $\mu \neq 0$. Sometimes it is possible to distinguish experimentally between cases (c) and (d). If by chemical substitution of a third

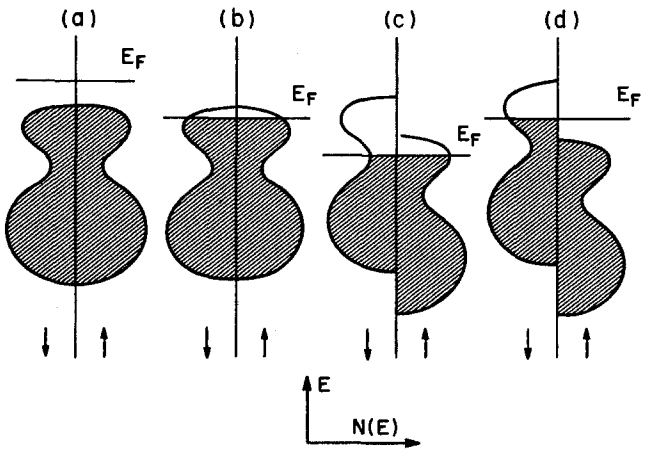

Fig. 10. Schematic representation of the density of states $N(E)$ of 3d electrons as a function of energy E. Spin down and spin up electrons are indicated by arrows. The position of the Fermi level is indicated by E_1.

component into the R–M compounds the total number of electrons contained in the 3d band can be raised situation (d) always leads to a decrease of μ. In case (c) $N(E_F)\downarrow$ is smaller than $N(E_F)\uparrow$. Upon further filling of the 3d band more electrons go into the spin up band thereby increasing the difference between the total number of spin up and spin down electrons. As a consequence μ will show an initial increase, a behaviour which is opposite to that expected in case (d).

In its simplest form the itinerant electron model predicts an exchange splitting between the two 3d sub-bands if the Stoner criterion (Stoner 1938) is satisfied

$$IN(E_F) - 1 \equiv \bar{I} - 1 > 0 \tag{31}$$

I is the effective Coulomb repulsion between the 3d electrons and $N(E_F)$ is the (paramagnetic) 3d electron density of states at the Fermi level. The Curie temperature is given in the Stoner–Wohlfarth model (Wohlfarth 1968) by

$$T_c^2 = T_F^2(\bar{I} - 1). \tag{32}$$

The degeneracy temperature T_F in this expression depends on the first and second energy derivatives of $N(E)$ at the paramagnetic Fermi level. This relation is strictly valid only for weak itinerant ferromagnets. In view of the comparatively large spatial extent of the 3d electron wave functions it can be presumed that the effect of externally applied pressure leads to larger effects on the electronic and magnetic properties than in the case of systems containing 4f electrons. In the itinerant electron model the pressure derivative of the Curie temperature (Wohlfarth 1969, Edwards and Bartel 1972) is given by

$$dT_c/dP = \tfrac{5}{3}\kappa T_c - \tfrac{5}{6}\kappa B/T_c. \tag{33}$$

The quantity κ represents the compressibility and B is a parameter determined by the intra-atomic Coulomb repulsion and the shape of the 3d band at the Fermi level.

It will be shown below that numerous properties of rare earth transition intermetallics bear features which can satisfactorily be described in the framework of the itinerant electron model. A priori it is not known how far the 3d moments in these compounds are localized or are due to itinerant 3d electrons. If they were strictly localized the same RKKY type description could be used as outlined for the 4f electrons in section 2.1. Friedel et al. (1961) have proposed a model for the 3d electron magnetism in which aspects of the localized as well as aspects of the itinerant model are combined. For the formation of localized moments on the transition metal atoms a similar criterion exists as that given by Stoner [eq. (31)]. The coupling between the localized moments is intimately related to the so-called Friedel oscillations that surround a transition metal moment. In many respects this coupling takes the same form as the RKKY coupling scheme. In Friedel's model the coupling is not mediated by conduction electrons of s character but rather by conduction electrons of d character. The spatially oscillating electron density variation responsible for this coupling is shown in fig. 11. The position of the nodes $r = \lambda, 2\lambda$ is determined by $\lambda \approx 1/k_F$, where k_F is measured now to the nearest 3d band extremum. If d is the

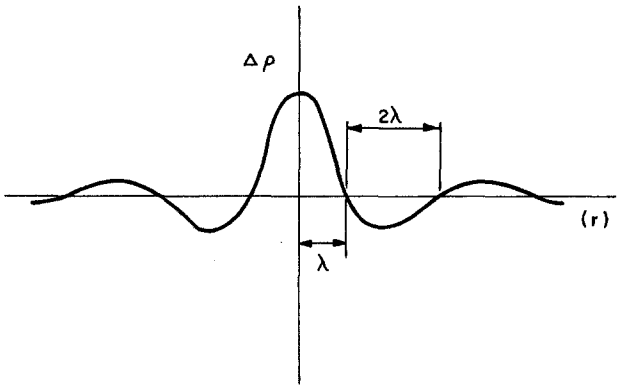

Fig. 11. Electron density variation $\Delta\rho$ around a local perturbation centered at $r = 0$.

interatomic distance between the transition metal atoms Friedel's model predicts ferromagnetism when $d < \lambda$; antiferromagnetism (including collinear as well as helical spin structures) is predicted when $d > \lambda$. A model dealing with itinerant as well as localized aspects of the 3d electron magnetism has also been proposed by Liu (1976) and by Stearns (1973). In the quasi spin model of Liu the 3d electrons reside in spin split energy bands in a way that there is a spin cloud around each atomic 3d site. When excited the spin cloud or quasi spin is assumed to precess rigidly. The moment per 3d atom is in general non-integral. The interaction between the quasi spins, in the large wave number limit, takes the form of the RKKY interaction. Since the band electrons include not only the s electrons but also the d electrons the coupling between the quasi spins will in general be more complex than is describable by means of simple analytical expressions like eq. (5).

Other models describing the 3d electron magnetism can be found in the papers of Edwards (1977) and Pettifor (1980).

3.2. Magnetic properties

3.2.1. Compounds with 3d transition elements

The magnetic properties of compounds with 3d transition metals are listed in table A.3. Recent years have seen the publication of a large number of papers reporting studies of the magnetic properties of rare earth transition intermetallics by means of the Mössbauer effect and NMR techniques. A detailed review of these results falls outside the scope of this chapter but has been given by Buschow (1977e).

In the various Ni compounds listed in table A.3a a substantial Ni moment is only found in R_2Ni_{17}. In R_2Ni_7 and RNi_3 the Ni moments are very small and fall below $0.1\mu_B$/Ni. In the other R–Ni compounds the Ni moments are virtually zero. It is understandable therefore that the magnetic ordering temperatures reach comparatively high values only in R_2Ni_{17}. That is is primarily the Ni–Ni

interaction which determines the ordering temperature is shown by the results on Y_2Ni_{17}, for which T_c is above 150 K. In view of the large electronegativity difference between Ni and the rare earths (Miedema et al. 1977) it is conceivable that considerable electron transfer may take place in the direction $R \rightarrow$ Ni. This would lead to a more complete filling of the Ni 3d band as well as to a reduction of the effective Coulomb repulsion between the 3d electrons. Both effects result in a decrease of the Ni moment. Specific heat measurements performed on $LaNi_2$ have shown the electronic coefficient of the specific heat to be equal to 12.5 millijoules/mole K (Wallace 1973). This value is close to that observed in $LaAl_2$. It indicates that the 3d band in RNi_2 is virtually full and contributes nothing or only a small portion to the density of states at the Fermi level. It is reasonable to assume that a similar situation is present in the compounds of higher R/Ni ratio. The absence of Ni moments in the compounds of lower Ni concentration than RNi_2 is therefore not surprising. Remarkable, on the other hand, is the absence of a Ni moment in RNi_5 (R = La, Lu or Y). Gignoux et al. (1976b) showed that $LaNi_5$ and YNi_5 are Pauli paramagnets with an exchange enhanced susceptibility. The results of magnetic measurements on $GdNi_{5\pm\delta}$ led them to suggest that the Fermi level in the 3d band in RNi_5 is located at a minimum in the density of states and this prevents exchange splitting between the two 3d sub-bands.

For the reasons mentioned above, magnetic ordering in RNi_n with $n \leqslant 2$ is primarily due to the indirect exchange interaction between the 4f moments. NMR data (Dormann and Buschow 1977) obtained on GdNi and related pseudo-binary compounds confirm this view. Similar data obtained on $Gd_{1-x}La_xNi_2$ indicate, however, that the contribution of the Ni 3d electrons to the indirect coupling between the Gd moments cannot be completely neglected, and that in the magnetically ordered state there should be an induced moment at the Ni sites in $GdNi_2$ of the order of a few hundredths of a Bohr magneton (Dormann and Buschow 1977). Experiments performed with polarized neutrons on a $TbNi_2$ single crystal have shown that in the paramagnetic state the nickel atoms do not carry a magnetic moment (Givord et al. 1976). Givord et al. also found that the Tb atoms produce a spatially non-uniform polarization of the conduction electrons which indicates that a substantial part of the Tb–Tb coupling proceeds via an RKKY-type coupling scheme. The easy direction of the magnetization in various RNi_2 compounds has been determined on Fe doped samples by means of the ^{57}Fe Mössbauer effect (Arif et al. 1977a).

In the R-rich R–Ni compounds in particular, the R atoms reside at crystallographic sites of low symmetry and crystal field effects are important. The magnetic properties of the R_3Ni and RNi compounds are therefore determined to a very large extent by the strong crystal field induced anisotropy. Neutron diffraction performed on several of these compounds (Bècle et al. 1970b) has shown that the magnetic structures can be rather complex. This has led Bècle et al. (1970b) to assume that the exchange interaction between the localized 4f moments is no longer isotropic but contains anisotropic contributions. The large magnetocrystalline anisotropy explains why the domain walls in these com-

pounds and related pseudobinary compounds are rather narrow. Their energy depends on the position of the wall centre with respect to the crystal lattice and varies periodically. This leads to a complex magnetization behaviour (Gignoux and Lemaire 1974) similar to that described for TbGa in section 2.3.1.

The magnetic properties of rare earth cobalt compounds are listed in tables A.3b and A.3c. There is a close correspondence between the 3d transition metal moments in R–Co and R–Ni compounds. In the cobalt compounds, too, a Co moment is only present at Co concentrations higher than in RCo_2. In compounds of lower Co concentration there are hardly any moments on the Co atoms or they occur only by virtue of the polarizing influence of the rare earth partner. In contradistinction to YNi_2, however, there are a still quite a large number of holes in the cobalt 3d band of YCo_2. The latter compound is a strongly exchange enhanced Pauli paramagnet. Depending on the polarizing power of the rare earth component the induced moment at the Co sites in RCo_2 can become fairly large (Moon et al. 1965, Gignoux et al. 1976a, 1977a, b) (about $1\mu_B$/Co in $GdCo_2$, see for instance Lemaire 1966a). The magnetic properties associated with the Co sublattice in RCo_2 give rise to a first order magnetic transition when R represents R = Dy, Ho or Er (Lemaire 1966a, Petrich and Mössbauer 1968, Givord and Shah 1972). In $GdCo_2$ and $TbCo_2$, where the exchange field due to the R moments is much stronger, the paramagnetic ferrimagnetic transition is of second order. This has been explained by Bloch et al. (1975) and by Cyrot et al. (1979) in terms of a model of itinerant electron metamagnetism. Gignoux et al. (1976a, 1977a, b) have performed a polarized neutron study on various RCo_2 single crystals. In the paramagnetic regime the temperature dependence of the Co sublattice magnetization was found to be in keeping with the enhanced paramagnetism model already referred to above (Bloch and Lemaire 1970, Bloch et al. 1975) and to be inconsistent with the localized moment description formerly proposed by Burzo (1972). Part of the data of Gignoux et al. is reproduced in fig. 12. In a more recent analysis Burzo (1976) uses a Co moment given by $\mu_{Co} = V_{Co}H_{ex}(Co)$ where $H_{ex}(Co)$ is the exchange field experienced by the Co atoms. The proportionality constant $V_{Co} = \frac{1}{3} \times 10^{-6}\mu_B$/G has the dimension of a susceptibility and this comes close to the description by Gignoux et al. (1976a, 1977a, b) where V_{Co} takes the form of a weakly temperature dependent susceptibility. Burzo (1976) does not state explicitly in how far the constant V_{Co} is sensitive to variations in temperature within the magnetically ordered and paramagnetic regimes considered.

Rare earth cobalt compounds in which the Co atoms have a magnetic moment of their own are tabulated in table A.3c. Magnetic measurements and in some cases neutron diffraction measurements can be interpreted on the assumption of a Co moment oriented antiparallel to the rare earth spin moment. This leads to ferromagnetism for the light rare earth compounds ($J = L - S$) and to ferrimagnetism for the heavy rare earth compounds ($J = L - S$). Roughly speaking, the ordering temperature in these R–Co compounds is determined by the Co–Co interaction (see also Wohlfarth 1979). Close to T_c the magnetization is primarily due to the Co sublattice magnetization. When the temperature is lowered the R sublattice magnetization increases together with the Co sublattice magnetization.

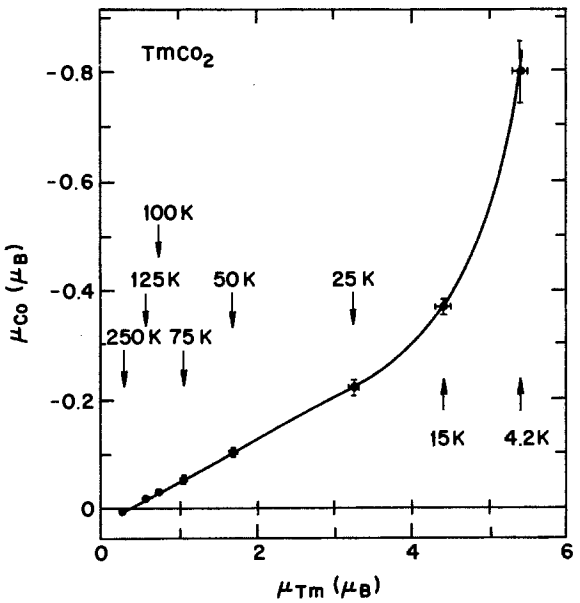

Fig. 12. Dependence of the Co moment on the polarizing influence of the Tm moments (Gignoux et al. 1976a, 1977a, b).

For several *R*–Co compounds in which *R* is a heavy rare earth, the former exceeds the latter at absolute zero. Since in these cases the *R*- and Co sublattice magnetizations are antiparallel, mutual compensation of both sublattice magnetizations should occur at some intermediate temperature (T_{comp}). Values of T_{comp} are also listed in table A.2c.

The effect of crystal fields on the magnetic properties is comparatively large in the rare earth rich compounds where it not only gives rise to a reduction of the rare earth sublattice magnetization at low temperatures but in addition has a large impact on the magnetization processes (Lemaire et al. 1968, Taylor 1971) in these compounds (for instance in Dy_3Co and Dy_4Co_3 the low temperature magnetic isotherms suggest magnetization processes which are largely governed by narrow domain wall propagation, 1979, Hendy and Lee 1978, as already discussed in section 2.3.1). In the cobalt rich *R*–Co compounds the effect of crystal fields is relatively less important, partly because the rare earth atoms reside at sites of higher symmetry and partly because a large portion of the magnetic properties is determined by the Co sublattice. The single ion crystal field anisotropy of the *R* component through the *R*–Co interaction still determines the direction of easy magnetization, at low temperature in particular. This holds a fortiori in the cubic compounds RCo_2, where the Co sublattice anisotropy is negligible (Dublon 1976, Dublon and Atzmony 1977, Atzmony et al. 1976, Gignoux et al. 1975). In RCo_3 a substantial influence of the Co sublattice anisotropy (Schweizer and Yakinthos 1969, Yakinthos and Mentzafos 1975,

Yakinthos and Rossat Mignod 1972, Georges et al. 1975, Kren et al. 1969) becomes apparent. This influence increases in compounds of still higher Co concentration such as RCo_5 (Ermolenko 1974, 1976, Klein et al. 1975) and R_2Co_{17} (Miller et al. 1976, Deryagin and Kudrevatykh 1975, Kazakov et al. 1975). In the stoichiometric compounds RCo_3, R_2Co_7, RCo_5 the Co sublattice favours an easy c-axis magnetization, whereas in R_2Co_{17} the easy magnetization direction is perpendicular to the c-axis. The single ion anisotropy of the R sublattice can in general be analyzed by means of crystal field theory outlined briefly in section 2.2. It can favour an easy direction either parallel or perpendicular to the c-axis, depending on the nature of the 4f wave function of a given R ion as well as on the nature of the site these ions occupy in the above compounds. At temperatures high compared to the overall crystal field splitting the single ion anisotropy is relatively small so that the easy magnetization direction is determined primarily by the Co sublattice anisotropy. At low temperatures the single ion contribution prevails. In cases where the contributions of R and Co differ in sign this can lead to changes in the easy direction at some intermediate temperature (Lemaire 1966b, Irkhin and Rozenfel'd 1974). In the case of $TbCo_{5.1}$ and $DyCo_{5.2}$ Ermolenko et al. (1976) found an anomalous change in the magnetization near the temperature where the transition from easy plane to easy axis magnetization occurs (see fig. 13). This has been explained by these authors in terms of a molecular field approach taking account of the change in magnetic energy levels due to the presence of the anisotropy.

The compound $SmCo_5$ is one of the few examples where the anisotropy due to both the R atoms and the Co atoms favours an easy c-axis. Experimental results obtained by different authors are shown in fig. 14b. These can be compared with the results of numerical calculations (Buschow et al. 1974b) in fig. 14a, where the stabilization energy ΔF of a moment alignment in the basal plane is given for various values of the second order crystal field parameter $A_2^0\langle r^2\rangle$ and the exchange field H_{ex} (see eqs. (10) and (25) of section 2.2). From a further analysis

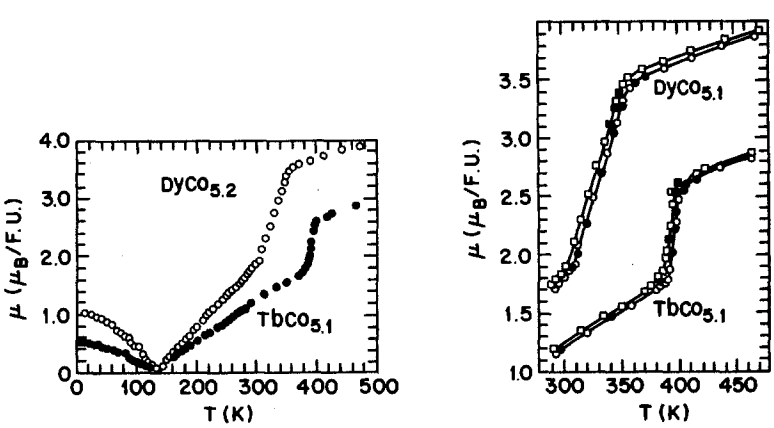

Fig. 13. Temperature dependence of the magnetic moment of several $CaCu_5$ type compounds. Open symbols: increasing temperature; full symbols: decreasing temperature (Ermolenko et al. 1976).

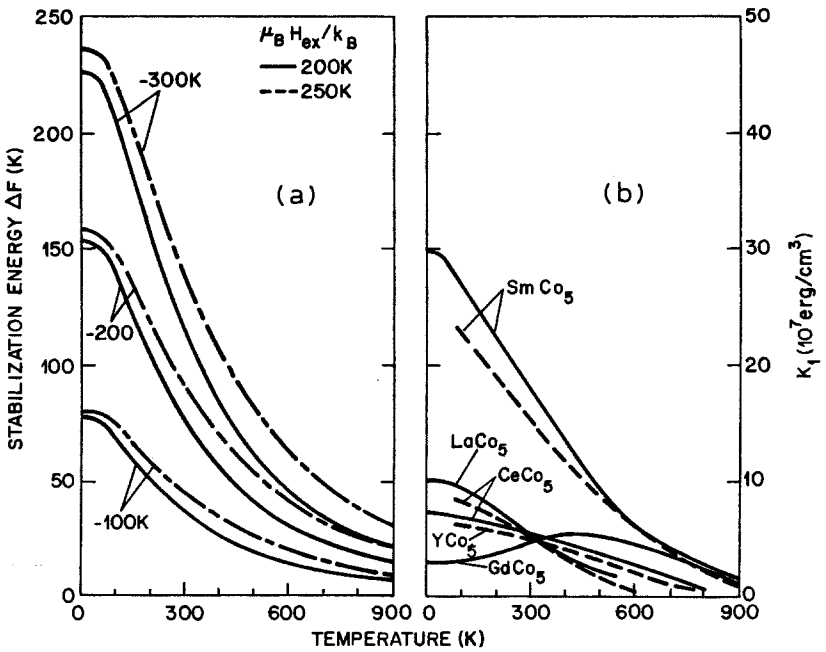

Fig. 14. (a) Dependence of the stabilization energy ΔF on the crystal field parameter $A_2^0\langle r^2\rangle$ and the exchange field H_{ex}. The parameters $A_4^0\langle r^4\rangle$ and $A_6^0\langle r^6\rangle$ were kept zero. (b) Temperature dependence of the anisotropy constant K_1 in various RCo_5 compounds (full lines: data of Ermolenko 1974; broken lines: data of Klein et al. 1975).

of the single ion anisotropy of Sm^{3+} it was derived that the higher order potentials appearing in eq. (19) of section 2.2 are relatively less important. Even if $A_6^6\langle r^6\rangle$ were of the same order of magnitude as $A_2^0\langle r^2\rangle$ the basal plane anisotropy is expected to be only a few percent of the axial anisotropy. This agrees with the fact that in $SmCo_5$ basal plane anisotropy could not be observed experimentally (Klein et al. 1975). In the compounds RCo_5 where the R ions are represented by La^{3+}, Ce^{4+}, Y^{3+} or Gd^{3+}, single ion anisotropy contributions are absent. It can be seen in fig. 14b that in these cases the anisotropy remains relatively small at low temperatures. The data of $GdCo_5$ in particular show that the anisotropy of dipolar origin, due to the magnetically ordered 4f moment at low temperatures, is of little importance (Buschow et al. 1974b). It is clear that the large single-ion anisotropy due to Sm^{3+} would be lost if Sm in $SmCo_5$ and Sm_2Co_{17} were to adopt the divalent state, as has been proposed by Orehotsky et al. (1977). More details regarding the magnetocrystalline anisotropy and the saturation magnetization in RCo_5 and R_2Co_{17} can be found in Buschow et al. (1974b), Sankar et al. (1975), Szpunar and Lindgård (1979), Streever (1979), Greedan and Rao (1973), Perkins and Nagel (1975), Perkins and Strässler (1977) and Deportes et al. (1976). Polarized neutron studies showed that the coupling between the Sm and Co moment remains ferromagnetic below 350 K (Givord et al. 1979).

Several of the above-mentioned compounds are suitable candidates for per-

manent magnet applications. Permanent magnets made from these materials have outstanding properties, such as a high coercive force, a high energy product and a high temperature stability (Martin and Benz 1971, Shur et al. 1975). More information regarding this class of materials is contained in Buschow (1977e) and in Vol. 3/4, of these handbooks (Rare earth based magnets, by K.J. Strnat).

From the results presented for R–Fe compounds in table A.3d it is seen that the magnetic ordering temperatures increase with decreasing Fe concentration, even though the magnetic moments per Fe atom decrease in the same direction (this latter fact can for instance be derived from the μ values listed for the Y–Fe compounds). The concentration dependence of T_c has a trend opposite to that observed in R–Co and R–Ni compounds. There is as yet no unique explanation for this peculiar behaviour (Buschow 1977e). The decrease in the Fe moment with decreasing Fe concentration can be ascribed to a weakening of the effective Coulomb repulsion and to the band filling mentioned earlier in connection with a similar 3d moment decrease in the R–Ni and R–Co series. An alternative interpretation, in terms of more localized 3d moments, is suggested by the results of numerous investigations of the R–Fe compound by means of the ^{57}Fe Mössbauer effect (Gubbens et al. 1978). It follows from these results that there is a considerable difference in effective hyperfine field (H_{eff}) between the Fe atoms occupying crystallographically non-equivalent positions in RFe_3, R_6Fe_{23} and R_2Fe_{17}. Gubbens et al. (1978) note that there seems to be no definite relation between H_{eff} and the nearest neighbour Fe–Fe separation at these Fe positions. A more or less linear decrease or increase of H_{eff} was found, however, when this quantity was plotted versus the relative number of first Fe neighbours (n_{Fe}) or versus the relative number of first R neighbours, respectively ($n_R = 1 - n_{Fe}$). These plots are reproduced in fig. 15a (R is trivalent Er or Y) and fig. 15b (R is tetravalent Ce or Th). Since H_{eff} is, under certain conditions, a measure of the magnetic moment of the corresponding Fe atoms, Gubbens et al. argue that the concentration dependent moment decrease in the R–Fe compounds could as well be explained on the basis of environmental changes. The magnetic measurements performed on R–Fe compounds in which R represents Y or Lu have shown that the strength of the Fe sublattice anisotropy is in general rather modest, so that the easy magnetization direction in these materials is determined primarily by the single ion anisotropy of the R component. Even in the cubic RFe_2-compounds the single ion anisotropy can be appreciable; studies on single crystals (Clark and Belson 1974, Abundi et al. 1979) (R = Tb, Dy, Ho and Er) made it clear that reliable values of the saturation magnetization cannot be obtained on polycrystalline samples even if the field strengths applied are in excess of 100 kOe. Apart from the above-mentioned studies on single crystals, information regarding the easy magnetization directions in RFe_2 compounds has been derived mainly from results of Mössbauer effect spectroscopy (Atzmony 1977, Atzmony and Dariel 1976, Atzmony et al. 1973a, Moriariu et al. 1976a, Van Diepen et al. 1973, Rosen et al. 1976). In many pseudobinary compounds, but also in $CeFe_2$, $SmFe_2$ and $HoFe_2$, the direction of the easy axis of magnetization is strongly temperature dependent and in a given temperature region does not coincide with one of the major cubic directions. Atzmony and Dariel analyzed

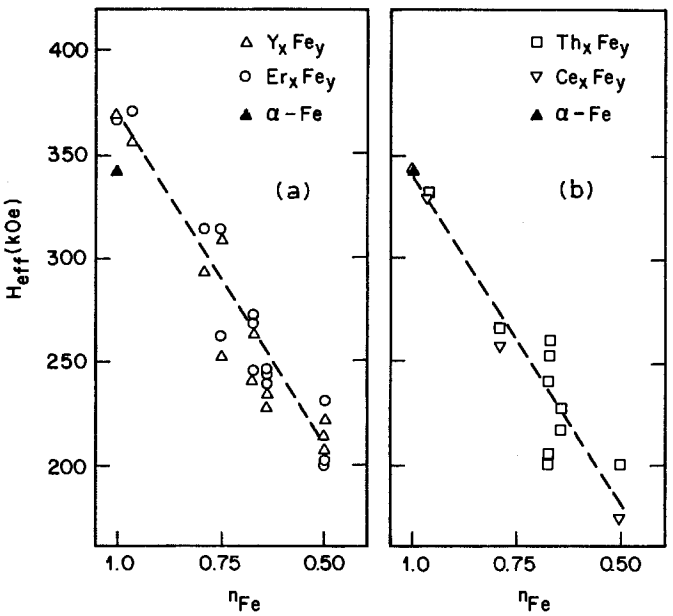

Fig. 15. Effective hyperfine fields, H_{eff}, at the various Fe sites in R_xFe_y as a function of the relative number of Fe neighbours (n_{Fe} = number of nn Fe atoms/[number of nn Fe atoms + number of nn R atoms]).

their data by means of crystal field theories (Atzmony 1977) (section 2.2, eqs. (26–28)) and showed that the single-ion model actually predicts these directions.

Polarized neutron studies were made on $HoFe_2$ by Fuess et al. (1979). The results show that the Fe atoms in this compound have a large stable moment of their own in addition to a small induced component due to the R–M interaction.

Elastic and magnetoelastic properties of RFe_2 compounds were studied by Klimker et al. (1974) by means of ultrasonic sound velocity measurements. These properties, together with the rather impressive magnetostrictive properties of binary and pseudobinary R–Fe compounds, are discussed in more detail in chapter 7 of this book (Magnetostrictive rare earth compounds, by Clark).

Mössbauer effect spectroscopy also proved to be useful in the determination of the easy magnetization directions in RFe_3 (Van der Kraan 1975, 1976, Arif et al. 1975) as well as in R_2Fe_{17} (Steiner and Haferl 1977, Gubbens et al. 1974a, b, 1977) correlation could be established between the easy directions observed in the various compounds and the sign of the coefficient θ_k of eq. (20) in section 2.2.

Several of the R_2Fe_{17} compounds are not simply ferro- or ferrimagnetic but have a non-collinear magnetic structure. The magnetization versus temperature curves shown in fig. 16 may help to illustrate the various possibilities that exist. The curve shown for Er_2Fe_{17} can be regarded as normal. The decreasing magnetization well below $T_c \approx 300$ K reflects the increasing ordering of the Er sublattice. Since the Fe sublattice magnetization still exceeds the Er sublattice magnetization at absolute zero no compensation temperature is expected nor is it observed. In Tm_2Fe_{17} too, the comparatively low magnetization at 0 K is in

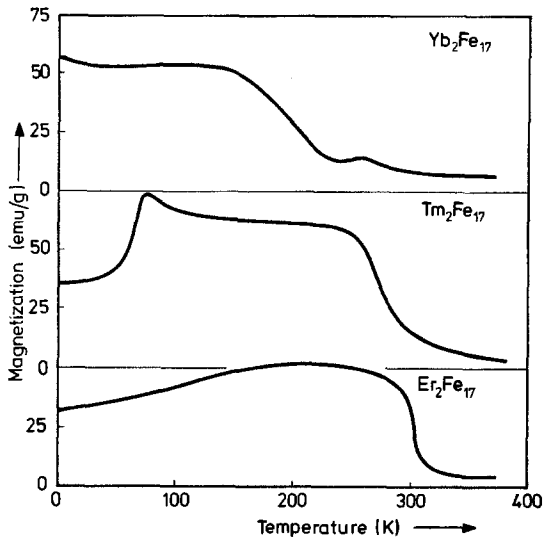

Fig. 16. Temperature dependence of the magnetization of three different R_2Fe_{17} compounds.

agreement with an antiparallel coupling between the Tm and Fe moment. This agrees with results of neutron diffraction (Givord and Lemaire 1972, 1973, 1974). The decreasing effect on the total magnetization of the increasing order of the Tm sublattice is obscured in this case by the change in easy direction from perpendicular with the c-axis ($T \geqslant 70$ K) to parallel with the c-axis ($T \leqslant 70$ K) (Givord and Lemaire 1972, Gubbens and Buschow 1973, 1974, Narasimhan and Wallace 1974). The curve shown in the top part of fig. 16 is more or less representative of the compounds Ce_2Fe_{17}, Yb_2Fe_{17} and Lu_2Fe_{17}. Magnetic ordering sets in close to the temperature where the M vs. T curve exhibits a small maximum. In these cases the magnetic ordering is not of a simple type but entails helimagnetic structures as well as fan structures (Givord and Lemaire 1972). In Tm_2Fe_{17} a helimagnetic structure has been observed only in the rather limited temperature range 275–235 K, whereas below 275 the magnetic structure is collinear (Givord and Lemaire 1972, Elemans and Buschow 1974). Comparison of the lattice constant in the c-direction of the R_2Fe_{17} compounds shows that comparatively low values are reached in the compounds with R representing Ce, Tm, Yb and Lu. In these cases the nearest neighbour Fe–Fe distance of the Fe atoms residing at the so-called dumb-bell sites (these are the sites indicated in table A.1 as 4(f) and 6(c) for the Th_2Ni_{17} structure and the Th_2Zn_{17} structure, respectively) are very short. Barbara et al. (1973) have correlated the presence of such short Fe–Fe distances with the occurrence of the non-collinear magnetic structures. According to these authors the short Fe–Fe distances correspond to negative exchange interactions on the Néel–Slater curve. These negative interactions stabilize a helical spin configuration below the ordering temperature. At lower temperatures the strength of the negative interactions decreases as a consequence of the spontaneous magnetostriction. In conjunction with an in-

creasing anisotropy this eventually leads to a transition from a helimagnetic structure to a fan structure.

Table A.3e summarizes the results of investigations performed on rare earth manganese compounds. The compounds RMn_2 crystallize in either the cubic $MgCu_2$ structure or the hexagonal $MgZn_2$ structure. From the results shown for YMn_2 and $LuMn_2$ it can be deduced that the Mn atoms do not have a magnetic moment of their own. The possibility of an induced moment exists in compounds where the R component possesses a sizable spin moment. Investigations of the ^{55}Mn NMR on $ErMn_2$ and $TmMn_2$ by Barnes and Lunde (1975) as well as neutron diffraction studies on $TmMn_2$ (Felcher et al. 1965) do not point to a magnetic moment on the Mn atoms in these compounds. They do have a magnetic moment, however, in $TbMn_2$ (Corliss and Hastings 1964). Neutron diffraction studies of this compound have shown that the Mn sublattice itself is antiferromagnetically ordered, so that essentially its magnetization is internally compensated. The Tb sublattice consists of ferromagnetically coupled Tb moments. The combination of the rare earth and manganese sublattices leads to a ferromagnetic spiral structure (Corliss and Hastings 1964). Unfortunately the neutron diffraction results do not allow the moment of the Mn atoms to be fixed, even within rather wide limits. It is reasonable to assume that the Mn sublattice magnetization in $GdMn_2$ is also internally compensated by antiferromagnetic ordering of the Mn moments, as in $TbMn_2$. It is not possible therefore to derive values of the Mn moments from the saturation magnetization, even if one assumes that the Gd moments in the Gd sublattice are ordered ferromagnetically. In view of the complicated magnetic ordering in RMn_2 compounds no definite conclusions can be reached regarding the sign of the R–Mn interaction.

Interesting results were reached in $PrMn_2$, obtained by Oesterreicher (1971) in the cubic Th_6Mn_{23} structure ($Pr_6Pr_4Mn_{19}$ or $Pr_6Pr_3Mn_{20}$) rather than in the hexagonal $MgZn_2$ structure. The structural change led to distinctly different magnetic properties (given in parentheses in table A.3e) with a magnetic ordering temperature ($T_c = 448$ K) close to that expected for compounds of the stoichiometric composition R_6Mn_{23} (see table A.3e).

The effective moments derived from the linear part of the temperature dependence of the reciprocal susceptibility in R_6Mn_{23} exceed the free R ion values considerably. This, and also the results obtained on Lu_6Mn_{23} and Y_6Mn_{23}, make it clear that the Mn atoms in R_6Mn_{23} bear a magnetic moment. In Gd_6Mn_{23} the saturation moment is close to $50\mu_B$ per Gd_6Mn_{23} which corresponds to $8.2\mu_B$ per Gd atom. Since the saturation magnetization of the Mn sublattice should have a value close to that found in Y_6Mn_{23} or Lu_6Mn_{23} the value $50\mu_B$ observed in Gd_6Mn_{23} is much too low to be explained by ferromagnetic ordering (Gd and Mn moments parallel). It also precludes simple ferrimagnetic ordering (Gd moments antiparallel to the Mn moments) (Buschow and Sherwood 1977b). From the results obtained in the magnetically ordered regime one can therefore reach no definite conclusions as to the sign of the R–Mn coupling. Measurements in the paramagnetic regime show that the reciprocal susceptibility in Gd_6Mn_{23} is approximately linear several hundred degrees above the magnetic

ordering temperature only (Kirchmayr 1966). Its form suggests ferrimagnetic ordering. An analysis of the magnetic data in terms of a molecular field model seems impossible, however, since it is not known how many different sublattices have to be included. If one assumes for instance the presence of two antiferromagnetically coupled Mn sublattices in conjunction with a ferromagnetic R sublattice, the change in sign of the asymptotic Curie temperature θ_p in going from the light to the heavy rare earths in R_6Mn_{23} would be indicative of an antiparallel coupling between the rare earth spin moment and the ferromagnetic moment component, induced by the R spin in the otherwise antiferromagnetically ordered Mn sublattice. It is clear that further experiments are needed to reach definite conclusions regarding the sign of the R–Mn interaction in these compounds.

The magnetic data of RMn_{12} listed at the end of table A.3e show that the magnetic ordering in these compounds is antiferromagnetic and occurs well below room temperature. No magnetic ordering in YMn_{12} is suggested by its field- and temperature independent susceptibility ($\chi = 3.7 \times 10^{-3}$ emu/mole). Neutron diffraction has shown, however, that antiferromagnetic ordering occurs below $T_N = 120$ K (Deportes et al. 1977). The mean magnetic moment per Mn is $0.4\mu_B$. A schematic representation of the non-collinear antiferromagnetic structure is given in fig. 17. Deportes et al. (1977) note that the symmetry of the magnetic structure is such that the molecular field produced by the M moments at the rare earth site cancels. The R and Mn sublattices are therefore not coupled magnetically and order more or less independently at temperatures T_R

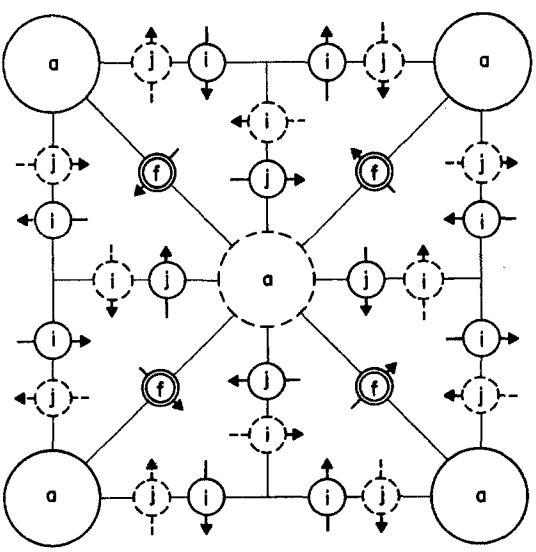

Fig. 17. Magnetic structure of YMn_{12}. Y atoms on the sites 2(a) and Mn atoms on the sites 8(i) and 8(j) lie in the planes $z = 0$ (full lines) or $z = \frac{1}{2}$ (dashed lines). Mn atoms on the site 8(f) lie in $z = \frac{1}{4}$ and $z = \frac{3}{4}$. (Taken from Desportes et al. 1977.)

and T_N, respectively ($T_R \ll T_N$). From a further analysis of the neutron diffraction data Deportes and Givord (1976) conclude that the magnetic interactions between the Mn moments in RMn_{12} vary strongly with the interatomic distance. Unfortunately the data on the RMn_{12} compounds do not reveal any information on the sign of the R–Mn coupling either.

3.2.2. Compounds with 4d and 5d transition elements

Attempts to determine the crystal structure of the various rare earth rich ruthenium compounds have not been very successful, although the stoichiometry of several of these compounds in the systems Gd–Ru, Dy–Ru and Y–Ru has been determined (Loebich and Raub 1976a). Magnetic data of R–Ru compounds are given in table A.3f. Curie temperatures have been reported only for RRu_2; the positive θ_p values in compounds of a composition R_3Ru, $R_{73}Ru_{27}$ and R_2Ru suggest that these latter are ferromagnetic, too. Several of the cubic Laves phase compounds become superconducting at low temperatures ($LuRu_2$, $CeRu_2$, $ThRu_2$) (Hillenbrand and Wilhelm 1972, Wilhelm and Hillenbrand 1971). Davidov et al. (1973b) investigated pseudobinary compounds of the type $Gd_xR_{1-x}Ru_2$ (R = La, Th, Ce) and found a correlation to exist between the normalized superconducting transition temperature and the thermal broadening of the EPR of the magnetic impurity. This was explained by assuming that the electrons which contribute to the superconductivity are also responsible for the thermal broadening (both properties depend on the square of the wave vector dependent exchange integral $\langle [J(q)]^2 \rangle$). Re-entrant critical field behaviour was studied in more detail in $Gd_xTh_{1-x}Ru_2$ (Davidov et al. 1973c).

Investigations of the magnetic properties of various Y–Rh compounds by Loebich and Raub (1975) have shown that the susceptibility of these compounds is lower than that of the parent materials and reaches a minimum for YRh. The diamagnetic character of YRh (see table 4.3f) suggests that no partly depleted 4d band due to the Rh atoms is left in this compound. Similar conclusions can also be drawn from the low electronic coefficient (γ) of the specific heat (Chamard-Bois 1974). In view of the large difference in electronegativity between Y and Rh, the disappearance of the open 4d band can be understood in terms of electron transfer from Y to Rh (Tamminga 1973). Charmard-Bois (1974) has used the band structure calculations available for the isostructural compound DyRh (Belakhovsky 1972) and attributed the low values of γ and χ to the presence of a minimum in the density of states at the Fermi surface.

Guided by the magnitude of the magnetic susceptibilities of the various Y–Rh compounds one might assume that the 4d electrons of the Rh atoms do not make a significant contribution in the determination of the magnetic properties of the rare earth rhodium compounds, with the possible exception of RRh_5. Rhodium behaves essentially as a non-magnetic partner element in the various R–Rh compounds, and one might expect the magnetic properties of these compounds to be governed by the RKKY mechanism. None of this is true, however. Inspection of the data contained in table A.3f shows that in the CsCl type compounds a change from ferromagnetism (R = Gd, Tb, Dy) to antiferromag-

netism (R = Ho, Er, Tm) occurs. This change is incompatible with the RKKY coupling scheme. Detailed investigations by means of spin echo NMR on GdRh and related pseudobinaries have shown that each of the two types of indirect exchange coupling between the Gd atoms (proceeding either via 4f–s or via 4f–d polarization as discussed in section 2.1) can be regarded as being small (Dormann and Buschow 1976). The change in magnetic properties in going from GdRh to TmRh is probably a shift in the relative importance of these coupling schemes. The mentioned change from ferromagnetism to antiferromagnetism has been used in Buschow et al. (1975e) to obtain materials (primarily based on $Gd_xEr_{1-x}Rh$) that have large heat capacities at low temperatures. From the cryogenic point of view these results seem quite valuable since there is a lack of materials that have high heat capacities in the range 4–10 K.

The other R–Rh compounds listed in table A.3f have not been so fully investigated as those of the CsCl type. Compounds of the type RRh_2 are ferromagnets whereas the data obtained on Gd_3Rh and Gd_7Rh_3 indicate that metamagnetic behaviour prevails in R_3Rh and R_7Rh_3 (Loebich and Raub 1975).

Of particular interest is the compound $EuRh_2$ and related pseudobinaries due to the intermediate valence state of Eu in these systems (Bauminger et al. 1974a). In $EuRh_{2-2x}Pt_{2x}$ the valence state of Eu was found to be strongly dependent on the local environment, including neighbours beyond the nearest shell (Nowik et al. 1977).

The diamagnetic character of the compounds RPd_3 with R = La, Y or Lu shows that the effect of the 4d electrons of Pd on the magnetic properties can be regarded as being negligible in RPd_3. This will probably also be the case in R–Pd compounds of even lower Pd concentration.

A comparatively high ferromagnetic ordering temperature is reached in Gd_5Pd_2 ($T_c \approx 334$ K, see table A.3f). It is somewhat surprising that the magnetic ordering temperatures in the remaining R_5Pd_2 compounds are much lower, even if one takes into account that the R component in these compounds has a lower spin moment than Gd. A possible reason for this could be a difference in crystal structure, since Gd_5Pd_2 was not observed to crystallize in the cubic Dy_5Pd_2 type (Fornasini and Palenzona 1974, Loebich and Raub 1973b). Extremely low magnetic ordering temperatures are observed in RPd_3. Furrer and Purwins (1976) have performed inelastic neutron scattering experiments on several of these compounds. Their measurements on $PrPd_3$ and $NdPd_3$ show that the energies and widths of the crystal field transitions are almost independent of the temperature. No crystal field transition has been observed in $CePd_3$. An intermediate valence state of the Ce ions in $CePd_3$ had been proposed before on the grounds of susceptibility data (Fornasini and Palenzona 1974). Furrer and Purwins have taken the absence of this transition as evidence that the 4f electron of Ce in $CePd_3$ has to be described by a virtual bound state near the Fermi energy rather than by a localized state, the width of the 4f electron state being comparable with or larger than the crystal field splitting.

Compounds obtained by combining rare earths with 5d transition metals have been the subject of only a few magnetic investigations. As can be seen in table

A.3g, these investigations have been focussed mainly on the Laves phases $R\mathrm{Os}_2$, $R\mathrm{Ir}_2$ and $R\mathrm{Pt}_2$. From the fact that LaOs_2 is a superconductor, and from the fact that the compounds of Ir and Pt with either La or Y are weakly Pauli paramagnetic or diamagnetic, it can be derived that there is at best only a very moderate contribution of the 5d electrons to the density of states at the Fermi level. For these reasons it can be expected that the 5d electrons of Os, Ir or Pt do not play a significant role in the exchange coupling between the rare earth moments. Spin echo NMR studies made on $\mathrm{Gd}_{1-x}\mathrm{La}_x\mathrm{Pt}_2$ have shown that the predominant interaction involves s conduction electrons (RKKY type). The somewhat higher ordering temperature in GdIr_2, if compared to GdPt_2, originates from a comparatively larger participation of the rare earth 5d electrons in the exchange coupling (Dormann et al. 1977a, b).

Harris et al. (1973) have shown that the cubic MgCu_2 type structure in several R–Pt binary systems can extend over an appreciable concentration range, including the composition $R\mathrm{Pt}_3$ (R = La to Tb). The X-ray diffraction measurements of the lattice spacing within this concentration range in GdPt_x have been interpreted by means of a model in which the Pt atoms substitute progressively into the Gd sites. At the stoichiometric composition GdPt_2 vacancies are believed to occur on Pt as well as on Gd sites (Harris et al. 1973, Taylor et al. 1976). Results of spin echo NMR of Gd^{155}, Gd^{157} and Pt^{195} performed on GdPt_x and related pseudobinary compounds (Dormann et al. 1977b) are in satisfactory agreement with the substitution scheme mentioned above, although they seem to indicate that the vacancy concentration is somewhat smaller than assumed by Taylor et al. (1976).

3.3. Discussion

There are numerous experimental facts which favour an interpretation of the magnetic properties of the R–M compounds described in section 3.2.1 in terms of itinerant 3d electrons. One of these is the gradual decrease of the transition metal moment in R–M compounds (M = Ni, Co, Fe) when the R/M ratio is increased. Several magnetic studies on pseudobinary compounds RM_n, where M is represented by $\mathrm{Fe}_{1-x}\mathrm{Co}_x$, have shown that the mean magnetic 3d moment passes through a maximum before decreasing with increasing x. On the other hand, if M represents $\mathrm{Co}_{1-x}\mathrm{Ni}_x$ or $\mathrm{Co}_{1-x}\mathrm{Cu}_x$ the magnetization displays a collapse-like decrease with increasing x (for more details regarding these pseudobinary systems we refer to the original papers cited in the reviews by Taylor (1971), Wallace (1973) and Buschow (1977e). The above-mentioned concentration dependences of the 3d sublattice magnetization have currently been interpreted by means of a rigid band approach, where the 3d electrons of the constituent 3d elements share a common 3d band: In the case of the pseudobinaries with $M = \mathrm{Fe}_{1-x}\mathrm{Co}_x$ a situation exists similar to that sketched in fig. 10c where the Fermi level of the 3d band is close to a minimum in the density of states of the spin down sub-band. Increasing x leads to a more complete filling of the 3d band. Since initially more electrons go into the spin up band than into the

spin down band this results in an initial increase of the magnetization. In pseudobinaries based on $M = Co_{1-x}Ni_x$ or $Co_{1-x}Cu_x$ the situation in fig. 10d applies. Increasing x corresponds to a filling up of the spin down sub-band and a simultaneous decrease in the magnetization. The (paramagnetic) density of states decreases towards the top of the band, so that eventually one reaches a situation where the Stoner criterion [eq. (31)] is no longer satisfied and the band splitting disappears (as in fig. 10b). Of particular interest in this latter respect is the series $Y_6(Fe_{1-x}Mn_6)_{23}$, in which the magnetization was found to vanish in the intermediate concentration range.

The itinerant nature of the 3d electrons is also supported by magnetovolume effects obtained on a variety of binary R–M compounds. The changes of the magnetic properties of R–M compounds and their amorphous counterparts obtained under applied pressure by various authors have been discussed by Buschow et al. (1977). Some representative sets of data, due to measurements of Brouha et al. (1973, 1974) are reproduced in fig. 18. Three examples are shown in this figure: the magnetic ordering temperature increases with 3d atom concentration (Gd–Co), it decreases with 3d atom concentration (Y–Fe), or it passes through a maximum with increasing 3d atom concentration (Th–Fe). In each of these cases the values of dT_c/dP are seen to be dependent only on the magnitude of T_c. A positive slope dT_c/dP is exhibited by the compounds with the highest T_c in each system. Lower T_c values lead to increasingly negative slopes. These features are explained in a satisfactory way by means of eq. (33) but are difficult to understand in a localized picture.

It is also possible, however, to produce experimental evidence that favours a description of the magnetic properties of the R–M compounds in terms of a localized model rather than in terms of itinerant 3d electrons. Burzo et al. (1974) pointed out already that the collapse-like decrease of the transition metal moment in $GdCo_{2-2x}Ni_{2x}$ can satisfactorily be explained by means of a model due to Jaccarino and Walker (1965) in which the decrease in moment with decreasing x can be ascribed to a loss of moment in those Co atoms that have an insufficient number of Co atoms as nearest neighbours. For each concentration x the probability of Co atoms having n Co atoms as nearest neighbours, out of a maximum number of N, is given by

$$P(x, n, N) = \frac{N!}{n!(N-n)!} x^n (1-x)^{N-n}. \tag{34}$$

The number N is determined by the crystal structure of a given series of compounds. With eq. (34) it is possible to calculate for each concentration x the number of Co atoms that is surrounded by at least j Co atoms as nearest neighbours from

$$P_j(x) = \sum_{n=j}^{n=N} P(x, n, N). \tag{35}$$

Since Co atoms having less than j nearest Co neighbours are assumed to have no exchange splittings, one has

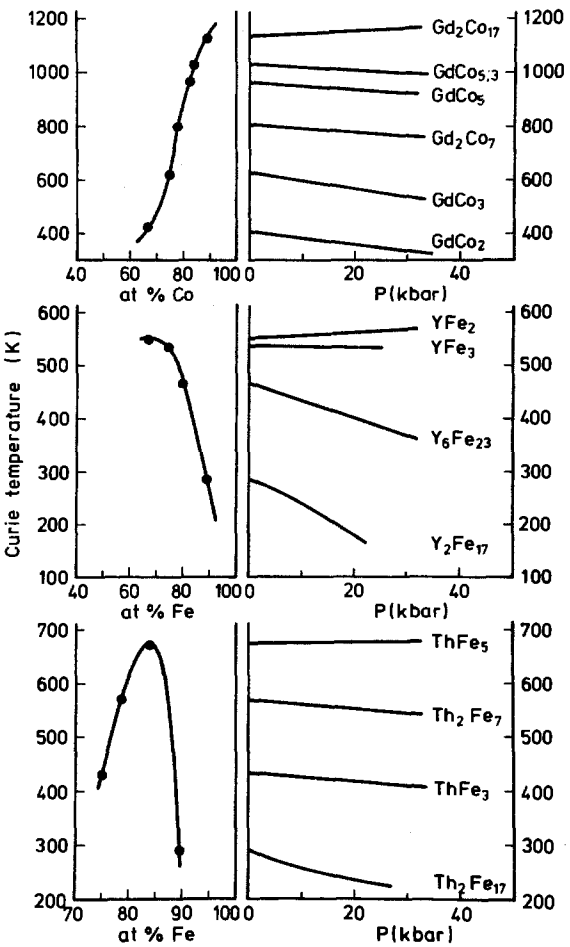

Fig. 18. Dependence of the Curie temperature (T_c) in various R–M compounds on M concentration (left hand parts) and on applied pressure (right hand parts).

$$\mu(x) = xP_j(x)\mu(x = 1). \tag{36}$$

Using the above formalism successful attempts to explain the concentration dependence of the 3d sublattice magnetization have been made in several other series of pseudobinaries such as $LaCo_{5-5x}Cu_{5x}$, $YCo_{5-5x}Ni_{5x}$ and $ThFe_{5-5x}Ni_{5x}$ (Buschow et al. 1977). All these examples show that the magnetic state of a given 3d atom is primarily determined by the local environment, i.e. its nearest neighbour shell. (More sophisticated models, taking also account of the mode of occupation of the shell of second neighbour 3d atoms (Besnus et al. 1978) or models where environmental changes lead to a stepwise decrease of the 3d moment (Van der Kraan et al. 1977) have been employed, too.) In this connection it is interesting that a similar analysis can explain the concentration

dependence of the 3d sublattice magnetization in amorphous rare earth transition metal alloys such as $Y_{1-x}Co_x$ (Buschow et al. 1977).

Investigations (Beckmann et al. 1976) of the system $Y_6(Fe_{1-x}Mn)_{23}$ made it clear that the disappearance of the 3d sublattice magnetization in the intermediate concentration range can also be understood in terms of localized 3d moments. According to Beckman et al. (1976) the introduction of Fe into Y_6Mn_{23} leads to a lattice contraction which enhances the antiferromagnetic Mn–Mn exchange. This in turn leads to a decrease of the magnetization and T_c. Starting from ferromagnetic Y_6Fe_{23}, lowering of the magnetization and T_c is due to the antiferromagnetic coupling of the Mn atoms with the host lattice. The disappearance of the magnetization in the intermediate concentration region was shown to originate predominantly from the magnetically inhomogenous nature of these materials (Beckmann et al. 1976, Hilscher et al. 1977).

Further support for the localized nature of the 3d moment comes from investigations using NMR or the Mössbauer effect. The ^{89}Y NMR in $YFe_{2-2x}Co_{2x}$ was investigated by Oppelt et al. (1976). The Y atoms themselves do not have a magnetic moment. Therefore the hyperfine field observed at the Y nuclei is a measure of the exchange fields produced by the surrounding magnetic Fe and Co atoms (transferred hyperfine field). In pure YFe_2 all Y sites are equivalent, so that only a single Y resonance line is observed. Oppelt et al. found that the substitution of Co for Fe gives rise to a well-developed satellite structure. The relative intensities of the various satellites are in agreement with the probabilities of the Y atoms having a nearest neighbour [nn] shell consisting of 12Fe [nn], 11Fe [nn] + 1Co [nn], 10Fe [nn] + 2Co [nn] and so forth. Without further analysis of the data the occurrence of this well-developed satellite structure reveals two important facts: (i) the 3d moments are fairly well localized, and (ii) there is a considerable difference in the magnitude of the Fe and Co moments. These results made it clear that the rigid band approach, where the 3d electrons of Co and Ni share a common band, is less well applicable on an atomic scale. This also follows from results of ^{57}Fe Mössbauer effect spectroscopy performed on the same pseudobinary series by Luijpen et al. (1977) who found that an Fe magnetic moment persists for Fe concentrations as low as 2% (YCo_2 is Pauli paramagnetic; see section 2). Mössbauer effect studies reported by Longworth and Harris (1975) on the analogous series $CeCo_{2-2x}Fe_{2x}$ even indicate the presence of an Fe moment for Fe concentrations as low as $\frac{1}{3}$%.

It was already mentioned in section 3.2.1 that the results of ^{57}Fe Mössbauer effect spectroscopy on R–Fe compounds of different composition and crystal structure (see fig. 14) can also be regarded as a demonstration of the localized character of the 3d moments in these binary compounds.

Finally it may be recalled from the results presented in section 3.2.1 that most of the R–M compounds in which there is a moment at the 3d sites can be characterized by the presence of ferromagnetically ordered 3d sublattices. The only exceptions were found in the iron rich compounds R_2Fe_{17} and in R–Mn compounds. In these cases the occurrence of the magnetic structure types

observed was explained by exchange interactions between localized moments whose sign and magnitude is strongly distance dependent. These results and those obtained by Crecelius et al. (1977) seem to indicate that the degree of 3d moment localization becomes stronger in the direction Ni, Co, Fe, Mn. This trend is also reflected in theoretical studies of 3d metals made by Pettifor (1980).

It will be clear from the above discussion that arguments can be given for the 3d electrons being either itinerant or localized. Neither the itinerant model nor the localized model are able to account fully for all aspects of the magnetic properties of the *R–M* compounds. This is undoubtedly inherent in the rather narrow 3d band in these compounds, which, in terms of the uncertainty principle, always constitutes a certain degree of localization of the 3d electrons.

Three schemes have been mentioned in section 3.1 for the magnetic coupling between the 3d and 4f moments. In the first scheme (Buschow 1971b, Wallace 1968) the coupling is considered to proceed via polarization of the s conduction electrons. The 4f–s interaction in this scheme is essentially of the RKKY type. Even if the s–3d interaction is taken to be the same in all the *R–M* compounds, the RKKY part may differ considerably in magnitude and sign from compound to compound in view of the expected differences of the lattice sum $\Sigma_i F(2k_F \cdot |r - R_i|)$ of eq. (4) in section 2.1. Since it was shown in section 3.2.1 that the *R–M* coupling is invariably antiferromagnetic, the RKKY-based coupling scheme seems less suited to deal with the extensive experimental material. In some cases it even leads to the wrong answer (Arif and McCausland 1975, McCausland 1975, Arif et al. 1977b). Especially the premise that the 3d–s interaction leads to a positive s electron polarization in *R–M* compounds (Wallace 1968) is not free from doubt. Spin echo NMR studies on YFe_3 reported by Oppelt et al. (1976) have shown that the hyperfine fields at the two crystallographic Y sites in this compound are both negative. As argued by Oppelt et al. this means that the s electron polarization produced by the Fe moments at the rare earth sites is also negative. As a matter of fact a glance at the data collected in table A.3a of Buschow (1977e) shows that a negative transferred hyperfine field at the rare earth site in *R–M* compounds is rather the rule than the exception. (A positive hyperfine field has been observed for Y as a solute in elemental Fe (Shirley et al. 1968). According to Stearns (1971) the positive sign of this field originated from the overlap of the too large solute atomic volume with the Fe matrix; it masks the negative contribution due to conduction electron polarization).

The NMR results discussed above make it difficult to believe that the coupling between the *R* and *M* moments in the various *R–M* compounds proceeds via 4f–s and 3d–s polarizations. These polarizations, however small, have a marked influence on hyperfine interactions in view of the fact that the hyperfine coupling constant of s electrons exceeds that of d electrons by an order of magnitude.

In the coupling scheme proposed by Campbell (1972) the 4f–3d coupling proceeds via polarization of the rare earth 5d electrons. Recently the results of

band structure calculations have become available (Malik et al. 1977a). These were made on several members of the RCo_5 family under the simplifying assumption of all Co sites being equivalent. The results of these calculations are indeed in favour of a strong coupling between the 3d electrons and the rare earth 5d electrons. The results of these band structure calculations and results of a Mössbauer-effect investigation by Tomala et al. (1977) disagree with the view of Gomes and Guimârães (1974) who assume a complete absence of d electrons at the rare earth site.

As outlined in section 3.1 Campbell's coupling scheme predicts an antiferromagnetic coupling between the 4f and 3d spin moments, independent of the R/M ratio and crystal structure. This is in agreement with the experimental data obtained hitherto on various R–Ni, R–Co and R–Fe compounds. Reliable data on the coupling between R and Mn in R–Mn compounds are not yet available. This is unfortunate in as much as in Campbell's coupling scheme the sign of the R–Mn interaction may differ from that of the interaction between R and Ni, Co or Fe. Antiferromagnetic coupling between 4f and 3d spin moments is also predicted in the calculations of Szpunar and Kozarzewski (1977) so that also in this case one can speak of agreement with the experimental data.

It follows from the results discussed in section 3.2.2 that there is virtually no influence on the magnetic properties of 4d or 5d electrons in rare earth compounds composed of Ru, Rh, Pd or Os, Ir, Pt, respectively. In itself this is not surprising since the d electron interaction in the pure 4d and 5d elements is rather weak compared with that in the 3d elements, and in several cases leads only to exchange-enhanced Pauli paramagnetism rather than to magnetic moments. In general magnetic moments could arise, however, upon combination of these elements with strongly polarizing rare earth elements. One would then have a situation analogous to that in YCo_2. The latter compound is Pauli paramagnetic but a moment on the Co atoms can be induced via the R–Co interaction as in $GdCo_2$ (see section 3.2.1). The electronegativity of the 4d and 5d elements is significantly larger, however, than that of the 3d elements. This means that the electron transfer from the rare earth atoms to the transition metal atoms would also be stronger. This latter effect presumably outweights the polarizing influence of the rare earth component and makes the 4d and 5d elements behave like non-magnetic components. Indeed, the compounds formed between rare earths and 4d or 5d transition elements have much more in common with the rare earth compounds involving a non-magnetic partner element, as reviewed in section 2.

4. Ternary compounds or hydrides

In recent years a considerable number of investigations has been reported in the literature in which the magnetic properties of ternary rare earth compounds were studied. It was already mentioned in the introduction that these ternary compounds differ from pseudobinary compounds in that all three constituent ele-

ments occur at crystallographically non-equivalent positions. The magnetic properties of the most common types of ternary compounds are listed in tables A.4.

Compounds of the type RNiAl and RCuAl crystallize in the hexagonal Fe_2P type structure (Dwight et al. 1968). As can be seen in table A.4a most of these compounds give rise to ferromagnetic ordering at low temperatures. In order to study the nature of the exchange interactions operative in these compounds magnetic dilution studies were performed on GdCuAl and GdPdIn (Buschow et al. 1971b, 1973b). A rather unusual variation of the paramagnetic Curie temperature θ_p was observed in the series $Gd_{1-x}Th_xCuAl$, passing through a maximum for $x = 0.3$. In the series $Gd_{1-x}Th_xPdIn$ a change in the sign of θ_p from positive to negative was observed at about the same Th concentration. Attempts have been made to explain these features, together with ^{27}Al NMR data on GdCuAl, in terms of the RKKY model (Buschow et al. 1971b, 1973b).

Rare earth metals and 3d transition metals can be combined in reasonably high concentrations in various compounds of the type RCo_2Ge_2, RFe_2Ge_2, RFe_2Si_2 and RMn_2Ge_2, all having the tetragonal $ThCr_2Si_2$ structure. The fact that $LuCo_2Ge_2$ and YCo_2Ge_2 are Pauli paramagnetic shows that Co has no moment, or at best only an induced moment in RCo_2Ge_2. The data listed for RCo_2Ge_2 in table A.4b reflect therefore mainly the nature of the R–R coupling. Antiferromagnetic ordering is seen to occur in most of these compounds, and a similar situation exists in compounds of the type RAu_2Si_2. The compounds of both series are isotypic and have about the same conduction electron concentration. It can be seen in table A.4b that there is a close resemblance in magnetic properties. In both series the magnetic ordering temperatures are rather low and of the Néel type. A fairly complicated situation seems to exist in the compounds RFe_2Si_2 and RFe_2Ge_2. The rare earth sublattice gives rise to antiferromagnetic ordering at temperatures slightly lower than, but comparable to, those in RCo_2Ge_2 and RAu_2Si_2. Above the Néel temperatures the magnetic susceptibility does not follow Curie–Weiss behaviour. The magnetization was found to be composed of a small spontaneous magnetization superimposed on the normal rare earth sublattice contribution. This spontaneous magnetization, also present in the cases where the R atoms do not carry a moment, has been ascribed to the Fe atoms. Neutron diffraction experiments performed on $NdFe_2Si_2$ confirmed the antiferromagnetic ordering within the Nd sublattice below $T_N = 15.6$ K but did not indicate the presence of magnetic ordering within the Fe sublattice (Pinto and Shaked 1973). Mössbauer effect spectroscopy (Bauminger et al. 1974b) showed that actually only a very small fraction of the Fe atoms participates in magnetic ordering (about 5% in RFe_2Si_2 and about 20% in RFe_2Ge_2) whilst the majority of Fe atoms remains paramagnetic. About the same fraction of magnetically ordered Fe atoms was found to be present and responsible for the spontaneous magnetization observed at high temperatures in RFe_2Si_2 and RFe_2Ge_2, mentioned earlier (Felner et al. 1975). As outlined in section 1, all these compounds crystallize in a structure derived from the tetragonal $BaAl_4$ type (see table A.1) where the Fe and Si(Ge) atoms are preferentially accommodated at

the 4(d) and 4(e)sites, respectively. However, complete atomic ordering will only occur in an ideal case. It is reasonable to assume that a very small fraction of Fe atoms has interchanged sites with Si or Ge atoms. Such a small deviation from ideal site occupancy is in general very difficult to observe by diffraction measurements. The slightly smaller R factor obtained by Pinto and Shaked (1973) when considering 9.8% interchange of Fe and Si in $R\mathrm{Fe_2Si_2}$ points nonetheless in this direction. The Fe atoms at Si(Ge) sites give rise to rather short Fe–Fe distances with the Fe neighbours at the normal Fe sites. It is conceivable therefore that the Fe atoms having this shorter nearest neighbour separation are responsible for the observed "weak" ferromagnetism at temperatures much in excess of T_N. In this connection it is interesting to note that Görlich et al. (1979) did not detect magnetic ordering in $\mathrm{DyFe_2Si_2}$ above 4.2 K. Apparently in their sample the site occupancies are rather perfect.

Compounds of the type $R\mathrm{Mn_2Ge_2}$ give rise to ferromagnetic ordering slightly above room temperature when R represents one of the light rare earth elements (Narasimhan et al. 1975). The moment per Mn atom in these compounds is about $1.5\mu_B$. A somewhat different behaviour is displayed in compounds where R is a heavy rare earth element. The results reported for $\mathrm{GdMn_2Ge_2}$ seem to indicate that in these compounds the Mn atoms tend to order antiferromagnetically. Nevertheless, ferromagnetic alignment occurs at lower temperatures, where, moreover, the rare earth sublattice becomes magnetically ordered. Narasimhan et al. (1975) conclude from their results that the magnetic coupling between the rare earth spin moment and the manganese moments is antiparallel. No T_N values have been determined for $R\mathrm{Mn_2Ge_2}$ compounds with R elements heavier than $R = \mathrm{Gd}$. The Curie temperatures listed for these latter compounds in table A.4b refer to ordering of the R sublattice.

Magnetic data obtained on ternary compounds of the tetragonal $\mathrm{CeMn_4Al_8}$ type (Zarechnyuk and Krypiakevich 1963) are collected in table A.4c. The main magnetic interaction in these compounds is due to the Fe atoms which carry a magnetic moment of about $0.7\mu_B$/Fe. It was mentioned in the introduction that the $\mathrm{CeMn_4Al_8}$ type is derived from the tetragonal $\mathrm{ThMn_{12}}$ type. A schematic representation of this structure is given in fig. 17. In $R\mathrm{Fe_4Al_8}$ the Fe atoms occupy the 8(f) positions. Magnetic ordering within the Fe sublattice is antiferromagnetic. Due to the low net magnetization it has not been possible to derive the magnetic ordering temperatures from magnetization measurements. The values listed in table A.4c have been determined by means of ^{57}Fe Mössbauer effect spectroscopy (Van der Kraan and Buschow 1977, Buschow and Van der Kraan 1978). Analysis of the magnetic data was performed by means of a molecular field model involving three sublattices, the R sublattice and the two antiparallel coupled Fe sublattices. Below T_N the molecular field contributions due to the two Fe sublattices cancel at the rare earth site. This leads to a more or less independent ordering of the rare earth sublattice at much lower temperatures (Bargouth et al. 1977). This situation is in fact not much different from that encountered in the binary compounds $R\mathrm{Mn_{12}}$ discussed in section 3.2.1.

Two different Cu sites are present in the $\mathrm{AuBe_5}$ type listed in table A.1.

Preferential ordering of different kinds of atoms on these two sites gives rise to the $MgCu_4Sn$ structure (Teslyuk and Krypiakevich 1961) adopted by several compounds of the type RCu_4Ag and $GdAu_4Ni$. Magnetic data of these compounds are given in table A.4d. Ferromagnetic ordering seems to occur in most of the $GdAu_4Ni$ compounds (Felner 1977). A change in ordering type has been reported to occur in the RCu_4Ag series (Takeshita et al. 1976). This behaviour would be difficult to explain if an RKKY coupling scheme alone were responsible for the magnetic interaction of the R moments in these compounds.

The ternary compounds of the type RRh_4B_4 form a quite interesting class of materials. For instance, $ErRh_4B_4$ becomes superconducting below 8.7 K. The return to the normal state at 0.9 K coincides with the occurrence of long range magnetic order (Matthias et al. 1977).

A separate class of ternary compounds is formed by the ternary hydrides. In general these ternary hydrides can be obtained by the absorption of hydrogen gas by intermetallic compounds of the type described in the preceding sections. A stable hydride (with a dissociation or equilibrium pressure at room temperature close to or below 1 atm) will be formed in most cases whenever one of the components of the original compound is strongly hydrogen attracting and if the compound itself is not particularly stable. For more details regarding these thermodynamic arguments we refer to textbooks (Mueller et al. 1968) and the original papers (Van Mal et al. 1974, Buschow et al 1975f). All but the most M rich R–M compounds described in section 3.2.1 satisfy the mentioned requirements to form a stable hydride. Instead of a complete survey of all the magnetic data available on ternary hydrides, only the changes in magnetic properties accompanying the hydrogen absorption will be briefly reviewed.

There have been relatively few magnetic investigations dealing with the hydrogen absorption in rare earth nickel compounds. Largely from NMR data concerning ternary hydrides based on $LaNi_5$ and related compounds, it can be concluded that Pauli paramagnetism is preserved after hydrogen absorption (Barnes et al. 1976, Halstead 1974, Halstead et al. 1976, Bauminger et al. 1977). EPR measurements performed on $LaNi_5$ doped with Gd seem to indicate that hydrogen absorption leads to a reduction of the 3d band susceptibility (Walsh et al. 1975). These results are in keeping with magnetization studies on $LaNi_5H_x$ reported by Busch and Schlapbach (1978).

Hydrogen absorption in R–Co compounds was found to give rise to a decrease in moment per Co atom and to a decrease in magnetic ordering temperature (Kuijpers 1973, Buschow 1977). Results obtained by Kuijpers (1973) on ternary hydrides of the type RCo_5H_x are shown in fig. 19. These results contrast strongly those obtained after hydrogen absorption in rare earth iron compounds. As can be seen in fig. 20, the 3d moment here considerably increases after uptake of hydrogen (Buschow 1976, Buschow and Van Diepen 1976, Van Diepen and Buschow 1977). The magnetic ordering temperature may decrease (YFe_2) or it may increase (Y_6Fe_{23}, $CeFe_2$). Since it is known from X-ray diffraction measurements that a considerable lattice expansion occurs upon H_2 absorption,

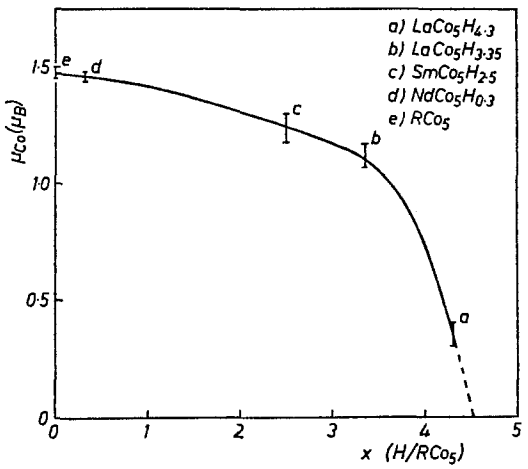

Fig. 19. H-concentration dependence of the Co moment in various RCo_5 compounds and their ternary hydrides. Results taken from Kuijpers (1973).

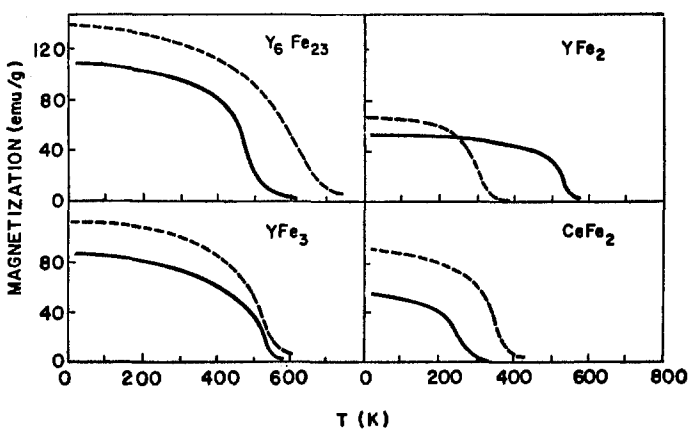

Fig. 20. Change of the magnetic properties of various rare earth iron compounds upon H_2-absorption. Full lines: before H_2-absorption; broken lines: after H_2 absorption.

successful attempts have been made to correlate the changes in T_c with data on magnetovolume effects available for the pure intermetallics. This is illustrated in fig. 21 where predictions regarding T_c in the hydrides can be made on the basis of the pressure effects reported by Buschow et al. (1977).

The most drastic changes in magnetic properties are found to accompany H_2 absorption in rare earth manganese compounds (Buschow and Sherwood 1977a, b, Malik et al. 1977b). These encompass hydrogen induced transitions from Pauli paramagnetism to ferromagnetism (YMn_2, $LuMn_2$, Th_6Mn_{23}) but also the reverse effect, i.e. transitions from ferromagnetism to Pauli paramagnetism (Y_6Mn_{23}). Most of the magnetically ordered ternary hydrides were found to exhibit pronounced thermomagnetic history effects at low temperatures (Bus-

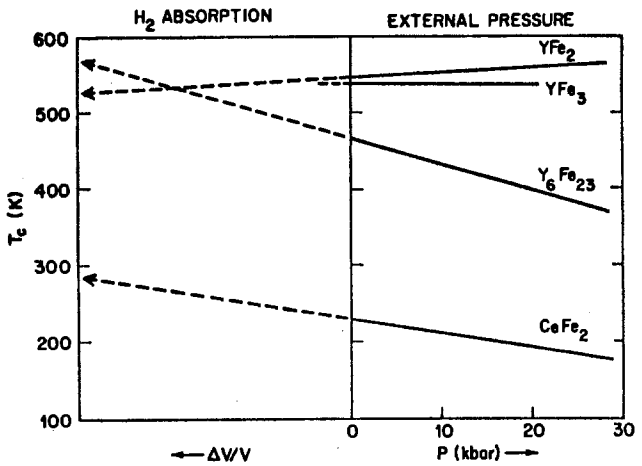

Fig. 21. Effect of the hydrogen absorption on the magnetic ordering temperature, predicted from the magnetovolume effects available for Y_6Fe_{23}, YFe_3, YFe_2 and $CeFe_2$.

chow and Sherwood 1977b). These features have been explained on the basis of partial atomic disorder originating from the metastable character of the ternary hydrides. Attempts have been made to correlate the presence or absence of a magnetic moment on the Mn atoms with a critical Mn–Mn distance in the *R*–Mn compounds and the corresponding hydrides. It was noted, however, in Buschow and Sherwood (1977) that the hydrogen absorbed may also exert its influence on the magnetic properties by means of electron transfer.

It is interesting to note that, even after the drastic changes in electronic properties associated with the hydrogen absorption, no change seems to occur in sign of the magnetic coupling between the rare earth- and 3d spins (Kuijpers 1973, Buschow 1977). Evidence was obtained, however, that this coupling can be reduced considerably (Gualtieri et al. 1976, Buschow 1977c, 1980).

Although it falls somewhat outside the scope of this review it is worthwhile to mention that several of the hydrogen absorbing compounds are important materials for several technical applications. These comprise hydrogen storage, energy conversion in solar heating and cooling, hydrogen compressors, cold accumulators and hydrogen based batteries. For more details the reader is referred to the various contributions on this subject contained in the book Hydrides for energy storage, edited by A.F. Andresen (1978).

Appendix

In table A.1 some details of the most common structure types encountered in rare earth intermetallics are listed. Magnetic characteristics of binary rare earth intermetallics are given in tables A.2a–n and A.3a–g. The former table pertains to intermetallics with non-magnetic partners, the latter to intermetallics in which the second component is a d transition metal. Magnetic properties of several series of ternary rare earth based intermetallics are listed in tables A.4a–e.

TABLE A.1

Most common structure types found with rare earth intermetallics. The position of the rare earth sites (R) and non-rare earth sites (M) is given in Wickoff notation. (For more details see text.) Compounds of the following lattice symmetry were considered: cubic (cub), hexagonal (hex), rhombohedral (rh), tetragonal (tetr) and orthorhombic (orth)

Structure type	Symmetry	Space group	R site(s)	M site(s)	M component in R_xM_y
$NaZn_{13}$	cub	Fm3c	8(a)	8(b); 96(i)	Be, Co, Zn
$ThMn_{12}$	tetr	I4/mmm	2(a)	8(f); 8(i); 8(j)	Mn, Zn
UB_{12}	cub	Fm3m	4(a)	48(i)	B
$BaHg_{11}$	cub	Pm3m	3(d)	1(b); 8(g); 12(i); 12(j)	Cd, Zn
Th_2Ni_{17}	hex	$P6_3/mmc$	2(b); 2(d)	6(g); 12(j); 12(k); 4(f)	Ni, Co, Fe, Mg
Th_2Zn_{17}	rh	$R\bar{3}m$	6(c)	6(c); 9(d); 18(f); 18(h)	Ni, Co, Fe, Zn
CaB_6	cub	Pm3m	1(a)	6(f)	B
$CeCu_6$	orh	Pnma	4(c)	8(d); $4(c_1)$; $4(c_2)$; $4(c_3)$; $4(c_4)$	Cu
$AuBe_5$	cub	$F\bar{4}3m$	4(a)	4(c); 16(e)	Cu
$CaCu_5$	hex	Pb/mmm	1(a)	2(c); 3(g)	Ni, Co, Cu, Ag, Au, Zn, Pt
$BaAl_4$	tetr	I4/mmm	2(a)	4(d); 4(e)	Al
UB_4	tetr	P4/mbm	4(g)	4(e); 4(h); 8(j)	B
Th_6Mn_{23}	tetr	Fm3m	24(e)	4(b); 24(d); $32(f_1)$; $32(f_2)$	Fe, Mn
Ce_2Ni_7	hex	$P6_3/mmc$	$4(f_1)$; $4(f_2)$	2(a); 4(e); 4(f); 6(h); 12(k)	Ni, Co
Gd_2Co_7	rh	$R\bar{3}m$	$6(c_1)$; $6(c_2)$	3(b); 6(c); 6(c); 9(e); 12(h)	Ni, Co
$CeNi_3$	hex	$P6_3/mmc$	2(c); 4(f)	2(a); 2(b); 2(d); 12(k)	Ni, Co
$PuNi_3$	rh	$R\bar{3}m$	3(a); 6(c)	3(b); 6(c); 18(h)	Ni, Co, Fe
$AuCu_3$	cub	Pm3m	1(a)	3(c)	Al, In, Sn, Tl, Pb, Pd, Pt

TABLE A.1 (*cont.*)

Structure type	Symmetry	Space group	*R* sites(s)	*M* site(s)	*M* component in R_xM_y
$SnNi_3$	hex	$P6_2/mmc$	2(c)	6(h)	Al, Hg
$BiLi_3$	cub	Fm3m	4(a)	4(b); 8(c)	Cd, Mg
$TiCu_3$	orh	Pmmm	2(a)	2(b); 4(f)	Au
$MgCu_2$	cub	Fd3m	8(a)	16(d)	Pt, Ir, P, Al, Ni, Co, Fe, Mn, Mg, Os, Rh, Ru
$MgZn_2$	hex	$P6_3/mmc$	4(f)	2(a); 6(h)	Os, Re, Ru, Mg, Mn
$CeCu_2$	orh	Imma	4(e)	8(h)	Cu, Ag, Au, Zn
AlB_2	hex	P6/mmm	1(a)	2(d)	B, Ga, Hg, Si
$ThSi_2$	tetr	$I4_1/amd$	4(a)	8(e)	Ge,Si
α-$GdSi_2$	orh	Imma	4(e)	4(e); 4(e)	Si
$MoSi_2$	tetr	I4/mmm	2(a)	4(e)	Ag, Au
CsCl	cub	Pm3m	1(a)	1(b)	Cd, Cu, Mg, Hg, Rh, Ag, Tl, Zn
CrB	orh	Cmcm	4(c)	4(c)	Ga, Ge, Ni
FeB	orh	Pnma	4(c)	4(c)	Cu, Ni
Mn_5Si_3	hex	$P6_3/mcm$	4(d); 4(g)	6(g)	Si, Ge
Zr_3Al_2	tetr	P4/mbm	2(a); 4(h)	4(g)	Al
$PbCl_2$	orh	Pnma	4(c)	$4(c_1)$; $4(c_2)$	Al
Th_7Fe_3	hex	$P6_3mc$	2(b); $6(c_1)$; $6(c_2)$	6(c)	Rh, Pd, Ni
Fe_3C	orh	Pnma	4(c); 8(d)	4(c)	Co, Ni

TABLES A.2a–n

Magnetic properties of intermetallic compounds of rare earths and non-magnetic metals. Details pertaining to the structure type listed in columns 3 are given in table A.1. The values of the effective moments (μ_{eff}) and saturation moments (μ) are expressed in Bohr magnetons per rare earth atom. Values for the paramagnetic Curie temperatures (θ_p) Curie temperatures (T_c) and Néel temperatures (T_N) are given in K. The magnetic structure types are indicated by F (ferromagnetic), AF (antiferromagnetic) or by C (complex). The references comprise three groups separated by semicolons. The first reference pertains to literature of the crystal structure and lattice constants. Usually only one reference has been chosen out of the collection of references available. The references given between the two semicolons pertain to the literature in which the values of μ_{eff}, θ_p, μ, T_c and T_N are reported. The references after the last semicolon correspond to neutron diffraction work. Since in most cases the values of μ_{eff}, θ_p, μ, T_c and T_N reported by different authors in literature are dissimilar, lower and higher limits have been listed. The values given for χ of Pauli paramagnetic compounds are room temperature values and not values attained at 4.2 K, since these latter may depend strongly on the amount of localized moment impurities present in the samples.

TABLE A.2a
Rare earth boron compounds

Compound	Symmetry	Crystal structure	μ_{eff}	θ_p	μ	T_c	T_N	Magnetic structure	References
TbB_2	hex	AlB_2	9.96	151	4.0	151		F	1; 1, 2; 2
DyB_2	hex	AlB_2	10.7	33	5.4	55			1; 1
HoB_2	hex	AlB_2	10.2	25	7.5	15			1; 1
ErB_2	hex	AlB_2	9.47	9	5.1	16			1; 1
Pr_2B_5	mon			14			15.1		3; 3
Nd_2B_5	mon			14			32.7		3; 3
Sm_2B_5	mon						23.5		3; 3
Gd_2B_5	mon						50		3; 3
LaB_4	tetr	UB_4	$\chi = -0.015 \times 10^{-3}$ cm^3/mole						4; 1, 4
CeB_4	tetr	UB_4	no C-W behaviour						4; 1, 3, 4
PrB_4	tetr	UB_4	3.53	5–27	1.54	24.2–25			4; 1, 3, 4
NdB_4	tetr	UB_4	3.61	−12			6.85–7		4; 1, 3, 4
SmB_4	tetr	UB_4	no C-W behaviour				31–57		4; 1, 3, 4
GdB_4	tetr	UB_4	7.94–8.07	−66–−50			42–45.3		4; 1, 3–7
TbB_4	tetr	UB_4	9.30–9.72	−43–−22			43–44.7		4; 1, 3–6
DyB_4	tetr	UB_4	10.26–10.6	−22–−11			20.7–22	AF	4; 1, 3–7; 7
HoB_4	tetr	UB_4	10.5–10.8	−21–−7			7–7.3		4; 1, 3–6
ErB_4	tetr	UB_4	9.52	−10–15			13–15	AF	4; 1, 3–6, 7
TmB_4	tetr	UB_4	7.6–7.68	−23–3			11.8		4; 1, 3–6
YbB_4	tetr	UB_4		−440			10		4; 1, 8
LuB_4	tetr	UB_4	$\chi = -0.046 \times 10^{-3}$ cm^3/mole						4; 3
YB_4	tetr	UB_4	$\chi = -0.032 \times 10^{-3}$ cm^3/mole						4; 4
LaB_6	cub	CaB_6	$\chi = -0.061 \times 10^{-3}$ cm^3/mole						9; 10
CeB_6	cub	CaB_6	2.49	−76			3.0		9; 11, 12
PrB_6	cub	CaB_6	3.56–3.59	−68–−44			7		9; 11–13
NdB_6	cub	CaB_6	3.54	−42			8.45–8.6		9; 11, 12, 14
SmB_6	cub	CaB_6	no C-W behaviour						9; 12
EuB_6	cub	CaB_6	8.1	8–9	8.5				9; 11–13
GdB_6	cub	CaB_6	7.28–8.01	−55–−60			13.5–18		9; 11, 12, 15, 16
TbB_6	cub	CaB_6	9.43	−35			23		9; 11, 12
DyB_6	cub	CaB_6	10.63	−21			21		9; 11, 12
HoB_6	cub	CaB_6					9		9, 11
YbB_6	cub	CaB_6		−161					9, 10,
LuB_6	cub	CaB_6							9;
YB_6	cub	CaB_6							9;
DyB_{12}	cub	UB_{12}	10.85	−23					17; 5
HoB_{12}	cub	UB_{12}					6.5		17; 11
ErB_{12}	cub	UB_{12}					6.5		17; 11
TmB_{12}	cub	UB_{12}					4.2		17; 11

1. Buschow (1977d)
2. Will et al. (1977a)
3. Bucher et al., unpublished
4. Buschow and Creijghton (1972)
5. Buschow, unpublished
6. Fisk et al. (1971)
7. Paderno and Pokrzywnicki (1967)
8. Sales and Wohlleben (1975)
9. Gschneidner (1961)
10. Etourneau et al. (1970)
11. Matthias et al. (1968)
12. Paderno et al. (1967)
13. Geballe et al. (1968)
14. Hacker and Liu (1968)
15. Coles and Griffith (1961)
16. Coles et al. (1962)
17. LaPlaca et al. (1961)

TABLE A.2b
Rare earth aluminium compounds

Compound	Symmetry	Crystal structure	μ_{eff}	θ_p	μ	T_c	T_N	Magnetic structure	References
Ce_3Al	hex	Ni_3Sn	2.52	−24					1; 2
Pr_3Al	hex	Ni_3Sn	3.62	2	1.16	16			1; 2
Pr_2Al	orh	Ni_2Si	3.59	4			18		3; 2
Gd_2Al	orh	Ni_2Si	8.02	150					3; 4
Gd_3Al_2	tetr	Zr_2Al_3	7.90–8.2	280–302	7.1–7.25	275 – 290			5; 4, 6, 7
Tb_3Al_2	tetr	Zr_2Al_3	9.6	125		203		C	5; 6; 8
Dy_3Al_2	tetr	Zr_2Al_3	10.8–11.2	31	5.9	76		C	5; 6, 9; 6
Ho_3Al_2	tetr	Zr_2Al_3	10.9	10		33			5; 6
Er_3Al_2	tetr	Zr_2Al_3	9.6	−3			9		5; 6
Tm_3Al_2	tetr	Zr_2Al_3	7.8	−10			3		5; 6
Y_3Al_2	tetr	Zr_2Al_3							5; 6
LaAl	orh	CeAl							10;
CeAl	orh	CeAl	2.34–2.54	−19–4			9–10		10; 6, 11, 12
PrAl	orh	DyAl	3.58	1–11			19–20		10; 6, 11,
NdAl	orh	DyAl	3.52–3.53	−4–13			25–29	C	10; 6, 11; 13
SmAl	orh	DyAl							10;
GdAl	orh	DyAl	5.69–8.52	64–260			42		10; 6, 7, 14
TbAl	orh	DyAl	10.0–10.11	10–24			72	C	10; 6, 14; 15
DyAl	orh	DyAl	10.6–11.15	17–25			20	C	10; 6, 14; 13
HoAl	orh	DyAl	10.7–11.15	17–22		26		C	10; 6, 14; 15
ErAl	orh	DyAl	9.45–10.05	23–28			13	C	10; 6; 13
TmAl	orh	DyAl	7.70	−2			10	C	10; 6; 13
YAl	orh	CrB							10;
$LaAl_2$	cub	$MgCu_2$	$\chi = 0.06 \times 10^{-3}$ cm^3/mole						16; 17
$CeAl_2$	cub	$MgCu_2$	2.53–2.64	−33–9			4–4.6		4, 6–9, 11, 12 16, 18–25
$PrAl_2$	cub	$MgCu_2$	3.46–3.5	30–32	2.60	31–37		F	16; 22, 26, 27; 27
$NdAl_2$	cub	$MgCu_2$	3.1–3.59	70	2.27–2.47	61–76		F	16; 26, 28, 29; 29
$SmAl_2$	cub	$MgCu_2$	no C-W		0.2	120–122			16; 22, 30
$EuAl_2$	cub	$MgCu_2$	7.84–8.05	−2–0	0.79–1.21		15		18, 31
$GdAl_2$	cub	$MgCu_2$	7.92–7.94	168–180	6.9–7.1	168–182			8; 7, 22, 26, 30, 32–35
$TbAl_2$	cub	$MgCu_2$	9.81–9.82	108–110	8.1–8.9	105–121		F	18; 22, 26, 32, 36; 37
$DyAl_2$	cub	$MgCu_2$	9.12–10.7	64	9.62–9.89	62–70		(F)	18; 22, 26, 29, 35, 38; 29
$HoAl_2$	cub	$MgCu_2$	10.7	30–36	9.16–9.18	27–42		F	18; 22, 39, 40; 37
$ErAl_2$	cub	$MgCu_2$	9.2–9.56	14–16	7.05–7.92	12–24		F	18; 22, 26, 27 32, 41, 42; 27, 43
$TmAl_2$	cub	$MgCu_2$			4.8	7			18; 22
$YbAl_2$	cub	$MgCu_2$	no C-W behaviour						18; 44–46
$LuAl_2$	cub	$MgCu_2$	$\chi = 0.075 \times 10^{-3}$ cm^3/mole						18; 47
YAl_2	cub	$MgCu_2$	$\chi = 0.103 \times 10^{-3}$ cm^3/mole						18; 22
$LaAl_3$	hex	Ni_3Sn	$\chi = 0.08 \times 10^{-3}$ cm^3/mole						19; 48
$CeAl_3$	hex	Ni_3Sn	2.52–2.63	−46–−25					19; 12, 49
$PrAl_3$	hex	Ni_3Sn	3.74	−14					19; 49
$NdAl_3$	hex	Ni_3Sn	4.11	+5					19; 49
$SmAl_3$	hex	Ni_3Sn	no C-W behaviour						19; 49, 50

TABLE A.2b (*cont.*)

Compound	Symmetry	Crystal structure	μ_{eff}	θ_p	μ	T_c	T_N	Magnetic structure	References
$GdAl_3$	hex	Ni_3Sn	8.29–8.35	−99.5–−89			17		19; 7, 49
$TbAl_3$	rh	$BaPb_3$	10.0	−64			21		19; 49
$DyAl_3$	rh	$HoAl_3$	10.85	−51			23		19; 49
$HoAl_3$	rh	$HoAl_3$	10.89	−26			9		19; 49
$ErAl_3$	cub	Cu_3Au	9.87	−16			5–5.1	AF	19; 49, 51; 43
$TmAl_3$	cub	Cu_3Au	7.88	−19					19; 51
$YbAl_3$	cub	Cu_3Au	4.62	−300					19; 52, 44, 46 49
YAl_3	rh	$BaPb_3$							19;
La_3Al_{11}	orh	La_3Al_{11}	$\chi = -0.48 \times 10^{-3}$ cm^3/mole						1; 53
Ce_3Al_{11}	orh	La_3Al_{11}	2.2–2.53	−24–−25	0.61	6–9			1; 2, 54, 56
Pr_3Al_{11}	orh	La_3Al_{11}	3.50–3.52	4	0.67		12.3		1; 2, 53
Nd_3Al_{11}	orh	La_3Al_{11}	3.62	−9					1; 53
$EuAl_4$	tetr	$BaAl_4$	7.75–7.79	12–14			13		20; 31; 53, 55

1. Buschow and Van Vucht (1967)
2. Mader and Wallace (1968a)
3. Buschow and Van der Goot (1971a)
4. Buschow (1975a)
5. Buschow (1965b)
6. Barbara et al. (1971a)
7. Stalinski and Pokrzywnicki (1966)
8. Barbara et al. (1968)
9. Buschow (1969)
10. Bècle and Lemaire (1967)
11. Kissel and Wallace (1966)
12. Niculescu (1972)
13. Bècle (1968)
14. Van Diepen et al. (1968)
15. Bècle et al. (1970)
16. Wernick and Geller (1960)
17. Buschow, unpublished
18. Harris et al. (1965)
19. Van Vucht and Buschow (1965)
20. Van Vucht and Buschow (1964)
21. Van Daal and Buschow (1970a)
22. Williams et al. (1962)
23. Van Daal and Buschow (1970b)
24. Walker et al. (1973)
25. Barbara et al. (1975a)
26. Swift and Wallace (1968)
27. Nereson et al. (1968)
28. Cock et al. (1974)
29. Nereson et al. (1966)
30. DeWijn et al. (1973)
31. Mader and Wallace (1968b)
32. Buschow et al. (1967)
33. Hacker et al. (1972)
34. Schäfer et al. (1972)
35. Barbara et al. (1977a)
36. Barbara et al. (1974)
37. Milhouse et al. (1972)
38. Oestereicher and Pitts (1972)
39. Barbara et al. (1977b)
40. Barbara et al. (1976)
41. Oestereicher (1973a)
42. Purwins et al. (1976)
43. Will and Bargouth (1972)
44. Havinga et al. (1973)
45. Klaasse et al. (1973)
46. Iandelli and Palenzona (1972)
47. Buschow, unpublished
48. Van Diepen et al. (1967)
49. Buschow and Fast (1966)
50. De Wijn et al. (1967)
51. Buschow (1968)
52. Sales and Wohlleben (1975)
53. Van Diepen et al. (1969)
54. Van Daal and Buschow (1970c)
55. Wernick et al. (1967)
56. Chouteau et al. (1978)

TABLE A.2c
Rare earth gallium compounds

Compound	Symmetry	Crystal structure	μ_{eff}	θ_p	μ	T_c	T_N	Magnetic structure	References
Ce_3Ga	cub	Cu_3Au	2.64	−56					1; 1
Gd_5Ga_3	tetr	Cr_5B_3	8.5	25			80		2; 2
Ce_3Ga_2			2.74	−40					3; 1
Gd_3Ga_2	tetr	Zr_3Al_2	8.23–8.51	−32–−23			53–55		2; 2, 4
CeGa	orh	CrB	2.73	−21					5; 1
NdGa	orh	CrB	3.40	34	1.93	45			5; 6
GdGa	orh	CrB	8.18–8.23	208–210	6.89	190–200			5; 2, 6
TbGa	orh	CrB	9.48	152	6.86	155–158		F, C	5; 6; 7, 8
DyGa	orh	CrB	10.47	88	5.28	116			5; 6
HoGa	orh	CrB	10.70	60	9.12	68			5; 6
ErGa	orh	CrB	9.51	18	5.39	34		C	5; 6; 8
TmGa	orh	CrB	7.72	10	4.42	15			5; 6
$LaGa_2$	hex	AlB_2							9;
$CeGa_2$	hex	AlB_2	2.76	−18					9; 1
$PrGa_2$	hex	AlB_2	3.6	9			11		9; 10
$NdGa_2$	hex	AlB_2	3.7	10			14		9; 10
$SmGa_2$	hex	AlB_2							9;
$EuGa_2$	hex	AlB_2	8.04	6					11; 11
$GdGa_2$	hex	AlB_2	7.93	−15					9; 2
$TbGa_2$	hex	AlB_2	9.8	−20			18		9; 10
$DyGa_2$	hex	AlB_2	10.7	−6			15	AF	9; 10
$HoGa_2$	hex	AlB_2	10.7	−2			10	AF	9; 10
$ErGa_2$	hex	AlB_2							9;
$TmGa_2$	hex	AlB_2							9;
$YbGa_2$	hex	AlB_2	no C-W behaviour						11; 12

1. Colombo and Olcese (1963)
2. Buschow and Van den Hoogenhof (1976)
3. Crystal structure unknown
4. Hacker and Gupta (1976)
5. Dwight et al. (1967)
6. Barbara et al. (1972)
7. Cable et al. (1964a)
8. Barbara et al. (1971b)
9. Haszko (1961)
10. Barbara et al. (1971c)
11. Iandelli (1964)
12. Klaasse et al. (1976)

TABLE A.2d
Rare earth indium compounds

Compound	Symmetry	Crystal structure	μ_{eff}	θ_p	μ	T_c	T_N	Magnetic structure	References
La_3In	cub	Cu_3Au							1;
Ce_3In	cub	Cu_3Au	2.68	−33					2; 2
Pr_3In	cub	Cu_3Au	3.4–3.48	9–22	1.43	56.5–62			1; 3, 4
Nd_3In	cub	Cu_3Au	3.4	10	0.37	114			1; 3
Gd_3In			8.8	196	5.2	213			5; 3
Dy_3In	tetr	$CuTi_3$	10.4	113	5.8	138			1; 3
Er_3In			9.6	31	5.2	51			5; 3
Ce_2In	hex	Ni_2In	2.62	−1					6; 2
Tb_2In	hex	Ni_2In	9.8	183		185		F	6; 7; 8
Ho_2In	hex	Ni_2In	10.7	95		112			6; 7
CeIn			2.63	+6					1; 2
GdIn	tetr	TbIn	8.1	−66–18			28		9; 9, 10
TbIn	tetr	TbIn		16			145–190	AF	9; 9, 11; 9, 11
DyIn	tetr	TbIn		10			120		9; 9
HoIn	tetr	TbIn		8			42	AF	9; 9
Ce_2In_3			2.73	−8					5; 2
$EuIn_2$	hex	$CaIn_2$	7.79	+8					12; 12
$LaIn_3$	cub	$AuCu_3$	$\chi = 0.27 \times 10^{-3}$ cm^3/mole						13; 14
$CeIn_3$	cub	$AuCu_3$	2.54	−46			11		13; 13
$PrIn_3$	cub	$AuCu_3$	3.58–3.72	−10–−9					13; 13, 15
$NdIn_3$	cub	$AuCu_3$	3.67–3.78	−17–−12			6.8–7	AF	13; 13, 15; 16
$SmIn_3$	cub	$AuCu_3$	no C-W behaviour				16		13; 13
$EuIn_3$				10			4.5–10		17; 18; 4
$GdIn_3$	cub	$AuCu_3$	8.20	−85			45–48		13; 4, 13
$TbIn_3$	cub	$AuCu_3$	10.05	−62			36	AF	13; 13; 19
$DyIn_3$	cub	$AuCu_3$	10.78	−35			23	AF	13; 13; 20
$HoIn_3$	cub	$AuCu_3$	10.65	−18			11		13; 13
$ErIn_3$	cub	$AuCu_3$	9.75	−10			6	AF	13; 13; 16
$TmIn_3$	cub	$AuCu_3$	7.6	−6					13; 13
$YbIn_3$	cub	$AuCu_3$	no C-W behaviour						13; 13, 21, 22
$LuIn_3$	cub	$AuCu_3$							17;
YIn_3	cub	$AuCu_3$	$\chi = 0.29 \times 10^{-3}$ cm^3/mole						17; 14

1. Moriarty et al. (1966)
2. Colombo and Olcese (1963)
3. Hutchens et al. (1973)
4. Stalinski (1974)
5. Crystal structure unknown
6. Palenzona (1968)
7. Kawano et al. (1974)
8. Umezaki et al. (1974)
9. Lethuillier and Percheron-Guegan (1976)
10. Sekizawa and Yasukochi (1964)
11. Cable et al. (1964a)
12. Iandelli (1964)
13. Buschow et al. (1969a)
14. Havinga et al. (1970)
15. Lethuillier and Chaussy (1976a)
16. Lethuillier (1974)
17. Kuzma and Markiv (1964)
18. Harris and Raynor (1965a)
19. Crangle (1964)
20. Arnold and Nereson (1969)
21. Klaasse et al. (1973)
22. Stalinski et al. (1974)

TABLE A.2e
Rare earth thallium compounds

Compound	Symmetry	Crystal structure	μ_{eff}	θ_p	μ	T_c	T_N	Magnetic structure	References
La_3Tl	cub	Cu_3Au							1;
Pr_3Tl	cub	Cu_3Au			0.7	11		F,C	1; 1; 2
Ce_2Tl			2.65	−33					3; 4
CeTl	cub	CsCl	2.58	−22					5; 4
EuTl	cub	CsCl	7.77	4					6; 6
GdTl	cub	CsCl	7.6	~0			220		6; 7
YbTl	cub	CsCl	$\chi = 0.28 \times 10^{-3}$ cm^3/mole						6; 6
$EuTl_2$	hex	$CaIn_2$	7.78	−10					8; 8
$CeTl_3$	cub	$AuCu_3$	2.40	−4					4; 4
$PrTl_3$	cub	$AuCu_3$	3.67						9; 7
$EuTl_3$	hex	Ni_3Sn					5.5–6.5		10; 10
$GdTl_3$	cub	$AuCu_3$					12–13		11; 10
$DyTl_3$	cub	$AuCu_3$	11.29	−20			11	AF	12; 12; 12
$YbTl_3$	hex	Ni_3Sn	no C-W behaviour						13; 13

1. Andres et al. (1972)
2. Birgenau et al. (1972)
3. Crystal structure unknown
4. Colombo and Olcese (1963)
5. Iandelli (1960)
6. Iandelli and Palenzona (1965)
7. Buschow, unpublished
8. Iandelli (1964)
9. Gschneidner (1961)
10. Stalinski (1974)
11. Bruzzone and Ruggiero (1963)
12. Olson et al. (1970)
13. Stalinski et al. (1974)

TABLE A.2f
Rare earth silicon compounds

Compound	Symmetry	Crystal structure	μ_{eff}	θ_p	μ	T_c	T_N	Magnetic structure	References
Ce_3Si			2.58	−60					1; 2
Ce_2Si	hex	Ni_2In	2.55	−46					1; 2
Ce_5Si_3	tetr	Cr_5B_3	2.61	−43					3; 2
Nd_5Si_3	hex	Mn_5Si_3	3.67	53.7					3; 4
Gd_5Si_3	hex	Mn_5Si_3	8.34	97					3; 4
Dy_5Si_3	hex	Mn_5Si_3	10.47	90					3; 4
Gd_5Si_4	orh	Sm_5Ge_4	8.15	349	7.24	336			3; 5
Tb_5Si_4	orh	Sm_5Ge_4	9.55	216	6.49	225			3; 5
Dy_5Si_4	orh	Sm_5Ge_4	10.35	133	7.08	140			3; 5
Ho_5Si_4	orh	Sm_5Ge_4	11.06	69	7.44	76			3; 5
Er_5Si_4	orh	Sm_5Ge_4	9.90	26	6.12	26			3; 5
CeSi	orh	FeB	2.50	−7					6; 2
GdSi	orh	FeB	8.23	5			50		6; 4
TbSi	orh	FeB	10.1	−8			57	AF	6; 7; 7
HoSi	orh	CrB	10.64	2	6.5		25	AF	6; 8; 8
ErSi	orh	CrB	9.38	−5	7.2		10	AF	6; 8; 8
TmSi	orh	CrB	7.45	10	6.0		10	AF	6; 8; 8
$CeSi_2$	tetr	$ThSi_2$	2.94	−299					6; 2
$PrSi_2$	tetr	$ThSi_2$				10.5			6; 9
$GdSi_2$	orh	$GdSi_2$	7.7–7.81	−58–−47			27		10; 10, 11
$TbSi_2$	orh	$GdSi_2$	9.8	−17			17		6; 11
$DySi_2$	orh	$GdSi_2$	10.3	−8			17		6; 11
$HoSi_2$	orh	$GdSi_2$	10.3	−5			18		6; 11
$ErSi_2$	hex	AlB_2	9.5	0					6; 11

1. Crystal structure unknown
2. Ruggiero et al. (1964)
3. Smith et al. (1967)
4. Ganapathy et al. (1976)
5. Holtzberg et al. (1967)
6. Parthé (1967)
7. Nguyen Van Nhung et al. (1970)
8. Nguyen Van Nhung et al. (1971)
9. Matthias et al. (1958)
10. Yaguchi (1966)
11. Sekizawa and Yasukochi (1966a)

TABLE A.2g
Rare earth germanium compounds

Compound	Symmetry	Crystal structure	μ_{eff}	θ_p	μ	T_c	T_N	Magnetic structure	References
Ce_3Ge			2.57	−41					1; 2
La_5Ge_3	hex	Mn_5Si_3	$\chi_0 = 0.46 \cdot 10^{-3}$ cm^3/mole						3; 4
Ce_5Ge_3	hex	Mn_5Si_3	2.54–2.66	−50–−26					3; 2
Pr_5Ge_3	hex	Mn_5Si_3	3.80	10			12		3; 3
Nd_5Ge_3	hex	Mn_5Si_3	3.73	20	1.92	45			3; 3 3; 1, 4–7
Sm_5Ge_3	hex	Mn_5Si_3	no C-W behaviour						3; 4
Gd_5Ge_3	hex	Mn_5Si_3	8.42	70			48		3; 3
Tb_5Ge_3	hex	Mn_5Si_3	9.98	93			85		3; 3
Dy_5Ge_3	hex	Mn_5Si_3	10.47	45			40		3; 3
Ho_5Ge_3	hex	Mn_5Si_3	11.10	10			10		3; 3
Er_5Ge_3	hex	Mn_5Si_3	9.48	35			31		3; 3
Gd_5Ge_4	orh	Sm_5Ge_4	8.15	94			15		5; 6
Tb_5Ge_4	orh	Sm_5Ge	9.63	80			30		5; 6
Dy_5Ge_4	orh	Sm_5Ge_4	10.58	43			40		5; 6
Ho_5Ge_4	orh	Sm_5Ge_4	10.74	16			21		5; 6
Er_5Ge_4	orh	Sm_5Ge_4	9.76	10			7		5; 6
LaGe	orh	FeB							7; 7
CeGe	orh	FeB	2.51	−19–0			10		7; 2, 7
PrGe	orh	CrB	3.69	+30	1.73	39			7; 7
NdGe	orh	CrB	3.74	+18	1.64	28			7; 7
SmGe	orh	CrB	no C-W behaviour				40		7; 7
GdGe	orh	CrB	8.21	−13			62		7; 7
TbGe	orh	CrB	9.76	−5			48		7; 7
DyGe	orh	CrB	10.60	~0			36		7; 7
HoGe	orh	CrB	10.77	−5			18		7; 7
ErGe	orh	CrB	10.0	−15			7		7; 7
YGe	orh	CrB							7;
$CeGe_2$	tetr	$ThSi_2$	2.46	5					8; 2
$PrGe_2$	tetr	$ThSi_2$	3.6	22	2.18	19			8; 9, 10
$NdGe_2$	tetr	$ThSi_2$	3.7	7		3.6			8; 9, 10
$SmGe_2$	tetr	$ThSi_2$	no C-W behaviour						8; 10
$GdGe_2$	orh		8.1	−54			28		10; 10
$TbGe_2$	orh		9.9	−48			42		10; 10
$DyGe_2$	orh		10.9	−26			28		10; 10
$HoGe_2$	orh		10.7	−4			11		10; 10
$ErGe_2$			9.4	20					10; 10

1. Crystal structure unknown
2. Ruggiero et al. (1964)
3. Buschow and Fast (1967)
4. Buschow, unpublished
5. Smith et al. (1967)
6. Holtzberg et al. (1967)
7. Buschow and Fast (1966)
8. Parthé (1967)
9. Matthias et al. (1958)
10. Sekizawa (1966)

TABLE A.2h
Rare earth tin and rare earth lead compounds

Compound	Symmetry	Crystal structure	μ_{eff}	θ_p	μ	T_c	T_N	Magnetic structure	References
Ce_2Sn			2.57	−13					1; 2
Sm_5Sn_3	hex	Mn_5Si_3	no C-W behaviour						3; 3
Ce_2Sn_3			2.55	−8					1; 2
Sm_2Sn_3	tetr		no C-W behaviour				11		3; 3
$LaSn_3$	cub	$AuCu_3$	$\chi_0 = 0.173 \times 10^{-3}$ cm^3/mole						4; 5
$CeSn_3$	cub	$AuCu_3$	2.78–2.8	−203					4; 2, 6, 7, 8
$PrSn_3$	cub	$AuCu_3$	3.42–3.55	−10–−5.2			8.5–8.6	AF	4; 2, 6, 7, 9; 8, 10
$NdSn_3$	cub	$AuCu_3$	3.6–3.63	−34–−22			4.6–4.7	AF	4; 2, 6, 7, 11; 10, 11
$SmSn_3$	cub	$AuCu_3$	no C-W behaviour				9–12		4; 3, 6
$EuSn_3$	cub	$AuCu_3$	7.65	−75–−60			38		4; 12, 13, 14
$GdSn_3$	cub	$AuCu_3$	8.0	−73			~35		4; 6
$YbSn_3$	cub	$AuCu_3$	$\chi_0 = -0.025 \times 10^{-6}$ cm^3/mole						2; 15
Ce_2Pb	hex	Ce_2Pb	2.4	−1					16; 2
Eu_2Pb	orh	$PbCl_2$	10.6	−7			32–42		17; 18
CePb			2.49	1					19; 2
$LaPb_3$	cub	$AuCu_3$	$\chi_0 = 0.114 \times 10^{-3}$ cm^3/mole						16; 5
$CePb_3$	cub	$AuCu_3$	2.3–2.74	−36–−17					16; 2, 6, 9, 18
$PrPb_3$	cub	$AuCu_3$	3.58–3.7	−10–−8					16; 9, 18
$NdPb_3$	cub	$AuCu_3$	3.5–3.61	−25–−22			2.7	AF	16; 9, 11, 18;
$SmPb_3$	cub	$AuCu_3$	no C-W behaviour				6		16; 18, 20
$EuPb_3$	cub	$AuCu_3$	7.5–7.81	−66–−25			19–22		17; 14, 18, 21, 22
$GdPb_3$	cub	$AuCu_3$	7.6	−60			17		23; 18
$TbPb_3$	cub	$AuCu_3$	9.21	−55			15		24; 18
$DyPb_3$	cub	$AuCu_3$	10.20	−29			11		24; 18
$HoPb_3$	cub	$AuCu_3$	10.0	−17			3.7		24; 18
$YbPb_3$	cub	$AuCu_3$	no C-W behaviour						24; 22
YPb_3	cub	$AuCu_3$	$\chi_0 = 0.085 \times 10^{-3}$ cm^3/mole						24; 5

1. Crystal structure unknown
2. Ruggiero et al. (1964)
3. Percheron and Lethuillier (1972)
4. Harris and Raynor (1965a)
5. Havinga et al. (1970)
6. Tsuchida and Wallace (1965)
7. Borsa et al. (1967)
8. Shenoy et al. (1970)
9. Lethuillier and Chaussy (1976a)
10. Lethuillier (1974)
11. Lethuillier et al. (1975)
12. Loewenhaupt and Hüfner (1969)
13. Percheron et al. (1973)
14. Loewenhaupt (1973)
15. Buschow, unpublished
16. Gschneidner (1961)
17. McMasters and Gschneidner (1967)
18. Hutchens and Wallace (1971)
19. Structure type now known
20. Lethuillier et al. (1973)
21. Stalinski (1974)
22. Stalinski et al. (1974)
23. McMasters and Gschneidner (1964)
24. Kuzma et al. (1964)

TABLE A.2i
Rare earth copper compounds

Compound	Symmetry	Crystal structure	μ_{eff}	θ_p	μ	T_c	T_N	Magnetic structure	References
CeCu	orh	FeB	2.15–2.60	−38–0			2.7		1; 1, 2
PrCu	orh	FeB	3.66	−11					1; 1
NdCu	orh	FeB	3.69	−2					1; 1
SmCu	orh	FeB	no C-W behaviour				40		1; 1
GdCu	cub	CsCl	8.3–8.46	−75–−26			41–140		3; 1, 4–8
TbCu	cub	CsCl	9.52–9.68	−22–−20			114–177	AF	3; 1, 8, 9; 9–11
DyCu	cub	CsCl	10.61–10.8	−26–−18			61–64	AF	3; 1, 12; 13
HoCu	cub	CsCl	10.73	−13–−18			28	AF	3; 1, 5; 10
ErCu	cub	CsCl					17–33	AF	3; 1; 14
TmCu	cub	CsCl	7.56	−8			11		3; 1
YbCu	orh	FeB	no C-W behaviour						15; 15
$LaCu_2$	hex	AlB_2							16;
$CeCu_2$	orh	$CeCu_2$	2.59	−48	0.8				16; 2, 17
$PrCu_2$	orh	$CeCu_2$	3.51	−10	2.3				16; 17–19
$NdCu_2$	orh	$CeCu_2$	3.56	−2	1.9				16; 17, 19
$SmCu_2$	orh	$CeCu_2$	no C-W		0.1				16; 17
$EuCu_2$	orh	$CeCu_2$	7.4		5.8		13–15		16; 17, 20
$GdCu_2$	orh	$CeCu_2$	8.4	11	6.0		41		16; 17, 19
$TbCu_2$	orh	$CeCu_2$	9.8	−6	7.4		54		16; 17, 19
$DyCu_2$	orh	$CeCu_2$	10.75	5	8.7		24		16; 17, 19
$HoCu_2$	orh	$CeCu_2$	10.5	−6	9.2		9		16; 17, 19
$ErCu_2$	orh	$CeCu_2$	9.35	4	5.6		11		16; 17, 19
$TmCu_2$	orh	$CeCu_2$	7.49	−4	4.2				16; 17, 19
$YbCu_2$	orh	$CeCu_2$	no C-W behaviour						16; 17, 21
$LuCu_2$	orh	$CeCu_2$			0.01				16; 17
$PrCu_5$	hex	$CaCu_5$							22; 23
$EuCu_5$	hex	$CaCu_5$	7.6	58	7.2		57		24; 24
$GdCu_5$	hex	$CaCu_5$	7.89	20	5.4		25		22; 24, 25
$TbCu_5$	cub	$AuBe_5$	9.6	2				15	22; 26
$DyCu_5$	cub	$AuBe_5$	10.9	2	6.5			7	22; 26
$HoCu_5$	cub	$AuBe_5$	10.8	~0	(7.6)				22; 26
$ErCu_5$	cub	$AuBe_5$	9.7	~0	(7.3)				22; 26
$TmCu_5$	cub	$AuBe_5$	7.4	~0	(4.9)				22; 26
$CeCu_6$	orh	$CeCu_6$	2.48–2.59	−40–−30					27; 2, 28
$PrCu_6$	orh	$CeCu_6$	3.59	12					27; 28, 29
$NdCu_6$	orh	$CeCu_6$	3.52	−4					27; 28
$SmCu_6$	orh	$CeCu_6$		−15					27; 28
$GdCu_6$	orh	$CeCu_6$	7.41–7.95	40–72					27; 28

1. Walline and Wallace (1965)
2. Olcese (1963a)
3. Chao et al. (1964)
4. De Wijn et al. (1968)
5. Pierre (1969)
6. Burzo et al. (1972)
7. Sekizawa and Yasukochi (1966b)
8. Pierre (1967)
9. Yashiro et al. (1976)
10. Pierre (1970)
11. Cable et al. (1964a)
12. Pierre and Pauthenet (1965)
13. Winterberger et al. (1971)
14. Cable et al. (1964b)
15. Debray et al. (1976)
16. Storm and Benson (1963)
17. Sherwood et al. (1964)
18. Tamminga (1973)
19. Sherwood, private communication
20. Wickman et al. (1968)
21. Klaasse (1973)
22. Buschow and van der Goot (1971b)
23. Andres et al. (1975b)
24. Van Steenwijk (1975a)
25. Van Steenwijk et al. (1977)
26. Buschow et al. (1970)
27. Buschow and van der Goot (1970)
28. Coldea and Pop (1974)
29. Andres and Bucher (1972)

TABLE A.2j
Rare earth silver and rare earth gold compounds

Compound	Symmetry	Crystal structure	μ_{eff}	θ_p	μ	T_c	T_N	Magnetic structure	References
LaAg	cub	CsCl	$\chi_0 = 0.086 \cdot 10^{-3}$ cm^3/mole						1; 2
CeAg	cub	CsCl	2.51–2.56	−20–−19	0.95	6.2–9			1; 3–6
PrAg	cub	CsCl	3.44	2–6	1.55		11–14	AF	1; 4, 7–9; 8
NdAg	cub	CsCl	3.64	−3			22	AF	1; 4; 10
SmAg	cub	CsCl	no C-W behaviour						1; 4
GdAg	cub	CsCl	8.24–8.6	−84–−70			138–150		1; 4, 11–13
TbAg	cub	CsCl	9.40–10.15	−36–−11			106	AF	1; 4, 13; 14
DyAg	cub	CsCl	10.45–10.58	−23			55–63	AF	1; 4, 13; 15
HoAg	cub	CsCl	9.93–10.25	−17–−4			32–33	AF, C	1; 4, 13; 16
ErAg	cub	CsCl	9.22	−9.5–15			18–21	AF, C	1; 4, 13; 16
TmAg	cub	CsCl	7.15–7.53	−7–−4			9.5–10		1; 4, 13
YbAg	orh	FeB	no C-W behaviour						17; 17
YAg	cub	CsCl	$\chi_0 = 0.0634$ cm^3/mole						18; 19
$CeAg_2$			2.41	14					20; 3
$EuAg_2$	orh	$CeCu_2$					12		21; 22
$GdAg_2$	tetr	$MoSi_2$		−47			24.6		23; 24
$TbAg_2$	tetr	$MoSi_2$		−31.5			34.4–35	AF	25; 24; 25
$DyAg_2$	tetr	$MoSi_2$	10.5	−25			9–15.0	C	26; 26, 27
$HoAg_2$	tetr	$MoSi_2$		−13.5			8.0	C	28; 24; 28
$ErAg_2$	tetr	$MoSi_2$		−5.0			5.2–5.5	C	29; 24; 29
$TmAg_2$	tetr	$MoSi_2$					<1.7		30; 30
$YbAg_2$	orh	$CeCu_2$	no C-W behaviour						18; 31
$EuAg_5$	hex	$CaCu_5$	7.43	19	6.3	19			32; 32
CeAu			2.60	−38					33; 3
PrAu	cub	CsCl							1;
NdAu	cub	CsCl							1;
SmAu	cub	CsCl							1;
EuAu									34;
GdAu	cub	CsCl	7.29	29			31, 37		1; 35
TbAu	cub	CsCl	9.54	23			40, 43		1; 35
DyAu	cub	CsCl	10.22	7			24–34		1; 35, 36
HoAu	cub	CsCl	10.50	0			10		1; 35
ErAu	cub	CsCl	9.42	−4			13–19		1; 35, 36
TmAu	cub	CsCl	7.32	−5			8–19		1; 35, 36
YbAu	orh	FeB	no C-W behaviour						17; 17
$CeAu_2$			3.03	−92					33; 3
$EuAu_2$	orh	$CeCu_2$		20			8.5		37; 22
$GdAu_2$	tetr	$MoSi_2$	8.38	−31.0			48–49.6		37; 24, 38
$TbAu_2$	tetr	$MoSi_2$	9.83	−21.0			55	C	37; 24, 38; 39
$DyAu_2$	tetr	$MoSi_2$	10.52–10.6	−13–24			31–33.8	C	37; 24, 26, 38; 27
$HoAu_2$	tetr	$MoSi_2$	10.97	−8.0			9–9.2	C	37; 24, 38; 40
$ErAu_2$	tetr	$MoSi_2$	9.45	−4.0			6–7.3	C	37; 24, 38; 41
$TmAu_2$	tetr	$MoSi_2$	7.62				3.2–3.5	C	37; 38; 30
$YbAu_2$	tetr	$MoSi_2$	4.35–4.5	−16–5			<1.7		37; 30, 31, 42

TABLE A.2j (*cont.*)

Compound	Symmetry	Crystal structure	μ_{eff}	θ_p	μ	T_c	T_N	Magnetic structure	References
$CeAu_3$			2.42	6					43; 3
$GdAu_3$	orh	$TiCu_3$	7.64	17.9					44; 45
$TbAu_3$	orh	$TiCu_3$	9.90	6.3					44; 45
$DyAu_3$	orh	$TiCu_3$	10.36	21.0					44; 45
$HoAu_3$	orh	$TiCu_3$	10.09	10.8					44; 45
$ErAu_3$	orh	$TiCu_3$	8.99	23.7					44; 45
$TmAu_3$	orh	$TiCu_3$	7.21	26.3					44; 45
$YbAu_3$	orh	$TiCu_3$	3.95-4.5	−10-33.5					44; 31, 42, 45
$ErAu_4$	tetr	$MoNi_4$	9.8	−6					44; 46
$TmAu_4$	tetr	$MoNi_4$	8.2	−6					44; 46
$YbAu_4$	tetr	$MoNi_4$	4.3-4.5	−9-15					44; 42, 46
$EuAu_5$	hex	$CaCu_5$	7.78	13		6.6	14		32; 32

1. Chao et al. (1963)
2. Goebel et al. (1975)
3. Olcese et al. (1963a)
4. Walline and Wallace (1964)
5. Olcese (1963b)
6. Ihrig and Methfessel (1976a)
7. Brun et al. (1974a)
8. Brun et al. (1976)
9. Brun et al. (1974b)
10. Buschow et al. (1975a)
11. Burzo et al. (1972)
12. Sekizawa and Yasukochi (1966b)
13. Pierre and Pauthenet (1965)
14. Cable et al. (1964a)
15. Arnold et al. (1967)
16. Nereson (1963)
17. Debray et al. (1976)
18. Moriarty (1966)
19. Weimann et al. (1972)
20. Crystal structure unknown
21. Köster and Meixner (1965)
22. Van Steenwijk (1976)
23. Baenziger and Moriarty (1961)
24. Kaneko et al. (1975)
25. Atoji (1968a)
26. Miura et al. (1971)
27. Atoji (1969a)
28. Atoji (1969b)
29. Atoji (1972a)
30. Atoji (1970)
31. Klaasse et al. (1976)
32. Van Steenwijk et al. (1977)
33. Crystal structure not known
34. Complex crystal structure, see Köster and Meixner (1965)
35. Kissel and Wallace (1966)
36. Chao (1966). (The T_N values listed are derived from resistivity measurements.)
37. Iandelli and Palenzona (1968).
38. Sill et al. (1973)
39. Atoji (1968b)
40. Atoji (1972b)
41. Atoji (1972c)
42. Iandelli and Palenzona (1969a)
43. Crystal structure not known
44. Sadagopan et al. (1968)
45. Sill and Prindeville (1975)
46. Sill et al. (1971)

TABLE A.2k
Rare earth beryllium compounds

Compound	Symmetry	Crystal structure	μ_{eff}	θ_p	μ	T_c	T_N	Magnetic structure	References
$LaBe_{13}$	cub	$NaZn_{13}$	$\chi = -0.024 \times 10^{-3}$ cm^3/mole						1; 1
$CeBe_{13}$	cub	$NaZn_{13}$	no C-W behaviour						1; 1–3
$PrBe_{13}$	cub	$NaZn_{13}$	3.58	−8					1; 1
$NdBe_{13}$	cub	$NaZn_{13}$	3.57–3.67	2.5–25			2.4–2.63		1; 1, 2
$SmBe_{13}$	cub	$NaZn_{13}$	no C-W behaviour				8.8		1; 1,
$EuBe_{13}$	cub	$NaZn_{13}$	no C-W behaviour						1; 1
$GdBe_{13}$	cub	$NaZn_{13}$	7.82–7.94	25–45	6.97	19–22	25.7		1; 1, 2, 4, 5
$TbBe_{13}$	cub	$NaZn_{13}$	9.7–9.71	14.0	9.0		15.3		1; 1, 4
$DyBe_{13}$	cub	$NaZn_{13}$	10.47–10.5	13	9.9		9–9.3		1; 1, 4
$HoBe_{13}$	cub	$NaZn_{13}$	10.57	6			5.45		1; 1
$ErBe_{13}$	cub	$NaZn_{13}$	9.53	6			2.37		1; 1
$TmBe_{13}$	cub	$NaZn_{13}$	7.55	1					1; 1
$YbBe_{13}$	cub	$NaZn_{13}$	no C-W behaviour						1; 1
$LuBe_{13}$	cub	$NaZn_{13}$	$\chi = -0.125 \times 10^{-3}$ cm^3/mole						1; 1

1. Bucher (1975)
2. Borsa and Olcese (1973)
3. Cooper et al. (1971)
4. Domngang and Herr (1973)
5. Heinrich and Meyer (1977)

TABLE A.2ℓ
Rare earth magnesium compounds

Compound	Symmetry	Crystal structure	μ_{eff}	θ_p	μ	T_c	T_N	Magnetic structure	References
LaMg	cub	CsCl							1;
CeMg	cub	CsCl	2.47	−10−−5			18–20		1; 1, 2
PrMg	cub	CsCl	3.39	−11−−9			45–47	AF	1; 1, 2; 3
NdMg	cub	CsCl	3.66	−14−−9			48–64	AF	1; 1, 2; 5
SmMg	cub	CsCl	no C-W behaviour						1;
GdMg	cub	CsCl	8.08–8.36	108–120	5.6–7.55	119–120		C	1; 1, 2, 4; 3
TbMg	cub	CsCl	9.73–9.94	83–84	5.7–7.7	81		C	1; 1, 2, 4–6; 4, 6
DyMg	cub	CsCl	10.54–10.7	25–48	6.4	22–46		AF	1; 1, 2; 2, 7
HoMg	cub	CsCl	10.6–10.77	24–25	6.8–8.9	21–25		C	1; 1, 2
ErMg	cub	CsCl	9.26–9.60	9–15	7.72	5.5–16		F, C	1; 1, 2; 2, 7
TmMg	cub	CsCl				<1.5			2; 4
YMg	cub	CsCl	$\chi = 0.171 \times 10^{-3}$ emu/mole						1; 2
$LaMg_2$	cub	$MgCu_2$	$\chi = 0.29 \times 10^{-3}$ emu/mole						8; 8
$CeMg_2$	cub	$MgCu_2$	2.51	−19	0.49	3.5			8; 8
$PrMg_2$	cub	$MgCu_2$	3.34	7	1.58	9.6			8; 8
$NdMg_2$	cub	$MgCu_2$	3.32	26	1.57	26			8; 8
$SmMg_2$	cub	$MgCu_2$	no C-W behaviour				26		8; 8
$EuMg_2$	hex	$MgZn_2$	8.52	19			30		8; 8
$GdMg_2$	cub	$MgCu_2$	8.90	100	7.23	81			8; 8
$TbMg_2$	hex	$MgZn_2$	10.11	83	5.69	88			8; 8
$DyMg_2$	hex	$MgZn_2$	10.82	56	5.03	66			8; 8
$HoMg_2$	hex	$MgZn_2$	10.74	23	6.05	27			8; 8
$ErMg_2$	hex	$MgZn_2$	9.86	7	4.3	19			8; 8
$TmMg_2$	hex	$MgZn_2$	7.46	3	2.7				8; 8
$YbMg_2$	hex	$MgZn_2$	$\chi = 0.11 \times 10^{-3}$ emu/mole						8; 8
YMg_2	hex	$MgZn_2$	$\chi = 0.18 \times 10^{-3}$ emu/mole						8; 8
$LaMg_3$	cub	Fe_3Al							9;
$CeMg_3$	cub	Fe_3Al	2.7	−46					9; 9
$PrMg_3$	cub	Fe_3Al	3.8	−42					9; 9
$NdMg_3$	cub	Fe_3Al	5.0	−124					9; 9
$SmMg_3$	cub	Fe_3Al	no C-W behaviour				6.5		9; 9
$GdMg_3$	cub	Fe_3Al	8.81	−240			16		9; 9, 10
$TbMg_3$	cub	Fe_3Al	9.56	−110			20–26	AF	9; 9, 10; 10
Gd_5Mg_{24}			8.55	−119					12;
Tb_5Mg_{24}	cub	α-Mn							11; 12
Dy_5Mg_{24}	cub	α-Mn	10.5	39					11; 12
Ho_5Mg_{24}	cub	α-Mn							11; 12
Er_5Mg_{24}	cub	α-Mn	10.02	11	7.1	13			11; 12
Tm_5Mg_{24}	cub	α-Mn	7.84	3	4.2	4			11; 12
Eu_2Mg_{17}	hex	Th_2Ni_{17}	8.66	−20			7.9		12; 12

1. Buschow (1973b)
2. Aleonard et al. (1976)
3. Morin et al. (1978a, b)
4. Aleonard et al. (1975)
5. Buschow et al. (1975c)
6. Schäfer et al. (1977)
7. Schäfer et al. (1976b)
8. Buschow et al. (1978)
9. Buschow (1976a)
10. Will et al. (1977b)
11. Krypiakevich et al. (1960)
12. Buschow, unpublished

TABLE A.2m
Rare earth zinc compounds

Compound	Symmetry	Crystal structure	μ_{eff}	θ_p	μ	T_c	T_N	Magnetic structure	References
LaZn	cub	CsCl	$\chi = 0.008 \cdot 10^{-3}$ cm^3/mole						1; 2
CeZn	cub	CsCl	2.14–2.48	−18–−2			29–36	AF	3; 3–5; 6
PrZn	cub	CsCl	3.26–3.43	10–13				AF	3; 3, 5; 7
NdZn	cub	CsCl	3.28–3.44	30–45			66–148	AF	3; 3, 5; 7.
SmZn	cub	CsCl	no C-W behaviour				110–125		3; 3, 5
EuZn	cub	CsCl	7.82	14					8; 8
GdZn	cub	CsCl		268	7.5	268–270			3; 3, 5
TbZn	cub	CsCl	9.19–9.2	190–203	8.9	204–207		F	3; 3, 5, 9, 10; 9, 11
DyZn	cub	CsCl	10.2	110–140	9.0	139–145			3; 3, 5, 10
HoZn	cub	CsCl	10.2	80	8.7	75–80			3; 3, 5, 10
ErZn	cub	CsCl	9.2	5–25	6.5–6.8	0–50			3; 3, 5, 10
TmZn	cub	CsCl							8;
YbZn	cub	CsCl	$\chi = 0.19 \times 10^{-3}$ cm^3/mole						8; 8, 12
LuZn	cub	CsCl							8;
YZn	cub	CsCl							1;
$LaZn_2$	orh	$CeCu_2$	$\chi = 10^{-5}$ emu/cm^3						13; 14
$CeZn_2$	orh	$CeCu_2$	2.25–2.72	−38–24			7–7.5	AF	15; 16, 17; 15
$PrZn_2$	orh	$CeCu_2$	3.56	14					13; 17
$NdZn_2$	orh	$CeCu_2$	3.40	28	1.82		24	C	13; 17, 18; 18
$SmZn_2$	orh	$CeCu_2$	no C-W behaviour				45		13; 17
$EuZn_2$	orh	$CeCu_2$	7.1–8.23	26.5–45			20–30		19; 8, 17, 19–21
$GdZn_2$	orh	$CeCu_2$	8.48	70	6.91	68			13; 17
$TbZn_2$	orh	$CeCu_2$	9.62	58			55	C	13; 17; 15
$DyZn_2$	orh	$CeCu_2$	10.45	31.5			35		13; 21
$HoZn_2$	orh	$CeCu_2$	9.71	26			12	C	22; 21; 22
$ErZn_2$	orh	$CeCu_2$	9.59	5.8		13		C	13; 21; 23
$TmZn_2$	orh	$CeCu_2$	6.48	11.5			5.2		13; 21
$YbZn_2$	orh	$CeCu_2$	no C-W behaviour						24; 21
$LuZn_2$	orh	$CeCu_2$							13;
$CeZn_5$	hex	$CaCu_5$	2.54	−44					25; 16
$EuZn_5$	hex	$CaCu_5$	7.99–8.06	−24–−78			10		19; 19, 26, 27
Ce_2Zn_{17}	rh	Th_2Zn_{17}	2.64	0					28; 16
Gd_2Zn_{17}	rh	Th_2Zn_{17}	7.84	−53			10		28; 29
Tb_2Zn_{17}	rh	Th_2Zn_{17}	9.84	−17			28		28; 29
Dy_2Zn_{17}	rh	Th_2Zn_{17}	11.01	−14					28; 29
Ho_2Zn_{17}	rh	Th_2Zn_{17}	10.08	−11.5					28; 29
Er_2Zn_{17}	rh	Th_2Zn_{17}	9.63	−4					28; 29
Tm_2Zn_{17}	rh	Th_2Zn_{17}	7.64	7					28; 29
Yb_2Zn_{17}	rh	Th_2Zn_{17}	0						28; 29

TABLE A.2m (*cont.*)

Compound	Symmetry	Crystal structure	μ_{eff}	θ_p	μ	T_c	T_N	Magnetic structure	References
$CeZn_{11}$	tetr	$BaCd_{11}$	2.54	26					28; 16
$YbZn_{11}$	tetr	$BaCd_{11}$	0						28; 29
$SmZn_{12}$	tetr	$ThMn_{12}$	0.74	−27.8			15		28; 29
$GdZn_{12}$	tetr	$ThMn_{12}$	8.40	−58			16	C	28; 29
$TbZn_{12}$	tetr	$ThMn_{12}$	10.14	−38			14		28; 29; 30
$ErZn_{12}$	tetr	$ThMn_{12}$	9.67	−3			2.8		28; 29
$EuZn_{13}$	cub	$NaZn_{13}$	7.50–7.94	2–18			3.19		19; 19, 27

1. Chao et al. (1964)
2. Goebel et al. (1975)
3. Eckrich et al. (1976)
4. Olcese (1963c)
5. Kanematsu et al. (1969)
6. Morin et al., unpublished
7. Buschow et al. (1975c)
8. Iandelli and Palenzona (1965)
9. Yashiro et al. (1976)
10. Morin and Pierre (1973)
11. Cable et al. (1964a)
12. Debray et al. (1976)
13. Fornasini and Merlo (1967)
14. Debray and Sakurai (1974)
15. Debray et al. (1970a)
16. Olcese (1963c)
17. Debray et al. (1970b)
18. Debray and Sougi (1973)
19. Buschow et al. (1975d)
20. Wickman et al. (1968)
21. Debray et al. (1975)
22. Debray and Sougi (1972)
23. Debray et al., unpublished
24. Michel and Ryba (1965)
25. Lott and Chiotti (1966)
26. Olcese (1963d)
27. Iandelli and Palenzona (1964)
28. Iandelli and Palenzona (1969b)
29. Stewart and Coles (1974)
30. Forsyth, unpublished

TABLE A.2n
Rare earth cadmium compounds and rare earth mercury compounds

Compound	Symmetry	Crystal structure	μ_{eff}	θ_p	μ	T_c	T_N	Magnetic structure	References
LaCd	cub	CsCl	$\chi = 0.060 \times 10^{-3}$ cm^3/mole						1; 1
CeCd	cub	CsCl	2.1–2.50	10–14	0.7	12–14			1; 1–3
PrCd	cub	CsCl	3.2–3.53	44–49	1.1	50	(50)		1; 1, 3
NdCd	cub	CsCl	3.3–3.82	70–83	2.2	105–121			1; 1, 3
SmCd	cub	CsCl	1.9	−12	0.03–0.05	194–196			1; 1, 3, 4
Eu_6Cd_5	cub	CsCl	7.89–7.97	−11–−3		30	75		5; 6, 7
GdCd	cub	CsCl	6–7.50	2 54	7.2	254–265			1; 1, 3, 8
TbCd	cub	CsCl	9.2–9.94	166–177	7.8	166–185			1; 1, 3
DyCd	cub	CsCl	9.5–10.7	80–92	8.3	90–105			1; 1, 3
HoCd	cub	CsCl	10–11.2	15–36	7.1	19–30			1; 1, 3
ErCd	cub	CsCl	9.2–9.69	−4–10		4–14			1; 1, 3
TmCd	cub	CsCl	7.78						6; 9
YbCd	cub	CsCl	(2.1)	(−42)					6; 3, 6
$CeCd_2$	hex	CdI_2	2.18	−75					2; 2
$EuCd_2$	orh	$CeCu_2$	7.82–7.95	35–50	7.05		35.5		10; 7
$GdCd_2$	hex	CeI_2	8.40	129					8; 8
$CeCd_3$	cub	$BiLi_3$	2.44	−29					11; 2
$GdCd_3$	hex	Ni_3Sn	7.76	12					8; 8
$GdCd_4$	cub	γ-brass	7.46	−6					8; 8
Gd_2Cd_9	hex	Pu_2Zn_9	8.18	−52					8; 8
$EuCd_6$	cub	$GdCd_6$	7.80	−16					7; 7
$GdCd_6$	cub	$GdCd_6$	7.65	3					8; 8
$CeCd_{11}$	tetr	$BaCd_{11}$	2.47	32					12; 2
$PrCd_{11}$	tetr	$BaCd_{11}$							12;
$EuCd_{11}$	tetr	$BaCd_{11}$	7.56–7.87	−7–18					7; 7, 13
CeHg	cub	CsCl	2.73	−32					2; 2
EuHg	cub	CsCl	7.63	11					6; 6
TbHg	cub	CsCl				80			6; 14
YbHg	cub	CsCl	$\chi_0 = 0.33 \times 10^{-3}$ cm^3/mole						6; 6
$CeHg_2$	hex	AlB_2	2.73	−33					2; 2
$EuHg_2$	hex	AlB_2	8.00	+29					13; 13
$CeHg_3$	hex	$MgCd_3$	2.93	−53					11; 2
$EuHg_3$	hex	$MgCd_3$	7.63	−69					13; 15
Ce_5Hg_{21}	cub	Ce_3Hg_{21}	3.03	−55					16; 2
$EuHg_5$			7.79	10					17; 13, 15

1. Buschow (1974)
2. Olcese (1963c)
3. Alfieri et al. (1967)
4. Stewart et al. (1974)
5. Köster and Meixner (1965)
6. Iandelli and Palenzona (1965)
7. Buschow and Van Steenwijk (1977)
8. Bruzzone et al. (1971)
9. Lüthi et al. (1973)
10. Complex crystal structure, see ref. 5
11. Iandelli (1955)
12. Iandelli and Ferro (1954)
13. Iandelli and Palenzona (1964)
14. Cable et al. (1964a)
15. Olcese (1963d)
16. Berndt (1967)
17. Crystal structure not known

TABLES A.3a–g

Magnetic properties of intermetallic compounds of rare earths and d-transition metals. Details pertaining to the structure type listed in columns 3 are given in table A.1. The values of the effective moments (μ_{eff}) and saturation moments (μ) are expressed in Bohr magnetons per rare earth ion and per formula unit, respectively. Values for the paramagnetic Curie temperatures (θ_p) Curie temperatures (T_c) and Néel temperatures (T_N) are given in K. The magnetic structure types are indicated by F (ferromagnetic), FF (ferrimagnetic) (AF (antiferromagnetic) or by C (complex). The references comprise three groups separated by semicolons. The first reference pertains to literature of the crystal structure and lattice constants. Usually only one reference has been chosen out of the collection of references available. The references given between the two semicolons pertain to the literature in which the value of μ_{eff}, θ_p, μ, T_c and T_N are reported. The references after the last semicolon correspond to neutron diffraction work. Since in most cases the values of μ_{eff}, θ_p, μ, T_c and T_N reported by different authors in literature are dissimilar, lower and higher limits have been listed. The values given for χ of Pauli paramagnetic compounds are room temperature values and not values attained at 4.2 K since these latter may depend strongly on the amount of localized moment impurities present in the samples.

Several of the Co- and Fe rich compounds give rise to a compensation temperature at which the rare earth and 3d sublattice magnetizations cancel. These temperatures are listed under T_{comp} and are given in K.

TABLE A.3a
Rare earth nickel compounds

Compound	Symmetry	Crystal structure	μ_{eff}	θ_p	μ	T_c	T_N	Magnetic structure	References
La_3Ni	orh	Fe_3C	$\chi = 0.30 \times 10^{-3}$ cm^3/mole						1;2
Pr_3Ni	orh	Fe_3C	3.7	−24	0.72		2		1;3,4
Nd_3Ni	orh	Fe_3C	3.6	0	0.7		15		1;3,4
Sm_3Ni	orh	Fe_3C	no C-W behaviour						1;3,4
Gd_3Ni	orh	Fe_3C	8.1	60	5.1–8.1		100		1;3–5
Tb_3Ni	orh	Fe_3C	10.0	−5	6.7		62		1;3–5
Dy_3Ni	orh	Fe_3C	10.6	29	3.7–5.7		33–35		1;3–5
Ho_3Ni	orh	Fe_3C	11.1	−6	5.3–7.3		20		1;3–5
Er_3Ni	orh	Fe_3C	9.8–9.9	−6–−5	7.1		5–9	C	1;2–5;4
Tm_3Ni	orh	Fe_3C	7.4	0	3.7	12			1;3,4
La_7Ni_3	hex	Th_7Fe_3	$\chi = 0.25 \times 10^{-3}$ emu/mole						6;6
Ce_7Ni_3	hex	Th_7Fe_3	2.16	13					6;6
Pr_7Ni_3	hex	Th_7Fe_3	3.55	23					6;6
Nd_7Ni_3	hex	Th_7Fe_3	3.33	48					6;6
LaNi	orh	CrB							7;
CeNi	orh	CrB			0				7;7
PrNi	orh	CrB	3.6–3.9	23	2.26–2.3	21–22			7;7,8
NdNi	orh	CrB	3.3–3.7	24	2.1–2.74	27–35		F	7;4;7,8;4
SmNi	orh	CrB	no C-W		0.23–0.3	45–47			7;7,8
GdNi	orh	CrB	8.1–8.2	77	7.2–7.40	71–73			7;7–9
TbNi	orh	CrB	9.7–9.8	40	4.0–7.9	50–52			7;4,7,8
DyNi	orh	CrB	10.7–10.8	64	7.8–8.75	48–62		C	8;7,8;10
HoNi	orh	CrB	10.4–10.7	36	7.0–9.2	32–37		C	7;4,7,8;4
ErNi	orh	FeB	9.8	13	8.10	11–13		C	7;4,7,8;4
TmNi	orh	FeB	7.4		5.1–5.2	8		C	7;7,8;10
YbNi	orh	FeB	4.5	15					11;12
LuNi	orh	FeB				4			7;
$LaNi_2$	cub	$MgCu_2$							13;14
$CeNi_2$	cub	$MgCu_2$	$\chi = 0.74 \times 10^{-3}$ emu/mole						15;16

TABLE A.3a (*cont.*)

Compound	Symmetry	Crystal structure	μ_{eff}	θ_p	μ	T_c	T_N	Magnetic structure	References
$PrNi_2$	cub	$MgCu_2$	3.53–3.57	4–8	0.86				15; 14, 17
$NdNi_2$	cub	$MgCu_2$	3.61–3.74	10–16.5	1.75–1.80	15.5–16			15; 14, 17
$SmNi_2$	cub	$MgCu_2$	no C-W		0.20–0.27	21–22			15; 14, 17, 18
$GdNi_2$	cub	$MgCu_2$	7.82–7.98	77–78	7.0–7.2	77–85			15; 17–19
$TbNi_2$	cub	$MgCu_2$	9.71–9.82	35–44	6.9–8.5	35–45		F	15; 14, 17, 19; 20, 21
$DyNi_2$	cub	$MgCu_2$	10.4–10.62	23–28	7.83–9.4	23–30			15; 14, 17, 19; 22
$HoNi_2$	cub	$MgCu_2$	10.5–10.64	12–18.5	7.55–9.2	16–22			15; 14, 17, 19; 23
$ErNi_2$	cub	$MgCu_2$	9.37–9.72	10–11	6.40–7.5	16–21			15; 2, 14, 17, 19
$TmNi_2$	cub	$MgCu_2$	7.28–7.56	0–2	3.2–3.34	13.5			15; 14, 17
$YbNi_2$	cub	$MgCu_2$				5.7			15; 24
$LuNi_2$	cub	$MgCu_2$	$\chi = 0.47 \times 10^{-3}$ cm^3/mole						15; 25
YNi_2	cub	$MgCu_2$	$\chi = 0.2 \times 10^{-3}$ cm^3/mole						15; 17
$LaNi_3$	rh	$PuNi_3$							26;
$CeNi_3$	hex	$CeNi_3$	$\chi = 0.6 \times 10^{-3}$ emu/mole						26;
$PrNi_3$	rh	$PuNi_3$		−24	1.57	20		F	26; 27; 28
$NdNi_3$	rh	$PuNi_3$		0	1.88	27		C	26; 27; 28
$SmNi_3$	rh	$PuNi_3$		60	0.33	85			26; 27
$GdNi_3$	rh	$PuNi_3$			6.55	115–116			26; 9, 27
$TbNi_3$	rh	$PuNi_3$		29	6.84	98–100		C	26; 9, 27; 28
$DyNi_3$	rh	$PuNi_3$		−6	7.0	69		C	26; 27; 28
$HoNi_3$	rh	$PuNi_3$		−5	7.84	66		F	26; 27; 29
$ErNi_3$	rh	$PuNi_3$	9.75–9.8	−5–15	5.77–6.4	62–66		C	26; 2, 27; 29
$TmNi_3$				0	3.86	43		F	27; 27; 28
$YbNi_3$	rh	$PuNi_3$			20	<20			11; 27
YNi_3	rh	$PuNi_3$			0.16	30–33		F	26; 27, 33; 33
La_2Ni_7	hex	Ce_2Ni_7							26;
Ce_2Ni_7	hex	Ce_2Ni_7			0.26	48			26; 30
Pr_2Ni_7					4.36	85			26; 30
Nd_2Ni_7	mixture of				4.14	87			26; 30
Sm_2Ni_7	hex(Ce_2Ni_7) and								26;
Gd_2Ni_7	hex(Gd_2Co_7)		6.8	58	12.65	116–118			26; 9, 30
Tb_2Ni_7					10.72	98–101			26; 9, 30
Dy_2Ni_7					13.30	80–81			26; 9, 30
Ho_2Ni_7	rh	Gd_2Co_7			12.57	70			26; 30
Er_2Ni_7	rh	Gd_2Co_7	9.56	22	11.0	67–74		C	26; 2, 30; 31
Y_2Ni_7	rh	Gd_2Co_7			0.41	58			26; 30
$LaNi_5$	hex	$CaCu_5$	$\chi = 2 \times 10^{-3}$ emu/mole						15; 32
$CeNi_5$	hex	$CaCu_5$	−2.6–2.65	−120–−90					15; 34, 35
$PrNi_5$	hex	$CaCu_5$	no C-W						15; 34, 36
$NdNi_5$	hex	$CaCu_5$	no C-W		2.2–2.27	13			15; 34, 37
$SmNi_5$	hex	$CaCu_5$	no C-W		0.7				15; 37
$EuNi_5$	hex	$CaCu_5$							2; 38
$GdNi_5$	hex	$CaCu_5$	7.7–7.94	30–31	6.0–6.9	27–33			15; 33, 34, 37, 32
$TbNi_5$	hex	$CaCu_5$			7	27		FF	15; 37; 39
$DyNi_5$	hex	$CaCu_5$			7.7	20			15; 37
$HoNi_5$	hex	$CaCu_5$	10.5	8	7.2–7.8	18–23			15; 34, 37

TABLE A.3a (*cont.*)

Compound	Symmetry	Crystal structure	μ_{eff}	θ_p	μ	T_c	T_N	Magnetic structure	References
$ErNi_5$	hex	$CaCu_5$	9.85	12	7.7	12		FF	15; 2, 37; 40
$TmNi_5$	hex	$CaCu_5$	7.88	60	6.7	22			; 34
$YbNi_5$	hex	$CaCu_5$							15;
$LuNi_5$	hex	$CaCu_5$							
YNi_5	hex	$CaCu_5$	$\chi = 2 \times 10^{-3}$ emu/mole						15; 32, 37
Sm_2Ni_{17}	hex	Th_2Ni_{17}			4.5–5.25	186			41; 42, 43
Eu_2Ni_{17}									44;
Gd_2Ni_{17}	hex	Th_2Ni_{17}	12.8	138	8.8–9.36	187–205			41; 42, 43, 45, 46
Tb_2Ni_{17}	hex	Th_2Ni_{17}		130	8.5–12.2	178		FF	41; 42, 43; 47
Dy_2Ni_{17}	hex	Th_2Ni_{17}		96	8.05–14.7	168–170		FF	41; 42, 43, 46; 48
Ho_2Ni_{17}	hex	Th_2Ni_{17}		73	12.2–13.8	162		FF	41; 42, 43; 49
Er_2Ni_{17}	hex	Th_2Ni_{17}		53	9.1–11.0	166		FF	41; 42, 43; 47
Tm_2Ni_{17}	hex	Th_2Ni_{17}		25	7.31	152		C	42; 42, 43; 47
Yb_2Ni_{17}	hex	Th_2Ni_{17}							11;
Lu_2Ni_{17}	hex	Th_2Ni_{17}			5.0	(601)			43; 43
Y_2Ni_{17}	hex	Th_2Ni_{17}			4.67–5	151–170		F	41; 9, 42, 43, 46, 49

1. Lemaire and Paccard (1967)
2. Buschow (1968)
3. Ferron et al. (1968)
4. Bècle et al. (1970)
5. Primavesi and Taylor (1972)
6. Olcese (1973)
7. Abrahams et al. (1964)
8. Walline and Wallace (1964)
9. Parviainen and Jaakkola (1975)
10. Barbara et al. (1973)
11. Buschow (1972)
12. Klaasse et al. (1976)
13. Mansey et al. (1968)
14. Farrell and Wallace (1966)
15. McMasters and Gschneidner (1964)
16. K.H.J. Buschow, unpublished results
17. Burzo and Laforest (1972)
18. Crangle and Ross (1964)
19. Voiron (1972)
20. Felcher et al. (1965)
21. Givord et al. (1976)
22. Gignoux and Givord (1977)
23. Gignoux et al. (1975)
24. Nowik and Dunlap (1973)
25. Scrabek and Wallace (1963)
26. Buschow and van der Goot (1970)
27. Paccard and Pauthenet (1967)
28. Yakinthos and Paccard (1972)
29. Paccard et al. (1971)
30. Lemaire et al. (1967)
31. Yakinthos and Rentzeperis (1974)
32. Gignoux et al. (1976b)
33. Gignoux et al. (1980)
34. Wallace and Aoyagi (1971)
35. Buschow et al. (1976a)
36. Andres et al. (1975c)
37. Nesbitt et al. (1962)
38. Oliver et al. (1978)
39. Lemaire and Paccard (1970)
40. Corliss and Hastings (1964)
41. Buschow (1966)
42. Laforest et al. (1967)
43. Carfagna and Wallace (1968)
44. Terekhova et al. (1967)
45. Steiner and Hrubec (1975)
46. Steiner et al. (1976)
47. Yakinthos (1977a)
48. Yakinthos and Roudeaux (1977)
49. Yakinthos (1977b)

TABLE A.3b
Rare earth cobalt compounds

Compound	Symmetry	Crystal structure	μ_{eff}	θ_p	μ	T_c	T_N	Magnetic structure	References
La_3Co	orh	Fe_3C	$\chi = 48 \times 10^{-3}$ cm^3/mole						1; 2
Pr_3Co	orh	Fe_3C		18	1.1	7			1; 3
Nd_3Co	orh	Fe_3C		35	1.7		14		1; 3, 4
Sm_3Co	orh	Fe_3C							
Gd_3Co	orh	Fe_3C		159	7.2–8.1		127–143		1; 3–5
Tb_3Co	orh	Fe_3C		85	5.3–8		76–82		1; 3, 4
Dy_3Co	orh	Fe_3C		65	5.4–6.4		45		1; 3, 4
Ho_3Co	orh	Fe_3C		44	5.9–7.6		23–24		1; 3, 4
Er_3Co	orh	Fe_3C		20	6–6.9	7	13	C	1; 3, 4; 6
Tm_3Co	orh	Fe_3C		0	5.3	5			; 3
Lu_3Co	orh	Fe_3C			~0	<2			1; 2, 7
Y_3Co	orh	Fe_3C			~0	<2			7; 7
Gd_4Co_3	hex	Ho_4Co_3	7.9–8.04	240–242	6.5–6.6	230–233			8; 5, 9
Tb_4Co_3	hex	Ho_4Co_3							8; 9
Dy_4Co_3	hex	Ho_4Co_3	10.6	62	5.2				8; 9
Ho_4Co_3	hex	Ho_4Co_3	10.6	50	7.4	44		FF	8; 9; 4
Er_4Co_3	hex	Ho_4Co_3	9.6	28	5.8	25		FF	8; 9; 4
Lu_4Co_3	hex	Ho_4Co_3			~0	<2			7; 7
Y_4Co_3	hex	Ho_4Co_3			0.03	<2			8; 7, 9
$CeCo_2$	cub	$MgCu_2$	$\chi = 1.72 \times 10^{-3}$ emu/mole						10; 11
$PrCo_2$	cub	$MgCu_2$			2.98–3.2	50			10; 12–15
$NdCo_2$	cub	$MgCu_2$		107	3.4–3.8	97–126		F	10; 12–18; 19
$SmCo_2$	cub	$MgCu_2$			1.26–2.0	211–259			10; 12–15
$GdCo_2$	cub	$MgCu_2$	8.58		4.31–5.3	395–420			10; 5, 13–17, 20–25
$TbCo_2$	cub	$MgCu_2$	10.02	228	4.38–6.7	226–256		(FF)	10; 5, 12–14, 17, 20, 21; 19
$DyCo_2$	cub	$MgCu_2$	11.3	129	6.72–7.6	123–169			10; 5, 12–14, 17, 20, 21
$HoCo_2$	cub	$MgCu_2$			7.17–8.0	74–111		(FF)	10; 5, 13, 14, 16, 17, 20, 21, 25, 26; 19
$ErCo_2$	cub	$MgCu_2$		28	5.6–7.56	32.5–48		(FF)	10; 5, 12–14, 17, 20, 21; 19
$TmCo_2$	cub	$MgCu_2$			2.5–5.8	7–33		FF	10; 14, 27; 28, 29
$YbCo_2$	cub	$MgCu_2$							30
$LuCo_2$	cub	$MgCu_2$	$\chi = 3.5 \times 10^{-3}$ cm^3/mole						10; 7
YCo_2	cub	$MgCu_2$	$\chi = 3.7 \times 10^{-3}$ cm^3/mole						10; 2, 14, 16

1. Buschow and van der Goot (1969a)
2. Buschow (1971a)
3. Ferron (1970)
4. Yakinthos (1977a, 1978)
5. Burzo (1972)
6. Gignoux et al. (1970)
7. Givord and Lemaire (1971)
8. Buschow (1970)
9. Lemaire et al. (1968)
10. McMasters and Gschneidner (1964)
11. Buschow and Sherwood, unpublished
12. Farrell and Wallace (1966)
13. Crangle and Ross (1964)
14. Wallace and Skrabek (1964)
15. Burzo (1973)
16. Lemaire (1966a)
17. Voiron and Bloch (1971)
18. Dublon et al. (1976)
19. Moon et al. (1965)
20. Cannon et al. (1972)
21. Chatterjee and Taylor (1971)
22. Tsuchida et al. (1975)
23. Burzo (1975)
24. Buschow (1977b)
25. Gignoux et al. (1975)
26. Steiner and Ortbauer (1975)
27. Deportes et al. (1974)
28. Schweizer (1968)
29. Gignoux et al. (1976a, 1977a, b)
30. Buschow (1972)

TABLE A.3c
Rare earth cobalt compounds

Compound	Symmetry	Crystal structure	μ	T_c	T_{comp}	Magnetic structure	References
$CeCo_3$	rh	$PuNi_3$	0.2	78			1; 2
$PrCo_3$	rh	$PuNi_3$	3.1	330–349		F	1; 2, 3; 4
$NdCo_3$	rh	$PuNi_3$	5.45–5.6	387–396		F	1; 2, 3, 5; 4
$SmCo_3$	rh	$PuNi_3$	3.1				1; 6
$GdCo_3$	rh	$PuNi_3$	2.2–2.3	611–612			1; 2, 7
$TbCo_3$	rh	$PuNi_3$	3.4	506		FF	1; 2; 4
$DyCo_3$	rh	$PuNi_3$	4.3	450	400	FF	1; 2, 8; 9
$HoCo_3$	rh	$PuNi_3$	5.3–5.6	418	326–330	FF	1; 2, 3, 5; 4
$ErCo_3$	rh	$PuNi_3$	3.9–4.5	389–401	224	FF	1; 2, 3, 10; 10
$TmCo_3$	rh	$PuNi_3$	3.0	370	115		1; 2
$YbCo_3$	rh	$PuNi_3$		345			11; 6
$LuCo_3$	rh	$PuNi_3$	1.8	362			12; 12
YCo_3	rh	$PuNi_3$	1.4–2.1	301		F	1; 3, 12–14; 14
La_2Co_7	hex	Ce_2Ni_7	6.9^r	490			1; 15, 16
Ce_2Co_7	hex	Ce_2Ni_7	0.9	50			1; 6
Pr_2Co_7	hex	Ce_2Ni_7	10.5^r	574			1; 16, 17
Nd_2Co_7	hex	Ce_2Ni_7	13.1^r	609			1; 16, 17
Sm_2Co_7	hex	Ce_2Ni_7	9.1^r	713			1; 16, 17
Gd_2Co_7	rh	Gd_2Co_7	2.4–2.6	767–775	428		1; 2, 7, 17
Tb_2Co_7	rh	Gd_2Co_7	5.3	717	410		1; 2, 17
Dy_2Co_7	rh	Gd_2Co_7		640	380		1; 6, 17
Ho_2Co_7	rh	Gd_2Co_7	6.0	647	230		1; 2, 17
Er_2Co_7	rh	Gd_2Co_7	7.5	623–670	140		1; 17, 18
Y_2Co_7	rh	Gd_2Co_7	7.4	639		F	1; 14; 19
La_5Co_{19}	rh	Pr_5Co_{19}	1.93^r	616			20; 21
Ce_5Co_{19}	rh	Pr_5Co_{19}	0.17^r	293			20; 21
Pr_5Co_{19}	rh	Pr_5Co_{19}	2.97^r	690			20; 21
Nd_5Co_{19}	rh	Pr_5Co_{19}	31.0^r	714			20; 21
$LaCo_5$	hex	$CaCu_5$	7.3	840			15; 15, 22
$CeCo_5$	hex	$CaCu_5$	5.7–7.4	737		F	15; 23, 24
$PrCo_5$	hex	$CaCu_5$	9.9–10.0	912			15; 23, 25
$NdCo_5$	hex	$CaCu_5$	9.5–11.7	910		F	15; 23–25
$SmCo_5$	hex	$CaCu_5$	6.0–6.8	1020			15; 23, 24
$GdCo_5$	hex	$CaCu_5$	1.2–1.5	1008–1020			15; 7, 23, 24, 26
$TbCo_{5.1}$	hex	$CaCu_5$	0.57–0.8	980	99–120	FF	15; 23, 24; 24, 27
$DyCo_{5.2}$	hex	$CaCu_5$	0.7–1.5	966	93–170	FF	15; 23–25; 24, 27
$HoCo_{5.5}$	hex	$CaCu_5$	1.1–2.0	1000–1066	71	FF	15; 23, 24, 26; 28
$ErCo_{5.9}$	hex	$CaCu_5$	0.46–2.1	986–1123			15; 18, 24, 26, 29
$TmCo_6$	hex	$CaCu_5$	1.5–1.9	1020			24; 23, 24
YCo_5	hex	$CaCu_5$	6.8–8.2	977–997		F	15; 14, 22–24; 14, 28

TABLE A.3c (*cont.*)

Compound	Symmetry	Crystal structure	μ	T_c	T_{comp}	Magnetic structure	References
Ce_2Co_{17}	rh	Th_2Zn_{17}	24.5–26.1	1074–1083			30; 2, 31
Pr_2Co_{17}	rh	Th_2Zn_{17}	31–32.8	1160–1200			30; 2, 31, 32
Nd_2Co_{17}	rh	Th_2Zn_{17}	30.5–31	1150–1183			30; 2, 31
Sm_2Co_{17}	rh	Th_2Zn_{17}	20.1–23.7	1190–1200			30; 2, 31, 32
Gd_2Co_{17}	rh	Th_2Zn_{17}	13.5–14.4	1209–1240			30; 2, 7, 31, 32
Tb_2Co_{17}	rh	Th_2Zn_{17}	8.4–10.7	1180–1195			30; 2, 31, 33
Dy_2Co_{17}	hex	Th_2Ni_{17}	7–8.3	1152–1188			30; 2, 31
Ho_2Co_{17}	hex	Th_2Ni_{17}	5.8–7.7	1173–1183			30; 2, 31, 33
Er_2Co_{17}	hex	Th_2Ni_{17}	9.5–10.6	1160–1200			30; 2, 18, 31–33
Tm_2Co_{17}	hex	Th_2Ni_{17}	11.3–13.2	1180–1185			; 2, 31
Yb_2Co_{17}	hex	Th_2Ni_{17}					11
Lu_2Co_{17}	hex	Th_2Ni_{17}	27.4–27.6	1192–1200			12; 12, 31
Y_2Co_{17}	hex	Th_2Ni_{17}	26.2–27.8	1167–1200			30; 2, 12, 31, 32
$LaCo_{13}$	cub	$NaZn_{13}$	20.5	1290			34, 15, 22

[r]oom temperature value.

1. Buschow (1970)
2. Lemaire (1966a)
3. Bloch and Chaissé (1969)
4. Schweizer and Yakinthos (1969)
5. Narasimhan et al. (1972)
6. Buschow, unpublished
7. Burzo (1972)
8. Narasimhan et al. (1973a)
9. Yakinthos and Mentzafos (1975)
10. Georges et al. (1975)
11. Buschow (1972)
12. Givord and Lemaire (1971)
13. Figiel et al. (1976)
14. Koen et al. (1969)
15. Velge and Buschow (1968)
16. Buschow (1973c)
17. Strnat and Ray (1970)
18. Buschow et al. (1968)
19. Kren et al. (1969)
20. Ray et al. (1973)
21. Ray and Strnat (1975)
22. Heidemann et al. (1975)
23. Nesbitt et al. (1962)
24. Lemaire (1966b)
25. Wallace et al. (1971)
26. Wallace and Swearingen (1973)
27. Ermolenko et al. (1976)
28. James et al. (1962)
29. Buschow and Fast (1967)
30. Buschow (1966)
31. Strnat et al. (1966)
32. Deryagin and Kudrevatykh (1975)
33. Miller et al. (1976)
34. Buschow and Velge (1976)

TABLE A.3d
Rare earth iron compounds

Compound	Symmetry	Crystal structure	μ	T_c	T_{comp}	Magnetic structure	References
$CeFe_2$	cub	$MgCu_2$	2.38–2.59	221–240			1; 1, 2
$SmFe_2$	cub	$MgCu_2$	2.50–2.8	676–700			1; 2–4
$GdFe_2$	cub	$MgCu_2$	2.8–3.75	785–810			1; 1, 2, 5–7
$TbFe_2$	cub	$MgCu_2$	3.68–5.8	696–711		FF	1; 1, 3, 7–9
$DyFe_2$	cub	$MgCu_2$	4.9–7.31	633–638			1; 1, 7, 8
$HoFe_2$	cub	$MgCu_2$	5.1–6.67	597–614		FF	1; 1, 7, 10; 10
$ErFe_2$	cub	$MgCu_2$	4.75–5.85	590–595	480–490	FF	1; 1, 3, 7, 8; 11
$TmFe_2$	cub	$MgCu_2$	2.52–2.7	566–610	255–248		12; 3, 7
$YbFe_2$	cub	$MgCu_2$	1.8–2.3		31		13; 14
$LuFe_2$	cub	$MgCu_2$	2.70–2.97	558–610			13; 3, 5, 6, 17
YFe_2	cub	$MgCu_2$	2.78–3.1	535–554			1; 1, 3, 5–7
$SmFe_3$	rh	$PuNi_3$	4.5	650–651			16; 16, 17
$GdFe_3$	rh	$PuNi_3$	1.6–1.99	728–733	615–621		16; 5, 16, 18
$TbFe_3$	rh	$PuNi_3$	2.66–3.6	648–655	595–626	FF	16; 16, 18, 19
$DyFe_3$	rh	$PuNi_3$	3.67–4.6	600–612	544–550		16; 2, 18, 20, 21
$HoFe_3$	rh	$PuNi_3$	4.2–4.8	565–580	383–405	FF	16; 10, 16, 18, 22; 22
$ErFe_3$	rh	$PuNi_3$	3.2–3.5	550–555	222–250	FF, C	16; 16, 18; 23, 22
$TmFe_3$	rh	$PuNi_3$	1.6	535–539			16; 16, 18
YFe_3	rh	$PuNi_3$	5.0–5.49	490–539			24; 5, 6, 18
Nd_6Fe_{23}	cub	Th_6Mn_{23}		429			; 18
Sm_6Fe_{23}	cub	Th_6Mn_{23}					
Gd_6Fe_{23}	cub	Th_6Mn_{23}	15.3	468–659			24; 18, 25
Tb_6Fe_{23}	cub	Th_6Mn_{23}		574	280		24; 17, 18
Dy_6Fe_{23}	cub	Th_6Mn_{23}	14.8–15.1	424–545	265–280		24; 18, 21, 26
Ho_6Fe_{23}	cub	Th_6Mn_{23}	14.6–15	501–560	205	FF	24; 10, 18, 26; 10
Er_6Fe_{23}	cub	Th_6Mn_{23}	5.3–7.2	493–495	105–120		24; 10, 18, 26
Tm_6Fe_{23}	cub	Th_6Mn_{23}	18.0	475			24; 18, 26
Yb_6Fe_{23}	cub	Th_6Mn_{23}	32	480			24; 17
Lu_6Fe_{23}	cub	Th_6Mn_{23}	43.9	471–491			24; 5, 18
Y_6Fe_{23}	cub	Th_6Mn_{23}	37.8–47.5	478–484			24; 5, 27
Ce_2Fe_{17}	rh	Th_2Zn_{17}	28.8–30.6	220–270		C	24; 28–31; 30
Pr_2Fe_{17}	rh	Th_2Zn_{17}	30.6	283			24; 29;
Nd_2Fe_{17}	rh	Th_2Zn_{17}	30.0	327			24; 29;
Sm_2Fe_{17}	rh	Th_2Zn_{17}		385–420			24; 29, 33, 34
Gd_2Fe_{17}	hex	Th_2Ni_{17}	21–21.5	460–485			24; 5, 29, 35, 36
Tb_2Fe_{17}	hex	Th_2Ni_{17}	17–18.8	408			24; 19, 29
Dy_2Fe_{17}	hex	Th_2Ni_{17}	15.4–17.0	363–380			24; 21, 29, 36
Ho_2Fe_{17}	hex	Th_2Ni_{17}	14.8	325		FF	24; 10, 29; 10

TABLE A.3d (*cont.*)

Compound	Symmetry	Crystal structure	μ	T_c	T_{comp}	Magnetic structure	References
Er_2Fe_{17}	hex	Th_2Ni_{17}	16.2–18	298.5–314			24; 29, 33, 37, 38
Yb_2Fe_{17}	hex	Th_2Ni_{17}	25.6	280		C	39; 39; 39
Tm_2Fe_{17}	hex	Th_2Ni_{17}		276		C	24, 29, 31; 31, 40
Lu_2Fe_{17}	hex	Th_2Ni_{17}	33.8–34.7	264–270		C	24; 5, 29, 31; 30
Y_2Fe_{17}	hex	Th_2Ni_{17}	30.0–34.7	302.5–332		F	24; 5, 6, 28, 29, 36, 41; 30

1. Buschow and Van Stapele (1971)
2. Miskinis et al. (1975)
3. Wallace and Skrabek (1964)
4. Dublon et al. (1975)
5. Givord et al. (1971)
6. Burzo and Givord (1970)
7. Burzo (1971)
8. Clark and Belson (1973)
9. Barbara et al. (1977f)
10. Moreau et al. (1971)
11. Will and Bargouth (1971)
12. McMasters and Gschneidner (1964)
13. Cannon et al. (1972)
14. Meyer et al. (1977)
15. James et al. (1979)
16. Buschow (1971b)
17. Buschow,unpublished
18. Salmans et al. (1968)
19. Oestereicher and Pitts (1973)
20. Narasimhan et al. (1973a)
21. Van der Goot and Buschow (1970)
22. Simmons et al. (1973)
23. Davis et al. (1977)
24. Ray (1968)
25. Kirchmayr (1969)
26. Nesbitt et al. (1962)
27. Hoffer and Salmans (1968)
28. Buschow and Van Wieringen (1970)
29. Strnat et al. (1966)
30. Givord and Lemaire (1972)
31. Givord and Lemaire (1974a)
32. Weik et al. (1964)
33. Deryagin et al. (1974)
34. Buschow (1971c)
35. Steiner and Hrubec (1975)
36. Steiner et al. (1976)
37. Buschow and Van der Goot (1969b)
38. Gubbens and Buschow (1973)
39. Elemans and Buschow, unpublished
40. Elemans and Buschow (1974)
41. Burzo (1975)

TABLE A.3e
Rare earth manganese compounds

Compound	Symmetry	Crystal structure	μ_{eff}	θ_p	μ	T_c	T_N	Magnetic structure	References
$PrMn_2$	hex	$MgZn_2$	2.6	−80	(0.92)	(448)			1; 2
$NdMn_2$	hex	$MgZn_2$	4.9	−90					1; 3
$GdMn_2$	cub	$MgCu_2$	8.86	45	4.8		10		4; 3, 5, 6
$TbMn_2$	cub	$MgCu_2$		20	8.0		40	C	4; 5, 7
$DyMn_2$	cub	$MgCu_2$	10.9	−15					4; 3
$HoMn_2$	hex	$MgZn_2$							4;
$ErMn_2$	hex	$MgZn_2$	9.6–10.1	−90–30	7.72–7.91	20		F	2; 2, 3, 8, 9; 8
$TmMn_2$	hex	$MgZn_2$			5.44			AF	10; 8, 9; 8
$LuMn_2$	hex	$MgZn_2$		$\chi = 0.71 \times 10^{-3}$ emu/mole					6; 6
YMn_2	cub	$MgCu_2$		$\chi = 1.28 \times 10^{-3}$ emu/mole					4; 6
Nd_6Mn_{23}	cub	Th_6Mn_{23}	5.23	60	9.6	416			12; 3, 13
Sm_6Mn_{23}	cub	Th_6Mn_{23}	5.04	85	3.0	439			12; 3, 13
Gd_6Mn_{23}	cub	Th_6Mn_{23}	10.04	−90	49–54.5	461–468			12; 3, 6, 11, 13
Tb_6Mn_{23}	cub	Th_6Mn_{23}	15.3	−360	44.4	455			14; 3, 13
Dy_6Mn_{23}	cub	Th_6Mn_{23}	11.47	25	49.8	443			12; 3, 13
Ho_6Mn_{23}	cub	Th_6Mn_{23}	11.83	~5	49.2	434			12; 3, 13
Er_6Mn_{23}	cub	Th_6Mn_{23}	10.56	−20–30	45.6	415			12; 3, 11, 13
Tm_6Mn_{23}	cub	Th_6Mn_{23}			30.8				10; 13
Lu_6Mn_{23}	cub	Th_6Mn_{23}		378	8.9–9.2	378			10; 13; 6
Y_6Mn_{23}	cub	Th_6Mn_{23}	2.35	475–486	13.2	486		FF	12; 3, 6, 11, 14; 11
$NdMn_{12}$	tetr	$ThMn_{12}$	8.6	−196			135		12; 3
$GdMn_{12}$	tetr	$ThMn_{12}$	8–17.2	−25					12; 3, 15
$TbMn_{12}$	tetr	$ThMn_{12}$	9.7				110	C	12; 15, 16; 15
$DyMn_{12}$	tetr	$ThMn_{12}$	10.4–16.3	−398			110	C	12; 3, 15; 15
$HoMn_{12}$	tetr	$ThMn_{12}$	10.5				95	C	12; 3, 15; 15
$ErMn_{12}$	tetr	$ThMn_{12}$	9.8–13.2	−65			87	C	12; 3, 15; 15
$TmMn_{12}$	tetr	$ThMn_{12}$	7.6						16; 15
YMn_{12}	tetr	$ThMn_{12}$		$\chi = 3.7 \times 10^{-3}$ emu/g			120	C	17; 15; 15, 18

1. Teslyuk et al. (1964)
2. Oesterreicher (1971)
3. Kirchmayr (1969)
4. McMasters and Gschneidner (1964)
5. Nesbitt et al. (1963)
6. Buschow and Sherwood (1977b)
7. Corliss and Hastings (1964)
8. Felcher et al. (1965)
9. Barnes and Lunde (1975)
10. Wang and Holden (1965)
11. Delapalme et al. (1979)
12. Kirchmayr (1967)
13. De Savage et al. (1965)
14. Buschow (1977)
15. Deportes et al. (1977)
16. Wang and Gilfrich (1966)
17. Kirchmayr and Lihl (1967)
18. Deportes and Givord (1976)

TABLE A.3f
Compounds of rare earths with ruthenium, rhodium and palladium

Compound	Symmetry	Crystal structure	μ_{eff}	θ_p	μ	T_c	T_N	Magnetic structure	References
Gd_3Ru			8.05	105					1; 2
Dy_3Ru			10.6	8					1; 2
Y_3Ru			$\chi = 0.21 \times 10^{-3}$ cm^3/mole						1; 2
$Gd_{73}Ru_{27}$			8.1	75					1; 2
$Dy_{73}Ru_{27}$			10.6	18					1; 2
$Y_{73}Ru_{27}$			$\chi = 5.09 \times 10^{-3}$ cm^3/mole						1; 2
Gd_2Ru			7.95	48					1; 2
Dy_2Ru			10.5	15					1; 2
Y_2Ru			$\chi = 0.18 \times 10^{-3}$ cm^3/mole						1; 2
$LaRu_2$	cub	$MgCu_2$	$\chi = 0.33 \times 10^{-3}$ cm^3/mole						3; 4
$CeRu_2$	cub	$MgCu_2$	$\chi = 0.72 \times 10^{-3}$ cm^3/mole						3; 4
$PrRu_2$	cub	$MgCu_2$			0.6	38–40			3; 5
$NdRu_2$	cub	$MgCu_2$				28–35			3; 5
$GdRu_2$	hex	$MgZn_2$	7.9	100	6.3–7.9	83			3; 5
$DyRu_2$	hex	$MgZn_2$	10.5	35					2; 2
$ErRu_2$	hex	$MgZn_2$				8			3; 2
YRu_2	hex	$MgZn_2$	$\chi = 0.40 \times 10^{-3}$ cm^3/mole						3; 2, 4
Gd_3Rh	orh	Fe_3C	8.05	150			115		6; 7
Dy_3Rh	orh	Fe_3C	10.6	72					6; 7
Y_3Rh	orh	Fe_3C	$\chi = 0.44 \times 10^{-3}$ cm^3/mole						6; 7
La_7Rh_3	hex	Th_7Fe_3	Pauli paramagnetic						8; 8
Ce_7Rh_3	hex	Th_7Fe_3	2.31	13					8; 8
Pr_7Rh_3	hex	Th_7Fe_3	3.39	37					8; 8
Nd_7Rh_3	hex	Th_7Fe_3	3.43	58					8; 8
Sm_7Rh_3	hex	Th_7Fe_3	no C-W						8; 8
Gd_7Rh_3	hex	Th_7Fe_3	7.92–8.35	134–173			142		8; 8; 7
Tb_7Rh_3	hex	Th_7Fe_3	10.16	55					8; 8
Dy_7Rh_3	hex	Th_7Fe_3	10.55	41					8; 8
Ho_7Rh_3	hex	Th_7Fe_3	10.30	34					8; 8
Er_7Rh_3	hex	Th_7Fe_3	9.22	26					8; 8
Y_7Rh_3	orh	Th_7Fe_3	$\chi = 0.65 \times 10^{-3}$ cm^3/mole						9; 7
Gd_5Rh_3			7.98	98					1; 7
Y_5Rh_3			$\chi = 0.52 \times 10^{-3}$ cm^3/mole						1; 7
Gd_3Rh_2			7.9	73					1; 7
Y_3Rh_2			$\chi = 0.30 \times 10^{-3}$ cm^3/mole						1; 7
Gd_4Rh_3			7.92	33					1; 7
GdRh	cub	CsCl	7.7	28	6.45–6.6	24–29.5			6; 10–12
TbRh	cub	CsCl	9.4	12	5.15	19.2			13; 11, 14
DyRh	cub	CsCl	10.4–10.6	2–8	6.38	4.8			6; 7, 11
HoRh	cub	CsCl	10.3–10.5	−3–3	5.80		3.2		11; 7, 11
ErRh	cub	CsCl	9.4	−4	5.55		3.3		11; 14
TmRh	cub	CsCl	7.1	−7	3.90		2.7		11; 11
YRh	cub	CsCl	$\chi = -0.006 \times 10^{-3}$ cm^3/mole						11; 11, 15
$LaRh_2$	cub	$MgCu_2$	$\chi = 0.073 \times 10^{-3}$ cm^3/mole						16; 4
$CeRh_2$	cub	$MgCu_2$	$\chi = 0.88 \times 10^{-3}$ cm^3/mole						6; 20

TABLE A.3f (*cont.*)

Compound	Symmetry	Crystal structure	μ_{eff}	θ_p	μ	T_c	T_N	Magnetic structure	References
$PrRh_2$	cub	$MgCu_2$			2.2	8			17; 17
$NdRh_2$	cub	$MgCu_2$			1.7	7			17; 17
$SmRh_2$	cub	$MgCu_2$			0.6	20			6; 17
$EuRh_2$	cub	$MgCu_2$		no C-W					18; 17, 18
$GdRh_2$	cub	$MgCu_2$	7.9	75–80	6.9	73			6; 7, 17
$TbRh_2$	cub	$MgCu_2$			7.1	39			6; 17
$DyRh_2$	cub	$MgCu_2$	10.5	30–35	8.1	27			6; 7, 17
$HoRh_2$	cub	$MgCu_2$	10.6	20–23	7.7	16			17; 7, 17
$ErRh_2$	cub	$MgCu_2$			7.2	7			17; 17
$YbRh_2$	cub	$MgCu_2$	4.50	−6					19; 20
YRh_2	cub	$MgCu_2$		$\chi = 0.012 \times 10^{-3}$ cm^3/mole					6; 20
$GdRh_3$	hex	$CeNi_3$	7.85	53					6; 7
YRh_3	hex	$CeNi_3$		$\chi = 0.287 \times 10^{-3}$ cm^3/mole					6; 7
$GdRh_5$	hex	$CaCu_5$	7.95	38					6; 7
YRh_5	hex	$CaCu_5$		$\chi = 0.754 \times 10^{-3}$ cm^3/mole					6; 7
Gd_5Pd_2			7.6–7.8	333–335	6.87	335			1; 21, 22
Tb_5Pd_2	cub	Dy_5Pd_2	10.63	65.3			63.5		23; 24
Dy_5Pd_2	cub	Dy_5Pd_2	11.0–11.38	39–44			38		23; 22, 24
Ho_5Pd_2	cub	Dy_5Pd_2	10.6–11.48	31–63			22.5		23; 22, 24
Er_5Pd_2	cub	Dy_5Pd_2	9.77	17			15		23; 24
Tm_5Pd_2	cub	Dy_5Pd_2	7.46	4.5			7		23; 24
La_7Pd_3	hex	Th_7Fe_3		$\chi = 0.5 \times 10^{-3}$ emu/mole					8; 8
Ce_7Pd_3	hex	Th_7Fe_3	2.31	29					8; 8
Pr_7Pd_3	hex	Th_7Fe_3	3.39	30					8; 8
Nd_7Pd_3	hex	Th_7Fe_3	3.34	49					8; 8
Sm_7Pd_3	hex	Th_7Fe_3		no C-W behaviour					25; 25
Sm_3Pd_2				no C-W behaviour					1; 22
Gd_3Pd_2	tetr	U_3Si_2	7.7	265					26; 22
Dy_3Pd_2	tetr	U_3Si_2	10.8	22					26; 22
Ho_3Pd_2	tetr	U_3Si_2	10.6	2					26; 22
Eu_2Pd			8.2	33					1; 27
SmPd	orh	CrB		no C-W behaviour					25; 25
EuPd	orh	CrB	8.2	0		4.8			28; 27, 28
GdPd	orh	CrB	8.2–8.31	40–46		39.5			29; 22, 29
DyPd	cub	CsCl	10.5	29					26; 22
HoPd	cub	CsCl	10.4	20					26; 22
Gd_4Pd_5			8	2					1; 22
Dy_4Pd_5			10.5	16					1; 22
Ho_4Pd_5			10.3	10					1; 22
Pr_3Pd_4	rh	Pu_3Pd_4	3.46	−17					30; 31
Nd_3Pd_4	rh	Pu_3Pd_4	3.42	8			9.5		30; 31
Sm_3Pd_4	rh	Pu_3Pd_4		no C-W behaviour					30; 31
Gd_3Pd_4	rh	Pu_3Pd_4	8.09	−11					30; 31
Tb_3Pd_4	rh	Pu_3Pd_4	10.0	−12			20		30; 31
Dy_3Pd_4	rh	Pu_3Pd_4	10.4	−6			14		30; 31
Ho_3Pd_4	rh	Pu_3Pd_4	10.4	−2			12		30; 31

TABLE A.3f (*cont.*)

Compound	Symmetry	Crystal structure	μ_{eff}	θ_p	μ	T_c	T_N	Magnetic structure	References
Er_3Pd_4	rh	Pu_3Pd_4	9.71	−4					30; 31
Tm_3Pd_4	rh	Pu_3Pd_4	7.39	−2					30; 31
$SmPd_2$			no C-W behaviour						32; 25
$EuPd_2$	cub	$MgCu_2$	7.8	80					33; 33
$GdPd_2$			8.1	−12					32; 22
$DyPd_2$			10.3	6					32; 22
$HoPd_2$			10.3	3					32; 22
$LaPd_3$	cub	$AuCu_3$	$\chi = -0.135 \times 10^{-3}$ emu/mole						34; 35, 36
$CePd_3$	cub	$AuCu_3$	no C-W behaviour						37; 36, 38
$PrPd_3$	cub	$AuCu_3$	3.4–3.69	−7–0			1.05		37; 36, 38
$NdPd_3$	cub	$AuCu_3$	3.4–3.50	−5–1					37; 36, 38
$SmPd_3$	cub	$AuCu_3$	no C-W behaviour						25; 25, 36
$EuPd_3$	cub	$AuCu_3$	no C-W behaviour						27; 27, 36
$GdPd_3$	cub	$AuCu_3$	8.0–8.03	1.5–3			7.5		37; 36, 38
$TbPd_3$	cub	$AuCu_3$	9.3–9.61	1–3			2.0–2.5		37; 36, 38
$DyPd_3$	cub	$AuCu_3$	10.1–10.51	0–2					37; 36, 38
$HoPd_3$	cub	$AuCu_3$	9.3–10.38	0–4					34; 36, 38
$ErPd_3$	cub	$AuCu_3$	9.40–9.5	0					37; 36, 38
$TmPd_3$	cub	$AuCu_3$	7.5	−1			0.20		34; 36, 38
$YbPd_3$	cub	$AuCu_3$	4.3	0					34; 36, 38
$LuPd_3$	cub	$AuCu_3$	$\chi = -0.075 \times 10^{-3}$ emu/mole						34; 36, 38
YPd_3	cub	$AuCu_3$	$\chi = -0.073 \times 10^{-3}$ emu/mole						34; 36, 38

1. Crystal structure not known
2. Loebich and Raub (1976a)
3. Compton and Matthias (1959)
4. Shaltiel et al. (1964)
5. Bozorth et al. (1959)
6. Ghassem and Raman (1973)
7. Loebich and Raub (1975)
8. Olcese (1973)
9. Loebich and Raub (1976b)
10. Dormann and Buschow (1976)
11. Chamard-Bois (1974)
12. Buschow et al. (1975e)
13. Dwight et al. (1965)
14. Chamard-Bois et al. (1972)
15. Tamminga (1973)
16. Singh and Raman (1965)
17. Crangle and Ross (1964)
18. Bauminger et al. (1974a)
19. Dwight (1964)
20. Buschow, unpublished
21. Berkowitz et al. (1964)
22. Loebich and Raub (1973a)
23. Fornasini and Palenzona (1974)
24. Yakinthos et al. (1977a)
25. Jordan and Loebich (1975)
26. Loebich and Raub (1973b)
27. Harris and Longworth (1971)
28. Longworth and Harris (1973)
29. Pierre and Siaud (1968)
30. Palenzona and Iandelli (1974)
31. Yakinthos et al. (1977b)
32. Crystal structure not known
33. Wickman et al. (1968)
34. Harris and Raynor (1965b)
35. Gardner et al. (1971)
36. Gardner et al. (1972)
37. Harris et al. (1973)
38. Hutchens et al. (1971)

TABLE A.3g
Compound of rare earths with osmium, iridium and platinum

Compound	Symmetry	Crystal structure	μ_{eff}	θ_p	μ	T_c	T_N	Magnetic structure	References
$CeOs_2$	cub	$MgCu_2$			0				1; 2
$PrOs_2$	hex	$MgZn_2$			1.1	28			1; 2
$NdOs_2$	hex	$MgZn_2$			1.3	23			1; 2
$SmOs_2$	hex	$MgZn_2$			0.1	35			1; 2
$GdOs_2$	hex	$MgZn_2$			6.7	66			1; 2
$TbOs_2$	hex	$MgZn_2$			7.3	34			1; 2
$DyOs_2$	hex	$MgZn_2$			6.7	15			1; 2
$HoOs_2$	hex	$MgZn_2$			6.0	9			1; 2
$ErOs_2$	hex	$MgZn_2$			5.3	3			1; 2
La_7Ir_3	hex	Th_7Fe_3		Pauli paramagnetic					3; 3
Ce_7Ir_3	hex	Th_7Fe_3	2.35	−32					3; 3
Pr_7Ir_3	hex	Th_7Fe_3	3.46	+34					3; 3
$LaIr_2$	cub	$MgCu_2$		$\chi = 0.060 \times 10^{-3}$ emu/mole					4; 5
$CeIr_2$	cub	$MgCu_2$		$\chi = 0.655 \times 10^{-3}$ emu/mole					4; 6
$PrIr_2$	cub	$MgCu_2$			2.0	16			4; 2
$NdIr_2$	cub	$MgCu_2$			1.5	12			4; 2
$SmIr_2$	cub	$MgCu_2$			0.2	37			2; 2
$EuIr_2$	cub	$MgCu_2$			(0.4)	(70)			7; 2
$GdIr_2$	cub	$MgCu_2$			6.8	88			4; 2
$TbIr_2$	cub	$MgCu_2$			6.9	43		F	7; 2; 8
$DyIr_2$	cub	$MgCu_2$			7.7	23			7; 2
$HoIr_2$	cub	$MgCu_2$			7.5	12		F	8; 2; 8
$ErIr_2$	cub	$MgCu_2$			6.1	3			9; 2
$TmIr_2$	cub	$MgCu_2$			2.9	1			9; 2
$YbIr_2$	cub	$MgCu_2$			1.7	~0			7; 2
YIr_2	cub	$MgCu_2$		$\chi = 0.0135 \times 10^{-3}$ cm^3/mole					9; 6
La_7Pt_3	hex	Th_7Fe_3		Pauli paramagnetic					3; 3
Ce_7Pt_3	hex	Th_7Fe_3	2.30	33					3; 3
Pr_7Pt_3	hex	Th_7Fe_3	3.53	23					3; 3
Nd_7Pt_3	hex	Th_7Fe_3	3.40	55					3; 3
$LaPt_2$	cub	$MgCu_2$		$\chi = -0.029 \times 10^{-3}$ cm^3/mole					9; 5
$CePt_2$	cub	$MgCu_2$	2.33–2.57	−26–5			1.6		10; 11, 12
$PrPt_2$	cub	$MgCu_2$	3.43	0	1.60–1.67	6–13.5			10; 10, 13
$NdPt_2$	cub	$MgCu_2$	3.60	0	1.60–2.11	4–10			10; 10; 13
$SmPt_2$	cub	$MgCu_2$			0.19	6			10; 6
$EuPt_2$	cub	$MgCu_2$	7.9	105					14; 14
$GdPt_2$	cub	$MgCu_2$	8.10–8.40	30–32	6.28–6.98	36–46.5			10, 15; 10, 13, 15–17

TABLE A.3g (*cont.*)

Compound	Symmetry	Crystal structure	μ_{eff}	θ_p	μ	T_c	T_N	Magnetic structure	References
$TbPt_2$	cub	$MgCu_2$	9.61	17	6.67–7.08	16–26			10; 10, 13
$DyPt_2$	cub	$MgCu_2$	10.58	7	6.40–7.34	14–25			10; 10, 13
$HoPt_2$	cub	$MgCu_2$	10.60	2	7.65–8.88	9–19			10; 10, 13
$ErPt_2$	cub	$MgCu_2$	9.50	1	7.26–7.48	3–15			10; 10, 13
YPt_2	cub	$MgCu_2$		$\chi = 0.00647 \times 10^{-3}$ cm^3/mole					9; 6
$LaPt_3$	cub	$MgCu_2$		$\chi = 0.298 \times 10^{-3}$ emu/mole					15; 18
$CePt_3$	cub	$MgCu_2$	2.92	−108					15; 18
$PrPt_3$	cub	$MgCu_2$	3.84	−22					15; 18
$TbPt_3$	cub	$AuCu_3$	9.94	17		20.5–22		AF	15; 15; 20
$DyPt_3$	cub	$AuCu_3$				13.2		AF	19; 19; 19
$LaPt_5$	hex	$CaCu_5$		diamagnetic					9; 21
$CePt_5$	hex	$CaCu_5$							9; 21
$PrPt_5$	hex	$CaCu_5$	4.8						9; 21
$NdPt_5$	hex	$CaCu_5$				18			9; 21

1. Gschneidner (1961)
2. Bozorth et al. (1959)
3. Olcese (1973)
4. Compton and Matthias (1959)
5. Shaltiel et al. (1964)
6. Buschow, unpublished
7. Elliot (1964)
8. Felcher and Koehler (1963)
9. McMasters and Gschneidner (1964)
10. Crangle and Ross (1964)
11. Joseph et al. (1972)
12. Vijayaraghavan et al. (1968)
13. Wallace and Vlasov (1967)
14. Wickman et al. (1968)
15. Harris et al. (1973)
16. Taylor et al. (1976)
17. Dormann et al. (1977b)
18. Grover et al. (1977)
19. Arnold and Nereson (1969)
20. Nereson and Arnold (1970)
21. Narasimhan et al. (1973b)

TABLES A.4a–e

Magnetic properties of ternary intermetallic compounds of rare earth metals. Details pertaining to the structure type listed in columns 3 are given in table A.1. The values of the effective moments (μ_{eff}) and saturation moments (μ) are expressed in Bohr magnetons per formula unit. Values for the paramagnetic Curie temperatures (θ_p) Curie temperatures (T_c) and Néel temperatures (T_N) are given in K. The references comprise two groups separated by semicolons. The first reference pertains to literature of the crystal structure and lattice constants. Usually only one reference has been chosen out of the collection of references available. The second reference pertains to the literature in which the values of μ_{eff}, θ_p, μ, T_c and T_N are reported. Since in most cases the values of μ_{eff}, θ_p, μ, T_c and T_N reported by different authors in literature are dissimilar, lower and higher limits have been listed. The values given for χ of Pauli paramagnetic compounds are room temperature values and not values attained at 4.2 K since these latter may depend strongly on the amount of localized moment impurities present in the samples.

TABLE A.4a
Compounds of the type *RAB* (A = Ni, Cu, Pd; B = Al, In, Ga)

Compound	Symmetry	Crystal structure	μ_{eff}	θ_p	μ	T_c	T_N	References
PrNiAl	hex	Fe_2P	3.73	−10				1; 2
NdNiAl	hex	Fe_2P	3.84	5	1.6	15–17		1; 1, 2
GdNiAl	hex	Fe_2P	8.50–8.90	53–70	7.38–7.42	61–70		1; 1–3
TbNiAl	hex	Fe_2P	10.1–10.2	45–52	7.48–8.01	57–65		1; 1, 2
DyNiAl	hex	Fe_2P	11.0–11.1	30	7.38–7.82	39–47		1; 1, 2
HoNiAl	hex	Fe_2P	10.6–10.8	11–12	7.25–8.86	25–27		1; 1, 2
ErNiAl	hex	Fe_2P	9.8–9.85	−1–0	7.39–7.40	15–16		1; 1, 2
TmNiAl	hex	Fe_2P	7.8	−11	4.72	12	4.2	1; 1
LuNiAl	hex	Fe_2P		Pauli paramagnetic				1; 1
PrCuAl	hex	Fe_2P			1.7	36		1; 1
NdCuAl	hex	Fe_2P			1.8	25		1; 1
GdCuAl	hex	Fe_2P	8.2	55–90	7.01	67–90		1; 1, 3
TbCuAl	hex	Fe_2P	10.1	42	7.41	52		1; 1
DyCuAl	hex	Fe_2P	11.0	29	8.66	35		1; 1
HoCuAl	hex	Fe_2P	10.9	13	8.59	23		1; 1
ErCuAl	hex	Fe_2P	10.0	3	7.27	17		1; 1
TmCuAl	hex	Fe_2P	7.6	−8	4.71	13		1; 1
YbCuAl	hex	Fe_2P		no C-W	$\chi = 13.3 \times 10^{-3}$ cm^3/mole			1; 4
LuCuAl	hex	Fe_2P		Pauli paramagnetic				1; 1
YCuAl	hex	Fe_2P		$\chi = 0.8 \times 10^{-3}$ cm^3/mole				1; 3
GdNiIn	hex	Fe_2P		80		83		3; 3
GdPdIn	hex	Fe_2P		103		102		3; 3
YPdIn	hex	Fe_2P		$\chi = 1.4 \times 10^{-3}$ cm^3/mole				3; 3
YbNiGa			4.5	0				4; 4
GdCuSn	hex	In_2Cu		−32	2.3		24	5; 5
GdAuSn	hex	In_2Cu		−10	1.6		35	5; 5

1. Oesterreicher (1973b)
2. Leon and Wallace (1970)
3. Buschow (1975b)
4. Klaasse et al. (1976)
5. Oesterreicher (1977b)

TABLE A.4b
Compounds of the type RA_2B_2 (A = Cu, Co, Fe, Mn, Au; B = Ge, Si)

Compound	Symmetry	Crystal structure	μ_{eff}	θ_p	μ	T_c	T_N	References
$LaCo_2Ge_2$	tetr	$ThCr_2Si_2$		$\chi \approx 3 \times 10^{-3}$ cm^3/mole				1; 1
$CeCo_2Ge_2$	tetr	$ThCr_2Si_2$	2.74	−151.9				1; 1
$PrCo_2Ge_2$	tetr	$ThCr_2Si_2$	2.87	−8.7			13.3	1; 1
$NdCo_2Ge_2$	tetr	$ThCr_2Si_2$	3.34	−32.5			28	1; 1
$SmCo_2Ge_2$	tetr	$ThCr_2Si_2$	1.12	−43.8				1; 1
$GdCo_2Ge_2$	tetr	$ThCr_2Si_2$	6.96	−39.5			40	1; 1
$TbCo_2Ge_2$	tetr	$ThCr_2Si_2$	9.27	−43.9			30	1; 1
$DyCo_2Ge_2$	tetr	$ThCr_2Si_2$	10.17	−4.7			14.5	1; 1
$HoCo_2Ge$	tetr	$ThCr_2Si_2$	10.38	6.0			8	1; 1
$ErCo_2Ge_2$	tetr	$ThCr_2Si_2$	7.60	8.7				1; 1
$TmCo_2Ge_2$	tetr	$ThCr_2Si_2$	5.89	−0.8				1; 1
$LuCo_2Ge$	tetr	$ThCr_2Si_2$		$\chi \approx 5 \times 10^{-3}$ cm^3/mole				1; 1
YCo_2Ge_2	tetr	$ThCr_2Si_2$		$\chi \approx 2 \times 10^{-3}$ cm^3/mole				1; 1
$LaFe_2Si_2$	tetr	$ThCr_2Si_2$				668		2; 2
$PrFe_2Si_2$	tetr	$ThCr_2Si_2$				693		2; 2
$NdFe_2Si_2$	tetr	$ThCr_2Si_2$				713	11	2; 2, 3
$SmFe_2Si_2$	tetr	$ThCr_2Si_2$				723		2; 2
$GdFe_2Si_2$	tetr	$ThCr_2Si_2$				738	7	4; 2
$TbFe_2Si_2$	tetr	$ThCr_2Si_2$			6.9	820	5.5	5; 5
$DyFe_2Si_2$	tetr	$ThCr_2Si_2$				753		2; 2
$HoFe_2Si_2$	tetr	$ThCr_2Si_2$			8.5	820		5; 5
$ErFe_2Si_2$	tetr	$ThCr_2Si_2$			7.7	825		5; 5
YFe_2Si_2	tetr	$ThCr_2Si_2$				790		5; 5
$CeFe_2Ge_2$	tetr	$ThCr_2Si_2$				605		4; 5
$PrFe_2Ge_2$	tetr	$ThCr_2Si_2$					14	6; 6
$NdFe_2Ge_2$	tetr	$ThCr_2Si_2$				665	13	2; 5; 5
$GdFe_2Ge_2$	tetr	$ThCr_2Si_2$				683	11	4; 5, 6
$TbFe_2Ge_2$	tetr	$ThCr_2Si_2$					7.5	6; 6
$ErFe_2Ge_2$	tetr	$ThCr_2Si_2$						6; 6
$LaMn_2Ge_2$	tetr	$ThCr_2Si_2$			3.0	306		7; 7
$CeMn_2Ge_2$	tetr	$ThCr_2Si_2$			3.10	316		7; 7
$PrMn_2Ge_2$	tetr	$ThCr_2Si_2$			3.90	334		7; 7
$NdMn_2Ge_2$	tetr	$ThCr_2Si_2$			6.00	334		7; 7
$GdMn_2Ge_2$	tetr	$ThCr_2Si_2$			3.60		365	7; 7
$TbMn_2Ge_2$	tetr	$ThCr_2Si_2$			6.02	33		7; 7
$DyMn_2Ge_2$	tetr	$ThCr_2Si_2$			3.50	47, 57		7; 7
$HoMn_2Ge_2$	tetr	$ThCr_2Si_2$			5.50	37		7; 7
$ErMn_2Ge_2$	tetr	$ThCr_2Si_2$			6.00	38		7; 7
$CeAu_2Si_2$	tetr	$ThCr_2Si_2$	2.3	−2.8			6.6	8; 8
$PrAu_2Si_2$	tetr	$ThCr_2Si_2$	3.3	−9.2				8; 8
$NdAu_2Si_2$	tetr	$ThCr_2Si_2$	3.6	−6.1				8; 8
$SmAu_2Si_2$	tetr	$ThCr_2Si_2$	0.63	2.5			15.9	8; 8
$EuAu_2Si_2$	tetr	$ThCr_2Si_2$	6.7	−5.0	1.5	15.5		8; 8
$GdAu_2Si_2$	tetr	$ThCr_2Si_2$	6.7	−4.9			5.7	8; 8
$TbAu_2Si_2$	tetr	$ThCr_2Si_2$	8.0	−14.8			14.8	8; 8
$DyAu_2Si_2$	tetr	$ThCr_2Si_2$	10.6	−3.6			7.5	8; 8
$HoAu_2Si_2$	tetr	$ThCr_2Si_2$	10.6	−2.1	4.5	14.8		8; 8
$ErAu_2Si_2$	tetr	$ThCr_2Si_2$	9.6	13.0	2.9	40.0		8; 8
YAu_2Si_2	tetr	$ThCr_2Si_2$						8; 8
$PrCu_2Si_2$	tetr	$ThCr_2Si_2$	3.41	−2	0.53		(15)	4; 9
$EuCu_2Si_2$	tetr	$ThCr_2Si_2$		no C-W behaviour				10; 10

TABLE A.4b (*cont.*)

Compound	Symmetry	Crystal structure	μ_{eff}	θ_p	μ	T_c	T_N	References
$GdCu_2Si_2$	tetr	$ThCr_2Si_2$	7.28	−10			(12)	4; 9
$TbCu_2Si_2$	tetr	$ThCr_2Si_2$	9.33	−12			(10)	4; 9
$PrCu_2Ge_2$	tetr	$ThCr_2Si_2$					16	4; 11
$GdCu_2Ge_2$	tetr	$ThCr_2Si_2$					11	4; 11
$CeMn_2Si_2$	tetr	$ThCr_2Si_2$	3.0	330			379	12; 12
$CeAg_2Si_2$	tetr	$ThCr_2Si_2$	2.55	−20				4; 13

1. McCall et al. (1973)
2. Felner et al. (1975)
3. Pinto and Shaked (1973)
4. Rieger and Parthé (1969)
5. Sankar et al. (1976)
6. Malik et al. (1976)
7. Narasimhan et al. (1975)
8. Felner (1975)
9. Oesterreicher (1976)
10. Bauminger et al. (1974a)
11. Oesterreicher (1977)
12. Siek et al. (1978)
13. Sampathkumaran et al. (1979)

TABLE A.4c
Compounds of the type RA_4B_8 (A = Fe, Mn; B = Al)

Compound	Symmetry	Crystal structure	μ_{eff}	θ_p	μ	T_c	T_N	References
$LaFe_4Al_8$	tetr	$CeMn_4Al_8$					135.4	1; 2
$CeFe_4Al_8$	tetr	$CeMn_4Al_8$					159.7	1; 2
$PrFe_4Al_8$	tetr	$CeMn_4Al_8$						1; 2
$NdFe_4Al_8$	tetr	$CeMn_4Al_8$					142	1; 2
$SmFe_4Al_8$	tetr	$CeMn_4Al_8$						1; 2
$GdFe_4Al_8$	tetr	$CeMn_4Al_8$			4.1		172.3	1; 2
$TbFe_4Al_8$	tetr	$CeMn_4Al_8$			4.0		165.3	1; 2, 3
$DyFe_4Al_8$	tetr	$CeMn_4Al_8$						1; 2
$HoFe_4Al_8$	tetr	$CeMn_4Al_8$						1; 2
$ErFe_4Al_8$	tetr	$CeMn_4Al_8$					183.0	1; 2, 3
$TmFe_4Al_8$	tetr	$CeMn_4Al_8$					186.6	1; 2
$YbFe_4Al_8$	tetr	$CeMn_4Al_8$						1; 2
$LuFe_4Al_8$	tetr	$CeMn_4Al_8$					197.3	1; 2
YFe_4Al_8	tetr	$CeMn_4Al_8$					184.7	1; 2
$GdMn_4Al_8$	tetr	$CeMn_4Al_8$	8.06	−10				1; 2
YMn_4Al_8	tetr	$CeMn_4Al_8$		$\chi = 6 \times 10^{-3}$ cm^3/mole				1; 2
$YbCr_4Al_8$	tetr	$CeMn_4Al_8$	4.7	−220				1; 4
$CeCu_4Al_8$	tetr	$CeMn_4Al_8$	2.3	−107				1; 4

1. Buschow et al. (1976b)
2. Van der Kraan and Buschow (1977)
   Buschow and Van der Kraan (1978)
3. Bargouth et al. (1977)
4. Buschow, unpublished

TABLE A.4d
Compounds of the type RA_4B (A = Cu, Au; B = Ag, Ni)

Compound	Symmetry	Crystal structure	μ_{eff}	θ_p	μ	T_c	T_N	References
$NdCu_4Ag$	cub	$MgCu_4Sn$	3.39	−9.0			7	1; 1
$SmCu_4Ag$	cub	$MgCu_4Sn$		no C-W behaviour			7	1; 1
$GdCu_4Ag$	cub	$MgCu_4Sn$	7.86	−7.0			9	1; 1
$TbCu_4Ag$	cub	$MgCu_4Sn$	9.38	9.5			16.5	1; 1
$DyCu_4Ag$	cub	$MgCu_4Sn$	9.65	20	8.8	25		1; 1
$HoCu_4Ag$	cub	$MgCu_4Sn$	9.91	12.0	8.33	22		1; 1
$GdAu_4Ni$	cub	$MgCu_4Sn$	8.1	22	5.9	38		2; 2
$TbAu_4Ni$	cub	$MgCu_4Sn$	9.6	12	4.5	28		2; 2
$DyAu_4Ni$	cub	$MgCu_4Sn$	11.4	5	5.4	23		2; 2
$HoAu_4Ni$	cub	$MgCu_4Sn$	11.9	4	6.1	14		2; 2
$ErAu_4Ni$	cub	$MgCu_4Sn$	10.3	4	5.0	24		2; 2
$TmAu_4Ni$	cub	$MgCu_4Sn$	9.8	−14				2; 2
$YbAu_4Ni$	cub	$MgCu_4Sn$	6.4					2; 2

1. Takeshita et al. (1976) 2. Felner (1977)

TABLE A.4e
Compounds of the type RRh_4B_4

Compound	Symmetry	Crystal structure	μ_{eff}	θ_p	μ	T_c	T_N	References
$NdRh_4B_4$	tetr	YRh_4B_4						1; 2
$SmRh_4B_4$	tetr	YRh_4B_4						1; 2
$GdRh_4B_4$	tetr	YRh_4B_4				5.62		1; 2
$TbRh_4B_4$	tetr	YRh_4B_4				7.08		1; 2
$DyRh_4B_4$	tetr	YRh_4B_4				12.03		1; 2
$HoRh_4B_4$	tetr	YRh_4B_4				6.56		1; 2
$ErRh_4B_4$	tetr	YRh_4B_4	9.62	1		0.9		1; 2, 3
$TmRh_4B_4$	tetr	YRh_4B_4						1; 2
$LuRh_4B_4$	tetr	YRh_4B_4						1; 2
YRh_4B_4	tetr	YRh_4B_4						1; 2

1. Van den Berg and Matthias (1977) 3. Moncton et al. (1977)
2. Matthias et al. (1977)

References

Abbundi, R., A.E. Clark and N.C. Koon, 1979, J. Appl. Phys. **50**, 1671.

Abrahams, S.C., J.L. Bernstein, R.C. Sherwood, J.H. Wernick and H.J. Williams, 1964, J. Phys. Chem. Solids **25**, 1069.

Akulov, N., 1936, Z. Phys. **100**, 197.

Alekseev, P.A., I.P. Sadikov, I.A. Markova, E.M. Savitskii, V.F. Terekhova and O.D. Chistyakov, 1976, Sov. Phys. Solid State **18**, 389.

Aleonard, R., P. Morin, J. Pierre and D. Schmitt, 1975, Solid State Comm. **17**, 599.

Aleonard, R., P. Morin, J. Pierre and D. Schmitt, 1976, J. Phys. F **6**, 1361–1373.

Alfieri, G.T., E. Banks and K. Kanematsu, 1966, J. Appl. Phys. **37**, 1254.

Alfieri, G.T., E. Banks, K. Kanematsu and T. Ohoyama, 1967, J. Phys. Soc. Japan **23**, 507.

Andres, K. and E. Bucher, 1972, J. Low Temp. Phys. **9**, 267.

Andres, K., E. Bucher, S. Darack and J.P. Maita, 1972, Phys. Rev. B **6**, 2716.

Andres, K., J.E. Graebner and H.R. Ott, 1975, Phys. Rev. Lett. **35**, 1779.

Andres, K., E. Bucher, P.H. Schmidt, J.P. Maita and S. Darack, 1975b, Phys. Rev. B **11**, 4364.

Andres, K., P.H. Schmidt and S. Darack, 1975c, AIP Conf. Proc. **24**, 238.

Andres, K., P.S. Wang, Y.H. Wong, B. Lüthi and H.R. Ott, 1976, AIP Conf. Proc. **34**, 222–223.

Arif, S.K. and M.A.H. McCausland, 1975, J. Phys. F **5**, L247.

Arif, S.K., D.St.P. Bunbury, G.J. Bowden and R.K. Day, 1975, J. Phys. F **5**, 1048–1063.

Arif, S.K., I. Sigalas and D.St.P. Bunbury, 1977a, Phys. Stat. Sol. (a) **41**, 585.

Arif, S.K., J.W. Ross and M.A.H. McCausland, 1977b, Physica **86–88B**, 158.

Arnold, G. and N. Nereson, 1969, J. Chem. Phys. **51**, 1495.

Arnold, G., N. Nereson and C. Olson, 1967, J. Chem. Phys. **46**, 4041.

Atoji, M., 1968a, J. Chem. Phys. **48**, 3380.

Atoji, M., 1968b, J. Chem. Phys. **48**, 560.

Atoji, M., 1969a, J. Chem. Phys. **51**, 3877.

Atoji, M., 1969b, J. Chem. Phys. **51**, 3882.

Atoji, M., 1970, J. Chem. Phys. **52**, 6433.

Atoji, M., 1972a, J. Chem. Phys. **57**, 851.

Atoji, M., 1972b, J. Chem. Phys. **57**, 2402.

Atoji, M., 1972c, J. Chem. Phys. **57**, 2407.

Atzmony, U., 1977, in Crystal field effects in metals and alloys (ed. A. Furrer) (Plenum Press, New York).

Atzmony, U. and M.P. Dariel, 1974, Phys. Rev. B **10**, 2060–2067.

Atzmony, U. and M.P. Dariel, 1976, Phys. Rev. B **13**, 4006.

Atzmony, U., M.P. Dariel, E.R. Bauminger, D. Lebenbaum, I. Nowik and S. Ofer, 1973a, Phys. Rev. B **7**, 4220.

Atzmony, U., M.P. Dariel, E.R. Bauminger, D. Lebenbaum, I. Nowik and S. Ofer, 1973b, Proc. 10th Rare Earth Research Conf. 605–611.

Atzmony, U., M.P. Dariel and G. Dublon, 1976, Phys. Rev. B **14**, 3713.

Baenziger, N.C. and J.L. Moriarty, 1961, Acta. Crystallogr. **14**, 948.

Barbara, B., C. Bècle, R. Lemaire and R. Pauthenet, 1968, J. Appl. Phys. **39**, 1084.

Barbara, B., C. Bècle, R. Lemaire and D. Paccard, 1971a, J. de Phys. **32**, C1-299.

Barbara, B., C. Bècle, N.N. Nguyen and E. Siaud, 1971b, Proc. Conf. Rare Earth and Actinides, digest no. 3 (The Institute of Physics, London) pp. 219.

Barbara, B., C. Bècle and E. Siaud, 1971c, J. de Phys. **32**, suppl. C1-1126.

Barbara, B., V.N. Nguyen and E.S. Siaud, 1972, C.R. Acad. Sci. (Paris) **274**, 1053.

Barbara, B., D. Gignoux, D. Givord, F. Givord and R. Lemaire, 1973, Int. J. Mag. **4**, 77.

Barbara, B., M.F. Rossignol, H.G. Purwins and E. Walker, 1974, Phys. Stat. Sol. (a) **22**, 553.

Barbara, B., M.F. Rossignol, H.G. Purwins and E. Walker, 1975a, Solid State Comm. **17**, 1525.

Barbara, B., M.F. Rossignol and J.X. Boucherle, 1975b, Phys. Lett. **55A**, 321.

Barbara, B., J.X. Boucherle, M.F. Rossignol and J. Schweizer, 1976, Proc. Conf. on Neutron Scattering, Gatlingburg (Tenn.) June 1976, vol. 1, pp. 452.

Barbara, B., M.F. Rossignol, H.G. Purwins and E. Walker, 1977a, in Crystal field effects in metals and alloys (ed. A. Furrer) (Plenum Press, New York).

Barbara, B., J.X. Boucherle, M.F. Rossignol and J. Schweizer, 1977b, Physica **86–88B**, 83.

Barbara, B., M.F. Rossignol and M. Uehara, 1977c, Physica **86–88B**, 183.
Barbara, B., M.F. Rossignol, H.G. Purwins and E. Walker, 1977d, in Crystal field effects in metals and alloys (ed. A. Furrer) (Plenum Press, New York).
Barbara, B., H. Bartholin, D. Florence, M.F. Rossignol and E. Walker, 1977e, Physica **86–88B**, 177.
Barbara, B., J.P. Giraud, J. Laforest, R. Lemaire, E. Siaud and J. Schweizer, 1977f, Physica **86–88B**, 155.
Bargouth, M.O., G. Will and K.H.J. Buschow, 1977, J. Mag. Mag. Mat. **6**, 129.
Barnes, R.G. and B.K. Lunde, 1975, AIP Conf. Proc. **24**, 217–218.
Barnes, R.G., W.C. Harper, S.O. Nelson, D.K. Thome and D.R. Torgeson, 1976, J. Less-Common Met. **49**, 483.
Bauminger, E.R., I. Felner, D. Froindlich, D. Levron, I. Novik, S. Ofer and R. Yanovsky, 1974a, J. de Phys. C6-61.
Bauminger, E.R., I. Felner, D. Froindlich, A. Grill, D. Lebenbaum, I. Mayer, I. Novik, S. Ofer and M. Schieber, 1974b, Proc. ICM-73 TOM V (Nauka Publ. Co., Moscow, 1974).
Bauminger, E.R., D. Davidov, I. Felner, I. Nowik, S. Ofer and D. Shaltiel, 1977, Physica **86–88B**, 201.
Beckman, C.A., K.S.V.L. Narasimhan, W.E. Wallace, R.S. Craig and R.A. Butera, 1976, J. Phys. Chem. Sol. **37**, 235.
Bècle, C., 1968, Thesis, University of Grenoble.
Bècle, C. and R. Lemaire, 1967, Acta. Crystallogr. **23**, 840.
Bècle, C., R. Lemaire and D. Paccard, 1970, J. Appl. Phys. **41**, 855–863.
Beille, J., D. Bloch and J. Voiron and G. Parisot, 1977, Physica **86–88B**, 231.
Belakhovsky, M., J. Pierre and D.K. Ray, 1972, Phys. Rev. B **6**, 939.
Belov, K.P., A.K. Zvezdin, A.M. Kadomtseva and R.Z. Levitin, 1977, Sov. Phys. Ups. **19**, 574.
Berkowitz, A.E., F. Holtzberg and S. Methfessel, 1964, J. Appl. Phys. **35**, 1030.
Berndt, A.F., 1967, J. Less-Common Met. **13**, 366.
Besnus, M.J., P. Bauer and J.M. Génin, 1978, J. Phys. F. **8**, 191.
Birgenau, R.J., J. Als-Nielsen and E. Bucher, 1972, Phys. Rev. B **6**, 2724.
Bloch, D. and F. Chaissé, 1969, C.R. Acad. Sc. (Paris) **268**, 660–663.
Bloch, D. and R. Lemaire, 1970, Phys. Rev. B **2**, 2648.
Bloch, D., D.M. Edwards, M. Shimizu and J. Voiron, 1975, J. Phys. F **5**, 1217.
Bloch, J.M., D. Davidov, I. Felner and D. Shaltiel, 1976, J. Phys. F **6**, 1979–1988.
Bloembergen, N. and T.J. Rowland, 1955, Phys. Rev. **97**, 1679.
Borsa, F. and G. Olcese, 1973, Phys. Stat. Sol. (a) **17**, 631.
Borsa, F., R.G. Barnes and R.A. Reese, 1967, Phys. Stat. Sol. **19**, 359.
Bowden, G.J., D.St.P. Bunbury and A.P. Guimârães and R.E. Snijder, 1968, J. Phys. C **1**, 1376–1387.
Bozorth, R.M., B.T. Matthias, H. Suhl, E. Corenzwit and D.D. Davis, 1959, Phys. Rev. **115**, 1595.
Brouha, M. and K.H.J. Buschow, 1973, J. Appl. Phys. **44**, 1813.
Brouha, M. and K.H.J. Buschow, 1975, J. Phys. F. **5**, 543–544.
Brouha, M., K.H.J. Buschow and A.R. Miedema, 1974, IEEE Trans. **MAG-10**, 182.
Brun, T.O., J.S. Kouvel, G.H. Lander and R. Aitken, 1974a, Solid State Comm. **15**, 1157.
Brun, T.O., G.H. Lander, D.L. Price, G.P. Felcher and J.F. Reddy, 1974b, Phys. Rev. B **9**, 248.
Brun, T.O., J.S. Kouvel and G.H. Lander, 1976, Phys. Rev. B **13**, 5007–5020.
Bruzzone, G. and A. Ruggiero, 1963, Atti. Acad. Naz. Lin. Rend. **33**, 465.
Bruzzone, G., M.L. Fornasini and F. Merlo, 1971, J. Less-Common Met. **25**, 295.
Bucher, E. and J.P. Maita, 1973, Solid State Comm. **13**, 215.
Bucher, E., J.P. Maita, G.W. Hull, R.C. Fulton and A.S. Cooper, 1975, Phys. Rev. B **11**, 440.
Bucher, E., P.H. Schmidt, R.N. Castellano and P. Dernier, unpublished results cited in Buschow (1977d).
Bührer, W., M. Godet, H.G. Purwins and E. Walker, 1973, Solid State Comm. **13**, 881.
Burzo, E., 1971, Z. Angew. Phys. **32**, 127.
Burzo, E., 1972, Phys. Rev. **86**, 2882–2887.
Burzo, E., 1973, Int. J. Mag. **3**, 161–170.
Burzo, E., 1975, Solid State Comm. **16**, 759–761.
Burzo, E., 1976, Solid State Comm. **20**, 569.
Burzo, E. and F. Givord, 1970, C.R. Acad. Sc. (Paris) **270B**, 1159–1161.

Burzo, E. and J. Laforest, 1972, Int. J. Mag. **3**, 171.
Burzo, E. and I. Ursu, 1971, Solid State Comm. **9**, 2289.
Burzo, E., I. Urzu and J. Pierre, 1972, Phys. Stat. Sol. (b) **51**, 463.
Burzo, E., D.P. Lazard and M. Ciorascu, 1974, Phys. Stat. Sol. (b) **65**, K145.
Busch, G. and L. Schlapbach, 1978, Helv. Phys. Acta **51**, 5.
Buschow, K.H.J., 1965a, J. Less-Common Met. **9**, 452.
Buschow, K.H.J., 1965b, J. Less-Common Metals **8**, 209.
Buschow, K.H.J., 1966, J. Less-Common Met. **11**, 204.
Buschow, K.H.J., 1968, Z. Phys. Chem. N.F. **59**, 21.
Buschow, K.H.J., 1969, Phys. Lett. **29A**, 12.
Buschow, K.H.J., 1970, Les elements de terres rare, I, CNRS p. 101–112.
Buschow, K.H.J., 1971a, J. Appl. Phys. **42**, 3433–3437.
Buschow, K.H.J., 1971b, Phys. Stat. Sol. (a) **7**, 199–210.
Buschow, K.H.J., 1971c, J. Less-Common Met. **25**, 131.
Buschow, K.H.J., 1972, J. Less-Common Met. **26**, 329.
Buschow, K.H.J., 1973a, J. Less-Common Met. **31**, 165.
Buschow, K.H.J., 1973b, J. Less-Common Met. **33**, 239.
Buschow, K.H.J., 1973c, J. Less-Common Met. **33**, 311–312.
Buschow, K.H.J., 1974, J. Chem. Phys. **61**, 4666.
Buschow, K.H.J., 1975a, J. Less-Common Met. **43**, 55.
Buschow, K.H. J., 1975b, J. Less-Common Met. **39**, 185.
Buschow, K.H.J., 1976a, J. Less-Common Met. **44**, 301–306.
Buschow, K.H.J., 1976b, Solid State Comm. **19**, 421.
Buschow, K.H.J. 1977a, Solid State Comm. **21**, 1031.
Buschow, K.H.J., 1977b, J. Less-Common Met. **51**, 173.
Buschow, K.H.J., 1977c, Physica **86–88B**, 79.
Buschow, K.H.J., 1977d, in Boron and refractory borides (ed. V.I. Matkovich) (Springer-Verlag, Berlin).
Buschow, K.H.J., 1977e, Reports Prog. Phys., **40**, 1170.
Buschow, K.H.J., 1978, in Hydrides for energy storage (ed. A.F. Andresen and A.J. Maeland) (Pergamon Press, Oxford).
Buschow, K.H.J. and J.H.N. Creijghton, 1972, J. Chem. Phys. **57**, 3910.
Buschow, K.H.J. and J.F. Fast, 1966, Z. Phys. Chem. **50**, 51.
Buschow, K.H.J. and J.F. Fast, 1966, Phys. Stat. Sol. **16**, 467.
Buschow, K.H.J. and J.F. Fast, 1967, Phys. Stat. Sol. **21**, 593.
Buschow, K.H.J. and A. Oppelt, 1974, J. Phys. F **4**, 1246–1255.
Buschow, K.H.J. and C.J. Schinkel, 1976, Solid State Comm. **18**, 609–612.
Buschow, K.H.J. and R.C. Sherwood, 1977a, IEEE Trans. Magn. **MAG-13**, 1571.
Buschow, K.H.J. and R.C. Sherwood, 1977b, J. Appl. Phys. **48**, 4643.
Buschow, K.H.J. and R.C. Sherwood, 1978, J. Appl. Phys. **49**, 1480.
Buschow, K.H.J. and W.W. van den Hoogenhof, 1976, J. Less-Common Met. **45**, 309.
Buschow, K.H.J. and A.S. van der Goot, 1969a, J. Less-Common Met. **18**, 309–311.
Buschow, K.H.J. and A.S. van der Goot, 1969b, Phys. Stat. Sol. **35**, 515–522.
Buschow, K.H.J. and A.S. van der Goot, 1970, J. Less-Common Met. **20**, 309.
Buschow, K.H.J. and A.S. van der Goot, 1971a, J. Less-Common Metals, 24, 117.
Buschow, K.H.J. and A.S. van der Goot, 1971b, Acta. Crystallogr. **B27**, 4085.
Buschow, K.H.J. and A.M. van der Kraan, 1978, J. Phys. F. **8**, 921.
Buschow, K.H.J. and A.M. van Diepen, 1976, Solid State Comm. **19**, 79.
Buschow, K.H.J. and R.P. van Stapele, 1971, J. Phys. **32**, suppl. C1, 672–674.
Buschow, K.H.J. and F.J. van Steenwŷk, 1977, Physica **85B**, 122–126.
Buschow, K.H.J. and J.H.N. van Vucht, 1967, Philips Res. Rep. **22**, 233.
Buschow, K.H.J. and J.S. van Wieringen, 1970, Phys. Stat. Sol. **42**, 231–239.
Buschow, K.H.J. and W.A.J.J. Velge, 1967, J. Less-Common Met. **13**, 11–17.
Buschow, K.H.J., J.F. Fast, A.M. van Diepen and H.W. De Wijn, 1967, Phys. Stat. Sol. 24, 715.
Buschow, K.H.J., J.F. Fast and A.S. van der Goot, 1968, Phys. Stat. Sol. **29**, 825–829.
Buschow, K.H.J., H.W. de Wijn and A.M. van Diepen, 1969a, J. Chem. Phys. **50**, 137.

Buschow, K.H.J., A. van der Goot and J. Birkhan, 1969b, J. Less-Common Met. **19**, 433–436.

Buschow, K.H.J., A.M. van Diepen and H.W. de Wijn, 1970, J. Appl. Phys. **41**, 4609.

Buschow, K.H.J., H.J. van Daal, F.E. Maranzana and P.B. van Aken, 1971a, Phys. Rev. B **3**, 1662.

Buschow, K.H.J., A.M. van Diepen and H.W. de Wijn, 1971b, J. Appl. Phys. **42**, 4315.

Buschow, K.H.J., A. Oppelt and E. Dormann, 1972, Phys. Stat. Sol. (b) **50**, 647.

Buschow, K.H.J., A.M. van Diepen and H.W. de Wijn, 1973a, Phys. Rev. B **8**, 5134.

Buschow, K.H.J., A.M. van Diepen and H.W. de Wijn, 1973b, Solid State Comm. **12**, 417.

Buschow, K.H.J., B. van Laar and J.B.A.A. Elemans, 1974a, J. Phys. F **4**, 1517.

Buschow, K.H.J., A.M. van Diepen and H.W. De Wijn, 1974b, Solid State Comm. **15**, 903.

Buschow, K.H.J., J.P. de Jong, H.W. Zandbergen and B. van Laar, 1975a, J. Appl. Phys. **46**, 1352.

Buschow, K.H.J., W.J. Huiskamp, F.J. van Steenwijk and R.C. Thiel, 1975b, J. Phys. F **5**, 1625–1636.

Buschow, K.H.J., M. Brouha and C. Langereis, 1975c, Solid State Comm. **16**, 789.

Buschow, K.H.J., W.J. Huiskamp, H.Th. LeFever, F.J. van Steenwŷk and R.C. Thiel, 1975d, J. Phys. F, **5**, 1625.

Buschow, K.H.J., J.F. Olijhoek and A.R. Miedema, 1975e, Cryogenics, May 1975, 261.

Buschow, K.H.J., H.H. van Mal and A.R. Miedema, 1975f, J. Less-Common Met. **42**, 163.

Buschow, K.H.J., M. Brouha, H.J. van Daal, and A.R. Miedema, 1976a, Proc. Int. Conf. on Valence Instabilities, Rochester (ed. R.D. Parks) (Plenum Press, New York 1977).

Buschow, K.H.J., J.H.N. van Vucht and W.W. van den Hoogenhof, 1976b, J. Less-Common Met. **50**, 145.

Buschow, K.H.J., M. Brouha, J.W.M. Biesterbos and A.G. Dirks, 1977a, Physica **91B**, 261.

Buschow, K.H.J., M. Campagna and G.K. Wertheim, 1977b, Solid State Comm. **24**, 253.

Buschow, K.H.J., F.S.L. Hsu, R.C. Sherwood and K. Knorr, 1978, J. Appl. Phys. **49**, 1510.

Buyers, W.J.L., T.M. Holden and A. Perreault, 1975, Phys. Rev. B 11, 266 (1975).

Cable, J.W., W.C. Koehler and E.O. Wollan, 1964a, Phys. Rev. A **136**, 240.

Cable, J.W., W.C. Koehler and E.O. Wollan, 1964b, Bull. Am. Phys. Soc. **9**, 213.

Callen, H.B. and E. Callen, 1971, J. Phys. Chem. Sol. **27**, 1271.

Campbell, I.A., 1972, J. Phys. F **2**, L47.

Cannon, J.F., D. Robertson and H.T. Hall, 1972, Mat. Res. Bull. **7**, 5.

Carfagna, P.D. and W.E. Wallace, 1968, J. Appl. Phys. **39**, 5259; Proc. 7th Rare Earth Research Conf. (Coronado, Cal., 1968) 105–115.

Chamard-Bois, R., 1974, Thesis, University of Grenoble CNRS AO no. 9748.

Chamard-Bois, R., Nguyen Van Nhung and J. Pierre, 1972, Phys. Stat. Sol. (b) **49**, 161.

Chao, C.C., 1966, J. Appl. Phys. **37**, 2081–2084.

Chao, C.C. and P. Duwez, 1966, J. Appl. Phys. **37**, 2631.

Chao, C.C., H.L. Luo and P. Duwez, 1963, J. Appl. Phys. **34** 1971–1973.

Chao, C.C., H.L. Luo and P. Duwez, 1964, J. Appl. Phys. **35**, 257.

Chatterjee, D. and K.N.R. Taylor, 1971, J. Less-Common Met. **25**, 423–426.

Chazalviel, J.N., M. Campagna, G.K. Wertheim and P.Y. Schmidt, 1976, Solid State Comm. **19**, 725.

Chiotti, P., J.T. Mason, 1965, Trans. AIME **233**, 786.

Chouteau, G., J. Flouquet, J.P. Keradac, J. Palleau, J. Peyrard and R. Tournier, 1978, J. de Phys. **39**, L-461.

Clark, A.E. and H.S. Belson, 1974, Proc. ICM-73 TOM IV (Nauka Publ. Co., Moscow, 1973) p. 335.

Cock, G.J., L.W. Roeland, H.G. Purwins, E. Walker and A. Furrer, 1974, Solid State Comm. **15**, 845.

Cohen, R.L., M. Eibschütz and K.W. West, 1970, Phys. Rev. Lett. **24**, 383.

Coldea, M. and I. Pop, 1974, Phil. Mag. **1974**, 881.

Coles, B.R. and D. Griffith, 1961, Proc. Phys. Soc. **77**, 213.

Coles, B.R., T. Cole, J. Lambe and N. Laurance, 1962, Proc. Phys. Soc. **79**, 84.

Colombo, L. and G.L. Olcese, 1963, Atti Lincei Rend. Sci. Fis. Mat. Nat. **35**, 12.

Compton, V.B. and B.T. Matthias, 1959, Acta. Crystallogr. **12**, 651.

Cooper, B.R., 1972, Phys. Rev. **B6**, 2730.

Cooper, J.R., R. Rizzuto and G. Olcese, 1971, J. de Phys. **32**, C1-1136–1138.

Corliss, L.M. and J.M. Hastings, 1964, J. Appl. Phys. **35**, 1051.
Corliss, L.M. and J.M. Hastings, 1964, Coll. Int. CNRS **126**, 133.
Crangle, J., 1974, Phys. Lett. **48A**, 370.
Crangle, J. and J.W. Ross, 1964, Proc. Int. Conf. Mag., Nottingham, pp. 240.
Crecelius, G., H. Maletta, J. Hauk, J. Fink, G. Czjzek and H. Schmidt, 1977, J. Mag. Mag. Mat. **4**, 40.
Creijghton, J.H.N., P.R. Locher and K.H.J. Buschow, 1973, Phys. Rev. **7**, 4829.
Cyrot, M. and M. Lavagna, 1979, J. de Phys. **40**, 763.
Cyrot, M., D. Gignoux, F. Givord and M. Lavagna, 1979, J. de Phys. **40**, C5-171.
Dariel, M.P., V. Atzmony and D. Lebenbaum, 1973, Proc. 10th Rare Earth Research Conf. (Carefree, Arizona) 439–448.
Davidov, D., K. Maki, R. Orbach, C. Rettori and E.P. Chock, 1970, Solid State Comm. **12**, 621–625.
Davidov, D., A. Chelkowski, C. Rettori, R. Orbach and M.B. Maple, 1973a, Phys. Rev. B 1029.
Davidov, D., C. Rettori, K. Baberschke, E.P. Chock and R. Orbach, 1973b, Phys. Lett. **45A**, 161.
Davidov, D., C. Rettori, K. Baberschke and R. Orbach, 1973c, Phys. Lett. **45A**, 163.
Davis, R.L., R.K. Day and J.B. Dunlop, 1977, J. Phys. F **7**, 1885.
Debray, D. and J. Sakurai, 1974, Phys. Rev. B **9**, 2129–2133.
Debray, D. and M. Sougi, 1972, J. Chem. Phys. **57**, 2156–2159.
Debray, D. and M. Sougi, 1973, J. Chem. Phys. **58**, 1783–1786.
Debray, D., M. Sougi and P. Meriel, 1970a, J. Chem. Phys. **56**, 4325.
Debray, D.K., W.E. Wallace and E. Ryba, 1970b, J. Less-Common Met. **22**, 19.
Debray, D., B.F. Wortmann and S. Methfessel, 1975, Phys. Stat. Sol. (a) **30**, 713.
Debray, D., B.F. Wortmann and S. Methfessel, 1976, Phys. Rev. B, **14**, 4009.
Debray, D., M. Sougi and D. Meriel, unpublished results cited in Debray et al. (1975).
Deenadas, C., A.W. Thompson, D.S. Craig and W.E. Wallace, 1971, J. Phys. Chem. Sol. **37**, 1853.
DeGennes, P.G., 1962a, J. Phys. Radium. **23**, 510.
DeGennes, P.G., 1962b, J. Phys. Radium. **23**, 630.
Delapalme, A., J. Déportes, R. Lemaire, K. Hardman and W.J. James, 1979, J. Appl. Phys. **50**, 1987.
Deportes, J. and D. Givord, 1976, Solid State Comm. **19**, 845.
Deportes, J., D. Gignoux and F. Givord, 1974, Phys. Stat. Sol. (b) **64**, 29 (1974).
Deportes, J., D. Givord, J. Schweizer and F. Tasset, 1976, IEEE Trans. **MAG-12**, 1000.
Deportes, J., D. Givord, R. Lemaire and H. Nagai, 1977, Physica **86–88B**, 69.
Deryagin, A.V. and N.V. Kudrevatykh, 1975, Phys. Stat. Sol. (a) **30**, K129.
Deryagin, A., A. Ulyanov, W. Kudrevatykh, E. Barabanova, Y. Bashkov, A. Andreev and E. Tarasov, 1974, Phys. Stat. Sol. (a) **23**, K15–18.
De Savage, B.F., R.M. Bozorth, F.E. Wang and E.R. Callen, 1965, J. Appl. Phys. **36**, 992–993.
Devine, R.A.B., 1974, J. Phys. C **7**, L71.
Devine, R.A.B. and D.K. Ray, 1977, Solid State Comm. **21**, 941–943.
de Wijn, H.W., A.M. van Diepen and K.H.J. Buschow, 1967, Phys. Rev. **161**, 253.
de Wijn, H.W., K.H.J. Buschow and A.M. van Diepen, 1968, Phys. Stat. Sol. **30**, 759.
de Wijn, H.W., A.M. van Diepen and K.H.J. Buschow, 1973, Phys. Rev. (B) **7**, 524.
de Wijn, H.W., A.M. van Diepen and K.H.J. Buschow, 1976a, Phys. Stat. Sol. (b) **76**, 11.
de Wijn, H.W., A.M. van Diepen and K.H.J. Buschow, 1976b, Phys. Stat. Sol. (b) **77**, 11.
Dixon, J.M., 1973, Solid State Comm. **12**, 789.
Domngang, S. and A. Herr, 1973, Solid State Comm. **13**, 197–199.
Dormann, E. and K.H.J. Buschow, 1976, J. Appl. Phys. **47**, 1662–1667.
Dormann, E. and K.H.J. Buschow, 1977, Physica **86–88B**, 75.
Dormann, E., K.H.J. Buschow, K.N.R. Taylor, G. Brown and M.A.A. Issa, 1973, J. Phys. F **3**, 220.
Dormann, E., L. Schaafhausen and K.H.J. Buschow, 1976, J. Mag. Mag. Mat. **2**, 177.
Dormann, E., M. Huck and K.H.J. Buschow, 1977a, J. Mag. Mag. Mat. **4**, 47–54.
Dormann, E., M. Huck and K.H.J. Buschow, 1977b, Z. Phys. B **27**, 141.
Dublon, G. and U. Atzmony, 1977, J. Phys. F **7**, 1069.

Dublon, G., M.P. Dariel and U. Atzmony, 1975, Phys. Lett. **51A**, 262–264.
Dublon, G., M. Kroupp, M.P. Dariel and U. Atzmony, 1976, Phys. Stat. Sol. (b) **76**, 669.
Dwight, A.E., 1964, ANL Report 6868.
Dwight, A.E., R.A. Conner and J.W. Downey, 1965, Acta Cryst. **18**, 836.
Dwight, A.E., J.W. Downey and R.A. Conner, 1967, Acta. Crystallogr. **23**, 860.
Dwight, A.E., M.H. Mueller, R.A. Conner, J.W. Downey and H. Knot, 1968, Trans. Met. Soc. AIME, **247**, 2075.
Eagles, D.M., 1975, Z. Phys. **B21**, 171.
Eckrich, K., E. Dormann, A. Oppelt and K.H.J. Buschow, 1973, Int. J. Mag. **5**, 75.
Eckrich, K., E. Dormann, A. Oppelt and K.H.J. Buschow, 1976, Z. Phys. **B23**, 157.
Edwards, D.M., 1977, Physica **91B**, 3.
Edwards, L.R. and L.C. Bartel, 1972, Phys. Rev. B **5**, 1064.
Elemans, J.B.A.A. and K.H.J. Buschow, 1974, Phys. Stat. Sol. (a) **24**, K125.
Elliot, R.P., 1964, in Rare earth research III (ed. L. Eyring) (Gordon and Breach, New York).
Elliot, R.P., 1965, Constitution of binary alloys, 1st suppl. (McGraw-Hill, New York).
Ermolenko, A.S., 1974, Proc. ICM-73 TOM I (Nauka Publ. Co. Moscow, 1974) 231.
Ermolenko, A.S., E.V. Rozenfel'd, Yu.P. Irkhin, V.V. Kelarev, A.F. Rozhda, S.K. Sidorov, A.N. Pirogov and A.P. Vokhmyanin, 1976, Sov. Phys. JETP **42**, 885.
Etourneau, J., J.P. Mercurio, R. Naslain and P. Hagenmuller, 1970, J. Solid State Chem. **2**, 333.
Farrell, J. and W.E. Wallace, 1966, J. Inorg. Chem. **5**, 105.
Felcher, G.P. and W.C. Koehler, 1963, Phys. Rev. **131**, 1518.
Felcher, G.P., L.M. Corliss and J.M. Hastings, 1965, J. Appl. Phys. **36**, 1001.
Felner, I., 1975, J. Phys. Chem. Solids **36**, 1063.
Felner, I., 1977, Solid State Comm. **21**, 267.
Felner, I., I. Mayer, A. Grill and M. Schieber, 1975, Solid State Comm. 16, 1005.
Ferron, J.L., 1970, Les elements des terres rares, II, CNRS p. 75.
Ferron, J.L., R. Lemaire, D. Paccard and D. Pauthenet, 1968, C.R. Acad. Sci. Paris, **267**, 371.
Figiel, H., A. Oppelt, E. Dormann and K.H.J. Buschow, 1976, Phys. Stat. Sol. (a) **36**, 275–283.
Fisk, Z., 1971, Phys. Lett. **34A**, 261.
Fisk, Z., R.H. Taylor and B.R. Coles, 1971, J. Phys. C **4**, L292.
Fornasini, M.L. and F. Merlo, 1967, Atti. Accad. Naz. Linc. Rc. **43**, 357.
Fornasini, M.L. and A. Palenzona, 1974, J. Less-Common Met. **38**, 77.
Forsyth, J.B., unpublished results cited in Stewart and Coles (1974).
Freeman, A.J., 1972, in Magnetic properties of rare earth metals (ed. R.J. Elliot) (Plenum Press, New York).
Freeman, A.J. and R.E. Watson, 1962, Phys. Rev. **127**, 2058.
Friedel, J., G. Lehman and S. Olszewski, 1961, J. Appl. Phys. **32**, 325S.
Fuess, H., D. Givord, A.R. Gregory and J. Schweizer, 1979, J. Appl. Phys. **50**, 2000.
Furrer, A., 1975, J. Phys. C **8**, 824–838.
Furrer, A. and H.G. Purwins, 1976, J. Phys. C **9**, 1491.
Ganapathy, E.V., K. Kugimiya, H. Steinfink and D.I. Tchernev, 1976, J. Less-Common Met. **44**, 245.
Garnder, W.E., J. Penfold and I.R. Harris, 1971, J. de Phys. **37**, C1-1139.
Gardner, W.E., J. Penfold, T.F. Smith and I.R. Harris, 1972, J. Phys. F **2**, 133.
Geballe, T.H., B.T. Matthias, K. Andres, J.P. Maita, A.S. Cooper and E. Corenzwit, 1968, Science **160**, 1443.
Georges, R., J. Schweizer and J. Yakinthos, 1975, J. Phys. Chem. Sol. **36**, 415–419.
Ghassem, H. and A. Raman, 1973, Z. Metallkde **64**, 197.
Gignoux, D. and F. Givord, 1977, Solid State Comm. **21**, 499.
Gignoux, D and R. Lemaire, 1974, Solid State Comm. **14**, 877.
Gignoux, D., R. Lemaire and D. Paccard, 1970, Solid State Comm. **8**, 391.
Gignoux, D., F. Givord and R. Lemaire, 1975, Phys. Rev. **12**, 3878.
Gignoux, D., D. Givord, F. Givord, W.C. Koehler and R.M. Moon, 1976a, Phys. Rev. **B14**, 162.
Gignoux, D., D. Givord and A. Del Moral, 1976b, Solid State Comm. **19**, 891.
Gignoux, D., F. Givord, W.C. Koehler and R.M. Moon, 1977a, J. Mag. Mag. Mat. **5**, 172.
Gignoux, D., F. Givord and J. Schweizer, 1977b, J. Phys. F **7**, 1823.
Gignoux, D., F. Givord, R. Perrier de la Bathie and F. Sayetat, 1979, J. Phys. F **9**, 763.

Gignoux, D., R. Lemaire and P. Molho (1980), J. Mag. Mag. Mat. (Proc. ICM 1979).
Givord, D. and R. Lemaire, 1972, C.R. Acad. Sc. (Paris) **274**, 1166–1169.
Givord, D. and R. Lemaire, 1973, Proc. ICM-73 TOM III, 492–496. (Nauka Publ. Co., Moscow, 1974).
Givord, D. and R. Lemaire, 1974, IEEE Trans. **MAG-10**, 109 (1974).
Givord, D., F. Givord and R. Lemaire, 1971, J. de Phys. Suppl. C1, 668–669.
Givord, D., F. Givord, D. Gignoux, W.C. Koehler and R.M. Moon, 1976, J. Phys. Chem. Solids **37**, 567–569.
Givord, D., J. Laforest, J. Schweizer and F. Tasset, 1979, J. Appl. Phys. **50**, 2008.
Givord, F. and R. Lemaire, 1971, Solid State Comm. **9**, 341–346.
Givord, F. and J.S. Shah, 1972, C.R. Acad. Sci. (Paris) B **274**, 923.
Glausinger, W.S., 1975, Phys. Stat. Sol. (b) **70**, K151.
Goebel, U., E. Dormann and K.H.J. Buschow, 1975, J. Phys. F **5**, 2198–2207.
Gomes, A.A. and A.P. Guimârães, 1974, J. Phys. F **4**, 1454.
Görlich, E.A., A.Z. Hrynkiewicz, K. Latka, R. Kmiec, A. Szytula and K. Tomala, 1979, J. de Phys. **40**, C2-656.
Greedan, J.E. and V.U.S. Rao, 1973, J. Solid State Chem. **6**, 387; **8**, 368.
Gross, W., K. Knorr, A. Murani and K.H.J. Buschow, 1977, in Crystal field effects in metals and alloys (ed. A. Furrer) (Plenum Press, New York).
Grover, A.K., L.C. Gupta and R. Vijayaraghavan, 1977, Physica **86–88B**, 81.
Gschneidner, K.A., 1961, Rare earth alloys (Van Nostrand, New York).
Gualtieri, D.M., K.S.V.L. Narasimhan and W.E. Wallace, 1976, AIP Conf. Proc. **34**, 219.
Gubbens, P.C.M. and K.H.J. Buschow, 1973, J. Appl. Phys. **44**, 3739.
Gubbens, P.C.M. and K.H.J. Buschow, 1974, Proc. ICM-73 TOM V (Nauka Publ. Co., Moscow, 1974) pp. 60–66.
Gubbens, P.C.M., J.H.F. van Apeldoorn, A.M. van der Kraan and K.H.J. Buschow, 1974a, J. Phys. F **4**, 921–927.
Gubbens, P.C.M., J.J. van Loef and K.H.J. Buschow, 1974b, J. de Phys. **35**, C6-617–620.
Gubbens, P.C.M., A.M. van der Kraan and K.H.J. Buschow, 1977, Physica **86–88B**, 199.
Gubbens, P.C.M., A.M. van der Kraan and K.H.J. Buschow, 1978, Solid State Comm. **26**, 107.
Guimârães, A.P., 1971, Ph.D. Thesis, Manchester.
Guimârães, A.P. and D. St. P. Bunbury, 1973, J. Phys. F **3**, 885–892.
Hacker, H. and R.M. Gupta, 1976, J. Less-Common Met. **45**, 331.
Hacker, H. and M.S. Liu, 1968, Solid State Comm. **6**, 379.
Hacker, H., R. Gupta and M.L. Shepard, 1972, Phys. Stat. Sol. (a) **9**, 601.
Halstead, T.K., 1974, Solid State Comm. **11**, 114.
Halstead, T.K., N.A. Abood and K.H.J. Buschow, 1976, Solid State Comm. **19**, 425.
Hansen, M., 1958, Constitution of binary alloys (McGraw-Hill, New York).
Harmon, B.N. and A.J. Freeman, 1974, Phys. Rev. B **10**, 1979.
Harris, I.R. and G. Longworth, 1971, J. Less-Common Met. **23**, 281.
Harris, I.R. and G.V. Raynor, 1965a, J. Less-Common Met. **9**, 7.
Harris, I.R. and G.V. Raynor, 1965b, J. Less-Common Met. **9**, 263.
Harris, I.R., R.C. Mansey and G.V. Raynor, 1965, J. Less-Common Metals **9**, 270.
Harris, I.R., W.E. Gardner and R.H. Taylor, 1973, J. Less-Common Met. **31**, 151.
Hasegawa, A. and J. Kübler, 1974, Z. Phys. **269**, 31–34.
Haszko, S.E., 1961, Trans. Met. Soc. AIME 221, 201.
Havinga, E.E., H. Damsma and M.H. van Maaren, 1970, J. Phys. Chem. Sol. **31**, 2653.
Havinga, E.E., K.H.J. Buschow and H.J. van Daal, 1973, Solid State Comm. **13**, 621.
Heidemann, A., D. Richter and K.H.J. Buschow, 1975, Z. Phys. B **22**, 367–372.
Heinrich, G. and A. Meyer, 1977, Solid State Comm. **21**, 21–24.
Hendy, P. and E.W. Lee, 1978, Phys. Stat. Sol(a) **50**, 101.
Henry, W.E., 1962, Bull. Am. Phys. Soc. **7**, 474.
Herbst, V., J. Schraub, E. Dormann and K.H.J. Buschow, 1974, Phys. Stat. Sol. (b) **61**, K101.
Hill, R.W. and J.M. Machado da Silva, 1969, Phys. Lett. **30A**, 13.
Hillenbrand, B. and M. Wilhelm, 1972, Phys. Rev. Lett. **40A**, 387.

Hilscher, G., N. Buis and J.J.M. Franse, 1977, Physica **91B**, 170.
Hilzinger, H.R. and H. Kronmüller, 1972, Phys. Stat. Sol(b) **54**, 593.
Hirst, L.L., 1970, Phys. Kond. Mat. **11**, 255.
Hoffer, G.L. and L.R. Salmans, 1968, Proc. 7th Rare Earth Conf. Coronado, Cal., p. 337.
Holtzberg, E., R.J. Gambino and T.R. McGuire, 1967, J. Phys. Chem. Sol. **28**, 2283.
Houmann, J.G., P. Bak, H.G. Purwins and E. Walker, 1974, J. Phys. C **7**, 2691.
Hutchens, R.D. and W.E. Wallace, 1971, J. Solid State Chem. **3**, 564.
Hutchens, R.D., V.U.S. Rao, J.E. Greedan, W.E. Wallace and R.S. Craig, 1971, J. Appl. Phys. **42**, 1293.
Hutchens, R.D., W.E. Wallace, R.S. Craig and V.U.S. Rao, cited in: W.E. Wallace, 1973, Rare earth intermetallics (Academic Press, New York).
Hutchings, M.T., 1964, Solid State Phys. **16**, 227.
Iandelli, A., 1955, Proc. 16e Congr. Int. Chim. Pure. Appl. Pans 1957, 35.
Iandelli, A., 1960, Acad. Nazl. Lincei Rend. Classe Sci. Fis. Mat. Nat. **29**, 62.
Iandelli, A., 1964, Z. Anorg. Allg. Chem. **330**, 221.
Iandelli, A., and R. Ferro, 1954, Gazz. Chim. Ital. **84**, 463.
Iandelli, A. and A. Palenzona, 1964, Atti. Accad. Naz. Lincei Rend. Sci. Fis. Mat. Nal **37**, 165.
Iandelli, A. and A. Palenzona, 1965, J. Less-Common Met. **9**, 1.
Iandelli, A. and A. Palenzona, 1968, J. Less-Common Met. **15**, 273.
Iandelli, A. and A. Palenzona, 1969a, J. Less-Common Met. **18**, 221.
Iandelli, A. and A. Palenzona, 1969b, J. Less-Common Met. **12**, 333.
Iandelli, A. and A. Palenzona, 1972, J. Less-Common Met. **29**, 293.
Ihrig, H. and S. Methfessel, 1976a, Z. Phys. B **24**, 385.
Ihrig, H. and S. Methfessel, 1976b, Z. Phys. B **24**, 381–383.
Ihrig, H., D.T. Vigren, J. Kübler and S. Methfessel, 1973, Phys. Rev. B **8**, 4525–4533.
Inoue, T., S.G. Sankar, R.S. Craig, W.E. Wallace and K.A. Gschneidner, 1977, in Crystal field effects in metals and alloys (ed. A. Furrer) (Plenum Press, New York).
Irkhin, Yu. P. and E.V. Rozenfel'd, 1974, Sov. Phys. Solid State **16**, 310.
Jaccarino, V. and L.R. Walker, 1965, Phys. Rev. Lett. **15**, 259.
Jaccarino, V., B.T. Matthias, M. Peter, H. Suhl and J.H. Wernick, 1960, Phys. Rev. Lett. **5**, 251.
James, W., R. Lemaire and F. Bertaut, 1962, C.R. Acad. Sci. Paris **255**, 896.
James, W.J., K. Hardmann, W. Yelon, J. Keem and J. Croat, 1979, J. Appl. Phys. **50**, 2006.
Jefferson, J.H. and K.H.W. Stevens, 1976, J. Phys. C. **9**, 2151.
Jordan, R.G. and O. Loebich, 1975, J. Less-Common Met. **39**, 55.
Joseph, R.R., K.A. Gschneidner and R.E. Hungsberg, 1972, Phys. Rev. B **5**, 1878.
Kaneko, T., S. Miura, M. Ohashi and H. Yamauchi, 1974, Proc. ICM-73 TOM V (Nauka Publ. Co., Moscow, 1974) pp. 370.
Kanematsu, K., G.T. Alfieri and E. Banks, 1969, J. Phys. Soc. Japan **26**, 244.
Kaplan, N., E. Dormann, K.H.J. Buschow and D. Lebenbaum, 1973, Phys. Rev. B **7**, 40.
Kaplan, T.A. and D.H. Lyons, 1963, Phys. Rev. **129**, 2072.
Kasuya, T., 1956, Prog. Theor. Phys. (Kyoto) **16**, 45.
Kawano, S., H. Umezaki and T. Shibata, 1974, An. Rep. Reactor Inst. Kyoto Univ. **7**, 99.
Kazakov, A.A., A.V. Deryagin, N.V. Kudrevatykh, and V.A. Reymer, 1975, Sov. Phys. Solid State **16**, 2429.
Kimball, C.W., A.E. Dwight, G.M. Kalvius, B. Dunlap and M.V. Nevitt, 1975, Phys. Rev. B **12**, 819–823.
Kirchmayr, H.R., 1966, IEEE Trans. **MAG-2**, 493.
Kirchmayr, H.R., 1967, Z. Kristallogr. **124**, 152–160.
Kirchmayr, H.R., 1969, Z. Angew. Phys. **27**, 18.
Kirchmayr, H. and F. Lihl, 1967, USAF report, AFML-TR-66-366.
Kissel, F. and W.E. Wallace, 1966, J. Less-Common Met. **11**, 417.
Klaasse, J.C.P., J.W.E. Sterkenburg, A.H.M. Bleyendaal and F.R. de Boer, 1973, Solid State Comm. **12**, 561.
Klaasse, J.C.P., W.C.M. Mattens, F.R. de Boer and P.F. de Chatel, 1976, AIP-Conf. Proc. **34**, 184.
Klein, H.P., A. Menth and R.S. Perkins, 1975, Physica **20B**, 153.

Klimker, H., M. Rosen, M.P. Dariel and U. Atzmony, 1974, Phys. Rev. B **10**, 2968.
Koen, E., J. Schweizer and F. Tasset, 1969, Phys. Rev. **186**, 479–483.
Köster, W. and J. Meixner, 1965, Z. Metallkde **56**, 695.
Kren, E., J. Schweizer and F. Tasset, 1969, Phys. Rev. **186**, 479.
Krypiakevich, P.I. and V.I. Evdokimenko, 1967, Z. Anorg. Allg. Chem. **355**, 104–112.
Krypiakevich, P.I., V.I. Evdokimenko and E.I. Gladyshevskii, 1960, Sov. Phys. Cryst. **9**, 330–331.
Kuijpers, F.A., 1973, Philips Res. Repts. Suppl. no. 2.
Kuzma, J.B. and V.J. Markiv, 1964, Soviet Phys. Cryst. **9**, 218.
Kuzma, J.B., R.V. Skolozdra, J.V. Markiv, 1964, Dopovidi Akad. Nauk. Ukr. RSR **1964**, 1070.
LaForest, J., R. Lemaire, D. Paccard and R. Pauthenet, 1967, C.R. Acad. Sci. (Paris) B **264**, 676–79.
LaPlaca, S., I. Binder and B. Post, 1961, J. Inorg. Chem. **18**, 113.
Lea, K.R., M.J. Leask and W.P. Wolf, 1962, J. Phys. Chem. Solids **23**, 1381.
Lemaire, R., 1966a, Cobalt **33**, 201.
Lemaire, R., 1966b, Cobalt **32**, 132.
Lemaire, R. and D. Paccard, 1967, Bull. Soc. Fr. Miner. Cristallogr. **90**, 311.
Lemaire, R. and D. Paccard, 1970, C.R. Acad. Sci. Paris **270**, B1131.
Lemaire, R., D. Paccard and R. Pauthenet, 1967, C.R. Acad. Sci. Paris **265**, B 1280.
Lemaire, R., C. Berthet-Columnas, J. LaForest, R. Pauthenet and J. Schweizer, 1968, Cobalt **39**, 97–101.
Leon, B. and W.E. Wallace, 1970, J. Less-Common Met. **22**, 1.
Lethuillier, R., 1974, Proc. ICM-73, TOM IV (Nauka Publ. Co., Moscow, 1974) pp. 50.
Lethuillier, P. and J. Chaussy, 1976a, J. de Phys. **37**, 123.
Lethuillier, P. and J. Chaussy, 1976b, Phys. Rev. B **13**, 3132.
Lethuillier, P. and A. Percheron-Guegan, 1976, J. Less-Common Met. **46**, 85.
Lethuillier, P., G. Quezel-Ambrunaz and A. Percheron, 1973, Solid State Comm. **12**, 105.
Lethuillier, P., J. Pierre, K. Knorr and W. Drexel, 1975, J. de Phys. **36**, 329.
Levy, M., 1971, J. Appl. Phys. **42**, 1702.
Levy, P.M., 1969, Solid State Comm. **7**, 1813.
Liu, S.H., 1976, Phys. Rev. B **13**, 3962.
Loebich, O. and E. Raub, 1973a, J. Less-Common. Met. **31**, 111.
Loebich, O. and E. Raub, 1973b, J. Less-Common Met. **30**, 47.
Loebich, O. and E. Raub, 1975, Mat. Res. Bull. **10**, 1017.
Loebich, O. and E. Raub, 1976a, J. Less-Common Met. **46**, 7.
Loebich, O. and E. Raub, 1976b, J. Less-Common Met. **46**, 1.
Loewenhaupt, M., 1973, Z. Phys. **258**, 209.
Loewenhaupt, M. and S. Hüfner, 1969, Phys. Lett. **30A**, 309.
Longworth, G. and I.R. Harris, 1973, J. Less-Common Met. **33**, 83.
Longworth, G. and I.R. Harris, 1975, J. Less-Common Met. **41**, 175–185.
Lott, B.G. and P. Chiotti, 1966, Acta. Cryst. **20**, 733.
Lueken, H., M. Meier, G. Klessen and W. Bronger, 1979, J. Less-Common Met. **63**, P 35.
Luijpen, M.G., P.C.M. Gubbens, A.M. van der Kraan and K.H.J. Buschow, 1977, Physica **86–88B**, 141.
Lüthi, B., M.E. Mullen, K. Andres, E. Bucher and J.P. Maita, 1973, Phys. Rev. B **8**, 2639–2648.
Mader, K.H. and W.E. Wallace, 1968a, J. Less-Common Met. **16**, 85.
Mader, K.H. and W.E. Wallace, 1968b, J. Chem. Phys. **49**, 1521.
Mahoney, J.V., W.E. Wallace and R.S. Craig, 1974, J. Appl. Phys. **45**, 2733.
Malik, S.K., R. Vijayaraghavan, S.K. Gaug and R.J. Ripmeester, 1974, Pure and Appl. Chem. **40**, 223.
Malik, S.K., S.G. Sankar, V.U.S. Rao and R. Obermyer, 1976, AIP Conf. Proc. **34**, 87.
Malik, S.K., F.J. Arlinghaus and W.E. Wallace, 1977a, Phys. Rev. B **16**, 1242.
Malik, S.K., T. Takeshita and W.E. Wallace, 1977b, Solid State Comm. **23**, 599.
Mansey, R.C., G.V. Raynor and I.R. Harris, 1968, J. Less-Common Met. **14**, 329.
Maple, M.B., 1969, Thesis, University of California.
Maranzana, F.E., 1970, Phys. Rev. Lett. **25**, 239.
Martin, D.L. and M.G. Benz, 1971, AIP Conf. Proc. **5**, 970.
Matthias, B.T., E. Corenzwit and W.H. Zachariasen, 1958, Phys. Rev. **112**, 89.

Matthias, B.T., T.H. Geballe, K. Andres, E. Corenzwit, G.W. Hull and J.P. Maita, 1968, Science **159**, 530.

Matthias, B.T., E. Corenzwit, J.M. van den Berg and H.E. Barz, 1977, Proc. Nat. Acad. Sci. U.S.A. **74**, 1336.

McCall, W.M., K.S.V.L. Narasimhan and R.A. Butera, 1973, J. Appl. Phys. **44**, 4724.

McHenry, M.R., B. Silbernagel and J.H. Wernick, 1972, Phys. Rev. B **5**, 2958.

McMasters, O.D. and K.A. Gschneidner, 1964, Nuclear Mettallurg. Series X, 93.

McMasters, O.D. and K.A. Gschneidner, 1967, J. Less-Common Met. **13**, 193.

Meyer, C., B. Srour, Y. Gros, F. Hartmann-Boutron and J.J. Capponi, 1977, J. Physique **38**, 1449.

Michel, D.J. and E. Ryba, 1965, Acta. Cryst. **19**, 687.

Miedema, A.R., R. Boom and F.R. de Boer, 1975, J. Less-Common Met. **41**, 283; 1976, **46**, 67.

Miedema, A.R., R. Boom and F.R. de Boer, 1977, Calphad 1, 341.

Milhouse, A.H., H.G. Purwins and E. Walker, 1972, Solid State Comm. **11**, 707.

Miller, A.E., T. D'Silva and H. Rodrigues, 1976, IEEE Trans. **MAG-12**, 1006.

Miskinis, E.T., K.S.V.L. Narasimhan, W.E. Wallace and R.S. Craig, 1975, J. Solid State Chem. **13**, 311–314.

Miura, S., T. Kaneko, M. Ohashi and K. Kancizaki, 1971, J. de Phys. **32** C1-1124.

Moncton, D.E., D.B. McWhan, J. Eckert, G. Shirane and W. Thomlison, 1977, Phys. Rev. Lett. **39**, 1164.

Moon, R.M., W.C. Koehler and J. Farrel, 1965, J. Appl. Phys. **36**, 978.

Moreau, J.M., C. Michel, M. Simmons, T.J. O'Keefe and W.J. James, 1971, J. de Phys. **32** Suppl. C1 670–671.

Moriariu, M., E. Burzo and D. Barb, 1976a, J. de Phys. **37** Suppl. C6-615.

Moriariu, M., E. Burzo and D. Barb, 1976b, Int. Conf. Mössbauer Spectroscopy, Corfu.

Moriarty, J.L., J.E. Humphreys, R.O. Gordon, N.C. Baenziger, 1966, Acta. Crystallogr. **21**, 840.

Morin, P. and A. de Combarieu, 1975, Solid State Comm. **17**, 975–978.

Morin, P. and J. Pierre, 1973, Phys. State Sol. (a) **17**, 479–482; Solid State Comm. **13**, 537–540.

Morin, P., J. LaForest, J. Pierre and J.S. Shah, 1973, C.R. Acad. Sc. (Paris) **277**, 353.

Morin, P., J. Pierre, J. Rossat-Mignod, K. Knorr and W. Drexel, 1974a, Phys. Rev. B **9**, 4932.

Morin, P., J. Pierre and J. Chaussy, 1974b, Phys. Stat. Sol. (a) **24**, 425–432.

Morin, P., J. Pierre and D. Schmitt, 1976, J. de Phys. **37**, 611–616.

Morin, P., J. Pierre and D. Schmitt, 1978a, Solid State Comm. **25**, 265.

Morin, P., J. Pierre, D. Schmitt and D. Givord, 1978b, Phys. Lett. **65A**, 156.

Morin, P., J. Pierre and D. Schmitt, 1975, unpublished results cited in Morin and de Combarieu.

Mueller, W.M., J.P. Blackledge and G.G. Libowitz, 1968, Metal hydrides (Academic Press, New York).

Murani, A.P., K. Knorr and K.H.J. Buschow, 1977, in Crystal fields in metals and alloys (ed. A. Furrer) (Plenum Press, New York).

Muraoka, Y., M. Shiga and Y. Nakamura, 1977, J. Phys. Soc. Japan **42**, 2067.

Narasimhan, K.S.V.L. and W.E. Wallace, 1974, IEEE Trans. **MAG-10**, 729.

Narasimhan, K.S.V.L., R.A. Butera and R.S. Craig, 1972, Phys. Lett. **40A**, 381–382.

Narasimhan, K.S.V.L., R.A. Butera and R.S. Craig, 1973a, J. Appl. Phys. **44**, 879–882.

Narasimhan, K.S.V.L., V.U.S. Rao and R.A. Butera, 1973b, AIP Conf. Proc. **10**, 1081.

Narasimhan, K.S.V.L., V.U.S. Rao, R.L. Bergner and W.E. Wallace, 1975, J. Appl. Phys. **46**, 4957.

Nereson, N., 1973, AIP Conf. Proc. **10**, 669; 1963, J. Appl. Phys. **44**, 4727.

Nereson, N. and G. Arnold, 1970, J. Chem. Phys. **53**, 2818.

Nereson, N., C. Olsen and G. Arnold, 1966, J. Appl. Phys. **37**, 4575.

Nereson, N., C. Olson and G. Arnold, 1968, J. Appl. Phys. **39**, 4605.

Nesbitt, E.A., H.J. Williams, J.H. Wernick and R.C. Sherwood, 1962, J. Appl. Phys. **33**, 1674–1678.

Nesbitt, E.A., H.J. Williams, J.H. Wernick and R.C. Sherwood, 1963, J. Appl. Phys. **34**, 1347.

Nguyen Than-Trang, L.B. Chiu, A.M. Stewart and K.N.R. Taylor, 1976, J. Phys. F **6**, 1399.

Nguyen Van Nhung, J. LaForest and J. Silvardiere, 1970, Solid State Comm. **8**, 23.

Nguyen Van Nhung, A. Barlet and J. LaForest, 1971, J. de Phys. **32**, C1-1133.

Niculescu, V., I. Pop and M. Rosenberg, 1972, Phys. Stat. Sol. (b) **53**, 701.
Nikitin, S.A., V.A. Vasilkovskii, H.M. Kovtum, A.K. Kupriyanov and V.F. Ostrovskii, 1975, Sov. Phys. JETP **41**, 285–286.
Nowik, I. and B.D. Dunlap, 1973, J. Phys. Chem. Sol. **34**, 465.
Nowik, I., M. Campagna and G.K. Wertheim, 1977, Phys. Rev. Lett. **38**, 43.
Oesterreicher, H., 1971, J. Less-Common Met. **23**, 7.
Oesterreicher, H., 1973a, J. Appl. Phys. **44**, 2350.
Oesterreicher, H., 1973b, J. Less-Common Met. **30**, 225.
Oesterreicher, H., 1976, Phys. Stat. Sol. (a) **34**, 723.
Oesterreicher, H., 1977a, Phys. Stat. Sol. (a) **39**, K75.
Oesterreicher, H., 1977b, J. Less-Common Met. **55**, 131.
Oesterreicher, H. and R. Pitts, 1972, J. Appl. Phys. **43**, 5174.
Oesterreicher, H. and R. Pitts, 1973, J. Appl. Phys. **44**, 5570–5574.
Oesterreicher, H., F.T. Parker and M. Misroch, 1977, Appl. Phys. **12**, 287.
Olcese, G.L., 1963a, Atti. Acad. Naz. Lincei Rend. Sci. Fiz. Mat. Nat. **34**, 1.
Olcese, G.L., 1963b, Atti. Acad. Naz. Lincei Rend. Sci. Fiz. Mat. Nat. **34**, 642.
Olcese, G.L., 1963c, Atti. Acad. Naz. Lincei Rend. Sci. Fiz. Mat. Nat. **35**, 7.
Olcese, G.L., 1963d, Atti. Acad. Naz. Lincei Rend. Sci. Fiz. Mat. Nat. **37**, 48.
Olcese, G.L., 1973, J. Less-Common Met. **33**, 71.
Oliver, F.W., K.W. West, R.L. Cohen and K.H.T. Buschow, 1978, J. Phys. F, **8**, 701.
Olson, C.E., G.P. Arnold and N.G. Nereson, 1970, Proc. 8th Rare Earth Research Conf., Reno, Nevada, pp. 63.
Oppelt, A. and K.H.J. Buschow, 1973, J. Phys. F **3**, L212–L215.
Oppelt, A. and K.H.J. Buschow, 1976, Phys. Rev. B **13**, 4698.
Oppelt, A., A. Merkel and K.H.J. Buschow, 1976, Phys. Stat. Sol. (a) **37**, K205.
Oppelt, A., E. Dormann and K.H.J. Buschow, 1972, Phys. Stat. Sol. (b) **51**, 275–282; Int. J. Mag. **3**, 55–57.
Orehotsky, J., S. Washo, J. Gerboc and T. Wahl, 1977, J. Appl. Phys. **48**, 823.
Paccard, D. and R. Pauthenet, 1967, C.R. Acad. Sci. Paris **264**, B1056.
Paccard, D., J. Schweizer and J. Yakinthos, 1971, J. de Phys. **32**, C-1, 663.
Paderno, Yu. B. and S. Pokrzywnicki, 1967, Phys. Stat. Sol. **24**, K11.
Paderno, Yu., S. Pokrzywnicki and B. Stalinski, 1967, Phys. Stat. Sol. **24**, K73.
Palenzona, A., 1966, J. Less-Common Met. **10**, 290.
Palenzona, A., 1968, J. Less-Common Met. **16**, 379.
Palenzona, A. and A. Iandelli, 1974, J. Less-Common Met. **34**, 121.
Parthé, E., 1967, Coll. Int. du CNRS **157**, 195.
Parviainen, S. and S. Jaakkola, 1975, EPS Conf. Abstr. **1**, A33.
Pearson, W.B., 1958, A handbook of lattice spacings and structures of metals and alloys (Pergamon Press, Oxford).
Pearson, W.B., 1972, The crystal chemistry and physics of metals and alloys (Wiley Interscience, New York).
Percheron, A. and P. Lethuillier, 1972, C.R. Acad. Sci. (Paris) **271**, 1129.
Percheron, A., O. Gorochov and J.C. Achard, 1973, C.R. Acad. Sci. (Paris) C **277**, 81.
Perkins, R.S. and H. Nagel, 1975, Physica **80B**, 143.
Perkins, R.S. and S. Strässler, 1977, Phys. Rev. B **15**, 477, 490.
Petrich, G. and R.L. Mössbauer, 1968, Phys. Lett. A **26**, 403.
Pettifor, D.G., 1980, J. Mag. Mag. Mat. (Proc. ICM 1979).
Pierre, J., 1969, Solid State Comm. **7**, 165.
Pierre, J., 1970, Proc. 8th Rare Earth Research Conf., Reno, Nevada, p. 1020.
Pierre, J., 1967, C.R. Acad. Sci. (Paris) (B) **265**, 1169.
Pierre, J. and R. Pauthenet, 1965, C.R. Acad. Sci. (Paris) **260**, 2739.
Pierre, J. and E. Siaud, 1968, C.R. Acad. Sci. (Paris) **266**, 1483.
Pierre, J., A. de Combarieu and R. Lagnier, 1979, J. Phys. F, **9**, 1271.
Pinto, H. and H. Shaked, 1973, Phys. Rev. B **7**, 3261.
Poldy, C.A. and H.R. Kirchmayr, 1974, Phys. Stat. Sol. (b) **65**, 553.
Primavesi, G.J. and K.N.R. Taylor, 1972, J. Phys. F **2**, 761.
Purwins, H.G., E. Walker, B. Barbara, M.F. Rossignol and A. Furrer, 1976, J. Phys. C **9**, 1025.

Radhakrishna, P. and F. Livet, 1976, unpublished resulted quoted in Ray and Silvadiere.
Ray, A.E., 1968, Proc. 7th Rare Earth Research Conf. Coronado, Cal., p. 473–484.
Ray, A.E. and K.J. Strnat, 1975, IEEE Trans. Mag. **MAG-11**, 1429.
Ray, A.E., A.T. Bierman, R.S. Harmer and J.E. Davison, 1973, Cobalt, 1036.
Ray, D.K., 1974, Solid State Comm. **15**, 1471–1474.
Ray, D.K. and J. Silvadiere, 1976, Solid State Comm. **19**, 1053–1057.
Rieger, W. and E. Parthé, 1969, Monatsh. Chem. **100**, 444.
Rosen, M., H. Klimker, U. Atzmony and M.P. Dariel, 1976, J. Phys. Chem. Sol. **37**, 513.
Ross, J.W. and J. Sigalas, 1976, J. Phys. F **5**, 1973–1973.
Ruderman, M.A. and C. Kittel, 1954, Phys. Rev. **96**, 99.
Ruggiero, A.F., G.L. Olcese and G.B. Bonino, 1964, Atti. Acad. Lincei Rend. Sci. Fiz. Mat. Nat. **37**, 169.
Sadagopan, V., B.C. Giessen and N.J. Grant, 1968, J. Less-Common Met. **14**, 279.
Sales, B.C. and D.K. Wohlleben, 1975, Phys. Rev. Lett. **35**, 1240.
Salmans, L.R., K. Strnat and G.I. Hoffer, 1968, Tech. Rept. AFML-CF-68-159.
Sampathkumaran, E.V., L.C. Gupta and V. Vÿayaraghavan, 1979, Phys. Lett. **70A**, 356.
Sanchez, J.P., J.M. Friedt, G.K. Shenoy, A. Percheron and J.C. Achard, 1976, J. Phys. C **9**, 2207.
Sankar, S.G., V.U.S. Rao, E. Segal, W.E. Wallace, W.G.D. Frederick and H.J. Garret, 1975, Phys. Rev. B 11, 435.
Sankar, S.G., S.K. Malik, V.U.S. Rao and R. Obermyer, 1976, AIP Conf. Proc. **34**, 236.
Sankar, S.G., S.K. Malik, V.U.S. Rao and W.E. Wallace, 1977, in Crystal field effects in metals and alloys (ed. A. Furrer) (Plenum Press, New York).
Savitsky, E.M. and V.F. Terekhova, 1975, Metallography of rare earth metals (Nauka Publ. Co., Moscow).
Schäfer, W., H.K. Schmidt, B. Elschner and K.H.J. Buschow, 1972, Z. Phys. **254**, 1.
Schäfer, W., G. Will and K.H.J. Buschow, 1976a, J. Chem. Phys. **64**, 1994.
Schäfer, W., G. Will and K.H.J. Buschow, 1976b, J. Phys. C **9**, L657–L661.
Schäfer, W., G. Will and K.H.J. Buschow, 1977, J. Mag. Mag. Mat. **4**, 28–35.
Schubert, K., 1964, Kristallstrukturen zweikomponentiger Phasen (Springer-Verlag, Berlin).
Schweizer, J., 1968, Thesis, University of Grenoble.
Schweizer, J. and J. Yakinthos, 1969, Coll. Internat. CNRS no. 180, Paris–Grenoble, pp. 239.
Scrabek, E.A. and W.E. Wallace, 1963, J. Appl. Phys. **34**, 1356.
Sekizawa, K., 1966, J. Phys. Soc. Japan **21**, 1137.
Sekizawa, K. and K. Yasukochi, 1964, Phys. Lett. **11**, 216.
Sekizawa, K. and K. Yasukochi, 1966a, J. Phys. Soc. Japan **21**, 274.
Sekizawa, K. and K. Yasukochi, 1966b, J. Phys. Soc. Japan **21**, 684–692.
Shaltiel, D., J.H. Wernick and V. Jaccarino, 1964, J. Appl. Phys. **35**, 978.
Shenoy, G.K., B.D. Dunlap, G.M. Kalvius, A.M. Toxen and R.J. Gambino, 1970, J. Appl. Phys. **41**, 1317.
Sherwood, R.C., H.J. Williams and J.H. Wernick, 1964, J. Appl. Phys. **35**, 1049.
Shirley, D.A., S.S. Rosenblum and E. Matthias, 1968, Phys. Rev. **170**, 363.
Shoemaker, D.P., R.E. Marsh, F.J. Ewring and L. Pauling, 1952, Acta. Crystallogr. **5**, 637.
Shunk, F.A., 1969, Constitution of binary alloys, 2nd suppl. (McGraw-Hill, New York).
Shur, Ya. S., O.I. Shiryayeva and V.G. Maykov, 1975, Fiz. Metal. Metalloved **39**, 1118.
Siek, S., A. Szytula and J. Leciejewics, 1978, Phys. Stat. Sol. (a) **29**, K101.
Sill, L.R. and B. Prindeville, 1975, AIP Conf. Proc. **24**, 420.
Sill, L.R., W.J. Mass, A.J. Fedro, J.C. Shaffer and C.W. Kimball, 1971, J. Appl. Phys. **42**, 1297.
Sill, L.R., S.R. Snow and A.J. Fedro, 1973, AIP Conf. Proc. **10**, 1060.
Simmons, M., J.M. Moreau, W.J. James, F. Givord and R. Lemaire, 1973, J. Less-Common Met. **30**, 75–82.
Singh, P.P. and A. Raman, 1965, Trans. AIME **245**, 1561.
Smith, G.S., A.G. Tharp and Q. Johnson, 1967, Acta. Crystallogr. **22**, 940.
Smith, T.F. and I.R. Harris, 1967, J. Phys. Chem. Sol. **28**, 1846.

Sperlich, G., K.H. Janneck and K.H.J. Buschow, 1973, Phys. Stat. Sol. (b) **57**, 701.
Stalinski, B., 1974, AIP-Conf. Proc. **18**, 490.
Stalinski, B. and S. Pokrzywnicki, 1966, Phys. Stat. Sol. **14**, K157.
Stalinski, B., A. Czopnik, I. Iliew and T. Mydlarz, 1974, Proc. ICM-73, TOM V (Nauka Publ. Co., Moscow, 1974) p. 349.
Stearns, M.B., 1971, Phys. Rev. B **4**, 4081.
Stearns, M.B., 1973, Phys. Rev. B **8**, 4383.
Steiner, W. and R. Haferl, 1977, Phys. Stat. Sol. (a) **42**, 739.
Steiner, W. and J. Hrubec, 1975, J. Less-Common Met. **41**, 165–174.
Steiner, W. and H. Ortbauer, 1975, Phys. Stat. Sol. (a) 31, K119–K123.
Steiner, W., A. Planck and G. Weihs, 1976, J. Less-Common Met. **45**, 143–153.
Stevens, K.W.H., 1953, Proc. Phys. Soc. **A65**, 209.
Stewart, A.M. and B.R. Coles, 1974, J. Phys. F, **4**, 458.
Stewart, A.M., G. Costa and G. Olcese, 1974, Aust. J. Phys. **27**, 383.
Stoner, E.C., 1938, Proc. Roy. Soc. A **165**, 372.
Storm, A. and K. Benson, 1963, Acta. Crystallogr. **16**, 701.
Streever, R.L., 1979, Phys. Rev. B **19**, 2704.
Strnat, K.J. and A.E. Ray, 1970, Z. Metallkde **61**, 461–470.
Strnat, K., G. Hoffer, W. Ostertag and J.C. Olson, 1966, J. Appl. Phys. **37**, 1252–1253.
Strnat, K., G.I. Hoffer and A.E. Ray, 1966, IEEE Trans. Mag. **2**, 489–493.
Swift, W.M. and W.E. Wallace, 1968, J. Phys. Chem. Sol. **29**, 2053.
Szpunar, B. and B. Kozarzewski, 1977, Phys. Stat. Sol. (b) **82**, 205.
Szpunar, B. and P.A. Lindgard, 1977, Phys. Stat. Sol. (b) **82**, 449.
Szpunar, B. and P.A. Lindgard, 1979, J. Phys. F, **9**, L55.
Takeshita, T., S.K. Malik, A.A. El-Attar and W.E. Wallace, 1976, AIP Conf. Proc. **34**, 230.
Tamminga, Y., 1973, Thesis, University of Amsterdam.
Tannous, C., D.K. Ray and M. Belakhovsky, 1976, J. Phys. F **5**, 2091–2096.
Taylor, K.N.R., 1971, Adv. Phys. **87**, 551.
Taylor, K.N.R. and J. Christopher, 1967, J. Phys. C 2237.
Taylor, R.H., 1975, Adv. Phys. **24**, 681; see also Fisk et al. (1971).
Taylor, R.H., I.R. Harris and W.E. Gardner, 1976, J. Phys. F **6**, 1125.
Tellenbach, U., A. Furrer and A.H. Millhouse, 1975, J. Phys. C **8**, 3833–3840.
Terekhova, V.F., P.I. Kripyakevich, D.P. Frankevich and R.S. Torchinowa, 1967, Russ. Met. **1**, 107–109.
Teslyuk, M. Yu. and P.I. Krypyakevich, 1961, Dopovidi Akad. Nauk. Ukr. RSK 1039.
Teslyuk, M.J., P.I. Krypiakevich and D.P. Frankevich, 1964, Soviet Phys. Cryst. **9**, 469.
Tomala, K., G. Czjzek, J. Fink and H. Schmidt, 1977, Solid State Comm. **24**, 857.
Tsuchida, T. and W.E. Wallace, 1965, J. Chem. Phys. **43**, 3811.
Tsuchida, T., S. Sugaki and Y. Nakamura, 1975, J. Phys. Soc. Japan **39**, 340–343.
Umezaki, H., S. Kawano, N. Achiwa and T. Shibata, 1974, Ann. Rep. Reactor Inst. Kyoto Univ. **7**, 94.
van Daal, H.J. and K.H.J. Buschow, 1969, Solid State Comm. **7**, 217; Phys. Rev. Lett. **23**, 408.
van Daal, H.J. and K.H.J. Buschow, 1970a, Phys. Stat. Sol. (a) **3**, 853.
van Daal, H.J. and K.H.J. Buschow, 1970b, Les elements des terres rares, II, CNRS pp. 551.
van Daal, H.J. and K.H.J. Buschow, 1970c, Phys. Lett. **31A**, 103.
van Daal, H.J., P.B. van Aken and K.H.J. Buschow, 1974, Phys. Lett. **49A**, 246.
van den Berg, J.M. and B.T. Matthias, 1977, Proc. Nat. Acad. Sci. U.S.A. **74**, 1336.
van den Broek, J.J. and H. Zijlstra, 1971, IEEE Trans. **MAG-7**, 226.
van der Goot, A.S. and K.H.J. Buschow, 1970, J. Less-Common Met. **21**, 151–157.
van der Kraan, A.M. and K.H.J. Buschow, 1977, Physica **86–88B**, 93.
van der Kraan, A.M. and P.C.M. Gubbens, 1974, J. de Phys. **12**, suppl. C6-469-472.
van der Kraan, A.M., P.C.M. Gubbens and K.H.J. Buschow, 1975, Phys. Stat. Sol. (a) **31**, 495–501.
van der Kraan, A.M., J.N.J. van der Velden, J.H.F. van Apeldoorn, P.C.M. Gubbens and K.H.J. Buschow, 1976, Phys. Stat. Sol. (a) **35**, 137–151.
van der Kraan, A.M., P.C.M. Gubbens and K.H.J. Buschow, 1977, Proc. Conf. Mössbauer Effect, Boekarest, pp. 121.
van Diepen, A.M. and K.H.J. Buschow, 1977, Solid State Comm. **22**, 113.

van Diepen, A.M., H.W. de Wijn and K.H.J. Buschow, 1967, J. Chem. Phys. **46**, 3489.
van Diepen, A.M., H.W. de Wijn and K.H.J. Buschow, 1968, Phys. Stat. Sol. **29**, 189.
van Diepen, A.M., K.H.J. Buschow and H.W. de Wijn, 1969, J. Chem. Phys. **51**, 5259.
van Diepen, A.M., H.W. de Wijn and K.H.J. Buschow, 1973, Phys. Rev. **8**, 1125–1129.
van Mal, H.H., K.H.J. Buschow and A.R. Miedema, 1974, J. Less-Common Met. **35**, 65.
van Steenwijk, F.J., 1976, Thesis, University of Leiden.
van Steenwijk, F.J., H.Th. LeFever, R.C. Thiel and K.H.J. Buschow, 1975a, Physica **79B**, 604.
van Steenwijk, F.J., H.Th. LeFever, R.C. Thiel and K.H.J. Buschow, 1975b, Physica **79B**, 607.
van Steenwijk, F.J., W.J. Huiskamp, H.Th. LeFever, R.C. Thiel and K.H.J. Buschow, 1977, Physica **B86–88**, 89.
van Vucht, J.H.N. and K.H.J. Buschow, 1964, Philips Res. Rep. **19**, 319.
van Vucht, J.H.N. and K.H.J. Buschow, 1965, J. Less-Common Metals, 10, 98.
Vasilkovskii, V.A., N.M. Kovtum, A.K. Kuprianov, S.A. Nikitin and V.F. Ostrovskii, 1974, Sov. Phys. JETP **38**, 342–344.
Velge, W.A.J.J. and K.H.J. Buschow, 1968, J. Appl. Phys. **39**, 1717–1720.
Vijayaraghavan, R., V.U.S. Rao, S.K. Malik and V. Marathe, 1968, J. Appl. Phys. **39**, 1086; see also the quotation in Joseph et al. (1972).
Voiron, J., 1972, C.R. Acad. Sci. Paris **274**, 589.
Voiron, J. and D. Bloch, 1971, J. de Phys. **32**, 949–952.
Vonsovskii, S.V., 1974, Magnetism (Wiley, New York).
Walker, E., H.G. Purwins, M. Landolt and F. Hullinger, 1973, J. Less-Common Met. **33**, 203.
Wallace, W.E., 1968, Prog. Rare Earth Sci. and Tech., III, 1–37.
Wallace, W.E., 1973, Rare earth intermetallics (Academic Press, New York).
Wallace, W.E. and M. Aoyagi, 1971, Monatshefte für Chemie **102**, 1455–1461.
Wallace, W.E. and E.A. Skrabek, 1964, Rare earth research, II, (ed. Vorres) (Gordon and Breach, New York) p. 431–441.
Wallace, W.E. and J.T. Swearingen, 1973, J. Solid State Chem. **8**, 37–38.
Wallace, W.E. and Y.G. Vlasov, 1967, J. Inorg. Chem. **6**, 2216.
Wallace, W.E., T.V. Volkmann and H.P. Hopkins, 1971, J. Solid State Chem. **3**, 510–514.
Walline, R.E. and W.E. Wallace, 1964, J. Chem. Phys. **41**, 3285.
Walline, R.E. and W.E. Wallace, 1965, J. Chem. Phys. **42**, 604.
Walsh, W.M., Jr., L.W. Rupp, Jr., P.H. Schmidt and L.D. Longinotti, 1975, AIP Conf. Proc. **29**, 686.
Wang, Y.L. and B.R. Cooper, 1969, Phys. Rev. **185**, 696.
Wang, F.E. and J. Gilfrich, 1966, Acta. Crystallogr. **21**, 476–481.
Wang, F.E. and J.R. Holden, 1965, Trans. Met. Soc. AIME **233**, 731–736.
Watson, R.E., 1967, in Hyperfine interactions (eds. A. Freeman and R.B. Frankel) (Academic Press, New York).
Weik, H., P. Fischer, W. Hälg and E. Stoll, 1964, Proc. 4th rare earth conf. pp. 20.
Weimann, G., B. Elschner, K.H.J. Buschow and R.P. van Stapele, 1972, Solid State Comm. **11**, 871.
Weimann, G., P.H. Bopp, B. Elschner and K.H.J. Buschow, 1973, Int. J. Magn. **5**, 1–3.
Wernick, J.H. and S. Geller, 1960, Trans. Met. Soc. AIME **218**, 866.
Wernick, J.H., H.J. Williams and A.C. Gossard, 1967, J. Phys. Chem. Sol. **28**, 271.
Wertheim, G.K., V. Jaccarino and J.H. Wernick, 1964, Phys. Rev. A **135**, 151–154.
Wickman, H.H., J.H. Wernick, R.C. Sherwood and C.F. Wagner, 1968, J. Phys. Chem. Solids **29**, 181.
Wilhelm, M. and B. Hillenbrand, 1971, Z. Naturforsch. **26a**, 141, 1684.
Will, G. and M.O. Bargouth, 1971, Phys. Kondens Materia **13**, 137.
Will, G. and M.O. Bargouth, 1972, Int. J. Mag. **3**, 87.
Will, G., V. Lehmann and K.H.J. Buschow, 1977a, J. Mag. Mag. Mat. **6**, 22.
Will, G., M.O. Bargouth and K.H.J. Buschow, 1977b, J. Mag. Mag. Mat. **6**, 131.
Williams, G. and L.L. Hirst, 1969, Phys. Rev. **185**, 407.
Williams, H.J., J.H. Wernick, E.A. Nesbitt and R.C. Sherwood, 1962, J. Phys. Soc. Japan **17**, suppl. B-1, 91.
Winterberger, M., R. Chamard-Bois, M. Belakhovsky and J. Pierre, 1971, Phys. Stat. Sol. (b) **48**, 705.

Wohlfarth, E.P., 1969, J. Phys. C **2**, 68.
Wohlfarth, E.P., 1979, J. Phys. F, **9**, L123.
Wood, V.E., 1971, Phys. Lett. **37A**, 357.
Wun, M. and N.E. Phillips, 1974, Phys. Lett. **50A**, 195.
Wybourne, B.G., 1965, Spectroscopic properties of rare earths (Interscience, New York).
Yaguchi, K., 1966, J. Phys. Soc. Japan **21**, 405.
Yakinthos, J.K., 1977a, Phys. Stat. Sol. (b) **82** 349.
Yakinthos, J.K., 1977b, Physica **86–88B**, 207.
Yakinthos, J.K., 1978, J. Phys. Chem. Sol. **39**, 485.
Yakinthos, J.K. and D.E. Mentzafos, 1975, Phys. Rev. **12**, 1928.
Yakinthos, J. and D. Paccard, 1972, Solid State Comm. **10**, 989.
Yakinthos, J.K. and P.J. Rentzeperis, 1974, Phys. Stat. Sol. (b) **64**, 643.
Yakinthos, J. and J. Rossat Mignod, 1972, Phys. Stat. Sol. (b) **50**, 747.
Yakinthos, J.K. and E. Roudeaut, 1977, Phys. Stat. Sol. (a) **39**, K151.
Yakinthos, J.K., T. Anagnostopoulos and P.F. Ikonomou, 1977a, J. Less-Common Met. **51**, 113.
Yakinthos, J.K., H. Gamari-Seale and J. Laforest, 1977b, Phys. Stat. Sol. (a) **40**, K105.
Yashiro, T., Y. Hamaguchi and H. Watanabe, 1976, J. Phys. Soc. Japan **40**, 63.
Yosida, K., 1957, Phys. Rev. **106**, 893.
Zarechnyuk, O.S. and P.I. Kripyakevitch, 1963, Sov. Phys. Crystallogr. **7**, 436.

chapter 5

ACTINIDE ELEMENTS AND COMPOUNDS

W. TRZEBIATOWSKI

Institute for Low Temperature and Structure Research
Polish Academy of Sciences
Wrocław
Poland

Ferromagnetic Materials, Vol. 1
Edited by E.P. Wohlfarth

CONTENTS

1. Introduction

The interest in the physical properties of actinides, elements and compounds is very large, because they include fissionable isotopes useful for energy production and because they offer the possibility of producing new transuranium elements either as byproducts of reactor processes or through nuclear reactions by means of accelerators. These elements are far less well-known than others, so that some details about their crystal and electronic structures will precede the description of their magnetic properties.

1.1. Electronic structure of actinides

The electronic structure of the actinides allows appreciable analogies to be drawn with that of the lanthanides. The Seaborg concept concerning the existence of a homologous family of the 5f elements has been once more directly confirmed by X-ray photoelectron spectroscopy of solids which identified the 5f band, for example, in UO_2 (Veal and Lam 1974). However, there exist distinct differences in the behaviour and properties of the 5f electrons in comparison to the 4f electrons. Thorium atoms, in contrast to cerium, do not contain the first 5f electron. Therefore thorium, according to its physical properties like the high melting point of the typical metallic fcc lattice, behaves rather as a transition d-metal.

The electronic structure of the actinide atoms (table 1) is quite similar to that of the lanthanides. But in the solid state the elements and their compounds differ in some particular features from the lanthanides, especially in the case of the lighter elements.

In spite of the fact that the band structure of actinide metals is complex, extensive theoretical calculations have been given, particularly for thorium, uranium, plutonium and others. The density of states and the Fermi surface have been calculated, concentrating naturally on the simpler allotropic forms such as α-Th, γ-U, δ-Pu, or γ-Np (Freeman and Koeling 1974, Freeman 1979, Koeling 1979).

The 5f electrons of the light actinides are delocalized and their bands significantly overlap their neighbours, hybridizing strongly with the 6d and 7s band. The calculated hybridized 5f-bandwidth is narrower than the d-bandwidths in the transition metals. Its half-widths diminish continuously from uranium to

TABLE 1
Electronic structure of the actinides

	Ra	Ac	Th	Pa	U	Np	Pu	Am	Cm	Bk	Cf	Es	Fm	Md	No	Lr
5d	10	10	10	10	10	10	10	10	10	10	10	10	10	10	10	10
5f	–	–	–	2	3	5	6	7	7	8	10	11	12	13	14	14
6s	2	2	2	2	2	2	2	2	2	2	2	2	2	2	2	2
6p	6	6	6	6	6	6	6	6	6	6	6	6	6	6	6	6
6d	–	1	2	1	1	–	–	–	1	1	–	–	–	–	–	1
7s	2	2	2	2	2	2	2	2	2	2	2	2	2	2	2	2

Sequence of lanthanide elements

	La	Ce	Pr	Nd	Pm	Sm	Eu	Gd	Tb	Dy	Ho	Er	Tm	Yb	Lu

americium metal (Kmetko and Hill 1970, Freeman and Koeling 1974, Koeling 1977).

The 5f electrons are also much more strongly influenced by the crystal field than the 4f electrons in the case of the lanthanides. These 5f states must also be considered as itinerant in contrast to the lanthanides which form narrow isolated bands of a localized character. With increasing atomic number the 5f band becomes more and more narrow and finally these electrons behave as those of the 4f family.

Such an electronic structure explains very often the physical properties of the actinide metals and compounds with increasing atomic number*.

1.2. Characteristic features of 5f electrons in the solid state

Metals of the first half of the actinide family exhibit, as mentioned above, a predominant itinerant character. These metals show no magnetic moments and their magnetic susceptibilities are practically independent of temperature; they recall the d-transition metals. This is a consequence of the more spatially extended nature of the 5f wave functions and their natural overlap. In contrast to the lighter actinide metals, curium and the following metals show distinctly localized 5f states.

Uranium and plutonium are the metals to which most attention has been paid, but great difficulties arise in the theoretical considerations because of their complex crystalline structures.

These circumstances arise even for the electronic states of uranium if their compounds are being considered. The larger the mutual separation of the magnetically active actinide atoms or ions in the lattice, the smaller are the interactions of their electrons so that the 5f electrons gradually occupy localized states and magnetic moments appear (Hill 1970a, b). The conditions for the appearance of magnetism in metallic actinide systems have been recently discussed by de Novion (1979), and for compounds by Suski (1979).

*An excellent review on the electronic structure of actinides and on their physical properties is given in the book "The Actinides", 1974, A.J. Freeman and J.B. Darby, Jr. eds. (Academic Press, New York).

1.3. Comparison of crystal structures of lanthanide elements and compounds with those of actinides

The crystal structure within the lanthanide family is characteristic of metallic lattice types like fcc, bcc and hcp, which occur especially at higher temperatures. The only exception is α-Sm which is rhombohedral. The hexagonal close packed (hcp) α-phases of numerous lanthanide metals occuring at normal temperatures mostly have their unit cells doubled along the c axis. The number of allotropic modifications do not usually exceed three unless a high static pressure is involved.

The crystal structure of actinide metals is often much more complicated, and the example of plutonium existing in as many as 6 allotropic modifications is quite unique. The first two representatives of this family, namely actinium and thorium, show the typical fcc metallic structure, but already α-Pa has a tetragonal unit cell and each of the three elements U, Np and Pu offer at least three allotropic modifications, often of an unconventional type. The heavier actinide metals have again simpler crystal structures, and double hexagonal unit cells (dhcp) such as occur among the lanthanides (table 2) are common.

From this point of view the actinide metals are divided into three subgroups: (1) Ac and Th – occurring in the typical transition metal structures, (2) Pa, U, Np, Pu – having numerous and often uncommon crystal lattice types, (3) Am and beyond – with the crystal structures corresponding to those of the lanthanides. Certainly it is the f-band which influences the crystal structure.

The subgroup (1) contains no f-electrons; within the subgroup (2) f, d, and s bands overlap, and within the subgroup (3) the localized character of the f-electrons prevails.

An interesting relationship also exists between the structure of a representative element of the 4f- and 5f-family. The fcc lattice of α-Ce transforms into α'-Ce under a pressure of 56 kb. The latter is orthorhombic and isostructural with α-U (Ellinger and Zachariasen 1974).

The crystal structure of the compounds generally depends on the kind of bonding forces and on the ratio of the components.

There is a particular interest in the compounds of uranium and plutonium with small interatomic An–An distances and refractory properties, suitable as reactor fuels, e.g. oxides, carbides, nitrides and others.

Attention will be paid here to the intermetallic or semimetallic compounds because they offer numerous examples of magnetic order. These compounds often belong to common lattice types such as NaCl, Cu_2Sb, AlB_2, $CuAl_2$, PbFCl, Mn_2O_3, CrB, β-W, $AuCu_3$, Laves phases and other types.

A large number of new types of crystal structure has been identified among the actinide compounds such as Th_3P_4, Th_2Zn_{17}, ThB_4, Th_6Mn_{23}, Th_7Fe_3, U_3Si, UZn_{12}, UB_{12}, UAl, UHg_3, U_3Si_2, Pu_3Co, Pu_2C_3, $PuAl_3$, $PuNi_3$, $PuAg_3$, $Pu_{11}Se_9$, U_3S_5 and others. They occur partly also among the lanthanide compounds.

The plot of atomic volumes against the atomic number of elements shows

TABLE 2
Crystal structure of actinide metals

Atomic number	Element	Melting point °C	Type system	Lattice constants Å			Transformation temperatures °C
				a	*b*	*c*	
89	Ac	1050	A_1	5.331			
90	α-Th		A_1	5.0843			1400
	β-Th	1690	A_2	4.11			
91	α-Pa		tetragonal	3.929		3.241	1170
	β-Pa	1560	A_1	3.81			
92	α-U		rhombic	2.8537	5.8695	4.9548	668
	β-U		tetragonal	10.763		5.652	772
	γ-U	1132	A_2	3.525	(805°)		
93	α-Np		rhombic	6.663	4.723	4.887	278
	β-Np		tetragonal	4.897		3.388	577
	γ-Np	637	A_2	3.52			
94*	α-Pu		monoclinic simple	6.183	4.822 ($\beta = 101.79°$)	10.963	115
	β-Pu		monoclinic body-centered	9.284	10.463 ($\beta = 92.13°$)	7.859	185
	γ-Pu		ortorhombic face-centered	3.159	5.768	10.162	310
	δ-Pu		A_2	4.637			458
	δ'-Pu		tetragonal body-centered	3.34		4.44	480
	ε-Pu	641	A_2	3.636			
95	α-Am		double-hexagonal	3.4680		11.241	1079
	β-Am	1175	A_1	4.894			
96	α-Cm		double-hexagonal	3.497		11.335	
	β-Cm	1340	A_1	5.039			
97	α-Bk		double-hexagonal	3.416		11.069	
	β-Bk	986	A_1	4.997			
98	α-Cf		A_1	5.743			
	β-Cf	900(?)	A_3	3.988		6.887	
99	Es	860(?)	A_1	5.75			

*After Taube (1974).

some interesting differences for the 3d-transition, the lanthanide and the actinide elements. As evident from fig. 1, the 4f-elements have the highest values of atomic volume with the very well known two maxima for europium and ytterbium ($Z = 63$ and 70). The intermediate plot represents the actinide elements, which at the beginning follows closely the curve of the 4f-elements and then lies between the curves of 3d and 4f elements. This also indicates the intermediate character of the 5f electrons as being responsible for this behaviour. The heavier transuranium elements again approach the atomic volumes of the 4f-elements (Julien et al. 1972).

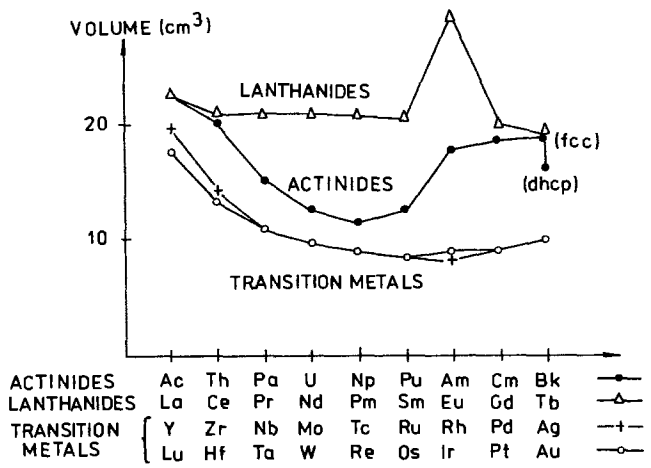

Fig. 1. Atomic volumes of 3d, 4f and 5f elements (after Julien et al. 1972).

1.4. Preparation of metals and compounds

The actinide elements are reactive metals and therefore their production must be carried out in a high vacuum or neutral gas atmosphere of the highest purity. Thorium and uranium are produced in large quantities mostly by calcium or magnesium reduction, in contrast to the other metals which, with the exception of plutonium, are available only on the gram or microgram scale.

The transuranium metals are α-emitters and because of their activity and toxicity glove-boxes must be used. Isotopes with shorter half-life periods, like curium-242 exhibit also strong self-heating effects which make precise physical measurements difficult.

Because the heavier transuranium elements are accessible only in very small quantities, magnetic and other physical measurements have so far been rather rare. Under these circumstances it is not surprising that the solid state investigations of the actinides were mostly performed on thorium, and especially on uranium, neptunium and plutonium compounds. Protactinium, curium, berkelium and californium as metals or as compounds have only rarely been studied; actinium still awaits its turn.

A common method of the production of uranium compounds consists in preparing fine uranium metal powder obtained by the hydrogenation of massive metal into UH_3 at 250°C, then by decomposition of the hydride by vacuum dissociation, and finally by reaction with the other nonmetallic component (Trzebiatowski et al. 1967a,b). The direct reaction of the metal hydride with the other elements (Naoumidis and Stocker 1967) or the reaction of metal with the gaseous nonmetallic hydride (e.g. PH_3) may also be carried out (Baskin 1966). Compounds with a lower content of the second component may be obtained by thermal dissociation, as in the case of pnictides or chalcogenides.

A volatile process may be applied which consists in heating the actinide metal with a suitable compound like Zn_3P_2 or ZnTe, producing the actinide phosphide or telluride simultaneously by volatilizing the zinc (Lovell et al. 1971). Other microscale preparation methods of transuranic compounds have been given recently by Damien et al. (1979).

For physical measurements single crystals are often required, and the metal single crystals are obtained by the known methods of Czochralski, Bridgman and others, which however necessitate the highest vacuum or a pure inert atmosphere and appropriate ceramics as crucible materials; e.g. alumina, beryllia, thorium dioxide or metallic tantalum.

Another method, especially applicable to the compounds of actinides with nonmetallic components, consists of vapour transport processes. This method uses the reactive gaseous substances like chlorine, bromine or iodine as a transporting agent acting on the polycrystalline samples and depositing small single crystals on the other side of a transport tube placed in a furnace with a constant temperature gradient. Examples are given by Henkie (1968), Buhrer (1969), Sevastianov et al. (1972), Wojakowski et al. (1972), Henkie and Klamut (1977), Spirlet (1979) and Calestani et al. (1979).

Recrystallization of the substance just below its melting point may produce single crystals; for example USb (Lander et al. 1976). Crystallization of intermetallic compounds like uranium dipnictides, chalcogenides or phosphides (U_3P_4) from low melting and nonreacting metallic melts such as bismuth or antimony also give positive results. Slow crystallizing of high melting compounds like US directly from the melts obtained by electric arc, electron beam or induction heating may also result in single crystals (Tillwick and du Plessis 1976a,b).

2. Survey of magnetic properties

The magnetic behaviour of actinide elements and their compounds is especially interesting because they show a wide variety of often complex magnetic properties. However, neither the simple band theory nor the localized electron theory are able to explain them completely. During the last 10 years a large number of contributions about the magnetic and electric properties of actinide compounds was published, so only a part of these can be cited in the following sections.

2.1. Magnetic properties of elements

The magnetic properties of actinide metals generally follow what is expected from their electronic structure (section 1.1). However, the magnetic susceptibilities are known only for a certain number of the actinides from thorium up to californium inclusively. Their room temperature values range from $+0.412 \times 10^{-6}$ emu/g for thorium to $+2.8 \times 10^{-6}$ emu/g for americium metal. Much larger values were observed for Cm, Bk and Cf (Gmelin 1976).

The other metals are still not available in the necessary quantities. According to expectations the lighter metals like Th, Pa, U, Np and Pu show practically temperature independent Pauli paramagnetism. The susceptibilities of thorium, uranium and the following metals increase slightly with temperature and some suppositions about low temperature transformations in uranium have been made. The phase transformations of elements are evident on the susceptibility–temperature curves and a small maximum in the susceptibility at 10 K and a minimum at 40–50 K were detected in plutonium, but no ordering effects could be proved, so they may be consequences of spin fluctuation effects.

Neptunium and americium behave similarly, although in the case of Am-metal it contains 3+ metallic ions with six f-electrons. This gives $J = 0$ and Van Vleck magnetism is responsible for the observed properties.

It is interesting to remark that americium is unexpectedly superconducting with $T_c = 0.6$ K (Smith et al. 1978).

Contrary to these metals, curium, berkelium and californium show a normal temperature dependence for the paramagnetic susceptibilities, yielding values of the magnetic moments $P_{eff} = 8.0\mu_B$, 8.2 and 8.8 μ_B, respectively. The first value agrees very well with that calculated for the f^7 electronic structure, also characteristic of Gd^{3+}. The data for berkelium metal is less certain and the homologous terbium ion Tb^{3+} has a moment of 9.7 μ_B. Californium metal has a magnetic moment of 9.7–9.8 μ_B, slightly lower than that calculated for both Cf^{2+} (10.18 μ_B) or Cf^{+3} (10.22 μ_B) ions.

Curium metal is especially interesting because it is the only actinide metal which is magnetically ordered (section 3.1), although among the homologous lanthanide metals a large number of ferro- and metamagnetics exist.

2.2. Magnetic properties of compounds

The magnetic properties of metallic or semimetallic actinide compounds are very interesting and the individual magnetic character of these elements shows up more distinctly in the compounds than in the elementary state, especially for the lighter members of this family. Contrary to the elements there exist a large number of magnetically ordered substances among the compounds.

The first magnetically ordered compound among the actinides was the ferromagnetic uranium hydride β-UH_3, identified by Trzebiatowski et al. (1952). Numerous other ordered uranium compounds such as chalcogenides and pnictides were discovered soon afterwards by the same authors (Trzebiatowski et al. 1967), and these formed a new family of magnetic materials similar to the hitherto well known lanthanides. One feature concerning these two groups of elements should be emphasised: The ordering temperatures of actinide compounds are commonly higher than in the case of lanthanides, although not so high as in the case of d-transition elements or compounds.

The localized magnetic moments occur if An–An distances are sufficiently large so as to diminish the overlap of the f-electron bands. After Hill (1970a,b), these critical minimal distances are 3.4–3.6 Å for uranium, 3.25 Å for neptunium

and 3.40 Å for plutonium compounds. If these values are exceeded, localized magnetic moments and possibly ordering effects may occur. But neither the simple band theory nor the localized electron theory may be applied.

Among the actinide compounds the following classes may be distinguished according to their magnetic properties:

(1) Without distinct magnetic moments and ordering.

(2) Paramagnetics obeying the Curie–Weiss law without established magnetic order.

(3) Ferromagnets or antiferromagnets.

The main interest in this context is focussed on ferromagnetics. Therefore only substances of this kind are presented in detail.

Isostructural compounds like US, UP, PuP often present different spin coupling, the kind of magnetic order depending primarily on the second component. Identical magnetic order exists between members of the groups of compounds shown in the following table.

TABLE 3
Magnetic families of actinide compounds

Crystal structure type	NaCl	NaCl	Th_3P_4	Cu_2Sb	NaCl	Th_3P_4
	UN					
	UP	US	U_3P_4	UP_2	PuP	Th_3P_4
	UAs	USe	U_3As_4	UAs_2	PuAs	Th_3As_4
	USb	UTe	U_3Sb_4	USb_2	PuSb	Th_3Sb_4
	UBi		U_3Bi_4	UBi_2		
Magnetic order	af	f	f	af	f	Weak magnetic

Grunzweig-Genossar and Kuznietz (1968) and Grunzweig-Genossar et al. (1968) tried to explain the kind of order existing in cubic uranium monopnictides or chalcogenides by considering U^{+4} ions with f^2 electrons and combining the Rudermann–Kittel–Kasuya–Yosida (RKKY) theory of exchange through the conduction band with a superexchange through the anions.

One observes that the Curie or Néel temperatures of isostructural compounds show correlations with the interatomic distances of the actinide component, as is evident from fig. 2.

The electrical transport in these actinide compounds is either semiconducting or metallic. For example, Th_3P_4 is a semiconductor (Price and Warren 1965) but U_3P_4 is a metallic conductor (Henkie and Bazan 1971, Bazan et al. 1977). By studying their solid solutions one may observe transitions between the different mechanisms of electrical conductivity (section 3.2.7).

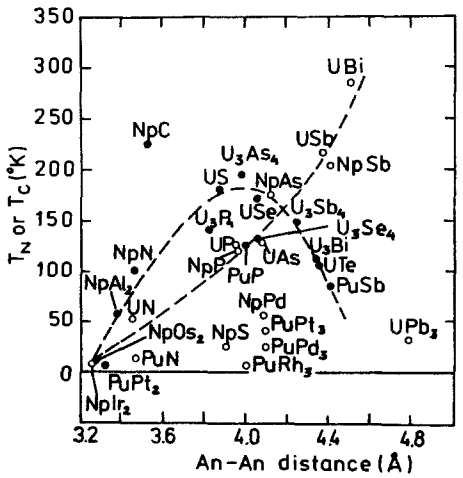

Fig. 2. The dependence of magnetic transformation temperatures on the An–An distances (after Lam and Aldred 1974).

3. Magnetic ordering in elements and compounds

Among the actinide compounds there now exist nearly 100 ferro- and antiferromagnets. Ferromagnets occur only rarely. Because magnetic research on transuranium compounds only started recently, interesting new examples of magnetic materials are very probable in the future. Thorium compounds do not belong to this class because the absence of the f-electrons excludes the appearance of magnetic moments. Therefore the discussion is concerned mostly with the ordered uranium compounds and to a lesser extent with compounds of plutonium, neptunium, curium and americium.

3.1. Elements

Fournier et al. [1977] identified curium as an antiferromagnetic with the Néel temperature of 52 K. Neutron diffraction studies have shown that the propagating vector is $q = (0, 0, \frac{1}{2})$ and further research on its magnetic order has been undertaken. This is the only actinide metal which is magnetically ordered.

3.2. Compounds

In the following sections the individual groups of compounds are reviewed taking into consideration the experimental and theoretical background.

3.2.1. Hydrides

As already mentioned (section 2.2) β-uranium hydride was identified as the first ferromagnetic actinide substance. β-UD_3 and α-UH_3 are similar types of ferro-

TABLE 4
Ferromagnetic actinide hydrides

Compound	Lattice type	Lattice constants Å	Curie temperature K	θ	Magnetic moment (μ_B) paramagnetic	ordered	References
α-UH_3	BiF_3	4.16	182	174	2.8	0.9	7, 9
β-UH_3	β-W	6.63	168–174	173	2.44	0.9–1.2	1, 2, 3, 4, 6, 10
β-UD_3	β-W	6.62	166–172	177	2.44	0.98	2, 5, 11, 12
PuH_{2+x}	CaF_2	5.56–5.34	107	5(x = 1.78) 85(x = 2.78)	–	0.24 at 76 K	8, 2
$PuD_{2.74}$	CaF_2	–	107	–	–	0.13	8, 2

1. Abraham et al. (1960)
2. Cinader et al. (1976)
3. Flotow et al. (1959)
4. Gruen (1955)
5. Henry (1958)
6. Lin and Kaufman (1956)
7. Mulford et al. (1954)
8. Olsen et al. (1963)
9. Sliwa and Trzebiatowski (1962)
10. Trebiatowski et al. (1952)
11. Trzebiatowski et al. (1954)
12. Ward et al. (1979)

magnets, as is also plutonium hydride PuH_{2+x}, which exist within the CaF_2 type of lattice in a wider composition range $0 < x < 0.7$. Thermodynamic functions for β-UH_3 (Flotow et al. 1959) and for β-UD_3 (Abraham et al. 1960) were determined. Magnetic and electronic properties of β-UD_3 have been recently reinvestigated (Ward et al. 1979). The plutonium hydride was investigated by nuclear magnetic resonance (Cinader et al. 1976) (table 4).

3.2.2. Chalcogenides

The class of actinide chalcogenides yield several magnets (table 5) and especially the monochalcogenides with NaCl structure. For example, the refractory uranium monosulphide US (melting temperature 2460°C) was investigated in detail. The U^{4+} ion, containing f^2 electrons with $J = 4$, was accepted as a component of this metallic conducting compound, representing below 178 K a simple ferromagnet. Neutron diffraction research at 4.2 K has confirmed the magnetic order of uranium moments along the [111] axis (Wedgwood 1972) and a large rhombohedral distortion was established by Marples (1970). There exists a large magnetic anisotropy with an estimated anisotropy field of $H_A = 3000$ kOe (Tillwick and du Plessis 1976a,b). The magnetic form factor was determined on single crystals with polarized neutrons and it follows the model assuming the ground state of the U^{4+} ion to be $^3H_4$ (Freeman et al. 1976).

The compounds USe and UTe exhibit ferromagnetic order, whereas NpS is antiferromagnetic and PuS is a temperature independent paramagnet.

Heat capacity measurements on US and USe within fairly large temperature ranges were carried out by Westrum et al. (1968), Takahashi et al. (1965), Flotow et al. (1971). Galvanomagnetic (Kanter and Kazmierowicz 1964) as well as electric properties of US were determined.

Uranium dichalcogenides UCh_2 do not exhibit a simple magnetic order within the investigated temperature range. USe_2 seems to be metamagnetic and a critical field of 15–18 kOe is sufficient to induce ferromagnetic order (Suski et al. 1972). It may be mentioned here that the surface conditions may influence the magnetic order (Popielewicz 1976).

Existing magnetic data on the orthorhombic uranium sesquichalcogenides U_2Ch_3 indicate that their magnetic behaviour is complex and more research, especially on single crystals, is necessary. In very low magnetic fields U_2S_3 behaves like a ferromagnet, but in higher magnetic fields maxima occur on the magnetization–temperature curves. Finally, U_2Se_3 and U_2Te_3 exhibit complicated behaviour, but their magnetic ordering cannot be established without neutron diffraction experiments (Suski et al. 1976).

U_3Te_4 seems to be ferromagnetic, at least in high magnetic fields, and U_3Se_4 shows more complicated properties (Suski et al. 1972) although there still exist some doubts. It may be mentioned that the phase diagrams of these systems are very complex so that phase changes within the investigated temperature range may occur. U_7Te_{12} may be regarded as ferromagnetic.

TABLE 5
Ferromagnetic actinide chalcogenides

Compound	Lattice type	Lattice constant Å	Curie temperature K	θ	Magnetic moment (μ_B)		References
					paramagnetic	ordered	
US	NaCl	5.487–5.490	172–180	173–180	2.22–2.31	1.20–1.76	2, 3, 4, 13, 14, 15
USe	NaCl	5.71–5.75	160.5–187	188	2.51	1.31–2.0	3, 4, 12
UTe	NaCl	6.146–6.161	102–110	104	2.84	1.10–2.20	3, 4, 6, 11, 15
U_2Te_3	Th_3P_4 (def)		122				17
U_3Te_4	Th_3P_4	9.40–9.42	38 ± 2	40	3.14	1.20	3, 4, 6, 10
U_7Te_{12}	Th_7Te_{12}	$a = 12.320$ $c = 4.293$	73	0	3.07	0.98	5
$UTe_{3.38}$		$a = 8.672$ $c = 13.014$	20				7, 16
$NpSe_3$	US_3 monoclinic	$a = 5.64–5.66$ $b = 4.01$ $c = 19.06–19.11$ $\beta = 79.36–78.30°$	18	−80.8	2.34		1
$NpTe_3$	$LnTe_3$ pseudotetragonal	$a = 4.355$ $c = 25.40$	25	9.8	2.26	0.39	1

1. Blaise et al. (1976)
2. Freeman et al. (1976)
3. Lam and Aldred (1974)
4. Dam et al. (1974)
5. Suski (1972)
6. Suski et al. (1972[b])
7. Suski (1976[b])
8. Tillwick and du Plessis (1976a)
9. Tillwick and du Plessis (1976b)
10. Troć et al. (1971)
11. Trzebiatowski and Sepichowska (1960)
12. Trzebiatowski and Suski (1961, 1962)
13. Trzebiatowski and Suski (1963)
14. Wedgwood (1972)
15. Wedgwood and Kutnietz (1972)
16. Yarembash et al. (1968)
17. Chechernikov et al. (1967)

Further interesting results regarding US may be deduced from its solid solutions (section 3.2.7).

Among the transuranium chalcogenides ferromagnetism has rarely been detected so far. Neptunium trichalcogenides $NpSe_3$ and $NpTe_3$ seem to belong to this class (Blaise et al. 1977), although for the monoclinic US_3 or USe_3 magnetic order has not been established by neutron diffraction. $UTe_{3.38}$ seems to have a ferromagnetic contribution below 20 K (Suski 1976). For the band calculation of An – monocompounds like US, ThP, NpSb, PuN, and others – see Davis (1974).

3.2.3. Pnictides

Among the actinide pnictides antiferromagnetic coupling is represented by the uranium mono- or dipnictides (table 6), but PuP is ferromagnetic. There exists an interesting and extensively investigated group of four ferromagnets within the U_3Pn_4 group (Pn = P, As, Sb, Bi) of cubic symmetry with the Th_3P_4 type of lattice, identified by Trzebiatowski, Troć and co-workers (1962, 1964). U_3P_4 and U_3As_4 show a large magnetocrystalline anisotropy (Buhrer 1969) along the [111] direction. Rhombohedral distortion for this kind of ferromagnet was provided by Przystawa (1970) and confirmed by Sampson et al. (1975). The parameters of magnetocrystalline anisotropy were also calculated by Zelený (1976). The magnetization of U_3As_4 was measured in pulsed fields of 230 kOe (Kačzer and Novotny 1977), giving anisotropy constants $K_1 = -2.67 \times 10^6$ erg/cm^3 and an extraordinary value for $K_2 = -3.45 \times 10^8$ erg/cm^3. The constants estimated by Bielow et al. (1973) for U_3P_4 and U_3As_4 were about $1\text{–}1.5 \times 10^7$ erg/cm^3. $NpAs_2$ is ferromagnetic below 23 K and antiferromagnetic between 180–23 K with longitudinal wave modulation (Fournier et al. 1973). The magnetic constants of the U_3Pn_4 series depend on the An–An distances (fig. 3).

Magnetoresistivity measurements were carried out on U_3P_4 single crystals between 1.8 and 4.2 K using magnetic fields up to 140 kOe. Bazan et al (1977) have suggested that U_3P_4 is a compensated metal and the free electron Fermi surface has been constructed for this substance.

A theory of noncollinear ferromagnetism for U_3Pn_4 ferromagnetics was given by Przystawa and Praweczki (1972) and the number of valency electrons was calculated for Th_3As_4 and U_3As_4 from positron annihilation experiments by Rosenfeld et al. (1974).

The electrical resistivity of single crystals of U_3P_4 and U_3As_4 along [100], [110] and [111] has been measured between 2–230 K (Henkie and Bazan 1971) and its electrical behaviour below and in the vicinity of the Curie temperature may indicate a more complex magnetic structure (Henkie and Klamut 1977). The Barkhausen effect was measured on U_3As_4 single crystals and the dynamics of the magnetization processes was discussed (Filka et al. 1977). From heat capacities of U_3As_4 and U_3Sb_4 thermal functions up to 950 K were derived (Westrum et al. 1976).

Neutron diffraction data show that both U_3P_4 and U_3As_4 exhibit a collinear structure (Leciejewicz et al. 1974).

TABLE 6
Ferromagnetic actinide pnictides

Compound	Lattice type	Lattice constant Å	Curie temperature K	θ	Magnetic moment (μ_B) paramagnetic	ordered	References
β-U_2N_3	La_2O_3	$a = 3.696–3.700$ $c = 5.826–5.840$	186		1.94		13, 15, 16, 20
U_3P_4	Th_3P_4	8.214	136.5–138	138–144	2.75–2.80	1.16–1.55	3, 6, 18, 21
U_3As_4	Th_3P_4	8.521	198	198–205	2.66–2.94	1.42–1.71	17, 18, 21, 22
U_3Sb_4	Th_3P_4	9.112	146	148–155	3.01–3.04	1.29	21, 22
U_3Bi_4	Th_3P_4	9.350	108	110	2.5–3.14	1.30–1.44	17, 19, 24
		9.368	112				
β-UBi	tetrag.	$a = 11.12$ $c = 10.55$	156	154	2.56	1.07	23
NpN	NaCl	4.898	82–100	82–100	2.13–2.44	1.4–2.2	1, 9, 12, 14
$NpAs_2$	Fe_2As	$a = 3.967$ $c = 8.115$	22	130	1.40	0.56	7
PuP	NaCl	5.651	125 126	130	1.06	0.42–0.77	10, 11
PuAs	NaCl	5.86	129	129	0.97	0.35	2
PuSb	NaCl	6.240	85	90	1.0	0.57	9
CmN	NaCl	5.041 5.027	109		7.02		4, 5, 8
CmAs	NaCl	5.905	88		6.58		4, 5, 8

1. Aldred et al. (1974)
2. Blaise et al. (1973)
3. Buhrer (1969)
4. Charvillat et al. (1975)
5. Charvillat et al. (1976)
6. Counsell et al. (1967)
7. Fournier et al. (1974)
8. Kanellakopulos et al. (1976)
9. Lam (1972)
10. Lam et al. (1969)
11. Lander and Lam (1970)
12. Lander and Mueller (1974)
13. Nasu et al. (1972)
14. de Novion and Lovenrelli (1968)
15. Masaki and Tagawa (1975)
16. Sasa and Atoda (1970)
17. Troć et al. (1971)
18. Staliński et al. (1966)
19. Sternbeck et al. (1971a)
20. Trezebiatowski et al. (1962)
21. Trzebiatowski and Troć (1963)
22. Trzebiatowski et al. (1964)
23. Trzebiatowski and Zygmunt (1966)
24. Troć et al. (1971)

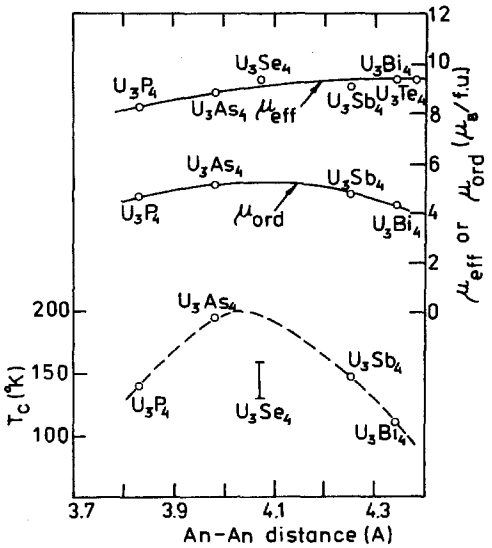

Fig. 3. Magnetic moments and Curie temperatures of U_3X_4 compounds in dependence of An–An distances (after Lam and Aldred 1974).

3.2.4. Compounds with IVA *and* IIIA *group elements*

To this group belong the carbides, silicides, germanides, stannides and plumbides, as well as borides or compounds with Ga, In and Tl (table 7).

The only ferromagnets hitherto known among the carbides are NpC_x and Np_2C_3 in contrast to U_2C_3 or Pu_2C_3, which are temperature independent paramagnets. $NpC_{0.89}$ seems to be antiferromagnetic between 220 and 310 K (Ross et al. 1967). Some germanides like U_3Ge_4, UGe_2 and $PuGe_2$ are again ferromagnetic. All these compounds possess structure types of lower symmetry than those of the analogous pnictide or chalcogenide compounds. Magnetic research on these compounds is rather scarce and more detailed investigations are awaited. Both tin and lead are true metals as are their actinide compounds, the stannides and plumbides; however, there is as yet no evidence regarding magnetic order in these compounds. Among the actinide compounds with IIIA elements the borides are the most characteristic, because boron is the last nonmetallic element going from VI to III group elements. Further, it is similar to the elements having small atomic volumes like hydrogen, nitrogen and carbon.

An interesting case of ferromagnetism occurs in the complex boride system containing uranium and lanthanide elements. The boride system $U_x(Y, La, Lu)_{1-x}B_4$ is ferromagnetic for $U_xLa_{1-x}B_4$ as example at $0.19 < x < 0.82$ although the pure components are not magnetically ordered (Hill et al. 1974). It was observed by nuclear magnetic resonance that only uranium atoms with coordination numbers equal to or smaller than four are magnetically active in this series. Also NpB_2 is ferromagnetic.

Examples of ferromagnetism in compounds with elements of the IIIA group

TABLE 7
Ferromagnetic actinide compounds with IIIA and IVA group elements

Compound	Lattice type	Lattice constant Å	Curie temperature K	θ	Magnetic moment (μ_B) paramagnetic	ordered	References
$U_x(Y, La, Lu)_{1-x}B_4$ $0.12 < x < 0.8$ (Y)	ThB_4		1.6–31				4,5
UGa_2	AlB_2	$a = 4.212$	126–133	125	3.12	1.50	1, 2, 9, 14,
		$c = 4.01$–4.024			3.56	2.1	15, 16
		$c/a = 0.954$				2.28	
U_2Ga_3	ortho-rhombic	$a = 7.583$	23	19	3.0	1.1	14
		$b = 9.398$		22.5	3.1		
		$c = 9.382$					
UGe_2	$ZrSi_2$	$a = 4.06$	52	−89	3.03	0.8	10, 12, 17
		$b = 15.8$					
		$c = 3.97$					
U_3Ge_4	ortho-rhombic	$a = 5.87$	94	67	2.83		17
		$b = 9.88$					
		$c = 8.98$					
NpB_2	AlB_2		99.5			0.3	16
NpC_x	NaCl	5.003 ($x = 0.95$)	190				11, 13
$x = 0.82$–0.98		4.992 ($x = 0.91$)	220			2.1	
		4.994 ($x = 0.89$)	220			1.4	
Np_2C_3	Pu_2C_3	8.1036	109	114	3.4	0.92	3, 6, 7
						1.83	
$PuGe_2$	$ThSi_2$	$a = 4.10$	35			0.14	12
		$c = 13.81$					

1. Ansorge and Menovsky (1968)
2. Buschow and Van Daal (1972)
3. Dunlap and Kalvius (1972)
4. Giorgi et al. (1974)
5. Hill et al. (1974)
6. Lam and Aldred (1974)
7. Lam and Aldred (1974b)
8. Lander et al. (1969)
9. Misiuk et al. (1972)
10. Nellis and Brodsky (1971)
11. de Novion and Lorenzelli (1968)
12. Olsen (1960)
13. Ross and Lam (1967)
14. Sechovsky et al. (1976)
15. Sternberk et al. (1971b)
16. Smith and Hill (1974b)
17. Trzebiatowski and Misiuk (1968)

occur in U_2Ga_3, UGa_2 and $NpAl_3$, but U(Ga, In, Tl, Pb)$_3$ are all antiferromagnets. Only UGa_2 has been investigated in greater detail.

An interesting case is represented by $NpSn_3$ because it is the first example of itinerant antiferromagnetism ($T_N = 9.5$ K) as established by Trainor et al. (1976).

3.2.5. Ternary compounds

There exist a large number of ternary compounds containing chalcogenide and pnictide atoms which exhibit ferromagnetic properties (table 8). Also double chalcogenides and the unique compound UNCl belong to this class of compounds. The compounds of AnPnCh composition are mostly of the PbFCl type of crystal structure related to the anti-Fe_2As type (Flahaut 1974). Many of them have been only roughly investigated, so that often discrepancies in the numerical values of the magnetic and crystallographic data exist. Detailed research on the magnetoresistance of UAsSe was carried out by Wojakowski et al. (1977). It was stated that on single crystals within the temperature range 77–135 K the magnetoresistance is negative and anisotropic. The results were compared with theoretical predictions of Yamada and Takada (1972, 1973).

In some analogous ternary neptunium and plutonium arsenide compounds with S, Se or Te ferromagnetism also occurs and symptoms of itinerant magnetism were established by Blaise et al. (1976).

Interesting magnetic properties are exhibited by the compounds derived from the antiferromagnetic uranium sesquinitride U_2N_3 by the substitution of one nitrogen atom by a V- or VI-group element. Tetragonal compounds like U_2N_2Bi, U_2N_2Sb and U_2N_2Te appear to be ferromagnetically ordered. The uranium-nitride-telluride is the first ferromagnet among actinides whose magnetic moment lies at an angle of $20 \pm 5°$ with the xy plane, as stated by Leciejewicz et al. (1977).

A class of ternary ferromagnetics which occur in systems containing, besides the uranium component, a transition d-metal has been discovered by Noël et al. (1976) (see table 8). Compounds like $CrUS_3$, $CrUSe_3$, $VUSe_3$, $CoUSe_{2.7}$ and FeU_2S_5 were identified as typical ferromagnets and the cobalt-uranium-selenide of variable composition is notable for its very high Curie temperature ($700 < T_C < 1100$).

3.2.6. Intermetallic compounds

At present a limited number of actinide intermetallic materials is known to be ferromagnetic (table 9). One may quote some examples belonging to the Laves phases of the $MgCu_2$-type, with iron or nickel as the second component, and also compounds containing platinum, like UPt or PuPt of the CrB lattice type (table 9). The example of UPt is interesting because the decrease of its interatomic distances through the application of 20 kbar pressure results in a decrease of the saturation moment of 90%, whereas the Curie temperature remains apparently constant (Huber et al. 1975). PuPt perhaps exhibits ferromagnetic properties (Smith and Hill 1974).

In certain cases like (U, Np, Pu, Am)Fe_2 the contributions of both components

TABLE 8
Ferromagnetic ternary actinide compounds

Compound	Lattice type	Lattice constant Å	Curie temperature K	θ	Magnetic moment (μ_B)		References
					paramagnetic	ordered	
UPS	anti-Fe_2As	$a = 3.813$ $c = 7.981$ $c/a = 2.093$	118	120	2.1	0.8	2, 7
UPSe	anti-Fe_2As	$a = 3.951$ $c = 8.185$ $c/a = 2.0716$	102–110	90	2.4	0.9 1.35 ± 0.1	2, 7, 22
UPTe	UGeTe	$a = 4.100$ $c = 17.026$ $c/a = 4.1525$	85	80 (80–300 K) −70 (300 K)	2.6 3.16	1.44 ± 0.15 1.74	20, 21
UAsS	anti-Fe_2As	$a = 3.884$ $c = 8.176$ $c/a = 2.1050$	128–124	−380	3.34	1.1–1.2	1, 2, 7, 13, 22
UAsSe	anti-Fe_2As	$a = 3.962$ $c = 8.422$ $c/a = 2.1256$	118–105	−195	3.41	1.4–1.5 1.36 1.5 ± 0.1	1, 2, 9, 16, 19
UAsTe	anti-Fe_2As	$a = 4.148$ $c = 17.256$ $c/a = 4.1600$	66–62	−95	3.34	1.59 ± 0.15 1.29	1, 2, 15, 19, 21
USbSe	anti-Fe_2As	$a = 4.173$ $c = 8.681$ $c/a = 2.080$	127	115	2.3–2.6	1.5 ± 0.1	7, 9
USbTe	anti Fe_2As	$a = 4.321$ $c = 9.063$ $c/a = 2.097$		110	3.0		7
UNTe	PbFCl	$a = 3.929$ $c = 7.617$ $c/a = 1.9386$	48				24

TABLE 8 (*cont.*)

Compound	Lattice type	Lattice constant Å	Curie temperature K	θ	Magnetic moment (μ_B) paramagnetic	Magnetic moment (μ_B) ordered	References
U_2N_2Sb	La_2O_2S I4/mmm	$a = 3.8925$ $c = 12.319$ $c/a = 3.1648$	166	161	1.78	1.80	15, 24
U_2N_2Bi	La_2O_2S I4/mmm	$a = 3.95$ $c = 12.65$ $c/a = 3.2025$	154	144	1.85	1.90	15, 24
U_2N_2Te	La_2O_2S I4/mmm	$a = 3.967$ $c = 12.581$ $c/a = 3.1714$	71	46	2.65	2.78 2.50 ± 0.05	10, 15, 24
UNCl	PbFCl	$a = 3.979$ $c = 6.811$ $c/a = 1.7117$	33				24
USSe	$PbCl_2$	$a = 7.3363$ $b = 4.1742$ $c = 8.6612$	25	$-12 + 25$	2.92		12, 23
USTe		$a = 7.543$ $b = 4.295$ $c = 8.897$	87	74	2.91–2.94	0.71	12, 14, 23
USeTe		$a = 7.770$ $b = 4.409$ $c = 9.079$	83		2.94	0.91	5, 23
UBiTe	anti-Fe_2As	$a = 4.434$ $c = 9.157$ $c/a = 2.065$		110			7
NpAsS	anti-Fe_2As	$a = 3.883$ $c = 8.344$ $c/a = 2.15$	30			0.15	3, 4
NpAsSe	anti-Fe_2As	$a = 3.972$ $c = 8.584$ $c/a = 2.16$	35			0.17	3, 4

TABLE 8 (*cont.*)

Compound	Lattice type	Lattice constant Å	Curie temperature K	θ	Magnetic moment μ_B paramagnetic	Magnetic moment μ_B ordered	References
NpAsTe	anti-Fe_2As	$a = 4.230$ $c = 8.982$ $c/a = 2.12$				0.65	3, 4
PuAsSe	anti-Fe_2As	$a = 4.002$ $c = 8.686$ $c/a = 2.17$	126		0.5	0.05	3, 4
PuAsTe	$a = 4.266$	$a = 4.266$ $c = 9.067$ $c/a = 2.12$	125		0.64–1.35	0.09	3, 4
$CrUS_3$	ortho-rhombic Pnam	$a = 7.163$ $b = 6.095$ $c = 8.851$	150	−165	5.6	0.46 (60 K)	17
$CrUSe_3$	ortho-rhombic Pnam	$a = 7.484$ $b = 6.382$ $c = 9.276$	110				11
$VUSe_3$	ortho-rhombic Pnam	$a = 7.278$ $b = 6.229$ $c = 9.063$	140				11
$CoUSe_{2.7}$	ortho-rhombic Pnam	$a = 7.338$ $b = 6.229$ $c = 9.063$	700–1100				11

TABLE 8 (*cont.*)

Compound	Lattice type	Lattice constant Å	Curie temperature K	θ	Magnetic moment (μ_B) paramagnetic	Magnetic moment (μ_B) ordered	References
FeU_2S_5	mono-clinic C2/c	$a = 14.697$ $b = 6.326$ $c = 7.024$ $= 96.5°$	250	−190	7.1	0.885 (4.2 K)	18

1. Bazan and Zygmunt (1972)
2. Bazan and Zygmunt (1973)
3. Blaise et al. (1977)
4. Charvillat et al. (1976)
5. Ellert and Slovianskich (1975)
6. Flahaut (1974)
7. Hulliger (1968)
8. Klein, Haneyeld and Jellinek (1969)
9. Leciejewicz and Zygmunt (1972)
10. Leciejewicz et al. (1977)
11. Noël et al. (1976)
12. Pletyushkin et al. (1971)
13. Pietraszko and Łukaszewicz (1975)
14. Rodier and Nicolas (1973)
15. Troć and Zolnierek (1973)
16. Wojakowski et al. (1972)
17. Wolfers et al. (1976)
18. Wolfers and Bacman (1976)
19. Zygmunt and Duczmal (1972)
20. Zygmunt and Czopnik (1973)
21. Zygmunt et al. (1974a)
22. Zygmunt et al. (1974b)
23. Zygmunt et al. (1977)
24. Zolnierek and Troć (1978)

TABLE 9
Ferromagnetic actinide intermetallics

Compound	Lattice type	Lattice constant Å	Curie temperature K	θ	Magnetic moment (μ_B) paramagnetic	ordered	References
$ThCo_5$	$ThNi_5$		290			2.84	6
UPt	CrB	$a = 3.721$ $b = 10.772$ $c = 4.410$	27				1, 2
UFe_2	$MgCu_2$	7.058	160	170	2,0	U: 0.06, Fe: 0.59	6, 7
UNi_2	$MgZn_2$	$a = 4.06$ $c = 8.25$	30	45	2.5	0.12	21
$UCo_{5.5}$	$R\bar{3}m$	$a = 4.76$ $c = 36.49$	360				8, 9, 10
$NpFe_2$	$MgCu_2$	7.144	500			Fe: 1.35, Np: 1.09	7, 11, 12
$NpAl_2$	$MgCu_2$	7.785	56	56	2.3	1.5	14
$NpAl_3$	$AuCu_3$	4.260	62.5			1.2	15, 16
$NpMn_2$	$MgCu_2$	7.230	18			0.3–0.4	11, 12
$NpNi_2$	$MgCu_2$	7.098	28–32	20		1.2	11, 12
$NpOs_2$	$MgCu_2$	7.528	7.5–8	−110	2.3	0.4	14, 17, 18
$NpOs_{2-x}Ru_x$	$MgCu_2$						20
$NpRe_2$	$MgZn_2$	$a = 4.96$ $c = 8.77$	47	47	2.1	0.9	22
PuPt	CrB	$a = 3.816$ $b = 10.694$ $c = 4.428$	19			0.22	3, 4
$PuPt_2$	$MgCu_2$	7.633	6	6	0.89	0.2	5
$PuFe_2$	$MgCu_2$	7.190	600			Pu: 0.45, Fe: 1.47 1.0 (Fe)	7
$AmFe_2$	$MgCu_2$	7.30	350–400			Fe: 1.7 1.5 (Fe)	13, 7

1. Huber et al. (1972)
2. Matthias et al. (1969)
3. Smith and Hill (1974)
4. Huber et al. (1975)
5. Harvey et al. (1973)
6. Chechernikov et al. (1970)
7. Lander et al. (1977a)
8. Derjagin and Andrejew (1976a)
9. Ermolenko et al. (1977)
10. Derjagin and Andrejew (1976b)
11. Aldred et al. (1975a)
12. Gal et al. (1973)
13. Aldred et al. (1976)
14. Aldred et al. (1974)
15. Aldred et al. (1973)
16. Mitchell and Lam (1974)
17. Dunlap et al. (1974)
18. Brodsky and Trainor (1977)
19. Aldred (1975)
20. Aldred et al. (1975)
21. Lam et al. (1974)
22. Brodsky et al. (1978)

to the ordered magnetic moment could be estimated. UFe_2 exhibits small anisotropy and a small uranium moment, so that an electron structure with partially delocalized 5f electrons may be accepted (Lander et al. 1977b). Further differences between these ferromagnetics exist, e.g. $NpAl_2$ has local 5f moments and those of $NpOs_2$ are of rather itinerant character (Aldred et al. 1977).

$NpOs_2$ is ferromagnetic, but on introducing ruthenium in solid solution the ordering gradually vanishes, because with diminishing Np–Np distances delocalization of the 5f electrons occurs (Aldred et al. 1975).

The properties of the iron compounds indicate an increasing localization of 5f electrons as the actinide component will be heavier (Aldred et al. 1976). $AmFe_2$ is especially interesting because neutron diffraction experiments indicate a small moment of $0.4\mu_B$ at the americium site, being antiparallel to the iron moment,

which amounts to 1.7 μ_B. Because the Am^{3+} ion ($f^6:{}^7F_0$) is nonmagnetic, only the Am^{2+} configuration ($f^7:{}^8S_{7/2}$) is likely to be responsible for this magnetic moment (Aldred et al. 1976). The pseudobinary intermetallic system $U_{1-x}Th_xAl_2$, which shows limited solubilities (up to about 30 at%) of the components belonging to the Laves phases type C15 and C32, respectively, exhibit ferromagnetic spin fluctuations as deduced by Trainor et al. (1976) from specific heat and electrical resistivity measurements.

The same kind of magnetism has been intensively studied on the pure compound UAl_2 (Brodsky and Trainor 1977, Fournier et al. 1979).

A ferromagnetic intermetallic compound of composition similar to the well known strong magnetic samarium compound $SmCo_5$ has been identified as $UCo_{5.5}$ (table 9).

3.2.7. Solid solutions

Isotypic actinide compounds often form continuous solid solutions which are the interesting subjects of numerous investigations, because they may be composed of components exhibiting different physical properties such as ferromagnets, antiferromagnets, diamagnets, temperature independent paramagnets. Further, they may be metallic or semiconducting. Most of the research was on systems containing monochalcogenides and pnictides of uranium or thorium. Examples of solid solutions which contain a ferromagnetic component are in table 10.

Neutron diffraction studies of such systems lead to the construction of magnetic phase diagrams. Many types of magnetic order occur in these systems, which contain an antiferromagnetic component depending on composition, temperature and magnetic field intensity.

The metallic system US–ThS was one of those investigated early (Chechernikov et al. 1968), being composed of a ferromagnet (US) and a weak paramagnet (ThS). This system was further investigated by many authors by the study of magnetization, specific heat and neutron diffraction (Danan et al. 1976). Ferromagnetic coupling was established up to the critical composition $U_{0.43}Th_{0.57}S$ and conclusions were drawn about the electronic structure of these alloys. The localized description is apparently in contradiction with the strong electronic specific heat and the band calculations which suggest a 5f–6d band crossing the Fermi level. The band model may therefore better describe the results of the physical measurements than the localized approach (section 3), and the course of

TABLE 10
Some solid solutions of ferromagnetic actinide compounds

NaCl-type		Th_3P_4-type
US–UP	USe–ThSe	U_3P_4–Th_3P_4
US–UAs	UTe–ThTe	U_3P_4–U_3As_4
US–ThS		U_3As_4–Th_3As_4
USe–UP		
USe–UAs		

the magnetization curves in uranium monopnictides, in uranium monosulphide and their mutual solid solutions was explained on this basis (Robinson and Erdös 1973, 1974). Haessler and de Novion (1977) also disagreed with a localized model proposing an electronic structure which is influenced by strong localized spin fluctuations associated with 5f virtual bound states on the uranium atoms.

The system UP–US (Trzebiatowski and Palewski 1969) whose schematic magnetic phase diagram is presented in fig. 4 shows typical behaviour, both from the magnetic measurements and from neutron diffraction measurements (Kuznietz et al. 1969a).

The ferromagnetic region of the UP–USe system extends up to 37 mol% USe, being enlarged by the application of high magnetic fields up to 320 kOe (Trzebiatowski et al. 1971, Suski et al. 1975, Leciejewicz et al. 1974, Schinkel et al. 1977). Metamagnetic behaviour was confirmed by Suski et al. (1975a,b) for 10 and 20 mol% USe.

The solid solutions UAs–US, first investigated by Trzebiatowski and Palewski (1971) are ferromagnetic in magnetic fields below 9.5 kOe if containing more than 20 mol% US. In higher magnetic fields the ferromagnetic region is extended and even at 8 mol% US one observes magnetic hysteresis (Mydlarz and Suski 1976, Mydlarz 1977).

Neutron diffraction in zero magnetic field revealed antiferromagnetic order at 25 mol% US and complex magnetic structures at 25–34 mol% US. Within those compositions the longitudinal spin waves (LSW) structure occurs, which may be understood as a modulation of the magnetic moment along the *c*-axis (Leciejewicz et al. 1971a,b, Lander et al. 1972).

Within the binary system UAs–USe (Trzebiatowski et al. 1967) the transition from the ferro- to the antiferromagnetic region is accompanied by the occurence

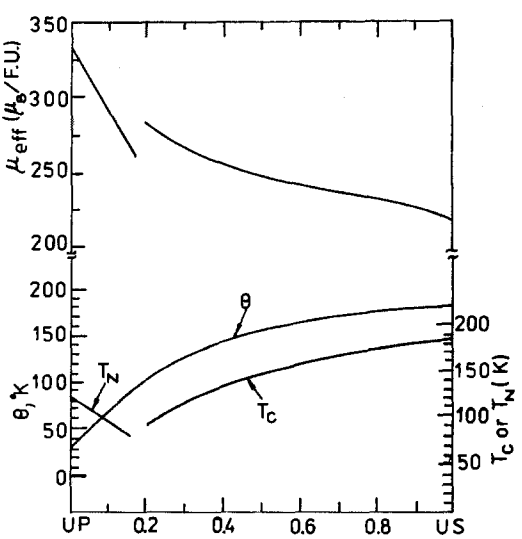

Fig. 4. Magnetic constants of the UP–US system (after Trzebiatowski and Palewski 1969).

of numerous magnetic structures of higher order. They possess magnetic unit cells, being N-multiples (N = 7–11) of the chemical unit cell along one direction. Within these the magnetic moment is cosinusoidally modulated with a periodicity of modulation $\frac{1}{2}N$ as established by Leciejewicz et al. (1971a,b). Samples containing more than 55 mol% USe are ferromagnetic in fields of 50 kOe, after Obolenski and Troe (1977), while solutions containing 33 mol% USe show the coexistence of anti- and ferromagnetism in fields of 80 kOe. Interesting magnetic properties at 25 mol% USe were observed on the magnetization, temperature curves by Palewski et al. (1972) for which sharp maxima occured. In pulsed magnetic fields of more than 100 kOe metamagnetism was observed by Biełow et al. (1973). A magnetic diagram (fig. 5) shows the extended ferromagnetic region in high magnetic fields (Suski 1976a).

Theoretical considerations by Robinson (1973, 1974) and Haessler et al. (1976), on the magnetic behaviour of monocompounds and their solid solutions indicate a complicated band structure. In addition, the possibility of a change in the uranium electronic structure from $5f^n$ to $5f^{n-1}$ exists as it may occur in the $UNi_{5-x}Cu_x$ alloys (Daal et al. 1975).

The model of Grunzweig-Genossar previously applied to the single monocompounds was also extended to solid solutions (Grunzweig-Genossar and Cahn 1973).

The continuous solid solutions of two ferromagnetic components U_3P_4 and U_3As_4 were investigated by Trzebiatowski and Misiuk (1970). The Weiss constants and Curie temperatures vary nearly linearly with composition. The electrical and magnetic properties of U_3P_4–Th_3P_4 solid solutions offer the interesting example of a transition between a metallic and a semiconducting state (Trzebiatowski et al. 1972). The preparation of U_3As_4–Th_3As_4 solid solutions causes some difficulties, but preliminary measurements of their magnetization have been carried out (Markowski, private communication).

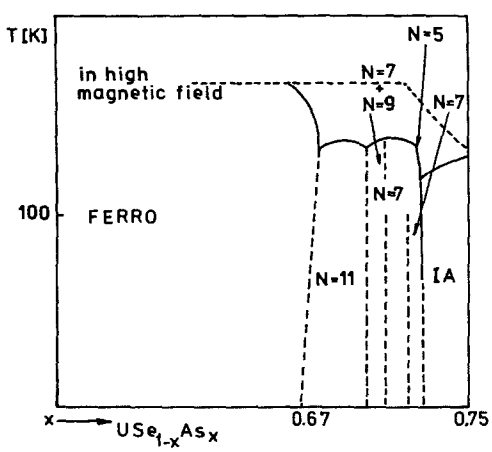

Fig. 5. Schematic magnetic phase diagram of the USe–UAs system (after Suski 1976a).

Further research on solid solutions of different components promises interesting results.

TABLE 11
Antiferromagnetic actinide compounds and intermetallics

Compound	Lattice type	T_N K	References	Compound	Lattice type	T_N K	References
UN	NaCl	52, 55	20, 30, 11	PuN	NaCl	13	30
UP	NaCl	122, 123	20, 39	Pu_3S_4	Th_3P_4	10	31
UAs	NaCl	128	20, 40	UGa	rhombic	27	33
USb	NaCl	213, 241	18, 40	UGa_3	$AuCu_3$	70	26
UBi	NaCl	285, 290	39, 16	UIn_3	$AuCu_3$	100	9
U_2N_3	Mn_2O_3	94, 96	10, 41	UTl_3	$AuCu_3$	80, 90	24
UP_2	Cu_2Sb	203, 206	4, 39	UPb_3	$AuCu_3$	32	22
UAs_2	Cu_2Sb	283	40	UPd_4	$AuCu_3$	30	25
USb_2	Cu_2Sb	206	40	UCu_5	$AuBe_5$	15, 16	8, 25, 27
UBi_2	Cu_2Sb	183	39	UMn_2	$MgCu_2$	260	19
UHg_2	AlB_2	70	24	$NpPd_3$	$AuCu_3$	55	14, 29
USe_2	US_2	11, 13	13, 35	$NpSn_3$	$AuCu_3$	9.5	38
U_2Te_3(?)	Sb_2S_3	106	36	$NpCo_2$	$MgCu_2$	15	3
UOS	PbFCl	55	5	$NpIr_2$	$MgCu_2$	7.5	2
UOSe	PbFCl	72	6	NpPt	CrB	27	32
UOTe	PbFCl	160, 162	33, 37	NpB_4	ThB_4	52.5	31
NpP	NaCl	130	1	$PuBe_{13}$	$NaZn_{13}$	11.5	7
NpAs	NaCl	175	1	$PuPd_3$	$AuCu_3$	24	29
NpSb	NaCl	207	1	$PuRh_3$	$AuCu_3$	6.2	28
NpS	NaCl	20	17	$PuPt_3$	$AuCu_3$	40	15, 28
$NpAs_2$	Cu_2Sb	180	14				

1. Aldred et al. (1974a)
2. Aldred et al. (1974b)
3. Aldred et al. (1975a)
4. Allbutt et al. (1964)
5. Ballestracci et al. (1963)
6. Boelsterli and Hulliger (1968)
7. Brodsky and Friddle (1975)
8. Brodsky and Bridger (1975)
9. Buschow and Van Daal (1972)
10. Counsell et al. (1966)
11. Curry (1965)
12. Fournier et al. (1973)
13. Grønvold et al. (1968)
14. Harvey et al. (1973a)
15. Harvey et al. (1973b)
16. Kuznietz et al. (1969b)
17. Lam et al. (1973)
18. Lander et al. (1976)
19. Lin and Kaufmann (1957)
20. Marples et al. (1975)
21. Misiuk et al. (1972a)
22. Misiuk et al. (1972b)
23. Misiuk et al. (1973)
24. Misiuk et al. (1972c)
25. Murasik et al. (1974a)
26. Murasik et al. (1975)
27. Murasik et al. (1974b)
28. Nellis and Brodsky (1972)
29. Nellis et al. (1974)
30. Raphael and de Novion (1969a)
31. Raphael and de Novion (1969b)
32. Smith and Hill (1974)
33. Staliński et al. (1963)
34. Sternberk et al. (1975)
35. Suski et al. (1972a)
36. Suski et al. (1976)
37. Trainor et al. (1976)
38. Trzebiatowski et al. (1961)
39. Trzebiatowski et al. (1964)
40. Trzebiatowski and Troć (1963)
41. Trzebiatowskiand Troć (1964)
42. Trzebiatowski and Zygmunt (1966)

3.2.8. Final remarks

As is evident from the preceding sections, actinide semi- or intermetallic compounds represent, by comparison with the d-transition and the lanthanide families, a new interesting class of magnetically ordered compounds.

Antiferromagnetic order exists in numerous compounds which are collected in table 11. The types of antiferromagnetic order have only rarely been determined so far. The order may be influenced by different factors, especially by alloying with a third component as well as by applying strong magnetic fields, so that neutron diffraction in magnetic fields promise interesting results.

All these compounds are therefore extremely useful for a wide variety of physical research, which may yield further insight into the specific behaviour and properties of 5f electrons in the solid state.

Acknowledgements

The Author is much indebted to Messr. W. Suski, R. Troć and A. Wojakowski for their assistance in preparing the manuscript.

Monographs and review articles on magnetic properties of actinide elements and semi- or intermetallic compounds

Trzebiatowski, W., 1967, Ferro- und antiferromagnetische Eigenschaften von Uranverbindungen in: Magnetismus, Struktur und Eigenschaften magnetischer Festkörper (VEB Deutscher Verlag für Grundstoffindustrie, Leipzig).

Trzebiatowski, W. and R. Troć, 1973, Recent investigations of the magnetic properties of some uranium compounds, Proc. Int. Conf. Magn. Moscow 1973, vol. IV, p.323–331.

Lam, D.J. and A.T.A. Aldred, 1974, Magnetic properties of actinide compounds in: The actinides, electronic structure and related properties, vols. I and II (A.J. Freeman and J.B. Darby, Jr., eds.) (Academic Press, New York).

Lam, D.J., 1976, Magnetic properties of actinides and their compounds, in The magnetism in metals (J. Lopuszański and J. Przystawa, eds.) (Plenum, New York).

Suski, W., 1976, Magnetic ordering in the actinide intermetallics, in plutonium and other actinides, p. 621–634 (H. Blank and R. Lindner, eds.) (North-Holland, Amsterdam).

Suski, W., 1977, Magnetic and structural properties of actinide compounds, Physica **86–88B**, 11.

Troć, R. and W. Suski, 1977, Magnetism of actinides, in Physics and chemistry of the solid state, ch. 2, p. 41–98 (in polish, PWN Wrocław).

Proceedings 2nd International Conference on the Electronic Structure of the Actinides, 1976, (J. Mulak, W. Suski and R. Troć, eds.) (Zakład Narodowy im. Ossolińskich, Wrocław, 1977).

3rd Int. Conf. on the electronic structure of the actinides, J. de Phys. Suppl. Fasc. 4, 1979.

Brodsky, M.B., 1978, Magnetic properties of the actinide elements and their metallic compounds, Rep. Prog. Phys. **41**, 1547.

Lander, G.H., 1978, Magnetic properties of the actinide systems, Inst. of Physics Conf. Ser. No. 37, 173.

References

Abraham, B.M., D.W. Osborne, H.E. Flotow and R.B. Marcus, 1960, J. Am. Chem. Soc. **82**, 1064.

Aldred, A.T., 1975, Phys. Rev. **B11**, 1169.

Aldred, A.T., B.D. Dunlap and D.J. Lam, 1973, AIP Conf. Proc. no. 18, 366.

Aldred, A.T., B.D. Dunlap, A.R. Harvey, D.J. Lam, G.H. Lander and M.H. Mueller, 1974a, Phys. Rev. **B9**, 3766.

Aldred, A.T., B.D. Dunlap, D.J. Lam, I. Nowik, 1974b, Phys. Rev. **B10**, 1011.

Aldred, A.T., B.D. Dunlap, D.J. Lam, G.H. Lander, M.H. Mueller, I. Nowik, 1975a, Phys. Rev. **B11**, 530.

Aldred, A.J., D.R. Lam, A.R. Harvey and B.D. Darby, 1975b, Phys. Rev. **B11**, 1169.

Aldred, A.T., D.J. Lam, A.R. Harvey and B.D. Dunlop, 1975c, Phys. Rev. **B11**, 1169.

Aldred, A.T., B.D. Dunlap, D.J. Lam and G.K. Shenoy, 1976, in Transplutonium Elements (W. Müller and R. Lindner, eds.) (North-Holland, Amsterdam) p. 191.

Aldred, A.T., B.D. Dunlap and G.H. Lander, 1977, in Proc. 2nd Int. Conf. Electr. Struct. Actinides (J. Mulak, W. Suski and R. Troc, eds.) (Ossolineum, Wrocław) p. 437.

Allbutt, M., A.R. Junkinson, R.M. Dell, in Compounds of interest in nuclear reactor technology, 1964, (J.T. Waber, P. Chiotti, W.N. Miner, eds.) (Met. Soc. AIME New York) pp. 65–81.

Ansorge, V., A. Menovsky, 1968, Phys. Stat. Sol. **30**, K31.

Ballestracci, R., E.F. Bertaut and R. Pauthenet, 1963, J. Phys. Chem. Solids **24**, 487.

Baskin, Y., 1966, J. Am. Cer. Soc. **49**, 511.

Bazan, C. and A. Zygmunt, 1972, Phys. Stat. Sol. (a) **12**, 649.

Bazan, C. and A. Zygmunt, 1973, Preprint Int. Lab. High Magn. Fields, Wrocław, No. 17.

Bazan, C., Z. Henkie and Z. Pawłowska, 1977, in Proc. 2nd Int. Conf. Electr. Struct. Actinides (J. Mulak, W. Suski and R. Troć, eds.) (Ossolineum, Wrocław) p. 431.

Bielow, K.P., A.S. Dmitriewskij, R.E. Levitin, T. Palewski, J.W. Popow, W. Suski, 1973, Zh. Teor. Eksp. Fiz. (Pisma) **17**, 81.

Blaise, A., J.M. Fournier, P. Salmon, 1973, Solid State Commun. **13**, 555.

Blaise, A., J.M. Fournier, P. Salmon and A. Wojakowski, 1976, in Plutonium and other actinides, (R. Blank and R. Lindner, eds.) (AIME, New York) p. 635.

Blaise, A., Charvillat, J.P., Salmon, P., Wojakowski, A., 1977, in Proc. 2nd Int. Conf. Electr. Struct. Actinides, (J. Mulak, W. Suski and R. Troć, eds.) (Ossolineum, Wrocław) p. 475.

Boelsterli, H.U. and F. Hulliger, 1968, J. Mat. Sciences **3**, 664.

Brodsky, M.B. and N.J. Bridger, 1973, AIP Conf. Proc. no 18, p. 357.

Brodsky, M.B. and R.J. Friddle, 1975, AIP Conf. Proc. no 24, p. 353.

Brodsky, M.B. and R.J. Trainor, 1977, Physica **86-88B**, 143; **91B**, 271.

Brodsky, M.B., R.J. Trainor, A.T. Aldred and C.H. Sevans, 1978, J. Appl. Phys. **49**, 1498.

Buhrer, C.F.J., 1969, Phys. Chem. Sol. **30**, 1273.

Buschow, K.W.H. and H.J. Van Daal, 1972, AIP Conf. Proc. no. 5, Magnetism and magnetic materials (C.O. Graham and J.J. Rhyne, eds.) p. 1464.

Calestani, G., J.C. Spirlet and W. Müller, 1979, J. de Phys. Suppl. 4, 106.

Chechernikov, W.I., A.W. Pechennikov, M.E. Barykin, W.K. Slovyanskich, E.I. Yarembash and G.W. Ellert, 1967, Zh. Eksp. Teor. Fiz. **52**, 854.

Cherchernikov, W.I., T.M. Shavishvili, W.A. Pletyushkin, W.K. Slovyanskich and G.V. Ellert, 1968, Zh. Teor. Eksp. Fiz. **27**, 921.

Chechernikov, W.I., W.A. Pletushkin, T.M. Shavishvili, W.K. Slovianskich, 1970, Zh. Eksp. Teor. Fiz. **58**, 80.

Charvillat, J.P., U. Benedict, D. Damien and W. Müller, 1975, Radioanal. Lett. **20**, 371.

Charvillat, J.P., U. Benedict, D. Damien, C.H. de Novion and A. Wojakowski, 1976, in Transplutonium Elements (W. Müller and R. Lindner, eds.) AIME, New York) p. 79.

Charvillat, J.P., A. Wojakowski, D. Damien, 1976, Proc. 2nd Int. Conf. Electr. Struct. Actinides (Ossolineum, Wrocław) p. 469.

Cinader, G., D. Zamir and Z. Hadari, 1976, Phys. Rev. **B14**, 91.

Counsell, J.F., R.M. Dell and J.F. Martin, 1966, Trans. Faraday Soc. **62**, 1736.

Counsell, J.F., Dell, R.M., Junkinson, A.R., Martin, J.F., Trans. Faraday Soc. **63**, 72 (1967).

Curry, N.A., Proc. Phys. Soc. London, **86**, 1193 (1965).

Daal, H.J. van., K.H.J. Buschow, P.B. Van Allen, M.H. Maaren, Phys. Rev. Lett. **34**, 1457 (1975).
Damien, C.A., R.G. Haire and J.R. Peterson, 1979, J. de Phys. Suppl. 4, 95.
Danan, J., C.H. de Novion, Y. Guerin, F.A. Wedgwood, M. Kuznietz, (1976), J. de Phys. **37**, 1169.
Davis, H.L., 1974, in The actinides, vol. II (A.J. Freeman and J.B. Darby, Jr., eds.) (Academic Press, New York) p. 1.
de Novion, G.H., 1979, J. de Phys. Suppl. 4, 1.
de Novion, C.H. and R. Lorenzelli, (1968) J. Phys. Chem. Sol. **29**, 1901.
Derjagin, A.W., A.B. Andrejew, (1976a), Zh. Eksp. Teor. Fiz. (Russ) **71**, 1166.
Derjagin, A.W., A.B. Andrejew, (1976b), Awtorskie swidetelstwa no. 37.
Dunlap, B.D. and G.M. Kalvius, (1972), Int. J. Magn. **1**, 231.
Dunlap, B.D., A.T. Aldred, D.J. Lam, G.R. Davidson, (1974), AIP Conf. Proc. no. 24.
Ellert, G.V., W.K. Slovianskich, (1974), Zh. Neorg. Chim. **19**, 1389, **20**, 504 (1975).
Ellinger, F.H., W.H. Zachariasen, (1971), Phys. Rev. Lett. **32**, 773.
Ermolenko, A.S., A.W. Iwanow, W.E. Komarow, L.M. Mahat, G.M. Makarowa, Ya.S. Shur, (1977), Fizika Metallow i Metallowed. **43**, 446.
Filka, S., A. Menovsky, A. Zentke, (1977), in Proc. 2nd Int. Conf. Electr. Struct. Actinides, (J. Mulak, W. Suski and R. Troc, eds.) (Ossolineum, Wrocław) p. 419.
Flahaut, J., (1974), J. Solid State Chem. **9**, 124.
Flotow, H.E., A.R. Lohr, B.M. Abraham, D.W. Osborne, (1959), J. Am. Chem. Soc. **81**, 3529.
Flotow, H.E., D.W. Osborne, R.R. Walters, (1971), J. Chem. Phys. **55**, 880.
Fournier, J.M. and J. Beille, 1979, J. de Phys. Suppl. 4, 145.
Fournier, M., A. Blaise, P. Salmon, (1973), Proc. Int. Conf. Magnetism, vol. VI, Moscow, p. 52.
Fournier, J.M., A. Blaise, P. Salmon, (1974), Proc. Int. Conf. Magnetism, vol. VI, Moscow, p. 65.
Fournier, J.M., A. Blaise, W. Müller, J.C. Spirlet, 1977, Physica **86–88B**, 30.
Freeman, A.J., 1979, J. de Phys. Suppl. 4, 84.
Freeman, A.J., D.D. Koeling, 1974, in The actinides: electronic structure and related properties (A.J. Freeman, J.B. Darby, Jr., eds.) (Academic Press, New York) p. 51.
Freeman, A.J., J.P. Desclaux, G.H. Lander, J. Faber Jr., 1976, Phys. Rev. **B13**, 1168.
Gal, I., Z. Hadari, E.R. Bauminger, I. Nowik, S. Ofer, M. Perkal, 1973, Phys. Rev. **B8**, 1901.
Giorgi A.L., E.G. Szklarz, R.W. White, H.H. Hill, 1974, J. Less-common. Met. **34**, 348.
Gmelin, ..., 1976, Handbuch der Anorganischen Chemie, VIII auflage Transurane metalle (Springer Verlag, Berlin).
Grønvold, F., Thurman-Moe T. Haraldsen, T. Tufte, 1968, J. Inorg. Nucl. Chem. **30**, 2117.
Gruen, D.M., 1955, J. Chem. Phys. **23**, 1708.
Grunzweig-Genossar, J., J.W. Cahn, 1973, Int. J. Mag. **4**, 193.
Grunzweig-Genossar, J., M. Kuznietz, 1968, J. Appl. Phys. **39**, 905.
Grunzweig-Genossar, J., M. Kuznietz, F. Friedman, 1968, Phys. Rev. **173**, 562.
Haessler, M., C.H. de Novion, 1977, J. Phys. C **10**, 589.
Haessler, M., C.H. de Novion, D. Damian, 1976, in Plutonium and other actinides, (H. Blank and R. Lindner, eds.) (AIME, New York) p. 649.
Harvey, A.R., W.J. Nellis, G.H. Lander, B.D. Dunlap, M.B. Brodsky, M.H. Mueller, 1973a, XIX Ann. Conf. Mag. and Mag. Mat., Boston.
Harvey, A.R., M.B. Brodsky, W.J. Nellis, 1973b, Phys. Rev. **B7**, 4137.
Henkie, Z., 1968, Roczn. Chem. **42**, 363.
Henkie, Z., C. Bazan, 1971, Phys. Stat. Sol. (a) **5**, 259.
Henkie, Z., J. Klamut, 1977, Physica **86–88B**, 991.
Henkie, Z., P.J. Markowski, 1977, J. Cryst. Growth, **41**, 303.
Henry, W.E., 1958, Phys. Rev. **109**, 1976.
Hill, H.H., 1970a, Nucl. Mat. **17**, 2.
Hill, H.H., 1970b, in Plutonium and other actinides (W.N. Miner, ed.) (AIME, New York) p. 2.
Hill, H.H., A.L. Giorgi, E.G. Sklarz and J.L. Smith, 1974, J. Less Common Met. **38**, 239.
Huber, J.G., M.B. Maple, D. Wohlleben, 1972, AIP Conf. Proc. no. 10, 1075.
Huber, J.G., M.B. Maple, D. Wohlleben, 1975, J. Mag. and Mag. Mat. **1**, 58.
Hulliger, F., 1968, J. Less-Common. Met. **16**, 113.
Jullien, R., d'Agliano E. Galleani, B. Coqblin, 1972, Phys. Rev. **B6**, 2139.

Kačzer, J., P. Novotny, 1977, Phys. Stat. Sol. A, **39**, 351.

Kamimoto, M., Y. Takahashi, T. Mukaibo, 1976, J. Nucl. Mat. **59**, 149.

Kanellakopulos, B., J.P. Charvillat, F. Maino, W. Müller, 1976, in Transplutonium elements (W. Müller and R. Lindner, eds.) (AIME, New York) p. 187.

Kanter, M.A., C.W. Kazmierowicz, 1964, J. Appl. Phys. **35**, 1053.

Klein Haneyeld, A.J., F. Jellinek, 1969, J. Less-common. Met. **18**, 123.

Kmetko, E.A., H.H. Hill, 1970, in Plutonium and other actinides (H. Blank and R. Lindner, eds.) (AIME, New York) p. 233.

Koeling, D.D., 1977, in Proc. 2nd Int. Conf. Electr. Struct. Actinides, (J. Mulak, W. Suski and R. Troć, eds.) (Ossolineum, Wrocław) p. 295.

Koeling, D.D., 1979, J. de Phys. Suppl. 4, 117.

Kuznietz, M., G.H. Lander, Y. Baskin, 1969a, J. Appl. Phys. **40**, 1030.

Kuznietz, M., G.H. Lander, F.P. Campos, 1969b, J. Phys. Chem. Solids, **30**, 1642.

Lam, D.J., 1972, AIP Conf. Proc. no. 5, 892.

Lam, D.J., A.T. Aldred, 1974a, in The Actinides: electronic structure and related properties, vols. I and II, (A.J. Freeman and J.B. Darby, Jr., eds.) (Academic Press, New York) pp. 109–179.

Lam, D.J., A.T. Aldred, 1974b, in The actinides: electronic structure and related properties (A.J. Freeman and J.B. Darby, Jr., eds.) (Academic Press, New York) p. 150.

Lam, D.J. and A.T. Aldred, 1979, Proc. AIP Conf. San Francisco No. **24**, 349.

Lam, D.J., F.Y. Fradin, O.L. Kruger, 1969, Phys. Rev. **187**, 606.

Lam, D.J., B.D. Dunlap, A.R. Harvey, M.H. Mueller, A.T. Aldred, I. Nowik, G.H. Lander, 1973, Proc. Int. Conf. Magnetism, Moscow.

Lam, D.J., J.B. Darby, Jr., M.V. Nevitt, 1974, in The actinides: electronic structure and related properties, vols. I and II, (A.J. Freeman and J.B. Darby, Jr., eds.) (Academic Press, New York) pp. 119–184.

Lam, D.J., M.H. Mueller, A.P. Paulikas, G.H. Lander, J. Phys. (Paris) Suppl. 32, C1-917.

Lander, G.H., D.J. Lam, 1970, Phys. Rev. **B14**, 4064.

Lander, G.H. W.H. Mueller, 1974, in The actinides: electronic structure and related properties, vol. I (A.J. Freeman and J.B. Darby, eds) (Academic Press, New York) p. 317.

Lander, G.H., L. Heaton, M.H. Mueller, K.D. Anderson, 1969, J. Phys. Chem. **30**, 733.

Lander, G.H., M.H. Mueller, J.F. Reddy, 1972, Phys. Rev. **B6**, 1880.

Lander, G.H., M.H. Mueller, D.M. Sperlin, O. Vogt, 1976, Phys. Rev. **B14**, 5035.

Lander, G.H., A.T. Aldred, B.D. Dunlap, G.K. Shenoy, 1977a, Physica **86–88B**, 152.

Lander, G.H., A.T. Aldred, B.D. Dunlap and G.H. Shenoy, 1977b, Physica **86–88B + C** 152.

Lander, G.H., M.H. Mueller, D.M. Sparlin, O. Vogt, 1976, Phys. Rev. **B14**, 5035.

Leciejewicz, J., A. Murasik, R. Troć, T. Palewski, 1971a, Phys. Stat. Sol. (b) **46**, 391.

Leciejewicz, J., R. Troć, A. Murasik, T. Palewski, 1971b, Phys. Stat. Sol. B, **48**, 445.

Leciejewicz, J., A. Zygmunt, 1972, Phys. Stat. Sol. A, **13**, 657.

Leciejewicz, J., R. Troć, T. Palewski, 1974, Phys. Stat. Sol. B, K57.

Leciejewicz, J., S. Ligenza, A. Misiuk, A. Murasik, W. Suski, R. Troc, A. Zygmunt, 1974, Proc. ICM, Nauka Moskwa, p. 479.

Leciejewicz, J. Z. Zołnierek, 1977, Troć R., Solid State Comm. 697.

Lin, S.T., A.R. Kaufman, 1956, Phys. Rev. **102**, 640.

Lin, S.T., A.R. Kaufmann, 1957, Phys. Rev. **108**, 1171.

Lovell, G.H.B., D.R. Perels, E.J. Britz, 1971, J. Nucl. Met. **39**, 393.

Marples, J.A., J. Phys. Chem. Solids, 1970, **31**, 2431.

Marples, J.A., C.F. Simpson, F.A. Wedgwood, M. Kuznietz, 1975, J. Phys. C **8**, 708.

Masaki, N., H. Tagawa, 1975, J. Nucl. Mat. **58**, 241.

Matthias, B.T., C.W. Chu, E. Corenzwit, D. Wohlleben, 1969, Proc. Nat. Acad. Sc. US **64**, 459.

Misiuk, A., J. Mulak, A. Czopnik, W. Trzebiatowski, 1972, Bull. Acad. Polon. Sci., Ser. Sci. Chim. **4**, 137.

Misiuk, A., J. Mulak, A. Czopnik, W. Trzebiatowski, 1972c, Bull. Acad. Polon. Sci., Ser. Sci. Chim., **20**, 337.

Misiuk, A., J. Mulak, A. Czopnik, 1972a, Bull. Acad. Polon. Sci., Ser. Sci. Chim. **20**, 891.

Misiuk, A., J. Mulak, A. Czopnik, 1972b, Bull. Acad. Polon. Sci., Ser. Sci. Chim., **20**, 459.

Misiuk, A., J. Mulak, A. Czopnik, 1973, Bull. Acad. Polon. Sci., Ser. Sci. Chim., **21**, 487.
Mitchell, A.W., D.J. Lam, 1974, J. Nucl. Mat. **52**, 125.
Mulford, R.W.R. F.H. Ellinger, W.H. Zachariasen, 1954, J. Am. Chem. Soc. **76**, 297.
Murasik, A., S. Ligenza, J. Leciejewicz, R. Troć, 1973, Phys. Stat. Sol. (a) **19**, K89.
Murasik, A., S. Ligenza, A. Zygmunt, 1974b, Phys. Stat. Sol. **23**, K163.
Murasik, A., J. Leciejewicz, S. Ligenza, A. Zygmunt, 1974a, Phys. Stat. Sol. **23**, K147.
Murasik, A., J. Leciejewicz, A. Zygmunt, 1975, Phys. Stat. Sol. **28**, K107.
Mydlarz, T., 1977, Thesis, Wrocław.
Mydlarz, T., W. Suski, 1976, preprint no. 30, Int. Lab. High Magn. Fields, Wrocław.
Nasu, S., M. Tanaki, H. Tagawa, T. Kikuchi, 1972, Phys. Stat. Sol. B **9**, 317.
Naoumidis, A., H.J. Stocker, 1967, Proc. Brit. Ceram. Soc. no. 8, 193.
Nellis, W.I., M.B. Brodsky, 1971, Phys. Rev. **B4**, 1594.
Nellis, W.J., M.B. Brodsky, 1972, AIP Conf. Proc. no. 5, p. 1483.
Nellis, W.J., A.R. Harvey, G.H. Lander, B.D. Dunlap, M.B. Brodsky, M.H. Mueller, J.F. Reddy, G.R. Davidson, 1974, Phys. **B9**, 1041.
Noël, H., P. Wolfers, G. Fillion, 1977, in Proc. 2nd Int. Conf. Electr. Struct. Actinides (J. Mulak, W. Suski and R. Troć, eds.))Ossolineum, Wrocław) p. 489.
Olsen, C.E., 1960, J. Appl. Phys. **31**, 340.
Olsen, C.E., T.A. Sandenaw, B.T. Matthias, 1963, J. Appl. Phys. **34**, 1358.
Obolenski, M., R. Troć, 1977, in Proc. 2nd Int. Conf. Electr. Struct. Actinides (J. Mulak, W. Suski and R. Troć, eds.) (Ossolineum, Wrocław) p. 397.
Palewski, T., W. Suski, T. Mydlarz, 1972, Int. J. Mag. **3**, 269.
Pietraszko, D., K. Łukaszewicz, 1975, Bull. Acad. Polon. Sci., Ser. Sci. Chim. **23**, 337.
Pletyushkin, V.A., V.J. Chechernikov, V.K. Slovyansky, 1971, Vest. Mosk. Univ. Fiz. Astron. **5**, 605.
Popielewicz, A., 1976, Phys. Stat. Sol. (b) **73**, 147; **74**, 383.
Price, C.E., I.H. Warren, 1965, J. Electrochem. Soc. **112**, 510.
Przystawa, J., 1970, J. Phys. Chem. Solids **31**, 2158.
Przystawa, J., E. Praweczki, 1972, J. Phys. Chem. Solids **33**, 1943.
Raphael, G., C.H. de Novion, 1969a, Solid State Commun. **7**, 791.
Raphael, G., C.H. de Novion, 1969b, J. Phys. (Paris), **30**, 261.
Robinson, J.M., P. Erdös, 1974, Phys. Rev. **B8**, 4333 (1973), Phys. Rev. **B9**, 2187 (1974).
Rodier, N., F. Nicolas, 1973, Bull. Soc. Fr. Minéral Crist. **96**, 356.
Rosenfeld, B., E.D. Bowska and Z. Henkie, 1976, J. Solid State Chem. **17**, 101.
Ross, J.W. and D.J. Lam, 1967, J. Appl. Phys. **38**, 1451.
Ross, J.W., D.J. Lam, 1967, J. Appl. Phys. **38**, 1451.
Sampson, C.F., F.A. Wedgwood, N.S. Satya-Murthy, 1975, J. Phys. C **9**, 4035.
Sasa Y., T. Atoda, 1970, J. Am. Ceram. Soc. **53**, 102.
Schinkel, C.J., W. Suski, T. Mydlarz, 1977, in Proc. Int. Conf. Electr. Struct. Actinides (J. Mulak, W. Suski and R. Troć, eds.) (Ossolineum, Wrocław) 1977 p. 403.
Sechovsky, V., Z. Smetana, A. Menovsky, 1976, in Plutonium and other actinides (H. Blank and R. Lindner, eds.) (AIME, New York) p. 641.
Sevastianov, V.G., G.V. Euert, W.K. Slovianskik, 1972, Zh. Neorg. Khimii, **17**, 16.
Śliwa, A., W. Trzebiatowski, 1962, Bull. Acad. Polon. Sci., Ser. Sci. Chim. **10**, 217.
Smith, J.L. and R.G. Haire, 1978, Science, **200**, 535.
Smith, J.L., H.H. Hill, 1974a, Phys. Stat. Sol. (b) **64**, 343.
Smith, J.L., A.M. Hill, 1974b, AIP Conf. Proc. no. 24.
Smith, J.L., G.R. Stewart, C.Y. Huang and R.G. Haire, 1979, J. de Phys. Suppl. 4, 138.
Spirlet, J.C., 1979, J. de Phys. Suppl. 4, 87.
Stalinski, B., J. Niemiec, Z. Biegański, 1963, Bull. Acad. Polon. Sci., Ser. Sci. Chim. **11**, 267.
Stalinski, B., Z. Biegański, R. Troć, 1966, Phys. Stat. Sol. **17**, K85.
Sternberk, J., A. Sorge, J. Hrebik, A. Menovsky, Z. Smetana, 1971a, Czech. J. Phys. **B21**, 969.
Sternberk, J., V. Ansorge, J. Hrebik, A. Menovsky, Z. Smetana, 1971b, J. Physique, **32**, C1-744.
Sternberk, J., A. Menovsky, T. Swec, A. Zentko, 1975, Phys. Stat. Sol. (a) **28**, K45.
Suski, W., 1972, Phys. Stat. Sol. (a) **13**, 675.

Suski, W., 1976a, in Plutonium and other Actinides (H. Blank and R. Lindner, eds.) (AIME, New York) p. 629.
Suski, W., 1976b, Bull. Acad. Polon. Sci., Sér. Sci. Chim. **24**, 75.
Suski, W., 1979, J. de Phys. Suppl. 4, 43.
Suski, W., A. Czopnik, T. Mydlarz, 1972a, Phys. Stat. Sol. (a) **12**, 525.
Suski, W., T. Mydlarz, V.U.S. Rao, 1972b, Phys. Stat. Sol. (a) **14**, K157.
Suski, W., T. Palewski, T. Mydlarz, 1975a, in Physique sous champs magnétiques intenses, CNRS p. 57.
Suski, W., A. Wojakowski, T. Palewski, 1975b, Phys. Stat. Sol. (a) **27**, K113.
Suski, W., A. Wojakowski, A. Blaise, P. Salmon, J.M. Fournier, T. Mydlarz, 1976, J. mag. Mat. **3**, 195.
Takahashi, and E.F. Westrum, 1965, J. Phys. Chem. **69**, 3618.
Taube, M., 1974, Plutonium-Verlag Chemie.
Tillwick, D.L., P. de V. du Plessis, 1976a, J. Mag. Mag. Mat. **3**, 319.
Tillwick, D.L., P. de V. du Plessis, 1976b, J. Mag. Mag. Mat. **3**, 329.
Trainor, R.J., M.B. Brodsky, B.D. Dunlap, G.K. Shenoy, 1976a, Phys. Rev. Lett. **37**, 1511.
Trainor, R.J., M.B. Brodsky, H.V. Culbert, 1976b, AIP Conf. Proc. no. 34, p. 224.
Troć, R., Z. Zołnierek, 1978, Proc. Int. Conf. Magnetism, vol. VI, Moscow, p. 59.
Troć, R., W. Suski, C. Bazan, 1971, in Conf. Dig. no. 3, Rare Earths and Actinides Durham (Inst. Phys., London) pp. 172–5.
Troć, R., J. Mulak, W. Suski, 1971, Phys. Stat. Sol. (b) **43**, 147.
Trzebiatowski, W., A. Misiuk, 1968, Rocz. Chem. **42**, 161.
Trzebiatowski, W., A Misiuk, Rocz. Chem. 1970, **44**, 695.
Trzebiatowski, W., T. Palewski, 1969, Phys. Stat. Sol. **34**, K51.
Trzebiatowski, W., T. Palewski, 1971, Bull. Acad. Polon. Sci., Sér. Sci. Chim. **19**, 83.
Trzebiatowski, W., A. Sępichowska, 1960, Bull. Acad. Polon. Sci., Ser. Sci. Chim. **8**, 457.
Trzebiatowski, W., W. Suski, 1961, Bull. Acad. Polon. Sci., Ser. Sci. Chim. **9**, 277.
Trzebiatowski, W. and W. Suski, 1962, Bull. Acad. Polon. Sci., Ser. Sci. Chim. **10**, 399.
Trzebiatowski, W., W. Suski, 1963, Rocz. Chem. **37**, 117.
Trzebiatowski, W., R. Troć, 1963, Bull. Acad. Polon. Sci., Ser. Sci. Chim. **11**, 661.
Trzebiatowski, W., R. Troć, 1964, Bull. Acad. Polon. Sci., Ser. Sci. Chim. **12**, 681.
Trzebiatowski, W., A. Zygmunt, 1966, Bull. Acad. Polon. Sci., Ser. Sci. Chim. **14**, 495.
Trzebiatowski, W., A. Śliwa, B. Stalinski, 1952, Rocz. Chem. **26**, 110.
Trzebiatowski, W., A. Śliwa, B. Stalinski, 1954, Rocz. Chem. **28**, 12.
Trzebiatowski, W., J. Niemiec, A. Sępichowska, 1961, Bull. Acad. Polon. Sci., Ser. Sci. Chim. **9**, 373.
Trzebiatowski, W., R. Troć, J. Leciejewicz, 1962, Bull. Acad. Polon. Sci., Ser. Sci. Chim. **10**, 395.
Trzebiatowski, W., A. Sępichowska, A. Zygmut, 1964, Bull. Acad. Polon. Sci., Ser. Sci. Chim. **12**, 687.
Trzebiatowski, W., T. Palewski, A. Sępichowska, R. Troć, A. Misiuk, W. Wojciechowski, A. Zygmunt, Coll. 1967a, Int. CNRS, Propriétés physiques et structurales des dérivés sémimetalliques, Paris, p. 499.
Trzebiatowski, W., A. Misiuk, T. Palewski, 1967b, Bull. Acad. Polon. Sci., Sér. Sci. Chim. **15**, 543.
Trzebiatowski, W., Z. Henkie, A. Misiuk, 1972, in Proc. 11th Int. Conf. Physics of Semiconductors, Warsaw, p. 1287.
Veal, B.W., D.J. Lam, 1974, Phys. Rev. **B10**, 4902.
Ward, J.W., L.E. Cox, J.L. Smith, G.R. Stewart and J.H. Wood, 1979, J. de Phys. Suppl. **4**, 15.
Wedgwood, F.A., 1972, J. Phys. C **5**, 2427.
Wedgwood, F.A., M. Kuznietz, 1972, J. Phys. C **5**, 3012.
Westrum, E.F. Jr., R.R. Walters, H.E. Flotow, D.W. Osborne, 1968, J. Chem. Phys. **48**, 155.
Westrum, E.F. Jr., F. Grønvold, 1977, in Proc. 2nd Int. Conf. Electr. Struct. Actinides (J. Mulak, W. Suski and R. Troć, eds.) (Ossolineum, Wrocław) p. 437.
Wojakowski, A., 1977, Acta. Phys. Polon. A52, 401.
Wojakowski, A., Z. Henkie, 1972, Acta Phys. Polon., in press.
Wojakowski, A., Z. Henkie, Z. Kletowski, 1972, Phys. Stat. Sol. (a) **14**, 517.
Wolfers, P., M. Bacman, 1976, in Proc. 2nd Int. Conf. Electr. Struct. Actinides (J. Mulak, W. Suski and R. Troć, eds.) (Ossolineum, Wrocław) p. 483.

Yamada, and Takada, 1972, Progr. Theor. Phys. **48**, 1828.

Yamada, and Takada, 1973, J. Phys. Soc. Jap. **34**, 51.

Yarembash, E.I., W.K. Slovyanskich, G.V. Ellert, 1968, Yeliseyev Neorg. Mat. **4**, 624.

Zelený, M., Czech. 1976, J. Phys. B **26**, 1174.

Zołnierek, Z., R. Troć, 1978, J. Mag. Mag. Mat., **8**, 210.

Zygmunt, A., A. Czopnik, 1973, Phys. Stat. Sol. (a) **18**, 731.

Zygmunt, A., M. Duczmal, 1972, Phys. Stat. Sol. (a) **9**, 659.

Zygmunt, A., A. Murasik, S. Ligenza, J. Leciejewicz, 1974a, Phys. Stat. Sol. (a) **22**, 75.

Zygmunt, A., S. Ligenza, H. Ptasiewicz, J. Leciejewicz, 1974b, Phys. Stat. Sol. (a) **25**, K77.

Zygmunt, A., W. Suski, T. Mydlarz, 1977, Rév. Chim. Minérale, **14**, 139.

chapter 6

AMORPHOUS FERROMAGNETS

F.E. LUBORSKY

General Electric Company
Research and Development Center
Schenectady, NY 12301
USA

Ferromagnetic Materials, Vol. 1
Edited by E.P. Wohlfarth

CONTENTS

1. Introduction

The terms amorphous solid and glass have no precise meaning. These terms are generally accepted to mean "not crystalline on any significant scale". Simple amorphous solids have random structures but with differing degrees of short range order depending on the nature of their atomic bonding. Thus amorphous metals in which nearest neighbor central forces dominate, form structures similar to the random packing of hard spheres. The principal order present is imposed by the roughly constant separation of nearest neighbors. Other types of order may also be present; for example directional ordering due to magnetic or stress annealing. However, not all disordered materials are amorphous since there are disordered crystalline alloys where different atoms irregularly occupy sites of a regular crystal lattice.

1.1. History

Because of the lack of atomic ordering it was believed for many years that ferromagnetism could not exist in amorphous solids. However, in 1960 Gubanov predicted, on the basis of theoretical analysis, that amorphous solids would be ferromagnetic. This was based on evidence that the electronic band structure of crystalline solids did not change in any fundamental way on transition to the liquid state. This implies that the band structure is more dependent on short-range, rather than long-range order so that ferromagnetism, which depends on short-range order, should not be destroyed in the corresponding amorphous solid.

The first report of an amorphous metallic alloy appears to have been made by Brenner et al. (1950). In this work they electro-deposited nickel–phosphorus alloys, observing only one broad diffuse peak in the X-ray scattering pattern in the non-magnetic high phosphorus alloys. Such alloys have been in use for many years as hard, wear and corrosion resistant, coatings. The present great interest in amorphous metals research stems from reports by Duwaz et al. (1960) on the preparation and properties of amorphous metallic alloys. They introduced two new methods of achieving very rapid quenching from the molten state. Both methods propelled a liquid alloy drop onto a cold surface where it would be spread into a thin film and thus rapidly solidify. Miroshnichenko and Salli (1959)

almost simultaneously reported a device for spreading such a liquid alloy sample between two mutually approaching pistons. These processes are now generally referred to by the onomatopoetic term "splat quenching." The new amorphous and metastable alloys prepared from such equipment were used in the early work to explore the many possibilities opened up by these new rapid quenching techniques. A real technological interest developed after Pond and Maddin (1969) reported on the preparation of continuous ribbons of amorphous alloy. Their method consisted essentially of directing a molten stream of the alloy onto the surface of a rapidly rotating drum. At this point it was now clear that amorphous metallic alloys could be prepared in large quantities at low cost.

The theoretically expected retention of ferromagnetic behavior in amorphous solids was first demonstrated by Mader and Nowick (1965) in work on vacuum deposited Co–Au alloys and soon thereafter by Tsuei and Duwez (1966) in work on splat-cooled Pd-20at.% Si containing some ferromagnetic element partially substituted for the Pd. The first alloy with a substantial magnetization, further confirming Gubanov's predictions, was $Fe_{75}P_{15}C_{10}$, reported by Duwez and Lin (1967). This appeared to be a typical soft ferromagnetic alloy with the large saturation magnetization of 7 kG [0.7 T]* and the relatively low coercive force of 3 Oe [240 A/m]. Simpson and Brambley (1971) appear to have been the first to point out that the amorphous alloys, expected to have no magnetocrystalline anisotropy, should have very low coercivities. However the early amorphous alloys of CoP, prepared by deposition methods had coercivities as high as 10–20 Oe [800–1600 A/m]. These high coercivities are now understood to arise from compositional inhomogeneities demonstrated by Chi and Cargill (1976) from small angle X-ray scattering analysis and from strain–magnetostriction anisotropy. The melt quenched alloys of Fe–P–C appeared to be compositionally much more homogeneous but still developed coercivities of a few oersteds [160 A/m]; many orders of magnitude higher than in the commercially available Fe–Ni alloys. It is now clear that this is the result of the large strain introduced by the rapid quenching in the splat technique. This gives rise to a large strain–magnetostriction anisotropy. Amorphous alloys of Fe–Ni–P–B prepared by the melt-quenching technique into ribbons by solidification on the surface of a rapidly rotating drum exhibited even lower coercivities, in the order of 0.1 Oe [8 A/m]. Luborsky et al. (1975) first demonstrated the reduction of coercivity in these alloys, down to less than 10 mOe [0.8 A/m] by suitable anneals and showed that the changes in properties correlated with the relief of internal strains. At about the same time Egami et al. (1975a) showed that annealing under tensile stress reduced the coercivity of an Fe–Ni–P–B–Si alloy to 3 mOe [0.3 A/m].

In the past few years there has been a literary explosion of both theoretical and experimental results on amorphous magnetic alloys. Many series of alloys have now been reported composed of the transition metal alloys with a wide variety of metalloids. Zero magnetostrictive alloys have been reported in the Fe–Co system; the study of the effects of the electron donor characteristics of the metalloids on magnetization and Curie temperature have led to the

*c.g.s. units will be used throughout with S.I. units in [ ].

development of high moment, high Curie temperature alloys; the studies of the mechanisms responsible for the low temperature embrittlement and magnetic anneal instability have led to the prediction and preparation of alloy compositions possessing greatly improved stability; by suitably annealing amorphous alloys, a variety of compositions have been demonstrated to have dynamic losses, permeabilities and magnetizations which make them competitive in quality to existing commercial alloys; the magnetic and structural stability has been evaluated at higher temperatures and found to be adequate for most foreseeable applications. These results will be described in detail in the main text. Three overlapping stages can be identified in the development of amorphous magnetic alloys as just summarized. The first stage was concerned with preparing this new state of matter by a variety of techniques, confirming its existence and the existence of ferromagnetism in the amorphous solids. The second stage started to systemize the results into an experimental and theoretical framework and then moved towards interest in particular properties. The third and perhaps present stage of work is showing an increased subdivision of interest prompted by an increased awareness of potential applications. For example, increased attention is being given to the production of wide ribbon filaments; to the preparation of alloys to compete for particular applications; to understanding the origins of the extrinsic properties so important in the practical application of a magnetic material; and to evaluating and understanding the long term stability of these alloys.

1.2. Theoretical and technological significance

Until recently the major efforts in solid state physics have been confined to understanding the properties of crystalline solids. Microscopic information has been obtained from studies of the properties of single crystals. Amorphous solids now represent a new state of matter. Some of their properties are entirely as predicted. Other properties have unexpected features and ambiguities. For example, although amorphous solids consist largely of random aggregates of atoms their densities are only slightly different from the density of crystals of the same composition.

The broad theoretical question is, how does the amorphous atomic structure affect all of the magnetic characteristics, e.g., the magnetization, Curie temperature, temperature dependence of magnetization, magnetostriction, spin waves, critical behavior, anisotropy, hysteresis, and coercive force. Each of these will be discussed in some detail in the forthcoming sections of this review. Much of our understanding has come from comparing the properties of the amorphous alloy with the same or similar crystalline alloy. However, this has only limited applicability because most of the interesting amorphous alloys have no simple or single crystalline counterpart. One of the singular advantages of studies on amorphous alloys is that we can vary the composition continuously, to prepare homogenous alloys which can be studied as a function of composition and temperature without complicating interference from structural phase transitions. Although, a few years ago, this statement was thought to be entirely

true, it has now been recognized that phase separation, diffusion of various species and structural relaxations all occur even though the alloy remains amorphous. That is, the amorphous phase is not a stable ground state of the solid. All of these changes can have effects on the observed properties. For example, the Curie temperatures and mechanical properties change on annealing at temperatures well below the crystallization temperature.

There are two technologically important classes of magnetic amorphous alloys; the transition metal–metalloid (TM–M) alloys and the rare earth–transition metal (RE–TM) alloys. The TM–M alloys typically contain about 80at.% Fe, Co or Ni with the remainder being B, C, Si, P, or Al. The RE–TM alloys are covered in vol. 2, ch. 5. The presence of the metalloids is necessary to lower the melting point making it possible to quench the alloy through its glass temperature rapidly enough to form the amorphous phase. Once made the same metalloids stabilize the amorphous phase but their presence drastically alters the magnetic properties of the alloy by donating electrons to the d-band and thus lowering M_s and T_c. The presumed isotropic character of the TM–M amorphous alloys had been predicted to result in very low coercivities and hysteresis loss and high permeabilities; all the properties of technological significance for application as soft magnetic materials. These good properties have been, more or less, achieved in some melt quenched alloys and we can account for their behavior by the same models as used for conventional crystalline soft magnetic materials taking into account the presence of the anisotropies mentioned above.

It is clear that many of the amorphous magnetic alloys will become useful soft magnetic materials. Some of the alloys have been treated to develop losses and permeabilities competitive with some of the very expensive Fe–Ni (Permalloy) alloys. Other alloys, with high magnetizations may compete in higher power transformer application where the Fe-3% Si steels are now used. These amorphous alloys have considerably lower losses, higher permeabilities and are expected to be competitive in cost, but unfortunately the reported alloys have a somewhat lower saturation magnetization than the Fe–3% Si.

1.3. Previous reviews

There have been a number of reviews covering the general phenomena of rapidly quenched metals. Duwez (1966, 1967) reviewed in some detail most of the early work, mainly done in his laboratory. Giessen (1969) alphabetically classified by alloy, work published up to the end of 1968. Giessen and Willens (1970) emphasized the underlying principles of the work reviewed and Anantharaman and Suryanarayana (1971) classified the information obtained from the alloy systems studied. Giessen and Wager (1972) reviewed the structure and properties of amorphous metallic phases produced mainly by quenching from the melt. Jones (1973) provided an extensive compilation of developments in splat-cooling and metastable phases. It included an analysis of the methods available for quenching from the melt and an understanding of how they work, the structural features obtained in both metastable crystalline and amorphous

phases, the response of the as-quenched structures to annealing, and finally the properties and applications of splat-cooled alloys. Jones and Suryanarayana (1973) published a comprehensive annotated bibliography covering the period up to near the end of 1972. The status of our knowledge of the structure of metallic alloy glasses, derived both experimentally and theoretically is covered by Cargill (1975a). Our understanding of the formation and stability of amorphous structures was reviewed by Takayama (1976).

Reviews have also been written covering specifically the magnetic properties of amorphous metallic materials. The properties and understanding of the behavior of almost pure transition metal amorphous films were critically evaluated by Wright (1976). The information available to evaluate amorphous metallic alloys for use as soft magnetic materials was reviewed by Egami et al. (1975a), Gyorgy et al. (1976), and by Luborsky (1977b). The state of understanding of the origin and behavior of ferromagnetism in amorphous solids was covered by Cargill (1975b), by Mizoguchi (1976), by Tsuei (1976), by Hasegawa et al. (1976b) and by Alben et al. (1977).

1.4. Scope of this review

In this review we will first describe the preparation of amorphous metallic solids. Our present state of understanding of the resultant atomic structures will then be described and the experimental methods used to obtain structural information. Finally, the magnetic properties reported will be presented and the origin of these properties will be discussed. The review is restricted to the ferromagnetic alloys possessing stability at least up to room temperature. This scope covers mainly the transition metal–metalloid alloys. The rare earth–transition metal alloys will be covered in vol. 2, ch. 5 of this series.

2. Preparation

Amorphous alloys are all in a metastable state. Their preparation, and stability at room temperature, thus depend on various kinetic barriers to growth of crystal nuclei, if nuclei are present, or to nucleation barriers which hinder formation of stable crystal nuclei. During quenching, the alloy must pass rapidly enough through the temperature range where nucleation can occur so as to prevent nucleation. Cohen and Turnbull (1964) have discussed the origins of these barriers and their dependence on the parameters of the materials. They argue that any liquid can be made into an amorphous solid if cooled rapidly enough. The various methods used to prepare amorphous metallic alloys, to be described next, allow a variety of different alloys to be prepared; alloys which require more or less rapid quenching to achieve the amorphous phase.

There are various techniques in use to determine whether a particular metallic alloy is amorphous, i.e. consisting of an atomic arrangement which has no long-range periodicity. Most often this is done by analyses of X-ray, electron or

neutron scattering experiments. However, the arrangements of the atoms cannot be uniquely determined from these analyses. Disagreement still exists concerning the evidence which is necessary to uniquely characterize a particular sample as amorphous. Strong inferences come from examination in the electron microscope at resolution of the order of a few angstroms, from density measurements and particularly from changes in properties on heating through the crystallization temperature. For example, at the crystallization temperature there are rapid changes in resistivity, heat evolution, magnetic coercive force, mechanical hardness and in other properties.

Amorphous materials such as common glasses and plastics are familiar articles of use to everyone. These are usually prepared by the direct solidification from the melt since they require easily attainable cooling rates to inhibit crystallization. All of the techniques to be described result in effective cooling rates orders of magnitude faster than used for conventional silicate glasses or for casting of ingots into molds. These higher cooling rates are a necessary condition for achieving the amorphous state in metallic alloys.

2.1. Vacuum deposition

The criteria for the formation of an amorphous phase by vapor deposition can be described in terms of whether the added atom is prevented from diffusing more than an atomic distance before it is fixed in position by additional atoms arriving. Vapor quenched amorphous alloys are almost always deposited onto a substrate at a temperature well below the glass temperature, T_g. At substrate temperatures below $\sim\frac{1}{3}T_g$ it is doubtful whether the liquid phase ever exists. When a stream of atoms arrives at a substrate at a temperature T_s, an equilibrium is set up between adsorbed and desorbed atoms. For metal atoms the thermal equilibration time is considerably shorter than the average desorption time. Thus virtually all of the atoms are adsorbed. After arriving at the surface an atom is free to diffuse until it is fixed in position for example by arrival of other atoms. Following Chopra (1969), the average distance traveled by an atom in time t is given by

$$\bar{x} = (2tD_s)^{1/2} \tag{1}$$

where D_s, the surface diffusion coefficient, is given by

$$D_s = a^2\nu \exp(-Q_d/kT_s) \tag{2}$$

where a is the atomic jump distance, approximately $2R$ here, Q_d is the activation energy for diffusion, ν is the vibration frequency, $= h/kT_s$, k is Boltzmann's constant and T_s substrate temperature. An atom can be taken to be free to move for a/R s where R is the deposition rate. Typical values of the parameters, from Scott and Maddin (1976), for representative cases, show that the adatom cannot diffuse more than an interatomic distance before it is frozen in position. Thus the disordered or amorphous phase is highly likely to be formed. The presence on the substrate of different adatoms might both reduce the mobility and increase

the distance that an individual atom would need to diffuse to form an ordered array.

The preparation of pure amorphous films of transition metal *elements* is difficult and produces films which crystallize well below room temperature. Thus deposition must be carried out at very low temperatures. Even then most results are suspect due to trapping of impurities from the vacuum into the film. Extrapolation of properties from results on "dirty" films unfortunately is often necessary. Wright (1976) has recently reviewed these results for the transition metal elements. Crystallization temperatures for these are summarized in table 1.

The alloys of amorphous metals are much more stable and therefore potentially useful. In particular, the rare earth–transition metal (RE–TM) alloys are of interest for magnetic bubble applications, as discussed in volume 2 ch. 5. Although these are usually made by sputtering, they have also been made by evaporation. The preparation of transition metal–metalloid alloys have not been investigated very extensively by vacuum deposition, partly because of the ease of preparing these alloys by the melt quenching techniques and partly because of the large difference in vapor pressure between the constituents. As an example Bagley and Turnbull (1970) have prepared Ni–P alloys, but flash evaporation was necessary.

2.2. *Sputter deposition*

The criteria for formation of an amorphous film by sputter deposition is the same as described for vacuum deposition. The advantage of sputtering is that the deposit composition will be essentially the same as the source material. Sputtering is typically carried out in a partial pressure of an inert gas, such as argon at 10^{-1} Torr using 14 MHz frequency. A power dissipation of 200 watts will give deposition rates of ~400 Å/min [0.7 nm/s]. Sputter deposition has been used

TABLE 1
Comparison of amorphous and crystalline saturation moments and Curie temperatures for the transition metal elements (Wright 1976)

Material	Crystallization Temperature, K	Comments	$\frac{M_s \text{ (amorphous)}}{M_s \text{ (crystalline)}}$	$\frac{T_c \text{ (amorphous)}}{T_c \text{ (crystalline)}}$
Fe	4 (150 Å thick)	Thinner films transform at higher temperatures; e.g., 25 Å at 50 K	0.2–0.6	<1 (in alloys)
Co	38	Increases with impurity content to 80 K at ~1%	0.95–1.00	<1 (in alloys)
Ni	70	Films with several percent of occluded gas	0.3–0.6	0.6–0.8

extensively to prepare rare earth–transition metal films for bubble memory applications as is discussed in volume 2 ch. 5.

2.3. Electrodeposition and chemical deposition

Both electrodeposition and chemical deposition have been used for many years to prepare binary, ternary and more complex amorphous alloys such as NiP, NiB, CoP, NiCoP, and NiCoFeP. The amorphous alloys are formed on deposition from conventional electrolytic or electroless baths provided a sufficiently high percentage of phosphorous or boron is deposited; in the region of 10–30at.%. Typical bath compositions and deposition parameters may be obtained from a number of reference sources, such as Brenner (1963) or Simpson and Brambley (1971). In contrast to the melt quenching and sputtering techniques where the solid product has the same composition as the melt, in both electrodeposition and chemical deposition, the deposit composition varies widely depending on the deposition conditions and bath composition. In addition, there is also a good chance of incorporating hydrogen into the deposit, which will change the magnetic properties and stability.

2.4. Quenching from the melt

To form the amorphous phase by any of the liquid quenching devices, the alloy must cool through the temperature range T_m to T_g, the melting temperature to the glass transition temperature, without crystallizing. The factors controlling T_g and crystallization are both structural and kinetic. The structural factors are concerned with atomic arrangement, bonding and atomic size effects. These factors tend to have limited predictive value, and kinetic factors tend to be dominant. The kinetic factors discussed by Turnbull (1969) and by Spaepen and Turnbull (1976) are the nucleation and crystal growth rate and diffusion rates compared to the cooling rate. The alloy must have a high resistance to homogenous nucleation of crystals and the T_g must occur at temperatures not too far below the liquidus. Thus a low eutectic temperature compared to the melting point of the metallic element coupled with a metal-rich eutectic composition favors the formation of the amorphous phase.

Much of the present interest in amorphous metals in general, and amorphous magnetic metals in particular, is concerned with their preparation by direct solidification from the melt. The interest in this method stems from the wide variety of alloys that can be made as well as from the potential low cost of preparation. Since the pioneering work of Duwez et al. (1960), a number of devices have been reported for obtaining the necessary high quenching rates and for producing continuous filaments. These are described next.

2.4.1. The gun

This technique, shown schematically in fig. 1, was developed by Duwez and Willens (1963). A small quantity, up to 100 mg, of the metal or alloy is melted in

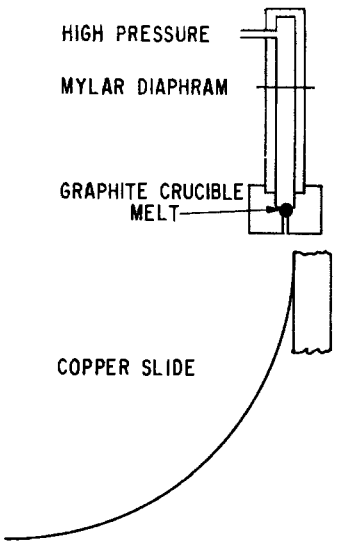

Fig. 1. Apparatus for splat cooling by the gun technique. After Duwez and Willens (1963).

a graphite crucible with an orifice of about 1 mm diameter at the bottom. The melt does not fall through the orifice because of high surface tension. Ejected by means of a shock wave, the molten metal passes through the orifice and spreads onto a copper substrate in the form of thin foils (up to 15μm in thickness). When desired, the substrate can be maintained at low temperatures. The shock wave is generated by the rupture of a thin myler diaphragm located between the high- and low-pressure chambers by means of an inert gas at high pressure. Graphite appears to be the best material for the container for metals and alloys which do not react with carbon. In case of reactive and refractory metals like tantalum, tungsten and zirconium, either a ceramic insert can be kept at the bottom of the crucible or the metal can be melted by radio-frequency induction-heating. The product is an irregular thin foil, porous in nature and with varying cross-sectional area. The thickness of the foils varies. Near the edges and holes, the foils are transparent to the electron beam and hence can be directly examined in an electron microscope. Because of their uneven cross-section, the foils obtained with the "gun" device are not easily suited for the measurement of either physical or mechanical properties.

2.4.2. Piston-and-anvil and double piston

The next technique, developed by Pietrokowsky (1963), utilizes the concept of catching a molten droplet between a stationary anvil and a fast-moving piston. During its fall the molten droplet cuts a beam of light, triggering the piston motion. Based on this simple model, a number of variations of this device with differences in either the melting technique or the process of releasing the piston have been developed over the years. A two-piston device using magnetic yokes

for driving, shown schematically in fig. 2, has recently been described by Cahn et al. (1976). The final product obtained in all the above cases is a foil of almost uniform thickness suited for both physical and mechanical property studies. The thickness may well be up to about 100μm, i.e., roughly ten times that obtained in the "gun" technique, but the cooling rate is considerably reduced. However, since the extraction of heat is from both the surfaces of the foil, the overall cooling rate in this technique is still of the order of 10^5 °C/s.

2.4.3. Centrifuge and rotary splat quencher

Kumar and Sinha (1968) built a simple apparatus to solidify a melt rapidly into foils. This was achieved by melting the material in a graphite crucible with a 0.6 mm diameter hole near the top, and then centrifuging the melt in the crucible. The centrifugal force thus developed ejects the metal onto a copper drum surrounding the crucible. Since the foils or flakes formed are quite thick, the cooling rates are expected to be at least two or three orders of magnitude less than those obtained by the "gun" technique. In the rotary splat quencher described by Cahn et al. (1976), a levitated melted drop falls onto a pair of rapidly rotating vanes in vacuo. The vanes atomize the drop and project it against a surrounding copper cylinder.

2.4.4. Torsion catapult

Roberge and Herman (1968) developed a technique based on a spring-loaded catapult device. In this technique the alloy is melted in a crucible placed at the end of a torsion bar and then catapulted against a cold copper substrate. During its motion, the torsion bar is abruptly stopped when it strikes a shock absorber, while the melt continues to travel at a high speed until it strikes the cold conducting substrate. With this device, bulk foil specimens were obtained, solidified at quenching rates comparable with those of the piston-and-anvil

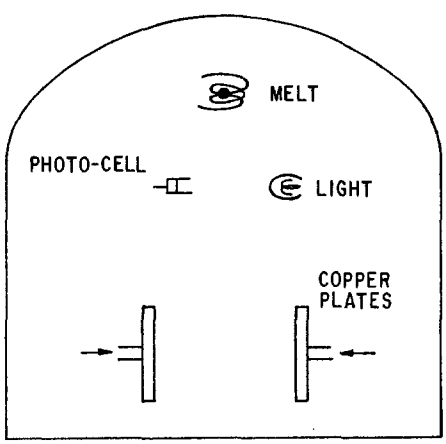

Fig. 2. Apparatus for the two-piston technique of splat cooling. Copper plates are forced together when activated by molten drop passing the photocell. After Cahn et al. (1976).

technique. The greatest advantage of this method is that foils, without any porosity, with an average thickness of 40 to 60μm and suitable for physical and mechanical tests can be obtained. In contrast to the piston-and-anvil technique, foils obtained by the catapult technique are free from effects of plastic deformation. In spite of the continuity of the foils, the thickness along their entire length tends to be irregular.

In all the techniques described so far, the size and amount of the product is limited. If very fast cooling rates have to be realized, the thickness of the foils will, necessarily, have to be small. But it is possible that there need not be any restrictions as regards the length of the sample. Some efforts made in this direction toward obtaining rapidly-quenched foils in large quantities are described next.

2.4.5. Plasma-jet spray

Moss et al. (1964) developed the plasma-jet spraying technique, with quenching rates of the order of 10^7 °C/s, producing material continuously at the rate of a few grams per minute. Both reactive and refractory metals can be quenched since there is no container problem. In this method, fine powder of the alloy is injected into a high-temperature plasma and the molten droplets impinge at a high velocity onto a cooled copper substrate. Although the products of this technique have been used for the measurement of mechanical properties, the fact that they are only 89% dense suggests that the mechanical properties may not be truly representative of the behavior of the material.

2.4.6. Filamentary casting

This technique of casting produces flat filaments with a thickness of 5 to 50μm. It was developed by Pond and Maddin (1969). In their technique, the molten alloy is forced through a sapphire orifice, from a graphite mould, and allowed to strike the interior of a spinning drum, as shown schematically in fig. 3. A

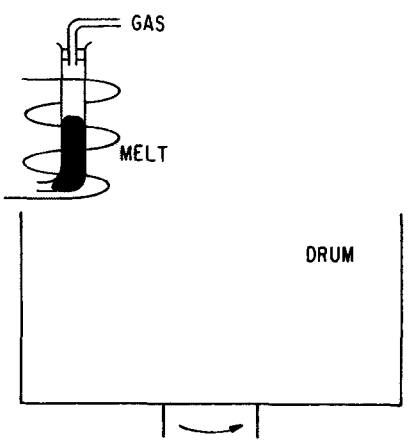

Fig. 3. Apparatus for continuous casting of ribbons. After Pond and Maddin (1969).

pneumatic cage raises the mould slowly so that the impinging melt does not hit the previously solidified ribbon.

Another development in this direction is due to Chen and Miller (1970). Their technique (fig. 4) consists of melting a few grams of alloy and then ejecting it into a pair of rapidly rotating steel rolls, held together under pressure. The drop solidifies while passing through the rollers. The cooling rate is estimated to be 10^5 °C/s. A similar technique, with rolls covered with a hard chrome surface rotating at a high speed has been reported by Babic et al. (1970). Thin uniform ribbons from 10 to 100μm thick are obtained. Variations of this technique are now in common use, for example, where the melt is ejected onto the outside of a drum or the inside tilted lip of a drum (fig. 5). In both cases, the solidified fiber is thrown off the drum as a continuous ribbon. Its length is limited only by the amount of material in the mold. By adjusting the process variables, such as orifice size, ejection pressure, drum velocity, melt temperature and others, the geometry of the filament can be controlled. This has been discussed qualitatively by Pond et al. (1974). Liebermann and Graham (1976) have derived the expression for the cross-section of the ribbon produced

$$A_r = \pi\phi^2(P/8\zeta)^{1/2}v_r \tag{3}$$

where ϕ is the ejection orifice diameter, P is pressure of ejection of the melt as supplied by an inert gas, ζ is the density of the molten alloy and v_r is the velocity of the ribbon which is essentially the surface velocity of the drum. The width of the ribbon is primarily controlled by the orifice diameter and shape. Thus wide ribbon may be produced simply by making the orifice rectangular or elliptical in

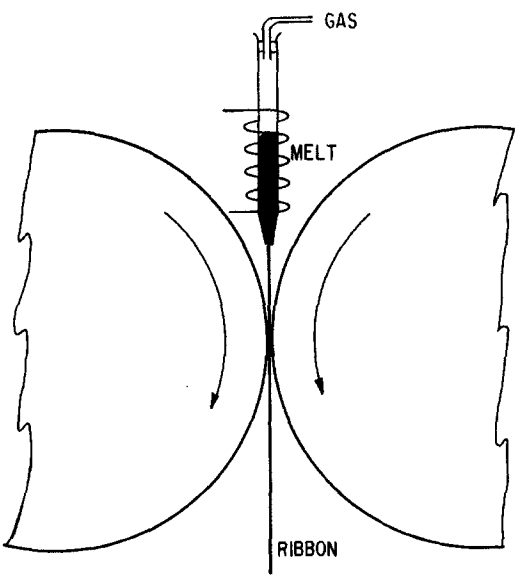

Fig. 4. Double roller casting of ribbons. After Babić et al. (1970).

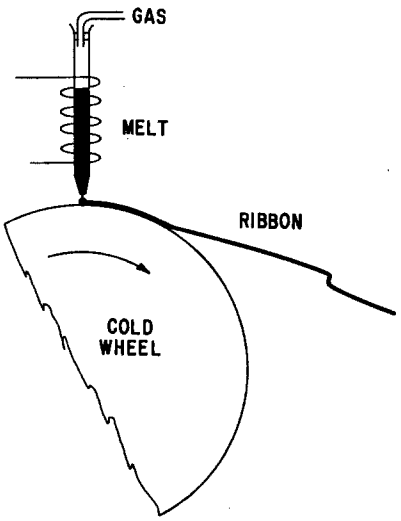

Fig. 5. Single roll casting of ribbons.

shape. Results by Liebermann and Graham (1976) on an Fe–Ni–P–B amorphous alloy agreed with the predictions of eq. (3). A more complete analysis of the casting of ribbons, as well as free jet casting, has been reported by Kavesh (1977) leading to expressions for both ribbon thickness and ribbon width. The various instabilities in the molten jet and solidifying puddle were described.

2.4.7. Melt extraction

There are two melt extraction techniques capable of producing amorphous fiber in a continuous manner; the crucible melt extraction technique and the pendant drop melt extraction technique. These were reported by Maringer and Mobley (1974) and by Maringer et al. (1976). A schematic diagram of the crucible melt technique is shown in fig. 6. The edge of the rapidly rotating disk contacts the clean surface of a molten metal alloy. As the periphery passes through the liquid metal, some metal solidifies, adheres to the disk and is brought up out of the liquid. As a result of thermal contraction and centrifugal force, the metal, now in the form of a fiber, is thrown free after some residence time on the disk. By varying the disk geometry, contact depth, speed, temperature of the melt and other parameters, a variety of ribbon geometries may be made. By introducing notches on the wheel, short fibers are produced directly. Care must be exercised to keep the surface clean of slag and other impurities by operating under an inert gas or in vacuum. The pendant drop melt extraction method is shown schematically in fig. 7 and is a very similar technique. The molten drop is supported by its own surface tension on the end of a rod of the same material. The great advantage of this is that it eliminates any orifices and crucibles and their attendant problems. Because of its simplicity, this technique is readily run in a vacuum system using an electron beam for heating.

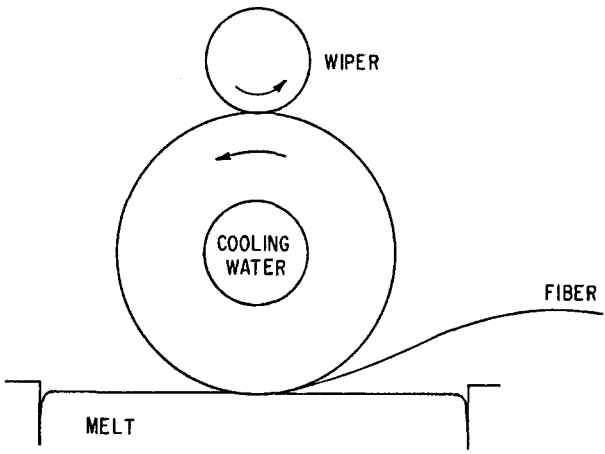

Fig. 6. Crucible melt extraction. After Maringer and Mobley (1974).

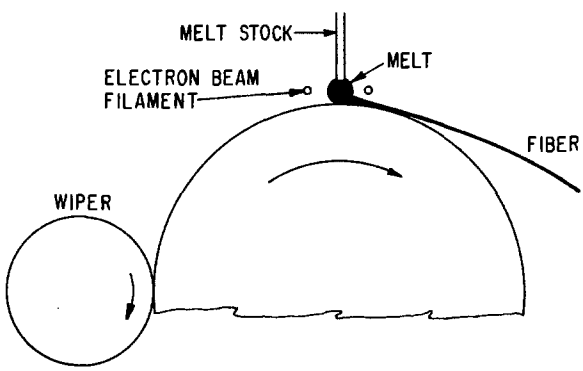

Fig. 7. Pendant drop melt extraction. After Maringer et al. (1976).

2.4.8. Free jet spinning

Free flight spinning involves the formation of a free jet of molten metal and the transformation of the jet to a solid. This procedure is commonly practiced to produce polymeric and oxide glass filaments where the materials have high viscosities and low surface tensions in the liquid state. A cylindrical jet of molten metal however is relatively unstable because of its low viscosity and high surface energy. Several processes are described by Kavesh (1974). Kavesh (1974) has described a process used for melt spinning of amorphous metallic alloys. It consisted of the steps of forming a free jet of molten alloy in a gaseous or evacuated chamber, traversal of the jet through an interface into a liquid medium where the liquid flows in the same direction as the jet and at essentially the same velocity, and finally the solidification of the jet. Water is satisfactory for alloys with melting points below about 700°C; above 700° a refrigerated brine is satisfactory.

3. The structure of amorphous metallic alloys

In order to understand the details of the magnetic properties, some understanding of the structure of these alloys is necessary. Comprehensive reviews of the structures of amorphous alloys have been given by Cargill (1975a, 1976).

3.1. Descriptions of structure

Structure can be discussed on many levels. For example, in terms of the external size and shape of the solid; in terms of cracks, voids, inclusions, composition gradients and other heterogeneities resolvable by optical microscopy or other techniques of similar resolution; in terms of voids and gradients resolvable only by electron microscopy or small angle scattering; and finally very short-range variations due to atomic size variations generally susceptible to examination only by X-ray, electron or neutron diffraction techniques. Most work on the structure of amorphous metallic alloys has, of course, been concerned with this short-range atomic order. However, more recently, attention is being given to larger scale structural effects which may strongly influence the technical and normally extrinsic magnetic properties such as coercive force, losses and permeability. Following Alben et al. (1977) we will distinguish between two types of disorder; structural and chemical. Structural disorder is the lack of crystallinity and refers to the global way in which atoms fit together. Chemical disorder is concerned with local environments; the chemical species and relative positions of the nearest neighbors to an atom. Since the most important magnetic interactions are dependent on what happens at quite short range, then atomic scale properties, such as magnetic moments, are controlled by chemical disorder.

A useful and accessible characterization of the structural arrangement of the atoms in amorphous solids can be given in terms of a radial distribution function, RDF(r). For identical atoms this describes the average number of atoms at distances between r and $r+\mathrm{d}r$ from some chosen atom as origin averaged by taking each atom in turn as the origin. The average number of atoms is then $4\pi r^2 P(r)\mathrm{d}r$, where $P(r)$ is the atomic distribution obtained from experimental X-ray or neutron scattering or by calculation from models. Then

$$\mathrm{RDF}(r) = 4\pi r^2 P(r). \tag{4}$$

Radial distribution functions are defined for systems of different atoms as weighted averages. The weighted averages depend on the composition and on the scattering factors of the individual species. The distribution functions are sometimes presented in slightly different forms as

$$G(r) = 4\pi r[P(r) - P_0] \qquad \text{and} \qquad W(r) = P(r)/P_0 \tag{5}$$

often called the "reduced radial distribution function" and the "pair correlation function" respectively, where P_0 is the average atomic density.

3.2. *Experimental techniques*

3.2.1. *X-ray, electron and neutron scattering*

Experimentally, the RDF(r) is obtained from X-ray, electron or neutron scattering intensities as a function of $K = 4\pi \sin\theta/\lambda$ where λ is the wavelength of the radiation and θ is the scattering angle. Measured intensities are corrected for background, for polarization, and for Compton modified scattering. The interference function $I(K)$ is then calculated using dispersion corrected atomic scattering factors for each atom present. The RDF is then,

$$\mathrm{RDF}(r) = 4\pi r^2 P(r) = 4\pi r^2 P_0 + (2r/\pi) \int_0^\infty K[I(K) - 1] \sin(Kr)\, \mathrm{d}K. \tag{6}$$

Some typical $I(K)$, RDF(r) and $G(r)$ spectra are shown in fig. 8 where r_1 is the value of r for the first diffuse peak. The common feature in all of these spectra is the shoulder on the high K side of the second peak. This shoulder represents the second nearest neighbor local configuration and is absent in interference functions from liquids. In many of these alloys oscillations occur in $G(r)$ out to ~15 Å [1.5 nm] indicating the existence of short-range order out to this distance. The area under the first peak in the RDF(r), called the first coordination number, is associated with the average number of near neighbors. The positions of each peak indicate the atom-to-atom separations involved in this short-range order. The positions of the maxima, r(max), vary slightly depending on the function

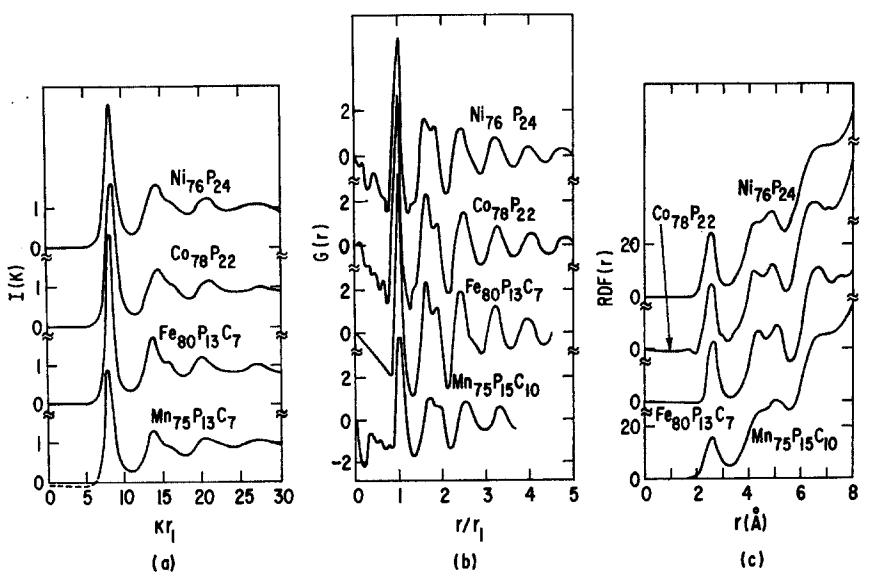

Fig. 8. Metal–metalloid alloys (a) $I(K)$ vs. Kr_1; (b) $G(r)$ vs. r/r_1; and (c) RFD(r) vs. r for alloys with only one metal atom. Cargill (1975a).

being examined

$$r(\max), \quad \mathrm{RDF} \geqslant r(\max), \quad G \geqslant r(\max), \quad W. \tag{7}$$

For the metallic glasses, these differences typically are less than 1% and thus may be ignored.

3.2.2. Electron microscopy

Electron microscope observations have yielded very little direct information about atomic arrangements in amorphous metallic solids. Normal high resolution bright field examination of thinned specimens are free of any features. This was normally interpreted as indicating the absence of crystalline regions; for example by Mader (1965), by Duwez (1967) and by Revcolevschi and Grant (1972). The electron microscope is very useful to detect the first appearance of crystallites on annealing, to follow their growth, and to identify their structure and composition by making use of selected area diffraction. Analyses have been reported for example by Bagley and Turnbull (1970) for crystallization of Ni–P, by Shingu et al. (1976) to study crystal growth in Fe–C and by Walter et al. (1977) to study crystalization of FeNiPB.

Dark field examination of amorphous alloys typically shows features or graininess on the order of 5–15 Å [0.5–1.5 nm] in size. In interference micrographs these features show up as clusters of parallel fringes. These observations were initially interpreted as evidence for a microcrystalline, rather than an amorphous structure in germanium. The graininess in the dark field micrographs of several amorphous metallic alloys was reported by Herd and Chaudhari (1974) although fringes in interference micrographs have not been reported for metallic alloys. These regions of contrast in dark field electron microscopy have been called "coherently scattering domains" by Chaudhari et al. (1972). Analysis by Chaudhari and Graczyk (1974) of dense random packing models for amorphous solids show that the atomic arrangements predicted by these models should produce the observed dark field contrast.

3.2.3. Calorimetry

Calorimetric studies of amorphous alloys have provided substantial fundamental information concerned with configurational entropy, atomic bonding, structural stability and glass formation criteria. Two topics are of particular interest here; crystallization and structural relaxation effects. The kinetics of the onset of crystallization have been studied calorimetrically by Clements and Cantor (1976) and both calorimetrically and magnetically by Luborsky (1977a) in a variety of magnetic alloys. These studies have been used to predict the useful life of the alloys. An irreversible change in heat capacity is observed by differential scanning calorimetry in a number of metallic glasses at temperatures well below crystallization. This has been associated with a structural relaxation and is accompanied by small changes in the Curie temperature. These Curie temperature changes have been reported by Chen et al. (1976) for a variety of alloys as shown in fig. 9.

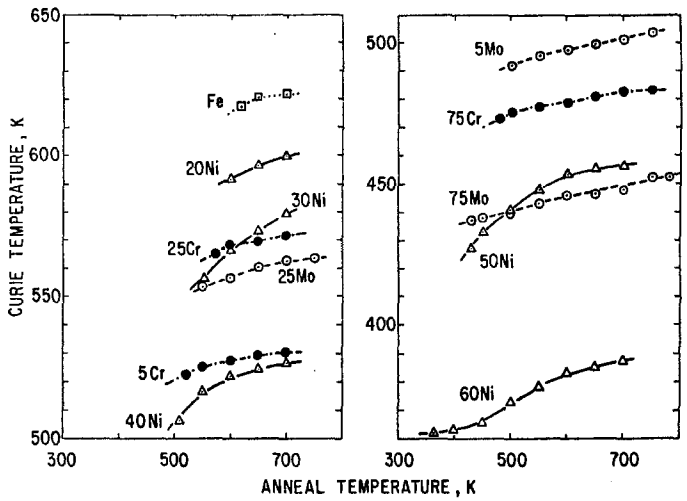

Fig. 9. Curie temperatures as a function of anneal temperature for amorphous alloys $(Fe_xT_{1-x})_{75}P_{16}B_6Al_3$. The value of $1-x$ is given on each curve. Samples heated at a rate of 20 K/min to each anneal temperature T_a in sequence and then immediately cooled. Chen et al. (1976).

3.2.4. Density

The accepted approach to modeling the atomic arrangements in metallic glasses is based on the structures formed by the dense random packing of hard spheres (DRPHS). Such structures are arrangements of rigid spheres (the atoms), dense in the sense that they contain no holes large enough to accommodate another sphere. They are random in that there are only weak correlations between spheres separated by five or more sphere diameters. On the basis of such models the packing fraction and thus the densities may be calculated. This requires specifying the atom radii. It appears best (Cargill 1975a) to use the 12-coordinated Goldschmidt radii for the metal atoms and tetrahedral covalent radii for the metalloid atoms. The calculated densities are usually within ±5% of the measured densities. Even better agreement between calculated and measured densities can be obtained by using the packing fraction, η, calculated from measured densities of closely related alloys. Measured densities and calculated packing fractions are given in table 2. Note that η varies only between 0.64 and 0.78 or $0.71 \pm 10\%$ with most of the values at $0.71 \pm 5\%$. This is somewhat larger than the value expected for the packing of hard spheres. Note also that the packing fractions vary linearly with metalloid or metal content. These density results illustrate the structural similarities between various amorphous alloy compositions. The amorphous alloys generally are only about 2% less dense than their corresponding equilibrium crystalline mixtures.

3.2.5. Resistivity

The low temperature electrical resistivity of amorphous ferromagnets exhibits an anomalous minimum with a logarithmic increase below the minimum which

TABLE 2
Measured densities and calculated atomic packing for some amorphous alloys (in part from Cargill 1975a)

Alloy	Composition x	ρ g/cm^3	ρ_0 at./Å^3	η^*	Reference
$Ni_{100-x}P_x$	18.6	8.00 ± 0.04	0.0900	0.678	Cargill (1970)
	21.1	7.93	0.0904	0.676	
	22.8	7.80	0.0897	0.667	
	24.0	7.79	0.0902	0.668	
	26.2	7.73	0.0905	0.665	
$Co_{100-x}P_x$	15.0	7.9	0.0869	0.677	Davis (1976)
	19.0	7.97 ± 0.04	0.0895	0.668	Cargill and
	20.3	7.94	0.0898	0.687	Cochrane (1974)
	22.0	7.89	0.0900	0.685	
	23.6	7.90	0.0909	0.688	
$Fe_{100-x}P_x$	14.5	7.252 ± 0.04	0.0836	0.681	Logan (1975)
	16.0	7.205	0.0837	0.678	
	18.4	7.128	0.0837	0.672	
	21.6	7.025	0.0838	0.665	
$Fe_{75}P_{15}C_{10}$	–	6.95	0.0882	0.658	Tsuei and Lillienthal (1976)
$Fe_{80}P_{16}C_3B_1$ #2615	–	7.7	0.091	0.735	Allied (1975a)
$Fe_{78}Mo_2B_{20}$ #2605A	–	7.39	0.0933	0.698	Allied (1975b)
$Fe_{75}P_{16}B_6Al_3$	–	7.10	0.0885	0.686	Chen (1975)
$Co_{75}P_{16}B_6Al_3$	–	7.29	0.0867	0.641	Sherwood et al. (1975)
$Ni_{75}P_{16}B_6Al_3$	–	7.71	0.0921	0.672	Chen (1975)
$Fe_{38}Ni_{39}P_{14}B_6Al_3$	–	7.6	0.0917	0.695	Davis (1976)
$Fe_{29}Ni_{49}P_{14}B_6Si_2$ #2826B	–	7.51	0.0896	0.671	Davis (1976)
$Fe_{32}Ni_{36}Cr_{14}P_{12}B_6$ #2826A	–	7.46	0.0887	0.680	Davis (1976)
$(Fe_xCo_{1-x})_{80}P_{13}C_7$	1.0	6.97 ± 0.05	0.0847	0.654	Lin and Duwez (1969)
	1.0	7.54	0.0917	0.708	Fujimori et al. (1976b)
	0.815	7.80	0.0940	0.720	
	0.63	7.64	0.0911	0.693	
	0.50	8.10	0.0960	0.726	
	0.415	8.33	0.0983	0.741	
	0.27	8.13	0.0954	0.714	

TABLE 2 (*cont.*)

Alloy	Composition x	ρ g/cm^3	ρ_0 at./Å^3	η*	Reference
$(Fe_xCo_{1-x})_{75}Si_{15}B_{10}$	0.265	8.13	0.100	0.752	Fujimori et al. (1976b)
	0.07	8.00	0.0982	0.728	
	0	8.46	0.1029	0.765	
	0	8.60	0.1045	0.777	Kazama et al. (1976)
$(Fe_xCo_{1-x})_{78}Si_{10}B_{12}$	0	8.43			
	0.5	8.06	calculated assuming $\eta = 0.75$		
	1.0	7.70			
$Pd_{80}Si_{20}$	–	10.25 ± 0.1	0.0680	0.678	Crewdson (1966)
$(Pd_{0.928}Cu_{0.072})_{100-x}Si_x$	15.5	10.54 ± 0.04	0.0693	0.694	Chen and Park (1973)
	16.5	10.48	0.0694	0.693	
	17.5	10.40	0.0695	0.691	
	18.5	10.33	0.0696	0.689	
	19.5	10.26	0.0697	0.688	
	20.5	10.19	0.0698	0.686	
$(Pd_{0.824}Si_{0.176})_{100-x}Cu_x$	0	10.57 ± 0.04	0.0687	0.691	Chen and Park (1973)
	2	10.53	0.0689	0.691	
	4	10.49	0.0691	0.691	
	6	10.49	0.0695	0.693	
	8	10.44	0.0696	0.693	
	10	10.42	0.0700	0.695	
	12	10.39	0.0702	0.695	
	14	10.35	0.0704	0.695	
$(Pt_{1-x}Ni_x)_{75}P_{25}$	0.2	15.71 ± 0.03	0.0708	0.651	Chen et al. (1973)
	0.3	15.85	0.0774	0.694	
$(Pd_{0.7}Mn_{0.3})_{100-x}P_x$	16	9.11 ± 0.05	0.0674	0.670†	Marzwell (1973)
	17	9.07	0.0676	0.669	
	18	9.00	0.0676	0.665	
	19	8.99	0.0681	0.666	
	20	8.91	0.0680	0.662	
	21	8.89	0.0684	0.662	
	22	8.84	0.0685	0.659	
	23	8.80	0.0687	0.658	
	24	8.78	0.0691	0.658	
	25	8.75	0.0694	0.657	
	26	8.71	0.0696	0.656	
$(Pd_{1-x}Mn_x)_{77}P_{23}$	0.15	9.51 ± 0.04	0.0689	0.660†	Marzwell (1973)
	0.17	9.36	0.0685	0.656	
	0.25	9.03	0.0687	0.658	
	0.30	8.80	0.0687	0.658	
	0.35	8.55	0.0685	0.656	
	0.37	8.46	0.0685	0.656	
	0.38	8.41	0.0685	0.658	

TABLE 2 (*cont.*)

Alloy	Composition x	ρ g/cm^3	ρ_0 at./Å^3	η*	Reference
$(Pd_{1-x}Ni_x)_{80}P_{20}$	0.20	10.08 ± 0.02	0.0725	0.674	Chen et al. (1973)
	0.30	9.97	0.0752	0.681	
	0.40	9.83	0.0778	0.688	
	0.50	9.48	0.0790	0.681	
	0.70	9.05	0.0844	0.689	
	0.80	8.75	0.0867	0.689	
$(Fe_xNi_{1-x})_{80}B_{20}$	0.25	7.94	0.0985	0.697	O'Handley et al. (1976a)
	0.375	7.83	0.0977	0.697	O'Handley et al. (1976a)
	0.50	7.14 ± 0.05	0.0897	0.645	Luborsky, unpublished
	0.50	7.72	0.0969	0.697	O'Handley et al. (1976a)
	0.625	7.65	0.0966	0.701	O'Handley et al. (1976a)
	0.75	7.53	0.0957	0.700	O'Handley et al. (1976a)
	0.875	7.46	0.0953	0.703	O'Handley et al. (1976a)
	1.0	7.05 ± 0.05	0.0907	0.674	Luborsky, unpublished
	1.0	7.39	0.0950	0.707	O'Handley et al. (1976a)
$(Fe_xNi_{1-x})_{80}P_{14}B_6$ # 2826	0.50	7.52 ± 0.05	0.0892	0.676	Luborsky et al. (1975)
	0.50	7.7	0.0913	0.692	Allied (1976a)
	0.625	7.21 ± 0.05	0.0860	0.657	Luborsky, unpubl.
	1.0	6.86 ± 0.05	0.0832	0.650	Luborsky, unpubl.
$(Fe_xCo_{1-x})_{80}B_{20}$	0	8.22	0.1004	0.714	O'Handley et al. (1976a)
	0.125	8.06	0.0991	0.709	
	0.25	7.93	0.0981	0.706	
	0.375	7.84	0.0976	0.706	
	0.50	7.70	0.0965	0.702	
	0.625	7.59	0.0957	0.700	
	0.75	7.52	0.0954	0.702	
	0.875	7.46	0.0953	0.705	
* 2605	1.0	7.39	0.0950	0.707	

* Packing fraction $\eta = (4\pi/3)\langle R^3\rangle\rho_0$, with $\langle R^3\rangle$ calculated using Godschmidt atomic radii (12-fold coordination) for metal atoms (from R.P. Elliot, "Constitution of Binary Alloys," First suppl., p. 870. McGraw-Hill, New York, 1965, except as noted) and "tetrahedral covalent radii" for metalloid atoms (from L. Pauling, "Nature of the Chemical Bond," 3rd ed., p. 246. Cornell Univ. Press, Ithaca, New York, 1960).

Allied Chemical Co. Metglas® alloy designation.

† Twelve-coordinated atomic radius for Mn was taken from W. Hume-Rothery, "The Structure of Metals and Alloys," p. 53. Institute for Metals, London, 1947: this value (1.37 Å) is larger than that given by Elliott (1.30 Å).

Cochrane et al. (1975) have shown to be non-magnetic in origin and to be associated with the amorphous structure. Similar measurements have been reported by a number of other workers as referenced by Cochrane et al. Although this behavior is also characteristic of the Kondo effect, Cochrane et al. showed that it was not caused by magnetic scattering.

One of the advantages of the amorphous metallic alloys for application in devices is the higher resistivity compared to the conventional metallic materials. This results in smaller eddy current contributions to the permeability and losses and is especially important at higher frequencies. Resistivities of the amorphous alloys are generally 2 to 4 times larger than the corresponding transition metal crystalline alloys without the glass formers. The temperature dependence of resistivity for a number of alloys is shown in fig. 10. These curves were obtained by heating at a constant rate; the initial sharp drop in resistivity indicates the beginning of crystallization, T_x, and is marked with an arrow. The first heating at temperatures below crystallization causes a structural relaxation which changes the resistivity slightly. Subsequent heating and cooling is then reversible if T_x is not exceeded. The available data for the change in resistivity with composition is shown in fig. 11.

3.3. Structural results

The principle source of information on the atomic arrangements in amorphous alloys comes from diffraction results. It is now clear that the dense random packing of hard spheres, DRPHS, model qualitatively accounts for the major features in the radial distribution functions. This comparison for NiP is shown in

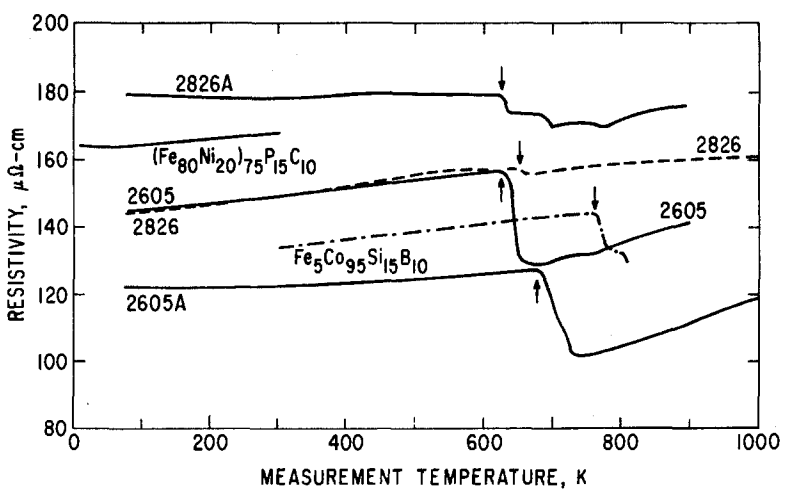

Fig. 10. Temperature dependence of resistivity of some amorphous alloys. Numbers refer to Allied Chemical Co. Metglas® compositions as listed in table 9 and measured by Teoh et al. (1977). FeNiPC, Hasegawa and Dermon (1973); FeCoSiB, Fujimori et al. (1976b).

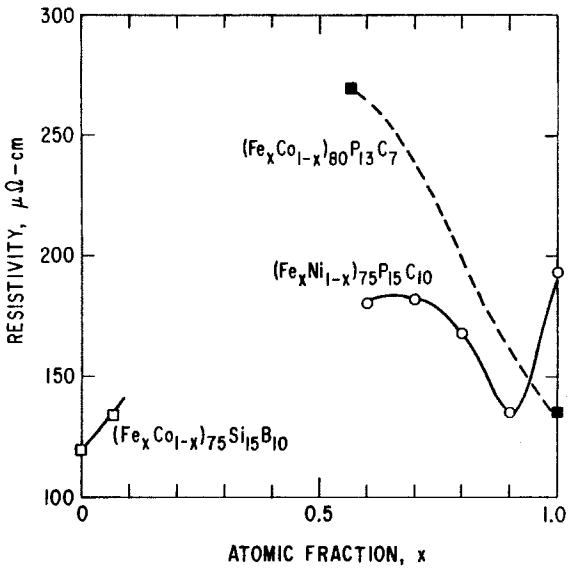

Fig. 11. Dependence of resistivity on composition for some amorphous alloys at room temperature. FeNiPC, Hasegawa and Dermon (1973); FeCoSiB and FeCoPC, Fujimori et al. (1976b).

fig. 12 from Cargill (1975a). However recent results reporting the partial interference functions associated with individual atomic pairs are not in complete agreement with the calculations of the DRPHS model, as discussed more recently by Cargill (1976).

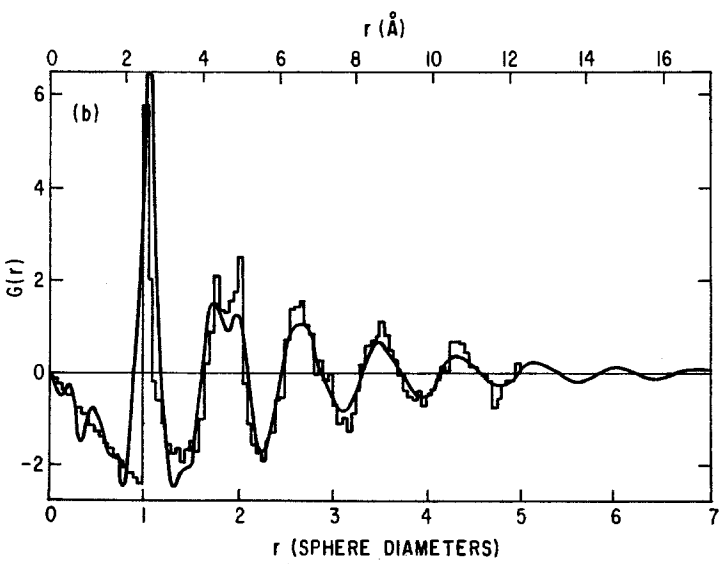

Fig. 12. Comparison of reduced radial distribution functions $G(r)$ for DRPHS structure and for amorphous $Ni_{76}P_{24}$. Cargill (1975a).

Annealing of amorphous structures reported by Waseda and Masumoto (to be published) indicates that detectable changes occur in the atomic structure in amorphous $Fe_{80}P_{13}C_7$ before any indication of crystallization is detected by transmission electron microscopy or by appearance of crystalline features in X-ray interference functions. The first two maxima in $I(K)$ become slightly higher after anneals at 300°C for varying times. The magnitude of oscillations at larger K values also appears to increase. Luborsky et al. (1976b), on the other hand, reported no detectable change in the diffuse X-ray scattering pattern from amorphous $Fe_{40}Ni_{40}P_{14}B_6$ both after cold rolling and after annealing to temperatures just below detectable crystallization.

Small angle X-ray scattering provides results related to compositional homogeneity. In the same paper Luborsky et al. (1976b) report that cold rolling the $Fe_{40}Ni_{40}P_{14}B_6$ alloy reduces the intensity of the small angle scattering, interpreted as improving the homogeneity, while annealing increased the small angle scattering, suggesting the possibility of phase separation taking place. More detailed analysis of these results by Walter et al. (1977) indicates that the scattering regions in the as-cast material are ~32 Å [3.2 nm] in diameter, ~250 Å [25 nm] apart, and constitute about 1% of the volume of the sample. Their size does not change on annealing but their number increases. These changes appear to have no direct effect on magnetic properties. Cold rolling produced a completely flat $I(K)$ versus K curve, indicating no inhomogenieties were present but subsequent annealing again developed scattering regions. The rolling also produced very large increases in coercivity and decreases in remanence. Subsequent annealing returned these parameters to values representative of annealed specimens which had not been rolled. Small angle X-ray scattering has also been used to characterize the inhomogeneities in Co–P. Chi and Cargill (1976) have interpreted their results as showing that this electroless deposit contained anisotropic inhomogeneities; ~100–300 Å [10–30 nm] in the film plane and $\geq$2000 Å [200 nm] normal to the film plane. It is believed that these regions influence the magnetic properties. On annealing, these inhomogenieties decreased in size in contrast to the results on the melt quenched $Fe_{40}Ni_{40}P_{14}B_6$.

3.4. Stability

There are three kinds of stability of significance for amorphous magnetic alloys: their resistance to the initiation of crystallization, structural relaxation effects and the relaxation or reorientation of directional order. These will each be discussed briefly here.

3.4.1. Crystallization

The formation and resultant stability of amorphous alloys are important topics both theoretically and technologically. The theoretical analysis of the factors controlling the ease of formation and the stability of the resultant amorphous alloys have been reviewed and discussed in many previous reviews, for example in the extensive general review by Jones (1973), from the thermodynamic

viewpoint by Turnbull (1974), and most recently by Takayama (1976). The ability of an alloy to be quenched into the glassy state is generally measured by the magnitude of the quantity

$$\Delta T_g = T_m - T_g \tag{8}$$

where T_m and T_g are the melting and glass temperature respectively. In a similar manner the stability of the glass after formation is generally measured by the magnitude of the quantity

$$\Delta T_x = T_x - T_g \tag{9}$$

where T_x is the temperature for the onset of crystallization. As the temperature decreases from T_m the rate of crystallization will increase rapidly but then fall rapidly as the temperature decreases below T_g. Thus if one quenched a molten alloy rapidly enough to a temperature below T_g a quasi-equilibrium amorphous phase is obtained. Note that there is no direct relation between the ease of formation and the resultant stability of an amorphous ally. Cohen and Turnbull (1961) noted that the composition most favorable for glass formation is near the eutectic; the deeper the eutectic the better is the glass forming ability. At such a point the liquid is particularly stable against crystallization.

There have been three approaches to relating the stability of the glass, i.e. its ability not to crystallize, to its microstructure. The first is based on Bernal's model of randomly packed hard spheres as developed by Cargill (1970), Bennett et al. (1971), Polk (1972) and Turnbull (1974). In this model the metal atoms are assumed to form a random network of close packed hard sheres and the smaller metalloid atoms fill the holes inherent in such a structure. The most stable configuration corresponds to the situation when all the holes are filled, corresponding to about 20at.%. This is near the eutectic composition of many of the alloys and is in the range of the stable glass compositions. Although this simple geometrical model has been successful in accounting for the observed glass-forming ability of many metallic alloys it would be surprising if only the atomic radii were important. In the second approach to understanding glass stability, Chen (1974) discusses the effect of atomic sizes and interatomic interactions, i.e., chemical bonding, and suggested that it is chemical bonds which are the dominating factor in glass formation and stability. The third approach was suggested by Nagel and Tauc (1975, 1976) and is based on the role of the electron gas. They showed that under certain circumstances a nearly free electron gas will produce a barrier against crystallization.

Luborsky (1977a) has clearly shown that the end-of-life as far as magnetic applications are concerned corresponds to the onset of crystallization. At the onset of crystallization, the coercive force and losses increase and the remanence and permeability decrease all at a very rapid rate for a small increase in temperature. All of the available information on the time–temperature behavior for the onset of crystallization in amorphous alloys of potential interest is summarized in fig. 13. The results were obtained by transmission electron microscopy and diffraction studies for FePC, CoSiB, and NiSiB. Calorimetric

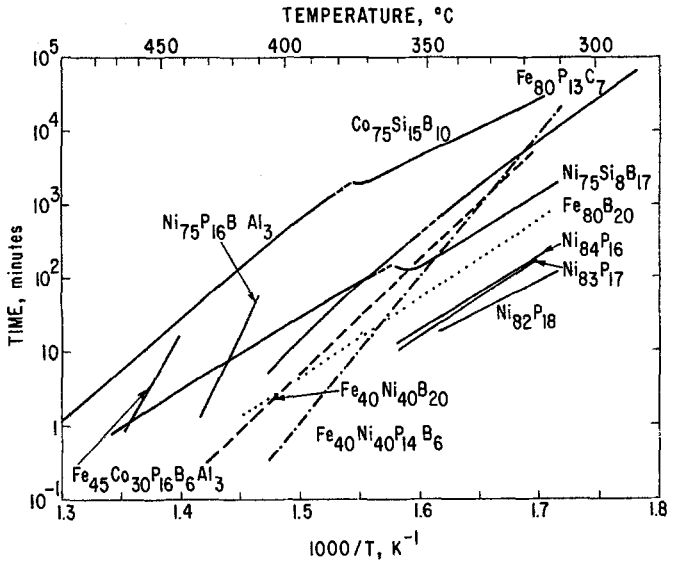

Fig. 13. Time for the start of crystallization as a function of temperature. FePC from Masumoto and Maddin (1975) and Masumoto et al. (1976); CoSiB, NiSiB from Masumoto et al. (1976); NiP from Clements and Cantor (1976); NiPBAl, FeCoPBAl from Coleman (1976); FeB, FeNiB, FeNiPB from Luborsky (1977a).

studies were used for the results on NiP, NiPBAl, and FeCoPBAl alloys. Both calorimetric and magnetic tests were used to obtain the crystallization results on FeB, FeNiB and FeNiPB. It is of interest to note that some of the t–T curves are discontinuous, e.g., the curves for CoSiB, NiSiB and FePC. These discontinuities are the result of the formation of different phases; at temperatures below the break a single metastable crystalline phase forms while at temperatures above the break small metastable crystals form in the amorphous phase. It is therefore apparent that extrapolation of high temperature results to lower temperatures may be very misleading.

The results in fig. 13 are close to straight lines represented by an Arrhenius relation for the time for the onset of crystallization

$$t_x = t_{o,x} \exp(\Delta E_x/kT). \tag{10}$$

These incubation times are a common feature of phase transformations. They may be considered to be the time required for a population of nuclei characteristic of the annealing temperature to be achieved. The existence of an incubation time therefore implies that no suitable sized nuclei exist in the as-quenched glass. Davies et al. (1974) applied this approach to the interpretation of the formation and stability of some glasses and Davies (1976) recently reviewed this subject. It can be readily shown that eq. (10) can be derived from transformation theory where ΔE_x is the activation energy for viscous flow, and other terms have been omitted because they have an insignificant temperature dependence in this region of temperature.

Luborsky (1977a) showed that the activation energies for the onset of crystallization, ΔE_x, obtained from the slopes of the lines in fig. 13, correlate well with the values of ΔT_x for the stability of amorphous alloys as given by eq. (9) and as obtained from scanning calorimetry. The values of ΔE_x also appear to correlate well with the number of atomic species in the alloy; the more complex the alloy the greater is ΔE_x. Some results are shown in table 3. Similar correlations between thermal stability as measured by ΔT_x and ΔE_x were discussed experimentally and theoretically by Chen (1976), but using the time of transformation to the peak in the exotherm, rather than to the start of the exotherm, to obtain ΔE_x. The effect of this difference in measurement on ΔE_x appears to be small.

The effect of alloying elements on the crystallization temperature has been studied by Naka et al. (1976) in the series $Fe_{80-x}M_xP_{13}C_7$ and by Luborsky (1977a) in $Fe_{80-x}Ni_xP_{14}B_6$ and $Fe_{80-x}Ni_xB_{20}$ alloys. Calorimetric measurements were made at a heating rate of 5 deg/min and 40 deg/min respectively, to determine T_x the temperature for the beginning of the crystallization exotherm.

TABLE 3
Activation energy for crystallization of various amorphous alloys (Luborsky 1977a)

Alloy	ΔE_x eV	T_g °C	$T_x - T_g$	Reference
$Ni_{75}P_{16}B_6Al_3$	6.5 6.7**	417	10†	Coleman (1976)
$Fe_{45}Co_{30}P_{16}B_6Al_3$	5.5	456	16	Coleman (1976)
$Fe_{75}P_{16}B_6Al_3$	4.8**	477	−50††	Chen (1976)
$Fe_{40}Ni_{40}P_{14}B_6$	3.9	405	9	Luborsky (1977a)
$Co_{75}P_{16}B_6Al_3$	3.2**	487	−87††	Chen (1976)
$Fe_{80}P_{13}C_7$	3.1 2.4*	–	–	Masumoto et al. (1976) Masumoto and Maddin (1975)
$Fe_{40}Ni_{40}B_{20}$	3.0	442	9†	Luborsky (1977a)
$Co_{75}Si_{15}B_{10}$	2.8 1.6*	–	–	Masumoto et al. (1976)
$Fe_{80}B_{20}$	2.1	441	7†	Luborsky (1977a)
$Ni_{75}Si_8B_{17}$	2.0 2.0*	–	–	Masumoto et al. (1976)
$Ni_{83}P_{17}$	2.0	–	–	Clements and Cantor (1976)
$Ni_{84}P_{16}$	1.9	–	–	Clements and Cantor (1976)
$Ni_{82}P_{18}$	1.6	–	–	Clements and Cantor (1976)

* The low temperature activation energy.
** Evaluated from time to reach peak in crystallization exotherm.
† T_x from DSC at 40 deg/min.
†† T_x from DSC at 20 deg/min by extrapolation.

Although the use of a constant rate of heating will give interesting correlations, the results cannot be extrapolated to other temperatures of interest and do not necessarily correlate with isothermal results as seen by comparing the 2 hour anneal results for the FeNiPB alloys with the scanning results in fig. 14; the trends are in opposite directions. Naka et al. concluded from their results that the atomic size of the alloying elements had little or no effect on T_x; second that the electronegativity also had little or no effect but; thirdly, the relative valency did seem to correlate with the trends in T_x. Their results of T_x as a function of average outer electron concentration show this correlation, taking for the number of outer electrons for Ti, V, Cr, Mn, Fe, Co, and Ni, 4 through 10 respectively. Thus they conclude that the crystallization temperature is predominantly governed by the nature and strength of the bonding of the atoms in these alloys.

3.4.2. Structural relaxation

Irreversible structural changes are observed at times and temperatures well below those necessary to initiate crystallization, and both magnetic and mechanical properties are drastically altered. Heating as-cast samples results in two broad peaks in differential scanning calorimetry, indicating two different modes of rearrangement as discussed by Chen and Coleman (1976). These structural changes produce a small change in Curie temperature (fig. 9) without a significant change in saturation moment. This change in T_c after structural relaxation is mostly the result of the change in the interatomic distances, but may also be affected by the change in average coordination number. An

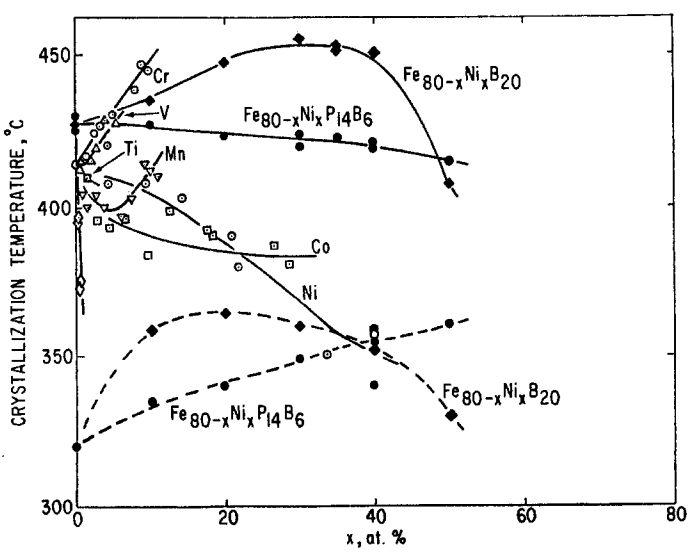

Fig. 14. Temperatures for the start of crystallization. For $Fe_{80-x}M_xP_{13}C_7$ alloys from Naka et al. (1976) using a 5°C/min heating rate, open symbols. For $Fe_{80-x}Ni_xP_{14}B_6$ ● and $Fe_{80-x}Ni_xB_{20}$ ◆ from Luborsky (1977a) at a 40°C/min heating rate and dashed lines for two hour anneals.

additional and major change occurs associated with the relaxation of internal strain, as first noted by Luborsky et al. (1975). By minimizing the internal strains, the strain–magnetostriction interaction, and the resultant anisotropy, is minimized leading to a reduction in coercive force and losses and an increase in permeability and loop squareness. This stress-relief occurs at temperatures below T_x in most alloys of interest. This will also be described more fully in a later section. Mechanical properties are also known to alter drastically during this low temperature annealing, but this is believed to be due in large measure to diffusion of certain atomic species over relatively large distances, as discussed by Walter et al. (1976) and Luborsky and Walter (1976).

3.4.3. Directional order relaxation

In contrast to the crystallization and structural relaxation effects which are irreversible processes, directional ordering is a reversible process. Directional ordering, produced either by annealing in a magnetic field or by annealing in a mechanically stressed condition, results in a magnetic anisotropy which can markedly influence the magnetic properties of the amorphous alloy. The relaxation or reorientation of this anisotropy can occur at quite low temperatures in some amorphous alloys, e.g., under the influence of its own self-demagnetizing field, externally applied field, or stressed condition. The rate at which this happens may limit the usefulness of some of the alloys in applications where the initial ordering direction is different from the resultant magnetic or stress fields encountered during use. This directional order arises from Fe–Fe and Ni–Ni pair ordering and from metalloid–metal ordering, both similar to that found in conventional crystalline alloys. This ordering again emphasizes the fact that these amorphous alloys are far from being homogenous structureless arrays of atoms. The origins and kinetics of directional ordering in amorphous alloys will be discussed more fully in section 6.3.

4. Fundamental magnetic properties

The intrinsic properties of amorphous ferromagnets are still not quantitatively understood. The basic problem is to incorporate into the existing theoretical approaches the structural distribution contained, for example, in the radial distribution functions described in the previous section. In a qualitative sense, the intrinsic properties (*magnetic moment*, M_s, *Curie temperature*, T_c, and *magnetostriction* λ) and the extrinsic properties (*coercive force*, H_c, *remanence-to-saturation* ratio, M_r/M_s, and *permeability*, μ, and *losses*, W, as a function of frequency) can all be understood using the same underlying physical principles applicable to crystalline alloys with appropriate modifications to take into account the differences in structure and composition.

The local environment around each atom in an amorphous solid differs from site-to-site in contrast to the regular crystalline lattice. Therefore the magnetic moment of an atom is not expected to be identical on every site. Thus the

hyperfine interactions will show a distribution of values. The effect of this distribution is not apparent in the magnetic moments, critical behavior or anisotropies, but is necessary to account for the details of the Mössbauer spectra and nuclear magnetic resonance. The major change in magnetic properties observed in amorphous alloys comes from the change in the electronic environment caused by the metalloids. These same metalloids are necessary for preparing and stabilizing the amorphous phase as discussed previously.

4.1. Magnetic moment and saturation magnetization

The saturation magnetization of a material at a temperature of 0 K is one of its basic properties. Measurements are usually expressed as average moment per magnetic atom in units of the Bohr magneton, μ_B, or as saturation magnetization for the alloy, M_s, in units of emu/cm^3 [Tesla]. The moments of most amorphous alloys are lower than those of the pure crystalline transition metals which they contain. However, the direct effect of the structural disorder on the moments is very small. The moments are lower because of the change in the local chemical environment provided by the presence of the metalloids.

Metallic glasses are rather poor conductors, but their 3d-electrons are just as "itinerant" as in crystalline transition metal alloys. Thus the 3d-electron magnetic moments should be discussed in terms of the band theory of magnetism. The band theory of magnetism is an approximate single particle picture whereby an electron interacts with other electrons through an effective potential which has a spin dependent part. A brief discussion of this approach, applied to amorphous alloys, may be obtained from Alben et al. (1977). The rigid band model is often used to correlate results, but it has no theoretical basis. The rigid band theory is based on the assumption that the d-bands do not alter on alloying; they just fill or empty. The success of rigid band theory in certain alloy systems is due to a fortuitous cancelling of errors and both theory and experiment show that the band structure does change shape. The addition of metalloids also changes the d-bands and does not simply transfer charge. Because the d-bands are not rigid the plotting of moment against average number of valence electrons, the Slater–Pauling curve, is without theoretical basis. However, the rigid band phenomenology will be used in much of the discussion of experimental results because of its simplicity in correlating data.

A better picture of magnetism in glassy alloys, discussed by Alben et al. (1977), follows from ideas of local chemical bonding. In atoms, states of high spin have low electron–electron Coulomb repulsion energies. Hence, by Hund's rules, atoms usually have large magnetic moments. When atoms interact, what were degenerate orbitals become split into low energy bonding orbitals and high energy antibonding orbitals. There is a competition between the reduction in Coulomb energy for high spin and the energy reduction in filling the lowest energy orbitals with pairs of electrons with zero total spin. When the Coulomb energy is large compared with the bonding interactions, the high spin atomic-like state is retained. When the bonding energy is comparable to the Coulomb

energy, as occurs between 3d orbitals in transition metals, a compromise is reached whereby the moments are reduced. Where bonding is still stronger, as occurs between transition metal 3d states and metalloid s and p states, the moment is further reduced or even eliminated.

The magnetic moments of the simple amorphous transition metal elements, Fe, Co and Ni would be the simplest to understand. However, these are very difficult to obtain and have usually been prepared only in an impure state, by vacuum deposition onto cold substrates. In most cases, in fact, information on the pure amorphous elements is obtained from impure films by extrapolating back to zero impurity or solute level. Some results for iron–metalloid and cobalt–metalloid amorphous alloys are shown in fig. 15 as a function of metalloid content. Data for related crystalline alloys are shown by the smooth curves with no data points. The simplified rules based on the rigid band model, that work reasonably well, indicate that the moment of the transition metal decreases linearly with additions of metalloid at a slope depending on the electrons available from the metalloid; approximately $3\mu_B$ for each P atom, $2\mu_B$ for each Si or C atom and $1\mu_B$ for each B atom. The results for the amorphous cobalt alloys all appear to fall approximately linearly as expected. The behavior of the amorphous iron alloys is very different. Apparently a small amount of impurity was necessary to stabilize the strong ferromagnetism in the amorphous FeSi reported by Felsch (1970), but this was not confirmed by the results of Shimada and Kojima (1976). Wright (1976) has recently reviewed the status of the

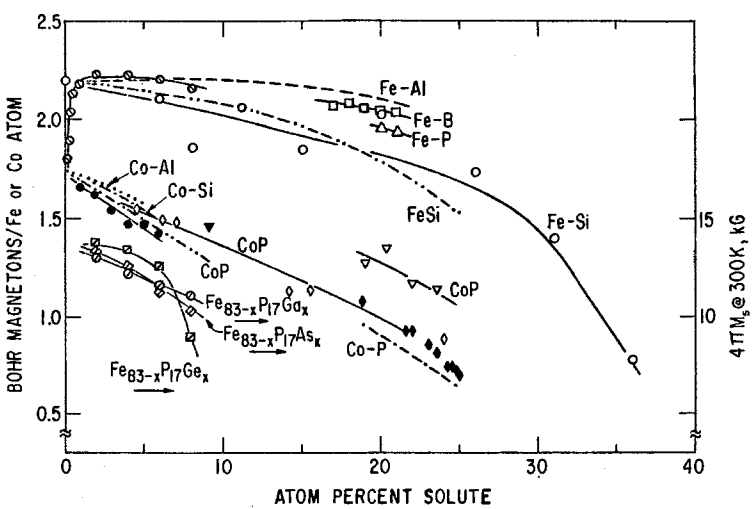

Fig. 15. Magnetic moments at 0 K as a function of solute concentration. Crystalline alloys shown by broken curves with no data points: FeAl, CoAl, CoSi Parsons et al. (1958); FeSi Shimada and Kojima (1976); CoP Pan and Turnbull (1974) and Simpson and Brambley (1971). Amorphous alloys shown by solid curves with data points: FeSi ○ Shimada and Kojima (1976) and Felsch (1970); CoP ◇ Kanabe and Kanematsu (1968). ◆ Pan and Turnbull (1974), ▽ Cargill and Cochrane (1974), ▽ Simpson and Brambley (1971); FeB □ Durand and Yung (1977); FeP △ Durand and Yung (1977); CoSi ● Felsch (1970). Magnetization in $4\pi M_s$ for FePGe, –As, –Ga ⊠, ◈ ⊘ Wiesner and Schneider (1974).

information available on "pure" amorphous elements. In all cases it appears that the saturation moment is the same or less than its value in the crystalline state (table 1).

There is considerably more information available for amorphous alloys than for pure elements, because of their greater stability. We can correlate the behavior of the magnetic moment in amorphous alloys containing 3d transition metals on the basis of the rigid band model, that is, by assuming that the metalloid atoms contribute some of their s, p electrons to fill the d band of the transition metal atoms. This accounts for the reduction of magnetization of both the crystalline and amorphous alloys with increasing metalloid content, as shown by the alloys in fig. 15. Thus we expect the magnetic moment of the transition metal, TM, atoms in the general amorphous alloy $(TM)_{1-z-y}F_zG_y$ to be expressed as

$$\mu = [m(1-z-y)-fz-gy]/(1-x-y) \tag{11}$$

or for the moment per atom of alloy as

$$\mu = m(1-z-y)-fz-gy \tag{12}$$

where F and G represent the metalloid or glass forming atomic species, m is the original number of unpaired spins in the transition metal alloy, and f and g are the number of electrons transferred from the F and G atoms respectively. Since the number of nearest neighbors in an amorphous alloy is essentially the same as in the fcc crystalline phase we can assume that m is the same. Thus $m = 0.6$, 1.6 and 2.6 for Ni, Co and Fe respectively. Using these values, the agreement between the observed and calculated values is usually quite good. Examples of the effects of the metalloid species and concentration on the moment in amorphous alloys are shown in figs. 16–18 and the effect of changing the transition metal alloy is shown in fig. 19. A variety of ternary alloys with a single transition metal element were reported by Yamauchi and Mizoguchi (1975), as shown in fig. 18. The data agree reasonably well with the rigid band model using the same moments of 0.6, 1.6 and 2.6 for Ni, Co and Fe and assigning an integral number of electrons transferred from the metalloids; 1 for B, 2 for C, 2 for Si and 3 for P.

Becker et al. (1977) studied the moment and Curie temperatures of amorphous alloys of $(Fe–Ni)_{80}(P–B)_{20}$. All of their data on the effect of the metalloid concentration, shown in fig. 18, and on the effect of the transition metal alloy composition, shown in fig. 19, are in quite good agreement with the rigid band model but using $\mu_{Ni} = 0.6$ Bohr magnetons, $\mu_{Fe} = 2.1$ Bohr magnetons and assuming that each phosphorus atom reduced the moment by 1.0 and each boron by 0.3 Bohr magnetons. Thus the moment per atom of alloy can be written as

$$\mu = 2.1x + 0.6b - 1.0z - 0.3y \tag{13}$$

in Bohr magnetons for $Fe_xNi_bP_zB_y$. Instead of using the rigid band model as above, Becker et al. (1977) showed that a somewhat more satisfying fit to the data was obtained using individual moments varying with composition, as

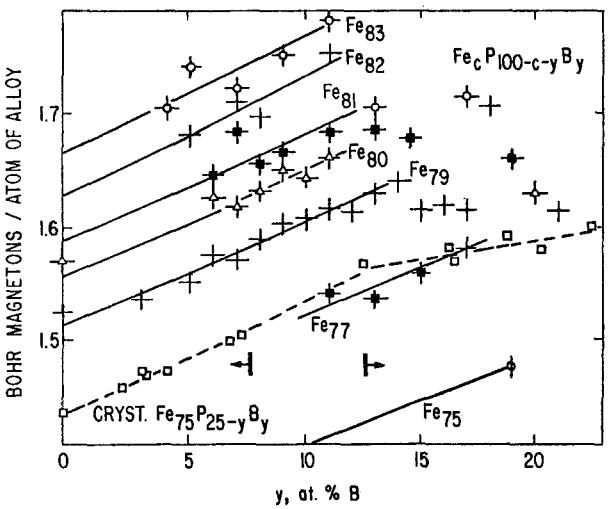

Fig. 16. Saturation moment per atom of alloy at 0 K for FePB amorphous alloys from Durand and Yung (1977). Dashed curve is for crystalline FePB from Fruchart et al. (1964).

described by Kouvel (1969) in his analysis of crystalline alloys. The individual atomic moments of Fe and Ni are then given by

$$\mu_{Fe} = 2.20 + 0.80(1 - x) \qquad \mu_{Ni} = 0.57 + 0.20x \tag{14}$$

in Fe_xNi_{1-x}. When this is done the best fit to the same data in the amorphous Fe–Ni–P–B alloys required that each phosphorus atom transfers 2.1 electrons and each boron atom 1.2 electrons. For the Fe rich alloys in the Fe–Ni series of

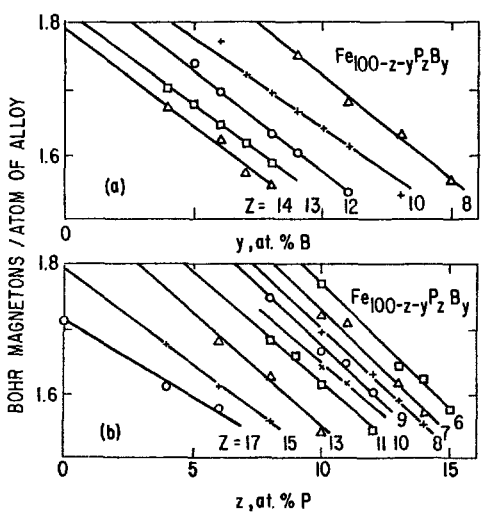

Fig. 17. Saturation moment per atom of alloy at 0 K (a) on substitution of B for Fe for various P contents. (b) on substitution of P for Fe for various B contents. Durand and Yung (1977).

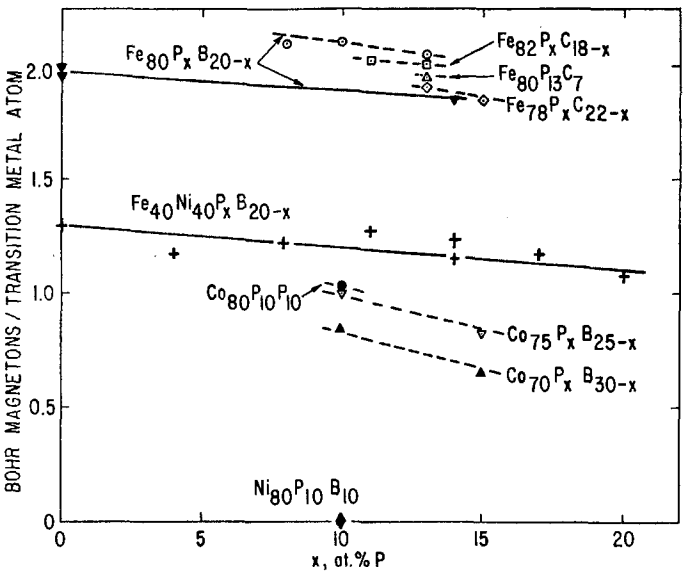

Fig. 18. Saturation moments per transition metal atom as a function of phosphorus for various amorphous alloys. ▼, + Becker et al. (1977); remainder of data from Yamauchi and Mizoguchi (1975).

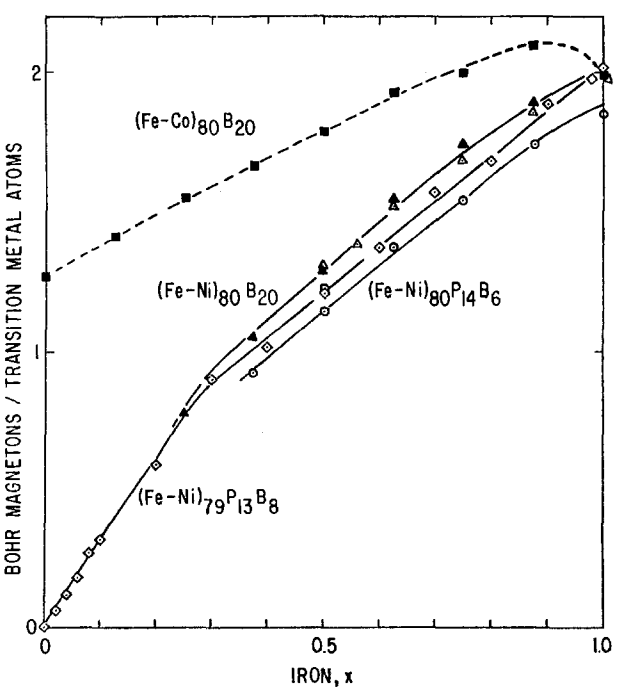

Fig. 19. Moment per transition metal atom at 0 K of amorphous alloys as a function of transition metal composition. FeCoB, O'Handley et al. 1976a; FeNiB, △ Becker et al. 1977, ▲ O'Handley et al. 1976a; FeNiPB ◇ Durand 1977; FeNiPB ○ Becker et al. (1977).

amorphous alloys the results for the various metalloids shown in fig. 19 are consistent. That is, the reduction in moment is greatest for $-P_{14}B_6$, less for $-P_{13}B_8$ and least for $-B_{20}$ alloys. The results for $Fe_xNi_{1-x}P_{13}B_8$ reported by Durand (1977) show a pronounced change in slope. This is interpreted on the basis of a roughly constant moment per Ni atom for $0.3 < x < 1$ but a progressive decrease in moment for $0 < x < 0.3$. Normal ferromagnetic ordering was reported only for $x > 10$at.%. Below this iron content various types of ordering appeared from mictomagnetic (superparamagnetic) to spin glass behavior as x decreased below 10at.%.

A very detailed investigation of the moments and Curie temperatures of amorphous alloys in the entire accessible region of Fe–P–B alloys was reported by Durand and Yung (1977). The result of replacing P by B for various constant Fe contents is shown in fig. 16. One of the remarkable features of these results, also shown by the Curie temperature results to be discussed later, is the change in slope as P replaces B. This change in slope is related to the change in slope exhibited by the crystalline alloys of $Fe_{75}P_{25-y}B_y$ reported by Fruchart et al. (1964) and shown by the square data points in fig. 16. These results suggest the existence of two different short-range orders in the amorphous alloys, probably corresponding to the ϵ and ϵ_1 crystal structures. Further results also reported by Durand and Yung (1977) for the change in moment when one metalloid substitutes for Fe, the other metalloid remaining constant, are shown in fig. 17. The extrapolation to "pure" amorphous Fe from both sets of data yields a value of $\sim 2.35 \mu_B$. Assuming that the electron transfer model is valid and independent of short range order variations the boron would donate 1.4 ± 0.2 electrons and the phosphorus 1.6 ± 0.2 electrons. These values for the number of electrons transferred are compared to other values reported in table 4. Note the rather large variation in the values reported for each element.

The magnetic moments for a wide variety of transition metal alloys with

TABLE 4
Electrons transferred from the metalloids in amorphous alloys based on the rigid band model

Alloy	B	C	Si	P	Reference
Fe–Ni–P–B	0.3			1.0	Becker et al. (1977)
Fe–Ni–B	1.2*			2.1	Becker et al. (1977)*
Fe–P–B	1.4			1.6	Durand and Yung (1977)
Fe–Co–B–P Fe–Ni–B–P	1.6			2.4	O'Handley et al. (1976a)
Co–P				5	Kanabe and Kanematsu (1968)
				2	Cargill and Cochrane (1974)
				<5	Pan and Turnbull (1974)
				<5	Simpson and Brambley (1971)
CoBP, FeBP FeCP, NiBP	1	2	2	3	Yamauchi and Mizoguchi (1975)

* Moment of transition metal varies linearly with alloy concentration.

$-P_{10}B_{10}$ glass formers from the work of Mizoguchi et al. (1973, 1974) are shown in fig. 20 as a function of the average number of outer electrons, N. This Slater–Pauling presentation is also shown for the crystalline alloys by the dashed curves. The approximate shape of the Slater–Pauling curve is retained for the amorphous alloys but the curve is shifted by the same assumed transfer of electrons from the P, B to the transition metals.

The room temperature saturation magnetizations are of more practical importance. These are shown in fig. 21 for a variety of alloys as a function of transition metal. The effect of the transition metal additions to amorphous Co–SiB is shown in fig. 22 from Fujimori et al. (1977). The relative number of electrons donated can be obtained from fig. 21. The number of electrons donated can be listed as $-P_{13}C_7 > -S_{15}B_{10} > -P_{16}B_6Al_3 > -P_{14}B_6 > -Si_9B_{13} > -B_{20}$ based on the relative magnitudes of $4\pi M_s$. The trend with transition metal content is the same as for the corresponding crystalline alloys although there are anomalies. For example crystalline Fe–Co alloys show a peak in magnetization at about 35% Co. The peak appears to be present in the Fe–Co–B, but at about 15% Co, while it appears to be absent in the other Fe–Co amorphous alloys. The origin of these differences has not been examined and is not understood. The trend with additions of other transition metal elements, e.g., Cr, Pd, V, and Mn as shown in figs. 20 and 22 is also approximately as observed in the crystalline alloys without the glass forming atoms. The saturation magnetizations at room temperature for a variety of alloys, most of which are not in any of the previous figures, are listed in table 5.

The effect of pressure on the moment of amorphous iron alloys was reported by Mizoguchi (1976). A microbomb technique was used. The value of $(d\bar{\mu}/dp)/\mu$ for $(Fe_{1-x}M_x)_{80}P_{10}B_{10}$ was found to be about -2×10^{-2} kbar^{-1} $[-2\times10^{-10}$

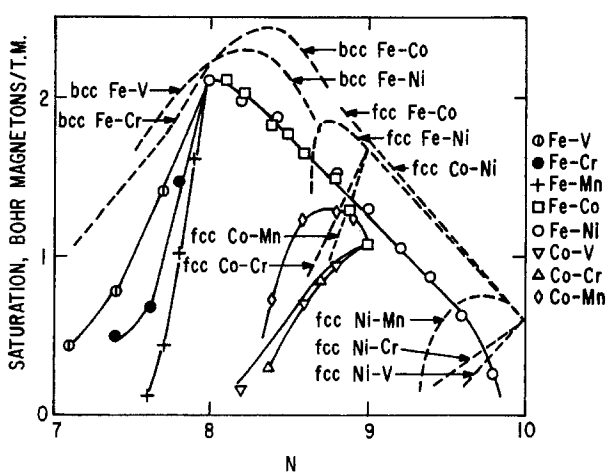

Fig. 20. The saturation magnetization of quasibinary amorphous alloys of 3d transition metals $(A_{1-x}B_x)_{80}P_{10}B_{10}$ shown by solid curves. The average moments per metallic atom, $A_{1-x}B_x$, are plotted as a function of outer electron concentration, N, of the metallic atoms. Mizoguchi et al. (1973, 1974). Crystalline alloys without P, B shown by dashed curves.

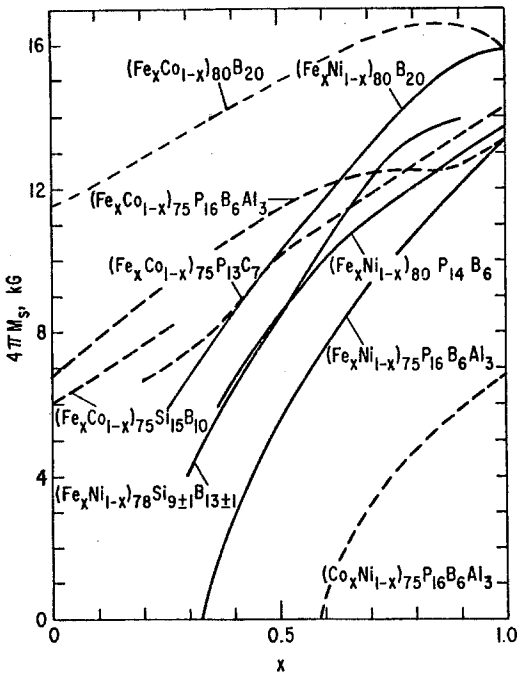

Fig. 21. Saturation magnetization at room temperature as a function of composition for Fe–Co–Ni amorphous alloys. FeNiB, FeNiPB Becker et al. (1977); FeNiSiB Masumoto et al. (1977); FeNiB, FeCoB O'Handley et al. (1976a, 1976b); FeCoPC, FeCoSiB Fujimori et al. (1976b); CoNiPBAl, FeCoPBAl, FeNiPBAl Gyorgy et al. (1976).

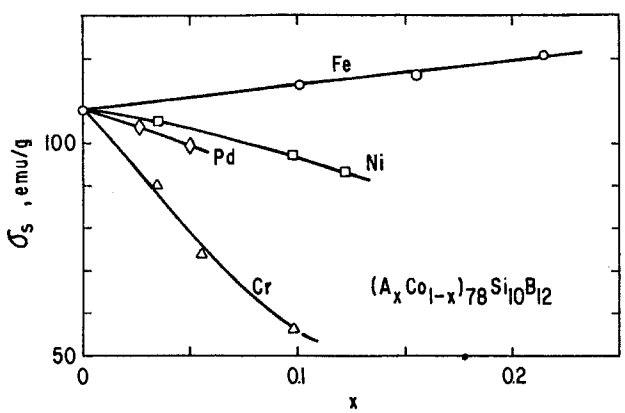

Fig. 22. Saturation magnetization per gram at room temperature for some amorphous –SiB alloys, Fujimori et al. (1977).

TABLE 5
Saturation magnetization and Curie temperatures of some* amorphous alloys

Alloy	$4\pi M_s$ at 300 K kG	μ_0 β/atom of alloy	M_0 emu/g	T_c K	Reference
$Fe_{75}P_{15}C_{10}$	–	–	–	619 (M)	Chien and Hasegawa (1976b)
	11.5	1.35	151	596.5	Tsuei and Lilienthal (1976)
$Fe_{80}P_{16}C_3B_1$	–	–	–	~590 (M)	Chien and Hasegawa (1976b)
#2615	14.9	1.68	187	565	Hasegawa and O'Handley (1976)
	17.1	–	–	–	Egami et al. (1975a)
	17.1	–	–	–	Flanders et al. (1975)
$Fe_{40}Ni_{40}P_{14}B_6$	–	–	–	537 (M)	Chien and Hasegawa (1976b)
#2826	8.7	–	–	–	Egami et al. (1975a)
	7.9	0.88	96.7	520	Hasegawa and O'Handley (1976)
$Fe_{40}Ni_{40}P_{14}B_6$	8.5	0.98	108	–	Becker et al. (1977)
$Fe_{80}B_{20}$	15.8	–	–	647	O'Handley et al. (1976a)
#2605	–	–	–	685 (M)	Chien and Hasegawa (1977)
	16.0	1.59	190	647	Hasegawa et al. (1976a, 1976b)
$Fe_{80}B_{20}$	15.8	1.55	185	651	Becker et al. (1977)
		1.63	194	652	Durand and Yung (1977)
$Fe_{29}Ni_{49}P_{14}B_6Si_2$ #2826B	4.9	–	–	–	Flanders et al. (1975)
$Fe_{80}P_{12.5}C_{7.5}$	14.0	1.68	186	586 (M)	Tsuei et al. (1968)
$Fe_{80}P_{13}C_7$	12.0	–	–	–	Fujimori et al. (1974)
	14.0	–	–	–	Fujimori et al. (1976b)
$Fe_{75}P_{16}B_6Al_3$	13.5	–	–	–	Sherwood et al. (1975)
$Co_{75}P_{16}B_6Al_3$	6.5	–	–	630	Sherwood et al. (1975)
$Co_{75}S_{15}B_{10}$	6.0	–	–	–	Fujimori et al. (1976b)
$Fe_{40}Co_{40}B_{20}$	15.0	1.43	166	>800	O'Handley et al. (1976a)
$Fe_{40}Ni_{40}B_{20}$	10.0	1.03	120	662	O'Handley et al. (1976a)
$Co_{80}B_{20}$	11.5	1.02	116	~765	O'Handley et al. (1976a)
$Fe_{45}Co_{35}C_{13}C_7$	10.7	–	–	673	Kikuchi et al. (1975)
$Fe_{4.5}Co_{70.5}Si_{15}B_{10}$	6.7	–	–	688	Kikuchi et al. (1975)
$Fe_3Co_{72}P_{16}B_6Al_3$	6.3	–	–	~600	Sherwood et al. (1975)
$Fe_6Co_{74}B_{20}$	11.8	–	–	~700	O'Handley et al. (1976b)
$Ni_{85}P_{15}$		0.04	4	190	Pan and Turnbull (1974)
		0.07	7		Simpson and Brambley (1972)
$Fe_{59}Ge_{41}$	12.8	–	–	–	Massenet et al. (1974)

TABLE 5 (*cont.*)

Alloy	$4\pi M_s$ at 300 K kG	μ_0 β/atom of alloy	M_0 emu/g	T_c K	Reference
$Fe_{44}Ge$	6.4	–	–	–	
$Fe_{35}Ge$	2.9	–	–	–	
$Fe_{30.5}Ge$	0.2	–	–	340 ± 30	
$Fe_{25.7}Ge$	0.0	–	–	35 ± 35	
$(Fe_{0.8}Ni_{0.2})_{78}Si_{10}B_{12}$	13.1	–	–	729	Masumoto et al. (1977)
$(Fe_{0.8}Ni_{0.2})_{78}Si_8B_{14}$	13.1	–	–	733	Masumoto et al. (1977)

Allied Chemical Co. Metglas® designation.
* Data for various alloy series are given in figures.
(M) Determined from Mössbauer spectra.

$(N/m^2)^{-1}$] when M = Fe, Co or Ni. For M = Cr or Mn it is about an order of magnitude greater. From the thermodynamic relation between the pressure dependence of magnetization and volume magnetostriction

$$\rho(dM/dp) = (1/V)(\partial V/\partial H) \tag{15}$$

where ρ is the density, the value of $(1/V)(\partial V/\partial H)$ is estimated to be about 10^{-9} Oe^{-1} [$\sim 10^{-7}(A/m)^{-1}$] for M = Fe, Co or Ni. This is about the same value as for crystalline Fe–Ni alloys.

4.2. Curie temperature

In spite of their chemical and structural disorder, amorphous ferromagnets most often have a well defined magnetic ordering "Curie" temperature, T_c. This has been confirmed from magnetization–temperature, Mössbauer and specific heat measurements. As with the M_s measurements, these results do not provide unambiguous answers concerning effects of structural disorder on T_c because chemical effects may be responsible for the differences. The coupling of moments in amorphous magnets, as in most other magnetic materials, is due to the exchange interaction. Only itinerant exchange between 3d moments is of importance in the transition metal–metalloid alloys. Itinerant exchange arises because the single site exchange taken together with the intersite electron hopping terms produce a correlation between moments on different sites. This mechanism depends on the band structure and can lead to ferromagnetism, antiferromagnetism or complex spin arrangements. The theoretical treatment of spin ordering in amorphous solids is a much more difficult problem than in regular crystalline lattices and has not been satisfactorily solved. If the molecular field approximation is used, even though its use is doubtful, the paramagnetic

Curie temperature can be expressed as

$$T_c = [2S(S+1)/3k] \sum_{ij} J_{ij} \tag{16}$$

where S is the spin number, k is Boltzmann's constant and J_{ij} is the exchange interaction between atoms at the position r_i and r_j and can be expressed in terms of the radial distribution function.

The Curie temperatures of amorphous transition metal–metalloid alloys are always found to be significantly lower than those of the pure crystalline transition metals. This reduction of T_c in the amorphous alloys appears to be largely the result of chemical composition and/or chemical disorder. A summary of some results from Wright (1976) for the pure transition metals was included in table 1. This shows the decrease in T_c for the amorphous elements compared to the crystalline elements. The results for some alloys are given in fig. 23 as a function of solute concentration for amorphous alloys of FeP, FeB, CoP and FePC compared to related crystalline alloys. The trends in T_c for the crystalline alloys are given by the broken curves with no data points; the solid curves for the amorphous alloys are shown with data points.

Curie temperatures vary with transition metal content as shown in fig. 24 for Fe–Ni alloys and in fig. 25 for Fe–Co and Co–Ni alloys both with a variety of glass formers. The variation of T_c with transition metal content for a fixed metalloid composition may be systematized using a phenomenological model as

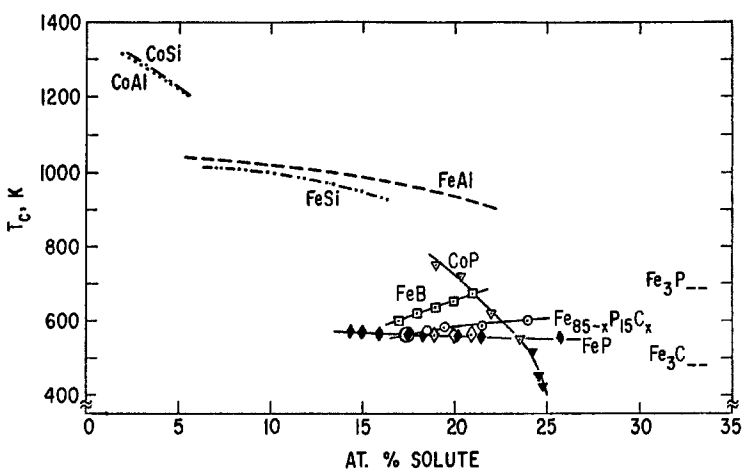

Fig. 23. Curie temperatures as a function of solute concentration. Crystalline alloys shown by the broken curves without data points; FeAl, FeSi, CoAl, CoSi Parsons et al. (1958); Fe_3P, Fe_3C Chen (1973). Amorphous alloys shown by solid curves with data points; CoP ▼ Pan and Turnbull (1974), ▽ Cargill and Cochrane (1974); $Fe_{85-x}P_{15}C_x$, ○ Chen (1973) where at.% solute = 15 + x; FeB □ and FeP ◇ Durand (1977); and electrodeposited FeP ◆ Logan and Sun (1976).

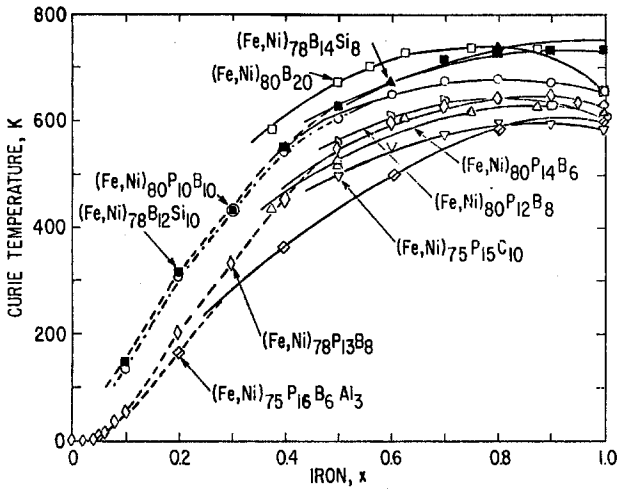

Fig. 24. Curie temperatures of amorphous Fe–Ni alloys as a function of transition metal composition. Solid lines calculated using phenomenological model; dashed lines follow the data. FeNiB and FeNiPB Becker et al. (1977); FeNiSiB Masumoto et al. (1977); FeNiPC Hasegawa and Dermon (1973); FeNiPBAl Gyorgy et al. (1976).

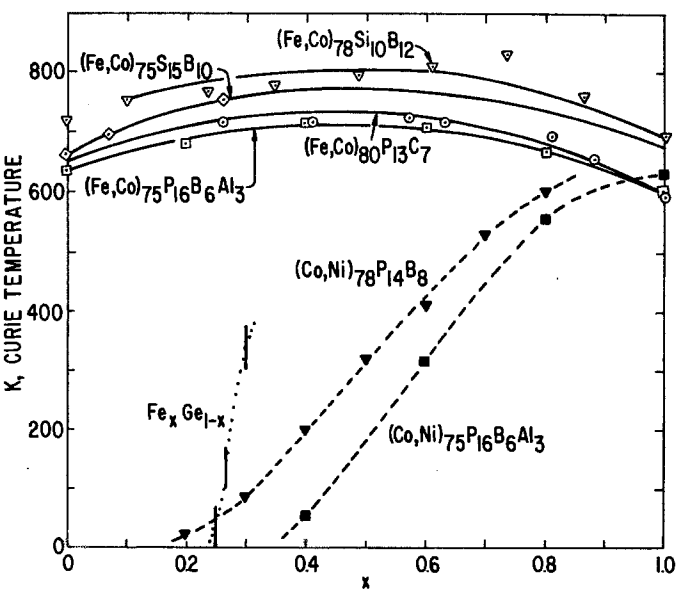

Fig. 25. Curie temperatures of amorphous Fe–Co and Co–Ni alloys as a function of transition metal content. Solid lines for Fe–Co alloys calculated using phenomenological model. FeCoSiB and FeCoPC Fujimori et al. (1976b); FeCoPBAl and CoNiPBAl Gyorgy et al. (1976); CoNiPB Amamou (1976); Fe_xGe_{1-x} Massenet et al. (1974).

described by Kouvel (1969). For this purpose it is adequate to use the molecular field model, suitably modified so that individual atomic moments vary in magnitude with their local environment. Only nearest neighbor interactions are considered. For the disordered crystalline alloy an explicit quadratic equation in T_c is derived whose physically meaningful solution is

$$T_c = \tfrac{1}{2}(T'_{AA} + T'_{BB}) + \{\tfrac{1}{4}(T'_{AA} - T'_{BB})^2 + T'_{AB}T'_{BA}\}^{1/2} \tag{17}$$

where T'_{AA}, T'_{BB}, T'_{AB} and T'_{BA} are interaction temperatures defined in terms of transition metal composition, magnetic moments, exchange coefficients, spin quantum numbers and number of nearest neighbors. If we neglect the variation of the individual atomic moments with changes in their local environment than eq. (17) reduces to

$$T_c = \tfrac{1}{2}[T_{AA}(1-x) + T_{BB}x] + \{\tfrac{1}{4}[T_{AA}(1-x) - T_{BB}x]^2 + T_{AB}^2 x(1-x)\}^{1/2} \tag{18}$$

assuming $T_{AB} = T_{BA}$ where x is the transition metal concentration in the case of binary alloy. Note that for

$$\begin{aligned} x &= 1, \quad T_c = T_{BB} \\ x &= 0, \quad T_c = T_{AA}. \end{aligned} \tag{19}$$

This approach does not predict a critical concentration for the onset of ferromagnetic behavior and thus cannot be applied to the Ni-rich amorphous alloys which become non-magnetic. The cubic equation in T_c of Foo and Wu (1972) is required for this latter case.

The solid curves in fig. 25 for the Fe–Co amorphous alloys were calculated using this equation. The interaction constants to obtain this best fit to the experimental results are given in table 6. The data for the Co–Ni alloys in the

TABLE 6
Curie temperature interaction constants

$(B_xA_{1-x})_yG_{100-y}$	T_{BB} K	T_{AB} K	T_{AA} K	Range of validity
$(Fe–Co)_{78}S_{10}B_{12}$	693	908	718	$0<x<1$
$(Fe–Co)_{75}Si_{15}B_{10}$	660	866	675	$0<x<1$
$(Fe–Co)_{75}P_{16}B_6Al_3$	600	804	635	$0<x<1$
$(Fe–Co)_{80}P_{13}C_7$	595	838	650	$0<x<1$
$(Fe–Ni)_{78}B_{14}Si_8$	753	790	−43	$0.4<x<1$
$(Fe–Ni)_{78}B_{12}Si_{10}$	731	780	134	$0.5<x<1$
$(Fe–Ni)_{80}B_{20}$	652	1029	−185	$0.35<x<1$
$(Fe–Ni)_{80}P_{10}B_{10}$	653	797	145	$0.5<x<1$
$(Fe–Ni)_{80}P_{12}B_8$	608	808	−93	$-<x<1$
$(Fe–Ni)_{79}P_{13}B_8$	627	799	−307	$0.45<x<1$
$(Fe–Ni)_{80}P_{14}B_6$	615	751	−219	$0.4<x<1$
$(Fe–Ni)_{75}P_{15}C_{10}$	585	693	−118	$-<x<1$
$(Fe–Ni)_{75}P_{16}B_6Al_3$	600	750	−1180	$0.3<x<1$
$(Co–Ni)_{75}P_{16}B_6Al_3$	630	–	–	no
$(Co–Ni)_{78}P_{14}B_8$	~670	–	–	no

same figure could not be fitted to eq. (18) because of the large change in atomic moments with compositon and the large critical concentration. The solid curves in fig. 24 for the Fe–Ni alloys were also calculated using eq. (18). This simplified equation could only be fitted to the data for $x \geq 0.4$, as shown by the solid lines. The dashed lines are simply drawn through the data points. The constants for the fitting are also given in table 6. Mizoguchi et al. (1973, 1974) has reported T_c values for a wide range of quasibinary transition metal amorphous alloys with the composition $(A_xB_{1-x})_{80}B_{10}P_{10}$. These are shown in fig. 26 plotted as a function of average outer electron concentration, N, together with the Curie temperatures of the corresponding transition metal crystalline alloys without the metalloids. There is a significant difference between T_c of crystalline bcc alloys and crystalline fcc alloys, suggesting the complexity of the effect of crystal structure on T_c. In the amorphous systems T_c is a smooth function of alloy composition over the entire range. We can compare the exchange interaction term in eq. (16) for various crystalline and amorphous alloys. For $Co_{80}B_{10}P_{10}$, taking into account the change in spin, S (cryst.) = 0.86 and S (amorp.) = 0.5, then ΣJ_{ij} (amorp.)/ΣJ_{ij} (cryst.) $\approx$ 1.1. Assuming only the short-range exchange interaction, the average J between nearest neighbor Co atoms seems to be the same in both pure hcp Co and in the amorphous alloy, since the coordination number is almost the same in both cases, i.e., $Z = 12$. However this is not the case for Fe. For $Fe_{80}B_{10}P_{10}$, ΣJ_{ij} (amorp.)/ΣJ_{ij} (cryst.) $\approx$ $12J$ (amorp.)/$8J$ (cryst.) $\approx$ 0.7. The nearest neighbor interaction, J, is estimated to be roughly half in the amorphous Fe compared to that in pure bcc Fe, taking into account the difference in coordination number.

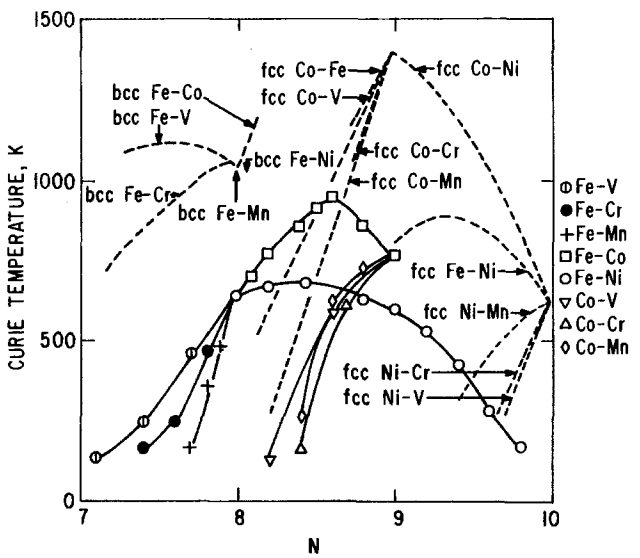

Fig. 26. Curie temperatures of quasibinary amorphous alloys of 3d transition metals $(A_{1-x}B_x)_{80}P_{10}B_{10}$ as a function of average outer electron concentration N of the metallic atom. Corresponding crystalline alloys, without P and B, are shown by the dashed curves. Mizoguchi et al. (1973, 1974).

The pressure dependence of T_c has been measured by Yamauchi (1975), as reported by Mizoguchi (1976). In the series $(Fe_xTM_{1-x})_{80}B_{10}P_{10}$ for TM = Mn or Cr, $dT_c/dp \simeq -2$ K/kbar $[-2\times10^{-8}$ K/N-m$^{-2}]$ and for TM = Ni, $dT_c/dp = -0.7$ K/kbar $[-0.7\times10^{-8}$ K/N-m$^{-2}]$.

In recent papers Durand (1976, 1977) and Durand and Yung (1977) studied the concentration dependence of the electronic and magnetic properties of Fe–Ni–P–B amorphous alloys. The results for the magnetization have already been discussed. The change in the magnetization and the change in Curie temperature when B substitutes for P in Fe–P–B at constant Fe concentration, shown in fig. 27, again suggests the existence of two different short-range orders in the amorphous alloys. One corresponds to the ϵ structure and the other to the ϵ_1 structure in crystalline $Fe_3P_{1-x}B_x$, as reported by Fruchart et al. (1964). This correspondence betwen the amorphous and crystalline characteristics is the clearest example of the retention of the short-range order in amorphous alloys.

Another interesting set of results reported by Durand and Yung (1977) on the Fe–P–B alloys is concerned with the concentration dependence of moment and Curie temperature when one of the metalloids is substituted for the iron. The results for the substitution of B for Fe at different fixed concentrations of P are shown in fig. 28a, and the results of substitution of P for Fe are shown in fig. 28b. By extrapolating the apparent linear trends of T_c with composition Durand

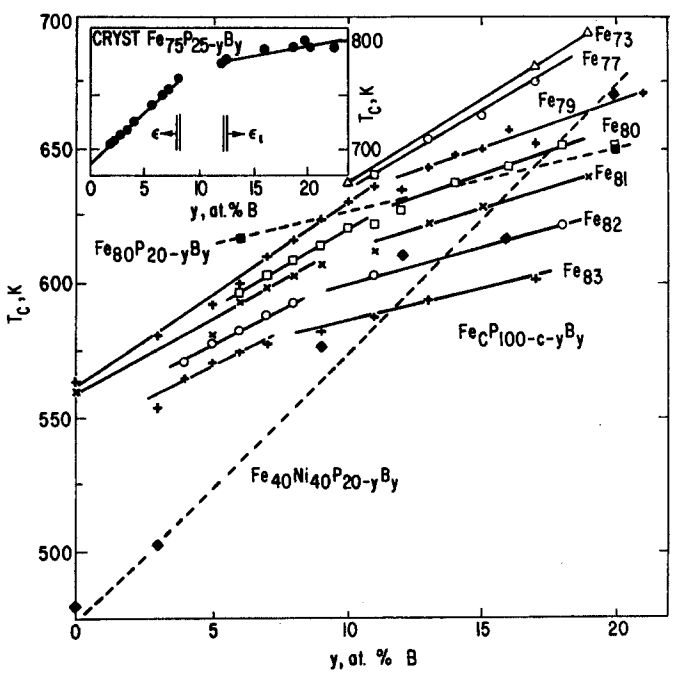

Fig. 27. Curie temperature of amorphous alloys as a function of glass-former composition. Solid lines for FePB Durand and Yung (1977). Dashed lines for FePB ■ and FeNiPB ◆ Becker et al. (1977). Crystalline FePB from Fruchart et al. (1964).

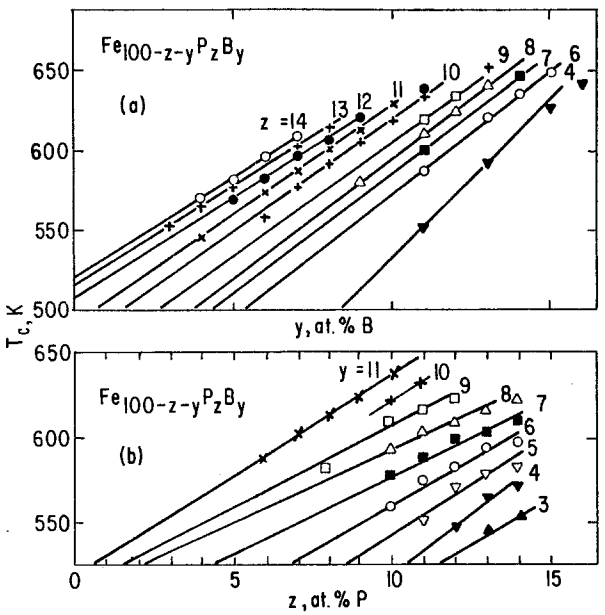

Fig. 28. Curie temperatures of amorphous Fe–P–B alloys as (a) boron or (b) phosphorus is substituted for iron. From Durand and Yung (1977).

and Yung (1977) obtain the value of $T_c = 320$ K for "pure amorphous Fe" from data on the Fe–B system and essentially the same value of $T_c = 335$ K from data on the Fe–P system. Curie temperatures of a number of alloys mostly not found in the figures are listed in table 5.

4.3. Temperature dependence of magnetization

The effect of measurement temperature on saturation magnetization is shown in fig. 29 for a variety of amorphous alloys and in fig. 30 for a series of $(Fe–Ni)_{80}B_{20}$ alloys reported by Luborsky and Walter (1977a). These curves appear superficially the same as observed for crystalline alloys. However, if we plot magnetization vs. temperature in reduced coordinates, as in fig. 31, we see that the amorphous alloys all fall below the theoretical curve, especially at low temperatures. This appears to be a general feature of the behavior of amorphous alloys. The mechanism responsible for this lowering is not clear. The theoretical treatments can be classified into two categories. In the first, a unique constant exchange interaction between the magnetic atoms is assumed and the amorphous nature of the alloy is taken into account by calculating a random distribution of the local anisotropy field. Such an approach has been described by Harris et al. (1973, 1974) and by Gubernatis and Taylor (1973). In the second approach to treating this problem, a distribution of exchange integrals is assumed in order to reflect the structural fluctuations in the amorphous alloy. This approach has been developed by Handrich (1969, 1972), Kobe (1977), Montgomery et al. (1970),

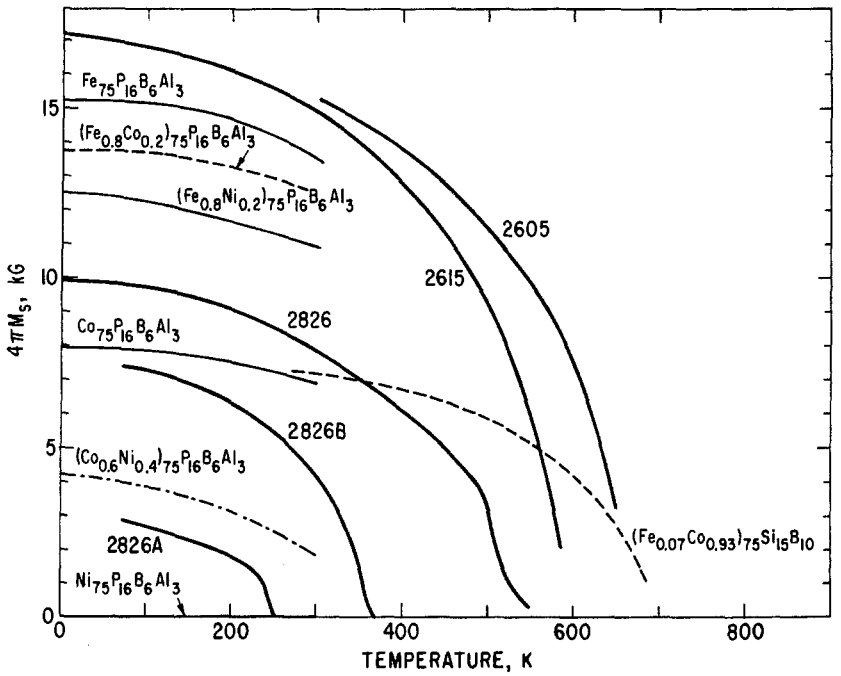

Fig. 29. Saturation magnetization as a function of temperature for various amorphous alloys. The numbers refer to the Allied Chemical Co. Metglas® alloys: 2605 is $Fe_{80}B_{20}$, Hasegawa et al. (1976a); 2615 is $Fe_{80}P_{16}C_3B_1$, Hasegawa and O'Handley (1976); 2826 is $Fe_{40}Ni_{40}P_{14}B_6$, Hasegawa (1976); is 2826B is $Fe_{29}Ni_{49}P_{14}B_6Si_2$, Egami and Flanders (1976); 2826A is $Fe_{32}Ni_{36}Cr_{14}P_{12}B_6$ Luborsky (unpublished). The $-P_{16}B_6Al_3$ alloys from Gyorgy et al. (1976); $(Fe_{0.07}Co_{0.93})_{75}Si_{15}B_{10}$ from Fujimori et al. (1976b).

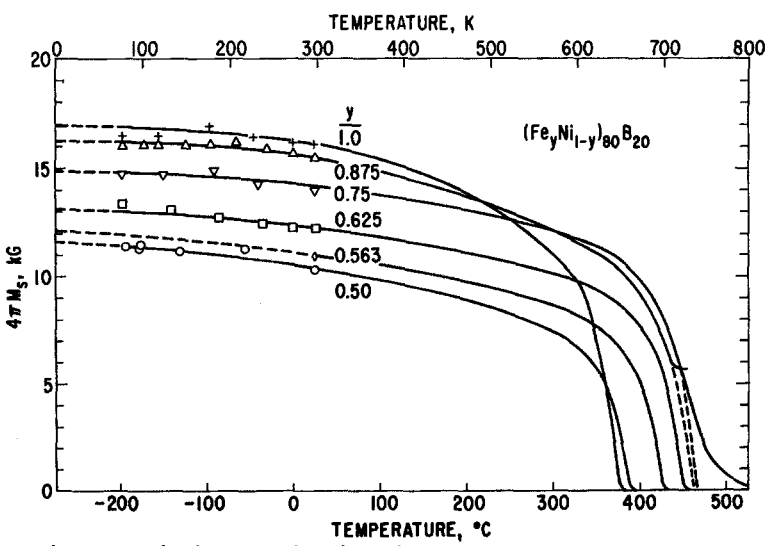

Fig. 30. Saturation magnetization as a function of temperature for Fe–Ni–B amorphous alloys. Luborsky and Walter (1977a).

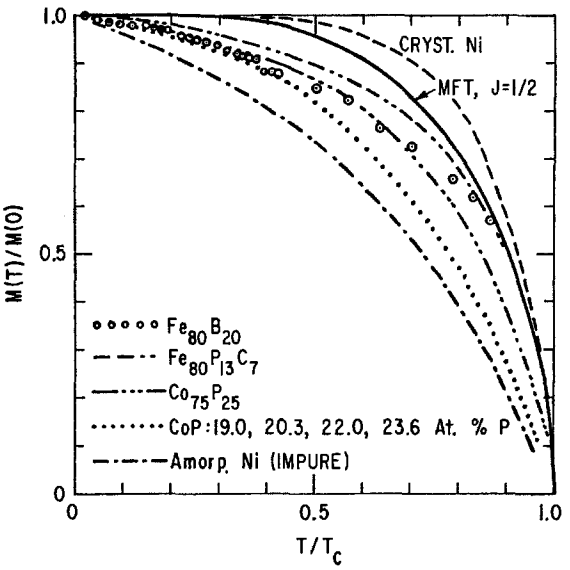

Fig. 31. Reduced magnetization–temperature dependence of various amorphous alloys compared to the molecular field theory calculation for $J = \frac{1}{2}$ and compared to crystalline Ni. FePC Tsuei et al. (1968); CoP Cargill and Cochrane (1974) and Pan and Turnbull (1974); amorphous Ni Wright (1976); FeB Chien and Hasegawa (1977).

Kaneyoshi (1973), Richter et al. (1975) and Yamada and Wohlfarth (1975). Both approaches predict that the M vs. T curve will fall below that for the crystalline counterpart. The first model however predicts that amorphous alloys should exhibit a structureless Mössbauer spectrum, contrary to the observed spectra. Thus the second approach is preferred. Of the various theories the molecular-field approach of Handrich (1969) or the approximate Green's function approach of Tahir-Kheli (1973) are the easiest to present although the band model of Yamada and Wohlfarth (1975) may be the most correct one. The effect of fluctuations in the exchange interaction leads to the equation for the reduced magnetization

$$\delta = M_T/M_0 = \tfrac{1}{2}\{B_s[(1+\delta)x] + B_s[(1-\delta)x]\} \tag{20}$$

where $x = [3S\sigma/(S+1)](T_c/T)$, B_s is the Brillouin function and δ is a measure of the degree of disorder. It is defined as the root mean square deviation from an average exchange integral between nearest neighbor spins.

$$\delta^2 = \langle \Delta J^2 \rangle / \langle J \rangle^2. \tag{21}$$

The larger the value of δ the larger the decrease in the reduced magnetization–temperature curve. Tsuei and Lillienthal (1976) have compared their results for $Fe_{75}P_{15}C_{10}$ to the theory. A value of $\delta = 0.3$ fit their magnetization results best, in good agreement with the hyperfine field distribution obtained from Mössbauer spectroscopy results. Also shown in fig. 31 is the curve calculated from molecular field theory (MFT) with $J = \frac{1}{2}$. For crystalline nickel, as shown, and for other

elements and alloys, reasonable agreement is obtained between the experimental and theoretical curves. Quantitative agreement between theory and experiment for amorphous magnetic metals is not expected since the Heisenberg localized moment models are generally not applicable to conductors and realistic models for the atomic arrangements of the amorphous alloys have not yet been used.

At low temperatures demagnetization in crystalline materials is attributed to thermal excitation of long wavelength spin waves. The spin wave behavior may be inferred from low temperature magnetic measurements and from inelastic neutron scattering measurements. From magnetization measurements directly, or from Mössbauer measurements, assuming that the hyperfine field H_{eff} is proportional to the magnetization M, the change in magnetization with temperature is given by

$$(M_0 - M_T)/M_0 = \Delta M/M_0 = BT^{3/2} + CT^{5/2} + \ldots \tag{22}$$

where M_0, M_T are the magnetizations at temperatures 0 and T and B and C are constants characteristic of the low temperature, long wavelength, spin waves. From neutron scattering, assuming a dispersion relation of the form

$$E(K) = DK^2 \tag{23}$$

the spin wave dispersion coefficient D may be determined. The values of D and B should be related by

$$B = \xi(\tfrac{3}{2})(g\mu/M)(k/4\pi D)^{3/2} \tag{24}$$

where g is the g-factor (~ 2.1), μ is the Bohr magneton in emu (9.27×10^{-21} emu), M is the magnetization in emu/Å^3, k is Boltzmann's constant (8.61×10^{-5} eV/K) with D in eV Å^2, to obtain B in $K^{-3/2}$. ξ is the zeta function, equal to 2.612. In crystalline ferromagnets the $T^{3/2}$ term is dominant. This appears to be the case also for amorphous ferromagnetics. For example, Chien and Hasegawa (1977) obtained for $Fe_{80}B_{20}$ $B = 22 \pm 1 \times 10^{-6}\,\text{deg}^{-3/2}$ and $C = 1.4 \pm 0.5 \times 10^{-8}\,\text{deg}^{-5/2}$. The values of B in amorphous alloys are typically larger (and D smaller) than related crystalline alloys; Cargill (1975b) and Kazama et al. (1976). The large value of B in amorphous alloys has been interpreted as a "softening" of the exchange interaction, while the small value of C/B implies that the exchange interactions damp out rapidly beyond the first nearest neighbors.

In crystalline ferromagnets of these alloys the values of B or D as determined from magnetization, Mössbauer and ferromagnetic resonance all agree with those evaluated from the spin wave dispersion coefficient from inelastic neutron scattering. Also, there is a reasonably good linear correlation between $T^{3/2}$ and $1/B$ (Cargill 1975b). In amorphous alloys the value of B determined from neutron scattering is always smaller, by as much as a factor of two, than the value obtained by the other techniques. Although there appears still to be a linear relation between $1/B$ and $T^{3/2}$ for amorphous alloys the curve falls well below the curve for crystalline ferromagnets. These discrepancies are not understood. The available results for the value of the spin wave coefficient D are

summarized in fig. 32 for values derived both from magnetic and neutron scattering results. Both appear to follow coincidently an approximate $T^{3/2}$ proportionality. Since it was previously noted that in crystalline alloys $1/B \propto T_c^{3/2}$ we would have expected $D^{3/2} \propto T_c^{3/2}$ i.e. $D \propto T_c$ in view of eq. (24) where $B \propto D^{-3/2}$. However a plot of D vs. T_c produces a non-linear relation.

4.4. *Magnetostriction*

The literature on magnetostriction of amorphous alloys is not very extensive. Simpson and Brambley (1971) prepared $Co_{91}P_9$ by electroless deposition and reported a value for linear magnetostriction λ of -4.3×10^{-6} for the as-deposited alloy. This increased on annealing even while remaining amorphous. The single phase crystalline alloy developed by further annealing had a value for λ of -11×10^{-6}. Sherwood et al. (1975) reported on the magnetostriction within the ternary region of the transition metals for roller quenched amorphous $(Fe–Ni–Co)_{75}P_{16}B_6Al_3$. A zero magnetostrictive composition occurred at $(Fe_{0.04}Co_{0.96})_{75}P_{16}B_6Al_3$. This has approximately the same Fe/Co content for which $\lambda = 0$ in crystalline alloys, i.e., Fe_8Co_{92}. With addition of nickel the iron content required for $\lambda = 0$ appeared to increase somewhat. Only qualitative observations of magnetostriction were made by observing changes in the hysteresis loop

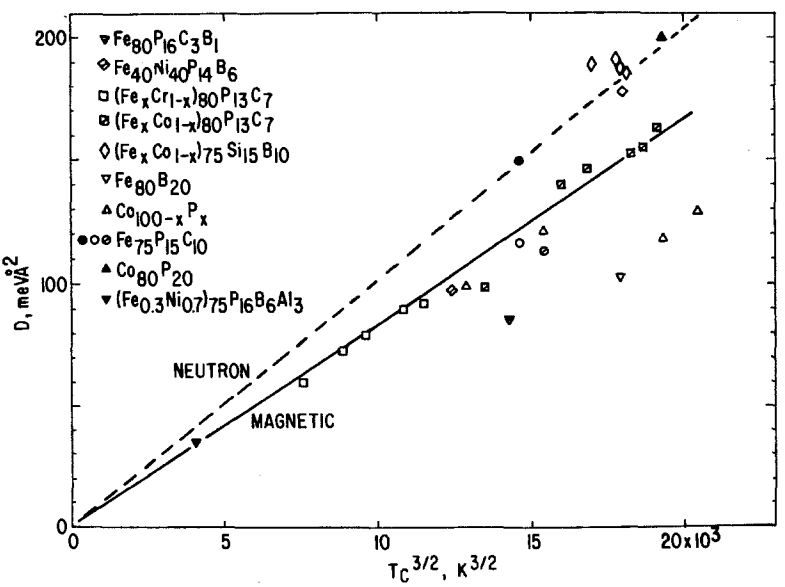

Fig. 32. Experimental correlation between the spin wave coefficient D and the Curie temperature of amorphous alloys. Solid symbols determined from inelastic neutron scattering; open symbols determined from magnetic measurements. FeCrPC □, FeCoPC ▨, FeCoSiB ◇, Kazama et al. (1976); FeB ▽, Chien and Hasegawa (1977); CoP △, Cargill and Cochrane (1974); FePC ●, Axe et al. (1975) and ○, Tsuei and Lillianthal (1976), CoP ▲, Mook et al. (1975); FeNiPBAl ▼, Lynn et al. (1976); FePC ⊘, FePCB ▽, FeNiPB ◇, Chien and Hasegawa (1976b).

caused by application of tension. Quantitative values of λ_s were reported by Brooks (1976) for the series $(Fe_{1-x}Co_x)_{75}P_{16}B_6Al_3$ from $0 \leq x \leq 0.97$. These results are shown in fig. 33. Tsuya et al. (1975) studied the magnetostriction of $Fe_{80}P_{13}C_7$ from −76°C to room temperature. The perhaps surprising result found was that the material did not appear to be isotropic; values of λ_s varied from 25×10^{-6} to 36×10^{-6} depending on the direction of field and measurement. A series of Ni–Co–Fe–P alloys were prepared by electroless deposition by Simpson and Clements (1975). The magnetizations all showed a composition dependence which was similar to that found in crystalline Ni–Co–Fe alloys. The magnetostriction constants however were all negative in sign (table 7) unlike the behavior observed in the related crystalline Ni–Co–Fe. These samples were all found to crystallize first to a metastable single phase with λ_s about half as large as in the amorphous phase but with amost no change in M_s. They conclude that the change in λ_s on crystallization could be accounted for by the change in Young's modulus. Magnetostriction was also studied by Arai et al. (1976) in three

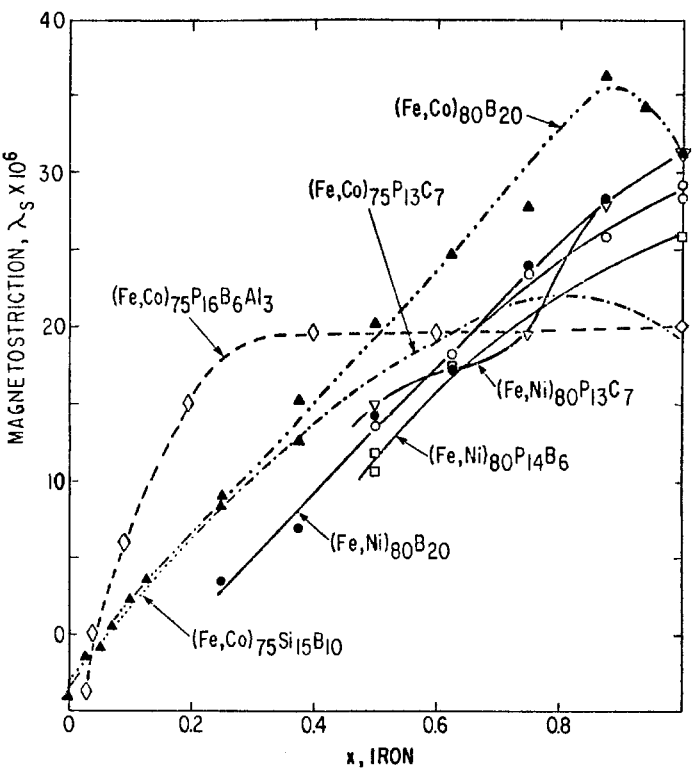

Fig. 33. Saturation magnetostriction for various amorphous alloys with changing transition metal composition. FeCoPBAl Brooks (1976), FeNiPC average of values from Arai et al. (1976), FeNiB Flanders and Luborsky (unpublished) and O'Handley (1977), FeNiPB Flanders and Luborsky (unpublished), FeCoPC and FeCoSiB Fujimori et al. (1976b), FeCoB O'Handley (1977).

TABLE 7
Magnetostriction of some* amorphous alloys at room temperature

Alloy	$\lambda_s \times 10^6$	Reference
$Co_{80}B_{20}$	−4.0	O'Handley (1977)
$Fe_{80}B_{20}$	31.0	O'Handley (1977)
#2605		
$Fe_{80}P_{10}B_1C_3$	30.0	O'Handley (1976)
#2615	29.0	Egami et al. (1975a, 1975b)
$Fe_{40}Ni_{40}P_{14}B_6$	11.0	O'Handley (1976)
#2826	11.0	Egami et al. (1975a, 1975b)
$Fe_{29}Ni_{49}P_{14}B_6Si_2$	3.0	O'Handley (1976)
#2826B	5.0	Egami et al. (1975a)
$Fe_{80}P_{13}C_7$	19.0	Fujimori et al. (1974)
	31.0	Tsuya et al. (1975)
	31.0	Arai et al. (1976)
$Co_{46.6}Ni_{31.1}P_{22.3}$	−9.0	Simpsons and Clements (1975)
$Fe_{0.6}Co_{35.2}Ni_{39.8}P_{24.4}$	−11.5	Simpson and Clements (1975)
$Fe_{0.7}Co_{46.9}Ni_{35.0}P_{17.4}$	−12.0	Simpson and Clements (1975)
$Fe_{3.9}Co_{36.5}Ni_{42.8}P_{16.8}$	−8.5	Simpson and Clements (1975)
$Fe_{4.3}Co_{39.9}Ni_{37.3}P_{18.5}$	−4.0	Simpson and Clements (1975)
$Fe_6Co_{74}B_{20}$	<0.4	O'Handley et al. (1976b)
$Fe_3Co_{72}P_{16}B_6Al_3$	~ 0	Sherwood et al. (1975)
$Fe_{4.7}Co_{70.3}Si_{15}B_{10}$	−0.1	Fujimori et al. (1976b)
$Co_{75}Si_{15}B_{10}$	−3	Arai et al. (1976)
$Co_{91}P_9$	−4.3	Simpson and Brambley (1971)

Allied Chemical Co. Metglas® designation.
* Values for other alloys given in the figures.

series of amorphous alloys: $Fe_{80-x}Ni_xP_{13}C_7$ $(0 \leq x \leq 40)$, $(Fe_{1-x}Co_x)_{80}P_{13}C_7$, $(0 \leq x \leq 0.7)$ and $(Fe_{1-x}Co_x)_{75}S_{15}B_{10}$ $(0.75 \leq x < 1)$ with the results also shown in fig. 33. Again λ_s was found to be not quite isotropic. The value of λ_s decreased nearly monotonically with increase in Ni from 31×10^{-6} for $Fe_{80}P_{13}C_7$ to 15×10^{-6} for $Fe_{40}Ni_{40}P_{13}C_7$. In the Fe–Co system the magnetostriction went through zero near 96at.% Co; at approximately the same composition as for alloys with other metalloids as shown in fig. 33. The temperature dependence of λ_s was not a simple function. For $Fe_{80}P_{13}C_7$ they found a broad maximum in λ_s near 130 K. In the Fe–Ni system the maximum was near 90 K for the compositions with $x = 0.2$ and 0.4. Some additional results on these same alloys were reported by Fujimori et al. (1976a) including the forced volume magnetostriction. A simple ternary

zero magnetostrictive alloy was reported by O'Handley (1976a) with the composition $Co_{74}Fe_6B_{20}$. This amorphous alloy has a higher saturation magnetization than the other zero magnetostrictive alloys so far reported (see table 7) which contain phosphorus and aluminum or silicon in addition to the boron. The magnetostrictions of the complete series of $(Fe–Ni)_{80}B_{20}$ and $(Fe–Co)_{80}B_{20}$ amorphous alloys were also reported by O'Handley (1977). These results are also shown in fig. 33. The saturation magnetostrictions reported in the above references are summarized in table 7, and in fig. 33 as a function of transition metal content, and in fig. 34 as a function of metalloid content.

O'Handley (1977) has discussed the possible origin of magnetostriction in amorphous alloys. Band models which adequately describe the magnetostriction of crystalline Fe–Ni alloys do not appear to apply to these Fe–Ni and Fe–Co amorphous alloys. A localized spin model, which sums the strain derivative of pseudodipolar interaction energies over nearest neighbors adequately describes the magnetostrictions of crystalline Fe and Co. When generalized to consider the amorphous alloys the model suggests that the short-range order of cobalt-rich amorphous alloys resembles that of their crystalline counterparts. Interpretation of the results in terms of a quantum-statistical mechanics theory suggests that one anisotropic mechanism for magnetostriction dominates in the Fe–Ni-based glasses while another mechanism is also important in Co-rich glasses.

4.5. Mössbauer spectroscopy results

Mössbauer spectroscopy yields information on the magnetic properties of individual atoms rather than on assemblies of atoms as in conventional magnetization measurements. Furthermore, it can yield information about the true zero field magnetization. Above the Curie temperature typical Mössbauer spec-

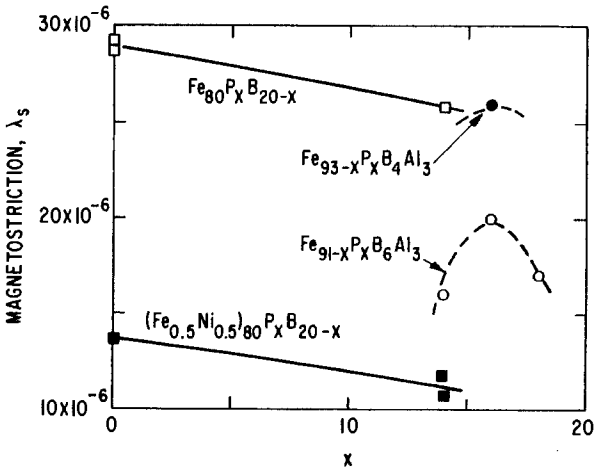

Fig. 34. Saturation magnetostriction for various amorphous alloys with changing glass former compositions. FePB and FeNiPB, Flanders and Luborsky (unpublished), FePBAl Brooks (1976).

tra for amorphous ferromagnetic alloys such as $Fe_{75}P_{15}C_{10}$ show two peaks characteristic of quadrupole splitting. Below the Curie temperature the spectra consist of six peaks symmetric with respect to their center but very broad compared to corresponding crystalline alloys. The broadening is attributed to the broad distribution of hyperfine fields. The distribution of hyperfine fields varies with the alloy for reasons that are not defined in detail but are related to the random nature of the structure. Thus amorphous $Fe_{80}B_{20}$ reported by Chien and Hasegawa (1977) has a narrower distribution of hyperfine fields than $Fe_{75}P_{15}C_{10}$ reported by Tsuei and Lilenthal (1976) and $Fe_{40}Ni_{40}P_{14}B_6$ reported by Chien and Hasegawa (1976a).

Mössbauer spectroscopy has also been used to determine the average direction of magnetization by using the well known fact that for Fe^{57} the intensities of the six lines of the hyperfine spectra have an area ratio of $3:b:1:1:b:3$. The value of b varies from 0 for the axis of magnetization perpendicular to the sample plane, to 4 for the axis of magnetization in the sample plane. Results by Chien and Hasegawa (1977) indicated that the magnetization stayed nearly completely in the plane of the ribbon for the as-prepared ribbon. The same conclusion was reached by Hasegawa et al. (1976a) using ferromagnetic resonance and scanning electron microscope measurements. Results for other alloys are not entirely consistent, undoubtedly because of the variability of the strains developed during the solidification of the ribbon. These strains interact with the magnetostriction resulting in an anisotropy which together with the other anisotropies present determines the average magnetization direction. These differences in magnetization direction have also been deduced from other observations. For example, from domain structures by Becker (1976), Fujimori et al. (1976b) and by Obi et al. (1976), and from magnetization measurements by Luborsky et al. (1975). On cooling these as-prepared samples the average direction of magnetization typically begins to tilt out of the ribbon plane presumably due to changes in strain, magnetostriction and other anisotropies.

The hyperfine field obtained from the Mössbauer spectra, assumed to be proportional to the magnetization, has a temperature dependence typical of amorphous ferromagnets. Results for M_s of $Fe_{80}B_{20}$ from Chien and Hasegawa (1977) are shown in fig. 31 compared to some other amorphous alloys.

5. Domain structure

It is clear from the preceding sections that the amorphous alloys are not magnetically isotropic. The anisotropy may arise from field or stress annealing, non-uniform strains, or from chemical inhomogeneities. The magnitude of the total anisotropy, K, from these sources will, of course, depend on the alloy, its preparation and thermal-mechanical treatments. This anisotropy, and its local variations, together with the sample shape then determines the domain structure. The motion of the domains under the influence of the internal material

parameters and the externally applied fields determine the static and dynamic magnetic properties. The domain configurations can be observed directly. Some typical domain structures in as-cast ribbon of $Fe_{40}Ni_{40}P_{14}B_6$ reported by Becker (1976) are shown in fig. 35, as revealed by Bitter solution. Similar domain structures were reported by Fujimori et al. (1976c). The patchy nature illustrates the irregular distribution of anisotropy. Their labyrinthine structure shown in the higher magnification views changes with strain and with field, as expected. These effects and their disappearance on annealing all suggest that their origin is due to internal strains. These strains produce a normal component of M which results in a low M_r/M_s value in the as-cast ribbons. Values between 0.3 and 0.6 are typically obtained in a variety of compositions. After annealing, to reduce the strains to zero, the labyrinth patches disappear and are replaced by a simple structure of only a few domain walls. The direction of magnetization is then determined only by the field applied during the anneal and by the sample geometry. Values of M_r/M_s of 0.8–0.9 measured in the easy axis direction and

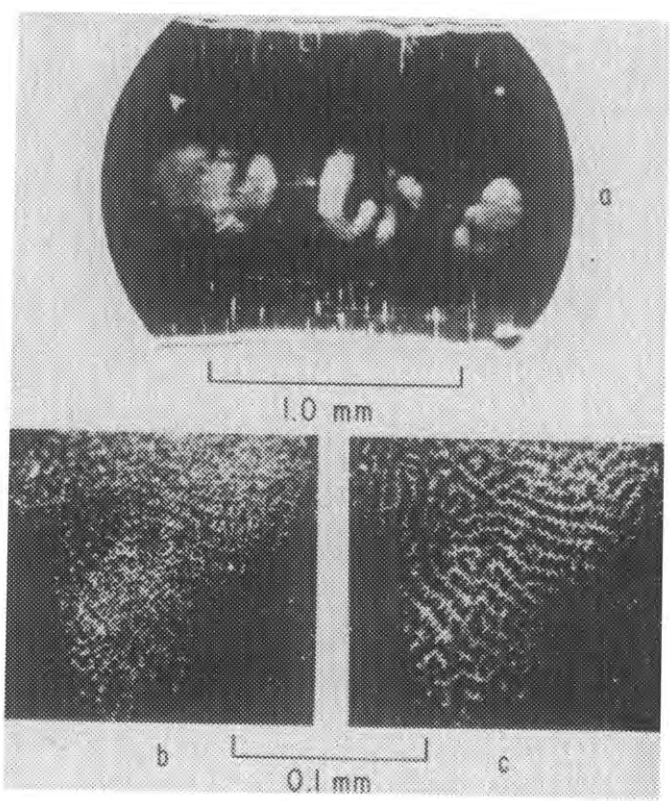

Fig. 35. Patches of fine domains observed on as-cast ribbon of $Fe_{40}Ni_{40}P_{14}B_6$. No applied field; ribbon axis horizontal. Ribbon thickness 40 mm. (a) low magnification, (b) higher magnification within patch in zero applied field, and (b) in 8 Oe along ribbon axis. Becker (1976).

less than 0.1 measured perpendicular to the easy axis, have been obtained. Results for some of the alloys are shown in table 8 and in fig. 36 as a function of temperature. The hysteresis loops measured in the easy axis direction, in the field annealed samples, are thus quite square and show a typical wall nucleation limited M–H loop with only a few Barkhausen jumps. Details of this have been reported by Becker (1975). Only a few walls are nucleated which are then free to sweep through the sample. This was confirmed by dynamic observation of the walls during reversal by Shilling (1976) and by measurements using a small ac field superimposed on the dc reversal field as described by O'Handley (1975).

6. Magnetic anisotropy

Amorphous solids usually are assumed to have no long-range order and thus should be isotropic on a macroscale. However, magnetic anisotropic behavior is observed. Its origin is varied and sometimes not completely understood. In many cases, it reflects the existence of short-range order in the amorphous alloy. In addition, it has become something like folklore that in an ideal amorphous alloy the atomic scale anisotropy would be averaged away so that there would be no anisotropy effects visible. Chi and Alben (1976) have shown from a simple model calculation that when the local random anisotropy is small the coercivity is indeed small but high coercivities are abruptly obtained as the local anisotropy increases and dominates the behavior. In the following sections the various anisotropies existing in amorphous alloys will be described.

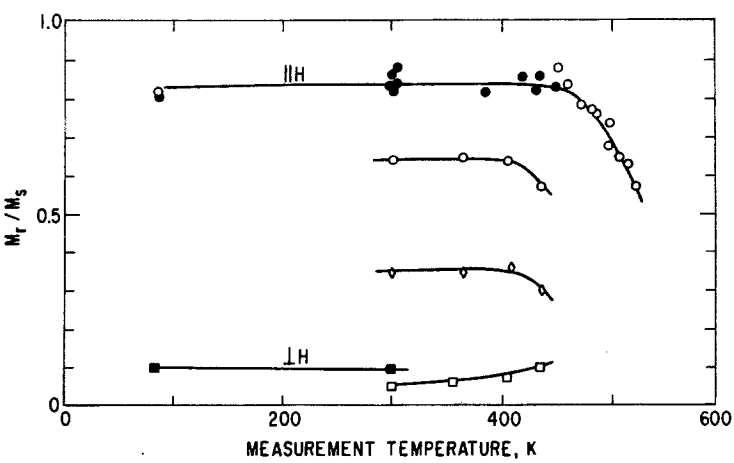

Fig. 36. Temperature dependence of the remanence to saturation ratio of $Fe_{40}Ni_{40}P_{14}B_6$. Sample annealed to obtain various values of M_r/M_s. ○ annealed in field along long axis of ribbon; □ annealed along width of ribbon; ○, ◇ incomplete anneal. Luborsky (unpublished).

TABLE 8
Static magnetic properties of some* amorphous alloys

Alloy	Sample shape	As-Cast H_c Oe	As-Cast M_r/M_s	As-Cast $\mu_{max} \times 10^{-3}$	Annealed H_c Oe	Annealed M_r/M_s	Annealed $\mu_{max} \times 10^{-3}$	Reference
$Fe_{80}B_{20}$	t				0.075	0.46		Luborsky (1977b)
#2605	t	0.08	0.51	100	0.04	0.77	300	O'Handley et al. (1976c)
	t				0.04	0.78		Hasegawa et al. (1976b)
$Fe_{40}Ni_{40}P_{14}B_6$	t	0.06	0.45	58	0.02	0.71	275	Luborsky et al. (1975)
#2826	t	0.05	0.44					Becker (1975)
	s	0.02–0.1						Becker (1975)
	s	0.010	0.90		0.009	0.89		Egami et al. (1975a)
	t				0.015–0.07	0.03–0.90		Luborsky et al. (1976a)
	s	0.017			0.012			O'Handley (1976)
	t	0.050	0.45	70	0.019	0.58	240	O'Handley (1976)
	s	0.065	0.36					Egami et al. (1975b)
	s	0.035						Hasegawa (1976)
	t	0.05 ±0.007	0.45 ±0.02	70	0.01	0.71	550	Mendelsohn et al. (1976)
	t				0.02	0.70		Luborsky (1977b)
$Fe_{29}Ni_{44}P_{14}B_6Si_2$	s	0.01	0.8		0.003 T	0.995 T		Egami et al. (1975a)
#2826B	s	0.013			0.006			O'Handley (1976)
	t	0.057	0.54	46	0.011	0.70	310	O'Handley (1976)
$Fe_6Co_{74}B_{20}$	s	0.035	0.83					O'Handley et al. (1976b)
$Fe_3Co_{72}P_{16}B_6Al_3$	t				0.015	0.82		Luborsky (1977b)
	t	0.023	0.45	120	0.013	0.71	340	Sherwood et al. (1975), Chen et al. (1975)
$Fe_{4.7}Co_{70.3}Si_{15}B_{10}$	s	0.013	0.36	190	0.006	0.63	700	Fujimori et al. (1976b)
	s	0.01	0.35	230	0.015	0.82	370	Kikuchi et al. (1975)
$Fe_{80}P_{13}C_7$	s	0.08	0.42	74	0.018	0.36	280	Fujimori et al. (1976b)
	t	0.12	0.42	42	0.06	0.40	80	Fujimori et al. (1974)

$Co_{75}Si_{15}B_{10}$	s	0.03	0.30	60				Kikuchi et al. (1975)
$Co_{80.8}P_{19.2}$	d	~1	0.01					Pan and Turnbull (1974)
$Co_{91}P_9$	s	9						Simpson and Brambley (1971)
$(Fe_{0.8}Ni_{0.2})_{78}S_{10}B_{12}$	s	0.04	0.44	145	0.015	0.93	800	Masumoto et al. (1977)
$(Fe_{0.8}Ni_{0.2})_{78}Si_8B_{14}$	s	0.018	0.41	300	0.006	0.95	2000	Masumoto et al. (1977)
$(Fe_{0.6}Ni_{0.4})_{78}Si_8B_{14}$		0.022	0.44	210	0.006	0.97	1700	Masumoto et al. (1977)
$(Fe_{0.4}Ni_{0.6})_{78}Si_8B_{14}$	s	0.024	0.46	120	0.005	0.76	950	Masumoto et al. (1977)
$Fe_{40}Ni_{40}P_{17}B_1$	t	0.046	0.52					Swift and Foster (1976)
$Fe_{45}Co_{35}P_{13}C_7$	s	0.19	0.51	40				Kikuchi et al. (1975)
	s	0.19	0.51	40				Fujimori et al. (1976b)
$Fe_{80}P_{16}C_3B_1$	s	0.080			0.068			O'Handley (1976)
#2615	t	0.062	0.40	96	0.050	0.42	130	O'Handley (1976)
	t				0.05	0.42	130	O'Handley et al. (1976c)
	t	0.19	0.30	26				Egami et al. (1975b)
$Fe_{60-70}Si_{40-30}$	d	~1	0.6–0.8					Shimada and Kojima (1976)
$Fe_{83-x}P_{17}Ga_x$: $2 < x < 8$	s	0.3–0.5						Wiesner and Schneider (1974)
$Fe_{83-x}P_{17}Ge_x$: $2 < x < 8$	s	0.2–0.5						Wiesner and Schneider (1974)
$Fe_{83-x}P_{17}As_x$: $2 < x < 8$	s	0.3–0.5						Wiesner and Schneider (1974)
$Fe_{40}Ni_{40}B_{20}$	t				0.090	0.68		Luborsky (1977b)
$Fe_{80}P_{14}B_6$	t				0.10	0.37		Luborsky (1977b)
$Fe_{50}Ni_{30}P_{14}B_6$	t				0.050	0.84		Luborsky (1977b)
$Fe_{40}Ni_{40}P_{14}B_6$	t				0.035	0.85		Luborsky (1977b)

d disk; s straight strip; t toroid; $\pm 1\sigma$; * values for other alloys are given in the figures; # Allied Chemical Co. Metglas® designation; T annealed under tension.

6.1. *Structural and compositional anisotropy*

Anisotropic microstructures can arise in amorphous alloys prepared by any of the techniques previously described. These microstructures may involve density or compositional fluctuations which produce internal shape effects, i.e. variations in magnetization. The resultant anisotropy field can then be no greater than that for long rods, namely $2\pi M_s$. The amorphous electrodeposited Co–P and CoNiP alloys have been studied in some detail. These alloys show a weak perpendicular anisotropy whose origin is believed due to such compositional fluctuations. Such fluctuations are often of the scale that can be seen by microprobe analysis or small angle X-ray scattering, i.e., in the range of 10–10000 Å [1–1000 nm]. Small angle X-ray scattering observations on these electrodeposited Co–P films have been interpreted by Chi and Cargill (1976) as showing the presence of oriented ellipsoidal scattering regions, assumed to be of high Co concentration. Annealing at temperatures well below crystallization reduced the perpendicular anisotropy and the small angle scattering suggesting that the annealing resulted in some homogenization of the alloy. In some amorphous alloys of Gd–Co, anisotropy fields greater than $2\pi M_s$ are observed even with no external stresses. The magnitude of K_u depends on the composition and conditions of preparation. The origin of this anisotropy in the rare earth–transition metal alloys is believed to involve short-range structural or compositional ordering developed during the preparation of the alloy, and is discussed in vol. 2, ch. 5.

6.2. *Strain–magnetostriction anisotropy*

Most amorphous ferromagnetic materials have non-zero magnetostriction, λ. Internal strains, σ, which may be uniform or non-uniform, arise from the original solidification or from subsequent fabrication. These strains couple with λ to produce an anisotropy, K_λ. Some values of λ reported for some of the commercially available alloys were listed in table 7. The changes in λ with composition for a variety of alloys were shown in figs. 33 and 34. Uniform strains are often induced in evaporated, sputtered or electrodeposited films due to the differential thermal expansion between the film and the substrate. The magnitude of λ and the direction and magnitude of σ will then determine the direction and magnitude of K_λ. An important example of non-uniform strains is observed on drum quenched alloys of the $(TM)_{80}(P, B, Al\ldots)_{20}$ type. The non-uniform strains develop during the preparation of the ribbon and result in a periodic fluctuation in the perpendicular component of anisotropy along the length of the tape. Thermal annealing removes the internal strains causing the anisotropy to disappear. The domain structure and their disappearance on annealing reflect this perpendicular K_λ and its removal. This has been discussed by Becker (1976) and Fujimori et al. (1976c).

6.3. *Directional order anisotropy*

As in crystalline alloys, the amorphous alloys also order under the influence of a magnetic field or stress, applied at a temperature below the Curie temperature. This results in a uniaxial anisotropy arising from the ordering of both the magnetic and non-magnetic atoms. Directional order theory predicts the dependence of the magnitude of the directional order anisotropy, K_u, on various parameters. It will be seen that the behavior of K_u in amorphous alloys is very similar to the behavior in thin films or bulk alloys of NiFe.

6.3.1. *Magnitude of magnetic ordering anisotropy*

In the case of magnetic ordering, following Slonczewski (1963), the magnitude of K_u is expected to be a function of the anneal temperature, θ, the magnetization at the anneal temperature, M_θ, at the measurement temperature, M_T, and at 0 K, M_0, and the concenetrations of the ordering atoms, C_A and C_B as given by

$$K_u = Af(c)(M_T/M_0)^2(M_\theta/M_0)^2/\theta \tag{25}$$

where A is a constant which depends on the atomic arrangement and the range of interactions considered. For dilute solutions for monatomic directional order $f(c) = c$ where c is the concentration of the ordering species. For diatomic order $f(c) = c_a^2$ where c_a is the concentration of the dilute species. If neither constituent is dilute, but assuming ideal solutions, i.e., for negligible non-magnetic interaction enrgy then

$$f(c) = \tfrac{1}{2}Nnc_a^2c_b^2 \tag{26}$$

where N is the number of atoms per unit volume and n is the number of possible orientations of each pair referred to a crystal lattice. For non-ideal solutions the effective non-magnetic interaction energy must be included in the expression for $f(c)$ as described by Luborsky and Walter (1977a). In amorphous alloys we expect the interaction energy to be negative, i.e., leading to precipitation. These relations for amorphous Fe–Ni–B alloys were studied in detail by Luborsky and Walter (1977a). The reported values of K_u are shown in fig. 37. The direction and magnitude of K_u can be changed reversibly by changing the field direction and anneal temperature. The non-zero value of K_u at $x = 1$ is interpreted as due to ordering of the boron. The temperature dependence observed fits the theoretically expected dependence on anneal temperature. The dependence of K_u on Fe–Ni composition follows the theoretical dependence for non-ideal solid solutions with a negative interaction energy, i.e., of the type leading to precipitation as expected.

Fujimori et al. (1977) studied the magnetically induced anisotropy in $(Fe_xCo_{1-x})_{78}Si_{10}B_{12}$ amorphous alloys. Their results for the maximum values of K_u obtained by annealing in a field for 15 min at increasing temperatures are shown by the solid circles in fig. 37. The same values were obtained by cooling in

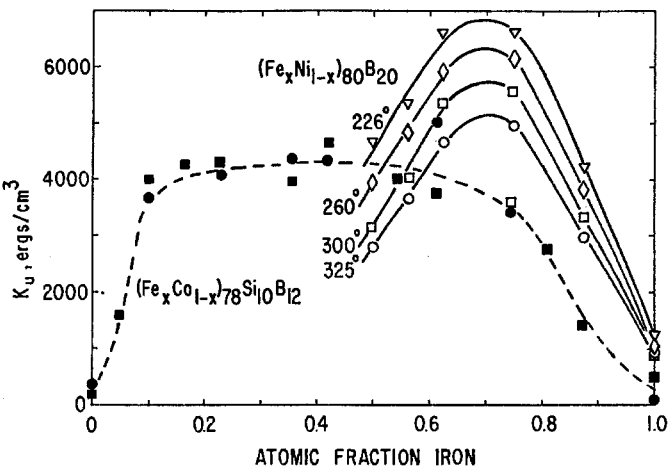

Fig. 37. Magnetically induced anisotropy as a function of composition. Developed by annealing to equilibrium at various temperatures given by open symbols from Luborsky and Walter (1977a). Solid symbols ● for maximum values obtained by heating 15 min at successively higher temperatures and ■ by colling from 380° at 1.6 deg/min, calculated from data of Fujimori et al. (1977).

a field at a rate of 1.6 deg/min as shown by the solid squares. Although these results are of interest from a practical viewpoint they are difficult to interpret quantitatively in terms of directional order theory because of the uncertainty as to the anneal temperature and the uncertainty as to whether equilibrium was achieved at any temperature. Directional order theory predicts a decrease in induced anisotropy as the anneal temperature increases, as observed by Fujimori. The decrease in K_u on further decreasing the anneal temperature is the result of the slower kinetics of orientation at low temperature, as will be discussed in the next section, suggesting that equilibrium was not achieved. The general requirement that two different metal atoms are necessary to obtain a large K_u was further demonstrated by Fujimori et al. (1977) by adding small amounts of Pd, Ni or Cr as well as the Fe to CoSiB. These results are shown in fig. 38.

6.3.2. Reorientation kinetics

There have been a few studies of the kinetics of the reorientation of K_u. The time constants for this reorientation for various amorphous alloys are shown in fig. 39 compared to similar crystalline alloys without the metalloid additions. It is clear that the amorphous alloys are more closely related in their behavior to the quenched crystalline alloys rather than to the annealed crystalline alloys. In the quenched alloys, the rate determining step in the reorientation has been associated with the excess vacancies present. It has thus been suggested that the disordered structure of the amorphous alloys has produced a similar atomic environment and thus similar kinetics for the reorientation. The $Fe_{40}Ni_{40}P_{14}B_6$ alloy surprisingly exhibited simple first order kinetics in the reorientation of its

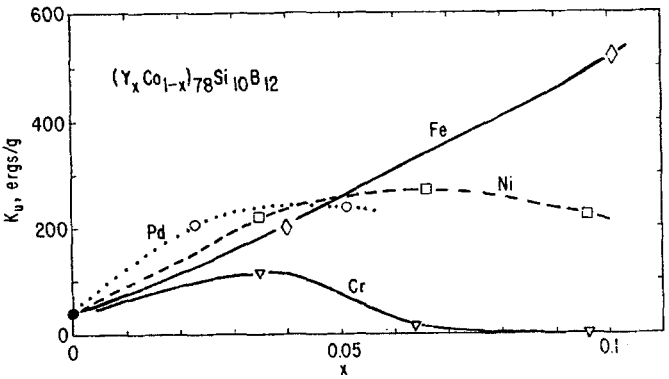

Fig. 38. The maximum magnetically induced anisotropy for small additions of Fe, Ni, Pd or Cr to CoSiB. Maximum values from heating 15 min at successively higher temperatures. From Fujimori et al. (1977).

anisotropy as measured by the changes in its remanent magnetization ratio M_r/M_s. This suggests that a uniform atomic environment exists around the reordering species. On the other hand the reorientation kinetics of the $Fe_{40}Ni_{40}B_{20}$ alloy did not exhibit simple first order kinetics; the kinetics could be fitted with a distribution of time constants or by second order kinetics with equal concentrations of the two species. Note that the time constants obtained for the

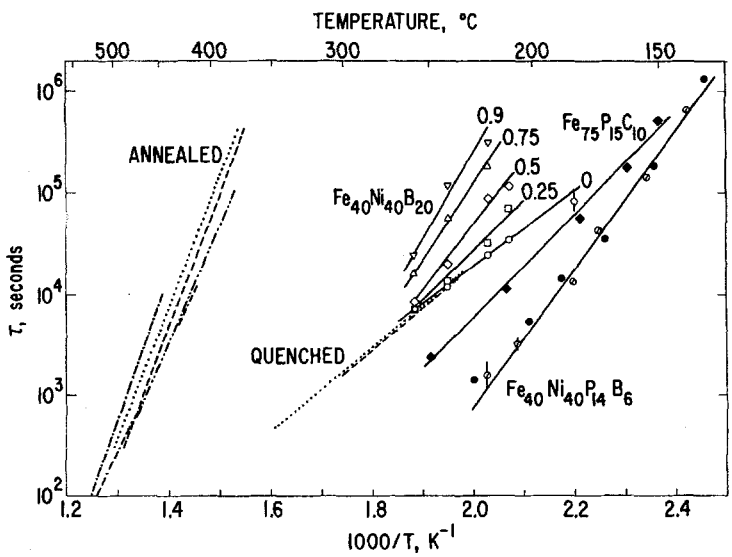

Fig. 39. Time constants for the reorientation of the induced anisotropy in some amorphous alloys shown by the solid curves with data points: FeNiPB ○ Luborsky (1976), ● Berry and Pritchet (1976); FePC Berry and Pritchet (1976); FeNiB Luborsky and Walter (1977b). Crystalline alloys shown by broken curves --- 40 Fe–60 Ni, · · · 15 Fe–85 Ni; —·— 20–50 Fe–Ni, —··— 16 Fe–84 Ni; —··—·— 20 Fe–20 Fe–20 Ni–60 Co, references given in Luborsky (1977b).

$Fe_{40}Ni_{40}P_{14}B_6$ alloy by Luborsky (1976) using magnetic measurements and by Berry and Pritchet (1976) using measurements of the ΔE effect using a vibrating reed, agree with each other.

6.3.3. Stress-induced order

These alloys are also susceptible to stress induced ordering as studied by Berry and Pritchet (1975, 1976) using internal friction measurements. As in crystalline alloys, this ordering presumably occurs via the interactions of the strain produced with the magnostriction. The activation energy for stress induced ordering, determined from the internal friction measurements, for $Fe_{75}P_{15}C_{10}$, $Fe_{40}Ni_{40}P_{14}B_6$ and $Fe_{80}B_{20}$ was 2.2, 2.6 and 2.6 eV [210, 250 and 250 kJ/mole] respectively. These activation energies are about twice as large as the values for magnetic ordering. It is thus concluded that stress induced directional ordering involves different atomic species or motions than those involved in magnetically induced ordering. In addition, the final state produced by the two ordering processes must be different.

6.4. Exchange anisotropy

Evidence for ferromagnetic–antiferromagnetic "exchange anisotropy" has been found in the amorphous alloy $Fe_{37.5}Mn_{37.5}P_{16}B_6Al_3$ by Sherwood et al. (1976). This appears to be the first demonstrated example of exchange anisotropy in an amorphous transition metal–metalloid alloy. This raises some interesting, and unanswered questions concerning the atomic arrangement necessary to develop this effect. By cooling in a field an asymmetric hysteresis loop was measured at 1.5 K. The intrinsic coercive force was near zero on one side and 7200 Oe [90 A/m] on the other. Cooling in zero field produced a symmetric loop with $H_{ci} = 1600$ Oe [20 A/m]. Magnetic saturation could not be achieved by any treatment; the magnetization at 15 kOe [190 A/m] was only 7.5 emu/g.

7. Coercive force

If we assume that magnetization reversal takes place by domain wall motion, there are several approaches to calculating the coercive force, H_c, in terms of the material parameters. See for example Gyorgy (1975) or Chikazumi (1974). In one approach given by Gyorgy et al. (1976) it was assumed that walls are pinned only at the surfaces. For 180° walls, the coercive force can be written from dimensional analysis, as

$$H_c = 4S(AK)^{1/2}/dM_s \tag{27}$$

where S is a constant determined by inclusion size and density, surface roughness, fluctuations in anisotropy or other factors; A is the exchange constant, K the anisotropy, d the ribbon thickness and M_s the saturation. In another approach Hasegawa (1976) wrote

$$H_c = (2K/M_s)f \tag{28}$$

if we assume reversal by domain wall motion where $f = \Sigma\, \Delta X/X$. Here ΔX stands for the fluctuation in X within a region corresponding to the domain wall width. The comparison of this functional relation to some results on an unannealed ribbon is shown in fig. 40 where temperature was varied to vary K and M_s. The solid line was obtained from the theoretical relation normalized to the room temperature value of H_c and K was determined from ferromagnetic resonance. The decrease in H_c on annealing results from the decrease in the strain–magnetostriction anisotropy. Results for H_c of other amorphous alloys are shown in fig. 41 as a function of transition metal content and in table 8 for alloys in the as-cast and in the annealed state. Note that the values of H_c for the annealed samples depend on their magnetic history. In the case of $(Fe, Co)_{75}Si_{15}B_{10}$ Fujimori et al. (1976c) assumed that the major contribution to the H_c arose from the strain–magnetostriction anisotropy fluctuations so that $H_c \propto \lambda_s/M_s$. Using measured values of λ_s and M_s, they calculated the solid and dashed curve in fig. 41 where the solid curve was normalized to fit the Fe, Co data at low concentrations and the dashed curve was normalized to the data at high Fe, Co concentrations. The agreement is not very satisfying. Other factors such as surface roughness, cracks, and stress may be varying from sample to sample.

The dynamic response of domain walls is of considerable practical as well as fundamental interest. When an ac field is applied, large enough to reverse the magnetization, with walls free of pinning sites, then the wall behavior is governed only by eddy current damping. The coercive force is then givn by

$$H_{ac} = (\pi f L H \beta/M_s)^{1/2} \tag{29}$$

where f is the frequency, L the domain wall spacing, H the maximum drive field, and β is the damping constant. Results for an amorphous alloy, in fig. 42,

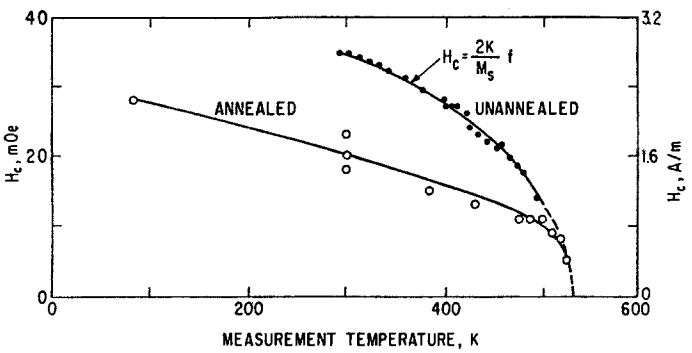

Fig. 40. Temperature dependence of coercive force for $Fe_{40}Ni_{40}P_{14}B_6$: ● unannealed sample, theoretical relation given by solid line, Hasegawa (1976); ○ annealed sample, Luborsky (unpublished).

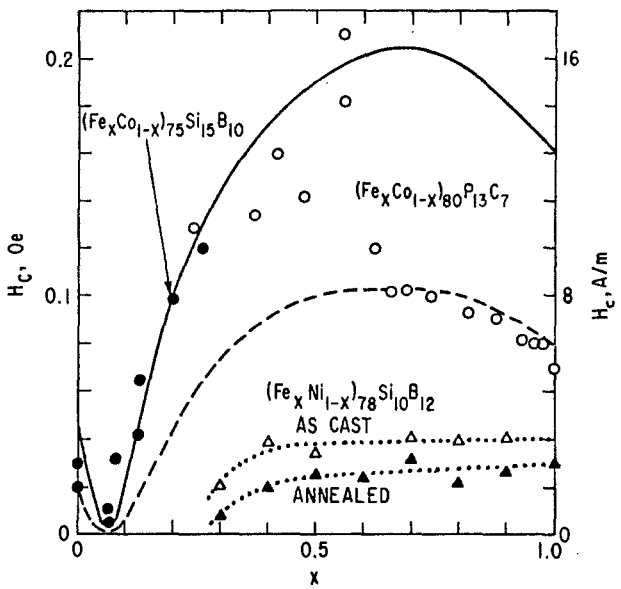

Fig. 41. Dependence of coercive force on composition. ● FeCoSiB and ○ FeCoPC as-cast Fujimori et al. (1976c). Solid line calculated by normalizing to fit FeCoSiB data; dashed line calculated by normalizing to fit FeCoPC data. △ ▲ FeNiSiB as-cast and annealed, Masumoto et al. (1977).

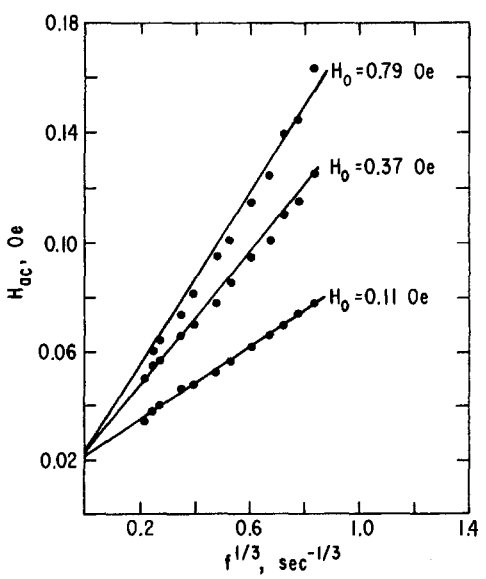

Fig. 42. The alternating current coercive force as a function of the drive field frequency at three field amplitudes, H_0. Gyorgy et al. (1976).

are very similar to results obtained on conventional SiFe and Permalloy. The slopes vary as $H_0^{1/2}$ as expected but an $f^{1/3}$ frequency dependence is found rather than $f^{1/2}$. This is due to a frequency dependence of the domain spacing L.

8. Remanence-to-saturation ratio

As in crystalline materials the remanence-to-saturation ratio of a magnetic material is important theoretically and technologically. Its value is determined by the magnitudes and directions of the anisotropies present. In amorphous alloys of the transition metal–metalloid type the anisotropies in the as-quenched ribbons appear to be dominated by the strain–magnetostriction interaction. Since the magnitude and the direction of the strain may vary with the details of the quenching the resultant anisotropy and thus M_r/M_s would be expected to vary, as is indeed the case. After a stress-relief anneal as first described by Luborsky et al. (1975) the dominant anisotropy remaining appears to be that due to directional order as described in a previous section of this chapter. The value of M_r/M_s is then determined by the direction and magnitude of the directional order anisotropy. In the $Fe_{40}Ni_{40}P_{14}B_6$ amorphous alloy, for example, Luborsky et al. (1976a) reported values of M_r/M_s from less than 0.1 to 0.9, as indicated in fig. 36, depending on the magnetic field and heat-treatment used. Typical values reported for M_r/M_s for some other alloys both before and after a stress relief anneal are listed in table 8 but these may also vary widely depending on their thermo-magnetic history.

9. Susceptibility and permeability

The low field susceptibility $\chi = M/H$, can be discussed in terms of a model similar to the one applied to discussing the coercive force. From the equation of motion of a wall and at low frequencies, considering the energy required to bow out the wall, it has been shown, for example by Gyorgy (1975), that the susceptibility

$$\chi = M_s^2 d/[18L(AK)^{1/2}] \tag{30}$$

where d is the sample thickness and L is the domain spacing. From the observed domain patterns for an annealed alloy, $L \approx 0.01$ cm and with $d = 2.5 \times 10^{-3}$ cm, χ(calc.) = 330; in reasonable agreement with values measured.

The permeability $\mu = B/H = (H + 4\pi M)/H$ of as-cast alloys is relatively low but improves with annealing at temperatures and times below crystallization, as reported by Luborsky et al. (1975). With decreasing magnetostriction the permeability of the as-cast alloys also improves considerably as measured in $Fe_{4.7}Co_{70.3}Si_{15}B_{10}$ by Fujimori et al. (1976b), in $Fe_3Co_{72}P_{16}B_6Al_3$ by Sherwood et al. (1975), in a variety of alloys by Luborsky (1977b), and in $Fe_6Co_{74}B_{20}$ by O'Handley et al. (1976b). Subsequent annealing of the low magnetostriction

alloys has little effect on their properties. The maximum dc permeability, often calculated as B_r/H_c, for a number of alloys in the as-cast and in the annealed state, are given in table 8. It should be noted again, however, that these results for the annealed specimens depend on the annealing history. Results from Luborsky (1977b) for a number of fully annealed amorphous alloys are shown as a function of frequency in fig. 43 compared to some conventional soft metallic magnetic materials. Luborsky et al. (1976a) showed that the losses and permeability could be controlled by control of the orientation as measured, for example, by M_r/M_s. The values of M_r/M_s and other charactertics of the samples whose permeabilities are shown in fig. 43 are given in table 9. The letter designations in the table are the same as given in the figure. The low frequency permeability of all of the amorphous alloys shown are less than the commercial Permalloys but higher than the FeSi. Improved permeabilities are expected for the amorphous alloys if smoother surfaces were prepared as is done for the commercial alloys. At higher frequencies the amorphous alloys compare somewhat more favorably to the crystalline alloys because of their higher resistivity.

10. Losses

At intermediate and high inductions, when core losses are significant in applications, the total power losses are often expressed as the sum of a hysteresis loss and eddy current loss as

$$W = \eta B^{1.6} f + eB^2 f^2 \tag{31}$$

when f is small, e.g., <100 Hz. At low inductions, B, the hysteresis loss term is

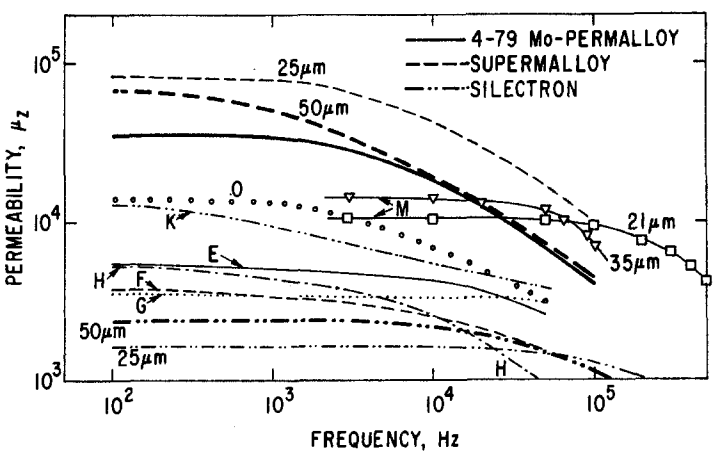

Fig. 43. Typical "initial" impedance permeability vs. frequency for amorphous alloys and commercial alloys. Amorphous alloys measured at $\Delta B = 100$ G; ▽, □ at 45 G; commercial alloys at 50 G. Luborsky (1977b).

TABLE 9
As-cast vs. annealed losses in amorphous alloys (from Luborsky 1977b)

Nominal Composition	Designation	Core loss at $B_m = 1$ kG, mW/cm³ As-cast Frequency, kHz 0.060	1	10	50	Annealed 0.060	1	10	50	Tape thickness μm	Annealed H_c Oe	M_r/M_s	Reference
$Fe_{80}B_{20}$ #2605	A	0.071	2.8	65	–	0.030	1.1	18	–	30–35[P]	0.040	0.78	Hasegawa et al. (1976b) O'Handley et al. (1976c)
$Fe_{80}P_{16}C_3B_1$ #2615	B	–	8.5	310	–	–	6.3	160†	–	40[P]	0.050	0.42	O'Handley (1976)
$Fe_{40}Ni_{40}P_{14}B_6$ #2826	C	–	13	250	–	–	1.8	42	–	50[P]	0.019	0.58	O'Handley (1976)
$Fe_{29}Ni_{49}P_{14}B_6Si_2$ #2826B	D	–	10	160	–	–	0.75	20	–	70[P]††	0.011	0.70	O'Handley (1976)
$Fe_5Co_{70}S_{15}B_{10}$	M	–	–	–	–	–	–	–	–	–	0.010	0.85	Kikuchi et al. (1975)
$Fe_{80}B_{20}$ #2605	E	0.10	5	350	1000	0.025	1.2	35	200	30	0.075	0.46	Luborsky (1977b)
$Fe_{40}Ni_{40}B_{20}$	F	0.07	4	450	2300	0.016	1.2	45	600	30	0.090	0.68	Luborsky (1977b)
$Fe_{80}P_{14}B_6$	G	0.04	2.5	80	950	0.014	1.1	28	200	25	0.10	0.37	Luborsky (1977b)
$Fe_{50}Ni_{30}P_{14}B_6$	H	0.09	5	380	1700	0.022	1.2	50	1000	30	0.050	0.84	Luborsky (1977b)
$Fe_{40}Ni_{40}P_{14}B_6$ #2826	K	0.07	4	400	3000	0.010	0.60	18	180	50	0.020	0.70	Luborsky (1977b)
$Fe_{40}Ni_{40}P_{14}B_6$	L	0.06	5.5	550	1300	0.014	0.92	49	820	36	0.035	0.85	Luborsky (1977b)
$Fe_3Co_{72}P_{16}B_6Al_3$	O	0.025	1	28	190	0.006	0.35	16	230	20	0.015	0.82	Luborsky (1977b)

Allied Chemical Co. Metglas® alloy designation.
† Could not be annealed at a high enough temperature to fully stress-relieve.
†† D-shaped cross section-maximum thickness.
[P] Private communication from R.C. O'Handley.

more nearly proportional to B^3f. At higher frequencies, the losses are controlled predominantly by eddy currents and are given by

$$W_e = \pi t B^2 f^\gamma / (\mu\Omega)^{1/2} \tag{32}$$

where f varies from f^2 at lower frequencies to $f^{3/2}$ at higher frequencies, t is the thickness, μ is the permeability and Ω the resistivity. Typical core loss results from Luborsky (1977b) are shown in fig. 44 for a variety of amorphous alloys at frequencies from 60 Hz to 50 kHz. All of the alloys have been stress relieved before measuring and are representative of the alloys with the M_r/M_s values listed in table 9. The considerable improvement in losses as the result of

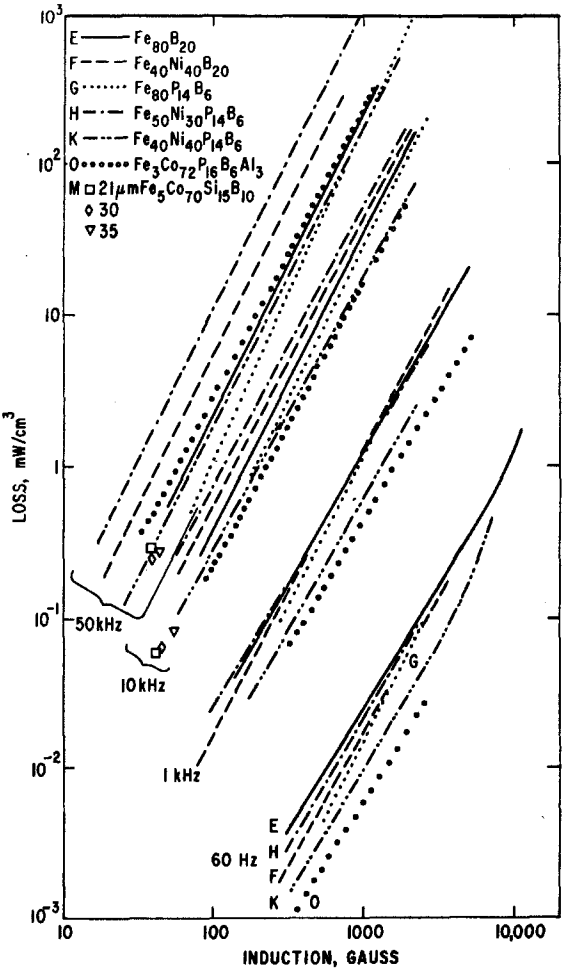

Fig. 44. Core loss vs. induction for amorphous alloys measured at various frequencies. All samples approximately 25–50μm thick. Luborsky (1977b).

annealing is shown in fig. 45 as a function of magnetostriction. The only data showing the thickness dependence of losses is for the FeCoSiB alloy shown. For thicknesses from 21 to 35μm, the change in loss is small. For comparison, we present results for conventional metallic soft magnetic materials in fig. 46, as obtained from commercial literature. Two thicknesses are shown: 25μm by the light lines and 50μm by the heavy lines. These thicknesses are in the range of thicknesses of the amorphous alloys measured. As an aid in comparing the results of the amorphous alloys to the conventional alloys, the losses of the amorphous alloys are shown at one point by their letter designations. All of these loss results for both the amorphous and crystalline alloys show the expected frequency and flux dependence given by

$$W \propto B^{\beta} f^{\gamma}. \tag{33}$$

The values of the exponents β and γ vary in a given alloy after stress relief, depending on the magnitude and direction of the induced anisotropy as described by Luborsky et al. (1976a). This is shown in fig. 47.

In many applications, the soft magnetic material is driven to saturation. The losses than increase faster than predicted by the straight line relations shown. Results from Luborsky (1977b) for two of the amorphous alloys are shown in fig. 48 tested using both sine H and sine B excitation. Results from the literature for two grades of crystalline oriented Fe-3.2% Si sheet steel are shown for comparison to the $Fe_{80}B_{20}$ amorphous alloy. The lower losses of the amorphous alloys are significant.

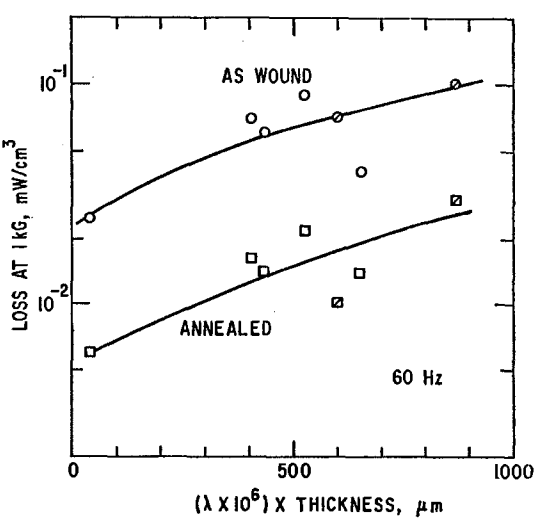

Fig. 45. Loss as a function of the product of magnetostriction and thickness for as-wound and annealed toroids. Luborsky (1977b). Material prepared by Luborsky, open symbols; material prepared by Allied Chemical Co., slashed symbols.

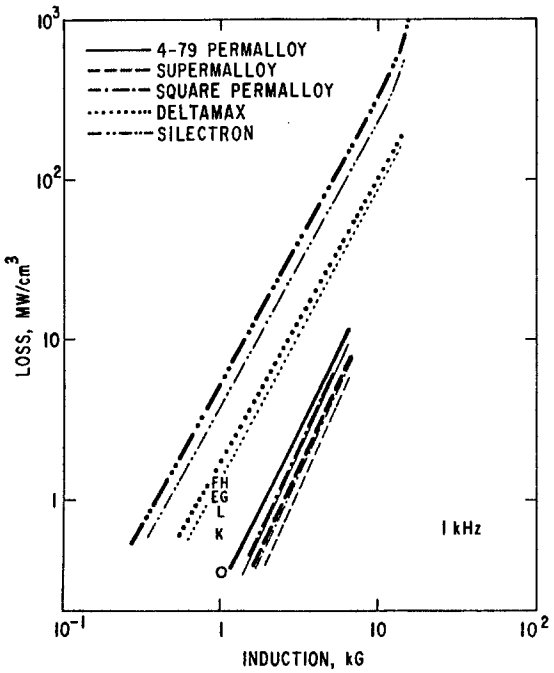

Fig. 46. Typical loss vs. induction characteristics at 1 kHz for conventional crystalline commercial alloys at 25μm (light lines) and 50μm (heavy lines). Loss of amorphous alloys shown here only at 1 kG for comparison. Luborsky (1976b).

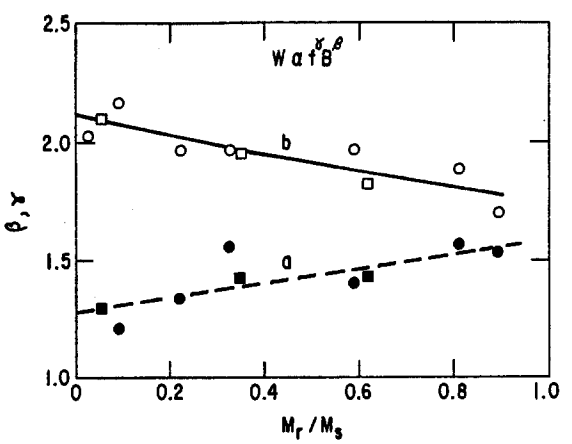

Fig. 47. Loss exponents for fully stress relieved amorphous $Fe_{40}Ni_{40}P_{14}B_6$ annealed in various fields to produce a variety of values of loop squareness. Two different samples shown. Luborsky et al. (1976a).

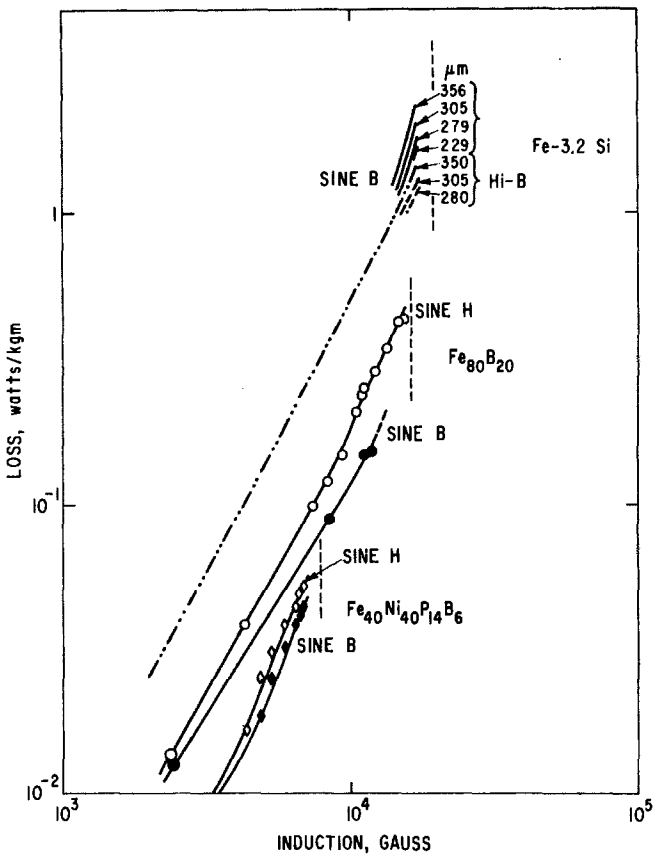

Fig. 48. Loss per kilogram vs. induction. Typical characteristics for Fe–3Si tapes at various frequencies and thicknesses. Conventional Fe-3Si sheet steel at 300μm is compared to the new "Hi B" sheet steel and the amorphous alloys all at 60 Hz. Luborsky (1977b).

11. Application as soft magnetic materials

Conventional soft magnetic materials are used in a wide variety of applications ranging from large power transformers and generators requiring many tons of SiFe to very small transformers and inductors in hybrid electronic circuits requiring only a few grams of one of the many available grades of FeNi, FeCo, or ferrites. The specific requirements of materials for these applications is also very varied. Thus in this section, we again will not present any details of specific device requirements for the materials. These may be found in detail from existing sources. Rather we will describe the amorphous material parameters which are generally significant to a variety of applications.

Possible applications of a material may be determined either by its static or dc properties, or by its dynamic or ac properties. In addition to the magnetic

properties required, the temperature coefficient of properties, the stability of properties and cost must be considered. The properties available in the amorphous alloys cover a wide range by changing alloy composition and heat treatment, as has been presented. Even for a given alloy, the properties are easily varied by changing the induced anisotropy, as also discussed. The wide range of dc and ac properties provide characteristics suitable for different types of applications. Samples with high M_r/M_s are particularly suited to devices such as switch cores, high-gain magnetic amplifiers, and low-frequency inverters, where the square loop characteristic is needed. Samples with intermediate M_r/M_s values, and thus minimum ac losses, are best applied in high-frequency inverters or transformers where minimum losses are important. This range is also useful in signal devices such as fluxmeters and ground fault detectors where the highest permeability is desired. Samples with M_r/M_s near zero are interesting for applications in which constant permeability is desired over a wide range of $4\pi M$ as in filter chokes or loading coils and some specialized transducers.

For application in small electronic devices, the amorphous alloys have somewhat poorer losses and permeabilities than the conventional Fe–Ni alloys but better than the Fe–Co and Fe–Si alloys. Where the design optimization requires the lower cost of the amorphous alloys, their higher induction compared to the Fe–Ni alloys or their lower losses compared to the Fe–Co, Fe–Si and the Fe–Ni at higher frequencies, all will favor the use of the amorphous alloys. For applications in large power equipment, the high moment $Fe_{80}B_{20}$, as thin tape, has about $\frac{1}{4}$ the sine B loss of the best quality grain oriented Fe–3.2% Si. However, because of the differences in thickness and the lower saturation flux of the Fe–B, it is not clear what the final cost/performance trade-off will be for the complete transformer.

The magnetic stability has to do with the change in the induced anisotropy, also discussed in an earlier section. This stability has been evaluated for $Fe_{40}Ni_{40}P_{14}B_6$ and $Fe_{40}Ni_{40}B_{20}$ amorphous alloys in a worst case situation from the reorientation kinetics. The worst case was taken as aging a toroid in a dc saturating circumferential field beginning from the low M_r/M_s state. Under these conditions, the lifetime is controlled by magnetic annealing, not by recrystallization. For the Fe–Ni–P–B alloy, at 140°C 10% reorientation of the magnetic anisotropy will take only 17 hours; extrapolated to 100°C, it will take ~ 1000 hours. Thus, application of the very low M_r/M_s state does not now appear reasonable for this alloy. However, improved stability is achieved by changing the alloy composition. For example, the time constants for magnetic reorientation of the Fe–Ni–B alloy are about 50 times larger (see fig. 39) and thus should pose no problem in most applications. Application of the high M_r/M_s state is quite reasonable since the domain orientation during most applications, as well as at rest, is the direction of the induced anisotropy.

The temperature coefficient of losses and permeability have been measured in a few amorphous alloys as reported by Luborsky (1977b). Because of the high Curie temperature, it is expected that the changes with measurement temperature will be small. Typical results, shown for a frequency of 1 kHz in fig. 49,

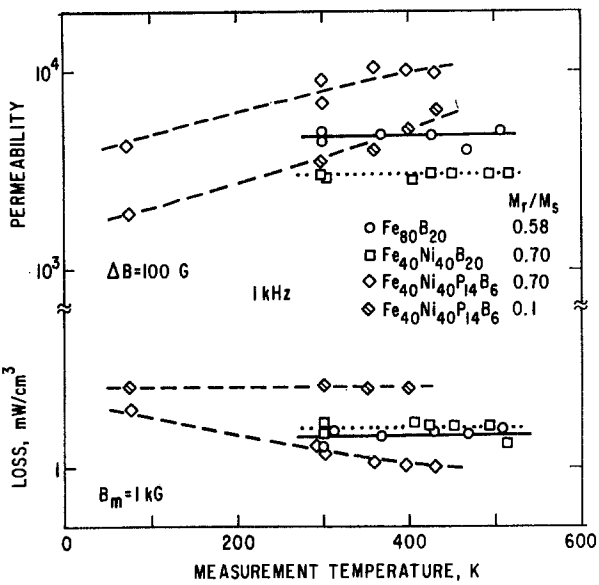

Fig. 49. Loss and permeability at 1 kHz of some amorphous alloys vs. measurement temperature. Luborsky (1977b).

confirm this. In general, these properties vary with temperature about the same as for the metallic crystalline soft alloys and are much less than for the soft ferrites.

It has been shown that at the onset of crystallization the coercivity of amorphous alloys, and thus their loss and permeability, change rapidly. As discussed in an earlier section in this chapter we have defined the irreversible end-of-life as the onset of crystallization. The available data from the literature and from our own work was summarized in fig. 13. The lifetimes at any temperature are, as expected, considerably shorter than for crystalline alloys where only recrystallization, oxidation or phase changes limit their life. The data define the maximum fabrication and operating time–temperature exposures. For example, we see that the $Fe_{80}B_{20}$ is the least stable of the alloys discussed as candidates for application. For this alloy, crystallization will start, if we assume a linear Arhennius extrapolation, at 175°C after 550 years or at 200°C after 25 years. This lifetime appears reasonable for all but the most severe application requirements.

References*

Alben, R., J.I. Budnick and G.S. Cargill III, 1977, in Metallic glasses (eds. H.S. Leamy and J.J. Gilman) (American Society for Metals, Metals Park, Ohio) ch. 12.

Allied Chemical Co., 1975a, Metglas® #2615. Data sheet 12–13–75.

*Bibliography search completed January 1977.

Allied Chemical Co., 1975b, Metglas® #2605A. Data sheet 12-23-75.
Allied Chemical Co., 1976a, Metglas® #2826. Data sheet 3-15-76.
Allied Chemical Co., 1976b, Metglas® #2605. Data sheet 2-18-76.
Amamou, A., 1976 IEEE Trans. Magnetics **MAG-12**, 948.
Anantharaman, T.R. and C. Suryanarayana, 1971, J. Materials Sci. **6**, 1111.
Arai, K., N. Tsuya, M. Yamada, H. Shirae, H. Fujimori, H. Saito and T. Masumoto, 1976, in Rapidly quenched metals, section 1 (eds. N.J. Grant and B.C. Giessen) (MIT Press, Cambridge, Mass.) p. 489.
Axe, J.D., L. Passel and C.C. Tsuei, 1975, AIP Conf. Proc. **24**, 119.
Babić, E., E. Girt, R. Krsnik and B. Leontić, 1970, J. Phys. E: Scientific Instruments **3**, 1015.
Bagley, B.G. and D. Turnbull, 1970, Acta Met. **18**, 857.
Becker, J.J., 1975, IEEE Trans. Magnetics **MAG-11**, 1326.
Becker, J.J., 1976, AIP Conf. Proc. **29**, 204.
Becker, J.J., F.E. Luborsky and J.L. Walter, 1977, IEEE Trans. Magnetics **MAG-13**, 988.
Bennett, C.H., D.E. Polk and D. Turnbull, 1971, Acta Met. **19**, 1295.
Berry, B.S. and W.C. Pritchet, 1975, Phys. Rev. Lett. **34**, 1022.
Berry, B.S. and W.C. Pritchet, 1976, AIP Conf. Proc. **34**, 292.
Brenner, A., 1963, Electrodeposition of alloys (Academic Press, New York).
Brenner, A., D.E. Couch and E.K. Williams, 1950, J. Res. Nat. Bureau Standards **44**, 109.
Brooks, H.A., 1976, J. Appl. Phys. **47**, 344.
Cahn, R.W., K.D. Krishnanand, M. Laridjani, M. Greenholtz and R. Hill, 1976, Materials Sci. Eng. **23**, 83.
Cargill III, G.S., 1970, J. Appl. Phys. **41**, 2248.
Cargill III, G.S., 1975a, Solid State Physics **30**, 227.
Cargill III, G.S., 1975b, AIP Conf. Proc. **24**, 138.
Cargill III, G.S., 1976, in Rapidly quenched metals, section 1 (eds. N.J. Grant and B.C. Giessen) (MIT Press, Cambridge, Mass.) p. 293.
Cargill III, G.S. and R.W. Cochrane, 1974, J. Phys. **35**, C4-269.
Chaudhari, P. and J.F. Graczyk, 1974, Bull. Amer. Phys. Soc. [2] **19**, 317.
Chaudhari, P., J.F. Graczyk and S.R. Herd, 1972, Phys. Stat. Sol. (b) **51**, 801.
Chen, H.S., 1973, Phys. Stat. Sol. (a) **17**, 561.
Chen, H.S., 1974, Acta Met. **22**, 1505.
Chen, H.S., 1975, Scripta Met. **9**, 411.
Chen, H.S., 1976, Appl. Phys. Lett. **29**, 12.
Chen, H.S. and E. Coleman, 1976, Appl. Phys. Lett. **28**, 245.
Chen, H.S. and C.E. Miller, 1970, Rev. Sci. Instrum. **41**, 1237.
Chen, H.S. and B.K. Park, 1973, Acta Met. **21**, 395.
Chen, H.S., J.T. Krause and E.A. Sigety, 1973, J. Non-Cryst. Solids **13**, 321.
Chen, H.S., S.D. Ferris, E.M. Gyorgy, H.J. Leamy and R.C. Sherwood, 1975, Appl. Phys. Lett. **26**, 405.
Chen, H.S., R.C. Sherwood, H.J. Leamy and E.M. Gyorgy, 1976, IEEE Trans. Magnetics **MAG-12**, 933.
Chi, M.C. and R. Alben, 1976, AIP Conf. Proc. **34**, 316.
Chi, G.C. and G.S. Cargill III, 1976, Materials Sci. Eng. **23**, 155.
Chien, C.L. and R. Hasegawa, 1976a, AIP Conf. Proc. **29**, 214.
Chien, C.L. and R. Hasegawa, 1976b, AIP Conf. Proc. **31**, 366.
Chien, C.L. and R. Hasegawa, 1977, in Amorphous Magnetism II (eds. R.A. Levy and R. Hasegawa) (Plenum Press, New York) p. 289.
Chikazumi, S., 1974, Physics of magnetism (Wiley, New York) p. 288.
Chopra, K.L., 1969, Thin film phenomena (McGraw-Hill, New York).
Clements, W.G. and B. Cantor, 1976, in Rapidly quenched metals, section 1 (eds. N.J. Grant and B.C. Giessen) (MIT Press, Cambridge, Mass.) p. 267.
Cochrane, R.W., R. Harris, J.O. Ström-Olson and M.J. Zuckermann, 1975, Phys. Rev. Lett. **35**, 676.
Cohen, M.H. and D. Turnbull, 1961, Nature **189**, 131.
Cohen, M.H. and D. Turnbull, 1964, Nature **203**, 964.
Coleman, E., 1976, Materials Sci. Eng. **23**, 161.
Crewdson, R.C., 1966, Ph.D. thesis, California Institute of Technology, Pasadena, Cal.
Davies, H.A., 1976, Phys. Chem. Glasses **17**, 159.
Davies, H.A., J. Aucote and J.B. Hull, 1974, Scripta Met. **8**, 1179.

Davis, L.A., 1976, in Rapidly quenched metals, section 1 (eds. N.J. Grant and B.C. Giessen) (MIT Press, Cambridge, Mass.) p. 369.
Durand, J., 1976, IEEE Trans. Magnetics **MAG-12**, 945.
Durand, J., 1977, in Amorphous magnetism II (eds. R.A. Levy and R. Hasegawa) (Plenum Press, New York) p. 305.
Durand, J. and M. Yung, 1977, in Amorphous magnetism II (eds. R.A. Levy and R. Hasegawa) (Plenum Press, New York) p. 275.
Duwez, P., 1966, in Progress in solid state chemistry, vol. 3 (ed. H. Reiss) (Pergamon Press, Oxford) pp. 377–406.
Duwez, P., 1967, Trans. Amer. Soc. Metals **60**, 607.
Duwez, P. and S.C.H. Lin, 1967, J. Appl. Phys. **38**, 4096.
Duwez, P. and R. Willens, 1963, Trans. Met. Soc. AIME **227**, 362.
Duwez, P., R.H. Willens and W. Klement, Jr., 1960, J. Appl. Phys. **31**, 1136.
Egami, T. and P.J. Flanders, 1976, AIP Conf. Proc. **29**, 220.
Egami, T., P.J. Flanders and C.D. Graham, Jr., 1975a, AIP Conf. Proc. **24**, 697.
Egami, T., P.J. Flanders and C.D. Graham, Jr., 1975b, Appl. Phys. Lett. **26**, 128.
Felsch, W., 1970, Z. Angew. Phys. **29**, 218.
Flanders, P.J. and F.E. Luborsky, unpublished.
Flanders, P.J., C.D. Graham, Jr. and T. Egami, 1975, IEEE Trans. Magnetics **MAG-11**, 1323.
Foo, E-Ni, and D. Wu, 1972, Phys. Rev. **B5**, 98.
Fruchart, E., A.M. Triquet and R. Fruchart, 1964, Ann. Chim. (Paris) **9**, 323.
Fujimori, H., T. Masumoto, Y. Obi, M. Kikuchi, 1974, Japan. J. Appl. Phys. **13**, 1889.
Fujimori, H., K.I. Arai, H. Shirae, H. Saito, T. Masumoto and N. Tsuya, 1976a, Japan. J. Appl. Phys. **15**, 705.
Fujimori, H., M. Kikuchi, Y. Obi, and T. Masumoto, 1976b, Sci. Repts. Res. Insts. Tohoku Univ. **A26**, 36.
Fujimori, H., Y. Obi, T. Masumoto and H. Saito, 1976c, Materials Sci. Eng. **23**, 281.
Fujimori, H., H. Morita, Y. Obi and S. Ohta, 1977, in Amorphous magnetism II (eds. R.A. Levy and R. Hasegawa) (Plenum Press, New York) p. 393.
Giessen, B.C., 1969, in Developments in the structural chemistry of alloy phases (ed. B.C. Giessen) (Plenum, New York) pp. 227–281.
Giessen, B.C. and C.N.J. Wagner, 1972, in Liquid metals (ed. S.Z. Beer) (Dekker, New York) p. 633.
Giessen, B.C. and R.H. Willens, 1970, in The use of phase diagrams in ceramic, glass and metal technology, vol. 3 (ed. A.M. Alper) (Academic Press, New York) pp. 103–141.
Gubanov, A.I., 1960, Fiz. Tver. Tel. **2**, 502.
Gubernatis, J.E. and P.L. Taylor, 1973, Phys. Lett. **A43**, 211.
Gyorgy, E.M., 1975, in Treatise on solid state chemistry, vol. 2 (ed. N.B. Hannay) (Plenum Press, New York).
Gyorgy, E.M., H.J. Leamy, R.C. Sherwood and H.S. Chen, 1976, AIP Conf. Proc. **29**, 198.
Handrich, K., 1969, Phys. Stat. Sol. **32**, K55.
Handrich, K., 1972, Phys. Stat. Sol. (b) **53**, K17.
Harris, R., M. Plischke and M.J. Zuckerman, 1973, Phys. Rev. Lett. **31**, 160.
Harris, R., M. Plischke and M.J. Zuckerman, 1974, J. Phys. (Paris) **35**, C4–265.
Hasegawa, R., 1970, Solid State Phys. **5**, 63 (in Japanese).
Hasegawa, R., 1976, AIP Conf. Proc. **29**, 216.
Hasegawa, R. and J.A. Dermon, 1973, Phys. Lett. **42A**, 407.
Hasegawa, R. and R.C. O'Handley, 1976, in Rapidly quenched metals, section 1 (eds. N.J. Grant and B.C. Giessen) (MIT Press, Cambridge, Mass.) p. 459.
Hasegawa, R., R.C. O'Handley, L. Tanner, R. Ray and S. Kavesh, 1976a, Appl. Phys. Lett. **29**, 219.
Hasegawa, R., R.C. O'Handley and L.I. Mendelsohn, 1976b, AIP Conf. Proc. **34**, 298.
Herd, S.R. and P. Chaudhari, 1974, Phys. Stat. Sol. (a) **26**, 627.
Jones, H., 1973, Rep. Prog. Phys. **36**, 1425.
Jones, H. and C. Suryanarayana, 1973, J. Materials Sci. **8**, 705.
Kanabe, T. and K. Kanematsu, 1968, J. Phys. Soc. Japan **24**, 1396.
Kaneyoshi, T., 1973, J. Phys. C **6**, L19.
Kavesh, S., 1974, US Patent 3 845 805 Nov. 5.
Kavesh, S., 1977, in Metallic glasses (eds. H.S. Leamy and J.J. Gilman) (American Society for Metals, Metals Park, Ohio 1977) to appear.
Kazama, N., M. Kameda and T. Masumoto, 1976, AIP Conf. Proc. **34**, 307.

Kikuchi, M., H. Fujimori, Y. Obi and T. Masumoto, 1975, Japan. J. Appl. Phys. **14**, 1077.

Kobe, S., 1977, in Amorphous Magnetism II (eds. R.A. Levy and R. Hasegawa) (Plenum Press, New York) pp. 529–534.

Kouvel, J.S., 1969, in Magnetism and metallurgy (eds. A.E. Berkowitz and E. Kneller) (Academic Press, New York) pp. 523–575.

Kumar, R. and A.N. Sinha, 1968, Trans. Ind. Inst. Metals **21**, (1) 9.

Liebermann, H.H. and C.D. Graham, Jr., 1976, IEEE Trans. Magnetics **MAG-12**, 921.

Lin, S.C.H. and P. Duwez, 1969, Phys. Stat. Sol. **34**, 469.

Logan, J., 1975, Phys. Stat. Sol. (a) **32**, 361.

Logan, J. and E. Sun, 1976, J. Non-Cryst. Solids **20**, 285.

Luborsky, F.E., 1976, AIP Conf. Proc. **29**, 209.

Luborsky, F.E., 1977a, Materials Sci. Eng. **28**, 139.

Luborsky, F.E., 1977b, in Amorphous magnetism II (eds. R.A. Levy and R. Hasegawa) (Plenum Press, New York) pp. 345–368.

Luborsky, F.E., unpublished.

Luborsky, F.E. and J.L. Walter, 1976, J. Appl. Phys. **47**, 3648.

Luborsky, F.E. and J.L Walter, 1977a, IEEE Trans. Magnetics **MAG-13**, 953.

Luborsky, F.E. and J.L. Walter, 1977b, Materials Sci. Eng. **28**, 77.

Luborsky, F.E., J.J. Becker and R.O. McCary, 1975, IEEE Trans. Magnetics **MAG-11**, 1644.

Luborsky, F.E., R.O. McCary and J.J. Becker, 1976a, in Rapidly quenched metals, section 1 (eds. N.J. Grant and B.C. Gressen) (MIT Press, Cambridge, Mass.) p. 467.

Luborsky, F.E., J.L. Walter and D.G. LeGrand, 1976b, IEEE Trans. Magnetics **MAG-12**, 930.

Lynn, J.W., G. Shirane, R.J. Birgeneau and H.S. Chen, 1976, AIP Conf. Proc. **34**, 313.

Mader, S., 1965, J. Vac. Soc. Technol. **2**, 35.

Mader, S. and A.S. Nowick, 1965, Appl. Phys. Lett. **7**, 57.

Maringer, R.E. and C.E. Mobley, 1974, J. Vac. Sci. Technol. **11**, 1067.

Maringer, R.E., C.E. Mobley and E.W. Collings, 1976, in Rapidly quenched metals, section 1 (eds. N.J. Grant and B.C. Giessen) (MIT Press, Cambridge, Mass.) p. 29.

Marzwell, N.I., 1973, Ph.D. thesis, California Institute of Technology, Pasadena, Cal.

Massenet, O., H. Daver and J. Geneste, 1974, J. de Physique **35**, C4–279.

Masumoto, T. and R. Maddin, 1975, Materials Sci. Eng. **19**, 1.

Masumoto, T., Y. Waseda, H. Kimura and A. Inoe, 1976, Sci. Repts. Res. Insts. Tohoku University **A26**, 21.

Masumoto, T., K. Watanabe, M. Mitera and S. Ohnuma, 1977, in Amorphous magnetism II (eds. R.A. Levy and R. Hasegawa) (Plenum Press, New York) p. 369.

Mendelsohn, L.I., E.A. Nesbitt and G.R. Bretts, 1976, IEEE Trans. Magnetics **MAG-12**, 924.

Miroshnichenko, I.S. and I.V. Salli, 1959, Ind. Lab. **25**, 1463 (in English) Fran Zavodskaya Lab. **25**, 1398 (1959).

Mizoguchi, T., 1976, AIP Conf. Proc. **34**, 286.

Mizoguchi, T., K. Yamauchi and H. Miyajima, 1973, in Amorphous magnetism (eds. H.O. Hooper and A.M. DeGraff) (Plenum, New York) p. 325.

Mizoguchi, T., K. Yamauchi and H. Miyajima, 1974, Proc. Int. Conf. Magnetism, vol. 2 (Moscow Aug. 1973) (Nauka, Moscow).

Montgomery, C.G., J.I. Krugler and R.M. Stubbs, 1970, Phys. Rev. Lett. **25**, 669.

Mook, H.A., D. Pan, J.D. Axe and L. Passell, 1975, AIP Conf. Proc. **24**, 112.

Moss, M., D.L. Smith and R.A. Lefever, 1964, Appl. Phys. Lett. **5**, 120.

Nagel, S.R. and J. Tauc, 1975, Phys. Rev. Lett. **35**, 380.

Nagel, S.R. and J. Tauc, 1977, Proc. Conf. Liquid Metals, Bristol, (eds. D.A. Greenwood and J. Tauc) Inst. Phys. Conf. Series **30**, 283.

Naka, M., S. Tomizawa, T. Watanabe and T. Masumoto, 1976, in Rapidly quenched metals, section 1 (eds. N.J. Grant and B.C. Giessen) (MIT Press, Cambridge, Mass.) p. 273.

Obi, Y., H. Fujimori and H. Saito, 1976, Jap. J. Appl. Phys. **15**, 611.

O'Handley, R.C., 1975, J. Appl. Phys. **46**, 4996.

O'Handley, R.C., 1976, AIP Conf. Proc. **29**, 206.

O'Handley, R.C., 1977, in Amorphous magnetism II (eds. R.A. Levy and R. Hasegawa) (Plenum Press, New York) p. 379.

O'Handley, R.C., R. Hasegawa, R. Ray and C.-P. Chou, 1976a, Appl. Phys. Lett. **29**, 330.

O'Handley, R.C., L.I. Mendelsohn and E.A. Nesbitt, 1976b, IEEE Trans. Magnetics **MAG-12**, 942.

O'Handley, R.C., L.I. Mendelsohn, R. Hase-

gawa, R. Ray, and S. Kavesh, 1976c, J. Appl. Phys. **47**, 4660.
Pan, D. and D. Turnbull, 1974, J. Appl. Phys. **45**, 1406.
Parsons, D., W. Sucksmith and J.E. Thompson, 1958, Phil. Mag **3**, 1174.
Pietrokowsky, P., 1963, Rev. Sci. Instr. **34**, 445.
Polk, D.E., 1972, Acta Met. **20**, 485.
Pond, R., Jr. and R. Maddin, 1969, Trans. Met. Soc. AIME **245**, 2475.
Pond, R.B., R.E. Maringer and C.E. Mobley, 1974, ASM Fall Precongress Seminar.
Revcolevschi, A. and N.J. Grant, 1972, Met. Trans. **3**, 1545.
Richter, J., K. Handrich and J. Schreiber, 1975, Phys. Stat. Sol. (b) **68**, K61.
Roberge, R. and H. Herman, 1968, Materials Sci. Eng. **3**, 62.
Scott, M.G. and R. Maddin, 1976, in Rapidly quenched metals, section 1 (eds. N.J. Grant and B.C. Giessen) (MIT Press, Cambridge, Mass.) p. 249.
Sherwood, R.C., E.M. Gyorgy, H.S. Chen, S.D. Ferris, G. Norman and H.J. Leamy, 1975, AIP Conf. Proc. **24**, 745.
Sherwood, R.C., E.M. Gyorgy, H.J. Leamy and H.S. Chen, 1976, AIP Conf. Proc. **34**, 325.
Shilling, J.W., 1976, AIP Conf. Proc. **29**, 222.
Shimada, Y. and H. Kojima, 1976, J. Appl. Phys. **47**, 4156.
Shingu, P.H., K. Shimomura, K. Kobayashi and R. Ozaki, 1976, Materials Sci. Eng. **23**, 183.
Simpson, A.W. and D.R. Brambley, 1971, Phys. Stat. Sol. (b) **43**, 291.
Simpson, A.W. and D.R. Brambley, 1972, Phys. Stat. Sol. (b) **49**, 685.
Simpson, A.W. and W.G. Clements, 1975, IEEE Trans. Magnetics **MAG-11**, 1338.
Slonczewski, J.C., 1963, in Magnetism, vol. I (eds. G. Rado and H. Suhl) (Academic Press, New York) ch. 5.
Spaepen, F. and D. Turnbull, 1976, in Rapidly quenched metals, section 1 (eds. N.J. Grant and B.C. Giessen) (MIT Press, Cambridge, Mass.) p. 205.
Swift, W.M. and K. Foster, 1976, Materials Sci. Eng. **23**, 267.
Tahir-Kheli, R.A., 1973, in Amorphous magnetism (eds. H.O. Hooper and A.M. deGraff) (Plenum, New York) p. 393.
Takayama, S., 1976, J. Materials Sci. **11**, 164.
Teoh, N., W. Teoh and S. Arajs, 1977, in Amorphous magnetism II (eds. R.A. Levy and R. Hasegawa) (Plenum, New York) p. 327.
Tsuei, C.C., 1976, in Rapidly quenched metals, section 1 (eds. N.J. Grant and B.C. Giessen) (MIT Press, Cambridge, Mass.) p. 441.
Tsuei, C.C. and P. Duwez, 1966, J. Appl. Phys. **37**, 435.
Tsuei, C.C. and H. Lilienthal, 1976, Phys. Rev. **B13**, 4899.
Tsuei, C.C., G. Longworth and S.C.H. Lin, 1968, Phys. Rev. **170**, 603.
Tsuya, N., K.I. Arai, Y. Shiraga, M. Yamada and T. Masumoto, 1975, Phys. Stat. Sol. (a) **31**, 557.
Turnbull, D., 1969, Contemp. Phys. **10**, 473.
Turnbull, D., 1974, J. de Physique **35**, C4–1.
Walter, J.L., P. Rao, E.F. Koch and S.F. Bartram, 1977, Met. Trans. 8A, 1141.
Walter, J.L., F. Bacon and F. Luborsky, 1976, Materials Sci. Eng. **24**, 239.
Walter, J.L., D.G. LeGrand and F.E. Luborsky, 1977, Materials Sci. Eng. **29**, 161.
Waseda, Y. and R. Masumoto, 1975, Z. Phys. **B22**, 121.
Wiesner, H. and J. Schneider, 1974, Phys. Stat. Sol. (a) **26**, 71.
Wright, J.G., 1976, IEEE Trans. Magnetics **MAG-12**, 95.
Yamada, H. and E.P. Wohlfarth, 1975, Phys. Lett. **51A**, 65.
Yamauchi, K., 1975, Ph.D. thesis, Gakishuin University.
Yamauchi, K. and T. Mizoguchi, 1975, J. Phys. Soc. Japan **39**, 541.

chapter 7

MAGNETOSTRICTIVE RARE EARTH–Fe_2 COMPOUNDS

A.E. CLARK

Naval Surface Weapons Center
White Oak Laboratory
Silver Spring, MD 20910
USA

Ferromagnetic Materials, Vol. 1
Edited by E.P. Wohlfarth

CONTENTS

1. Introduction

By the early 1960's, it was widely recognized that the rare earths possessed many extraordinary magnetic properties. Neutron diffraction measurements, for example, showed that the spin structures were much more complex than those of any of the classical ferromagnets or antiferromagnets. More importantly, in the heavy rare earth metals, the parallel coupling of large orbital and large spin angular momenta yielded huge magnetic moments of $9\mu_B$ and $10\mu_B$, dwarfing the conventional values of 0.6 for Ni and 2.2 for Fe. Enormous magnetic anisotropies were also encountered in the heavy rare earth elements. In 1963, a breakthrough in magnetostrictive materials occurred with the measurement of the basal plane magnetostrictions of Tb and Dy at low temperatures (Legvold et al. 1963, Clark et al. 1963, 1965, Rhyne and Legvold 1965). These basal plane strains are 100 to 10000 times typical magnetostrictions and still remain today the largest known ($\sim 1\%$). Over wide temperature ranges, thermal expansions are dominated by the temperature dependences of the magnetostrains. Elastic moduli were found to be strongly influenced by the unprecedented magnetoelastic interactions. However, because of the low ordering temperatures of the rare earths the application of these magnetostrictive properties to devices operating at room temperature could not be achieved with the elements. Only Gd, which is essentially non-magnetostrictive, possesses a Curie point as high as room temperature.

In 1971 a search for magnetostrictive materials with high magnetostriction at room temperature was started. Highly magnetostrictive rare earths, Tb and Dy, were combined with the magnetic transition metals, Ni, Co and Fe, by direct compound synthesis and by rapid sputtering into amorphous alloys. The cobalt rich R_2Co_{17} compounds (R = rare earth) possess Curie temperatures as high as 1200 K, and exhibit moderate magnetostrictions at room temperature. The remaining Co compounds, which are richer in rare earths, plus all the Ni compounds, possess lower ordering temperatures and very low room temperature magnetostrictions. In contrast to the normal Curie temperature behavior of the Ni and Co compounds, the Curie temperatures of the rare earth–iron compounds *increase* with increasing rare earth concentration. The highest ordering temperatures are found for the Laves phase RFe_2 compounds. Both the high concentration of rare earth and the high Curie temperatures of

these compounds are responsible for huge room temperature magnetostrictions in $TbFe_2$ and in $SmFe_2$. Non-crystalline Tb_xFe_{1-x} ($x \cong \frac{1}{3}$) alloys also possess comparatively high Curie temperatures and large room temperature magnetostrictions.

Magnetic anisotropy plays an important role in magnetostrictive materials. First, it is important to recognize that there is no linear magnetostriction if the anisotropy is independent of the state of strain of the crystal. In effect, the crystal deforms spontaneously whenever to do so lowers the anisotropy energy. On the other hand, the existence of magnetic anisotropy itself may be a hindrance to the technical usefulness of a magnetostrictive material. Large fields may be required to attain the large magnetostriction. In fact, $TbFe_2$ possesses an anisotropy energy $>10^7$ ergs/cm^3 and an anisotropy field >100 kOe, about two orders of magnitude larger than that of conventional cubic metals.

In addition to the conventional static magnetoelastic property (i.e. magnetostriction), elastic phenomena, both static and dynamic can be dominated by magnetoelastic effects. Elastic constants in single crystal RFe_2 compounds are modified by as much as 60% by the strong magnetoelastic interaction. In polycrystal and amorphous alloys, the high symmetry of cubic and isotropic samples is clearly broken. In $Sm_{0.88}Dy_{0.12}Fe_2$, the degeneracy between shear waves is removed by the magnetoelastic coupling producing two shear modes whose moduli differ by 30%.

This chapter presents an overview of the magnetoelastic properties of the highly magnetostrictive rare earth–Fe_2 alloys. In section 2 a general treatment of magnetostriction is given for the cases of hexagonal and cubic symmetry, which is applicable to the rare earth elements and the rare earth–iron compounds. The expressions for the magnetostriction up to sixth order in the direction cosines of the magnetization are given in Appendix A. In section 3 the magnetostriction of binary rare earth–iron alloys is presented. The magnetostriction of single crystal and polycrystal RFe_2 compounds are compared to other magnetostrictive materials at room temperature. A possible source of a startling magnetostriction anisotropy ($\lambda_{111} \gg \lambda_{100}$) is discussed. Magnetization, sublattice magnetization and magnetic anisotropy measurements are presented in sections 4 and 5. Measurements on single crystals are compared to those on polycrystals. In section 6 the magnetostrictive properties of pseudobinary Tb-based and Sm-based RFe_2 alloys are examined. The effects of the strong magnetoelastic coupling on sound velocities and elastic moduli are reported in sections 7 and 8. Extraordinarily large ΔE effects and changes in sound velocity are observed in single crystals, polycrystals and amorphous rare earth–Fe_2 alloys. The role of intrinsic (intradomain) as well as extrinsic (domain wall induced) effects are discussed. Low signal linear transduction properties of certain highly magnetostrictive materials are given in section 8. Finally, in section 9, recent measurements of linear and volume magnetostriction on the amorphous form of the RFe_2 alloys are presented.

The objective of this chapter is to focus on the magnetostrictive RFe_2 alloys. For a broad review of the magnetic properties of the rare earth–transition metal alloys, the reader is referred to chapters 3 and 4 of this volume and references therein.

2. Phenomenology of magnetostriction

Akulov (1928) and Becker and Döring (1939) developed simple expressions to describe the magnetostriction of cubic crystals. A commonly accepted expression, utilizing five constants, has the form

$$\begin{aligned}\Delta l/l = {} & h_1(\alpha_x^2\beta_x^2 + \alpha_y^2\beta_y^2 + \alpha_z^2\beta_z^2 - \tfrac{1}{3}) \\ & + 2h_2(\alpha_x\alpha_y\beta_x\beta_y + \alpha_y\alpha_z\beta_y\beta_z + \alpha_z\alpha_x\beta_z\beta_x) \\ & + h_4(\alpha_x^4\beta_x^2 + \alpha_y^4\beta_y^2 + \alpha_z^4\beta_z^2 + \tfrac{2}{3}s - \tfrac{1}{3}) \\ & + 2h_5(\alpha_x\alpha_y\alpha_z^2\beta_x\beta_y + \alpha_y\alpha_z\alpha_x^2\beta_y\beta_z + \alpha_z\alpha_x\alpha_y^2\beta_z\beta_x) \\ & + h_3 s \qquad [\text{ or } h_3(s - \tfrac{1}{3}].\end{aligned} \tag{2.1}$$

Here α_i denote the direction cosines of the magnetization with respect to the crystal axes; β_i the direction cosines of the measurement direction with respect to the crystal axes, and $s = \alpha_x^2\alpha_y^2 + \alpha_y^2\alpha_z^2 + \alpha_z^2\alpha_x^2$.

Frequently the magnetostriction is empirically fitted by the two lowest order terms. Denoting by λ_{100} the change in length along [100] when the magnetization is also in that direction, and by λ_{111} the change in length along [111] when the magnetization is along [111], the magnetostrictive strain reduces to

$$\begin{aligned}\Delta l/l = {} & \tfrac{3}{2}\lambda_{100}(\alpha_x^2\beta_x^2 + \alpha_y^2\beta_y^2 + \alpha_z^2\beta_z^2 - \tfrac{1}{3}) \\ & + 3\lambda_{111}(\alpha_x\alpha_y\beta_x\beta_y + \alpha_y\alpha_z\beta_y\beta_z + \alpha_z\alpha_x\beta_z\beta_x).\end{aligned} \tag{2.2}$$

In the special case of an isotropic body (whether polycrystal or amorphous)

$$\Delta l/l = \tfrac{3}{2}\lambda_s(\cos^2\theta - \tfrac{1}{3}) \tag{2.3}$$

where θ denotes the angle between the magnetization and the measurement direction.

The linear magnetostriction described here originates because the magnetic anisotropy energy depends upon strain. The crystal therefore deforms to minimize the total energy. In the following, the general form of the magnetostriction for both cubic and hcp systems is derived. The cubic expressions are appropriate for many metals, including the RT_2 and R_6T_{23} rare earth (R) transition metal (T) compounds. The hexagonal expressions apply to RT_3, R_2T_{17} and to many of the rare earth elements.

The total energy must be invariant under the symmetry operations of the crystal lattice. It can conveniently be written

$$E = E_0 + E_a + E_{me} + E_{el}. \tag{2.4}$$

E_0 denotes the part of the magnetic energy which is independent of magnetization direction. E_a, the anisotropy energy, can be expressed in terms of polynomials of the direction cosines which transform according to the fully symmetric representation of the crystal, i.e. the cubic or hexagonal harmonics. These polynomials are listed in table 1 (Bell 1954). The polynomials which keep the crystal symmetry intact are identified by α. Letting $K^{\alpha,l}$ denote the anisotropy constants and $S^{\alpha,l}$, the symmetry polynomials

TABLE 1
Basis functions for cubic and hexagonal lattices (taken from Bell 1954)

Cubic		Hexagonal	
$S^{\alpha,0}$	$\alpha_x^2+\alpha_y^2+\alpha_z^2=1$	$S^{\alpha,0}$	$\alpha_x^2+\alpha_y^2+\alpha_z^2=1$
$S\gamma^{,2}$	$\frac{1}{2}(2\alpha_z^2-\alpha_x^2-\alpha_y^2)$	$S^{\alpha,2}$	$\alpha_z^2-\frac{1}{3}$
$S^{\gamma,2}$	$(\sqrt{3}/2)(\alpha_x^2-\alpha_y^2)$	$S\gamma^{,2}$	$\frac{1}{2}(\alpha_x^2-\alpha_y^2)$
$S_1^{\epsilon,2}$	$\alpha_y\alpha_z$	$S_2^{\gamma,2}$	$\alpha_x\alpha_y$
$S_2^{\epsilon,2}$	$\alpha_z\alpha_x$	$S_1^{\epsilon,2}$	$\alpha_z\alpha_x$
$S_3^{\epsilon,2}$	$\alpha_x\alpha_y$	$S_2^{\epsilon,2}$	$\alpha_z\alpha_y$
$S^{\alpha,4}$	$\alpha_x^4+\alpha_y^4+\alpha_z^4-\frac{3}{5}$	$S^{\alpha,4}$	$\alpha_z^4-\frac{6}{7}(\alpha_z^2-\frac{1}{3})-\frac{1}{5}$
$S\gamma^{,4}$	$2\alpha_z^4-\alpha_x^4-\alpha_y^4-\frac{6}{7}(2\alpha_z^2-\alpha_x^2-\alpha_y^2)$	$S\gamma^{,4}$	$\frac{1}{2}(\alpha_z^2(\alpha_x^2-\alpha_y^2)-\frac{1}{7}(\alpha_x^2-\alpha_y^2))$
$S\gamma^{,4}$	$\sqrt{3}((\alpha_x^4-\alpha_y^4)-\frac{6}{7}(\alpha_x^2-\alpha_y^2))$	$S\gamma^{,4}$	$\alpha_z^2\alpha_x\alpha_y-\frac{1}{7}\alpha_x\alpha_y$
$S_1^{\epsilon,4}$	$\alpha_z^2\alpha_x\alpha_y-\frac{1}{7}\alpha_x\alpha_y$	$S\gamma^{,4'}$	$\frac{1}{4}(\alpha_x^4-6\alpha_x^2\alpha_y^2+\alpha_y^4)$
$S_2^{\epsilon,4}$	$\alpha_x^2\alpha_y\alpha_z-\frac{1}{7}\alpha_x\alpha_y$	$S\gamma^{,4'}$	$(\alpha_y^2-\alpha_x^2)\alpha_x\alpha_y$
$S_3^{\epsilon,4}$	$\alpha_y^2\alpha_z\alpha_x-\frac{1}{7}\alpha_z\alpha_x$	$S_1^{\epsilon,4}$	$\alpha_z^3\alpha_x-\frac{3}{7}\alpha_z\alpha_x$
$S^{\alpha,6}$	$\alpha_x^2\alpha_y^2\alpha_z^2+\frac{1}{22}(\alpha_x^4+\alpha_y^4+\alpha_z^4-\frac{3}{5})-\frac{1}{105}$	$S_2^{\epsilon,4}$	$\alpha_z^3\alpha_y-\frac{3}{7}\alpha_z\alpha_y$
$S\gamma^{,6}$	$2\alpha_z^6-\alpha_x^6-\alpha_y^6-\frac{15}{11}(2\alpha_z^4-\alpha_x^4-\alpha_y^4$	$S^{\alpha,6}$	$\alpha_z^6-\frac{15}{11}(\alpha_z^4-\frac{6}{7}(\alpha_z^2-\frac{1}{3})-\frac{1}{5})-\frac{5}{7}(\alpha_z^2-\frac{1}{3})-\frac{1}{7})$
	$-\frac{6}{7}(2\alpha_z^2-\alpha_x^2-\alpha_y^2))-\frac{5}{7}(2\alpha_z^2-\alpha_x^2-\alpha_y^2)$	$S^{\alpha,6'}$	$\alpha_x^6-15\alpha_x^4\alpha_y^2+15\alpha_x^2\alpha_y^4-\alpha_y^6$
$S\gamma^{,6}$	$\sqrt{3}(\alpha_x^6-\alpha_y^6-\frac{15}{11}(\alpha_x^4-\alpha_y^4-\frac{6}{7}(\alpha_x^2-\alpha_y^2)))$	$S\gamma^{,6}$	$\frac{1}{2}(\alpha_z^4-\frac{6}{11}(\alpha_z^2-\frac{1}{7})-\frac{1}{21})(\alpha_x^2-\alpha_y^2)$
	$-\frac{5}{7}(\alpha_x^2-\alpha_y^2))$	$S\gamma^{,6}$	$(\alpha_z^4-\frac{6}{11}(\alpha_z^2-\frac{1}{7})-\frac{1}{21})\alpha_x\alpha_y$
$S_1^{\epsilon,6}$	$(\alpha_x^4-\frac{6}{11}(\alpha_x^2-\frac{1}{7})-\frac{1}{21})\alpha_y\alpha_z$	$S\gamma^{,6'}$	$\frac{1}{4}(\alpha_z^2-\frac{1}{11})(\alpha_x^4-6\alpha_x^2\alpha_y^2+\alpha_y^4)$
$S_2^{\epsilon,6}$	$(\alpha_y^2-\frac{6}{11}(\alpha_y^2-\frac{1}{7})-\frac{1}{21})\alpha_z\alpha_x$	$S\gamma^{,6'}$	$(\alpha_z^2-\frac{1}{11})(\alpha_y^2-\alpha_x^2)\alpha_x\alpha_y$
$S_3^{\epsilon,6}$	$(\alpha_z^2-\frac{6}{11}(\alpha_z^2-\frac{1}{7})-\frac{1}{21})\alpha_x\alpha_y$	$S_1^{\epsilon,6}$	$(\alpha_z^4-\frac{10}{11}(\alpha_z^2-\frac{3}{7})-\frac{5}{21})\alpha_z\alpha_x$
$S_1^{\epsilon,6'}$	$(\alpha_y^4+\alpha_z^4-\frac{10}{3}\alpha_y^2\alpha_z^2)\alpha_y\alpha_z$	$S_2^{\epsilon,6}$	$(\alpha_z^4-\frac{10}{11}(\alpha_z^2-\frac{3}{7})-\frac{5}{21})\alpha_z\alpha_y$
$S_2^{\epsilon,6'}$	$(\alpha_z^4+\alpha_x^4-\frac{10}{3}\alpha_z^2\alpha_x^2)\alpha_z\alpha_x$	$S_1^{\epsilon,6'}$	$(\alpha_x^4-10\alpha_x^2\alpha_y^2+5\alpha_y^4)\alpha_z\alpha_x$
$S_3^{\epsilon,6'}$	$(\alpha_x^4+\alpha_y^4-\frac{10}{3}\alpha_x^2\alpha_y^2)\alpha_x\alpha_y$	$S_2^{\epsilon,6'}$	$(5\alpha_x^4-10\alpha_y^2\alpha_x^2+\alpha_y^4)\alpha_z\alpha_y$

$$E_a=\sum_l K^{\alpha,l}S^{\alpha,l}.$$

To lowest degree in α_i

$$E_a|_{\text{cubic}}=K^{\alpha,4}(\alpha_x^4+\alpha_y^4+\alpha_z^4-\tfrac{3}{5}),\quad \text{or}$$
$$=K_1(\alpha_x^2\alpha_y^2+\alpha_y^2\alpha_z^2+\alpha_z^2\alpha_x^2)+\text{constant} \tag{2.5a}$$

and

$$E_a|_{\text{hex}}=K^{\alpha,2}(\alpha_z^2-\tfrac{1}{3}). \tag{2.5b}$$

The magnetoelastic energy, E_{me}, arises from the strain dependence of the anisotropy energy and for small strains takes the form: $E_{me}\sim\epsilon f(\alpha)$. This term, in order to possess the correct transformation properties of the crystal, must be a direct product of strain components and direction cosine polynomials which transform according to the *same* symmetry representation (Callen and Callen 1963). In the cubic system the symmetry strain components fall into the three irreducible representations given in table 2 and designated by α, γ, and ϵ. The subscript denotes the components of the same irreducible representation. In the hexagonal system, the strain components consist of two fully symmetric components, designated by α 1 and $\alpha 2$, and two 2-dimensional representations γ and ϵ.

Thus taking the direct product of the symmetry strains and the direction

TABLE 2
Symmetry strain components for cubic and hexagonal lattices

Cubic		Hexagonal	
ϵ^{α}	$\epsilon_{xx}+\epsilon_{yy}+\epsilon_{zz}$	$\epsilon^{\alpha 1}$	$\epsilon_{xx}+\epsilon_{yy}+\epsilon_{zz}$
ϵ_1^{γ}	$\frac{1}{2}(2\epsilon_{zz}-\epsilon_{xx}-\epsilon_{yy})$	$\epsilon^{\alpha 2}$	$\frac{1}{2}(2\epsilon_{zz}-\epsilon_{xx}-\epsilon_{yy})$
ϵ_2^{γ}	$(\sqrt{3}/2)(\epsilon_{xx}-\epsilon_{yy})$	ϵ_1^{γ}	$\epsilon_{xx}-\epsilon_{yy}$*
ϵ_1^{ϵ}	ϵ_{yz}	ϵ_2^{γ}	ϵ_{xy}
ϵ_2^{ϵ}	ϵ_{zx}	ϵ_1^{ϵ}	ϵ_{yz}
ϵ_3^{ϵ}	ϵ_{xy}	ϵ_2^{ϵ}	ϵ_{zx}

* In this table the strains are defined by $\Delta x = \epsilon_{xx}x+\frac{1}{2}\epsilon_{xy}y+\frac{1}{2}\epsilon_{xz}z$. Note: $\epsilon^{\gamma}=\frac{1}{2}(\epsilon_{xx}-\epsilon_{yy})$ if the strains were defined by $\Delta x = \epsilon_{xx}x+\epsilon_{xy}y+\epsilon_{zz}z$.

cosine polynomials, E_{me} becomes

$$E_{me}|_{cubic} = \sum_l [B^{\alpha,l}\epsilon^{\alpha}S^{\alpha,l} + B^{\gamma,l}\sum_i \epsilon_i^{\gamma}S_i^{\gamma,l} + B^{\epsilon,l}\sum_i \epsilon_i^{\epsilon}S_i^{\epsilon,l}] \tag{2.6a}$$

$$E_{me}|_{hex} = \sum_l [B^{\alpha 1,l}\epsilon^{\alpha 1}S^{\alpha,l} + B^{\alpha 2,l}\epsilon^{\alpha 2}S^{\alpha,l} + B^{\gamma,l}\sum_i \epsilon_i^{\gamma}S_i^{\gamma,l} + B^{\epsilon,l}\sum_i \epsilon_i^{\epsilon}S_i^{\epsilon,l}]. \tag{2.6b}$$

In terms of the conventional cartesian strains

$$\begin{aligned} E_{me}|_{cubic} = \sum_l \Big[& \left(B^{\alpha,l}S^{\alpha,l} + B^{\gamma,l}\left(-\frac{1}{2}S_1^{\gamma}+\frac{\sqrt{3}}{2}S_2^{\gamma}\right)\right)\epsilon_{xx} \\ & + \left(B^{\alpha,l}S^{\alpha,l} + B^{\gamma,l}\left(-\frac{1}{2}S_1^{\gamma}-\frac{\sqrt{3}}{2}S_2^{\gamma}\right)\right)\epsilon_{yy} \\ & + (B^{\alpha,l}S^{\alpha,l} + B^{\gamma,l}S_1^{\gamma})\epsilon_{zz} + B^{\epsilon,l}(S_1^{\epsilon,l}\epsilon_{yz} + S_2^{\epsilon,l}\epsilon_{zx} + S_3^{\epsilon,l}\epsilon_{xy})\Big] \end{aligned} \tag{2.7a}$$

$$\begin{aligned} E_{me}|_{hex} = \sum_l [& B^{\alpha 1,l}(\epsilon_{xx}+\epsilon_{yy}+\epsilon_{zz})S^{\alpha,l} + B^{\alpha 2,l}(2\epsilon_{zz}-\epsilon_{xx}-\epsilon_{yy})S^{\alpha,l} \\ & + B^{\gamma,l}((\epsilon_{xx}-\epsilon_{yy})S_1^{\gamma,l} + \epsilon_{xy}S_2^{\gamma,l}) + B^{\epsilon,l}(\epsilon_{zx}S_1^{\epsilon,l} + \epsilon_{yz}S_2^{\epsilon,l})]. \end{aligned} \tag{2.7b}$$

Or for $l = 0, 2$

$$\begin{aligned} E_{me}|_{cubic} = {} & b_0(\epsilon_{xx}+\epsilon_{yy}+\epsilon_{zz}) + b_1(\alpha_x^2\epsilon_{xx}+\alpha_y^2\epsilon_{yy}+\alpha_z^2\epsilon_{zz}) \\ & + b_2(\alpha_x\alpha_y\epsilon_{xy}+\alpha_y\alpha_z\epsilon_{yz}+\alpha_z\alpha_x\epsilon_{zx}) \end{aligned} \tag{2.8a}$$

$$\begin{aligned} E_{me}|_{hex} = {} & b_{11}(\epsilon_{xx}+\epsilon_{yy}) + b_{12}\epsilon_{zz} + b_{21}(\alpha_z^2-\tfrac{1}{3})(\epsilon_{xx}+\epsilon_{yy}) + b_{22}(\alpha_z-\tfrac{1}{3})\epsilon_{zz} \\ & + b_3(\tfrac{1}{2}(\alpha_x^2-\alpha_y^2)(\epsilon_{xx}-\epsilon_{yy}) + \alpha_x\alpha_y\epsilon_{xy}) + b_4(\alpha_z\alpha_x\epsilon_{zx}+\alpha_y\alpha_z\epsilon_{yz}). \end{aligned} \tag{2.8b}$$

The relationships between the conventional magnetoelastic constants (Kittel 1949) and the symmetry constants are given in table 3.

In a similar fashion, the elastic energy, E_{el}, takes the following form in terms

of symmetry strains

$$E_{el}|_{cubic} = \tfrac{1}{2}c^{\alpha}(\epsilon^{\alpha})^2 + \tfrac{1}{2}c^{\gamma}((\epsilon_1^{\gamma})^2 + (\epsilon_2^{\gamma})^2) + \tfrac{1}{2}c^{\epsilon}((\epsilon_1^{\epsilon})^2 + (\epsilon_2^{\epsilon})^2 + (\epsilon_3^{\epsilon})^2) \tag{2.9a}$$

$$E_{el}|_{hex} = \tfrac{1}{2}c_{11}^{\alpha}(\epsilon^{\alpha 1})^2 + c_{12}^{\alpha}(\epsilon^{\alpha 1})(\epsilon^{\alpha 2}) + \tfrac{1}{2}c_{22}^{\alpha}(\epsilon^{\alpha 2})^2 + \tfrac{1}{2}c^{\gamma}((\epsilon_1^{\gamma})^2 + (\epsilon_2^{\gamma})^2) + \tfrac{1}{2}c^{\epsilon}((\epsilon_1^{\epsilon})^2 + (\epsilon_2^{\epsilon})^2). \tag{2.9b}$$

Transforming to the cartesian strains

$$E_{el}|_{cubic} = \tfrac{1}{2}c_{11}(\epsilon_{xx}^2 + \epsilon_{yy}^2 + \epsilon_{zz}^2) + c_{12}(\epsilon_{yy}\epsilon_{zz} + \epsilon_{zz}\epsilon_{xx} + \epsilon_{xx}\epsilon_{yy}) + \tfrac{1}{2}c_{44}(\epsilon_{xy}^2 + \epsilon_{yz}^2 + \epsilon_{zx}^2) \tag{2.10a}$$

$$E_{el}|_{hex} = \tfrac{1}{2}c_{11}(\epsilon_{xx}^2 + \epsilon_{yy}^2) + c_{12}\epsilon_{xx}\epsilon_{yy} + \tfrac{1}{2}c_{33}\epsilon_{zz}^2 + c_{13}(\epsilon_{xx}\epsilon_{zz} + \epsilon_{yy}\epsilon_{zz}) + \tfrac{1}{2}c_{44}(\epsilon_{yz}^2 + \epsilon_{zx}^2) + \tfrac{1}{4}(c_{11} - c_{12})\epsilon_{xy}^2. \tag{2.10b}$$

The relationships between the symmetry constants and the conventional elastic constants are given in table 3.

The magnetostriction, $\Delta l/l$, is determined in the conventional way from the definition (Kittel 1949)

$$\Delta l/l = \sum_{i \geq j} \epsilon_{ij}^{eq}\beta_i\beta_j \tag{2.11}$$

where the ϵ_{ij}^{eq} are the equilibrium strains determined from

$$\delta E/\delta\epsilon_{ij} = 0. \tag{2.12}$$

For the cubic case

$$\epsilon_{ii}^{eq} = -b_1\alpha_i^2/(c_{11} - c_{12}) - b_0/(c_{11} + 2c_{12}) + c_{12}b_1/(c_{11} + 2c_{12})(c_{11} - c_{12})$$
$$\epsilon_{ij}^{eq} = -b_2\alpha_i\alpha_j/c_{44}. \tag{2.13a}$$

TABLE 3
Relation between symmetry and cartesian elastic constants and magnetoelastic constants

Cubic	Hexagonal
$c_{11} = c^{\alpha} + c^{\gamma}$	$c_{11} = c_{11}^{\alpha} - c_{12}^{\alpha} + \frac{1}{4}c_{22}^{\alpha} + c^{\gamma}$
$c_{12} = c^{\alpha} - \frac{1}{2}c^{\gamma}$	$c_{12} = c_{11}^{\alpha} - c_{12}^{\alpha} + \frac{1}{4}c_{22}^{\alpha} - c^{\gamma}$
$c_{44} = c^{\epsilon}$	$c_{33} = c_{11}^{\alpha} + 2c_{12}^{\alpha} + c_{22}^{\alpha}$
	$c_{13} = c_{11}^{\alpha} + \frac{1}{2}c_{12}^{\alpha} - \frac{1}{2}c_{22}^{\alpha}$
	$c_{44} = c^{\epsilon}$
$b_0 = B^{\alpha} - \frac{1}{2}B^{\gamma,2}$	$b_{11} = B^{\alpha 1,0} - B^{\alpha 2,0}$
$b_1 = \frac{3}{2}B^{\gamma}$	$b_{12} = B^{\alpha 1,0} + 2B^{\alpha 2,0}$
$b_2 = B^{\epsilon,2}$	$b_{21} = B^{\alpha 1,2} - B^{\alpha 2,2}$
	$b_{22} = B^{\alpha 2,2} + 2B^{\alpha 2,2}$
	$b_3 = B^{\gamma,2}$
	$b_4 = B^{\epsilon,2}$

For the hexagonal case

$$\epsilon_{xx}^{eq} = \frac{-b_{11}c_{33}+b_{12}c_{13}}{D} + \frac{(-b_{12}c_{33}+b_{22}c_{13})(\alpha_z^2-\frac{1}{3})}{D} - \frac{b_3(\alpha_x^2-\alpha_y^2)}{2(c_{11}-c_{12})}$$

$$\epsilon_{yy}^{eq} = \frac{-b_{11}c_{33}+b_{12}c_{13}}{D} + \frac{(-b_{12}c_{33}+b_{22}c_{13})(\alpha_z^2-\frac{1}{3})}{D} + \frac{b_3(\alpha_x^2-\alpha_y^2)}{2(c_{11}-c_{12})}$$

$$\epsilon_{zz}^{eq} = \frac{2c_{13}b_{11}-(c_{11}+c_{12})b_{12}}{D} + \frac{(2c_{13}b_{21}-(c_{11}+c_{12})b_{22})(\alpha_z^2-\frac{1}{3})}{D}$$

$$\epsilon_{xy}^{eq} = \frac{-b_3\alpha_x\alpha_y}{\frac{1}{2}(c_{11}-c_{12})} \qquad \epsilon_{yz}^{eq} = \frac{-b_4\alpha_y\alpha_z}{c_{44}} \qquad \epsilon_{zx}^{eq} = \frac{-b_4\alpha_z\alpha_x}{c_{44}} \tag{2.13b}$$

where $D = c_{33}(c_{11}+c_{12}) - 2c_{13}^2$.

Substituting these expressions into eq. (2.11), we find to second degree in α_i

$$\Delta l/l|_{\text{cubic}} = \lambda^{\alpha} + \tfrac{3}{2}\lambda_{100}(\alpha_x^2\beta_x^2 + \alpha_y^2\beta_y^2 + \alpha_z^2\beta_z^2 - \tfrac{1}{3}) + 3\lambda_{111}(\alpha_x\alpha_y\beta_x\beta_y + \alpha_y\alpha_z\beta_y\beta_z + \alpha_z\alpha_x\beta_z\beta_x) \tag{2.14a}$$

where

$$\lambda^{\alpha} = -3b_0/(c_{11}+c_{12}) + 3c_{12}b_1/(c_{11}+2c_{12})(c_{11}-c_{12})$$

$$\lambda_{100} = -2b_1/3(c_{11}-c_{12})$$

$$\lambda_{111} = -b_2/3c_{44}$$

and

$$\Delta l/l|_{\text{hex}} = \lambda^{\alpha 1,0}(\beta_x^2+\beta_y^2) + \lambda^{\alpha 2,0}\beta_z^2 + \lambda^{\alpha 1,2}(\alpha_z^2-\tfrac{1}{3})(\beta_x^2+\beta_y^2) + \lambda^{\alpha 2,2}(\alpha_z^2-\tfrac{1}{3})\beta_z^2 + \lambda^{\gamma,2}[\tfrac{1}{2}(\alpha_x^2-\alpha_y^2)(\beta_x^2-\beta_y^2) + 2\alpha_x\alpha_y\beta_x\beta_y] + 2\lambda^{\epsilon,2}[\alpha_y\alpha_z\beta_y\beta_z + \alpha_z\alpha_x\beta_z\beta_x] \tag{2.14b}$$

where

$$\lambda^{\alpha 1,0} = (b_{11}c_{33}+b_{12}c_{13})/D$$

$$\lambda^{\alpha 2,0} = (2b_{11}c_{13} - b_{12}(c_{11}+c_{12}))/D$$

$$\lambda^{\alpha 1,2} = (-b_{21}c_{33}+b_{22}c_{13})/D$$

$$\lambda^{\alpha 2,2} = (2b_{21}c_{13} - b_{22}(c_{11}+c_{12}))/D$$

$$\lambda^{\gamma,2} = -b_3/(c_{11}-c_{12})$$

$$\lambda^{\epsilon,2} = -b_4/2c_{44}.$$

The symmetry modes are depicted in fig. 1. Expressions for the magnetostriction up to α_i^6 are given in Appendix A.

When the crystals are free to strain under magnetization rotation (constant external stress), the presence of magnetoelasticity gives rise to a contribution to the anisotropy not included in E_a. (For a clamped lattice, there is no magnetostrictive contribution to the anisotropy.) For a cubic system, the magnetostriction affects the lowest order anisotropy expression. Substituting ϵ_{ii}^{eq} and

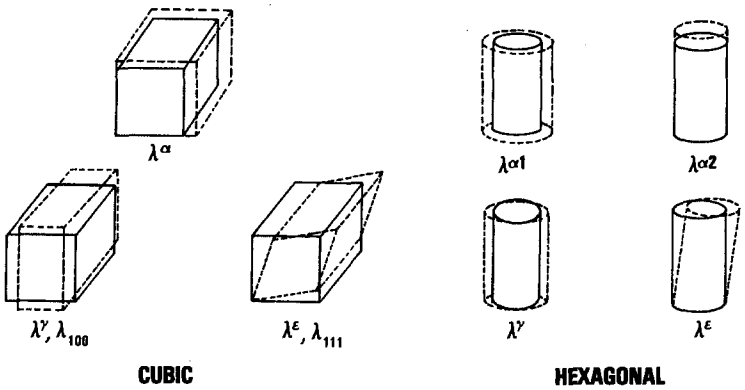

Fig. 1. Magnetostriction modes for cubic and hexagonal symmetries.

ϵ_{ij}^{eq} from eq. (2.13a) into eqs. (2.8a) and (2.10a), the total energy at constant stress (σ) becomes

$$E^{\sigma} = E_0 + K_1'(\alpha_x^2\alpha_y^2 + \alpha_y^2\alpha_z^2 + \alpha_z^2\alpha_x^2) \tag{2.15}$$

where

$$K_1' = K_1 + b_1^2/(c_{11} - c_{12}) - b_2^2/2c_{44}.$$

In the hexagonal system, the lowest order anisotropy constant is not affected by the magnetostriction.

3. Magnetostriction of binary rare earth–iron alloys

The heavy rare earth elements, Tb and Dy, display the largest known magnetostrictions (Rhyne and Legvold 1965, Clark et al. 1965). Below their ordering temperatures, the magnetically induced strains overwhelm the conventional thermal expansion of the crystal axes (fig. 2). These large magnetostrictions are a direct consequence of the huge strain dependence of the magnetic anisotropy. In the heavy rare earth metals, J is a good quantum number, and for Tb and Dy, the intrinsic magnetostrictions ($\lambda^{\gamma,2}$ (0 K)) are almost identical to each other, in agreement with Stevens' equivalent operator calculations (Tsuya et al. 1964). The magnetostriction and anisotropy of the rare earths, however, are huge *only* at cryogenic temperatures. All of the magnetostrictive rare earths possess ordering temperatures below room temperature. Because of this, only a small paramagnetic magnetostriction ($\lambda \propto H^2$) exists at room temperature, even for Tb and Dy.

To achieve highly magnetostrictive materials at room temperature, alloys of the type R_xT_{1-x}, where R = Sm, Tb, Dy, Ho, Er, Tm, and T = Ni, Co and Fe, were investigated. The addition of Ni, Co and Fe to the rare earths produces compounds and amorphous alloys which in some cases have higher Curie temperatures than the elements, and in others, much lower ones (see Taylor

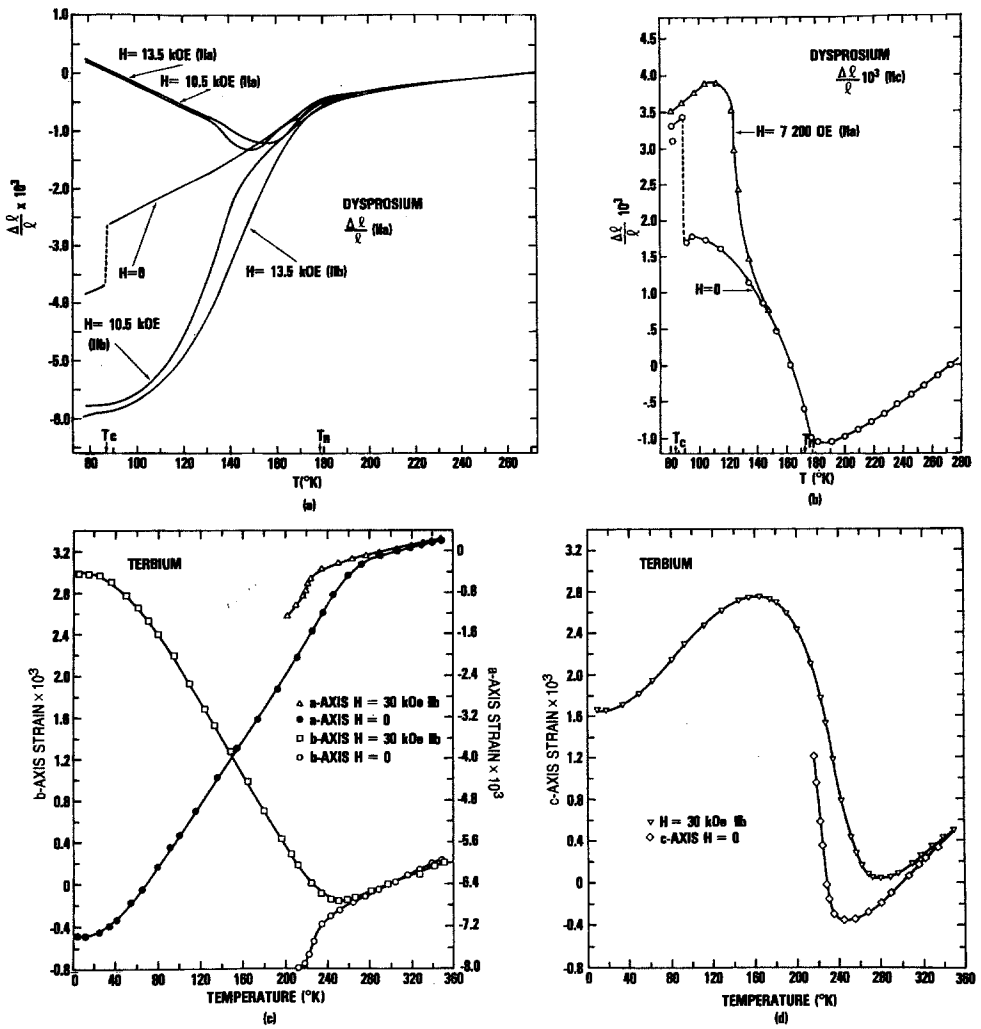

Fig. 2. Magnetostriction of dysprosium and terbium single crystals (Dy, taken from Clark et al. 1965; Tb, taken from Rhyne and Legvold 1965).

1971, Rhyne 1978). In fact, all the Ni compounds have Curie temperatures below 200 K. The Curie temperatures of the Co compounds span a wide range from the high T_C of 1200 K for Tb_2Co_{17} to near 0 K for Er_3Co. The R_xFe_{1-x} compounds have an anomalous Curie temperature dependence on composition x, in which the most Fe rich compound (R_2Fe_{17}) possesses the lowest T_C and the least iron rich (RFe_2) possesses the highest. Amorphous rare earth transition metal alloys produced both by rapid sputtering and evaporation techniques also possess a wide range of ordering temperatures, some of which are higher than their crystalline counterparts (most Co alloys) and some of which are lower (most Fe

alloys). In view of this, the R_xT_{1-x} alloys with the greatest potential to achieve large room temperature magnetostrictions are the cubic Laves phase RFe_2 compounds with R = Tb and Dy.

The first compound observed to exhibit a large magnetostriction ($\sim 2 \times 10^{-3}$) at room temperature was $TbFe_2$ (Clark and Belson 1972). This compound possesses the largest room temperature magnetostriction known to date. In table 4 are gathered the room temperature magnetostrictions of some typical ferro- and

TABLE 4
Magnetostriction of some polycrystalline materials at room temperature*

Material	$10^6\lambda_s$	Reference	Material	$10^6\lambda_s$	Reference
Ni	−33	a	$TbFe_2$	1753	h
Co	−62	b	$TbNi_{0.4}Fe_{1.6}$	1151	k
Fe	−9	c	$TbCo_{0.4}Fe_{1.6}$	1487	k
60% Co 40% Fe	68	d	$TbFe_2$(amorphous)	308	h
60% Ni 40% Fe	25	e	$DyFe_2$	433	h
$NiFe_2O_4$	−26	f	$DyFe_2$(amorphous)	38	k
$Co_2Fe_2O_4$	−110	f	$HoFe_2$	80	l
Fe_3O_4	40	f	$ErFe_2$	−299	h
$Y_3Fe_5O_{12}$	−2	g	$TmFe_2$	−123	h
Tb_2Ni_{17}	−4	h	$SmFe_3$	−211	m
YCo_3	0.4	h	$TbFe_3$	693	m
$TbCo_3$	65	h	$DyFe_3$	352	m
Y_2Co_{17}	80	i	$HoFe_3$	57	m
Pr_2Co_{17}	336	i	$ErFe_3$	−69	m
Tb_2Co_{17}	207	i	$TmFe_3$	−43	m
Dy_2Co_{17}	73	i	Ho_6Fe_{23}	58	m
Er_2Co_{17}	28	i	Er_6Fe_{23}	−36	m
$Tb_{0.04}(Co_{0.5}Fe_{0.5})$	95	j	Tm_6Fe_{23}	−25	m
85 Wt % Tb			Sm_2Fe_{17}	−63	m
15 Wt % Fe	539	h	Tb_2Fe_{17}(as cast)	131	m
70 Wt % Tb			Tb_2Fe_{17}	−14	m
30 Wt % Fe	1590	h	Dy_2Fe_{17}	−60	m
YFe_2	1.7	h	Ho_2Fe_{17}	−106	m
$SmFe_2$	−1560	h	Er_2Fe_{17}	−55	m
$GdFe_2$	39	m	Tm_2Fe_{17}	−29	m

* For the rare earth compounds, λ_s denotes $\frac{2}{3}(\lambda_\parallel - \lambda_\perp)$ at some large field (see references below).

[a] Went (1951).
[b] Yamamoto and Miyasawa (1965).
[c] Weil and Reichel (1954).
[d] S.R. Williams (1932).
[e] Masiyama (1931).
[f] See: Ferrites by Smit and Wijn (1959).
[g] Clark et al. (1963b).
[h] Clark (1974). Here λ_s denotes $\frac{2}{3}(\lambda_\parallel - \lambda_\perp)$ at 25 kOe.
[i] A.E. Miller, unpublished. Here λ_s denotes $\frac{2}{3}(\lambda_\parallel - \lambda_\perp)$ at 14 kOe.
[j] Sato et al. (1976).
[k] A.E. Clark and R. Abbundi, unpublished.
[l] Koon et al. (1974).
[m] Abbundi and Clark (1978). Also Naval Surface Weapons Center TR78-88, Dahlgren, V.A. λ_s denotes $\frac{2}{3}(\lambda_\parallel - \lambda_\perp)$ at 25 kOe.

ferrimagnets, some rare earth–cobalt compounds and some rare earth–iron compounds. While the RFe_2 compounds $TbFe_2$ and $SmFe_2$ possess the largest room temperature magnetostrictions, large magnetostrictions are also found in some RFe_3 and R_2Co_{17} compounds. Contrary to expectations, $DyFe_2$ possesses a much smaller magnetostriction than $TbFe_2$.

In figs. 3, 4, 5 and 6 the magnetostrictions of the rare earth–iron compounds are plotted vs. applied field. Here $\lambda_\parallel - \lambda_\perp$ denotes the fractional change in length as an applied field is rotated from perpendicular to parallel to the measurement direction. For isotropic polycrystals $\lambda_\parallel - \lambda_\perp = \frac{3}{2}\lambda_s$.

$TbFe_2$ and $SmFe_2$ possess the largest strains by far and are the basis of the multicomponent systems of sections 6, 7, and 8. For $SmFe_2$, $\lambda_\parallel - \lambda_\perp < -2000 \times 10^{-6}$; for $TbFe_2$, $\lambda_\parallel - \lambda_\perp > 2000 \times 10^{-6}$. In both of these compounds the rare earth ion is highly anisotropic (Sm – most prolate in form; Tb – most oblate in form) and the rare earth–iron exchange is large, which keeps the rare earth sublattice magnetization nearly intact at room temperature. Thus the large magnetostriction does not fall appreciably from its low temperature value. Unlike the elements, where the magnetostriction of Tb and Dy are similar, the magnetostriction of $DyFe_2$ is much smaller than that of $TbFe_2$ and exhibits a

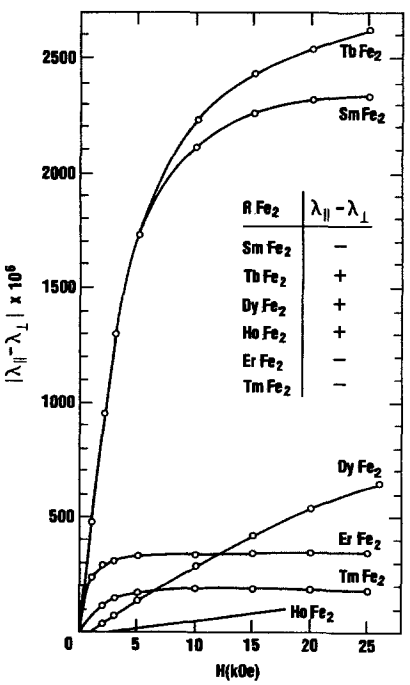

Fig. 3. Room temperature magnetostriction of rare earth–Fe_2 polycrystals ($SmFe_2$, $TbFe_2$, $DyFe_2$, $ErFe_2$ and $TmFe_2$ taken from Clark 1974; $HoFe_2$ taken from Koon et al. 1974).

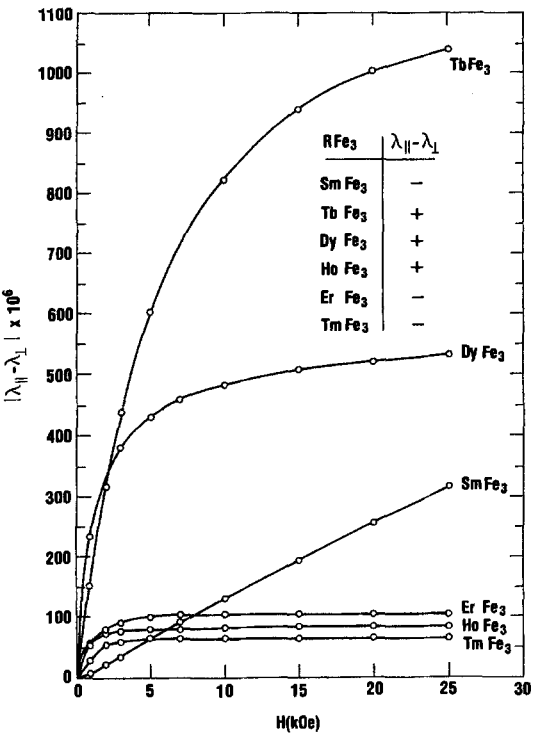

Fig. 4. Room temperature magnetostriction of rare earth-Fe_3 polycrystals (taken from Abbundi and Clark 1978).

slow increase with magnetic field (fig. 3). This is indicative of a very large magnetocrystalline anisotropy. As will be shown in section 5, the anisotropy is indeed large at room temperature. While the magnetostrictions of $DyFe_2$ and $HoFe_2$ are far from saturation at room temperature with laboratory fields, the magnetostrictions of the remaining RFe_2 compounds display rather well defined knees. In the compounds $SmFe_2$, $TbFe_2$, $ErFe_2$ and $TmFe_2$, the magnetization lies along the [111] whereas for the $DyFe_2$ and $HoFe_2$ compounds, it lies parallel to [100] (see section 4). Because of this, the absence of a large magnetostriction at low fields for $DyFe_2$ and $HoFe_2$ leads to the conjecture that $\lambda_{111} \geqslant \lambda_{100}$ at room temperature (Clark 1974). The increasing magnetostriction with increasing field in the case of polycrystalline $DyFe_2$ and $HoFe_2$ is attributed to the sensing of a large λ_{111} as the magnetic moments in the crystallites are rotated away from their easy [100] axes. The magnetostriction of the Sm, Tb, Er and Tm compounds is large at low fields, directly reflecting the large λ_{111}. Similar field dependences were found below room temperature in polycrystalline $TbFe_2$ and $DyFe_2$ (Clark and Belson 1972) and in polycrystalline $DyFe_2$, $HoFe_2$ and $ErFe_2$ (Koon et al. 1971).

In fig. 7, the effect of replacing Fe by Co in $TbFe_2$ is illustrated. Since the Curie temperature does not fall appreciably in $TbFe_{2(1-x)}Co_{2x}$ for $x < 0.5$, the

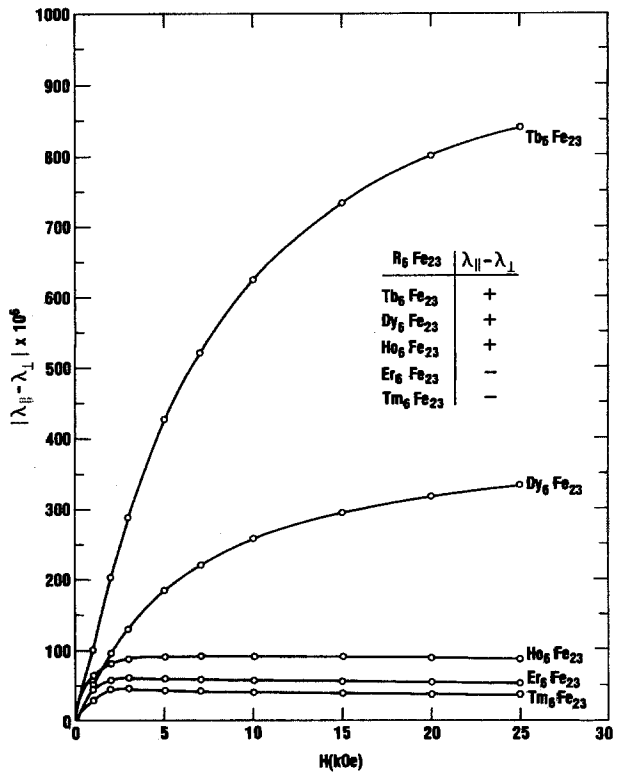

Fig. 5. Room temperature magnetostriction of R_6Fe_{23} polycrystals (taken from Abbundi and Clark 1978). Tb_6Fe_{23} and Dy_6Fe_{23} are not completely single phase.

relative magnetostriction, as measured by the distortion of the cubic cell (Dwight and Kimball 1974) remains almost constant over this concentration range. Strain gage measurements by Belov et al. (1975) show a more rapid decrease in magnetostriction with increasing Co concentration. This may be due to preferred orientation of their polycrystalline samples.

Single crystals of $TbFe_2$, $DyFe_2$, $HoFe_2$, $ErFe_2$ and $TmFe_2$ have been prepared by Bridgman, Czochralski and induction zoning methods (McMasters, unpublished, 1978, Williams and Koon 1975, Milstein 1976). In fig. 8, values of λ_{111} are shown for $TbFe_2$, $ErFe_2$ and $TmFe_2$ at room temperature. In these crystals [111] is the easy magnetization direction. The compounds $DyFe_2$ and $HoFe_2$, on the other hand, possess [100] as the easy magnetization axis. In these materials therefore λ_{100}, rather than λ_{111}, is sensed at technical saturation. Room temperature field dependences of λ_{100} are shown in fig. 9. In remarkable contrast to the large values of λ_{111} for $TbFe_2$ and $ErFe_2$, for $DyFe_2$, $\lambda_{100} = 4 \times 10^{-6}$ and for $HoFe_2$, $\lambda_{100} = -59$ to -66×10^{-6} (Clark et al. 1976, Koon, unpublished, Abbundi et al. 1979). Such a highly anisotropic magnetostriction ratio, $|\lambda_{111}/\lambda_{100}| \gg 1$, is uncommon. It reveals the immense importance of grain orientation in achieving high magnetostriction in

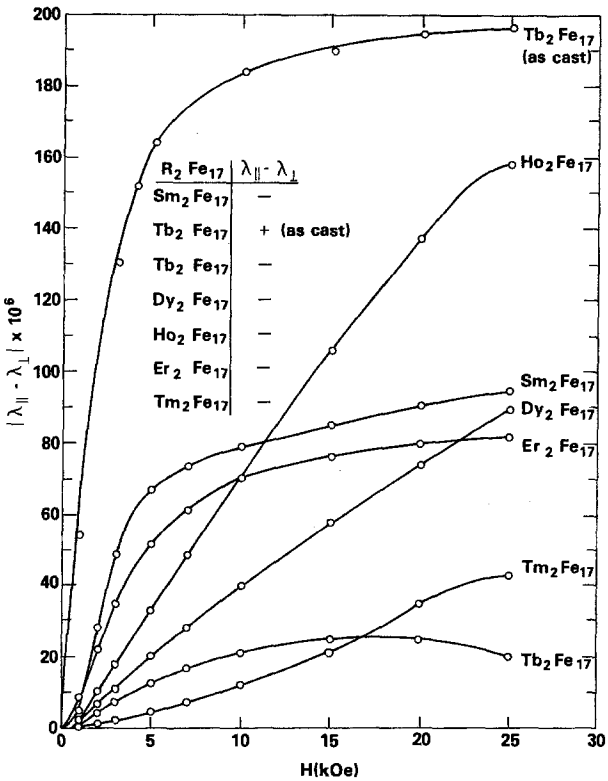

Fig. 6. Room temperature magnetostriction of R_2Fe_{17} polycrystals (taken from Abbundi and Clark 1978). Tb_2Fe_{17} and Dy_2Fe_{17} contain both rhombohedral and hexagonal phases. With the exception of Tb_2Fe_{17} (as cast), all samples were heat treated at 1000°C.

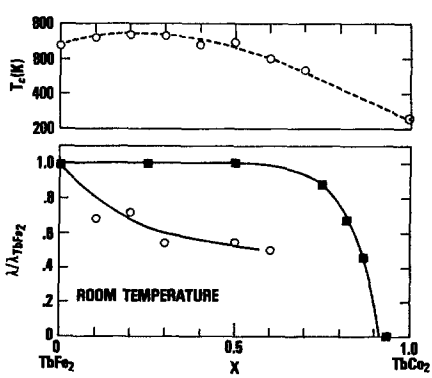

Fig. 7. Curie temperature and relative magnetostriction of $TbFe_{2(1-x)}Co_{2x}$ (taken from ■ Dwight and Kimball 1974, and ○ Belov et al. 1975).

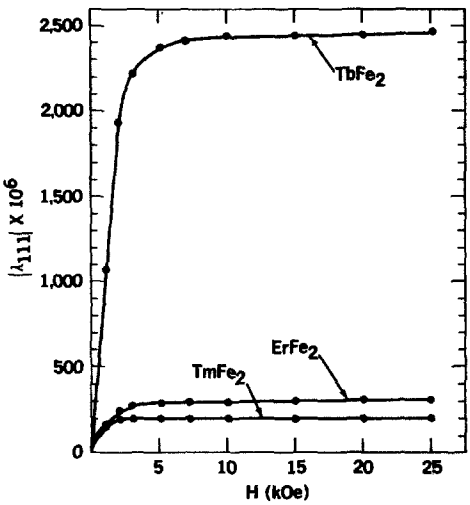

Fig. 8. Room temperature magnetostriction $|\lambda_{111}|$ for single crystal $TbFe_2$, $ErFe_2$ and $TmFe_2$ (taken from Clark et al. 1975, Abbundi and Clark 1978). For $TbFe_2$, $\lambda_{111} > 0$; for $ErFe_2$ and $TmFe_2$, $\lambda_{111} < 0$.

polycrystal RFe_2 materials. In an optimally oriented polycrystal, $\lambda_s \simeq \lambda_{111}$; in an isotropic polycrystal, $\lambda_s \simeq 0.6\lambda_{111}$; and in a poorly textured polycrystal, $\lambda_s \simeq 0$. The effect of crystallite orientation can be two-fold beneficial. In addition to the increase in magnetostriction constant, λ_s, a preferentially oriented polycrystal possesses the major advantage of far lower internal losses at grain boundaries. This is important in applications where a high magnetostriction at low applied fields is required.

In fig. 10, $\lambda_{111}(T)$ of $TbFe_2$ and $\lambda_{100}(T)$ of $DyFe_2$ are contrasted (Clark et al.

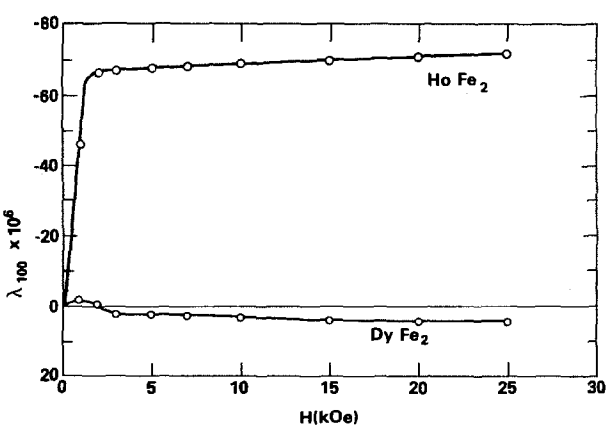

Fig. 9. Room temperature magnetostriction (λ_{100}) for single crystal $DyFe_2$ and $HoFe_2$ (taken from Abbundi, Clark and Koon, unpublished).

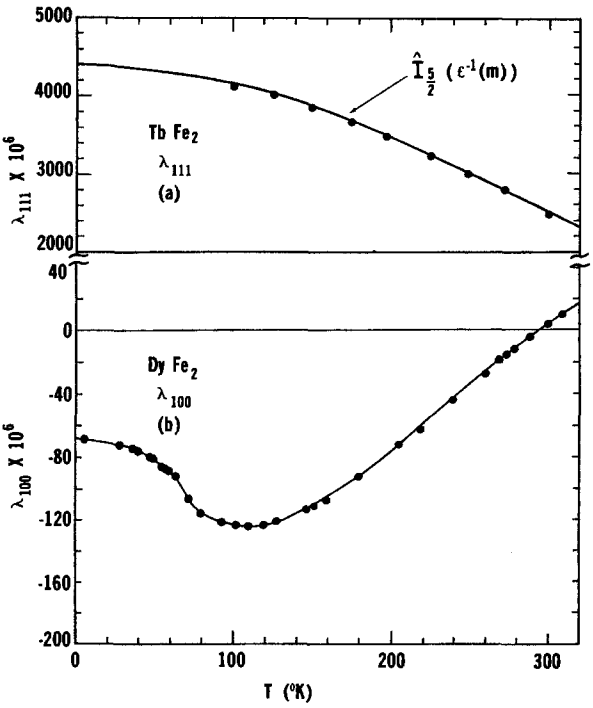

Fig. 10. Temperature dependence of the magnetostriction for single crystal $TbFe_2$ and $DyFe_2$ (taken from Clark et al. 1977).

1977). $\lambda_{111}(T)$ is well behaved. The magnetostriction monotonically decreases with increasing temperature according to the single-ion temperature dependence (Callen and Callen 1963) (see section 4). At absolute zero, $\lambda_{111}(0) = 4400 \times 10^{-6}$ for $TbFe_2$ the largest known value for a cubic material. On the other hand, $\lambda_{100}(T)$ is small for $DyFe_2$ and cannot be fit by a simple single-ion function. This is also true for $HoFe_2$ where $|\lambda_{100}|$ is much larger [$\lambda_{100}(0) = -7{\cdot}45 \times 10^6$]. See Abbundi et al. (1979).

$TmFe_2$ possesses a comparatively small magnetostriction at room temperature. This, however, reflects the weak Tm–Fe exchange and low room temperature Tm magnetization, rather than a small intrinsic magnetoelastic coupling. In fig. 11, the rapid rise of $|\lambda_{111}|$ with decreasing temperature to a value approaching that of $TbFe_2$ at 4 K is illustrated. A fit to the data with single-ion theory (section 4) is excellent. Over this range, the magnetostriction changes by a factor of 15. The dip in the observed magnetostriction of $TmFe_2$ at 235 K is a consequence of the cancellation of sublattice magnetizations at its compensation temperature, where the moments lie perpendicular to the applied field direction. The forced magnetostriction is observed to change sign at this temperature as the Tm moment rotates from parallel to the applied field direction for $T < T_{comp}$ to antiparallel to the applied field direction for $T > T_{comp}$.

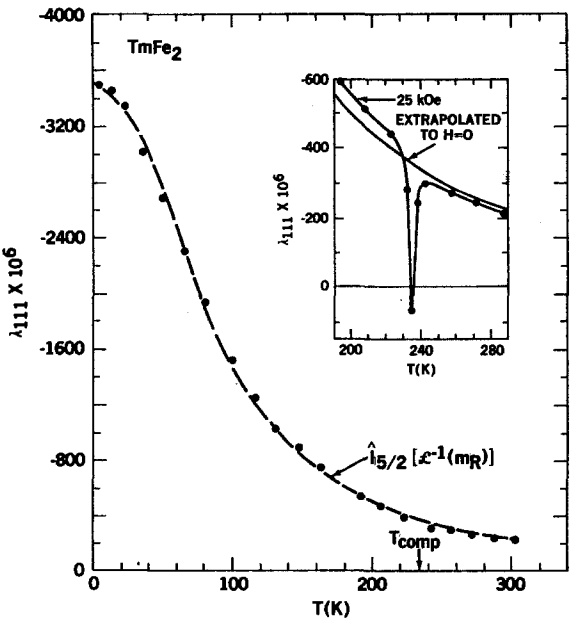

Fig. 11. Magnetostriction (λ_{111}) of single crystal $TmFe_2$ (taken from Abbundi and Clark 1978).

A large magnetoelastic coupling, b_2, is also inferred for $SmFe_2$. No single crystal measurements have yet been reported. In fig. 12 the magnetostriction of polycrystal $SmFe_2$, taken from Rosen et al. (1974), is plotted as a function of temperature. The magnetoelastic coupling indeed is high. However, an analysis of the temperature dependence is difficult because of a low lying $J = \frac{7}{2}$ multiplet. A

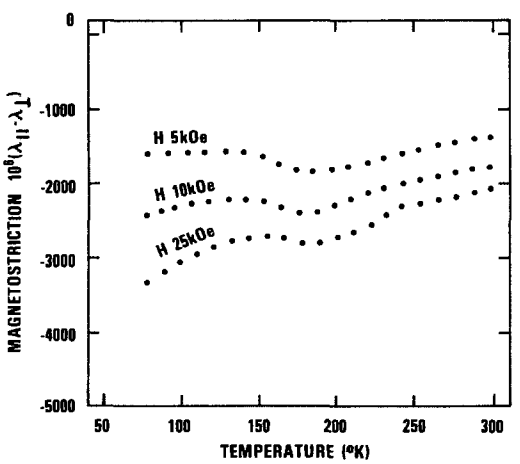

Fig. 12. Magnetostriction of $SmFe_2$ (taken from Rosen et al. 1974).

broad peak in $|\lambda_{\parallel} - \lambda_{\perp}|$ is observed between 140 K and 240 K where the easy axis of magnetization rotates from [110] to [111] with increasing temperature.

An atomic model for the anisotropic magnetostriction based upon the structure of the cubic Laves phase C15 compounds was proposed by Clark et al. (1976) and Cullen and Clark (1977). In this model, potentially huge values of λ_{100}, arising from the asymmetry of the rare earth 4f electron shell, are effectively shorted out because of the high tetrahedral ($\bar{4}3m$) symmetry at the rare earth sites. On the other hand, huge λ_{111}'s are allowed because two inequivalent tetrahedral sites exist in the C15 structure which permit internal distortions along [111] directions. *This internal distortion lowers the symmetry and drives an external rhombohedral distortion* (λ_{111}). In fig. 13, the distortion is illustrated for $TbFe_2$ and other RFe_2 compounds containing rare earths with oblate 4f charge distributions. The two inequivalent sites, situated at 0, 0, 0 and $\frac{1}{4}, \frac{1}{4}, \frac{1}{4}$ are denoted by A (or A') and B (or B') respectively. The iron atoms are not shown. λ_{111} signifies the fractional change in length along the [111] direction when the material is magnetized along this direction. In fig. 13a, the magnetization is directed along [111]. The oblate 4f electron cloud ($-e$) lies perpendicular to the magnetization axis. Considering only the electrostatic coulomb interaction, the closer proximity of the 4f electron cloud on A to atoms B', than to atom B, causes an extension of the A–B bond, the magnitude of which depends upon the internal A–B modulus. The resultant increase in a exceeds a small decrease in b, yielding a net positive external magnetostriction along [111]. Conversely, for compounds with rare earths possessing prolate 4f charge densities, e.g. for $SmFe_2$, $ErFe_2$ and $TmFe_2$, a contraction of a occurs, producing the observed negative magnetostrictions (λ_{111}). A large rhombohedral distortion thus exists

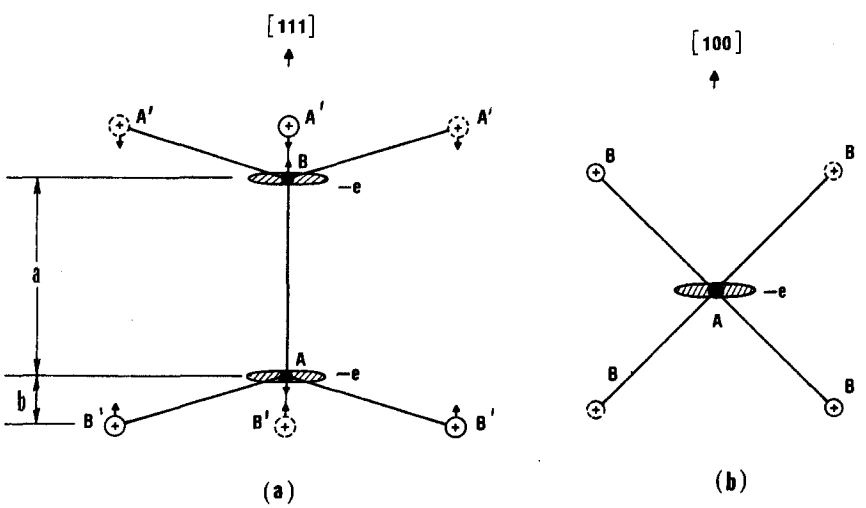

Fig. 13. Model of magnetostriction in Laves phase RFe_2 compounds: (a) $M \| [111]$, (b) $M \| [100]$. Open circles, ○, denote atoms above plane of figure; broken circles, ◌, denote atoms below (taken from Clark et al. 1976).

whenever the magnetization points along [111], i.e. for $TbFe_2$, $SmFe_2$, $ErFe_2$ and $TmFe_2$. The alternate case of [100] easy, i.e. for $DyFe_2$ and $HoFe_2$, is depicted in fig. 13b. With the easy direction of magnetization parallel to the [100] direction, the 4f electron cloud becomes equidistant to all rare earth nearest neighbors, allowing no magnetostrictively driven internal distortion via point charge electrostatic interactions. All A–B bonds are equivalent, the symmetry remains high, and the potentially huge magnetostriction constant, λ_{100}, does not appear. To date these internal distortions have not yet been verified.

Of the total of fifteen lanthanide rare earths, only a few form highly magnetostrictive RFe_2 compounds at room temperature. In table 5 are listed the rare earth elements in order of the increasing number of 4f electrons. La with no 4f electrons and Lu with a full shell of fourteen 4f electrons are omitted. It is possible to calculate the intrinsic ($T = 0$ K) magnetostrictive contribution of each 3^+ rare earth ion for a particular compound (assuming its existence) given the magnetostriction of at least one compound (e.g. $TbFe_2$). The theory utilizes the Stevens' equivalent operator method. According to Stevens (1952), the ratio of the intrinsic magnetostriction of one rare earth to another is given by the ratio of $\alpha J\ (J - \frac{1}{2})\langle r_f^2\rangle$ where α is the lowest order Stevens' factor, J is the ground state angular momentum for the 3^+ ion and $\langle r_f^2\rangle$ is the average radius squared of the 4f electron shell. Here the effect of screening (Freeman and Waton 1962) is neglected, In table 5, the values of J, α, and $\langle r_f^2\rangle$ are given along with the calculated values of λ_{111} for RFe_2 compounds, normalized to 4400×10^{-6} for $TbFe_2$. The estimated uncertainty

TABLE 5
Magnetostriction of RFe_2 compounds

R	$\alpha \times 10^{2}$[a]	J	$\langle r_f^2\rangle$[b]	$\lambda_{111} \times 10^6$(calc)* 0 K	$\lambda_{111} \times 10^6$(exp) room temperature
Ce*	−5.72	$\frac{5}{2}$	1.20	6000	–
Pr*	−2.10	4	1.086	5600	–
Nd*	−0.643	$\frac{9}{2}$	1.001	2000	–
Pm*	0.772	4	0.942	−1800	–
Sm	4.13	$\frac{5}{2}$	0.883	−3200	−2100[e]
Eu*	0	0	0.834	0	–
Gd	0	$\frac{7}{2}$	0.785	0	–
Tb	−1.01	6	0.756	4400	2460[d]
Dy	−0.635	$\frac{15}{2}$	0.726	4200	1260[e]
Ho	−0.222	8	0.696	1600	185[c], 200[g]
Er	−0.254	$\frac{15}{2}$	0.666	−1500	−300[d]
Tm	1.01	6	0.639	−3700	−210[f]
Yb*	3.18	$\frac{7}{2}$	0.613	−3600	–

* Calculated for cubic Laves phase $R^{3+}Fe_2$ compounds. For R = Ce, Nd, Pm, Eu and Yb, this compound has not yet been synthesized. $PrFe_2$ has been synthesized only under high pressure.

[a] Stevens (1952).
[b] Freeman and Watson (1962).
[c] Koon and Williams (1977).
[d] Clark et al. (1975).
[e] Clark et al. (1976).
[f] Abbundi and Clark (1978).
[g] Abbundi et al. (1979).

in the absolute magnitude of $\lambda_{111}(0)$ is ± 15%. Note that the largest positive intrinsic magnetostrictions are those calculated for $CeFe_2$, $PrFe_2$, $TbFe_2$, and $DyFe_2$; the largest negative magnetostrictions are those calculated for $SmFe_2$, $TmFe_2$ and $YbFe_2$. However, not all of these compounds have been synthesized. Ce and Yb are not found in their trivalent states. The calculated magnetostrictions of quadrivalent Ce and divalent Yb are zero. $PrFe_2$ and $NdFe_2$ do not readily form the cubic Laves phase compounds. While both $DyFe_2$ and $TmFe_2$ have high incipient magnetostrictions, the large magnetostriction is not realized in $DyFe_2$ since [111] is magnetically hard, and the large magnetostriction of $TmFe_2$ is realized only at low temperatures because of a weak thulium–iron exchange interaction. Thus only $TbFe_2$ and $SmFe_2$ emerge with large room temperature magnetostrictions. Experimental values of λ_{111} measured at room temperature are given in table 5 for the binary compounds $SmFe_2$, $TbFe_2$, $DyFe_2$ (see section 6), $HoFe_2$, $ErFe_2$ and $TmFe_2$.

It is clear from the foregoing that since in many cases $\lambda_{111} \gg \lambda_{100}$, care must be taken in interpreting measurements on polycrystals. Typical preparation techniques yield samples which are far from isotropic. Crystallites grow anisotropically, most rapidly along a direction near [211] (McMasters unpublished).

4. Magnetization and sublattice magnetization of RFe_2 compounds

Magnetization measurements on a large number of RFe_2 binary and pseudobinary polycrystals have been reported on the literature. Extensive measurements over a wide range of temperatures have been made by Buschow and Van Stapele (1970, 1971) and Burzo (1971). It is clear from this work and the earlier work of Wallace and Skrabek (1964) that the rare earth and iron moments couple antiferromagnetically. Within the last few years, magnetization measurements in high fields and on single crystals have become available (Clark et al. 1974, 1977, 1978, Abbundi et al. 1979). In this section, comparison will be made between single crystal and polycrystal data. Single crystal magnetizations will be used to calculate theoretical temperature dependences of the magnetostriction utilizing a theory formulated by Callen and Callen (1963).

In figs. 14 through 18, the magnetic moment along the easy magnetization direction is compared to data taken on polycrystalline samples for $TbFe_2$, $DyFe_2$, $HoFe_2$, $ErFe_2$ and $TmFe_2$. Although the compounds are cubic and only moderate anisotropies were initially expected, it is clear that the full saturation magnetization is not achieved in any of the polycrystal specimens at low temperatures. Instead, large cubic anisotropies were measured in all compounds (see section 5). The easy directions of magnetization are consistent with those predicted by the earlier Mössbauer measurements (Wertheim et al. 1964, Bowden et al. 1968, Guimaraes 1971, Atzmony et al. 1973). In a polycrystal in which crystallites are distributed uniformly over all directions, if the [111] axis is easy, and if the magnetization lies along the [111] axis in each crystallite closest to the external field, the polycrystal remanent moment is 0.866 of the aligned saturation moment (Chikazumi and Charap 1964). This is close to the observed polycrystal/single crystal

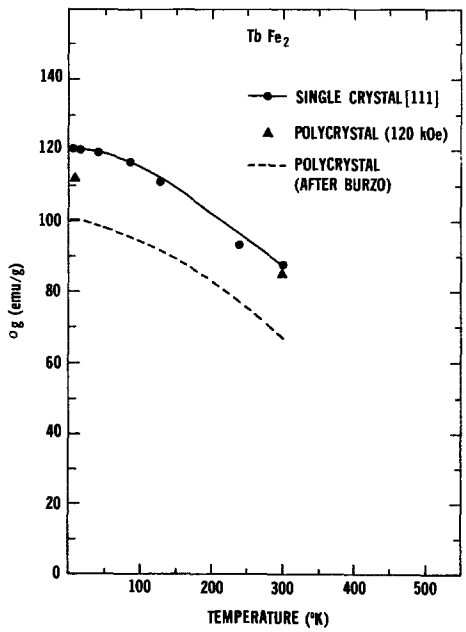

Fig. 14. Magnetic moment of $TbFe_2$ (taken from Clark et al. 1978, Burzo 1971).

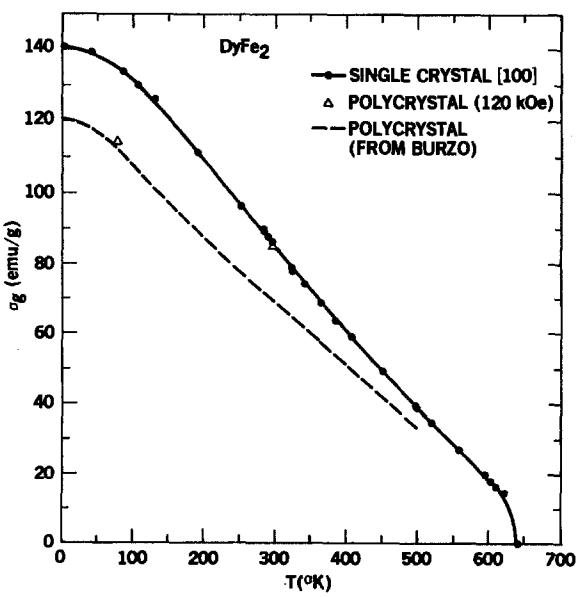

Fig. 15. Magnetic moment of $DyFe_2$ (taken from Clark et al. 1978, Burzo 1971).

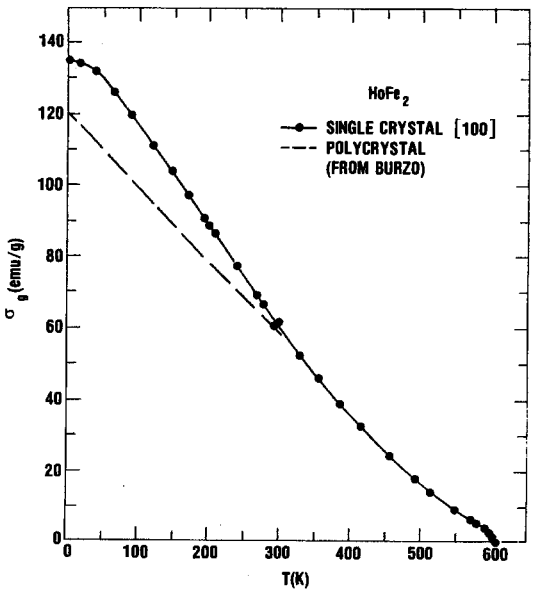

Fig. 16. Magnetic moment of $HoFe_2$ (taken from Abbundi et al. 1979, Burzo 1971).

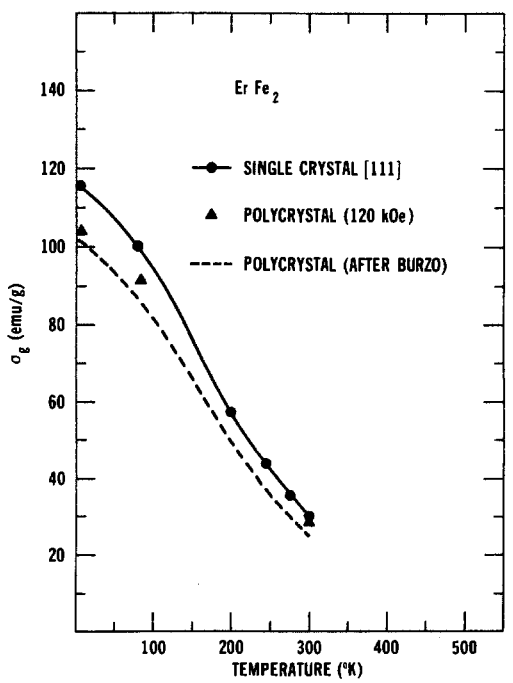

Fig. 17. Magnetic moment of $ErFe_2$ (taken from Clark 1974, Burzo 1971).

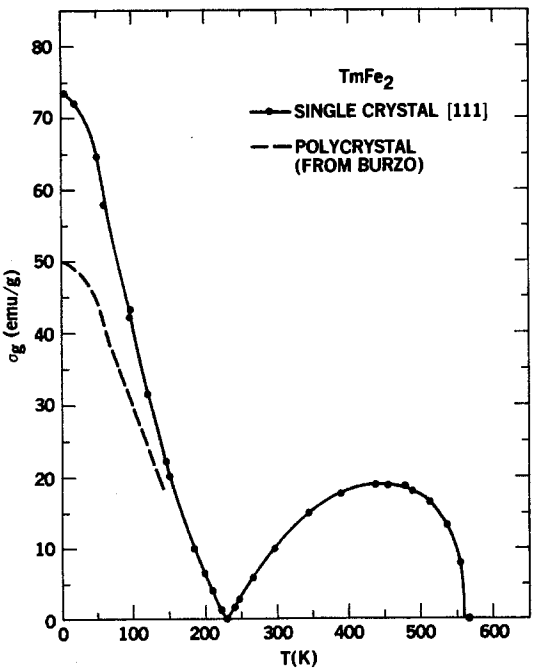

Fig. 18. Magnetic moment of $TmFe_2$ (taken from Clark et al. 1978, Burzo 1971).

moment ratio at 4 K for $TbFe_2$ and $ErFe_2$. When [100] is easy, the corresponding calculated ratio is 0.832. In $DyFe_2$ and $HoFe_2$, the ratios are ~0.87, only slightly higher than the calculated value. No moments have been reported to date for single crystal $SmFe_2$. In table 6 are collected Curie temperatures, atomic magnetic moments, magnetizations and theoretical densities for these compounds. Similar values of iron sublattice moments ($1.61 \pm 0.04 \mu_B$) at 0 K are calculated from the single crystal magnetization measurements assuming that the rare earth moments equal gJ. They are remarkably close to those adduced from nuclear hyperfine fields by Wallace (1968).

Unlike the magnetostrictions of the transition metals Ni, Co and Fe, the magnetostrictions of the rare earth elements follow a rather simple single-ion temperature dependence. Callen and Callen (1963, 1965) developed a formulation which directly relates the temperature dependence of the magnetostriction to the temperature dependence of the rare earth magnetization. This formulation is valid in the molecular field approximation, spin wave approximation and various Green's function theories (Callen and Shtrickman 1965). They find

$$\lambda^{\mu,l}(T) = \lambda^{\mu,l}(0)\hat{I}_{l+1/2}(x) \tag{4.1}$$

where $\hat{I}_{l+1/2}$ is the ratio of the hyperbolic Bessel function of order $l+\frac{1}{2}$ to the hyperbolic Bessel function of order $\frac{1}{2}$. The argument x is related to the normalized magnetization $m = M/M_s$ through the relationship

TABLE 6
Magnetic moments and Curie temperatures of RFe_2

RFe_2	σ(emu/g) 0 K	σ(emu/g) 300 K	ρ g/cm^3	M(emu/cm^3) 0 K	M(emu/cm^3) 300 K	n_b 0 K	n_b 300 K	n_{bFe}[e]	n_{bFe}[f]	T_C K
$TbFe_2$[a]	120	88	9.06	1090	800	5.81	4.26	1.60	1.75	697,711[g]
$DyFe_2$[b]	140	87	9.28	1300	810	6.87	4.27	1.57	1.60	635
$HoFe_2$[c]	135	62	9.44	1274	590	6.70	3.06	1.65	1.55	606
$ErFe_2$[b]	116	29	9.62	1120	280	5.79	1.45	1.61	1.60	590,597[g]
$TmFe_2$[a]	74	10	9.79	725	98	3.72	0.49	1.64	1.55	560
$SmFe_2$[d]	48	47	8.53	410	400	2.25	2.20	–	–	676

[a] Taken from single crystal data (Clark et al. 1978).
[b] Taken from single crystal data (Clark 1974 Clark et al. 1978).
[c] Taken from single crystal data (Abbundi et al. 1979).
[d] Taken from polycrystal data (Buschow, unpublished).
[e] Calculated from single crystal data assuming $n_{bR} = gJ$.
[f] Calculated from Mössbauer spectra (see Wallace 1968).
[g] Taken from polycrystal data (Buschow and Van Stapele 1971, Burzo 1971).

$$m = \hat{I}_{3/2}(x). \tag{4.2}$$

Since $\hat{I}_{3/2}$ is the familiar Langevin function, $\mathscr{L}(x) = \coth x - 1/x$, $\hat{I}_{l+1/2}$ $(l > 1)$ can be considered to be "higher order" Langevin functions (Callen and Callen 1965, Keffer 1955). In molecular field theory, $x = \mu H/kT$, where μ is the magnetic moment/ion and H is the total (effective + external) magnetic field. In a more general sense, however, x can be defined through eq. (4.2). Thus, expressing the magnetostriction in terms of the normalized magnetization $m(T, H)$

$$\lambda^{\mu,l}(T) = \lambda^{\mu,l}(0)\hat{I}_{l+1/2}[\mathscr{L}^{-1}(m(T, H))]. \tag{4.3}$$

For the lowest order ($l = 2$) magnetostriction, e.g. λ_{100} and λ_{111}, we find $\lambda^{\mu,2}(T) \simeq \lambda^{\mu,0}(0)m^3(T)$ at low temperatures and $\lambda^{\mu,2}(T) \simeq 0.6\lambda^{\mu,2}(0)m^2(T)$ at high temperatures. The functional dependence of $\hat{I}_{l+1/2}$ on m is given for $l = 2$, 4 and 6 in Appendix B. To test the applicability of eq. (4.3) to the RFe_2 compounds, the rare earth sublattice magnetizations, m_R's, must be known.

These sublattice magnetizations, m_R's, can be obtained directly by Mössbauer and by neutron diffraction methods, and indirectly by subtracting the Fe magnetization from the total magnetization. The results are shown in fig. 19. For $DyFe_2$ good agreement is found between the values of m_{Dy} calculated from Mössbauer measurements (Bowden et al. 1968) and those obtained from the total magnetization measurements (Clark 1974). Similarly, good agreement is found between the neutron diffraction results (Rhyne, unpublished) and total magnetization results for $HoFe_2$ (Abbundi et al. 1979) and $ErFe_2$ (Clark 1974). For $TbFe_2$ the neutron diffraction data (Rhyne, unpublished) is higher than that calculated from the magnetization over the entire temperature range. Both these measurements, however, fall within the uncertainty cited by Barbara et al. (1977) in their neutron diffraction data on $TbFe_2$. For $TmFe_2$ the neutron diffraction

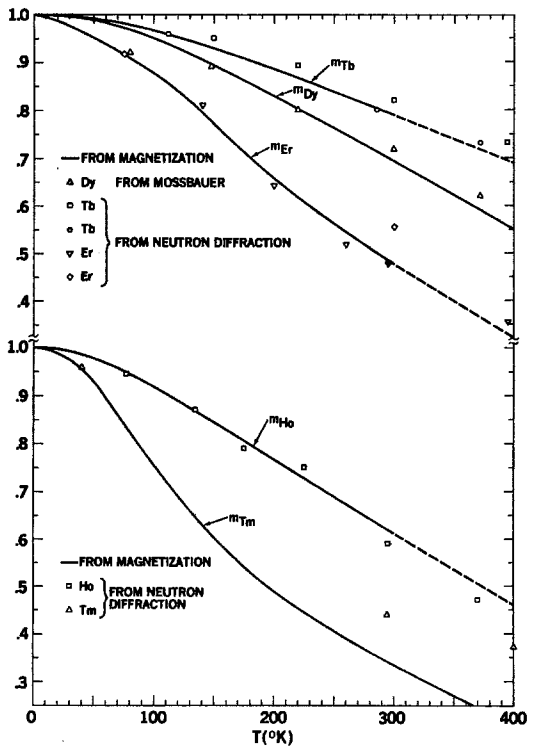

Fig. 19. Normalized rare earth sublattice magnetizations in RFe_2. (△ (Mössbauer) Bowden et al. 1968; □ ▽△ Rhyne, unpublished, ○ Barbara et al. 1977, ◇ Bargouth and Will 1971). The solid lines were calculated from single crystal magnetizations minus the iron sublattice magnetizations (Bowden et al. 1968) normalized to the respective Curie temperatures of the compounds.

data (Rhyne, unpublished, Barbara et al. 1977) are not in agreement with the total magnetization results, leading to incorrect magnetizations and compensation temperatures. Thus the currently available neutron diffraction data for $TmFe_2$ are considered unsatisfactory.

The temperature dependence of the magnetostrictions were calculated from eq. (4.3) using the rare earth sublattice magnetizations of fig. 19. Excellent agreement between the measured temperature dependences and those calculated from the lowest order ($l = 2$) single-ion theory were found for $TbFe_2$ (fig. 10) and $TmFe_2$ (fig. 11). The Callen–Callen single-ion theory was found insufficient to account for the (small) λ_{100} of $DyFe_2$ and $HoFe_2$ (fig. 9 and 10).

5. Magnetic anisotropy of binary RFe_2 compounds

The largest magnetic anisotropies occur in uniaxial crystals. The hexagonal rare earth elements possess the largest known magnetic anisotropies at low temperatures. The high Curie temperature compounds RCo_5 and R_2Co_{17} possess the

largest known magnetic anisotropy energies at room temperature. Smaller anisotropies are found in the cubic RFe_2 compounds. However, recent measurements have shown that they possess by far the largest known anisotropies of cubic crystals. Depending upon the strength of the rare earth–iron exchange, this large anisotropy sometimes persists to room temperature.

Anisotropy constants were experimentally determined by both magnetization and magnetic torque measurements on single crystals of the binary RFe_2 compounds (Clark et al. 1973, 1978, Williams and Koon 1975). The room temperature anisotropy constants K_1 of $TbFe_2$, $DyFe_2$, $HoFe_2$, $ErFe_2$ and $TmFe_2$ are compared to some typical cubic ferro- and ferrimagnets in table 7. The decrease in Curie temperature with increasing atomic number is directly reflected in the room temperature value of the rare earth sublattice magnetization m_R (fig. 19) and thus in the magnitude of the room temperature magnetic anisotropy. In $TbFe_2$, anisotropy fields are in excess of 100 kOe at room temperature, while in $TmFe_2$, saturation is achieved below 12 kOe (see fig. 20). The easy axes are consistent with the earlier Mössbauer spectra measurements (see compilation by Taylor 1971).

The total anisotropy is a sum of both intrinsic and magnetoelastic contributions (see section 2). In table 8 are shown the calculated contributions to the anisotropy from the magnetoelastic coupling, as obtained from $\Delta K_1 = -\frac{9}{2}c_{44}\lambda_{111}^2$. Subtracting these values from the total anisotropies of table 7, the intrinsic anisotropies $K_1^{int}(300)$ and $K_1^{int}(0)$ were inferred. For $TbFe_2$, $DyFe_2$ and $TmFe_2$, where the intrinsic magnetostriction, $\alpha J(J-\frac{1}{2})$ is large, $\Delta K_1(300)/K_1(300) \simeq 20\%$; for $HoFe_2$ and $ErFe_2$, where the magnetostriction is smaller, $\Delta K_1(300)/K_1(300) \leq 6\%$.

According to single-ion theory (see Appendix B), the temperature dependence

TABLE 7
Anisotropy constants of some cubic metals and ferrites at room temperature

Metal	$10^{-4}K_1$(ergs/cm^3)	Ferrite	$10^{-4}K_1$(ergs/cm^3)
Fe	45[a]		
Ni	−5[a]		
70% Fe–Co	−43[b]	$Ga_{0.44}Fe_{2.54}O_4$	−81[g]
65% Co–Ni	−26[c]	$CoFe_2O_4$	260[h]
$TbFe_2$	−7600[d]	$Co_{0.8}Fe_{2.2}O_4$	290[i]
$DyFe_2$	2100[d]	$Co_{0.3}Zn_{0.2}Fe_{2.2}O4$	150[j]
$HoFe_2$	580[e], 550[j]		
$ErFe_2$	−330[d]		
$TmFe_2$	−53[f]		

[a] Hoffman (1967).
[b] McKeehan (1937).
[c] Shih (1936).
[d] Clark et al. (1972, 1975).
[e] Williams et al. (1978).
[f] Abbundi and Clark (1978).
[g] Pearson (1960).
[h] Perthel et al. (1966).
[i] Bozorth et al. (1955).
[j] Abbundi et al. (1979).

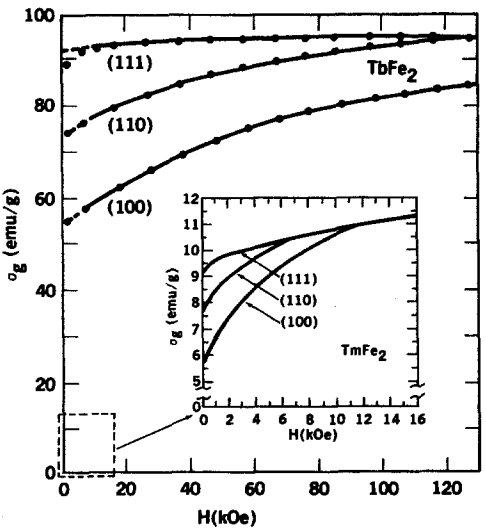

Fig. 20. Magnetic moment of $TbFe_2$ and $TmFe_2$ at room temperature (taken from Clark et al. 1975, Abbundi and Clark 1978).

TABLE 8
Intrinsic, K_1^{int}, and magnetoelastic, ΔK_1, contributions to the magnetic anisotropy (ergs/cm³)

RFe_2	$\Delta K_1(300)$* $\times 10^{-4}$	$K_1^{int}(300)$ $\times 10^{-4}$	$\frac{\Delta K_1(300)}{K_1^{int}(300)}$	$K_1^{int}(0)$** $\times 10^{-8}$
$SmFe_2$	−970	–	–	–
$TbFe_2$	−1330	−6300	0.21	−5.2
$DyFe_2$	−350	2450	−0.14	4.7
$HoFe_2$	−7.5	590	−0.01	2.7
$ErFe_2$	−20	−310	0.06	−5.4
$TmFe_2$	−9.7	−43	0.22	−3.8

* Calculated from $\frac{9}{2}c_{44}\lambda_{111}^2$ taking $c_{44} = 4.87 \times 10^{11}$ dynes/cm² from Rinaldi et al. (1977).
** Extrapolated to $T = 0$ using single-ion theory.

of the lowest order (intrinsic) anisotropy constant in cubic crystals is given by

$$K^{\alpha,4}(T)/K^{\alpha,4}(0) = \hat{I}_{9/2}[\mathscr{L}^{-1}(m_R)] \tag{5.1}$$

or

$$K_1(T)/K_1(0) = \hat{I}_{9/2}[\mathscr{L}^{-1}(m_R)] \tag{5.2}$$

whenever $|K_2| \ll |11\, K_1|$.

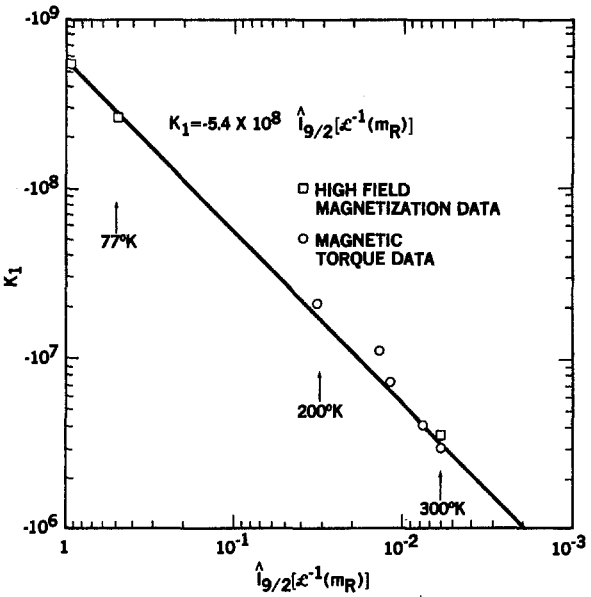

Fig. 21. Magnetic anisotropy K_1 of $ErFe_2$ vs. single-ion theory (taken from Clark et al. 1974).

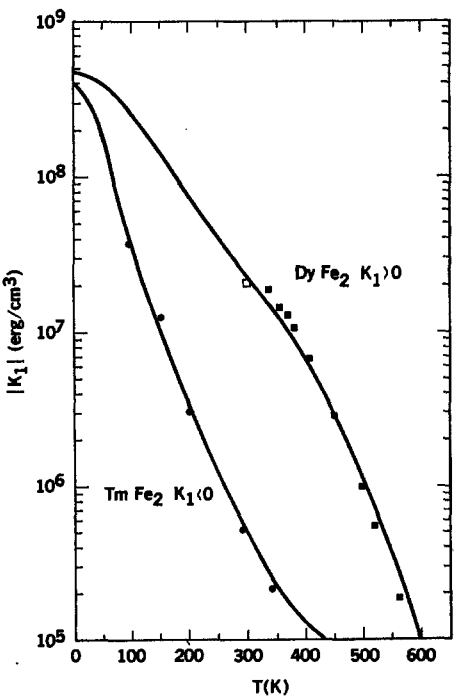

Fig. 22. Anisotropy constant K_1 for $DyFe_2$ and $TmFe_2$ as a function of temperature (taken from Clark et al. 1978). The solid curves are calculated from single-ion theory.

Figure 21 shows that the experimentally observed anisotropy of $ErFe_2$, in which $\Delta K/K$ is negligible, conforms rather well to the simple theory, as given by eq. (5.2). The temperature dependence of the anisotropy constants (K_1) for $DyFe_2$ and $TmFe_2$ are plotted in fig. 22. The anisotropy spans three decades. Again satisfactory agreement between experiment and theory is found. With one adjustable constant, $K_1^{int}(0)$, the fit to the data is within 20% over the entire temperature range. The values of $K_1^{int}(0)$ calculated from eq. (5.2), utilizing higher temperature measured values and the sublattice magnetizations m_R from section 4, are given in table 8. All anisotropy magnitudes exceed 2×10^8 erg/cm^3 at $T = 0$ K and agree with each other within a factor of two.

Higher order anisotropy terms also contribute to the total anisotropy energy, particularly at low temperatures. Evidence for their existence can be found from spin reorientation diagrams of pseudobinary RFe_2 compounds (Atzmony et al. 1973, 1977; Atzmony and Dariel 1976) and from torque magnetometry measurements in the $Tb_xHo_{1-x}Fe_2$ system (Williams and Koon 1975, 1978). Temperature dependences of the anisotropy constants are in general complex and require the inclusion of the large magnetoelastic contribution (Koon and Williams 1978).

The binary RFe_2 compounds $TbFe_2$, $DyFe_2$, $HoFe_2$, $ErFe_2$ and $TmFe_2$ have only one easy direction at all temperatures. However anisotropy compensation and spin reorientation can be achieved with suitable rare earth alloying into compounds of the form $R_x^{(1)}R_y^{(2)}\ldots Fe_2$ $(x + y \ldots = 1)$. Spin reorientation diagrams and anisotropy measurements for some pseudobinary RFe_2 compounds are discussed in section 6.

6. Magnetostriction of pseudobinary RFe_2 compounds

In the hexagonal rare earths, the lowest order anisotropy and magnetostriction arises from the same degree of spin operator ($l = 2$). In contrast, in the RFe_2 compounds, because they are cubic, the anisotropy arises from $l = 4$ terms and the magnetostriction from $l = 2$ terms. This makes it possible to tailor compounds with optimum magnetostriction and anisotropy properties simultaneously. For certain magnetostrictive materials applications, high strains at low fields are necessary. In these cases a low anisotropy is important in order to maximize domain wall mobility and easy domain rotation at low fields.

Table 9 shows the signs of λ, $K^{\alpha,4}$ and $K^{\alpha,6}$ for the binary RFe_2 compounds taken from the signs of the Stevens' equivalent operator coefficients. Using this table, pseudobinary compounds can be constructed in such a way as to minimize the magnetic anisotropy while still maintaining a large positive (or negative) magnetostriction. It is preferable to alloy binary compounds with the same magnetostriction sign but with opposite signs of anisotropy. Ternary compounds yielding large positive magnetostrictions at room temperature must contain Tb. Hence acceptable anisotropy compensating systems are $Tb_{1-x}Dy_xFe_2$, $Tb_{1-x}Ho_xFe_2$ and $Tb_{1-x}Pr_xFe_2$. Experimental spin reorientation diagrams for $Tb_{1-x}Dy_xFe_2$ and $Tb_{1-x}Ho_xFe_2$ are shown in fig. 23. The region of

TABLE 9
Polarity of λ, $K^{\alpha,4}$ and $K^{\alpha,6}$

	$PrFe_2$[a]	$SmFe_2$	$TbFe_2$	$DyFe_2$	$HoFe_2$	$ErFe_2$	$TmFe_2$	$YbFe_2$[a]
λ	+	−	+	+	+	−	−	−
$-K^{\alpha,4}$, $K_1 + K_2/11$	+	−	−	+	+	−	−	+
$K^{\alpha,6}$, K_2	−	0	+	−	+	−	+	−

[a] The binary $PrFe_2$ and $YbFe_2$ compounds are not readily synthesized.

spin reorientation and anisotropy compensation are clearly identified from 0 K to 300 K. Ternary compounds possessing a large negative magnetostriction at room temperature must possess Sm. However Yb, the only suitable element with the correct sign distribution, is not available in a trivalent state. Fortunately, the ratio of λ/K is much larger for Sm than for the heavy rare earth compounds.

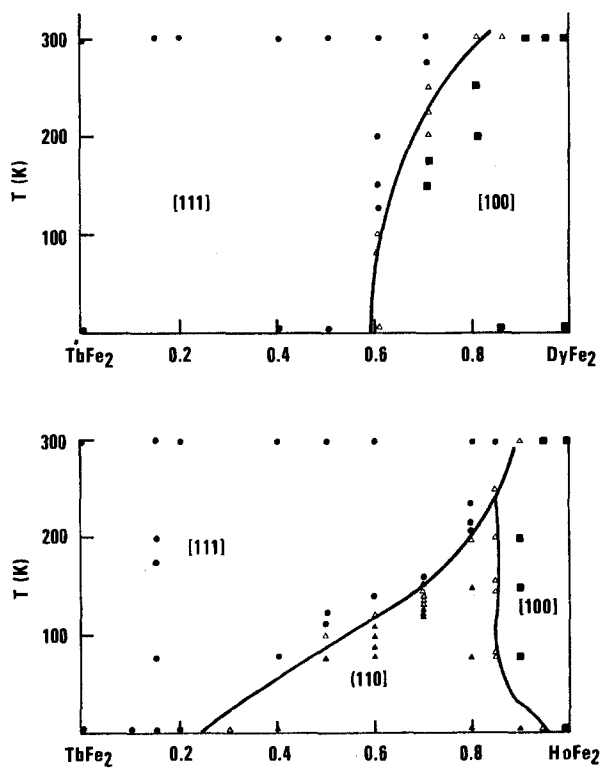

Fig. 23. Spin orientation of $Tb_{1-x}Dy_xFe_2$ and $Tb_{1-x}Ho_xFe_2$ systems (taken from Atzmony et al. 1973). Filled circles, triangles and squares correspond to [111], [110] and [100] axes of magnetization respectively. Open triangles correspond to intermediate directions.

Hence certain ternary alloys, such as $Sm_{1-x}Dy_xFe_2$ and $Sm_{1-x}Ho_xFe_2$, are attractive candidates for anisotropy minimization.

The $Tb_{1-x}Dy_xFe_2$ system has been investigated in detail. In fig. 24, are shown the magnetostrictions at room temperature of polycrystalline samples of $Tb_{1-x}Dy_xFe_2$ for $H = 10$ kOe and $H = 25$ kOe. Near $x = 0.7$, the magnetostrictions at these fields exhibit a peak, reflecting the near zero magnetic anisotropy at this concentration. Figure 25 illustrates how the single crystal magnetostriction constant λ_{111} varies with Dy concentration. λ_{111} was determined by X-ray techniques, utilizing a method developed (Dwight and Kimball 1974, Clark et al. 1975) to accurately determine the magnetostriction at the point of spin reorientation. When [111] is easy, a large rhombohedral distortion (λ_{111}) occurs contributing to a large X-ray splitting of the (440) and (620) lines. When [100] is easy, only a tiny distortion is realized ($\lambda_{100} \simeq 0$) and X-ray splittings are not observed. The concentration at which the magnetostriction disappears clearly identifies the point of anisotropy minimization. At the spin reorientation $\lambda_{111} = 1600 \times 10^{-6}$. The extrapolated value of λ_{111} for $DyFe_2$ is 1260×10^{-6}.

The magnetostriction of single crystal $Tb_{0.27}Dy_{0.73}Fe_2$ has been measured through the anisotropy compensation region (Abbundi and Clark 1977). A spectacular "turning on" of a huge rhombohedral (magnetostrictive) strain by a rise in temperature occurs. At low temperatures, $M \| [100]$, and no significant

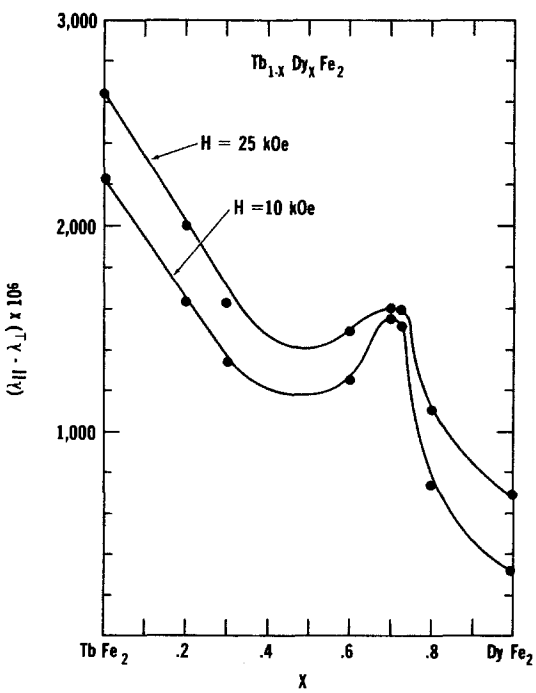

Fig. 24. Magnetostriction of $Tb_{1-x}Dy_xFe_2$ at room temperature (taken from Clark 1974).

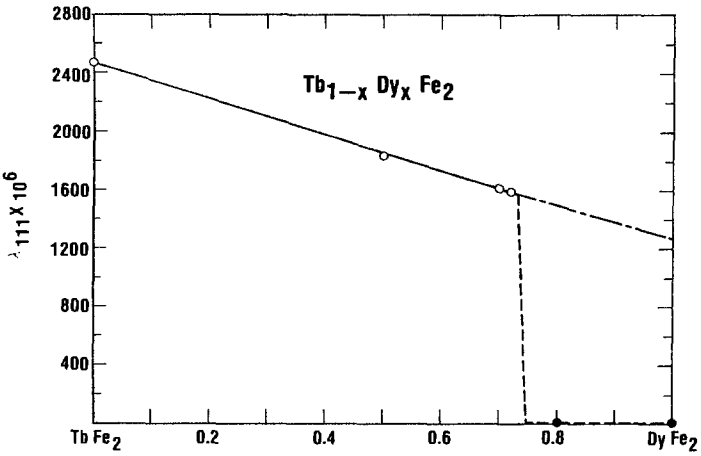

Fig. 25. λ_{111} of $Tb_{1-x}Dy_xFe_2$ at room temperature. Open circles are λ_{111}; solid circles denote region where no spontaneous λ_{111} exists (taken from Clark et al. 1976).

magnetostrain exists. Rather abruptly, at the anisotropy compensation temperature, magnetization rotation takes place and a large rhombohedral distortion (λ_{111}) develops. The effective linear thermal expansion coefficient $\alpha_\ell = d\lambda_{111}/dT$ reaches 110 ppm in this region (see fig. 26). The region of the anomalous thermal expansion can be shifted in temperature by application of an external magnetic field. The fields required for magnetization saturation through the compensation region are shown in fig. 27.

In fig. 28, the room temperature saturation magnetostriction measurements of Koon et al. (1974) for $Tb_{1-x}Ho_xFe_2$ are shown as a function of composition x. Since the anisotropy of Ho is smaller than that of Dy at room temperature, compensation occurs at a larger value of x than in the $Tb_{1-x}Dy_xFe_2$ system. In $Tb_{1-x}Ho_xFe_2$, compensation occurs near $x = 0.85$ as indicated by the anisotropy measurements of Williams and Koon (1975). At this concentration, $\lambda_{111} = 500 \times 10^{-6}$ (Koon and Williams 1977).

Figure 29 shows the effect of the addition of $PrFe_2$ to $TbFe_2$. Here the magnetostriction remains very high, but complete anisotropy compensation cannot be reached. Beyond 20% substitution, non-cubic phases appear.

In multicomponent pseudobinary systems, such as $Tb_xDy_yHo_zFe_2$, $Tb_xDy_yPr_zFe_2$ and $Tb_xDy_yHo_zPr_wFe_2$, values of x, y, z and w can be selected to achieve maximum magnetostriction with the simultaneous minimization of two or more anisotropy constants. Williams and Koon (1977) have successfully determined the alloy composition of the $(Tb_{0.3}Dy_{0.7}Fe_2)_x(Tb_{0.14}Ho_{0.86}Fe_2)_{1-x}$ pseudobinary for simultaneously minimization of the *two* lowest order anisotropy constants. They found low anisotropy for $x \simeq 0.32$ and calculated a still lower anisotropy for $Tb_{0.20}Dy_{0.22}Ho_{0.58}Fe_2$. For this compound, $\lambda_s = 530 \times 10^{-6}$. The three lowest symmetry anisotropy constants κ_4, κ_6 and κ_8, calculated from a least square fit to torque data, are illustrated in fig. 30.

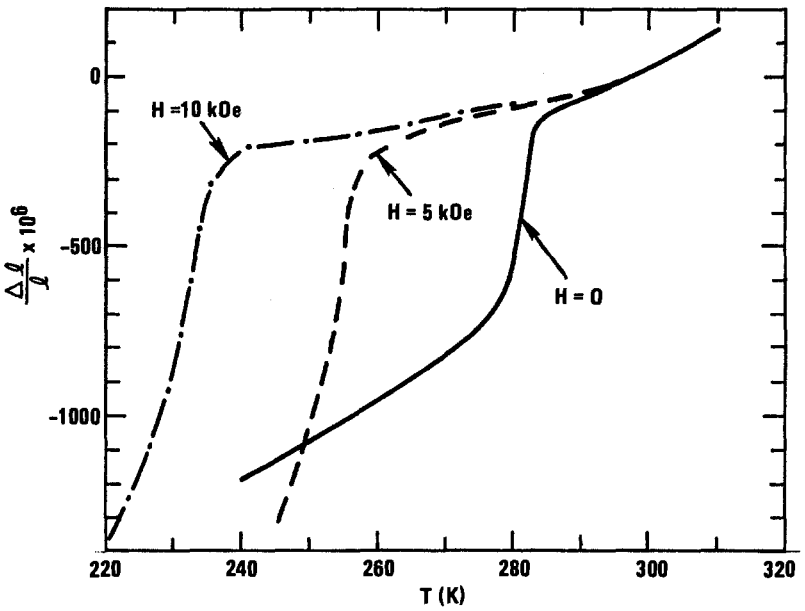

Fig. 26. Thermal expansion along [111] in single crystal $Tb_{0.27}Dy_{0.73}Fe_2$ (taken from Abbundi and Clark 1977).

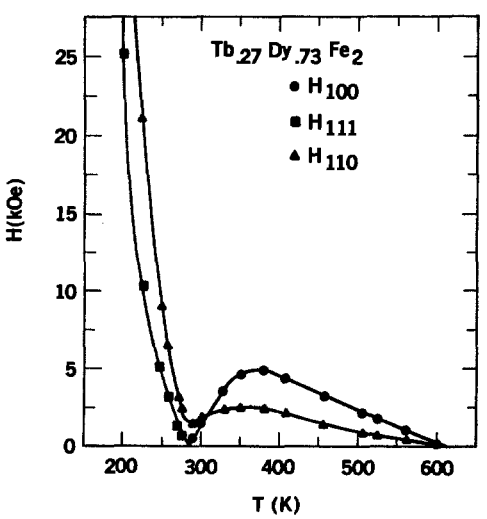

Fig. 27. Fields required for magnetic saturation along the principal directions in single crystal $Tb_{0.27}Dy_{0.73}Fe_2$ (taken from Clark et al. 1978).

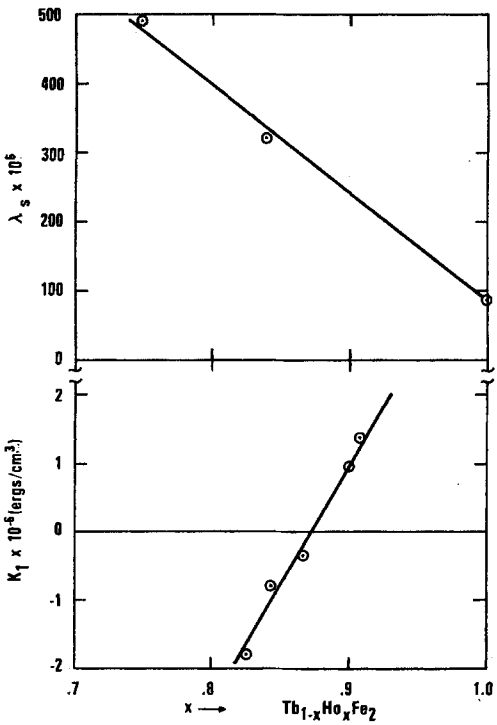

Fig. 28. Magnetostriction, λ_s, and magnetic anisotropy of $Tb_{1-x}Ho_xFe_2$ (taken from Koon et al. 1974, Williams, private communication).

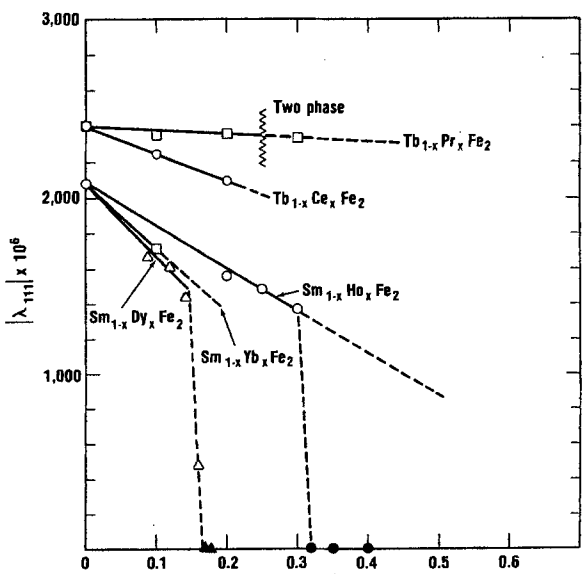

Fig. 29. λ_{111} of some $Tb_{1-x}R_xFe_2$ and $Sm_{1-x}R_xFe_2$ alloys. Open symbols are $|\lambda_{111}|$; solid symbols denote region where no spontaneous λ_{111} exists (taken from Clark et al. 1977).

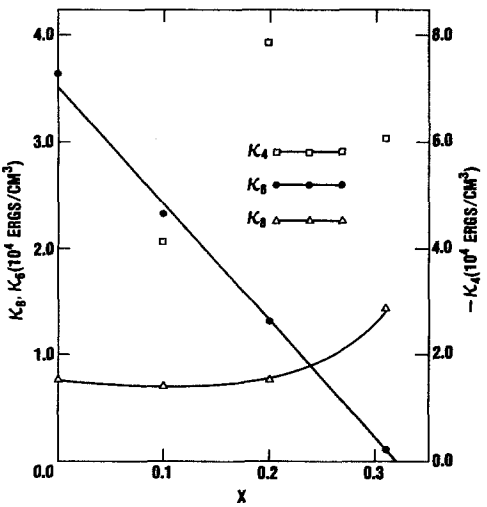

Fig. 30. Anisotropy constants κ_4, κ_6 and κ_8 for the compound $(Ho_{0.86}Tb_{0.14}Fe_2)_{1-x}(Dy_{0.7}Tb_{0.3}Fe_2)_x$ (taken from Williams and Koon 1977).

Values of the magnetostriction for some quaternary compounds are listed in table 13 of section 8.

In fig. 29, the absolute value of λ_{111} is plotted vs. x $(0 < x < 0.4)$ for the two Sm alloys $Sm_{1-x}Dy_xFe_2$ and $Sm_{1-x}Ho_xFe_2$. In these systems, both λ_{111} and K_1 compensate, as can be seen from the sign distribution in table 9. However, because of the relatively small anisotropy of $SmFe_2$, only small additions of Dy and Ho are needed for spin reorientation and anisotropy minimization. X-ray measurements show that reorientation occurs near $x = 0.12$ for $Sm_{1-x}Dy_xFe_2$ and near $x = 0.3$ for $Sm_{1-x}Ho_xFe_2$. The values of magnetostriction at these concentrations are large and negative. In both alloys, $|\lambda_{111}| > 1200 \times 10^{-6}$.

RFe_2 bimetallic strips composed of highly magnetostrictive alloys of both positive and negative polarity can exhibit huge flexural strains. The extent of the motion depends upon the magnetostrictions, strip length and strip thickness.

7. Elastic properties of RFe_2 compounds

Room temperature sound velocities, densities and moduli are listed in table 10 for polycrystalline $TbFe_2$, $ErFe_2$, YFe_2 and $TbFe_3$. The moduli are midway between those of the soft rare earth elements and the stiffer magnetic transition metals, such as Fe and Ni. The moderate magnitudes of the moduli and the huge magnitudes of the magnetostrictions combine to yield huge magnetoelastic forces and energies for these compounds. Values of λ_s, $E\lambda_s$ and the energy density, $\frac{1}{2}E\lambda_s^2$, are shown in table 10. They are compared to those of elemental Ni, a typical magnetostrictive material. The quantity $E\lambda_s$ is a measure of the pressure exerted by a constrained bar of the material which is magnetized to

TABLE 10
Elastic and magnetoelastic properties[a)]

	$TbFe_2$	$ErFe_2$	YFe_2	$TbFe_3$	Ni
v_l(m/sec)	3940	4120	4340	4230	–
v_s(m/sec)	1980	2180	2720	2320	–
ρ(g/cm^3)	9.1	9.7	6.7	9.4	–
$E \times 10^{-10}$ (newton/m^2)	9.4	12.1	12.7	13.1	21[b)]
$\lambda_s \times 10^6$	1750	−229	–	693	−31[c)]
$E\lambda_s \times 10^{-7}$ (newton/m^2)	17	2.8	–	9	0.7
$E\lambda_s^2/2 \times 10^{-3}$ (joule/m^3)	145	3.2	–	32	0.1

[a)] Clark et al. (1973b).
[b)] "Nickel", The International Nickel Co., Inc., (1951).
[c)] Went (1951).

saturation. The energy density, $\frac{1}{2}E\lambda_s^2$, represents the amount of magnetic energy which can be transformed to elastic energy per unit volume of the material. For $TbFe_2$ this energy is about 1000 times that of earlier magnetostrictive materials, such as Ni.

Rosen et al. (1973, 1974) have determined the Young's modulus and the shear modulus ultrasonically for the ternary $Tb_{1-x}Ho_xFe_2$ system and for $SmFe_2$ as a function of temperature. Their values are illustrated in fig. 31. Clearly defined depressions in the moduli occur where easy axis rotation takes place. (Refer to the spin reorientation diagram of fig. 23 and the magnetostriction data of fig. 12.) Young's moduli for a large number of binary RFe_2 compounds as a function of temperature are given in fig. 32 (Klimker et al. 1974).

Unprecedented changes in elastic moduli with magnetic field (ΔE effect) have been observed in the highly magnetostrictive RFe_2 compounds. In figs. 33 and 34 are plotted the relative changes in Young's modulus with field, $E_H - E_0$, normalized to the modulus at zero field E_0. ΔE effects are huge for the highly magnetostrictive $TbFe_2$ and $Tb_{0.3}Dy_{0.7}Fe_2$ compounds. Conventional ΔE effects, i.e. reductions in the modulus from their intrinsic high field values, have been generally associated with domain wall motion (see Bozorth 1951). However, in the RFe_2 compounds, the moduli continue to change far above technical saturation. Thus the major source of the field dependences cannot be attributed to the motion of domains, but to an intrinsic softening of the lattice due to local atomic magnetoelastic interactions. In this section we shall derive an expression for the softening in the shear modulus, c_{44}, by the second order contribution of the large magnetoelastic coupling, b_2.

It was shown in section 2 that a magnetostrictive system, composed of magnetic anisotropy, magnetoelastic energy and elastic energy components leads to the equilibrium strains

$$\epsilon_{ij}^{eq} = -(b_2/c_{44}^0)\alpha_i\alpha_j \tag{7.1}$$

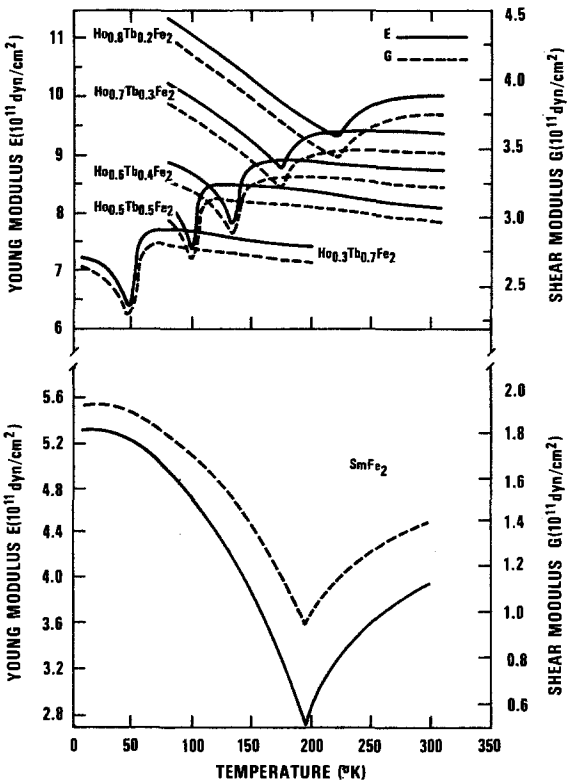

Fig. 31. Temperature dependence of Young's modulus, E, and shear modulus, G, for $Tb_{1-x}Ho_xFe_2$ and $SmFe_2$ (taken from Rosen et al. 1973, 1974).

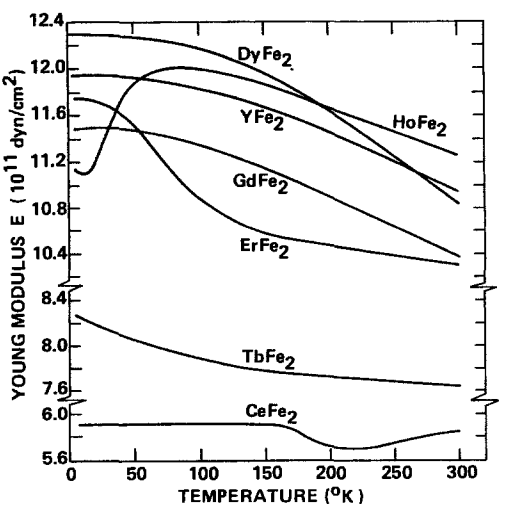

Fig. 32. Temperature dependence of the Young's moduli for the RFe_2 compounds (taken from Klimker et al. 1974).

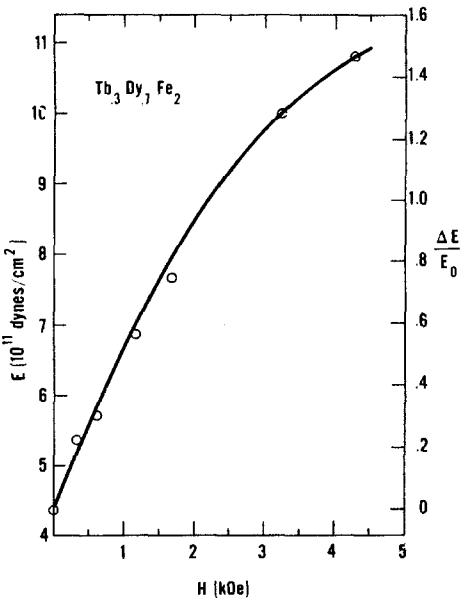

Fig. 33. Young's modulus and ΔE effect at room temperature for $Tb_{0.3}Dy_{0.7}Fe_2$, $\Delta E = E_H - E_0$ (taken from Clark and Savage 1975).

and to an effective anisotropy constant K_1'

$$K_1' = K_1 - (b_2^2/2c_{44}^0) \tag{7.2}$$

whenever $b_2 \gg b_1$. (The superscript "0" is added to c_{44} to label the "intrinsic" stiffness.) Thus as a function of the magnetization cosines, α_i, the total energy at constant stress (including magnetoelastic and elastic terms) becomes simply

$$E^\sigma = K_1'(\alpha_x^2\alpha_y^2 + \alpha_y^2\alpha_z^2 + \alpha_x^2\alpha_y^2) + \text{constant} \tag{7.3}$$

The dependent variables, the strains, have been eliminated. Only an effective anisotropy constant remains.

In like manner the effect of the magnetoelastic interaction on the elastic moduli and sound velocity can be readily calculated. Here, instead of the strains, ϵ_{ij}, being the dependent variables, the magnetization direction cosines, α_1, are the dependent variables and the elastic strains are the independent variables. To determine c_{44} we consider an arbitrary ϵ_{xy} strain, produced, for example, by an ultrasonic transducer, and calculate the equilibrium values of α_x, α_y and α_z. This ϵ_{xy} strain can be visualized as a shear wave polarized in the x [100] crystalline direction and propagating in the y [010] direction. In the following we: (1) assume $b_2 \gg b_1$, and (2) introduce the effect of an external field applied along x, such that the moment is nearly parallel to x ($\alpha_x \simeq 1$). For this case, the total energy expression [eq. (2.4)] becomes

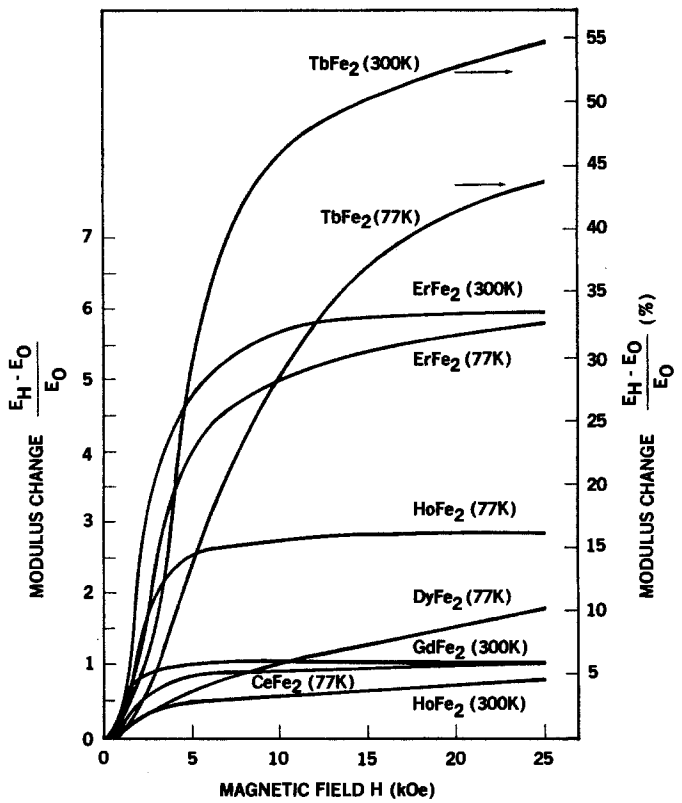

Fig. 34. Magnetic field dependence of the modulus change $(E_H - E_0)/E_0$ of the RFe_2 compounds (taken from Klimker et al. 1974).

$$E = K_1(\alpha_x^2\alpha_y^2 + \alpha_y^2\alpha_z^2 + \alpha_z^2\alpha_x^2) - HM\alpha_x + b_2\alpha_x\alpha_y\epsilon_{xy} + \tfrac{1}{2}c_{44}^0\epsilon_{xy}^2$$
$$+ b_2(\alpha_y\alpha_z\epsilon_{yz}^{eq} + \alpha_z\alpha_x\epsilon_{zx}^{eq}) + \tfrac{1}{2}c_{44}^0(\epsilon_{yz}^{eq\,2} + \epsilon_{zy}^{eq\,2}) \qquad (7.4)$$
$$+ \text{elastic terms in } \epsilon_{xx}, \epsilon_{yy} \text{ and } \epsilon_{zz}.$$

To determine the equilibrium values of α_i, the torque is set equal to zero. From the z component of the torque, it follows that

$$\alpha_x^{eq}\alpha_y^{eq} = -\frac{b_2}{2K_1 + MH}\epsilon_{xy}. \qquad (7.5)$$

From the y component, it follows (to lowest order)

$$\alpha_z^{eq} = 0. \qquad (7.6)$$

The equilibrium value α_x^{eq} can be approximated from eq. (7.5) using the relationship: $\alpha_x^2 = 1 - \alpha_y^2$. Thus

$$\alpha_x^{eq} \simeq 1 - \tfrac{1}{2}\alpha_y^2 = 1 - \frac{1}{2}\frac{b_2^2}{(2K_1 + MH)^2}\epsilon_{xy}^2. \qquad (7.7)$$

Substituting for $\alpha_x^{eq}\alpha_y^{eq}$ and for α_x^{eq} into eq. (7.4)

$$E = \frac{1}{2}\left(c_{44}^0 - \frac{b^2}{2K_1 + MH}\right)\epsilon_{xy}^2 - MH. \tag{7.8}$$

The coefficient of $\frac{1}{2}\epsilon_{xy}^2$, i.e. the effective elastic constant is

$$c_{44}^{eff} \equiv c_{44}^0 - \frac{b_2^2}{2K_1 + MH}. \tag{7.9}$$

For large b_2^2/K_1, the softening of the modulus can almost be complete. In terms of the measured anisotropy, K_1', eq. (7.9) becomes

$$\Delta c_{44} \equiv c_{44}^0 - c_{44}^{eff} = c_{44}^0\left(1 - \frac{K_1'}{K_1}\right)\left(\frac{1}{1 + MH/2K_1}\right). \tag{7.10}$$

The minimum c_{44} occurs when $K_1 = \frac{1}{2}b_2^2/c_{44}$, i.e. at the condition of magnetic isotropy ($K_1' = 0$). Equation (7.10) is valid for $H\|$ shear polarization, p. For the case of $H \perp p$, there is no magnetoelastic effect to lowest order ($\alpha_x = 0$) and the elastic modulus c_{44} remains stiff. Note that in metals, where eddy currents play a significant role, H must be replaced by $H + 4\pi M$.

In fig. 35 is plotted $(c_{44}^0 - c_{44}^{eff})^{-1}$ vs. H as measured by Cullen et al. (1978) in $Tb_{0.3}Dy_{0.7}Fe_2$. Here H is applied parallel to the shear polarization, p. The large b_2 has a profound effect on c_{44} and the corresponding sound velocity. From eq. (7.9) it is possible to determine both b_2^2 and K_1 graphically. They find $|b_2| = 2.3 \times 10^9$ erg/cm^3 and $K_1 = -3 \times 10^6$ erg/cm^3, which are in excellent agreement with the static measurements reported in section 3. In fig. 36, the coupled ($H\|p$) and uncoupled ($H \perp p$) moduli are plotted vs. H. For the c_{44} mode, the reduction in the intrinsic modulus is ~55%. The change in modulus is of the same order as

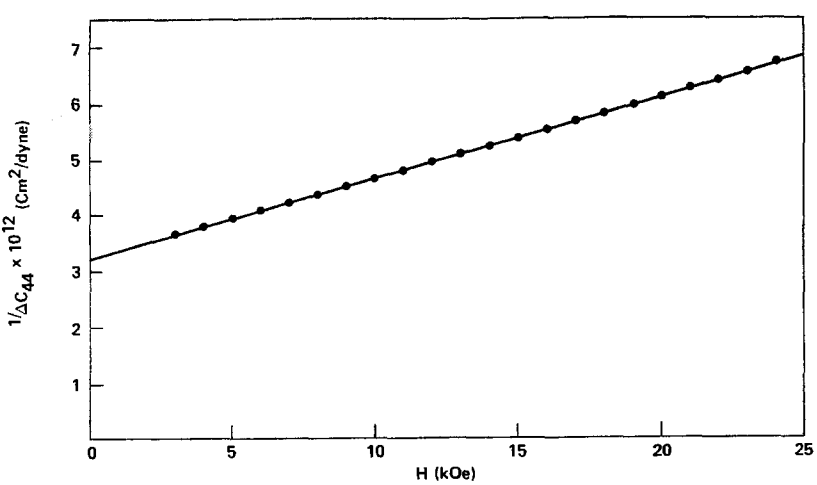

Fig. 35. The reciprocal of the difference in shear modulus, $1/(c_{44}^0 - c_{44})$ vs. magnetic field for $Tb_{0.3}Dy_{0.7}Fe_2$ (taken from Cullen et al. 1978).

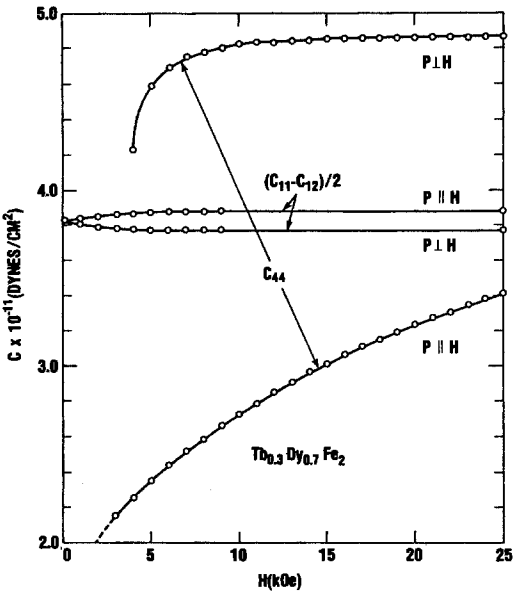

Fig. 36. Shear moduli c_{44} and $\frac{1}{2}(c_{11}-c_{12})$ for $Tb_{0.3}Dy_{0.7}Fe_2$ vs. magnetic field strength. The magnetic field was applied parallel and perpendicular to the shear polarization direction P (taken from Cullen et al. 1978).

the modulus itself. In contrast, the $\frac{1}{2}(c_{11}-c_{12})$ mode, for which the appropriate magnetoelastic coupling is b_1, has a small magnetoelastic contribution. (In fact, for this case, the coupled modulus is higher than the uncoupled modulus. This cannot be attributed to the lowest order magnetoelastic effects considered above.) Note that $c_{44}^0 > \frac{1}{2}(c_{11}-c_{12}) > c_{44}^{\text{eff}}$ at low fields. Thus elastic *isotropy* can be achieved with $H \| p$ at a sufficiently large applied magnetic field. Elastic isotropy can also be achieved for lower fields applied along intermediate directions. Experiments on $Tb_{0.3}Dy_{0.7}Fe_2$ by Rinaldi et al. (1977) have shown that as a field H is rotated from $H \| p$ to $H \perp p$, the modulus rises smoothly from the lower strongly coupled value to the higher uncoupled value. Thus by rotation of the magnetic field, the elastic anisotropy can be nullified and even inverted, with the application of a very low applied magnetic field.

The uncoupled elastic constants as measured ultrasonically on $Tb_{0.3}Dy_{0.7}Fe_2$ by Rinaldi et al. (1977) are given in table 11.

In-depth studies of the magnetoelastic behavior of the shear moduli and the sound velocity have also been made in the polycrystalline RFe_2 compounds at room temperature. Here, instead of a continuous change in shear modulus with field direction, the (degenerate) shear mode in the isotropic polycrystal breaks up into two modes, one polarized normal to the field and the other perpendicular (Cullen et al. 1978). Experimentally, two independent sound modes propagate whose intensities depend only upon field direction. Ultrasonic echo patterns taken for fields at various angles, θ, with respect to the direction of polarization of the

TABLE 11
Elastic constants of RFe_2 compounds* ($\times 10^{-11}$ dynes/cm^2)

	c_{11}	$\frac{1}{2}(c_{11}-c_{12})$	c_{44}°
$DyFe_2$	14.58	3.89	4.70
$Tb_{0.3}Dy_{0.7}Fe_2$	14.1	3.81	4.87

* Taken from Rinaldi et al. (1977, unpublished). c_{44} is a strong function of field. c_{44}° denotes the pure (uncoupled) elastic modulus (see text).

impinging sound wave, are shown in fig. 37 for amorphous $TbFe_2$. For $\theta = 0°$ and 90°, a single train of echoes is observed with those for $\theta = 0°$ reflecting the slower velocity. At intermediate angles, a superposition of the two patterns is observed, indicating the simultaneous propagation of two shear waves. The isotropy of the amorphous sample with respect to shear waves is broken by the magnetoelastic coupling.

The magnetic field dependences of both shear waves were measured in polycrystalline $Tb_{0.27}Dy_{0.73}Fe_2$, $Sm_{0.88}Dy_{0.12}Fe_2$, $Sm_{0.7}Ho_{0.3}Fe_2$ and amorphous $TbFe_2$ (a-$TbFe_2$) by Cullen et al. (1978) (see fig. 38). Two clearly separated modes

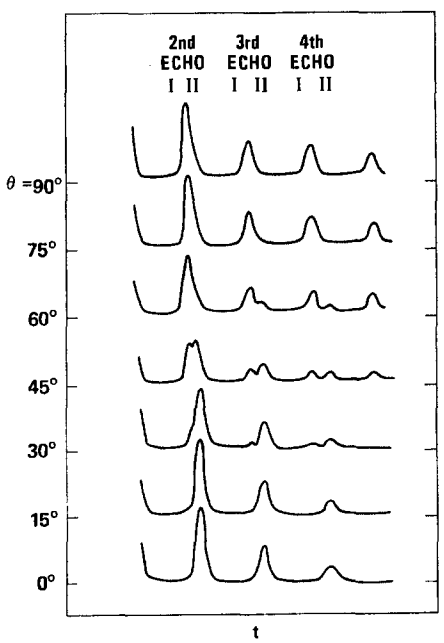

Fig. 37. Echo pattern for shear waves propagating perpendicular to the applied field H in amorphous $TbFe_2$. The changes in the amplitudes of the peaks as the angle θ between the direction of H and the polarization is varied indicate the presence of two normal modes with polarization parallel and perpendicular to H (taken from Cullen et al. 1978).

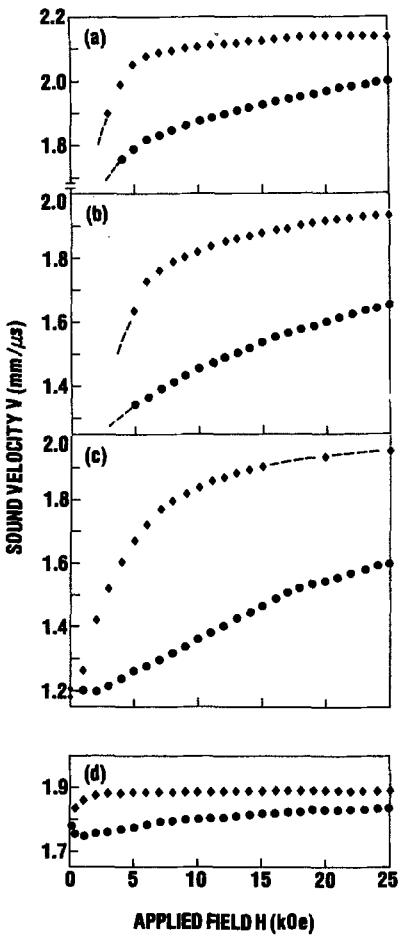

Fig. 38. Sound velocity as a function of applied field H for H parallel and perpendicular to the polarization p (● $H \| p$, ◆ $H \perp p$) in (a) $Tb_{0.3}Dy_{0.7}Fe_2$, (b) $Sm_{0.88}Dy_{0.12}Fe_2$, (c) $Sm_{0.7}Ho_{0.3}Fe_2$ and (d) a-$TbFe_2$ (taken from Cullen et al. 1978).

were observed. The velocity of the slow modes could not be saturated even at 25 kOe. By plotting the velocities of the fast mode vs. $1/H$, the intrinsic (uncoupled) elastic shear moduli, μ^0, were obtained. The values obtained in this way, along with the values of b_p calculated from the slope of $(\mu^0 - \mu)^{-1}$ vs. H plots are given in table 12.

In the preceding single crystal work it was assumed that $b_2 \gg b_1$. However, $b_1 \neq 0$. In a magnetostrictive system with b_1 and b_2 non-zero, the customary break in the shear degeneracy by the cubic crystal symmetry into the well known normal modes with polarization along the crystalline axes, may not occur. The magnitude and direction of the applied field, as well as the crystal symmetry, determine the normal modes.

TABLE 12
Uncoupled elastic moduli, μ^0, and magnetoelastic coupling, b_p, for polycrystalline RFe_2 at room temperature (M_s is in emu/cm^3, μ_0 in 10^{11} dynes/cm^2 and b_p in 10^9 ergs/cm^3)*

RFe_2	M_s	μ_0	b_p
$Tb_{0.3}Dy_{0.7}Fe_2$	780	4.3	1.3
$Sm_{0.88}Dy_{0.12}Fe_2$	360	3.4	1.4
$Sm_{0.7}Ho_{0.3}Fe_2$	145	3.5	0.9
a-$TbFe_2$	390	2.9	0.5

* Taken from Cullen et al. (1978).

For the general case of $b_1 \neq 0$ and $b_2 \neq 0$, the expressions for the shear velocities and moduli as a function of field angle θ and magnitude H are given by Rinaldi and Cullen (1978). For propagation along [1$\bar{1}$0] they find

$$v_{\pm}^2 = \tfrac{1}{2}(C + C') \pm [(\tfrac{1}{4}(C + C')^2 + B^2]^{1/2} \tag{7.11}$$

where

$$C = c_{44}^0/\rho - b_2^2 \cos^2\theta/HM_s\rho$$
$$C' = \tfrac{1}{2}(c_{11}^0 - c_{12}^0)/\rho - b_1^2 \sin^2\theta/HM_s\rho$$
$$B = b_1 b_2 \sin\theta \cos\theta/HM_s\rho.$$

θ is the angle of the applied field with respect to the [001] direction.

If $B = 0$, the two conventional transverse shear waves are polarized along [100] and [110] directions with velocities $C^{1/2}$ and $C'^{1/2}$. When $B \neq 0$, the polarization is determined by the strength of B according to the following expression

$$\tan\Phi_{\pm} = B/[\tfrac{1}{2}(C' - C) \pm (\tfrac{1}{4}(C' - C)^2 + B^2)^{1/2}] \tag{7.12}$$

where Φ is the angle of the polarization with respect to the [001] axis.

In fig. 39 are plotted the values of Φ and v vs. the field angle θ for $Tb_{0.27}Dy_{0.73}Fe_2$, taking $b_2 = -2.3 \times 10^9$ ergs/cm^3 and assuming $b_1 = 0.1b_2$. Note that the large change in Φ occurs over a small change in θ near $\theta = 45°$ for $H = 8$ kOe. This pulling of the polarization away from the crystal axis has been demonstrated in $Tb_{0.3}Dy_{0.7}Fe_2$ by Cullen et al. (1978).

8. Magnetomechanical coupling of RFe_2 compounds

Because of their large magnetostriction the rare earth–Fe_2 compounds have potential as high power transduction elements. In this section the low signal linear properties of these compounds will be examined.

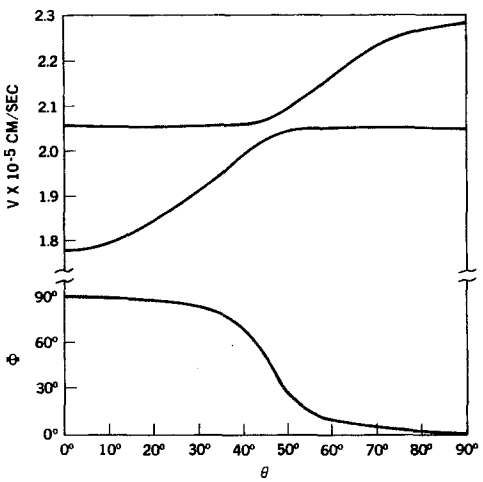

Fig. 39. Calculated dispersion and direction of polarization of one of the shear normal modes vs. the orientation of the magnetization for [110] propagation in $Tb_{0.3}Dy_{0.7}Fe_2$. The magnetization is in the (110) plane at an angle θ from the [001]. $H = 8$ kOe (taken from Cullen et al. 1978).

The single most important low signal transducer parameter is the magneto-mechanical coupling factor, k. For a magnetomechanical vibrator with no loss or radiation, k^2 denotes the fraction of magnetic energy which can be converted to mechanical (elastic) energy per cycle, or conversely, the fraction of stored mechanical (elastic) energy which can be converted to magnetic energy. For a mechanically driven system $(1-k^2)E_{el} = k^2 E_{mag}$. The relation between k^2 and the conventional linear properties of a magnetomechanically coupled system can be obtained starting with the definition of the compliance s^H, permeability μ^T and coupling d through the following equations

$$\epsilon = s^H T + dH \tag{8.1a}$$

$$B = dT + \mu^T H. \tag{8.1b}$$

Here ϵ, B, T and H symbolically represent components of the strain, magnetic induction, stress and magnetic field (see for example Berlincourt et al. 1964). Eliminating T and H respectively from eq. (8.1)

$$B = (d/s^H)\epsilon + \mu^T(1 - d^2/s^H\mu^T)H \tag{8.2a}$$

$$\epsilon = s^H(1 - d^2/s^H\mu^T)T + (d/\mu^T)B. \tag{8.2b}$$

Thus, defining the permeability at constant strain μ^ϵ and the compliance at constant induction s^B (blocked conditions), it follows that

$$\mu^\epsilon = (1 - d^2/s^H\mu^T)\mu^T \tag{8.3}$$

$$s^B = (1 - d^2/s^H\mu^T)s^H. \tag{8.4}$$

Writing eq. (8.4) in terms of moduli $c \equiv 1/s$

$$c^H = (1 - d^2/s^H\mu^T)c^B. \tag{8.5}$$

In effect, the permeability is reduced from its intrinsic value μ^T whenever energy is transferred to the elastic system. At constant strain the maximum energy is stored in the elastic system. Likewise, the intrinsic (uncoupled) elastic stiffness, c^B, is reduced to a lower value c^H when energy is transferred from the elastic to the magnetic system. Energy is transferred whenever the moment is rotated from its equilibrium value by an applied stress. The maximum fraction of magnetic energy which can be transformed is

$$\frac{\frac{1}{2}\mu^T H^2 - \frac{1}{2}\mu^\epsilon H^2}{\frac{1}{2}\mu^T H^2} = \frac{\mu^T - \mu^\epsilon}{\mu^T} = \frac{d^2}{s^H\mu^T} = k^2. \tag{8.6}$$

Similarly the maximum fraction of elastic energy which can be transformed is

$$\frac{\frac{1}{2}c^B\epsilon^2 - \frac{1}{2}c^H\epsilon^2}{\frac{1}{2}c^B\epsilon^2} = \frac{c^B - c^H}{c^B} = \frac{d^2}{s^H\mu^T} = k^2. \tag{8.7}$$

The magnetomechanical coupling k is conventionally obtained by measuring the complex impedance of a coil containing the magnetostrictive material. A material coupling factor k_{33} is defined which is geometry independent. For a torroid $k_{33} = k$; for a slender rod $k_{33} \cong (\pi/\sqrt{8})k$. A successful method was developed by Savage et al. (1975) to determine the complex impedance for the low permeability $R\text{Fe}_2$ alloys as a function of frequency. The magnetomechanical coupling k_{33}, quality factor Q and permeability μ for $\text{Tb}_{0.3}\text{Dy}_{0.7}\text{Fe}_2$ calculated this way are shown

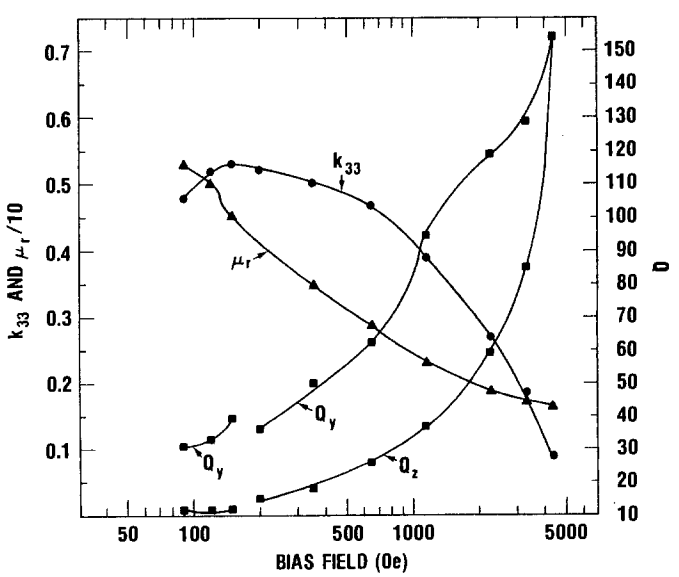

Fig. 40. Coupling factor k_{33}, Q factor and relative permeability μ_r, of $\text{Tb}_{0.3}\text{Dy}_{0.7}\text{Fe}_2$ as a function of bias field. Q_z, the quality factor at constant current drive, includes both mechanical and electrical losses, whereas Q_y, the quality factor at constant voltage drive, includes only mechanical losses (taken from Savage et al. 1975).

in fig. 40 as a function of magnetic bias. The coupling factor is high when the field is between 100 and 500 Oe. Note that the permeability is low, a necessary consequence of a highly magnetostrictive *polycrystal.*

In fig. 41 are plotted the resonant and antiresonant frequencies of a 10 cm thin rod of $Tb_{0.3}Dy_{0.7}Fe_2$ driven magnetically. The resonant frequency differs from the antiresonant frequency at each bias field by an amount related to the coupling. At resonance (maximum change in magnetic induction with fixed magnetic drive H), the bar executes motion at frequency $f^H = v^H/\lambda = (c^H/\rho)^{1/2}/\lambda$, whereas at antiresonance B executes minimum oscillation and the bar vibrates at $f^B = v^B/\lambda = (c^B/\rho)^{1/2}/\lambda$. Thus, from eq. (8.7), neglecting loss terms

$$k^2 = 1 - (f^H/f^B)^2. \tag{8.8}$$

Also, as seen in fig. 41, in a highly magnetostrictive polycrystal both f^B and f^H depend strongly upon applied magnetic field. The change in f^B and f^H with magnetic field reflects the moduli change (ΔE effect) discussed in section 7. It is solely magnetoelastic in origin. The change can be divided into two parts, one macroscopic, due to domain wall motion, and the other microscopic, due to the atomic interaction between the magnetic moment and the local strain field within the domain. In most conventional materials, e.g. Ni, the major contribution arises during the magnetization process by a redistribution of the domains. This induced redistribution due to the pressure field causes a reduction in the modulus. The domain free material at technical saturation is stiffer. Above technical saturation, an externally imposed elastic stress rotates the moment slightly from its aligned condition, allowing the storage of energy in the magnetic system. The amount of rotation depends upon the externally applied field and

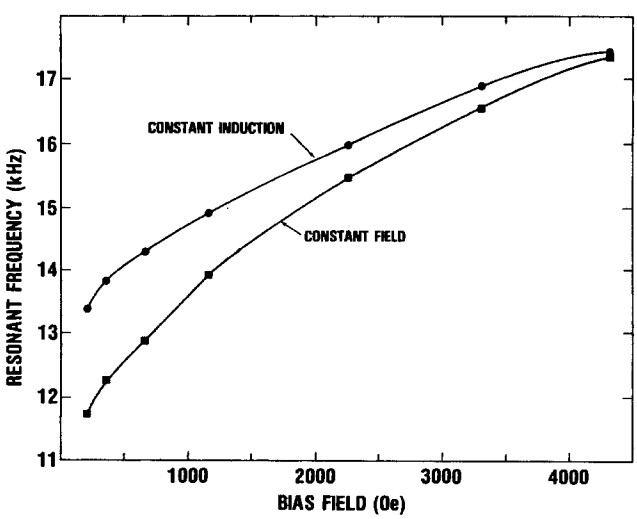

Fig. 41. Resonant frequency (at constant induction and constant field) vs. bias field of a 10 cm bar of $Tb_{0.3}Dy_{0.7}Fe_2$ (taken from Savage et al. 1975).

any magnetocrystalline anisotropy. Only when the magnetic system is blocked ($H \to \infty$) is it possible to keep the energy totally within the elastic system and obtain the stiff modulus, c^B. The modulus and ΔE effect at constant field, calculated from f^H for $Tb_{0.3}Dy_{0.7}Fe_2$ is plotted in fig. 33. The increase in modulus is about 150%.

In fig. 42, k_{33} is plotted vs. x for the ternary $Tb_{1-x}Dy_xFe_2$ and $Tb_{1-x}Ho_xFe_2$ alloys. With the addition of $DyFe_2$ and $HoFe_2$ to $TbFe_2$, the values of k_{33} increase to a peak $k_{33} \simeq 0.6$ for $Tb_{0.26}Dy_{0.74}Fe_2$ and $k_{33} \simeq 0.44$ for $Tb_{0.25}Ho_{0.75}Fe_2$. Further increases in k_{33} are observed in the quaternary $Tb_xDy_yHo_zFe_2$ system. In table 13, are listed the magnetomechanical coupling factors for a number of rare earth–Fe_2 materials along with those of a few typical magnetostrictive materials. The largest coupling factors are found in grain oriented RFe_2 alloys.

Eddy current losses, which exist in metallic transducers, become important for high frequency applications. In fig. 43 electrical resistivity measurements for $TbFe_2$ are plotted as a function of temperature. At room temperature, its value, while comparable to that of the rare earth elements, is much larger than that of Ni and Fe.

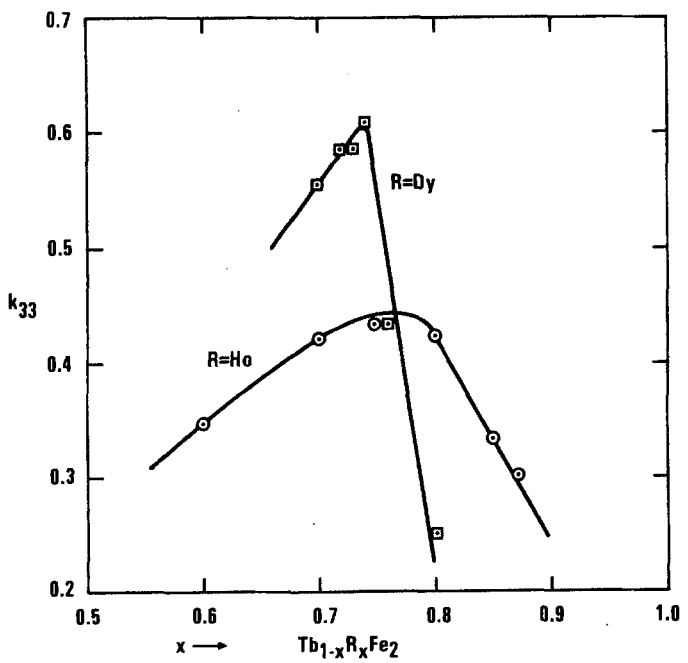

Fig. 42. Magnetomechanical coupling, k_{33}, for $Tb_{1-x}Dy_xFe_2$ and $Tb_{1-x}Ho_xFe_2$ (taken from Savage et al. 1975, Timme 1976).

TABLE 13
Maximum magnetomechanical coupling factor and magnetostriction

	k_{33}	$\lambda_{100} \times 10^6$	$\lambda_{111} \times 10^6$	Reference
Ni	0.31	−51	−23	a, c
13% Al 87% Fe		70	8	b, c
50% Co 50% Fe	0.35	30	160	d, c
4.5% Co 95.5% Ni	0.51	−30	−40	e, f
$(NiO)_{0.913}(CoO)_{0.027}$ $(FeO)_{0.06}(Fe_2O_3)$	0.36	–	–	g
$TbFe_2$	0.35	–	2450	h
$Tb_{0.5}Dy_{0.5}Fe_2$	0.51	–	1840	h
$Tb_{0.27}Dy_{0.73}Fe_2$	0.53–0.60	–	1620	i
$Tb_{0.23}Dy_{0.35}Ho_{0.42}Fe_2$	0.61–0.62	–	1130	i
$Tb_{0.20}Dy_{0.22}Ho_{0.58}Fe_2$	0.60–0.66	–	820	i
$Tb_{0.19}Dy_{0.18}Ho_{0.03}Fe_2$	0.59	–	810	i
$SmFe_2$	0.35	–	−2100	h
$Sm_{0.88}Dy_{0.12}Fe_2$	0.55	–	−1620	j
$Sm_{0.7}Ho_{0.3}Fe_2$	0.35	–	−1370	j
$Tb_{0.23}Ho_{0.77}Fe_2$(oriented)	0.76	–	710	k
$Tb_{0.27}Dy_{0.73}Fe_2$(oriented)	0.74	–	1620	h

[a] Bozorth and Hamming (1953).
[b] Hall (1959).
[c] See Davis (1977).
[d] Hall (1960).
[e] Yamamoto and Nakamichi (1958).
[f] Clark (1956).
[g] Ferebee and Davis (1958).
[h] Savage and Clark, unpublished.
[i] Savage et al. (1977).
[j] Savage and Clark (1977).
[k] Timme, unpublished.

9. Amorphous RFe_2 alloys

Sputtered alloys of composition RFe_2 are both structurally and magnetically amorphous (see Rhyne et al. 1972). Curie temperatures range from below room temperature to ~400 K. A most striking feature of these alloys is the large coercivity at low temperatures (Clark 1973, Rhyne et al. 1974). This is attributed to the combination of high anisotropy and the absence of crystal structure. The maximum energy product calculated for amorphous $TbFe_2$ at 4 K is 29.5×10^6 GOe, which is comparable to the largest measured value for Sm–Co alloys. While the intrinsically high magnetic anisotropy of the rare earth persists to room temperature, the thermal energy is too high to inhibit magnetization reversal. Consequently coercivities of only ~100 Oe are observed at room temperature.

Like the anisotropy, large magnetostrictions are found in the amorphous state (Clark 1973). Forester et al. (1978) have reported magnetostrictions greater than 200×10^{-6} for $0.25 < x < 0.45$ in amorphous Tb_xFe_{1-x}. The room temperature magnetostrictions of amorphous $TbFe_2$, $Tb_{0.3}Dy_{0.7}Fe_2$ and $DyFe_2$ are shown in fig. 44. $TbFe_2$ has a large unsaturated magnetostriction and $DyFe_2$ has a spontaneous

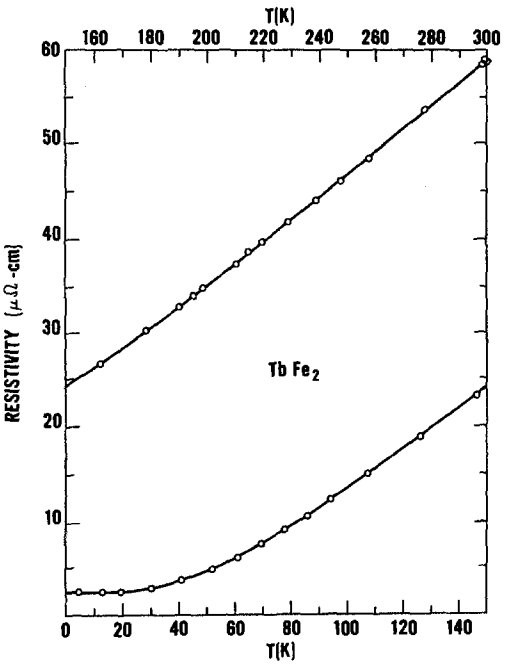

Fig. 43. Resistivity of $TbFe_2$ vs. temperature (taken from Savage; see Clark 1974).

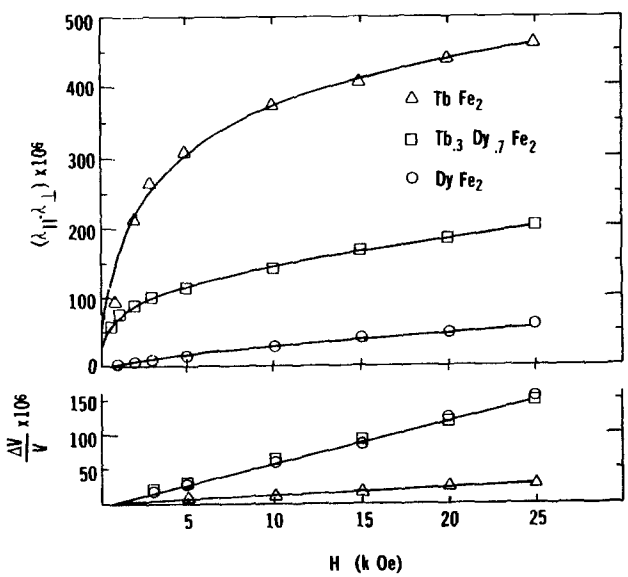

Fig. 44. Magnetostriction of amorphous $TbFe_2$, $Tb_{0.3}Dy_{0.7}Fe_2$ and $DyFe_2$ at room temperature (taken from Clark 1973, unpublished).

magnetostriction near zero. This difference is accounted for by the difference in Curie temperatures. For amorphous $TbFe_2$, $T_C >$ room temperature; for amorphous $DyFe_2$, $T_C <$ room temperature. Unlike crystalline $DyFe_2$, where $d\lambda/dT < 0$, the magnetostriction of amorphous $DyFe_2$ increases rapidly with decreasing temperature (fig. 45). Similar to the RFe_2 compounds, the highly magnetostrictive amorphous alloys can also exhibit a large forced magnetostriction at room temperature.

10. Summary

The RFe_2 alloys (R = Sm Tb, ...) derive their magnetostrictive effects from the large anisotropic 4f charge density of the R^{3+} ions. Because of strong Fe–Fe and Fe–R exchange interactions, the large intrinsic zero temperature magnetostriction is preserved more-or-less intact up to room temperature. An unusual magnetostriction anisotropy ($|\lambda_{111}/\lambda_{100}| \gg 1$) characterizes many of these compounds. Thus in polycrystalline materials, the magnetostriction and magnetomechanical coupling is strongly dependent upon crystallite orientation. The high anisotropy of the 4f electron cloud and high Curie temperatures lead to huge cubic magnetocrystalline anisotropies at room temperature as well as large magnetostrictions. In $TbFe_2$ and $DyFe_2$ the anisotropy is over an order of magnitude larger than that of conventional ferro- and ferrimagnetic cubic materials. The strong magnetoelastic coupling also manifests itself in huge magnetically

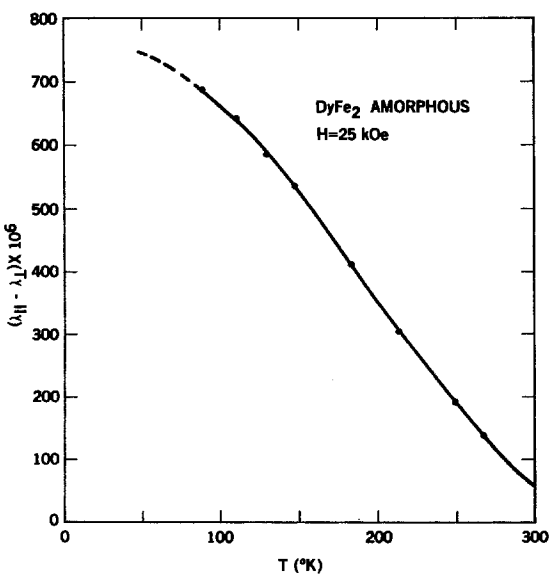

Fig. 45. Magnetostriction of amorphous $DyFe_2$ vs. temperature (taken from Abbundi and Clark, unpublished).

induced moduli changes. This huge "ΔE effect" reflects the $|\lambda_{111}/\lambda_{100}| > 1$ anisotropy. Because of the cubic symmetry of the Laves phase RFe_2 compounds (unlike the hexagonal heavy rare earth elements), the lowest order anisotropy and magnetostriction possess different sign sequences as R is changed from one element to another. Thus pseudobinary RFe_2 compounds, where R is composed of various rare earths, can be synthesized to exhibit a wide assortment of magnetic properties.

Acknowledgements

The author would like to thank his many co-workers: H.S. Belson, H.T. Savage, J.R. Cullen, R. Abbundi, E. Callen, N. Tamagawa and K. Sato, whose assistance made this chapter possible. Special thanks are due to E. Callen and R. Abbundi for critically reading the manuscript. The author is particularly grateful to N.C. Koon, C.M. Williams, J.J. Rhyne, R.W. Timme and A.E. Miller for many valuable discussions and for permission to include their work prior to publication.

Appendix A: Magnetostriction and magnetic anisotropy of cubic and hexagonal crystals

In computing the crystal field matrix elements for the rare earth ions, $\langle 4f|V_c|4f\rangle$, the required integrals are of the form: $\int \Psi_{4f} V_{l'}^{m} \Psi_{4f}\, d\Omega$. For the rare earths, where $l = 3$, the integrals vanish for $l' > 6$. While in many cases it is possible to fit the experimental data with the lowest order magnetostriction constants, e.g. λ_{100} and λ_{111}, within first order perturbation theory we can expect terms to exist up to sixth degree. The proper expression for the magnetostriction for a particular symmetry can be determined by taking the direct product of the basis functions of the same irreducible representation, one function in the strain space and the other in the space of the magnetization. In this way magnetostriction and magnetic anisotropy expressions are generated which not only manifestly reflect the crystal symmetry, but are also orthogonal. Using orthogonal functions has the advantage that the coefficients of the lower order terms do not change as higher order terms are added. In addition, the coefficients of these terms possess characteristic temperature dependences (Callen and Callen 1963).

Expressions for the magnetostriction and magnetic anisotropy to sixth degree in the direction cosines of the magnetization are given below. They are derived from the cubic and hexagonal basis functions of table 1. (Bell 1954).

(a) Cubic:

$$\begin{aligned}\Delta l/l = {} & \lambda^{\alpha,0} + \lambda^{\alpha,4}\{\alpha_x^4 + \alpha_y^4 + \alpha_x^4 - \tfrac{3}{5}\} \\ & + \lambda^{\alpha,6}\{\alpha_x^2\alpha_y^2\alpha_z^2 + \tfrac{1}{22}[\alpha_x^4 + \alpha_y^4 + \alpha_z^4 - \tfrac{3}{5}] - \tfrac{1}{105}\} \\ & + \lambda^{\gamma,2}\{\alpha_x^2\beta_x^2 + \alpha_y^2\beta_y^2 + \alpha_z^2\beta_z^2 - \tfrac{1}{3}\} \\ & + \lambda^{\gamma,4}\{\alpha_x^4\beta_x^2 + \alpha_y^4\beta_y^2 + \alpha_z^4\beta_z^2 - \tfrac{1}{3}[\alpha_x^4 + \alpha_y^4 + \alpha_z^4] \\ & \qquad - \tfrac{6}{7}[\alpha_x^2\beta_x^2 + \alpha_y^2\beta_y^2 + \alpha_z^2\beta_z^2 - \tfrac{1}{3}]\}\end{aligned}$$

$$+\lambda^{\gamma,6}\{\alpha_x^6\beta_x^2+\alpha_y^6\beta_y^2+\alpha_z^6\beta_z^2-\tfrac{1}{3}[\alpha_x^6+\alpha_y^6+\alpha_z^6]$$
$$-\tfrac{15}{11}[\alpha_x^4\beta_x^2+\alpha_y^4\beta_y^2+\alpha_z^4\beta_z^2-\tfrac{1}{3}(\alpha_x^4+\alpha_y^4+\alpha_z^4)]$$
$$+\tfrac{5}{11}(\alpha_x^2\beta_x^2+\alpha_y^2\beta_y^2+\alpha_z^2\beta_z^2-\tfrac{1}{3})\}$$
$$+\lambda^{\epsilon,2}\{\alpha_x\alpha_y\beta_x\beta_y+\alpha_y\alpha_z\beta_y\beta_z+\alpha_z\alpha_x\beta_z\beta_x\}$$
$$+\lambda^{\epsilon,4}\{(\alpha_z^2-\tfrac{1}{7})\alpha_x\alpha_y\beta_x\beta_y+\text{C.P.}\}$$
$$+\lambda^{\epsilon,6}\{[\alpha_z^2-\tfrac{6}{11}\alpha_z^2+\tfrac{1}{33}]\alpha_x\alpha_y\beta_x\beta_y+\text{C.P.}\}$$
$$+\lambda^{\epsilon,6'}\{[\alpha_x^4+\alpha_y^4-\tfrac{10}{3}\alpha_x^2\alpha_y^2]\alpha_x\alpha_y\beta_x\beta_y+\text{C.P.}\}.$$

Note for $l\leq 2$, $\lambda_{100}=\frac{2}{3}\lambda^{\gamma,2}$ and $\lambda_{111}=\frac{1}{3}\lambda^{\epsilon,2}$.

$$E_a=K^{\alpha,4}\{\alpha_x^2\alpha_y^2+\alpha_y^2\alpha_z^2+\alpha_z^2\alpha_x^2-\tfrac{1}{5}\}$$
$$+K^{\alpha,6}\{\alpha_x^2\alpha_y^2\alpha_z^2-\tfrac{1}{11}(\alpha_x^2\alpha_y^2+\alpha_y^2\alpha_z^2+\alpha_z^2\alpha_x^2-\tfrac{1}{5})-\tfrac{1}{105}\}.$$

The conventional cubic anisotropy constants K_1 and K_2 are related to the symmetry constants by $K_1=-K^{\alpha,4}-\frac{1}{11}K^{\alpha,6}$ and $K_2=K^{\alpha,6}$.

(b) Hexagonal:

$$\Delta l/l=\{\lambda_1^{\alpha,0}+\lambda_1^{\alpha,2}(\alpha_z^2-\tfrac{1}{3})+\lambda_1^{\alpha,4}(\alpha_z^4-\tfrac{6}{7}\alpha_z^2+\tfrac{3}{35})$$
$$+\lambda_1^{\alpha,6}(\alpha_z^6-\tfrac{15}{11}\alpha_z^4+\tfrac{5}{11}\alpha_z^2-\tfrac{5}{231})$$
$$+\lambda_1^{\alpha,6'}(\alpha_x^6-15\alpha_x^4\alpha_y^2+15\alpha_x^2\alpha_y^4-\alpha_y^6)\}(\beta_x^2+\beta_y^2)$$
$$+\{\lambda_2^{\alpha,0}+\lambda_2^{\alpha,2}(\alpha_z^2-\tfrac{1}{3})+\lambda_2^{\alpha,4}(\alpha_z^4-\tfrac{6}{7}\alpha_z^2+\tfrac{3}{35})$$
$$+\lambda_2^{\alpha,6}(\alpha_z^6-\tfrac{15}{11}\alpha_z^4+\tfrac{5}{11}\alpha_z^2-\tfrac{5}{231})$$
$$+\lambda_2^{\alpha,6'}(\alpha_x^6-15\alpha_x^4\alpha_y^2+15\alpha_x^2\alpha_y^4-\alpha_y^6)\}\beta_z^2$$
$$+\{\lambda^{\gamma,2}+\lambda^{\gamma,4}(\alpha_z^2-\tfrac{1}{7})+\lambda^{\gamma,6}(\alpha_x^4-\tfrac{6}{11}\alpha_z^2+\tfrac{1}{33})\}$$
$$\times\{\alpha_x\alpha_y\beta_x\beta_y+\tfrac{1}{4}(\alpha_x^2-\alpha_y^2)(\beta_x^2-\beta_y^2)\}$$
$$+\{\lambda^{\gamma,4'}+\lambda^{\gamma,6'}(\alpha_z^2-\tfrac{1}{11})\}$$
$$\times\{\alpha_x\alpha_y(\alpha_y^2-\alpha_x^2)\beta_x\beta_y+\tfrac{1}{8}(\alpha_x^4-6\alpha_x^2\alpha_y^2+\alpha_y^2)(\beta_x^2-\beta_y^2)\}$$
$$+\{\lambda^{\epsilon,2}+\lambda^{\epsilon,4}(\alpha_z^2-\tfrac{3}{7})+\lambda^{\epsilon,6}(\alpha_z^4-\tfrac{10}{11}\alpha_z^2+\tfrac{5}{33})\}$$
$$\times\{\alpha_z\alpha_x\beta_z\beta_x+\alpha_z\alpha_y\beta_z\beta_y\}$$
$$+\lambda^{\epsilon,6'}\{\alpha_z\alpha_x(\alpha_x^4-10\alpha_x^2\alpha_y^2+5\alpha_y^4)\beta_z\beta_x+\alpha_z\alpha_y(5\alpha_x^4-10\alpha_x^2\alpha_y^2+\alpha_y^4)\beta_z\beta_y\}.$$

$$E_a=K^{\alpha,2}\{\alpha_z^2-\tfrac{1}{3}\}+K^{\alpha,4}\{\alpha_z^4-\tfrac{6}{7}\alpha_z^2+\tfrac{3}{35}\}$$
$$+K^{\alpha,6}\{\alpha_z^6-\tfrac{15}{11}\alpha_z^4+\tfrac{5}{11}\alpha_z^2-\tfrac{5}{231}\}$$
$$+K^{\alpha,6'}\{\alpha_x^6-15\alpha_x^4\alpha_y^2+15\alpha_x^2\alpha_y^4-\alpha_y^6\}.$$

Appendix B: Temperature dependences of magnetostriction and magnetic anisotropy for single-ion models

The magnetostriction and magnetocrystalline anisotropy of a magnetic system derive from spin operators which have the functional form of the basis functions found in table 1, of section 2 (see Callen and Callen 1963). The temperature

dependences of these quantities depend upon the thermal averages of these operators over the allowed energy states. Thus a calculation of temperature dependences require the quantum statistical averages of such quantities as (Stevens 1952)

$$\langle J_z^2 - J(J+1)\rangle,$$
$$\langle 35J_z^4 - 30J(J+1)J_z^2 + 25J_z^2 - 6J(J+1) + 3J^2(J+1)^2\rangle \quad \text{and}$$
$$\langle 231J_z^6 - 315J(J+1)J_z^4 + 735J_z^4 + 105J^2(J+1)^2J_z^2 - 525J(J+1)J_z^2 + 294J_z^2 - 5J^3(J+1)^3 + 40J^2(J+1)^2 - 60J(J+1)\rangle,$$

for $l = 2$, $l = 4$ and $l = 6$ respectively. Callen and Shtrickman (1965) have shown that for a large number of theories of ferromagnetism, these averages can be expressed in terms of the moment $\langle J_z\rangle$ itself. These (single-ion) theories include not only molecular field theory, but those collective excitation theories (i.e., spin waves, random field approximation, other Green's function decoupling) in which the quasiparticle levels are equally spaced and ordered like J_z quantum states. In the limit of large J, in the molecular field approximation, these averages take the simple form of the following hyperbolic Bessel functions

$$\langle J_z\rangle \quad \to \mathcal{L}(x) = -1/x + \operatorname{ctnh} x = m$$
$$\langle J_z^2 - J(J+1)\rangle \to \hat{I}_{5/2}(x) = (3/x^2 + 1) - (3/x)\operatorname{ctnh} x$$
$$\langle 35J_z^4 \ldots\rangle \quad \to \hat{I}_{9/2}(x) = (105/x^2 + 45/x + 1) - (105/x^3 + 10/x)\operatorname{ctnh} x$$

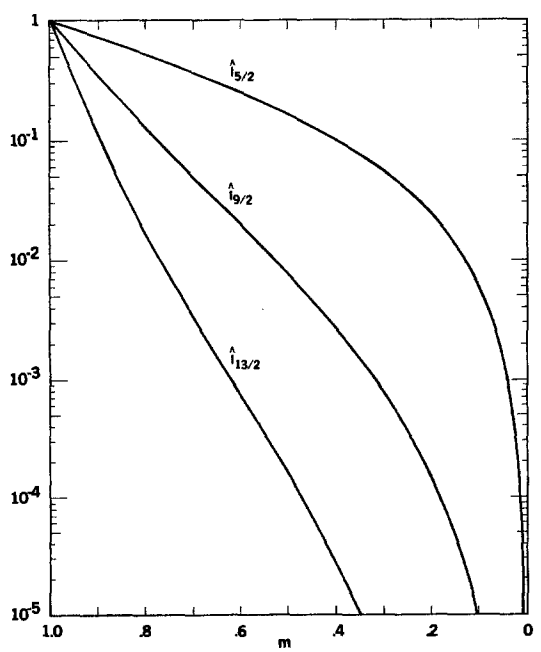

Fig. 46. Normalized hyperbolic Bessel functions $\hat{I}_{5/2}$, $\hat{I}_{9/2}$ and $\hat{I}_{13/2}$ vs. the normalized magnetization, m.

$$\langle 231 J_z^6 \ldots \rangle \quad \rightarrow \hat{I}_{13/2}(x) = (11{\cdot}945/x^6 + 4725/x^4 + 210/x^2 + 1) - (11{\cdot}945/x^5 + 1210/x^3 + 21/x)\,\mathrm{ctnh}\,x.$$

The parameter "x" can be eliminated from these relationships, yielding expressions of the form $\hat{I}_{l+1/2}[\mathcal{L}^{-1}(m)]$ from which eq. (4.3) and eq. (5.1) follow directly.

In fig. 46, $\hat{I}_{5/2}$, $\hat{I}_{9/2}$ and $\hat{I}_{13/2}$ are plotted vs. the reduced magnetization, m. All expressions are normalized to one at $T = 0$ K. From this figure the temperature dependences of the magnetostriction and anisotropy can be directly related to the temperature dependence of the empirically determined magnetization. *The temperature dependences found in this way are independent of the details of the magnetic model.* The hyperbolic Bessel function is a good approximation for the heavy rare earth ions with large J.

References

Abbundi, R. and A.E. Clark, 1977, IEEE Trans. Mag. **MAG–13**, 1519.

Abbundi, R. and A.E. Clark, 1978, J. Appl. Phys. **49**, 1969. Also NSWC/WOL/TR 78-88, Naval Surface Weapons Center, Dahlgren, VA 22448, USA; Proc, Int. Conf. on Magnetism ICM–79, Munich, Sept. 1979.

Abbundi, R., A.E. Clark and N.C. Koon, 1979, J. Appl. Phys. **50**, 1671.

Akulov, N.S., 1928, Z. Physik **52**, 389.

Atzmony, U., M. Dariel, E. Bauminger, D. Lebenbaum, I. Nowik and S. Offer, 1973, Phys. Rev. **B7**, 4220.

Atzmony, V. and M. Dariel, 1976, Phys. Rev. **B13**, 4006.

Atzmony, V., M. Dariel and G. Dublon, 1977, Phys. Rev. **B15**, 3565.

Barbara, B., J. Giraud, J. La Forrest, R. LeMaire, E. Siaud and J. Schweitzer, 1977, Physica **86–88B**, 155.

Bargouth, M. and G. Will, 1971, J. de Physique **32**, C1-675.

Becker, R. and W.D. Doring, 1939, Ferromagnetismus (Springer, Berlin).

Bell, D.G., 1954, Rev. Mod. Phys. **26**, 311.

Belov, K.P., O.P. Yelyutin, G.I. Katayev, D. Kim, S.A. Nikitin, G.V. Pshechenkova, L.I. Solntseva, G.N. Surovaya, and V.P. Taratynov, 1975, Phys. Met. Metallogr. **39**, 50.

Berlincourt, D.A., D.R. Curran and H. Jaffe, 1964, Physical Acoustics, IA, (by W.P. Mason ed.) (Academic Press, New York).

Bowden, G., D. St. P. Bunbury, A.P. Guimares and R.E. Snyder, 1968, J. Phys. C (Proc. Phys. Soc.) **1**, 1376.

Bozorth, R.M., 1951, Ferromagnetism (Van Nostrand, New York).

Bozorth, R.M. and R.W. Hamming, 1953, Phys. Rev. **89**, 865.

Bozorth, R.M., E.R. Tilden, and A.J. Williams, 1955, Phys. Rev. **99**, 1788.

Burzo, E., 1971, Z. Angew. Phys. **32**, 127.

Buschow, K. and R. Van Stapele, 1970, J. Appl. Phys. **41**, 4066.

Buschow, K. and R. Van Stapele, 1971, J. de Physique **32**, C1-672.

Callen, E. and H.B. Callen, 1963, Phys. Rev. **129**, 578.

Callen, E. and H.B. Callen, 1965, Phys. Rev. **139**, A455.

Callen, H.B. and S. Shtrickman, 1965, Solid State Comm. **3**, 5.

Chikazumi, S. and S. Charap, 1964, Physics of Magnetism (Wiley, New York).

Clark, A., 1973, Appl. Phys. Lett. **11**, 642.

Clark, A., 1974, AIP Conf. Proc. No. 18 (American Institute of Physics, New York) p. 1015. Also Proc. 11th Rare Earth Research Conf. (U.S.A.E.C. Tech. INF. Center, Oak Ridge) p. 972.

Clark, A.E. and H. Belson, 1972, AIP Conf. Proc. no. 5 (American Institute of Physics, New York) p. 1498; Phys. Rev. **B5**, 3642; IEEE Trans. Mag. **MAG-8**, 477.

Clark, A.E. and H.T. Savage, 1975, IEEE Trans. on Sonics and Ultrasonics **SU-22**, 50.

Clark, A.E., R. Bozorth and B. DeSavage, 1963, Phys. Lett. **5**, 100.

Clark, A.E., B.F. DeSavage, W. Coleman, E. Callen and H. Callen, 1963b, J. Appl. Phys. **34**, 1296.

Clark, A.E., B. DeSavage and R. Bozorth, 1965, Phys. Rev. **138**, A216.
Clark, A., H. Belson and N. Tamagawa, 1973a, AIP Conf. Proc. no. 10 (American Institute of Physics, New York) p. 749. Also Phys. Lett. **42A**, 160.
Clark, A.E., H.S. Belson, and R.E. Strakna, 1973b, J. Appl. Phys. **44**, 2913.
Clark, A.E., H.S. Belson, N. Tamagawa and E. Callen, 1974, Proc. Int. Conf. on Magnetism **ICM-73**, Moscow, Sept. 1973, volume IV, p. 335.
Clark, A., J. Cullen and K. Sato, 1975, AIP Conf. Proc. no. 24 (American Institute of Physics, New York) p. 670.
Clark, A.E., J. Cullen, O. McMasters and E. Callen, 1976, AIP Conf. Proc. no. 29 (American Institute of Physics, New York) p. 192.
Clark, A.E., R. Abbundi, O. McMasters and H. Savage, 1977, Physica **86-88B**, 73.
Clark, A.E., R. Abbundi and W.G. Gillmor, 1978, IEEE Trans. Mag. **MAG-14**, 542.
Clark, C.A., 1956, Brit. J. Appl. Phys. **7**, 355; 1961, J. Acoust. Soc. Am. **33**, 930.
Cullen, J. and A. Clark, 1977, Phys. Rev. **B15**, 4510.
Cullen, J.R., S. Rinaldi and G.V. Blessing, 1978, J. Appl. Phys. **49**, 1960.
Davis, C.M., 1977, Proc. Workshop on Magnetostrictive Materials, Naval Research Laboratory, Orlando, Florida, p. 39.
Dwight, A. and C. Kimball, 1974, Acta. Crys. **B30**, 2791.
Ferebee, S.F. and C.M. Davis, 1958, J. Acoust. Soc. Am. **30**, 747.
Forester, D., C. Vittoria, J. Schelleng and P. Lubitz, 1978, J. Appl. Phys. **49**, 1966.
Freeman, A. and R. Watson, 1962, Phys. Rev. **127**, 2058.
Guimaraes, A., Ph.D. dissertation. See K.N.R. Taylor, 1971, Adv. in Physics **20**, 551.
Hall, R.C., 1959, J. Appl. Phys. **30**, 816.
Hall, R.C., 1960, Trans. TMS-AIME **218**, 268.
Hoffman, U., 1967, Z. Angew Phys. **22**, 106.
Keffer, F., 1955, Phys. Rev. **100**, 1692.
Kittel, C., 1949, Rev. Mod. Phys. **21**, 541.
Klimker, H., M. Rosen, M.P. Dariel and U. Atzmony, 1974, Phys. Rev. **B10**, 2968.
Koon, N.C., A. Schindler and F. Carter, 1971, Phys. Lett. **37A**, 413.
Koon, N.C., A. Schindler, C. Williams and F. Carter, 1974, J. Appl. Phys. **45**, 5389.
Koon, N.C. and C.M. Williams, 1977, NRL Report 8137, Naval Research Laboratory, Washington, D.C.
Koon, N.C. and C.M. Williams, 1978, J. Appl. Phys, **49**, 1948.
Legvold, S., J. Alstad and J. Rhyne, 1963, Phys. Rev. Lett. **10**, 509.
Masiyama, Y., 1931, Sci. Rep. Tohoko Univ. **20**, 574.
McKeehan, L.W., 1937, Phys. Rev. **51**, 136.
McMasters, O.D., G.E. Holland and K.A. Gscheidner Jr., 1978, J. Crystal Growth **43**, 577.
Milstein, J., 1976, AIP Conf. Proc. no. 29 (American Institute of Physics, New York) p. 592.
Pearson, R.F., 1960, J. Appl. Phys. **31**, 160S.
Perthel, R., G. Elbinger, and W. Keilig, 1966, Phys. Status Solidi **17**, 151.
Rhyne, J. and S. Legvold, 1965, Phys. Rev. **138**, A507.
Rhyne, J., S. Pickart and H. Alperin, 1972, Phys. Rev. Lett. **29**, 1562.
Rhyne, J., J. Schelleng and N. Koon, 1974, Phys. Rev. **B10**, 4672.
Rhyne, J., 1978, Handbook on the physics and chemistry of the rare earths, vol. 2 (K. Gschniedner, Jr. and L. Eyring, eds.) (North-Holland, Amsterdam).
Rinaldi, S., J. Cullen and G. Blessing, 1977, Phys. Lett. **61A**, 465.
Rinaldi, S., and J.R. Cullen, 1978, Phys. Rev. **18**, 3677.
Rosen, M., H. Klimker, U. Atzmony and M. Dariel, 1973, Phys. Rev. **B8**, 2366.
Rosen, M., H. Klimker, U. Atzmony and M. Dariel, 1974, Phys. Rev. **B9**, 254.
Sato, K., E. Callen and N. Tamagawa, 1976, J. College of Liberal Arts, Toyama University **9**, 19.
Savage, H.T. and A.E. Clark, Conf. on Rare Earths and Actinides, 1977, Durham, England, July 1977.
Savage, H.T., A.E. Clark and J. Powers, 1975, IEEE Trans. Mag. **MAG-11**, 1355.
Savage, H.T., A.E. Clark, N.C. Koon and C.M. Williams, 1977, IEEE Trans. Mag. **MAG-13**, 1517.
Shih, J.W., 1936, Phys. Rev. **50**, 376.
Smit, J. and H.P.J. Wijn, 1959, Ferrites (Wiley, New York) p. 169.
Stevens, K.W.H., 1952, Phys. Soc. **65**, 209.
Timme, R., 1976, J. Acoust. Soc. Am. **59**, 459. Also NRL Report 8064.
Taylor, K., 1971, Adv. Phys. **20**, 551.

Tsuya, N., A. Clark and R. Bozorth, 1964, Proc. Int. Conf. on Magnetism, Nottingham (Inst. of Phys. and Physical Society, London) p. 250.
Wallace, W.E. and E. Skrabek, 1964, Rare Earth Research II (Gordon and Breach, New York) p. 431.
Wallace, W.E., 1968, Prog. Rare Earth Sci. Technol. **3**, 1.
Wallace, W.E., 1973, Rare earth intermetallics (Academic Press, New York).
Weil, L. and K. Reichel, 1954, J. Phys. Radium **15**, 725.
Went, J.J., 1951, Physica **17**, 98.
Wertheim, G., V. Jaccarino and J. Wernick, 1964, Phys. Rev. **A135**, 151.
Williams, C. and N. Koon, 1975, Phys. Rev. **B11**, 4360.
Williams, C. and N. Koon, 1977, Physica **86-88B**, 14.
Williams, C. and N. Koon, 1978, Solid State Commun. **27**, 81.
Williams, C., N. Koon and J. Milstein, 1978, J. Phys. Chem. Solids **39**, 823.
Williams, S.R., 1932, Rev. Sci. Instrum. **3**, 675.
Yamamoto, M. and R. Miyasawa, 1965, Sci. Rep. Tohoku Univ. **A5**, 22.
Yamamoto, M. and T. Nakamichi, 1958, J. Phys. Soc. Japan **2**, 228.

SUBJECT INDEX

MATERIALS INDEX

*R = rare earth metal, M_n = non-magnetic metal, M_d = d-transition metal